Petrogenesis of the Ferrogabbroic Intrusions and Associated Fe-Ti-V-P Mineralization within the McFaulds Greenstone belt, Superior Province, Canada

Benjamin Nick Kuzmich

Submitted in partial fulfillment of

the requirements for the degree of

M.Sc. – Geology

Supervisor: Dr. Pete Hollings

Department of Geology

Lakehead University

Thunder Bay, Ontario

December 2014

Abstract

The McFaulds Lake area (commonly known as the Ring of Fire), has been the site of much recent exploration within northern Ontario. The area represents a recently discovered Archean greenstone belt which is host to world class chromite deposits along with significant Cu-Zn VMS, magmatic Ni-Cu-PGE and Fe-Ti-V occurrences. Much emphasis has been placed on the chromite mineralized ultramafic intrusions with little attention focused on the Fe-Ti-V mineralized ferrogabbroic intrusions.

The Butler and Thunderbird intrusions represent the best described intrusions within the volumetrically significant ferrogabbroic suite within the McFaulds Lake area. These intrusions are characterized by a suite of well layered magnetite-ilmenite rich rocks which are dominantly composed of gabbroic to anorthositic units with lesser stratigraphically conformable units composed of pure magnetite-ilmenite. The Fe-Ti oxide rich layers contain variable vanadium mineralization and low chromium contents within magnetite (up to 2.45 V_2O_5 wt. %, 0.99 % Cr_2O_3 wt. %) and ilmenite (up to 0.57 V_2O_5 wt. %). The massive and semi-massive oxide layers occur as basal members of repeated cycles characterized by sharp lower contacts which grade upwards into oxide-rich pyroxenite, followed by oxide-bearing leucogabbros and/or anorthosites. The layers are believed to be caused dominantly by magmatic convection currents within a system which is at least partially open to oxygen. No evidence has been found to suggest multiple pulses of magma. Oxide-silicate liquid immiscibility is thought to only occur within the evolved, apatite-bearing margins of the Thunderbird intrusion; however, additional drilling may reveal further apatite mineralization.

The ferrogabbroic intrusions are thought to have originated from a shallow depleted mantle source, possibly related to a plume event. The ferrogabbros have likely undergone a two stage differentiation to account for the extreme iron enrichments. The first stage is characterized by an anhydrous, tholeiitic melt, within the upper mantle (above the garnet stability field, <110 Km) which underwent Fe-Ti enrichment due to the crystallization of Fe-poor phases (e.g., olivine, plagioclase, etc.) within a system closed to oxygen. The second stage is considered to be a very shallow intrusion within the McFaulds Lake mafic-felsic volcanic rocks. This final stage is characterized by a system which was at least partially open to oxygen from an originally reduced magma (<QFM buffer). These magmas initially crystallized Cr-V-rich magnetite-ilmenite horizons and gradationally evolved into Cr-V-poor, apatite-bearing ferrogabbros. These ferrogabbros likely share a parental magma with the coeval Cr-Ni-PGE-bearing ultramafic intrusions of the McFaulds Lake greenstone belt. Additionally, spatial and geochronological evidence suggests that abundant VMS-style mineralization within the McFaulds Lake area may be a result of a thinned lithosphere during plume tectonics.

Table of Contents

List of Figures

List of Tables

List of Equations

1. Introduction

1.1. Background

The McFaulds Lake area of Northern Ontario has been the focus of recent exploration for base and precious metals (Metsaranta and Houlé, 2012). This area is commonly known as the Ring of Fire, and includes several significant deposits, such as the Eagles Nest (Ni-Cu-PGE), Black Thor (Cr), Blackbird (Cr), Black Horse (Cr), Black Creek (Cr), Big Daddy (Cr), McFaulds Lake and Butler (Cu-Zn VMS) and the Thunderbird (Fe-Ti-V; Mungall et al., 2011).

Initial mapping in the McFaulds Lake area took place between 1960 and 1962, with the Geological Survey of Canada's "Roads to Resource" program, which focused on mapping and interpreting the geology of the area (Bostock, 1962). A later mapping project was conducted through the Ontario Department of Mines in 1969 based on helicopter reconnaissance (Bennet and Riley, 1969) and summarized by Thurston et al. (1979).

The initial economic interest in the area was focused on exploration for diamonds, which began in 1959 and continued intermittently until 1988, when Monopros Ltd. discovered the first diamondiferous kimberlites (Mungall et al., 2010). Increased exploration activities for kimberlite bodies led to the accidental discovery of the McFaulds Lake VMS in April of 2002 by Spider Resources Inc. (Mungall et al., 2010). Since 2002, the McFaulds Lake area has been heavily explored and the discovery of major chromite, Ni-Cu-PGE, VMS, and Fe-Ti-V occurrences have been reported (Mungall et al., 2010).

1.2. Objective

The purpose of this thesis was to better understand the petrogenesis of the ferrogabbros which host Fe-Ti-V-P mineralization within the McFaulds Lake area. Petrographic and geochemical analysis of the ferrogabbros of the Butler intrusions, held by MacDonald Mines Exploration, and the Thunderbird intrusion, held by Noront Resources Ltd., and their associated Fe-Ti-V-P mineralization will aid in the understanding of the ferrogabbros, and the McFaulds Lake intrusive rocks as a whole.

The study of ferrograbbros within the McFaulds Lake area has implications for the regional geology, tectonics, and large igneous provinces globally. This study also investigated possible genetic links with other magmatic deposits within the Ring of Fire, and the development of enhanced exploration models.

1.3. Oxide Mineralogy

In this study, a strong emphasis was placed on the abundance and characterization of the oxide minerals present within the Thunderbird and Butler intrusions. The term oxide in this thesis refers to the common iron-titanium oxide (Fe-Ti-oxide) series, which is present in the ferrogabbroic suite. Due to the importance of the oxide species, the chemical and crystallographic variations within the intrusions must be fully understood in order to properly interpret petrographic relationships.

Oxide minerals are categorized based on the number of different sites they possess, and can be divided into simple or multiple oxides according to the Dana classification of minerals (Gaines et al., 1997). The simple oxides are generally dominated by a single cation

site, whereas the multiple oxides generally contain two or more different sites, usually one with a 4-coordination and the other with a 6-coordination (Dyar et al., 2008). Within this study, the rhombohedra group of simple oxides and the spinel group of multiple oxides are of particular relevance.

The spinel group of minerals is characterized by a general formula of $A^{2+}B_2^{3+}O_2^{2-}$, where A is a divalent cation (Mg, Mn, Fe, Zn, Co, Cu, and/or Ge), and B is a trivalent cation (Al, Fe, Cr, and/or V; Dyar et al., 2008). The spinel group is characterized by a cubic (isometric) crystal system with the oxide anions arranged in a cubic close-packed lattice and the cations (A and B) occupying some, or all of the octahedral and tetrahedral sites (Dyar et al., 2008). Although the spinel group contains numerous end members, it can be divided into three major series; aluminum spinels, iron spinels, and chromium spinels. The aluminum spinels are characterized by the B (i.e., trivalent) cation space being occupied by an aluminum atom (e.g., $FeAl_2O_4$-Hercynite), iron spinels by an iron atom (e.g., $TiFe_2O_4$-Ulvöspinel), and chromium spinels with a chromium atom (e.g., $FeCr_2O_4$-chromite).

The rhombohedral group of minerals is defined by a hexagonal close-packed array of oxygen atoms with the metal cations in octahedral interstices (Stormer, 1983). These simple oxides contain a large range of formulae but in general are either $A^{2+}O$, $A^{1+}O_2$, or $A_2^{3+}O_3$ (Dyar et al., 2008). Of particular interest are the corundum and the ilmenite groups of oxides. The corundum group is characterized by a 3+ cation (e.g., Al^{3+}, Cr^{3+}, Fe^{3+}, V^{3+}) and includes the common iron oxide, hematite. The ilmenite group is with the corundum group with a lower symmetry due to alternations of the A cation with the Ti^{4+} unit cell (Dyar et al., 2008). The ilmenite group is characterized by a general formula of $ATiO_3$, where A can be Fe^{2+}, Mg^{2+}, Mn^{2+}, Zn^{2+}, or Sb^{5+} (Dyar et al., 2008).

1.4. FeO-Fe_2O_3-TiO_2

The iron-titanium oxides relevant to this study exhibit complex interrelationships between mineralogical characteristics which have been well studied in the past (e.g., Buddington and Lindsley, 1964). The pioneering work of Buddington and Lindsley (1964) was focused on the controls of ulvöspinel-magnetite, and hematite-ilmenite exsolution textures in order to determine the primary and secondary conditions which affected the preserved textures. This work led to a better understanding of the origins of Fe-Ti-oxides, the conditions for formation and a formula which can be used to determine the temperature and oxygen fugacity of a crystalizing magma which contains Fe-Ti-oxide grains.

The FeO-Fe_2O_3-TiO_2 system can be divided into a spinel series and a rhombohedral series of minerals. The spinel series is characterized by a solid solution (denoted as: ss) between magnetite and ulvöspinel, whereas the rhombohedral series is characterized by a solid solution between hematite and ilmenite (Fig. 1.1; Buddington and Lindsley, 1964). In an attempt to address the geologically common exsolution of ilmenite grains within magnetite Buddington and Lindsley (1964) theorized that either the magnetite and/or ilmenite grains were the result of secondary processes, rather than a primary intergrowth of minerals as observed in some silicate minerals (e.g., perthite). This theory was supported by limited experimental work which demonstrated that the solubility of ilmenite in magnetite is too small to account for the majority of ilmeno-magnetites by simple exsolution (Lindsley, 1962, 1963). Furthermore, Buddington and Lindsley (1964) proposed that both $magnetite_{ss}$-$ulvöspinel_{ss}$ and $hematite_{ss}$-$ilmenite_{ss}$ occur with each other in equilibrium to generally form titanomagnetite, and that upon cooling of the solid solution series, exsolution at submagmatic

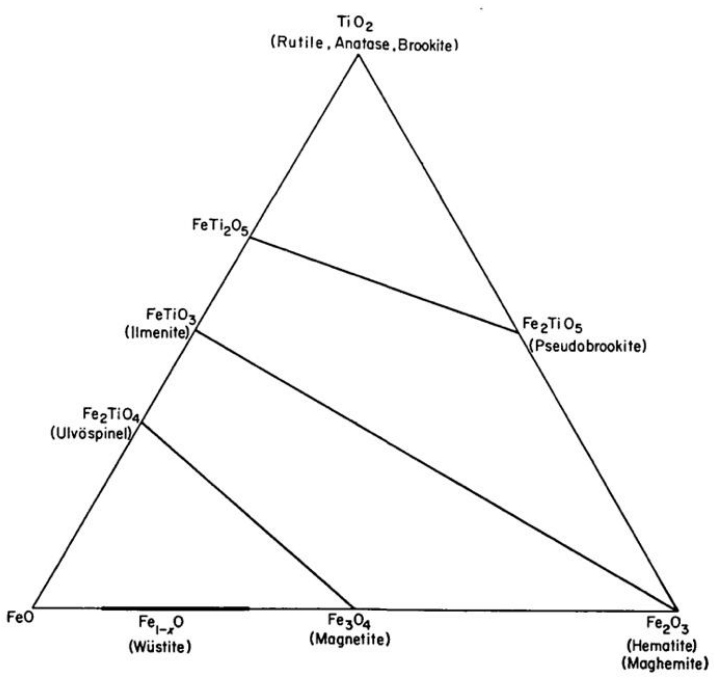

Figure 1.1. FeO-Fe_2O_3-TiO_2 system (from Buddington and Lindsley, 1964)

temperatures (as low as 500°C) occurs to produce dominantly magnetite-ilmenite pairs with variable titanium concentrations within magnetite and Fe_2O_3 in ilmenite. The titanium-rich magnetite (titanomagnetite) can be separated into two phases largely controlled by temperature and oxygen fugacity of the magma, which are approximately dependent on one another (Buddington and Lindsley, 1964). It is thought that in most igneous and metamorphic rocks, exsolution of ilmenite lamellae is probably contemporaneous or pene-contemporaneous with the oxidation of Fe_2TiO_4 (ulvöspinel; Buddington and Lindsley, 1964). This theory is supported by experimental data which demonstrated the formation of magnetite-ilmenite grains from an orignal ulvöspinel crystal in a closed system with increased oxygen fugacity (Buddington and Lindsley, 1964).

Variations within the compositions of resulting pairs of $magnetite_{ss}$-$ulvöspinel_{ss}$ and $hematite_{ss}$-$ilmenite_{ss}$ is believed to be caused by oxygen fugacity and/or temperature (e.g.,

Buddington and Lindsley, 1964; Stormer, 1983). It has been shown that at constant temperatures, an increase in oxygen fugacity results in a decrease in the percentage of TiO_2 in the magnetite, and an increase in the MnO and Fe_2O_3 of the ilmenite (Buddington and Lindsley, 1964). The oxygen fugacity also has a major role in the distribution of minor elements, particularly vanadium (Mallmann and O'Neil, 2009). This dependence upon the oxygen fugacity is exemplified in V due to the large range of valance states which may occur within a magma (V^{2+},V^{3+},V^{4+},V^{5+}, and/or V^{6+}; Mallmann and O'Neil, 2009). This is in contrast to homovalent elements which are compatible within the Fe-Ti-oxide grains (e.g., Sc, Ga, Y ,Zr, etc.), and therefore independent of the oxygen fugacity (Mallmann and O'Neil, 2009). It has been proposed that an increase in temperature corresponds to an increase in TiO_2 within the primary titanomagnetite; however, oxygen fugacity is considered a more important parameter due to the relatively large variations in oxygen fugacity over short ranges of temperature for a given redox buffer (Buddington and Lindsley, 1964).

Textural relationships within magnetite-ilmenite pairs have also been shown to correspond to variations in oxygen fugacity and cooling rates (Bowles, 1977). It has been established that upon a relatively fast quenching of a iron-titanium-oxide bearing magma (e.g. thoeliitic basalt), the primary $magnetite_{ss}$-$ulvöspinel_{ss}$ can be completely preserved as a homogenous, exsolution-free oxide grain (Stormer, 1983). However, during slower cooling of a magma, oxidation of the primary oxides produces a titanium-bearing magnetite, and a ferrous-bearing ilmenite exsolution (Buddington and Lindsley, 1964). This oxidation may be caused internal processes (e.g. decoupling of hydrous phases) or external processes (e.g., contamination by highly oxidized material). The progression of oxidation within the Fe-Ti-oxides reaches a maximum endmember of pure magnetite and pure ilmenite upon very slow cooling and sufficient oxidisation (Buddington and Lindsley, 1964). It has also been suggested

that the form of exsolution is dependent on the rate of cooling, in which external/granule exsolution occurs at high temperatures and slow cooling, whereas thin ilmenite lamellae within magnetite occur at lower temperatures (Buddington and Lindsley, 1964).

2. Regional Geology

2.1. Superior Province

The Superior Province of North America comprises 23% of the world's exposed Archean crust, spanning approximately 1 572 000Km^2, making it the largest Archean craton in the world (Thurston et al., 1991).The Superior Province is bound to the north, east, and west by rocks of Paleoproterozoic age, and to the southeast by the Mesoproterozoic Grenville Province (Fig. 2.1).

The Superior Province is interpreted to have formed through the amalgamation of discrete continental fragments during the Kenoran Orogeny, which occurred between 2.72 and 2.68 Ga (Percival et al., 2002). Card and Ciesielski (1986) originally classified these assemblages as subprovinces and recognized four broad types i) volcano-plutonic, ii) metasedimentary, iii) plutonic, and iv) high grade gneissic, all of which were bound by lithospheric scale faults. The volcano-plutonic sequences are dominated by subaqueous mafic volcanic flows interpreted to represent island-arc settings (Thurston and Chivers, 1990) which are surrounded or cut by later felsic intrusive batholiths (Card and Ciesielski, 1986). The metasedimentary units are dominated by clastic sedimentary sequences which were later intruded by large S-type granites and have been metamorphosed from greenschist to granulite facies (Thurston et al., 1991). The plutonic, or gneissic sequences are characterized by tonalitic gneiss with very little supracrustal rocks (Beakhouse, 1985). The high grade gneissic regions are composed of amphibolite to granulite facies metamorphic rocks cut by felsic intrusive rocks, such as the Kapuskasing Structural Zone (Thurston et al., 1991).

Since the original subprovince classification proposed by Card and Ciesielski (1986), there has been much debate regarding the boundaries and classification of subdivisions within

the Superior Province. Stott et al. (2010) have recently revised the boundaries and terminology of the craton based on geochronology, seismic data, mapping, isotopic data and aeromagnetic data. The use of the term terrane has replaced in favour of subprovince to represent a tectonically bounded region with internal characteristics distinct from those in adjacent regions prior to Neoarchean assembly of the Superior Province (Stott et al., 2010). The term superterrane is applied to an amalgamation of multiple terranes prior to Neoarchean assemblage (Stott et al., 2010). Terranes may be subdivided into domains, which are a typically younger, yet distinct part of a terrane which either share a common basement or contain juvenile crust (Stott et al., 2010). The resulting classification subdivides the Superior Province into numerous, distinct regions with their own tectonic characteristics (Fig. 2.1).

Within the newly revised Superior Province, there remains the need for further correlation between terranes. Stott et al. (2010) suggested that the Uchi Domain and the Oxford-Stull Domain (Fig. 2.1) may actually be a single domain, which continues eastward across the James Bay Lowlands as indicated by aeromagnetic data. Furthermore, there are also geological similarities (stratigraphic, magnetic, etc.) between the Opatica Subprovince and the Quetico basin (Lacroix, 1987), which is similar to the relationship between the English River and Winnipeg River terranes (Williams, 1991).

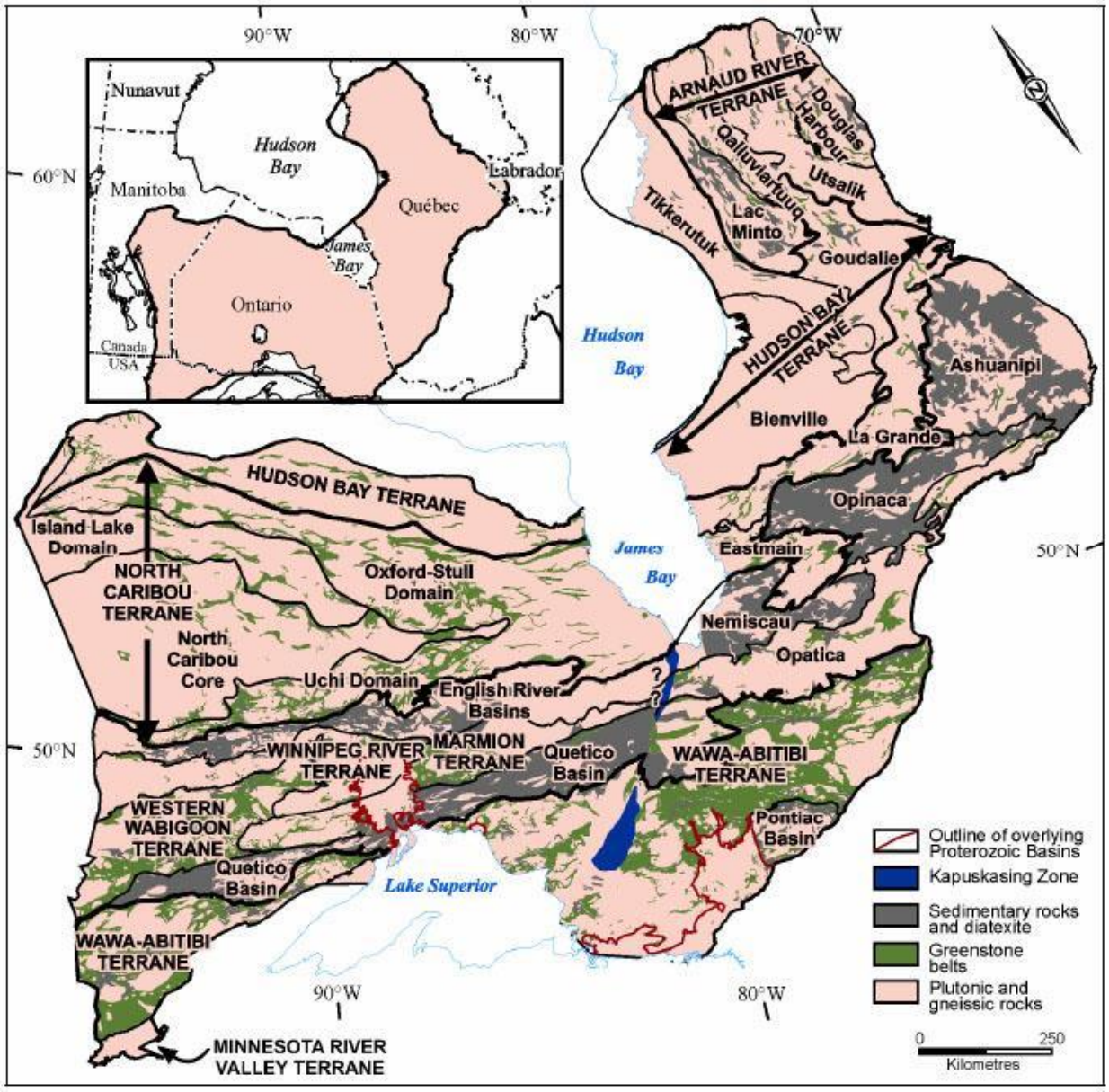

Figure 2.1. Divisions of the Superior Province (From Stott et al., 2007)

2.2. North Caribou Terrane

The North Caribou Terrane (NCT) is located in the northern Ontario portion of the Superior Province (Fig. 2.1). The NCT was originally classified by Card and Ciesielski (1986) as the combination of the Sachigo subprovince, Berens River subprovince, and the Uchi subprovince. However, recent data including aeromagnetic surveys, crustal formation ages,

and Nd model ages have redefined the boundaries of the NCT (Percival et al., 2006; Stott et al., 2007, 2010).

The North Caribou terrane is largely comprised of massive felsic plutonic rocks (e.g., the North Caribou batholith), with minor mafic volcanic greenstone belts (Stott et al., 1989). The greenstone belts contain minor komatiite flows intercalated with mature quartzite beds which are interpreted to be the result of plume related magmatism (Percival et al., 2006). The NCT also consists of a rare and diverse group of rocks which include stromatolitic-bearing sandstones interpreted to have formed in shallow subaqueous environment (e.g., Muskrat Dam Lake greenstone belt; Thurston et al., 1991) to volcanic rocks with a shoshonitic affinity (North Spirit Lake greenstone belt; Smith and Longstaffe, 1974).

The North Caribou is the largest Mesoarchean terrane of the Superior Province and displays widespread evidence for mantle extraction ages of ~3.0 Ga (Percival et al., 2006). Greenstone belts within the NCT have preserved ages from 2.9 to 3.0 Ga (e.g., Red Lake and North Caribou Lake greenstone belts) as well ~2.9 Ga rift sequences which occur locally within the central NCT and contain detrital zircons ranging from 2.97 to 3.048 Ga (Stott et al., 2010). The NCT has recorded two broad episodes of plutonic and metamorphic activity which span 2.89 to 2.895 Ga and 2.85 to 2.86 Ga (Stott et al., 2010). The North Caribou terrane forms a core onto which Neoarchean crust has amalgamated along the northern and southern margins (Stott et al., 2010). The recent classification of Stott et al. (2010) has subdivided the NCT into the Island Lake domain, Oxford-Stull domain, and the Uchi domain, all of which border the North Caribou core. The amalgamation of these domains is believed to have occurred prior to 2.87 Ga (Percival et al., 2006).

2.2.1. Island Lake Domain

The Island Lake domain is located on the northern margin of the older North Caribou Core and is characterized by a complex Meso- and Neoarchean crustal history (Stott et al., 2010). The Island Lake domain is composed of oceanic arc greenstone belts (e.g., Island Lake greenstone belt) within a series of granite plutons which overlap the provincial boundary between Ontario and Manitoba (Thurston et al., 1991). The Island Lake domain as it is currently defined had been previously divided into the Island Lake terrane to the northwest and the east, the Muskrat Dam terrane in the central portion, and the Munro Lake terrane to the southeast (Card and Ciesielski, 1986).

The majority of studies of the Island Lake domain have largely focused on the Island Lake greenstone belt (ILGB). The Island Lake greenstone belt is separated from the North Caribou Core to the south by the Savage Island shear zone (Parks et al., 2006). The western ILGB is characterized by 2852 Ma dacitic tuffs and 2744 Ma granites with ε_{Nd} values ranging from -2.0 to -0.4, and model ages that range from 2.97 to over 3.0 Ga (Stevenson and Turek, 1992) and is interpreted to represent a Mesoarchean crustal component within the ILGB (Parks et al., 2006). The ILGB spans approximately 200 million years (Parks et al., 2006) and is composed of volcano-sedimentary assemblages which have been intruded by felsic plutonic rocks (e.g., Bella Lake pluton). The lowermost unit within the ILGB is the Island Lake Group which is composed of turbidite sequences which contain detrital zircons ranging in age from 2920 to 2712 Ma in the eastern portion and 2938 to 2722 Ma in the western portion (Corfu and Lin, 2000). The Island Lake Group is lithologically similar to the Timiskaming Group in the Abitibi greenstone belt, and it has been suggested that the sedimentary sequences may have formed within a late orogenic basin which is consistent with the theory that the Island Lake

domain collision with the North Caribou terrane occurred over 20-40 million years as proposed by Percival et al. (2006). The Island Lake Group has also been interpreted to be the result of infilling of a basin caused by continental rifting (Thurston et al., 1991).

2.2.2. Uchi Domain

The Uchi Domain roughly corresponds to the original boundaries of the Uchi subprovince as defined by Card and Ciesielski (1986). It is currently thought that the Uchi domain shares a common basement with the North Caribou Core, and was consequently termed a domain (Stott et al., 2010).

The Uchi Domain is an approximately linear belt, composed of a supracrustal volcanic-sedimentary assemblage with younger felsic plutons (Stott and Corfu, 1991). The volcanic rocks are dominated by two distinct trends; a tholeiitic basalt, with lesser komatiite, and calc-alkaline andesite, dacite and rhyolite (Stott and Corfu, 1991).The tholeiitic series (e.g., the Balmer assemblage) is considered to represent an oceanic mafic sequence, likely in a back-arc setting; whereas the calc-alkaline series (e.g., the Confederation assemblage) represents continental or oceanic-arc settings (Stott and Corfu, 1991). Plutonism within the domain is largely felsic, and occurs as syn-volcanic intrusions, (e.g., the Dobie Lake pluton; Stott and Wilson, 1986), pre- to syn-tectonic (e.g., the North Bamaji pluton; Wallace, 1985), or post-tectonic intrusions (e.g., the Williams suite; Stott and Corfu, 1991). The late to post-tectonic plutons are generally massive granite to granodiorite in composition, and are volumetrically the most significant (Stott and Corfu, 1991).

The crustal growth of the Uchi domain formed in pulses from approximately from 2.69 Ga to 3 Ga, and shows a general southward younging (Stott and Corfu, 1991). Widespread magmatic U/Pb zircon ages and Nd model ages indicate the presence of 2.8 to 2.9 Ga crust

which is comparable to the Island Lake domain (Stott et al., 2010). The eastern portion of the Uchi domain is tentatively interpreted to extend along the eastern margin of the North Caribou Core and transition into the Oxford-Stull domain (Stott G. , Superior Province: terrances, domains and autochthons, 2008).

2.2.3. The North Caribou Core

The North Caribou Core (NCC) is located in the western portion of the North Caribou terrane (Fig. 2.1). The region was originally classified by Card and Ciesielski (1986) as the western part of the Sachigo and Berens River subprovinces. The NCC forms a Mesoarchean core upon which the subsequent Neoarchean domains have been added to the southern and northern margins (Stott et al., 2010).

The NCC is largely dominated by Mesoarchean granitoid intrusions, with several narrow greenstone belts (e.g., the North Caribou greenstone belt) which range in age from 2.9 to 3.0 billion years (Stott et al., 2010). The North Caribou Lake greenstone belt (NCGB) is characterized by seven assemblages which developed through two episodes of volcanism and sedimentation between 2981 +/- 1.8 and 2932 +/- 3 Ma (Breaks et al., 2001). These supracrustal rocks were deposited on a dominantly 2990 +/- 1 Ma tonalitic basement (Breaks et al., 2001). Volcanic rocks within the NCGB range from arc-related mafic rocks (Breaks et al., 2001) with intercalated felsic units (Hollings et al., 1999) which have been dated by U-Pb at 2972.4 +/- 0.8 and 2982.4 +/- 1.0 (Biczok et al., 2012), and intermediate flows formed through supra-subduction processes, with rare ultramafic flows of plume origin (Hollings and Kerrich, 1999). Thin quartzite-komatiite packages have been preserved within NCC which is consistent with a plume related rifting event at circa 2.9 Ga (e.g., Stott et al., 2010). The NCGB felsic intrusive tonalite-trondhjemite-granite suits range in age from relatively older material at 2869

+/- 3.6 Ma (DeKemp, 1987) and 2864 +/- 1.1 Ma (Davis and Stott, 2001) to younger intrusions such as the North Caribou Lake batholith emplaced at 2725.8 +/- 3 Ma (Klipfel, 2002) along with granitic dykes as young as 2668.8 +/- 1.1 Ma (Biczok et al., 2012).

2.2.4. The Oxford-Stull Domain

The Oxford-Stull Domain (OSD) of the North Caribou terrane was originally defined by Card and Ciesielski (1986) to include the northern and eastern portions of the Sachigo subprovince. The domain is characterized by ~2.830 to 2.71 Ga metavolcanic and metaplutonic rocks which may represent material accreted onto the North Caribou core (Lin et al., 2006). The domain is bound to the north by the North Kenyon fault which contacts with the Hudson Bay terrane and to the south by the Stull-Wunnummin fault with the NCC as defined by Stott et al. (2010). The OSD is host to the McFaulds Lake greenstone belt (Metsaranta and Houlé, 2012) and has been the site of and academic research.

The volcanic and plutonic rocks of the OSD typically have Neoarchean to Mesoarchean Nd model ages, and positive ε_{Nd}, indicative of relatively juvenile crustal growth (Skulski et al., 2000; Rayner and Stott, 2005). Across the OSD, U-Pb zircon ages have yielded Neoarchean volcanic and pluton dates as young as 2710 Ma near the Manitoba-Ontario border (Stott et al., 2010), and 2737 to 2969 Ma near the James Bay Lowlands in Ontario (Skulski et al., 2000; Rayner and Stott, 2005).

The Hayes River group in the western OSD occurs along the southern margin with the Island Lake domain, and represents one of the best studied areas within the domain (Stott et al., 2010). The group is composed of volcanic rocks which range from 2870 to 2830 Ma, and show a geochemical gradation through time evolving from a sequence which is MORB-like, to island-arc, then a variably contaminated non-arc, a non-arc with a possibly contaminated back-

arc basin basalt, then picrites (Stott et al., 2010). These volcanic rocks are unconformably overlain by greywackes, iron formations, and pebble to cobble conglomerates with 2707- 3500 million-year-old detrital zircons (Stott et al., 2010).

2.3. The McFaulds Lake Greenstone Belt

The McFaulds Lake greenstone belt is located within the western portion of the OSD within the NCT (Stott et al., 2010). Based on preliminary investigation of drill holes and limited outcrops, the greenstone belt has been shown to contain five distinct Archean supracrustal rock assemblages (Fig. 2.2; Metsaranta and Houlé, 2012; 2013).

Through the collaboration of the Targeted Geosciences Initiative-four (TGI-4) and the Ontario Geological Survey (OGS), a three year regional mapping project of the McFaulds Lake area has been undertaken to update the regional bedrock geology, characterize major lithological units, and improve our geological understanding of the McFaulds Lake region (Metsaranta and Houlé, 2012; 2013).

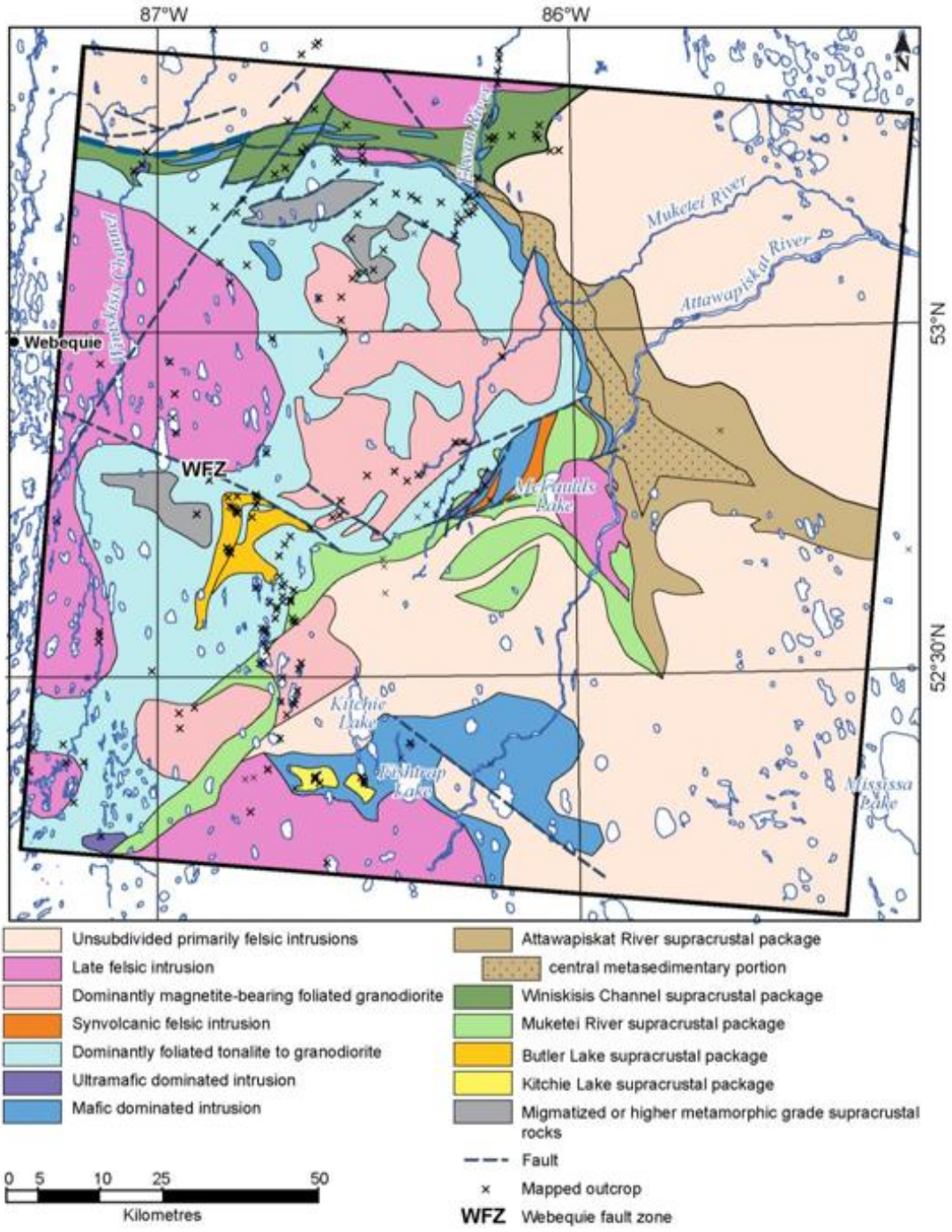

Figure 2.2. Preliminary bedrock geology of the McFaulds Lake area (Metsaranta and Houlé, 2012)

2.3.1. Kitchie Lake Supracrustal Assemblage

The Kitchie Lake supracrustal assemblage is a roughly 15km long, east-striking metavolcanic-dominated succession (Fig. 2.2). The assemblage is largely composed of fine- to medium-grained amphibole-plagioclase-biotite +/- garnet schist, along with lesser quartz-biotite-plagioclase schist interpreted to represent mafic and felsic metavolcanic rocks respectively (Metsaranta and Houlé, 2013). The metavolcanic sequences contain rare fine-grained, bedded quartz-biotite-plagioclase schist which is interpreted to represent metasedimentary rocks (Metsaranta and Houlé, 2013).

The Kitchie Lake supracrustal assemblage is also characterized by late mafic and ultramafic layered intrusions (e.g., Highbank-Fishtrap) and possibly related metagabbroic and metapyroxenitic dykes which cross cut the metasedimentary rocks (Metsaranta and Houlé, 2013). The Highbank Lake intrusion had yielded a zircon age of circa 2808 Ma which is the interpreted age of crystallization (Stott G. , Superior Province: terrances, domains and autochthons, 2008); however, preliminary detrital zircon date from the sedimentary rocks of the eastern Kitchie Lake supracrustal assemblage yielded an age of circa 2725 to 2730 Ma (Metsaranta and Houlé, 2013). The age of the Highbank Lake intrusion is contradictory to the field relations described by Metsaranta and Houlé (2013), and may represent contamination by inherited zircon rather than a crystallization age. Therefore, the age of crystallization for the Highbank intrusion remains to be determined (Metsaranta and Houlé, 2013).

The Kitchie Lake surpracrustal assemblage has been recently explored for base and precious metal mineralization (Metsaranta and Houlé, 2013). Nielsen (2010) reported zinc and copper mineralization within sulphide-bearing felsic metavolcanic rocks which suggests that the assemblage has the potential to host VMS-style base metal mineralization. As well, the

Highbank-Fishtrap intrusive complex has the potential to host Ni-Cu-PGE and Fe-Ti-V mineralization (Metsaranta and Houlé, 2012).

2.3.2. Butler Lake Supracrustal Assemblage

The Butler Lake supracrustal assemblage is bounded to the north by the Webequie regional scale dextral shear zone and is surrounded by older tonalitic and migmatized rocks (Metsaranta and Houlé, 2012). The assemblage has been divided by Metsaranta and Houlé (2012) into western and eastern portions which merge in the southwest, and is separated by a central magnetic low (likely a tonalite to quartz-diorite).

The western portion strikes north to northeast for approximately 30km, and is 3 to 4km wide (Fig. 2.2; Metsaranta and Houlé, 2012). The area is dominantly composed of felsic metavolcanic rocks with subordinate mafic and ultramafic metavolcanic rocks with late mafic dominated intrusions (Metsaranta and Houlé, 2012). The eastern portion strikes northeast and is 4 to 5kms wide and is largely composed of high-magnesium mafic metavolcanic rocks with minor felsic metavolcanic rocks and iron formation (Metsaranta and Houlé, 2012). The eastern portion is characterized by a variety of ultramafic (dunite and peridotite) and mafic (magnetite-rich gabbro, magnetite-poor gabbro) intrusive units.

Copper-zinc VMS-style mineralization has been identified within the western portion, and gabbro-hosted nickel-copper-PGE mineralization within the eastern portion of the Butler Lake supracrustal assemblage (Metsaranta and Houlé, 2012). Both areas have been shown to host significant iron-titanium-vanadium mineralization (Metsaranta and Houlé, 2012).

2.3.3. Muketei River Supracrustal Assemblage

The Muketei River supracrustal assemblage strikes roughly northeast, and extends for up to 110km (Fig. 2.2). The area is truncated to the north by the Attawapiskat River supracrustal assemblage, and is surrounded to the south, east, and west by various pre- and post-tectonic tonalitic and granitic rocks (Metsaranta and Houlé, 2012). The assemblage is also transected by numerous northeast-trending dextral shear zones, and north- and northwest-trending faults (Metsaranta and Houlé, 2012).

The Muketei River assemblage is dominantly composed of mafic and felsic metavolcanic successions with minor iron formation and clastic metasedimentary units, which have been intruded by mafic and ultramafic rocks (Metsaranta and Houlé, 2012). The volcanic rocks have been shown to consist of at least two strata; a felsic dominated sequence dated at 2737+/-7 Ma (Rayner and Stott, 2005) and an ultramafic sequence dated at 2770.7 +/-0.8 Ma (Mungall et al., 2010).

The Muketei River supracrustal assemblage is of interest as it hosts several world-class chromite deposits (e.g., Black Thor, Big Daddy, etc.), magmatic nickel-copper-PGE (e.g., Eagle's Nest) deposits, several VMS deposits (e.g., McFaulds #1, and #3), along with iron-titanium-vanadium deposits (e.g., Thunderbird; Metsaranta and Houlé, 2012).

2.3.4. Winiskisis Channel Supracrustal Assemblage

The Winiskisis Channel supracrustal assemblage is east-striking, 80 to 90km long, and 5 to 10km wide (Fig. 2.2; Metsaranta and Houlé, 2012). The assemblage is surrounded by tonalitic and granitic rocks except to the southeast, where it shares a faulted contact with the Muketei River supracrustal assemblage (Metsaranta and Houlé, 2012). The geochronology of

the Winiskisis Channel is incomplete, however, detrital zircons collected from a tuffaceous unit have yielded ages as young as circa 2714 (Buse et al., 2009), which is younger then the Muketei River supracrustal assemblage.

The Winiskisis Channel supracrustal assemblage is subdivided into western, central and eastern portions, all of which have limited outcrop and consequently interpretations are largely based on drill core data (Metsaranta and Houlé, 2013). The western portion is comprised of steeply dipping, sheared, tuffaceous metasedimentary rocks and schistose to gneissic, felsic to intermediate rocks which may represent metasedimentary or metavolocanic rocks (Metsaranta and Houlé, 2013). Within regions of lesser deformation, interbedded greywacke, black siltstone or shale, felsic tuffaceous sandstones, quartz-phyric felsic flows, and mafic flows are shown in drill core (Metsaranta and Houlé, 2013). Rare thin beds of silicified pyrite-pyrrhotite mineralized and chert-magnetite iron formations are also present within the western portion (Metsaranta and Houlé, 2013). The central portion of the Winiskisis supracrustal assemblage is dominated by felsic to intermediate volcanic successions which are interpreted to underlie the mafic metavolcanic sequences described in the eastern portion (Metsaranta and Houlé, 2013). The felsic to intermediate metavolcanic rocks are characterized by moderately to strongly deformed quartz +/- biotite +/- garnet +/- amphibole schist and lesser interlayered fine-grained amphibolite which are interpreted to represent mafic metavolcanic flows. The eastern portion is dominantly comprised of pillowed mafic metavolcanic rocks which are variably deformed (Metsaranta and Houlé, 2013).

The assemblage of supracrustal rocks are host to significant VMS style mineralization within heavily altered felsic and mafic metavolcanic rocks (e.g., Northern Star Eagle; Metsaranta and Houlé, 2012). Potential exists within the magnetite gabbro to host iron-

titanium-vanadium mineralization, and magmatic chromium-nickel-copper-PGE mineralization within the ultramafic assemblage (Metsaranta and Houlé, 2012).

2.3.5. Attawapiskat River Supracrustal Assemblage

The Attawapiskat River Supracrustal assemblage is overlain by Paleozoic strata, and has been divided into three portions based on limited data (Metsaranta and Houlé, 2012). The western portion is dominantly composed of fine- to medium-grained amphibolites, or fine-grained schistose rocks and lesser sericite or biotite schist which sometimes display fine-grained quartz and/or feldspar phenocrysts, interpreted as mafic and felsic metavolcanic rocks respectively (Metsaranta and Houlé, 2013). The western portion also contains subordinate thin sulphide zones within the felsic to intermediate rocks (Palmer, 2007) and has been intruded by ferrogabbroic sills and dykes (Metsaranta and Houlé, 2012). The central portion is not exposed and has been defined solely through drill core (Metsaranta and Houlé, 2013). The central portion is inferred to consist dominantly of clastic metasedimentary units which locally display primary load structures, graded bedding and rare cross-laminations (Metsaranta and Houlé, 2013). Detrital zircons from the sandstone unit have yielded ages of circa 2702 Ma to 2816 Ma (Metsaranta and Houlé, 2012), suggesting the sedimentary succession was not exclusively derived from a local volcanic source (Metsaranta and Houlé, 2013). The eastern portion of the Attawapiskat River supracrustal assemblage is largely comprised of massive and pillowed mafic metavolcanic flows, graphitic and pyritic mudstone and siltstone with rare thin bands of felsic to intermediate tuffaceous rocks (Metsaranta and Houlé, 2013). The mafic volcanic rocks are cross-cut by gabbroic sills which have been interpreted to represent synvolcanic intrusions (Metsaranta and Houlé, 2013).

The Attawapiskat River supracrustal assemblage contains several small VMS style deposits within the felsic volcanic rocks. These are spatially associated with the ferrogabbroic sills that have potential to host iron-titanium-vanadium mineralization (Metsaranta and Houlé, 2012). The area is also prospective for gold in brecciated porphyritic tonalite to quartz diorite intrusions associated with carbonatization, sericitization, silicification and sulphide mineralization (Metsaranta and Houlé, 2012).

3. Methods

3.1. Whole Rock and Trace Element Geochemistry

One hundred samples were collected from the Butler East, Butler West, and Thunderbird intrusions in order to characterize the lithologies and determine possible magmatic stratigraphy (data available in Appendix D). The 100 samples were cut, crushed and milled to −200 mesh in an agate ring mill so as to reduce risk of contamination of trace elements (Jenner, 1996). Tools and working surfaces were cleaned with acetone between each sample. Samples were analyzed for major elements by X-ray fluorescence (XRF) and for trace and rare earth elements by inductively coupled plasma mass spectrometry (ICP-MS) and inductively coupled plasma atomic emission spectrometry (ICP-AES) at the Geoscience Laboratories (Geo Labs) of the Ministry of Northern Development and Mines in Sudbury, Ontario. Selected trace elements (e.g., Zr and Y) were analyzed by XRF using a pressed pellet to allow comparison with data generated by ICP-MS. Totals for major element oxide data were generally 100±2% and have been recalculated to a 100% volatile-free basis. Detection limits for major elements are 0.01 weight % and relative standard deviations of duplicate analyses are within 5%. Trace elements, including the REE and HFSE analyzed at the GeoLabs were completed on a PerkinElmer Elan 9000 ICP-MS following a variation on the protocol described by Burnham and Schweyer (2004) and Tomlinson et al. (1998). Twenty four trace elements were determined using a 200mg aliquots of powder digested by a two stage procedure involving an initial decomposition in a closed beaker by a mixture of HF with lesser HCl and $HClO_4$ followed by a second mixture of dilute HCl and $HClO_4$ as described by Burnham et al. (2002). Detection limits for some critical elements, defined as 3σ of the procedural blank, are as follows: Th (0.032 ppm), Nb (0.044 ppm), Hf (0.085 ppm), Zr (3.2 ppm), La (0.048 ppm) and

Ce (0.08 ppm) (Burnham and Schweyer, 2004). All analyses performed during the course of this study utilized standards, duplicate samples and blanks, both in-house as part of the normal procedures of the analytical facilities, as well as standards submitted for replicate analyses.

Whole rock major and trace element data were used to characterize samples, to determine the major oxide evolution and to interpret possible fractionation trends within the ferrogabbroic intrusions. Within the studied lithologies large concentrations of iron, titanium and vanadium were analyzed. The highest concentrations of iron correspond to negative loss on ignition values due to the oxidation of Fe^{2+} to Fe^{3+} and ultimately a gain in mass. Titanium content was determined by XRF and ICP-AES which yielded values of TiO_2 (wt. %) and Ti (ppm) respectively. Of the samples collected 22% of the analyses were above the upper detection limit for XRF (7.69 wt. %), in which case the TiO_2 wt. % was calculated from the stoichiometric conversion of Ti (ppm) as determined by ICP-AES. Vanadium contents were analyzed by ICP-AES and ICP-MS and were converted to V_2O_5 wt. % based on stoichiometric mass balance.

3.2. Magnetite-Ilmenite Oxybarometer

3.2.1. Introduction

The three phase FeO-TiO_2-Fe_2O_3 system represents two solid solution series; the spinel, and rhombohedral series (Buddington and Lindsley, 1964). The spinel series ranges in composition from magnetite with an ideal composition of $Fe^{2+}(Fe^{3+})_2O_4$, to an ideal ulvöspinel with a composition of $(Fe^{2+})_2Ti^{4+}O_4$ (Fig. 1.1 :Buddington and Lindsley, 1964). The rhombohedral series is characterized by hematite of composition $(Fe^{3+})_2O_3$ and ilmenite of composition $Fe^{2+}Ti^{4+}O_3$ (Buddington and Lindsley, 1964). Solid solution between the end-members is characterized by varying degrees of titanium concentrations within each series. For

simplification, the term titanomagnetite will be used to describe a mineral which is dominantly composed of magnetite, with a lesser ulvöspinel component. Conversely, hemoilmenite is a grain which is dominated by ilmenite, with a lesser hematite composition.

3.2.2. Theory

The theory behind the oxybarometer (oxygen barometer) is based on the concept that the concentration of titanium within the FeO-Fe_2O_3 series causes a cation disorder which is largely dependent on temperature, and indirectly the oxygen fugacity of the crystallizing magma (Navrotsky and Kleppa, 1967). This requires an accurate determination of the composition of two grains which both represent the solid solution series (e.g., ulvöspinel and ilmenite) and have crystallized cogenetically (Buddington et al., 1955). This also requires that the original mineralogy has not undergone alteration, particularly oxy-exsolution (Buddington Lindsley, 1964). The process of oxy-exsolution is very common within slow cooling (i.e., plutonic) rocks in which metastable spinel phases exsolve rhombohedral phases through a solid state oxidation processes (Buddington and Lindsley, 1964). In such cases, the determined temperature and oxygen fugacity of the system determined by the Fe-Ti-oxide minerals would represent the cessation of oxy-exsolution, rather than the primary crystallizing conditions (Bowles, 1977).

Due to the known effects of multicomponent substitution (e.g., Mn, Mg, Cr, V, etc.), it would be logical to calculate the vanadiferous magnetite-ilmenites using a oxybaromenter which accounted for this effect. The model used to determine and calculate the oxybarometer in this research is based on an adaptation of the methods described by Stormer (1983) and

Spencer and Linsley (1981) to include vanadium as a significant substitution competent, particularly within the spinel phase.

The model proposed by Spencer and Lindsley (1981) assumes that (1) ilmenite$_{ss}$ behaves as a binary asymmetric Margules solution; (2) titanomagnetite behaves as a binary asymmetric Margules solution below 800^{o}C and as an ideal binary solution above 800^{o}C; (3) configurational entropy terms can be approximated by a molecular mixing model for magnetite, and by Rumble's (1977) model B (disorder of Fe^{3+}) for ilmenite and; (4) only ordered (R3) ilmenite solutions are present. It can then be assumed that the compositions of coexisting magnetite$_{ss}$ and ilmenite$_{ss}$ are governed by a temperature-dependent exchange reaction, and an oxidation reaction (Rumble, 1970). A hypothetical exchange reaction could be written as:

Equation 3.1

$$Fe_3O_4\ (Mt) + FeTiO_3\ (Ilm) = Fe_2TiO_4\ (Mt) + Fe_2O_3\ (Ilm)$$

And the Oxidation reaction as:

Equation 3.2

$$4Fe_3O_4\ (Mt) + O_2 = 6Fe_2O_3\ (Ilm)$$

Considering the Gibbs free energy, a total free energy of the solid solutions are:

Equation 3.3

$$G_{total}(Usp_{ss}) = \mu^{o}_{Usp}X_{Usp} + \mu^{o}_{Mt}X_{Mt} + \alpha RT(X_{Usp}\ln X_{Usp} + X_{Mt}\ln X_{Mt}) + X^{G}_{Usp}X^{2}_{Mt}X_{Usp} + X^{G}_{Mt}X^{2}_{Usp}X_{Mt}$$

Equation 3.4

$$G_{total}(Ilm_{ss}) = \mu^{o}_{Ilm}X_{Ilm} + \mu^{o}_{Hem}X_{Hem} + \alpha RT(X_{Ilm}\ln X_{Ilm} + X_{Hem}\ln X_{Hem}) + X^{G}_{Ilm}X^{2}_{Hem}X_{Ilm} + X^{G}_{Hem}X^{2}_{Ilm}X_{Hem}$$

Where α is equal to 2 for ilmenite, and 1 for titanomagnetite in accordance with configurational entropy expressions (Rumble, 1977). Calculations of temperature and oxygen fugacity rely on estimates of the original mole fractions of ulvöspinel and ilmenite compositions. These solid solution series have been known to contain considerable impurities

which are assumed to largely be controlled by the local charge (Bloss, 1971). The compositions and can be expressed as:

Equation 3.5

$$X_{Usp} = (n_{Ti,F})(x_{Fe2+,S2+}) /[(0.5\ n_{Fe3+,F})(X_{Fe3+,S3+}) + (n_{Ti,F})(x_{Fe2+,S2+})]$$

Equation 3.6

$$X_{Ilm} = [(n_{Ti,F})(n_{Fe2+,F2+})]^{1/2} /[(0.5\ n_{Fe3+,F}) + ((n_{Fe2+,F})(n_{Ti,F}))^{1/2}]$$

Where n represents the number of atoms in the formula (e.g., $n_{Ti,F}$= number of Ti in the formula), and s represents the number of atoms relative to the sum of all elements with a similar charge (e.g. $x_{Fe2+,S2+}$ is the composition of all Fe^{2+} relative to the sum of all 2+ cations).

The temperature can then be calculated using the equation:

Equation 3.7

$$T(^oK)= (-A1xW_H^{Usp}- A2xW_H^{Mt}+ A3xW_H^{Ilm}+ A4xW_H^{Hem}+\Delta H^o_{exch})/$$
$$(-A1xW_S^{Usp}- A2xW_S^{Mt}+ A3xW_S^{Ilm}+ A4xW_S^{Hem}+\Delta S^o_{exch}- RxlnK^{exch})$$

Where ΔH^o_{exch} = 27799 Joules/mole

ΔS^o_{exch} = 4.1920 Joules/mole

$A1 = -3X^2_{Usp} + 4X_{Usp} -1$

$A2 = 3X^2_{Usp} - 2X_{Usp}$

$A3 = -3X^2_{Ilm} + 4X_{Ilm} -1$

$A4 = 3X^2_{Ilm} - 2X_{Ilm}$

$K^{exch}= (X_{Usp}x\ X^2_{Hem})/(X_{Mt}xX^2_{Ilm})$

And oxygen fugacity can be calculated following the relationship:

Equation 3.8

$$Log_{10}fo_2 = MH + (12ln(1-X_{Ilm}) – 4ln(1-X_{Usp}) + (1/RT)(8X^2_{Usp}(X_{Usp}-1)xW_G^{Usp} + 4X^2_{Usp}(1-2X_{Usp})xW_G^{Mt} + 12X^2_{Ilm}(1-X_{Ilm})xW_G^{Ilm} – 6X^2_{Ilm}(1-2X_{Ilm})xW_G^{Hem}))/2.303$$

Where MH is the Haas value for the log oxygen fugacity at the magnetite-hematite buffer at the specific temperature of interest calculated from equation 3.7, where $\log_{10}MH = 13.966 - 24634/T$.

3.2.3. Considerations

From the 30 samples analyzed for magnetite-ilmenite pairs by microprobe, a reconstruction of the oxygen fugacity and temperature can be calculated based on the theory described by Buddington and Lindsley (1964). However, since the original work on oxybarometer it has been demonstrated that the effects of cation impurities within the Fe-Ti-oxide series have a profound effect on the calculated conditions of formation (e.g., Stormer, 1983). There has also been discrepancies within the data orignally collected in the work of Buddington and Linsley (1964), as demonstrated by Spencer and Lindsley (1981). In addition to analytical differences, the effects of ΔH and ΔS within the magma have been assumed to be contant over a large range of temperatues (Buddington and Lindsley, 1964), which has been shown to affect the geobarometer calculations (Spencer and Linsley, 1981).

3.2.4. Procedure

Stormer (1983) summarises the calculation procedure for multicomponent calculations for the temperature and oxygen fugacity as follows: (1) Calculate the molar proportions of all cations in the analysis for both the rhombohedral and spinel phases; (2) Normalize the cations in the spinel phase to a formula unit of 3 sites, and the cations in the rhombohedral phase to a formula unit of 2 sites; (3) Calculate the sum of the cationic charges per formula unit and subtract 8 for the spinel phase. For the rhombohedral phase subtract 6. The resulting numbers are the cation charge deficiencies (or excess); (4) Convert Fe^{2+} to Fe^{3+} to eliminate the charge

deficiency. If it is not possible to balance the charges, the analysis cannot represent a stoichiometeric oxide phase; (5) Using the moles of each cation per formula unit, calculate the mole fraction of Fe^{2+} relative to the sum of all 2+ cation, and the mole fraction of Fe^{3+} relative to all 3+ cations in the spinel phase; (6) calculate theX_{Usp} and X_{Ilm}; (7) Determine temperature and oxygen fugacity based on the relationships put forth by Spencer and Lindsley (1981).

It is important to note that the calculations of Fe_2O_3 wt.% and FeO wt. % were based on the simple stoichiometry calculations (Carmichael, 1967). It was also assumed that the dominant vanadium species within the oxides was present as V^{3+} which is consistent with the assumptions of vanadium substitution (Mallmann and O'Neil, 2009).

3.3. Samarium-Neodymium isotopes

A total of fifteen samples were analyzed for Sm-Nd isotopes and are presented in Appendix E. The samples were chosen based on the rare earth element primitive mantle plots which outlined trends and series within the separate intrusions. The samples were analyzed at the Isotope Geochemistry and Geochronology Research Centre at Carleton University, Ottawa, Ontario. Sm and Nd were separated on Eichrom Ln Resin chromato-graphic columns containing Teflon powder coated with HDEHP (di(2-ethylhexyl)) orthophosphoric acid (Richard et al., 1976). Total procedural blanks for Nd were <50 picograms, and <6 picograms for Sm. Samples were spiked with a mixed ^{148}Nd–^{149}Sm spike prior to dissolution. Concentrations are precise to ±1%, but $^{147}Sm/^{144}Nd$ ratios are reproducible to 0.5%. Sm and Nd samples were loaded with H_3PO_4 on one side of a Re double filament for analysis. Isotope ratios were normalized to $^{146}Nd/^{144}Nd = 0.72190$. Analyses of the USGS standard BCR-1 yielded Nd = 29.02 ppm, Sm = 6.68 ppm, and $^{146}Nd/^{144}Nd = 0.512668 \pm 20$ (n = 4). The La Jolla standard produced: $^{143}Nd/^{144}Nd$

= 0.511847 ± 7, n = 26 (Feb 2005–Jun 2007) and an internal Nd metal lab standard = 0.511818 ± 8, n = 28 (Feb 2005–Jun 2007) and 0.511819 ± 10 n = 94 (Feb 2005–Aug 2009).

3.4. Electron Microprobe

Samples were prepared at Lakehead University and sent to Geo Labs in Sudbury Ontario to be analyzed by the Cameca SX-100 Electron Probe Micro Analyzer (EPMA). Samples were selected based on stratigraphic and mineralization characteristics. The EPMA is equipped with five wavelength dispersive (WD) spectrometers which allow for a wide array of large area diffraction crystals to produce high sensitivity during quantitative mineral analysis.

Major and trace element compositions were determined using focused beam with variable current and count time (table 3.2). Total iron content (FeO^t) was expressed as FeO and Fe^{3+} / Fe^{2+} proportions were calculated based on the oxygen arrangement of the mineral analyzed (Droop, 1987). The limit of detection (L.O.D.) was defined as three times the standard deviation of the total accumulated background counts, and the limit of quantitation (L.O.Q.) is defined as ten times the standard deviation of the total accumulated background counts. The L.O.D. for V_2O_5 may be affected by the overlap correction for Ti Kb on V Ka, and the L.O.D. determined will be achieved in samples that have low concentrations of titanium.

All microprobe analyses have been verified with in-house standards with the exception of magnetite and ilmenite pairs from samples MM-V1-3, MM-V1-4, MM-V1-5, MM-V5-3, MM-V8-2, MM-V8-3, NO-2G21-6, NO-2G21-7, NO-2G21-11, NO-2G25-3, NO-2G25-4, NO-2G25-5, NO-2G25-6, NO-2G46-1, NO-2G46-2, NO-2G47-8 and NO-2G47-9.

Table 3.1 Beam current and count times for the oxide species analyzed by EPMA (beam current measured in nA and count time in seconds).

Oxide	Magnetite		Ilmenite		Feldspar		Pyroxene/ Amphibole	
	Beam Current	Count time	Beam Current	Count time	Beam Current	Count time	Beam Current	Count time
SiO_2	200	10	200	10	20	10	20	10
TiO_2	200	15	20	10	20	15	20	15
Al_2O_3	200	10	200	10	20	10	20	10
V_2O_5	200	15	200	15	n/a	n/a	n/a	n/a
Cr_2O_3	200	15	200	15	n/a	n/a	20	15
Nb_2O_3	n/a	n/a	200	15	n/a	n/a	n/a	n/a
MgO	200	10	200	10	20	10	20	10
CaO	n/a	n/a	n/a	n/a	20	10	20	10
MnO	200	15	200	15	20	15	20	15
FeO^t	20	20	20	10	20	15	20	15
CoO	200	15	200	15	n/a	n/a	n/a	n/a
NiO	200	15	200	15	n/a	n/a	n/a	n/a
CuO	200	15	200	15	n/a	n/a	n/a	n/a
ZnO	200	15	200	15	n/a	n/a	n/a	n/a
SrO	n/a	n/a	n/a	n/a	20	10	n/a	n/a
BaO	n/a	n/a	n/a	n/a	20	10	n/a	n/a
Na_2O	n/a	n/a	n/a	n/a	20	30	20	15
K_2O	n/a	n/a	n/a	n/a	20	10	20	10
F	n/a	n/a	n/a	n/a	n/a	n/a	20	15
Cl	n/a	n/a	n/a	n/a	n/a	n/a	20	10

Feldspar and pyroxene recalculations were based on atomic units as described by Brady and Perkins (2012) and data are presented in Appendix F. Feldspar was classified based on the three end members of anorthite-albite-orthoclase in an eight oxygen arrangement. Pyroxene was classified according to the wollastonite-enstatite–ferrosilite end members and a six oxygen arrangement. The M2 site was assumed to be occupied by Fe^{2+}, Mn, Ca and Na, the M1 site by Ti, Al, Cr, Fe^{3+}, Fe^{2+}, and Mg, and the T site occupied by Si and Al (Brady et al., 2012).

The amphibole groups of minerals are characterized by extremely complex and diverse chemistries and structures which makes recalculation difficult. Considerable attention has recently been focused on the reclassification of amphibole minerals from the International

Mineralogical Association in 2012 (IMA: Hawthorne et al. 2012; Oberti et al. 2012). This thesis followed the recalculation scheme outlined by Locock (2014) which accounts for the IMA classification and is based on a general amphibole formula of $AB_2C_6T_8O_{22}W_2$ where A= Na,K,Ca,Pb,Li; B=Na, Ca, Mn^{2+}, Fe^{2+}, Mg, Li; C=Mg, Fe^{2+}, Mn^{2+}, Zn, Ni^{2+}, Co^{2+}, Fe^{3+}, Mn^{3+}, Cr^{3+}, V^{3+}, Sc, Al, Ti, Zr, Li; T= Si, Al, Ti^{4+}, Be; and W= OH^-, F^-, Cl^-, O^{2-} (Hawthorne, et al., 2012). The method recalculates the loss of data in the light elements (e.g., OH, Li, ect.), and the valence state of common cations (e.g., Fe^{3+}, Mn^{3+}, ect.) based on neutral electronegativity (Locock, 2014). The method described my Locock (2014) requires a number of assumptions which must be individualized for each analysis: 1. orthorhombic or monoclinic symmetry; 2. use initial M^{3+}/Σ M; 3. OH=2-2Ti and; 4.require initial 'H_2O+?'. Assumptions (1) about amphibole symmetry are accounted for by petrographic investigations and since valance state of common anions (Fe, Mn) were not determined; the calculation did not use the initial M^{3+}/Σ M. H_2O cannot be determined with the EMPA and thus the OH was assumed to be largely controlled by the titanium content and thus OH=2-2Ti. As a result the initial "H_2O+?" cannot be assumed.

Amphibole calculations commonly (50% of the samples) exhibited low totals (96-98 %) and as such should be considered to be less accurate than samples which contain the accepted normal totals (98-102 %: Locock, 2014). The cause for the low totals may be a number of factors including errors in assumptions, inaccuracies of the assumptions (e.g., Fe^{2+}/Fe^{3+} ratios), and/or the lack of complete analysis of the constituent elements (V^{3+}, P, etc.).

4. Results

4.1. Field Relations

Detailed graphic core logging was undertaken on the Butler and Thunderbird Intrusions followed by selective sampling for geochemical and petrographic analysis. Detailed graphic logging was the preferred method to investigate the intrusions due to the layered nature of the lithologies, and best represents large scale variations. Due to the high Fe-Ti oxide (magnetite-ilmenite) contents within the ferrogabbroic units, a modification was employed in the identification of the silicate host rocks which were based on the IUGS classification. The rock units were first categorized by the major silicate minerals with a prefix modifier which is based on the proportions of magnetite and ilmenite (Fig. 4.1). This rock classification was used both during core logging and petrographic study (Appendix C).

4.1.1. Butler Intrusions

A seven day property visit to the Butler Intrusions, currently held by MacDonald Mines Exploration Ltd. was conducted in May of 2012. Ben Kuzmich was accompanied by Riku Metsaranta of the Ontario Geological Survey (OGS), and Michel Houlé of the Geological Survey of Canada (GSC). The purpose of the site visit to the Butler Intrusion was to collect geochemical and petrographic samples, and to complete detailed graphic drill logs for representative drill holes. A total of ten drill holes were examined (1801m) and 133 representative samples from the intrusions were collected for further study.

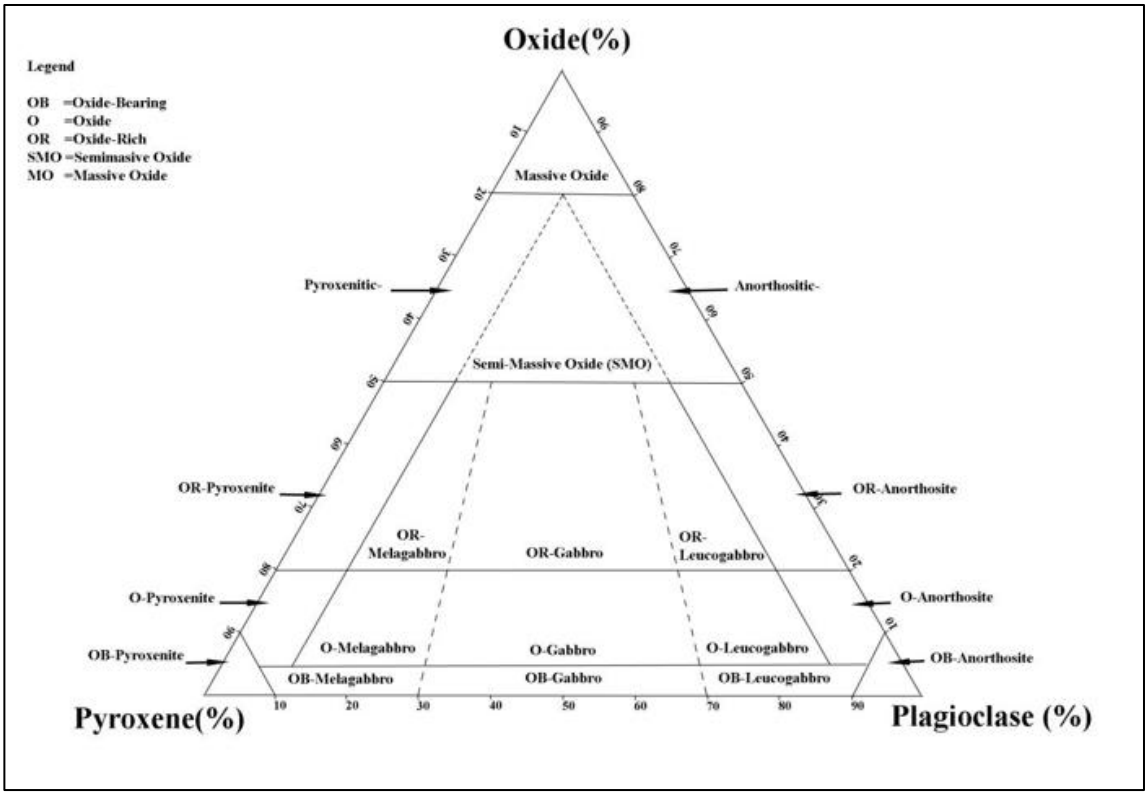

Figure 4.1. Rock classification chart (Oxide= magnetite+ilmenite).

4.1.1.1. Lithology

The Butler Intrusions have been subdivided into the Butler East, and Butler West intrusion as defined by aeromagnetic surveys (Fig. 4.2). Both intrusions are composed of a ferrogabbroic suite which ranges in composition from melagabbro to anorthosite with highly variable proportions of magnetite and ilmenite. The intrusions are characterized by both sharp and gradational lithological contacts, however, in many sections a repeated sequence of massive oxide grading into anorthosite is common with sharp lower contacts along the massive oxide units (Appendix C).

The melagabbro, gabbro and leucogabbro units are texturally similar with variable proportions of hornblende and plagioclase (Fig. 4.3 A,B). These rocks are dark to medium

green, medium-grained, massive to weakly foliated and typically contain subhedral plagioclase, anhedral amphibole, and trace fine- to medium-grained anhedral magnetite+ilmenite (though they can host semi-massive oxide proportions) and trace fine-grained anhedral pyrite, pyrrhotite and/or chalcopyrite. Rare coarse-grained heterogeneous leucogabbro has been intersected and compositionally transitions into anorthosite and gabbro (Fig 4.3 C). These

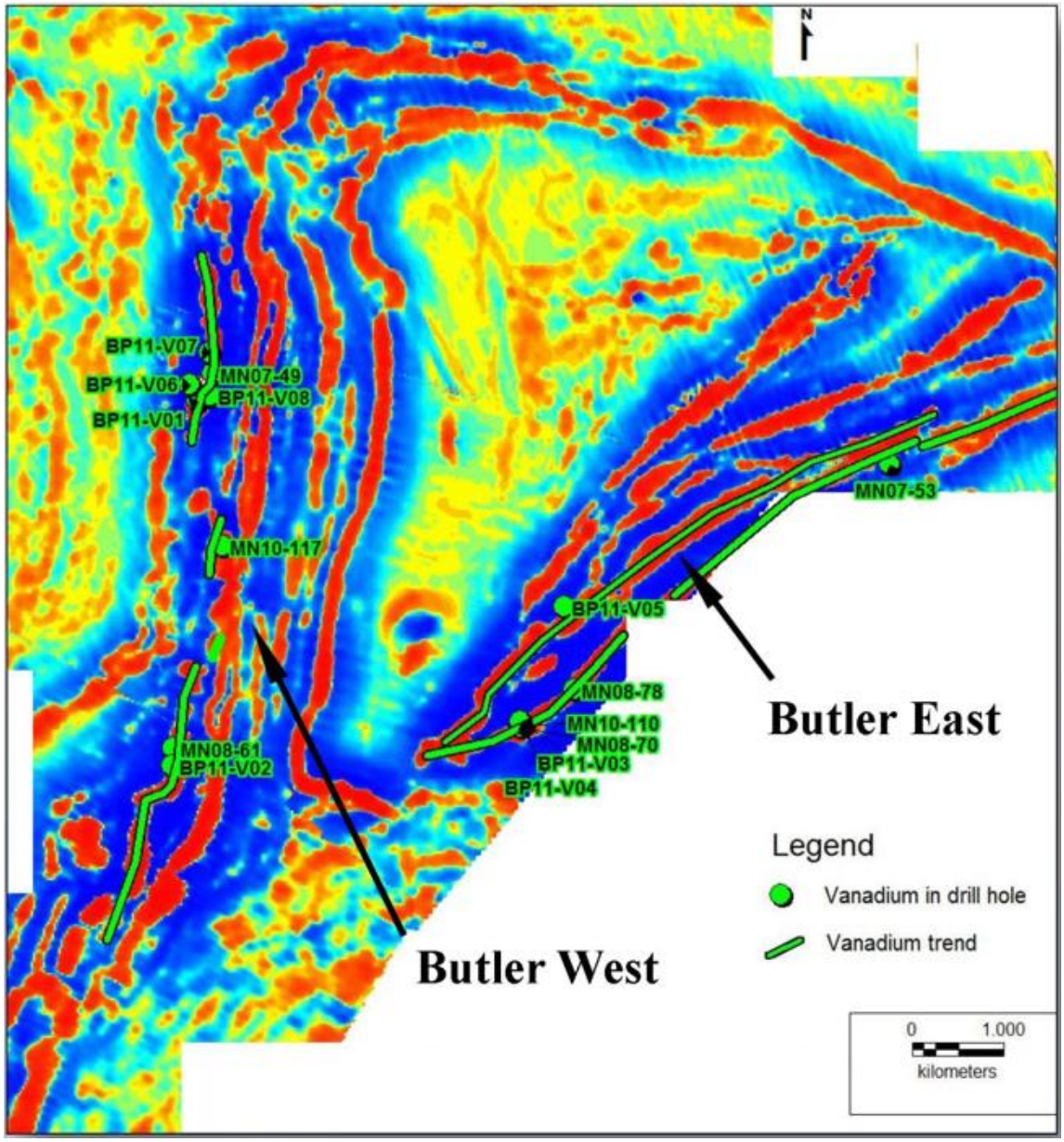

Figure 4.2. First vertical derivative airborne magnetic map of the Butler Intrusion showing location of vanadium-bearing drill holes and interpreted mineralized trend (Modified from MacDonald Mines Exploration Limited, 2012)

coarse-grained gabbro-anorthosite units typically contain diffuse contacts with the medium-grained ferrogabbro, and contain trace to absent magnetite-ilmenite. In contrast, thick successions of homogenous pegmatitic gabbro have been intersected (e.g., MN08-117) and are characterized by euhedral hornblende and plagioclase grains ranging from 2-4 cm in length and contain brecciated plagioclase crystals (Fig 4.3D).

The Butler intrusions are cross-cut by a series of felsic to intermediate and rare ultramafic dikes which exhibit sharp contacts and local ferrogabbroic magmatic breccia (Fig. 4.3 E, F). The felsic units are subdivided into: pegmatitic salmon-pink massive granite, a medium-grained biotite-bearing massive tonalite, and a white variably magnetic, medium-grained massive biotite-hornblende-bearing diorite. All the felsic units cross cut the ferrogabbroic intrusion and locally contain chill margins. The ultramafic dikes are composed of a serpentinized fine-grained massive peridotite/dunite which contains massive oxide breccia (Fig. 4.3 F). The peridotite dykes are variably magnetic and contain both xenolithic magnetite along the contacts of the dike (angular fragments), and fine-grained disseminated anhedral magnetite within the core.

4.1.1.2. Mineralization

Magnetite-ilmenite mineralization within the East and West Butler intrusions occurs both as disseminated and massive textures. The massive and semi-massive oxides are restricted to stratigraphically conformable units which occur along the basal portions of the melagabbro-anorthosite cycles. The massive and semi-massive units vary in thickness from millimeters (Fig. 4.3 G), to a maximum core length of 23.88 meters (Fig. 4.3 H) and typically contain sharp lower contacts with gradational upper contacts. In contrast, the disseminated units display highly variable proportions of magnetite-ilmenite and are characterized by

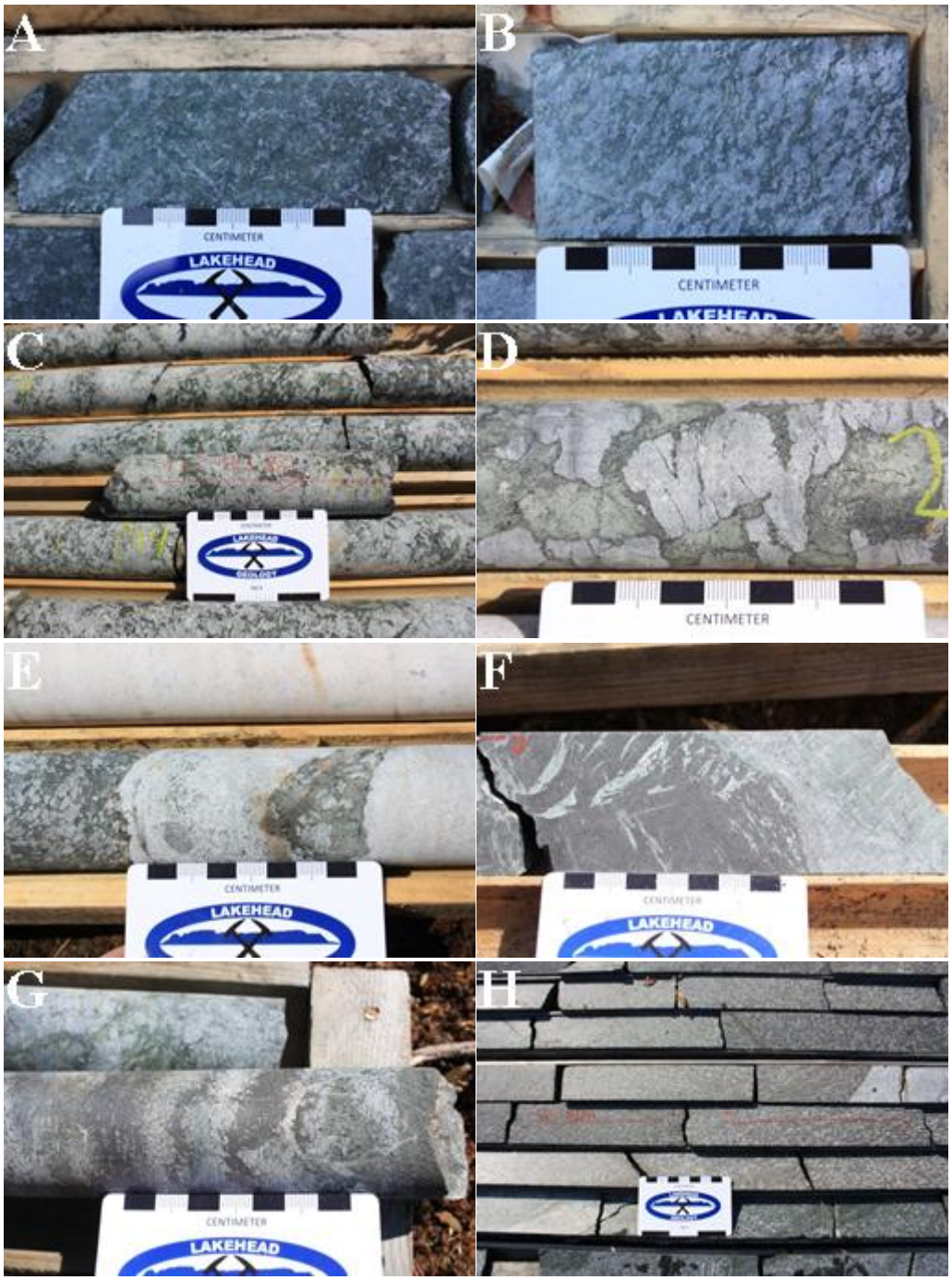

Figure 4.3 Representative core photos from the Butler Intrusions. A) Massive, medium-grained melagabbro; B) weakly foliated medium-grained leucogabbro; C) coarse-grained leucogabbro; D) pegmatitic gabbro with fractured plagioclase crystals; E) ferrogabbro xenolith within dioritic dyke; F) magnetite and ultramafic dyke contact with brecciation of ferrogabbroic unit; G) centimeter-scale layering of massive-oxide and anorthositic units; H) meter-scale intercept of semi-massive oxides.

gradational contacts. The disseminated magnetite-ilmenite units have a greater variance in the silicate host rock compositions and range from medium-grained, massive pyroxenite, to medium-grained massive anorthosite. The silicate mineralogy within the massive and semi-massive units is dominantly composed of euhedral medium-grained plagioclase and chlorite with lesser pyroxene and/or hornblende.

4.1.1.3. Alteration

The Butler East and Butler West intrusions contain pervasive chlorite, epidote and amphibole metamorphism. Chlorite occurs within all ferrogabbro lithologies and ranges from trace amounts in anorthosites, to chlorite schists (Fig. 4.4A). Recrystallization textures are also present within the pegmatitic gabbro, and talc-serpentine alteration within the peridotite dikes. Along with the regional metamorphism observed within the Butler intrusions, local biotite, quartz, K-feldspar and garnet have been observed. These local alterations are typically focused within narrow intervals (<1m) and are largely observed within the southern portion of the Butler East intrusion. The garnet-bearing and silicified gabbros (Fig. 4.4B) are restricted to local shear zones which exhibit a strong foliation and rapid gradation into massive units (Fig. 4.4C). The shear zones postdate the felsic intrusions in the southern portion of Butler East and have preserved boudinage texture (Fig 4.4D).

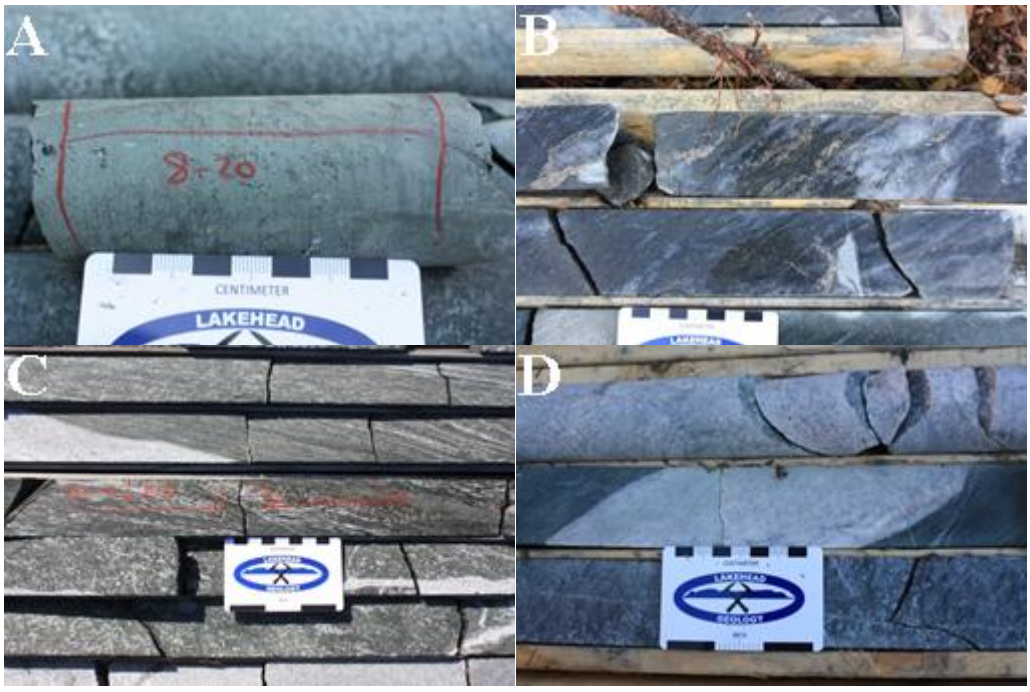

Figure 4.4 Representative alteration and deformation within the Butler Intrusions. A) Intense chlorite altered gabbro; B) silicified gabbro; C) weakly to strongly foliated garnet-bearing gabbro; D) boudinage cross cutting granitic intrusion.

4.1.2. Thunderbird Intrusion

Field work on the Thunderbird intrusion commenced during the fall of 2012 for seven days under the supervision of Peter Hollings (Lakehead University). The entire core examined was on site at the Esker camp which is currently held by Noront Resources Ltd. During the property visit, a total of five drill holes (2037m), recommended by Noront staff, were logged in detail (see Appendix C) . The distribution of drill core represents the core and marginal facies of the Thunderbird intrusion and a total of 130 core samples were collected during the visit (Fig. 4.5)

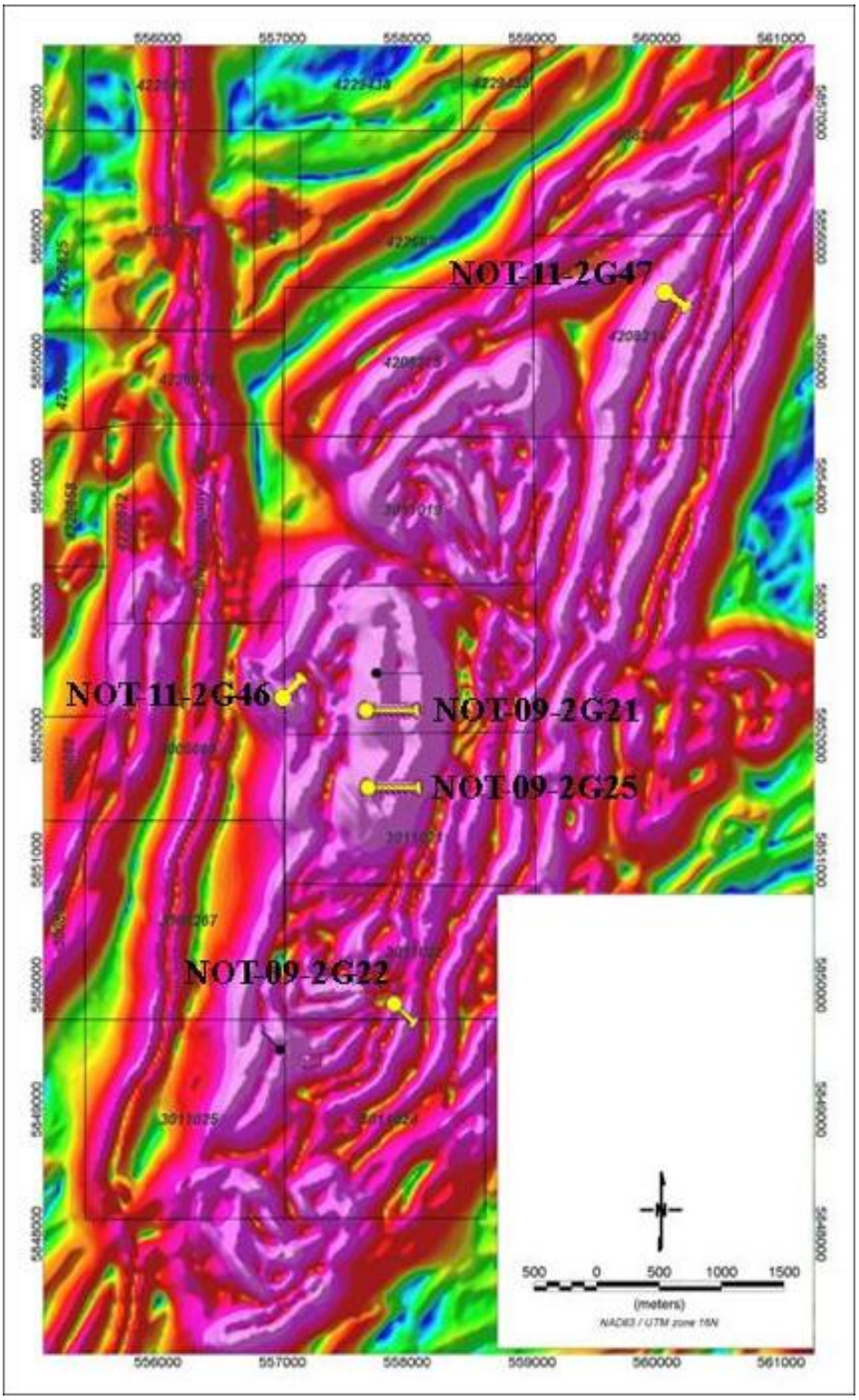

Figure 4.5. Horizontal derivative magnetic map of the Thunderbird intrusion with highlighted drill holes and their orientation (courtesy of Noront Resources).

4.1.2.1. Lithology

Similar to the Butler intrusions, the Thunderbird intrusion is largely composed of dark to light green, medium-grained, massive to weakly foliated melagabbro-anorthosite units (Fig. 4.6A, B). These rocks contain variable proportions of magnetite and ilmenite which range from absent to massive stratigraphically conformable units (Fig. 4.6C). Lesser units of the Thunderbird intrusion include pyroxenites, pegmatitic gabbro (Fig. 4.6D), and chlorite-calcite schists (Fig. 4.6E) which have been cross cut by dykes of micro-ferrogabbro, basalt, pegmatitic tourmaline veins, quartz veins, tonalites, and granites. The Thunderbird intrusion comprises a poorly to very well layered sequence of ferrogabbro units which typically exhibit sharp lower contacts and gradational upper contacts. These sequences occur as partial to complete repeated layers which are composed of sulphides (dominantly pyrite with lesser chalcopyrite and/or pyrrhotite) followed by massive magnetite and ilmenite, melagabbro, and then anorthosite (Fig. 4.6F).

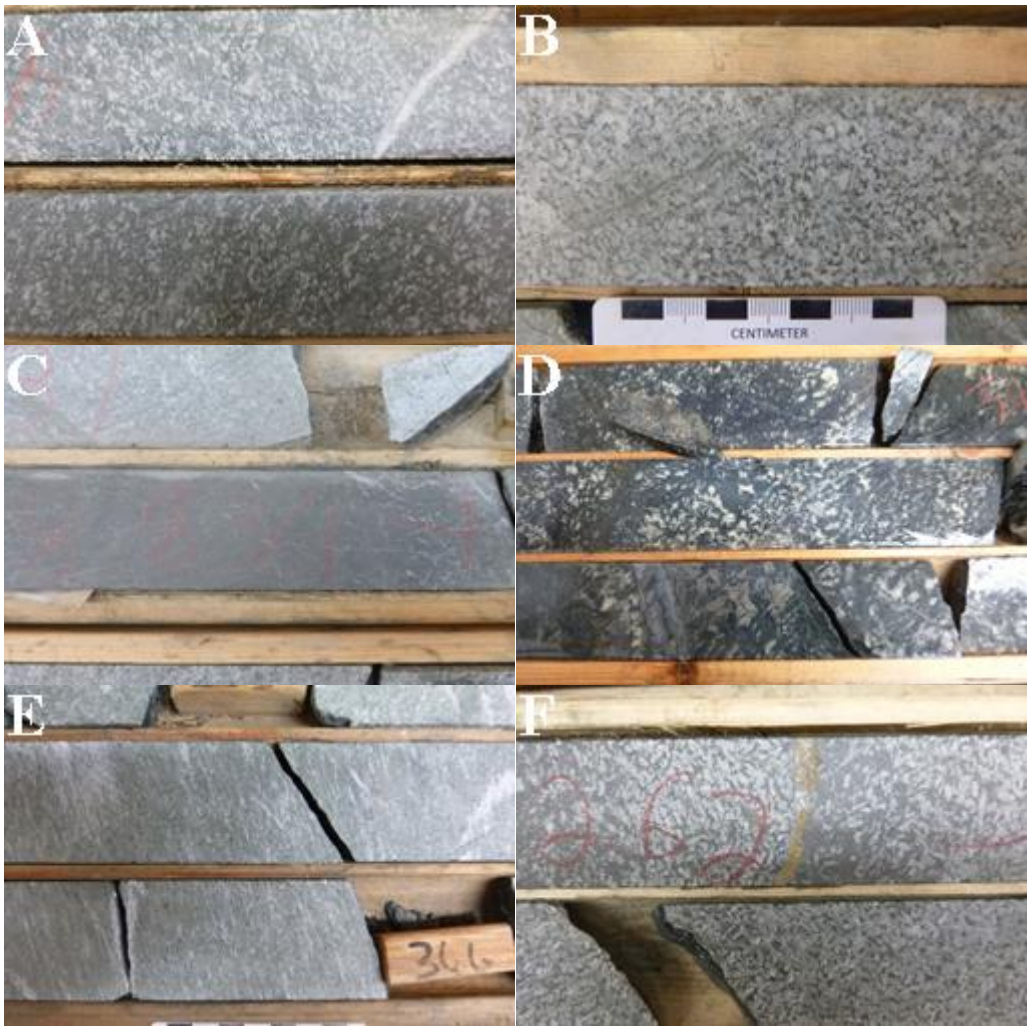

Figure 4.6. Representative lithologies within the Thunderbird intrusion. A) Massive, medium-grained gabbro; B) massive, medium-grained anorthosite; C) fine-grained magnetite; D) pegmatitic melagabbro; E) chlorite-carbonate schist; F) layered pyrite, magnetite+ ilmenite, and plagioclase.

4.1.2.2. Mineralization

The Thunderbird intrusion is mineralized with highly variable proportions of magnetite and ilmenite which occurs as fine-grained anhedral crystals within the ferrogabbro (Fig. 4.7A). The Fe-Ti-oxides typically occur as disseminated grains between 2-5 modal percent; however, they also occur as layers of massive or semi-massive magnetite and ilmenite (Fig. 4.7B). The thickest massive oxide unit intersected within the Thunderbird intrusion had a 0.45 meter core

interval from drill hole NOT-09-2G21. A small intercept of anorthosite within the drill core from NOT-09-2G25 is mineralized with centimeter scale anhedral blebs of Fe-Ti oxides which contain no fine-grained disseminated magnetite-ilmenite, and is atypical for the mineralization observed elsewhere within the Thunderbird intrusion (Fig. 4.7C).

The Thunderbird intrusion also contains large intercepts of apatite mineralization which has been observed in drill core from holes NOT-11-2G46 and NOT-11-2G47. These drill holes occur along the extremities of the intrusion as outlined by the magnetic map in Figure 4.5. The phosphate mineralization is hosted within stratigraphically conformable, dark green, medium-grained, homogenous, apatite-magnetite-ilmenite-bearing melagabbros which range in thickness from 48 meters (NOT-11-2G46) to 4 meters (NOT-11-2G46). The apatite occurs as very fine- to fine-grained tabular crystals and varies in proportions from trace to 10%. Due to the fine-grained and translucent nature of the apatite, it is difficult to estimate the concentrations of apatite within a dark green host rock in drill core (Fig. 4.7D).

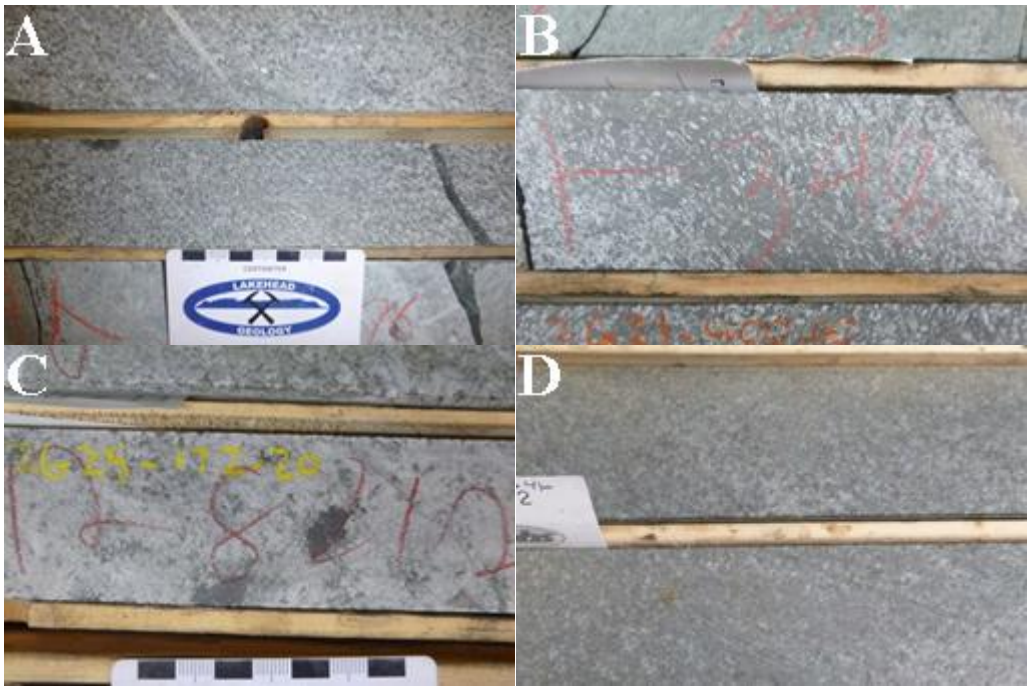

Figure 4.7. Varying styles of Fe-Ti-oxide mineralization within the Thunderbird intrusion. A) fine-grained disseminated magnetite-ilmenite; B) semi-massive magnetite-ilmenite with gradational contacts; C) coarse-grained bleb of magnetite-ilmenite; D) fine-grained clear apatite mineralization within melagabbro.

4.1.2.3. Alteration

The Thunderbird intrusion has undergone pervasive weak to moderate chlorite-epidote- amphibole metamorphism. Minor intervals within the Thunderbird intrusion have also undergone intense amounts of amphibole-chlorite alteration which has partially to completely replace the primary plagioclase and pyroxene grains (Fig. 4.8A, B). In addition, intense epidote and/or calcite alteration is commonly observed along the basal contacts of layered magnetite-ilmenite-rich sequences (Fig. 4.8C). Lesser alteration intersected within the intrusion include hematite veinlets (Fig. 4.8D) which are common near the surface (generally <50 meters), gypsum veinlets (Fig 4.8E), potassic, and/or biotitic alterations.

The Thunderbird intrusion generally exhibits a massive to weakly foliated texture; however, narrow intervals of strongly foliated schists occur throughout the intrusion (Fig.

4.6E). Within the sheared units, chlorite-epidote alteration is generally stronger than in the massive counterparts (Fig. 4.8F).

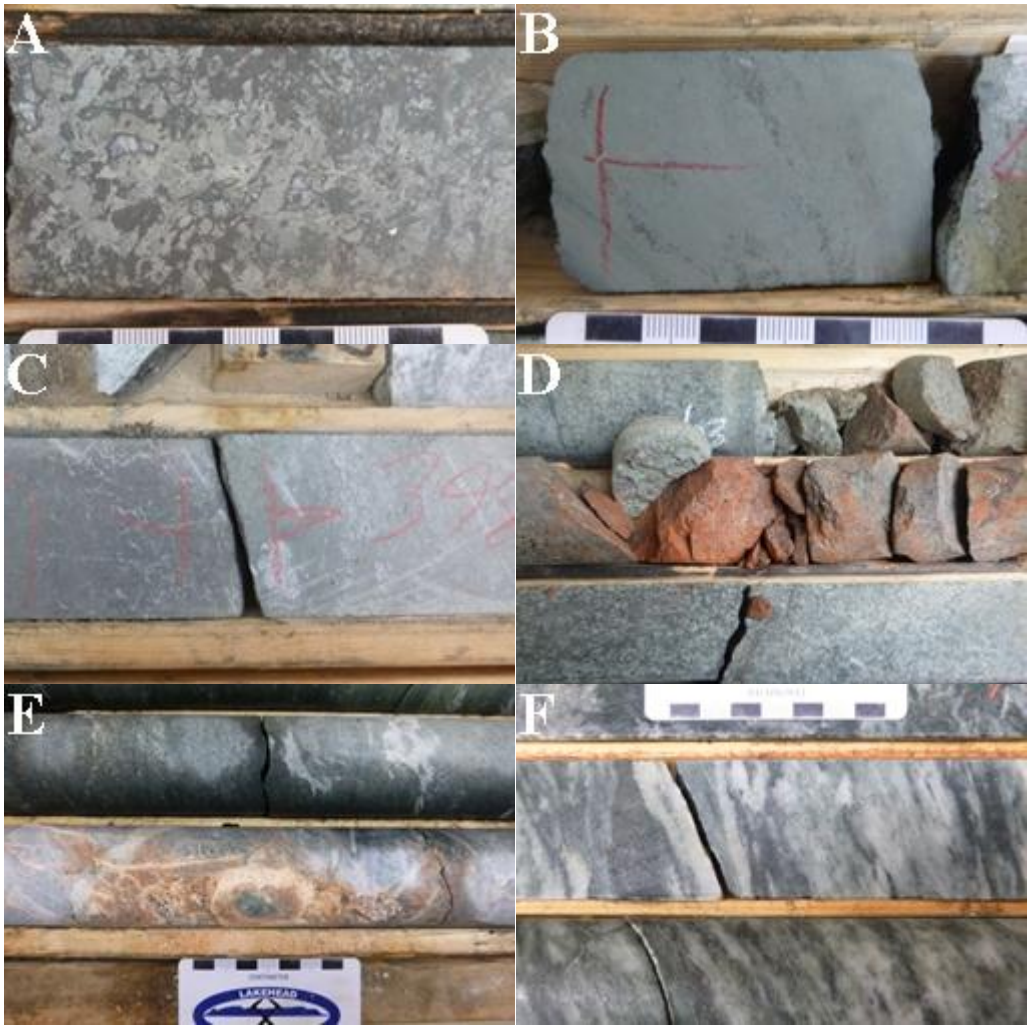

Figure 4.8. Photos of drill core representative of the alteration observed within the Thunderbird intrusion. A) Moderate chlorite alteration; B) intense chlorite alteration; C) intense epidote-carbonate alteration associated with the contacts with massive oxide units; D) hematite-rich fractures; E) gypsum veinlets, F) well foliated chlorite-epidote altered gabbro/leucogabbro.

4.2. Petrography

4.2.1. Butler Intrusions

The Butler intrusions are composed of a suite of magnetite- and ilmenite-rich units which range from anorthosites to pyroxenites (Fig. 4.9). A total of 56 samples have been examined with detailed descriptions in Appendix A.

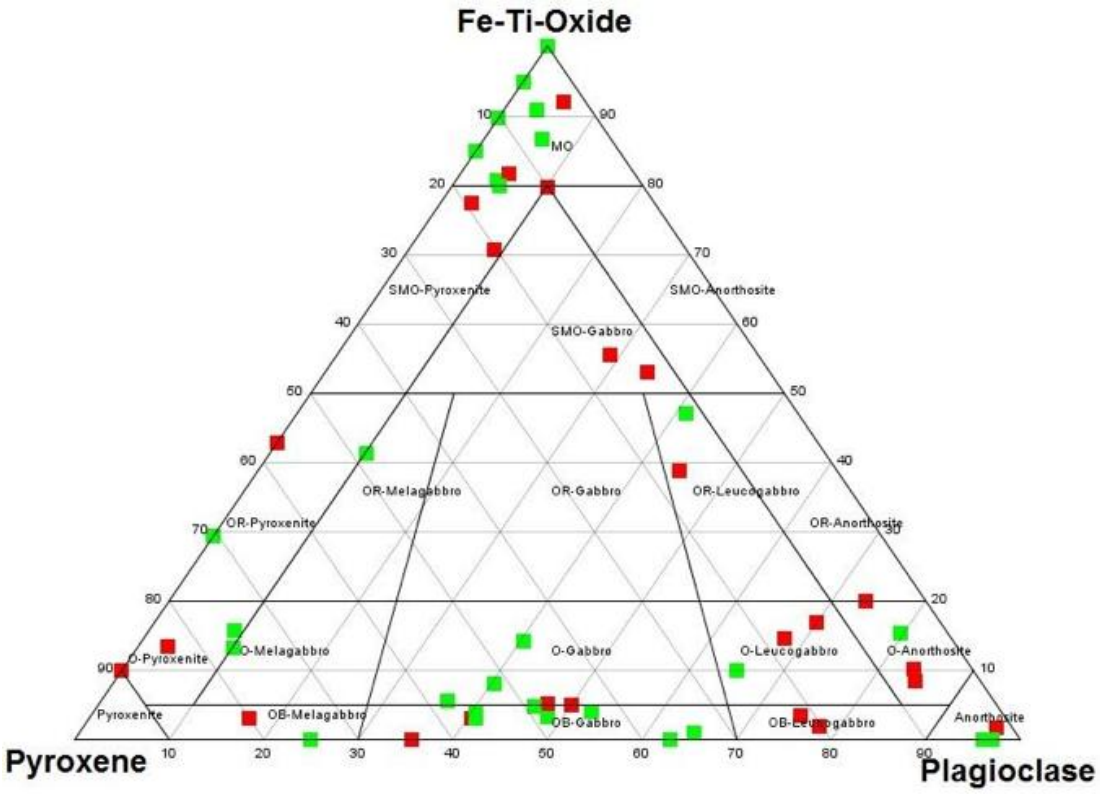

Figure 4.9. Sample distribution based on interpreted primary mineralogy for the Butler East (red) and Butler West (green) intrusions.

4.2.1.1. Alteration

The Butler intrusions have experienced pervasive weak to moderate amphibole-chlorite-epidote metamorphism. As a result of this metamorphism, the primary mineralogy has been interpreted based on alteration assemblages and textures to accurately assign primary lithological titles to the units. Below is a discussion of the degree of alteration and metamorphism observed within the Butler intrusions and for the remainder of this thesis will refer to the interpreted primary mineralogy of the intrusions rather that the observed alteration.

Plagioclase is a major rock forming mineral within the Butler intrusion. Plagioclase typically occurs as medium-grained euhedral laths which commonly exhibit deformation twins (Fig. 4.10A), simple twins, and sericite +/- epidote +/- clinozoisite alteration (Fig. 4.10B), and rarely contain compositional zoning. Locally plagioclase grains display recrystallization textures which frequently are associated with very fine-grained quartz (Fig. 4.10C).

Clinopyroxene and rarely orthopyroxene is the second dominant primary mineral within the ferrogabbro units examined. The medium-grained anhedral to subhedral pyroxene grains have generally been partially to completely replaced by secondary amphibole and/or Fe-poor chlorite and/or epidote. The pyroxene grains typically display a corona texture of very fine- to fine-grained blue to pale green amphibole (Fig. 4.10 D). Aphanitic to very fine-grained pyroxene (now altered to amphibole) also occurs as needle-like inclusions within plagioclase grains and are oriented parallel to the crystallographic planes (Fig. 4.10 E).

The Butler intrusions also contain significant abundances of titanomagnetite and ilmenite grains. These oxide minerals have generally remained unaltered; however, annealing textures and coronas of Fe-rich chlorite, biotite and/or epidote are common in the semi-

massive to massive lithologies (Fig. 4.10F). Anhedral very fine-grained titanite also occurs rarely in trace amounts which are either disseminated or occur along titanomagnetite-ilmenite grains (Fig. 4.10G). Titanite contents generally increase in the presence of carbonate and hematite lamellae within ilmenite. Ilmenite also occurs as rare skeletal grains within amphibole (Fig. 4.10 H). This texture is particularly evident in drill core from holes MN08-110 and MN08-117 and occurs as fine- to medium-grained crystals which commonly contain blebs of very fine-grained magnetite along the grain boundaries.

The Butler intrusions also display local carbonate, biotite, garnet, serpentine, quartz, and/or muscovite alteration. The carbonate grains typically occur as very fine- to fine-grained anhedral blebs which are disseminated throughout the rock. Biotite occurs both as randomly oriented, brown to red fine-grained crystals, or fine- to medium-grained strongly foliated shear zones. The shear zones commonly contain carbonate within the matrix, and the biotite is partially replaced by chlorite. Fine-grained euhedral garnet occurs within drill core BP11-V01 where it is typically associated with massive to semi-massive oxide units. The garnet has also undergone brittle deformation and locally contains fractures (Fig. 4.10 I). Serpentine occurs dominantly as pervasive replacement of the ultramafic dyke which crosscuts the ferrogabbro in drill core BP11-V05 (Fig. 4.10J). The serpentine is largely evident within the cross-cutting ultramafic dykes (MM-V5-4, MM-V5-5), and associated with very fine-grained disseminated magnetite which exhibits no ilmenite oxy-exsolution textures. Serpentine occurs less commonly within pyroxene-rich ferrogabbro units of the Butler intrusions. The quartz and muscovite (sericite) alteration is associated with the replacement of plagioclase laths and occur as trace to minor amounts.

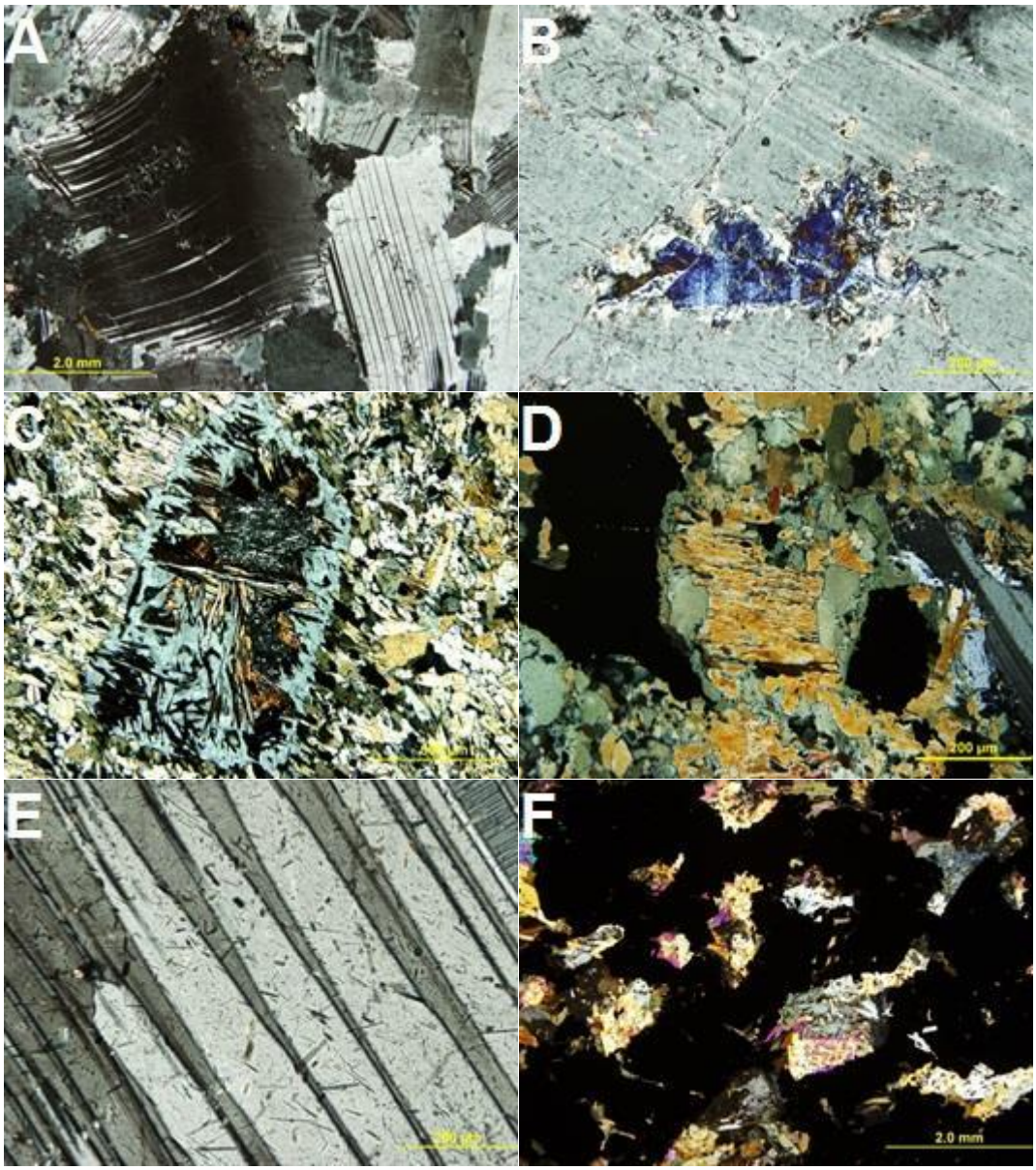

Figure 4.10. Transmitted light photo micrographs of representative alterations within the Butler Intrusions. A) deformation twins within plagioclase (XPL); B) clinozoisite after plagioclase (XPL); C) Relict plagioclase grain with quartz-albite alteration along the rim (XPL); D) amphibole after pyroxene (XPL); E) deformation twins within plagioclase and very fine-grained amphibole needles (XPL); F) epidote and minor biotite within a massive-oxide (opaque; XPL).

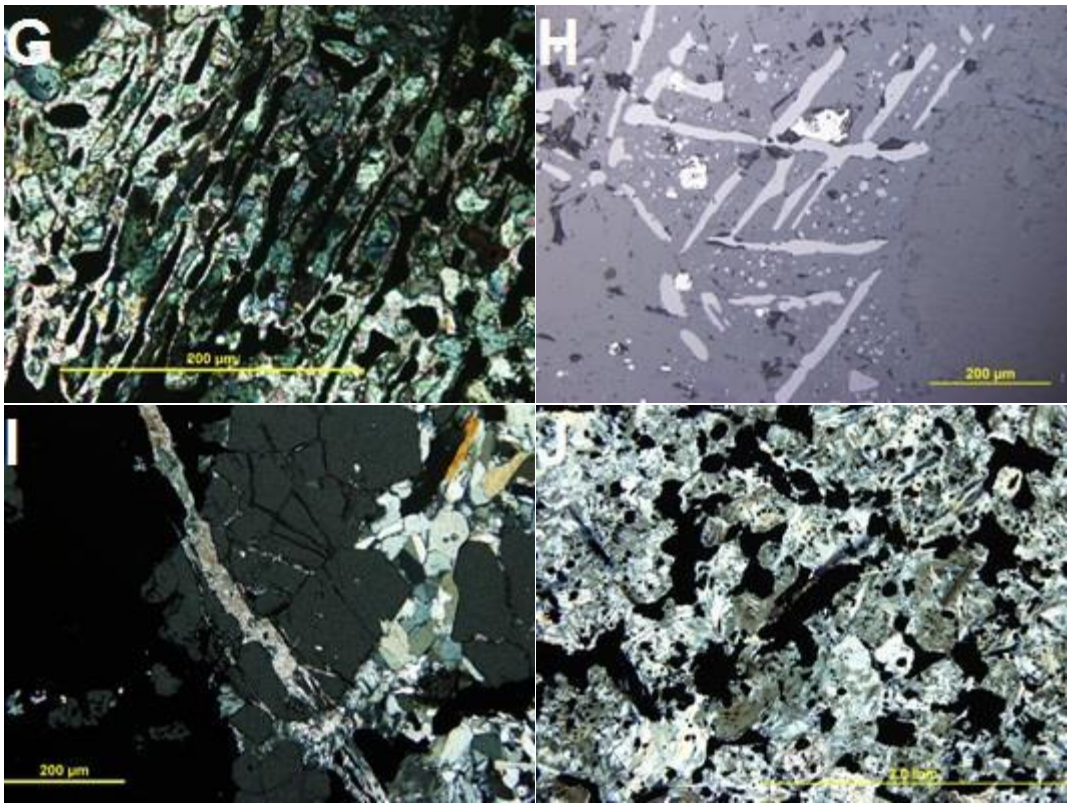

Figure 4.10 (cont.) Transmitted light photo micrographs of representative alterations within the Butler Intrusions. G) ilmenite lamellae (opaque) with a corona of very fine-grained sphene; H) Ilmenite lamellae within pyroxene (reflected light, XPL); I) metamorphic garnets with cross cutting carbonate veinlets (XPL); serpentine altered ultramafic intrusive with anhedral magnetite (opaque; XPL).

4.2.1.2. Lithology and Mineralization

The Butler intrusions are composed of a suite of massive to weakly foliated anorthosites to gabbros which host variable magnetite and ilmenite mineralization (Fig. 4.9). The anorthosites are characterized by equigranular medium-grained plagioclase laths with accessory anhedral to subhedral fine-grained amphibole. Gabbroic rocks are characterized by medium-grained, equigranular to subophitic plagioclase with anhedral medium-grained pyroxene, partially to completely altered to amphibole and/or chlorite.

The Butler intrusions contain subordinate layers of pyroxenite (largely altered to amphibolites), pegmatitic gabbro, peridotite, and micro-gabbroic rocks. The pyroxenites and

pegmatitic gabbros are stratigraphically conformable with the ferrogabbroic sequence, whereas the peridotites and micro-gabbros occur as dykes with clear cross cutting relationships (e.g., Fig. 4.3F). The peridotites are dominantly composed of very fine-grained serpentine (and/or grunerite) and up to 15% disseminated very fine-grained sub-rounded magnetite which does not contain ilmenite lamellae (Fig. 4.11A). Pegmatitic gabbros are characterized by subhedral to euhedral plagioclase laths (3cm long) and anhedral to subhedral clinopyroxene grains which exhibit coronas of amphibole, and aggregates of fine- to medium-grained magnetite-ilmenite grains. The micro-gabbro dykes contain sharp contacts with the ferrogabbro sequences and are characterized by fine-grained, massive, biotite-bearing gabbros, which generally contain 2-5% magnetite and ilmenite (Fig. 4.11B).

The anorthosite-gabbro suite contains between trace to nearly massive areas of magnetite and ilmenite. Textures within the Fe-Ti oxides vary considerably when present in smaller concentrations (<20% magnetite+ ilmenite). Within the oxide-bearing- to oxide-ferrogabbroic rocks, the magnetite and ilmenite generally occur as disseminated fine- to medium-grained anhedral blebs (Fig. 4.11C). The magnetite typically contains fine (1-10μm) to coarse (25-50μm) ilmenite exsolution lamellae which range from trace to 10% ilmenite. The ilmenite lamellae generally exhibit a trellis texture which is characterized by fine lamellae oriented along all of the octahedral planes within magnetite, though less commonly only along one set of planes (111). These ilmenite lamellae contain sharp contacts with the magnetite host and typically contain tapered terminations (Fig. 4.11D) and rarely intersect one another. In magnetite grains which host ilmenite lamellae in only one set of planes, the ilmenite grains exhibit synchronous extinction. Ilmenite lamellae also rarely exhibit sandwich textures which are defined by coarse, parallel oriented grains which do not contain tapered terminations, and may extend beyond the magnetite host into the silicate groundmass. Ilmenite also occurs as

fine- to medium-grained discrete anhedral to euhedral crystals, and not solely as lamellae within magnetite (Fig. 4.11E). These discrete ilmenite grains contain rare trace to 2% hematite lamellae which occur as very fine (1-3µm) parallel oriented lamellae (Fig. 4.11F). The hematite lamellae within the ilmenite are analogous to the trellis texture observed within the magnetite hosts with the exception that hematite lamellae occur only along one crystallographic plane. Ilmenite occurs rarely as symplectic to graphic intergrowths within primary pyroxene grains which have been altered to fine-grained amphibole and resulted in skeletal textured ilmenite (Fig. 4.10G). This ilmenite-silicate intergrowth occurs rarely within the Butler intrusions, however, it is particularly common within drill core from hole MN08-117.

Textural variance within the Fe-Ti oxide minerals is considerably less within the oxide-rich, semi-massive oxide, and massive oxide units. These iron-titanium-rich ferrogabbro rocks are characterized by net textured (Fig. 4.11H) to massive textured oxides (Fig. 4.11I) and the mineralogy is characterized by fine to coarse ilmenite lamellae within magnetite hosts which contain trellis and sandwich textures. Additionally, the semi-massive and massive oxide units exhibit composite/granule exsolution textures which are characterized by very fine- to fine-grained euhedral to subhedral tabular ilmenite grains which occur as internal and external crystals within fine- to medium-grained magnetite (Fig. 4.11E).

The Butler intrusions typically contain trace to 2% sulphide minerals, and locally up to 39% (sample MM-V4-6). The sulphides are composed dominantly of pyrite with lesser pyrrhotite and/or chalcopyrite and occur as very fine- to fine-grained disseminated crystals. The sulphides commonly occur concentrated within oxide-rich portions of the samples, and can also exhibit net-textured pyrrhotite and chalcopyrite in massive oxide units (sample MM-V4-1: Fig. 4.11 J). Pyrite typically occurs as anhedral blebs, though locally may exhibit a sub-cubic

habit. Pyrrhotite and chalcopyrite occur solely as anhedral blebs spatially associated with pyrite. Pyrrhotite also occurs rarely as very fine-grained flames/lamellae within pyrite and vice versa.

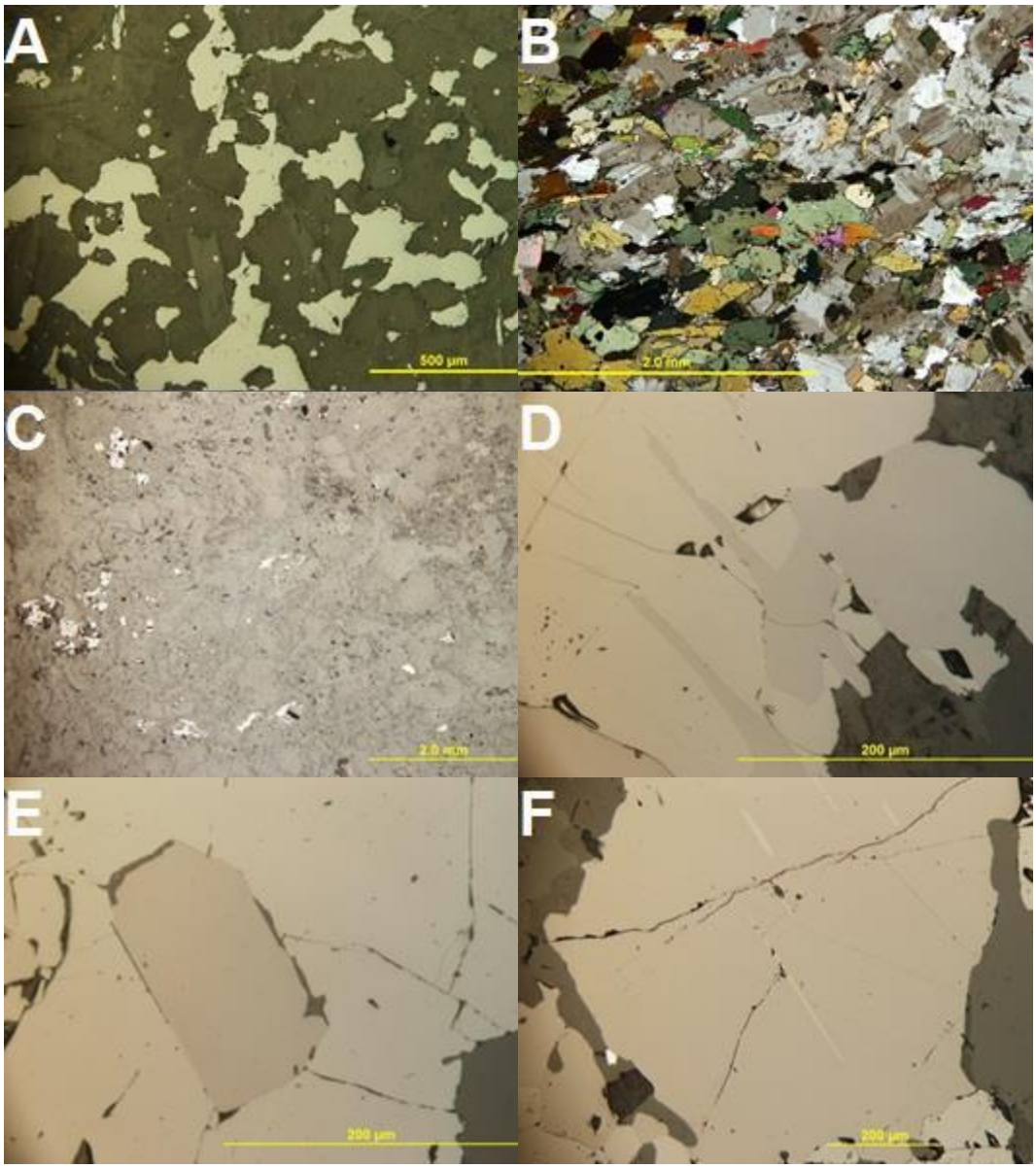

Figure 4.11. Transmitted light photomicrograph of typical textures and lithologies within the Butler intrusions. A) Magnetite within cross-cutting ultramafic dykes with no ilmenite exsolution (reflected light; XPL); B) cross cutting microgabbro dyke (XPL); C) fine-grained disseminated magnetite (reflected light; XPL); D) ilmenite lamellae within magnetite displaying tapered lamellae terminations (reflected light; XPL); E) euhedral ilmenite surrounded by magnetite (reflected light: XPL); F) ilmenite grain with very fine-grained hematite exsolution lamellae (reflected light; XPL)

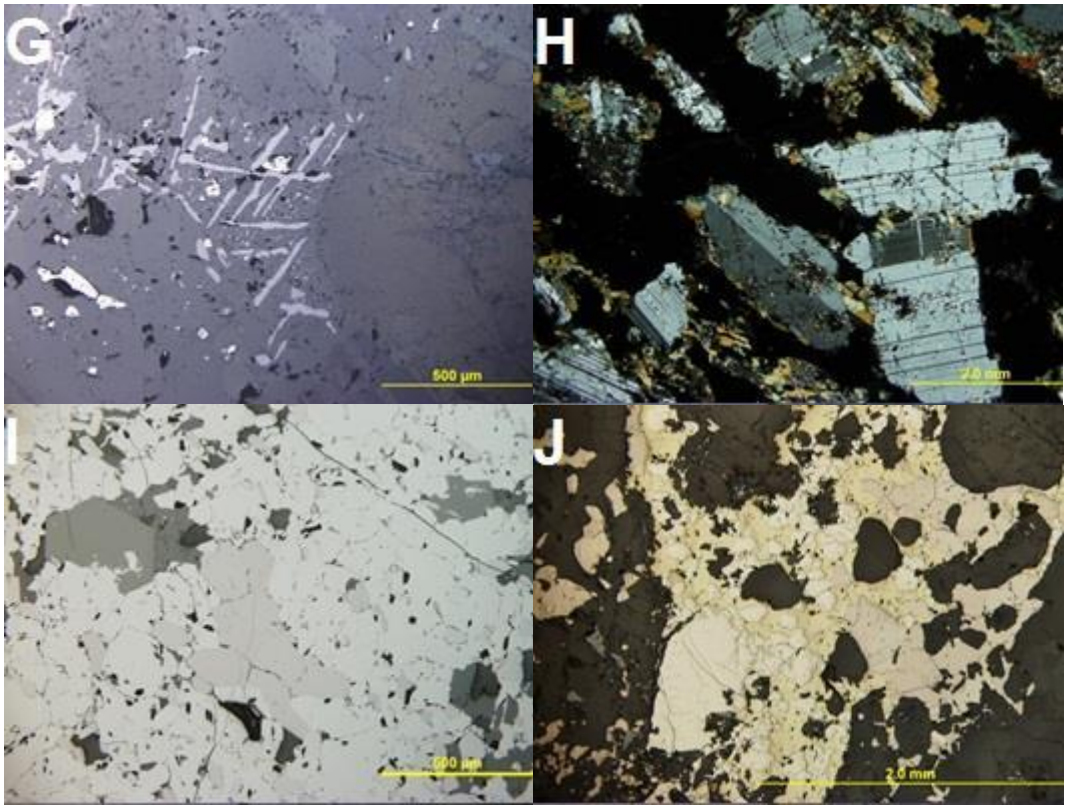

Figure 4.11. (cont.). Transmitted light photomicrograph of typical textures and lithologies within the Butler intrusions. G) ilmenite lamellae within amphibole (reflected light; XPL); H) net textured magnetite-ilmenite (opaque: XPL); I) massive magnetite and ilmenite (reflected light; XPL); J) net textured pyrite-pyrrhotite-chalcopyrite (PPL; reflected light).

4.2.2 Thunderbird Intrusion

The Thunderbird intrusion has been described in detail using 44 polished thin sections with detailed descriptions in Appendix A. The Thunderbird intrusion is characterized by a suite of medium-grained, massive to weakly foliated magnetite-ilmenite-rich pyroxenite-anorthosite units (Fig. 4.12).

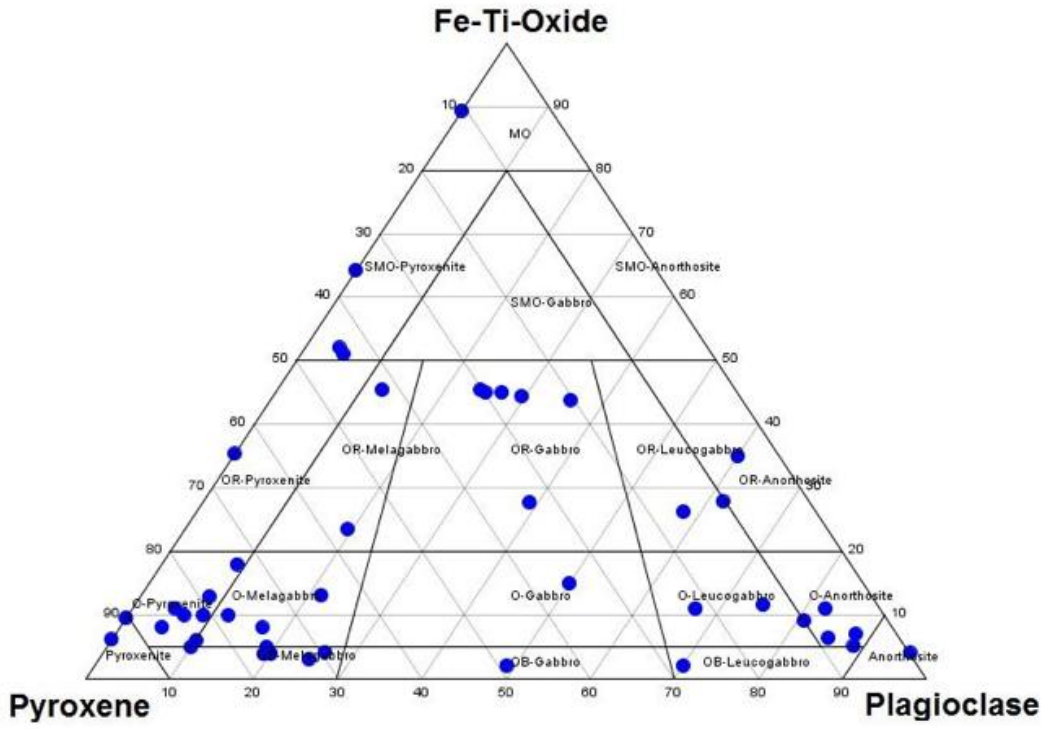

Figure 4.12. Sample distribution based on interpreted primary mineralogy for the Thunderbird intrusion

4.2.2.1. Alteration

The Thunderbird intrusion has been subject pervasive weak to moderate amphibole-chlorite-epidote metamorphism. The metamorphism has largely replaced the primary mineralogy and the text below is a description of the metamorphism/alteration of the primary minerals as interpreted from textures and compositions.

The Thunderbird intrusion is characterized by abundant medium-grained, anhedral to euhedral laths of plagioclase. The plagioclase generally exhibits deformation twinning (Fig. 4.13A), simple twining, recrystallization textures, and rare compositional zoning. Locally, plagioclase is partially to completely replaced by sericite ± epidote ± clinozoisite and when

altered, is often accompanied by very fine-grained quartz which exhibit triple junction boundaries (Fig. 4.13A).

Clinopyroxene occurs dominantly as fine- to medium-grained anhedral to subhedral laths which are partially to completely replaced by blue-green amphibole and/or chlorite (Fig. 4.13C). Clinopyroxene grains are rarely oikocrystic with inclusions of plagioclase, magnetite, pyrrhotite, pyrite and/or chlorite. Clinopyroxene (now altered to epidote, chlorite, and/or amphibole) rarely exhibits a symplectic intergrowth with magnetite and/or ilmenite and locally contains concentrations of up to 50% iron-titanium oxide (Fig. 4.13D).

Titanomagnetite crystals are characterized by fine- to medium-grained anhedral blebs which have undergone sub solidus oxy-exsolution to produce a magnetite host which contains varying concentrations of ilmenite exsolution. The ilmenite ranges from very fine-grained trellis-type exsolutions (<10µm: Fig. 4.13E), to coarse sandwich-type laths, to amoeboidal shaped inclusions (Fig. 4.13F) which range from fine- (<10µm) to medium-grained (10-20µm). The amoeboidal ilmenite exsolutions typically occur within the core of the titanomagnetite and gradationally transition into trellis and/or rarely sandwich-type exsolutions. Titanomagnetite rarely contains a corona of fine-grained chlorite and epidote, whereas ilmenite may contain very fine-grained titanite coronas. Ilmenite is also observed as fine- to medium-grained subhedral to euhedral crystals which may exhibit trace exsolutions of hematite. Hematite lamellae have only been observed within these distinct ilmenite grains, and not in the ilmenite exsolution lamellae within the magnetite grains.

The Thunderbird intrusion exhibits a generally massive to weakly foliated texture and locally highly sheared mylonitic texture. Areas of high strain are typically accompanied by

increased carbonate, chlorite, amphibole, epidote, clinozoisite, quartz, sericite /muscovite and/or biotite alteration.

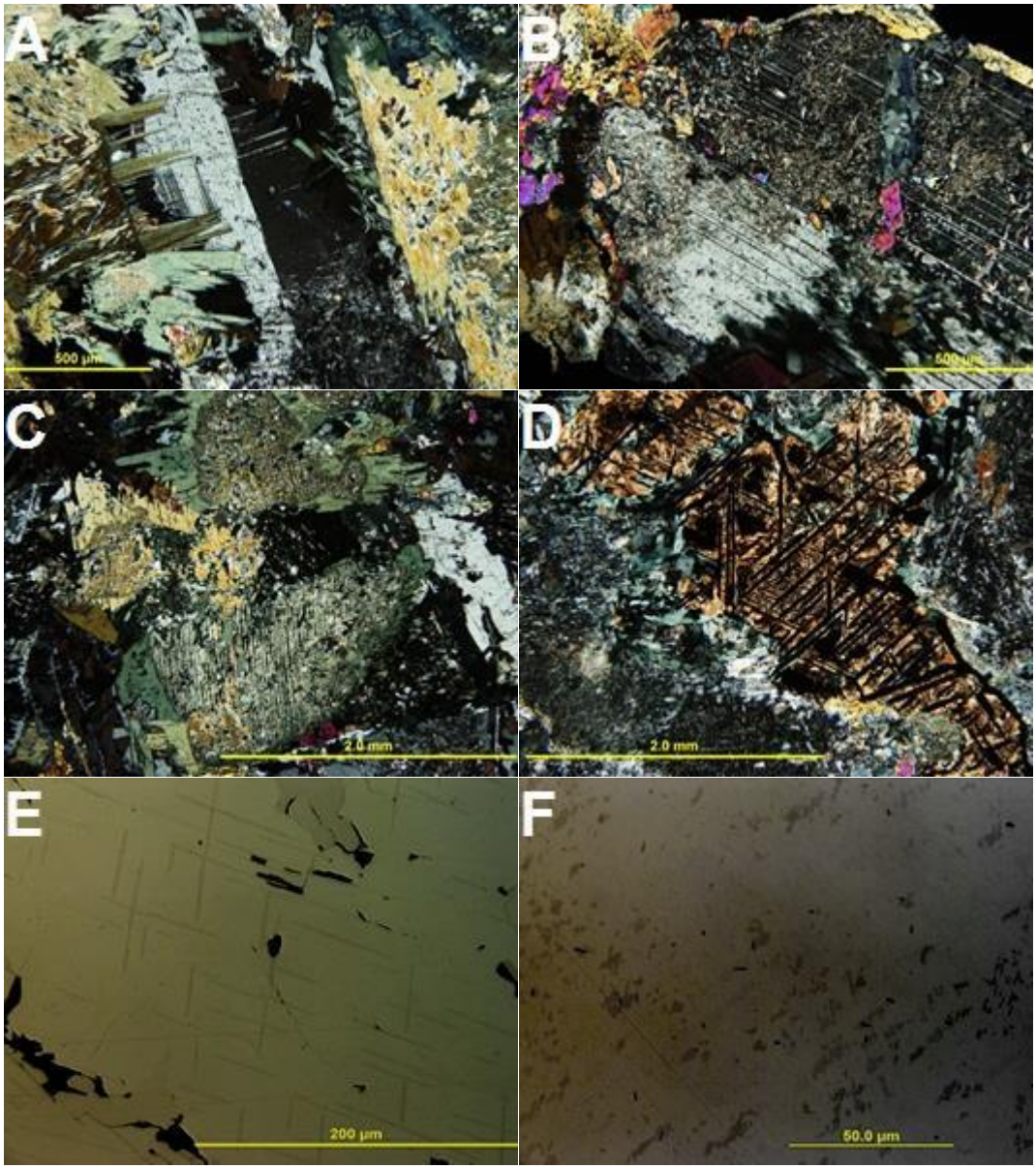

Figure 4.13. Transmitted light photomicrographs of representative textures within the Thunderbird intrusion. A) deformation twinning within plagioclase (XPL); B) sericite alteration after plagioclase (XPL); C) amphibole after pyroxene (XPL); D) Ilmenite (opaque) within amphibole after pyroxene (XPL); E) fine-grained ilmenite lamellae within magnetite (reflected light; XPL); F) ilmenite blebs within magnetite (reflected light; XPL).

4.2.2.2. Lithology and Mineralization

The Thunderbird intrusion is characterized by a suite of variably well-layered magnetite-ilmenite-rich gabbro-anorthosite rocks (Fig. 4.11). The anorthosites typically occur as translucent blue to milky white, medium-grained, equigranular, massive rocks dominantly composed of plagioclase with minor clinopyroxene, magnetite, ilmenite, pyrite, chalcopyrite and/or pyrrhotite. The gabbros are characterized by dark green, fine- to medium-grained massive subophitic to equigranular rocks which are composed of approximately equal proportions of euhedral plagioclase laths and anhedral to subhedral clinopyroxene with minor amounts of magnetite, ilmenite, pyrite, chalcopyrite and/or pyrrhotite (Fig. 4.14A). The layered anorthosite-gabbro units frequently exhibit compositions which range in plagioclase and pyroxene proportions which are intermediate between anorthosite and gabbro. These units have been termed leucogabbro and are dominantly composed of euhedral medium-grained plagioclase laths with lesser fine- to medium-grained anhedral to subhedral clinopyroxene and trace magnetite, ilmenite, pyrite, chalcopyrite, and/or pyrrhotite.

The Thunderbird intrusion is also composed of rare stratigraphically conformable massive oxides, pyroxenites, pegmatitic gabbros and leucogabbros, and cross-cutting microgabbros. The pyroxenites are dominantly composed of massive, fine- to medium-grained subhedral clinopyroxene with minor plagioclase laths, magnetite, ilmenite, pyrite, chalcopyrite, and/or pyrrhotite (Fig. 4.14B). The pegmatitic gabbro and leucogabbro rocks are compositionally similar to their fine- to medium-grained counter parts, but differ in the fact that their grain size is greater than or equal to 3cm. The microgabbros are composed of very fine- to fine-grained anhedral plagioclase and clinopyroxene with trace amounts of magnetite, ilmenite and pyrite (Fig. 4.14C).

The massive oxides are in part an end member of the magnetite-ilmenite mineralized suite of rocks. The massive oxides are dominantly composed of fine- to medium- grained anhedral blebs of magnetite which commonly display fine-grained (1-10µm) and rarely medium-grained (10-20µm) trellis style ilmenite exsolution lamellae, and rarely sandwich, and/or composite/granule ilmenite exsolution. Ilmenite within the massive oxides typically occur as fine- to medium-grained anhedral to subhedral tabular grains which contain fine-grained (<5µm) trace hematite exsolution lamellae with a parallel orientation and display synchronous extinction. Ilmenite also occurs as exsolution within magnetite, but does not display any hematite exsolution lamellae. The semi-massive oxide rocks are characterized by a ferrogabbro host which contains between 50-80% magnetite and ilmenite. The semi-massive oxide units are texturally similar to the massive oxide units; however, the magnetite grains lack the composite/granule ilmenite exsolution which is rarely observed within the massive oxides. The oxide-bearing to oxide-rich units are characterized by magnetite which displays fine- to medium-grained trellis style ilmenite exsolution and lacks of sandwich or composite/granule ilmenite exsolution. The ilmenite occurs both as exsolution lamellae within magnetite and/or as discrete fine- to medium-grained anhedral to subhedral tabular grains which commonly exhibit trace fine-grained (<3µm) hematite exsolution lamellae which are analogous to the ilmenite observed within the massive and semi-massive oxide units. Within all the magnetite-ilmenite-bearing units of the Thunderbird intrusion, rare fine-grained (<5µm) anhedral blebs of ilmenite occurs within the cores of medium-grained magnetite which grade into trellis ilmenite exsolution lamellae along the cores of the magnetite.

Drill core from holes NOT-11-2G46 and NOT-11-2G47 have intersected broad horizons of apatite mineralization. The apatite occurs as fine-grained euhedral prismatic crystals which are spatially associated with fine-grained anhedral magnetite and ilmenite (Fig. 4.14 D). The

apatite occurs solely within dark to light green leucogabbro to melagabbros and is very difficult to identify in hand sample due to the translucent nature and grain size; although concentrations locally reach as much as 15% apatite (sample NO-2G46-6).

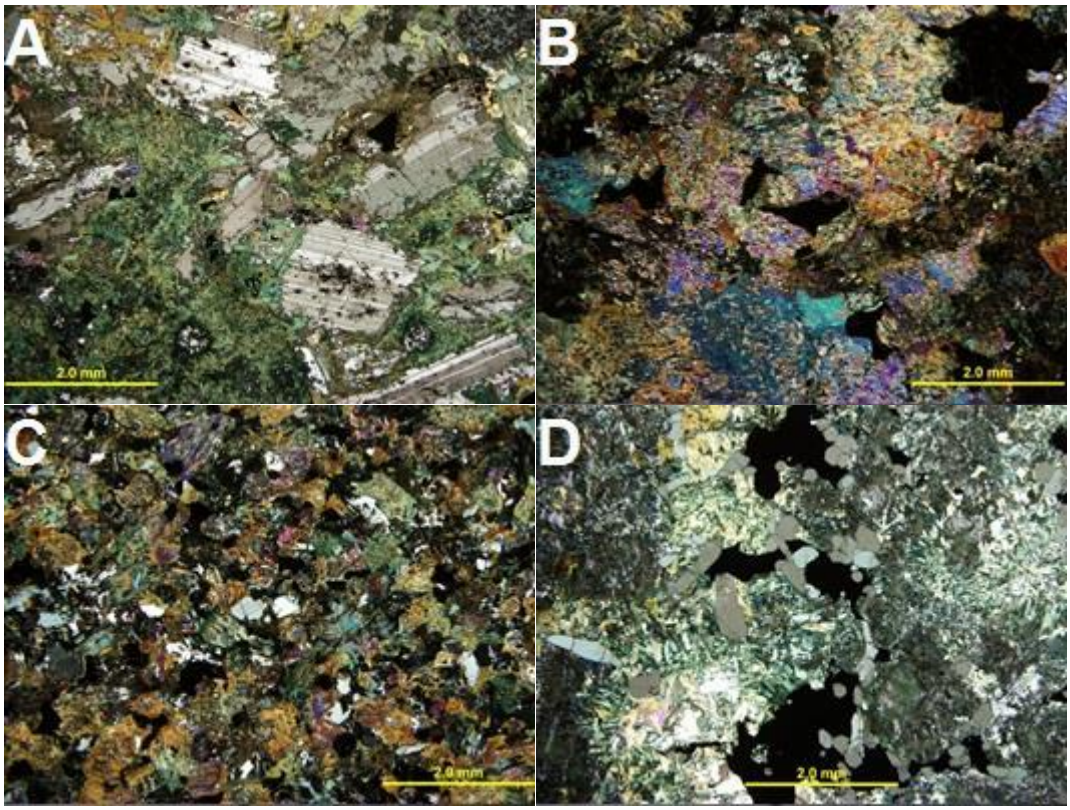

Figure 4.14. Transmitted light photomicrographs of representative lithologies from the Thunderbird intrusion. A) Gabbro (XPL); B) pyroxenite(XPL); C) microgabbro (XPL); apatite (tabular grey) displaying an association with magnetite-ilmenite (opaque; XPL).

4.3 Geochemistry

Due to the high abundances of cumulate magnetite and ilmenite within the Butler and Thunderbird intrusions, major oxide proportions cannot be used to classify the lithologies in the typical manner (e.g., TAS diagram). Furthermore, due to the high compatibility of high field strength elements in magnetite (Nielsen and Beard, 2000), trace element compositions cannot be accurately used to characterize the samples. Petrography of the Butler and Thunderbird intrusions has been used to describe them as a suite of rocks which range from anorthosite to pyroxenite with highly variable concentrations of magnetite and ilmenite. The lithologies of the samples have been characterized by their mineralogy rather than chemistry; however, geochemical trends are evident within Harker diagrams (Fig. 4.15).

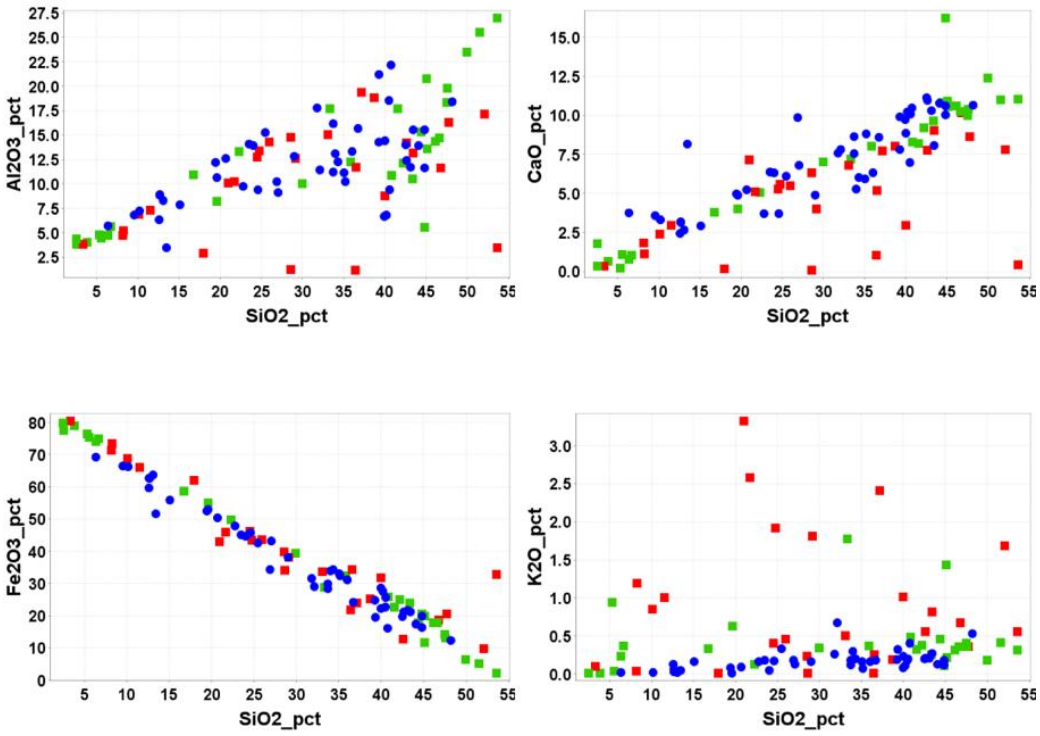

Figure 4.15. Harker variation diagrams of SiO_2 versus major element oxides (Red square= Butler East intrusion, Green Square= Butler West intrusion, Blue circle= Thunderbird intrusion).

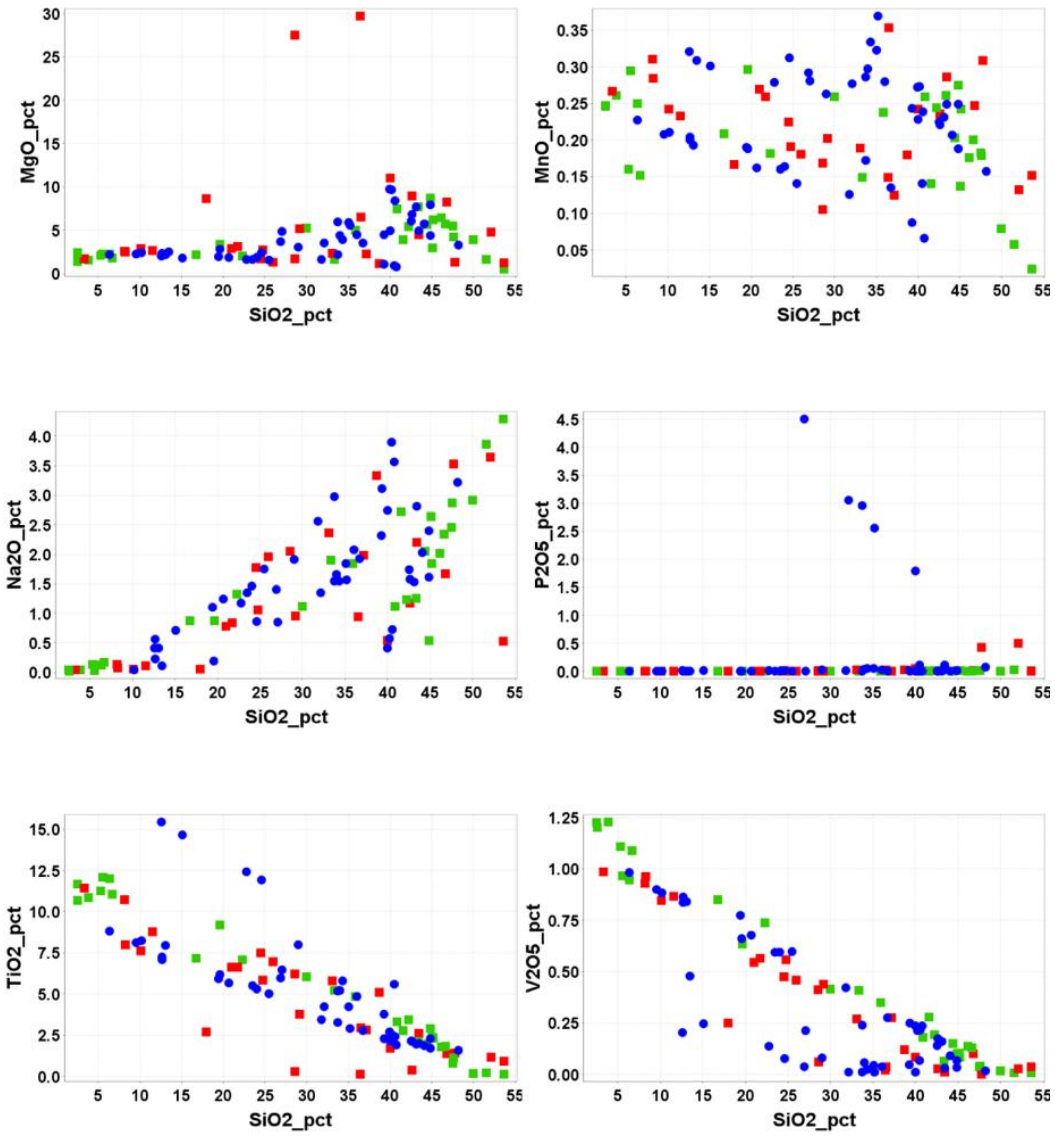

Figure 4.15 (cont.). Harker variation diagrams of SiO_2 versus major element oxides (Red square= Butler East intrusion, Green Square= Butler West intrusion, Blue circle= Thunderbird intrusion).

4.3.1. Butler Intrusions

4.3.1.1. Major and Trace Element Geochemistry

Fifty-four samples have been analyzed for major and trace element geochemistry from the Butler intrusions (Appendix E) of these, 26 samples are from the Butler East intrusion and 28 samples from the Butler West intrusion.

The Butler intrusions are comprised of a suite of Fe-Ti-rich lithologies which range in composition from anorthosite to pyroxenite with highly variable proportions of magnetite and ilmenite. Both intrusions display strong depletions in TiO_2, V_2O_5, and Fe_2O_3(t) with strong enrichments in Al_2O_3, CaO, and Na_2O with respect to SiO_2 (Fig. 4.15). The K_2O and MnO concentrations lack any obvious trend and correspond with variable degrees of alteration within the samples as determined through petrography. MgO within the Butler intrusions displays the highest abundances within a range of ~40-50 wt.% SiO_2 and corresponds to oxide-free and oxide-bearing gabbros and pyroxenites. Samples MM-V5-4 and MM-V5-5 collected from the Butler east intrusion represent cross-cutting ultramafic dykes and contain the highest concentrations of MgO (27 and 29 wt. %, respectively). P_2O_5 typically occurs as trace contents in the Butler intrusions with the exception of samples MM-71B-3 and MM-110-2 which contain 0.423 and 0.496 wt. % P_2O_5 (respectively), the remainder of the samples contain <0.052 wt. % P_2O_5 and are apatite-undersaturated. The phosphorous within the Butler East is concentrated within the oxide-bearing gabbro and leucogabbro which also contain relatively higher concentrations of SiO_2 (Fig. 4.15).

Although evolutionary trends are better demonstrated on Harker diagrams with respect to SiO_2 wt. %, mineralization trends are more evident when compared to Fe_2O_3(t) wt.% (Fig. 4.16). Fe_2O_3(t) wt % is a rough proxy for the amount of magnetite+ilmenite, and to a lesser

extent the concentration of Fe-bearing silicates (e.g., amphibole, pyroxene, epidote, etc.), particularly within Fe-rich samples where the concentration of iron is largely controlled by the concentration of Fe-Ti-oxide minerals. Strong positive trends are evident on plots of TiO_2, V_2O_5, Cr, Ni, Zn, and Co with respect to Fe_2O_3(t) in both Butler intrusions (Fig. 4.16). Scatter within the chalcophile elements (copper and zinc) are caused by variable amounts of sulfur within the sample. As a result of the highly elevated zinc values within samples MM-V4-1 (4409 ppm, Zn) and MM-110-3 (1376 ppm Zn) were excluded and correspond to sulfur-rich samples (12.4%, and 1.78 % S respectively). Zinc, nickel and cobalt are typically associated with the mineralization of sulphide minerals; however, within magnetite-rich samples these elements display a more prominent siderophile nature as shown by clear positive trends with total iron (Fig. 4.16). Copper values do not display any discernable trends with respect to Fe_2O_3 (t), and scatter is likely due to the highly chalcophile nature of copper. Chromium values are generally low and correspond to higher concentrations of magnetite and ilmenite, however, two anomalous oxide-anorthosite samples from the Butler East intrusion (MM-110-4: 2787 ppm and MM-V5-7: 1270 ppm) contain elevated chromium contents for their respective Fe_2O_3 (t) contents. Phosphorous concentrations do not display any correlation with Fe_2O_3 (Fig. 4.16), however, it is notable that all samples which contain phosphorous mineralization contain magmatic oxides as determined through petrographic analysis, where apatite grains are spatially associated with magnetite and ilmenite grains.

Trace element data from the Butler East and Butler West intrusions are presented on Figure 4.17. The data represent the interquartile range of the primary lithologies within the Butler intrusions and thus samples from cross-cutting ultramafic dykes (MM-V5-4 and MM-V5-5) were excluded, as was sample MM-V4-6 due to intense silicification. Samples MM-71B-3 and

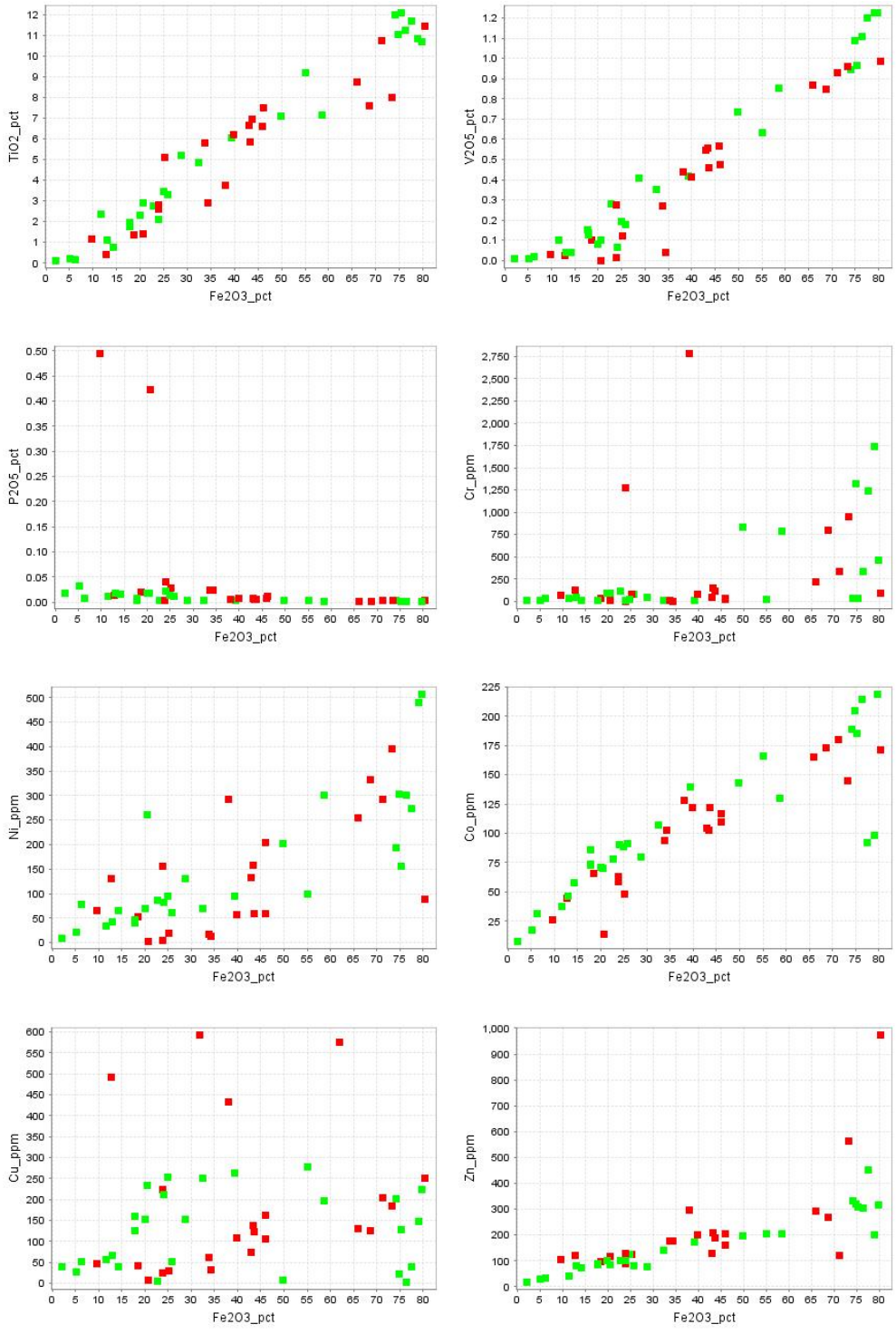

Figure 4.16. Harker variation diagrams of Fe_2O_3 (t) versus major element oxides in weight percent and trace elements in ppm (Red square= Butler East intrusion, Green Square= Butler West intrusion)

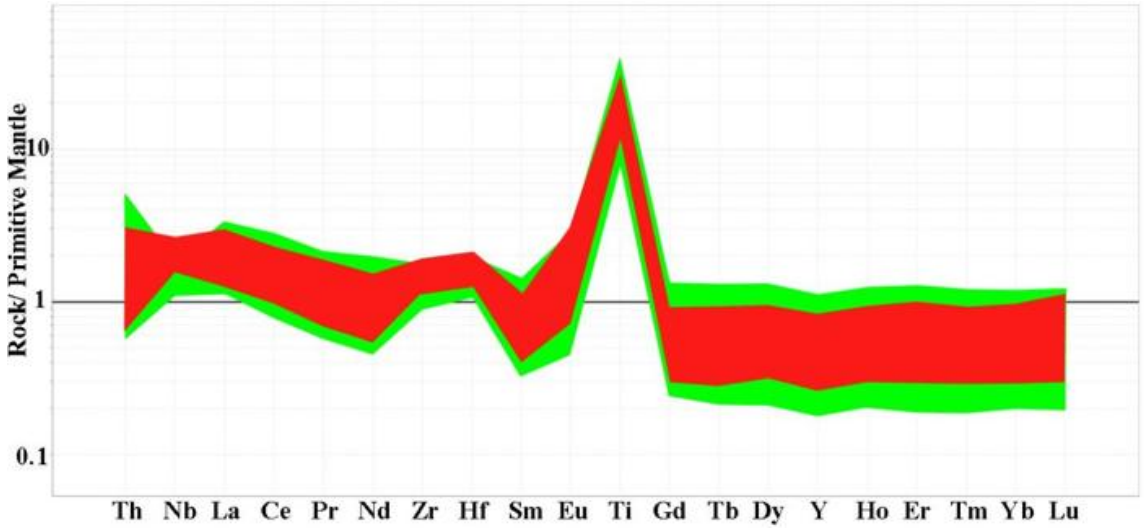

Figure 4.17. Primitive mantle normalized plot of the Butler East (red) and Butler West (green) intrusions with the first and third quartile range of elements (samples MM-V4-6, MM-V5-4, MM-V5-5, MM-71B-3, and MM-110-2 excluded); normalizing values from Sun and McDonough, 1989

MM-110-2 were also omitted due to the anomalously high trace element contents which correlate to trace amounts of apatite mineralization and are shown in Figure 4.19.

The Butler East intrusion is characterized by generally positive titanium anomalies, weakly enriched LREE (La/Sm_{pm}=2.93) and flat HREE (Gd/Yb_{pm}=1.16; Fig. 4.17). Butler East displays flat to slightly positive Zr (Zr/Zr*=1.07) and Hf (Hf/Hf*=1.27) anomalies and weak negative Y anomalies. The magnetite and ilmenite-rich lithologies (massive oxides, semi-massive oxides and oxide-rich: Fig. 4.18) are characterized by lower rare earth element abundances along with positive Zr (Zr/Zr*= 1.55) and Hf (Hf/Hf*=1.90) anomalies, and enriched LREE (La/Sm_{pm}=3.25) with flat HREE (Gd/Yb_{pm}=0.98) and Nb (Nb/Nb*=1.06). Sample MM-V4-1 is a massive oxide which displays an anomalously positive HREE slope (Gd/Yb_{pm}=0.20) which corresponds to presence of altered olivine and spinel. The oxide, and oxide-bearing lithologies are characterized by gentle sloping LREE (La/Sm_{pm}=2.60), HREE (Gd/Yb_{pm}=1.44), negative Zr (Zr/Zr*=0.55), Hf (Hf/Hf*=0.60), and Nb (Nb/Nb*=0.36) anomalies.

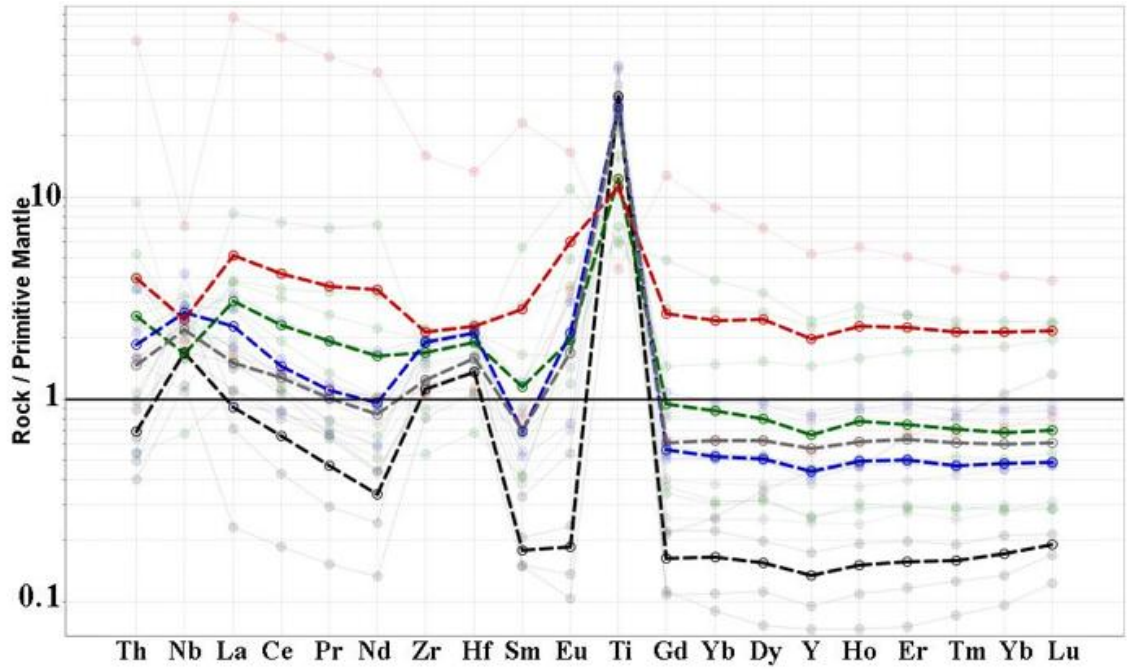

Figure 4.18. Butler East intrusion average trace element abundances for massive oxides (black), semi-massive oxide (grey), oxide-rich (blue), oxide (green), oxide-bearing (red). Highlighted plots are averages whereas faded plots are samples (Normalizing values from Sun and McDonough, 1989).

Apatite-bearing units within the Butler East intrusion are presented on Figure 4.19. Although the samples contain similar P_2O_5 contents (MM-110-2 =0.495 %, MM-71B-3=0.423 %) they display a large variance within REEs. These samples (particularly MM-110-2) contain high levels of REEs due to the strong partitioning of these elements within apatite (Prowatke and Klemme, 2006), but are broadly similar to the other ferrogabbroic units with negative Nb, Zr, Hf, and Y anomalies and weakly depleted HREE trends.

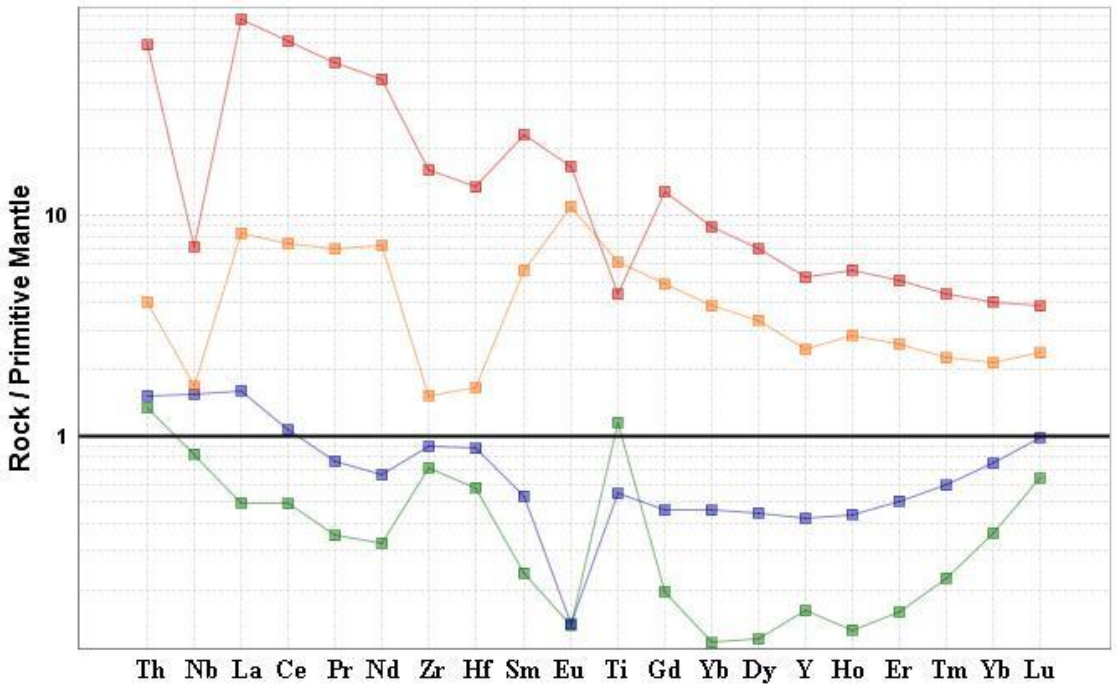

Figure 4.19. Primitive mantle normalized plot for apatite-bearing units (Red: MM-110-2, Orange: MM-71B-3) and ultramafic dykes within the Butler East intrusion (Blue: MM-V5-5, Green: MM-V5-4): normalizing values from Sun and McDonough, 1989)

The ultramafic dykes which cross-cut the Butler East intrusion are displayed on Figure 4.19 and are represented by samples MM-V5-4, and MM-V5-5. These two samples were collected from the same dyke which was intruded along the contact between a massive oxide and an oxide-bearing gabbro. The ultramafic dyke was sampled along the upper contact (MM-V5-4) which exhibited large massive magnetite-ilmenite xenoliths, and within the center of the dyke (MM-V5-5) which was mineralized with very fine-grained disseminated magnetite and ilmenite. Both samples display low concentrations of REEs and are characterized by positive Zr and Hf anomalies, and negative Eu anomalies with variable Y and Ti anomalies. The ultramafic dyke is also characterized by enriched HREE which is uncharacteristic of much of the Butler intrusions.

The Butler West intrusion is characterized by generally positive titanium anomalies, enriched LREE (La/Sm_{pm}= 3.10) and flat HREE (Gd/Yb_{pm}= 1.19; Fig. 4.20). Butler West displays positive Zr (Zr/Zr*=1.21) and Hf (Hf/Hf*=1.46) anomalies and negative Y (Y/Y*=0.45) anomalies. The magnetite and ilmenite-rich lithologies (massive oxides, semi-massive oxides and oxide-rich: Fig. 4.20) are characterized by lower abundances in heavy rare earth elements along with positive Zr (Zr/Zr*= 2.37), Hf (Hf/Hf*=2.94) and Nb (Nb/Nb*=1.41) anomalies, and steep LREE patterns (La/Sm_{pm}=3.99) with flat HREE (Gd/Yb_{pm}=1.18). The oxide, and oxide-bearing lithologies are characterized by enriched LREE (La/Sm_{pm}=2.53), flat HREE (Gd/Yb_{pm}=1.19), and negative Zr (Zr/Zr*=0.47), Hf (Hf/Hf*=0.50), and Nb (Nb/Nb*=0.19) anomalies.

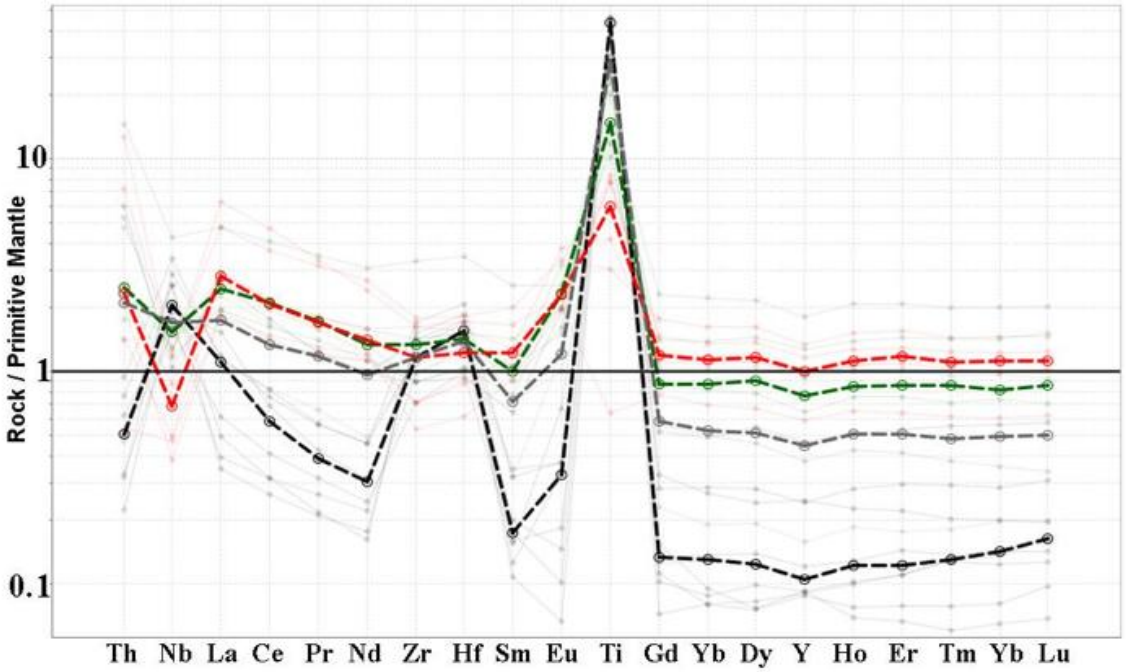

Figure 4.20. Butler West intrusion average trace element abundances for massive oxides (black), semi-massive oxide (grey), oxide (green), oxide-bearing (red): normalizing values from Sun and McDonough, 1989.

4.3.1.2. Mineral Chemistry

Select samples from the Butler intrusions have been analyzed by electron microprobe in order to determine the elemental compositions of the major mineral phases. A summary of the mineral phases and drill core analyzed can be found in Table 4.1 with the complete results presented in Appendix D. The electron microprobe work was focused on the characterization of the oxide and silicate minerals, and the determination of the trace element compositions for petrogenetic and mineralization trends within the Butler intrusions.

Table 4.1 Electron microprobe spot analysis totals for the Butler East and Butler West intrusions.

Sample	Magnetite	Ilmenite	Pyroxene	Plagioclase	Amphibole
MM-V1-1	14	3	0	0	0
MM-V1-2	13	3	0	24	0
MM-V1-3	19	6	0	0	0
MM-V1-4	17	6	0	0	0
MM-V1-5	20	7	0	0	0
MM-V1-6	2	5	0	0	0
MM-V4-1	0	0	11	0	0
MM-V4-7	0	0	3	19	8
MM-V5-1	21	12	0	0	0
MM-V5-2	15	12	0	0	0
MM-V5-3	14	9	0	0	0
MM-V5-4	10	0	0	0	0
MM-V8-1	0	0	6	17	7
MM-V8-2	13	13	0	0	0
MM-V8-3	13	11	0	0	0
MM-V8-4	16	11	0	0	0
MM-70-2	0	0	0	19	3
MM-71B-2	0	0	0	17	9
MM-117-1	0	0	7	14	8
MM-117-2	17	10	0	0	0
MM-117-6	0	0	3	15	10
Total	*204*	*108*	*30*	*125*	*45*

The oxide minerals examined within the Butler intrusions were focused on the characterization of magnetite and ilmenite (Fig. 4.21). Both magnetite and ilmenite contain very little solid solution with ulvöspinel and hemenite (respectively). The oxide minerals display

lower values of FeO compared to the ideal compositions of magnetite and ilmenite. This observation is consistent with the presence of impurities (e.g., V, Cr, Mn) within the ilmenite and magnetite crystals (Figs. 4.22 and 4.23).

Magnetite grains within the Butler intrusions are characterized by highly variable proportions of impurities (Table 4.2). The magnetite from the Butler West is characterized by higher contents of SiO_2, Al_2O_3, V_2O_5, Cr_2O_3, MgO, CoO, and NiO than the Butler East intrusion, and lower Fe_2O_3 and FeO* contents with similar FeO, CuO, ZnO and Fe_2O_3/FeO ratios (Table 4.2). Cations which are believed to substitute with a 3^+ valance state such as V , Cr and Al (Stormer, 1983), display a very weak negative trend with increasing Fe^{3+}/Fe^{2+} (Fig. 4.22). Cations which are thought to exist dominantly with a 2^+ valence state such as Si, Mg, Mn, Zn (Stormer, 1983), Ni, Co, and Cu (Liang et al., 2013) do not display any discernable trends (Fig 4.22). Titanium which exists as the 4^+ cation occupies the Fe^{2+} site within the magnetite which requires a second substitution of Fe^{2+} with Fe^{3+} to maintain charge balance

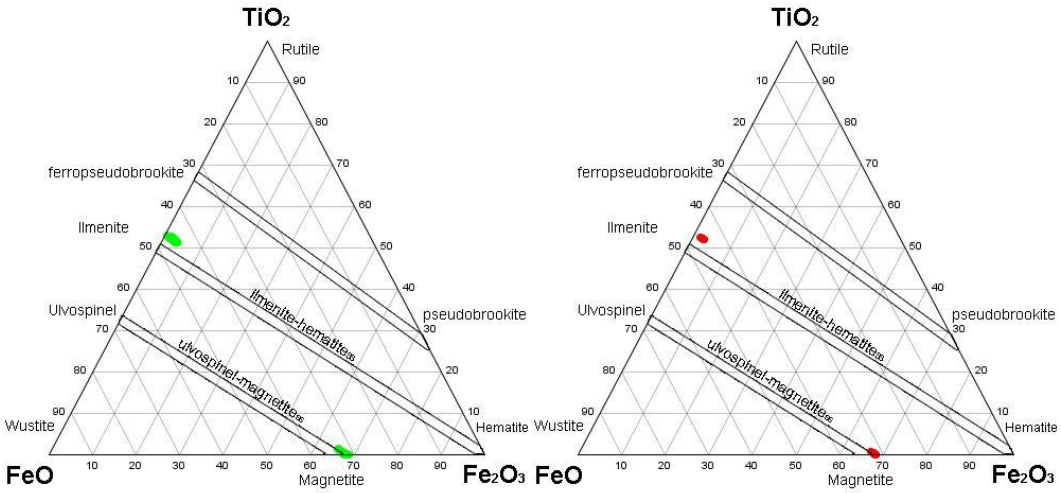

Figure 4.21. FeO-Fe_2O_3-TiO_2 characterization diagram for the oxide minerals within the Butler East (Red) and Butler West (Green) intrusions (modified from Taylor, 1964)

Table 4.2 Compositions of magnetite grains analyzed from the Butler East and Butler West intrusions (FeO*=total measured iron; S.D.= standard deviation for the population).

Oxide % Magnetite	Butler West				Butler East			
	Maximum	*Minimum*	*Average*	*S.D.*	*Maximum*	*Minimum*	*Average*	*S.D.*
SiO_2	0.064	0.007	0.024	0.009	0.119	0.004	0.019	0.016
TiO_2	1.428	0.039	0.251	0.257	0.954	0.014	0.242	0.207
Al_2O_3	0.636	0.073	0.270	0.117	0.116	0.031	0.066	0.021
V_2O_5	2.209	0.000	1.784	0.266	1.791	1.349	1.585	0.109
Cr_2O_3	0.617	0.003	0.251	0.136	0.216	0.121	0.166	0.025
MgO	0.050	0.000	0.006	0.008	0.014	0.000	0.002	0.003
MnO	0.023	0.000	0.007	0.005	0.023	0.000	0.007	0.004
FeO*	93.033	89.058	90.627	0.598	91.714	90.399	91.056	0.330
CoO	0.034	0.000	0.015	0.008	0.026	0.000	0.008	0.007
NiO	0.045	0.000	0.020	0.015	0.026	0.000	0.011	0.008
CuO	0.009	0.000	0.000	0.001	0.007	0.000	0.000	0.001
ZnO	0.031	0.000	0.006	0.007	0.037	0.000	0.006	0.007
Fe_2O_3	68.786	63.939	65.948	0.726	67.166	65.159	66.477	0.403
FeO	32.734	30.772	31.287	0.284	31.877	30.874	31.240	0.232
Fe_2O_3/FeO	2.148	1.989	2.106	0.035	2.161	2.045	2.128	0.024

(Lindsley, 1976). Titanium displays a strong negative correlation with increasing Fe^{3+}/Fe^{2+} in the magnetite, and is largely affected by the ulvöspinel content within the magnetite and thus trends within the Fe^{3+}/Fe^{2+} are reflective of oxy-exsolution processes (Lindsley, 1976). FeO* (total iron) displays a weak positive correlation with the Fe^{3+}/Fe^{2+} ratio and is effectively a measure of the total amount of elemental substitution/impurities of (dominantly V and to a lesser extent Ti) within the magnetite.

Sample MM-V1-6 was excluded from Figure 4.22 due to anomalously low concentrations of elements (e.g., V_2O_5=0.008 %), the high Fe_2O_3/FeO ratios and the limited magnetite grains for analysis (n=2). Additionally, MM-V5-4 was excluded since the sample was collected from the cross cutting ultramafic dyke and not stratigraphically conformable.

Due to the absence of ilmenite within the ultramafic dykes of the Butler East intrusion, only magnetite grains were analyzed. These magnetites contain elevated Cr_2O_3 (up to 3.904 %), MnO (0.192%), MgO (0.223%) and NiO (0.137%), with low V_2O_5 (0.197%) and comparable SiO_2, TiO_2, Al_2O_3, CoO, ZnO, and Fe_2O_3/FeO ratios with respect to the Butler intrusions.

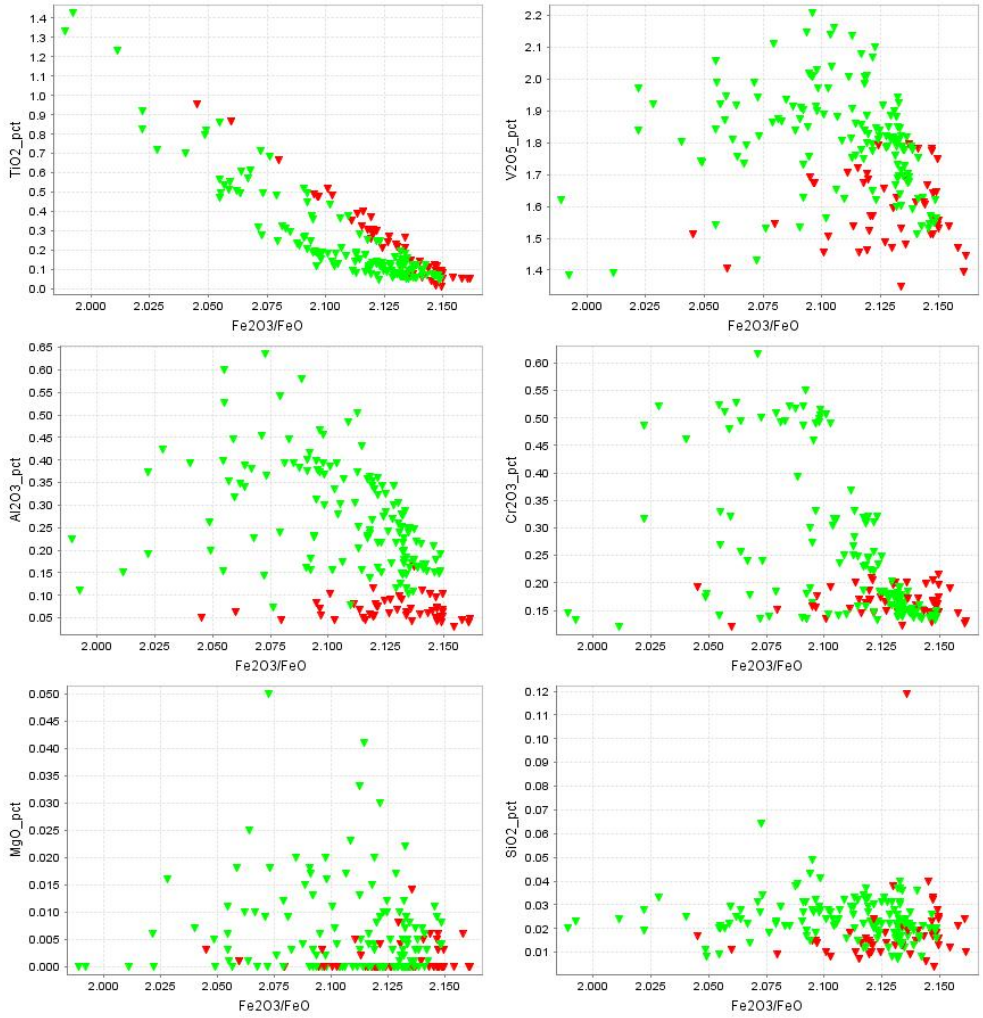

Figure 4.22. Magnetite analysis from the Butler East (red) and Butler West (green) intrusions (samples MM-V5-4 and MM-V1-6 excluded: n=192).

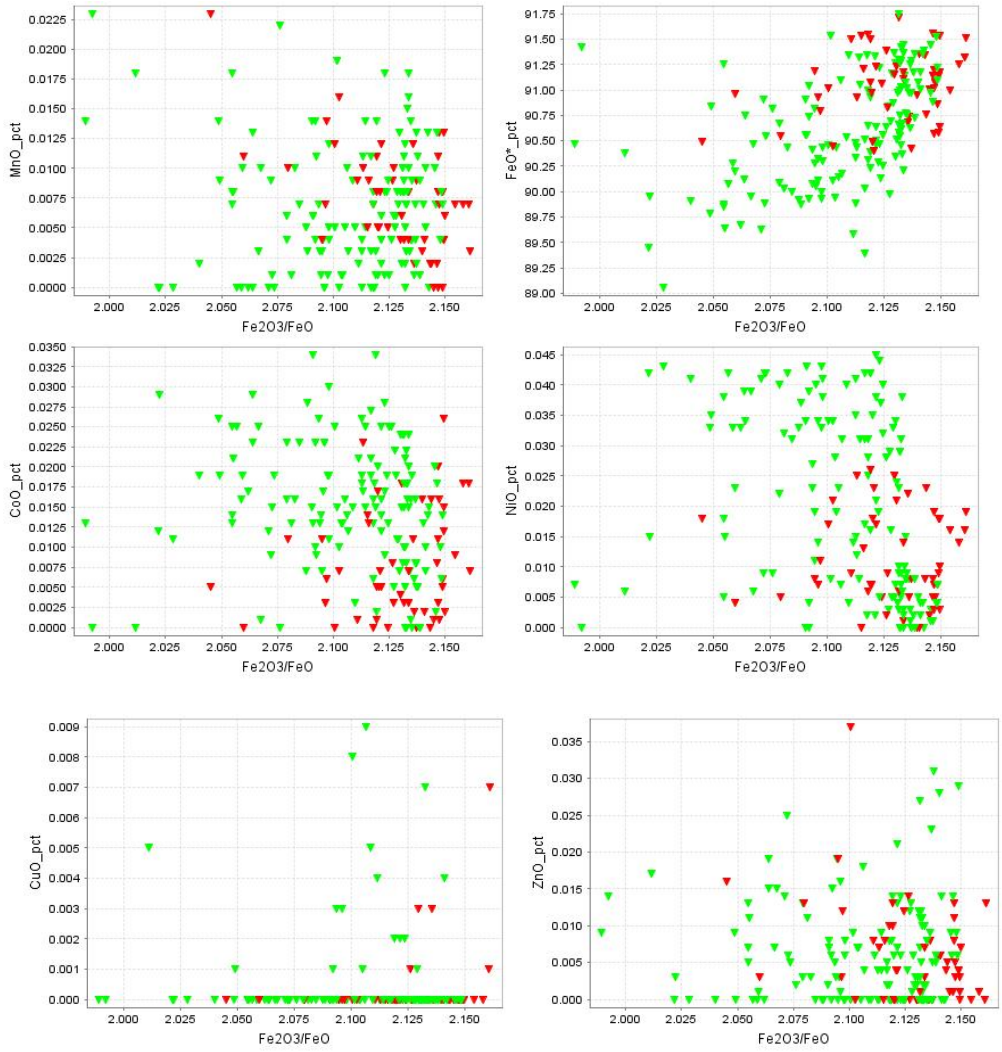

Figure 4.22 (cont.). Magnetite analysis from the Butler East (red) and Butler West (green) intrusions (samples MM-V5-4 and MM-V1-6 excluded: n=192).

The Butler intrusions are characterized by abundant ilmenite, and as a result microprobe analyses were focused on the ilmenite-hematite series (Fig. 4.23). Ilmenite ($Fe^{2+}Ti^{4+}O_3$) forms a complete solid solution series with hematite ($Fe_2^{3+}O_3$) at magmatic temperatures (Lindsley, 1976), and thus the ratio of Fe_2O_3 / FeO is an approximate measure of the amount of hematite solid solution within the ilmenite. Weak positive trends are observed within FeO* (total iron) along with negative TiO_2 contents with increasing hematite contents.

The other elements analyzed do not display any systematic trends with respect to hematite contents.

Ilmenite from the Butler West intrusion is characterized by elevated MgO, CoO, NiO, Fe_2O_3 and FeO (Table 4.3). However, ilmenite from the Butler East intrusion contains elevated MnO and ZnO (Table 4.3). Ilmenite from both intrusions contains similar concentrations of TiO_2, Al_2O_3, Cr_2O_3, V_2O_5, Nb_2O_3 and Fe_2O_3/FeO ratios.

Table 4.3 Compositions of ilmenite grains analyzed from the Butler East and Butler West intrusions (FeO*=total iron; S.D.= standard deviation).

Oxide % Ilmenite	Butler West				Butler East			
	Maximum	*Minimum*	*Average*	*S.D.*	*Maximum*	*Minimum*	*Average*	*S.D.*
SiO_2	0.030	0.000	0.009	0.007	0.045	0.000	0.008	0.008
TiO_2	51.924	50.320	51.033	0.319	51.776	50.526	51.052	0.287
Al_2O_3	0.053	0.000	0.018	0.008	0.062	0.000	0.013	0.011
V_2O_5	0.363	0.000	0.274	0.086	0.363	0.194	0.305	0.038
Cr_2O_3	0.048	0.000	0.027	0.009	0.037	0.013	0.027	0.006
Nb_2O_3	0.015	0.000	0.001	0.003	0.008	0.000	0.000	0.001
MgO	0.410	0.009	0.096	0.109	0.050	0.004	0.024	0.012
MnO	1.824	0.332	1.067	0.407	1.556	1.172	1.405	0.126
FeO*	47.733	45.748	46.908	0.420	47.337	46.184	46.661	0.272
CoO	0.039	0.000	0.014	0.010	0.025	0.000	0.010	0.007
NiO	0.011	0.000	0.003	0.003	0.006	0.000	0.002	0.002
CuO	0.017	0.000	0.001	0.003	0.008	0.000	0.001	0.002
ZnO	0.025	0.000	0.008	0.006	0.032	0.001	0.018	0.008
Fe_2O_3	3.749	0.477	2.523	0.596	3.459	1.582	2.477	0.394
FeO	45.587	43.987	44.637	0.328	44.929	44.048	44.433	0.239
Fe_2O_3/FeO	0.085	0.010	0.057	0.014	0.078	0.035	0.055	0.009

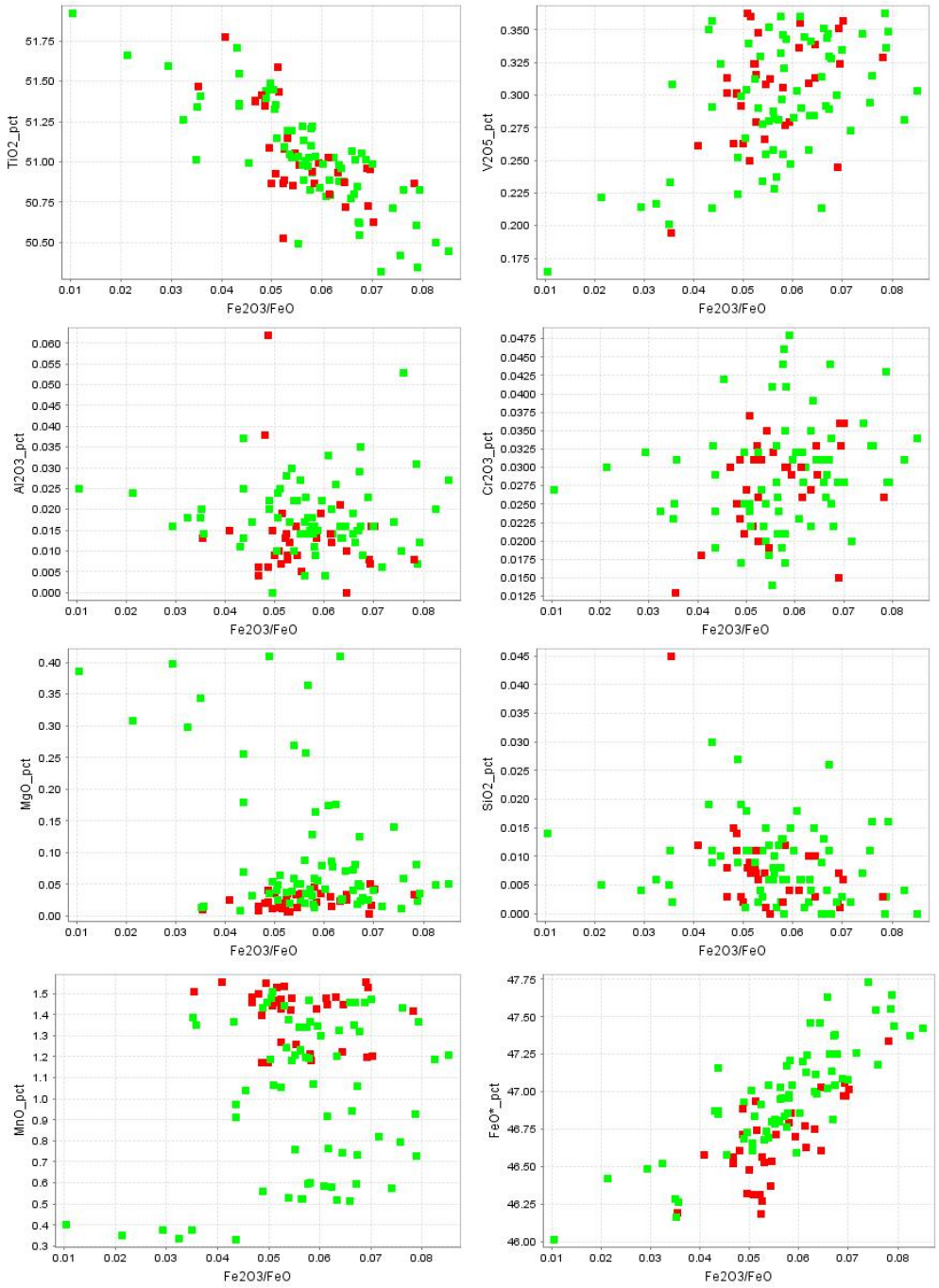

Figure 4.23. Ilmenite analysis from the Butler East (red) and Butler West (green) intrusions (n=108).

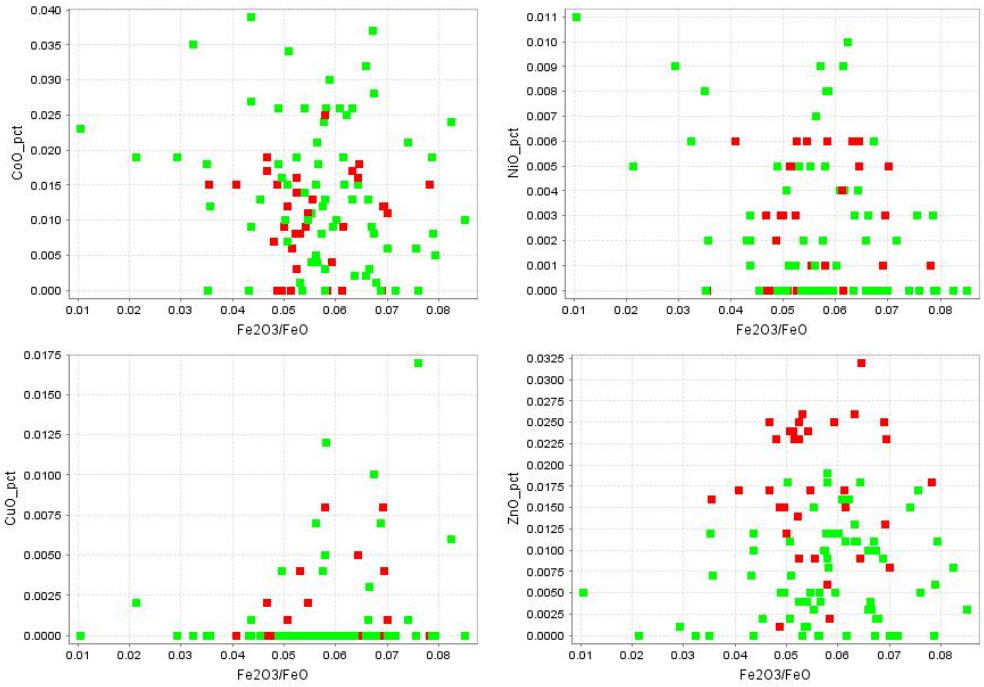

Figure 4.23 (cont.). Ilmenite analysis from the Butler East (red) and Butler West (green) intrusions (n=108).

Silicate analyses on the Butler intrusions were focused on the characterization of feldspar and to a lesser extent pyroxene and amphibole compositions due to the high amount of alteration observed within primary pyroxene grains (Table 4.1). A total of 55 spot analyses of feldspar from the Butler East intrusion and 70 from the Butler West intrusions were recalculated to determine the compositions of the anorthite-albite-orthoclase end members (Fig. 4.24).

Feldspar from the Butler East intrusion has been characterized by three samples which were identified as plagioclase with variable anorthite contents (28 to 81 An %). Sample MM-71B-2 is characterized by 28-50 An % and is generally restricted to 37-48 An% which is identified as andesine plagioclase. The variable compositions of plagioclase are coincident with heterogeneous alteration within the sample and appear to decrease in An% with higher degrees of alteration. Sample MM-70-2 ranges from 51-81 An% and generally ranges from 53-

55 An% which has been identified as labradorite plagioclase. Sample MM-V4-7 is a very homogenous sample which exhibits simple twinning but no alteration and is characterized by 50 to 53 An % and has been classified as labradorite plagioclase.

Plagioclase grains from the Butler West intrusion display highly variable An % and the anomalous values coincide with alteration of the mineral analyzed. Sample MM-117-1 ranges from 59-73 An % but is generally restricted to 60-66 An % and is identified as labradorite plagioclase. Sample MM-117-6 collected down hole from MM-117-1 ranges from 58-64 % An (labradorite). Sample MM-V1-2 ranges from 56 to 85 An%, though is largely restricted to 58-59 An% (labradorite). Sample MM-V8-1 displays a very homogenous composition and ranges from 54-56 An % which coincides with labradorite plagioclase.

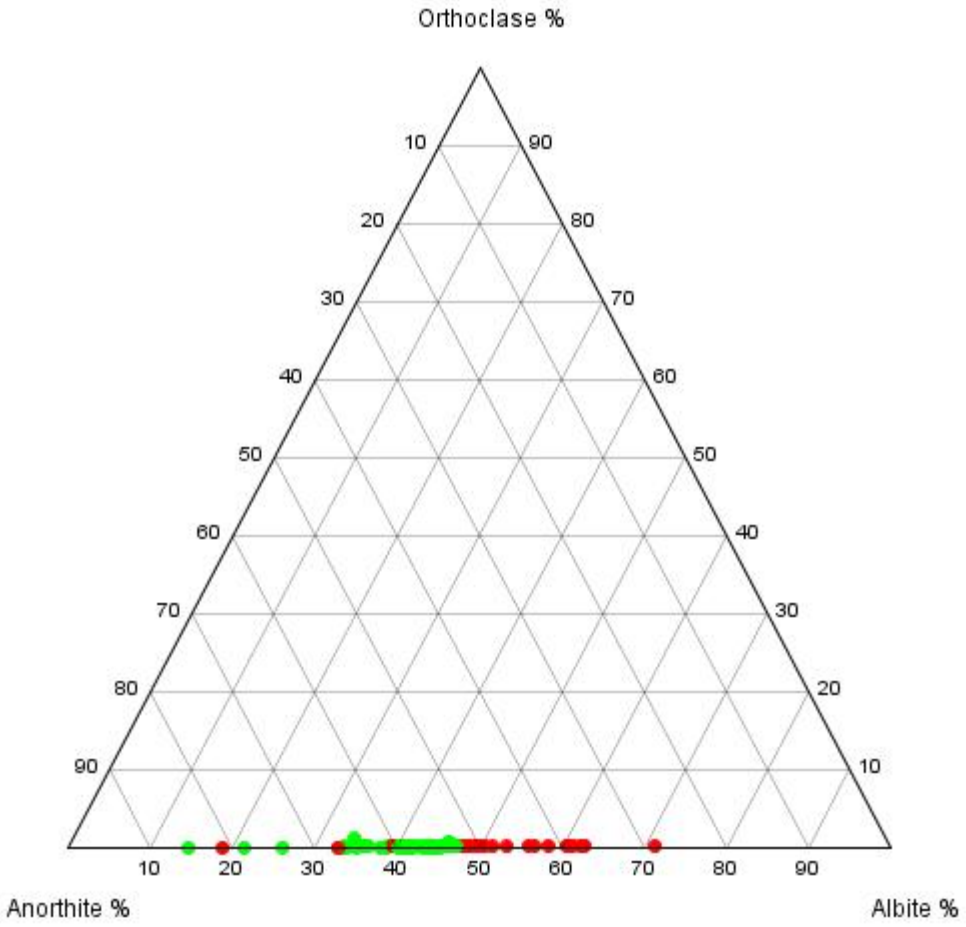

Figure 4.24. Feldspar compositions as determined by EMPA of the Butler East (Red) and Butler West (green)

Pyroxene compositions were determined by electron microprobe and recalculated to the end-member group of the wollastonite-enstatite-ferrosilite group. Due to the presence of pervasive secondary amphibolite within the Butler intrusions, pyroxene grains are uncommon and only a few samples contained enough pyroxene to be analyzed. Sixteen pyroxene grains were analyzed from the Butler West intrusion and 14 analyses from the Butler East intrusion from a total of four samples (Table 4.1).

The Butler East intrusion is characterized by samples MM-V4-1 and MM-V4-7. Pyroxenes from MM-V4-1 display no compositional zoning and are restricted to a narrow range of augite compositions (Fig. 4.25). Sample MM-V4-7 which was collected down hole from MM-

V4-1 similarly displays no compositional zoning and has been identified as clinoenstatite (Fig. 4.25). The Butler West intrusion is characterized by three samples. Samples MM-117-1 and MM-V8-1 have been identified as augite whereas pyroxene from MM-117-6 displays an intermediate composition between clinoenstatite and clinoferrosilite (Fig. 4.25).

Amphibole analysis of the Butler intrusions was a minor focus of the study and comprises by 20 analyses from the Butler East intrusion and 25 analyses from the Butler West (Table 4.1). All the amphiboles belong to the OH, F, Cl group and the Ca subgroup as defined by the International Mineralogical Association (Locock, 2014).

Amphibole analyses from the Butler East intrusion were conducted on drill core samples from MN08-71B, MN08-70 and BP11-V04. Samples MM-71B-2 and MM-V4-7 were characterized by a ferro-pargasite and ferro-hornblende assemblage. Three points were analyzed from MM-70-2 and display a highly variable composition ranging from magnesio-hornblende to tschermakite to ferro-hornblende.

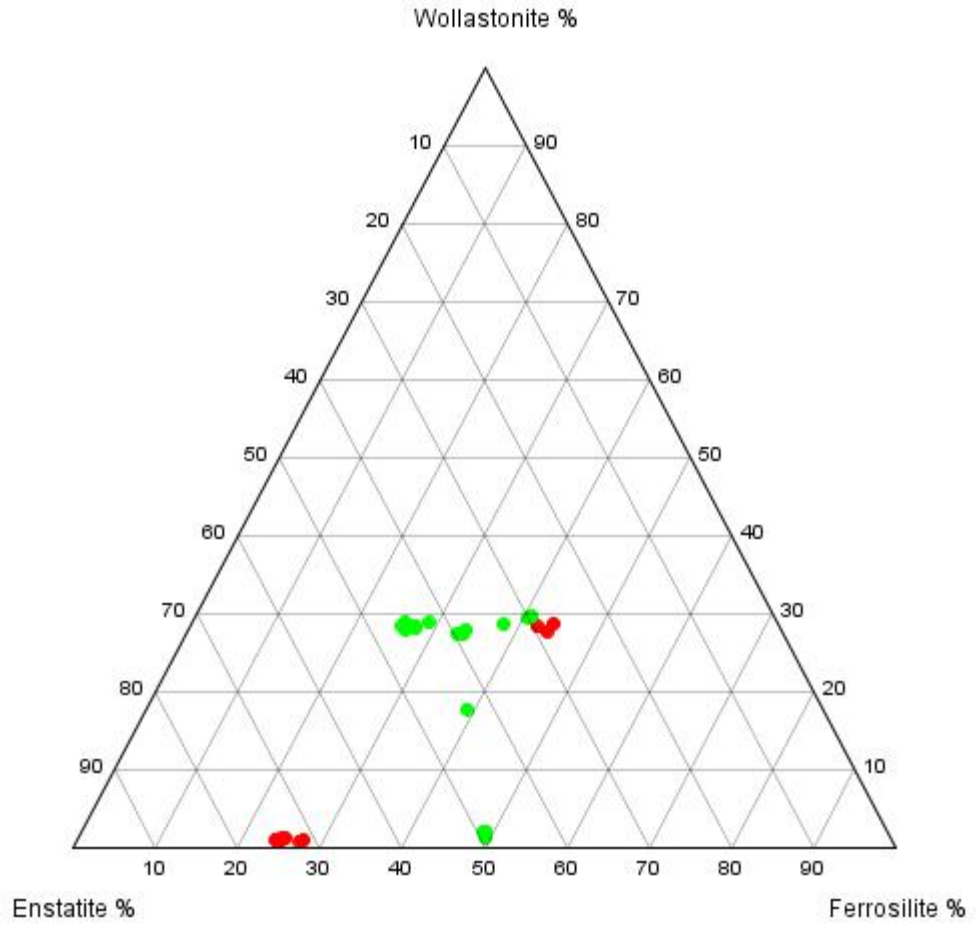

Figure 4.25. Pyroxene compositions as determined by EMPA of the Butler East (red) and Butler West (green) intrusions.

The Butler West intrusion amphibole analyses were focused on samples from drill holes MN10-117 and BP11-V08. Sample MM-117-1 is characterized dominantly by magnesio-hornblende and lesser actinolite, whereas sample MM-117-6 is composed dominantly of magnesio-hornblende with lesser magnesio-ferri-hornblende and ferro-hornblende. Sample MM-V8-1 is characterized by an assemblage of magnesio-hornblende, ferro-pargasite and ferro-hornblende.

4.3.1.3. Samarium-Neodymium Isotope Geochemistry

Sample selection for Sm-Nd isotope analysis was limited to samples which contained > 1 ppm Nd and displayed limited alteration. Five samples were selected from the Butler East and Butler West intrusion. The ε_{Nd} of the samples were calculated to an age of 2733.6 Ma based on preliminary geochronology from the Thunderbird intrusion (McNicoll, pers. comm., 2014). The Butler East intrusion displays a wide range of ε_{Nd} values from -2.80 and +11.23 and initial $^{143}Nd/^{144}Nd$ ratios from 0.508947 to 0.509661 (Table 4.4). Model ages within the Butler East range from 1896 to 10187 Ma (Table 4.4). The Butler West intrusion is characterized by a relatively narrow range of ε_{Nd} values from -3.34 to +4.01 and initial $^{143}Nd/^{144}Nd$ ratios 0.508920 to 0.509294 (Table 4.4). Model ages calculated from the Butler West intrusion range from 2565 to 3398 Ma (Table 4.4).

Table 4.4 Sm-Nd isotopic values from the Butler intrusions.

Sample	Intrusion	$^{143}Nd/^{144}Nd$ current	εNd_{2733}	Model Age (Ma)	$^{143}Nd/^{144}Nd$ initial
MM-V4-1	Butler East	0.513496	+8.76	10187	0.509536
MM-V4-6	Butler East	0.512346	+5.51	2379	0.509370
MM-V5-1	Butler East	0.512358	-2.80	4578	0.508947
MM-110-3	Butler East	0.512202	+11.23	1896	0.509661
MM-110-4	Butler East	0.511612	+4.84	2594	0.509336
MM-V2-5	Butler West	0.511771	+1.60	2913	0.509171
MM-V8-2	Butler West	0.512186	-0.28	3379	0.509076
MM-V8-4	Butler West	0.511417	-3.34	3398	0.508920
MM-60-4	Butler West	0.511817	+1.89	2885	0.509186
MM-117-7	Butler West	0.512524	+4.01	2565	0.509294

4.3.2. Thunderbird Intrusion

4.3.2.1. Major and Trace Element Geochemistry

Forty four samples of the Thunderbird intrusion have been analyzed for whole rock and trace element geochemistry (Appendix E). The samples were selected to characterize petrographic and mineralization trends within the intrusion.

The Thunderbird intrusion displays broad positive trends of Al_2O_3, CaO, K_2O, and Na_2O, along with negative Fe_2O_3 (t), MnO, TiO_2, and V_2O_5 with increasing SiO_2 wt. % (Fig. 4.26). P_2O_5 contents are generally low; however, anomalous concentrations were intersected within drill cores NOT11-2G46 and NOT11-2G47. If present, the P_2O_5 displays a negative trend with increasing SiO_2 (Fig. 4.26). Within the Thunderbird intrusion, two broad geochemical trends are observed within drill cores and can be subdivided into vanadium-rich and phosphorous-rich trends. The vanadium-rich trends are observed within drill holes NOT09-2G21, NOT09-2G22, and NOT09-2G25, whereas phosphorous-rich trends have been observed in NOT11-2G46 and NOT11-2G47.

Vanadium-rich trends are characterized by higher concentrations of compatible elements for their respective Fe_2O_3 (t): V_2O_5, Cr, Ni, Co, and Cu (Fig. 4.26) along with flat HREE patterns (Fig. 4.27). The phosphorous-rich trend is characterized by elevated TiO_2, and P_2O_5 along with elevated HREE (Fig. 4.27). Both trends display similar Zn concentrations (Fig. 4.26) variable Nb anomalies, and positive Ti anomalies (Fig. 4.27).

Due to the geochemical variation within the vanadium-rich and phosphorous-rich trends of the Thunderbird intrusion, they will be examined as discrete groups. The vanadium-rich trend displays enriched LREE (La/Sm_{pm}= 3.00) and flat HREE (Gd/Yb_{pm}= 1.36), along with positive Zr (Zr/Zr*= 2.06), Hf (Hf/Hf*= 2.61), and highly variable Nb (Nb/Nb*= 0.18 to 4.68)

anomalies (Fig. 4.27). The phosphorous trend displays enriched LREE (La/Sm_{pm}= 2.96) and HREE (Gd/Yb_{pm}= 2.51), along with highly variable Zr (Zr/Zr*=0.03 to 19.12), Hf (Hf/Hf*=0.04 to 14.66), and Nb (Nb/Nb*= 0.06 to 5.27) anomalies (Fig. 4.27).

Sample NO-2G25-1 was collected from a cross-cutting fine-grained ferrogabbro dyke and is characterized by depleted LREE (La/Sm_{PM}= 0.77), and flat HREE (Gd/Yb_{PM}= 1.35), along with negative Nb (Nb/Nb*= 0.45), Zr (Zr/Zr*= 0.45) and Hf (Hf/Hf*= 0.79) anomalies and a positive Ti anomaly (Fig. 4.28).

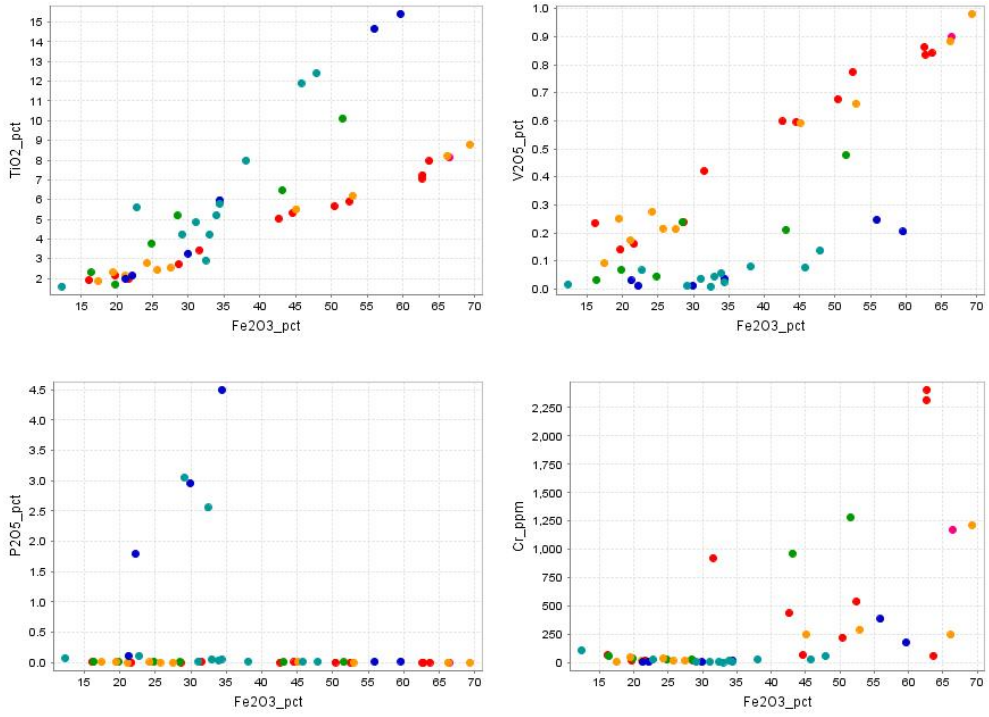

Figure 4.26. Harker variation diagram for the Thunderbird intrusion with Fe_2O_3 wt. % on the x-axis (Dark blue=NOT11-2G47, light blue=NOT11-2G46, red= NOT09-2G21, green = NOT09-2G22, orange= NOT09-2G25).

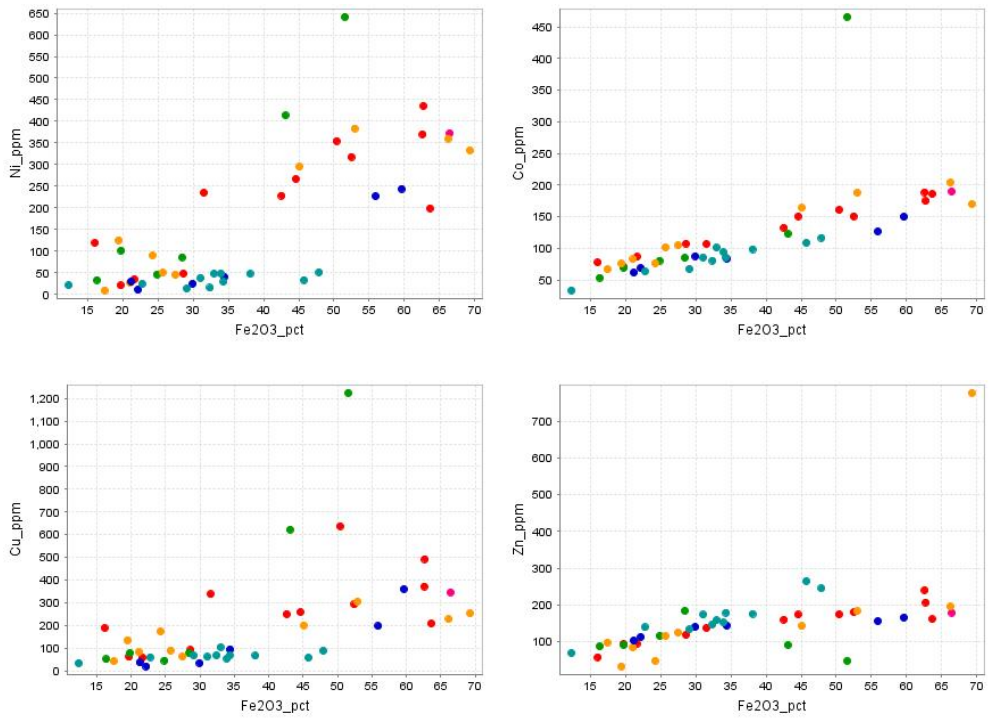

Figure 4.26 (cont.). Harker variation diagram for the Thunderbird intrusion with Fe_2O_3 wt. % on the x-axis (Dark blue=NOT11-2G47, light blue=NOT11-2G46, red= NOT09-2G21, green = NOT09-2G22, orange= NOT09-2G25).

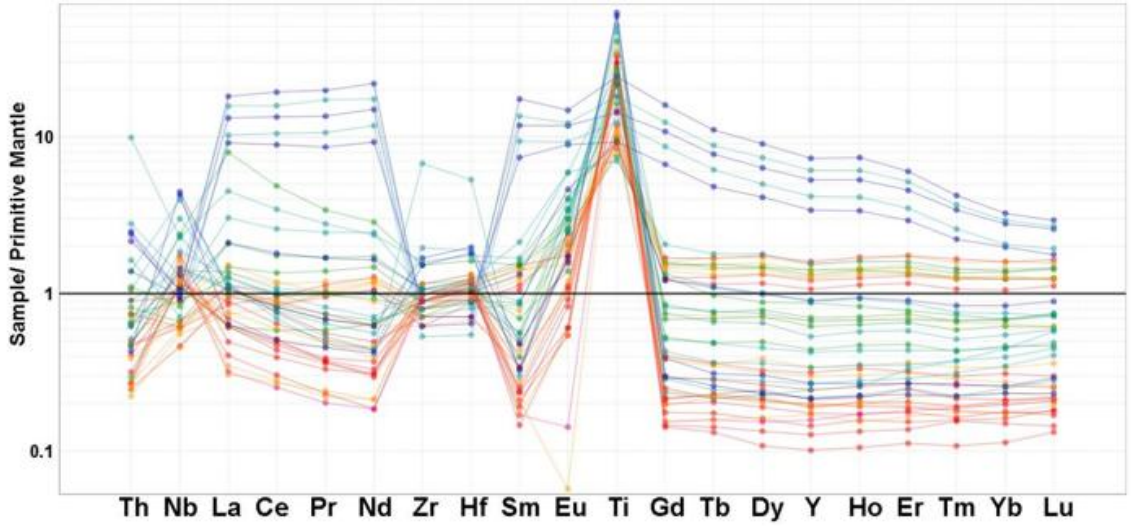

Figure 4.27. Primitive mantle normalized plot of the Thunderbird intrusion (Dark blue=NOT11-2G47, light blue=NOT11-2G46, red= NOT09-2G21, green = NOT09-2G22, orange= NOT09-2G25: normalizing values from Sun and McDonough, 1989).

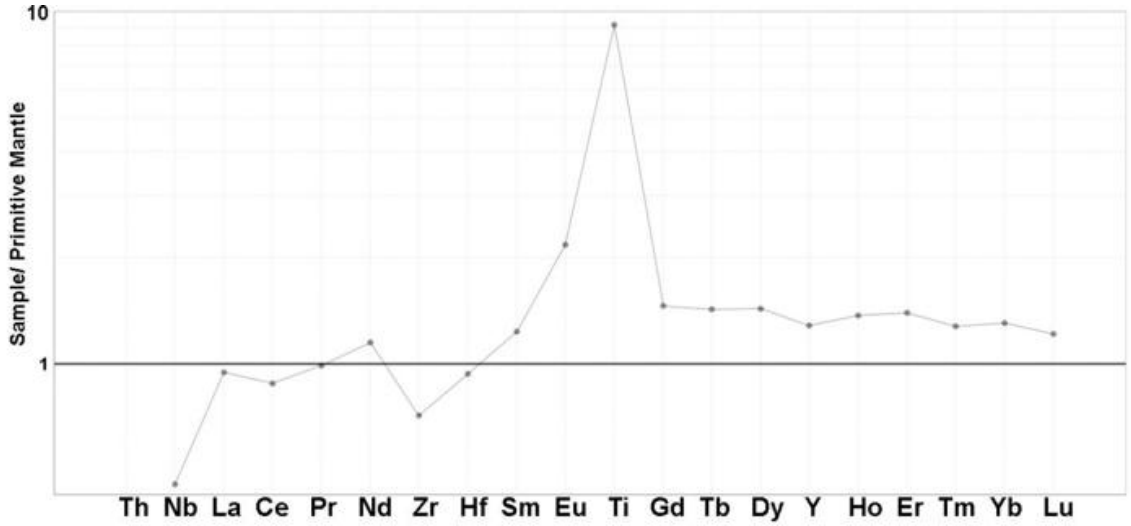

Figure 4.28 Primitive mantle normalized plot for sample NO-2G25-1, a ferrogabbro dyke from the Thunderbird intrusion (normalizing values from Sun and McDonough, 1989).

4.3.2.2. Mineral Chemistry

Oxide and silicate minerals from the Thunderbird intrusion were analyzed by electron microprobe to determine major and trace element compositions (Table 4.5). Oxide minerals were focused on magnetite and ilmenite, whereas the silicates were focused on pyroxene, plagioclase, and amphibole based on the high abundance of these minerals (Table 4.5). The results of the microprobe analysis can be found in Appendix D.

The oxide minerals within the Thunderbird intrusion are composed of nearly end-member magnetite and ilmenite of the magnetite-ulvöspinel and ilmenite-hematite solid solution series (Fig. 4.29). Both magnetite and ilmenite grains display lower values of FeO than the ideal compositions, and as a result shift the elemental proportions towards the TiO_2 and Fe_2O_3 corner of the ternary diagram (Fig. 4.29).

Table 4.5 Electron microprobe spot analysis totals for the Thunderbird.

Sample	Magnetite	Ilmenite	Pyroxene	Plagioclase	Amphibole
NO-2G21-1	0	0	0	0	36
NO-2G21-2	0	0	16	2	0
NO-2G21-5	0	0	3	11	0
NO-2G21-6	14	9	0	0	0
NO-2G21-7	13	12	0	0	0
NO-2G21-9	11	13	0	0	0
NO-2G21-10	13	15	0	0	0
NO-2G21-11	16	15	0	0	0
NO-2G22-4	0	0	0	29	18
NO-2G25-3	21	12	0	0	0
NO-2G25-4	23	6	0	0	0
NO-2G25-5	18	9	0	0	0
NO-2G25-6	15	7	0	0	0
NO-2G46-1	13	12	0	0	0
NO-2G46-2	11	16	0	0	0
NO-2G46-3	0	18	4	15	0
NO-2G47-2	0	0	10	17	3
NO-2G47-3	0	0	0	23	7
NO-2G47-5	0	0	7	16	0
NO-2G47-6	9	14	0	0	0
NO-2G47-7	13	14	0	0	0
NO-2G47-8	13	14	0	0	0
NO-2G47-9	*12*	21	0	0	0
Total	*215*	*207*	*40*	*113*	*64*

Magnetite grains within the Thunderbird intrusion display variable compositions based on their respective mineralization trends (i.e., vanadium or phosphorous: Table 4.6). Magnetite within the vanadium trend is characterized by elevated compatible elements such as V_2O_5, Cr_2O_3, CoO, and NiO. Magnetite grains from the phosphorous trend are characterized by elevated SiO_2, TiO_2, Al_2O_3, FeO (t), Fe_2O_3, FeO, and display higher Fe_2O_3/FeO ratios than the vanadium trend. Both trends display similar MnO and very low ZnO concentrations.

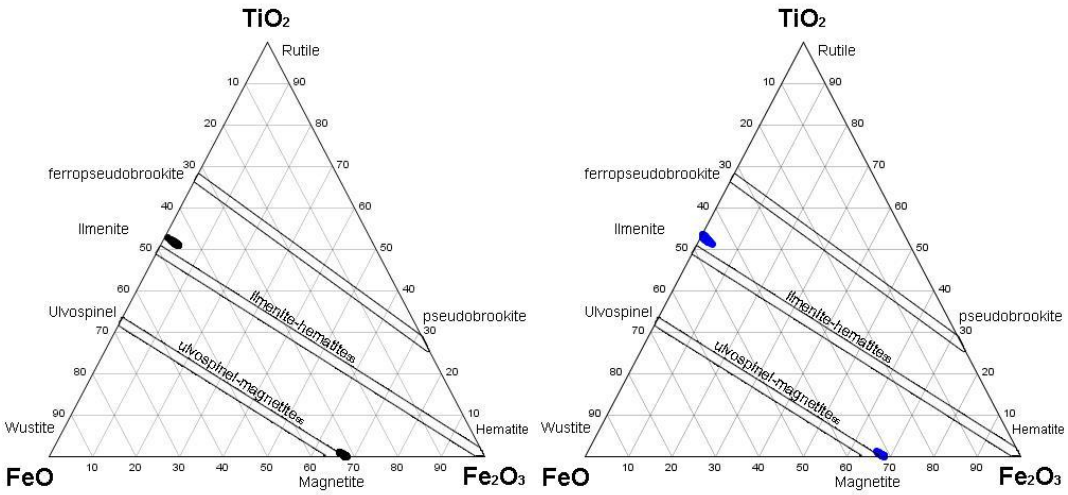

Figure 4.29. FeO-Fe_2O_3-TiO_2 characterization diagram for the oxide minerals within the Thunderbird intrusion (black= vanadium trend, blue= phosphorous trend; modified from Taylor, 1964)

Magnetite grains display decreasing TiO_2, Cr_2O_3, and NiO concentrations and increasing FeO* (total iron) with increasing Fe_2O_3/FeO ratios (Fig. 4.30). Considerable scatter is evident within Al_2O_3, MgO, SiO_2, MnO, CoO, CuO, and ZnO contents and they display no discernable relationship with Fe_2O_3/FeO ratios (Fig. 4.30). The vanadium-trend within the Thunderbird intrusion contains a lower TiO_2, FeO*, SiO_2, with higher V_2O_5, Cr_2O_3, and NiO contents with respect to the Fe_2O_3/FeO ratios. Conversely, the phosphorous trend displays higher TiO_2, FeO*, SiO_2, with lower V_2O_5, Cr_2O_3, and NiO contents (Fig. 4.30).

Table 4.6 Compositions of magnetite grains analyzed from the Thunderbird intrusion (FeO*=total iron; S.D.= standard deviation for the population).

Oxide % **Magnetite**	Vanadium trend				Phosphorous trend			
	Maximum	*Minimum*	*Average*	*S.D.*	*Maximum*	*Minimum*	*Average*	*S.D.*
SiO_2	0.139	0.000	0.021	0.019	0.225	0.006	0.041	0.035
TiO_2	1.059	0.023	0.338	0.260	1.270	0.062	0.486	0.294
Al_2O_3	0.236	0.024	0.086	0.033	0.203	0.033	0.097	0.032
V_2O_5	2.463	1.426	1.787	0.246	0.679	0.123	0.418	0.179
Cr_2O_3	0.989	0.161	0.332	0.184	0.336	0.013	0.108	0.082
MgO	0.039	0.000	0.002	0.006	0.036	0.000	0.002	0.006
MnO	0.020	0.000	0.007	0.004	0.018	0.000	0.007	0.005
FeO*	91.848	89.926	90.976	0.431	92.688	90.763	92.045	0.316
CoO	0.024	0.000	0.009	0.006	0.020	0.000	0.007	0.005
NiO	0.030	0.000	0.014	0.006	0.016	0.000	0.004	0.004
CuO	0.013	0.000	0.001	0.002	0.008	0.000	0.000	0.002
ZnO	0.026	0.000	0.006	0.006	0.022	0.000	0.005	0.006
Fe_2O_3	67.360	64.548	66.184	0.516	68.307	65.751	67.259	0.519
FeO	34.240	30.851	31.455	0.298	32.420	31.011	31.525	0.324
Fe_2O_3/FeO	2.158	2.014	2.103	0.031	2.199	2.046	2.134	0.036

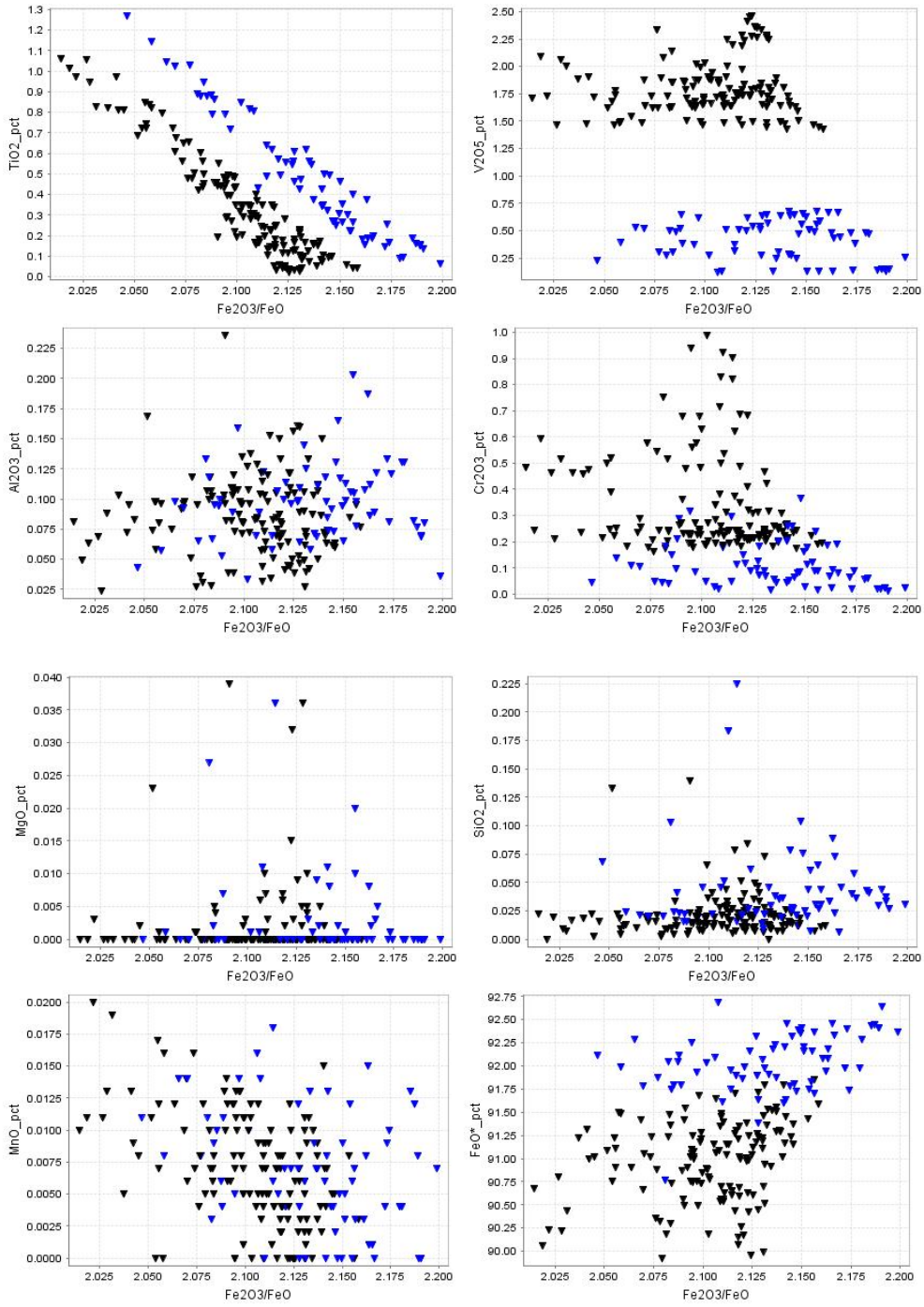

Figure 4.30. Magnetite analysis from the Thunderbird intrusion showing the vanadium- (black) and phosphorous - trends (blue).

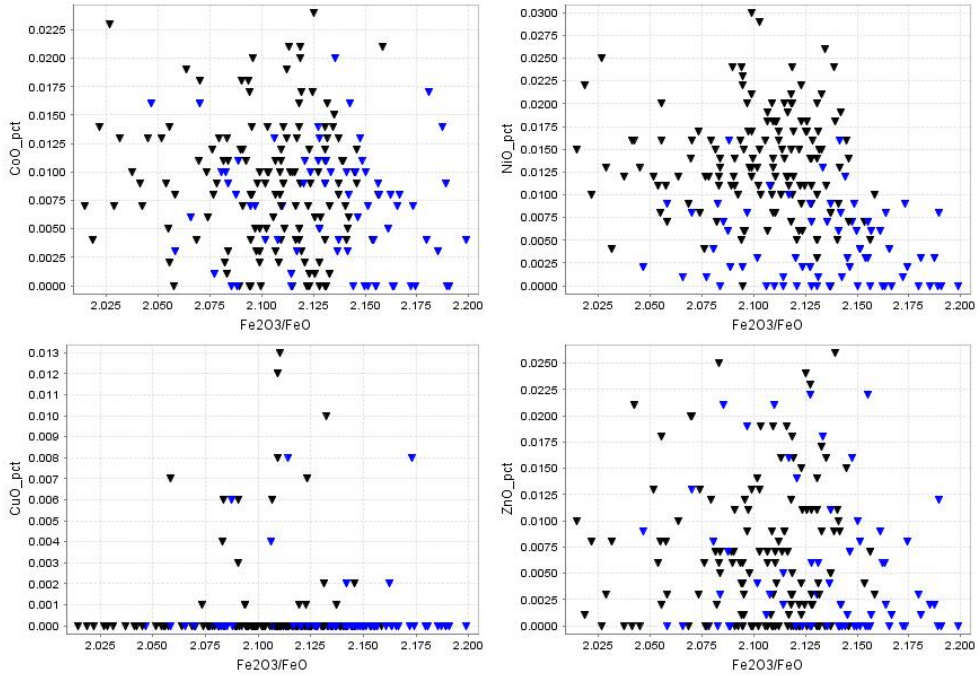

Figure 4.30 (cont.). Magnetite analysis from the Thunderbird intrusion showing the vanadium- (black) and phosphorous -trends (blue).

Ilmenite compositions vary considerably between the vanadium and phosphorous trends in the Thunderbird intrusion. The vanadium trend is characterized by higher V_2O_5, Cr_2O_3, FeO*, Fe_2O_3, CoO and Fe_2O_3/FeO ratios, whereas the phosphorous trend displays higher TiO_2, MgO and FeO (Table 4.7). Both trends display scatter of Al_2O_3, Nb_2O_3, NiO, CuO, and ZnO. The Thunderbird intrusion is characterized by positive trends of V_2O_5, Cr_2O_3 and FeO* along with negative trends of TiO_2 and MnO with increasing Fe_2O_3/ FeO (Fig. 4.31). Similar to the magnetite grains, the V_2O_5 contents display a distinct separation between the vanadium and phosphorous trends as defined by whole rock analysis. Furthermore, the MnO contents are highly elevated within the phosphorous trend, particularly samples with low Fe_2O_3/ FeO ratios (Fig. 4.31). Both trends exhibit scatter of Al_2O_3, MgO, SiO_2, CoO, NiO, CuO, and ZnO (Fig. 4.31).

Table 4.7 Compositions of ilmenite grains analyzed from the Thunderbird intrusion (FeO*=total iron; S.D.= standard deviation of the population).

Oxide % Ilmenite	Vanadium trend				Phosphorous trend			
	Maximum	*Minimum*	*Average*	*S.D.*	*Maximum*	*Minimum*	*Average*	*S.D.*
SiO_2	0.065	0.000	0.009	0.008	0.041	0.000	0.010	0.008
TiO_2	52.292	49.989	50.861	0.400	52.726	50.565	51.689	0.396
Al_2O_3	0.053	0.000	0.012	0.007	0.034	0.000	0.012	0.005
V_2O_5	0.567	0.165	0.351	0.065	0.095	0.000	0.033	0.028
Cr_2O_3	0.097	0.019	0.048	0.014	0.028	0.000	0.008	0.007
Nb_2O_3	0.006	0.000	0.000	0.001	0.006	0.000	0.000	0.001
MgO	0.041	0.000	0.014	0.009	0.069	0.000	0.027	0.018
MnO	1.142	0.790	0.941	0.081	1.961	0.742	1.071	0.325
FeO*	48.168	46.620	47.457	0.337	47.932	45.349	46.821	0.607
CoO	0.030	0.000	0.011	0.007	0.030	0.000	0.006	0.006
NiO	0.010	0.000	0.002	0.002	0.008	0.000	0.001	0.002
CuO	0.016	0.000	0.002	0.004	0.024	0.000	0.001	0.003
ZnO	0.023	0.000	0.009	0.006	0.025	0.000	0.009	0.007
Fe_2O_3	4.246	0.705	2.999	0.625	3.447	0.137	1.628	0.649
FeO	45.986	43.877	44.759	0.365	46.084	44.558	45.355	0.351
Fe_2O_3/FeO	0.096	0.015	0.067	0.014	0.077	0.003	0.036	0.014

Silicate analysis on the Thunderbird intrusion focused on the characterization of the feldspar and to a lesser extent the pyroxene and amphibole compositions (Table 4.5). A total of 42 spot analyses of feldspar from the vanadium trend and 71 from the phosphorous trend have been recalculated to determine the compositions of the anorthite-albite-orthoclase end members (Fig. 4.32).

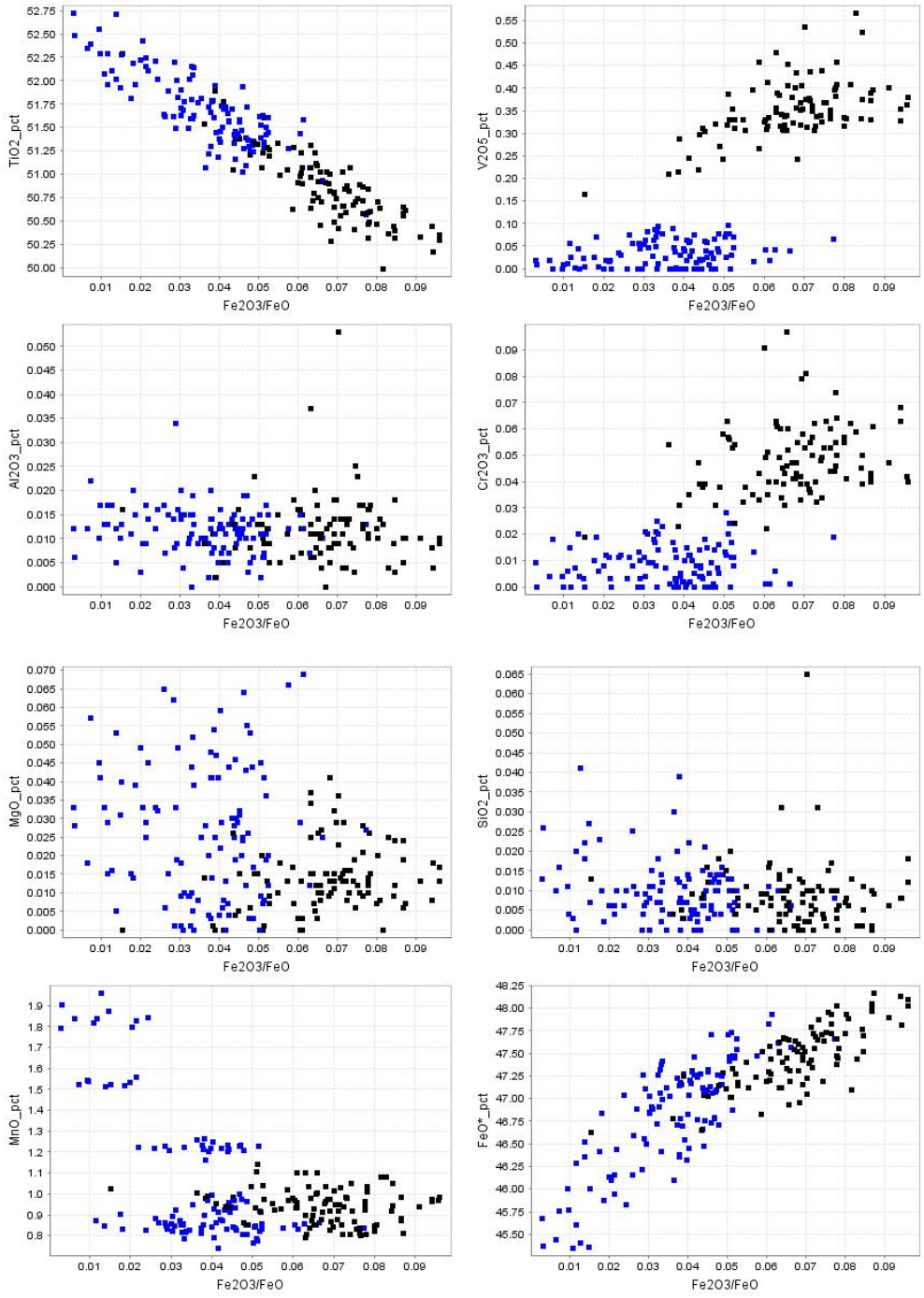

Figure 4.31. Ilmenite analysis from the Thunderbird intrusion showing the vanadium-trend (black) and phosphorous trend (blue).

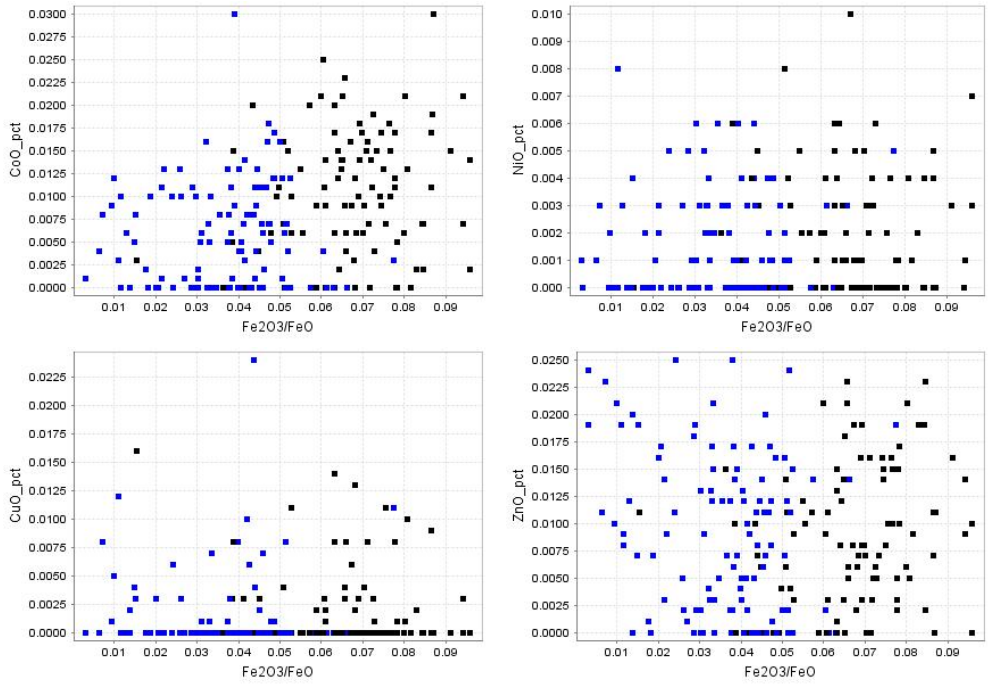

Figure 4.31 (cont.). Ilmenite analysis from the Thunderbird intrusion showing the vanadium-trend (black) and phosphorous trend (blue).

Feldspar from the vanadium trend have been identified as plagioclase feldspar which ranges from 1 to 60 An %. Sample NO-2G22-4 ranges from 3 to 57 % An but generally is restricted to a narrow range of 53-55 An% which coincides with labradorite feldspar. One anomalously low analysis (3% An) was collected from an albite altered of the labradorite, which formed a corona around the primary grain. Sample NO-2G21-2 exhibits high amounts of alteration resulting in the albitization of plagioclase. Only two analyses were conducted on NO-2G21-2 and are nearly pure albite (1 % An). Sample NO-2G21-5 is characterized by labradorite plagioclase and ranges from 53-60 An%.

Plagioclase grains from the phosphorous-trend within the Thunderbird intrusion generally display lower anorthite contents than the vanadium-trend (Fig. 4.32). Sample NO-2G46-3 ranges from 47-51 % An and has been identified as andesine plagioclase. Sample NO-2G47-2 ranges from 47-55 An% but generally is restricted to 48-49 % An (andesine plagioclase). Sample NO-2G47-3 contains andesine plagioclase and ranges from 47-50 % An. Sample NO-

2G47-5 ranges from 45-50 % An but is generally restricted to 46-47 An% which contains the lowest anorthite content of all the plagioclase analyzed.

Pyroxene compositions have been determined for the vanadium (19 analyses) and phosphorous trends (21 analyses) within the Thunderbird intrusion (Fig. 4.33). Due to alteration of the pyroxene grains and the limited number of analysis, compositional zoning was not identified within any of the pyroxene grains.

The vanadium trend is represented by samples from drill core NOT09-2G21. Analysis from sample NO-2G21-2 has been identified as augite with constant Wo proportions (26-28%) but variable En (33-53%) and Fs (19-37%). A single coarse-grained subhedral pyroxene was analyzed from sample NO-2G21-5 and was identified as wollastonite and exhibits no compositional zoning.

Samples from drill core from NOT11-2G46 and NOT11-2G47 of the phosphorous trend. Sample NO-2G46-3 exhibits moderate to high degrees of amphibole alteration and has been characterized by three analyses which range from pigeonite to augite in composition. Sample NO-2G47-2 is composed of augite pyroxene which contains constant Wo proportions (28%) but variable En (27-36%) and Fs (35-44%) proportions. Sample NO-2G47-5 largely falls within the diopside field and exhibits a relatively homogenous composition (Fig. 4.33).

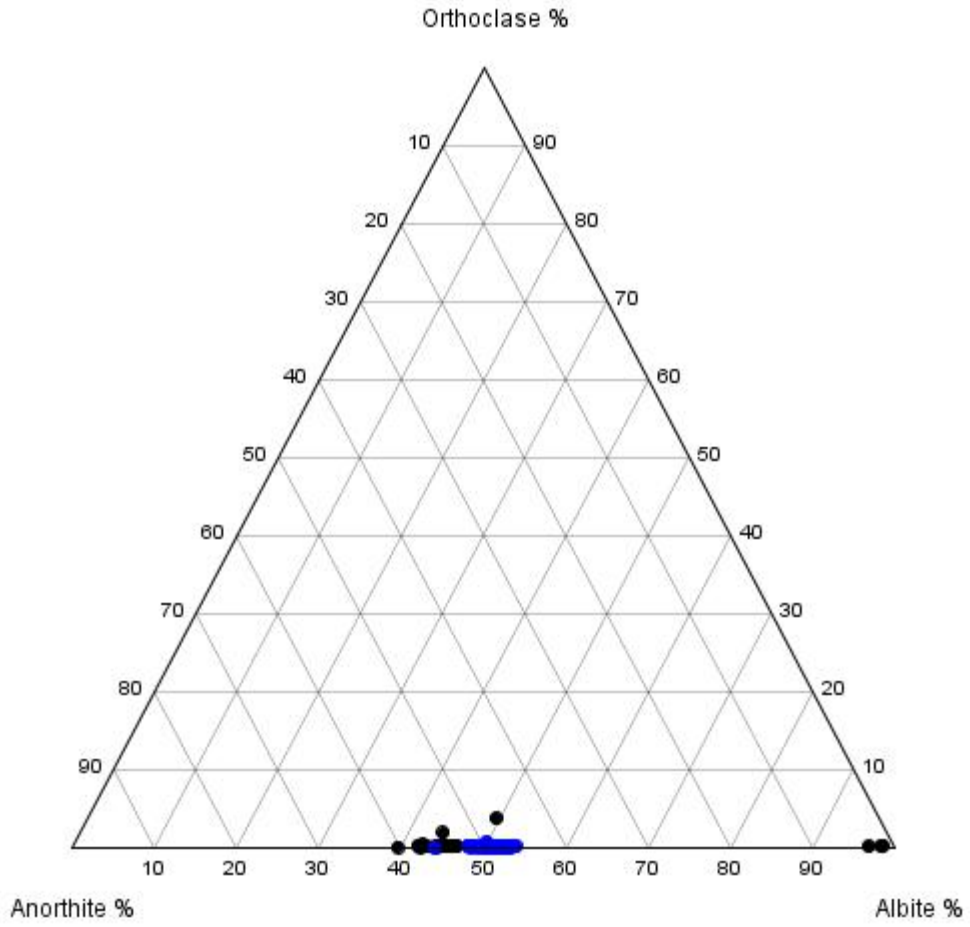

Figure 4.32. Feldspar compositions as determined by EMPA of the vanadium-trend (black) and the phosphorous-trend (blue).

Amphibole analyses within the Thunderbird intrusion examined the vanadium and phosphorous trends to investigate possible compositional differences. A total of 64 analyses were conducted on the Thunderbird intrusion, of which 54 were from the vanadium trend and 10 from the phosphorous trend (Table. 4.5).

The vanadium trend samples were collected from holes NOT-09-2G21and NOT-09-2G22. Sample NO-2G21-1 was composed of abundant amphibole and as a result was examined in detail. This sample was characterized by an assemblage of magnesio-hornblende, actinolite

and ferro-hornblende with lesser ferro-pargasite. Similarly, sample NO-2G22-4 was composed almost entirely of ferro-hornblende with minor ferro-pargasite.

The phosphorous trend was not as extensively analyzed as the vanadium trend and comprised only samples from drill core of holes NOT-11-2G46 and NOT-11-2G47. Sample NO-2G46-3 is dominantly composed of ferro-pargasite with lesser ferro-hornblende. Sample NO-2G47-2 displays a highly variable composition with limited analysis, and is composed of ferro-hornblende, ferro-actinolite, and ferro-hornblende. Similarly, NO-2G47-3 is characterized by highly variable compositions and range from ferro-sadanagaite to ferro-tschermakite.

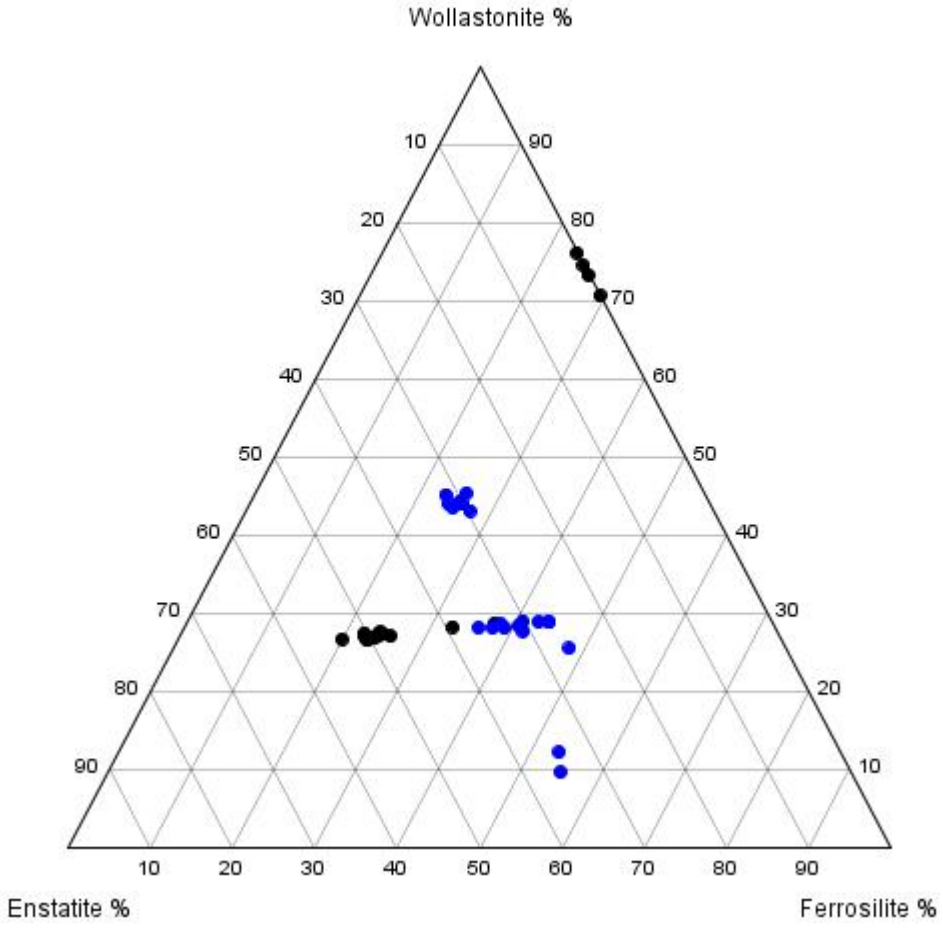

Figure 4.33. Pyroxene compositions as determined by EMPA of the vanadium-trend (black) and the phosphorous-trend (blue).

4.3.2.3. Samarium-Neodymium Isotope Chemistry

Sample selection for Sm-Nd isotope analysis was limited to samples which contained >1 ppm Nd. Five samples were selected based on the concentrations of Nd and were determined through petrography to exhibit lower degrees of alteration (particularly carbonate). The samples were dominantly collected from the phosphorous-trend (drill holes NOT11-2G46, NOT11-2G47) and a single sample from the vanadium-trend (hole NOT09-2G22).The ε_{Nd} values were calculated to an age of 2733.6 Ma based on preliminary geochronology from the Thunderbird intrusion (McNicoll, pers. comm., 2014). ε_{Nd} values range from +0.03 to +1.52 and the initial $^{143}Nd/^{144}Nd$ ratios range from 0.509091 to 0.509167 (Table 4.8). Model ages within the Thunderbird intrusion vary from 3048 to 4831 Ma (Table 4.8).

Table 4.8 Sm-Nd isotopic values from the Thunderbird intrusion.

Sample	$^{143}Nd/^{144}Nd$ current	εNd_{2733}	Model Age (Ma)	$^{143}Nd/^{144}Nd$ initial
NO-2G22-2	0.512788	+0.42	4831	0.509111
NO-2G46-3	0.512119	+0.03	3265	0.509091
NO-2G46-6	0.512003	+0.43	3133	0.509112
NO-2G47-2	0.512273	+1.52	3048	0.509167
NO-2G47-5	0.512004	+0.44	3132	0.509112

5. Discussion

5.1. Stratigraphy, Geochemistry and Petrography of the McFaulds Lake Ferrogabbro Intrusions

5.1.1. Butler Intrusions

The Butler intrusions have been separated into the Butler East and Butler West, as mapped by geophysical data (Fig. 5.1). Based on lithological and spatial associations, it is likely that the intrusions are coeval; however, due to a lack of geochronological data this remains unresolved. The Butler intrusions are characterized by a suite of iron-titanium-rich gabbros and anorthosites termed ferrogabbro. The Butler East intrusion has an approximate strike length of 9km and is ~2km wide. The Butler West intrusion appears to have been folded and is dominated by a north trending limb that is approximately 10km long and 3km wide, and an east-south-east trending limb that is approximately 8km long and 1km wide and thins towards the east. The Butler West intrusion appears to truncate the Butler East along the east portion of the northern limb as interpreted through geophysical mapping (Fig. 5.1). The ferrogabbros are interpreted to have intruded the mafic- to felsic-volcanic rocks of the Butler supracrustal assemblage of the McFaulds Lake greenstone belt (Metsaranta and Houlé, 2012). With the exception of a few outcrops, the Butler East intrusion has only been observed in drill core, and thus the true extent and geometry of the intrusion is solely interpreted through geophysical surveys and drill core.

The Butler intrusions contain highly variable proportions of vanadium-titanium-iron mineralization which occur as stratigraphically conformable layers composed of nearly pure, fine-grained magnetite and ilmenite. These layers have been interpreted to extend for up to 9km in the Butler East, and as much as 18km in the Butler West as based on magnetic

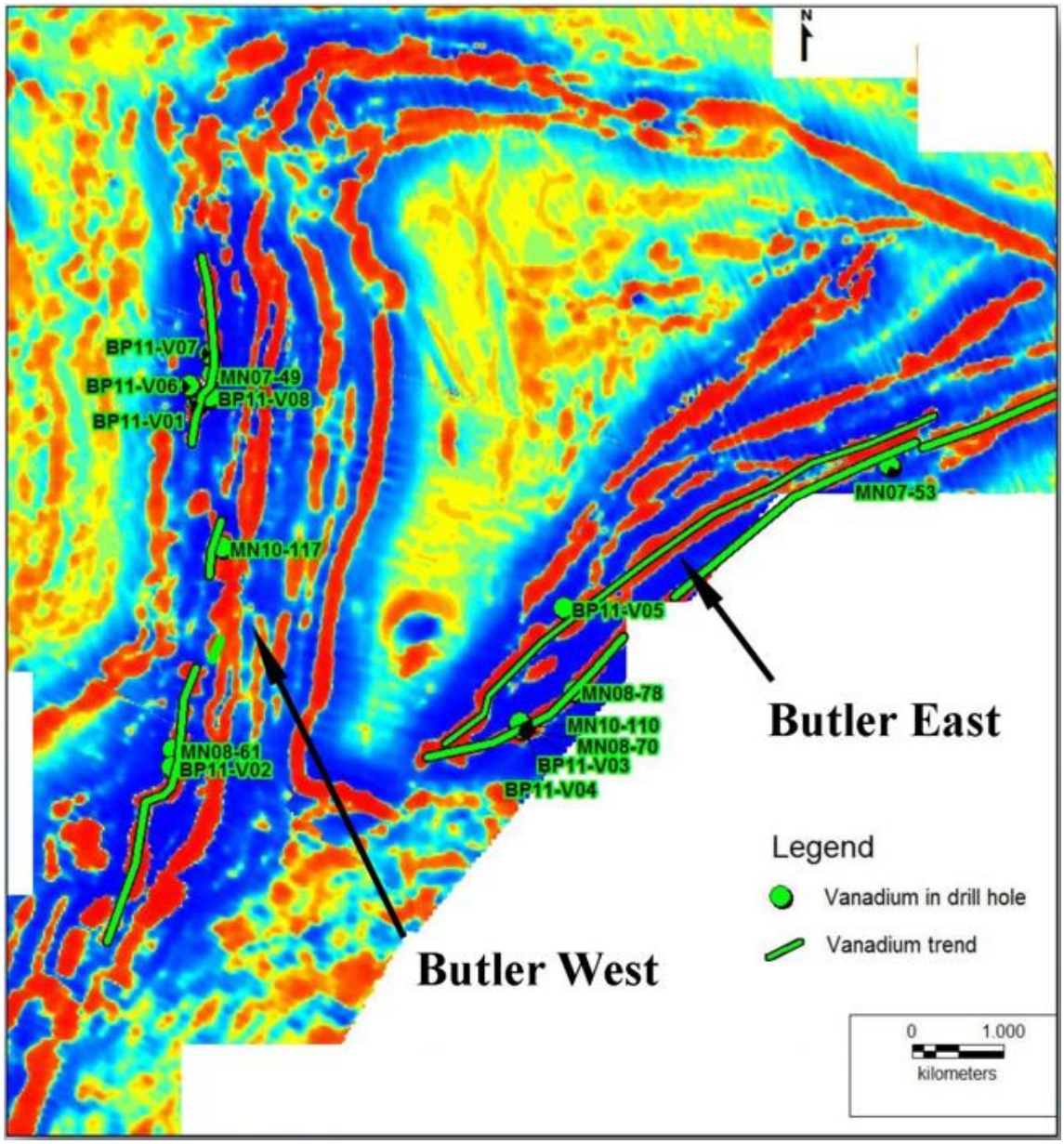

Figure 5.1. First derivative magnetic map of the Butler East and Butler West intrusions. Drill holes which intersected Fe-Ti-V mineralization have been highlighted and labeled along with inferred vanadium trends (courtesy of MacDonald Mines Exploration Limited).

anomalies (Fig. 5.1). The main magnetite-ilmenite mineralization occurs within the basal members of the repetitive oxide-silicate layers which vary from centimeter to meter scale cycles characterized by pure oxides (magnetite and ilmenite) with sharp lower contacts that grade upward into semi-massive oxide pyroxenites, followed by net textured or disseminated gabbro. Near the top of each cycle, the rocks are generally composed of oxide-bearing anorthosites. These cycles may occur as complete or partial packages (Fig. 5.2). Hole BP11-V04 displays many of the typical characteristics of the Butler East intrusion. Massive magnetite-ilmenite horizons (>80% oxide) exhibit sharp contacts with the overlying oxide-bearing anorthosite. These units grade into a semi-massive oxide gabbro, to an oxide-rich gabbro, and lastly into an interlayered oxide anorthosite to oxide-bearing leucogabbro. This gradual transition from massive magnetite-ilmenite to disseminated magnetite-ilmenite can be observed geochemically through the decreasing Fe_2O_3(t), TiO_2, and V_2O_5 contents (Fig. 5.2). Throughout the oxide-rich and oxide-poor cycles, the TiO_2/V_2O_5 ratio steadily increases regardless of silicate mineralogy and/or the total amount of magnetite-ilmenite present (Fig. 5.2). The increase in TiO_2/V_2O_5 ratio is expected within an evolving ferrogabbroic system (see chapter 5.3) and thus, drill core from BP11-V04 is interpreted to young down hole (i.e., towards the south-south-east).

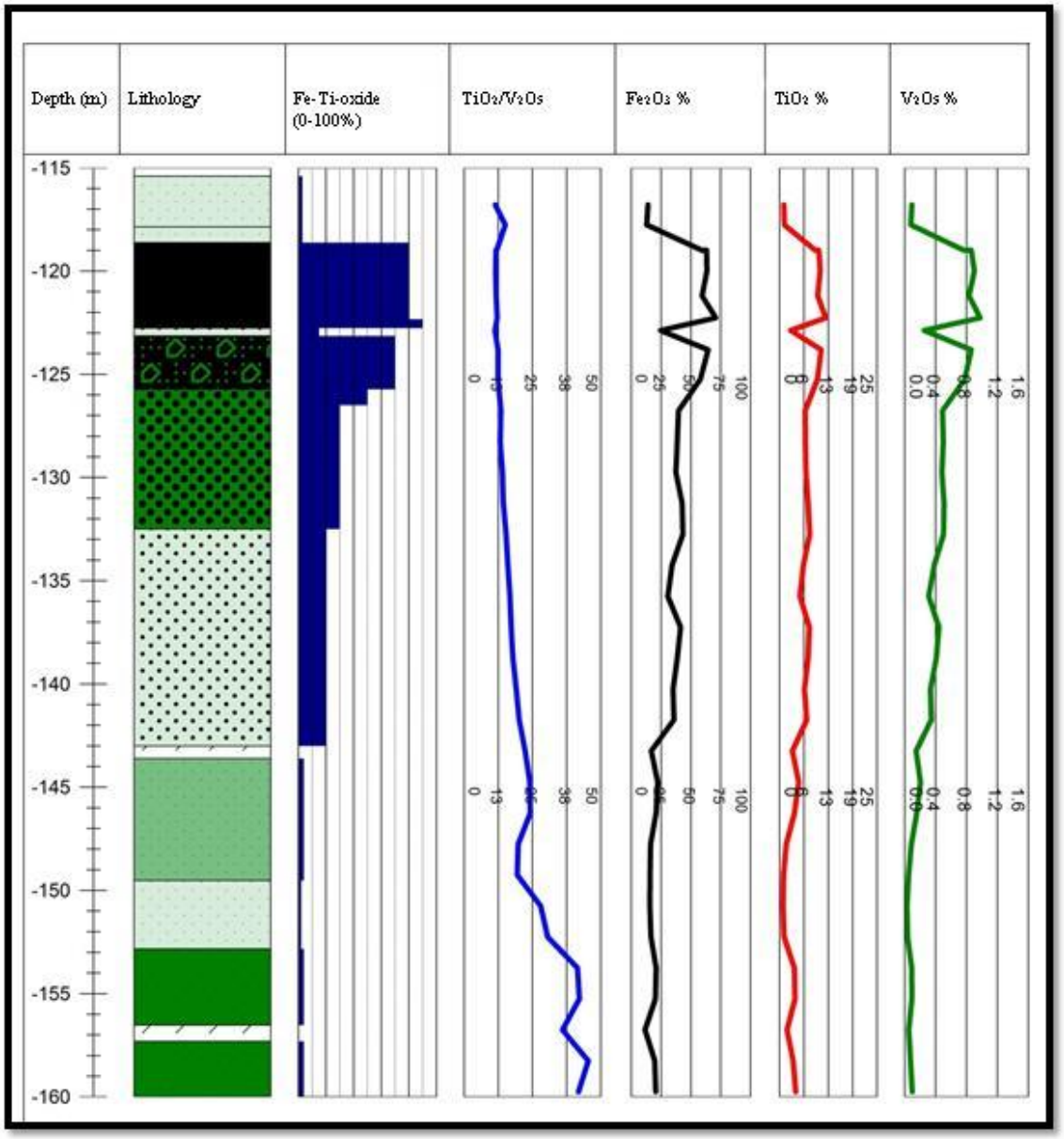

Figure 5.2. Core log excerpt from drill hole BP11-V04 of the Butler East intrusion displaying decreasing Fe_2O_3, TiO_2, V_2O_5 wt. %, and magnetite-ilmenite contents down hole, with increasing TiO_2/V_2O_5 values which is typical of oxide-rich cycles and interpreted to young down hole (115 to 160 m depth). Lithology legend available in Appendix B.

Throughout individual drill holes, very limited textural variation is observed within the oxide minerals (Figs. 5.3, 5.4). Furthermore, the silicate minerals have largely been replaced by secondary minerals and primary textures are difficult to identify. However, oxide minerals

appear to be relatively unaltered and consequently are the most suitable phases to model magmatic evolution. Throughout the Butler intrusion it is observed that the ratio of ilmenite to magnetite generally increases up stratigraphy, in addition textural variations within ilmenite grains have been observed (e.g., trellis, granular). The increase of ilmenite: magnetite ratio has also been observed in experimental work on rocks believed to represent the primary Skaergaard intrusion magma, and is consistent with an evolving ferrogabbroic system (Toplis and Carrol, 1996). Within the basal massive and semi-massive oxide units of the layered cycle of the Butler intrusions, the ilmenite occurs as discrete anhedral fine- to medium-grained crystals which commonly exhibit very fine (1-3µm) hematite exsolution lamellae, and as subhedral to tabular fine-grained crystals which occur within or bordering magnetite grains. The ilmenite grains which exhibit hematite exsolution lamellae are interpreted to have formed through the primary crystallization of the Butler intrusions as the lamellae suggest an original ilmenite-hematite solid solution which has undergone sub-solidus oxy-exsolution (Haggerty, 1976). The ilmenite grains which occur as fine-grained subhedral to tabular crystals are termed granular/composite textured (e.g., Buddington and Lindsley, 1964; Haggerty, 1976). This composite textured ilmenite could have formed through either primary crystallization, or through moderate to high degrees of oxidation from a primary titanomagnetite grain (Haggerty, 1976). Within these massive and semi-massive oxide units, magnetite grains typically contain no trellis textured ilmenite lamellae, and have been determined by microprobe analysis to be nearly pure end-member magnetite. It is suggested that the textures observed within the massive and semi-massive oxide units are largely controlled by sub-solidous reactions, with only minor primary oxide textures preserved (e.g., hematite lamellae within ilmenite). As the system evolves towards the oxide- and oxide-bearing units, the

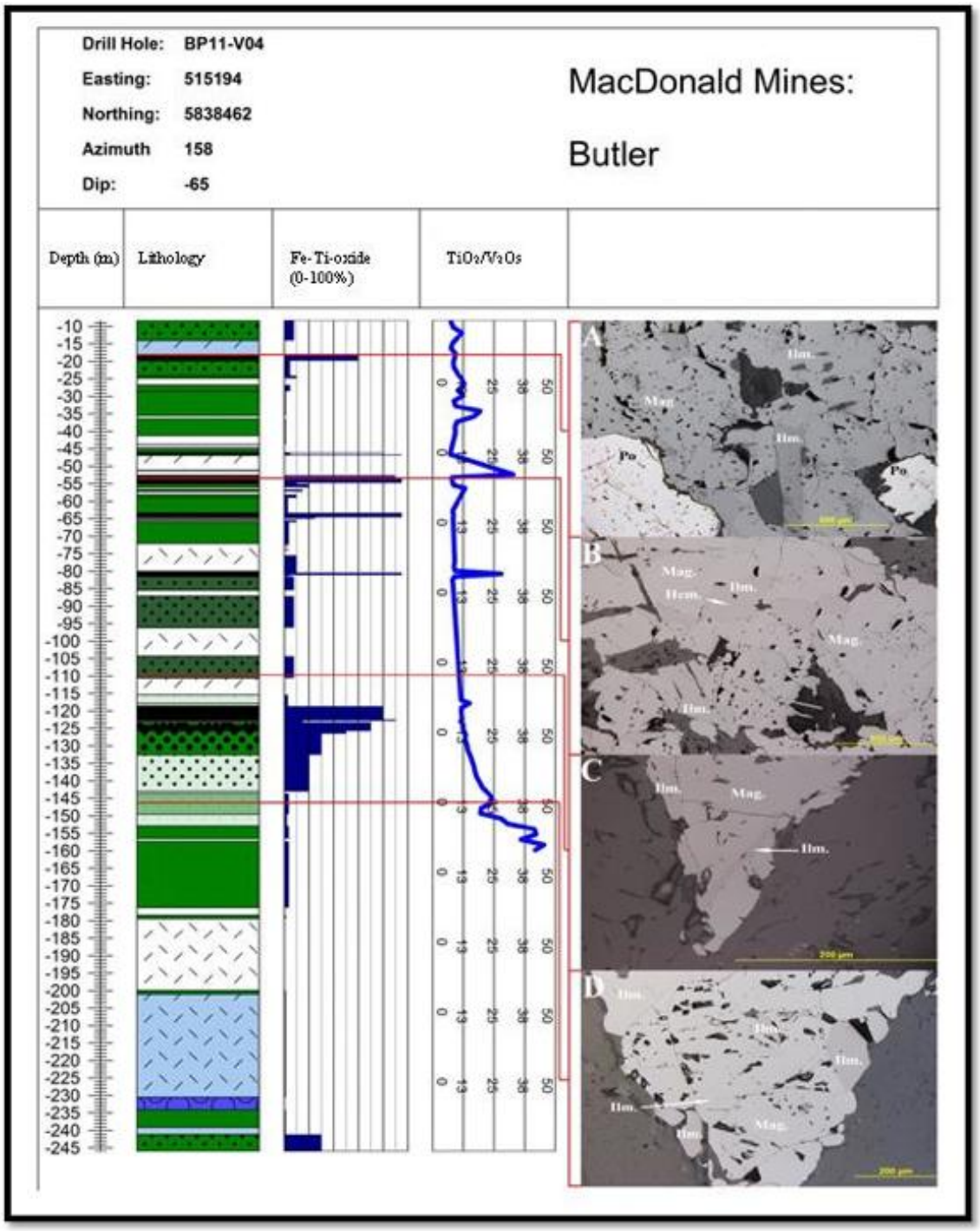

Figure 5.3. Core log from hole BP11-V04 of the Butler East intrusion displaying lithology, estimated Fe-Ti oxide %, down hole TiO_2/V_2O_5 ratios and reflected light images of the Fe-Ti-oxides (A=MM-V4-1; B=MM-V4-2; C=MM-V4-5; D=MM-V4-6). The drill core displays increasing TiO_2/V_2O_5 values and ilmenite: magnetite ratios down hole, suggesting the intrusion youngs down hole. Lithology scale available in Appendix B.

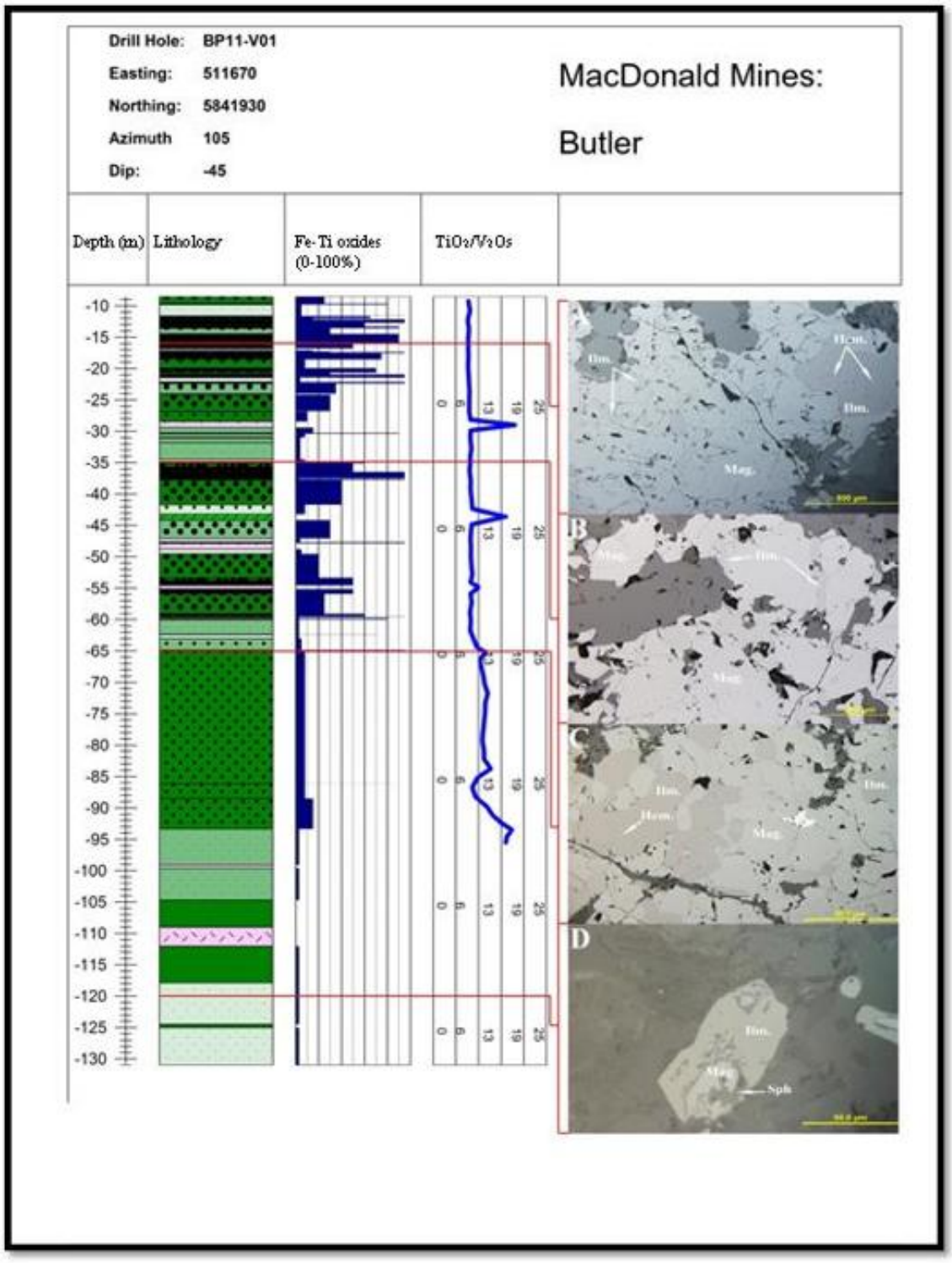

Figure 5.4. Core log from hole BP11-V01 of the Butler West intrusion displaying lithology, estimated Fe-Ti oxide %, down hole TiO_2/V_2O_5 ratios and reflected light images of the Fe-Ti-oxides (A=MM-V1-2; B=MM-V1-3; C=MM-V1-5; D=MM-V1-6). The drill core displays increasing TiO_2/V_2O_5 values and ilmenite: magnetite ratios down hole, suggesting the intrusion youngs down hole. Lithology scale available in Appendix B.

presence of trellis-textured ilmenite lamellae within magnetite becomes more prevalent at the expense of granule/composite ilmenite (Fig. 5.3). This may be caused by variable degrees of oxy-exsolution, or by our poor understanding of the nature of granule/composite textured ilmenite which may actually represent primary fine-grained euhedral ilmenite precipitates (Haggerty, 1976). Additionally, the ilmenite:magnetite ratio of the intrusions increases and the width of the ilmenite lamellae gradationally decreases during the evolution of the magma (Fig. 5.4). The variable widths of the ilmenite lamellae within magnetite are more likely a result of the degree of oxidation than primary conditions as a system progressivly evolves from fine-grained ilmenite lamellae to coarse-grained lamellae and lastly as composite ilmenite as oxidation proceeds (Haggerty, 1976). It is suggested that the increasing ilmenite:magnetite ratios from BP11-V04 from the Butler East (Fig. 5.3) and BP11-V01 from the Butler West (Fig. 5.4) may be useful tools in the determination of stratigraphy. Both drill holes display textural evidence in drill core (i.e., sharp lower contacts of massive-oxide grading into oxide-rich gabbro), mineralogy (increasing ilmenite:magnetite ratio), and geochemistry (increasing TiO_2/V_2O_5 ratios) which suggests the intrusion youngs down hole.

Eales and Cawthorn (1996) reported that vanadium contents within the massive and semi-massive oxide units decrease significantly over short stratigraphic intervals within the Upper Zone of the Bushveld complex, possibly reflecting stratigraphic variations within evolving magmas. In the Butler East intrusion this phenomenon is exemplified in samples MM-V5-1 (85.5 m) and MM-V5-2 (86.27 m) which were collected 77 centimeters apart from each other. Sample MM-V5-1 represents the basal massive oxide unit which exhibits a sharp lower contact and is characterized by increasing plagioclase contents downhole (Fig. 5.5). The increase in plagioclase content represents material which is less dense in the magmatic system and therefore it is suggested that the dense magnetite-ilmenite may have

crystallized/concentrated lower in the stratigraphy (e.g., Zhou et al., 2005b). Sample MM-V5-2 is a down hole continuation of MM-V5-1 and is a semi-massive oxide anorthosite. Microprobe analysis of the magnetite grains from the two samples show lower contents of compatible elements within sample MM-V5-2 (Fig. 5.6). This observation is consistent with the sharp lower contact observed within MM-V5-1 and the gradation from massive oxide to semi-massive oxide anorthosite in MM-V5-2. This trend is not unique within the Butler intrusions, and downhole variations within compatible elements are also seen in the Butler West intrusion (e.g., BP11-V01; Fig. 5.7). Within the drill core from BP11-V01 (Butler West) magnetite grains analyzed from six samples display a steady decrease in the TiO_2 and Cr_2O_3 contents and a general decrease in V_2O_5 down hole. Variations of V_2O_5 may be caused by fluctuations in oxygen fugacity as this will affect the compatibility of V within magnetite (Toplis and Corgne, 2002). However, down hole depletions in Cr which is highly compatible within magnetite will not be affected by oxygen fugacity due to the divalent nature of chromium (Toplis and Corgne, 2002). The decrease in Cr contents of the magnetite suggests a down hole younging direction, whereas variations in V contents may be affected by oxygen fugacity (Mallmann and O'Neil, 2009). Magnetite and ilmenite grains display weak compositional zoning within individual grains. Both magnetite and ilmenite are generally characterized by higher Al_2O_3, V_2O_3 and Cr_2O_3 contents within the cores and lower contents along the margins of the grains (Fig. 5.8). TiO_2 contents within magnetite are highly variable throughout the Butler intrusions and are anomalously high within magnetite grains which are in contact with ilmenite, possibly reflecting a diffusional process during metamorphism of the Butler East intrusion (Fig. 5.8; Oliver, 1978). Based on the geochemical signatures within oxide minerals (decreasing compatible elements) and textural characteristics (decreasing plagioclase contents) observed within samples MM-V5-1 and MM-V5-2, the younging direction is interpreted to be down hole

(towards the south east). Similarly, based on decreasing TiO_2, Cr_2O_3 and V_2O_5 contents of the magnetite, drill hole BP11-V01 (from the Butler East intrusion) is interpreted to young downhole (towards the east).

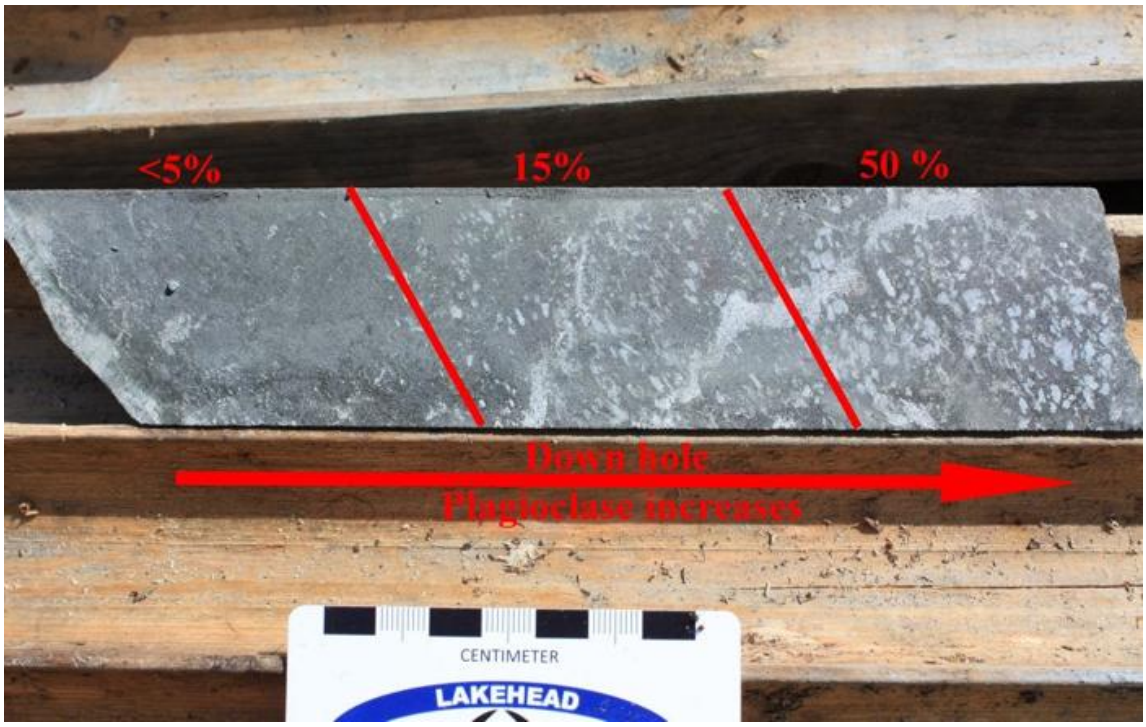

Figure 5.5 Sample MM-V5-1 displaying the approximate proportions of plagioclase within the massive to semi-massive oxide anorthosite. Depth and plagioclase modal % increases to the right and the unit is interpreted to young to the right (i.e., downhole).

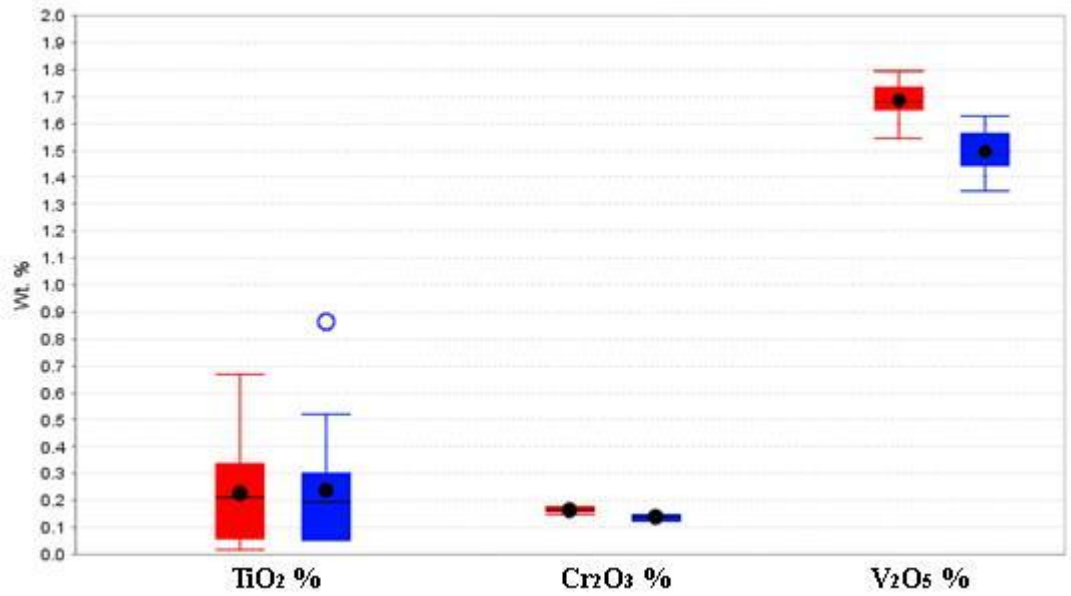

Figure 5.6. Box and whisker plot from magnetite grains analyzed by EMP. Data were collected from samples MM-V5-1 (Red) and MM-V5-2 (Blue) from the Butler East intrusion. Sample MM-V5-2 displays lower values of TiO_2, Cr_2O_3 and V_2O_5 which is interpreted to be more evolved. Black lines represent median values, filled box represents interquartile range, Whiskers represent data within the upper quartile range, open circle represents outliers in the 95th percentile.

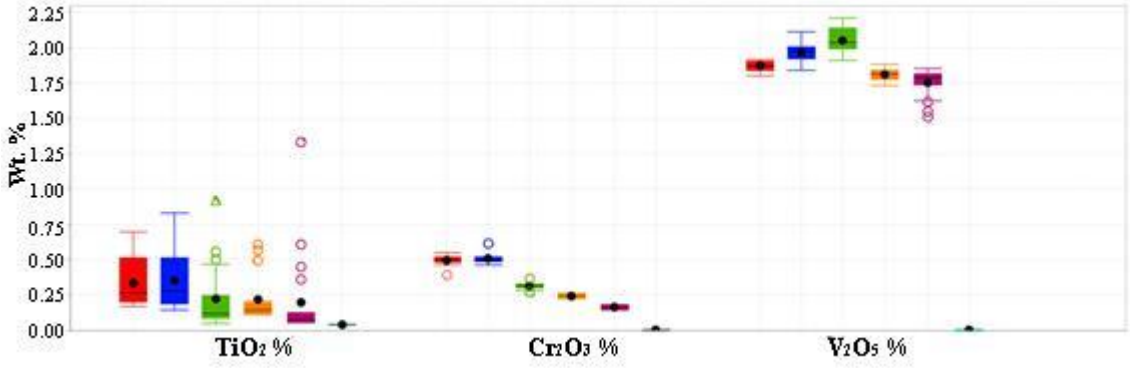

Figure 5.7. Box and whisker plot from magnetite grains analyzed by EMP. Data was collected from samples MM-V1-1 (Red), MM-V1-2 (Blue), MM-V1-3 (Green), MM-V1-4 (Orange), MM-V1-5 (Purple), and MM-V1-6 (Cyan) from the Butler West intrusion. Black lines represent median values, filled box represents interquartile range, Whiskers represent data within the upper quartile range, open circle represents outliers in the 95th percentile and triangles represent data within the 98th percentile.

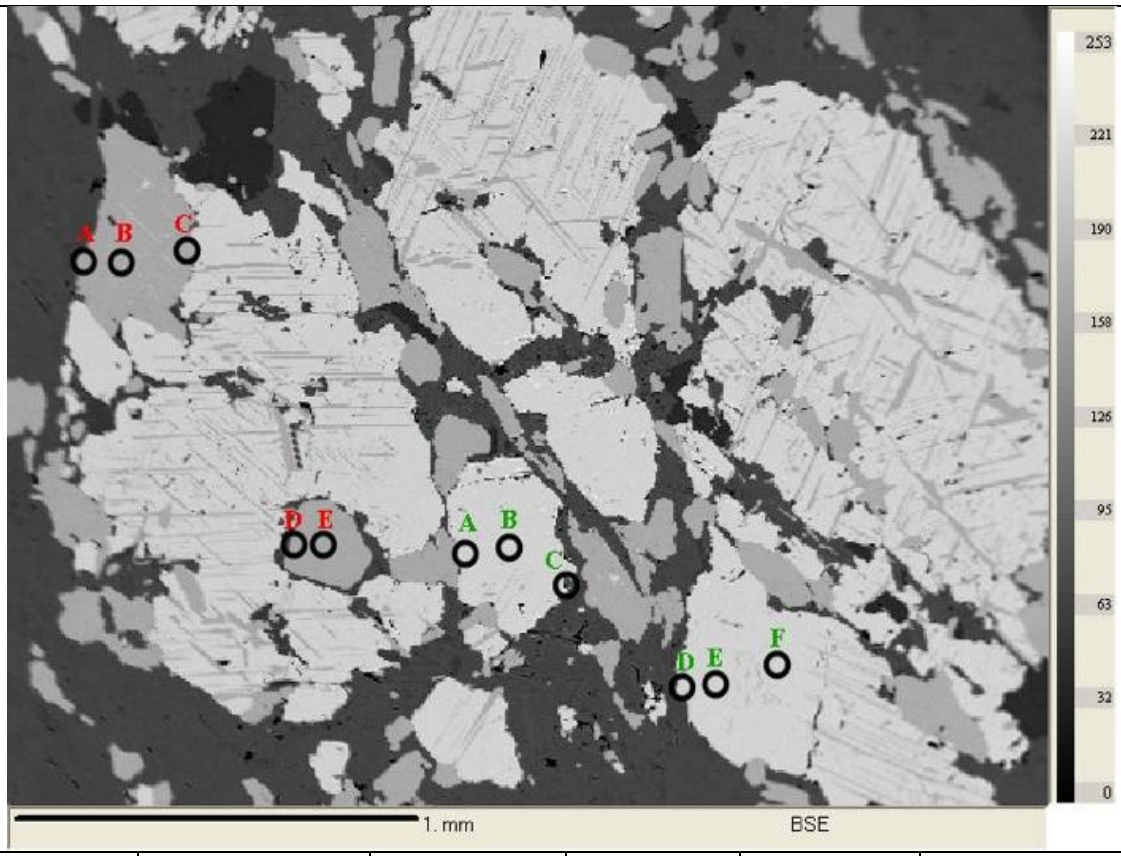

Analysis	Mineral	TiO_2	V_2O_5	Cr_2O_3	Al_2O_3
A	Ilmenite	50.959	0.245	0.015	0.008
B	Ilmenite	50.952	0.324	0.033	0.016
C	Ilmenite	51.027	0.336	0.030	0.014
D	Ilmenite	51.088	0.292	0.021	0.015
E	Ilmenite	51.148	0.348	0.031	0.012
A	Magnetite	0.325	1.721	0.170	0.051
B	Magnetite	0.018	1.773	0.166	0.070
C	Magnetite	0.087	1.640	0.164	0.051
D	Magnetite	0.043	1.667	0.147	0.066
E	Magnetite	0.022	1.783	0.167	0.073
F	Magnetite	0.061	1.783	0.172	0.112

Figure 5.8. Backscattered electron (BSE) image from sample MM-V5-1 with select analysis locations and values (Red = ilmenite analysis, green = magnetite analysis).

The Butler East intrusion is unique among the McFaulds Lake ferrogabbroic intrusions as it is cross cut by a peridotite dyke/sill which has a core length of 14.3 meters. The ultramafic intrusion is a dark green, massive, fine-grained rock which has undergone intense serpentine and chlorite alteration. The dyke/sill intruded along the basal contact of a massive oxide unit

and has caused local brecciation of the Butler East intrusion (Fig. 4.3F) and is therefore interpreted to have been intruded after the crystallization of the Butler East intrusion. The cross-cutting nature of the peridotite has implications for the sequence of events within the Butler intrusions and possibly within McFaulds Lake greenstone belt. It has been suggested that the ferrogabbroic suites represent an evolved end member of the voluminous ultramafic intrusions (e.g., Black Thor), and thus formed after or during the emplacement of the ultramafic units (Mungall et al., 2010).

The peridotite dyke contains abundant partially digested massive-oxide breccia which imparted a magnetic feature to the unit (Fig. 4.3F). The oxide minerals within the breccia were analyzed by microprobe and are characterized by highly elevated and variable chromium contents relative to the Butler intrusions (1.5-3.9 Cr_2O_3 wt. %). The oxides are characterized by very fine-grained disseminated to banded textures which may have formed due in part to the pervasive serpentinization of the olivine to produce magnetite as a by-product. The incorporated magnetite within the peridotite intrusion may have undergone an exchange with the chromium in the magma and variably replaced iron for chromium. This would be analogous to the tentative model for chromium mineralization within the Black Thor intrusion whereby Cr-rich ultramafic magma may have been contaminated by magnetite from the country rocks and undergone a magnetite-chromite$_{ss}$ exchange (Pers. Comm. Carson, 2014). The variable chromium contents within the magnetite analyzed within the peridotite may be a function of variable degrees of interaction between the magnetite and the magma.

Magnetite-ilmenite mineral pairs which have co-precipitated were analyzed to investigate the temperatures and oxygen fugacity at the time of crystallization (Table 5.1). The conditions during formation have been calculated using an adaption of the Spencer and

Lindsley (1981) and Stormer (1983) geothermometers and oxygen fugacity calculations as described in Chapter 3.2. Small variations of temperature and oxygen fugacity (Fig. 5.9) along with similar mole % ulvöspinel and ilmenite compositions within the Butler East intrusion have been calculated (Table 5.1). In contrast, the Butler West intrusion is characterized by two broad populations i) a group of values nearly identical to those of the Butler East, and ii) a low temperature, low oxygen fugacity suite which displays considerable scatter (Fig. 5.9). The group of tightly clustered values similar to those calculated for the Butler East is suggested to be more representative of the Butler West intrusion, whereas the low temperature low oxygen fugacity samples correspond to higher degrees of alteration within the sample. Temperatures calculated for the Butler intrusions are far too low for the crystallization of a gabbroic magma and are suggested to represent the temperature of oxy-exsolution, rather than crystallization. This is supported by work done on metamorphic and plutonic rocks whereby the oxy-barometer and geo-thermometer may be reset so that the calculated temperatures and oxygen fugacity reflect the conditions during exsolution, not crystallization (Haggerty, 1976; Oliver, 1978; Stormer, 1983).

Table 5.1. Average calculated values from magnetite-ilmenite pairs for the Butler Intrusions (Usp=ulvöspinel, Ilm=ilmenite).

Sample	Intrusion	Mole % Usp	Mole % Ilm	Temperature (^{o}C)	Oxygen Fugacity
MM-V5-1	Butler East	0.70	97.50	462	-25.73
MM-V5-2	Butler East	0.73	97.78	455	-26.49
MM-V5-3	Butler East	0.83	97.47	469	-25.53
MM-V1-1	Butler West	1.06	98.91	421	-30.94
MM-V1-2	Butler West	1.12	98.58	439	-29.12
MM-V1-3	Butler West	0.71	97.26	458	-25.41
MM-V1-4	Butler West	0.68	97.51	461	-25.78
MM-V1-5	Butler West	0.63	97.07	470	-24.79
MM-V1-6	Butler West	0.12	97.94	397	-28.41
MM-V8-2	Butler West	0.73	97.56	462	-25.85
MM-V8-3	Butler West	1.00	97.42	476	-25.27
MM-V8-4	Butler West	0.74	97.37	468	-25.35
MM-117-2	Butler West	0.68	97.54	460	-25.87

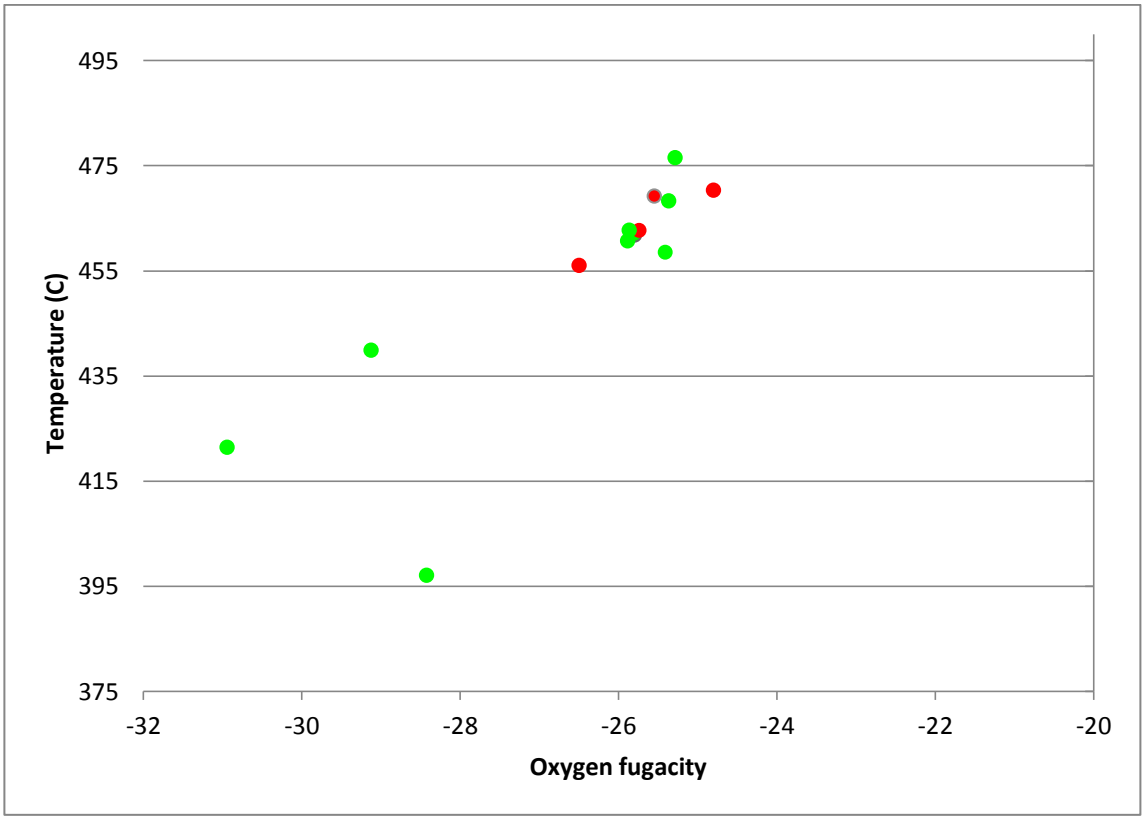

Figure 5.9. Temperature and oxygen fugacity values calculated for the Butler East (Red) and Butler West (Green) intrusions based on EMPA data from co-precipitated magnetite-ilmenite pairs.

Plagioclase compositions within the Butler East intrusion have been determined for three samples (MM-71B-2, MM-70-2 and MM-V4-7). The plagioclase display trends of decreasing anorthite % with decreasing whole rock Zr and TiO_2/V_2O_5, (Fig. 5.10). These trends are consistent with the evolution of gabbroic magmas (e.g., Bushveld intrusion) whereby incompatible elements (e.g., Zr) increase as the plagioclase evolves towards the albite end member (Eales and Cawthorn, 1996). This interpretation is supported by an increase in TiO_2/V_2O_5 values which are suggested in this work to increase during evolution. Sample MM-70-2 is characterized by bytownite (An% 70-90)-labradorite (An% 50-70) and represents the most primitive plagioclase within the Butler East intrusion (Fig. 5.10). Sample MM-71B-2

characterized by labradorite-andesine (An% 30-50) represents the most evolved plagioclase analyzed with MM-V4-7 being intermediate. It should be noted however, that large variations within individual samples have been calculated which likely represent variable degrees of albitization. However, the broad trends observed with anorthite contents and whole rock geochemistry (Zr, TiO_2/V_2O_5) support the interpretation that MM-70-2 represents the most primitive plagioclase, followed by MM-V4-7 and MM-71B-2 being the most evolved.

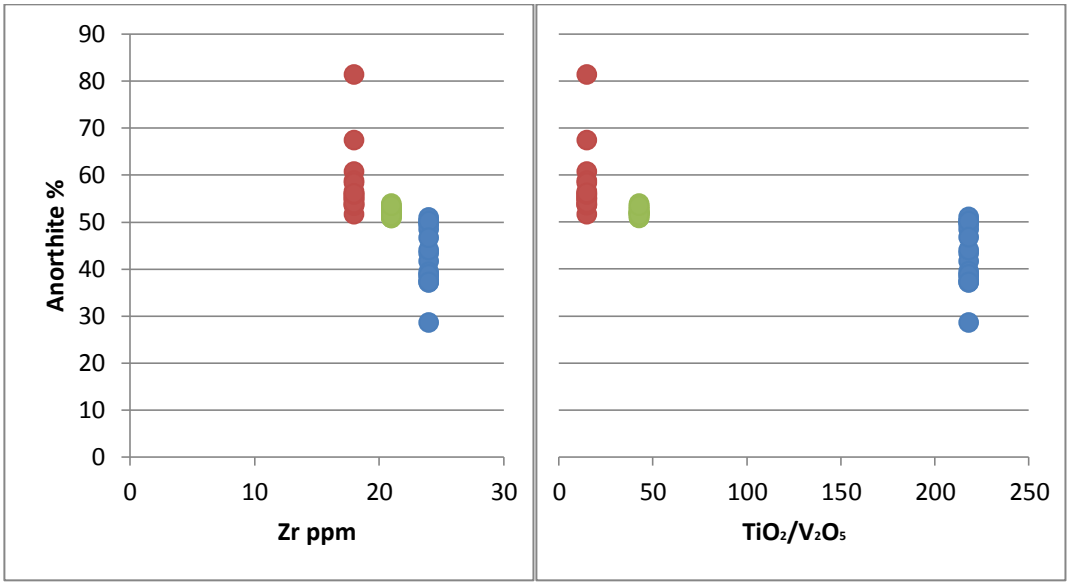

Figure 5.10. Zr (ppm) and TiO_2/V_2O_5 values from whole rock data against anorthite % of plagioclase from the Butler East intrusion (Red: MM-70-2, Green: MM-V4-7, Blue: MM-71B-2). Lower An% of plagioclase corresponds to lower Zr and TiO_2/V_2O_5 values in whole rock interpreted to represent relatively primitive samples.

Plagioclase compositions within the Butler West intrusion display similar trends to those observed within the Butler East intrusion. Trends of increasing Zr (ppm) and TiO_2/V_2O_5 values with decreasing anorthite % of plagioclase are observed which are interpreted to reflect fractionation (Fig. 5.11). Sample MM-117-6 appears not to follow the general trends observed throughout the Butler intrusions. However, sample MM-117-6 was collected 170.28 meters down hole from MM-117-1 (drill hole MM10-117) and displays decreasing Zr, TiO_2/V_2O_5 and lower An% values downhole. Sample MM-117-6 displays higher values of Zr, TiO_2/V_2O_5, and

more albitic plagioclase compared to MM-117-1 and is thus interpreted to represent a more evolved plagioclase and may be a useful tool in determinations of stratigraphy of drill hole MM10-117. This is particularly significant as geochemical data from MM10-117 is poor due to limited sampling. Assuming that the more evolved plagioclase of MM-117-6 is representative of a more evolved magma, the drill hole is interpreted to young downhole (towards the east), which is consistent with the younging direction of the Butler West intrusion.

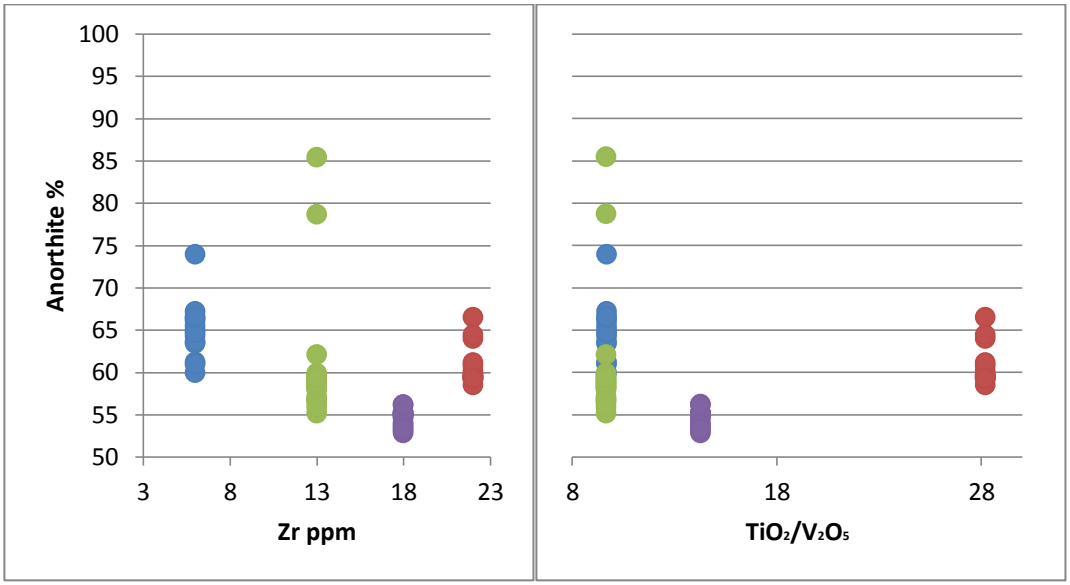

Figure 5.11. Zr (ppm) and TiO_2/V_2O_5 values from whole rock data against anorthite % of plagioclase from the Butler West intrusion (Blue: MM-117-1, Green: MM-V1-2, Purple: MM-V8-1, Red: MM-117-6). Lower An% of plagioclase corresponds to lower Zr and TiO_2/V_2O_5 values in whole rock interpreted to represent relatively primitive samples.

Microprobe analysis of pyroxene grains are very limited within the Butler intrusions, however, with the incomplete data available broad interpretations may be possible. Pyroxene grains analyzed in samples MM-V4-1 and MM-V4-7 from the Butler East have been identified as clinoenstatite and augite (respectively). Sample MM-V4-7 was collected 141.5 meters down hole from MM-V4-1 and exemplifies the evolution of orthopyroxene (clinoenstatite) to clinopyroxene (augite). The transition from orthopyroxene to clinopyroxene is a well-

documented phenomenon in evolving mafic-ultramafic systems such as the Skaergaard, Stillwater and Bushveld Intrusions (Raedeke and McCallum, 1984; McBirney, 1996; Eales and Cawthorn, 1996). The orthopyroxene-bearing upper portion of the drill hole and the clinopyroxene-bearing lower portion is consistent with increased TiO_2/V_2O_5 ratios, and textural evidence observed in drill core (i.e., increasing plagioclase contents down hole, sharp lower contacts of magnetite-ilmenite rich horizons, etc.). Consequently it is proposed that drill hole BP11-V04 youngs down hole (i.e., towards the south-east). Pyroxene grains from the Butler West intrusion are characterized by samples MM-117-1, MM-117-6 and MM-V8-1 and have been identified as augite, clinoenstatite/ferrosilite, and augite (respectively). Sample MM-117-6 (orthopyroxene) has been interpreted to be stratigraphically higher than MM-117-1 (augite), based on plagioclase compositions and textural variations observed within drill core. This trend of orthopyroxene after augite is not consistent with the earlier interpretation in drill hole BP11-V04 from the Butler East intrusion. However, MgO % within pyroxene grains of MM-117-1 (12-13%) and MM-117-6 (15%) are very similar but the CaO varies significantly (7-12% and 1% in MM-117-1 and MM-117-6 respectively). Similar trends of alternating clinopyroxene and orthopyroxene layers have been observed within the Sept Isle layered intrusion where orthopyroxene occurs within all members of the intrusion (Namur et al., 2010). It is then possible that within the Butler intrusions, orthopyroxene and clinopyroxene may occur throughout the intrusion, and due to sparse sampling and intense alteration, the primary pyroxene compositions may not be accurately represented.

Five samples from the Butler East and Butler West intrusions were analyzed for Sm-Nd isotopes. Large variations within ε_{Nd} and model ages are present within both intrusions, and although the Sm-Nd system is generally thought to be robust (Dickin, 2005), obvious discrepancies exist within the data. Both intrusions are characterized by a dominantly positive

ε_{Nd} which suggests a mantle derived magma (DePaolo and Wasserburg, 1976). Model ages are highly variable, ranging from 1896 to 10187 Ma (Fig. 5.12). These values are clearly incorrect as the U-Pb age of the ferrogabbro suite is circa 2735 Ma (Mungall et al., 2010), and the Thunderbird intrusion which is suggested to be contemporaneous and has been dated at 2733.6 Ma (Pers. Comm., McNicoll 2014). It is suggested that pervasive metamorphism and local alterations (possibly related to VMS hydrothermal systems within the Butler supracrustal assemblage: Metsaranta and Houlé, 2012) may have distrupted the Sm-Nd isotopic system providing some scatter within the values. However, the Butler intrusions are characterized dominantly by a mantle ε_{Nd} signature which overlaps with the depleted mantle ε_{Nd} value of approximatly +4 (calculated using methods decribed by DePaolo, 1981).

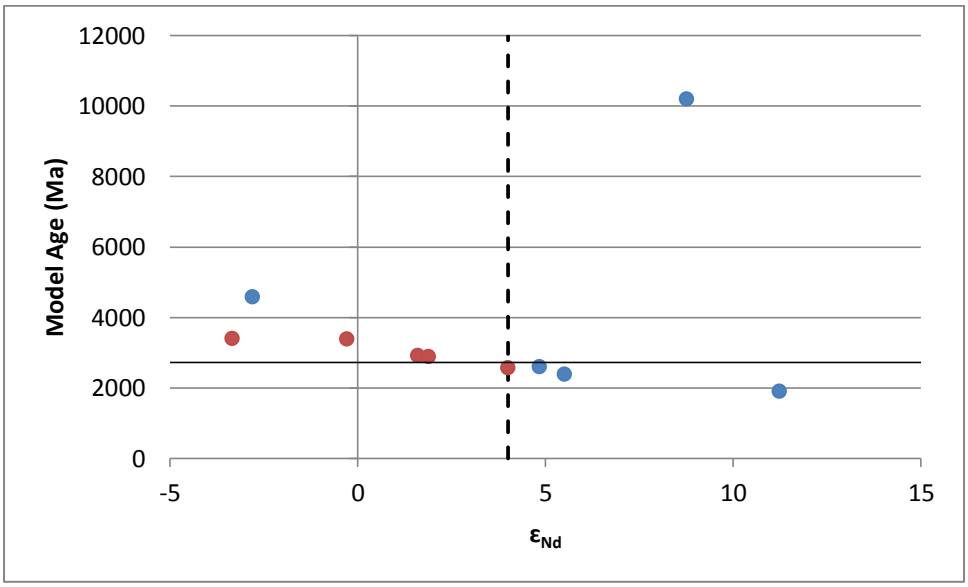

Figure 5.12. Calculated εNd_{2733} and model ages from the Butler East (Blue) and Butler West (red) intrusions. Solid horizontal line corresponds to the age of crystallization of the Thunderbird intrusion at 2733.6 Ma (Pers. Comm. McNicoll, 2014) and dashed line represents depleted mantle at T=2735 (DePaolo, Neodymium isotopes in the Colorado Front Range and crust - mantle evolution in the Proterozoic, 1981).

Based on textural variations, lithological associations, and the geochemistry of minerals and whole rock analysis (TiO_2/V_2O_5), the younging direction of the Butler intrusions have been reconstructed from the drill core. The Butler East intrusion is interpreted to young towards the

south east, and the Butler West intrusion is interpreted to young towards the east consistent with tentative younging directions proposed by Metsaranta and Houle (2013). The determinations of the younging direction vary in confidence levels and are dependent on the data available. The younging directions were largely reconstructed using the TiO_2/V_2O_5 ratio which increases during evolution, and stratigraphic/textural relationships (i.e., sharp lower contact of basal massive-oxides). The TiO_2/V_2O_5 ratio however is reliant on data provided from the company (MacDonald Mines Exploration Ltd.) and thus the method of analysis was tailored for exploration purposes. This is a source of error in some holes where titanium and vanadium were analyzed as elemental concentrations by 4 acid ICP-OES and were converted to oxide proportions for the use of the ratio whereas the data in this study was determined through XRF and ICP-AES. The majority of the data though, has been determined using XRF and is less susceptible to inaccurate analysis of Fe-Ti-V refractory phases.

5.1.2. Thunderbird Intrusion

The Thunderbird Intrusion is characterized by a suite of well layered iron-titanium rich ferrogabbros. The Thunderbird is a north-east trending diamond shaped intrusion with a strike length of approximately 12 km and width of 5 km (Fig. 5.13). The ferrogabbroic intrusion is hosted within the Muketei River supracrustal assemblage which is characterized dominantly by mafic metavolcanic rocks with lesser iron formations and felsic volcanic rocks of ~2770 Ma (Mungall et al., 2010), this is broadly similar in appearance to rocks within the eastern portion of the Butler Lake supracrustal assemblage. Ferrogabbroic rocks within the Muketei River supracrustal have been interpreted by Mungall et al. (2010) to be coeval with the voluminous Cr-Ni-PGE mineralized ultramafic rocks (e.g., Black Thor, Big Daddy, Eagles Nest, etc.). The ferrogabbroic (e.g.,Thunderbird intrusion) and ultramafic intrusive rocks are interpreted to be

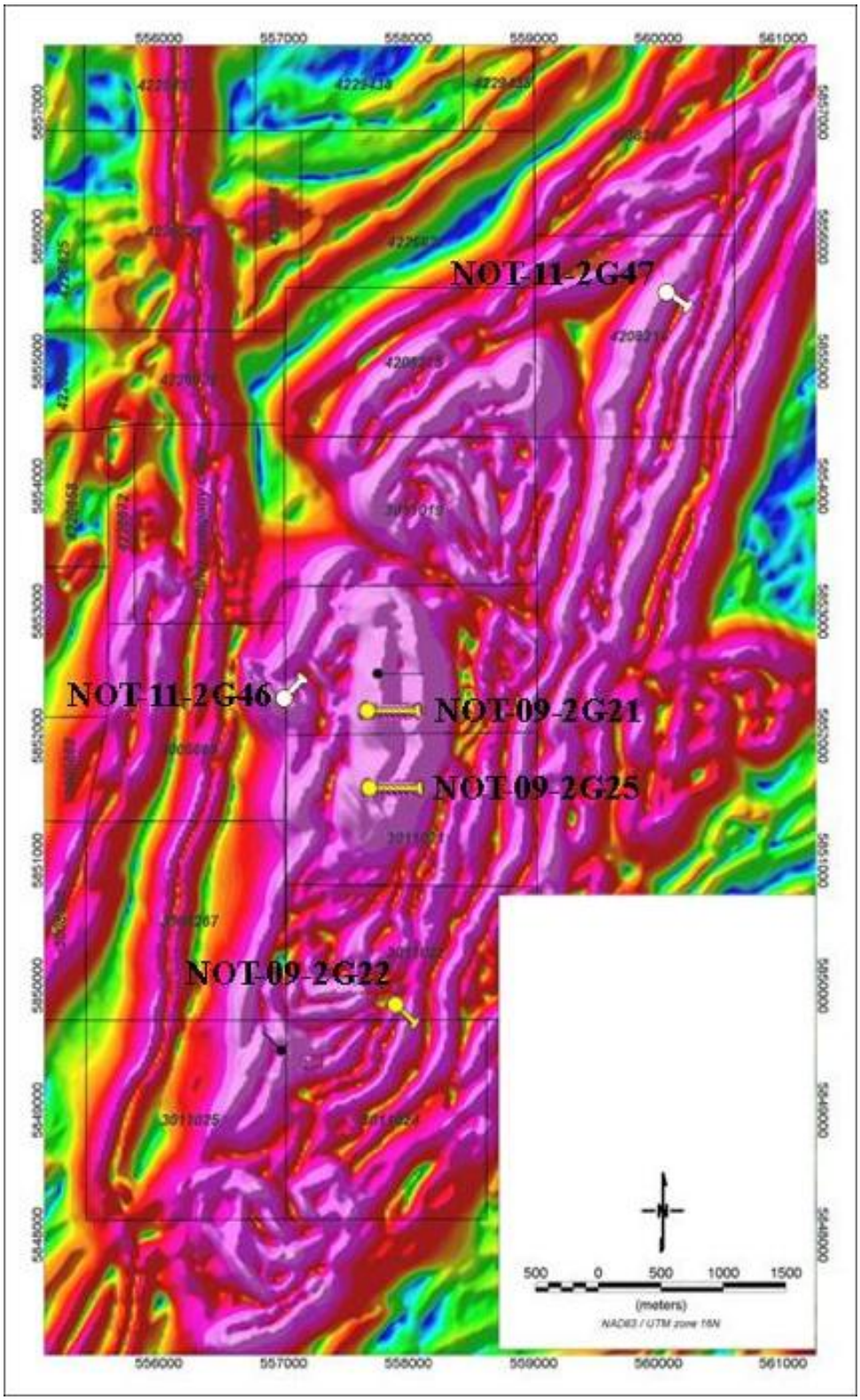

Figure 5.13. Total Horizontal Derivative magnetic map of the Thunderbird intrusion. Drill holes from the Vanadium-trend/ central portion of the Thunderbird highlighted in yellow and the phosphorous-trend/ marginal series highlighted in white (courtesy of Noront Resources).

coeval with the circa 2737 Ma intermediate and felsic volcanic rocks and associated VMS mineralization (e.g., McFaulds Lake VMS: Mungall et al., 2010).

The Thunderbird intrusion is largely composed of well layered medium-grained, equigranular gabbros, leucogabbros and anorthosites which typically contain 1-5% magnetite+ ilmenite. Lesser units within the intrusion include stratigraphically conformable semi-massive and massive oxide units, melanogabbros and pyroxenites. The Thunderbird intrusion is characterized by partial to complete repetitive cycles of massive and semi-massive oxide units which typically occur within discrete horizons and display sharp lower contacts which grade into oxide-rich pyroxenites, followed by oxide-bearing gabbro and lastly oxide-bearing anorthosites. Within these repetitive cycles, variable amounts of sulphide minerals are present (dominantly pyrite with lesser pyrrhotite and/or chalcopyrite). When present, the sulphide minerals occur as massive to semi-massive layers along the basal contacts or as disseminated grains within the anorthositic upper members of the cycles and range from 0.5-3 %. In contrast to the layered portions of the intrusion, large intercepts of relatively homogenous, poorly layered gabbroic to anorthositic units which contain variable magnetite + ilmenite contents display broad gradational contacts ranging from 0-10 % magnetite + ilmenite. Apatite mineralization occurs within these relatively homogenous rocks, which is unlike the vanadium mineralization concentrated within the basal magnetite-ilmenite horizons of the cyclic members of the Thunderbird intrusion.

The magmatic stratigraphy has been inferred based on lithological contacts (i.e., magmatic layering), whole-rock geochemistry (i.e., TiO_2/V_2O_5), mineralogy and mineral chemistry (e.g., magnetite compositions). Magmatic layering as determined through detailed core logging, has not been particularly effective for determining younging directions within the

Thunderbird intrusion. For example, highly layered portions of the intrusion display variable contact relationships and do not necessarily follow the general patterns observed within the McFaulds Lake ferrogabbros (i.e., sharp lower contacts and gradational upper contacts) as observed within the Butler intrusions. These contact relationships can at times be contradictory within the same drill core and must be used with caution in determinations of magmatic stratigraphy (Fig. 5.14). Geochemistry however, has been a useful tool in the determination of magmatic stratigraphy. TiO_2/V_2O_5 variations have been useful for determining stratigraphy, particularly within the Thunderbird intrusion which contains a large geochemical dataset. Drill hole NOT09-2G25 exemplifies the magmatic evolution as modelled through TiO_2/V_2O_5 variations (Fig. 5.15). The drill core displays two trends, i) decreasing ratio downhole between 0 and ~175 m, and ii) increasing ratio downhole between ~175 and 550 m (Fig. 5.15). Within each trend, the slope is remarkably consistent with anomalous values corresponding to sampling contaminations (e.g., late granitic dykes with evolved values). The contrasting trends observed within the TiO_2/V_2O_5 ratios suggests an initial upper member (<175 meters) which youngs up hole, and a lower member (>175 m) which youngs down hole. This two-tiered trend is interpreted to represent an anticline with the most primitive (stratigraphically lowest) portion occurring at the inflection point (~175 m depth). Magnetite chemistry has also proven to be a useful tool in the determination of magmatic stratigraphy as demonstrated by drill hole NOT11-2G47 (Fig. 5.16). Magnetite grains analyzed by EMP display a trend of decreasing V_2O_5 and Cr_2O_3 wt. % content downhole. Based on the high compatibilities of vanadium and chromium within magnetite, it has been suggested that the decrease of these elements could be used to model magmatic evolution (McCarthy and Cawthorn, 1983). If this is the case, drill hole NOT11-2G47 youngs down hole (towards the south-east). Plagioclase compositions within the Thunderbird intrusion also display a marked difference from labradorite dominated

plagioclase within the central portions of the intrusion, and andesine plagioclase within the marginal portions of the intrusion (Fig. 5.17). However, only limited mineral chemistry data is available and thus multiple methods of interpretation are used (texture, geochemical ratios, mineral chemistry, etc.). This is suggestive of a more evolved marginal series within the Thunderbird intrusion. The appearance of apatite mineralization restricted to the marginal series, supports the notion of a more evolved magma towards the margins of the intrusion based on the late stage appearance of apatite within ferrogabbroic melts (e.g., Namur et al., 2012; Tollari et al., 2006; Toplis et al., 1994). In light of the geochemical and mineralogical trends observed, it is suggested that the Thunderbird intrusion may represet a folded anticlinal structure (whale back) which contains the more primitive and stratigraphically lowermost units within the central portions, and the highly evolved units along the extremities. Alternatively, the Thunderbird may represent a relatively undeformed intrusion which is characterized by a primitive core and evolved margins, however, the steeply dipping nature of the igneous layers suggest a deformed geometry and thus the anticline model is preferred. Additional drilling with oriented core may help resolve this issue.

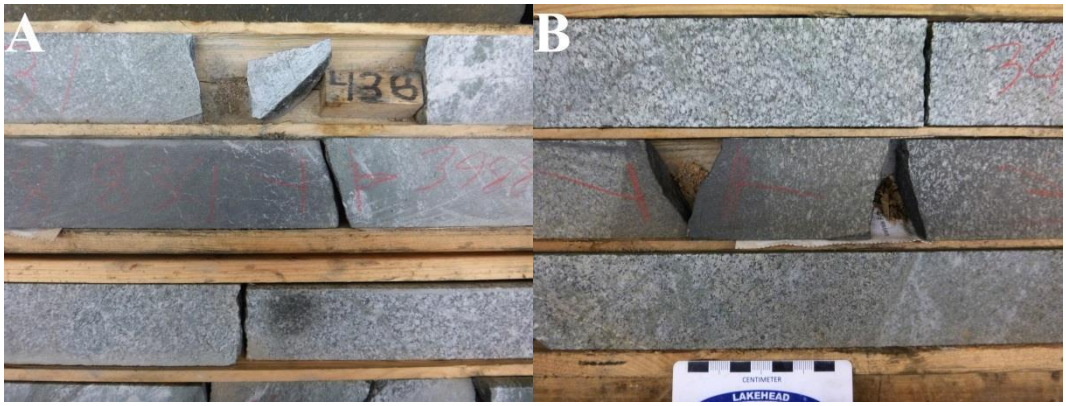

Figure 5.14. Photos of drill core from hole NOT09-2G21 displaying the variable contact relationships with their overlying and underlying ferrogabbro (down hole direction is bottom right). A. Massive oxide with sharp lower contact down hole (439 meters). B. Semi-massive oxide with sharp lower contact up hole (493 meters).

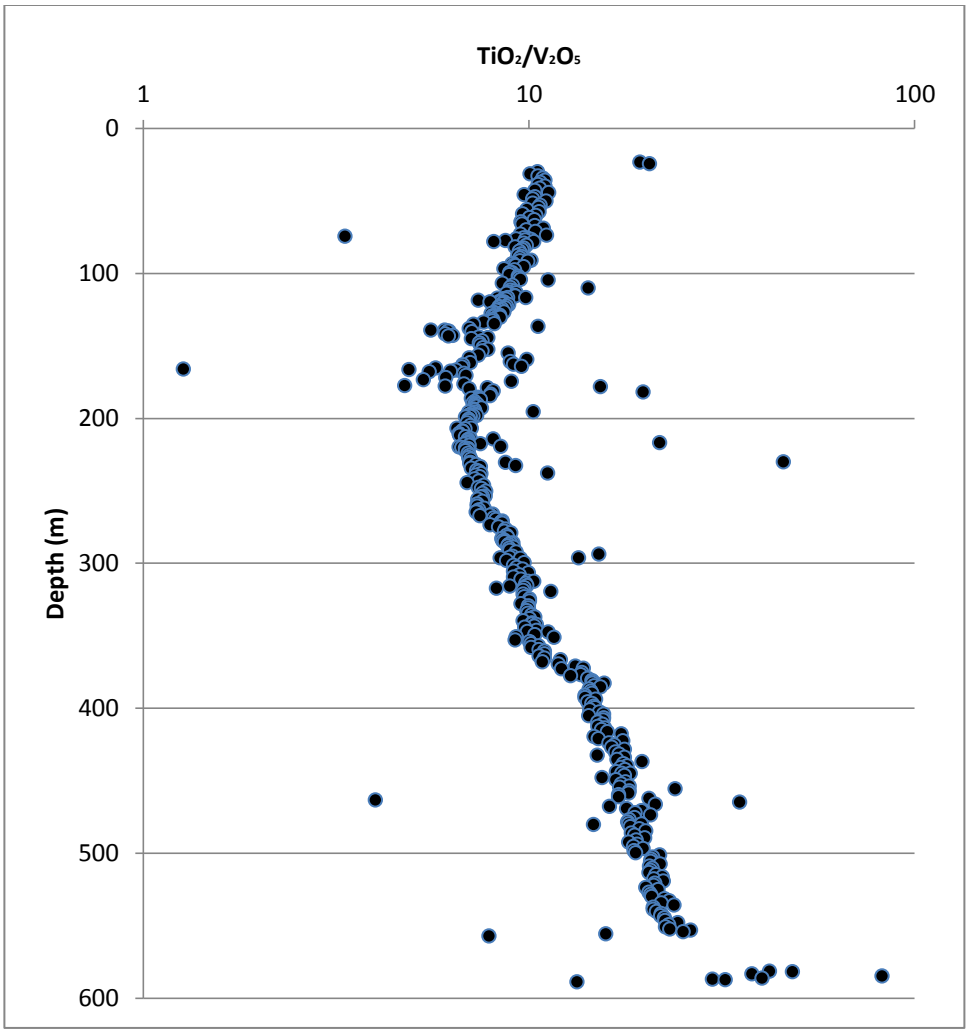

Figure 5.15. TiO_2/V_2O_5 variations against depth from drill hole NOT09-2G25. Intrusion youngs up hole between 0-175 meters, and youngs down hole >175 meters as interpreted from the TiO_2/V_2O_5 ratios.

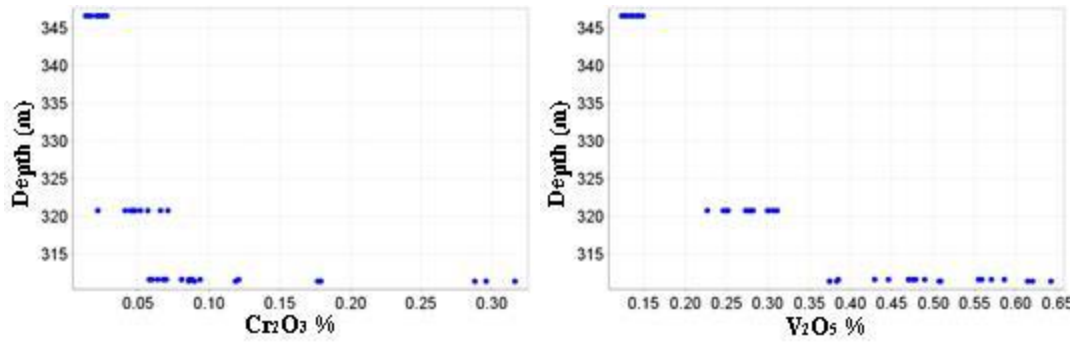

Figure 5.16. Down hole variations in Cr_2O_3 and V_2O_3 wt. % of magnetite grains as determined by EMP from the lower members of drill hole NOT11-2G47. Decreases in vanadium and chromium contents in magnetite suggest a down hole younging direction.

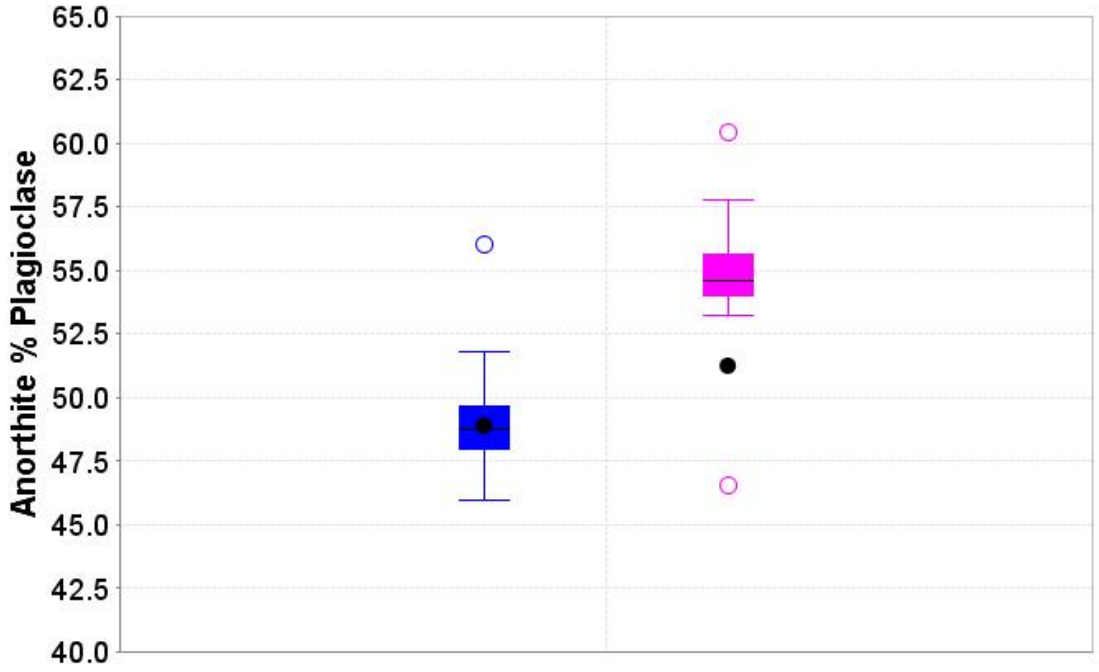

Figure 5.17. Box and whisker plot for the plagioclase compositions from the central drill holes (Pink: NOT09-2G21, NOT09-2G22, NOT09-2G25) and the marginal drill holes (Blue: NOT11-2G46, NOT11-2G47) from the Thunderbird intrusion.

Magnetite-ilmenite mineral pairs which have co-precipitated were analyzed by electron microprobe and the values have been used to interpret the temperatures and oxygen fugacity at the time of crystallization (Table 4.8). The conditions during formation have been calculated using an adaption of Spencer and Lindsley (1981) and Stormer (1983) geothermometers and oxygen fugacity calculations as described in Chapter 3.2. The Thunderbird intrusion has been subdivided into the vanadium trend (i.e., core of the intrusion) and the phosphorous trend (margins of the intrusions). The vanadium trend displays values of higher oxygen fugacity, with only slightly higher temperatures compared to the phosphorous trend (Fig. 5.18). The phosphorous trend which occurs along the margins of the intrusion has been interpreted to represent the more evolved portion of the Thunderbird intrusion and is characterized by more reduced oxygen fugacity (Fig. 5.18). The relatively reduced evolved portion of the intrusion is consistent with increasing ilmenite: magnetite ratios observed within

the McFaulds Lake ferrogabbros, and similar observations within the Baima (Zhang et al., 2012) and Skaergaard intrusions (Toplis and Carrol, 1996). However, even small concentrations of phosphorous have been experimentally proven to significantly reduce the oxygen fugacity of the magma (Toplis et al., 1994). This observation is consistent with apatite mineralization within the marginal series, as the presence of phosphorous will increase the ilmenite: magnetite ratio by destabilizing magnetite in favor of ilmenite (Toplis et al., 1994). It should also be considered that the temperatures and oxygen fugacity have been calculated on Archean rocks which have undergone metamorphism, which may have affected the results (Stormer, 1983; Oliver, 1978).

Table 5.2. Average values from magnetite-ilmenite pairs for the Thunderbird intrusion.

Sample	Trend	Mole % Usp	Mole % Ilm	Temperature (^{o}C)	Oxygen Fugacity
NO-2G21-6	Vanadium	1.37	96.86	501	-23.76
NO-2G21-7	Vanadium	0.59	97.27	463	-25.31
NO-2G21-9	Vanadium	1.72	96.93	507	-23.74
NO-2G21-10	Vanadium	0.93	96.89	487	-24.11
NO-2G21-11	Vanadium	1.27	97.11	492	-24.34
NO-2G25-3	Vanadium	0.64	96.98	472	-24.58
NO-2G25-4	Vanadium	1.31	96.98	496	-24.04
NO-2G25-5	Vanadium	0.74	97.05	476	-24.61
NO-2G25-6	Vanadium	1.23	97.26	487	-24.73
NO-2G46-1	Phosphorous	2.48	98.51	465	-28.24
NO-2G46-2	Phosphorous	1.03	98.29	449	-27.95
NO-2G47-6	Phosphorous	2.32	97.84	490	-25.81
NO-2G47-7	Phosphorous	0.65	98.39	431	-28.71
NO-2G47-8	Phosphorous	1.96	98.09	476	-26.73
NO-2G47-9	Phosphorous	1.10	98.31	450	-27.97

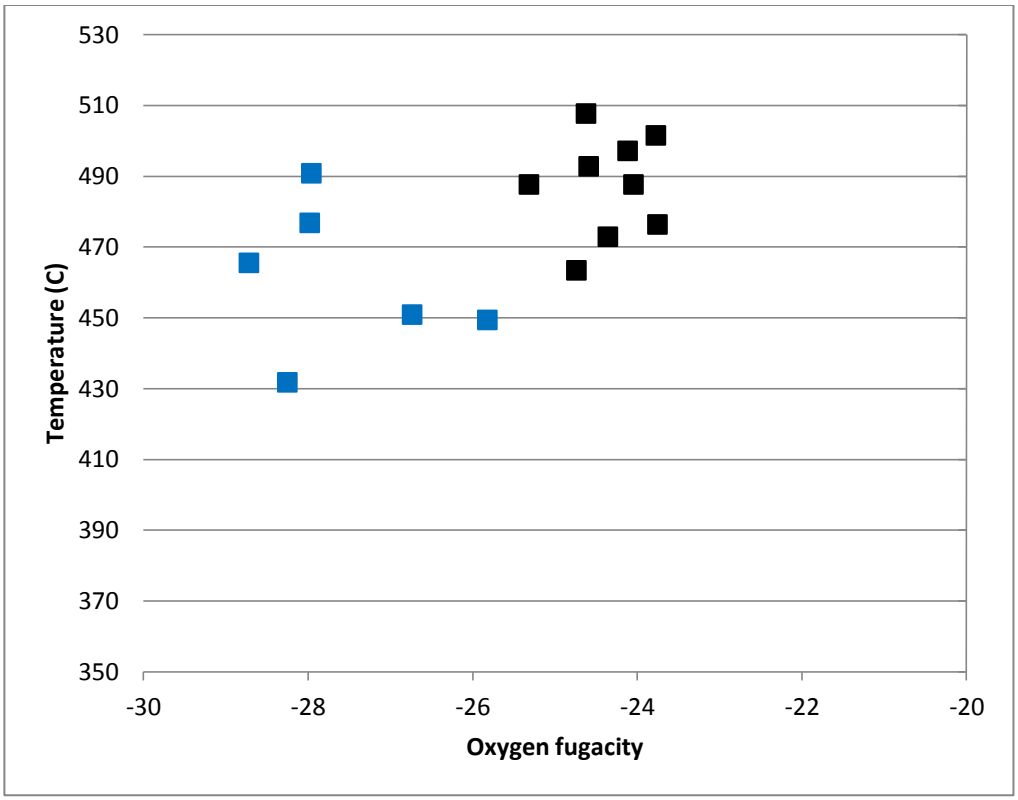

Figure 5.18. Temperature and Oxygen fugacity values for the Thunderbird intrusion (black= vanadium trend, blue=phosphorous trend).

Five samples from the Thunderbird intrusion were analyzed for Sm-Nd isotopes. Four of these samples were collected from the phosphorous-trend/marginal portions of the intrusion, and a single sample was collected from the vanadium-trend/central portion. The Thunderbird intrusion is characterized by positive ε_{Nd} values and model ages which dominantly range from 3048 to 3265 Ma (Fig. 5.19). Isotopic data from the Thunderbird intrusion is considerably less variable and scattered than the Butler Intrusions. However, overlap between the three intrusions is evident (e.g., positive ε_{Nd}) and suggests the less altered values from the Thunderbird may be used to verify discrepancies within altered rocks from the Butler intrusions. The Thunderbird intrusion is suggested to have formed from a mantle derived source with ε_{Nd} values slightly enriched from the Archean depleted mantle (ε_{Nd} =+4 calculated using methods decribed by DePaolo, 1981).

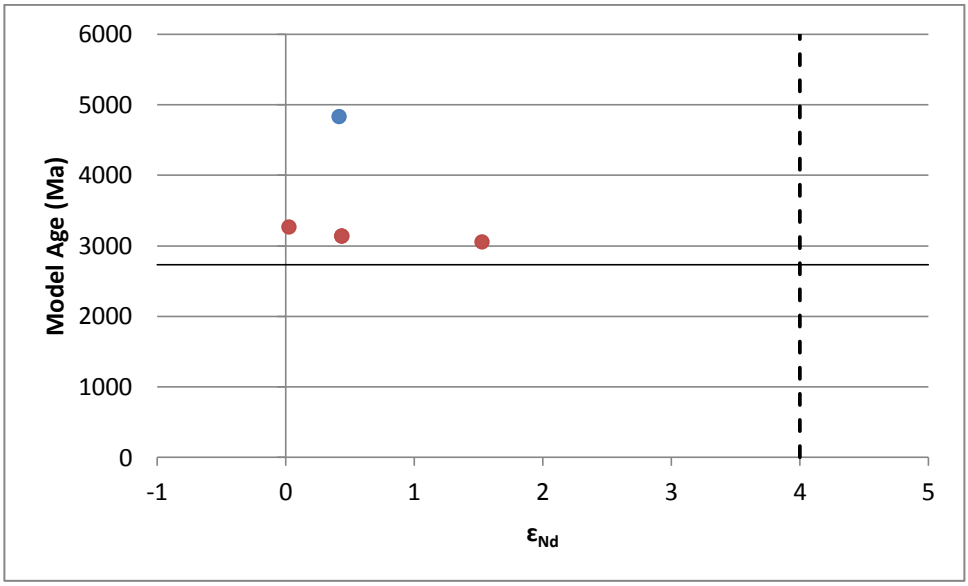

Figure 5.19 Calculated εNd_{2733} and model ages from the Thunderbird intrusion. Solid horizontal line corresponds to the age of crystallization of the Thunderbird intrusion at 2733.6 Ma (Pers. comm. McNicoll, 2014) and dashed line represents depleted mantle at T=2735 (DePaolo, Neodymium isotopes in the Colorado Front Range and crust - mantle evolution in the Proterozoic, 1981).

5.2. Petrogenesis of the Ferrogabbro Intrusions

This study represents the first detailed analysis of the Butler and Thunderbird intrusions and has implications for the regional geology of the McFaulds Lake greenstone belt. Furthermore, ferrogabbro intrusions may host large reserves of Fe-Ti-V mineralization with the potential to host Cr-Ni-Cu-PGE mineralization (Zhou et al., 2008). Understanding the petrogenesis of the McFaulds Lake ferrogabbro intrusions is fundamental to developing models for both targeting and exploring for Fe-Ti-V-P mineralization. A summary of the Butler and Thunderbird characteristics are displayed in Table 5.3.

Table 5.3. Characteristics of the Butler and Thunderbird intrusions (*Metsaranta and Houlé, 2012,approximated dimensions based on available magnetic maps, *** selective values based on least altered samples, **** Pers. comm. McNicoll 2014).**

Intrusion	Butler East	Butler West	Thunderbird
Country rock*	Dominantly high-Mg mafic volcanic with lesser iron formation and felsic volcanic rocks	Dominantly felsic volcanic with subordinate mafic to ultramafic metavolcanics	Bimodal mafic-felsic metavolcanic rocks.
Strike length (km)**	9	>18	12
Width (km)**	2	1-3	5
Younging direction	East	South-East	Outward (anticlinal dome)
Dominate plagioclase	Labradorite	Labradorite	Labradorite-Andesine
ε_{Nd}***	+4.84	+1.61 to +1.9	+0.03 to +1.53
Model Age***	2594	2885-2913	3048-3265
Intrusion Age (Ma)****	N/A	N/A	2733.6
Dominate oxide	Magnetite	Magnetite	Magnetite
Mineralization	Fe-Ti-V	Fe-Ti-V	Fe-Ti-V and Fe-Ti-P
Mineralization style (in order of abundance)	Massive, Semi-massive, disseminated	Massive, Semi-massive, disseminated	Disseminated, Semi-massive, disseminated

5.2.1. Origin of Layering

The formation of igneous layering is an enigmatic problem within even the most highly studied mafic-ultramafic intrusion (e.g., Bushveld: Eales and Cawthorn, 1996). This is likely due to the large variations within the types of layering (grain size, mineralogy, texture, geochemistry, etc.), and within inherent variations such as thickness, length and lateral variations, along with the nature of the layer boundaries (Naslund and McBirney, 1996). In addition, variations within the layers often suggest that more than one mechanism may be responsible for the formation of layering (Naslund and McBirney, 1996). The nature of layering does not always involve an open system with the addition of new magma but can also occur in closed systems, such as the layered ferrogabbros of the upper cycle of the Bushveld intrusion (Eales and Cawthorn, 1996). Below is a discussion and evaluation of different mechanisms which may have had a role in the formation of layering in the Butler and Thunderbird intrusions.

5.2.1.1. Magma Emplacement

An important concept to consider when studying magmatic intrusions is that the initial magma may not be a homogenous liquid; rather it may contain variable amounts of phenocrysts (Naslund and McBirney, 1996). The notion of a magma with suspended minerals has been a proposed to explain the chromium-rich deposits such as the UG2 chromite layer within the Bushveld intrusion (Mondal and Mathez, 2007) and has been extended to the mineralization of magnetite-ilmenite rich horizons (Duke, 1995). This phenomenon is observed commonly within volcanic flows and may have an effect on the flow dynamics of an intruding magma (Naslund and McBirney, 1996). Magmas which are crystal-rich liquids during

emplacement may develop rough layering caused by internal flow banding (Naslund and McBirney, 1996). Flow banding, or mechanical sorting within a magma has been proposed as the cause of an olivine-rich layer within the Palisades diabase sill (New Jersey) which ranges from 1-10 m and is traceable for over 40km strike length (Walker, 1969). The olivine grains were distributed chaotically within a homogenous plagioclase-augite matrix, which was used as evidence for mechanical sorting (Gorring and Naslund, 1995). These crystal-rich magmas typically produce thick sequences of phenocryst-rich and liquid-rich zones with gradational upper and lower contacts and may have bimodal grain-size distributions (Naslund and McBirney, 1996). Similar textures have been observed within the Thunderbird and Butler intrusions; however, they remain equigranular and display stratigraphic variations which would not be expected within a phenocrysts-rich melt.

Mafic-ultramafic intrusions which host economic sulphide and chromite deposits commonly exhibit variable degrees of magmatic layering (e.g., Stillwater: Irvine, 1987). The layering is typically interpreted as the result of magma recharge of a primitive melt (Irvine, 1977; Duke, 1995; Mondal and Mathez, 2007). Layers have been historically attributed to separate injections of magma of differing compositions; however, it has been suggested that the bulk composition of many layers could not have been liquid at a reasonable magmatic temperature and that injection of hot primitive magma cannot be a plausible explanation (Naslund and McBirney, 1996). The injection of a primitive melt into a partially crystalline magma chamber has been cited as the cause for layering within the Muskox intrusion, Nunavut (Irvine and Smith, 1967). The lower member of the Muskox intrusion is characterized by repetitive sequences of basal dunite, followed by harzburgite and an upper member of orthopyroxenite (Irvine and Smith, 1967). Within each sequence there is an observed decrease in the chromite content along with decreases in Ni in olivine, and an increase in Fe towards the

top of the intrusion (Irvine and Smith, 1967). The progressive decrease of compatible elements along with sharp contacts and primitive basal members of each unit has been interpreted to be the result of an influx of primitive magma (Irvine and Smith, 1967). This interpretation has been questioned due to the remarkable regularity of the layers and mass balance issues since chromium is typically only an accessory mineral within ultramafic intrusions (Brandeis, 1992). Rather an internal convection may have caused the observed sequence of layering (Brandeis, 1992). Regardless, the formation of chromite-rich layers is widely cited as the result of magma mixing with a less evolved magma (e.g., Lipin, 1993). Irvine (1977) has demonstrated that through magma mixing, in a primary assemblage of crystallizing olivine and chromite, the stability field of chromite expands at the expense of olivine which effectively ceases to crystallize to produce pure chromite. This could produce layers or segregations of nearly pure chromite (Irvine, 1977) and has been extended to the mineralization of stratigraphically continiuous Fe-Ti-oxides in a method analogous to the formation of chromite (Duke, 1995). The formation of expansive layers of chromitite of roughly equal thickness within the Bushveld intrusion requires a different mechanism of formation (Naslund and McBirney, 1996), and will be discused later.

5.2.1.2. Magma Convection

Convection is a phenomenon with variable importance within magma chambers and is hypothesized to occur both as a continuous and an intermittent process (Naslund and McBirney, 1996). Convection currents occur within magma chambers due to heat transfer during the cooling of the magma (Naslund and McBirney, 1996). The transfer of cool and hot magma creates currents which can suspend minor concentrations of crystalline minerals within the magma, so long as their settling velocities are lower than their turbulent fluid velocities

(Marsh and Maxey, 1985). However, if the concentration of crystals overcomes the suspension caused by convecting magma, the crystals will settle out leaving behind a mass of crystals along with a crystal-free magma (Naslund and McBirney, 1996). Convection can occur as a continuous process which is largely controlled by buoyancy variations during cooling, or can occur as discrete or intermittent episodes of convection caused by complexities within magma chambers (Naslund and McBirney, 1996). Intermittent convection is believed to be the cause of the layering observed within the Middle Zone of the Skaergaard intrusion which is characterized by alternating plagioclase-rich and pyroxene-rich layers (Naslund et al., 1991). These layers exhibit sharp upper and lower contacts which range from 0.3 to 6 m in thickness and can be traced for up to 2km (Naslund et al., 1991). It has been proposed that the plagioclase-rich layers formed during periods of stagnations and have settled out of suspension, whereas the pyroxene-rich layers were deposited during episodes of convection (Naslund et al., 1991). The intermittent convection is thought to produce layers which exhibit sharp boundaries with variable thicknesses and may occur with variable lateral extents; indicative of a system which abruptly and randomly turned on or off (Naslund and McBirney, 1996).

Double diffusive convection is a particular style of convection which requires two components of vertical differences working in opposition based on density contrasts (Naslund and McBirney, 1996). These components are not limited to, but are typically considered to be temperature and composition (Naslund and McBirney, 1996). Variations in the components cause a difference in density/buoyancy within the magma which produces stratification and may cause the magma to overturn (McBirney, 1985). The magmas are thought to solidify as a crystalline front which propagates upwards with the stratified liquid remaining in front of the front (McBirney, 1985). However, it is not clear as to how a layered liquid can crystallize as a

layered solid (Naslund and McBirney, 1996). Additionally, the effectiveness of horizontal double diffusive convection cells are considered to be insignificant within magmas near their liquidus, since temperature and compositions are not independent variables and would require extreme superheating or undercooling (McBirney, 1985). These large temperature variations would be unlikely to occur within large or slow cooling magma chambers (Naslund and McBirney, 1996) and may be applicable to the Thunderbird or Butler intrusions, but require further defining as to the size and extent of the intrusions before interpreting cooling rates. Double diffusive convection has been interpreted to produce the some of the layering within the Stillwater intrusion (Irvine et al., 1983), Honnigsvåg intrusive suite (Robins et al., 1987), and the upper member of the Bushveld complex (McCarthy and Cawthorn, 1983). These layers exhibit distinct lateral variations which appear to be the defining characteristic (Naslund and McBirney, 1996).

5.2.1.3. Mechanical Sorting

Mechanical sorting within magma chambers is largely analogous to fluvial sedimentary processes and involves erosion and deposition within a liquid medium. It has been suggested that crystals in suspension will settle due to gravity so long as the crystal overcomes the yield strength of the magma (McBirney and Noyes, 1979). The yield strength can be measured based on Stoke's Law and which experimental studies have shown to increase with time and SiO_2 content and decrease with increasing temperature and H_2O contents (McBirney and Noyes, 1979). Additionally, the effects of P_2O_5 within magma have been shown to drastically affect the viscosity of the liquid when present in considerable amounts, but this is a poorly understood parameter (Toplis et al., 1994). Gravity settling within a stagnant magma chamber may produce a series of graded layers which exhibit grain size and/or density sorting (Naslund and

McBirney, 1996). The layers are characterized by coarse and/or dense minerals which occur along the base of the layer and grade into finer and/or less dense minerals, as in the Imilik gabbro of Greenland (Brown and Farmer, 1971). The yield strength will be drastically decreased within a flowing magma (McBirney and Noyes, 1979). Centimeter to meter scale trough structures observed within the upper member of the Skaergaard intrusion have been attributed to internal magmatic currents and have deposited a dense assemblage of olivine-magnetite-ilmenite-pyroxene within a predominantly anorthositic rock (Irvine, 1987). These troughs are thought to have formed through depositional processes of dense minerals associated with internal magmatic currents, resulting in linear lens shaped structures which exhibit grain size and density grading (Irvine, 1987).

Mechanical sorting of crystals within a magma may also occur during magmatic deformation and compaction (Naslund and McBirney, 1996). Deformation within a crystallizing magma differs from that of a liquid due to an inherit anisotropy (Naslund and McBirney, 1996). During deformation the liquid matrix absorbs more stress than the entrained crystals (Naslund and McBirney, 1996). The deformation results in crystals with little strain, whereas the liquid exhibits high strain and a planer foliation of the crystals (Naslund and McBirney, 1996). Magmatic deformation is more common within the margins of an intrusion and produces lenses or schlieren of layered zones (Naslund and McBirney, 1996). Deformation has been proposed as the cause of minor layering within the Sept Iles anorthosite intrusion of Quebec (Higgins, 1991). Compaction of crystal mush is a poorly understood process which is thought to occur when gravity produces a consolidated crystal layer (Naslund and McBirney, 1996). The compaction results in a loss of pore space liquid and may even cause deformation within the crystals such as pressure dissolution in extreme cases (McBirney and Hunter, 1995). However, no such evidence has been observed within the Butler or Thunderbird intrusions.

5.2.1.4. Intensive Parameters

Intensive parameters are physical characteristics (pressure, temperature, oxygen fugacity, etc.) which are independent of the size or mass of an intrusion. Of particular interest in magmatic oxide deposits are the constraints on oxygen fugacity, as the crystallizing mineral phase and mineral chemistry may be controlled by this parameter (Ulmer, 1969). Experimental studies have shown that a system crystallizing plagioclase, pyroxene, and olivine at low oxygen fugacity (10^{-11}), will only precipitate pyroxene at higher oxygen fugacity (10^{-9}: Ulmer, 1969). It has also been shown that olivine and pyroxene which precipitate at higher oxygen fugacities have higher Mg#s (Ulmer, 1969) and the partition coefficients of hetrovalent elements (e.g., V) vary as a function of oxygen fugacity (Mallmann and O'Neil, 2009). Oxygen fugacity may fluctuate through numerous processes such as the assimilation of water-rich or CO_2-rich country rocks, gas release through volcanic vents and/or diffusion, temperature fluctuations, convection or fractionation of oxide-rich phases (Naslund and McBirney, 1996). It has been suggested that variations in oxygen fugacity have caused alternating silicate-rich and oxide-rich layers such as the chromite layers of the Lower Bushveld or the magnetite layers of the Upper Bushveld (Cameron, 1975; 1977). Variations in oxygen fugacity have also been proposed to affect the stable silicate phases resulting in modal layering, as in the norite I layer within the Stillwater intrusion where anorthositic layers are interpreted to have formed through the reduction of pyroxene during periods of increased oxygen fugacity (Ryder, 1984). Through experimental studies, it has been demonstrated that large variations in stable mineral phases and mineral chemistry have been observed under differing oxygen fugacities (e.g., Ulmer, 1969; Mallmann and O'Neil, 2009; Toplis and Carroll, 1995), yet it remains unclear as to how

changes in oxygen fugacity could occur over large distances such as in the magnetite horizons of the Upper Bushveld intrusion (Naslund and McBirney, 1996).

Variations in liquid pressure have been a popular mechanism by which large, continious, homogenous layers have formed (e.g., chromite layers in the Bushveld: Eales and Cawthorn, 1996). Variations in total pressure or vapour pressure would simultaneously effect the entire magma chamber and may be the result of exsolution or expansion of a vapour phase (Lipin, 1993), emplacement of a new magma into an exisiting magma chamber, convective overturn (Jackson, 1961), volcanic eruptions from the magma chamber (Sorensen and Larsen, 1987), tectonic stress (Cameron, 1977) and fracturing of the overlying crust (Naslund and McBirney, 1996). Experimental studies show that an increase in pressure will expand the stability field of spinel and orthopyroxene and may result in the precipitation of a different mineral assemblage (Osborn, 1978; Sen and Presnall, 1984). It has been suggested that an increase in pressure could result in chromite, magnetite or orthopyroxene-rich layers, while a pressure decrease could result in anorthositic or dunitic layers (Naslund and McBirney, 1996). Pressure variations have been proposed to explain the alternating layers of aegirine, arfvedsonite and eudialyte in the Ilimaussaq intrusion of southern Greenland (Ferguson and Pulvertaft, 1963). It has been suggested that inversly graded layers formed during periods of gradually increasing pressure, whereas the normally graded layers formed during periods of gradually decreasing pressure (Ferguson and Pulvertaft, 1963).

It has been proposed that evolved mafic magmas which achieve extreme iron enrichments may separate into two immiscible liquids, one rich in silica, alumina and alkalies, are the other would be rich in iron and other mafic cations (McBirney, 1975; McCarthy and Cawthorn, 1983). Immiscibility may be triggered by high concentrations of Fe_2O_3, FeO, P_2O_5 and

TiO_2 but low concentrations of MgO, CaO and Al_2O_3 along with high ratios of Fe_2O_3/FeO, K_2O/Na_2O and $(Na_2O + K_2O)/ Al_2O_3$ (Naslund, 1983). Liquid imiscibility has been suggested to have occurred within the Upper Zone up the Skaergaard intrusion, where dykes, sills, layers and pods of Fe-Ti-oxide and apatite-rich layers (nelsonite) occur (Philpotts, 1967; Jakobsen et al., 2011). It has also been also been suggested that three zones of Fe-Ti-oxide and apatite-rich horizons of the upper Bushveld intrusion may have been formed through the process of liquid immiscibility (Reynolds, 1985). The thickness of the three zones is approximatly two meters and they are composed of nearly pure apatite-magnetite-ilmenite in a roughly 70% Fe-Ti-oxide to 30% apatite ratio (Reynolds, 1985), which is a similar proportion to nelsonites reported elsewhere (Naslund and McBirney, 1996).

5.2.1.5. Layering within the Ferrogabbros

Igneous layering within the Butler and Thunderbird intrusions is widespread with large variations in the scale of layering (cm to meter), contact relationships, mineral phases present and grain size. Due to the highly variable nature of the layering, it is possible that multiple mechanisms have produced these layers. The limited number of drills holes means that the lateral extent and true thickness of the layers (particularly within the Butler intrusions). Large scale layering is thus largely based on first derivative magnetic maps which illustrate linear magnetic features interpreted to represent magnetite-rich ferrogabbro (Figs. 5.1; 5.13).

Two styles of layering have been observed within the ferrogabbro intrusions. The first style occurs as repetitive sequences of sulphides (pyrite +/- pyrrhotite +/- chalcopyrite), oxides (magnetite+ ilmenite), mafic silicates (pyroxene+/- amphibole) +/-oxides, and plagioclase+/- mafic silicates +/- oxides. These sequences occur as partial to complete cycles which exhibit sharp lower contacts and gradational internal contacts (Fig. 5.5). However, similar

mineralogical sequences exhibit gradational lower contacts where massive intervals of magnetite+ ilmenite occur as typically thin (<10cm) stratigraphically conformable horizons. Cycles range from a few centimeters (Fig. 4.3G) to several meters in core length (Fig. 4.3F). Layering has also been observed within large intervals of gabbro with highly variable proportions of pyroxene/amphibole and plagioclase which display gradational contacts and variable amounts of magnetite+ ilmenite (typically 0-10%). The second style of layering has been observed within the Butler West intrusion and is characterized by stratigraphically conformable oxide-bearing pegmatitic gabbros which exhibit gradational contacts with coarse-grained oxide-bearing leucogabbros. These pegmatitic units are mineralogically and chemically identical to the oxide-bearing gabbros observed throughout the ferrogabbro intrusions with the exception of fractured plagioclase grains speculated to have formed during either a plagioclase phenocryst-rich magma injection, or within a turbulent, volatile-rich, tectonically deformed portion of the Butler West intrusion.

Trace element data has been used by previous workers to provide insight into the nature and cause of layering as with the vanadium-bearing magnetite layers of the Upper Bushveld intrusion (McCarthy and Cawthorn, 1983). McCarthy and Cawthorn (1983) analyzed magnetite grains and observed that large depletions of chromium within short intervals and also noted abundant ‘reversals’ within the stratigraphy (Fig. 5.20). The Upper Bushveld intrusion is thought to have crystallized within a closed magma chamber (Eales and Cawthorn, 1996), and thus the reversals in chromium content could not have formed through addition of primitive magma. Chromium reversals are generally associated with the appearance of layers composed of massive magnetite which display either sharp or gradational upper and/or lower contacts. The reversals have been proposed to have formed by convection cells which supplied the crystallizing front with relatively undepleted magma (McCarthy and Cawthorn, 1983).

Similar trends are present within the Butler East intrusion, along with reversals in vanadium and chromium (Fig. 5.7). The TiO_2/V_2O_5 ratio generally increases down hole and displays a stepped pattern (Fig. 5.21). The ratio sharply increases over short intervals associated with chromium and vanadium mineralization but only gradually increases over intervals of weak mineralization (Fig. 5.20). This trend is interpreted to represent a closed system as the ratio displays no sign of reversal as would be expected from the injection of a primitive magma. The layers may have formed through a similar process of convection currents as proposed for the Upper Bushveld intrusion (McCarthy and Cawthorn, 1983) as no evidence to date suggests multiple pulses of primitive magma injection as the magmatic layers are characterized by local

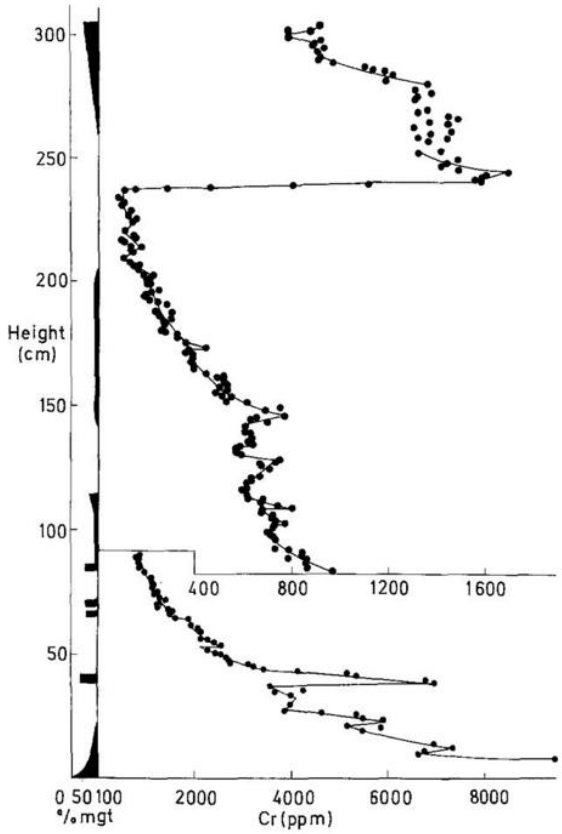

Figure 5.20 Upper Zone of the Bushveld intrusion displaying chromium variations and magnetite contents with depth (From McCarthy and Cawthorn, 1983).

increase of compatible elements (Cr,V) within the base of oxide rich layers. However, the geometry of these massive oxide layers is vital in understanding the process of layer formation. Convection cells within the Bushveld intrusion have been advocated due to the immense volume of magma which would produce long-lived convection (Naslund and McBirney, 1996) and brings into question the longevity of convection cells within the Butler and Thunderbird intrusions. If the layering within the Butler and Thunderbird intrusions is continuous over large distances then it is possible that the repeated sequences of massive oxide and silicates may have formed from pressure fluctuations (Naslund and McBirney, 1996) possibly related to tectonic activity related to the coeval and spatially associated VMS occurrences (Mungall et al., 2010; Metsaranta and Houlé, 2012). This is significant as VMS deposits occur on the ocean floor and require highly fractured host rocks (Mumin et al., 2007) which may cause pressure fluctuations during tectonic movement (Naslund and McBirney, 1996).

Layers of nearly pure magnetite and ilmenite may have formed through oxide-silicate liquid immiscibility as has been proposed for the Panzhihua (Zhou et al., 2005b; Zhou et al., 2013) and Skaergaard intrusions (Humphreys, 2011; Jakobsen et al., 2011).These layers are characterized by apatite mineralized and fluid-bearing systems which have been shown to greatly enhance the formation of oxide immiscible melts (Jakobsen et al., 2011; Zhou et al., 2013). Although the Panzhihua and Skaergaard intrusions display similar textures within silicate minerals (e.g., equigranular medium-grained gabbro-anorthositic rocks: Zhou et al., 2005b; Jakobsen et al., 2011) and oxide-rich bodies occur as stratigraphically conformable layers (some with sharp upper and lower contacts), they differ in there presence of oxide-rich dykes, pods and/or sills which have not been observed within the Butler or Thunderbird intrusions. There also remains little evidence of apatite-rich (nelsonite) or fluid-rich melts within the Butler and Thunderbird intrusions with the exception of the pegmatitic phases of the Butler West

intrusion which may indicate fluid-rich melts, and the apatite-bearing phases of the Thunderbird intrusion. These phases currently appear to be localized and would not explain the similarlities (mineralogy, chemistry, contact relationships, etc.) in layering observed within the Butler and Thunderbird intrusions.

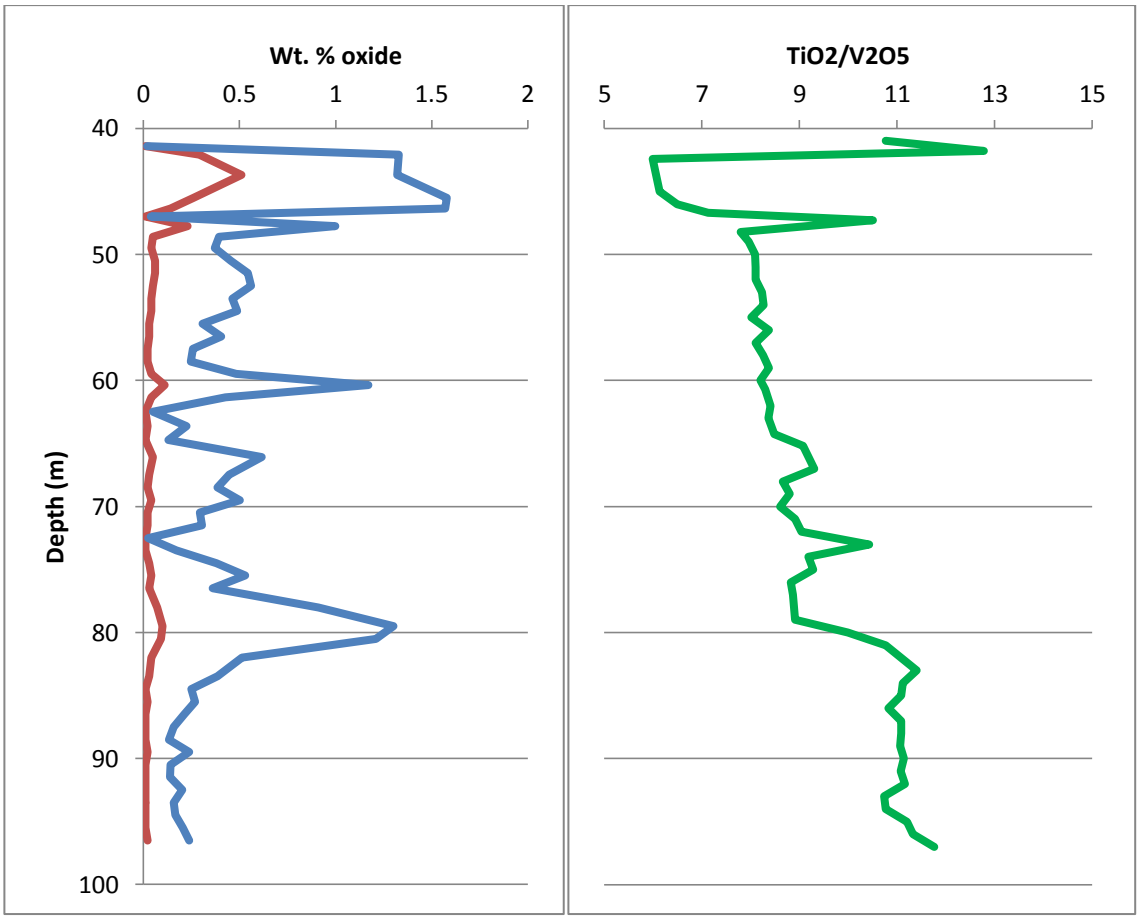

Figure 5.21. Downhole variations in V_2O_5 (blue), Cr_2O_3 (red), and TiO_2/V_2O_5 with depth in BP11-V07-Butler West (n=53). Increased TiO_2/V_2O_5 values with depth suggest the intrusion youngs down hole.

Pegmatitic phases within the Butler West intrusion are exclusive to the ferrogabbros studied, as all the other units are characterized by equigranular medium-grained plagioclase and pyroxene/amphibole. The pegmatitic gabbros are compositionally and mineralogically identical to the other gabbros except they are characterized by >3cm plagioclase and pyroxene/amphibole with fractured plagioclase crystals. Fractured plagioclase is unique within

the pegmatitic unit and interpreted to be a primary feature as the rock exhibits no evidence of anomalous secondary deformation and remains a competent unit. The texture is interpreted to represent brecciation of a plagioclase phenocryst-rich melt prior to the crystallization of pyroxene. The fracturing may have occurred within a turbulent crystal mush during tectonic activity, or by injection of a new magma of similar composition. These pegmatites are similar to those described in the Smartville (Beard and Day, 1986) intrusive complex and the Panzhihua intrusion (Zhou et al., 2013). The pegmatites occur as stratigraphically conformable units and are characterized by gabbroic to pyroxenitic cores and leucogabbro to anorthositic rims and are compositionally identical to the surrounding gabbroic units (Beard and Day, 1986). The Smartville pegmatites are interpreted to have crystallized in place within a shallow chamber rich in a hydrous phase (Beard and Day, 1986).

It is proposed that the observed layering within the Butler and Thunderbird intrusions have been caused by various mechanisms. The very well layered portions characterized by massive oxide and semi-massive basal members and upper members of oxide-poor leucogabbro to anorthosite which display sharp lower contacts and gradational internal contacts are interpreted to represent closed system convection cells. The oxide-rich portions represent dense materials which were transported and concentrated along the base of the crystallizing front and were initially high in compatible elements (Cr and V) and decrease upwards. Magnetite and ilmenite contents gradationally decrease upwards within the cycles as they represent more dense material. New cycles are thought to have formed during magmatic overturns which abruptly transported new relatively primitive, oxide-rich material to the base of the intrusion and as a result produce sharp lower contacts with the underlying layered cycle. Alternatively, apatite-magnetite-ilmenite mineralized members observed within the margins of the Thunderbird intrusion are interpreted to have formed through liquid immiscibility as a

nelsonite melt. The observed net-textured apatite-ilmenite-magnetite is analogous to net textured sulphides observed within magmatic sulphide deposits and interpreted to be the product of sulphide-silicate liquid immiscibility (e.g., Veksler, 2004). The Fe-Ti-P mineralized melagabbro within the Thunderbird intrusion is characterized by approximately the same proportions as in many nelsonites oberserved within evolved ferrogabbro intrusions (Naslund and McBirney, 1996). This interpretation is supported by experimental evidence of phosphorous-bearing Fe-Ti-rich systems which greatly expand the immicibility gap for oxide-silicate liquids (Toplis and Carroll, 1995; Veksler, 2009). Oxide-silicate liquid immiscibility is interpreted to be a minor phenoenom within the Thunderbird and absent within the Butler intrusions, however, many linear magnetitic anomalies remain untested and it is possible that they may host stratigraphically conformable nelsonite layers, as obsered within the Sept Iles intrusion (Namur et al., 2010; Namur et al., 2012).

Pegmatite units of the Butler West are interpreted to have formed within a plagioclase-phyric crystal mush likely with a fluid component. Fluid-bearing magmas have been experimentally shown to induce the crystallization of pegmatitic phases (Jahns and Burnham, 1969). The fluid phase may have exsolved from the crystallizing magma during an episode of decreased pressure, of possibly through an external contaminant. The fluid phase would have also significantly lowered the viscosity of the magma (Naslund and McBirney, 1996) and may increase the turbidity of the crystal mush. Fragmentation only occurs within plagioclase grains and thus these are interpreted to be the only mineral phase precipitated prior to deformation. The fragmentation may have been caused by local tectonic activity, possibly related to proximal VMS systems within the belt.

5.3. TiO_2/V_2O_5 Ratio

The ratio of TiO_2 to V_2O_5 has been demonstrated through the study of the Butler and Thunderbird intrusions, to be an instrumental and potentially more broadly useable tool in the interpretation of original stratigraphic polarity and as a result, in the identification of areas that are prospective for mineralization within ferrogabbroic intrusions. Titanium and vanadium were selected for study due to their high concentration within the magnetite-ilmenite oxide species and relative incompatibility within the silicate facies (e.g., Mallmann and O'Neil, 2009; Toplis and Corgne, 2002).

The TiO_2/V_2O_5 ratio is suggested to evolve during the crystallization of magma and as a result, can be a measure of how primitive a crystallizing magma was. The change in ratio is due to the assumed higher compatibility of V_2O_5 within the ferrogabbroic magma, compared to TiO_2 (McCarthy and Cawthorn, 1983). This assumption however, is only valid once magnetite is on the liquidus phase. As the magnetite crystalizes, the vanadium is incorporated preferentially over titanium into the oxide phases, and as a result the TiO_2/V_2O_5 ratio increases. This ratio can be then be applied to large geochemical datasets to interpret possible way up directions of ferrogabbroic intrusions. The drill core from hole BP11-V08 exemplifies the use of the ratio where an extensive set of geochemical data (64 samples) is plotted continuously down hole (Fig. 5.22). The TiO_2/V_2O_5 ratios display both gradual and local variations which are independent of whole-rock major oxides (e.g., Fe_2O_3: Figure 5.23), and are interpreted to reflect how primitive a magma is.

The TiO_2/V_2O_5 ratio can be applied in mineral exploration to determine vanadium-rich magnetite-bearing lithologies, from vanadium-poor lithologies. A compilation of 2288 samples

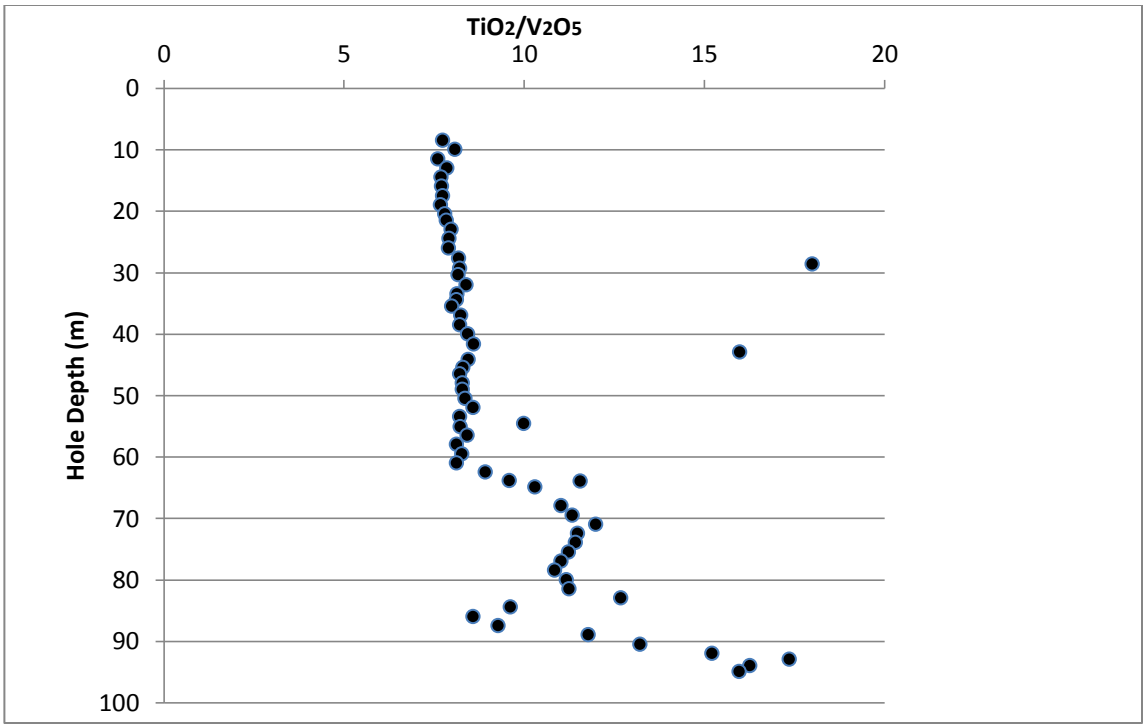

Figure 5.22. TiO_2/V_2O_5 values down hole of MM08-V01 from the Butler West Intrusion. Down hole variations display a stepped pattern of broadly weak evolution (i.e., 9-60 meters) along with sudden increases in ratio (i.e., 60-70 meters). The general increased ratio suggests a down hole younging direction.

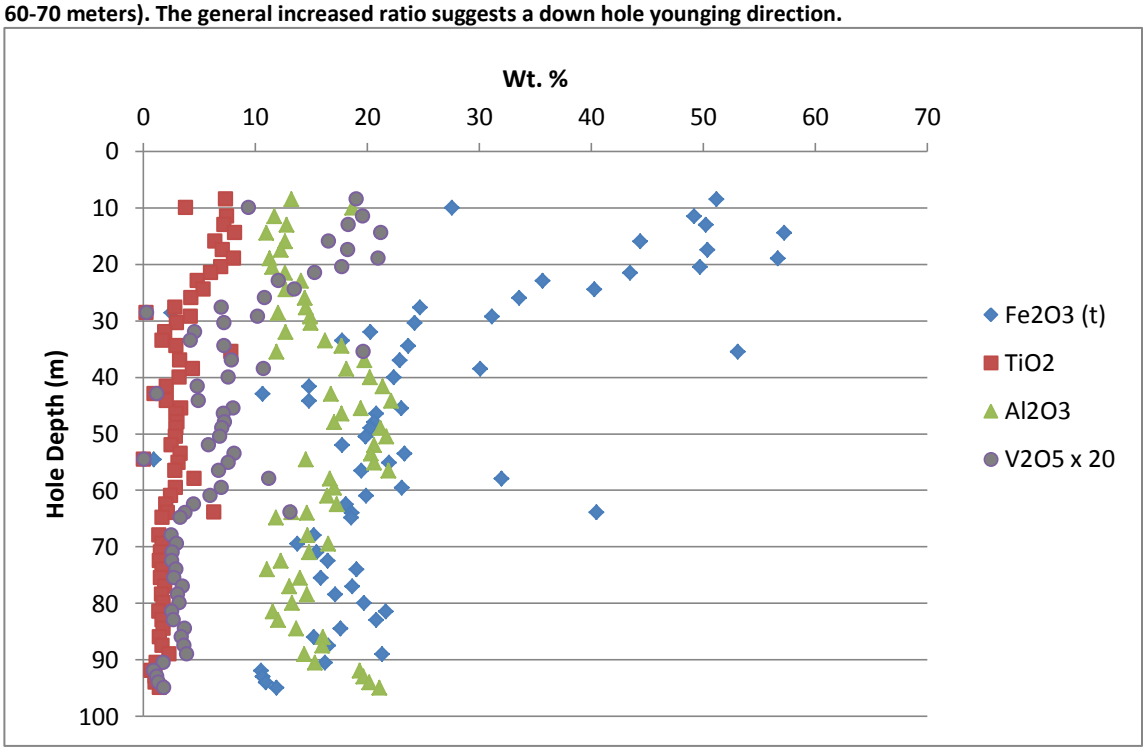

Figure 5.23. Whole-rock values down hole of MM08-V01 from the Butler East Intrusion which display a general decrease in Fe_2O_3 , V_2O_5, and TiO_2 contents which model approximate Fe-Ti-oxide contents along with local variations caused by meter-scale oxide-silicate layering. Al_2O_3 approximates the relative feldspar proportions and displays an approximately inverse relationship to Fe_2O_3 , V_2O_5, and TiO_2 contents.

which have been analyzed for vanadium and titanium from the Butler and Thunderbird intrusions, reveal that the samples which are considered to contain 'high grade' vanadium mineralization (>0.50 wt. % V_2O_5), are restricted to a relatively narrow range of TiO_2/V_2O_5 values between ~5-15 (Fig. 5.24). Within this range, the magnetite grains are considered to be vanadium-rich, and the absolute V_2O_5 of the sample is a function of the amount of oxides present. This tool can be applied to determine the content of vanadium within the oxides present, while not being influenced by the total vanadium within the sample. This method can be used to distinguish fertile vanadium-bearing magnetite horizons from depleted or less favorable horizons. The ratio can also be applied to exploration for phosphate (apatite)-bearing horizons within a layered intrusion. Figure 5.25 is a plot which compares the TiO_2/V_2O_5 to the total P_2O_5 within 2288 samples from the Butler and Thunderbird intrusions. The distribution of phosphate is restricted to ilmenite-rich horizons with evolved TiO_2/V_2O_5 ratio values (>100) and contain vanadium-poor magnetites.

The TiO_2/V_2O_5 also displays trends of increasing values with deceasing anorthite % of plagioclase (Fig. 5.26). This trend is consistent with models of decreasing anorthite and increasing albite content within an evolving melt observed within many intrusions (e.g., Bushveld: Mitchell, 1990). Figure 5.26 shows that the primitive bytownite and labradorite plagioclase with lower TiO_2/V_2O_5 values (~<100) and coincides with vanadium mineralization in Figure 5.26. Similarly, the relatively evolved andesine plagioclase is associated with higher TiO_2/V_2O_5 values (>100) and coincides with phosphorous mineralization (Fig. 5.25). It is suggested that using the TiO_2/V_2O_5 values from whole rock data, it is possible to make inferences as to the plagioclase compositions (Fig. 5.26). It should be noted that the silicate minerals (e.g., plagioclase, pyroxene, etc.) within the McFaulds Lake ferrogabbro intrusions

have undergone metamorphism and variable albitization of primary plagioclase which is evident in the little scatter observed within Figure 5.26. However, plagioclase compositions were largely analyzed from the unaltered cores and are interpreted to represent accurate An% values. Low TiO_2/V_2O_5 values are interpreted to represent ferrogabbros which contain relatively primitive, vanadium-rich magnetites, and coincide with lower anorthite contents within the plagioclase. This is consistent with microprobe analysis of magnetite and plagioclase grains within the Bushveld intrusion where precipitated magnetite plagioclase grains display positive correlations with increasing V_2O_5 wt. % within magnetite, and higher An % in plagioclase (Kruger and Smart, 1987; Eales and Cawthorn, 1996).

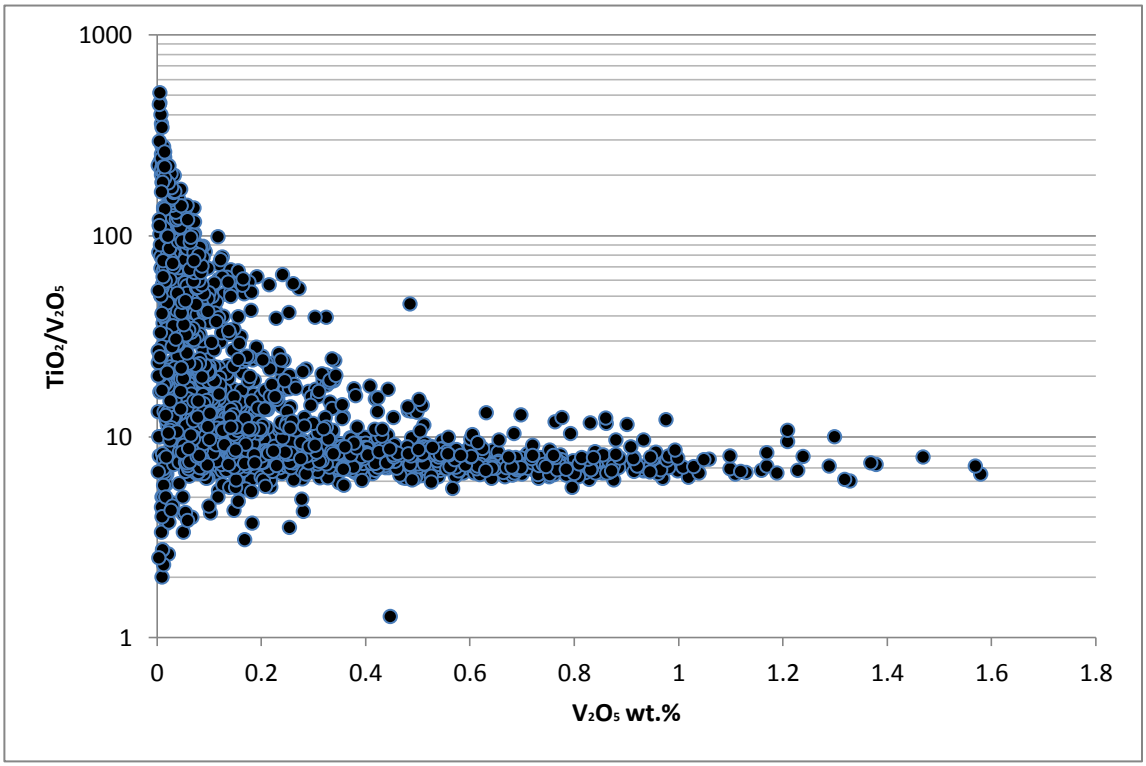

Figure 5.24. Complied TiO_2/V_2O_5 and V_2O_5 values from the Butler and Thunderbird intrusions (n=2288: courtesy of Noront Resources Ltd. and Macdonald Mines Exploration Ltd.)

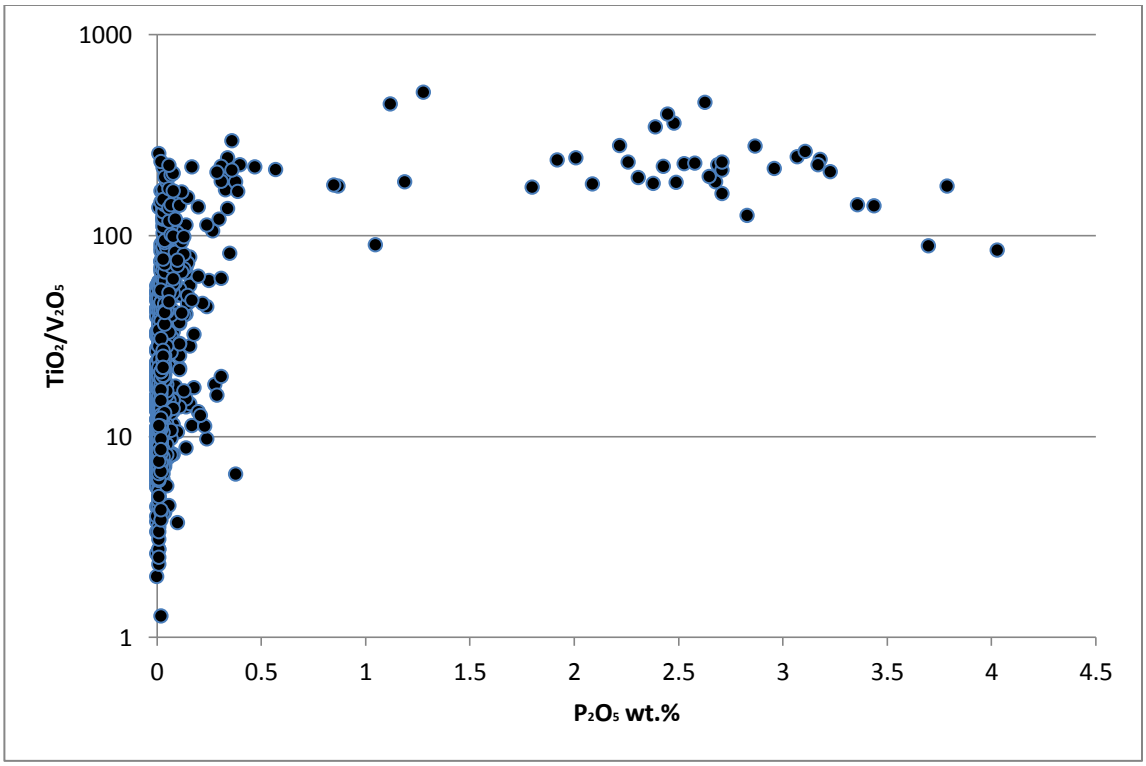

Figure 5.25. Compiled TiO_2/V_2O_5 and P_2O_5 values from the Butler and Thunderbird intrusion (n=2288: courtesy of Noront Resources Ltd. and Macdonald Mines Exploration Ltd.).

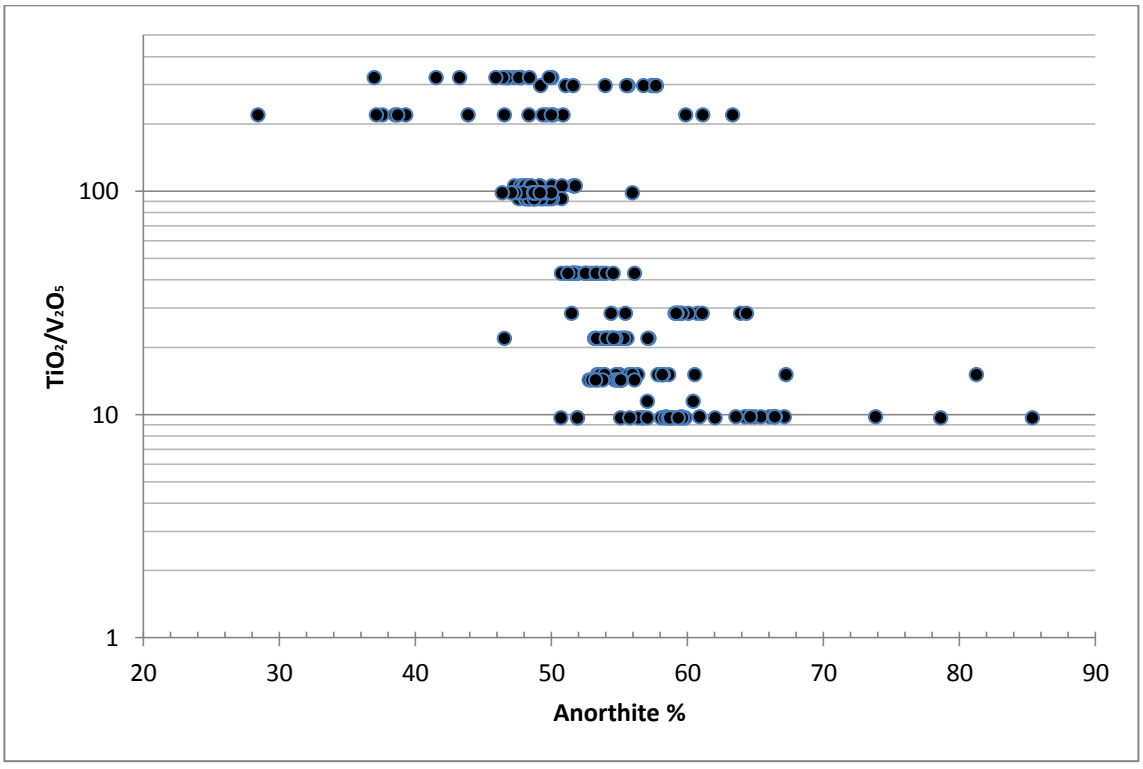

Figure 5.26. Compiled TiO_2/V_2O_5 from whole rock XRF and An % values of plagioclase from microprobe analysis from the Thunderbird and Butler intrusions.

It is proposed that the TiO_2/V_2O_5 ratio can give insight into the evolution of ferrogabbroic rocks. This ratio is a potentially transferable tool for the interpretation of magmatic stratigraphy, mineralization and mineral chemistry (plagioclase compositions) as summarized in Figure 5.27. This ratio is particularly useful in metamorphosed rocks where the silicate mineralogy may be highly deformed and altered, but the oxides remain largely unaltered (with the exception of oxy-exsolution). The use of this ratio in mineral exploration is proposed for vanadium and phosphorous mineralization, but may be extrapolated to chromium exploration in a similar method to that described for vanadium (i.e., target lower, primitive ratios). The ratio, calculated from whole-rock data (XRF) can be used to measure the degree of evolution within a magnetite-ilmenite bearing ferrogabbro intrusion. The lower values are interpreted to represent more primitive units and are suggested to have a higher potential to host vanadium-rich magnetite and labradorite dominate plagioclase (Fig. 5.27). Based on a compilation of 2288 samples from the Butler and Thunderbird intrusions, it is suggested that the highest whole-rock V_2O_5 contents are restricted to a range of values between ~5-15 which correspond to approximately 1.5 % V_2O_5 within massive oxide units, and sharply decrease with increasing TiO_2/V_2O_5 values (Fig. 5.27). Within the vanadium-rich, labradorite dominant, primitive ferrogabbro, apatite mineralization has not been observed (<0.5 P_2O_5 wt. %; Fig. 5.27). However, apatite is expected to occur within the evolved ferrogabbroic suite which can be modeled using the TiO_2/V_2O_5 values from whole rock data (>100: Fig. 5.27). Within the apatite mineralized units, andesine is the dominant plagioclase at the gradual expense of labradorite. Within the apatite-mineralized units, it is suggested that nelsonite magmas (immiscible Fe-Ti-P liquids) may be the dominate style of mineralization. Future applications should be focused more on the relationships of such mineral chemistries of pyroxene and olivine, and their relationship to the TiO_2/V_2O_5 ratio.

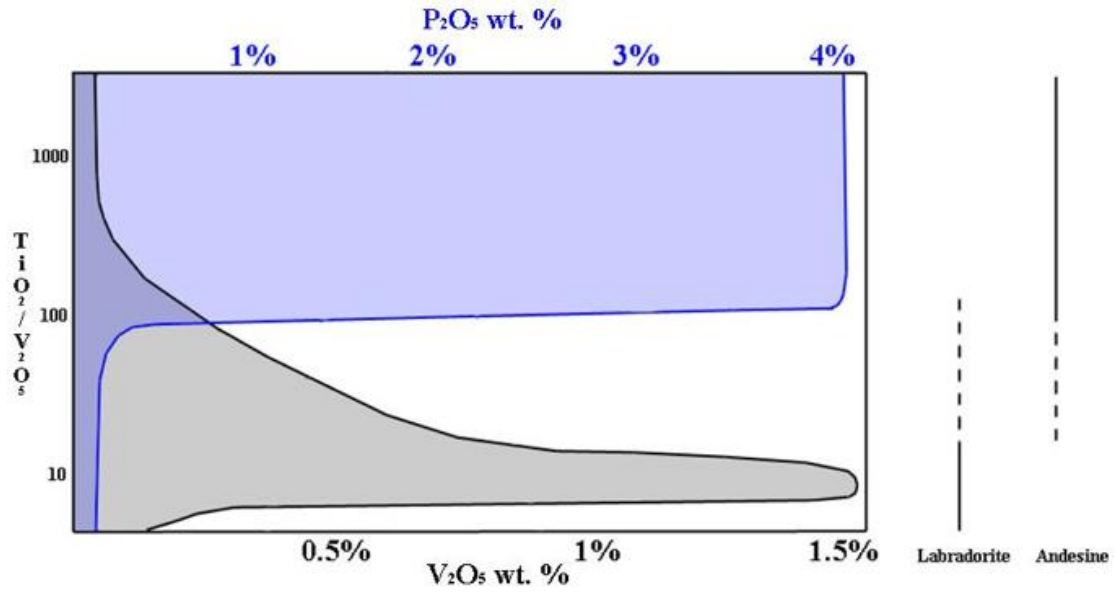

Figure 5.27. Model for the maximum vanadium and phosphorous values along with plagioclase composition in relationship to the TiO_2/V_2O_5 ratio.

5.3.1. Mineralization

5.3.1.1. Magnetite-Ilmenite-Hematite Oxy-Exsolution

Due to the pervasive occurrence of ilmenite exsolution within the magnetite, it is suggested that the primary mineralogy of these magnetite grains contained considerable ulvöspinel in solid solution, and are more accurately described as titanomagnetites. Titanomagnetite rarely occurs in plutonic environments due to the inherent instability of the ulvöspinel solid solution component and undergoes exsolution into ilmenite and magnetite phases (Bowles, 1977). This process typically occurs at subsolidious temperatures, and this study has approximated the final stages of exsolution within the McFaulds Lake ferrogabbros to have occurred at approximately 400-500^{o}C. However, it should be noted that large variations within samples and drill holes were observed. The process of titanomagnetite oxy-exsolution requires the addition of an oxidizing fluid (Buddington and Lindsley, 1964). This is typically considered to be caused by the disassociation of magmatic fluids which penetrate the rock and provide the necessary oxidation during magmatic cooling (Buddington and Lindsley, 1964). However, plutonic rocks have been proposed to exsolve as low as ~600^{o}C (Lindsley, Experimental Studies of Oxide Minerals, 1976) which is considerably higher than the temperatures calculated for the McFaulds Lake ferrogabbro. Thus, the temperatures of oxide equilibration may be the result of metamorphic overprinting. This interpretation is consistent with the amphibole + chlorite +/- garnet+/- biotite metamorphic assemblage observed throughout the intrusions, which overlaps with the temperatures of upper greenschist facies metamorphism during hydrous conditions at 450-550^{o}C (Keesman et al., 1971; Winter, 2010). The metamorphism of the ferrogabbroic intrusions was a secondary process which may have further refined the magnetite-ilmenite end members, producing nearly stoichiometrically

proportional Fe_2O_3 in magnetite and FeO-free ilmenite. It is suggested that this secondary process may have affected the vanadium contents within the primary titanomagnetite, whereby the two stage refining process (sub magmatic exsolution along with metamorphism) may have preferientially exsolved V^{3+} into the magnetite phase, and V^{4+} within the ilmenite phase (Bordage et al., 2011). If this assumption is valid, and that the oxidation state of the vanadium species is the control on the distribution of vanadium within the mineral phases, it can then be infered that the dominate vanadium species is V^{3+} and is approximatley an order of magnetitude more prevalent within the cystallizing magma (based on microprobe analysis from magnetite vs. ilmenite).

5.3.1.2. Parental Magma and Magma Dynamics

Magnetite and ilmenite are common accessory minerals in many igneous rocks (Guastoni and Appiani, 2005). The Butler and Thunderbird intrusions exhibit thick, stratigraphically conformable layers of massive and semi-massive oxides. Such iron-rich gabbroic and anorthositic intrusions have been observed globally to have originated from iron-rich parental melts that are typically associated with mantle plumes (e.g., Bushveld intrusion: Eales and Cawthorn, 1996) and/or rifting events (e.g., Sept Iles Intrusion: Namur et al., 2010). The process of iron-titanium enrichment within magmas is poorly understood, however, parental magma, oxygen fugacity, and internal processes are often cited as major controlling factors in the mineralization of these intrusions (e.g., Toplis and Carroll, 1995: Zhang et al., 2012: Hou et al., 2013). The Panzhihua ferrogabbroic intrusion is interpreted to have been derived from a slightly enriched asthenospheric melt generated from a mantle plume (Zhou et al., 2005a). The Bushveld intrusion is characterized by an Upper Zone of ferrogabbroic rocks (Eales and Cawthorn, 1996), and although the parental magma of the Bushveld is highly

debated (e.g., Gibson and Stevens, 1998; Kruger, 2002, 2005) and complicated by multiple pulses of magma (Eales and Cawthorn, 1996), the predominant theory is that the magmatism is plume related but has undergone crustal interaction (Hatton, 1995; Kinnaird, 2014). The parental magma of the McFaulds Lake ferrogabbroic rocks requires further study and detailed regional examinations. However, a Fe-Ti-rich parental magma is a prevailing theme within similar intrusions. The source of Fe-Ti enrichment within these intrusions is controlled by serveral factors, of which oxygen fugacity, pressure, and volatiles are significant parameters and are inter-related (Snyder et al., 1993; Toplis and Carrol, 1996; Veksler, 2009).

Iron enrichment along the tholeittic trend has been demonstrated through many experiments to occur within cooling mafic magmas under low pressures which favour the crystallization of plagioclase and olivine (e.g., Toplis and Carrol, 1996; Veksler, 2009). Crystallization of Fe-poor phases results in Fe-rich melts which reach their maximum Fe contents prior to the onset of magnetite crystallization (Toplis and Carrol, 1996). If a melt is to experience extreme amounts of Fe enrichment, the melt must be anhydrous and relatively reduced (fo_2 <FMQ) both conditions supress the crystallization of magnetite (Veksler I. , 2009). An Fe-Ti-rich mafic melt under reduced conditions will crystallize ilmenite prior to magnetite (e.g., Panzhihua, Skaergaard; Zhou et al., 2005a; Veksler, 2009) which results in a slight depletion of Fe contents, but more importantly increases the Fe^{3+}/Fe^{2+} ratio (i.e. oxygen fugacity) by crystallizing out Fe^{2+} within ilmenite (Zhou et al., 2005a; Veksler, 2009). As the oxygen fugacity increases, magnetite will eventually become a stable mineral phase afterwhich the magma follows a granitic-anorthositic evolution trend and a decrease in iron contents (Toplis and Carroll, 1995; Zhou et al., 2005a).

Of particular interest within Fe-Ti-rich mafic melts are the roles of phosphorous and system dynamics with regards to oxygen fuacity (Toplis et al., 1994;Toplis and Carroll, 1995, 1996). Oxygen fugacity is a significant parameter from the stability of magnetite, and as a result, controls the extent of iron enrichment within a melt (Veksler I. , 2009). Phosphorous within a ferrogabbroic melt behaves as an incompatible cation until the onset of apatite crystallization during the later stages of differentiation (Toplis et al., 1994). The concentration of phosphorous within a magma has a dramatic effect on the ferric/ferrous ratio and will cause a reduction of Fe^{3+} to Fe^{2+} which may result in the destabilization of the magnetite phase (Toplis et al., 1994). Oxygen fugacity is a dynamic variable within ferrogabbroic magmas and may either evolve within closed or open systems (Toplis and Carrol, 1996). It has been demonstrated through experimental work from Toplis and Carrol (1995; 1996), that systems closed to oxygen fugacity typically result in magnetite and ilmenite which occurs dominantly as disseminated mineralization. These systems are typically considered to be plutonic enviroments (Toplis and Carrol, 1996), and have intruded into a non-reactive host rock. Closed systems have been suggested to contain variations within Fe^{3+}/Fe^{2+} ratios during crystallization, while maintaining a fixed $Fe^{3+}+Fe^{2+}$ concentration (Toplis and Carrol, 1995; 1996). This is caused by the relative incompatability of ferric iron during the early stage crystallization of olivine, pyroxene, ilmenite, and plagioclase, thus increasing the Fe^{3+}/Fe^{2+} (i.e. oxygen fugacity). This trend of increasing Fe^{3+}/Fe^{2+} will be limited and possibly reversed by the crystallization of Fe-Ti-oxides (e.g., magnetite, hematite, ect.). In closed systems, the oxygen fugacity follows a uniquly defined trend with decreasing temperature, and is not expected to follow a predictive solid-gas buffer such as the FMQ buffer (Toplis and Carrol, 1996). Conversely, systems open to oxygen experience variations in the contents of Fe^{3+} and Fe^{2+} (with constant Fe_{total}) but will contain a constant Fe^{3+}/Fe^{2+} ratio with falling temperature (Toplis and Carrol, 1996). Open systems are

typically considered to be volcanic and generally are thought to parallel the FMQ buffer +/- 2 units (Toplis and Carrol, 1996).

The extent of iron enrichment within mafic magmas is complex and poorly understood (Toplis and Carrol, 1995; Veksler, 2009). Tholeiitic lavas typically exhibit enriched values up to ~15 wt. % FeO^t and as high as ~19 wt.% (Brooks et al., 1991), whereas residual melt compositions for the Skaergaard and Kiglapait intrusions have been suggested to contain up to 30 wt. % FeO^t (McBirney and Naslund, 1990). However, Hunter and Sparks (1987, 1990) demonstrated that the maximum iron enrichment is ~20 wt. % FeO^t and this has been experimentally verified by Toplis and Carrol (1996) with systems closed or open to oxygen, and in fractional crystallization or equillibrium crystallization. It has been suggested that intrusions with calcualted parental magma compositions containing FeO^t contents >~20 wt.% are caused by errors within the MELTS program which poorly constains Fe-Ti oxide phases (particularly ilmenite and magnetite stabilities), and the complexity associated with phosphorous (Toplis and Carrol, 1996). Regardless, it is generally acepted that a magma contains the highest proportions of FeO^t just prior to the onset crystallization of Fe-Ti oxides, whereby the magma continually decreases afterwards (Toplis and Carroll, 1995; 1996; Veksler, 2009).

The temperature at which a typical ferrogabbroic magma (based on the Skaergaard intrusion) crystallizes magnetite is dependent on the system dynamics. In closed systems, the magma crystallizes out a lesser proportion of magnetite and is generally independent of the oxidation state of the magma (Toplis and Carrol, 1996). However, the onset of magnetite crystallization is significantly affected by the oxygen fugacity within systems open to oxygen (Fig. 5.28 :Toplis and Carrol, 1996). In systems open to oxygen, the temperature of magnetite crystallization may varry as much as 50^oC between the FMQ +1 and FMQ-1 buffers (Fig. 5.28).

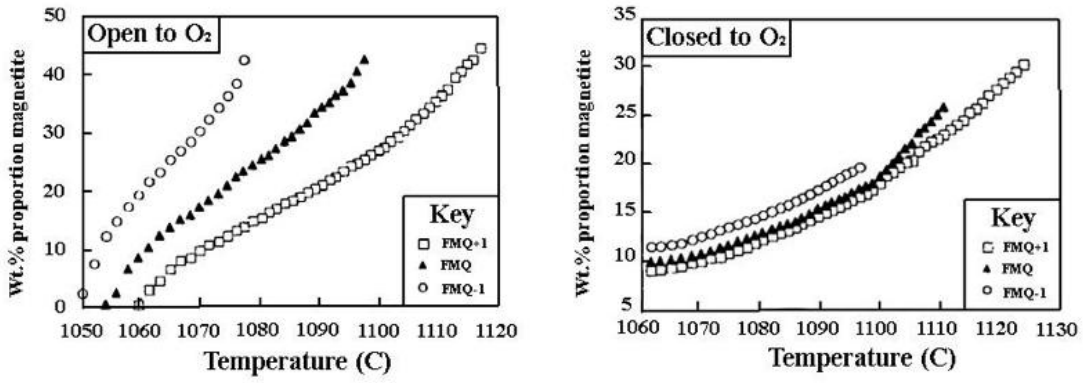

Figure 5.28 Experimentally determined Wt. % proportion of magnetite during fractional crystallization in systems open and closed of oxygen (Toplis and Carrol, 1996).

It is suggested that the Butler and Thunderbird magmas may have undergone a series of distinct evolutions (at least two stages) in order to offer an explanation to the layering and extreme iron enrichment which characterizes the intrusions. The ferrogabbroic intrusions studied are characterized by mantle-derived, positive ε_{Nd} values which are slightly enriched compared to the depleted mantle at 2735 Ma (DM ε_{Nd}= +4: DePaolo, 1981). The intrusions also display flat HREE patterns which suggests the initial melt was not in equilibrium with garnet and thus formed at depths shallower than the stability field (<60km: Wyllie, 1979). The intrusions are characterized by trace element geochemistry similar to the trends of enriched mid-ocean ridge basalt magmas (E-MORB), albeit with lower element contents (Fig. 5.29). It is proposed that the initial magma differentiated from an anhydrous, tholeiitic, reduced (<FQM buffer) source within a system closed to oxygen fugacity which would be requirements for the high degree of iron enrichment evident within the intrusions. This magma was sourced from interactions between depleted mantle and plume magma which resulted similar to that of E-MORB. Within this early first stage chamber, differentiation caused by the crystallization of Fe-poor phases (olivine and plagioclase) caused iron-titanium enrichment

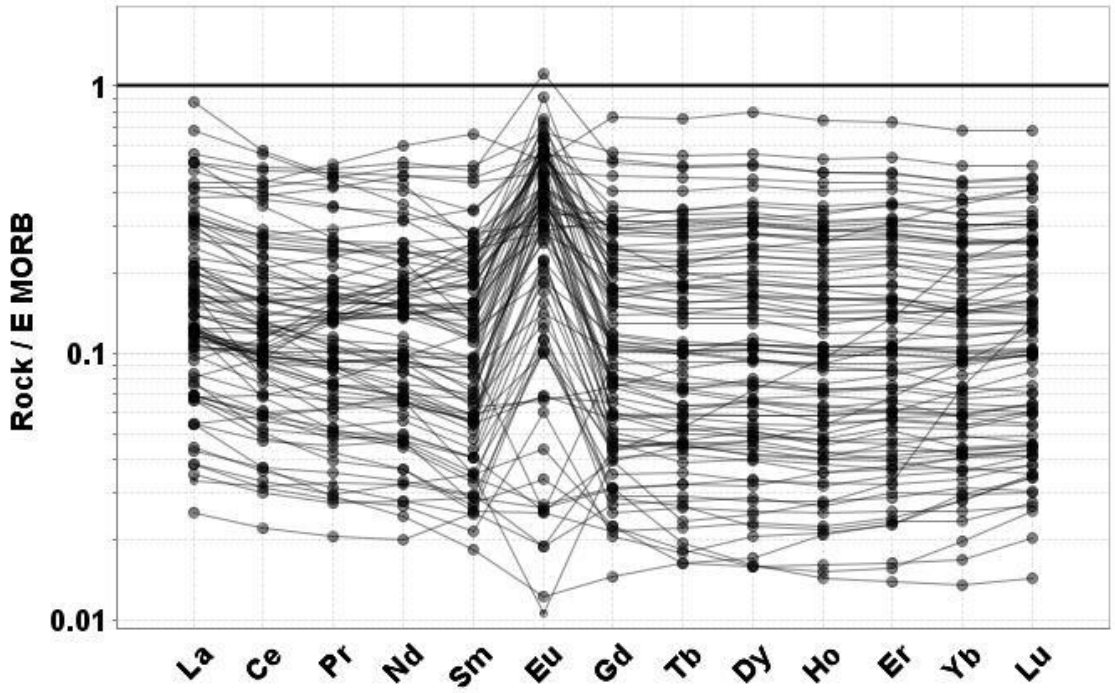

Figure 5.29 Rare Earth spider diagram displaying all samples from the Butler and Thunderbird intrusions (normalizing values from Sun and McDonough, 1989) .

within the liquid. The system is interpreted to be closed to oxygen which suppressed the onset of Fe-Ti oxide crystallization due to reducing conditions thus allowing higher degrees of iron enrichment within the liquid (Toplis and Carrol, 1996). The second and final stage is characterized by the emplacement of the Butler and Thunderbird magmas into near-surface chambers within the mafic-felsic dominated volcanic sequences of the McFaulds Lake greenstone belt. In this final stage, the system was coincident with VMS hydrothermal systems which suggests a highly fractured host rock effectively produced open system behavior with respect to oxygen, causing oxidation of the intrusions and precipitating early Cr-V-rich Fe-Ti oxides. With the onset of Fe-Ti oxide precipitation, the magma decreases in iron content and likely followed the QFM buffer. However, during the final stages of crystallization, variations within the QFM buffer will likely occur with the increase in phosphorous contents of the liquid, which has been experimentally demonstrated to reduce the oxygen fugacity of the magma

(Toplis and Carrol, 1994). This two stage model has been proposed previously for the mantle derived Panzhihua ferrogabbro intrusion (Zhou et al., 2005b; Zhou et al., 2013). Zhou et al. (2005a) suggested that the Panzihihua intrusion has been sourced from mantle material which segregated and underwent differentiation into an ultramafic and Fe-rich mafic component. The mafic melt differentiated into an extreme iron-rich melt due to the onset of plagioclase+olivine crystallization and intruded into the shallow crust (Zhou et al., 2005a). Zhou et al. (2005a) suggested the ultramafic portion was related to the coeval and abundant Fe-Cu-Ni -PGE mineralized intrusions. Alternatively, the Bushveld intrusion displays many of the same lithological and tectonic characteristics as the Panzihihua intrusion, except the differentiation occurred dominantly within a single magma chamber (Eales and Cawthorn, 1996). Within the Bushveld intrusion, a primitive Cr-PGE mineralized ultramafic basal member may be the early differentiate to the Fe-Ti-V-P mineralized ferrogabbroic Upper Zone (Eales and Cawthorn, 1996; Kruger, 2005). It is possible that the ultramafic series within the McFaulds Lake greenstone belt characterized by world class Cr (Farhangi et al., 2013; Weston and Shinkle, 2013) and significant Ni-Cu-PGE deposits (Mungall et al., 2010), may be genetically related to the Butler and Thunderbird intrusion as supported by geochronology. It is possibile that the ferrogabbroic and ultramafic intrusions of *circa* 2735 (Mungall et al., 2010), may share a common parental source that had undergone segregation into an ultramafic member, and an evolved Fe-Ti rich mafic member characterized by the Butler and Thunderbird intrusions.

5.3.1.3. Fe-Ti-V-P Mineralization

Fe-Ti-V mineralization within the Butler and Thunderbird intrusions is restricted to variable amounts of cumulate magnetite and ilmenite. These Fe-Ti oxides occur as disseminated to massive stratigraphically conformable units and typically display sharp lower

contacts which grade into plagioclase-rich gabbros and anorthosites. The exact geometry and extent of these Fe-Ti-rich layers is unknown, however, based on limited geophysical data, large linear highly magnetic features may approximate the geometry (Figs. 5.1 and 5.13). Due to the large spacing between drill holes, it is difficult to identify individual mineralized horizons.

Vanadium contents within magnetite generally exhibit positive trends of NiO and Cr_2O_3 along with negative trends with SiO_2, and Fe_2O_3 (Fig. 5.30). Ilmenite chemistry displays trends of increasing Cr_2O_3 and Fe_2O_3 with increasing vanadium and decreasing TiO_2 and FeO (Fig. 5.31). In both oxide minerals, vanadium is positively correlated with increasing chromium content which is highly compatible (Bordage et al., 2011; Liang et al., 2013), thus vanadium must behave similarly to chromium. The V-Cr-rich oxides are interpreted to have crystallized from a relatively primitive melt, rich in compatible elements (e.g., Cr and V). This is supported by elevated Ni contents in V-rich magnetite as this is believed to concentrate within early formed magnetite (Liang et al., 2013). Decreases in Fe_2O_3 within magnetite and TiO_2 and FeO within ilmenite may be caused by competition of V^{3+} and Fe^{3+} within magnetite along with V^{4+} and V^{2+} with Ti^{4+} and Fe^{2+} in ilmenite. SiO_2 contents within V-poor magnetite are likely due to the higher activity of silica within the magma during the late stage crystallization (Toplis et al., 1994) of the Thunderbird intrusion whereby the Si^{2+} substitutes for Fe^{2+}. Based on the positive trends of highly compatible elements (Cr and Ni) and vanadium within magnetite and ilmenite, it is suggested that the vanadium-rich oxides are the result of early magnetite crystallization. This observation is consistent with magnetite layers of the Bushveld and Baima intrusions, where stratigraphically lower magnetite horizons contain higher concentrations of vanadium and chromium and decrease during evolution (McCarthy and Cawthorn, 1983; Zhang et al., 2012).

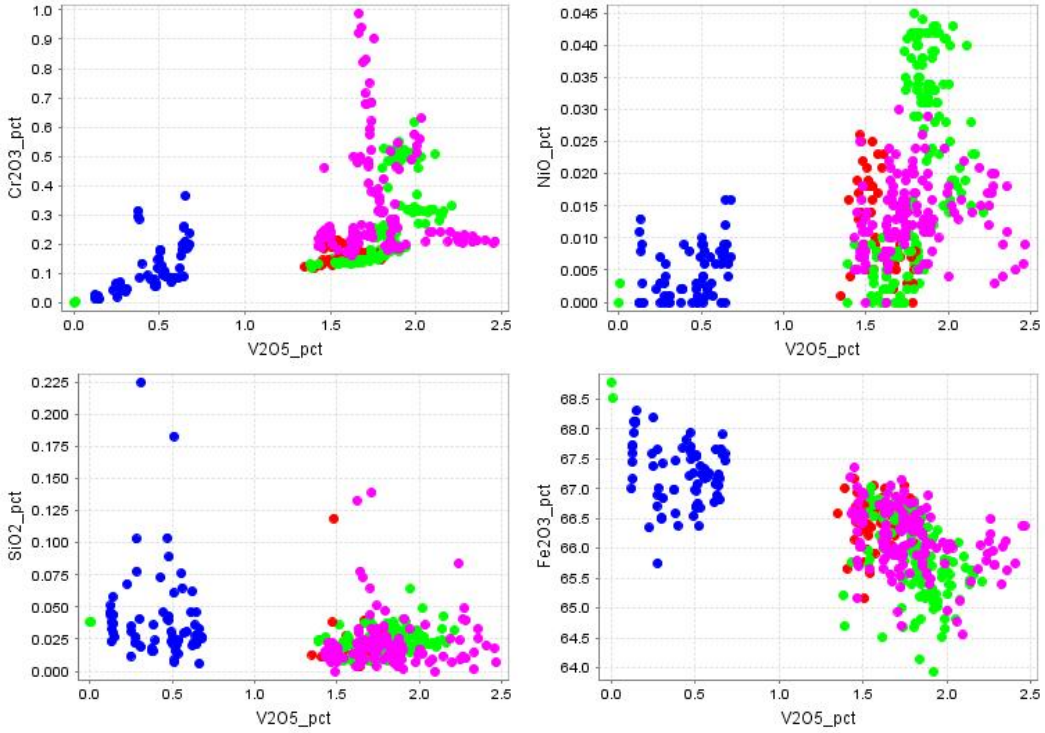

Figure 5.30. Magnetite analysis from the Butler East (red), Butler West (green), Thunderbird-V trend (pink), and Thunderbird-P trend (blue).

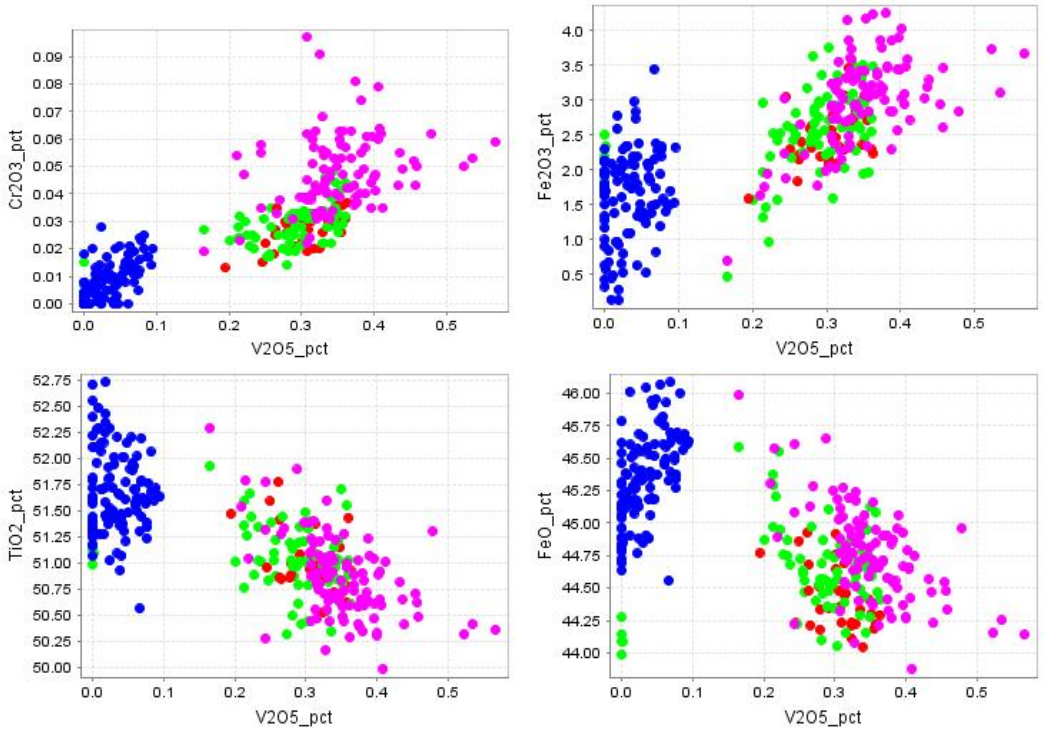

Figure 5.31. Ilmenite analysis from the Butler East (red), Butler West (green), Thunderbird-V trend (pink), and Thunderbird-P trend (blue).

Vanadium concentrations have been experimentally proven to be in part controlled by the oxygen fugacity of the crystallizing magma (e.g., Toplis and Corgne, 2002; Mallmann and O'Neil, 2009; Bordage et al., 2011). It has been demonstrated by Toplis and Corgne (2002) that vanadium partion coefficents within magnetite can decrease an order of magnetude with increasing oxygen fugacity between the NNO-7 to NNO+2.6 buffer. Their work also demonstrated that vanadium concentrations within magnetite decrease within P-bearing systems, and that divalent cations (e.g., Cr, Ni and Mn) are independent of oxygen fugacity of the magma, and thus can be proxies from the primitiveness of the magma. It has been suggested that magnetites which crystallize in reducing conditions (and lower temperatures), have a higher partition coefficient for vanadium and that vanadium contents of the magma sharpy decrease after magnetite crystallization (Toplis and Corgne, 2002). This suggests that magnetite which crystallized within relatively reducing conditions (i.e., primitive magnetite) may contain higher concentrations of V_2O_5.

Phosphorous mineralization has currently only been observed within the margins of the Thunderbird Intrusion, although anomalous phosphorous values have been observed within the Butler East (e.g., sample MM-110-2: 0.495 wt. % P_2O_5). Phosphorous mineralization within the Thunderbird intrusion reached values of up to 4.5 wt. % P_2O_5 (NO-2G46-6) along with four samples between 1.79 and 3.05 wt. % P_2O_5 in drill core from holes NOT-11-2G46 and NOT-11-2G47. Drill holes NOT-11-2G46 and NOT-11-2G47 define the phosphorous mineralized-trend, where large intersections of anomalous contents of P_2O_5 have been oberseved. Within NOT-11-2G46, a gabbroic interval averaged 2.63 wt. % P_2O_5, 28.2 % Fe_2O_3*, and 35.8 % SiO_2 over 42 meters, whereas NOT-11-2G47 averaged 2.20 wt. % P_2O_5, 26.3 % Fe_2O_3*, and 39.7 % SiO_2 over 29.86 meters. Phosphorous occurs as fine-grained, euhedral, translucent, apatite grains typically associated with anhedral fine-grained disseminated to net-textured magnetite

and ilmenite (Fig. 4.14D). Apatite mineralization is a common cumulate mineral associated with late stage differentiaion of ferrobasaltic melts (Toplis et al., 1994; Tollari et al., 2006). In extreme cases of phosphorous enrichment, a nearly pure apatite-magnetite-ilmenite assemblage (nelsonite) may occur within ferrogabbroic rocks, such as the upper part of the layered series in the Sept Iles intrusion (Tollari et al., 2008). These nelsonites are commonly believed to have formed through liquid-immicibility processes during late stage differentiaion (e.g., Hebert et al., 2005; Tollari et al., 2008; Namur et al., 2012, etc.). No such true nelsonites have been observed to date within the McFaulds Lake ferrogabbros. However, the Thunderbird intrusion contains net textured apatite-magnetite-ilmenite mineralization in a roughly 30:70 ratio (apatite:Fe-Ti oxide) which is the same aproximate proportions as many nelsonites (Reynolds, 1985; Naslund and McBirney, 1996) and are interpreted to represent an immiscibile nelsonite melt within a silicate unit (melagabbro). This Fe-Ti-P rich association offers the only possible evidence of oxide-silicate liquid immicibilty within the ferrogabbroic intrusions, though potential exisits within the margins of the Thunderbird intrusion to host true nelsonites.

Phosphorous mineralization has implications for the chemistry and dynamics of the crystallizing magma (Toplis et al., 1994). Phosphorous is considered to be generally incompatible within a ferrobasaltic melt until the late stages of crystallization when the system becomes saturated in P_2O_5 (Tollari et al., 2006). These late stage melts may contain weight percent concentrations of P_2O_5 before saturation has occurred, such as in the Skaergaard Intrusion where the melt is estimated to have contained a maximum of 1.3-1.75 wt. % P_2O_5 prior to apatite crystallization (McBirney and Naslund, 1990; Wager and Brown, 1968). Experiments have shown phosphorous to i) reduce Fe^{3+} contents in basaltic melts, ii) increase viscosity, iii) reduce denisty (Toplis et al., 1994), iv) affect the trace element chemistry of oxides

(e.g., V content in magnetite; Toplis and Corgne, 2002), and v) increase the oxide-silicate immiscibility gap (Visser and Koster, 1979; Ryerson, 1980). The reduction of ferric iron within the melt has a large effect on the stability of magnetite, whereby a P-bearing melt may be too reduced for magnetite, and favour ilmenite crystallization (Toplis et al., 1994). Phosphorous-bearing systems have been described as complex systems where the reduction of ferric iron initally results in a small change in viscosity and further addition of phosphorous results in a strong increase in viscosity (Toplis et al., 1994). The viscosity has implications for fluid dynamics within the melt (e.g. Campbell, 1996), and has been experimentally shown to increase the viscosity on the order of 15% relative per wt. % P_2O_5 at temperatures between 1100-1200^{o}C (Toplis et al., 1994). Phosphorous largely reduces the density of ferrobasaltic melts, but also counteracts the strong association of Fe-Ti oxides (Toplis et al., 1994). Phosphorous-bearing systems typically contain V-poor magnetites (Toplis and Corgne, 2002; Namur et al., 2010) which may be either related to the abundance of vanadium in an apatite-saturated melt, or due to the oxygen fugacity during crystallization which has been shown to have a large effect on trace element partioning into Fe-Ti oxides (Toplis and Corgne, 2002; Mallmann and O'Neil, 2009). At any rate, P-bearing melts are characterized by V-poor magnetite within relativly reduced conditions. These P-bearing melts have also been proposed to be more susceptible to oxide-silicate liquid immicibility than their P-free melts (Ryerson, 1980). This may be due in part to the P-Fe^{3+} polymerization (Toplis et al., 1994) which increases the Fe and P contents and promotes liquid immiscibilty (Naslund, The effect of oxygen fugacity on liquid immiscibility in iron-bearing silicate metls, 1983), particularly near the solidous temperature of a melt (Charlier and Grove, 2012).

5.4. Regional Interpretations

The McFaulds Lake greenstone belt was described by Percival et al., (1999) and with the exception of the preliminary work done by the OGS and GSC (Metsaranta and Houlé, 2012; 2013), no detailed regional compilations have been undertaken. The McFaulds Lake greenstone has been characterized as an assemblage of Neoarchean mafic to felsic volcanic rocks and subordinate metasedimentary units which have been intruded by mafic to ultramafic rocks (Mungall et al., 2010; Metsaranta and Houlé, 2012; 2013). All the lithological units and styles of mineralization within the McFaulds Lake greenstone belt must be considered in the regional interpretations in order to assess the geologic setting of the ferrogabbros.

The McFaulds Lake Cu-Zn VMS deposits weres discovered in 2003 (Mungall et al., 2010), occurs approximately 5km to the east of the Thunderbird intrusion; as well, several VMS occurences have been identified within the Butler supracrustal assemblage which are underlain by the ferrogabbroic rocks in this study. The McFaulds Lake VMS is hosted within a felsic dominated volcano-sedimentary sequence (Franklin, 2003). The rhyolites which host the VMS occurrence have been classified as dominantly FII with lesser FIII (Franklin, 2003) and to have crystallized at 2737±7 Ma (Rayner and Stott, 2005). The presence of FII rhyolites implies a high temperature rhyolitic magma which has equilibrated with plagioclase-amphibole residua at 10-30km depth, whereas FIII magma has equilibrated with a plagioclase-dominated, garnet-amphibole-free residua at <15km depth (Hart et al., 2004). This suggests a moderate (10-15km) to shallow (<10km) heat source responsible for the VMS mineralization (Hart et al., 2004).

The abundant ultramafic intrusive units hosted within the Meketi supracrustal assemblage have received the most attention within the McFaulds Lake area due to the extensive chromite and Ni-Cu-PGE mineralization (e.g., Mungall et al., 2010; Laarman et al.,

2012; Carson et al., 2013). The Black Thor intrusive complex (BTIC) has been described by Carson et al. (2013) and is tentatively composed of a lower peridoititic and dunitic zone, overlain by a chromitiferous dunitic intermediate zone, and a peridotitic to pyroxenitic to gabbroic upper zone. The BTIC formed in a conduit system from high-chromium, low-magnesium komatiitic magma (Carson et al., 2013). The BTIC is host to an indicated and inferred resource of > 102 million tonnes of chromite with thicknesses of up to 100 meters and strike lengths of up to 3km with an average grade of 31% Cr_2O_3 (Weston and Shinkle, 2013). The BTIC was later intruded by a second pulse of pyroxenite which caused brecciation of the host pyroxenite and resulted in magmatic breccia associated with Cu-Ni-PGE mineralization of the F2-Zone and NW Breccia Zone (Farhangi et al., 2013). Additionally there are zones of similar Ni-Cu-PGE mineralization possibly associated with the primary BTIC which have been termed the AT-12, AT-12 Extension and Basal Contact zones (Farhangi et al., 2013). The BTIC has been dated using U/Pb zircon from a ferrogabbro which is stratigraphically on top of the AT12 feeder dike and yielded an age of 2734.5±1.0 Ma (Mungall et al., 2010). The tonalite intrusion which forms the footwall of the BTIC was dated at 2773.37±0.9 Ma from U/Pb zircon (Mungall et al., 2010) and the hanging wall produced an age of 2770.7±0.8 Ma composed of acr-related rhyolites (Mungall et al., 2011)

Although attempts were made to date two felsic volcanic samples and a ferrogabbro of the Butler supracrustal assemblage, no age has yet been produced from this area (Metsaranta and Houlé, 2012). It is tentatively suggested that the age of volcanics (*circa* 2770 Ma), BTIC (*circa* 2734), and VMS hosted rhyolites (*circa* 2737 Ma) within the Butler are of similar age to those elsewhere in the McFaulds greenstone belt. A sample from this study for the ongoing regional work of Metsaranta (OGS) and Houlé (GSC) was collected from the Thunderbird intrusion and using U/Pb zircon produced an age of 2733.6 Ma (McNicoll pers. comm.) and is

currently the only age for the Thunderbird intrusion. It is clear from geochronological work in the McFaulds Lake area that the BTIC, Thunderbird, and McFaulds Lake VMS occurrence are broadly coeval and possibly magmatically related. Furthermore, it has been suggested by Mungall et al. (2010) that the Ni-Cr mineralization within the Bird River complex (Theyer, 1991) which was intruded along the southern margins of the same microcontinent at 2745±5 Ma (Timmins et al., 1991), may coincide with the age span of a single plume-related large igneous province.

It is suggested here that the large occurrence of highly voluminous ferrogabbro intrusions, ultramafic intrusive and volcanic rocks (Metsaranta and Houlé, 2013) and coeval FII/FIII rhyolite hosted VMS occurrences (Franklin, 2003) may be explained through a plume-related model similar to that previously proposed by Mungall et al. (2010). The plume is interpreted to have punctured the thin margins of the Oxford-Stull Domain approximately 15 million years prior to the collision of the North Caribou superterrane at circa 2720 Ma (Mungall et al., 2010). This interpretation is consistent with other ferrogabbroic intrusions which are proposed to have formed through anhydrous mantle plume processes, such as the Bushveld intrusion (Eales and Cawthorn, 1996), Midcontinent rift (Miller and Ripley, 1996), and the Emeishan large igneous province (Luo et al., 2006). The chemistry of the ferrogabbro intrusions suggests interation between a plume and depleted mantle sources which produced magmas with an E-MORB affinity. This magma mixing is thought to occur within a relativity shallow (<60km) chamber, possibly along the edges of the plume head. The voluminous ultramafic intrusions are thought to be derived from the same plume responsible for the ferrogabbro intrusions possibly from the hotter core of the plume. It is proposed that the plume was also the heat source for the VMS mineralization based on identical ages and the common association of ferrogabbroic units which underlies many VMS occurences (e.g. VMS

occurences in the Butler supracrustal assemblage and McFaulds Lake VMS: Metsaranta and Houle, 2012; 2013). Furthermore, shallow emplacement (<15km depth) of the plume caused partial melting of the crust at circa 2735 Ma and produced the FII and FIII rhyolites which host the McFaulds Lake VMS.

6. Conclusion

Fe-Ti rich gabbroic to anorthositic plutonic rocks, termed ferrogabbro, are a volumetrically significant intrusive rock within the McFaulds Lake area (e.g., Metsaranta and Houlé, 2011; 2012; 2013). Within the ferrogabbroic rocks of the McFaulds Lake area, the Butler and Thunderbird intrusions represent the best studied occurrences and have implications for ferrogabbroic rocks in the region.

The Butler and Thunderbird intrusions are largely composed of well layered medium-grained gabbroic to anorthositic rocks which typically contain between 1-5% magnetite and ilmenite. These intrusions are characterized by stratigraphically conformable massive magnetite-ilmenite horizons which exhibit variable Fe-Ti-V-P mineralization, similar to those described within the Bushveld (Eales and Cawthorn, 1996) and Panzhihua intrusions (Zhou et al., 2013). The massive Fe-Ti oxide layers typically exhibit sharp lower contacts with the underlying ferrogabbro, and grade upwards into a semi-massive oxide, to an oxide-rich pyroxenite, oxide gabbro, and lastly to an oxide-bearing leucogabbro or anorthosite. The cycles occur as partial to complete sequences and range from cm to m scale in thickness. Within these cycles, decreases in the vanadium and chromium content of the magnetite have been documented, along with general decreases in vanadium and chromium throughout the intrusion during evolution. However, TiO_2/V_2O_5 ratios within the intrusions display steady evolution trends which suggests a lack of multiple magma injections. The layering is interpreted to have been caused largely by internal convection cycles within a shallow chamber in a system which is at least partially open to oxygen. The only strong evidence for oxide-silicate liquid immiscibility within the ferrogabbros has been observed within apatite-ilmenite-magnetite bearing melagabbros within the margins of the Thunderbird intrusion. These Fe-Ti-P

mineralized sections of the Thunderbird intrusion occur as thick sequences of relatively homogenous melagabbro which contain <25% apatite+magnetite+ilmenite, but exhibit roughly the same proportions of apatite:oxide as nelsonites reported within similar ferrogabbro intrusions (Naslund and McBirney, 1996).

The ferrogabbroic intrusions are interpreted to have been sourced from an interaction between depleted mantle and a plume magma at shallow depths (<60km) which resulted in a primary composition with an E-MORB affinity. The intrusions are characterized by flat HREE patterns and positive ε_{Nd} values which are slightly enriched compared to depleted mantle at 2735 Ma. It is proposed that the initial magma was tholeiitic, anhydrous, Fe-Ti rich, and relatively reduced (compared to the QFM buffer). This primitive magma likely underwent at least a two stage differentiation characterized by contrasting environments. The first stage would have been in a closed system, relatively shallow (above the garnet stability field), and underwent differentiation due to the crystallization of Fe^{3+}-poor phases (plagioclase, olivine). The precipitation of Fe-poor phases effectively increases the Fe content of the liquid. The second stage involed the intrusion of the magmas into the McFaulds Lake greenstone belt at relativly shallow depths within a system that was open, or partially open to oxygen. Within this final stage, the ferrogabbroic rocks exhibit magnetite saturation likely due to increased oxygen fugacity caused by open system behaviour and the increase of Fe^{3+}/Fe^{2+} ratio due to crystallization of earlier Fe^{2+} phases (e.g., ilmenite, fayallite, etc.). The precipitation of early formed magnetite-ilmenite is characterized by high V-Cr values, labradorite plagioclase, and low TiO_2/V_2O_5 ratios. As the system evolves, the ilmenite:magnetite and TiO_2/V_2O_5 ratio increases, V-Cr contents within magnetite decrease, andesine plagioclase becomes increasingly dominant and apatite becomes a cumulous phases (as observed within the evolved margins of the Thunderbird intrusion).

The regional geology within the McFaulds Lake area is poorly understood (Mungall et al., 2010). The greenstone belt is characterized by two ages of volcanic strata circa 2770 and 2737 Ma(Metsaranta and Houlé, 2012). The older strata are more mafic dominated and coeval with some tonalitic intrusions (Mungall et al., 2010), whereas the younger volcanic rocks are characterized by intermediate to felsic compositions (Mungall et al., 2010; Metsaranta and Houlé, 2012, 2013). The younger volcanic strata has been interpreted to be coeval with the abundant ultramafic and ferrogabbroic intrusives and VMS mineralization (Mungall et al., 2010). Ferrogabbroic rocks, interpreted to occur stratigraphically above the ultramafic Cr-Cu-Ni-PGE mineralized Black Thor Igneous Complex have been dated at 2734.5 ± 1.0 Ma (Mungall et al., 2010) which is consistent with preliminary age dates from the Thunderbird intrusion at 2733.6 Ma (Pers. comm., McNicoll, 2014). These intrusions overlap with the ages of felsic volcanic strata that host the McFaulds Lake Cu-Zn VMS occurrence at 2737 ± 7 Ma (Rayner and Stott, 2005). It is worth noting the many VMS occurrences within McFaulds Lake greenstone belt are commonly underlain by ferrogabbro intrusions (Metsaranta and Houlé, 2011). The geochronological and spatial associations suggest that the mafic-ultramafic intrusives, VMS occurrences, and younger volcanic strata are genetically related. It is proposed that the ultramafic-mafic intrusive and volcanic rocks are plume sourced (which may have undergone variable contamination with depleted mantle sources) and may have subsequently thinned the Archean lithosphere, increasing heat to the crust and producing coeval VMS-style mineralization and associated felsic volcanic rocks. This is consistent with the large igneous province model proposed by Mungall et al. (2010) who attributed the ultramafic-mafic Bird River complex to possibly be related. The Bird River complex intruded the southern margins of the same microcontinent at 2745 ± 5 Ma (Timmins et al., 1991) which is prior to the collision of the North Caribou super terrance at 2720 Ma (Mungall et al., 2010). Ferrogabbro rocks are

commonly considered to be related to evolved portions of mafic-ultramafic suites such as the Panizihihua (Zhou et al., 2005a; Zhou et al., 2005b; Zhou et al., 2008), Bushveld (Eales and Cawthorn, 1996; Kruger, 1990; Tegner et al., 2006), Skaergaard (Humphreys, 2011; Hunter and Sparks, 1987; McBirney and Naslund, 1990), Stillwater (Ryder, 1984), and Sept Ilse intrusions (Higgins, 1991; Namur et al., 2010; Namur et al., 2012). In many intrusions (e.g., Panzihihua, Bushveld, etc.), a mantle sourced model has been proposed (Hatton and von Gruenewaldt, 1987; Zhou et al., 2005b), similar to the McFaulds Lake ferrogabbros.

The ferrogabbroic rocks which occur throughout the greenstone belt represent a volumetrically significant intrusive phase which may be genetically related to the abundant Cr-Cu-Ni-PGE bearing ultramafic intrusives and VMS-style mineralization. These ferrogabbroic rocks are poorly understood on a regional scale and this study represents the first detailed examination of Butler and Thunderbird intrusions.

References

Ashwal, L., Webb, S., & Knoper, M. (2005). Magmatic stratigraphy in the Bushveld Northern Lobe: continuous geophysical and mineralogical data from the 2950 m Bellevue drill core. *South African Journal of Geology*, pp. 199-232.

Beakhouse, G.P., McNutt, R.H., & Krogh, T.E., (1988) Comparative Rb-Sr and U-Pb zircon geochronology of late- to post-tectonic plutons in the Winnipeg River belt, northwestern Ontario, Canada. *Chemical Geology, vol. 72,* pp. 337-51.

Beard, J., & Day, H. (1986). Origin of gabbro pegmatite in the Smartville intrusive complex, northern Sierra Nevada, California. *American Mineralogist, vol. 71,* pp. 1085-99

Bennet, G., & Riley, R. (1969). Operation Lingman Lake. *Ontario Department of Mines Miscellaneous Paper 27*.

Biczok, J., Hollings, P., Klipfel, P., Heaman, L., Maas, R., Hamilton, M., Kamo, S., Friedman, R. (2012). Geochronology of the North Caribous greenstone belt, Superior Province Canada: Implications for tectonic history and gold mineralization at the Musselwhite mine. *Precambrian Research*, pp. 209-30.

Bloss, F. (1971). *Crystallography and crystal chemistry.* New York: Holt.

Bordage, A., Balan, E., Villiers, J., Cromarty, R., Juhin, A., Carvallo, C., Calas, G., Raju, S., Glatzel,P. (2011). V oxidation state in Fe-Ti oxides by high-energy resolution fluorescence-detected X-ray absorption spectroscopy. *Physics and Chemistry of Minerals, vol. 38*, pp. 449-58.

Bostok, H. (1962). Geology Lansdowne House Ontario: Ontario Geological Survey Map 4.

Bowles, J. (1977). A Method of tracing the temperature and oxygen-fugacity histories of complex magnetite-ilmenite grains. *Mineralogical Magazine, vol. 41*, pp. 103-9.

Brady, J., S., C., & Perkins, D. (2012). *Mineral Formulae Recalculation*. Retrieved April 7, 2014, from http://serc.carleton.edu/research_education/equilibria/mineralformulaerecalculation.html

Brandeis, G. (1992). Constraints on the formation of cyclic units in ultramafic zones of large basaltic chambers. *Contributions to Mineralogy and Petrology vol.112,* pp. 312-28.

Breaks, F., Osmani, I., & deKemp, E. (2001). Geology of the North Caribou Lake Area, Northwestern Ontario. *Ontario Geological Survey, Open File Report 6023*.

Brooks, C., Larsen, L., & Nielsen, T. (1991). Importance of iron-rich tholeiitic magmas at divergent plate margins: a reappraisal. *Geology, vol. 19,* pp. 269-72.

Brown, P., & Farmer, D. (1971). Size-graded layering in the Imilik gabbro, East Greenland. *Geologic Magazine, vol. 108*, pp. 456-76

Buddington, A., & Lindsley, D. (1964). Iron-Titanium Oxide Minerals and Synthetic Equivalents. *Journal of Petrology, vol. 5,* pp. 310-57

Buddington, A., Fahey, J., & Vlisidis, A. (1955). Thermometric and petrogentic significance of titaniferous magnetite. *American Journal of Science, vol. 254*, pp. 506-15.

Burnham, O., Hecler, J., Semenyna, L., & Schweyer, J. (2002). Mineralogical controls on the determination of trace elements following mixed acid dissolution. In *Summary of field work and other activities.* Ontario Geological Survey.

Burnham, O., & Schweyer, J. (2004). Trace element analysis of geological samples by ICP-MS at the Geoscience Laboratories: Revised capabilities due to improvements to instrumentation. In *Summary of field work and other activities 2004.* Ontario Geological Survey.

Buse, S., Smar, L., Stott, G., & McIlraith, S. (2009). Precambrian geology of the Winisk Lake area; Preliminary Map P.3607, scale 1:100 000. Ontario Geological Survey.

Cameron, E. (1975). Postcumulus and subsolidus equilibration of chromite and coexisting silicates in the Eastern Bushveld Complex. *Geochem. Cosmochim.*(39), pp. 1021-33.

Cameron, E. (1977). Chromite in the central sector, eastern Bushveld Complex, South Africa. *American Mineralogist* (62), pp. 1082-96.

Cameron, E. (1978). The Lower Zone of the Eastern Bushveld complex in the Olifants River trough. *Journal of Petrology*, pp. 437-62.

Campbell, I. (1996). Fluid Dynamic Processes in Basaltic Magma Chambers. In R. Cawthorn (Ed.), *Layered Intrusions* (pp. 45-76). Amsterdam: Elsevier Science, pp. 45-76.

Card, K., & Ciesielski, A. (1986). Subdivisions of the Superior Province of the Canadian Shield. *Geoscience Canada*, pp. 5-13.

Carmichael, D. (1967). The iron-titanium oxides of salic volcanic rocks and thier associated ferrmagnesian silicates. *Contributions to Mineralogy and Petrology, vol. 14*, pp. 36-64.

Carson, H., Lesher, C., Houle, M., Weston, R., & Shinkle, D. (2013). Stratigraphy, Geochemistry and Petrogenesis of the Black Thor Intrusive Complex and Associated Chromium and Nickel-Copper-Platnium Group Element Mineralization, McFaulds Lake Greenstone Belt, Ontario. In *Summary of Field Work and Other Activities 2013, Ontario Geological Survey Open File Report 6290*, pp. 521-35.

Cawthorn, R., Meyer, P., & Kruger, F. (1991). Major addition of magma at the Pyroxenite Marker in the western Bushveld Complex, South Africa. *Journal of Petrology, vol. 32*, pp. 739-63.

Charlier, B., & Grove, T. (2012). Experiments on liquid immiscibility along tholeiitic liquid lines of descent. *Contributions to Mineralogy and Petrology vol.* 164, pp. 27-44.

Chung, S., & Jahn, B. (1995). Plume-lithosphere interaction in generation of Emeishan flood basalts at the Permian-Triassic boundary. *Geology, vol. 23*, pp. 889-92.

Coffin, M., & Eldholm, O. (1994). Large igneous provinces: crustal structure, dimensions, and external consequences. *Reviews of Geophysics*, pp. 1-36.

Corfu, F., & Lin, S. (2000). Geology and U-Pb geochronology of the Island Lake greenstone belt, northwestern Superior Province, Manitoba. *Canadian Journal of Earth Sciences, vol. 37*, pp.1275-86.

Cortis, A., Ayres, L., & Thurston, P. (1989). A quartz-rich Archean fan delta, Sandy Lake, Ontario. In *Geological Association of Canada-Mineralogical Assocaition of Canada*, pp. A36.

Davis, D., & Stott, G. (2001). Geochronology of several greenstone belts in the Sachigo Subprovince, northwestern Ontario. *Ontario Geological Survey, ORF 6070.018*.

DeKemp, E. (1987). Stratigraphy, provenance and geochronology of Archean supracrustal rocks of western Eyapamikama Lake area, northwestern Ontario. *Unpublished MSc thesis, Carleton University, Ottawa, Ontario*, pp. 98

DePaolo, D., & Wasserburg, G. (1976). Nd isotopic variations and petrogenetic models. *Geophysical Research Letters, vol. 3*, pp. 249-52.

DePaolo, D. (1981). Neodymium isotopes in the Colorado Front Range and crust - mantle evolution in the Proterozoic. *Nature, vol. 291*, pp. 193-9.

Dickin, A. (2005). *Radiogenic Isotope Geology* (2 ed.). Cambridge University Press.

Droop. (1987). A general equation for estimating Fe (super 3+) concentrations in ferromagnesian silicates and oxides from microprobe analyses, using stoichiometric criteria. *Mineralogical magazine, vol. 51*, pp. 431-35.

Duke, J. (1995). Mafic/ultramfic-hosted chromite. In O. Eckstrant, W. Sinclair, & R. Thorpe (Eds.), *Geology of Canadian Mineral deposit types* (pp. 615-24). Geological Survey of Canada.

Dyar, M., Gunter, M., & Tasa, D. (2008). *Mineralogy and Optical Mineralogy* (1st ed.). Mineralogical Society of America.

Eales, H., & Cawthorn, R. (1996). The Bushveld Complex. In R. Cawthorn, *Layered Intrusions 15 Developments in Petrology*. Amsterdam: Elsevier Science B.V., pp. 181-230

Engelbrecht, J. (1985). The Chromites of the Bushveld Complex in the Nietverdiend area. *Economic Geology, vol. 80*, pp. 896-910.

Farhangi, N., Lesher, C., & Houle, M. (2013). Mineralogy, Geochemistry and Petrogenesis of Nickel-Copper-Platnium Group Mineralization in the Black Thor Intrusive Complex, McFaulds Lake Greenstone Belt, Ontario. In *Summary of Field Work and Other Activities, Ontario Geological Survey Open File Report 6290*, pp. 549-55.

Ferguson, J., & Pulvertaft, T. (1963). Contrasted styles of igneous layering in the Garder Province of South Greenland. *Mineralogical Society of America Special Paper* (1), pp. 10-21

Franklin, J. (2003). *Preliminary Review of a VMS Occurence McFauld's Lake Area, N.W Ontario For Spider Resources Inc.* Retrieved 05 26, 2014, from http://www.ucresources.net/_resources/McFaulds_VMS_Report.pdf

Gaines, R., Skinner, H., Foord, E., Mason, B., Rosenzweig, A., King, V., & Dowty, R. (1997). *Dana's New Mineralogy.* New York: John Wiley and Sons.

Gibson, R., & Stevens, G. (1998). Regional metamorphism due to anorogenic intracratonic magmatism. What drives Metamorphism and metamorphic Reactions? *Geological Socierty of London*, pp. 121-35.

Gilber, H. (1985). Geology of the Knee Lake-Gods Lake area. *Manitoba Energy and Mines Geological Report, 83-IB*, pp. 76

Gorring, M., & Naslund, H. (1995). Geochemical reversals within the lower 100m of the Palisades sill, New Jersey. *Contributions to Minerology and Petrology*, pp. 263-76.

Guastoni, A., & Appiani, R. (2005). *Minerals* (1st ed.). Richmond Hill, Ontario, Canada: Firefly Books Ltd.

Haggerty, S. E. (1976). Oxidation of Opaque Mineral Oxides in Basalts. In D. I. Rumble (Ed.), *Oxide Minerals* (pp. Hg1-98). Blacksburg, Virginia: Mineralogical Society of America, pp. Hg1-98.

Hart, T., Gibson, H., & Lesher, C. (2004). Trace element geochemistry and petrogenesis of felsic volcanic rocks associated with volcanogenic massive Cu-Zn-Pb sulfide deposits. *Economic Geology, vol. 99*, pp. 1003-13.

Hatton, C., & von Gruenewaldt, A. (1987). The geological setting and petrogenesis of the Bushveld chromite layers. In C. Stower (Ed.), *Evolution of chromium ore fields*. New York: Van Nostrand Reinhold Co, pp. 109-143.

Hatton, C. (1995). Mantle plume origin for the Bushveld and Venterdorp magmatic provinces. *Journal of African Earth Sciences, vol. 21*, pp. 571-77.

Hawthorne, F., Orberti, R., Harlow, G., Maresch, W., Martin, R., Schumacher, J., & Welch, M. (2012). IMA report, nomenclature of the amphibole supergroup. *American Mineralogist, vol. 97*, pp. 2031-48.

Hebert, C., Cadieux, A.-M., & Breemen, O. (2005). *Temporal evolution and nature of Ti-Fe-P mineralization in the anorthosite-mangerite-charnockite-granite (AMCG) suites of the south-central Grenville Province, Saguenay - Lac St. Jean area, Quebec, Canada*. Retrieved 2 15, 2014, from http://cjes.nrc.ca

Higgins, M. (1991). The origin of laminated and massive anorthosite, Sept Iles Layered intrusion, Quebec, Canada. *Contributions to Mineralogy and Petrology* vol. 106, pp. 340-54.

Hilliard, H. (1994). *The Materials Flow of Vanadium in the United States.* U.S. Department of the interior.

Hollings, P., & Kerrich, R. (1999). Trace element systematics of ultramafic and mafic volcanic rocks from the 3 Ga North Caribou greenstone belt, northwestern Superior Province. *Precambrian Research, vol. 93*, pp. 257-79.

Hollings, P., Wyman, D., & Kerrich, R. (1999). Komatiite-basalt-rhyolite volcanic associations in Northern Superior Province greenstone belts: significance of plume-arc interaction in the generation of the proto continental Superior Province. *Elsevier, vol. 46*, pp. 137-61.

Hou, T., Zhang, Z., & Piranjno, F. (2012). A new metallogenic model of the Panzhihua giant V-Ti-iron oxide deposit (Emeishan Large Igneous Province) based on high-Mg olivine-bearing wehrlite and new field evidence. *International Geology Review, vol. 54*, pp. 1721-45.

Hou, T., Zhang, Z., & Encarnacion, J. (2013). The role of recycled oceanic crust in magmatism and metallogeny: Os-Sr-Nd isotopes, U-Pb geochronology and geochemistry of picritic dykes in the Panzhihua giant Fe-Ti oxide deposit, central Emeichan large igneous province, SW China. *Contributions to Mineralogy and Petrology* vol. 165, pp. 805-22.

Hulbert, L., & von Gruenewaldt, G. (1985). Textural and compositional features of chromite in the Lower and Critical Zones of the Bushveld, south Potgietersrus. *Economic Geology, vol. 77*, pp. 1296-1306.

Humphreys, M. (2011). Silicate liquid immiscibility within the crystal mush: evidence from Ti in plagioclase from the Skaergaard intrusion. *Journal of Petrology, vol. 52*, pp. 147-74.

Hunter, R., & Sparks, R. (1987). The differentiation of the Skaergaard Intrusion. *Contributions to Mineralogy and Petrology, vol. 95*, pp. 451-61.

Hunter, R., & Sparks, R. (1990). The differentiation of the Skaergaard Intrusion. Reply to McBirney and Naslund. *Contributions to Mineralogy and Petrology, vol. 106*, pp. 248-54.

Irvine, T., & Smith, C. (1967). The ultramafic rocks of the Muskox inturion, Northwest Territories, Canada. In P. Wyllie (Ed.), *Ultramafic and Related Rocks*. New York: Wiley and Sons, pp. 38-49.

Irvine, T. (1977). Origin of chromite layers in the Muskox intrusion and other stratiform intrusions: a new interpretation. *Geology vol. 5,* pp. 273-7.

Irvine, T., Keith, D., & Todd, S. (1983). The J-M platnium-palladium reef of the Stillwater complex, Montana: II Origin by double diffusive convective magma mixing and implications for the Bushveld complex. *Economic Geology vol. 78,* pp. 1287-334.

Irvine, T. (1987). Layering and related structures in the Duke Island and Skaergaard intrusions: a new interpretation. *Geology vol. 5,* pp. 273-7.

Jackson, E. (1961). Primary textures and mineral associations in the ultramafic zone of the Stillwater complex, Montana. *U.S. Geological Survey Professional Paper vol. 358,* pp. 1-106.

Jahns, R., & Burnham, C. (1969). Experimental studies of pegmatite genesis: A model for the derivation and crystallization of granitic pegmatite. *Economic Geology, vol. 64*, pp. 843-64.

Jakobsen, J., Veksler, I., Tegner, C., & Brooks, K. (2011). Crystallization of the Skaergaard Intrusion from an Emulsion of Immiscible Iron- and Silica-rich Liquids: Evidence from Melt inclusions in Plagioclase. *Journal of Petrology, vol. 52*, pp. 345-73.

Jenner, G. (1996). Trace element geochmistry of igneous rocks: geochemical nomenclature and analytical geochemistry In:Trace element geochmistry of volcanic rocks: applications for massive sulphide exploration. Geological Association of Canada, Short Course Notes, 12.

Keesman, I., Matthes, S., Schreyer, W., & Seifert, F. (1971). Stability of Almandine in the System FeO-(Fe2O3)-Al2O3-SiO2-(H2O) at Elevated Pressures. *Contributions to Mineralogy and Petrology vol. 34,* pp. 132-44.

Kinnaird, J. A. (2014). The Bushveld Large Igneous Province. *School of Geosciences, University of the Witwatersrand*. Retrieved 06 2, 2014, from http://www.largeigneousprovinces.org/sites/default/files/BushveldLIP.pdf

Klipfel, P. (2002). Musselwhite U-Pb zircon and Ar-Ar dates: synthesis and interpretation Internal report prepared for Placer Dome. 23, pp. 23.

Kruger, F., & Smart, R. (1987). Diffusion of trace elements during bottom crystallization of double-diffusive convection systems: the magnetitite layers of the Bushveld Complex. *Journal of Volcanology and Geothermal Resources, vol. 34*, pp. 133-42.

Kruger, F., Cawthorn, R., & Walsh, K. (1987). Strontium isotopic evidence against magma addition in the Upper Zone of the Bushveld Complex. *Earth and Planetary Science Letters, vol. 84*, pp. 51-58

Kruger, F. (1990). The stratigraphy of the Bushveld Complex: a reappraisal of the Main Zone boundaries. *South African Journal of Geology, vol. 93*, pp. 376-81.

Kruger, F. (2002). Isotopic constraints on the origin of the Bushveld Complex magmas in a back-arc enviroment. *Geochimica et Cosmochimica, vol. 66*, pp. A420.

Kruger, F. (2005). Filling the Bushveld Complex magma chamber: lateral expansion, roof and floor interation, magmatic unconformities, and formation of giant chromitite, PGE and Ti-V magnetitite deposits. *Mineralium Deposita*, pp. 451-72.

Laarman, J., Barnett, R., & Duke, N. (2012). Preliminary Results of Chromite Geochemistry at the Black Label, Black Thor and Big Daddy Chromite Deposits, McFaulds Lake Greenstone Belt, Ontario. In *Summary of Field Work and Other Activities 2012: Ontario Geological Survey, Open File Report6280*, pp. 432-9.

Lacroix, S. (1987). Sillon Harricana-Turgeon (Project #37); Rapport d'activities 87. *Direction de la recherche Geologique Quebec*.

Lee, C. (1996). A Review of Mineralization in the Bushveld Complex and some other Layered Mafic intrusions. In R. Cawthorn (Ed.), *Layered Intrusions*. Amsterdam: Elsevier Science B.V., pp. 103-46.

Liang, X., Zhong, Y., Zhu, S., He, H., Yuan, P., Jianxi, Z., & Jiang, Z. (2013). The valence and site occupancy of substituting metals in magnetite spinel structure Fe3-xMxO4 (M=Cr,Mn,Co, and Ni) and thier influence on thermal stability: An XANES and TG-DSC inverstigation. *Solid state sciences, vol. 15*, pp. 122-55.

Lin, S., Corkery, M., Bailes, A., & Davis, D. (2006). Geology and geochronology of the Gods Lake Narrows area, Gods Lake greenstone belt, NW Superior Province. *Canadian Journal of Earth Sciences, vol. 43*. Pp. 749-65.

Lindsley, D. (1962). Investigations in the system FeO-Fe2O3-TiO2. *Carnegie Inst. Wash.Yearb., vol. 61*, pp. 100-6.

Lindsley, D. (1963). Equilibrium relations of coexisting pairs of Fe-Ti oxides. *Ibid., vol. 62*, pp. 60-66.

Lindsley, D. (1976). Experimental Studies of Oxide Minerals. In D. Rumble (Ed.), *Oxide Minerals: Mineralogical Societry of America Short Course Notes* . Washingston, D.C.: Mineralogical Association of America, pp. L61-88.

Lindsley, D. (1976). The crystal chemistry and structure of oxide minerals as exemplified by the Fe-Ti-oxides. In D. Rumble (Ed.), *Oxide Minerals*. Washingston ,D.C.: Mineralogical Society of America, pp. L-15.

Lipin, B. (1993). Presure inceases, the formation of chromite seams, and the development of the ultramafic series in the Stillwater Complex, Montana. *Journal of Petrography vol. 34,* pp. 955-76.

Locock, A. (2014). An Excel spreadsheet to classify chemical analyses of amphiboles following the IMA 2012 recommendations. *Computers and Geosciences, vol. 62*, pp. 1-11.

Luo, Z.-Y., Xu, Y.-G., He, B.-L., & Shi, Y. (2006). A-type granite and syenite intrusions in Emeishan large igneous provinces: products of the Emeishan plume? *International Coference on Continental Volcanism Abstracts and Program, Guangzhou, China*, pp. 63

Ma, Y., Ji, X., Li, J., Huang, M., & Min, Z. (2003). Mineral resources of Panzhihua, Sichuan Province, SW China. *Chengdu University of Technology*, *vol. 275,* pp. 275

MacDonald Mines Exploration Limited. (2012, February). *www.macdonaldmines.com.* Retrieved September 29, 2013, from http://www.macdonaldmines.com/investors/presentation

Mallmann, G., & O'Neil, H. (2009). The crystal/melt partitioning of V during mantle melting as a function of oxygen fugacity caompared with some other elements (Al,P,Ca,Sc,Ti,Cr,Fe,Ga,Y,Zr and Nb). *Journal of Petrography, vol. 50,* pp. 1765-94.

Marsh, B., & Maxey, M. (1985). On the distribution and seperation of crystals in convecting magma. *Journal of Volcanic Geothermal Resources vol. 24, pp.* 95-150.

McBirney, A. (1975). Differentiation of the Skaergaard intrusion. *Nature vol. 253,* pp. 691-4.

McBirney, A., & Noyes, R. (1979). Crystallization and layering of the Skaergaard intrusion. *Journal of Petrology vol. 20,* pp. 487-554.

McBirney, A. (1985). Further considerations of double-diffusive stratification and layering in the Skaergaard intrusion. *Journal of Petrology vol. 26,* pp. 993-1001.

McBirney, A., & Naslund, H. (1990). The differentiation of the Skaergaard Intrusion. A discussion of Hunter and Sparks. *Contributions to Mineralogy and Petrology, vol. 104*, pp. 235-40.

McBirney, A., & Hunter, R. (1995). The cumulate paradigm reconsidered. *Journal of Geology vol. 103, pp. 122-44.*

McBirney, A. (1996). The Skaergaard Intrusion. In R. Cawthorn (Ed.), *Layered Intrusions*. Amsterdam, The Netherlands: Elsevier Science, pp. 147-80.

McCarthy, T., & Cawthorn, R. (1983). The Geochemistry of Vanadiferous Magnetite in the Bushveld complex: Implications for Crystallization Mechanisms in Layered Complexes. *Mineralium Deposita vol. 18,* pp. 505-18.

Metsaranta, R., & Houle, M. (2011). McFaulds Lake Area Regional Compilation and Bedrock Mapping Project Update. In R. Easton, O. Burnham, B. Berger, G. Beakhouse, A. Bajc, J. Parker, . . . E. Debicki (Eds.), *Summary of Field Work and Other Activities*. Ontario Geological Survey, Open File Report 6270, pp. 12-1 to 12-12.

Metsaranta, R., & Houlé, M. (2012). Progress on the McFaulds Lake ("Ring of Fire") Region Data Compilation and Bedrock Geology Mapping Project. *Ontario Geological Survey, Open File Report*, pp. 43-1 to 43-12.

Metsaranta, R., & Houlé, M. (2013). An Update on Regional Bedrock Geology Mapping in the McFaulds Lake ("Ring of Fire") Region. *Summary of Field Work and Other Activities*, pp. 496-504.

Miller, J., & Ripley, E. (1996). Layered intrusions of the Duluth Complex, Minnesota, USA. In R. Cawthorn (Ed.), *Layered Intrusions*. Amsterdam, The Netherlands: Elsevier Science, pp. 257-302.

Mitchell, A. (1990). The straigraphy, petrology and mineralogy of the Main Zone of the Northwestern Bushveld. *South African Journal of Geology*, pp. 818-31.

Molyneux, T. (1974). A geological investigation of the Bushveld Complex in Sekhukhuneland and part of the Steelpoort valley. *Transinternational Geological Soceity of South Africa , vol. 77,* pp. 329-38.

Mondal, S., & Mathez, E. (2007). Origin of the UG2 chromitite layer, Bushveld Complex. *Journal of Petrology, vol. 18,* pp. 495-510.

Mumin, A., Scott, S., Somarin, A., & Oran, K. (2007). Structural Controls on Massive Sulfide Deposition and Hydrothermal Alteration in the South Sturgeon Lake Caldera, Northwestern Ontario. *Canadian Institute of Mining, Metallurgy and Petroleum, vol. 16,* pp. 83-107.

Mungall, J., Azar, B., & Hamilton, M. (2010). Eagle's Nest: a magmatic Ni-Cu-PGE deposit in the James Bay Lowlands, Ontario, Canada. *SEG Special Publication vol. 15*, pp. 539-57.

Mungall, J., Azar, B., & Hamilton, M. (2011). Ni-Cu-PGE-Cr-Fe-Ti-V and VMS Mineralization of the Ring of Fire Intrusive Suite, Ontario. Ottawa: Geological Association of Canada-Mineralogical Association of Canada, Joint Annual Meeting.

Namur, O., Charlier, B., Toplis, M., Higgins, M., Liegeois, J.-P., & Auwera, J. (2010). Crystallization Sequence and Magma Chamber Processes in the Ferrobasaltic Sept Iles Layered Intrusion, Canada. *Journal of Petrology, vol. 51, pp.* 1203-36.

Namur, O., Charlier, B., & Holness, M. (2012). Dual origin of Fe-Ti-P gabbros by immiscibility and fractional crystallization of evolved tholeiitic basalts in the Sept Iles Layered intrusion. *Lithos, vol. 154,* pp. 100-14.

Naslund, H. (1983). The effect of oxygen fugacity on liquid immiscibility in iron-bearing silicate melts. *American Journal of Science vol. 86,* pp. 359-67.

Naslund, H. (1983). The effect of oxygen fugacity on liquid immiscibility in iron-bearing silicate metls. *American Journal of Science, vol. 283*, pp. 1034-59.

Naslund, H., Turner, P., & Keith, D. (1991). Crystallization and Layered Formation in the Middle Zone of the Skaergaard intrusion. *Bulletin of Geologic Society Denmark* vol. 38, pp. 359-67.

Naslund, H., & McBirney, A. (1996). Mechanisms of Formation of Igneous Layering. In R. Cawthorn (Ed.), *Layered Intrusions*. Elsevier Science, pp. 1-76.

Navrotsky, A., & Kleppa, O. (1967). The thermodynamics of cation distributions in simple spinels. *Journal of Inorganic and Nuclear chemistry, vol. 29*, pp. 791-802.

Nielsen, P. (2010). *Drill report on the Fishhook property, BMA 523863 BMA524864 BMA 523864 and BMA 524863 areas, Thunder Bay and Porcupine Mining divisions, Ontario, Canada.* Thunder Bay North Resident Geologist's Office, assessment file AFRO# 2.44148 (AFRI# 20000005881).

Nielsen, R., & Beard, J. (2000). Magnetite-melt HFSE partitioning. *Chemical Geology, Chemical Geology vol. 164*, pp. 21-37.

Northern Shield Resources, I. (2012). *Highbank Lake Property*. Retrieved 12 3, 2012, from http://www.northern-shield.com/properties/highbank

Oberti, R., Cannillo, E., & Toscani, G. (2012). How to name amphiboles after the IMA2012 report: rules of thumb and a new PC program for monoclinic amphiboles. *Periodico di Mineralogia, vol. 81*, pp. 257-67.

Oliver, G. (1978). Ilmenite-magnetite geothermometry and oxygen barometry in granulite and amphibolite facies gneisses from Doubtful Sound, Fiordland, New Zealand. *Lithos, vol. 11*, pp. 147-53

Osborn, E. (1978). Changes in phase relations in response to change in pressure from 1 atm. to 10 kbar for the system Mg2SiO4-iron oxide-CaAl2Si2O8-SiO2. *Yrbk. Carnegie Inst. Wash. vol. 77,* pp. 784-90.

Palmer, D. (2007). *Probe Mines Limited, Victory Project, James Bay Lowlands, Ontario, report on assessment work 2005.* Thunder Bay North Resident Geologist's Office, assessment file AFRO# 2.34620.

Parks, J., Lin, S., Davis, D., & Corkery, T. (2006). New high-precision U-Pb ages for the Island Lake greenstone belt, northwestern Superior Province: implications for regional stratigraphy and the extent of the North Caribou terrane. *Canadian Journal of Earth Science, vol. 43*, pp. 780-803.

Percival, J., Breaks, F., Brown, J., Corkery, M., Devaney, J., Dube, B., McNicoll, V., Parker, J.R., Rogers, N., Sanborn-Barrie, M., Sasseville, C., Skulski, T., Stone, D., Stott, G.M., Syme, E.C., Thurston, P.C., Tomlinson, K.Y.,Whalen, J. (1999). Project 95034. Evolution of Archean continental and oceanic domains in the Western Superior province: 1999 NATMAP results. *Ontario Geological Survey Open File Report 6000, Summary of Field Work and Other Activities*, pp. 17-1 to 17-16.

Percival, J., Walen, J., Tomlinson, K., McNicoll, V., & Stott, G. (2002). Geology and tectonostratigraphic assemblages,north-central Wabigoon Subprovince, Ontario. *Geological Survey of Canada*.

Percival, J., Sanborn-Barrie, M., Skulski, T., Stott, G., Helmstaedt, H., & White, D. (2006). Tectonic evolution of the Western Superior Province from NATMAP and lithoprobe studies. *Canadian Journal of Earth Sceince, vol. 43*, pp. 1085-1117

Philpotts, A. (1967). Origin of certian iton-titanium oxide and apatite rocks. *Economic Geology vol. 63,* pp. 305-15.

Polyak, D. (2013). Vanadium. In *Mineral Commodity Summaries 2013* (pp. 178-180). Reston, Virginia: U.S. Geological Survey, pp. 178-80.

Prowatke, S., & Klemme, S. (2006). Trace element partitioning between apatite and silicate metls. *EGeochimica, vol. 70*, pp. 4513-27.

Raedeke, L., & McCallum, I. (1984). Investigations of the Stillwater Complex: Part II. Petrology and petrogenesis of the ultramafic series. *Journal of Petrology, vol. 25*, pp. 395-420.

Rayner, N., & Stott, G. (2005). Discrimination of Archean domains in the Sachigo Subprovince: a progress report on the geochronology. In C. Baker, E. Debicki, R. Kelly, J. Ayer, R. Easton, & Z. Madon (Eds.), *Summary of Field Work and Other Activities*. Ontario Geological Survey, pp. 10-11.

Reynolds, I. (1985). Contrasting mineralogy and textural relationships in the uppermost titaniferous magnetite layers of the Bushveld Complex in the Bierkraal area north of Rustenburg. *Economic Geology vol. 80,* pp. 1027-48.

Richard, P., Shimizu, N., & Allegre, C. (1976). 143Nd/147Nd, a natural tracer: an application to oceanic basalts. *Earth and Planetary Science Letters , vol. 31*, pp. 269-73.

Robins, B., Haukvik, L., & Jansen, S. (1987). The organization and internal structure of cyclic units in the Honningvag intrusive suite, North Norway: implications for intrusive mechanisms, double-diffusive convection and pore-magma infiltration. In I. Parsons (Ed.), *Origins of Igneous Layering*. Dordrecht Reidel, pp. 287-312.

Rumble III, D. (1970). Thermodynamic analysis of phase equilibria in the system Fe2TiO4=Fe3O4-TiO2. *Carnegie Institution of Washington Year Book, vol. 69*, pp. 198-207.

Rumble III, D. (1977). Configurational entropy of magnetite-ulvospinel and hematite-ilmenite. *Carnegie Institution of Washington Year Book, vol. 76*, pp. 581-4.

Ryder, G. (1984). Oxidation and layering in the Stillwater intrusion. *Geological Society of America* vol. 16, pp. 642.

Ryerson, F. (1980). The role of P2O5 in silicate melts. *Geochemica et Cosmochemica Acta, vol. 44*, pp. 611-24.

SACS. (1980). Stratigrphy of South Africa. *Geological Survey of South Africa* vol. 8, pp. 690.

Scoates, J., & Friedman, R. (2008). Precise age of the platiniferous Merensky Reef, Bushveld Complex, Southern Africa, by the U-Pb zircon chemical abrasion ID-TIMS technique. *Econmic Geology*, pp. 465-71.

Sen, G., & Presnall, D. (1984). Liquidusphases relationships on the join anorthite-forsterite-quarts and 10 kbar with applications to basalt genesis. *Contributions to Mineralogy and Petrology* vol. 85, pp. 4004-8.

Skulski, T., Corkery, M., Stone, D., Whalen, J., & Stern, R. (2000). Geological and geochemical investigations in the Stull Lake - Edmund Lake greenstone belt and granitoid rocks of the northwestern Superior Province. *Manitoba Industry, Trade and Mines, Manitoba Geological Survery*, pp. 12.

Smith, T., & Longstaffe, F. (1974). Archean rocks of shoshonitic affinities at Bijou Point, northwestern Ontario. *Canadian Journal of Earth Sciences, vol. 11,* pp. 1407-13.

Snyder, D., Carmichael, I., & Wiebe, R. (1993). Experimental study of liquid evolution in an Fe-rich, layered mafic intrusion: contraints of Fe-Ti oxide precipitation on the T-fO2 and T-p paths of tholeiitic magmas. *Contributions o Mineralogy and Petrology, vol. 113,* pp. 73-86.

Song, X., Zhou, M.-F., Hou, Z., Cao, Z., Wang, Y., & Li, Y. (2001). Geochemical contraints on the mantle source of the Upper Permian Emeishan continental flood basalts, southwestern China. *Internations Geology Review, vol. 43*, pp. 213-25.

Sorensen, H., & Larsen, L. (1987). Layering in the Ilimaussaq Alkaline intrusion South Greenland. In I. Parsons (Ed.), *Origins of Igneous Layering*. Dordrecht: Reidel, pp. 1-28.

Spencer, K., & Linsley, D. (1981). A solution model for coexisting iron-titanium oxides. *American Mineralogist, vol. 66*, pp. 1189-1291.

Stevenson, R., & Turek, A. (1992). An isotope study of the Island Lake Greenstone Belt, Manitoba: curstal evolution and progressive cratonization in the late Archean. *Canadian Journal of Earth Sciences, vol. 29*, pp. 2200-10.

Stormer, J. (1983). The effects of recalculation on estimates of temperature and oxygen fugacity from analysis of multicomponent iron-titanium oxides. *American Mineralogist, vol. 68*, pp. 586-94.

Stott, G., & Wilson, A. (1986). Precambrian geology of the Muskegsagagen-Bancroft lakes area;Ontario Geological Survey, Map 2507, scale 1:50 000.

Stott, G., Corfu, F., Breaks, F., & Thurston, P., (1989) Multiple oogenesis in northwestern Superior Province; Geological Association of Canada-Mineralogical Association of Canada, Program with Abstracts, vol. 14.

Stott, G., & Corfu, F. (1991). Uchi subprovince. In P. Thurston, H. Williamsn, R. Sutchliffe, & G. Stott (Eds.), *Geology of Ontario*. Ontario Geological Survery, pp. 145-238.

Stott, G. T., Leclair, A., Boily, M., & Percival, J. (2007). A revised terrane map for the Superior Province as interpreted from aeromagnetic data. *Institute on Lake Superior Geology, vol. 53*, pp. 74-5.

Stott, G. (2008). Superior Province: terrances, domains and autochthons. Thunder Bay.

Stott, G., Corkery, M., Percival, J., Simard, M., & Goutier, J. (2010). A revised terrane subdivion of the Superior Province. *Summary of Field Work and Other Activities*.pp. 20-1 to 20-10

Sun, S., & McDonough, W. (1989). Chemical and isotopic systematics of oceanic basalts: implications for mantle composition and processes. *Geological Societry, London, Special Publications, vol. 42*, pp. 313-45

Tang, H. (1984). The Panzhihua V-Ti-magnetite deposits. In *Panxi Geological Team of Sichuan Geological Survey.* Research Report of Metallogeny and its Prediction (unpublished).

Taylor, R. (1964). Phase equilibria in the system FeO-Fe2O3-TiO2 at 1300^{o} C.*The American Mineralogist, vol. 49*, pp. 1016-30.

Tegner, C., Cawthorn, R., & Kruger, F. (2006). Cyclicity in the Main and Upper Zones of the Bushveld Complex, South Africa: Crystallization from a Zoned Magma Shear. *Journal of Petrology*, *vol. 47,* pp. 2257-79.

Teigler, B. (1990). *Minerology, petrology, and geochemistry of the Lower and Lower Critical Zones, Northwestern Bushveld Complex.* Grahamstown: Unpublished Ph.D. thesis Rhodes University.

Theyer, P. (1991). Petrography, chemistry and distribution of platnium and palladium in ultramafic rocks of the Bird River Sill, SE Manitoba, Canada. *Mineralium Deposita, vol. 26*, pp. 165-74.

Thurston, P., Sage, R., & Siragusa, G. (1979). Geology of the Winisk Lake area, District of Kenora, Patricia Portion. *Ontario Geological Survey Report vol. 193*, pp. 169.

Thurston, P., & Chivers, K. (1990). Secular variation in greenstone sequence development emphasizing Superior Province, Canada. *Precambrian Research*, pp. 21-58.

Thurston, P., Osmani, I., & Stone, D. (1991). Northwestern Superior Province:Review and terrane analysis. In P. H. Thurston, R. Sutcliffe, & G. Stott, *Geology Ontario: Ontario Geological Survey Special Volume 4, Part 1.* Ontario Geological Survey.

Timmins, E., Turek, A., & Symons, D. (1991). U-Pb zircon geochronology and paleomagnetism of the Bird River greenstone belt, Manitoba. Geological Societry of Canada/Mineralogical Association of Canada Program with Abstracts.

Tollari, N., Toplis, M., & Barnes, S.-J. (2006). Predicting phosphate saturation in silicate magmas: An experimental study of the effects of melt composition and temperature. *Geochimica, vol. 70,* pp. 1518-36.

Tollari, N., Barnes, S.-J., Cox, R., & Nabil, H. (2008). Trace element concentrations in apatites from the Sept-Iles Intrusive Suite, Canada-Implications for the genesis of nelsonites. *Chemical Geology, vol. 252*, pp. 180-90

Tomlinson, K., Bowins, R., & Heshler, J. (1998). Refinement of hafnium (Hf) and zirconium (Zr) analysis by improvement in the sample digestion procedure. *Ontario Geological Survey, Miscellaneous Paper vol. 169*, pp. 189-92.

Toplis, M., Dingwell, D., & Libourel, G. (1994). The effect of phosphorus on the iron redox ratio, viscosity, and density of an evolved ferro-basalt. *Contributions to Mineralogy and Petrology vol. 117,* pp. 293-304.

Toplis, M., & Carroll, M. (1995). An Experimental Study of the Influence of Oxygen Fugacity on Fe-Ti-Oxide Stability, Phase Relations, and Mineral-Melt Equilibrium in Ferro-Basaltic Systems. *Journal of Petrology, vol. 36*, pp. 1137-70.

Toplis, M., & Carrol, M. (1996). Differentiation of Ferro-Basaltic Magmas under Conditions Open and Closed to Oxygen: Implications for the Skaergaard Intrusion and Other Natural Systems. *Journal of Petrology, vol. 37*, pp. 837-58.

Toplis, M., & Corgne, A. (2002). An experimental study of element partitioning between magnetite, clinopyroxene and iron-bearing silicate liquids with particular emphasis on vanadium. *Contributions to Mineralogy and Petrology, vol. 144*, pp. 22-37.

Turek, A., Carson, T., Smith, P., Van Schmus, W., & Weber, W. (1986). U-Pb zircon ages for rocks from the Island Lake greenstone belt, Manitoba. *Canadian Journal of Earth Sciences, vol. 23*, pp. 92-101.

Ulmer, G. (1969). Experimental investigations of chromite spinels. In H. Wilson (Ed.), *Magmatic Ore Deposits*. Economic Geology Monograph 4, pp. 114-31.

Veksler, I. (2004). Liquid immiscibility and its role at the magmatic-hydrothermal transistion: a summary of experimental studies. *Chemical Geology, vol. 210*, pp. 1270-98.

Veksler, I. (2009). Extreme iron enrichment and liquid immiscibility in mafic intrusions: Experimental evidence revisited. *Lithos*, pp. 72-82.

Vermaak, C. (1976). The Merensky Reef-thoughts on its environment and genesis. *Economic Geology*, *vol. 71*, pp. 1270-98.

Villeneuve, M. (2011). An overview of Natural Resrouces Canada's Targeted Geoscience Initiative 4: enhancing the effectivness of deep exploration. In *Summary of Field Work and Other Activities*. Ontario Geological Survey, pp. 36-41.

Visser, W., & Koster, G. (1979). Effects of P2O5 and TiO2 on liquid-liquid equilibria in the system K2O-FeO-Al2O3-SiO2. *American Journal of Science, vol. 279*, pp. 970-88.

von Gruenewaldt, G. (1973). The Main and Upper Zone of the Bushveld in the Roossenekal area, eastern Transvaal. *Transinternational Geological Society of South Africa, vol. 76*, pp. 207-27.

Wager, L., & Brown, G. (1968). *Layered Igneous Rocks.* Edinburgh: Oliver and Boyd.

Walker, L. (1969). The Palisades sill, New Jersey: a reinvestigation. *Geologic Society of America Special Paper*, pp. 1-178.

Wallace, H. (1985). Geology of the Slate Falls area; Ontario Geological Survey, Report 232.

Weston, R., & Shinkle, D. (2013). Geology and stratigraphy of the Black Thor and Black Label chromite deposits, James Bay Lowlands, Ontario, Canada. Uppsala, Sweden: Society for Geology Applied to Minerals, 12th SGA Biennial Meeting.

White, J. (1994). The Potgietersrus prospect- geology and exploration history. In C. Anhaeusser (Ed.), *Proc. XVth CMMI Congress*. Johannesburg: South African Institute of Mining Metal. *vol. 3,* pp. 173-81.

Williams, H. (1991). Quetico Subprovince. In P. Thurston, H. Williams, R. Sutcliffe, & G. Stott (Eds.), *Geology of Ontario.* Geological Survey of Canada.

Wilson, J., Robins, B., Nielsen, F., Duchesne, J., & Vander Auwere, J. (1996). The Bjerkreim-Sokndal Layered Intrusions, Southwest Norway. In R. Cawthorn (Ed.), *Layered Intrusions*. Amsterdam, The Netherlands: Elsevier Science, pp. 231-56.

Winter, J. (2010). *Principles of Igneous and Metamorphic Petrology* (2nd ed.). Upper Saddle River, New Jersey: Pearson Education, Inc.

Wyllie, P. (1979). Magmas and volatile components. *American Mineralogist, vol. 64*, pp. 469-500

Wyman, D., Hollings, P., & Biczok, J. (2011). Crustal evolution in a cratonic nucleus: Granitoids and felsic volcanic rocks of the North Caribous Terrane, Superior Province Canada. *Lithos*, pp.37-49.

Xu, Y., Chung, S., Jahn, B., & Wu, G. (2001). Petrologic and geochemical constrints on the petrogenesis of Permian-Triassic Emeishan flood basalts in southwestern China. *Lithos, vol. 58*, pp. 145-68.

Zhang, X., Lou, Y., & Yang, X. (1988). The Panxi Rift: Beijing. *Geological Press*, pp. 422.

Zhang, X.-Q., Song, X.-Y., Chen, L.-M., Xie, W., Yu, S.-Y., Zheng, W.-Q., Deng, Y.-F., Zhang, J.-F., Gui, S.-G. (2012). Fractional crystallization and the formation of thick Fe-Ti-V oxide layers in the Baima Layered Intrusion, SW China. *Ore Geology Reviews vol. 49,* pp. 96-108.

Zhou, M.-F., Yang, Z., Song, X., Keays, R., & Lesher, C. (2002). Magmatic Ni-Cu-(PGE) sulfide deposits in China. In L. Cabri (Ed.), *The Geology, Geochemistry, Mineralogy, Mineral*

Beneficiation of the Platnium-Group Elements. Canadian Institute of Mining, Metallurhy and Petroleum, pp. 619-36.

Zhou, M.-F., Wang, C., Pang, K.-N., & Shellnutt, G. (2005a). Origin of giant Fe-Ti-V oxide deposits in layered gabbroic intrusions, Pan-Xi district, Sichuan Province, SW China. *Springer*, pp. 511-3

Zhou, M.-F., Robinson, P., Lesher, M., Keys, R., Zhang, C.-J., & Malpas, J. (2005b). Geochemistry, Petrogenesis and Metallogenesis of the Panzhihua Gabbroic Layered Intrusion and Associated Fe-Ti-V Oxide Depoits, Sichuan Province, SW China. *Journal of Petrology, vol. 46*, pp. 2253-80.

Zhou, M.-F., Arndt, N., Malpas, J., Wang, C., & Kennedy, A. (2008). Two magma series and associated ore deposit types in the Permian Emeishan large igneous province, SW China. *Lithos, vol. 103*, pp. 352-68.

Zhou, M.-F., Chen, W., Wang, C., Prevec, S., Pingping, L., & Howarth, G. (2013). Two stages of immiscible liquid seperation in the formation of Panzhihua-type Fe-Ti-V oxide despoits, SW China. *Geoscience Frontiers vol. 4,* pp. 481-502.

Appendix A

Petrographic descriptions

List of Abbreviations

Vy-Fn	Very-Fine
Fn	Fine
Md	Medium
Cs	Coarse
Peg	Pegmatitic
Tr	Trace

Slide#	Rock Type
MM-V1-1	SMO-Melagabbro

Transmitted

Mineral	%	Grain size	Habit	Comments
Plagioclase	4	Md	Euhedral	Plagioclase exhibits deformation twins, undulose extinction, and subgrain boundaries. The grains also contain numerous very fine-grained inclusions of amphibole crystals.
Amphibole	13	Fn	Subhedral	Anhedral to subhedral fine to very fine-grained blue/green (PPL) amphibole occur throughout sample and exhibits subgrain boundaries, simple twins, and compositional zoning.
Biotite	2	Fn	Euhedral	Brown (PPL) biotite laths occur throughout sample.
Garnet	5	Fn	Euhedral	Inclusion-free euhedral garnet occur spatially associated with magnetite-ilmenite grains.
Chlorite	1	Vy-Fn	Subhedral	Chlorite occurs throughout and replaces amphiboles.

Reflected

Mineral	%	Grain size	Habit	Comments
Magnetite	40	Fn	Subhedral	Rounded magnetite aggregates contain abundant tabular to rounded ilmenite grains.
Ilmenite	35	Fn	Subhedral	Ilmenite occurs as tabular to rounded grains within a magnetite matrix. Rare medium-grained ilmenite contains exsolution lamellae of magnetite.
Chalcopyrite	tr	Vy-Fn	Anhedral	Very fine-grained chalcopyrite occurs disseminated throughout.

General Notes:

The sample is a massive, fine- to medium-grained, garnet-bearing semi-massive oxide melagabbro. The sample is characterized by euhedral plagioclase grains within very fine-grained needle-like amphibole grains and intercumulous magnetite-ilmenite.

The oxides are magnetite dominant with granular to tabular ilmenite which occurs within a matrix of rounded magnetite grains. Rare medium-grained subhedral grains of ilmenite contains exsolution lamellae of hematite

Slide#	Rock Type
MM-V1-2	OR-Leucogabbro

Transmitted

Mineral	%	Grain size	Habit	Comments
Plagioclase	35	Md	Euhedral	Plagioclase commonly contains deformation twins and/or minor compositional zoning. The grains typically contian~5% inclusions of very fine-grained amphibole needles.
Amphibole	10	Fn	Subhedral	Occurs as inclusions within plagioclase, and as fine- to medium grains distinct blue/green grains.
Clinopyroxene	Tr.	Fn	Euhedral	Typically is spatially associated with magnetite-ilmenite grains.
Biotite	2	Fn	Euhedral	Disseminated throughout.
Garnet	12	Fn	Euhedral	Perfect euhedral crystals which are contacting Fe-Ti oxides grains.
Carbonate	Tr	Fn	Anhedral	Occurs within sub mm cross cutting veinlets.

Reflected

Mineral	%	Grain size	Habit	Comments
Magnetite	30	Fn	Anhedral	Occurs as blebs with inclusions of ilmenite. The surface is pervasively pitted.
Ilmenite	10	Fn	Subhedral	Occurs both as anhedral blebs and subhedral laths within, and surrounding magnetite grains. Ilmenite contains minor magnetite exsolutions (<2%).
Pyrite	Tr	Vy-Fn	Anhedral	Blebs of pyrite occur disseminated.
Chalcopyrite	tr	Vy-Fn	Anhedral	Occurs alongside pyrite grains.

General Notes:

The sample is largely composed of medium-grained euhedral plagioclase within a net textured massive oxide. The oxides are dominantly composed of anhedral magnetite with ilmenite laths and blebs. The oxides are surrounded by euhedral crystals of garnet. Plagioclase contains ~5% very fine-grained inclusions of amphibole crystals.

Slide#	Rock Type
MM-V1-3	O-Leucogabbro

Transmitted

Mineral	%	Grain size	Habit	Comments
Plagioclase	65	Md	Euhedral	Plagioclase occurs as 'bent' grains with deformation twins and rare undulose extinction.
Amphibole	20	Fn	Euhedral	Euhedral to subhedral, and occurs as a replacement mineral after pyroxene.
Clinopyroxene	5	Fn	Euhedral	Occurs as clusters completely surrounded by secondary amphibole grains.
Biotite	Tr	Fn	Euhedral	Disseminated brown/red laths.

Reflected

Mineral	%	Grain size	Habit	Comments
Magnetite	6	Fn	Anhedral	Occurs as disseminated fine grains of magnetite.
Ilmenite	4	Fn	Subhedral	Almost lath shaped, ilmenite occurs in proximity to magnetite and rarely contains very fine-grained hematite exsolutions.
Hematite	Tr.	Vy-Fn	Lamellae	Hematite occurs solely as very fine lamellae within ilmenite grains.

General Notes:

Clinopyroxene occurs as clusters surrounded by secondary amphibole. Plagioclase is commonly 'bent' with abundant deformation twins. Magnetite and ilmenite occurs as disseminated grains, typically distinct with only minor very fine-grained hematite exsolutions within ilmenite laths.

Slide#	Rock Type
MM-V1-4	Massive oxide

Transmitted

Mineral	%	Grain size	Habit	Comments
Plagioclase	tr	Vy-Fn	Anhedral	Partially to completely replaced by epidote and clinozoisite within relict medium-grained plagioclase boundaries.
Amphibole	7	Fn	Subhedral	Green-blue amphibole partially replaced by chlorite.
Almandine	2	Fn	Euhedral	Red euhedral garnet occurs dominantly in clusters and contains only trace aphanitic inclusions of silicate minerals.
Chlorite	Tr	Fn	Subhedral	Partially replaces amphibole.
Biotite	Tr	Fn	Anhedral	Red biotite occurs within magnetite-ilmenite aggregates.
Epidote	6	Vy-Fn	Subhedral	Pale green epidote occurs throughout but dominantly within relict plagioclase boundaries.
Clinozoisite	Tr	Vy-Fn	Anhedral	Colourless (PPL) with anomalous blue (XPL) and associated with epidote.

Reflected

Mineral	%	Grain size	Habit	Comments
Magnetite	70	Md	Anhedral	Magnetite blebs contain no ilmenite lamellae.
Ilmenite	15	Fn	Euhedral	Subhedral to euhedral ilmenite occurs as tabular crystals within massive magnetite.
Pyrite	Tr	Fn	Anhedral	Partially replacing pyrrhotite.
Pyrrhotite	Tr	Fn	Anhedral	
Chalcopyrite	Tr	Fn	Anhedral	Occurs as inclusions within pyrrhotite.

General Notes:

The sample is a fine-grained, garnet-bearing massive oxide. The oxides are magnetite dominated which contain no ilmenite lamellae. The ilmenite occurs as discrete euhedral tabular crystals within massive magnetite. The primary plagioclase has partially to completely been replaced by secondary epidote, clinozoisite, and chlorite.

Slide#	Rock Type
MM-V1-5	Massive Oxide

Transmitted

Mineral	%	Grain size	Habit	Comments
Plagioclase	3	Md	Euhedral	Plagioclase is partially replaced, and contains minor deformation twins.
Clinopyroxene	tr	Fn	Euhedral	Fine- to very fine-grained clinopyroxene occurs throughout the sample and commonly exhibits simple twins.
Almandine	10	Md	Euhedral	Fine- to medium-grained and commonly fractured.
Amphibole	5	Fn	Subhedral	Blue-green amphibole occurs as very fine- to fine-grained subhedral crystals.
Biotite	tr	Fn	Euhedral	Red/brown biotite occurs proximal to amphibole and clinopyroxene.
Chlorite	tr	Fn	Euhedral	Green chlorite occurs disseminated throughout, and as micro veinlets.

Reflected

Mineral	%	Grain size	Habit	Comments
Magnetite	60	Md	Anhedral	Contains minor (<5%) fine ilmenite exsolution.
Ilmenite	20	Md	Anhedral	Ilmenite occurs within magnetite as exsolution lamellae, but dominantly as medium-grained anhedral/subhedral crystals.
Pyrite	2	Fn	Anhedral	Disseminated throughout sample.
Chalcopyrite	Tr	Fn	Anhedral	Disseminated throughout sample.

General Notes:

The sample is a fine- to medium-grained massive oxide dominantly composed of magnetite. The ilmenite dominantly occurs as discrete fine- to medium-grained crystals, and to a lesser extent as exsolution within magnetite. Almandine garnet occurs throughout and is commonly fractured. Plagioclase is partially replaced and contains deformation twins.

Slide#	Rock Type
MM-V1-6	Anorthosite

Transmitted

Mineral	%	Grain size	Habit	Comments
Plagioclase	95	Md-Cs	Euhedral	Contains abundant deformation twins, with lesser simple twins and weak compositional zoning. Grains also contain ~3-5% very fine-grained inclusions of amphibole needles.
Amphibole	4	Fn	Subhedral	Blue-green amphibole occurs as disseminated grains, as sub-mm veins, and as inclusions within plagioclase.
Epidote	1	Fn	Subhedral	Occurs only within sub-mm veinlets.
Chlorite	Tr	Fn	Euhedral	Occurs both disseminated and within sub-mm veinlets.
Biotite	Tr	Fn	Euhedral	Disseminated throughout.
Carbonate	Tr	Fn	Anhedral	Occurs only within sub-mm veinlets.

Reflected

Mineral	%	Grain size	Habit	Comments
Pyrite	Tr	Vy-Fn	Euhedral	Cubic, very fine-grained disseminated grains.

General Notes:

The sample is a massive anorthosite with commonly deformed plagioclase grains which are also host to numerous very fine-grained inclusions of amphibole with preferential orientations along the crystal structure. Late stage sub millimeter veinlets cross cut the sample composed of carbonate, clinopyroxene, and amphibole. The sample also contains no magnetite or ilmenite.

Slide#	Rock Type
MM-V2-1	Massive Oxide

Transmitted

Mineral	%	Grain size	Habit	Comments
Chlorite	15	Fn	Anhedral	Green (PPL) blue/purple (XPL) chlorite occurs as fibrous very fine- to fine-grained crystals.
Carbonate	Tr	Fn	Anhedral	Carbonate occurs within cross cutting sub-millimeter veinlets.

Reflected

Mineral	%	Grain size	Habit	Comments
Magnetite	50	Fn	Subhedral	Rounded magnetite contains triple junctions and rare ilmenite exsolution lamellae.
Ilmenite	34	Fn	Subhedral	Rounded to anhedral ilmenite contains triple junctions and rarely occurs as exsolution lamellae within magnetite.
Pyrite	1	Fn	Anhedral	Pyrite occurs as intercumulous crystals within magnetite-ilmenite grains.
Chalcopyrite	Tr	Vy-Fn	Anhedral	Chalcopyrite occurs strictly as inclusions within pyrite grains.

General Notes:

The sample is a massive textured, massive-oxide unit and is dominated by fine-grained magnetite and ilmenite which exhibit triple junctions and rare ilmenite exsolutions within magnetite. Chlorite occurs as fibrous intercumulous grains between magnetite and ilmenite, and sulphide minerals are restricted to an anhedral habit within oxide-rich portions.

Slide#	Rock Type
MM-V2-2	Massive Oxide

Transmitted

Mineral	%	Grain size	Habit	Comments
Chlorite	10	Fn	Anhedral	Green (PPL) Blue/purple (XPL) chlorite occurs as fibrous very fine- to fine-grained crystals.
Carbonate	2	Fn	Anhedral	Carbonate occurs within sub millimeter veinlets, and as medium-grained blebs.
Epidote	Tr	Vy-Fn	Subhedral	Very fine-grained epidote disseminated throughout sample. Grains are possibly amphibole grains.

Reflected

Mineral	%	Grain size	Habit	Comments
Magnetite	58	Fn	Subhedral	Rounded magnetite contains triple junctions and rare ilmenite exsolution lamellae.
Ilmenite	29	Fn	Subhedral	Rounded to anhedral ilmenite contains triple junctions and rarely occurs as exsolution lamellae within magnetite.
Pyrite	1	Fn	Anhedral	Pyrite occurs as intercumulous crystals within magnetite-ilmenite grains.
Chalcopyrite	Tr	Vy-Fn	Anhedral	Chalcopyrite occurs strictly as inclusions within pyrite grains.

General Notes:

The sample is a massive textured, massive-oxide unit and is dominated by fine-grained magnetite and ilmenite which exhibit triple junctions and rare ilmenite exsolutions within magnetite. Chlorite occurs as fibrous intercumulous grains between magnetite and ilmenite, and sulphide minerals are restricted to an anhedral habit within oxide-rich portions.

Slide#	Rock Type
MM-V2-3	O-Anorthosite

Transmitted

Mineral	%	Grain size	Habit	Comments
Sericite	70	Vy-Fn	Euhedral	Aphanitic sericite has completely replaced medium-grained euhedral plagioclase laths which retain the relic plagioclase grain boundaries.
Epidote	10	Fn	Subhedral	Epidote occurs as anhedral to subhedral grains which completely surround magnetite-ilmenite grains.
Amphibole	5	Fn	Subhedral	Blue-green (PPL) amphibole occurs as elongate grains.
Carbonate	Tr	Vy-Fn	Anhedral	Carbonate occurs as very fine grained vein controlled crystals.
Titanite	Tr	Vy-Fn	Anhedral	Occurs within carbonate veinlets and rims magnetite-ilmenite grains which are in contact with carbonate.

Reflected

Mineral	%	Grain size	Habit	Comments
Magnetite	8	Fn	anhedral	Fine- to medium-grained magnetite exhibits coarse-grained ilmenite exsolution lamellae.
Ilmenite	7	Fn	Subhedral	Rounded to tabular ilmenite occurs as discrete grains and as exsolution lamellae within magnetite.
Hematite	0.5	Vy-Fn	Anhedral	Hematite occurs as very fine-grained blebs within magnetite.
Pyrite	0.5	Fn	Anhedral	Pyrite contains blebs of chalcopyrite and subtabular very fine-grained inclusions of hematite.
Chalcopyrite	Tr	Vy-Fn	Anhedral	Blebs of chalcopyrite are present within and rimming pyrite.

General Notes: The sample is a massive, medium-grained oxide- anorthosite. The unit is largely composed of completely sericitized medium-grained plagioclase laths with intercumulate magnetite-ilmenite grains. Epidote occurs as a very thin rim along magnetite-ilmenite, and titanite partially replaces ilmenite. The oxides are composed of magnetite, ilmenite, and to a much lesser extent, hematite. Hematite occurs as anhedral wormy, localized replacement after magnetite. Rare medium-grained magnetite exhibits coarse ilmenite exsolution lamellae, however it is generally fine-grained and contains triple junctions with ilmenite. Pyrite contains minor hematite as very fine-grained sub tabular crystals within a pseudo tabular pyrite grain.

Slide#	Rock Type
MM-V2-4	O-Melagabbro

Transmitted

Mineral	%	Grain size	Habit	Comments
Plagioclase	10	Fn	Anhedral	Contains numerous deformation twins, subgrain boundaries and abundant inclusions of amphibole.
Amphibole	30	Fn	Euhedral	Dark green/blue to yellow/orange, observed partially replacing clinopyroxene grains.
Clinopyroxene	30	Fn to Vy-Fn	Euhedral	Occurs as aggregates which are rimmed with amphibole crystals.
Chlorite	15	Fn	Euhedral	Occurs as massive mats which are surrounded by amphibole grains.
Biotite	2	Fn	Euhedral	Associated with massive magnetite-ilmenite aggregates.
Quartz	Tr	Fn	Anhedral	Strong undulose extinction and subgrains, with no inclusions.

Reflected

Mineral	%	Grain size	Habit	Comments
Magnetite	3	Fn-Md	Anhedral	Has a very 'rough' texture with abundant silicate inclusions and composed of approximately 10-20% ilmenite exsolutions.
Ilmenite	8	Vy-Fn to Fn	Subhedral	Occurs largely as discrete grains, and as laths within magnetite.
Hematite	2	Fn	Anhedral	Occurs as discrete grains within and around magnetite-ilmenite.
Pyrite	tr	Vy-Fn	Anhedral	Disseminated specks.

General Notes:

The sample is a fine- to medium-grained uralized melagabbro. The sample contains abundant clinopyroxene which have been partially altered to a green/blue to yellow/orange amphibole, and secondary chlorite is common. The magnetite has a very 'rough' texture with numerous inclusions of pyroxene, and amphibole along with ilmenite exsolutions. The ilmenite however, is largely competent and inclusion free. Hematite occurs as fine-grained anhedral crystals which are disseminated throughout and along magnetite-ilmenite grains. The Fe-Ti-oxides are concentrated in very course-grained 'pods/smears' within the sample, and to a lesser extent disseminated throughout.

Slide#	Rock Type
MM-V2-5	Leucogabbro

Transmitted

Mineral	%	Grain size	Habit	Comments
Plagioclase	60	Md	Anhedral	Plagioclase contains deformation twins, sub grains, undulose extinction and is replaced by patchy sericite. Plagioclase grains also contain ~5% very fine-grained amphibole grains which are aligned to the crystal planes.
Amphibole	30	Fn-Md	Euhedral	Both green/blue and yellow/orange crystals. Commonly oikocrystic with inclusions of round very fine potassium feldspar. Amphibole commonly has subgrains and undulose.
Clinopyroxene	tr	Vy Fn	Anhedral	Clinopyroxene is nearly completely replaced by amphibole and chlorite, and only exists as very fine-grained anhedral crystals.
Chlorite	7	Fn	Euhedral	Chlorite is associated with amphibole grains.
Muscovite	2	Vy Fn	Euhedral	Occurs as an alteration after plagioclase and is rimmed with sericite.
K-feldspar	1	Vy Fn	Anhedral	Only present as very fine-grained inclusions within amphibole grains, and contains strong compositional zoning.

Reflected

Mineral	%	Grain size	Habit	Comments
Magnetite	Tr	Vy Fn	Anhedral	Rims ilmenite grains.
Ilmenite	tr	Vy Fn	Anhedral	Surrounded by magnetite grains.

General Notes:

The sample is a weakly foliated medium-grained leucogabbro with trace magnetite-ilmenite. Plagioclase is partially replaced by sericite, and locally muscovite has developed as discrete grains. The amphibole grains contain numerous very fine-grained inclusions of potassium feldspar which contain strong compositional zoning.

Slide#	Rock Type
MM-V4-1	O-Pyroxenite

Transmitted

Mineral	%	Grain size	Habit	Comments
Enstatite	42	Md	Subhedral	Supported within a magnetite-ilmenite-pyrrhotite matrix. Commonly exhibits undulose extinction and/or subgrain boundaries.
Actinolite	1	Md	Subhedral	Nearly fibrous to robust habit.
Chlorite	5	Fn	Euhedral	Fibrous steel grey chlorite occurs dominantly along magnetite-ilmenite grains.
Rutile	1	Fn	Anhedral	Blebs of rutile occur throughout but dominantly alongside magnetite-ilmenite grains.
Spinel	tr	Fn	Anhedral	Light green (PPL), non pleochroic and isotropic. Occurs within magnetite-ilmenite grains.

Reflected

Mineral	%	Grain size	Habit	Comments
Magnetite	15	Md	Anhedral	Pitted magnetite contains only minor (<1%) ilmenite exsolution, and contains numerous fine- to medium-grained inclusions of chlorite, rutile, ilmenite and/or spinel.
Ilmenite	5	Fn	Anhedral	Occurs as rims alongside magnetite, or as inclusions.
pyrrhotite	30	Md	Anhedral	Net-textured
Chalcopyrite	1	Fn	Anhedral	Exclusively hosted within pyrrhotite.

General Notes:

The sample is massive, relatively unaltered, net textured sulphide, oxide pyroxenite. The sample is dominated by a magnetite-pyrrhotite matrix with subhedral Enstatite with lesser spinel, chlorite, actinolite, and ilmenite.

Slide#	Rock Type
MM-V4-2	Massive Oxide

Transmitted

Mineral	%	Grain size	Habit	Comments
Biotite	1	Fn	Anhedral	Red-brown biotite has been partially to completely been replaced by chlorite.
Epidote	5	Md	Euhedral	Contains very high relief, prismatic to tabular habit, and up to second order colour birefringence. Commonly exhibits simple twins.
Chlorite	13	Fn	Euhedral	Grey-brown (XPL) fibrous chlorite occurs as matts throughout the sample and replaces biotite.
Clinozoisite	Tr	MD	Anhedral	Anomalous blue (XPL) and spatially associated with epidote.

Reflected

Mineral	%	Grain size	Habit	Comments
Magnetite	60	Md	Anhedral	Magnetite contain ilmenite exsolution lamellae (<3%), and exhibits a pitted texture.
Ilmenite	20	Fn	Subhedral	Occurs as discrete fine- to medium-grains and as exsolution lamellae within magnetite.
Pyrite	1	Fn	Subhedral	Subcubic pyrite disseminated throughout.

General Notes:

The sample is a fine- to medium-grained massive oxide. Magnetite is the dominate oxide where is occurs as massive medium-grained aggregates with minor ilmenite exsolution. Ilmenite also occurs as subhedral, tabular grains within the magnetite.

Epidote is medium-grain and euhedral forming prismatic and tabular grains. Chlorite replaces biotite and has a grey-brown (XPL) colour.

Slide#	Rock Type
MM-V4-4	OR-Leucogabbro

Transmitted

Mineral	%	Grain size	Habit	Comments
Plagioclase	40	Md	Euhedral	Commonly exhibits deformation twinning, and contains ~5% very fine-grained amphibole inclusions.
Amphibole	5	Fn	Subhedral	Disseminated blue/green (PPL). Also occurs as inclusions within plagioclase.
Clinopyroxene	10	Fn	Euhedral	Prismatic clinopyroxene spatially associated with oxide aggregates. Rarely contains secondary amphibole rims.
Biotite	10	Fn	Euhedral	Disseminated.
Chlorite	Tr	Fn	Euhedral	Rarely occurs as alteration along biotite grains.

Reflected

Mineral	%	Grain size	Habit	Comments
Magnetite	25	Fn	Anhedral	Semi-net textured magnetite with an often pitted surface.
Ilmenite	10	Fn	Subhedral	Occurs as anhedral blebs alongside, and within magnetite grains, or as subhedral laths. Ilmenite grains contain minor magnetite exsolutions.
Pyrite	Tr	Vy-Fn	Anhedral	Disseminated very fine-grained pyrite.

General Notes:

The sample is a weakly- to moderately-foliated unit, with semi-net textured Fe-Ti-oxides. Ilmenite contains only minor (<2%) magnetite exsolutions and occurs as anhedral blebs, or subhedral laths. Plagioclase contains numerous~5% very fine-grained inclusions of amphibole crystals with a preferential orientation along the plagioclase crystal structure.

Slide#	Rock Type
MM-V4-3	Massive Oxide

Transmitted

Mineral	%	Grain size	Habit	Comments
Chlorite	10	Fn	Anhedral	Pale green (PPL) to brown-grey (XPL) occurs as fibrous mineral within magnetite-ilmenite grains.
Epidote	10	Fn	Subhedral	Anhedral to euhedral epidote grains typically rim magnetite-ilmenite grains and contain minor simple twins.

Reflected

Mineral	%	Grain size	Habit	Comments
Magnetite	52	Fn	Anhedral	Blebs of magnetite contain thin ilmenite exsolution lamellae (~10%). Magnetite also occurs as exsolution within ilmenite.
Ilmenite	27	Fn	Subhedral	Rounded to sub tabular ilmenite occurs as discrete grains which exhibit triple junction boundaries with contacted ilmenite and/or magnetite. Ilmenite also occurs and fine-grained blebs and exsolution lamellae within magnetite.
Pyrite	1	Fn	Subhedral	Sub cubic to anhedral pyrite occurs throughout, but is largely vein controlled.

General Notes:

The sample is a massive, fine-grained massive-oxide which contains fine-grained secondary intercumulous chlorite and epidote. The oxides are magnetite dominate which occur as anhedral blebs along which exhibit triple junction boundaries with sub rounded ilmenite. Both the magnetite and ilmenite contain very thin exsolution lamellae of each respective oxide species.

Slide#	Rock Type
MM-V4-5	OB-Gabbro

Transmitted

Mineral	%	Grain size	Habit	Comments
Plagioclase	40	Md	Euhedral laths	Sporadic fibrous fine-grained amphibole inclusions and secondary fibrous plagioclase rimming primary euhedral laths. Plagioclase contains ~2% very fine grained green needle-like amphibole inclusions
Amphibole	45	Fn-Md	Subhedral	Occurs as fine-grained aggregates or as medium-grained crystals after clinopyroxene.
Clinopyroxene	5	Md	Euhedral	Almost completely amphibole altered, and is exclusively rimmed by secondary amphibole.
Chlorite	6	Fn	Subhedral	Chlorite occurs as a secondary alteration often as laths surrounding amphibole, or as laths within plagioclase.
Biotite	1	Fn	Subhedral	Often transitional with chlorite grains and commonly associated with magnetite and amphibole.
titanite	Tr.	Vy-Fn	Subhedral	Occurs as inclusions within amphibole and magnetite.
Garnet	Tr.	Fn	Euhedral	Euhedral garnet occur exclusively contacting magnetite or as inclusions.

Reflected

Mineral	%	Grain size	Habit	Comments
Magnetite	3	Fn-Md	Anhedral	Blebs of magnetite with minor inclusions of ilmenite and rimmed with minor hematite.
Ilmenite	Tr.	Fn	Subhedral	Occurs as thin lamellae within magnetite, or as distinct euhedral laths.
Pyrite	Tr.	Vy-Fn	Anhedral	Disseminated.
Hematite	Tr.	Vy-Fn	Anhedral	Occurs exclusively as rims along magnetite grains.

General Notes:

Sample is heavily amphibolized and has nearly replaced all primary clinopyroxene. Plagioclase laths have a relic euhedral habit but are rimmed with fibrous secondary plagioclase. Magnetite contains exsolution lamellae of ilmenite, and in places rimmed with trace hematite.

Slide#	Rock Type
MM-V4-6	Silicified OB-gabbro

Transmitted

Mineral	%	Grain size	Habit	Comments
Plagioclase	1	Fn	Euhedral	Contains minor sericite alteration and deformation twins.
Quartz	55	Fn	Anhedral	Varies from fine- to coarse-grained, contains subgrain boundaries and undulose extinction.
Biotite	2	Fn	Euhedral	Weakly aligned red-brown biotite.
Chlorite	1	Fn	Euhedral	Occurs as aligned mats of chlorite.
Garnet	Tr	Fn	Subhedral	Pale red, only one observed grain.
Carbonate	1	Vy-Fn	Anhedral	Occurs within concentrations of biotite.
Epidote	Tr	Vy-Fn	Anhedral	Disseminated very fine-grained epidote.

Reflected

Mineral	%	Grain size	Habit	Comments
Ilmenite	1	Fn	Subhedral	Possibly brecciated fine- to very fine-grained ilmenite.
Pyrrhotite	35	Md	Anhedral	Heterogeneously distributed throughout sample into ‘smears’.
Pyrite	3	Fn	Subhedral	Possibly brecciated subcubic grains associated with chalcopyrite.
Chalcopyrite	1	Fn	Subhedral	Hosted within pyrrhotite, and spatially associated with pyrite.

General Notes:

The sample is weakly to moderately foliated, silicified semi-massive sulphide, oxide-bearing gabbro. The original mineralogy is difficult to distinguish due to the high degree of silification and biotite-chlorite-garnet alterations. The sulphides are pyrrhotite dominated, and subhedral pyrite appears brecciated. Ilmenite is the only observed oxide present and as well appears brecciated.

Slide#	Rock Type
MM-V4-7	O-Leucogabbro

Transmitted

Mineral	%	Grain size	Habit	Comments
Plagioclase	80	Md	Euhedral	Commonly exhibits deformation twins and/or simple twins. All plagioclase grains contain ~5-10% very fine-grained amphibole inclusions which preferentially grow along crystal planes.
Amphibole	5	Fn	Subhedral	Blue-green (XPL) and contains minor quartz inclusions.
Clinopyroxene	1	Vy-Fn	Euhedral	Occurs as distinct grains and partially replaced by amphibole.
Biotite	2	Fn	Euhedral	Brown-red laths spatially associated with oxides
Quartz	2	Vy-Fn	Euhedral	Occurs as dense clusters surrounded by amphibole grains.
Carbonate	tr	Fn	Anhedral	Occurs solely as a sub mm cross cutting veinlet.

Reflected

Mineral	%	Grain size	Habit	Comments
Magnetite	7	Fn-Md	Anhedral	Pitted with minor silicate inclusions.
Ilmenite	3	Fn	Subhedral	Occurs as blebs in contact with magnetite or as separate tabular grains. Occasional very fine-grained magnetite exsolutions.
Pyrite	1	Fn	Euhedral	Cubic and partially replaced by pyrrhotite.
Pyrrhotite	Tr	Vy-Fn	Anhedral	Occurs only as a secondary alteration after pyrite.

General Notes:

Sample is moderately deformed with common deformation and simple twins within plagioclase grains, and late stage sub-mm carbonate veinlets. Plagioclase contains numerous very fine-grained inclusions of amphibole grains which preferential orientation along crystal planes. Quartz is very fine-grained and occurs as clusters within amphibole oikocrysts. Both ilmenite and magnetite typically occur as distinct grains with only minor exsolution.

Slide#	Rock Type
MM-V5-1	OR-Biotite Schist

Transmitted

Mineral	%	Grain size	Habit	Comments
Amphibole	2	Md	Euhedral	Fine- to medium-grained amphibole reaches first ordered-orange interference color.
Biotite	60	Fn	Euhedral	Brown, partially replaced by chlorite.
Chlorite	4	Fn	Euhedral	Chlorite occurs in clots and partially to completely replace biotite.
Carbonate	8	Md	Anhedral	Carbonate occurs throughout sample.
Clinozoisite	1	Md	Subhedral	Partially replaced amphibole-looking. Light blue in XPL, moderate-strong relief.

Reflected

Mineral	%	Grain size	Habit	Comments
Magnetite	15	Md	Anhedral	Magnetite varies in texture from an ilmenite exsolution lamellae-bearing core, to an exsolution-free rim. Magnetite typically contains ~5% ilmenite exsolution.
Ilmenite	9	Md	Subhedral	Ilmenite occurs as subhedral grains with 2-3% magnetite exsolution, as fine-grained exsolution-free grains, and as exsolution within magnetite.
Pyrite	1	Fn	Subhedral	Sub-cubic pyrite disseminated throughout.
Pyrrhotite	Tr	Vy-Fn	Anhedral	Spatially associated with pyrite.
Chalcopyrite	Tr	Vy-Fn	Anhedral	Spatially associated with pyrite.

General Notes:

The sample is a fine- to medium-grained, moderately foliated oxide-rich biotite schist. The original composition of the sample is difficult to estimate due to pervasive biotite-chlorite-carbonate alteration.

The oxides are magnetite dominated which occurs in three varies of texture i) medium-grained anhedral crystals with ilmenite exsolution lamellae, ii) exsolution-free magnetite rims, and iii) as exsolution lamellae within ilmenite. The medium-grained ilmenite contains 2-3% magnetite exsolution, whereas the fine-grained ilmenite is exsolution-free.

Slide#	Rock Type
MM-V5-2	OR-Biotite schist

Transmitted

Mineral	%	Grain size	Habit	Comments
Plagioclase	2	Vy-Fn	Anhedral	Plagioclase only exists as very fine-grained crystals within sericitized medium-grained relict plagioclase grain boundaries.
Biotite	45	Fn	Euhedral	Brown Biotite occurs throughout the sample.
Carbonate	10	Fn	Anhedral	Carbonate occurs throughout the sample.
Chlorite	7	Fn	Euhedral	Chlorite partially replaces biotite grains, and also present within altered plagioclase.
Sericite	10	Vy-Fn	Euhedral	Sericite has nearly completely replaced primary plagioclase grains.
Quartz	Tr	Fn	Anhedral	Associated with sericitized plagioclase.
Epidote	Tr	Fn	Euhedral	Epidote occurs throughout sample/
Clinozoisite	1	Vy-Fn	Anhedral	Aggregates of very fine-grained clinozoisite occur within altered plagioclase grains.

Reflected

Mineral	%	Grain size	Habit	Comments
Magnetite	15	Md	Anhedral	Contains ~5% very thin ilmenite exsolution. Magnetite is also present as exsolution lamellae within ilmenite.
Ilmenite	10	Md	Subhedral	Occurs as subhedral medium-grains, or as exsolution lamellae within magnetite.
Pyrite	tr	Fn	Anhedral	Disseminated throughout.

General Notes:

The sample is weakly foliated, fine- to medium-grained, oxide-rich biotite schist. The sample has been heavily altered by biotite, carbonate, and sericite with lesser quartz and epidote. The primary, medium-grained plagioclase crystals retain relict grain boundaries, but are almost completely composed of sericite.

The oxides are magnetite dominated with contains very fine ilmenite exsolution lamellae. Likewise, the ilmenite contains very fine-grained magnetite exsolution.

Slide#	Rock Type
MM-V5-3	SMO-Gabbro

Transmitted

Mineral	%	Grain size	Habit	Comments
Chlorite	20	Fn	Anhedral	Pale-green (PPL) to brown (XPL) occurs throughout the samples a s a fibrous outgrown along magnetite-ilmenite.
Epidote	9	Fn	Subhedral	Epidote occurs as very fine-grained euhedral grains and as fine-grained anhedral grains.

Reflected

Mineral	%	Grain size	Habit	Comments
Magnetite	45	Md	Anhedral	Magnetite varies in texture from an ilmenite exsolution lamellae-bearing core, to an exsolution-free rim. Magnetite typically contains ~5% ilmenite exsolution. Medium-grained magnetite commonly is poikilitic with inclusions of chlorite.
Ilmenite	25	Md	Subhedral	Ilmenite occurs as subhedral grains with 2-3% magnetite exsolution, as fine-grained exsolution-free grains, and as exsolution within magnetite.
Pyrite	1	Fn	Subhedral	Sub-cubic pyrite disseminated throughout.
Pyrrhotite	Tr.	Vy-Fn	Anhedral	Spatially associated with pyrite.
Chalcopyrite	Tr	Vy-Fn	Anhedral	Spatially associated with pyrite.

General Notes:

The sample is a massive, fine-grained semi-massive oxide gabbro. The sample is dominated by fine-grained anhedral to subhedral magnetite and ilmenite (respectively) which display a variety of forms and textures. The magnetite ranges from a medium-grained, ilmenite exsolution lamellae-bearing phase with rims of exsolution-free magnetite, to a fine- to medium-grained ilmenite lamellae-bearing phase. Ilmenite occurs as subhedral grains which variably contain magnetite exsolution. The sample contains inter cumulate fibrous chlorite and epidote grains.

Slide#	Rock Type
MM-V5-4	O-Peridotite

Transmitted

Mineral	%	Grain size	Habit	Comments
Serpentine	65	Vy-Fn	Anhedral	Occurs as a massive textured aggregate.
Grunerite	20	Fn	Subhedral	Fibrous grunerite occurs throughout.
Titanite	Tr	Fn	Anhedral	Single grain of anhedral titanite

Reflected

Mineral	%	Grain size	Habit	Comments
Magnetite	14	Fn	Anhedral	Magnetite occurs as aggregates of partially digested fine-grained ilmenite lamellae-bearing (<1%) crystals. The edges of rare, medium-grained magnetite crystals contain anomalously high concentrations of very fine-grained ilmenite blebs. The magnetite is also cross cut by fibrous grunerite grains.
Ilmenite	1	Vy-Fn	Anhedral	Ilmenite occurs as thin exsolution lamellae within magnetite, and as very fine-grained blebs within the rims of medium-grained magnetite.
Pyrrhotite	Tr	Fn	Anhedral	Blebs of very fine-grained pyrrhotite occur throughout.

General Notes:

The sample is a fine-grained, massive, serpentine-grunerite altered oxide peridotite. The serpentine occurs as massive, fibrous aggregates and the grunerite occurs as fine- to medium-grained fibrous crystals which cross cut magnetite grains.

The oxides are largely composed of anhedral fine- to medium-grained magnetite which exhibit partially digested grain boundaries. The magnetite also contains rare ilmenite exsolution lamellae and within medium-grained magnetite, ilmenite occurs as very fine-grained blebs along the contacts within silicate minerals.

Slide#	Rock Type
MM-V5-5	O-Serpentinite

Transmitted

Mineral	%	Grain size	Habit	Comments
Serpentine	80	Vy-Fn	Anhedral	Occurs as a massive textured aggregate.
Carbonate	15	Vy-Fn	Anhedral	Carbonate occurs disseminated throughout the sample and as millimeter scale veinlets which cross-cut the sample.

Reflected

Mineral	%	Grain size	Habit	Comments
Magnetite	5	Fn	Anhedral	Magnetite occurs as anhedral, partially digested grains which have been cross cut but serpentine-altered silicate minerals.
Pentlendite	Tr	Vy-Fn	Anhedral	Pentlendite occurs along the edges of magnetite aggregates.

General Notes:

The sample is a massive serpentinte-oxide. The carbonate occurs both as disseminated grains throughout the sample, and as cross-cutting millimeter scale veinlets. Magnetite occurs as anhedral crystals which may have preserved relict possibly olivine grain boundaries. The oxide exhibits partially digested grain boundaries, and is often cross cut by fibrous, very fine-grained silicate minerals which have been altered to serpentine.

Slide#	Rock Type
MM-V5-6	Gabbro

Transmitted

Mineral	%	Grain size	Habit	Comments
Chlorite	45	Fn	Subhedral	Fine- to very fine-grained green (PPL) green/brown (XPL) chlorite occurs as fibrous grains.
Quartz	25	Vy-Fn	Anhedral	Very-fine grained quartz occurs throughout sample.
Carbonate	30	Fn	Anhedral	Fine- to medium-grained carbonate occurs disseminated throughout and as cm-thick carbonate rich (90%) bands.
Titanite	Tr	Vy-Fn	Subhedral	Mylonitized titanite occurs surrounded by chlorite grains.
Epidote	Tr	Fn	Anhedral	Occurs disseminated throughout sample

Reflected

Mineral	%	Grain size	Habit	Comments
Magnetite	Tr	Vy-Fn	Anhedral	Very fine-grained magnetite occurs disseminated throughout sample.

General Notes:

The sample is a very well foliated chlorite-carbonate-quartz schist. The sample exhibits a banded texture with cm-thick carbonate rich (90%) bands within chlorite-quartz bands. The titanite has been mylonitised and is completely surrounded by chlorite-rich bands. The sample likely represents a highly deformed gabbro with trace magnetite which may have formed prior to, or during alteration.

Slide#	Rock Type
MM-V5-7	O-Anorthosite

Transmitted

Mineral	%	Grain size	Habit	Comments
Plagioclase	80	Md	Euhedral	Plagioclase laths have been completely replaced by very fine-grained sericite alteration.
Amphibole	5	Fn	Subhedral	Green (PPL) to green-yellow (XPL) amphibole occurs as fine-grained aggregates.
Epidote	5	Vy-Fn	Anhedral	Epidote rims magnetite-ilmenite grains and exhibits a corona texture.
Chlorite	2	Fn	Anhedral	Pale green (PPL) to blue (XPL) fibrous chlorite occurs throughout.

Reflected

Mineral	%	Grain size	Habit	Comments
Magnetite	5	Fn	Anhedral	Magnetite occurs as anhedral grains which contains rare, coarse ilmenite exsolution, and very fine-grained ilmenite blebs.
Ilmenite	3	Fn	Anhedral	Anhedral ilmenite occurs as fine-grained crystals spatially associated with magnetite, and contain variable (0-50%) wormy hematite intergrowths. Ilmenite lamellae within magnetite also contain hematite.
Hematite	0.5	Vy-Fn	Anhedral	Hematite occurs as a wormy intergrowth within ilmenite grains.
Pyrite	0.5	Vy-Fn	Anhedral	Blebs of pyrite occur throughout sample.

General Notes:

The sample is a massive, medium-grained oxide-anorthosite. The plagioclase has been completely replaced by very fine-grained sericite, and the magnetite-ilmenite grains are partially to completely rimmed by a corona of epidote. The magnetite contains exsolution of ilmenite which occurs as blebs and lamellae and has been variably replaced by wormy hematite (up to 50%).

Slide#	Rock Type
MM-V8-1	O-Gabbro

Transmitted

Mineral	%	Grain size	Habit	Comments
Plagioclase	50	Md	Euhedral	Plagioclase laths contain deformation twins, simple twins and minor subgrain boundaries. Plagioclase grains also contain very fine-grained inclusions of amphibole which are oriented along crystallographic planes.
Amphibole	40	Fn	Subhedral	Blue-green amphibole grains occur as fine- to medium-grained subhedral crystals with minor inclusions of possible plagioclase/quartz and magnetite blebs.
Chlorite	5	Fn	Subhedral	Green chlorite occurs as a replacement mineral after amphibole
Epidote	Tr	Vy-fn	Subhedral	Sub prismatic very fine-grained epidote crystals occur throughout the sample

Reflected

Mineral	%	Grain size	Habit	Comments
Magnetite	3	Fn	Anhedral	Magnetite blebs occur disseminated throughout the sample and contain trace ilmenite exsolution and tabular ilmenite. Magnetite occurs as very fine-grained blebs within amphibole grains which are proximal to medium-grained magnetite blebs.
Ilmenite	2	Fn	Euhedral	Ilmenite occurs as subhedral to euhedral grains within and proximal magnetite grains.
Pyrite	1	Fn	Anhedral	Occurs disseminated throughout.
Chalcopyrite	tr	Vy-Fn	Anhedral	Occurs within pyrite grains.

General Notes:

The sample is a medium-grained, massive, oxide-gabbro. The primary pyroxene has been completely replaced by fine- to medium-grained amphibole and chlorite which preserved the relict grain boundaries within euhedral plagioclase laths. The magnetite occurs largely as fine- to medium-grained blebs which exhibit trace ilmenite lamellae and fine-grained euhedral ilmenite crystals. Magnetite also occurs as rounded blebs within amphibole grains which are proximal to larger magnetite blebs, as well, the magnetite also contains minor amphibole inclusions.

Slide#	Rock Type
MM-V8-2	O-Gabbro

Transmitted

Mineral	%	Grain size	Habit	Comments
Plagioclase	40	Md	Euhedral	Medium- to course-grained euhedral plagioclase exhibits simple twins, deformation twins, undulose extinction, and weak sericite and clinozoisite alteration.
Amphibole	51	Md	Euhedral	Fine- to medium-grained green-yellow amphibole contains subgrains and undulose extinction. Minor amphibole is oikocrystic with aphanitic inclusions of possible plagioclase/quartz.
Clinozoisite	tr	Vy-Fn	Anhedral	Occurs exclusively within the core of altered plagioclase.

Reflected

Mineral	%	Grain size	Habit	Comments
Magnetite	5	Fn	Anhedral	Anhedral to subhedral magnetite exhibits ilmenite exsolution lamellae and blebs. Magnetite also occurs within ilmenite as exsolution lamellae.
Ilmenite	3	Fn	Anhedral	Ilmenite occurs as exsolution within magnetite and as fine-grained discrete anhedral grains. Ilmenite contains very thing exsolution lamellae of magnetite.
Pyrite	1	Vy-Fn	Subhedral	Anhedral to subhedral cubic pyrite occurs throughout.

General Notes:

The sample is a massive, medium- to course-grained oxide-gabbro. The plagioclase and amphibole grains exhibit undulose extinction, subgrain boundaries, and/or deformation and simple twins.

The oxides are magnetite-dominated which occur as fine-grained anhedral crystals. Both magnetite and ilmenite contain exsolution lamellae of their respective oxides.

Slide#	Rock Type
MM-V8-3	OB-Gabbro

Transmitted

Mineral	%	Grain size	Habit	Comments
Plagioclase	40	Md	Euhedral	Commonly exhibits subgrains and deformation twins. Plagioclase also contains numerous very fine-grained amphibole inclusions.
Amphibole	40	Fn	Subhedral	Blue-green amphibole surrounds clinopyroxene. Some amphibole clusters contain abundant very fine-grained magnetite.
Clinopyroxene	10	Md	Euhedral	Partially to completely replaced by amphibole and chlorite, however primary euhedral grains can still be distinguished.
Chlorite	5	Fn	Subhedral	Occurs along with amphibole and surrounds clinopyroxene.

Reflected

Mineral	%	Grain size	Habit	Comments
Magnetite	2	Fn	Anhedral	Contains well formed ilmenite exsolution lamellae and displays a pitted texture. Magnetite occurs as discrete pitted grains, and as very fine-grained inclusions within amphibole.
Ilmenite	2	Fn	Anhedral	Ilmenite occurs as anhedral blebs associated with magnetite, and within magnetite as exsolution.
Pyrite	1	Fn	Anhedral	Disseminated throughout sample.

General Notes:

The sample is a massive, medium-grained oxide-bearing gabbro. The primary clinopyroxene has partially to completely been replaced by amphibole and to a lesser extent, chlorite. Plagioclase exhibits subgrain boundaries and deformation twins.

Magnetite and ilmenite occur is roughly equal proportions. Magnetite occurs as discrete grains with ilmenite exsolution, and as very fine-grained inclusions within amphibole.

Slide#	Rock Type
MM-V8-4	OR-Melanogabbro

Transmitted

Mineral	%	Grain size	Habit	Comments
Plagioclase	10	Md	Euhedral	Oikocrystic euhedral plagioclase contains undulose extinction, subgrain boundaries, and compositional zoning. Typically contains very fine-grained amphibole micro-veinlets.
Amphibole	46	Fn	Subhedral	Blue-green amphibole is supported within a magnetite-ilmenite matrix. Amphibole exhibit undulose extinction and subgrain boundaries.
Biotite	1	Fn	Euhedral	Red-brown biotite occurs throughout the sample.
Chlorite	1	Fn	Euhedral	Green (PPL), partially replacing biotite and amphibole.
Carbonate	tr	Vy-Fn	Anhedral	Disseminated throughout sample.

Reflected

Mineral	%	Grain size	Habit	Comments
Magnetite	25	Fn	Anhedral	Pitted magnetite contains minor (<2%) ilmenite exsolution lamellae.
Ilmenite	15	Fn	Anhedral	Occurs dominantly as discrete grains and to a lesser extent within magnetite.
Pyrite	2	Vy-Fn	Anhedral	Disseminated throughout sample.
Chalcopyrite	tr	Vy-Fn	Anhedral	Occurs alongside, and within pyrite

General Notes:

The sample is a massive, fine-grained magnetite-ilmenite net textured oxide-rich melanogabbro. Oikocrystic plagioclase contains deformation twins, undulose extinction, and subgrain boundaries. The blue-green amphibole is likely a replacement after pyroxene, however none is preserved.

The oxides are magnetite dominated, although ilmenite-rich, and unusually fine-grained. The magnetite contains only minor ilmenite exsolution lamellae.

Slide#	Rock Type
MM-V8-5	OB-Gabbro

Transmitted

Mineral	%	Grain size	Habit	Comments
Plagioclase	40	Md	Euhedral	Plagioclase laths contain deformation twins, simple twins and minor subgrain boundaries. Plagioclase grains also contain very fine-grained inclusions of amphibole which are oriented along crystallographic planes.
Amphibole	50	Fn	Subhedral	Blue-green amphibole grains occur as fine- to medium-grained subhedral crystals with minor inclusions of possible plagioclase/quartz and magnetite blebs.
Chlorite	5	Fn	Subhedral	Green chlorite occurs as a replacement mineral after amphibole
Epidote	Tr	Vy-fn	Subhedral	Sub prismatic very fine-grained epidote crystals occur throughout the sample
Clinozoisite	Tr	Vy-Fn	Anhedral	Occurs exclusively within plagioclase grains.
Carbonate	Tr	Vy-fn	Anhedral	Occurs disseminated throughout sample.

Reflected

Mineral	%	Grain size	Habit	Comments
Magnetite	2	Fn	Anhedral	Magnetite blebs occur disseminated throughout the sample tabular ilmenite. Magnetite occur occurs as very fine-grained blebs within amphibole grains which are proximal to medium-grained magnetite blebs.
Ilmenite	1	Fn	Euhedral	Ilmenite occurs as subhedral to euhedral grains within and proximal magnetite grains.
Pyrite	1	Fn	Anhedral	Occurs disseminated throughout.
Chalcopyrite	tr	Vy-Fn	Anhedral	Occurs within pyrite grains.

General Notes:

The sample is a medium-grained, massive, oxide-gabbro. The primary pyroxene has been completely replaced by fine- to medium-grained amphibole and chlorite which preserved the relict grain boundaries within euhedral plagioclase laths. The magnetite occurs largely as fine- to medium-grained blebs which contain fine-grained euhedral ilmenite crystals. Magnetite also occurs as rounded blebs within amphibole grains which are proximal to larger magnetite blebs, as well, the magnetite also contains minor amphibole inclusions.

Slide#	Rock Type
MM-60-1	Massive-Oxide

Transmitted

Mineral	%	Grain size	Habit	Comments
Epidote	5	Fn	Euhedral	Prismatic euhedral epidote exhibits minor simple twins.
Chlorite	15	Fn	Euhedral	Green (PPL)-Brown (XPL) fibrous chlorite occurs within cumulous magnetite-ilmenite grains.

Reflected

Mineral	%	Grain size	Habit	Comments
Magnetite	55	Md	Anhedral	Magnetite occurs as fine- to medium-grained anhedral crystals which contains minor ilmenite exsolution lamella and/or blebs.
Ilmenite	25	Fn	Subhedral	Ilmenite occurs as fine-to medium-grained rounded crystals largely within a magnetite matrix. Ilmenite also occurs to a much lesser extent as exsolution textures within magnetite.
Pyrrhotite	tr	Fn	Anhedral	Pyrrhotite blebs occur disseminated throughout sample and contains pyrite 'flames'
Pyrite	Tr	Vy-Fn	Anhedral	Occurs solely as exsolution 'flames' within pyrrhotite.
Chalcopyrite	Tr	Vy-Fn	Anhedral	Chalcopyrite occurs as very fine-grained blebs which boarder pyrrhotite.

General Notes:

The sample is a medium-grained, massive oxide which is dominantly composed of magnetite and ilmenite with intergranular chlorite and epidote. The fine- to medium-grained magnetite is the dominate oxide present and contains minor (<2%) ilmenite exsolution lamellae and/or rounded anhedral blebs. The Ilmenite occurs largely as discrete fine- to medium-grained rounded subhedral crystals within a magnetite matrix. The ilmenite grains approximately go extinct at parallel orientations and may indicate a possible exsolution origin for the subhedral ilmenite.

Slide#	Rock Type
MM-60-2	Oxide-Melanogabbro

Transmitted

Mineral	%	Grain size	Habit	Comments
Plagioclase	5	Md	Euhedral	Mylonitised medium-grained plagioclase laths occur largely within magnetite-poor regions, and contain deformation twins and simple twins.
Amphibole	40	Fn	Subhedral	Blue-green amphibole grains occur throughout the sample and contain minor magnetite-ilmenite inclusions, deformation twins, and weak compositional zoning.
Biotite	10	Fn	Euhedral	Biotite is spatially associated with magnetite-ilmenite grains within the oxide-poor regions of the sample where it is partially replaced by green (XPL) chlorite.
Chlorite	27	Fn	Subhedral	Chlorite occurs throughout the sample and varies from brown (XPL) within magnetite-rich regions, to green(XPL) within magnetite-poor regions, it also partially replaces biotite.
Carbonate	Tr	Md	Anhedral	Anhedral carbonate occurs throughout
Epidote	3	Fn	Euhedral	Tabular/prismatic epidote occurs spatially associated within magnetite-rich regions.

Reflected

Mineral	%	Grain size	Habit	Comments
Magnetite	5	Fn	Anhedral	Anhedral magnetite grains occurs throughout the sample as magnetite-rich, and poor bands. The magnetite contains minor (<5%) ilmenite exsolution blebs.
Ilmenite	9	Fn	Subhedral	Ilmenite occurs as fine-grained rounded crystals and to a lesser extent as exsolution within magnetite.
Pyrrhotite	1	Fn	Anhedral	Pyrrhotite occurs as disseminated grains and within fractures.
Pyrite	Tr	Fn	Anhedral	Occurs as exsolution within pyrrhotite grains.
Chalcopyrite	tr	Vy-Fn	Anhedral	Occurs along pyrrhotite grain boundaries.

General Notes: The sample is a moderately- to well foliated oxide-melanogabbro which has been subject to mylonitization, chlorite, amphibole, and biotite alterations. The oxides are ilmenite dominated and pyrrhotite occurs as crosscutting fractures which rim oxide grains and also as disseminated crystals which exhibit pyrite exsolutions.

Slide#	Rock Type
MM-60-3	OB-Gabbro

Transmitted

Mineral	%	Grain size	Habit	Comments
Plagioclase	20	Md	Euhedral	Plagioclase laths contain abundant deformation twins, simple twins, and minor subgrain boundaries. The laths also are commonly bent.
Amphibole	40	Md	Subhedral	Fine-to medium-grained subhedral blue/green (PPL) amphibole grains are commonly oikocrystic with inclusions of euhedral magnetite, quartz, and/or biotite-chlorite. Few amphibole grains contain abundant magnetite-ilmenite exsolution.
Chlorite	5	Fn	Anhedral	Green (PPL) fibrous chlorite occurs throughout.
Biotite	5	Fn	Euhedral	Red-brown(PPL) biotite occurs throughout.
Quartz	15	Fn	Anhedral	Quartz occurs within relict plagioclase grain boundaries and exhibits undulose extinction, and common subgrain boundaries.
Carbonate	Tr	Fn	Anhedral	Carbonate occurs disseminated throughout.
Epidote	10	Fn	Subhedral	Epidote occurs between amphibole and plagioclase grains and exhibits high relief and a prismatic habit.

Reflected

Mineral	%	Grain size	Habit	Comments
Magnetite	1	Fn	Euhedral	Magnetite occurs as fine-grained anhedral blebs and as very fine-grained euhedral prismatic crystals.
Ilmenite	2	Fn	Euhedral	Occurs as disseminated grains, and as exsolution lamellae within amphibole grains.
Pyrrhotite	1	Fn	Anhedral	Occurs disseminated throughout sample but is more concentrated spatially along with magnetite-ilmenite.
Chalcopyrite	Tr	Vy-Fn	Anhedral	Occurs alongside pyrrhotite grains.
Pyrite	tr	Vy-Fn	Subhedral	Occurs exclusively as ‘flames’ within pyrrhotite grains.

General Notes: The sample is a medium-grained, weakly to moderately foliated oxide-bearing gabbro. Plagioclase is partially replaced by deformed fine-grained quartz. Amphibole has completely replaced pyroxene and commonly contains inclusions of euhedral magnetite, and exsolution lamellae of ilmenite. Oxides exhibit a box-texture, and are ilmenite-dominated which are restricted to the mafic minerals (amphibole) and are surrounded by a reaction rim of epidote.

Slide#	Rock Type
MM-60-4	OB-Gabbro

Transmitted

Mineral	%	Grain size	Habit	Comments
Plagioclase	65	Md	Euhedral	Medium- to coarse-grained plagioclase laths exhibit deformation twins, simple twins and weak sericite alteration (<5%).
Amphibole	30	Fn	Euhedral	Green-blue (PPL) hornblende partially to complete replaces medium-grained clinopyroxene crystals. Amphibole rarely contains simple twins.
Pyroxene	2	Md	Euhedral	Clinopyroxene is partially to completely replaced by secondary fine-grained amphibole.
Chlorite	2	Fn	Euhedral	Fibrous Green (PPL) brown (XPL) chlorite occurs as a replacement after pyroxene and amphibole grains.
Clinozoisite	Tr	Vy-Fn	Anhedral	Very fine-grained crystals occur within plagioclase laths.
Biotite	Tr	Fn	Euhedral	Red-brown (PPL) biotite occurs partially replaced by chlorite.

Reflected

Mineral	%	Grain size	Habit	Comments
Ilmenite	1	Fn	Euhedral	Ilmenite occurs as exsolution lamellae within amphibole crystals.
Chalcopyrite	Tr	Vy-Fn	Anhedral	Chalcopyrite blebs occur alongside pyrrhotite blebs.
Pyrrhotite	tr	Vy-Fn	Anhedral	Pyrrhotite occurs disseminated throughout sample.

General Notes:

The sample is a medium- to coarse-grained, massive oxide-bearing gabbro. Primary clinopyroxene has been partially to completely replaced by amphibole, chlorite, and/or biotite. The plagioclase grains exhibit deformation twins, sericite alteration, and trace clinozoisite replacement.

No magnetite was observed within the sample, and ilmenite occurs as exsolution lamellae within amphibole grains and as very fine-grained disseminated crystals.

Slide#	Rock Type
MM-60-5	Anorthosite

Transmitted

Mineral	%	Grain size	Habit	Comments
Plagioclase	85	Md	Euhedral	Medium- to coarse-grained plagioclase exhibits deformation twins, simple twins, and subgrain boundaries. All the grains have been slightly sericite altered.
Amphibole	2	Fn	Subhedral	Blue-green amphibole occurs throughout. Few medium-grained crystals as oikocrystic with inclusions of quartz.
Quartz	10	Fn	Anhedral	Quartz occurs in clusters, and commonly between plagioclase grains.
Chlorite	1	Vy-Fn	Subhedral	Green (PPL) chlorite occurs after amphibole grains.
Epidote	1	Fn	Anhedral	Pale green with high relief.
Clinozoisite	1	Fn	Anhedral	Similar to epidote but colorless and contains anomalous blue interference.
Carbonate	Tr	Vy-Fn	Anhedral	Anhedral carbonate occurs in very fine-grained blebs.

Reflected

Mineral	%	Grain size	Habit	Comments
Magnetite	Tr	Vy-Fn	Anhedral	Very fine-grained anhedral magnetite is completely surrounded by ilmenite.
Ilmenite	Tr	Vy-Fn	Anhedral	Occurs as a rim around magnetite
Pyrite	tr	Vy-Fn	Euhedral	Cubic in form.

General Notes:

The sample is a medium- to coarse-grained anorthosite. The plagioclase exhibits deformation twins, simple twins and subgrain boundaries. Both magnetite and ilmenite were only observed as one grain whereby ilmenite surrounded magnetite completely.

Slide#	Rock Type
MM-70-1	Massive Oxide

Transmitted

Mineral	%	Grain size	Habit	Comments
Chlorite	5	Fn	Anhedral	Pale green (PPL), steel grey (XPL) fibrous chlorite occurs disseminated throughout.

Reflected

Mineral	%	Grain size	Habit	Comments
Magnetite	74	Fn	Subhedral	Round, exsolution and inclusion-free. Annealing textures common.
Ilmenite	20	Fn	Anhedral	Anhedral to subhedral ilmenite occurs as discrete grains with no magnetite exsolution, and minor chlorite inclusions. Possible subgrains present.
Pyrrhotite	1	Fn	Anhedral	Pyrrhotite hosts very fine-grained pyrite.
Pyrite	Tr	Vy-Fn	Anhedral	Occurs exclusively within pyrrhotite.

General Notes:

The sample is a Massive oxide unit. The oxides are magnetite dominated, and neither ilmenite nor magnetite contains any exsolution textures. Ilmenite occurs as granular grains with rare chlorite inclusions. Annealing texture is pervasive within magnetite and ilmenite.

Slide#	Rock Type
MM-70-2	O-Anorthosite

Transmitted

Mineral	%	Grain size	Habit	Comments
Plagioclase	70	Md	Euhedral	Medium-grained plagioclase laths exhibit deformation twins and simple twins and are commonly poikilitic within very fine-grained inclusions of amphibole crystals.
Amphibole	13	Fn	anhedral	Blue-green (PPL) sub prismatic to anhedral amphibole grains dominantly as intercumulous minerals and contain simple twins.
Biotite	Tr	Vy-Fn	Subhedral	Very fine-grained biotite occurs throughout.
Chlorite	Tr	Fn	Subhedral	Pale green (PPL) to purple/blue (XPL) chlorite forms as fine-grained rims along magnetite-ilmenite grains in contact with plagioclase.
Carbonate	Tr	Vy-Fn	Anhedral	Very fine-grained disseminated carbonate occurs throughout.
Titanite	Tr	Vy-Fn	Anhedral	Occurs alongside few magnetite-ilmenite grains.

Reflected

Mineral	%	Grain size	Habit	Comments
Magnetite	7	Fn	Anhedral	Magnetite occurs as fine-grained anhedral blebs with minor (5%) ilmenite exsolution lamellae, and as exsolution lamellae/blebs within subhedral ilmenite.
Ilmenite	10	Fn	Subhedral	Ilmenite occurs as fine- to medium-grained anhedral to subhedral crystals with minor (5%) magnetite exsolution lamellae/blebs.
Pyrrhotite	tr	Fn	Anhedral	Occurs as disseminated blebs spatially associated with oxides grains and contains pyrite ‘flames’.
Pyrite	tr	Vy-Fn	Subhedral	Occurs exclusively as ‘flames’ within pyrrhotite.
Chalcopyrite	tr	Vy-Fn	Anhedral	Very-fine grained and disseminated, associate with pyrrhotite.

General Notes:

The sample is a massive, medium-grained oxide-anorthosite. The sample is composed of euhedral cumulous plagioclase laths within an intercumulous amphibole-ilmenite-magnetite matrix. The oxides are ilmenite dominant, and both magnetite and ilmenite contain exsolution lamellae and exsolution blebs of each respective oxide. Chlorite occurs as a reaction rim along magnetite-ilmenite grains which contact plagioclase.

Slide#	Rock Type
MM-70-3	O-Anorthosite

Transmitted

Mineral	%	Grain size	Habit	Comments
Plagioclase	70	Md	Euhedral	Medium-grained plagioclase laths exhibit deformation twins and simple twins and are commonly poikilitic within very fine-grained inclusions of amphibole crystals.
Amphibole	tr	Fn	anhedral	Blue-green (PPL) sub prismatic to anhedral amphibole grains dominantly as intercumulous minerals and contain simple twins.
Biotite	5	fn	Subhedral	Biotite is spatially associated with crosscutting veinlets carbonate veinlets.
Chlorite	6	Fn	Subhedral	Pale green (PPL) to purple/blue (XPL) chlorite forms as fine-grained rims along magnetite-ilmenite grains in contact with plagioclase.
Carbonate	Tr	Vy-Fn	Anhedral	Carbonate occurs as sub millimeter cross cutting veinlets

Reflected

Mineral	%	Grain size	Habit	Comments
Magnetite	8	Fn	Anhedral	Magnetite occurs as fine-grained anhedral blebs with minor (5%) ilmenite exsolution lamellae, and as exsolution lamellae/blebs within subhedral ilmenite.
Ilmenite	11	Fn	Subhedral	Ilmenite occurs as fine- to medium-grained anhedral to subhedral crystals with minor (5%) magnetite exsolution lamellae/blebs.
Pyrrhotite	tr	Fn	Anhedral	Occurs as disseminated blebs spatially associated with oxides grains and contains pyrite 'flames'.
Pyrite	tr	Vy-Fn	Subhedral	Occurs exclusively as 'flames' within pyrrhotite.
Chalcopyrite	tr	Vy-Fn	Anhedral	Very-fine grained and disseminated, associate with pyrrhotite.

General Notes: The sample is a massive, medium-grained oxide-anorthosite. The sample is composed of euhedral cumulous plagioclase laths within an intercumulous ilmenite-magnetite matrix which have been cross cut but sub mm biotite-carbonate veinlets (which may be a local feature). The oxides are ilmenite dominant, and both magnetite and ilmenite contain exsolution lamellae and exsolution blebs of each respective oxide. Chlorite occurs as a reaction rim along magnetite-ilmenite grains which contact plagioclase.

Slide#	Rock Type
MM-70-4	O-Leucogabbro

Transmitted

Mineral	%	Grain size	Habit	Comments
Plagioclase	65	Md	Euhedral	Medium-grained plagioclase laths exhibit deformation twins, subgrain boundaries, and weak sericite alteration. Plagioclase contains numerous very fine-grained amphibole rod-shaped inclusions which are oriented parallel to crystallographic planes.
Amphibole	15	Fn	Subhedral	Sub-prismatic blue-green (PPL) amphibole grains exhibit weak compositional zoning and are rarely oikocrystic with inclusions of magnetite.
Biotite	3	Fn	Euhedral	Brown-red biotite laths occur throughout the sample.
Chlorite	2	Vy-Fn	Anhedral	Green (PPL), blue-grey (XPL) chlorite occurs disseminated throughout and along carbonate-epidote veinlets.
Carbonate	Tr	Fn	Anhedral	Carbonate occurs within sub mm veinlets along with epidote and chlorite.
Epidote	Tr	Fn	Anhedral	Occurs exclusively within carbonate veinlets.

Reflected

Mineral	%	Grain size	Habit	Comments
Magnetite	9	Fn	Anhedral	Magnetite blebs occur throughout the sample and contain no ilmenite exsolution lamellae, though grains commonly contain ilmenite inclusions.
Ilmenite	5	Fn	Subhedral	Ilmenite occurs both as tabular fine-grained inclusions within magnetite, and as anhedral blebs along magnetite grain boundaries.
Pyrite	1	Fn	Subhedral	Pyrite occurs disseminated throughout sample and exhibits a sub cubic form.
Chalcopyrite	tr	Vy-Fn	Anhedral	Occurs spatially associated with pyrite.

General Notes:

The sample is a massive, medium-grained oxide-leucogabbro. The sample is largely composed of cumulate plagioclase laths with intercumulous amphibole, magnetite, and ilmenite and late stage cross-cutting carbonate-chlorite-epidote veinlets. The oxides are magnetite dominate, and contains no ilmenite exsolution lamellae.

Slide#	Rock Type
MM-71B-1	O-Pyroxenite

Transmitted

Mineral	%	Grain size	Habit	Comments
Amphibole	70	Md	Subhedral	Blue-green, partially replacing primary clinopyroxene.
Clinopyroxene	15	Fn	Subhedral	Clinopyroxene occurs as aggregates which are surrounded by secondary amphibole grains.
Chlorite	5	Md	Pseudomorphic	Pale green (PPL) to steel grey (XPL) completely replaced primary olivine while preserving relict grain boundaries.
Quartz	Tr	Fn	Anhedral	Only occurs within a cross cutting sub mm veinlet.

Reflected

Mineral	%	Grain size	Habit	Comments
Magnetite	4	Fn	Anhedral	Magnetite occurs as anhedral blebs, and as very fine-grained exsolution lamellae within ilmenite.
Ilmenite	6	Md	Subhedral	Ilmenite occurs as a fine-grained exsolution free phase, and as medium-grained subhedral crystals which contain minor (<5%) magnetite exsolution lamellae.
Pyrite	tr	Fn	Anhedral	Pyrite occurs as very fine-grained blebs disseminated.

General Notes:

The sample is a massive, medium-grained oxide pyroxenite. Chlorite occurs throughout the sample and has completely replaced a fine-grained euhedral mineral with a hexagonal form (possibly olivine). Clinopyroxene is partially to completely replaced by amphibole, and quartz occurs as a very thin cross cutting veinlets.

The oxides are ilmenite dominate which occur as fine-grained exsolution free grains, and as medium-grained magnetite lamellae-bearing grains. The anhedral magnetite is spatially associated with ilmenite and contains no ilmenite exsolution.

Slide#	Rock Type
MM-71B-2	OB-Melanogabbro

Transmitted

Mineral	%	Grain size	Habit	Comments
Plagioclase	15	Md	Euhedral	Occurs as medium-grained laths with deformation and simple twinning, subgrain boundaries, and compositional zoning.
Amphibole	80	Fn	Euhedral	Blue-green, fine-grained amphibole commonly contains very fine-grained inclusions of quartz and local simple twinning.
Quartz	2	Vy-Fn	Anhedral	Occurs solely as very fine-grained inclusions within fine-grained amphibole.
Calcite	tr	Vy-Fn	Anhedral	Very weak pervasive calcite alteration

Reflected

Mineral	%	Grain size	Habit	Comments
Magnetite	tr	Fn	Anhedral	Magnetite occurs along ilmenite grains.
Ilmenite	3	Fn	Subhedral	Anhedral to sub tabular ilmenite occurs as aggregates along with magnetite.
Pyrite	Tr	Fn	Anhedral	Pyrite occurs disseminated throughout sample.

General Notes:

The sample is a massive oxide-bearing melanogabbro with deformed plagioclase and amphibole grains. Calcite occurs as a very weak pervasive alteration. Amphibole commonly contains abundant inclusions of very fine-grained quartz/plagioclase.

The oxides are ilmenite dominate with only trace amounts of magnetite. The magnetite and ilmenite occur alongside each other where ilmenite occurs as anhedral to subhedral grains, and magnetite as anhedral only grains.

Slide#	Rock Type
MM-71B-3	OB-Gabbro

Transmitted

Mineral	%	Grain size	Habit	Comments
Plagioclase	45	Fn-Md	Subhedral	Minor compositional zoning within most grains. Deformation twins are common along with undulose extinction and 'bent' grains. Plagioclase is oikocrystic with ~2% very fine-grained euhedral amphibole crystals.
Amphibole	45	Fn-Md	Subhedral	All grains are blue-green and contain compositional zoning.
Apatite	5	Vy-Fn	Euhedral	Occurs are very fine-grained clusters within masses of amphibole and do not contact plagioclase grains.

Reflected

Mineral	%	Grain size	Habit	Comments
Magnetite	4	Fn	Anhedral	Often pitted and contains minor ilmenite inclusions.
Ilmenite	1	Vy-Fn	Anhedral	Occurs as minor magnetite inclusions or as distinct grains.
Pyrite	Tr.	Vy-Fn	Anhedral	Disseminated throughout.

General Notes:

The sample is an equigranular fine- to medium-grained gabbro. Compositional zoning within plagioclase and amphibole is consistent within all crystals. Apatite occurs as very fine-grained aggregates surrounded by amphibole. Plagioclase contains~2% very fine-grained inclusions of amphibole, but may contain upwards of 10% euhedral inclusions. Magnetite only contains minor exsolutions of ilmenite and is anhedral.

Slide#	Rock Type
MM-110-1	Massive oxide

Transmitted

Mineral	%	Grain size	Habit	Comments
Biotite	13	Fn	Subhedral	Dark brown (PPL) biotite is partially replaced by chlorite.
Chlorite	2	Fn	Subhedral	Pale green (PPL) to brown (XPL) chlorite partially replaces biotite.
Epidote	4	Fn	Anhedral	Anhedral aggregates of epidote occur throughout sample.
Muscovite	1	Fn	Subhedral	Fine to very fine-grained muscovite laths occur as aggregates within the sample.
Carbonate	1	Fn	Anhedral	Carbonate blebs occur disseminated.

Reflected

Mineral	%	Grain size	Habit	Comments
Magnetite	60	Md	Anhedral	Medium-grained magnetite blebs contain very fine- to coarse-grained ilmenite exsolution lamellae, and anhedral inclusions of chlorite and/or epidote.
Ilmenite	20	Fn	Subhedral	Rare subhedral fine-grained ilmenite contains very fine-grained magnetite exsolution. Ilmenite is dominantly present as lamellae within magnetite.
Chromite	tr	Vy-Fn	Anhedral	Very fine grained chromite occurs alongside magnetite and contains abundant pyrite inclusions (~15%).
Pyrite	Tr	Fn	Subhedral	Anhedral to sub cubic pyrite occurs throughout.
Chalcopyrite	Tr	Vy-Fn	Anhedral	Blebs of chalcopyrite occur alongside pyrite grains.

General Notes:

The sample is a massive, fine-grained massive oxide which has been subject to biotite, chlorite, and epidote alteration. The fine- to medium-grained magnetite and ilmenite is surrounded by biotite and epidote. The oxides are dominated by magnetite which contains abundant fine- to coarse- ilmenite exsolution lamellae which accounts for the majority of ilmenite within the sample. Rare fine-grained subhedral ilmenite grains contain very thin exsolution lamellae of magnetite.

Slide#	Rock Type
MM-110-2	OB-Leucogabbro

Transmitted

Mineral	%	Grain size	Habit	Comments
Plagioclase	55	Fn-Md	Subhedral	Plagioclase exhibits moderated deformation twinning and subgrain boundaries. Weak compositional zoning within larger grains.
Amphibole	15	Fn	Euhedral	Blue-green amphibole with few magnetite inclusions.
Orthopyroxene	2	Fn	Anhedral	Partially replaced with amphibole and/or chlorite.
Apatite	1	Fn	Euhedral	Prismatic apatite with undulose extinction.
Quartz	5	Fn	Anhedral	Commonly exhibits subgrain boundaries and undulose extinction.
Biotite	8	Fn-Md	Euhedral	Brown-orange biotite partially replaced by chlorite.
Chlorite	2	Fn	Euhedral	Partially replacing biotite and orthopyroxene.
Clinozoisite	1	Vy-Fn	Anhedral	Disseminated throughout, often associated with calcite.
Epidote	5	Vy-Fn	Anhedral	Occurs disseminated throughout, as a massive alteration veins (1mm)
Titanite	1	Vy-Fn	Euhedral	Prismatic Titanite.
Calcite	tr	Vy-Fn	Anhedral	Occurs as disseminated blebs.

Reflected

Mineral	%	Grain size	Habit	Comments
Magnetite	3	Fn	Subhedral	Magnetite occurs as sub prismatic disseminated grains.
Ilmenite	Tr	Fn	Subhedral	Ilmenite occurs as sub tabular grains which exhibit a wormy to blebby intergrowth of hematite.
Hematite	Tr	Vy-Fn	Anhedral	Hematite occurs strickly within ilmenite grains.
Pyrite	2	Vy-Fn	Subhedral	Sub cubic pyrite occurs disseminated throughout sample.

General Notes: The sample was collected as a late cross cutting microgabbroic dyke. The microgabbro has an oxide-Leucogabbro composition which is massive, fine-grained and exhibits textures of amphibolite-facies metamorphism. The oxides are magnetite dominate which occurs as exsolution-free subhedral disseminated grains. The ilmenite occurs as sub-tabular grains which have blebs and wormy intergrowth of hematite.

Slide#	Rock Type
MM-110-3	O-Pyroxenite

Transmitted

Mineral	%	Grain size	Habit	Comments
Plagioclase	3	Fn	Subhedral	Fine to very fine-grained plagioclase has been partially to completely replaced by sericite alteration.
Clinopyroxene	63	Fn	Subhedral	Elongate colorless (PPL) clinopyroxene commonly exhibits simple twins.
Orthopyroxene	15	Fn	Subhedral	Elongate to rectangular orthopyroxene commonly exhibits undulose extinction.
Amphibole	2	Fn	Anhedral	Blue-green (XPL) amphibole occurs as anhedral to subhedral fine grained crystals.
Serpentine	2	Fn	Anhedral	Serpentine occurs within possible relict fine- to medium grained olivine crystals.
Titanite	tr	Vy-Fn	Anhedral	Rutile blebs occur alongside magnetite-ilmenite.

Reflected

Mineral	%	Grain size	Habit	Comments
Magnetite	9	Md	Anhedral	Fine- to medium-grained magnetite contains thin ilmenite exsolution lamellae.
Ilmenite	4	Fn	Subhedral	Sub tabular ilmenite occurs as a fine-grained magnetite exsolution-free phase, and as a medium-grained sub tabular phase with very thin magnetite exsolution lamellae.
Pyrite	1	Fn	Anhedral	Pyrite occurs as very fine-grained anhedral grains, in places approaching net texture with chalcopyrite and pyrrhotite.
Chalcopyrite	tr	Fn	Anhedral	Chalcopyrite is generally a very-fine grained anhedral crystal which boarders pyrite, and less commonly as atoll textured within plagioclase.
Pyrrhotite	1	Fn	Anhedral	Pyrrhotite occurs alongside pyrite and chalcopyrite.

General Notes:

The sample is a moderately foliated, fine-grained oxide pyroxenite. The sample contains rounded, medium-grained relict crystals (possibly olivine) which have been completely replaced by serpentine. The sulphides and oxides are very heterogeneously distributed and in places approach net textured to massive. Very fine-grained chalcopyrite forms an atoll structure around plagioclase laths.

Slide#	Rock Type
MM-110-4	OR-Leucogabbro

Transmitted

Mineral	%	Grain size	Habit	Comments
Plagioclase	10	Vy-Fn	Anhedral	Plagioclase as very fine-grained anhedral crystals which have been heavily altered by sericite and epidote.
Amphibole	tr	Vy-Fn	Anhedral	Blue-green (PPL) amphibole grains occur disseminated.
Biotite	5	Fn	Euhedral	Brown/red biotite laths which occurs dominantly as a cross cutting band and to a lesser extent as disseminated laths which have been partially to completely replaced by chlorite.
Chlorite	11	Fn	Euhedral	Pale green (PPL) to brown/grey (XPL) fibrous chlorite occurs disseminated throughout and concentrated along magnetite-ilmenite grains.
Carbonate	5	Vu-Fn	Anhedral	Very fine-grained carbonate occurs disseminated throughout but higher concentrations occur along with biotite-bands.
Epidote	19	Fn	Subhedral	Euhedral to anhedral epidote-clinozoisite grains occur as massive aggregates within magnetite-ilmenite grains.

Reflected

Mineral	%	Grain size	Habit	Comments
Magnetite	32	Md	Anhedral	Magnetite occurs as medium-grained blebs with exsolution blebs/ granular exsolution of ilmenite.
Ilmenite	13	Fn	Subhedral	Ilmenite occurs as an exsolution product of magnetite.
Pyrite	tr	Vy-Fn	Subhedral	Disseminated pyrite occurs as anhedral to sub cubic grains.
Chalcopyrite	Tr	Vy-Fn	Anhedral	Blebs of chalcopyrite occur alongside pyrite.

General Notes:

The thin section was cut along the contact of a semi-massive oxide layer, and an oxide-bearing leucogabbro. The unit is a weakly foliated oxide-rich leucogabbro. The plagioclase has largely been replaced by epidote, as well secondary biotite, chlorite and carbonate are present. The oxides are dominated by medium-grained anhedral magnetite which contains ilmenite exsolution granules and blebs.

Slide#	Rock Type
MM-117-1	OB-Leucogabbro

Transmitted

Mineral	%	Grain size	Habit	Comments
Plagioclase	75	Md	Euhedral	Contains strong to moderate deformation twins and locally sutured edges. Plagioclase is oikocrystic with very fine-grained euhedral green amphibole grains.
Amphibole	20	Fn-Md	Euhedral	Blue-green amphibole occurs as fine-grained massive aggregates and as oikocrystic medium grains with plagioclase inclusions. Medium-grained amphibole exhibits suture edges. Local exsolution of amphibole and ilmenite.
Clinozoisite	2	Fn	An-euhedral	Commonly exhibits anomalous blue in cross polarized light, and occurs as massive anhedral very fine-grained grains associated with calcite, and as euhedral fine grained discrete grains.
Calcite	Tr.	Vy-Fn	Anhedral	Calcite occurs within sub mm veinlets, and as pervasive blebs associated with Clinozoisite.

Reflected

Mineral	%	Grain size	Habit	Comments
Ilmenite	2	Fn	Euhedral	Ilmenite occurs as laths within deformed anhedral amphibole grains and form a box-texture, and to a lesser extent as very fine-grained randomly oriented inclusions.
Pyrite	1	Vy-Fn	Anhedral	Disseminated pyrite occurs throughout.

General Notes:

The sample is a massive, medium-grained Oxide-bearing Leucogabbro which has experienced amphibolite facies metamorphism. Plagioclase exhibits strong to moderate deformation twinning and commonly contains sutured edges. Medium-grained amphibole contains abundant plagioclase inclusions and locally ilmenite lamellae which form a box texture. Clinozoisite is strongly associated with blebby pervasive calcite alteration.

Slide#	Rock Type
MM-117-2	O-Gabbro

Transmitted

Mineral	%	Grain size	Habit	Comments
Plagioclase	40	Fn-Cs	Euhedral	Plagioclase occurs as fine-grained subhedral crystals, and as euhedral course-grained crystals with abundant deformation and mechanical twinning.
Amphibole	40	Fn	Subhedral	Fine-grained blue-green amphibole with common twinning.
Clinopyroxene	4	Fn-Md	Subhedral	Colorless needle-like clinopyroxene partially replaced by amphibole.
Orthopyroxene	1	Fn	Anhedral	Colorless anhedral grains almost completely altered to amphibole.
Biotite	Tr.	Fn	Euhedral	Often transitional into chlorite, and typically associated with more massive magnetite-ilmenite.
Chlorite	Tr	Fn	Euhedral	Transitional into biotite, amphibole, and pyroxenes.
epidote	Tr.	Md	Subhedral	Anhedral to subhedral fine- to medium-grained epidote occurs throughout.

Reflected

Mineral	%	Grain size	Habit	Comments
Magnetite	10	Md	Anhedral	Magnetite occurs as medium-grained blebs with exsolution blebs/ granular exsolution of ilmenite.
Ilmenite	4	Fn	Subhedral	Ilmenite occurs as an exsolution product of magnetite.
Pyrite	1	Fn	Anhedral	Pyrite blebs occur throughout.
Chalcopyrite	tr	Vy-Fn	Anhedral	Chalcopyrite occurs alongside pyrite grains.

General Notes:

The sample is a weakly foliated medium-grained oxide-gabbro which has experienced amphibolite facies metamorphism. The thin section is very heterogeneous with a transitional oxide-rich half (~40% magnetite+ ilmenite), and an oxide poor half (~5% magnetite+ ilmenite). Plagioclase occurs as two distinct varieties, as fine-grained subhedral crystals, and as course-grained euhedral crystals with abundant deformation twinning.

Slide#	Rock Type
MM-117-3	OB-Pegmatitic Gabbro

Transmitted

Mineral	%	Grain size	Habit	Comments
Plagioclase	5	Vy-Cs	Subhedral	Subhedral plagioclase is partially to completely replaced by secondary clinozoisite, chlorite, and sericite
Clinopyroxene	45	Peg	Euhedral	Clinopyroxene occurs as very coarse-grained crystals with fine-grained amphibole coronas and abundant chlorite-amphibole alterations which are oriented along crystallographic planes.
Amphibole	20	Fn	Subhedral	Very fine- to fine-grained blue/green (PPL) amphibole grains occur within clinopyroxene and rimming pyroxene
Chlorite	10	Fn	Anhedral	Fibrous pale green (PPL) replacing pyroxene.
Clinozoisite	20	Fn	Subhedral	Anhedral to elongated clinozoisite occurs within relict plagioclase grains and has partially to completely replaced plagioclase.
Titanite	Tr	Vy-Fn	Anhedral	Titanite occurs exclusively as an anhedral corona around magnetite-ilmenite.

Reflected

Mineral	%	Grain size	Habit	Comments
Magnetite	tr	Fn	Anhedral	Magnetite blebs occur within titanite grains.
Ilmenite	Tr	Vy-Fn	Subhedral	Ilmenite lamellae occur within titanite grains.
Pyrite	tr	Vy-Fn	Anhedral	Pyrite occurs disseminated throughout sample.

General Notes:

The sample is a massive, pegmatitic oxide-bearing gabbro. The sample is characterized by clinopyroxene grains (3cm) which contains numerous inclusions of chlorite and amphibole. The clinopyroxene is also rimmed by a corona of very fine-grained amphibole grains. The plagioclase has largely been replaced by clinozoisite, and the magnetite-ilmenite has been largely replaced by titanite where blebs of magnetite and lamellae of ilmenite occur within titanite.

Slide#	Rock Type
MM-117-4	Massive Oxide

Transmitted

Mineral	%	Grain size	Habit	Comments
Serpentine	6	Vy-Fn	Subhedral	Serpentine occurs as fibrous matts within magnetite-ilmenite grains.
Spinel	3	Vy-Fn	Anhedral	Green (PPL) isotropic spinel occurs as very fine-grained anhedral crystals throughout sample. Spinel contains aphanitic inclusions of possible magnetite.
Epidote	Tr	Vy-Fn	Anhedral	Very fine-grained anhedral grains disseminated throughout.

Reflected

Mineral	%	Grain size	Habit	Comments
Magnetite	69	Md	Anhedral	Blebs of magnetite occur throughout and comprise the majority of the sample. Magnetite contains abundant very fine-grained granule (tabular) ilmenite exsolution, and rare lamellae.
Ilmenite	22	Fn	Anhedral	Ilmenite occurs both as fine-grained rounded blebs which contain triple junction boundaries with magnetite, and also as very fine-grained tabular crystals within magnetite grains.
Pyrrhotite	Tr	Fn	Anhedral	Anhedral pyrrhotite occurs disseminated throughout and exhibits lamellae of pyrite.
Pyrite	Tr	Vy-Fn	Euhedral	Pyrite occurs as lamellae within pyrrhotite.
Chalcopyrite	Tr	Fn	Anhedral	Blebs of chalcopyrite occur throughout and typically associated within pyrrhotite.

General Notes:

The sample is a massive textured, fine- to medium-grained massive oxide. The sample is dominantly composed of anhedral magnetite which contains abundant ilmenite granule exsolution and rare lamellae, and ilmenite which occurs as fine-grained anhedral blebs. The sample also contains serpentine and spinel which occur within massive magnetite and ilmenite.

Slide#	Rock Type
MM-117-5	O-Pegmatitic gabbro

Transmitted

Mineral	%	Grain size	Habit	Comments
Plagioclase	40	Vy-Cs	Subhedral	Laths of plagioclase exhibit deformation twins and subgrain boundaries. Plagioclase is cross cut by fine-grained amphibole which are oriented along crystallographic planes.
Clinopyroxene	30	Fn	Subhedral	Fine- to medium-grained clinopyroxene is partially completely replaced by secondary amphibole.
Amphibole	33	Fn	Subhedral	Blue/green (PPL) to green-yellow (XPL) amphibole occurs as fine- to medium-grained crystals which partially replace clinopyroxene and form a corona texture.
Quartz	Tr	Vy-Fn	Anhedral	Very fine-grained quartz occurs in medium-grained oikocrystic amphibole grains.
Epidote	Tr	Vy-Fn	Anhedral	Occurs disseminated throughout.

Reflected

Mineral	%	Grain size	Habit	Comments
Magnetite	3	Fn	Subhedral	Magnetite occurs as subhedral fine-grained crystals within a fine-grained amphibole matrix, and as a fine-grained blebby to skeletal habit with ilmenite lamellae, in a fine-grained amphibole matrix.
Ilmenite	3	Fn	Subhedral	Ilmenite dominantly occurs as a skeletal habit within a fine-grained amphibole matrix, and to a lesser extent as lamellae within magnetite.
Pyrrhotite	1	Fn	Anhedral	Disseminated throughout.
Chalcopyrite	Tr	Fn	Anhedral	Disseminated and typically contacts pyrrhotite.

General Notes:

The sample is a massive, pegmatitic oxide gabbro. The sample is characterized by deformed subhedral plagioclase grains which are >3cm in length, and clinopyroxene which has been partially to completely replaced by fine-grained amphibole. The masses of amphibole locally contain very course-grained skeletal forms of magnetite and ilmenite which likely represent a primary clinopyroxene which had originally contained lamellae of magnetite and ilmenite.

Slide#	Rock Type
MM-117-6	OB-Gabbro

Transmitted

Mineral	%	Grain size	Habit	Comments
Plagioclase	45	Cs	Euhedral	Course-grained poikilitic plagioclase with abundant very fine-grained inclusions of needle-like green amphibole.
Amphibole	45	Fn	Euhedral	Occurs as blue-green, fine-grained massive aggregates. Grains also occasionally contain fine-grained quarts inclusions and magnetite/ilmenite.
Clinopyroxene	5	Fn	Euhedral	Partially replaced by secondary amphibole.
Quartz	2	Vy-Fn	Anhedral	Occurs only as inclusions within amphibole.

Reflected

Mineral	%	Grain size	Habit	Comments
Magnetite	2	Fn	Anhedral	Magnetite occurs as anhedral fine-grained crystals within a fine-grained amphibole matrix, and as a fine-grained blebby to skeletal habit with ilmenite lamellae, in a fine-grained amphibole matrix.
Ilmenite	3	Fn	Subhedral	Ilmenite dominantly occurs as a skeletal habit within a fine-grained amphibole matrix, and to a lesser extent as lamellae within magnetite.
Pyrrhotite	Tr	Vy-Fn	Anhedral	Pyrrhotite occurs disseminated throughout sample.
Chalcopyrite	tr	Vy-Fn	Anhedral	Chalcopyrite occurs alongside pyrrhotite.

General Notes:

The sample is a massive, very course-grained Oxide-bearing gabbro which has been subject to amphibolite facies metamorphism. Plagioclase occurs as very course-grained euhedral laths with numerous very fine-grained green amphibole crystals. Blue/green amphibole comprises the matrix and is observed partially replacing clinopyroxene in a corona texture.

The oxides typically exhibit a skeletal habit within a matrix of fine-grained amphibole. The magnetite grains are generally anhedral and contain abundant coarse ilmenite lamellae.

Slide#	Rock Type
MM-117-7	OB-Pegmatitic Gabbro

Transmitted

Mineral	%	Grain size	Habit	Comments
Plagioclase	50	Peg	Subhedral	Subhedral plagioclase is partially to completely replaced by secondary clinozoisite, chlorite, and sericite. Plagioclase contains abundant deformation twins and subgrains.
Amphibole	41	Fn	Subhedral	Very fine- to fine-grained blue/green (PPL) amphibole grains exhibit compositional zoning.
Chlorite	1	Fn	Anhedral	Fibrous pale green (PPL) replacing pyroxene. Locally kink banding is observed.
Clinozoisite	1	Fn	Subhedral	Anhedral to elongated clinozoisite occurs within relict plagioclase grains and has partially to completely replaced plagioclase.
Biotite	3	Fn	Subhedral	Brown (PPL) biotite occurs within a cross-cutting veinlet.
Carbonate	Tr	Fn	Anhedral	Carbonate occurs along with biotite in veinlets.

Reflected

Mineral	%	Grain size	Habit	Comments
Ilmenite	4	Vy-Fn	Subhedral	Ilmenite occurs solely as a skeletal habit within fine-grained amphibole masses.
Pyrite	Tr.	Vy-Fn	Anhedral	Disseminated pyrite occurs throughout sample.

General Notes:

The sample is a massive, pegmatitic oxide-bearing gabbro. The sample is characterized by deformed subhedral plagioclase grains which are >3cm in length, and clinopyroxene which has been partially to completely replaced by fine-grained amphibole. The masses of amphibole locally contain very medium-grained skeletal forms of ilmenite which likely represent a primary clinopyroxene which had originally contained lamellae of ilmenite.

Slide#	Rock Type
NO-2G21-1	OB-Melanogabbro

Transmitted

Mineral	%	Grain size	Habit	Comments
Clinopyroxene	20	Fn	Euhedral	Partially to completely replaced by secondary chlorite and/or amphibole. Commonly contains very fine-grained inclusions of plagioclase, and contains compositional zoning.
Amphibole	35	Fn	Subhedral	Blue-green amphibole (actinolite var.) occurs as robust and fibrous grains after pyroxene. Commonly poikilitic with inclusions of plagioclase and magnetite-ilmenite.
Plagioclase	5	Md	Anhedral	Plagioclase has almost be completely replaced by very fine grained sericite and epidote, however relict grains can be observed.
Chlorite	30	Md	Anhedral	Blue-green chlorite occurs as fibrous aggregates surrounding pyroxene and amphibole grains.
Epidote	5	Fn	Anhedral	Fine-grained epidote occurs proximal to amphibole and chlorite.

Reflected

Mineral	%	Grain size	Habit	Comments
Magnetite	3	Fn	Anhedral	Contains minor <5% ilmenite exsolution blebs.
Ilmenite	2	Fn	Anhedral	Occurs as along rims of magnetite, and as inclusions within magnetite.
Pyrite	Tr	Fn	Anhedral	Disseminated blebs.

General Notes:

The sample is a heavily amphibolised and chloritised oxide-bearing melanogabbro. The primary plagioclase content is underestimated due to subsequent alteration. The primary mineralogy has been nearly completely replaced by amphibole, chlorite, epidote, and sericite.

The oxides are magnetite dominant where is occurs as blebs. Ilmenite occurs as minor exsolution blebs within magnetite, and also as anhedral rims along magnetite grains.

Slide#	Rock Type
NO-2G21-2	O-Pyroxenite

Transmitted

Mineral	%	Grain size	Habit	Comments
Clinopyroxene	60	Md	Subhedral	Partially to completely replaced by secondary chlorite and/or amphibole. Commonly contains very fine-grained inclusions of chlorite which occur along crystallographic planes.
Amphibole	5	Fn	Subhedral	Blue-green (PPL) amphibole occurs as robust and fibrous grains after pyroxene.
Quartz	5	Fn	Anhedral	Very fine- to fine-grained anhedral quartz occurs within relict plagioclase grains.
Chlorite	10	Md	Anhedral	Blue-green (PPL) to brown (XPL) chlorite occurs as fibrous aggregates surrounding pyroxene and amphibole grains.
Epidote	1	Fn	Anhedral	Fine-grained epidote occurs proximal to amphibole and chlorite.
Carbonate	Tr	Fn	Anhedral	Carbonate occurs as fine-grained aggregates.
Titanite	Tr	Vy-Fn	Anhedral	Very thin rims of titanite form a corona along magnetite and ilmenite grains.

Reflected

Mineral	%	Grain size	Habit	Comments
Magnetite	5	Md	Anhedral	Pitted magnetite contains abundant ilmenite exsolution lamellae (~10%), and is rimmed by titanite.
Ilmenite	4	Md	Anhedral	Ilmenite occurs as lamellae within magnetite, and as discrete, magnetite exsolution-free grains which occur alongside magnetite.
Pyrite	Tr	Fn	Anhedral	Anhedral to sub cubic pyrite occurs throughout sample.
Chalcopyrite	tr	Vy-Fn	Anhedral	Chalcopyrite occurs along and within pyrite grains.

General Notes: The sample is a mass, medium-grained oxide pyroxenite. The clinopyroxene is partially replaced by chlorite and fibrous amphibole. Epidote and chlorite also occur within relict medium-grained laths to rounded grain boundaries. Titanite occurs as a very fine-grained mineral forming a corona texture along magnetite and ilmenite grains.

The oxides are composed of magnetite which contain ilmenite exsolution lamellae, and ilmenite which occurs as medium-grained exsolution-free grains.

Slide#	Rock Type
NO-2G21-3	O-Anorthosite

Transmitted

Mineral	%	Grain size	Habit	Comments
Plagioclase	80	Md	Euhedral	Plagioclase contains undulose extinction, subgrain boundaries, and is partially replaced by epidote-clinozoisite.
Chlorite	5	Fn	Subhedral	Pale green (PPL) to grey (XPL) chlorite occurs in association with epidote alteration.
Epidote	6	Fn	Anhedral	Epidote occurs along magnetite-ilmenite grains and as massive aggregates of rounded epidote grains.
Clinozoisite	2	Vy-Fn	Anhedral	Very fine-grained clinozoisite occurs within altered plagioclase grains.
Biotite	Tr	Vy-Fn	Anhedral	Biotite occurs exclusively within box work magnetite-ilmenite grains.
Carbonate	Tr	Fn	Anhedral	Carbonate occurs as disseminated grains.

Reflected

Mineral	%	Grain size	Habit	Comments
Magnetite	5	Fn	Anhedral	Magnetite has been partially to completely replaced by epidote, and contains ilmenite exsolution lamellae (5%).
Ilmenite	2	Vy-Fn	Subhedral	Ilmenite occurs exclusively as lamellae within magnetite.
Pyrite	Tr	Fn	Anhedral	Anhedral to sub cubic pyrite occurs throughout sample.
Chalcopyrite	tr	Vy-Fn	Anhedral	Chalcopyrite occurs along and within pyrite grains.

General Notes:

The sample is a massive, medium-grained, oxide anorthosite. The sample exhibits pervasive replacements of plagioclase and magnetite by epidote, chlorite, and clinozoisite. Locally magnetite has been completely replaced; however, the ilmenite lamellae are unaltered.

Slide#	Rock Type
NO-2G21-4	OR-Leucogabbro

Transmitted

Mineral	%	Grain size	Habit	Comments
Plagioclase	2	Md	Euhedral	Medium-grained plagioclase laths have been partially to completely replaced by epidote-chlorite alteration.
Chlorite	30	Fn	Euhedral	Pale green (PPL) to grey (XPL) chlorite occurs throughout the sample as massive aggregates within relict grain boundaries.
Epidote	22	Fn	Anhedral	Anhedral to subhedral epidote occurs throughout and locally rims magnetite-ilmenite grains.
Carbonate	1	Fn	Anhedral	Carbonate aggregates occur throughout sample.

Reflected

Mineral	%	Grain size	Habit	Comments
Magnetite	35	Md	Anhedral	Magnetite occurs as anhedral blebs which contain abundant very fine-grained ilmenite lamellae and blebs (10%). Magnetite is rimmed by epidote and is partially replaced.
Ilmenite	10	Fn	Anhedral	Ilmenite dominantly occurs as exsolution lamellae within magnetite, and less commonly as discrete fine-grained anhedral blebs.
Pyrite	1	Fn	Anhedral	Anhedral to sub cubic pyrite occurs throughout sample.
Pyrrhotite	Tr.	Fn	Anhedral	Pyrrhotite occurs throughout and often contacts pyrite.
Chalcopyrite	Tr.	Vy-Fn	Anhedral	Chalcopyrite occurs along and within pyrite grains and along the contacts of pyrite and pyrrhotite.

General Notes:

The sample is a massive, medium-grained oxide-rich leucogabbro. The primary plagioclase has largely been altered by fine-grained anhedral epidote, which also replaces magnetite grains. Chlorite occurs as a fibrous aggregate and may have completely replaced a primary mafic phase (e.g. pyroxene). The oxides are dominated by medium-grained magnetite which contains abundant ilmenite exsolution lamellae. Ilmenite also occurs to a lesser extent as discrete fine-grained blebs alongside magnetite. Pyrite has partially to completely replaced pyrrhotite and locally chalcopyrite occurs within the contact of the sulphides.

Slide#	Rock Type
NO-2G21-5	OR-Anorthosite

Transmitted

Mineral	%	Grain size	Habit	Comments
Plagioclase	20	Md	Euhedral	Medium-grained plagioclase laths have been partially to completely replaced by epidote-chlorite-sericite alteration. Plagioclase also contains deformation twins and subgrain boundaries.
Chlorite	5	Fn	Euhedral	Pale green (PPL) to grey (XPL) chlorite occurs throughout the sample as massive aggregates within relict grain boundaries.
Epidote	40	Fn	Anhedral	Anhedral to subhedral epidote occurs throughout and locally rims magnetite-ilmenite grains.

Reflected

Mineral	%	Grain size	Habit	Comments
Magnetite	24	Md	Anhedral	Heavily pitted magnetite occurs as anhedral blebs which contain abundant very fine-grained ilmenite lamellae and blebs (10%). Magnetite is rimmed by epidote and is partially replaced.
Ilmenite	11	Fn	Anhedral	Ilmenite dominantly occurs as exsolution lamellae within magnetite, and less commonly as discrete fine-grained anhedral blebs.
Pyrite	1	Fn	Anhedral	Anhedral to sub cubic pyrite occurs throughout sample.
Chalcopyrite	Tr.	Vy-Fn	Anhedral	Chalcopyrite occurs along and within pyrite grains.

General Notes:

The sample is a massive, medium-grained oxide-rich anorthosite. The primary plagioclase has largely been altered by fine-grained anhedral epidote, which also replaces magnetite grains. Chlorite occurs as a fibrous aggregate and may have completely replaced a primary mafic phase (e.g. pyroxene).

The oxides are dominated by medium-grained magnetite which contains abundant ilmenite exsolution lamellae. Ilmenite also occurs to a lesser extent as discrete fine-grained blebs alongside magnetite.

Slide#	Rock Type
NO-2G21-6	OR-Anorthosite

Transmitted

Mineral	%	Grain size	Habit	Comments
Plagioclase	30	Fn	Anhedral	Fine- to very fine-grained plagioclase exists as anhedral grains within sericitized medium-grained relict euhedral plagioclase boundaries.
Chlorite	15	Fn	Euhedral	Grey-Blue chlorite occurs as fibrous veinlets, and disseminated throughout.
Epidote	20	Fn	Subhedral	Very fine-grained anhedral epidote occurs within relict plagioclase grains, but dominantly as fine- to medium-grained crystals rimming magnetite-ilmenite. Commonly contains compositional zoning and/or simple twins.
Sericite	5	Vy-Fn	Euhedral	Partially replacing euhedral medium-grained plagioclase grains.
Carbonate	5	Fn	Anhedral	Spatially associated with sericite and fine-grained epidote.

Reflected

Mineral	%	Grain size	Habit	Comments
Magnetite	18	Md	Anhedral	Pitted magnetite contains numerous (~5%) well-formed ilmenite exsolution lamellae
Ilmenite	7	Fn	Anhedral	Occurs as discrete fine-grained crystals, and as exsolution within magnetite
Pyrite	Tr	Fn	Anhedral	Disseminated throughout.
Chalcopyrite	Tr	Vy-Fn	Anhedral	Occur within pyrite grains.

General Notes:

The sample is a massive, fine- to medium-grained oxide-rich anorthosite. The primary euhedral medium-grained plagioclase exhibit relict grain boundaries and are largely replaced with sericite, epidote, chlorite, carbonate, and fine-grained anhedral plagioclase. Chlorite occurs as veinlets cross cutting the sample, and as an alteration of plagioclase.

The oxides are magnetite dominated which contain well formed ilmenite exsolution lamellae (~5%). Ilmenite also occurs as fine-grained euhedral crystals.

Slide#	Rock Type
NO-2G21-7	SMO-Gabbro

Transmitted

Mineral	%	Grain size	Habit	Comments
Plagioclase	5	Vy-Fn	Anhedral	Plagioclase is almost completely altered by chlorite and carbonate however it retains relict grain boundaries.
Clinopyroxene	10	Fn	Anhedral	Clinopyroxene is partially to completely replaced by chlorite
Chlorite	33	Fn	Subhedral	Steel-blue (XPL) fibrous mats of chlorite replace clinopyroxene and plagioclase.
Carbonate	2	Fn	Anhedral	Carbonate occurs throughout but primarily associated with altered plagioclase.

Reflected

Mineral	%	Grain size	Habit	Comments
Magnetite	35	Fn	Anhedral	Magnetite contains abundant well-formed ilmenite exsolutions (15%), and in places appears to have brecciated boundaries.
Ilmenite	15	Fn	Subhedral	Approximately half of the ilmenite occurs within magnetite as exsolution, and the other half as subhedral grains spatially associated within magnetite.
Pyrite	1	Fn	Euhedral	Cubic pyrite is uncommon and dominantly occurs as disseminated blebs.
Pyrrhotite	Tr.	Vy-fn	Anhedral	Disseminated blebs occur with other sulphides.
Chalcopyrite	Tr.	Vy-fn	Anhedral	Disseminated blebs occur with other sulphides.

General Notes:

The sample is a massive, medium-grained semi-massive oxide gabbro. The original composition of the rock has been significantly altered as much of the original plagioclase and clinopyroxene has been replaced. Chlorite is the dominate silicate present and has partially to completely replaced the original mineralogy however the relict grain boundaries remain.

Magnetite is the dominate oxide present and contains approximately half of the ilmenite as well-formed exsolution lamellae. Magnetite, unlike ilmenite contains a weak pitted texture.

Slide#	Rock Type
NO-2G21-8	OB-Anorthosite

Transmitted

Mineral	%	Grain size	Habit	Comments
Plagioclase	85	Md	Euhedral	Cumulate plagioclase grains have been heavily replaced by sericite (~50-70%) with lesser epidote, clinozoisite, and quartz. Relict grain boundaries are well preserved.
Chlorite	Tr.	Fn	Subhedral	Light green chlorite occurs typically along magnetite-ilmenite grains.
Epidote	5	Fn	Subhedral	Granular epidote occurs throughout but concentrated along magnetite-ilmenite grain boundaries.
Clinozoisite	5	Vy-Fn	Anhedral	Occurs disseminated throughout the altered plagioclase grains.
Quartz	Tr.	Fn	Anhedral	Quartz occurs in granular patches associated with altered plagioclase.

Reflected

Mineral	%	Grain size	Habit	Comments
Magnetite	3	Md	Anhedral	Pitted magnetite contains inclusions of epidote and chlorite and abundant very fine-grained ilmenite lamellae. Magnetite is partially replaced by epidote which rims the magnetite grains.
Ilmenite	1	Fn	Subhedral	Ilmenite occurs as blebs to sub tabular grains associated with magnetite, and as lamellae within magnetite.
Pyrite	1	Fn	Anhedral	Fine- to medium-grained pyrite occurs throughout sample and is partially replaced by pyrrhotite.
Pyrrhotite	Tr.	Vy-Fn	Anhedral	Pyrrhotite occurs within the cores of pyrite and is partially to completely replaced by pyrite.

General Notes:

The sample is a massive, medium-grained oxide-bearing anorthosite which has been subjected to pervasive alteration. The plagioclase retains primary grain boundaries; however they have been largely replaced by sericite (50-70%), with lesser epidote, clinozoisite, and quartz. Magnetite contains abundant very fine-grained ilmenite lamellae, and is partially replaced by chlorite and epidote. The ilmenite also occurs as fine- to medium-grained anhedral to subtabular grains. Pyrite partially to completely replaces pyrrhotite.

Slide#	Rock Type
NO-2G21-9	Massive Oxide

Transmitted

Mineral	%	Grain size	Habit	Comments
Chlorite	10	Fn	Anhedral	Fibrous steel-blue (XPL) chlorite occurs within massive magnetite-ilmenite.
Carbonate	5	Fn	Anhedral	Carbonate blebs occur throughout sample.
Quartz	Tr.	Fn	Anhedral	Occurs within matts of chlorite and contains undulose extinction and subgrains.

Reflected

Mineral	%	Grain size	Habit	Comments
Magnetite	70	Fn	Anhedral	Contains pervasive ilmenite exsolution 10%. Few magnetite grains contain silicate intergrowths along cleavage planes which have now been replaced by chlorite. Few magnetite rims are exsolution-free and approaching euhedral crystal boundaries.
Ilmenite	14	Fn	Subhedral	Dominantly occurs as massive aggregates, and to a lesser extent within magnetite as exsolution.
Pyrite	1	Fn	Anhedral	Disseminated pyrite occurs as blebs throughout.

General Notes:

The sample is a massive to weakly sheared massive oxide unit. The original silicates have been completely replaced within chlorite carbonate and trace quartz.

The oxides are magnetite dominated. The magnetite however, contains abundant ilmenite exsolution lamellae (~10%). The magnetite also displays various ilmenite exsolution textures ranging from ilmenite blebs, to lamellae. Few rims of magnetite are exsolution-free and approach a euhedral magnetite habit. Ilmenite also occurs as discrete aggregates along with exsolution.

Slide#	Rock Type
NO-2G21-10	OR-Anorthosite

Transmitted

Mineral	%	Grain size	Habit	Comments
Plagioclase	Tr.	Vy-Fn	Anhedral	Medium- to coarse-grained relict plagioclase has been heavily altered and only present as very fine-grained anhedral crystals.
Quartz	25	Fn	Anhedral	Occurs within relict plagioclase boundaries.
Epidote	5	Fn	Subhedral	Epidote occurs as fine-grained euhedral crystals alongside magnetite-ilmenite grains, and as a very fine-grained crystal within relict plagioclase grains.
Chlorite	30	Fn	Subhedral	Chlorite occurs as fine-grained subhedral crystals alongside magnetite-ilmenite grains, as a very fine-grained crystal within relict plagioclase grains and/or as micro veins.
Sericite	5	Vy-Fn	Euhedral	Sericite occurs throughout relict plagioclase grains.

Reflected

Mineral	%	Grain size	Habit	Comments
Magnetite	17	Md	Anhedral	Contains various proportions of ilmenite exsolution lamellae (0-10), which range from well-formed lamellae, to a very fine-grained disseminated blebs. Rare euhedral magnetite grain boundaries are ilmenite-free.
Ilmenite	8	Md	Anhedral	Ilmenite dominantly occurs within magnetite as exsolution lamellae, and to a lesser extent as medium-grained anhedral crystals.
Pyrite	Tr.	Fn	Anhedral	Fine- to medium-grained pyrite throughout and partially replaced by pyrrhotite.
Pyrrhotite	Tr.	Fn	Anhedral	Associated with pyrite.
Chalcopyrite	Tr.	Fn	Anhedral	Associated with pyrite.

General Notes:

The sample is a massive, medium-grained oxide-rich anorthosite. The primary plagioclase has been heavily altered and largely replaced by a combination of quartz, epidote, chlorite, and sericite; however the relict plagioclase grain boundaries remain unaltered. Magnetite contains varying textures and ilmenite exsolution. Ilmenite contains rims of chlorite inclusions.

Slide#	Rock Type
NO-2G21-11	OR-Anorthosite

Transmitted

Mineral	%	Grain size	Habit	Comments
Plagioclase	2	Vy-Fn	Anhedral	Medium- to coarse-grained relict plagioclase has been heavily altered and only present as very fine-grained anhedral crystals.
Quartz	Tr.	Fn	Anhedral	Occurs within relict plagioclase boundaries.
Epidote	30	Fn	Subhedral	Epidote occurs as fine-grained euhedral crystals alongside magnetite-ilmenite grains, and as a very fine-grained crystal within relict plagioclase grains.
Chlorite	28	Fn	Subhedral	Chlorite occurs as fine-grained subhedral crystals alongside magnetite-ilmenite grains, as a very fine-grained crystal within relict plagioclase grains and/or as micro veins.
Carbonate	Tr.	Fn	Anhedral	Carbonate aggregates occur throughout.

Reflected

Mineral	%	Grain size	Habit	Comments
Magnetite	40	Md	Anhedral	Aggregates of pitted magnetite blebs contain both coarse-grained and very fine-grained ilmenite lamellae.
Ilmenite	8	Vy-Fn	Subhedral	Ilmenite only occurs as lamellae within magnetite blebs.
Pyrite	Tr.	Fn	Anhedral	Pyrite occurs within as blebs and along the contacts of pyrrhotite grains.
Pyrrhotite	2	Fn	Anhedral	Pyrrhotite contains lamellae and blebs of pyrite.
Chalcopyrite	Tr.	Vy-Fn	Anhedral	Chalcopyrite occurs alongside pyrite and chalcopyrite.

General Notes:

The sample is a massive to weakly foliated, medium-grained oxide-rich anorthosite. The primary plagioclase has almost completely been replaced by epidote and quartz which occur within medium- to coarse-grained relict plagioclase boundaries. Chlorite occurs as a corona alongside medium-grained magnetite aggregates which contain both very fine-grained ilmenite lamellae, and rare coarse-grained ilmenite lamellae. Pyrrhotite is partially replaced by pyrite.

Slide#	Rock Type
NO-2G21-12	OR-Anorthosite

Transmitted

Mineral	%	Grain size	Habit	Comments
Plagioclase	10	Vy-Fn	Anhedral	Medium- to coarse-grained relict plagioclase has been heavily altered and only present as very fine-grained anhedral crystals.
Quartz	10	Fn	Anhedral	Occurs within relict plagioclase boundaries.
Epidote	15	Fn	Subhedral	Epidote occurs as fine-grained euhedral crystals alongside magnetite-ilmenite grains, and as a very fine-grained crystal within relict plagioclase grains.
Chlorite	20	Fn	Subhedral	Chlorite occurs as fine-grained subhedral crystals alongside magnetite-ilmenite grains, as a very fine-grained crystal within relict plagioclase grains and/or as micro veins.

Reflected

Mineral	%	Grain size	Habit	Comments
Magnetite	30	Md	Anhedral	Aggregates of pitted magnetite blebs contain both coarse-grained and very fine-grained ilmenite lamellae and rare blebs.
Ilmenite	13	Md	Anhedral	Fine- to medium-grained blebs of ilmenite occur alongside magnetite and contain very fine-grained magnetite lamellae (1%)
Pyrite	2	Fn	Anhedral	Pyrite occurs disseminated throughout the sample
Pyrrhotite	Tr.	Fn	Anhedral	Pyrrhotite occurs alongside pyrite.
Chalcopyrite	Tr.	Vy-Fn	Anhedral	Chalcopyrite occurs alongside pyrite and chalcopyrite.

General Notes:

The sample is a massive to weakly foliated, medium-grained oxide-rich anorthosite. The primary plagioclase has almost completely been replaced by epidote and quartz which occur within medium- to coarse-grained relict plagioclase boundaries. Chlorite occurs as a corona alongside medium-grained magnetite aggregates which contain both very fine-grained ilmenite lamellae, and rare coarse-grained ilmenite lamellae. Ilmenite occurs also as discrete fine- to medium-grained crystals which contain very fine-grained magnetite lamellae.

Slide#	Rock Type
NO-2G21-13	OB-Melanogabbro

Transmitted

Mineral	%	Grain size	Habit	Comments
Plagioclase	10	Md	Euhedral	Plagioclase has nearly been completely replaced by epidote; however the relict crystal boundaries remain.
Amphibole	70	Fn	Subhedral	Green amphibole has partially to completely replaced primary pyroxene. Amphibole contains minor compositional zoning within medium-grained crystals.
Clinopyroxene	5	Fn	Euhedral	Clinopyroxene is exclusively surrounded by secondary amphibole.
Chlorite	5	Fn	Anhedral	Fibrous chlorite is spatially associated with magnetite-ilmenite and amphibole.
epidote	10	Vy-Fn	Anhedral	Semi-massive epidote occurs after plagioclase and less commonly within chlorite.
Quartz	Tr.	Fn	Anhedral	Quartz contains undulose extinction and subgrains.

Reflected

Mineral	%	Grain size	Habit	Comments
Magnetite	2	Fn	Anhedral	Magnetite contains minor <5% ilmenite exsolution lamelea, and often has a pitted texture.
Ilmenite	2	Fn	Anhedral	Occurs as discrete grains and within magnetite as exsolution.
Pyrite	1	Fn	Anhedral	Blebs of disseminated pyrite throughout.
Chalcopyrite	Tr.	Fn	Anhedral	Blebs of chalcopyrite associated with pyrite.

General Notes:

The sample is an amphibole-epidote-chlorite altered medium-grained weakly foliated oxide-bearing melanogabbro. Epidote has nearly completely replaced plagioclase grains. Amphibole and chlorite has partially to completely replaced clinopyroxene.

Magnetite and ilmenite occur in roughly equal proportions. Magnetite contains a pitted texture with exsolution lamellae of ilmenite.

Slide#	Rock Type
NO-2G22-1	OR-Melanogabbro

Transmitted

Mineral	%	Grain size	Habit	Comments
Plagioclase	3	Vy-Fn	Anhedral	Plagioclase occur as anhedral very fine-grained crystals within relict fine- to medium-grained plagioclase boundaries which have been replaced with chlorite-epidote-quartz.
Pyroxene	1	Vy-Fn	Euhedral	Dusty pyroxene is completely rimmed with amphibole grains. Cannot be distinguished between clino or orthopyroxene.
Amphibole	40	Fn	Subhedral	Anhedral to sub prismatic blue/green (PPL) amphibole rims pyroxene grains and is partially replaced by chlorite.
Quartz	1	Vy-Fn	Anhedral	Quartz occurs within relict plagioclase grains as anhedral very fine-grained crystals.
Epidote	15	Fn	Subhedral	Anhedral to subhedral epidote occurs throughout and partially rims magnetite-ilmenite grains.
Chlorite	15	Fn	Subhedral	Pale green (PPL) to grey (XPL) chlorite occurs throughout and partially rims amphibole, magnetite, and ilmenite.

Reflected

Mineral	%	Grain size	Habit	Comments
Magnetite	15	Md	Anhedral	Aggregates of pitted magnetite blebs contain both coarse-grained and very fine-grained ilmenite lamellae.
Ilmenite	8	Fn	Subhedral	Fine- to medium-grained sub-tabular ilmenite occurs alongside magnetite.
Pyrite	2	Fn	Anhedral	Blebs of pyrite occur disseminated throughout.
Chalcopyrite	Tr.	Vy-Fn	Anhedral	Chalcopyrite occurs alongside pyrite grains.

General Notes:

The sample is a massive, medium-grained oxide-rich melanogabbro. The sample has been heavily altered to amphibole, epidote, and chlorite after pyroxene and to a lesser extent, magnetite and plagioclase. Relict grain boundaries of plagioclase and pyroxene are abundant and the magnetite is rimmed by a chlorite-epidote assemblage.

The oxides are dominated by medium-grained blebs of magnetite which contain ilmenite lamellae. Ilmenite also occurs as discrete grains which are magnetite lamellae-free.

Slide#	Rock Type
NO-2G22-2	O-Melanogabbro

Transmitted

Mineral	%	Grain size	Habit	Comments
Plagioclase	15	Md	Euhedral	Plagioclase laths have been partially replaced by epidote and chlorite grains. The plagioclase contains deformation twins and simple twins.
Clinopyroxene	35	Md	Subhedral	Primary clinopyroxene contains coronas of amphibole grains and exhibits fine-grained abundant chlorite-amphibole alteration along crystal planes.
Amphibole	35	Fn	Anhedral	Blue/green (PPL) amphibole partially to completely replaces clinopyroxene and forms a corona texture.
Epidote	4	Fn	Subhedral	Sub tabular to rounded epidote occurs throughout sample
Chlorite	6	Fn	Subhedral	Pale green (PPL) to grey (XPL) chlorite replaces clinopyroxene and is associated with amphibole replacement.

Reflected

Mineral	%	Grain size	Habit	Comments
Magnetite	2	Fn	Anhedral	Magnetite occurs as disseminated fine- to medium-grained ilmenite lamellae-bearing (10%) crystals, and as lamellae within ilmenite.
Ilmenite	3	Fn	Anhedral	Ilmenite occurs largely as discrete magnetite lamellae-bearing (2%) crystals and to a lesser extent as lamellae within magnetite.
Pyrite	Tr.	Fn	Anhedral	Blebs of pyrite occur disseminated throughout.

General Notes:

The sample is a massive, medium-grained oxide melanogabbro. The primary clinopyroxene has been partially to completely altered to amphibole and chlorite, and the plagioclase has been partially altered to epidote and chlorite. The oxides are ilmenite dominant and both magnetite and ilmenite contain exsolution lamellae of their respective oxide species.

Slide#	Rock Type
NO-2G22-4	O-Anorthosite

Transmitted

Mineral	%	Grain size	Habit	Comments
Plagioclase	66	Md	Euhedral	Medium grained plagioclase laths exhibit deformation twins, undulose extinction, and subgrain boundaries. The plagioclase is rimmed by very fine-grained anhedral quartz.
Amphibole	2	Fn	Subhedral	Blue/green (PPL) amphibole occurs as elongate and fibrous fine-grained crystals which generally rim magnetite-ilmenite grains.
Epidote	7	Fn	Euhedral	Subhedral to euhedral tabular epidote occurs throughout sample and contains simple twins.
Chlorite	4	Fn	Subhedral	Pale green (PPL) fibrous chlorite partially replaces amphibole grains.
Quartz	2	Vy-Fn	Anhedral	Quartz occurs exclusively as very fine-grained anhedral corona textured grains which surround plagioclase laths.
Carbonate	Tr.	Vy-Fn	Anhedral	Disseminated carbonate occurs throughout.

Reflected

Mineral	%	Grain size	Habit	Comments
Magnetite	5	Fn	Anhedral	Aggregates of fine- to medium-grained magnetite occur throughout the sample and contain abundant ilmenite lamellae and blebs (10%).
Ilmenite	5	Fn	Subhedral	Fine- to medium-grained subhedral to anhedral ilmenite occurs alongside magnetite and contains very fine-grained hematite lamellae (2%).
Hematite	Tr.	Vy-Fn	Euhedral	Hematite occurs exclusively as very thin lamellae within ilmenite grains.
Pyrite	1	Fn	Anhedral	Blebs of pyrite occur throughout the sample.

General Notes:

The sample is a massive, medium-grained oxide anorthosite. The sample is dominantly composed of euhedral plagioclase laths with intercumulus magnetite and ilmenite. The plagioclase contains numerous very fine-grained amphibole needles which are oriented along the crystallographic planes, and have been partially altered by epidote. The magnetite and ilmenite contain a corona of chlorite. The oxides occur as anhedral blebs and the magnetite contains abundant ilmenite lamellae and blebs, and the ilmenite contains minor amounts of hematite lamellae.

Slide#	Rock Type
NO-2G22-5	OB-Gabbro

Transmitted

Mineral	%	Grain size	Habit	Comments
Plagioclase	45	Md	Euhedral	Plagioclase laths exhibit deformation twins, undulose extinction, and subgrain boundaries.
Clinopyroxene	1	Md	Euhedral	Primary clinopyroxene is has been partially to completely replaced by amphibole.
Amphibole	45	Md	Subhedral	Blue/green (PPL) amphibole occurs as elongate and fibrous fine-grained crystals which rim clinopyroxene grains.
Epidote	3	Fn	Euhedral	Subhedral to euhedral tabular epidote occurs throughout sample and contains simple twins.
Chlorite	2	Fn	Subhedral	Pale green (PPL) fibrous chlorite partially replaces clinopyroxene grains.
Carbonate	1	Fn	Anhedral	Fine-grained carbonate occurs within mm-scale veinlets.
Quartz	Tr.	Fn	Anhedral	Quartz occurs exclusively as very fine-grained euhedral corona textured grains which surround plagioclase laths.

Reflected

Mineral	%	Grain size	Habit	Comments
Magnetite	Tr.	Vy-Fn	Anhedral	Magnetite occurs as very fine-grained blebs alongside ilmenite and has been partially to completely replaced by chlorite and epidote.
Ilmenite	2	Fn	Subhedral	Ilmenite occurs as discrete fine- to medium-grains with minor hematite lamellae (1%), and to a lesser extent as lamellae within pyroxene and amphibole.
Hematite	Tr.	Vy-Fn	Euhedral	Hematite occurs exclusively as lamellae within ilmenite.
Pyrite	1	Vy-Fn	Anhedral	Pyrite occurs disseminated throughout.

General Notes: The sample is a massive, medium-grained oxide-bearing gabbro. The primary plagioclase has been partially replaced by epidote and quartz, and the clinopyroxene has partially to completely been replaced by amphibole. The amphiboles contain abundant inclusions of blebby carbonate, and chlorite, and 60^{o}-120^{o} oriented lamellae of ilmenite. The oxides are dominated by ilmenite, which contains minor hematite exsolution lamellae. Magnetite occurs in trace amounts as very fine-grained blebs alongside ilmenite, and is partially to completely altered by epidote and chlorite.

Slide#	Rock Type
NO-2G22-6	O-Melanogabbro

Transmitted

Mineral	%	Grain size	Habit	Comments
Plagioclase	7	Vy-Fn	Euhedral	The plagioclase is forms anhedral inter granular crystals which have largely been replaced by anhedral epidote.
Clinopyroxene	5	Md	Euhedral	Primary clinopyroxene is has been partially to completely replaced by amphibole. Pyroxene also is commonly oikocrystic with euhedral opaque minerals and carbonate grains.
Amphibole	63	Md	Subhedral	Blue/green (PPL) amphibole occurs as elongate and fibrous fine-grained crystals which rim clinopyroxene grains. Amphibole exhibits undulose extinction and subgrains.
Epidote	3	Fn	Subhedral	Subhedral to euhedral tabular epidote occurs throughout sample and contains simple twins.
Chlorite	15	Fn	Subhedral	Pale green (PPL) to grey (XPL) fibrous chlorite partially replaces clinopyroxene grains.
Carbonate	1	Fn	Anhedral	Very fine-grained carbonate occurs within oikocrystic pyroxene
Quartz	Tr.	Fn	Anhedral	Quartz occurs exclusively as very fine-grained euhedral corona textured grains which surround plagioclase laths.

Reflected

Mineral	%	Grain size	Habit	Comments
Magnetite	2	Fn	Anhedral	Pitted magnetite contains abundant very fine-grained ilmenite blebs and lamellae.
Ilmenite	4	Fn	Anhedral	Fine- to medium-grained ilmenite occurs as anhedral to subhedral grains which contain trace hematite lamellae.
Hematite	Tr.	Vy-Fn	Euhedral	Hematite occurs as lamellae in ilmenite.
Pyrite	Tr.	Vy-Fn	Anhedral	Very fine-grained blebs of pyrite occur disseminated throughout.

General Notes: The sample is a massive, medium-grained, oxide melanogabbro. The primary clinopyroxene has been partially to completely replaced by amphibole and chlorite grains, and the plagioclase has been recrystallized and altered to epidote and quartz. The oxides are dominantly composed of anhedral to subhedral ilmenite grains which contain trace hematite lamellae. The magnetite contains abundant ilmenite blebs and lamellae.

Slide#	Rock Type
NO-2G25-1	O-Melanogabbro

Transmitted

Mineral	%	Grain size	Habit	Comments
Plagioclase	15	Fn	Anhedral	Fine-grained anhedral plagioclase exhibits undulose extinction, simple twins, and is partially replaced by sericite.
Clinopyroxene	25	Fn	Euhedral	Pyroxene is partially to completely replaced by amphibole and is completely rimmed by amphibole.
Amphibole	42	Fn	Subhedral	Blue/green (PPL) amphibole partially to completely replaces pyroxene and pseudomorphs pyroxene.
Chlorite	8	Fn	Anhedral	Pale green (PPL) to grey (XPL) chlorite is associated with amphibole alteration.
Epidote	2	Fn	Anhedral	Epidote occurs as cross cutting veinlets.
Carbonate	Tr.	Vy-Fn	Anhedral	Carbonate occurs within the core of epidote veinlets.
Titanite	Tr.	Vy-Fn	Anhedral	Titanite occurs as a corona mineral along ilmenite grains.

Reflected

Mineral	%	Grain size	Habit	Comments
Magnetite	4	Fn	Anhedral	Fine-grained blebs of magnetite occur throughout sample and contain coarse-grained ilmenite lamellae.
Ilmenite	4	Fn	Anhedral	Ilmenite occurs alongside magnetite as discrete grains which are rimmed by titanite, and also as lamellae within magnetite. Ilmenite contains rare, very fine-grained lamellae of hematite.
Hematite	Tr.	Vy-Fn	Euhedral	Hematite occurs exclusively as lamellae within ilmenite.
Pyrite	Tr.	Vy-Fn	Anhedral	Pyrite occurs as disseminated blebs.

General Notes:

The sample is a massive, fine-grained oxide melanogabbro. The unit is composed of clinopyroxene which has partially to completely been replaced by amphibole and chlorite, and plagioclase which has been partially altered to sericite and epidote. Ilmenite is rimmed with a very thin corona of titanite, and the ilmenite contains rare hematite exsolution lamellae. The magnetite occurs as fine-grained blebs throughout the sample and exhibit coarse lamellae of ilmenite.

Slide#	Rock Type
NO-2G25-2	O-Pyroxenite

Transmitted

Mineral	%	Grain size	Habit	Comments
Plagioclase	3	Vy-Fn	Anhedral	The plagioclase is forms anhedral inter granular crystals which have largely been replaced by anhedral epidote.
Clinopyroxene	15	Md	Subhedral	Primary clinopyroxene is has been partially to completely replaced by amphibole. Pyroxene also is commonly oikocrystic with euhedral opaque minerals and carbonate grains.
Amphibole	58	Md	Anhedral	Blue/green (PPL) amphibole occurs as elongate and fibrous fine-grained crystals which rim clinopyroxene grains. Amphibole exhibits undulose extinction and subgrains.
Epidote	2	Fn	Anhedral	Subhedral to euhedral tabular epidote occurs throughout sample and contains simple twins.
Chlorite	10	Fn	Anhedral	Pale green (PPL) to brown (XPL) fibrous chlorite partially replaces clinopyroxene grains.
Quartz	Tr.	Vy-Fn	Anhedral	Quartz occurs alongside altered plagioclase grains, and associated with chlorite alteration.
Titanite	Tr.	Vy-Fn	Anhedral	Titanite occurs as a corona mineral along oxides.

Reflected

Mineral	%	Grain size	Habit	Comments
Magnetite	5	Fn	Anhedral	Fine-grained blebs of magnetite occur throughout sample and contain coarse-grained ilmenite lamellae.
Ilmenite	6	Md	Anhedral	Ilmenite occurs alongside magnetite as discrete grains which are rimmed by titanite, and also as lamellae within magnetite. Ilmenite contains rare, very fine-grained lamellae of hematite.
Hematite	Tr.	Vy-Fn	Euhedral	Hematite occurs as lamellae within ilmenite.
Pyrrhotite	1	Vy-Fn	Anhedral	Pyrrhotite occurs as disseminated grains.
Pyrite	Tr.	Vy-Fn	Subhedral	Sub cubic pyrite occurs alongside pyrrhotite.
Chalcopyrite	Tr.	Vy-Fn	Anhedral	Blebs of chalcopyrite occur along pyrrhotite and pyrite grain boundaries.

General Notes:The sample is a massive, medium-grained oxide pyroxenite. The primary clinopyroxene has been partially to completely altered to amphibole and chlorite. Plagioclase has been altered to quartz and epidote.

Slide#	Rock Type
NO-2G25-3	O-Anorthosite

Transmitted

Mineral	%	Grain size	Habit	Comments
Plagioclase	50	Md	Euhedral	Plagioclase is partially replaced by epidote and has destroyed many primary textures.
Orthoclase	15	Fn	Anhedral	Occurs as aggregates of very-fine to fine-grained crystals with subgrain boundaries and undulose extinction.
Epidote	15	Vy-Fn	Anhedral	Selectively replaces plagioclase grains, often associated with chlorite.
Chlorite	8	Fn	Anhedral	Blue-green chlorite occurs as fibrous matts largely along magnetite-ilmenite grains, and as disseminated grains along with epidote.
Carbonate	5	Fn	Anhedral	Blebs of carbonate are disseminated throughout and contain subgrains.

Reflected

Mineral	%	Grain size	Habit	Comments
Magnetite	2	Fn	Anhedral	Contains a pitted texture. Occurs within ilmenite, but dominantly as a pitted grain.
Ilmenite	4	Fn	Subhedral	Ilmenite contains minor magnetite exsolution blebs and is typically a discrete grain spatially associated with magnetite.
Pyrite	1	Fn	Anhedral	Blebs of disseminated fine-grained pyrite throughout.

General Notes:

The sample is a heavily epidote-chlorite-orthoclase altered oxide anorthosite. Much of the primary plagioclase has been replaced by an epidote-chlorite-carbonate assemblage. Orthoclase occurs as very fine-grained to fine-grained mats with subgrains.

The oxides are ilmenite dominated which contain minor magnetite exsolution blebs. Magnetite contains a pitted texture and commonly is associated with ilmenite grains.

Slide#	Rock Type
NO-2G25-4	OR-Anorthosite

Transmitted

Mineral	%	Grain size	Habit	Comments
Plagioclase	14	Vy-Fn	Anhedral	Medium- to coarse-grained relict plagioclase has been heavily altered and only present as very fine-grained anhedral crystals.
Quartz	25	Vy-Fn	Anhedral	Occurs within relict plagioclase boundaries.
Epidote	20	Fn	Euhedral	Epidote occurs as fine-grained euhedral crystals alongside magnetite-ilmenite grains, and as a very fine-grained crystal within relict plagioclase grains.
Chlorite	10	Fn	Subhedral	Chlorite occurs as fine-grained subhedral crystals alongside magnetite-ilmenite grains, and as a very fine-grained crystal within relict plagioclase grains.
Sericite	1	Vy-Fn	Euhedral	Sericite occurs throughout relict plagioclase.
Clinozoisite	Tr.	Fn	Anhedral	Clinozoisite occurs as anhedral blebs which partially replace plagioclase grains.

Reflected

Mineral	%	Grain size	Habit	Comments
Magnetite	20	Md	Anhedral	Contains various proportions of ilmenite exsolution lamellae (0-10), which range from well-formed lamellae, to a very fine-grained disseminated blebs. Rare euhedral magnetite grain boundaries are ilmenite-free.
Ilmenite	7	Md	Anhedral	Ilmenite dominantly occurs within magnetite as exsolution lamellae, and to a lesser extent as medium-grained anhedral crystals.
Pyrite	2	Fn	Anhedral	Fine- to medium-grained pyrite throughout and partially replaced by pyrrhotite.
Pyrrhotite	1	Fn	Anhedral	Associated with pyrite.
Chalcopyrite	Tr.	Fn	Anhedral	Associated with pyrite.

General Notes:

The sample is a massive, medium-grained oxide-rich anorthosite. The primary plagioclase has been heavily altered and largely replaced by a combination of quartz, epidote, chlorite, and sericite, however the relict plagioclase grain boundaries remains unaltered. Magnetite contains varying textures and ilmenite exsolution.

Slide#	Rock Type
NO-2G25-5	OR-Gabbro

Transmitted

Mineral	%	Grain size	Habit	Comments
Clinopyroxene	10	Fn	Euhedral	Pyroxene is partially to completely replaced by chlorite and reaches first order blue/red birefringence. Pyroxene also contains compositional zoning and deformation twins.
Quartz	10	Fn	Anhedral	Occurs as fine to very fine-grained crystals with undulose extinction and subgrain boundaries.
Chlorite	27	Fn	Euhedral	Green (PPL) with strong anomalous blue interference colors (XPL). Chlorite occurs as massive fibrous matts and replaces pyroxene.
Carbonate	10	Fn	Anhedral	Blebs of carbonate occur throughout but are spatially associated with quartz.
Epidote	1	Vy-Fn	Anhedral	Occurs with chlorite-altered clinopyroxene.

Reflected

Mineral	%	Grain size	Habit	Comments
Magnetite	25	Md	Anhedral	Contains well-formed ilmenite lamella exsolution and exhibits a 'brecciated' grain boundary
Ilmenite	15	Fn	Anhedral	Occurs as discrete fine-grains crystals and as exsolution within magnetite.
Pyrite	2	Fn	Subhedral	Subhedral cubic pyrite occurs throughout the sample
Pyrrhotite	Tr.	Fn	Anhedral	Typically rims pyrite
Chalcopyrite	Tr.	Vy-Fn	Anhedral	Very fine-grained disseminated chalcopyrite occurs within pyrite and pyrrhotite.

General Notes:

The sample is a medium-grained, massive to weakly foliated oxide-rich gabbro which has been subject to strong pervasive chlorite-carbonate-epidote alteration which has almost completely replaced the primary mineralogy. Clinopyroxene is partially to completely replaced and where present, contains compositional zoning and deformation twins.

The oxides are magnetite dominated and contain which formed ilmenite exsolution lamellae. Ilmenite also occurs as discrete anhedral grains.

Slide#	Rock Type
NO-2G25-6	SMO-Gabbro

Transmitted

Mineral	%	Grain size	Habit	Comments
Chlorite	25	Fn	Anhedral	Pale green (PPL) – grey/blue (XPL) fibrous chlorite occurs throughout the sample and in largely concentrated within chlorite-oxide-rich bands and is an interstitial mineral within magnetite-ilmenite grains.
Carbonate	30	Fn	Anhedral	Very fine- to fine-grained carbonate occurs throughout the sample but is largely concentrated in chlorite-oxide-poor bands.
Quartz	Tr.	Fn	Anhedral	Trace anhedral quartz occur within carbonate-rich bands.

Reflected

Mineral	%	Grain size	Habit	Comments
Magnetite	25	Fn	Anhedral	Fine- to medium-grained magnetite blebs contain abundant (10%) very fine-grained ilmenite exsolution lamellae.
Ilmenite	20	Vy-Fn	Euhedral	Ilmenite occurs as exsolution lamellae within magnetite, but is dominantly present as very fine-grained tabular crystals which are randomly oriented.
Chalcopyrite	Tr.	Fn	Anhedral	Chalcopyrite is the dominate sulphide and occurs as an intercumulate mineral within magnetite and ilmenite.
Pyrite	Tr.	Vy-Fn	Anhedral	Pyrite occurs alongside chalcopyrite

General Notes:

The sample is a well foliated chlorite-magnetite- carbonate-ilmenite schist. The primary silicate mineralogy has been completely replaced by chlorite, carbonate, and trace amounts of quartz which are concentrated into bands, and may have reflected an originally gabbroic lithology. The magnetite occurs as medium-grained anhedral blebs with abundant very fine-grained ilmenite lamellae. The ilmenite occurs dominantly as very fine-grained tabular grains which are randomly oriented.

Slide#	Rock Type
NO-2G25-7	SMO-Gabbro

Transmitted

Mineral	%	Grain size	Habit	Comments
Chlorite	28	Fn	Subhedral	Pale green (PPL) to grey/blue (XPL) chlorite occurs throughout sample.
Epidote	22	Fn	Anhedral	Epidote blebs occur throughout sample and appear to have a strong association with quartz.
Quartz	5	Vy-Fn	Anhedral	Very fine-grained quartz grains appear to be within relict plagioclase laths.

Reflected

Mineral	%	Grain size	Habit	Comments
Magnetite	25	Md	Anhedral	Fine- to medium-grained magnetite blebs contain abundant (10%) very fine-grained ilmenite exsolution lamellae.
Ilmenite	20	Md	Anhedral	Ilmenite occurs as exsolution lamellae within magnetite, and as discrete fine- to medium-grained anhedral to sub tabular grains.
Pyrite	5	Fn	Anhedral	Blebs of pyrite occur throughout.
Pyrrhotite	2	Fn	Anhedral	Pyrrhotite contains flames of pyrite.
Chalcopyrite	Tr.	Vy-Fn	Anhedral	Anhedral chalcopyrite occurs alongside pyrite and pyrrhotite.

General Notes:

The sample is a massive, fine- to medium-grained semi-massive oxide gabbro. The primary plagioclase has been completely replaced by epidote and quartz which occur within relict medium-grained plagioclase boundaries. Magnetite and ilmenite have been partially replaced by epidote and chlorite.

The oxides are dominantly composed of magnetite grains which contain abundant very fine-grained ilmenite lamellae and blebs. Ilmenite also occurs as discrete, lamellae-free grains. Pyrrhotite has been partially to completely replaced by pyrite.

Slide#	Rock Type
NO-2G25-8	O-Anorthosite

Transmitted

Mineral	%	Grain size	Habit	Comments
Plagioclase	70	Vy-Fn	Anhedral	Plagioclase occurs as very fine-grained recrystallized minerals within medium-grained plagioclase lath relict boundaries.
Epidote	7	Fn	Anhedral	Rounded epidote occurs as fine- to medium-grained crystals.
Chlorite	6	Fn	Anhedral	Pale green (PPL) to grey (XPL) chlorite rims magnetite-ilmenite grains.
Clinozoisite	10	Vy-Fn	Anhedral	Very fine-grained clinozoisite occurs as clusters within plagioclase grains.

Reflected

Mineral	%	Grain size	Habit	Comments
Magnetite	2	Fn	Anhedral	Magnetite has been partially replaced by chlorite, and contains abundant (10%) coarse ilmenite lamellae.
Ilmenite	3	Fn	Anhedral	Ilmenite blebs occur throughout sample and have not been replaced by chlorite. Ilmenite contains rare hematite lamellae.
Hematite	Tr.	Vy-Fn	Euhedral	Occurs exclusively within ilmenite.
Pyrite	1	Fn	Anhedral	Blebs of pyrite occur throughout.
Pyrrhotite	Tr.	Vy-Fn	Anhedral	Pyrrhotite contains flames of pyrite.

General Notes:

The sample is a massive, medium-grained oxide anorthosite. The unit is dominantly composed of medium-grained plagioclase laths which have been recrystallized into very fine-grained crystals and partially replaced by epidote and clinozoisite. Magnetite contains abundant coarse ilmenite lamellae and has been partially replaced by chlorite. Ilmenite also occurs as discrete grains which contain rare hematite exsolution lamellae.

Slide#	Rock Type
NO-2G25-9	O-Pyroxenite

Transmitted

Mineral	%	Grain size	Habit	Comments
Clinopyroxene	10	Md	Euhedral	Primary clinopyroxene is has been partially to completely replaced by amphibole which form a corona. Pyroxene also is commonly oikocrystic with chlorite and amphibole grains.
Amphibole	80	Md	Subhedral	Blue/green (PPL) amphibole occurs as elongate and fibrous fine-grained crystals which rim clinopyroxene grains. Amphibole exhibits undulose extinction and subgrains.
Chlorite	2	Fn	Anhedral	Pale green (PPL) to brown (XPL) fibrous chlorite partially replaces clinopyroxene grains.
Quartz	Tr	Vy-Fn	Anhedral	Very fine-grained anhedral quartz occurs alongside carbonate grains.
Carbonate	1	Fn	Anhedral	Fine-grained carbonate occurs throughout sample.

Reflected

Mineral	%	Grain size	Habit	Comments
Magnetite	3	Fn	Anhedral	Magnetite has been partially replaced by chlorite, and contains abundant (10%) coarse ilmenite lamellae.
Ilmenite	3	Md	Anhedral	Ilmenite occurs throughout sample as lamellae within magnetite, and as discrete fine- to medium-grains. Ilmenite contains rare hematite lamellae.
Hematite	Tr.	Vy-Fn	Euhedral	Occurs exclusively within ilmenite.
Pyrrhotite	1	Fn	Anhedral	Blebs of pyrrhotite occur throughout.

General Notes:

The sample is a massive, medium-grained oxide pyroxenite. The primary clinopyroxene has been partially to completely altered to amphibole and chlorite. Magnetite has partially been altered to chlorite. The magnetite also contains abundant, coarse ilmenite lamellae. The ilmenite is also present as discrete fine- to medium-grained hematite lamellae-bearing grains.

Slide#	Rock Type
NO-2G25-10	OB-Gabbro

Transmitted

Mineral	%	Grain size	Habit	Comments
Plagioclase	3	Vy-Fn	Anhedral	The plagioclase is forms anhedral inter granular crystals which have largely been replaced by anhedral epidote and clinozoisite.
Clinopyroxene	2	Fn	Subhedral	Primary clinopyroxene is has been partially to completely replaced by amphibole which form a corona. Pyroxene also is commonly oikocrystic with quartz and carbonate grains.
Amphibole	64	Md	Subhedral	Blue/green (PPL) amphibole occurs as elongate and fibrous fine-grained crystals which rim clinopyroxene grains. Amphibole exhibits undulose extinction and subgrains.
Epidote	5	Fn	Anhedral	Epidote alters from plagioclase
Clinozoisite	10	Vy-Fn	Anhedral	Clinozoisite alters from plagioclase.
Chlorite	10	Fn	Subhedral	Pale green (PPL) to brown (XPL) fibrous chlorite partially replaces clinopyroxene grains.
Quartz	2	Vy-Fn	Anhedral	Quartz occurs alongside altered plagioclase grains, and associated with chlorite alteration.
Titanite	1	Vy-Fn	Anhedral	Titanite partially to completely replaces magnetite and ilmenite.

Reflected

Mineral	%	Grain size	Habit	Comments
Magnetite	3	Md	Anhedral	Magnetite has been partially replaced by chlorite, and contains abundant (10%) coarse ilmenite lamellae.
Ilmenite	1	Fn	Anhedral	Ilmenite occurs throughout sample as lamellae within magnetite, and as discrete fine- to medium-grains. Ilmenite contains rare hematite lamellae.
Pyrrhotite	Tr.	Vy-Fn	Anhedral	Very fine-grained pyrrhotite occurs disseminated.
Chalcopyrite	Tr.	Vy-Fn	Anhedral	Blebs of chalcopyrite occur alongside pyrrhotite.

General Notes: The sample is a massive, medium-grained oxide-bearing gabbro. The primary clinopyroxene has been partially to completely altered to amphibole and chlorite. Magnetite has partially been altered to chlorite. The magnetite also contains abundant, coarse ilmenite lamellae. The ilmenite is also present as discrete fine- to medium-grains which have been partially to completely altered to titanite.

Slide#	Rock Type
NO-2G46-1	SMO-Pyroxenite

Transmitted

Mineral	%	Grain size	Habit	Comments
Chlorite	22	Fn	Anhedral	Pale green (PPL) to steel grey (XPL) chlorite occurs as radial to fibrous grains within intercumulate magnetite-ilmenite.
Amphibole	10	Vy-Fn	Anhedral	Dark green/blue amphibole occurs exclusively as very fine-grained coronas along magnetite-ilmenite grains.
Epidote	3	Vy-Fn	Anhedral	Very fine-grained epidote occurs within very fine-grained magnetite-ilmenite aggregates.

Reflected

Mineral	%	Grain size	Habit	Comments
Magnetite	3	Md	Anhedral	Blebs of pitted magnetite contain abundant (20%) ilmenite lamellae. Magnetite is also partially replaced by chlorite and contains inclusions of pyrite.
Ilmenite	35	Md	Anhedral	Ilmenite occurs as medium-grained discrete exsolution-free grains, and also as lamellae within magnetite. Ilmenite also contains inclusions of fine-grained pyrite.
Pyrite	2	Fn	Anhedral	Pyrite occurs as very fine- to fine-grained disseminated grains along the edges of magnetite and ilmenite, and also as inclusions within magnetite and ilmenite. Pyrite is also locally replaced by ilmenite.
Chalcopyrite	Tr.	Vy-Fn	Anhedral	Very fine-grained chalcopyrite occurs alongside pyrite.

General Notes:

The sample is a massive, fine- to medium-grained semi-massive oxide pyroxenite. The primary pyroxene has been completely replaced by iron-rich chlorite, amphibole, and epidote. Relict grain boundaries of primary pyroxene are preserved, however are now composed of a core of chlorite with an outer rim of amphibole. The sample is ilmenite dominate and is observed as fine- to medium-grained discrete grains, as lamellae within magnetite, and as a secondary replacement after pyrite. Ilmenite also occurs as semi-massive very fine-grained inclusions within massive epidote-pyrite aggregates. Magnetite occurs as anhedral medium-grained blebs which host abundant ilmenite lamellae.

Slide#	Rock Type
NO-2G46-3	OB-Gabbro

Transmitted

Mineral	%	Grain size	Habit	Comments
Plagioclase	25	Md	Euhedral	Plagioclase is brecciated, contains subgrain boundaries, undulose extinction, and compositional zoning.
Amphibole	60	Fn	Euhedral	Occurs as green (PPL) fibrous matts which partially to completely replace clinopyroxene.
Clinopyroxene	3	Fn	Euhedral	Clinopyroxene has partially to completely been replaced by amphibole and chlorite.
Chlorite	9	Fn	Euhedral	Blue-green chlorite rims amphibole and pyroxene grains.

Reflected

Mineral	%	Grain size	Habit	Comments
Magnetite	1	Fn	Anhedral	Pitted magnetite contains ilmenite exsolution lamellae.
Ilmenite	2	Fn	Anhedral	Occurs as exsolution within magnetite, and as discrete grains.
Pyrite	Tr.	Vy-Fn	Euhedral	Cubic pyrite is disseminated throughout the sample.

General Notes:

The sample is a weakly to moderately foliated, fine- to medium-grained oxide-bearing gabbro. The sample has been subject to weak mylonitization and strong amphibole-chlorite alteration. Plagioclase exhibits evidence of strong deformation (i.e. subgrain boundaries, undulose extinction, compositional zoning, and brecciated edges).

The oxides are ilmenite dominated, which is present as distinct grains and as exsolution within magnetite. The magnetite is pitted and contains well formed ilmenite exsolution.

Slide#	Rock Type
NO-2G46-4	OB-Gabbro

Transmitted

Mineral	%	Grain size	Habit	Comments
Amphibole	55	Fn	Anhedral	Blue-green amphibole occurs throughout the sample as fibrous matts.
Plagioclase	25	Md	Euhedral	Plagioclase has been partially to completely replaced by chlorite and sericite. Commonly contains deformation twins.
Apatite	5	Fn	Euhedral	Hexagonal apatite occurs throughout sample.
Chlorite	11	Fn	Euhedral	Contains strong anomalous blue interference and rims plagioclase.

Reflected

Mineral	%	Grain size	Habit	Comments
Magnetite	1	Fn	Anhedral	Magnetite contains a 'pitted' texture and contains ilmenite exsolution lamellae.
Ilmenite	3	Fn-Md	Anhedral	Occurs as discrete grains, and to a lesser extent within magnetite.
Pyrite	Tr.	Vy-Fn	Anhedral	Pyrite occurs as very fine-grained blebs throughout.

General Notes:

The sample is a massive, medium-grained oxide-bearing gabbro. The sample has been extensively and pervasively altered by secondary amphibole and chlorite. Plagioclase is distinguishable, however it is partially to completely replaced by chlorite. Apatite occurs as euhedral hexagonal grains throughout the sample.

The oxides are ilmenite-dominated which occurs as discrete anhedral grains, and within magnetite as exsolution lamellae. Magnetite occurs as fine-grained anhedral blebs.

Slide#	Rock Type
NO-2G46-5	O-Melanogabbro

Transmitted

Mineral	%	Grain size	Habit	Comments
Amphibole	15	Md	Euhedral	Amphibole occurs as fibrous medium-grained crystals which reach up to first order blue interference colors.
Apatite	6	Fn	Euhedral	Hexagonal apatite occurs throughout although seems to be associated spatially with magnetite-ilmenite. Apatite contains minor undulose extinction.
Chlorite	70	Fn	Euhedral	Chlorite occurs as blue-green fibrous matts with a steel blue birefringence, and as typical green chlorite.

Reflected

Mineral	%	Grain size	Habit	Comments
Magnetite	3	Md	Anhedral	Spatially associated with ilmenite.
Ilmenite	6	Fn	Anhedral	Occurs as discrete grains alongside magnetite.

General Notes:

The sample is a medium-grained, massive oxide melanogabbro which has been completely amphibolized and chloritised. The sample is dominated by secondary fibrous amphibole and two distinct varieties of chlorite which likely are related to the respective primary mineral. The blue-chlorite is believed to have a higher iron content, and thus likely correspond to Fe-rich mafic silicate minerals. The apatite contains undulose extinction and partially brecciated boundaries.

The oxides are ilmenite-dominated and spatially associated with magnetite. Both the oxides are exsolution-free.

Slide#	Rock Type
NO-2G46-6	Oxide-Melanogabbro

Transmitted

Mineral	%	Grain size	Habit	Comments
Plagioclase	2	Fn	Euhedral	Plagioclase has almost been completely replaced by sericite, epidote, and chlorite. Grains contain abundant deformation twins and subgrains.
Amphibole	15	Md	Euhedral	Amphibole occurs as fibrous medium-grained crystals which reach up to first order blue interference colors.
Apatite	15	Fn	Euhedral	Hexagonal apatite occurs throughout although seems to be associated spatially with magnetite-ilmenite. Apatite contains minor undulose extinction.
Chlorite	52	Fn	Euhedral	Chlorite occurs as blue-green fibrous matts with a steel blue birefringence, and as typical green chlorite.
Epidote	5	Vy-Fn	Anhedral	Occurs as massive medium-grained clots with very fine-grained abundant magnetite-ilmenite crystals.

Reflected

Mineral	%	Grain size	Habit	Comments
Magnetite	2	Vy-Fn	Anhedral	Occurs as very fine-grained specks within epidote clusters, and as fine-grained grains with ilmenite exsolution lamellae (~10%).
Ilmenite	9	Fn	Anhedral	Dominantly occurs as fine- to medium-grained crystals with numerous very fine-grained magnetite exsolution (~5%). Also occurs as very fine-grained disseminated grains associated with epidote.

General Notes:

The sample is a heavily amphibole-chlorite-epidote altered oxide melanogabbro. The primary composition has largely been altered by secondary amphibole, chlorite, and epidote which have partially to completely replaced plagioclase and pyroxene. Apatite is common throughout sample and commonly associated with magnetite-ilmenite. The oxides are ilmenite-dominated which contain very fine-grained magnetite exsolutions. The magnetite occurs with abundant well formed ilmenite exsolution, and within massive epidote aggregates.

Slide#	Rock Type
NO-2G47-1	O-Melanogabbro

Transmitted

Mineral	%	Grain size	Habit	Comments
Plagioclase	12	Vy-Fn	Anhedral	Plagioclase occurs as recrystallized very fine-grained crystals within medium-grained relict plagioclase lath boundaries.
Clinopyroxene	3	Mf	Subhedral	Primary clinopyroxene is has been partially to completely replaced by amphibole which form a corona. Pyroxene also is commonly oikocrystic with amphibole and magnetite-ilmenite.
Amphibole	52	Fn	Subhedral	Blue/green (PPL) amphibole occurs as elongate and fibrous fine-grained crystals which rim clinopyroxene grains.
Chlorite	23	Fn	Subhedral	Pale green (PPL) to steel grey (XPL) and occurs largely within relict plagioclase laths

Reflected

Mineral	%	Grain size	Habit	Comments
Magnetite	2	Fn	Anhedral	Very fine- to fine-grained magnetite contains abundant, coarse ilmenite lamellae and typically found alongside ilmenite grains.
Ilmenite	8	Md	Anhedral	Fine- to medium-grained ilmenite contains trace to 2% lamellae of hematite. Ilmenite also occurs as lamellae within magnetite.
Hematite	Tr.	Vy-Fn	Euhedral	Hematite occurs exclusively as very thin lamellae within ilmenite.
Pyrite	1	Fn	Anhedral	Very fine- to fine-grained pyrite occurs disseminated throughout sample.

General Notes:

The sample is a massive to weakly foliated oxide-melanogabbro. The primary plagioclase has been largely recrystallized as very fine-grained plagioclase within relict medium-grained lath-like boundaries. The clinopyroxene has been partially to completely replaced by secondary amphibole and chlorite. Few grains of clinopyroxene contain abundant (20%) inclusions of very fine-grained ilmenite and/or pyrite.

The dominate oxide is ilmenite which occurs as medium-grained hematite lamellae-bearing discrete grains, and as a lesser extent as lamellae within magnetite. The magnetite is generally fine-grained and partially replaced by chlorite.

Slide#	Rock Type
NO-2G47-2	OB-Leucogabbro

Transmitted

Mineral	%	Grain size	Habit	Comments
Plagioclase	66	Md	Euhedral	Fine- to medium-grained plagioclase laths exhibit undulose extinction, deformation twins, compositional zoning, and subgrain boundaries.
Clinopyroxene	8	Fn	Subhedral	Clinopyroxene is rimmed by amphibole and chlorite grains.
Amphibole	15	Fn	Subhedral	Blue/green amphibole partially to completely replaces clinopyroxene.
Chlorite	5	Fn	Subhedral	Chlorite rims clinopyroxene and is associated with amphibole grains.
Epidote	3	Vy-Fn	Anhedral	Very fine-grained epidote occurs in clusters within plagioclase laths.
Clinozoisite	1	Vy-Fn	Anhedral	Very fine-grained clinozoisite occurs as clusters within plagioclase laths and spatially associated with epidote.
Quartz	Tr.	Vy-Fn	Anhedral	Very-fine-grained quartz occur as inclusions within secondary amphibole.
Titanite	Tr.	Vy-Fn	Anhedral	Very thin rims of titanite occur as a corona along all ilmenite grains.

Reflected

Mineral	%	Grain size	Habit	Comments
Ilmenite	2	Fn	Anhedral	Ilmenite blebs occur throughout the sample and are partially to completely replaced by coronas of titanite.
Pyrite	tr	Vy-fn	Subhedral	Very fine-grained pyrite blebs, and locally sub cubic pyrite occurs disseminated throughout sample.

General Notes:

The sample is a massive to weakly foliated oxide-bearing leucogabbro. The plagioclase exhibits simple twins, compositional zoning, deformation twins, undulose extinction, subgrains boundaries, and it partially replaced by clinozoisite, and epidote. The clinopyroxene has been partially to completely altered by amphibole and chlorite.

The only oxide species present is ilmenite which is partially to completely replaced by titanite which occurs as very thin coronas along the grain boundaries of each ilmenite grain.

Slide#	Rock Type
NO-2G47-3	O-Leucogabbro

Transmitted

Mineral	%	Grain size	Habit	Comments
Plagioclase	64	Md	Euhedral	Fine- to medium-grained plagioclase laths exhibit undulose extinction, deformation twins, compositional zoning, and subgrain boundaries.
Clinopyroxene	2	Md	Subhedral	Clinopyroxene has been partially to completely replaced by amphibole.
Amphibole	20	Vy-Fn	Subhedral	Blue/green amphibole occurs as radiating very fine-grained crystals which surround clinopyroxene and magnetite-ilmenite grains.
Sericite	1	Vy-Fn		Sericite occurs as patchy alteration within the cores of plagioclase laths.
Epidote	2	Vy-Fn	Anhedral	Epidote occurs as very fine-grained aggregates within magnetite-ilmenite inclusion-rich relict grain boundaries.

Reflected

Mineral	%	Grain size	Habit	Comments
Magnetite	2	Vy-Fn	Anhedral	Magnetite occurs as very fine-grained needle-like, and or fibrous inclusions within massive aggregates of very fine-grained epidote, and as very fine-grained rounded blebs alongside ilmenite which contains trace ilmenite exsolution blebs.
Ilmenite	9	Md	Anhedral	Fine- to medium-grained ilmenite occurs throughout the sample and contains trace hematite exsolution lamellae.
Hematite	Tr.	Vy-Fn	Euhedral	Hematite occurs exclusively as very fine-grained lamellae within ilmenite.
Pyrite	Tr.	Fn	Anhedral	Pyrite blebs occur disseminated throughout the sample.

General Notes: The sample is a massive, medium-grained oxide leucogabbro. The sample is dominantly composed of medium-grained cumulate plagioclase laths which have been extensively altered and partially replaced by sericite and epidote. The clinopyroxene has partially to completely been replaced by amphibole. The oxides are dominated by medium-grained hematite exsolution-bearing ilmenite grains. Magnetite occurs as very fine-grained fibrous/ needle-like aggregates along with very fine-grained chlorite, amphibole and epidote within relict medium-grained anhedral grain boundaries.

Slide#	Rock Type
NO-2G47-4	O-Melanogabbro

Transmitted

Mineral	%	Grain size	Habit	Comments
Plagioclase	9	Md	Euhedral	Fine- to medium-grained plagioclase laths exhibit undulose extinction, deformation twins, compositional zoning, and subgrain boundaries.
Amphibole	52	Vy-Fn	Subhedral	Blue/green amphibole occurs as radiating very fine-grained crystals which surround magnetite-ilmenite grains.
Chlorite	21	Fn	Subhedral	Pale green (PPL) to steel grey (XPL) chlorite rims amphibole grains and within magnetite-ilmenite grains.
Epidote	Tr	Vy-Fn	Anhedral	Epidote occurs as very fine-grained aggregates within magnetite-ilmenite inclusion-rich relict grain boundaries.

Reflected

Mineral	%	Grain size	Habit	Comments
Magnetite	5	Fn	Anhedral	Magnetite occurs as very fine-grained needle-like, and or fibrous inclusions within massive aggregates of very fine-grained epidote, and as fine-grained rounded blebs alongside ilmenite which contain abundant ilmenite exsolution granules and coarse lamellae.
Ilmenite	13	Md	Anhedral	Fine- to medium-grained ilmenite occurs throughout the sample and contains trace hematite exsolution lamellae.
Hematite	tr	Vy-Fn	Euhedral	Hematite occurs exclusively as very fine-grained lamellae and/or blebs within ilmenite.
Pyrite	tr	Vy-Fn	Anhedral	Pyrite blebs occur disseminated throughout the sample.

General Notes: The sample is a massive, medium-grained oxide melanogabbro. The sample is composed of medium-grained cumulate plagioclase laths which have been extensively altered and partially replaced by sericite and epidote. The clinopyroxene has partially to completely been replaced by amphibole. The oxides are dominated by medium-grained hematite exsolution-bearing ilmenite grains. Magnetite contains both fine-grained ilmenite granules and/or lamellae and occurs as very fine-grained fibrous / needle-like aggregates along with very fine-grained chlorite, amphibole and epidote within relict medium-grained anhedral grain boundaries.

Slide#	Rock Type
NO-2G47-4B	O-melanogabbro

Transmitted

Mineral	%	Grain size	Habit	Comments
Plagioclase	9	Fn	Euhedral	Fine- to medium-grained plagioclase laths exhibit undulose extinction, deformation twins, compositional zoning, and subgrain boundaries.
Clinopyroxene	2	Vy-Fn	Anhedral	Clinopyroxene has been partially to completely replaced by amphibole.
Amphibole	61	Vy-Fn	Subhedral	Blue/green amphibole occurs as radiating very fine-grained crystals which surround magnetite-ilmenite grains.
Chlorite	18	Fn	Anhedral	Pale green (PPL) to steel grey (XPL) chlorite rims amphibole grains and is within magnetite-ilmenite grains.

Reflected

Mineral	%	Grain size	Habit	Comments
Magnetite	2	Fn	Anhedral	Magnetite occurs alongside ilmenite aggregates and contains ilmenite lamellae.
Ilmenite	8	Fn	Anhedral	Fine- to medium-grained ilmenite occurs throughout sample as discrete grains, and as lamellae within magnetite.
Pyrite	Tr.	Vy-Fn	Anhedral	Blebs of very fine-grained pyrite occur throughout the sample.

General Notes:

The sample is a weakly foliated, medium-grained oxide melanogabbro. The primary plagioclase and pyroxene have been heavily deformed and replaced by chlorite and amphibole (respectively). The magnetite has partially to completely been replaced by aggregates of chlorite and amphibole, which rim the magnetite and exhibit a fibrous outgrowth of amphibole. The oxides are dominantly composed of fine- to medium-grained ilmenite which occurs as discrete grains, and to a lesser extent as lamellae within magnetite.

Slide#	Rock Type
NO-2G47-5	O-Leucogabbro

Transmitted

Mineral	%	Grain size	Habit	Comments
Plagioclase	71	Md	Euhedral	Fine- to medium-grained plagioclase laths exhibit undulose extinction, deformation twins, compositional zoning, and subgrain boundaries.
Clinopyroxene	6	Fn	Anhedral	Clinopyroxene has been partially to completely replaced by amphibole.
Amphibole	5	Vy-Fn	Anhedral	Blue/green amphibole occurs as radiating very fine-grained crystals which surround magnetite-ilmenite grains.
Apatite	5	Fn	Euhedral	Tabular apatite grains are spatially associated with higher concentrations of oxide minerals.
Chlorite	2	Vy-Fn	Anhedral	Pale green (PPL) to steel grey (XPL) chlorite forms a corona around oxides and clinopyroxene

Reflected

Mineral	%	Grain size	Habit	Comments
Magnetite	3	Fn	Anhedral	Magnetite occurs as very fine-grained needle-like, and or fibrous inclusions within massive aggregates of very fine-grained epidote, and as fine-grained rounded blebs alongside ilmenite which contain abundant ilmenite exsolution granules and coarse lamellae.
Ilmenite	8	Md	Anhedral	Fine- to medium-grained ilmenite occurs throughout the sample and contains trace hematite exsolution lamellae.
Hematite	Tr.	Vy-Fn	Euhedral	Hematite occurs exclusively as very fine-grained lamellae and/or blebs within ilmenite.
Pyrite	Tr.	Fn	Anhedral	Pyrite blebs occur disseminated throughout the sample.

General Notes: The sample is a massive, medium-grained apatite-bearing, oxide leucogabbro. The sample is relatively unaltered, and clinopyroxene has largely remained intact as anhedral crystals within cumulate plagioclase grains. Apatite occurs as tabular fine-grained crystals which are generally associated with ilmenite and magnetite aggregates. The oxides are dominated by medium-grained hematite exsolution-bearing ilmenite grains. Magnetite occurs both as fine-grained ilmenite exsolution granules and lamellae-bearing grains, and as very fine-grained fibrous/ needle-like aggregates along with very fine-grained chlorite, amphibole within possible primary olivine grain boundaries.

Slide#	Rock Type
NO-2G47-6	Oxide-Gabbro

Transmitted

Mineral	%	Grain size	Habit	Comments
Plagioclase	45	Md	Euhedral	All grains contain deformation and simple twins. Plagioclase commonly contains rims of orthoclase and are compositionally zoned.
Amphibole	15	Fn	Subhedral	Blue-green amphibole is partially replaced by chlorite and contains compositional zoning.
Orthoclase	5	Fn	Anhedral	Occurs as rims along primary plagioclase, as a very fine-grained aggregates.
Chlorite	20	Fn	Subhedral	Blue chlorite occurs as fibrous intergrowths after amphibole grains.

Reflected

Mineral	%	Grain size	Habit	Comments
Magnetite	5	Md	Anhedral	Occurs with a pervasive pitted texture with ~5% ilmenite lamella exsolutions
Ilmenite	10	Md	Subhedral	Occurs within magnetite grains, but dominantly as discrete ilmenite crystals.
Pyrite	Tr.	Fn	Anhedral	Disseminated throughout sample

General Notes:

The sample is a medium-grained oxide-gabbro, with moderate pervasive chlorite alteration. Blue fibrous chlorite has partially, to completely replaced the amphibole grains and suggests the original composition was gabbroic. Plagioclase contains compositional zoning and abundant deformation twins, with common rims of orthoclase.

The oxides dominated by ilmenite which occurs as discrete grains and as minor exsolution within magnetite. The magnetite occurs as a heavily ‘pitted’ mineral, unlike the ilmenite.

Slide#	Rock Type
NO-2G47-7	O-Anorthosite

Transmitted

Mineral	%	Grain size	Habit	Comments
Plagioclase	80	Md	Euhedral	Contains numerous very fine-grained inclusions of amphibole, weak compositional zoning, deformation twins, and subgrains.
Amphibole	5	Fn	Subhedral	Fibrous amphibole occurs as matts associated with chlorite.
Chlorite	5	Fn	Euhedral	Blue-green (PPL) chlorite occurs along with amphibole.
Carbonate	1	Fn	Anhedral	Occurs with quartz within cross cutting veinlets (<1mm).
Quartz	tr	Fn	Anhedral	Occurs with Carbonate within cross cutting veinlets (<1mm).

Reflected

Mineral	%	Grain size	Habit	Comments
Magnetite	3	Fn	Anhedral	Magnetite is very 'pitted' and contains well formed ilmenite exsolution.
Ilmenite	6	Md	Subhedral	Occurs as subhedral grains, and as exsolution within magnetite.
Pyrite	Tr.	Fn	Subhedral	Pyrite is sub-cubic and occurs throughout.
Pyrrhotite	Tr.	Vy-Fn	Anhedral	Occurs alongside of pyrite and magnetite.

General Notes:

The sample is a massive, medium-grained oxide anorthosite. Plagioclase contains deformation twins, compositional zoning, and subgrains. The sample is crosscut by sub millimeter carbonate-quartz veinlets.

The oxides are ilmenite dominated which primarily occurs as subhedral crystals, and to a lesser extent as exsolution within pitted anhedral magnetite.

Slide#	Rock Type
NO-2G47-8	OR-Gabbro

Transmitted

Mineral	%	Grain size	Habit	Comments
Plagioclase	25	Md	Euhedral	Contains abundant deformation twins, subgrain boundaries, and undulose extinction.
Amphibole	15	Fn	Anhedral	Blue-green amphibole commonly rims magnetite-ilmenite.
Chlorite	15	Fn	Anhedral	Fibrous matts of steel-blue (XPL) chlorite occur throughout the sample and partially replace amphibole.
Carbonate	Tr.	Fn	Anhedral	Blebs of carbonate occur disseminated throughout the sample.

Reflected

Mineral	%	Grain size	Habit	Comments
Magnetite	20	Md	Anhedral	Magnetite is heavily pitted and contains abundant ilmenite exsolution lamellae (10%). Magnetite is also present in trace amounts as exsolution within ilmenite. Magnetite also occurs as massive (80%) aphanitic inclusions within silicates which have been dominantly replaced by chlorite.
Ilmenite	25	Md	Anhedral	Ilmenite occurs as anhedral grains within trace magnetite exsolution, as exsolution lamela within magnetite, and as fine-grained euhedral tabular crystals.
Pyrite	Tr.	Fn	Anhedral	Disseminated pyrite occurs throughout sample

General Notes:

The sample is a medium-grained, massive oxide-rich gabbro which has been amphibolized. Plagioclase exhibits strong deformation features such as deformation twins, subgrain boundaries, and undulose extinction. Chlorite occurs as fibrous matts and is replacing amphibole crystals.

The oxides are slightly ilmenite dominant which contain minor magnetite exsolution lamellae. The ilmenite also occurs as euhedral tabular fine-grain crystals. The magnetite contains ilmenite exsolution and often exhibits a strong pitted texture. The magnetite is also observed as aphanitic, massive (80%) inclusions within silicates which have been completely chloritised.

Slide#	Rock Type
NO-2G47-9	O-Melanogabbro

Transmitted

Mineral	%	Grain size	Habit	Comments
Plagioclase	4	Vy-Fn	Anhedral	Relict euhedral medium-grained plagioclase is completely replaced by chlorite with minor rims of anhedral plagioclase remaining.
Amphibole	80	Fn	Euhedral	Blue-green amphibole partially replaced by chlorite
Chlorite	6	Fn	Euhedral	Occurs both as grey/blue (XPL) matts within relict plagioclase grains, and as blue-green-yellow grains partially to completely replacing amphibole.
Orthoclase	1	Fn	Anhedral	Possible quartz, but too fine-grained to identify.
Epidote	Tr.	Fn	Anhedral	Disseminated throughout the sample.
Carbonate	Tr.	Fn	Anhedral	Disseminated throughout sample.

Reflected

Mineral	%	Grain size	Habit	Comments
Magnetite	3	Fn	Anhedral	Occurs as pitted anhedral grains with abundant (>10%) ilmenite exsolution lamellae.
Ilmenite	5	Md	Subhedral	Occurs as medium- to coarse-grained subhedral crystals, and as exsolution within magnetite.
Pyrite	1	Fn	Anhedral	Disseminated throughout.
Chalcopyrite	Tr.	Vy-Fn	Anhedral	Occurs within and rimming pyrite.

General Notes:

The sample is a fine- to medium-grained well foliated oxide melanogabbro. The sample is dominantly composed of amphibole, magnetite, and ilmenite. The protlith originally contained more plagioclase then preserved as suggested by the relict grain boundaries.

The oxides are ilmenite dominated, which occurs as medium-grained subhedral crystals. The magnetite is pitted and contains numerous ilmenite exsolution lamellae.

Slide#	Rock Type
NO-2G47-10	O-Gabbro

Transmitted

Mineral	%	Grain size	Habit	Comments
Chlorite	55	Fn	Subhedral	Pale green (PPL) to steel grey (XPL) chlorite is partially replaced by biotite.
Biotite	2	Fn	Euhedral	Green/brown (PPL) biotite occurs as lamellae within chlorite grains.
Apatite	6	Fn	Subhedral	Tabular to rounded apatite grains exhibit very thin fractures which have been in filled by carbonate.
Carbonate	7	Fn	Anhedral	Carbonate occurs disseminated throughout and present within strain shadows of apatite grains and magnetite-ilmenite.
Quartz	18	Fn	Anhedral	Quartz occurs disseminated throughout and present within strain shadows of apatite grains and magnetite-ilmenite.

Reflected

Mineral	%	Grain size	Habit	Comments
Magnetite	3	Fn	Anhedral	Magnetite occurs as fine-grained anhedral blebs which occur alongside ilmenite, and contains coarse ilmenite lamellae.
Ilmenite	8	Md	Anhedral	Fine- to medium-grained ilmenite blebs occur throughout the sample and are occurs as lamellae within magnetite.
Pyrite	1	Fn	Anhedral	Blebs of pyrite occur disseminated throughout the sample.

General Notes:

The sample is a very well foliated chlorite-quartz, apatite-bearing, oxide schist. The protolith was likely composed of a gabbroic lithology, however, the primary plagioclase and pyroxene has been completely altered. The apatite and ilmenite are commonly brecciated and contain in filling of chlorite.

Appendix B

Drill logs

Core Log Legend

Ferrogabbro Suite

- Anorthosite
- Oxide-Bearing Anorthosite
- Oxide Anorthosite
- Oxide-Rich Anorthosite
- Semi-Massive Oxide Anorthosite
- Leucogabbro
- Oxide-Bearing Leucogabbro
- Oxide Leucogabbro
- Oxide-Rich Leucogabbro
- Semi-Massive Oxide Leucogabbro
- Gabbro
- Oxide-Bearing Gabbro
- Oxide Gabbro
- Oxide-Rich Gabbro
- Semi-Massive Oxide Gabbro
- Melagabbro
- Oxide-Bearing Melagabbro
- Oxide Melagabbro
- Oxide-Rich Melagabbro
- Semi-Massive Oxide Melagabbro
- Micro-Gabbro
- Massive Oxide
- Pegmatitic Gabbro

Ultramafic Suite

- Peridotite
- Pyroxenite

Country Rock

- Basalt

Late Felsic Intrusives

- Tonalite
- Granite
- Diorite

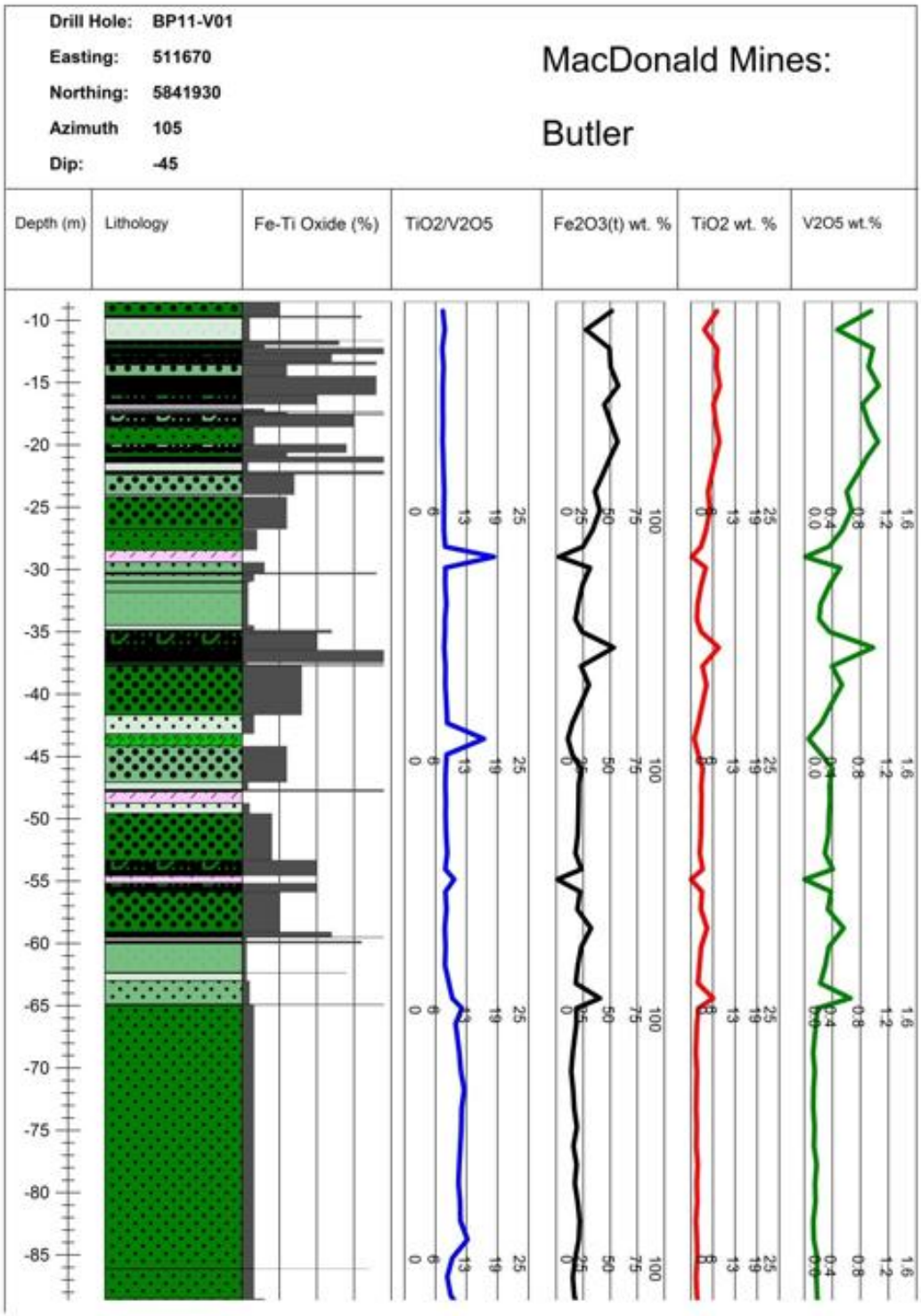
Drill Hole: BP11-V01
Easting: 511670
Northing: 5841930
Azimuth 105
Dip: -45
MacDonald Mines:
Butler
Depth (m)
Lithology
Fe-Ti Oxide (%)
TiO2/V2O5
Fe2O3(t) wt. %
TiO2 wt. %
V2O5 wt.%
-10
-15
-20
-25
-30
-35
-40
-45
-50
-55
-60
-65
-70
-75
-80
-85

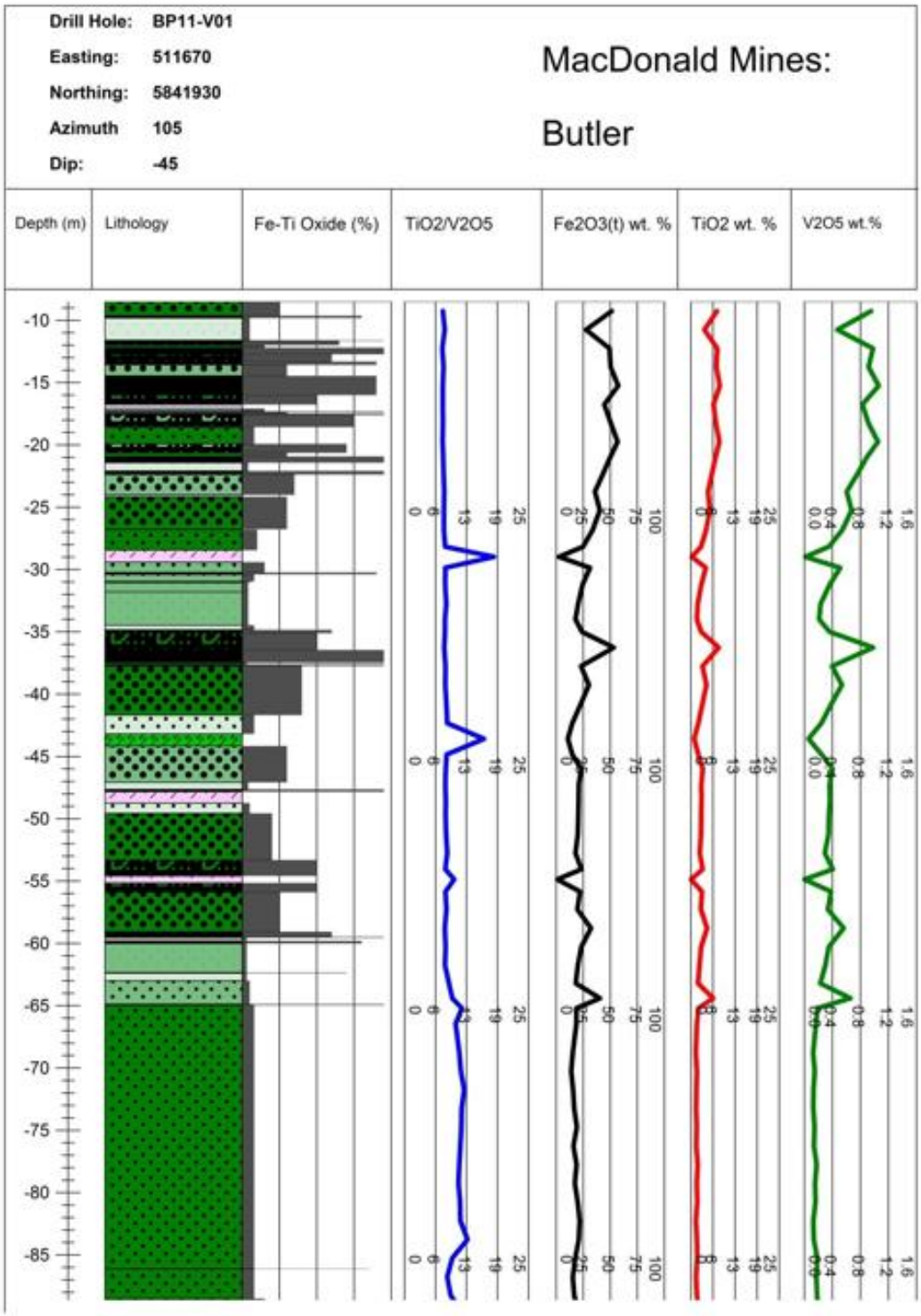
Drill Hole: BP11-V01
Easting: 511670
Northing: 5841930
Azimuth 105
Dip: -45
MacDonald Mines:
Butler
Depth (m)
Lithology
Fe-Ti Oxide (%)
TiO2/V2O5
Fe2O3(t) wt. %
TiO2 wt. %
V2O5 wt.%
-10
-15
-20
-25
-30
-35
-40
-45
-50
-55
-60
-65
-70
-75
-80
-85

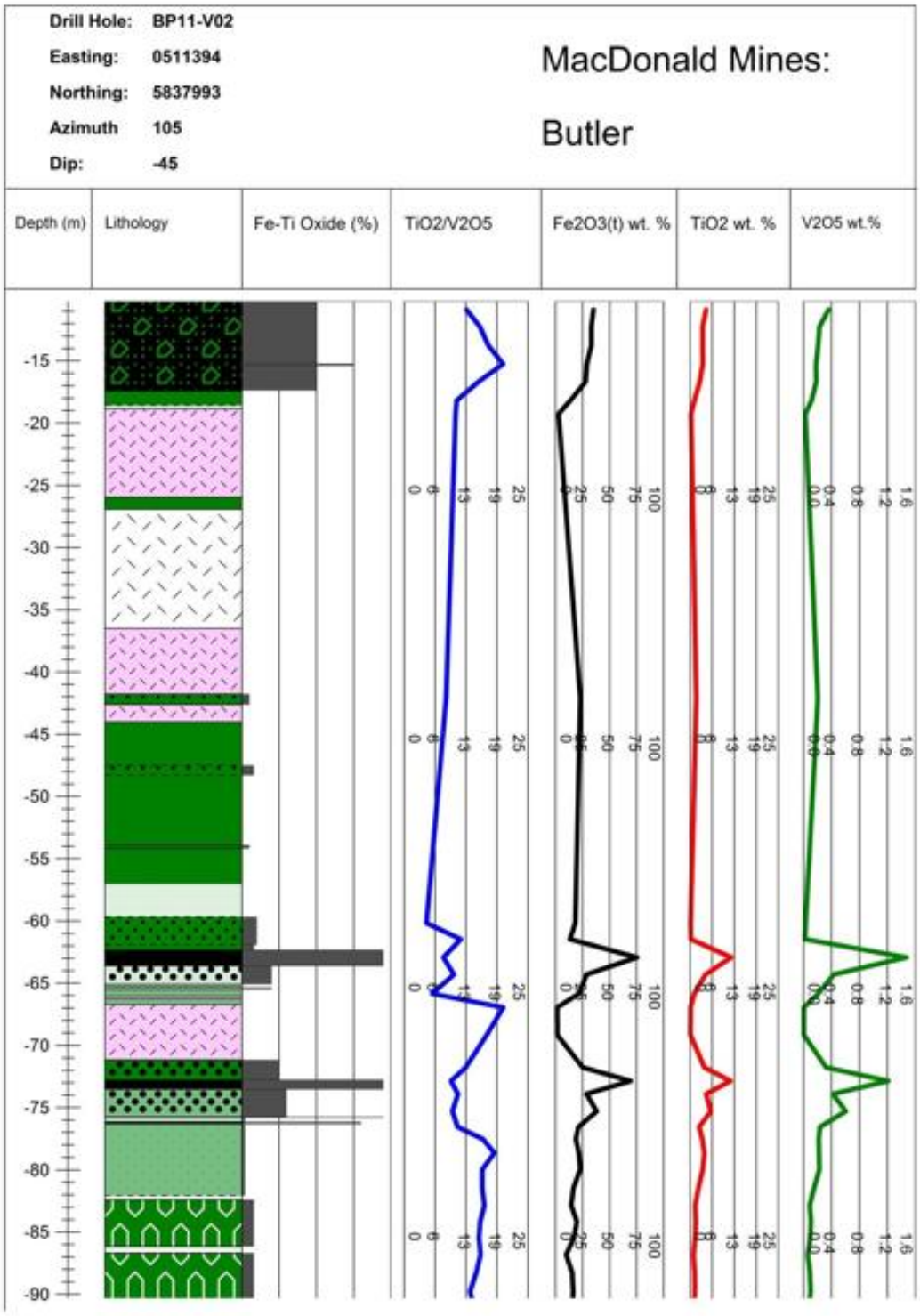
Drill Hole: BP11-V02
Easting: 0511394
Northing: 5837993
Azimuth 105
Dip: -45
MacDonald Mines:
Butler
Depth (m)
Lithology
Fe-Ti Oxide (%)
TiO2/V2O5
Fe2O3(t) wt. %
TiO2 wt. %
V2O5 wt.%
-15
-20
-25
-30
-35
-40
-45
-50
-55
-60
-65
-70
-75
-80
-85
-90

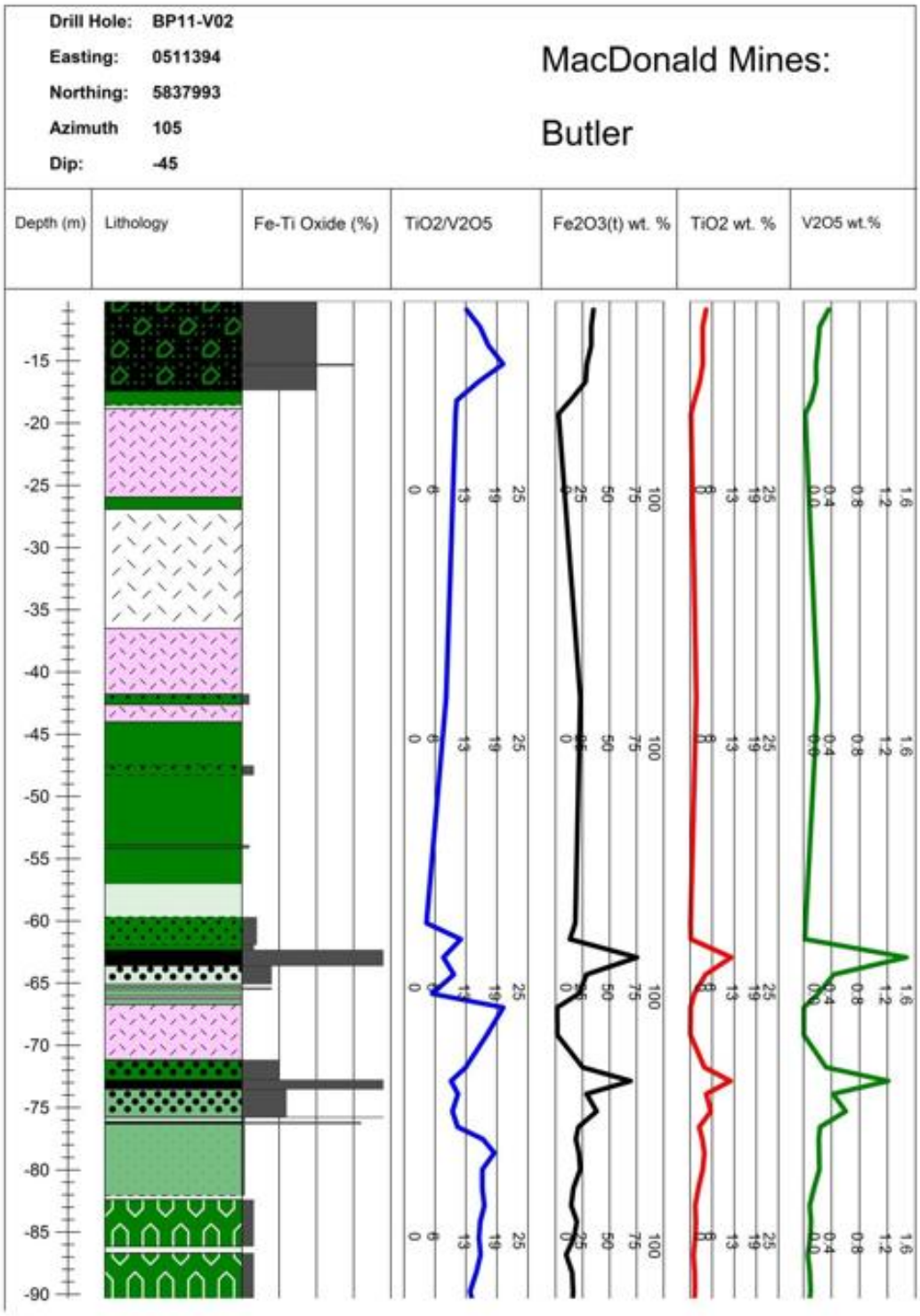
Drill Hole: BP11-V02
Easting: 0511394
Northing: 5837993
Azimuth 105
Dip: -45
MacDonald Mines:
Butler
Depth (m)
Lithology
Fe-Ti Oxide (%)
TiO2/V2O5
Fe2O3(t) wt. %
TiO2 wt. %
V2O5 wt.%
-15
-20
-25
-30
-35
-40
-45
-50
-55
-60
-65
-70
-75
-80
-85
-90

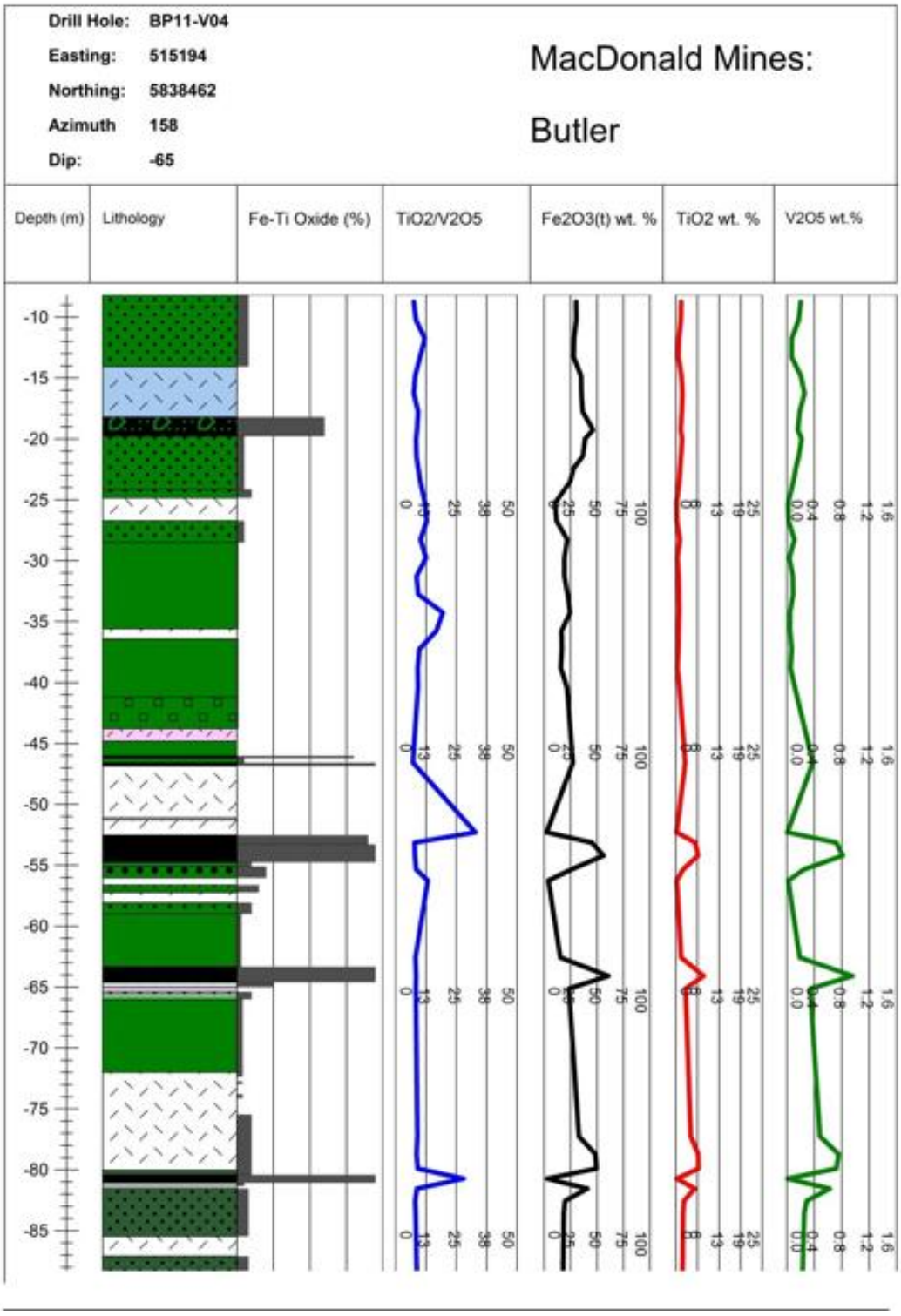
Drill Hole: BP11-V04
Easting: 515194
Northing: 5838462
Azimuth 158
Dip: -65
MacDonald Mines:
Butler
Depth (m)
Lithology
Fe-Ti Oxide (%)
TiO2/V2O5
Fe2O3(t) wt. %
TiO2 wt. %
V2O5 wt.%
-10
-15
-20
-25
-30
-35
-40
-45
-50
-55
-60
-65
-70
-75
-80
-85

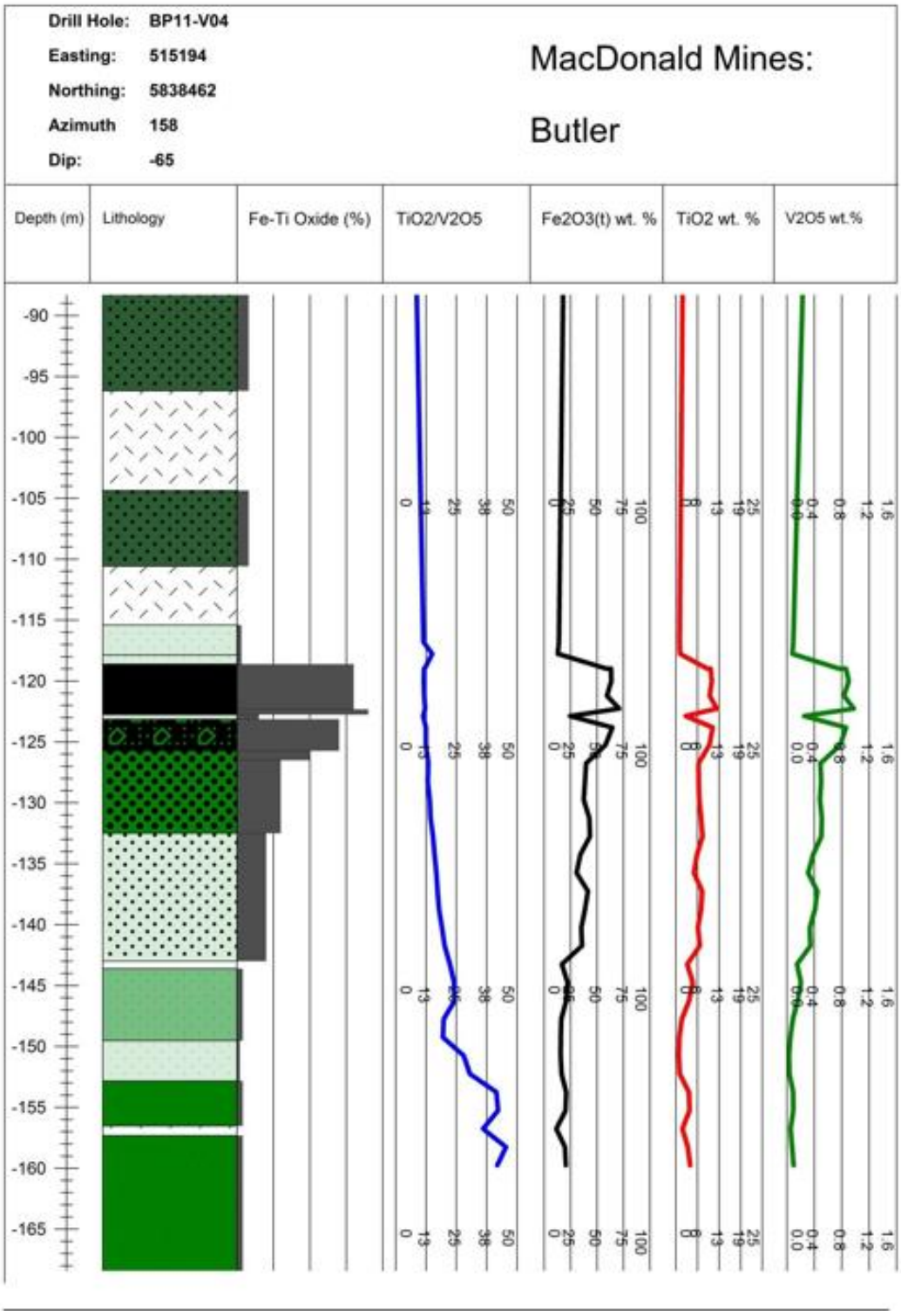
Drill Hole: BP11-V04
Easting: 515194
Northing: 5838462
Azimuth 158
Dip: -65
MacDonald Mines:
Butler
Depth (m)
Lithology
Fe-Ti Oxide (%)
TiO2/V2O5
Fe2O3(t) wt. %
TiO2 wt. %
V2O5 wt.%
-90
-95
-100
-105
-110
-115
-120
-125
-130
-135
-140
-145
-150
-155
-160
-165

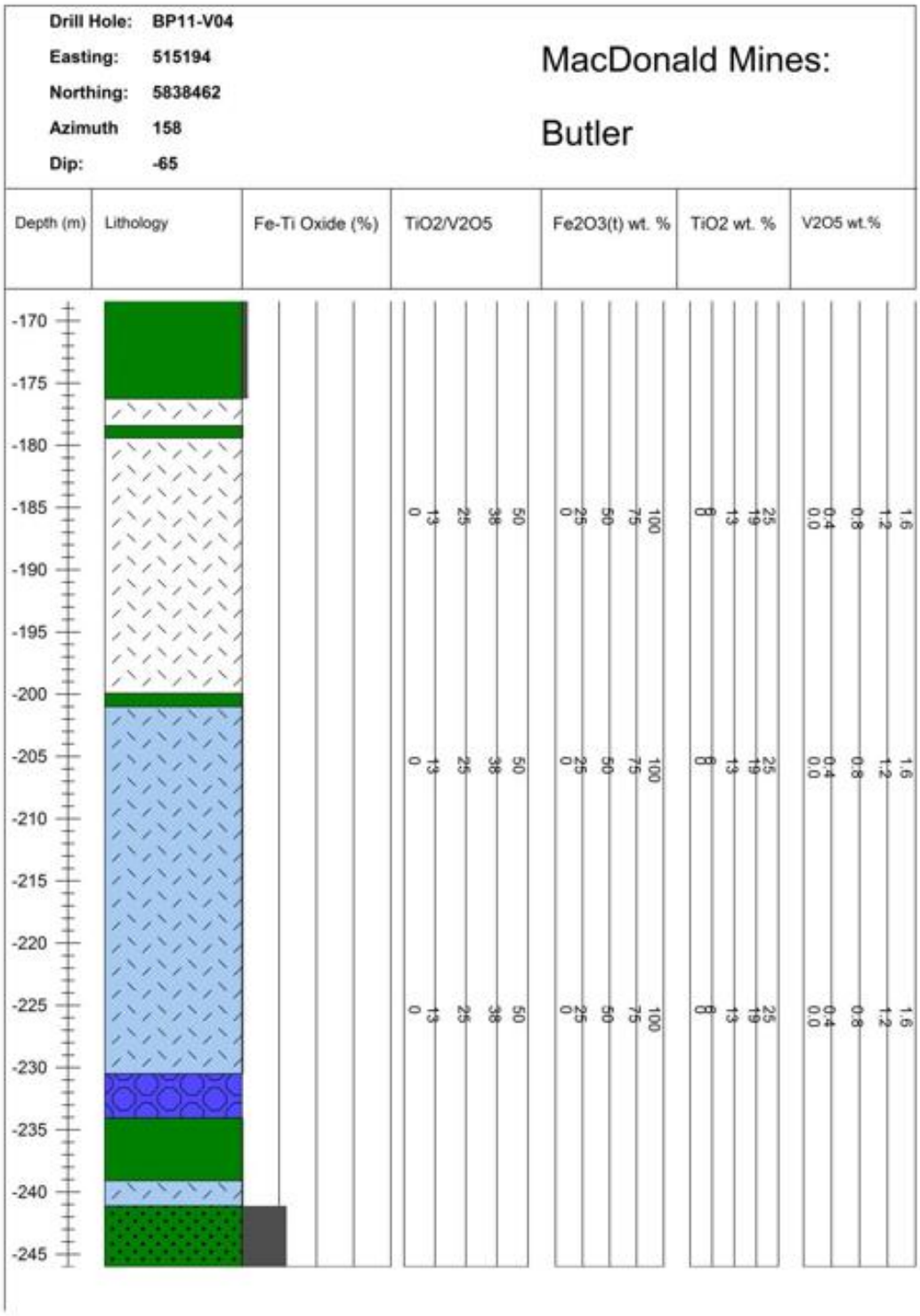
Drill Hole: BP11-V04
Easting: 515194
Northing: 5838462
Azimuth 158
Dip: -65
MacDonald Mines:
Butler
Depth (m)
Lithology
Fe-Ti Oxide (%)
TiO2/V2O5
Fe2O3(t) wt. %
TiO2 wt. %
V2O5 wt.%
-170
-175
-180
-185
-190
-195
-200
-205
-210
-215
-220
-225
-230
-235
-240
-245
0 13 25 38 50
0 25 50 75 100
8 13 19 25
0.0 0.4 0.8 1.2 1.6

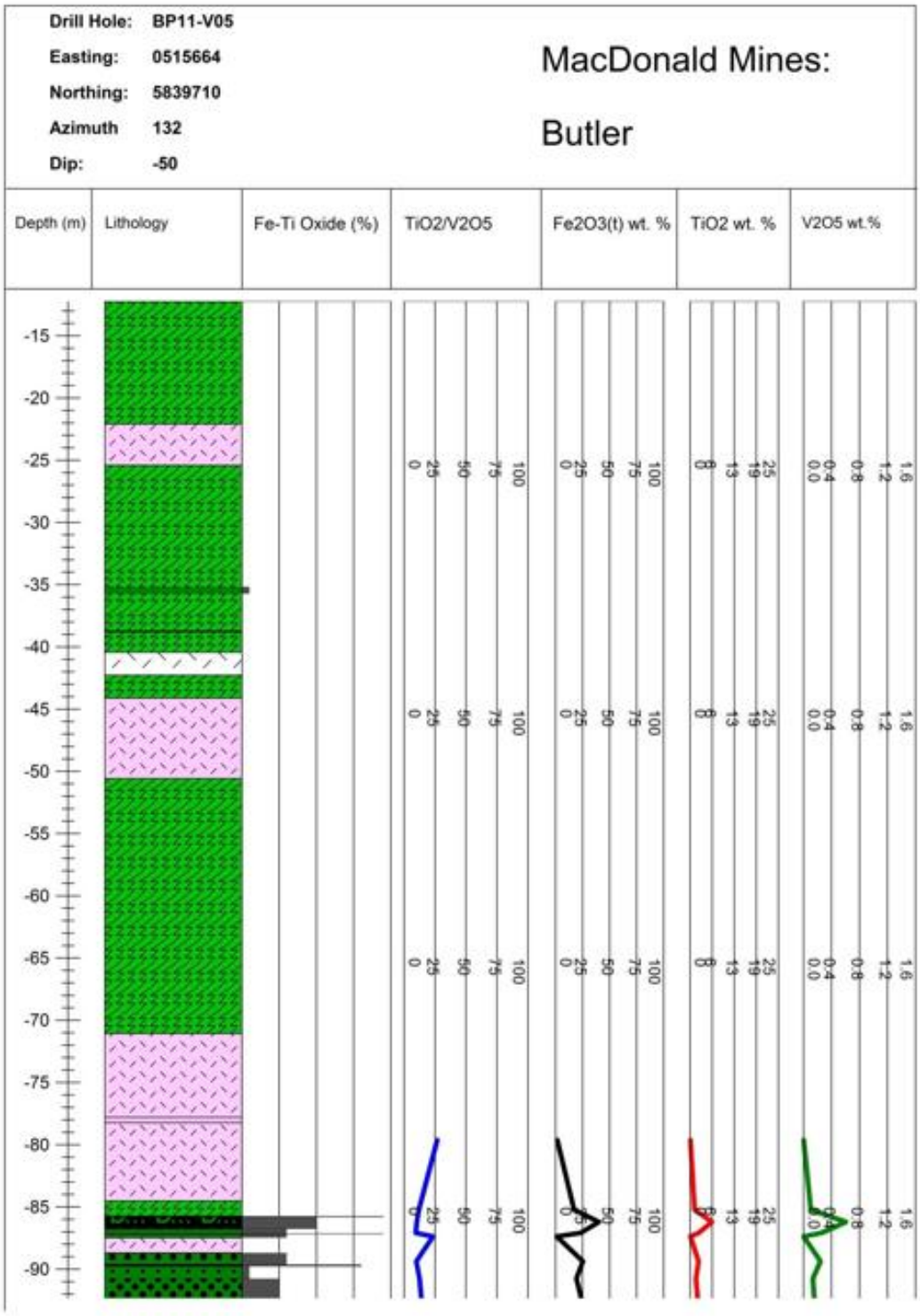
Drill Hole: BP11-V05
Easting: 0515664
Northing: 5839710
Azimuth 132
Dip: -50
MacDonald Mines:
Butler
Depth (m)
Lithology
Fe-Ti Oxide (%)
TiO2/V2O5
Fe2O3(t) wt. %
TiO2 wt. %
V2O5 wt.%
-15
-20
-25
-30
-35
-40
-45
-50
-55
-60
-65
-70
-75
-80
-85
-90

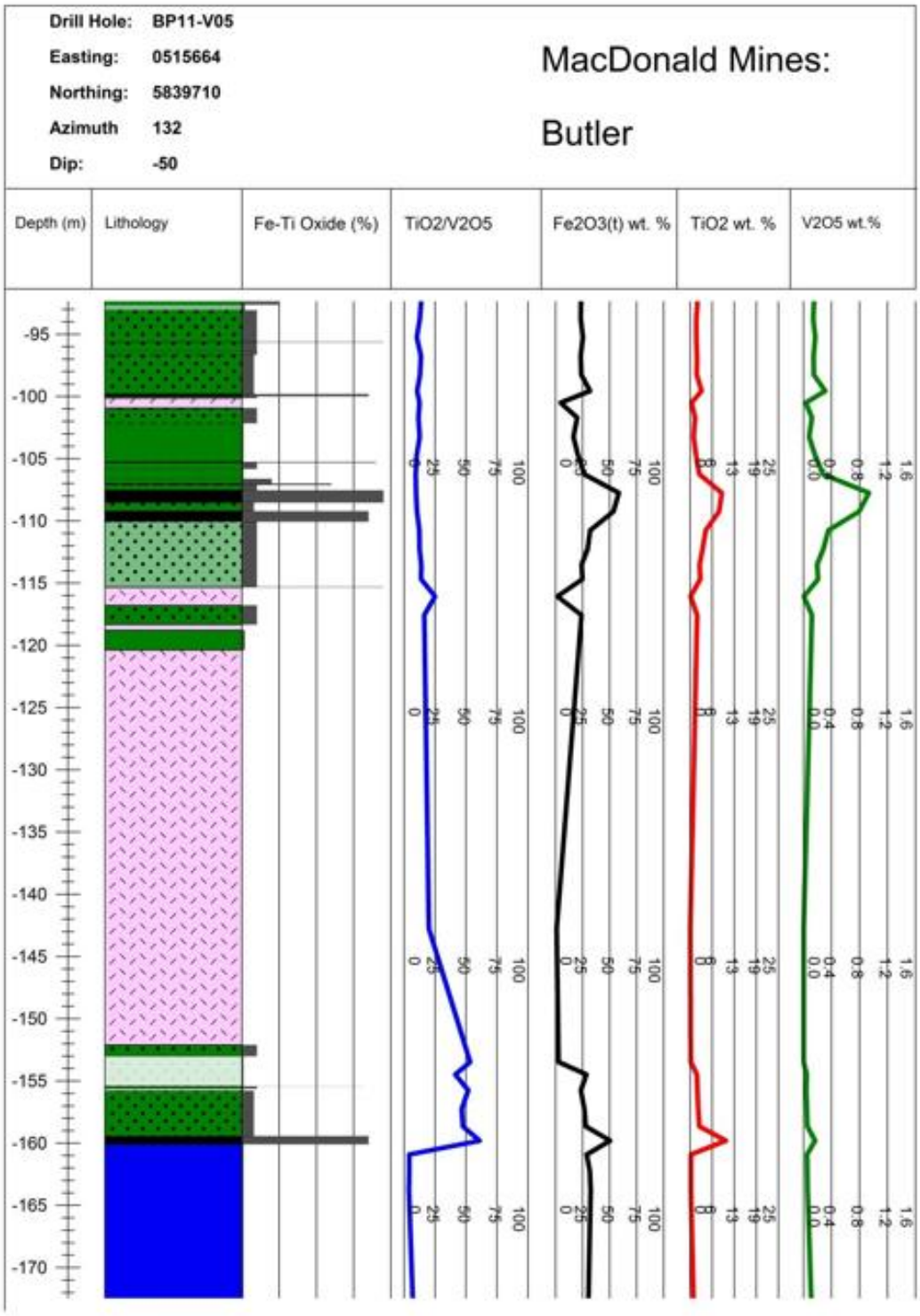
Drill Hole: BP11-V05
Easting: 0515664
Northing: 5839710
Azimuth 132
Dip: -50
MacDonald Mines:
Butler
Depth (m)
Lithology
Fe-Ti Oxide (%)
TiO2/V2O5
Fe2O3(t) wt. %
TiO2 wt. %
V2O5 wt.%
-95
-100
-105
-110
-115
-120
-125
-130
-135
-140
-145
-150
-155
-160
-165
-170

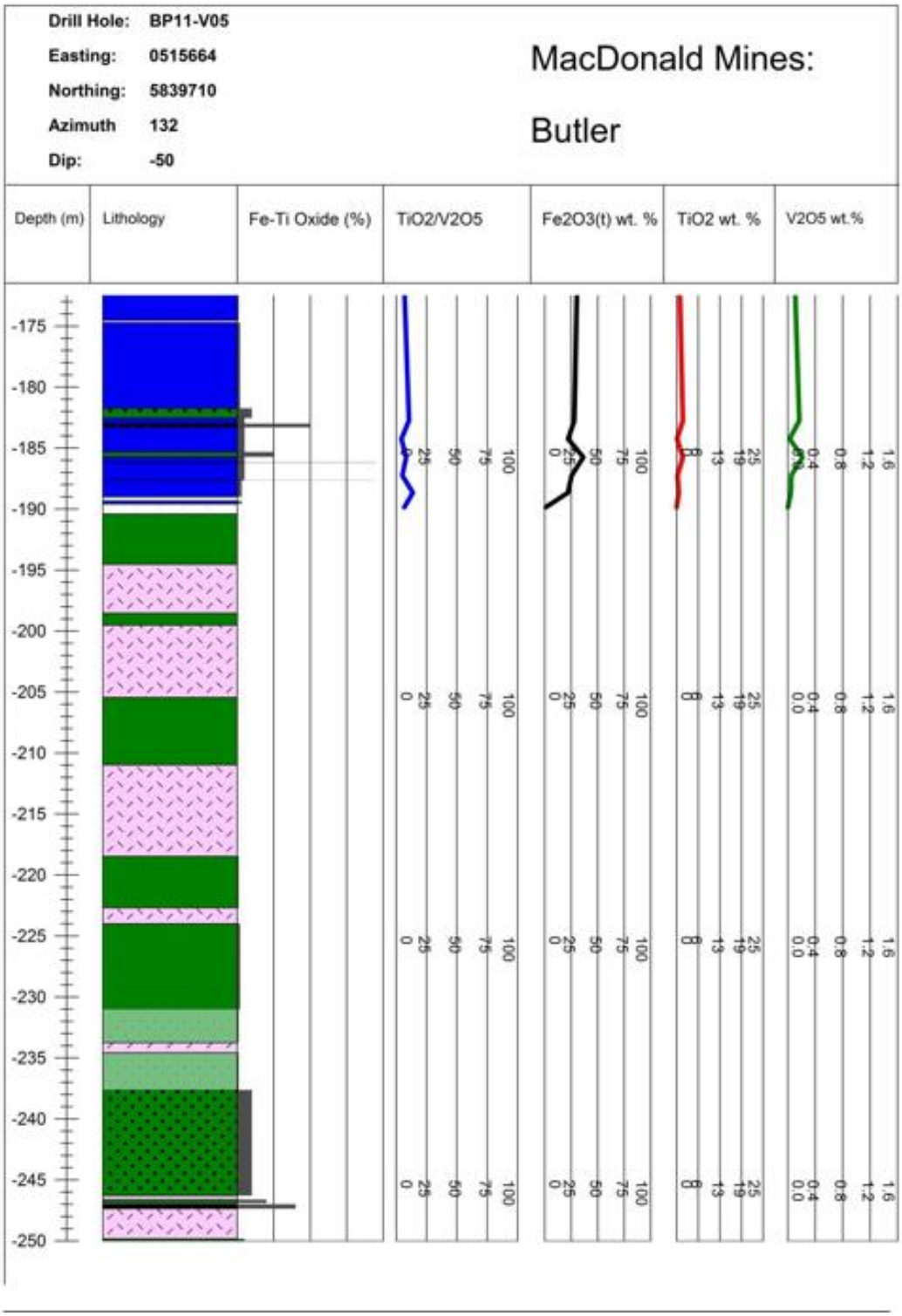
Drill Hole: BP11-V05
Easting: 0515664
Northing: 5839710
Azimuth 132
Dip: -50
MacDonald Mines:
Butler
Depth (m)
Lithology
Fe-Ti Oxide (%)
TiO2/V2O5
Fe2O3(t) wt. %
TiO2 wt. %
V2O5 wt.%
-175
-180
-185
-190
-195
-200
-205
-210
-215
-220
-225
-230
-235
-240
-245
-250

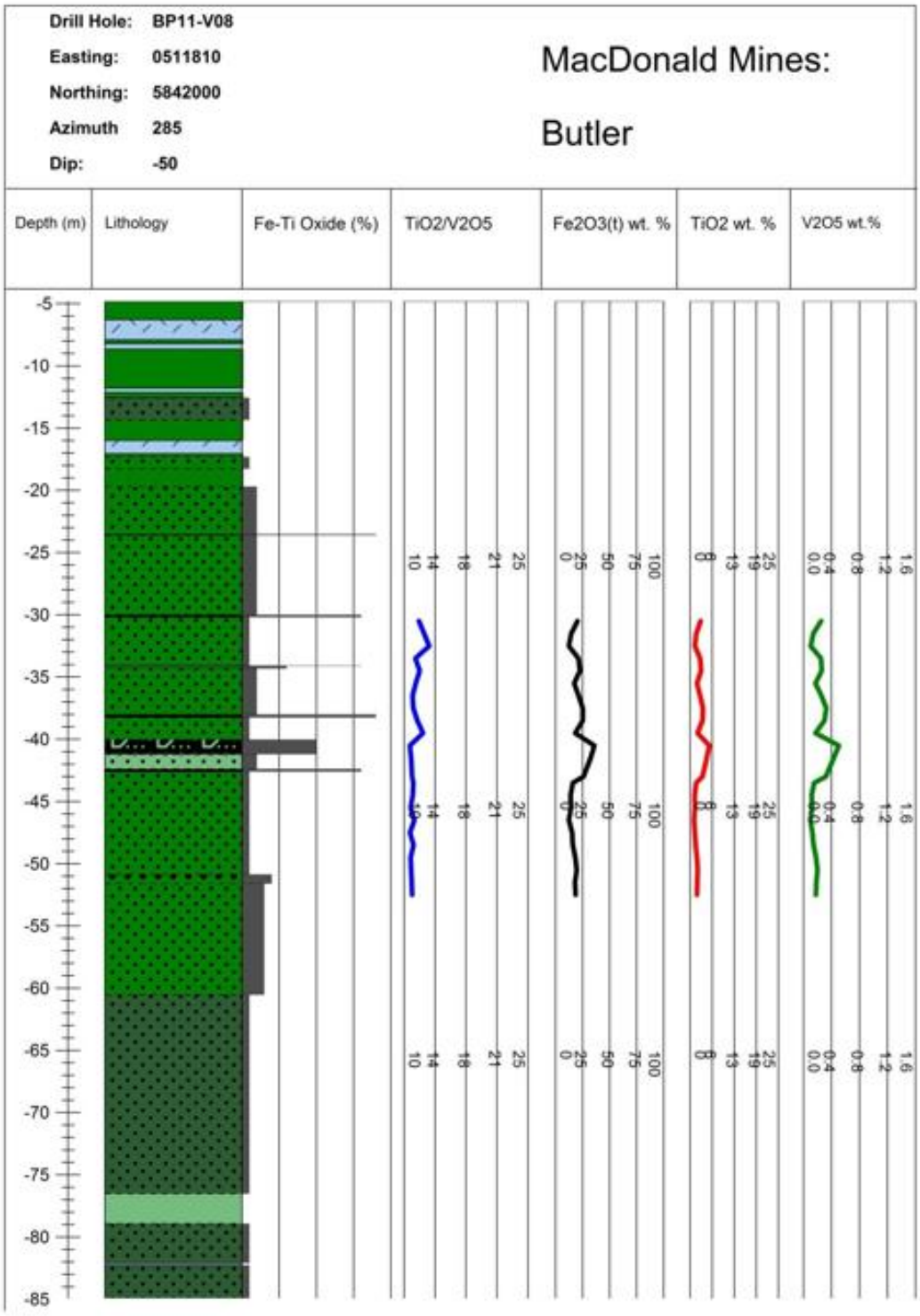
Drill Hole: BP11-V08
Easting: 0511810
Northing: 5842000
Azimuth 285
Dip: -50
MacDonald Mines:
Butler
Depth (m)
Lithology
Fe-Ti Oxide (%)
TiO2/V2O5
Fe2O3(t) wt. %
TiO2 wt. %
V2O5 wt.%
-5
-10
-15
-20
-25
-30
-35
-40
-45
-50
-55
-60
-65
-70
-75
-80
-85

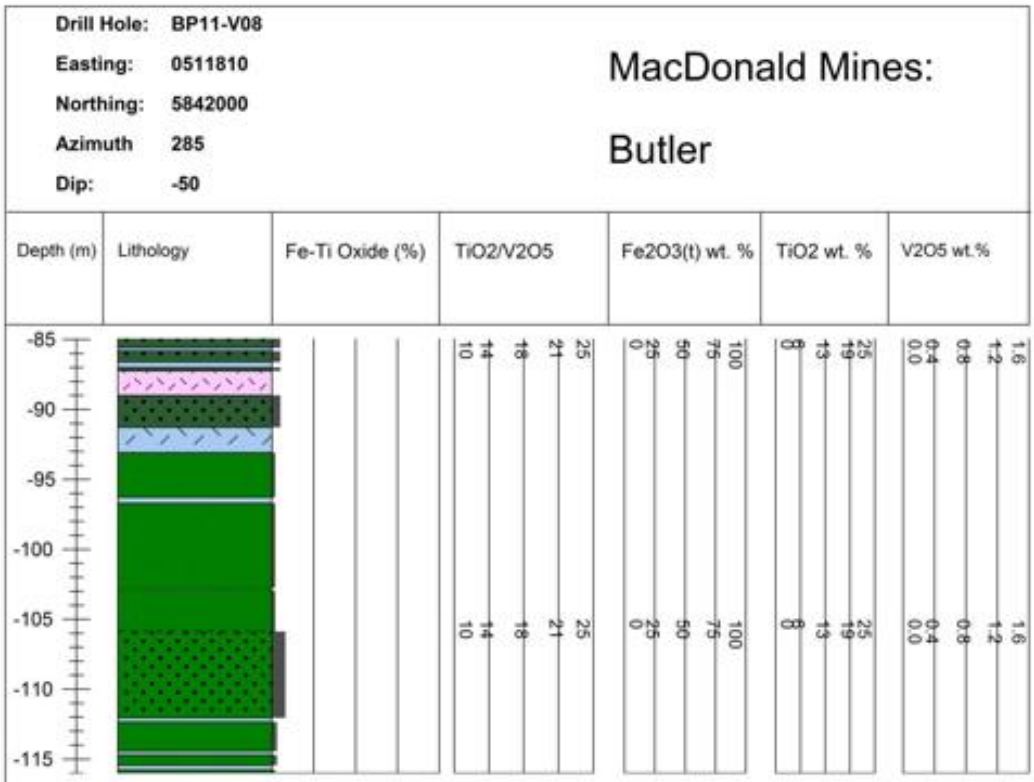
Drill Hole: BP11-V08
Easting: 0511810
Northing: 5842000
Azimuth 285
Dip: -50
MacDonald Mines:
Butler
Depth (m)
Lithology
Fe-Ti Oxide (%)
TiO2/V2O5
Fe2O3(t) wt. %
TiO2 wt. %
V2O5 wt.%
-85
-90
-95
-100
-105
-110
-115
10 14 18 21 25
0 25 50 75 100
0 6 13 19 25
0.0 0.4 0.8 1.2 1.6

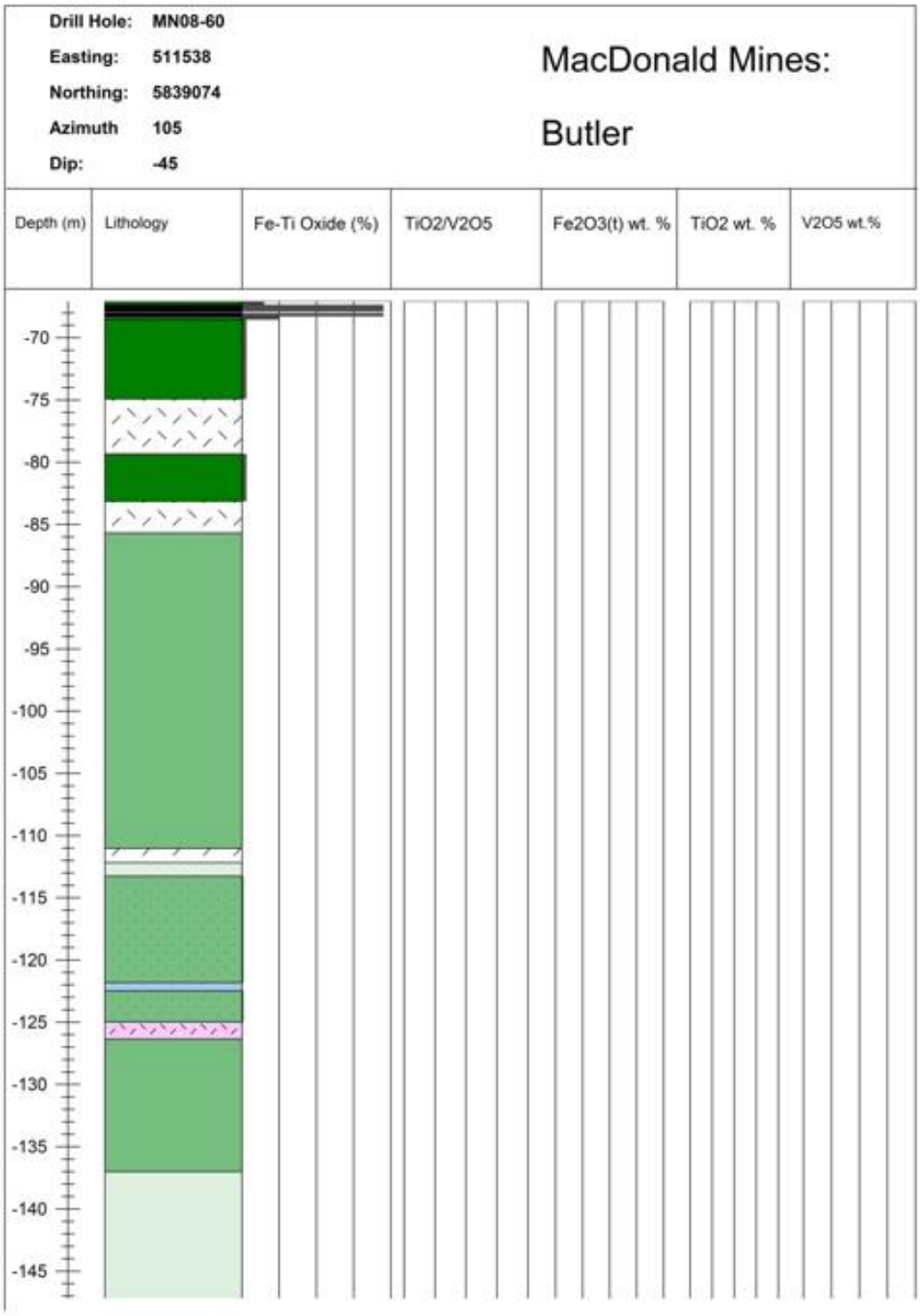
Drill Hole: MN08-60
Easting: 511538
Northing: 5839074
Azimuth 105
Dip: -45
MacDonald Mines:
Butler
Depth (m)
Lithology
Fe-Ti Oxide (%)
TiO2/V2O5
Fe2O3(t) wt. %
TiO2 wt. %
V2O5 wt.%
-70
-75
-80
-85
-90
-95
-100
-105
-110
-115
-120
-125
-130
-135
-140
-145

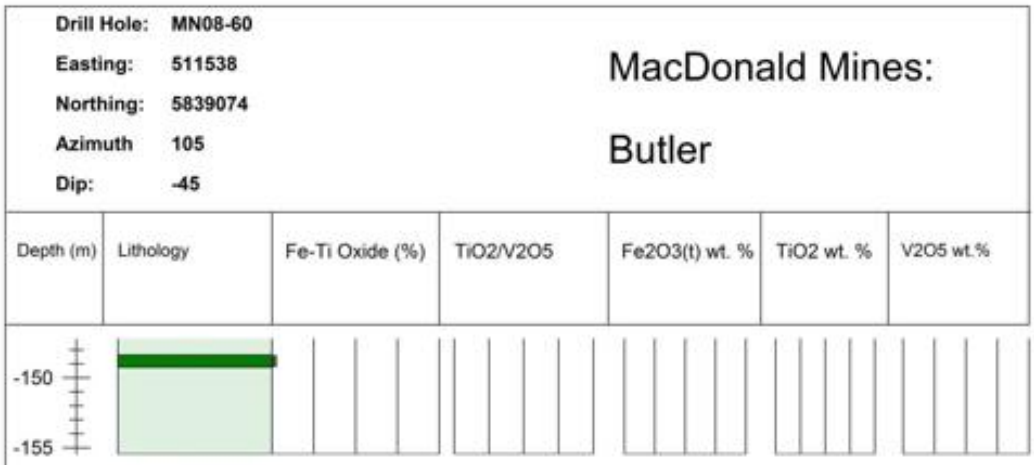
Drill Hole: MN08-60
Easting: 511538
Northing: 5839074
Azimuth 105
Dip: -45
MacDonald Mines:
Butler
Depth (m)
Lithology
Fe-Ti Oxide (%)
TiO2/V2O5
Fe2O3(t) wt. %
TiO2 wt. %
V2O5 wt.%
-150
-155

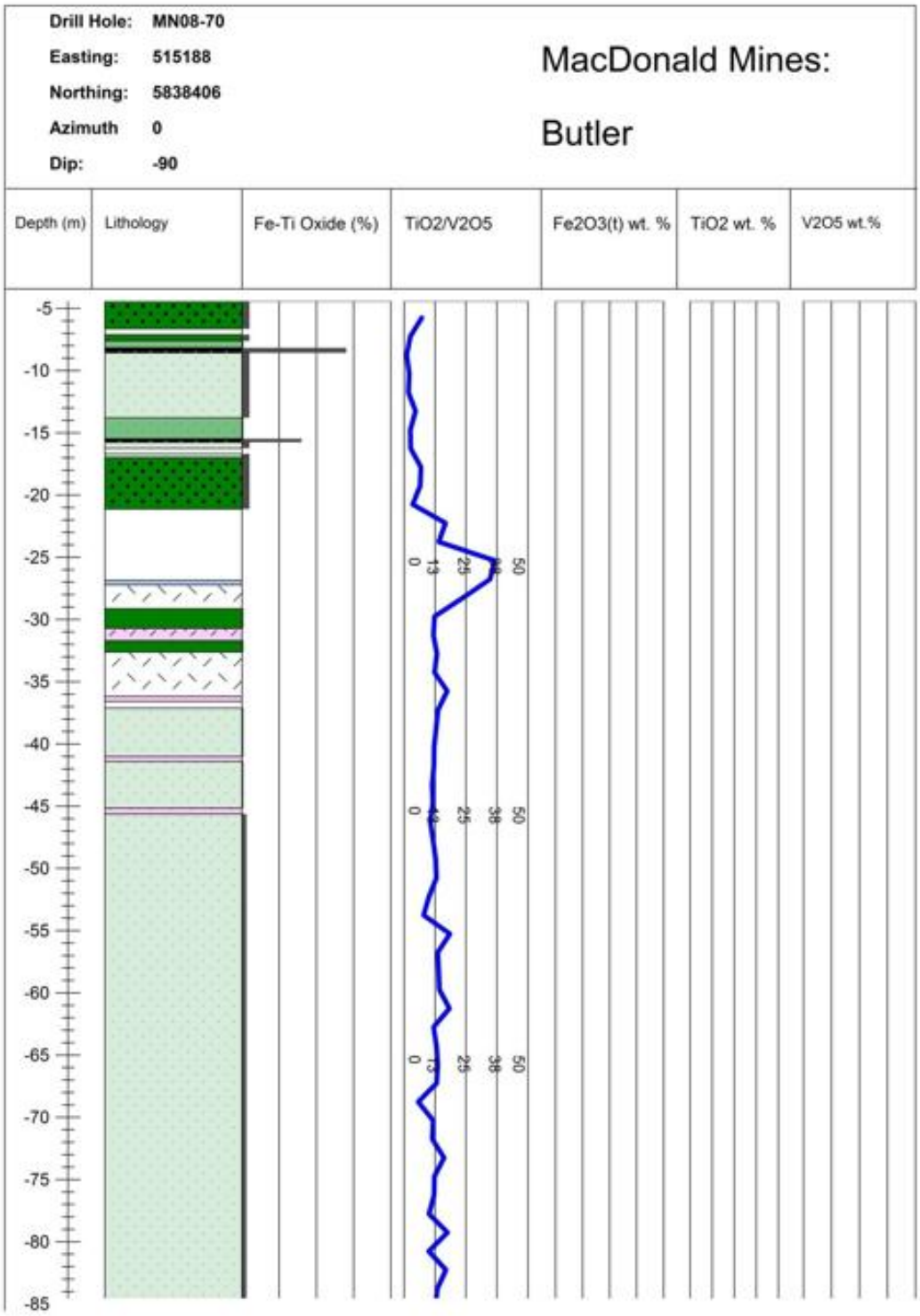
Drill Hole: MN08-70
Easting: 515188
Northing: 5838406
Azimuth 0
Dip: -90
MacDonald Mines:
Butler
Depth (m)
Lithology
Fe-Ti Oxide (%)
TiO2/V2O5
Fe2O3(t) wt. %
TiO2 wt. %
V2O5 wt.%
-5
-10
-15
-20
-25
-30
-35
-40
-45
-50
-55
-60
-65
-70
-75
-80
-85
0
13
25
38
50

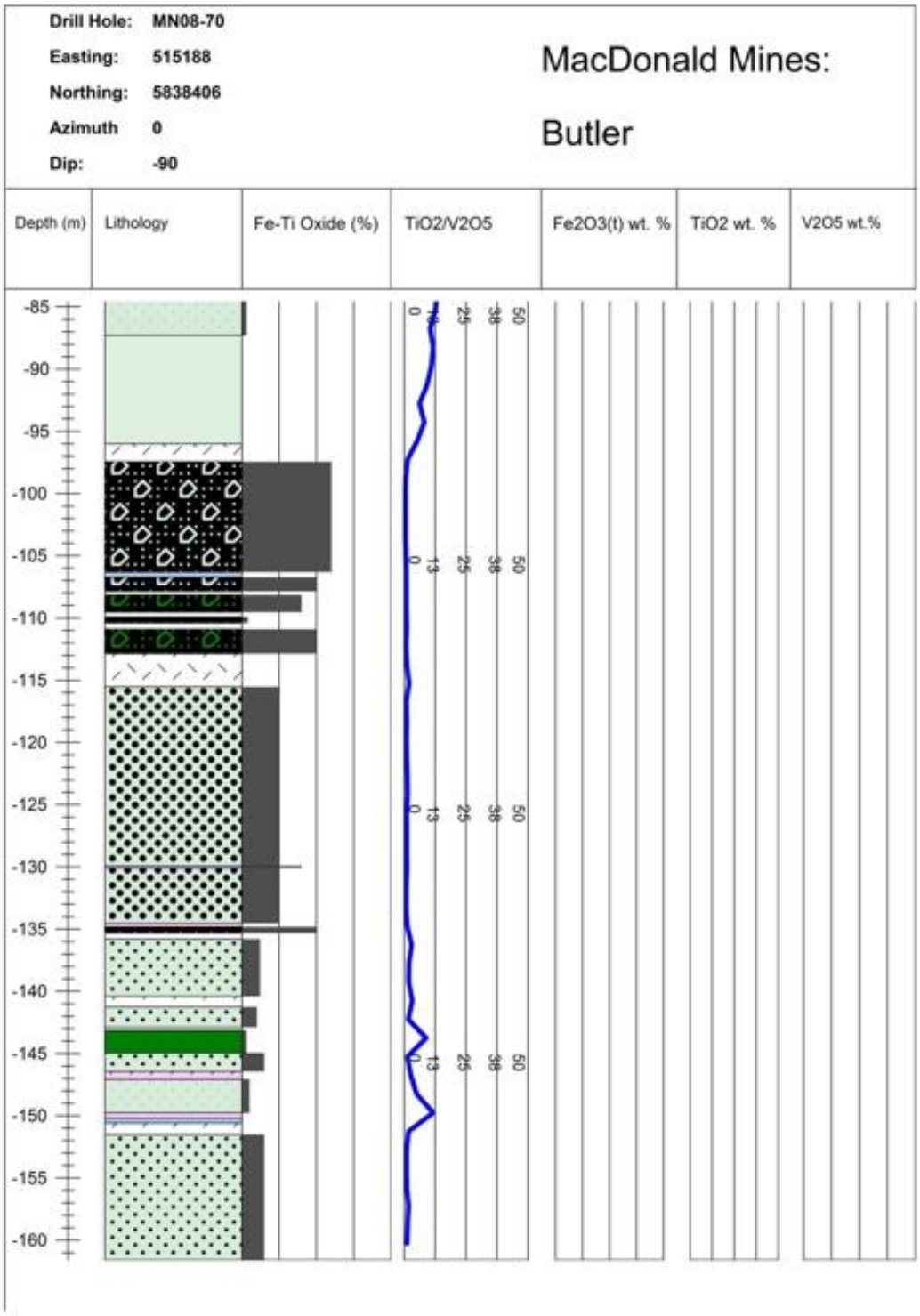
Drill Hole: MN08-70
Easting: 515188
Northing: 5838406
Azimuth 0
Dip: -90
MacDonald Mines:
Butler
Depth (m)
Lithology
Fe-Ti Oxide (%)
TiO2/V2O5
Fe2O3(t) wt. %
TiO2 wt. %
V2O5 wt.%
-85
-90
-95
-100
-105
-110
-115
-120
-125
-130
-135
-140
-145
-150
-155
-160
0
13
25
38
50

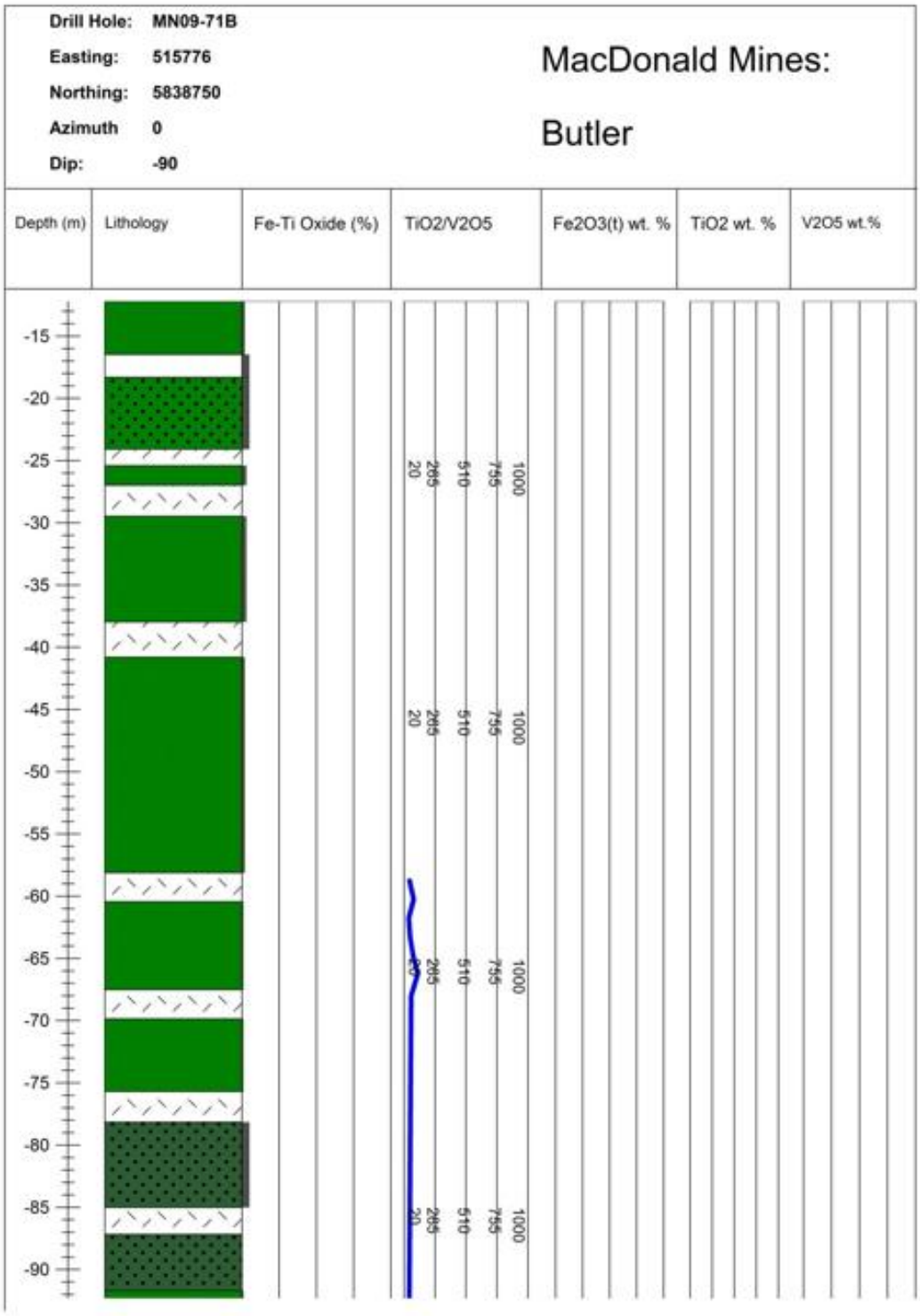
Drill Hole: MN09-71B
Easting: 515776
Northing: 5838750
Azimuth 0
Dip: -90
MacDonald Mines:
Butler
Depth (m)
Lithology
Fe-Ti Oxide (%)
TiO2/V2O5
Fe2O3(t) wt. %
TiO2 wt. %
V2O5 wt.%
-15
-20
-25
-30
-35
-40
-45
-50
-55
-60
-65
-70
-75
-80
-85
-90
20
265
510
755
1000

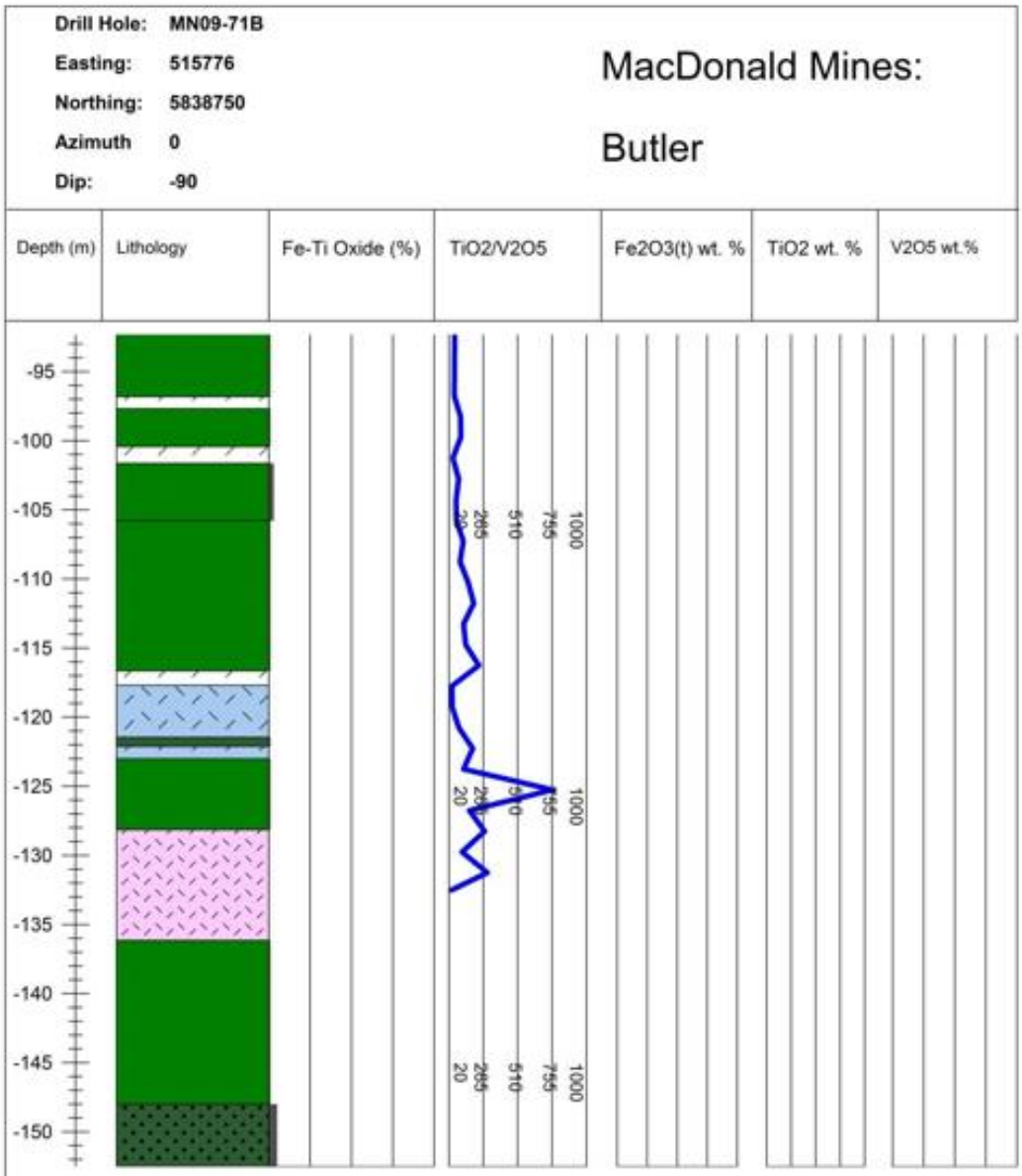
Drill Hole: MN09-71B
Easting: 515776
Northing: 5838750
Azimuth 0
Dip: -90
MacDonald Mines:
Butler
Depth (m)
Lithology
Fe-Ti Oxide (%)
TiO2/V2O5
Fe2O3(t) wt. %
TiO2 wt. %
V2O5 wt.%
-95
-100
-105
-110
-115
-120
-125
-130
-135
-140
-145
-150
20
285
510
755
1000

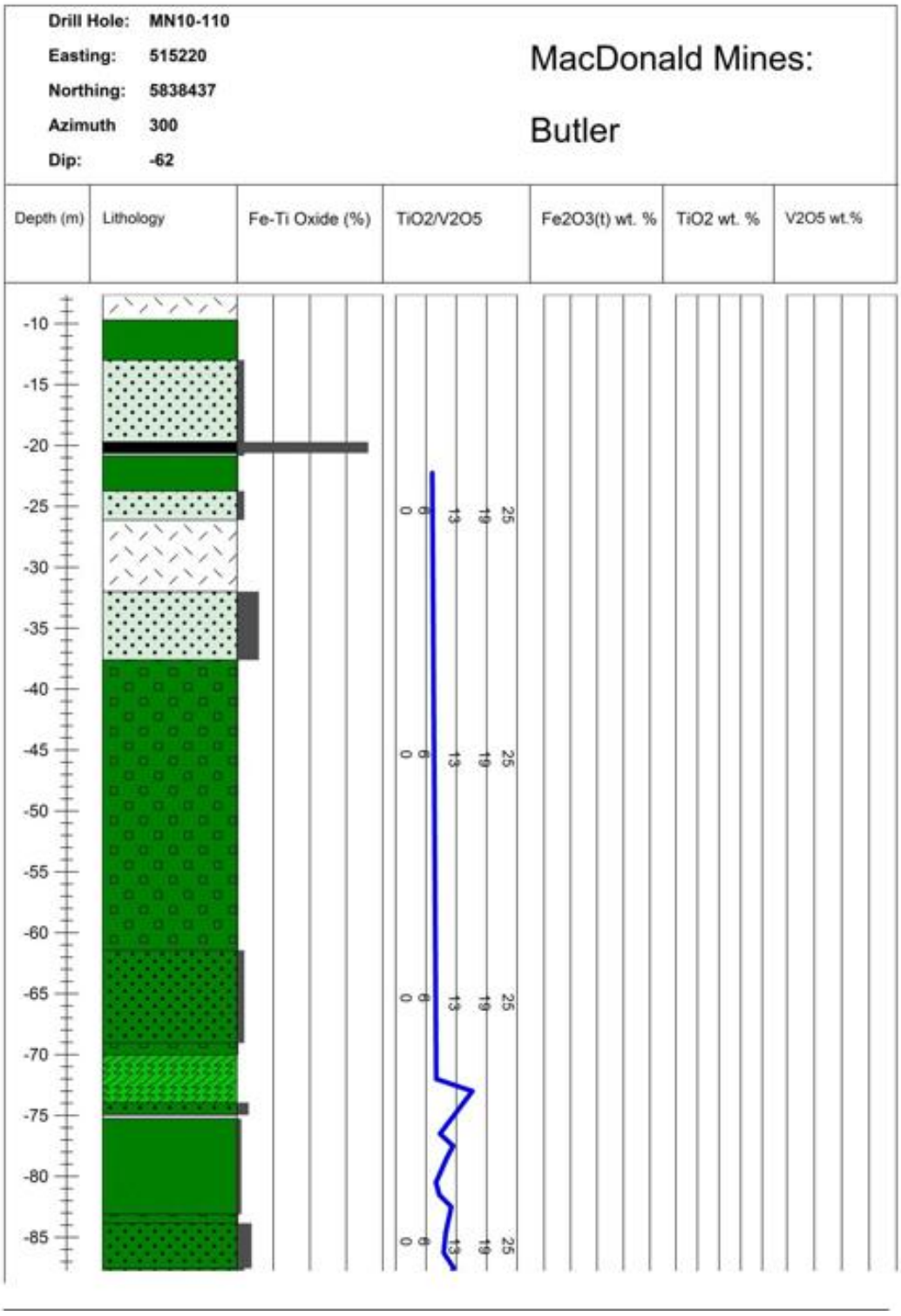
Drill Hole: MN10-110
Easting: 515220
Northing: 5838437
Azimuth 300
Dip: -62
MacDonald Mines:
Butler
Depth (m)
Lithology
Fe-Ti Oxide (%)
TiO2/V2O5
Fe2O3(t) wt. %
TiO2 wt. %
V2O5 wt.%
-10
-15
-20
-25
-30
-35
-40
-45
-50
-55
-60
-65
-70
-75
-80
-85
0
6
13
19
25

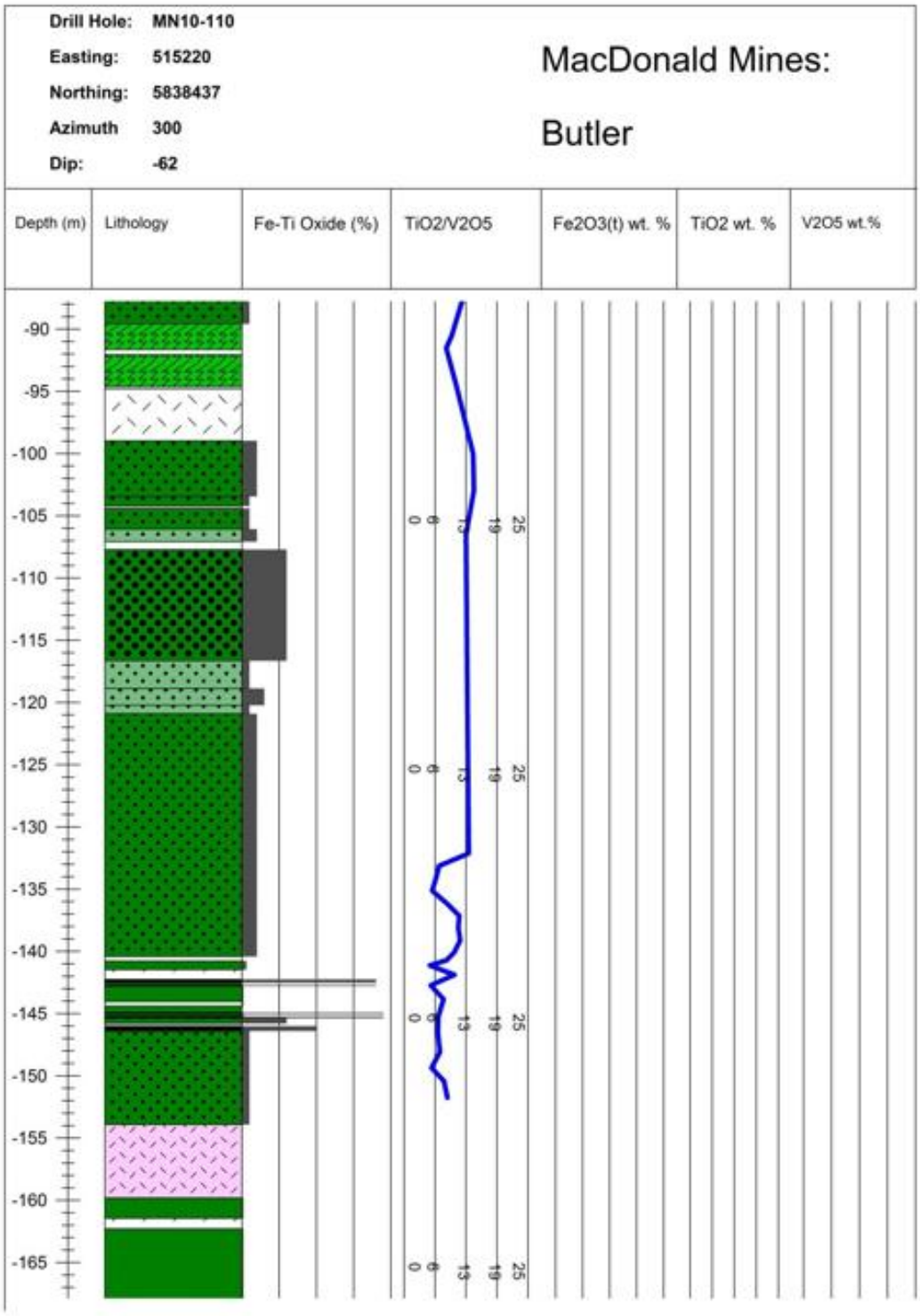
Drill Hole: MN10-110
Easting: 515220
Northing: 5838437
Azimuth 300
Dip: -62
MacDonald Mines:
Butler
Depth (m)
Lithology
Fe-Ti Oxide (%)
TiO2/V2O5
Fe2O3(t) wt. %
TiO2 wt. %
V2O5 wt.%
-90
-95
-100
-105
-110
-115
-120
-125
-130
-135
-140
-145
-150
-155
-160
-165
0
6
13
19
25

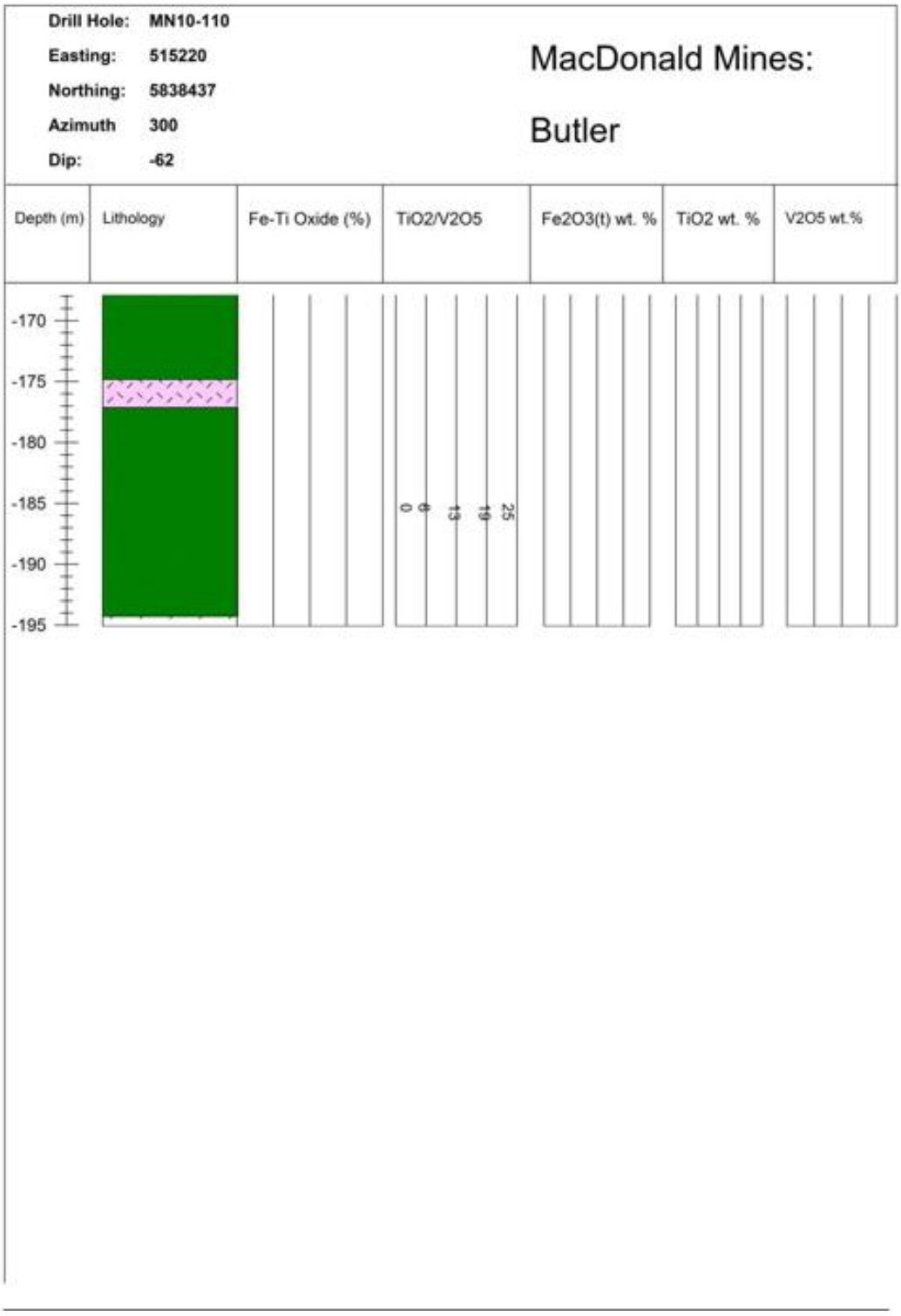
Drill Hole: MN10-110
Easting: 515220
Northing: 5838437
Azimuth 300
Dip: -62
MacDonald Mines:
Butler
Depth (m)
Lithology
Fe-Ti Oxide (%)
TiO2/V2O5
Fe2O3(t) wt. %
TiO2 wt. %
V2O5 wt.%
-170
-175
-180
-185
-190
-195
0
8
13
19
25

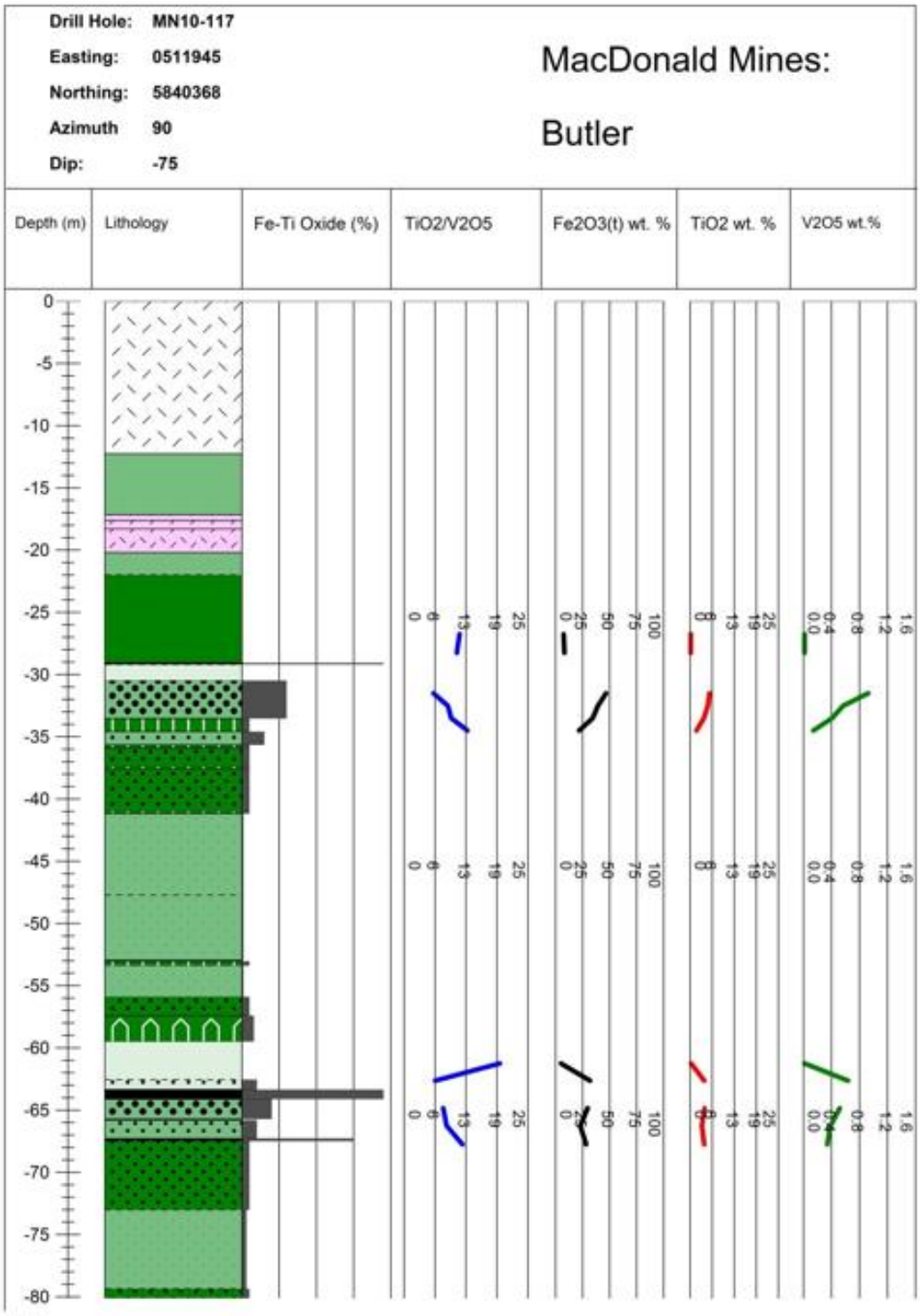
Drill Hole: MN10-117
Easting: 0511945
Northing: 5840368
Azimuth 90
Dip: -75
MacDonald Mines:
Butler
Depth (m)
Lithology
Fe-Ti Oxide (%)
TiO2/V2O5
Fe2O3(t) wt. %
TiO2 wt. %
V2O5 wt.%
0
-5
-10
-15
-20
-25
-30
-35
-40
-45
-50
-55
-60
-65
-70
-75
-80

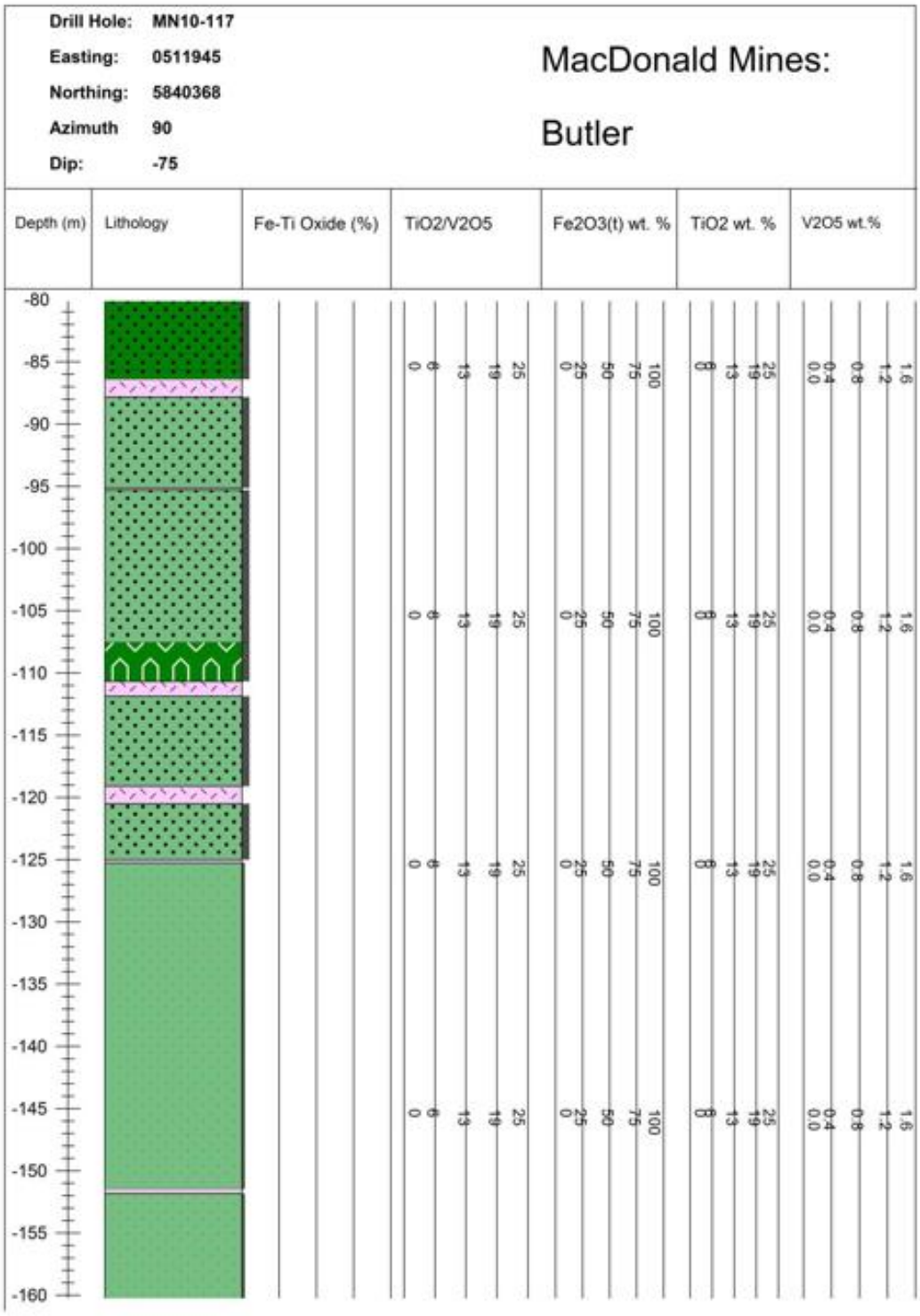
Drill Hole: MN10-117
Easting: 0511945
Northing: 5840368
Azimuth 90
Dip: -75
MacDonald Mines:
Butler
Depth (m)
Lithology
Fe-Ti Oxide (%)
TiO2/V2O5
Fe2O3(t) wt. %
TiO2 wt. %
V2O5 wt.%
-80
-85
-90
-95
-100
-105
-110
-115
-120
-125
-130
-135
-140
-145
-150
-155
-160

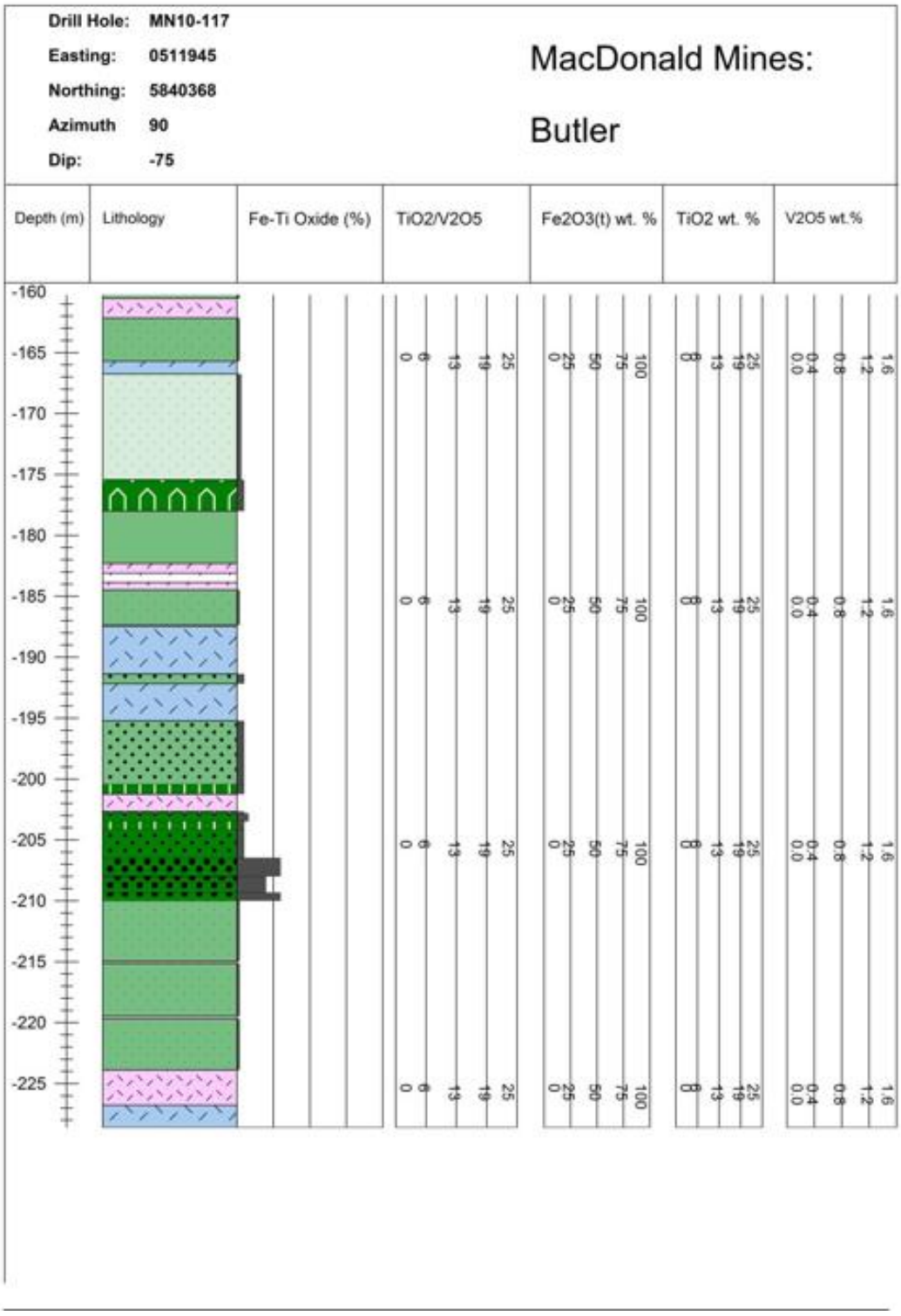
Drill Hole: MN10-117
Easting: 0511945
Northing: 5840368
Azimuth 90
Dip: -75
MacDonald Mines:
Butler
Depth (m)
Lithology
Fe-Ti Oxide (%)
TiO2/V2O5
Fe2O3(t) wt. %
TiO2 wt. %
V2O5 wt.%
-160
-165
-170
-175
-180
-185
-190
-195
-200
-205
-210
-215
-220
-225

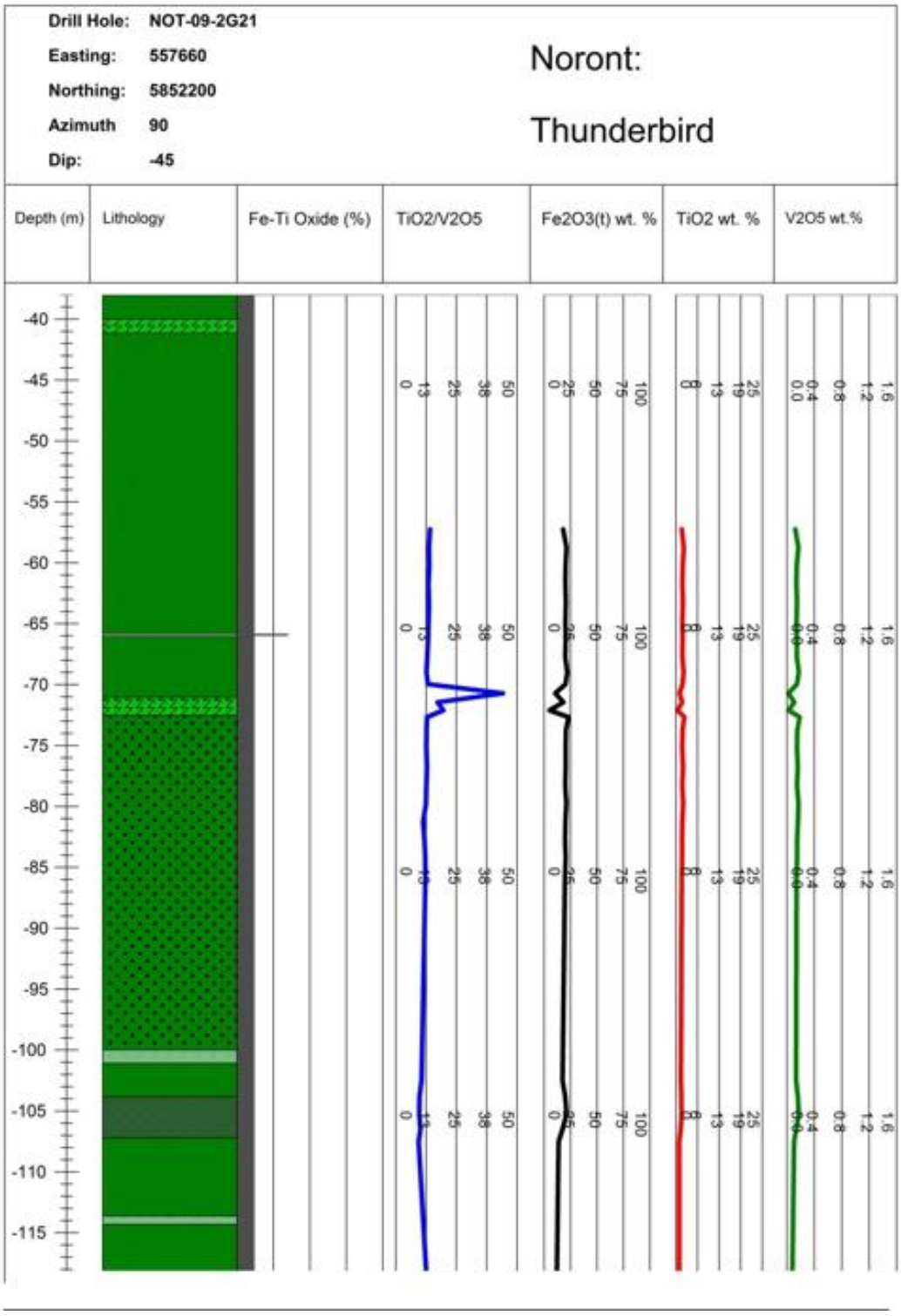
Drill Hole: NOT-09-2G21
Easting: 557660
Northing: 5852200
Azimuth 90
Dip: -45
Noront:
Thunderbird
Depth (m)
Lithology
Fe-Ti Oxide (%)
TiO2/V2O5
Fe2O3(t) wt. %
TiO2 wt. %
V2O5 wt.%
-40
-45
-50
-55
-60
-65
-70
-75
-80
-85
-90
-95
-100
-105
-110
-115

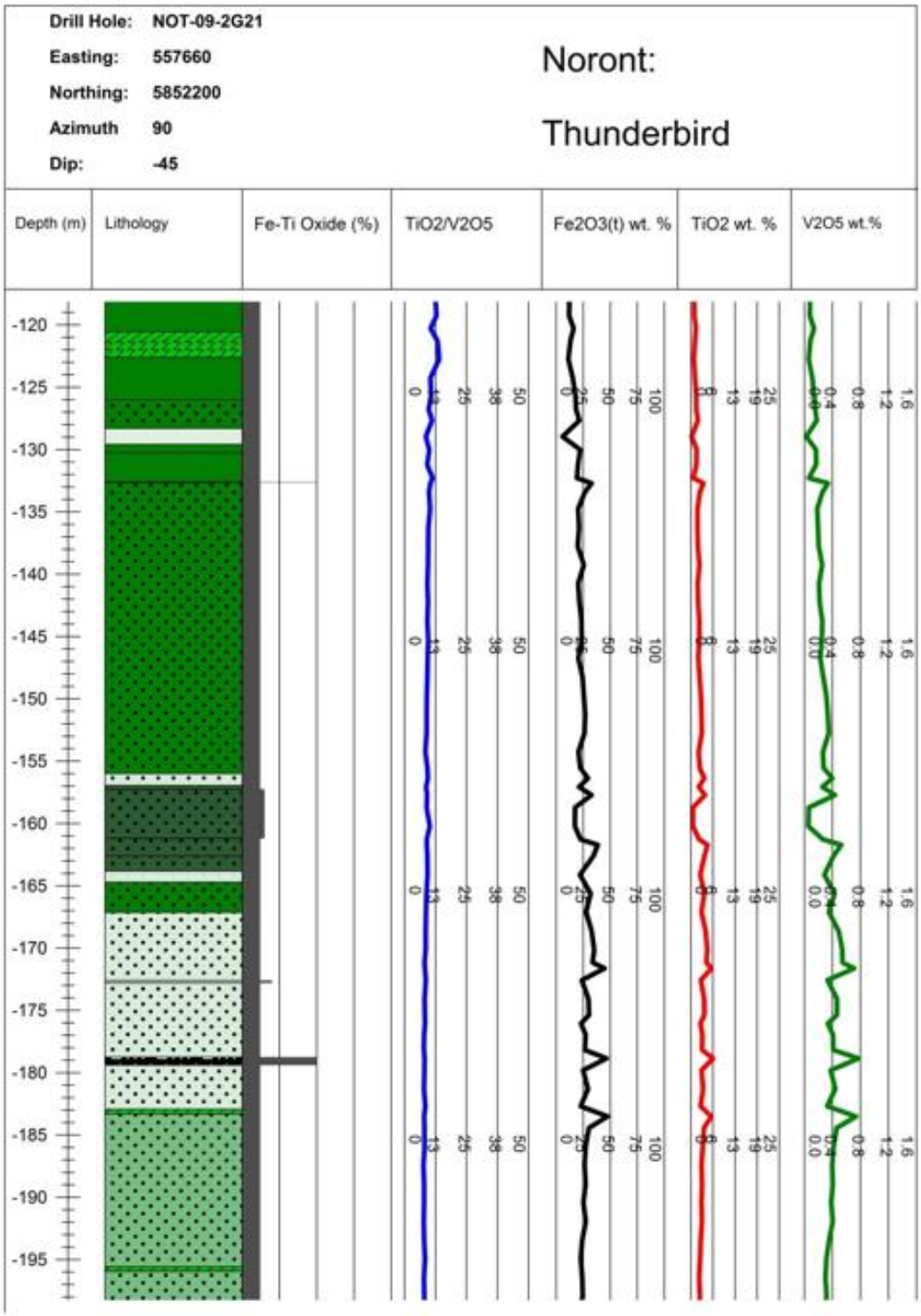
Drill Hole: NOT-09-2G21
Easting: 557660
Northing: 5852200
Azimuth 90
Dip: -45
Noront:
Thunderbird
Depth (m)
Lithology
Fe-Ti Oxide (%)
TiO2/V2O5
Fe2O3(t) wt. %
TiO2 wt. %
V2O5 wt.%
-120
-125
-130
-135
-140
-145
-150
-155
-160
-165
-170
-175
-180
-185
-190
-195

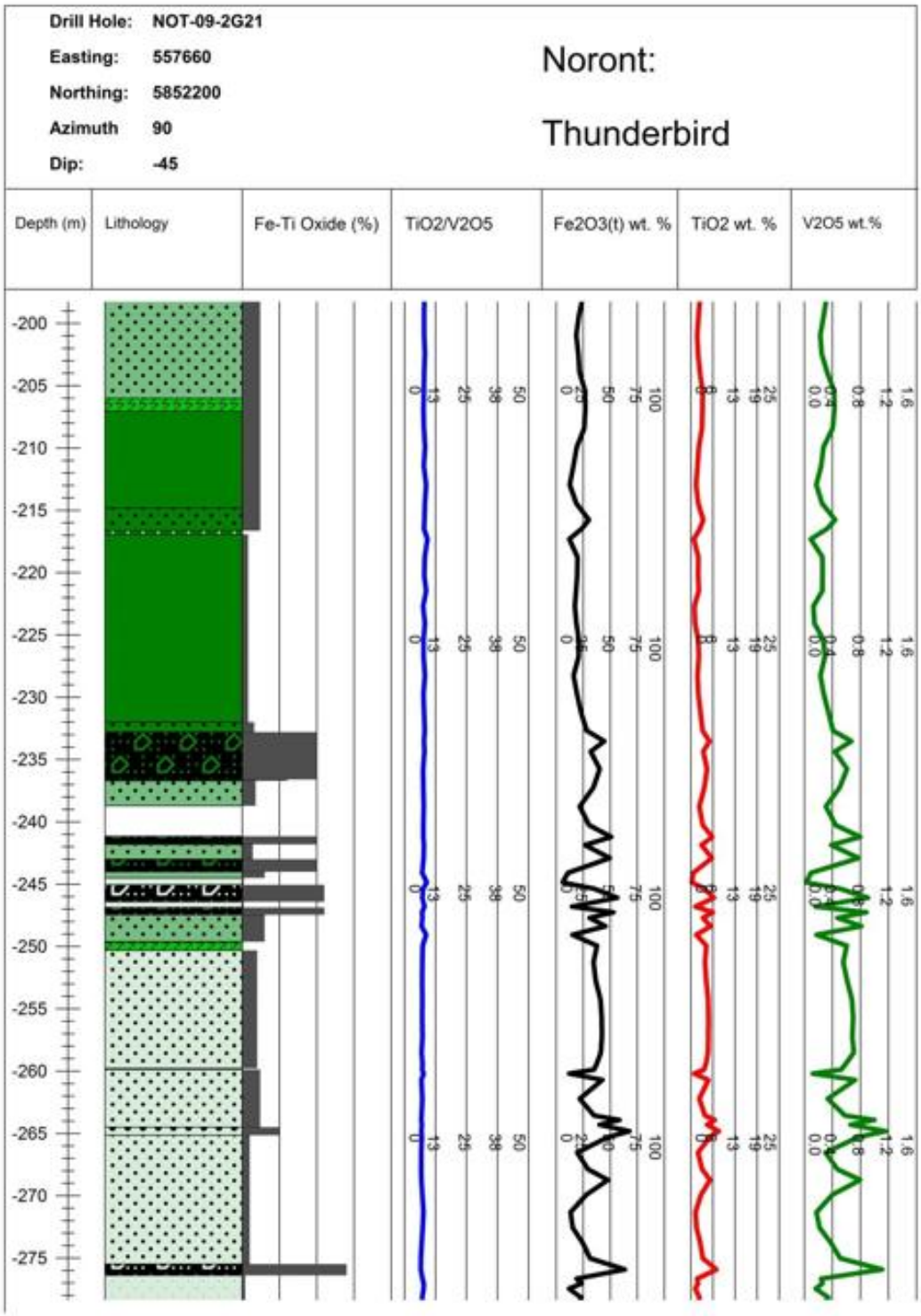
Drill Hole: NOT-09-2G21
Easting: 557660
Northing: 5852200
Azimuth 90
Dip: -45
Noront:
Thunderbird
Depth (m)
Lithology
Fe-Ti Oxide (%)
TiO2/V2O5
Fe2O3(t) wt. %
TiO2 wt. %
V2O5 wt.%
-200
-205
-210
-215
-220
-225
-230
-235
-240
-245
-250
-255
-260
-265
-270
-275

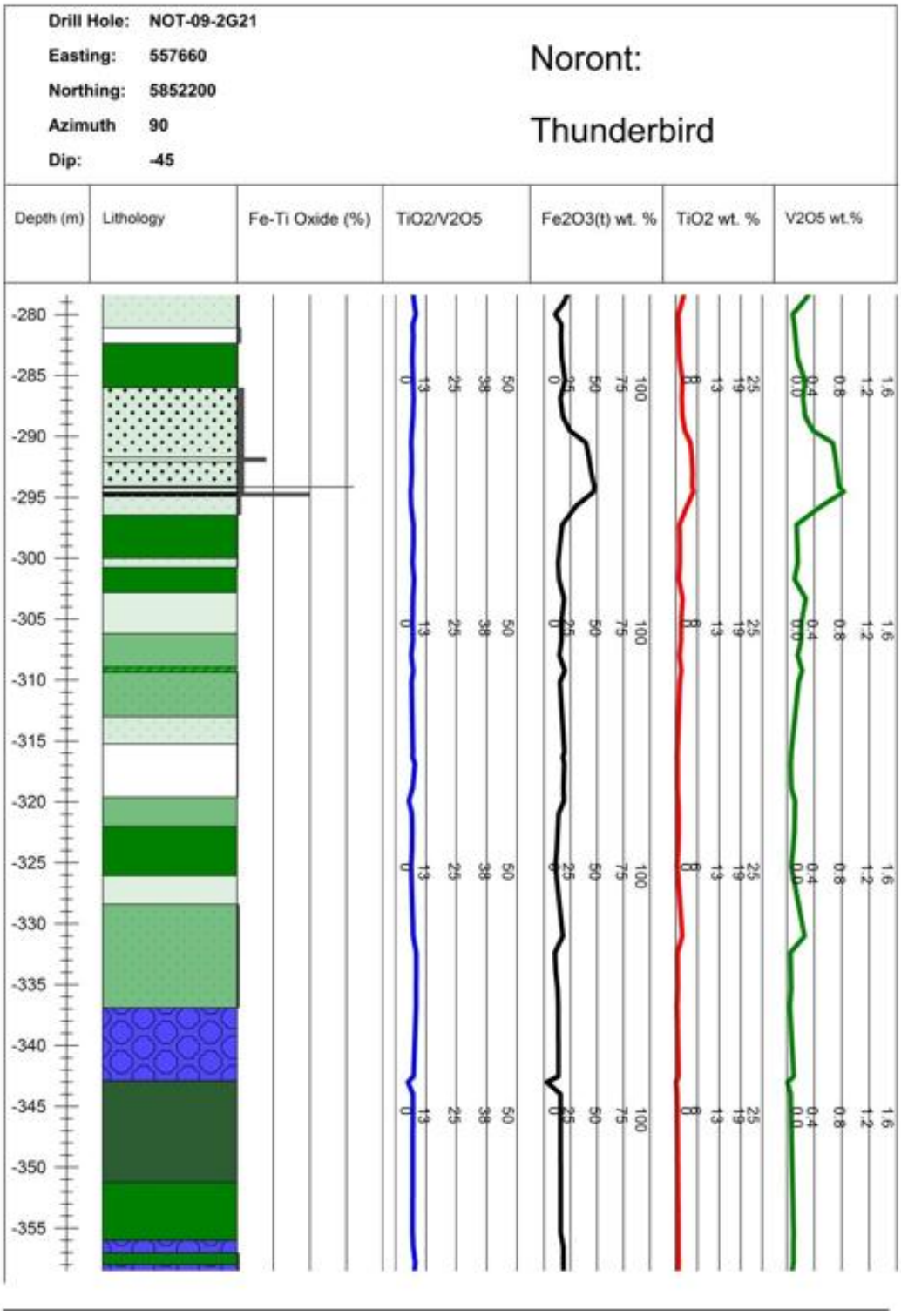
Drill Hole: NOT-09-2G21
Easting: 557660
Northing: 5852200
Azimuth 90
Dip: -45
Noront:
Thunderbird
Depth (m)
Lithology
Fe-Ti Oxide (%)
TiO2/V2O5
Fe2O3(t) wt. %
TiO2 wt. %
V2O5 wt.%
-280
-285
-290
-295
-300
-305
-310
-315
-320
-325
-330
-335
-340
-345
-350
-355

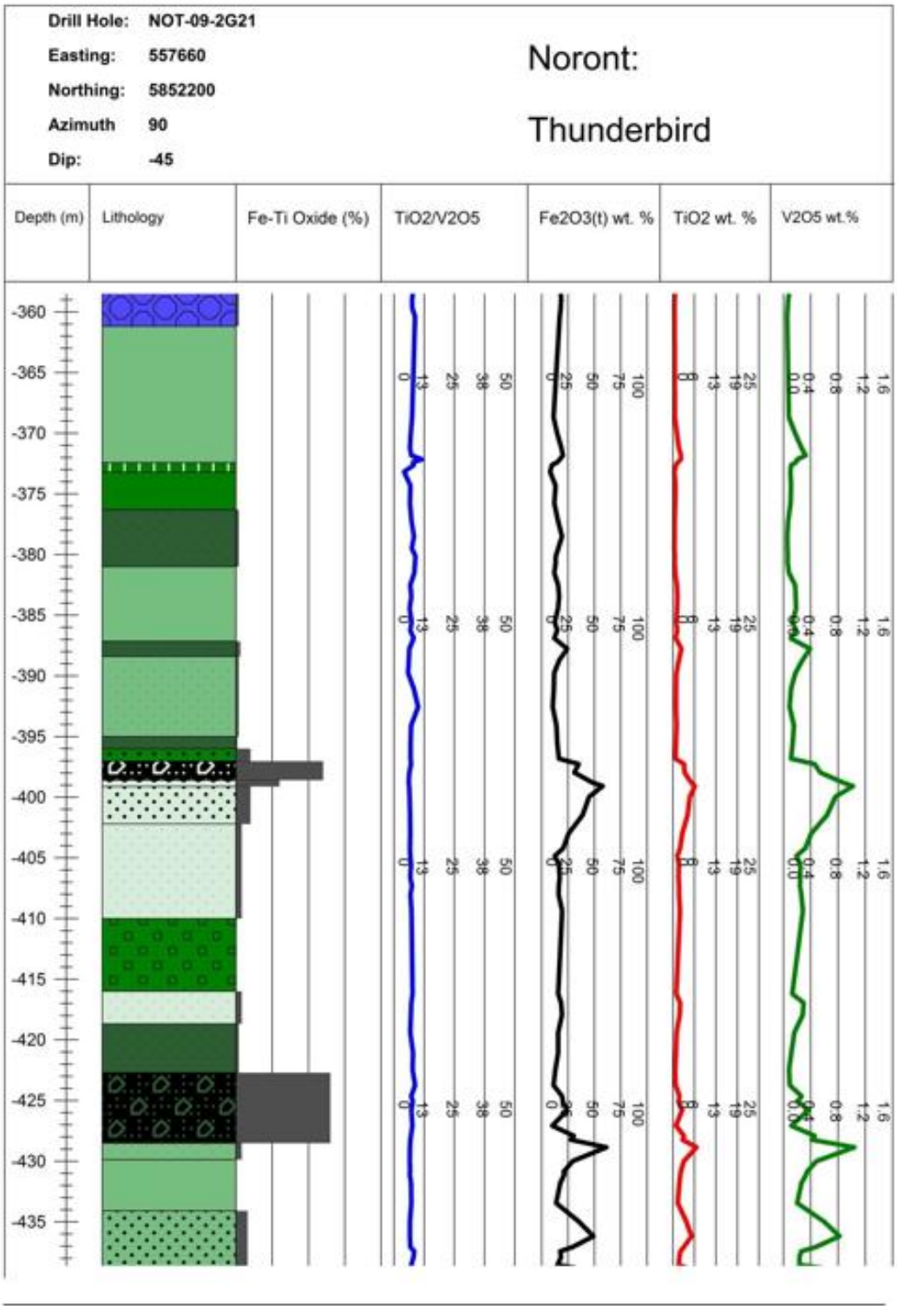
Drill Hole: NOT-09-2G21
Easting: 557660
Northing: 5852200
Azimuth 90
Dip: -45
Noront:
Thunderbird
Depth (m)
Lithology
Fe-Ti Oxide (%)
TiO2/V2O5
Fe2O3(t) wt. %
TiO2 wt. %
V2O5 wt.%
-360
-365
-370
-375
-380
-385
-390
-395
-400
-405
-410
-415
-420
-425
-430
-435

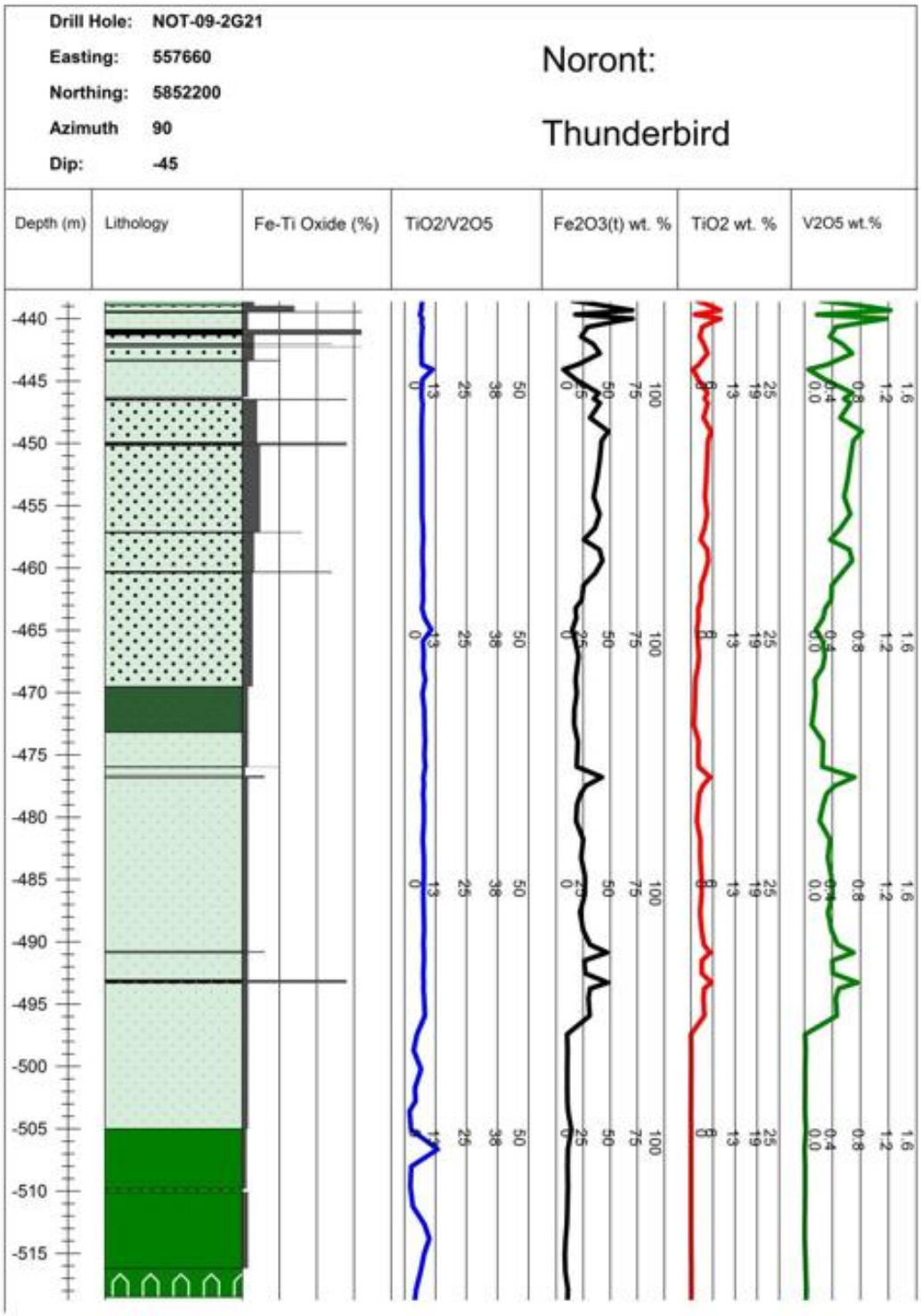
Drill Hole: NOT-09-2G21
Easting: 557660
Northing: 5852200
Azimuth 90
Dip: -45
Noront:
Thunderbird
Depth (m)
Lithology
Fe-Ti Oxide (%)
TiO2/V2O5
Fe2O3(t) wt. %
TiO2 wt. %
V2O5 wt.%
-440
-445
-450
-455
-460
-465
-470
-475
-480
-485
-490
-495
-500
-505
-510
-515


Drill Hole: NOT-09-2G21
Easting: 557660
Northing: 5852200
Azimuth 90
Dip: -45
Noront:
Thunderbird
Depth (m)
Lithology
Fe-Ti Oxide (%)
TiO2/V2O5
Fe2O3(t) wt. %
TiO2 wt. %
V2O5 wt.%
-520

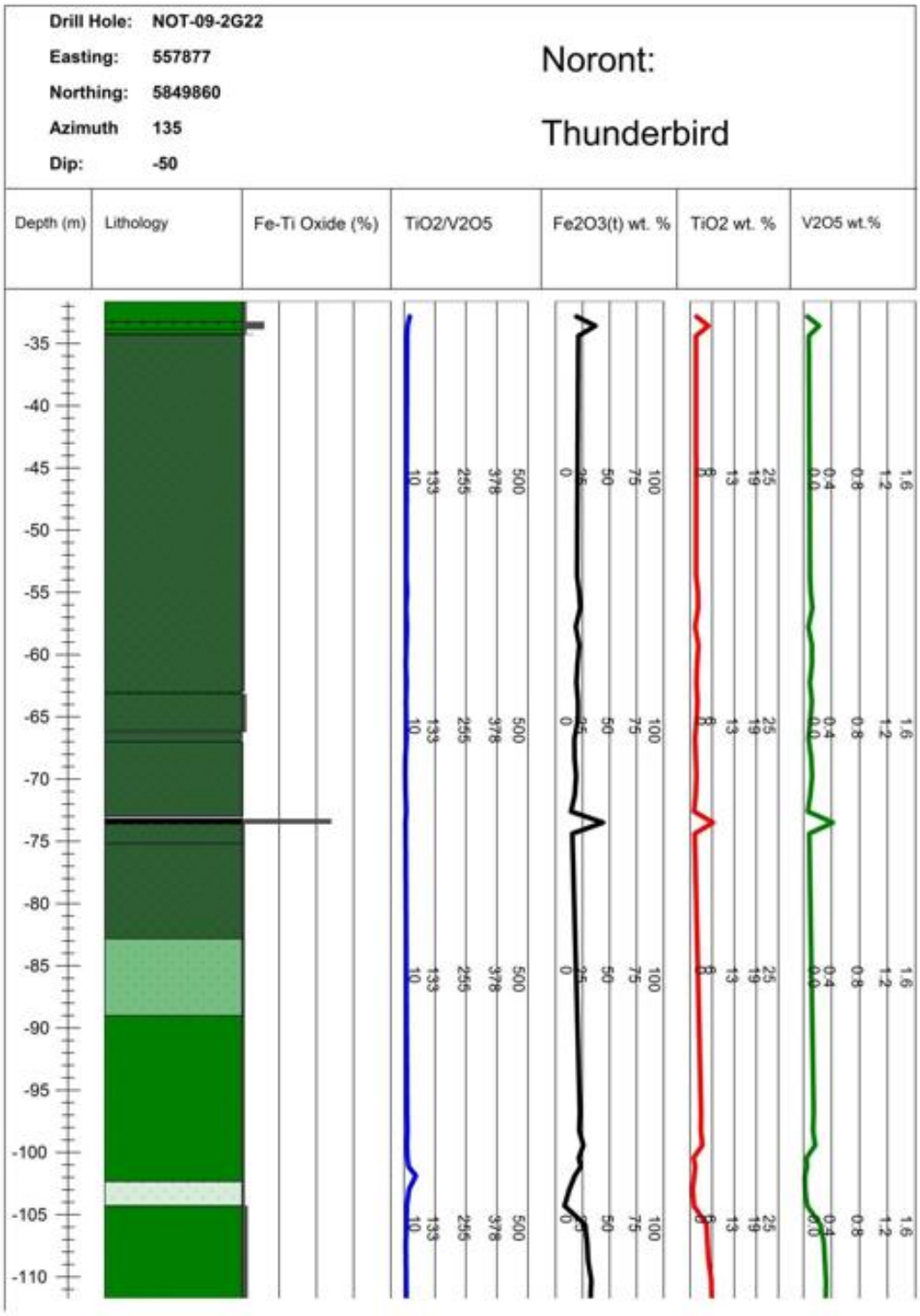
Drill Hole: NOT-09-2G22
Easting: 557877
Northing: 5849860
Azimuth 135
Dip: -50
Noront:
Thunderbird
Depth (m)
Lithology
Fe-Ti Oxide (%)
TiO2/V2O5
Fe2O3(t) wt. %
TiO2 wt. %
V2O5 wt.%
-35
-40
-45
-50
-55
-60
-65
-70
-75
-80
-85
-90
-95
-100
-105
-110

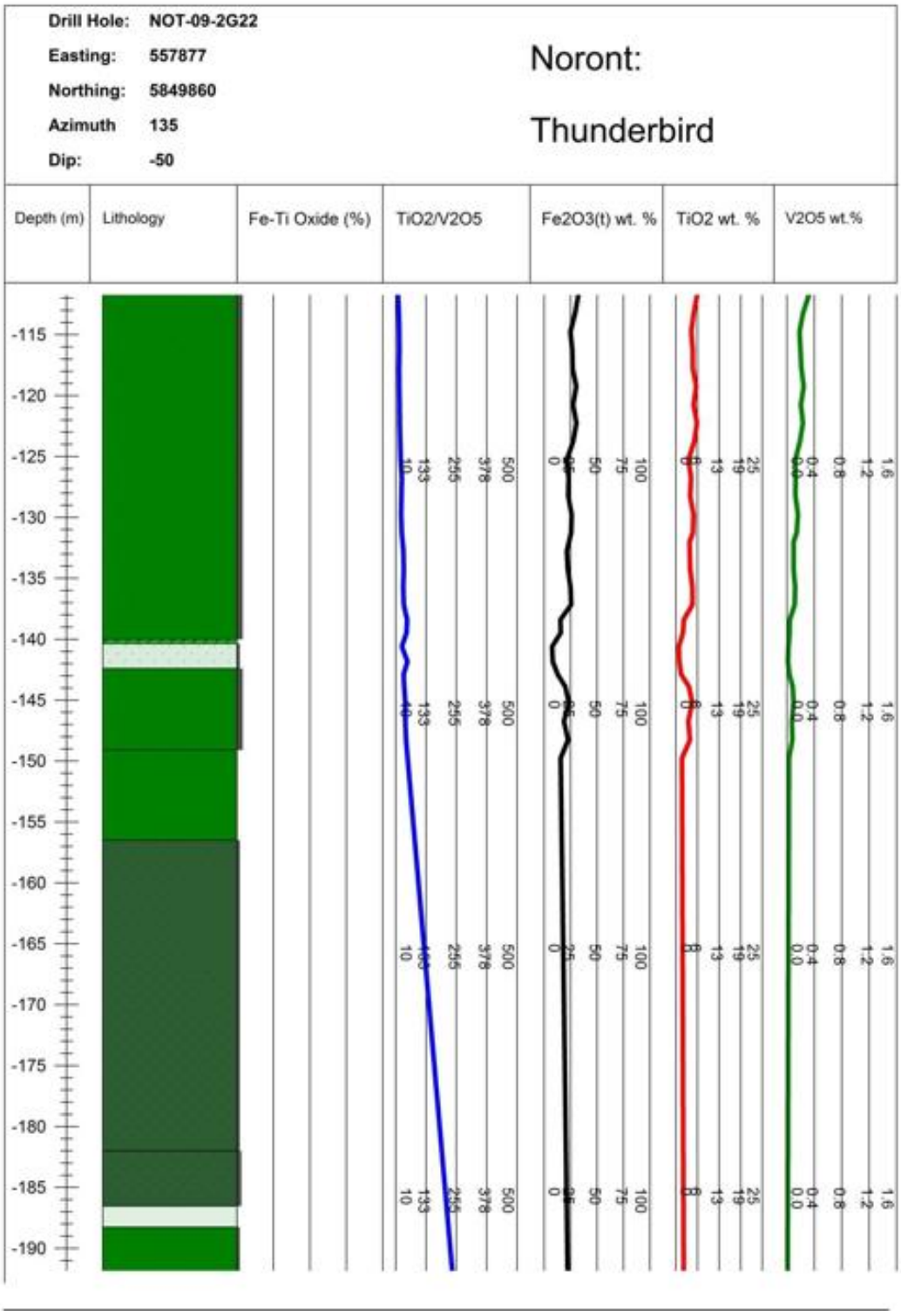
Drill Hole: NOT-09-2G22
Easting: 557877
Northing: 5849860
Azimuth 135
Dip: -50
Noront:
Thunderbird
Depth (m)
Lithology
Fe-Ti Oxide (%)
TiO2/V2O5
Fe2O3(t) wt. %
TiO2 wt. %
V2O5 wt.%
-115
-120
-125
-130
-135
-140
-145
-150
-155
-160
-165
-170
-175
-180
-185
-190

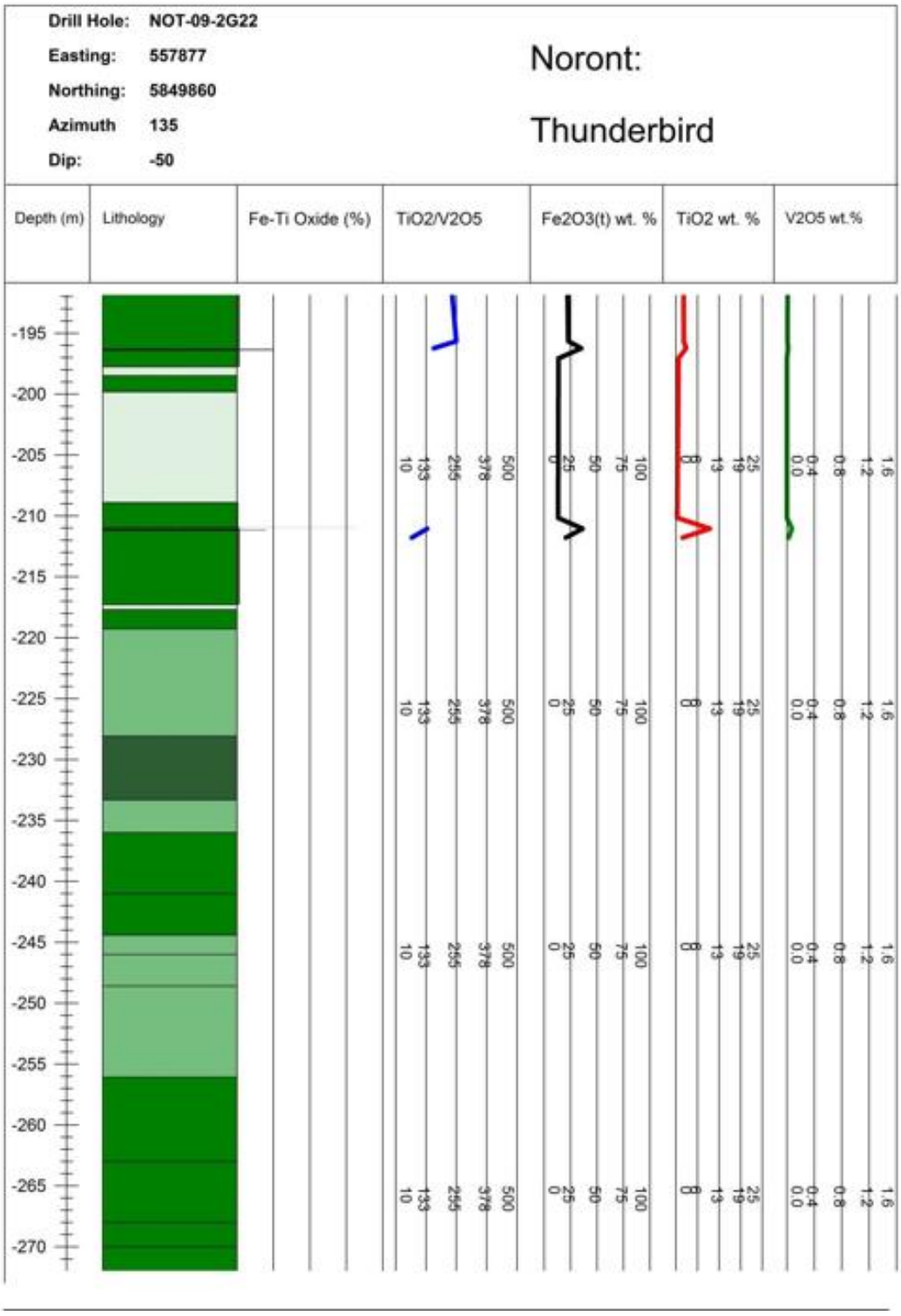
Drill Hole: NOT-09-2G22
Easting: 557877
Northing: 5849860
Azimuth 135
Dip: -50
Noront:
Thunderbird
Depth (m)
Lithology
Fe-Ti Oxide (%)
TiO2/V2O5
Fe2O3(t) wt. %
TiO2 wt. %
V2O5 wt.%
-195
-200
-205
-210
-215
-220
-225
-230
-235
-240
-245
-250
-255
-260
-265
-270

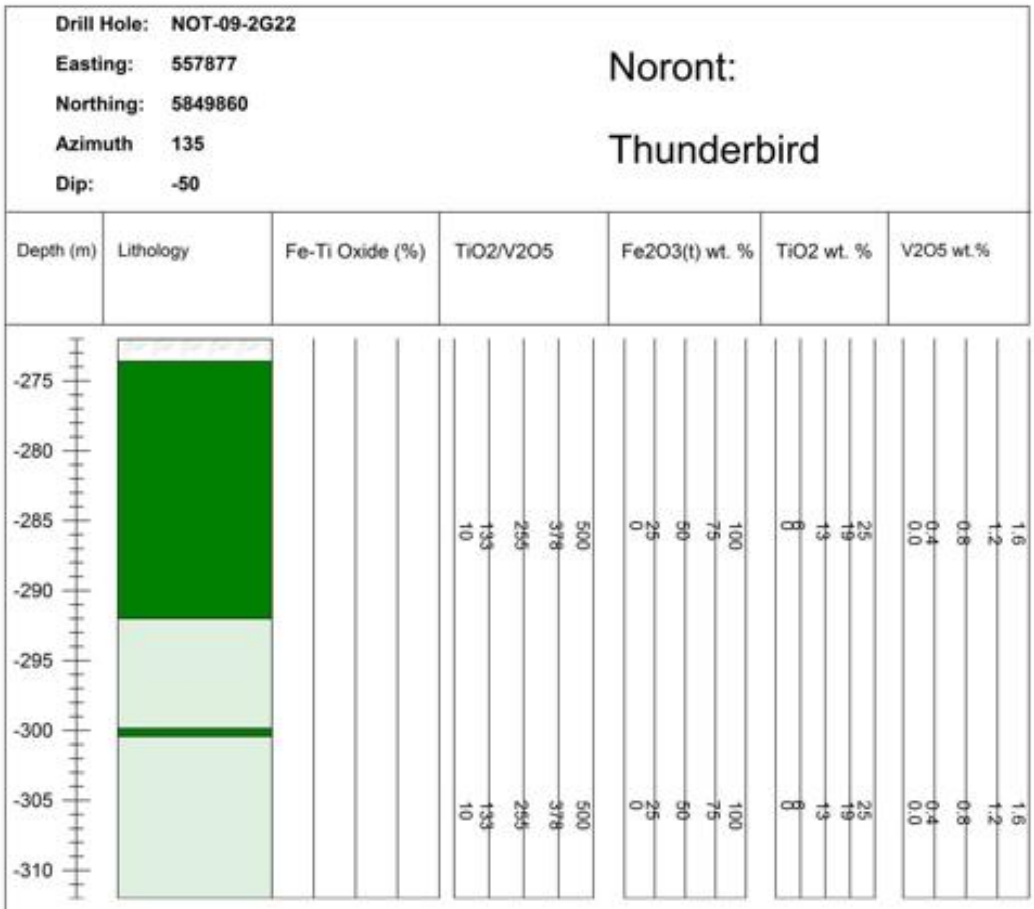
Drill Hole: NOT-09-2G22
Easting: 557877
Northing: 5849860
Azimuth 135
Dip: -50
Noront:
Thunderbird
Depth (m)
Lithology
Fe-Ti Oxide (%)
TiO2/V2O5
Fe2O3(t) wt. %
TiO2 wt. %
V2O5 wt.%
-275
-280
-285
-290
-295
-300
-305
-310
10
133
255
378
500
0
25
50
75
100
0
8
13
19
25
0.0
0.4
0.8
1.2
1.6

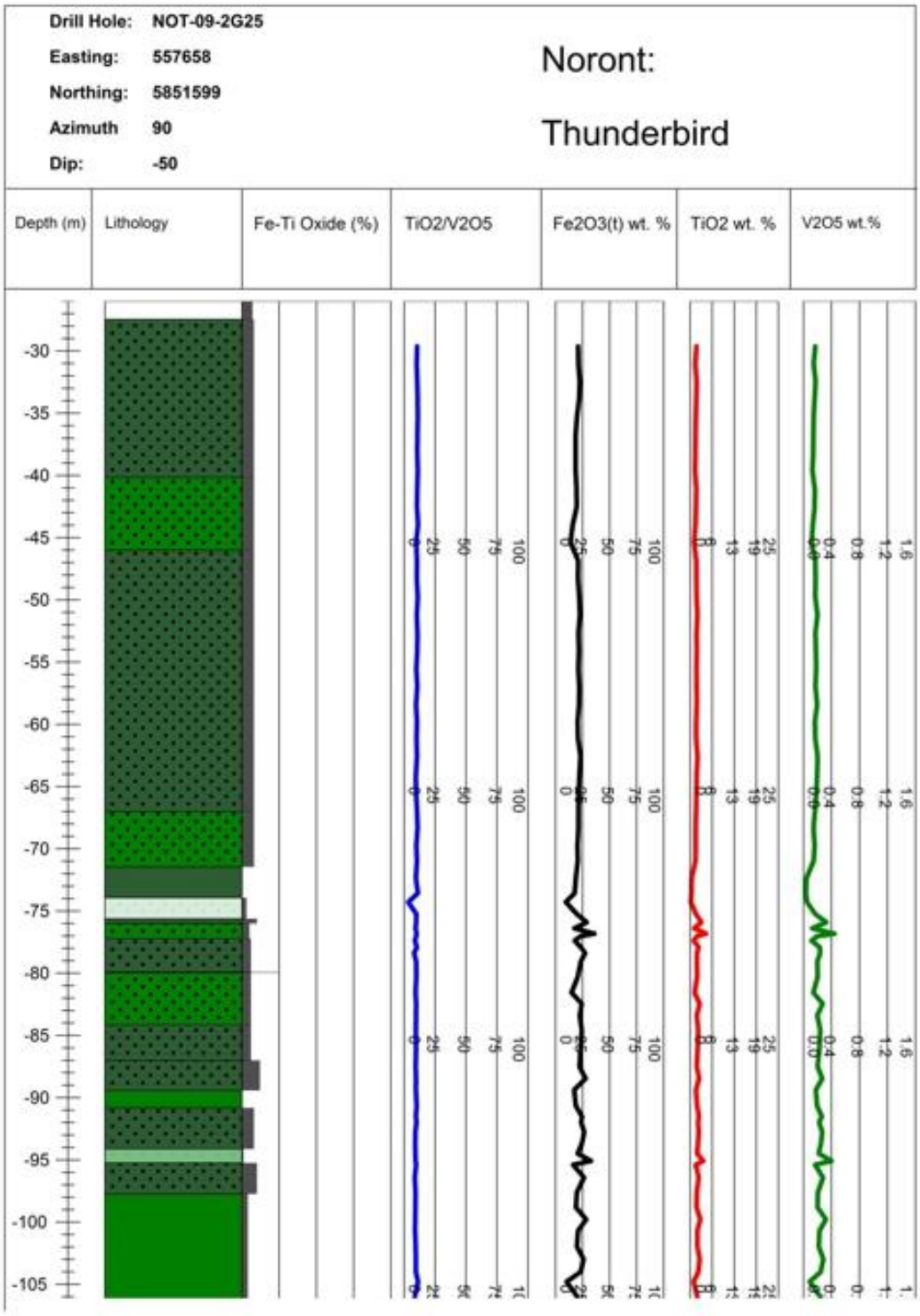
Drill Hole: NOT-09-2G25
Easting: 557658
Northing: 5851599
Azimuth 90
Dip: -50
Noront:
Thunderbird
Depth (m)
Lithology
Fe-Ti Oxide (%)
TiO2/V2O5
Fe2O3(t) wt. %
TiO2 wt. %
V2O5 wt.%
-30
-35
-40
-45
-50
-55
-60
-65
-70
-75
-80
-85
-90
-95
-100
-105

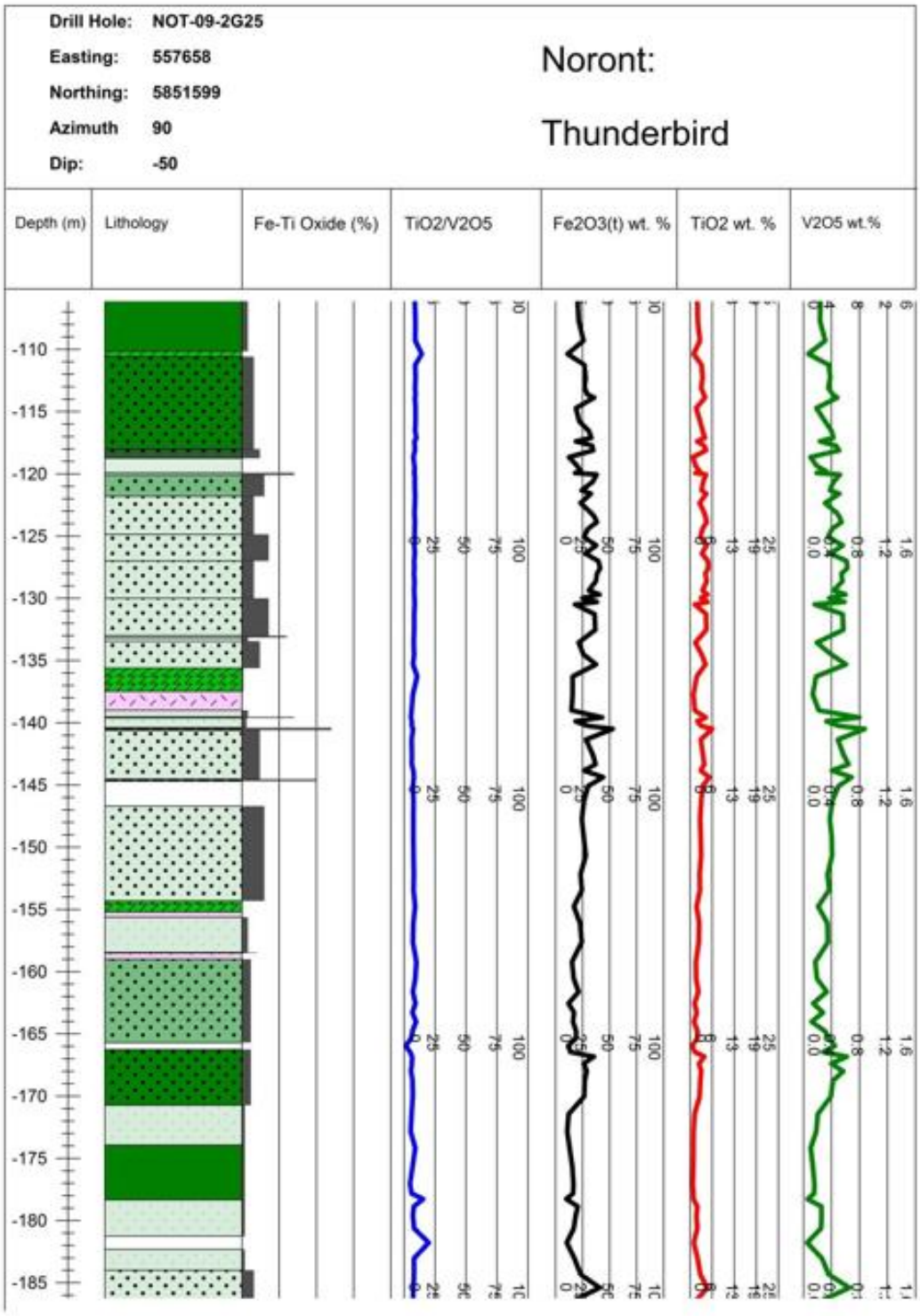
Drill Hole: NOT-09-2G25
Easting: 557658
Northing: 5851599
Azimuth 90
Dip: -50
Noront:
Thunderbird
Depth (m)
Lithology
Fe-Ti Oxide (%)
TiO2/V2O5
Fe2O3(t) wt. %
TiO2 wt. %
V2O5 wt.%
-110
-115
-120
-125
-130
-135
-140
-145
-150
-155
-160
-165
-170
-175
-180
-185

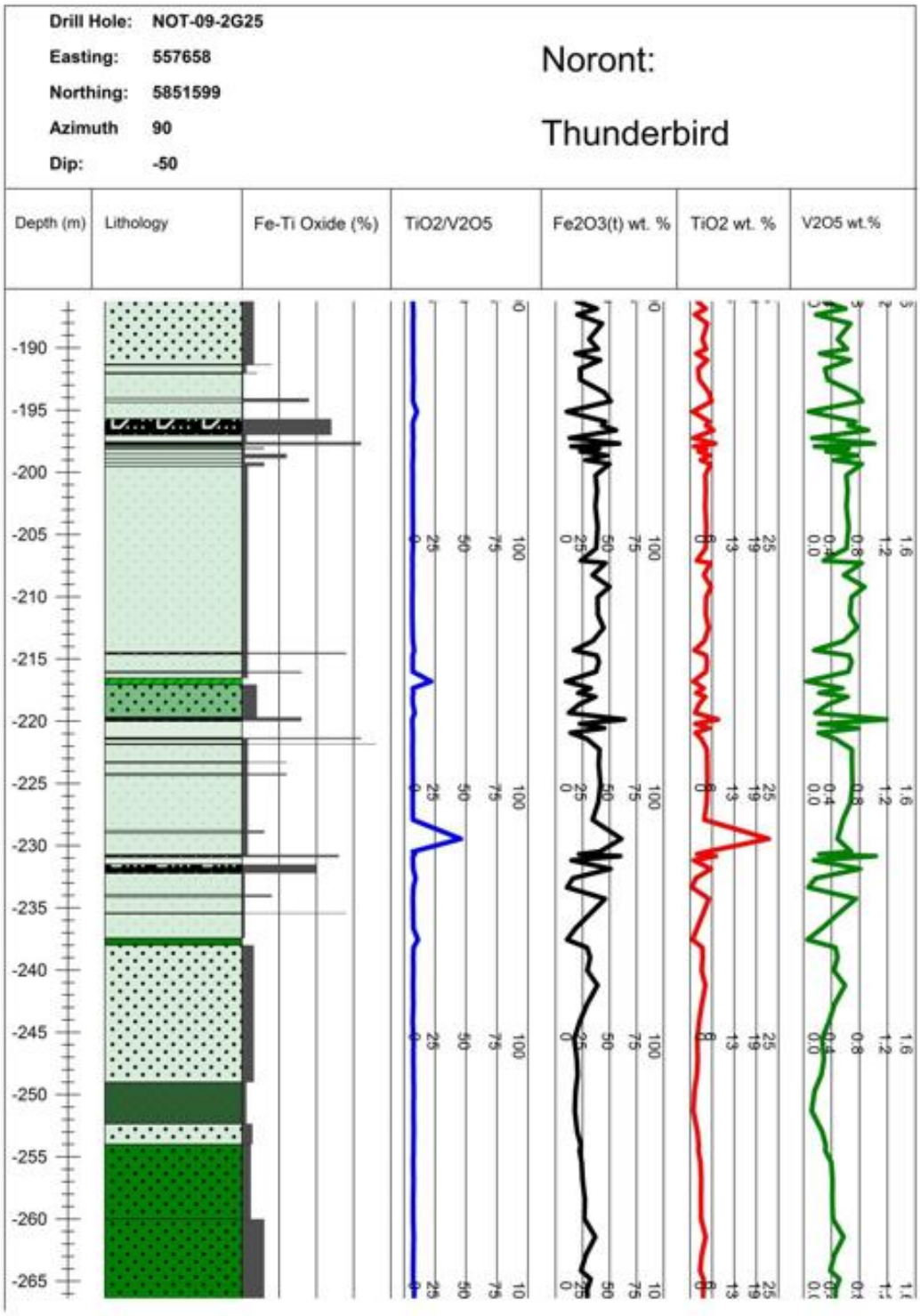
Drill Hole: NOT-09-2G25
Easting: 557658
Northing: 5851599
Azimuth 90
Dip: -50
Noront:
Thunderbird
Depth (m)
Lithology
Fe-Ti Oxide (%)
TiO2/V2O5
Fe2O3(t) wt. %
TiO2 wt. %
V2O5 wt.%
-190
-195
-200
-205
-210
-215
-220
-225
-230
-235
-240
-245
-250
-255
-260
-265

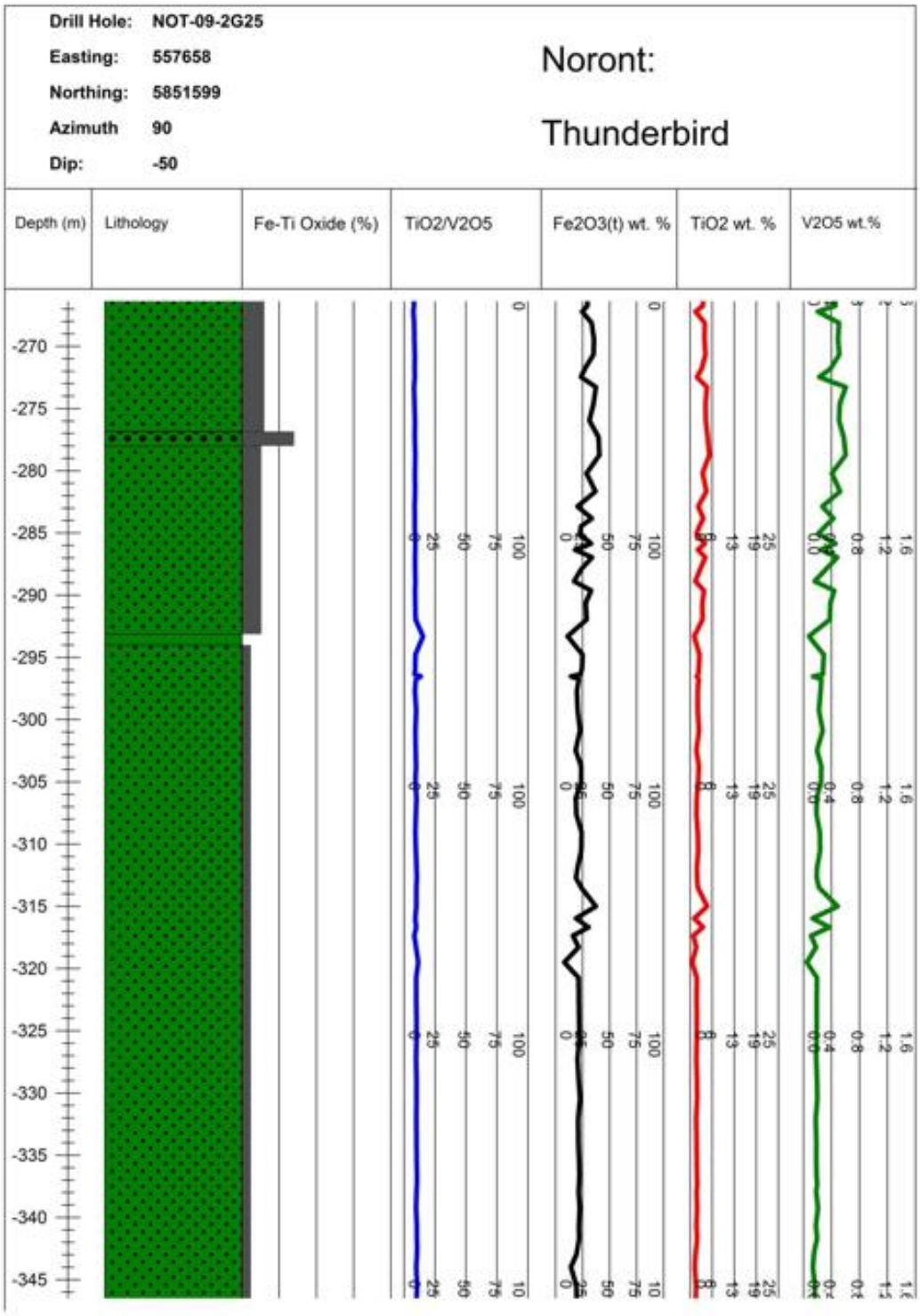
Drill Hole: NOT-09-2G25
Easting: 557658
Northing: 5851599
Azimuth 90
Dip: -50
Noront:
Thunderbird
Depth (m)
Lithology
Fe-Ti Oxide (%)
TiO2/V2O5
Fe2O3(t) wt. %
TiO2 wt. %
V2O5 wt.%
-270
-275
-280
-285
-290
-295
-300
-305
-310
-315
-320
-325
-330
-335
-340
-345

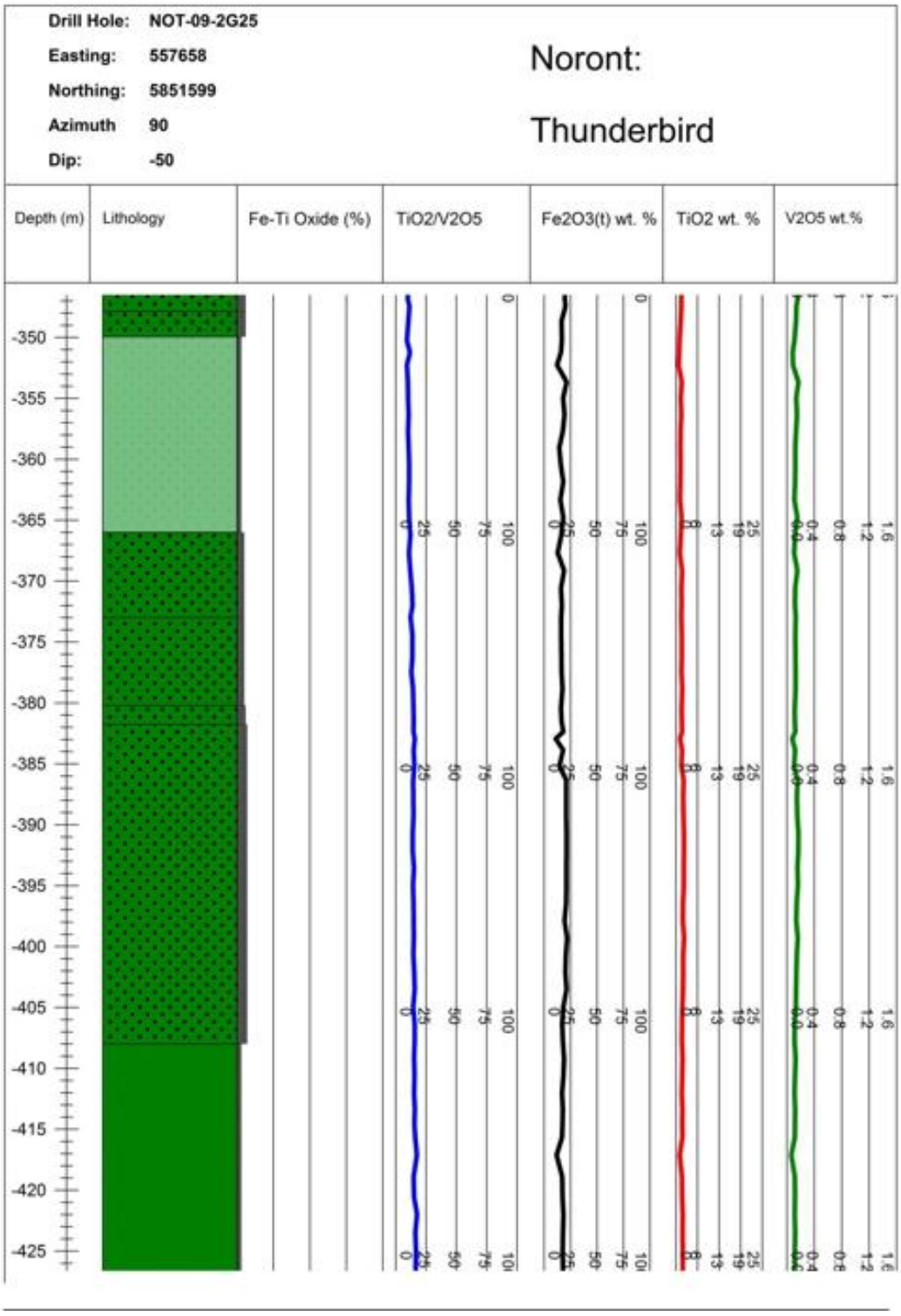
Drill Hole: NOT-09-2G25
Easting: 557658
Northing: 5851599
Azimuth 90
Dip: -50
Noront:
Thunderbird
Depth (m)
Lithology
Fe-Ti Oxide (%)
TiO2/V2O5
Fe2O3(t) wt. %
TiO2 wt. %
V2O5 wt.%
-350
-355
-360
-365
-370
-375
-380
-385
-390
-395
-400
-405
-410
-415
-420
-425

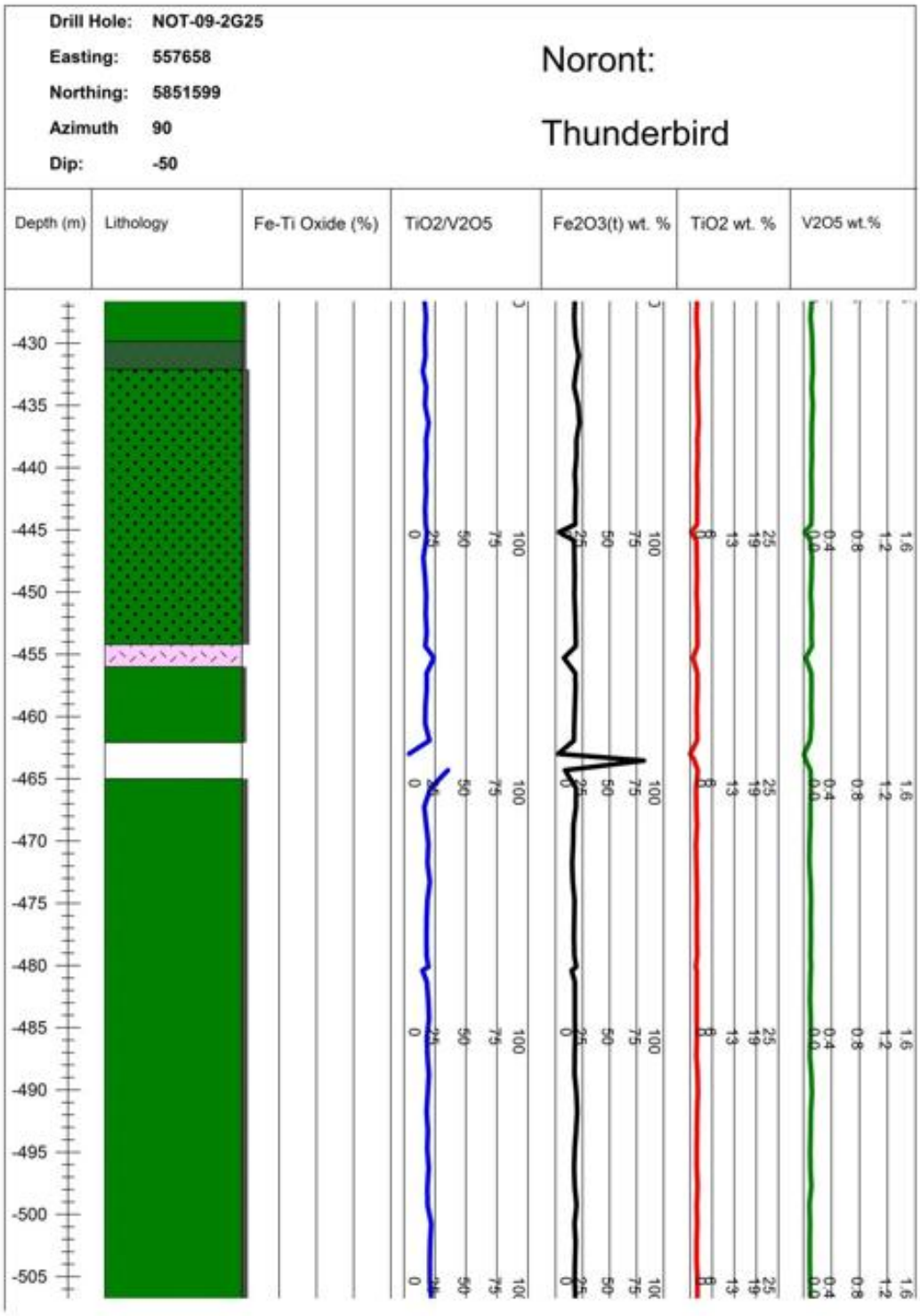
Drill Hole: NOT-09-2G25
Easting: 557658
Northing: 5851599
Azimuth 90
Dip: -50
Noront:
Thunderbird
Depth (m)
Lithology
Fe-Ti Oxide (%)
TiO2/V2O5
Fe2O3(t) wt. %
TiO2 wt. %
V2O5 wt.%
-430
-435
-440
-445
-450
-455
-460
-465
-470
-475
-480
-485
-490
-495
-500
-505

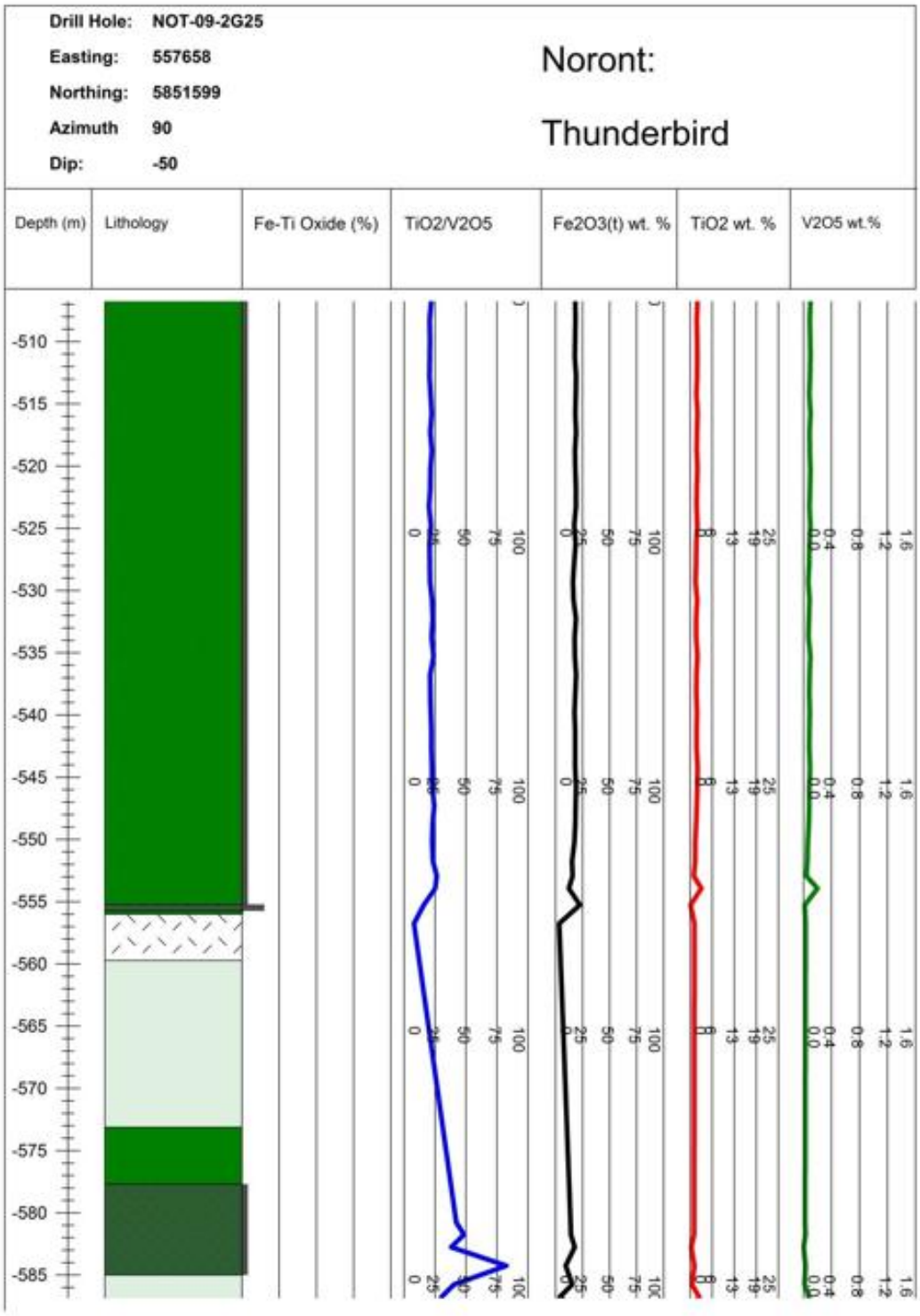
Drill Hole: NOT-09-2G25
Easting: 557658
Northing: 5851599
Azimuth 90
Dip: -50
Noront:
Thunderbird
Depth (m)
Lithology
Fe-Ti Oxide (%)
TiO2/V2O5
Fe2O3(t) wt. %
TiO2 wt. %
V2O5 wt.%
-510
-515
-520
-525
-530
-535
-540
-545
-550
-555
-560
-565
-570
-575
-580
-585

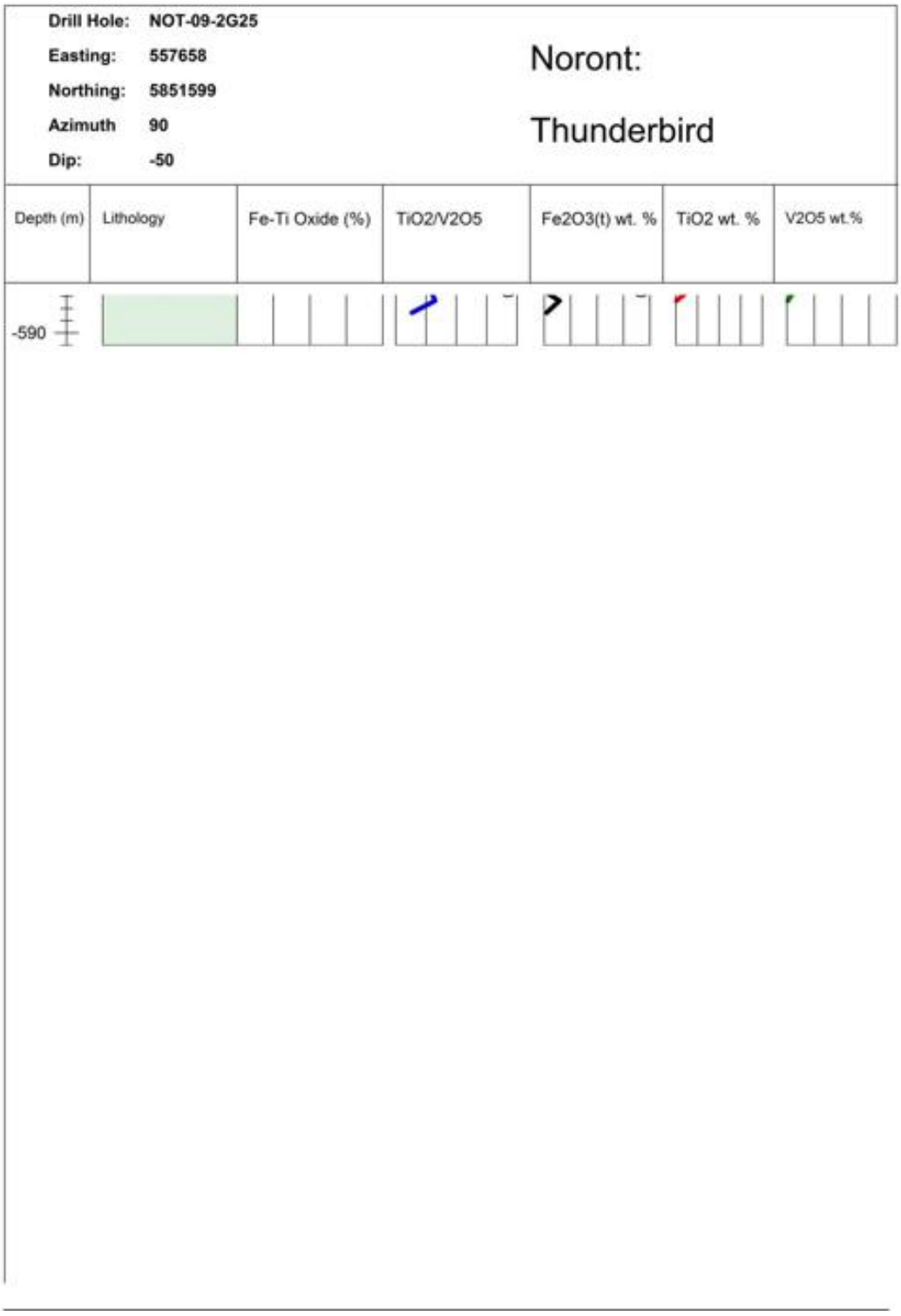
Drill Hole: NOT-09-2G25
Easting: 557658
Northing: 5851599
Azimuth 90
Dip: -50
Noront:
Thunderbird
Depth (m)
Lithology
Fe-Ti Oxide (%)
TiO2/V2O5
Fe2O3(t) wt. %
TiO2 wt. %
V2O5 wt.%
-590

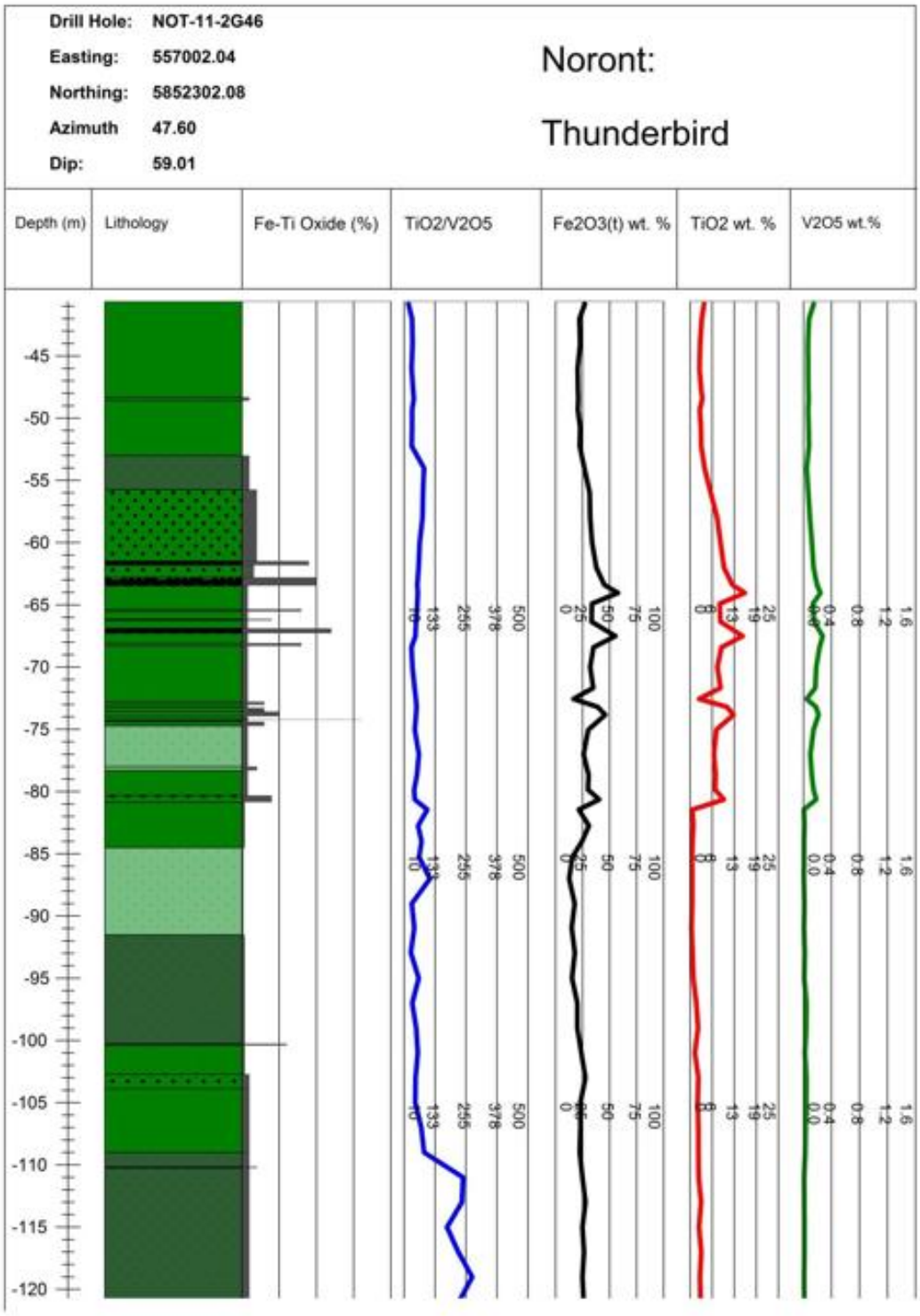
Drill Hole: NOT-11-2G46
Easting: 557002.04
Northing: 5852302.08
Azimuth 47.60
Dip: 59.01
Noront:
Thunderbird
Depth (m)
Lithology
Fe-Ti Oxide (%)
TiO2/V2O5
Fe2O3(t) wt. %
TiO2 wt. %
V2O5 wt.%
-45
-50
-55
-60
-65
-70
-75
-80
-85
-90
-95
-100
-105
-110
-115
-120

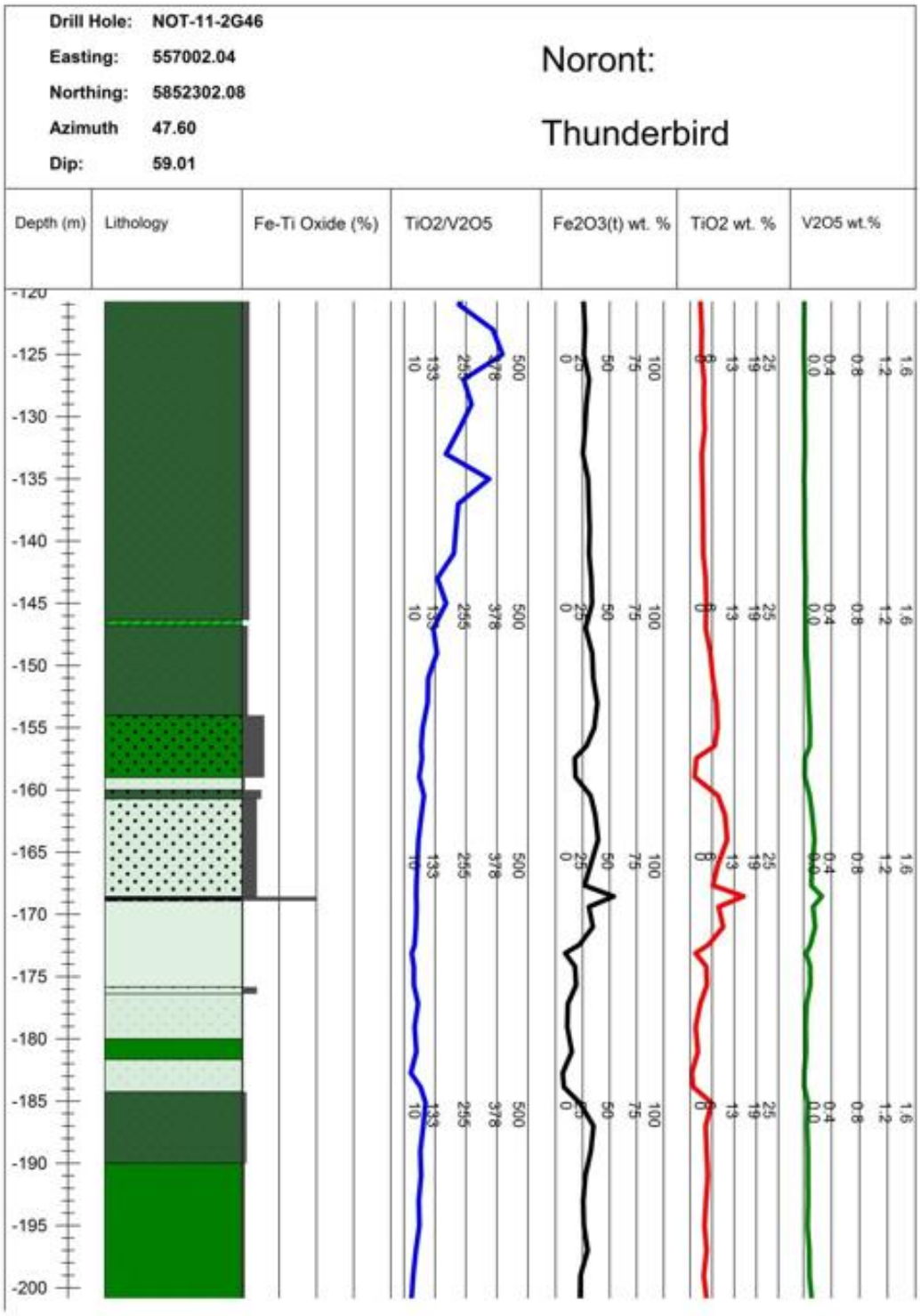
Drill Hole: NOT-11-2G46
Easting: 557002.04
Northing: 5852302.08
Azimuth 47.60
Dip: 59.01
Noront:
Thunderbird
Depth (m)
Lithology
Fe-Ti Oxide (%)
TiO2/V2O5
Fe2O3(t) wt. %
TiO2 wt. %
V2O5 wt.%
-120
-125
-130
-135
-140
-145
-150
-155
-160
-165
-170
-175
-180
-185
-190
-195
-200

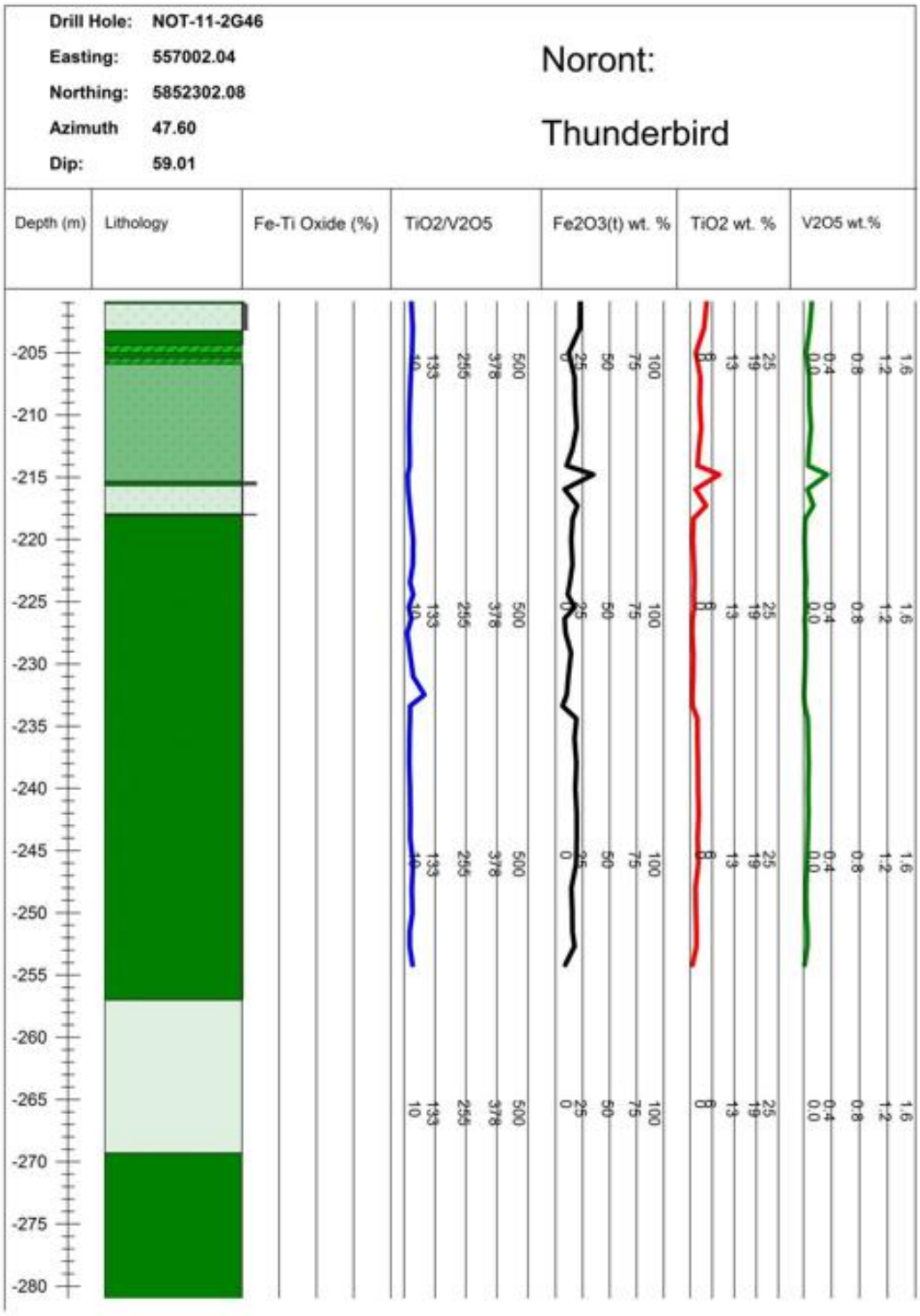
Drill Hole: NOT-11-2G46
Easting: 557002.04
Northing: 5852302.08
Azimuth 47.60
Dip: 59.01
Noront:
Thunderbird
Depth (m)
Lithology
Fe-Ti Oxide (%)
TiO2/V2O5
Fe2O3(t) wt. %
TiO2 wt. %
V2O5 wt.%
-205
-210
-215
-220
-225
-230
-235
-240
-245
-250
-255
-260
-265
-270
-275
-280

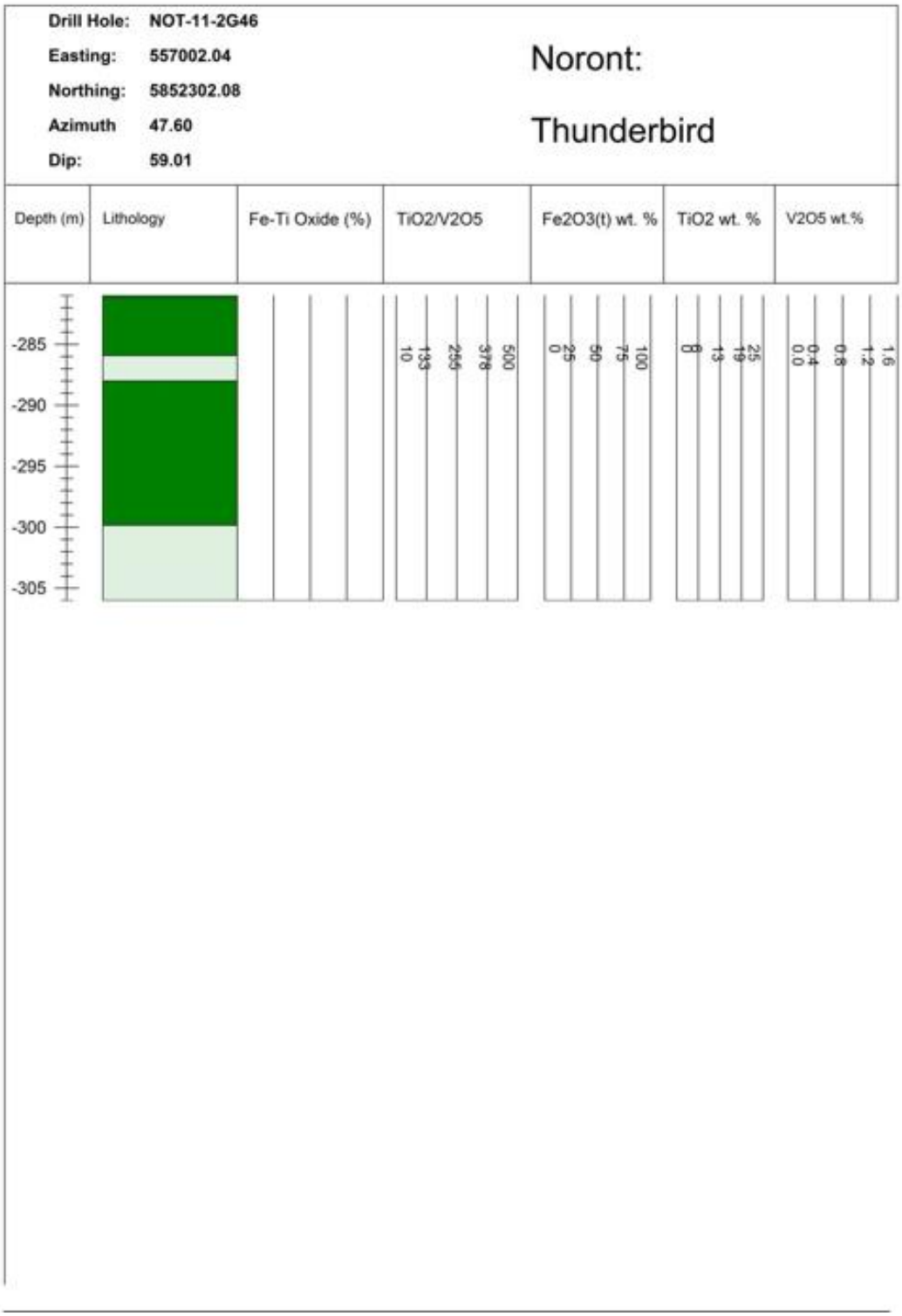
Drill Hole: NOT-11-2G46
Easting: 557002.04
Northing: 5852302.08
Azimuth 47.60
Dip: 59.01
Noront:
Thunderbird
Depth (m)
Lithology
Fe-Ti Oxide (%)
TiO2/V2O5
Fe2O3(t) wt. %
TiO2 wt. %
V2O5 wt.%
-285
-290
-295
-300
-305
10
133
255
378
500
0
25
50
75
100
0
13
19
25
0.0
0.4
0.8
1.2
1.6

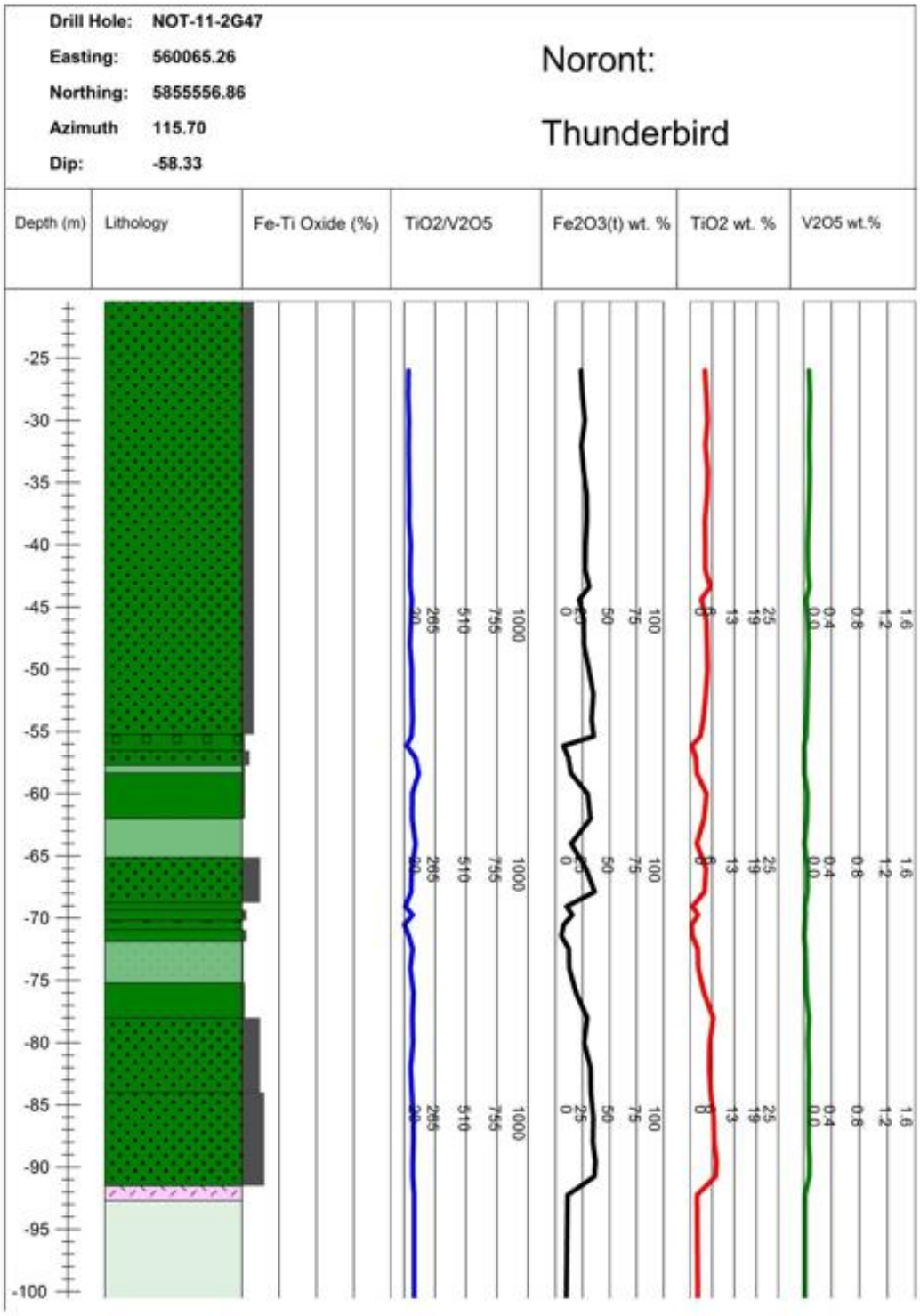
Drill Hole: NOT-11-2G47
Easting: 560065.26
Northing: 5855556.86
Azimuth 115.70
Dip: -58.33
Noront:
Thunderbird
Depth (m)
Lithology
Fe-Ti Oxide (%)
TiO2/V2O5
Fe2O3(t) wt. %
TiO2 wt. %
V2O5 wt.%
-25
-30
-35
-40
-45
-50
-55
-60
-65
-70
-75
-80
-85
-90
-95
-100

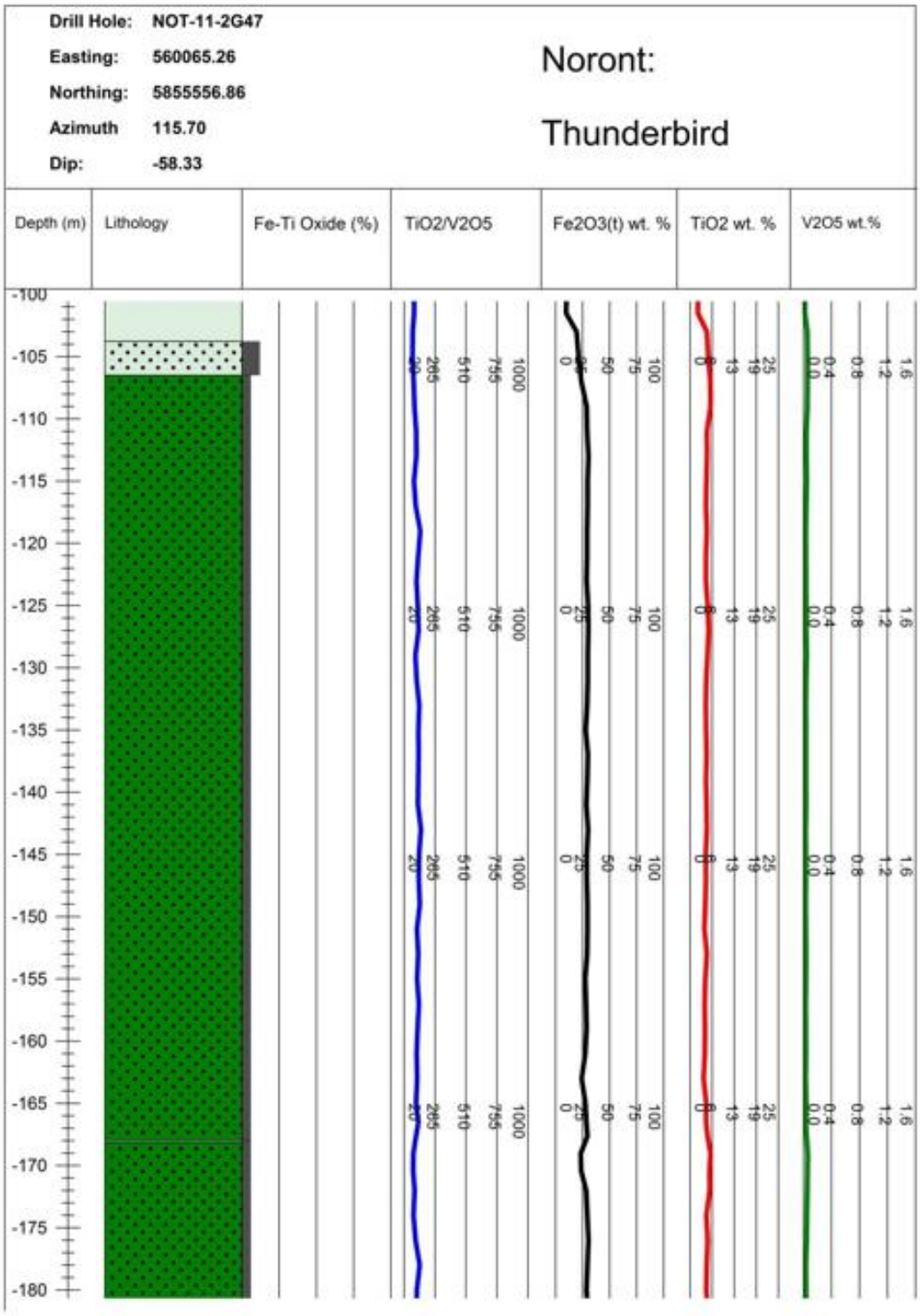
Drill Hole: NOT-11-2G47
Easting: 560065.26
Northing: 5855556.86
Azimuth 115.70
Dip: -58.33
Noront:
Thunderbird
Depth (m)
Lithology
Fe-Ti Oxide (%)
TiO2/V2O5
Fe2O3(t) wt. %
TiO2 wt. %
V2O5 wt.%

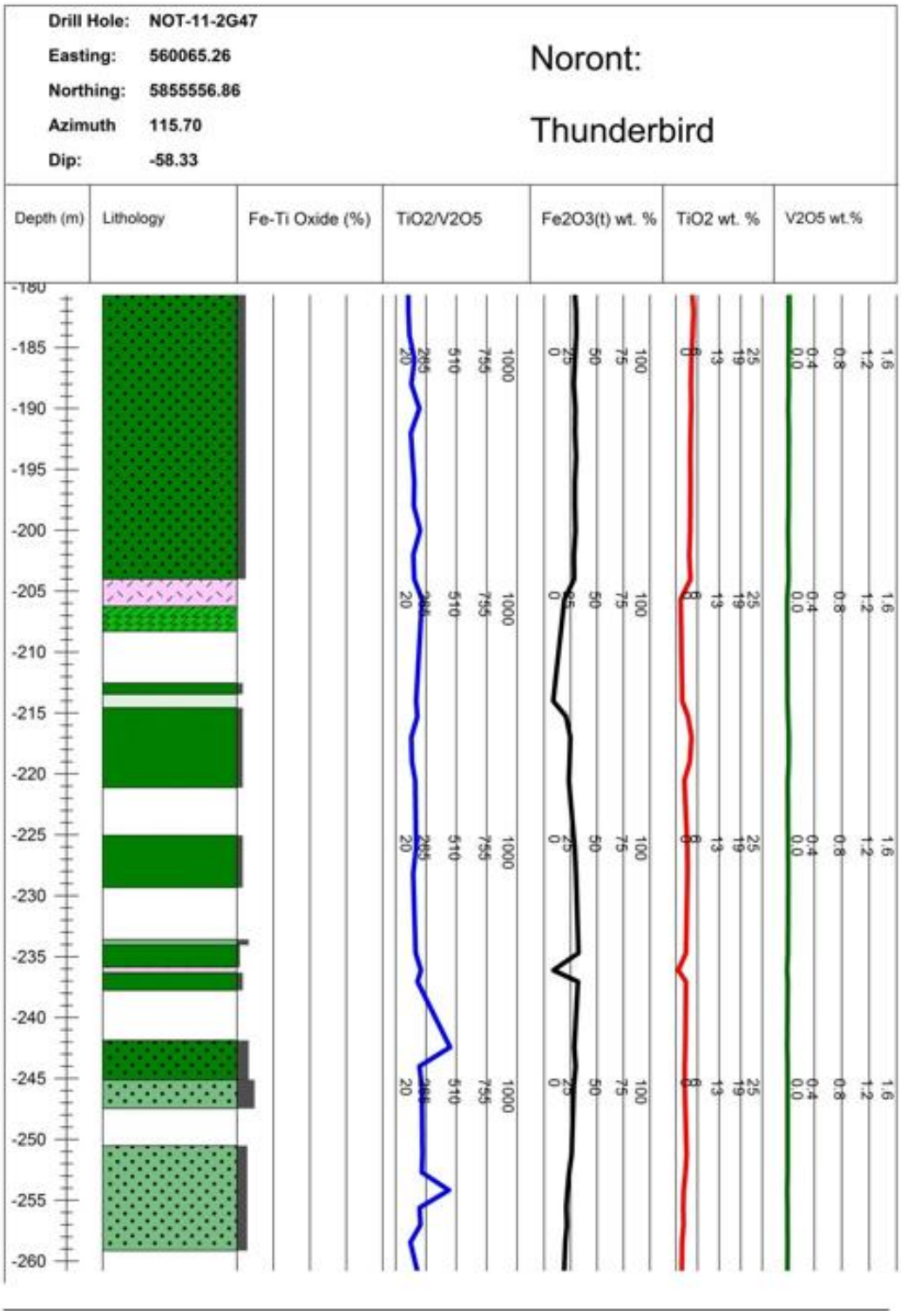
Drill Hole: NOT-11-2G47
Easting: 560065.26
Northing: 5855556.86
Azimuth 115.70
Dip: -58.33
Noront:
Thunderbird
Depth (m)
Lithology
Fe-Ti Oxide (%)
TiO2/V2O5
Fe2O3(t) wt. %
TiO2 wt. %
V2O5 wt.%
-180
-185
-190
-195
-200
-205
-210
-215
-220
-225
-230
-235
-240
-245
-250
-255
-260

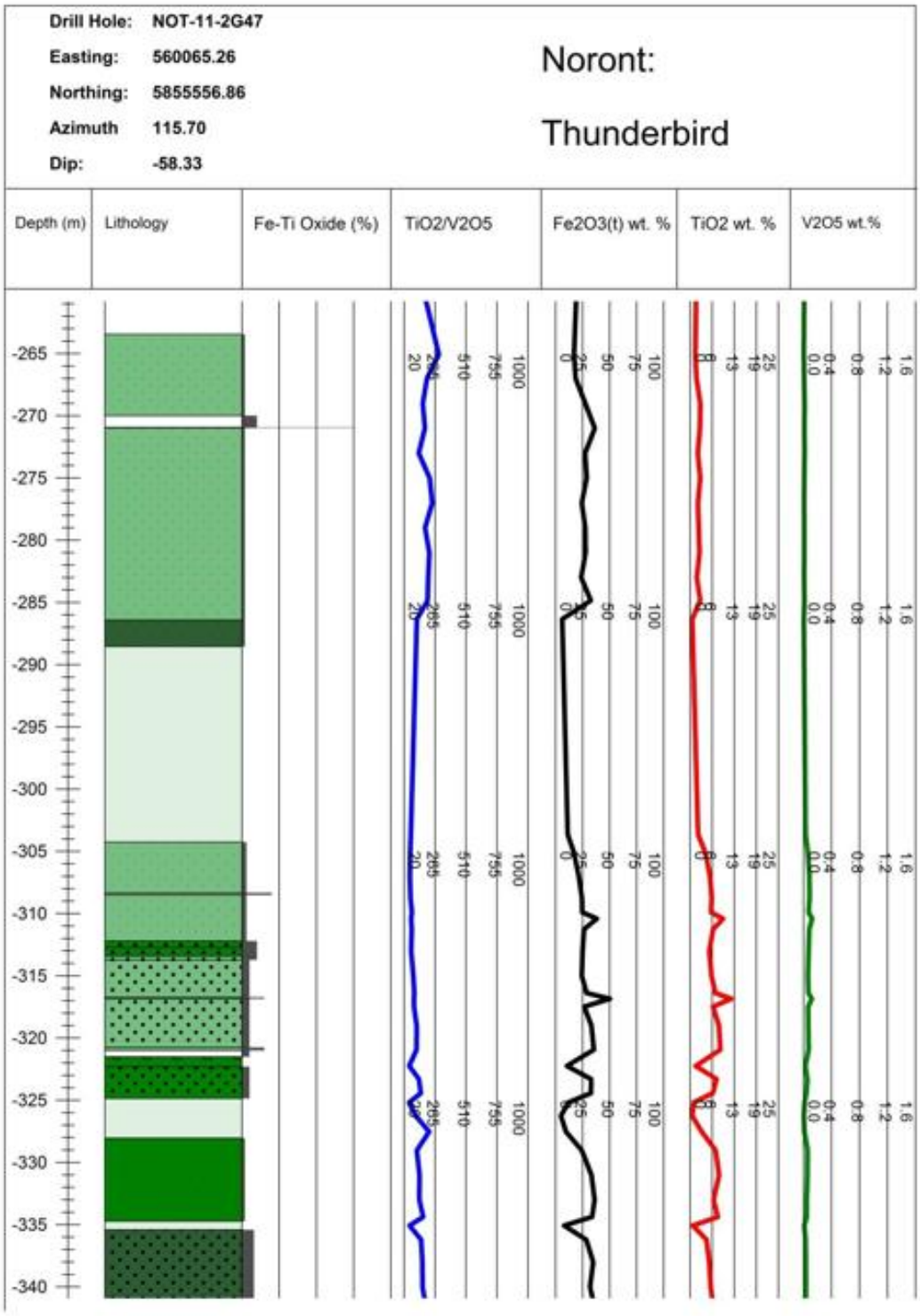
Drill Hole: NOT-11-2G47
Easting: 560065.26
Northing: 5855556.86
Azimuth 115.70
Dip: -58.33
Noront:
Thunderbird
Depth (m)
Lithology
Fe-Ti Oxide (%)
TiO2/V2O5
Fe2O3(t) wt. %
TiO2 wt. %
V2O5 wt.%
-265
-270
-275
-280
-285
-290
-295
-300
-305
-310
-315
-320
-325
-330
-335
-340

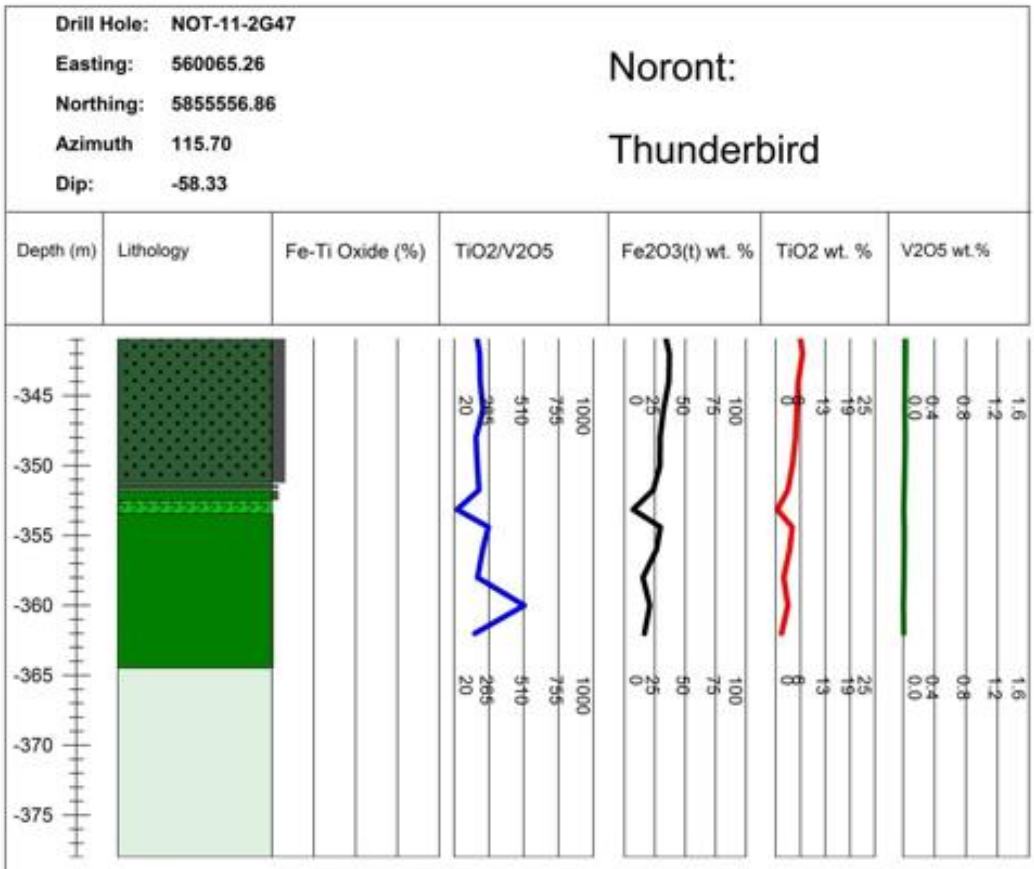
Drill Hole: NOT-11-2G47
Easting: 560065.26
Northing: 5855556.86
Azimuth 115.70
Dip: -58.33
Noront:
Thunderbird
Depth (m)
Lithology
Fe-Ti Oxide (%)
TiO2/V2O5
Fe2O3(t) wt. %
TiO2 wt. %
V2O5 wt.%
-345
-350
-355
-360
-365
-370
-375

Appendix C

Microprobe analysis

Intrusion	Sample	Mineral	Sample Label	SiO2	TiO2	Al2O3	V2O3	Cr2O3	Nb2O3
Butler East	MM-70-2	Plagioclase	MM-70-2a-1	53.826	0.005	29.041	n.d.	n.d.	n.d.
Butler East	MM-70-2	Plagioclase	MM-70-2a-2	54.035	0.071	28.862	n.d.	n.d.	n.d.
Butler East	MM-70-2	Plagioclase	MM-70-2a-3	55.097	0.000	28.239	n.d.	n.d.	n.d.
Butler East	MM-70-2	Plagioclase	MM-70-2a-4	54.156	0.020	28.681	n.d.	n.d.	n.d.
Butler East	MM-70-2	Plagioclase	MM-70-2b-9	51.051	0.012	31.074	n.d.	n.d.	n.d.
Butler East	MM-70-2	Plagioclase	MM-70-2b-10	54.151	0.000	29.054	n.d.	n.d.	n.d.
Butler East	MM-70-2	Plagioclase	MM-70-2b-11	53.948	0.022	28.915	n.d.	n.d.	n.d.
Butler East	MM-70-2	Plagioclase	MM-70-2c-14	54.402	0.000	28.915	n.d.	n.d.	n.d.
Butler East	MM-70-2	Plagioclase	MM-70-2c-15	54.042	0.000	28.713	n.d.	n.d.	n.d.
Butler East	MM-70-2	Plagioclase	MM-70-2c-16	52.663	0.022	30.331	n.d.	n.d.	n.d.
Butler East	MM-70-2	Plagioclase	MM-70-2d-1	54.198	0.000	28.852	n.d.	n.d.	n.d.
Butler East	MM-70-2	Plagioclase	MM-70-2d-2	54.037	0.030	29.225	n.d.	n.d.	n.d.
Butler East	MM-70-2	Plagioclase	MM-70-2d-3	53.337	0.013	29.654	n.d.	n.d.	n.d.
Butler East	MM-70-2	Plagioclase	MM-70-2e-1	53.631	0.000	29.040	n.d.	n.d.	n.d.
Butler East	MM-70-2	Plagioclase	MM-70-2e-2	54.487	0.000	28.729	n.d.	n.d.	n.d.
Butler East	MM-70-2	Plagioclase	MM-70-2e-3	53.567	0.000	29.452	n.d.	n.d.	n.d.
Butler East	MM-70-2	Plagioclase	MM-70-2f-1	47.951	0.000	33.381	n.d.	n.d.	n.d.
Butler East	MM-70-2	Plagioclase	MM-70-2f-2	54.313	0.000	28.993	n.d.	n.d.	n.d.
Butler East	MM-70-2	Plagioclase	MM-70-2f-3	54.001	0.015	29.075	n.d.	n.d.	n.d.
Butler East	MM-70-2	Amphibole	MM-70-2a-1red	42.545	0.617	13.733	n.d.	0.032	n.d.
Butler East	MM-70-2	Amphibole	MM-70-2a-2red	43.044	0.502	13.411	n.d.	0.007	n.d.
Butler East	MM-70-2	Amphibole	MM-70-2a-3red	41.173	0.586	16.196	n.d.	0.003	n.d.
Butler East	MM-71B-2	Plagioclase	MM-71B-2a-1	58.964	0.002	26.099	n.d.	n.d.	n.d.
Butler East	MM-71B-2	Plagioclase	MM-71B-2a-2	57.646	0.000	27.100	n.d.	n.d.	n.d.
Butler East	MM-71B-2	Plagioclase	MM-71B-2a-3	57.907	0.008	26.772	n.d.	n.d.	n.d.
Butler East	MM-71B-2	Plagioclase	MM-71B-2a-4	55.704	0.000	28.159	n.d.	n.d.	n.d.
Butler East	MM-71B-2	Plagioclase	MM-71B-2a-5	55.214	0.001	28.292	n.d.	n.d.	n.d.
Butler East	MM-71B-2	Plagioclase	MM-71B-2c-6	55.723	0.000	28.083	n.d.	n.d.	n.d.
Butler East	MM-71B-2	Plagioclase	MM-71B-2c-7	55.097	0.031	28.393	n.d.	n.d.	n.d.
Butler East	MM-71B-2	Plagioclase	MM-71B-2c-8	55.792	0.000	27.861	n.d.	n.d.	n.d.
Butler East	MM-71B-2	Plagioclase	MM-71B-2d-1	58.512	0.000	26.382	n.d.	n.d.	n.d.
Butler East	MM-71B-2	Plagioclase	MM-71B-2d-2	58.450	0.011	26.234	n.d.	n.d.	n.d.
Butler East	MM-71B-2	Plagioclase	MM-71B-2d-3	58.304	0.013	26.422	n.d.	n.d.	n.d.
Butler East	MM-71B-2	Plagioclase	MM-71B-2e-1	55.320	0.005	28.151	n.d.	n.d.	n.d.
Butler East	MM-71B-2	Plagioclase	MM-71B-2e-2	57.041	0.000	27.326	n.d.	n.d.	n.d.
Butler East	MM-71B-2	Plagioclase	MM-71B-2e-3	61.230	0.000	24.408	n.d.	n.d.	n.d.
Butler East	MM-71B-2	Plagioclase	MM-71B-2f-1	56.415	0.000	27.467	n.d.	n.d.	n.d.
Butler East	MM-71B-2	Plagioclase	MM-71B-2f-2	58.364	0.000	26.287	n.d.	n.d.	n.d.
Butler East	MM-71B-2	Plagioclase	MM-71B-2f-3	59.070	0.000	26.225	n.d.	n.d.	n.d.
Butler East	MM-71B-2	Amphibole	MM-71B-2a-1red	41.387	1.268	11.782	n.d.	0.006	n.d.
Butler East	MM-71B-2	Amphibole	MM-71B-2a-3red	42.180	1.270	11.215	n.d.	0.004	n.d.
Butler East	MM-71B-2	Amphibole	MM-71B-2b-5red	42.200	0.770	10.584	n.d.	0.000	n.d.
Butler East	MM-71B-2	Amphibole	MM-71B-2a-2red	41.533	1.243	11.482	n.d.	0.002	n.d.
Butler East	MM-71B-2	Amphibole	MM-71B-2b-7red	42.385	0.964	10.917	n.d.	0.000	n.d.
Butler East	MM-71B-2	Amphibole	MM-71B-2b-9red	42.189	0.621	10.875	n.d.	0.004	n.d.
Butler East	MM-71B-2	Amphibole	MM-71B-2a-4red	41.518	1.295	11.859	n.d.	0.022	n.d.
Butler East	MM-71B-2	Amphibole	MM-71B-2c-12red	42.027	0.982	11.002	n.d.	0.000	n.d.
Butler East	MM-71B-2	Amphibole	MM-71B-2c-15red	40.989	1.353	11.844	n.d.	0.001	n.d.
Butler East	MM-V4-1	Pyroxene	MM-V4-1a-1green	56.357	0.052	1.940	n.d.	0.016	n.d.
Butler East	MM-V4-1	Pyroxene	MM-V4-1a-2green	55.803	0.039	2.023	n.d.	0.010	n.d.
Butler East	MM-V4-1	Pyroxene	MM-V4-1a-3green	56.398	0.052	1.890	n.d.	0.018	n.d.
Butler East	MM-V4-1	Pyroxene	MM-V4-1a-6green	56.068	0.064	1.939	n.d.	0.016	n.d.
Butler East	MM-V4-1	Pyroxene	MM-V4-1b-7green	55.817	0.053	2.229	n.d.	0.008	n.d.
Butler East	MM-V4-1	Pyroxene	MM-V4-1b-8green	55.653	0.076	2.179	n.d.	0.000	n.d.
Butler East	MM-V4-1	Pyroxene	MM-V4-1b-10green	55.888	0.105	2.230	n.d.	0.000	n.d.
Butler East	MM-V4-1	Pyroxene	MM-V4-1c-11green	55.359	0.063	1.995	n.d.	0.008	n.d.
Butler East	MM-V4-1	Pyroxene	MM-V4-1c-12green	56.766	0.037	1.413	n.d.	0.001	n.d.
Butler East	MM-V4-1	Pyroxene	MM-V4-1c-13green	55.254	0.045	1.739	n.d.	0.001	n.d.

MgO	MnO	FeO^t	CoO	NiO	CuO	ZnO	Fe2O3	FeO	CaO	SrO	BaO	Na2O	K2O	TOTAL
0.000	0.003	0.021	n.d.	n.d.	n.d.	n.d.	n.d.	n.d.	11.660	0.000	0.000	5.147	0.041	94.556
0.000	0.015	0.147	n.d.	n.d.	n.d.	n.d.	n.d.	n.d.	11.405	0.000	0.000	5.252	0.047	94.535
0.000	0.000	0.044	n.d.	n.d.	n.d.	n.d.	n.d.	n.d.	10.798	0.091	0.000	5.594	0.031	94.269
0.000	0.002	0.083	n.d.	n.d.	n.d.	n.d.	n.d.	n.d.	11.215	0.076	0.018	5.389	0.032	94.233
0.000	0.000	0.088	n.d.	n.d.	n.d.	n.d.	n.d.	n.d.	14.033	0.038	0.000	3.765	0.010	96.296
0.000	0.000	0.044	n.d.	n.d.	n.d.	n.d.	n.d.	n.d.	11.525	0.107	0.022	5.206	0.021	94.881
0.000	0.009	0.126	n.d.	n.d.	n.d.	n.d.	n.d.	n.d.	11.569	0.122	0.000	5.189	0.044	94.711
0.007	0.000	0.067	n.d.	n.d.	n.d.	n.d.	n.d.	n.d.	11.296	0.015	0.000	5.380	0.050	94.702
0.000	0.003	0.027	n.d.	n.d.	n.d.	n.d.	n.d.	n.d.	11.564	0.000	0.000	5.257	0.029	94.349
0.000	0.003	0.101	n.d.	n.d.	n.d.	n.d.	n.d.	n.d.	12.698	0.015	0.017	4.543	0.040	95.833
0.000	0.000	0.091	n.d.	n.d.	n.d.	n.d.	n.d.	n.d.	11.219	0.000	0.000	5.335	0.039	94.360
0.027	0.010	0.209	n.d.	n.d.	n.d.	n.d.	n.d.	n.d.	11.667	0.031	0.000	5.062	0.032	95.236
0.000	0.000	0.187	n.d.	n.d.	n.d.	n.d.	n.d.	n.d.	12.266	0.000	0.000	4.754	0.036	95.457
0.000	0.003	0.039	n.d.	n.d.	n.d.	n.d.	n.d.	n.d.	11.851	0.061	0.000	5.045	0.034	94.625
0.013	0.000	0.105	n.d.	n.d.	n.d.	n.d.	n.d.	n.d.	11.274	0.061	0.000	5.279	0.056	94.669
0.000	0.006	0.144	n.d.	n.d.	n.d.	n.d.	n.d.	n.d.	12.314	0.091	0.009	4.860	0.033	95.574
0.000	0.011	0.049	n.d.	n.d.	n.d.	n.d.	n.d.	n.d.	16.562	0.000	0.000	2.109	0.002	97.954
0.013	0.008	0.072	n.d.	n.d.	n.d.	n.d.	n.d.	n.d.	11.655	0.008	0.003	5.095	0.030	95.062
0.011	0.000	0.070	n.d.	n.d.	n.d.	n.d.	n.d.	n.d.	11.682	0.015	0.045	5.042	0.046	94.869
7.894	0.343	22.102	n.d.	n.d.	n.d.	n.d.	n.d.	n.d.	8.969	n.d.	n.d.	1.456	0.360	98.051
7.734	0.377	23.439	n.d.	n.d.	n.d.	n.d.	n.d.	n.d.	8.524	n.d.	n.d.	1.336	0.318	98.692
5.795	0.272	22.786	n.d.	n.d.	n.d.	n.d.	n.d.	n.d.	10.120	n.d.	n.d.	1.743	0.376	99.050
0.000	0.003	0.033	n.d.	n.d.	n.d.	n.d.	n.d.	n.d.	7.841	0.121	0.000	7.341	0.048	93.063
0.004	0.002	0.047	n.d.	n.d.	n.d.	n.d.	n.d.	n.d.	9.077	0.152	0.000	6.553	0.033	94.028
0.000	0.000	0.025	n.d.	n.d.	n.d.	n.d.	n.d.	n.d.	8.852	0.174	0.004	6.856	0.040	93.738
0.000	0.000	0.049	n.d.	n.d.	n.d.	n.d.	n.d.	n.d.	10.421	0.038	0.000	5.816	0.033	94.371
0.000	0.006	0.074	n.d.	n.d.	n.d.	n.d.	n.d.	n.d.	10.576	0.076	0.000	5.769	0.045	94.239
0.002	0.004	0.047	n.d.	n.d.	n.d.	n.d.	n.d.	n.d.	10.363	0.137	0.000	5.841	0.045	94.359
0.000	0.008	0.124	n.d.	n.d.	n.d.	n.d.	n.d.	n.d.	10.671	0.038	0.000	5.665	0.035	94.362
0.000	0.000	0.064	n.d.	n.d.	n.d.	n.d.	n.d.	n.d.	10.123	0.069	0.000	5.954	0.028	93.909
0.000	0.000	0.020	n.d.	n.d.	n.d.	n.d.	n.d.	n.d.	7.956	0.099	0.000	7.267	0.048	92.969
0.000	0.000	0.022	n.d.	n.d.	n.d.	n.d.	n.d.	n.d.	8.211	0.136	0.006	7.203	0.060	93.064
0.025	0.012	0.093	n.d.	n.d.	n.d.	n.d.	n.d.	n.d.	8.320	0.106	0.000	7.064	0.042	93.295
0.000	0.001	0.048	n.d.	n.d.	n.d.	n.d.	n.d.	n.d.	10.457	0.183	0.000	5.740	0.048	94.165
0.000	0.006	0.041	n.d.	n.d.	n.d.	n.d.	n.d.	n.d.	9.238	0.061	0.000	6.496	0.037	93.713
0.000	0.008	0.073	n.d.	n.d.	n.d.	n.d.	n.d.	n.d.	6.038	0.105	0.006	8.364	0.041	91.862
0.000	0.000	0.004	n.d.	n.d.	n.d.	n.d.	n.d.	n.d.	9.757	0.152	0.000	6.165	0.026	93.795
0.000	0.000	0.055	n.d.	n.d.	n.d.	n.d.	n.d.	n.d.	8.102	0.098	0.008	7.052	0.045	92.906
0.003	0.006	0.176	n.d.	n.d.	n.d.	n.d.	n.d.	n.d.	7.838	0.136	0.000	7.287	0.065	93.454
5.580	0.282	24.448	n.d.	n.d.	n.d.	n.d.	n.d.	n.d.	11.004	n.d.	n.d.	1.345	0.832	97.934
5.873	0.282	24.455	n.d.	n.d.	n.d.	n.d.	n.d.	n.d.	10.928	n.d.	n.d.	1.292	0.769	98.268
5.942	0.295	24.785	n.d.	n.d.	n.d.	n.d.	n.d.	n.d.	10.829	n.d.	n.d.	1.312	0.760	97.477
5.635	0.292	24.445	n.d.	n.d.	n.d.	n.d.	n.d.	n.d.	10.984	n.d.	n.d.	1.388	0.846	97.850
5.880	0.300	24.940	n.d.	n.d.	n.d.	n.d.	n.d.	n.d.	10.981	n.d.	n.d.	1.304	0.756	98.427
5.935	0.308	25.065	n.d.	n.d.	n.d.	n.d.	n.d.	n.d.	10.914	n.d.	n.d.	1.367	0.774	98.052
5.557	0.277	24.489	n.d.	n.d.	n.d.	n.d.	n.d.	n.d.	11.038	n.d.	n.d.	1.379	0.848	98.282
5.588	0.323	24.619	n.d.	n.d.	n.d.	n.d.	n.d.	n.d.	11.098	n.d.	n.d.	1.383	0.859	97.881
5.315	0.286	24.718	n.d.	n.d.	n.d.	n.d.	n.d.	n.d.	10.963	n.d.	n.d.	1.369	0.963	97.801
24.630	0.392	14.182	n.d.	n.d.	n.d.	n.d.	n.d.	n.d.	0.471	n.d.	n.d.	0.198	0.016	98.254
24.442	0.355	14.002	n.d.	n.d.	n.d.	n.d.	n.d.	n.d.	0.507	n.d.	n.d.	0.235	0.007	97.423
24.392	0.362	14.579	n.d.	n.d.	n.d.	n.d.	n.d.	n.d.	0.466	n.d.	n.d.	0.199	0.010	98.366
24.317	0.373	14.503	n.d.	n.d.	n.d.	n.d.	n.d.	n.d.	0.507	n.d.	n.d.	0.195	0.006	97.988
23.943	0.362	14.224	n.d.	n.d.	n.d.	n.d.	n.d.	n.d.	0.517	n.d.	n.d.	0.274	0.001	97.428
24.511	0.391	14.195	n.d.	n.d.	n.d.	n.d.	n.d.	n.d.	0.488	n.d.	n.d.	0.271	0.006	97.770
23.667	0.343	14.409	n.d.	n.d.	n.d.	n.d.	n.d.	n.d.	0.535	n.d.	n.d.	0.457	0.044	97.678
23.185	0.396	15.876	n.d.	n.d.	n.d.	n.d.	n.d.	n.d.	0.456	n.d.	n.d.	0.206	0.002	97.546
24.793	0.344	14.310	n.d.	n.d.	n.d.	n.d.	n.d.	n.d.	0.461	n.d.	n.d.	0.153	0.000	98.278
23.861	0.375	15.994	n.d.	n.d.	n.d.	n.d.	n.d.	n.d.	0.380	n.d.	n.d.	0.189	0.000	97.838

Intrusion	Sample	Mineral	Sample Label	SiO2	TiO2	Al2O3	V2O3	Cr2O3	Nb2O3
Butler East	MM-V4-1	Pyroxene	MM-V4-1c-14green	56.095	0.028	2.067	n.d.	0.005	n.d.
Butler East	MM-V4-7	Plagioclase	MM-V4-7a-1	54.986	0.042	28.579	n.d.	n.d.	n.d.
Butler East	MM-V4-7	Plagioclase	MM-V4-7a-2	55.099	0.000	28.378	n.d.	n.d.	n.d.
Butler East	MM-V4-7	Plagioclase	MM-V4-7a-3	55.419	0.000	28.372	n.d.	n.d.	n.d.
Butler East	MM-V4-7	Plagioclase	MM-V4-7b-4	55.349	0.000	28.592	n.d.	n.d.	n.d.
Butler East	MM-V4-7	Plagioclase	MM-V4-7b-5	55.204	0.002	28.342	n.d.	n.d.	n.d.
Butler East	MM-V4-7	Plagioclase	MM-V4-7b-6	55.237	0.000	28.522	n.d.	n.d.	n.d.
Butler East	MM-V4-7	Plagioclase	MM-V4-7b-7	55.495	0.004	28.312	n.d.	n.d.	n.d.
Butler East	MM-V4-7	Plagioclase	MM-V4-7c-9	55.011	0.009	28.668	n.d.	n.d.	n.d.
Butler East	MM-V4-7	Plagioclase	MM-V4-7c-10	54.927	0.001	28.743	n.d.	n.d.	n.d.
Butler East	MM-V4-7	Plagioclase	MM-V4-7c-11	55.277	0.000	28.554	n.d.	n.d.	n.d.
Butler East	MM-V4-7	Plagioclase	MM-V4-7d-1	55.266	0.000	28.589	n.d.	n.d.	n.d.
Butler East	MM-V4-7	Plagioclase	MM-V4-7d-2	54.973	0.025	28.630	n.d.	n.d.	n.d.
Butler East	MM-V4-7	Plagioclase	MM-V4-7d-3	54.806	0.000	28.917	n.d.	n.d.	n.d.
Butler East	MM-V4-7	Plagioclase	MM-V4-7e-1	55.247	0.000	28.389	n.d.	n.d.	n.d.
Butler East	MM-V4-7	Plagioclase	MM-V4-7e-2	55.085	0.005	28.388	n.d.	n.d.	n.d.
Butler East	MM-V4-7	Plagioclase	MM-V4-7e-3	55.206	0.033	28.567	n.d.	n.d.	n.d.
Butler East	MM-V4-7	Plagioclase	MM-V4-7f-1	55.067	0.018	28.603	n.d.	n.d.	n.d.
Butler East	MM-V4-7	Plagioclase	MM-V4-7f-2	55.393	0.000	28.403	n.d.	n.d.	n.d.
Butler East	MM-V4-7	Plagioclase	MM-V4-7f-3	54.650	0.045	28.883	n.d.	n.d.	n.d.
Butler East	MM-V4-7	Pyroxene	MM-V4-7a-1green	42.438	0.943	13.160	n.d.	0.000	n.d.
Butler East	MM-V4-7	Pyroxene	MM-V4-7a-2green	42.505	0.883	13.156	n.d.	0.000	n.d.
Butler East	MM-V4-7	Pyroxene	MM-V4-7a-3green	42.604	0.841	13.174	n.d.	0.000	n.d.
Butler East	MM-V4-7	Amphibole	MM-V4-7a-1red	41.930	0.691	14.046	n.d.	0.006	n.d.
Butler East	MM-V4-7	Amphibole	MM-V4-7a-2red	42.504	0.892	13.132	n.d.	0.000	n.d.
Butler East	MM-V4-7	Amphibole	MM-V4-7a-3red	42.340	1.030	12.817	n.d.	0.000	n.d.
Butler East	MM-V4-7	Amphibole	MM-V4-7b-4red	41.944	0.955	13.391	n.d.	0.018	n.d.
Butler East	MM-V4-7	Amphibole	MM-V4-7b-5red?	42.637	0.734	13.098	n.d.	0.000	n.d.
Butler East	MM-V4-7	Amphibole	MM-V4-7b-6red	42.277	0.817	13.368	n.d.	0.012	n.d.
Butler East	MM-V4-7	Amphibole	MM-V4-7c-7red	41.786	0.622	14.023	n.d.	0.000	n.d.
Butler East	MM-V4-7	Amphibole	MM-V4-7c-8red	41.539	0.634	14.170	n.d.	0.004	n.d.
Butler East	MM-V5-1	Magnetite	MMV5-1-mag1a	0.010	0.210	0.089	1.791	0.174	n.d.
Butler East	MM-V5-1	Magnetite	MMV5-1-mag1b	0.019	0.145	0.043	1.682	0.171	n.d.
Butler East	MM-V5-1	Magnetite	MMV5-1-mag1c	0.014	0.478	0.056	1.675	0.177	n.d.
Butler East	MM-V5-1	Magnetite	MMV5-1-mag2a	0.033	0.018	0.070	1.773	0.166	n.d.
Butler East	MM-V5-1	Magnetite	MMV5-1-mag2b	0.007	0.325	0.051	1.721	0.170	n.d.
Butler East	MM-V5-1	Magnetite	MMV5-1-mag2c	0.004	0.087	0.051	1.640	0.164	n.d.
Butler East	MM-V5-1	Magnetite	MMV5-1-mag3a	0.019	0.061	0.112	1.783	0.172	n.d.
Butler East	MM-V5-1	Magnetite	MMV5-1-mag3b	0.032	0.022	0.073	1.783	0.167	n.d.
Butler East	MM-V5-1	Magnetite	MMV5-1-mag3c	0.040	0.043	0.066	1.667	0.147	n.d.
Butler East	MM-V5-1	Magnetite	MMV5-1-mag5a	0.024	0.014	0.063	1.748	0.173	n.d.
Butler East	MM-V5-1	Magnetite	MMV5-1-mag5b	0.018	0.241	0.060	1.657	0.165	n.d.
Butler East	MM-V5-1	Magnetite	MMV5-1-mag6a	0.015	0.488	0.083	1.692	0.157	n.d.
Butler East	MM-V5-1	Magnetite	MMV5-1-mag6b	0.014	0.287	0.055	1.684	0.169	n.d.
Butler East	MM-V5-1	Magnetite	MMV5-1-mag7a	0.015	0.260	0.116	1.703	0.170	n.d.
Butler East	MM-V5-1	Magnetite	MMV5-1-mag7b	0.016	0.304	0.057	1.675	0.164	n.d.
Butler East	MM-V5-1	Magnetite	MMV5-1-mag8a	0.015	0.475	0.070	1.674	0.156	n.d.
Butler East	MM-V5-1	Magnetite	MMV5-1-mag8b	0.018	0.351	0.081	1.705	0.154	n.d.
Butler East	MM-V5-1	Magnetite	MMV5-1-mag8c	0.018	0.057	0.053	1.645	0.157	n.d.
Butler East	MM-V5-1	Magnetite	MMV5-1-mag9a	0.015	0.143	0.059	1.614	0.160	n.d.
Butler East	MM-V5-1	Magnetite	MMV5-1-mag9b	0.009	0.666	0.045	1.545	0.152	n.d.
Butler East	MM-V5-1	Magnetite	MMV5-1-mag9c	0.028	0.073	0.041	1.553	0.161	n.d.
Butler East	MM-V5-1	Ilmenite	MMV5-1-ilm1a	0.007	51.436	0.019	0.360	0.031	0.000
Butler East	MM-V5-1	Ilmenite	MMV5-1-ilm2a	0.001	50.952	0.016	0.324	0.033	0.000
Butler East	MM-V5-1	Ilmenite	MMV5-1-ilm2b	0.002	50.959	0.008	0.245	0.015	0.000
Butler East	MM-V5-1	Ilmenite	MMV5-1-ilm2c	0.004	51.027	0.014	0.336	0.030	0.000
Butler East	MM-V5-1	Ilmenite	MMV5-1-ilm3a	0.006	51.148	0.012	0.348	0.031	0.000
Butler East	MM-V5-1	Ilmenite	MMV5-1-ilm3b	0.003	51.088	0.015	0.292	0.021	0.000

MgO	MnO	FeO^t	CoO	NiO	CuO	ZnO	Fe2O3	FeO	CaO	SrO	BaO	Na2O	K2O	TOTAL
24.575	0.376	14.134	n.d.	n.d.	n.d.	n.d.	n.d.	n.d.	0.483	n.d.	n.d.	0.238	0.004	98.005
0.008	0.005	0.101	n.d.	n.d.	n.d.	n.d.	n.d.	n.d.	10.854	0.000	0.016	5.531	0.032	94.575
0.000	0.024	0.069	n.d.	n.d.	n.d.	n.d.	n.d.	n.d.	10.910	0.000	0.003	5.548	0.039	94.480
0.000	0.000	0.082	n.d.	n.d.	n.d.	n.d.	n.d.	n.d.	10.645	0.000	0.000	5.691	0.037	94.518
0.000	0.009	0.043	n.d.	n.d.	n.d.	n.d.	n.d.	n.d.	10.696	0.000	0.000	5.614	0.061	94.689
0.008	0.002	0.025	n.d.	n.d.	n.d.	n.d.	n.d.	n.d.	10.805	0.030	0.000	5.541	0.047	94.418
0.000	0.010	0.051	n.d.	n.d.	n.d.	n.d.	n.d.	n.d.	10.895	0.023	0.000	5.546	0.061	94.738
0.000	0.012	0.028	n.d.	n.d.	n.d.	n.d.	n.d.	n.d.	10.637	0.061	0.000	5.668	0.044	94.549
0.007	0.000	0.046	n.d.	n.d.	n.d.	n.d.	n.d.	n.d.	11.036	0.038	0.019	5.372	0.058	94.815
0.000	0.000	0.016	n.d.	n.d.	n.d.	n.d.	n.d.	n.d.	11.146	0.061	0.000	5.350	0.035	94.894
0.004	0.024	0.034	n.d.	n.d.	n.d.	n.d.	n.d.	n.d.	10.880	0.091	0.000	5.534	0.031	94.864
0.000	0.000	0.021	n.d.	n.d.	n.d.	n.d.	n.d.	n.d.	10.816	0.084	0.000	5.564	0.045	94.776
0.000	0.000	0.033	n.d.	n.d.	n.d.	n.d.	n.d.	n.d.	11.045	0.091	0.018	5.456	0.032	94.797
0.000	0.000	0.098	n.d.	n.d.	n.d.	n.d.	n.d.	n.d.	11.283	0.084	0.000	5.332	0.048	95.188
0.000	0.000	0.043	n.d.	n.d.	n.d.	n.d.	n.d.	n.d.	10.825	0.053	0.002	5.598	0.027	94.557
0.000	0.007	0.053	n.d.	n.d.	n.d.	n.d.	n.d.	n.d.	10.773	0.114	0.000	5.551	0.047	94.425
0.001	0.000	0.086	n.d.	n.d.	n.d.	n.d.	n.d.	n.d.	10.950	0.000	0.000	5.455	0.031	94.843
0.000	0.000	0.040	n.d.	n.d.	n.d.	n.d.	n.d.	n.d.	10.945	0.008	0.000	5.447	0.032	94.681
0.000	0.007	0.044	n.d.	n.d.	n.d.	n.d.	n.d.	n.d.	10.747	0.015	0.017	5.620	0.051	94.609
0.010	0.006	0.151	n.d.	n.d.	n.d.	n.d.	n.d.	n.d.	11.184	0.000	0.004	5.386	0.040	94.929
7.262	0.296	20.916	n.d.	n.d.	n.d.	n.d.	n.d.	n.d.	10.683	n.d.	n.d.	1.644	0.561	97.903
7.636	0.345	20.816	n.d.	n.d.	n.d.	n.d.	n.d.	n.d.	10.318	n.d.	n.d.	1.555	0.519	97.733
7.953	0.288	20.395	n.d.	n.d.	n.d.	n.d.	n.d.	n.d.	10.672	n.d.	n.d.	1.590	0.524	98.041
6.653	0.217	21.670	n.d.	n.d.	n.d.	n.d.	n.d.	n.d.	11.060	n.d.	n.d.	1.478	0.564	98.315
6.986	0.320	21.436	n.d.	n.d.	n.d.	n.d.	n.d.	n.d.	10.410	n.d.	n.d.	1.687	0.533	97.900
6.798	0.285	21.709	n.d.	n.d.	n.d.	n.d.	n.d.	n.d.	10.684	n.d.	n.d.	1.573	0.495	97.731
7.078	0.302	21.452	n.d.	n.d.	n.d.	n.d.	n.d.	n.d.	10.585	n.d.	n.d.	1.736	0.520	97.981
7.694	0.322	21.003	n.d.	n.d.	n.d.	n.d.	n.d.	n.d.	9.919	n.d.	n.d.	1.628	0.514	97.549
7.355	0.290	20.759	n.d.	n.d.	n.d.	n.d.	n.d.	n.d.	10.752	n.d.	n.d.	1.759	0.541	97.930
6.679	0.335	21.721	n.d.	n.d.	n.d.	n.d.	n.d.	n.d.	10.569	n.d.	n.d.	1.787	0.507	98.029
7.424	0.268	20.207	n.d.	n.d.	n.d.	n.d.	n.d.	n.d.	11.000	n.d.	n.d.	1.706	0.578	97.530
0.000	0.005	91.062	0.000	0.005	0.000	0.012	66.442	31.277	n.d.	n.d.	n.d.	n.d.	n.d.	100.015
0.000	0.002	90.742	0.002	0.005	0.000	0.008	66.336	31.053	n.d.	n.d.	n.d.	n.d.	n.d.	99.465
0.000	0.014	90.790	0.006	0.011	0.000	0.012	65.949	31.449	n.d.	n.d.	n.d.	n.d.	n.d.	99.841
0.000	0.011	91.201	0.003	0.007	0.000	0.011	66.786	31.106	n.d.	n.d.	n.d.	n.d.	n.d.	99.984
0.000	0.005	91.532	0.014	0.000	0.000	0.000	66.687	31.527	n.d.	n.d.	n.d.	n.d.	n.d.	100.506
0.000	0.007	91.069	0.001	0.005	0.000	0.003	66.695	31.056	n.d.	n.d.	n.d.	n.d.	n.d.	99.713
0.005	0.004	91.359	0.002	0.000	0.000	0.006	66.836	31.220	n.d.	n.d.	n.d.	n.d.	n.d.	100.219
0.006	0.000	91.020	0.020	0.003	0.000	0.013	66.654	31.045	n.d.	n.d.	n.d.	n.d.	n.d.	99.817
0.000	0.000	91.006	0.001	0.002	0.000	0.001	66.623	31.058	n.d.	n.d.	n.d.	n.d.	n.d.	99.648
0.000	0.004	91.532	0.012	0.003	0.000	0.001	67.055	31.196	n.d.	n.d.	n.d.	n.d.	n.d.	100.292
0.000	0.009	91.383	0.008	0.002	0.001	0.014	66.699	31.367	n.d.	n.d.	n.d.	n.d.	n.d.	100.241
0.000	0.004	91.190	0.011	0.008	0.000	0.019	66.215	31.609	n.d.	n.d.	n.d.	n.d.	n.d.	100.301
0.000	0.005	90.975	0.017	0.007	0.000	0.000	66.331	31.290	n.d.	n.d.	n.d.	n.d.	n.d.	99.859
0.000	0.008	91.070	0.001	0.007	0.000	0.010	66.394	31.328	n.d.	n.d.	n.d.	n.d.	n.d.	100.012
0.000	0.007	91.549	0.000	0.006	0.000	0.010	66.729	31.506	n.d.	n.d.	n.d.	n.d.	n.d.	100.474
0.003	0.007	90.927	0.003	0.007	0.000	0.003	66.041	31.503	n.d.	n.d.	n.d.	n.d.	n.d.	99.957
0.005	0.009	91.498	0.001	0.009	0.000	0.008	66.615	31.557	n.d.	n.d.	n.d.	n.d.	n.d.	100.513
0.000	0.000	90.863	0.005	0.007	0.000	0.004	66.557	30.975	n.d.	n.d.	n.d.	n.d.	n.d.	99.477
0.001	0.003	90.947	0.016	0.000	0.000	0.006	66.524	31.088	n.d.	n.d.	n.d.	n.d.	n.d.	99.629
0.000	0.010	90.547	0.011	0.005	0.000	0.013	65.585	31.534	n.d.	n.d.	n.d.	n.d.	n.d.	99.574
0.000	0.008	90.580	0.006	0.009	0.000	0.004	66.354	30.874	n.d.	n.d.	n.d.	n.d.	n.d.	99.111
0.012	1.527	46.743	0.006	0.005	0.000	0.023	2.300	44.673	n.d.	n.d.	n.d.	n.d.	n.d.	100.399
0.017	1.530	46.974	0.012	0.003	0.004	0.023	3.070	44.211	n.d.	n.d.	n.d.	n.d.	n.d.	100.197
0.004	1.556	46.975	0.000	0.001	0.000	0.025	3.050	44.231	n.d.	n.d.	n.d.	n.d.	n.d.	100.096
0.030	1.479	46.771	0.000	0.004	0.000	0.017	2.712	44.330	n.d.	n.d.	n.d.	n.d.	n.d.	99.984
0.007	1.533	46.531	0.008	0.000	0.004	0.026	2.354	44.413	n.d.	n.d.	n.d.	n.d.	n.d.	99.890
0.012	1.547	46.324	0.000	0.003	0.000	0.015	2.194	44.350	n.d.	n.d.	n.d.	n.d.	n.d.	99.540

Intrusion	Sample	Mineral	Sample Label	SiO2	TiO2	Al2O3	V2O3	Cr2O3	Nb2O3
Butler East	MM-V5-1	Ilmenite	MMV5-1-ilm4a	0.003	50.865	0.008	0.329	0.026	0.000
Butler East	MM-V5-1	Ilmenite	MMV5-1-ilm4b	0.001	51.051	0.009	0.308	0.019	0.000
Butler East	MM-V5-1	Ilmenite	MMV5-1-ilm5a	0.006	50.797	0.012	0.355	0.026	0.000
Butler East	MM-V5-1	Ilmenite	MMV5-1-ilm5b	0.011	51.080	0.008	0.316	0.020	0.000
Butler East	MM-V5-1	Ilmenite	MMV5-1-ilm6a	0.003	51.378	0.004	0.313	0.030	0.000
Butler East	MM-V5-1	Ilmenite	MMV5-1-ilm7a	0.008	50.924	0.010	0.363	0.037	0.000
Butler East	MM-V5-2	Magnetite	MMV5-2-mag1a	0.021	0.215	0.062	1.531	0.142	n.d.
Butler East	MM-V5-2	Magnetite	MMV5-2-mag1b	0.014	0.398	0.044	1.456	0.146	n.d.
Butler East	MM-V5-2	Magnetite	MMV5-2-mag1c	0.024	0.052	0.039	1.393	0.127	n.d.
Butler East	MM-V5-2	Magnetite	MMV5-2-mag2a	0.017	0.192	0.090	1.629	0.147	n.d.
Butler East	MM-V5-2	Magnetite	MMV5-2-mag2b	0.017	0.111	0.061	1.614	0.149	n.d.
Butler East	MM-V5-2	Magnetite	MMV5-2-mag2c	0.021	0.055	0.044	1.468	0.145	n.d.
Butler East	MM-V5-2	Magnetite	MMV5-2-mag4a	0.025	0.056	0.103	1.557	0.147	n.d.
Butler East	MM-V5-2	Magnetite	MMV5-2-mag4c	0.011	0.864	0.062	1.405	0.121	n.d.
Butler East	MM-V5-2	Magnetite	MMV5-2-mag5a	0.018	0.121	0.049	1.512	0.129	n.d.
Butler East	MM-V5-2	Magnetite	MMV5-2-mag6a	0.023	0.094	0.096	1.564	0.143	n.d.
Butler East	MM-V5-2	Magnetite	MMV5-2-mag6b	0.010	0.518	0.103	1.454	0.134	n.d.
Butler East	MM-V5-2	Magnetite	MMV5-2-mag7a	0.024	0.300	0.075	1.569	0.146	n.d.
Butler East	MM-V5-2	Magnetite	MMV5-2-mag7b	0.014	0.270	0.090	1.487	0.149	n.d.
Butler East	MM-V5-2	Magnetite	MMV5-2-mag8	0.013	0.268	0.056	1.349	0.123	n.d.
Butler East	MM-V5-2	Magnetite	MMV5-2-mag9	0.010	0.051	0.047	1.446	0.131	n.d.
Butler East	MM-V5-2	Ilmenite	MMV5-2-ilm2a	0.010	50.931	0.021	0.309	0.027	0.000
Butler East	MM-V5-2	Ilmenite	MMV5-2-ilm2b	0.008	51.374	0.006	0.302	0.030	0.000
Butler East	MM-V5-2	Ilmenite	MMV5-2-ilm3	0.008	50.867	0.013	0.324	0.033	0.000
Butler East	MM-V5-2	Ilmenite	MMV5-2-ilm4a	0.015	51.412	0.038	0.263	0.025	0.000
Butler East	MM-V5-2	Ilmenite	MMV5-2-ilm4b	0.045	51.470	0.013	0.194	0.013	0.008
Butler East	MM-V5-2	Ilmenite	MMV5-2-ilm4c	0.012	51.776	0.015	0.261	0.018	0.000
Butler East	MM-V5-2	Ilmenite	MMV5-2-ilm5a	0.007	50.887	0.009	0.279	0.026	0.000
Butler East	MM-V5-2	Ilmenite	MMV5-2-ilm5b	0.003	50.719	0.010	0.339	0.029	0.000
Butler East	MM-V5-2	Ilmenite	MMV5-2-ilm6a	0.007	50.851	0.016	0.266	0.035	0.000
Butler East	MM-V5-2	Ilmenite	MMV5-2-ilm6b	0.004	50.996	0.019	0.279	0.029	0.000
Butler East	MM-V5-2	Ilmenite	MMV5-2-ilm6c	0.009	51.591	0.007	0.250	0.022	0.000
Butler East	MM-V5-2	Ilmenite	MMV5-2-ilm7	0.011	51.374	0.062	0.302	0.023	0.000
Butler East	MM-V5-3	Magnetite	MMV5-3-mag1a	0.013	0.092	0.052	1.542	0.216	n.d.
Butler East	MM-V5-3	Magnetite	MMV5-3-mag1b	0.012	0.059	0.031	1.537	0.190	n.d.
Butler East	MM-V5-3	Magnetite	MMV5-3-mag1c	0.009	0.371	0.053	1.461	0.187	n.d.
Butler East	MM-V5-3	Magnetite	MMV5-3-mag2a	0.013	0.216	0.097	1.594	0.200	n.d.
Butler East	MM-V5-3	Magnetite	MMV5-3-mag2b	0.006	0.113	0.102	1.607	0.198	n.d.
Butler East	MM-V5-3	Magnetite	MMV5-3-mag2c	0.013	0.295	0.075	1.570	0.205	n.d.
Butler East	MM-V5-3	Magnetite	MMV5-3-mag2d	0.010	0.391	0.068	1.536	0.200	n.d.
Butler East	MM-V5-3	Magnetite	MMV5-3-mag3	0.008	0.483	0.044	1.507	0.192	n.d.
Butler East	MM-V5-3	Magnetite	MMV5-3-mag4a	0.016	0.081	0.069	1.532	0.197	n.d.
Butler East	MM-V5-3	Magnetite	MMV5-3-mag4b	0.017	0.119	0.043	1.512	0.204	n.d.
Butler East	MM-V5-3	Magnetite	MMV5-3-mag4c	0.038	0.231	0.069	1.471	0.197	n.d.
Butler East	MM-V5-3	Magnetite	MMV5-3-mag5	0.119	0.081	0.071	1.481	0.200	n.d.
Butler East	MM-V5-3	Magnetite	MMV5-3-mag6a	0.017	0.954	0.051	1.511	0.192	n.d.
Butler East	MM-V5-3	Magnetite	MMV5-3-mag6b	0.010	0.305	0.081	1.525	0.210	n.d.
Butler East	MM-V5-3	Ilmenite	MMV5-3-ilm1a	0.002	50.941	0.011	0.306	0.030	0.000
Butler East	MM-V5-3	Ilmenite	MMV5-3-ilm1b	0.014	51.345	0.006	0.301	0.031	0.000
Butler East	MM-V5-3	Ilmenite	MMV5-3-ilm1c	0.002	50.867	0.009	0.263	0.027	0.000
Butler East	MM-V5-3	Ilmenite	MMV5-3-ilm2	0.007	50.728	0.007	0.351	0.036	0.000
Butler East	MM-V5-3	Ilmenite	MMV5-3-ilm3	0.010	50.872	0.000	0.313	0.033	0.000
Butler East	MM-V5-3	Ilmenite	MMV5-3-ilm4a	0.008	50.526	0.014	0.324	0.020	0.000
Butler East	MM-V5-3	Ilmenite	MMV5-3-ilm4b	0.006	50.625	0.016	0.357	0.036	0.000
Butler East	MM-V5-3	Ilmenite	MMV5-3-ilm4c	0.000	50.980	0.005	0.312	0.032	0.000
Butler East	MM-V5-3	Ilmenite	MMV5-3-ilm4d	0.012	50.863	0.013	0.277	0.030	0.000
Butler East	MM-V5-4	Magnetite	MMV5-4-mag1	0.010	0.512	0.016	0.163	3.527	n.d.
Butler East	MM-V5-4	Magnetite	MMV5-4-mag2	0.009	0.004	0.000	0.000	0.000	n.d.

MgO	MnO	FeO^t	CoO	NiO	CuO	ZnO	Fe2O3	FeO	CaO	SrO	BaO	Na2O	K2O	TOTAL
0.034	1.419	47.337	0.015	0.001	0.000	0.018	3.459	44.225	n.d.	n.d.	n.d.	n.d.	n.d.	100.402
0.014	1.480	46.537	0.011	0.006	0.002	0.017	2.418	44.362	n.d.	n.d.	n.d.	n.d.	n.d.	99.697
0.015	1.445	46.627	0.009	0.000	0.000	0.015	2.715	44.184	n.d.	n.d.	n.d.	n.d.	n.d.	99.579
0.007	1.428	46.561	0.016	0.000	0.000	0.023	2.332	44.462	n.d.	n.d.	n.d.	n.d.	n.d.	99.704
0.009	1.457	46.565	0.019	0.000	0.002	0.017	2.086	44.688	n.d.	n.d.	n.d.	n.d.	n.d.	100.006
0.014	1.442	46.315	0.012	0.000	0.001	0.024	2.246	44.294	n.d.	n.d.	n.d.	n.d.	n.d.	99.375
0.000	0.008	91.177	0.007	0.014	0.000	0.007	66.629	31.224	n.d.	n.d.	n.d.	n.d.	n.d.	99.860
0.000	0.009	91.205	0.013	0.013	0.000	0.008	66.458	31.406	n.d.	n.d.	n.d.	n.d.	n.d.	99.965
0.000	0.007	91.315	0.018	0.016	0.001	0.000	67.014	31.015	n.d.	n.d.	n.d.	n.d.	n.d.	99.706
0.000	0.004	91.714	0.003	0.006	0.000	0.001	66.998	31.429	n.d.	n.d.	n.d.	n.d.	n.d.	100.516
0.000	0.002	91.348	0.000	0.008	0.000	0.004	66.854	31.192	n.d.	n.d.	n.d.	n.d.	n.d.	100.012
0.006	0.007	91.256	0.018	0.014	0.000	0.001	66.942	31.021	n.d.	n.d.	n.d.	n.d.	n.d.	99.742
0.003	0.006	91.178	0.002	0.010	0.000	0.007	66.798	31.073	n.d.	n.d.	n.d.	n.d.	n.d.	99.787
0.001	0.011	90.960	0.000	0.004	0.000	0.003	65.662	31.877	n.d.	n.d.	n.d.	n.d.	n.d.	100.021
0.000	0.002	91.140	0.008	0.005	0.000	0.001	66.736	31.090	n.d.	n.d.	n.d.	n.d.	n.d.	99.671
0.005	0.008	91.560	0.011	0.008	0.000	0.008	67.046	31.231	n.d.	n.d.	n.d.	n.d.	n.d.	100.237
0.000	0.012	91.013	0.000	0.017	0.000	0.037	66.152	31.489	n.d.	n.d.	n.d.	n.d.	n.d.	99.926
0.004	0.012	91.227	0.005	0.017	0.000	0.004	66.533	31.360	n.d.	n.d.	n.d.	n.d.	n.d.	100.049
0.000	0.010	90.831	0.003	0.009	0.000	0.000	66.301	31.173	n.d.	n.d.	n.d.	n.d.	n.d.	99.506
0.000	0.004	91.112	0.003	0.001	0.000	0.003	66.581	31.202	n.d.	n.d.	n.d.	n.d.	n.d.	99.603
0.000	0.003	91.513	0.007	0.019	0.007	0.013	67.166	31.076	n.d.	n.d.	n.d.	n.d.	n.d.	99.977
0.023	1.482	46.748	0.017	0.006	0.000	0.026	2.793	44.234	n.d.	n.d.	n.d.	n.d.	n.d.	99.880
0.015	1.482	46.524	0.017	0.003	0.000	0.025	2.084	44.649	n.d.	n.d.	n.d.	n.d.	n.d.	99.995
0.015	1.459	46.312	0.008	0.001	0.000	0.014	2.307	44.236	n.d.	n.d.	n.d.	n.d.	n.d.	99.285
0.021	1.497	46.610	0.007	0.000	0.000	0.023	2.146	44.679	n.d.	n.d.	n.d.	n.d.	n.d.	100.126
0.010	1.511	46.195	0.015	0.000	0.000	0.016	1.582	44.771	n.d.	n.d.	n.d.	n.d.	n.d.	99.649
0.025	1.555	46.577	0.015	0.006	0.000	0.017	1.831	44.929	n.d.	n.d.	n.d.	n.d.	n.d.	100.460
0.036	1.472	46.269	0.014	0.006	0.000	0.025	2.319	44.182	n.d.	n.d.	n.d.	n.d.	n.d.	99.262
0.033	1.446	46.607	0.018	0.006	0.000	0.032	2.844	44.048	n.d.	n.d.	n.d.	n.d.	n.d.	99.527
0.034	1.423	46.370	0.009	0.000	0.000	0.024	2.396	44.214	n.d.	n.d.	n.d.	n.d.	n.d.	99.275
0.035	1.429	46.702	0.004	0.000	0.000	0.025	2.628	44.337	n.d.	n.d.	n.d.	n.d.	n.d.	99.785
0.021	1.468	46.933	0.000	0.005	0.000	0.024	2.300	44.864	n.d.	n.d.	n.d.	n.d.	n.d.	100.560
0.022	1.397	46.713	0.000	0.000	0.000	0.015	2.177	44.754	n.d.	n.d.	n.d.	n.d.	n.d.	100.137
0.000	0.004	91.136	0.026	0.018	0.000	0.003	66.763	31.062	n.d.	n.d.	n.d.	n.d.	n.d.	99.791
0.000	0.007	90.998	0.009	0.016	0.000	0.000	66.715	30.967	n.d.	n.d.	n.d.	n.d.	n.d.	99.543
0.000	0.011	91.500	0.005	0.026	0.000	0.013	66.709	31.475	n.d.	n.d.	n.d.	n.d.	n.d.	100.320
0.004	0.006	91.228	0.018	0.021	0.000	0.000	66.631	31.273	n.d.	n.d.	n.d.	n.d.	n.d.	100.073
0.006	0.002	90.761	0.016	0.023	0.000	0.005	66.431	30.986	n.d.	n.d.	n.d.	n.d.	n.d.	99.495
0.000	0.008	90.399	0.007	0.023	0.000	0.004	65.922	31.082	n.d.	n.d.	n.d.	n.d.	n.d.	99.204
0.002	0.010	90.922	0.023	0.025	0.000	0.007	66.223	31.334	n.d.	n.d.	n.d.	n.d.	n.d.	99.829
0.000	0.016	90.447	0.007	0.021	0.000	0.000	65.761	31.275	n.d.	n.d.	n.d.	n.d.	n.d.	99.314
0.000	0.013	90.638	0.015	0.018	0.000	0.000	66.401	30.889	n.d.	n.d.	n.d.	n.d.	n.d.	99.232
0.003	0.013	90.568	0.016	0.019	0.000	0.005	66.324	30.889	n.d.	n.d.	n.d.	n.d.	n.d.	99.164
0.008	0.004	91.150	0.004	0.025	0.003	0.000	66.566	31.253	n.d.	n.d.	n.d.	n.d.	n.d.	99.869
0.014	0.012	90.682	0.011	0.022	0.003	0.000	66.287	31.036	n.d.	n.d.	n.d.	n.d.	n.d.	99.337
0.003	0.023	90.489	0.005	0.018	0.000	0.016	65.159	31.858	n.d.	n.d.	n.d.	n.d.	n.d.	99.807
0.000	0.005	90.494	0.005	0.018	0.000	0.000	65.985	31.120	n.d.	n.d.	n.d.	n.d.	n.d.	99.264
0.045	1.212	46.796	0.025	0.001	0.008	0.006	2.579	44.476	n.d.	n.d.	n.d.	n.d.	n.d.	99.641
0.041	1.173	46.884	0.015	0.002	0.000	0.001	2.182	44.920	n.d.	n.d.	n.d.	n.d.	n.d.	100.032
0.036	1.172	46.480	0.009	0.003	0.000	0.012	2.222	44.481	n.d.	n.d.	n.d.	n.d.	n.d.	99.103
0.050	1.199	47.059	0.012	0.000	0.008	0.013	3.064	44.302	n.d.	n.d.	n.d.	n.d.	n.d.	99.777
0.026	1.224	47.026	0.016	0.005	0.005	0.009	2.863	44.450	n.d.	n.d.	n.d.	n.d.	n.d.	99.826
0.026	1.271	46.184	0.003	0.003	0.000	0.009	2.308	44.107	n.d.	n.d.	n.d.	n.d.	n.d.	98.619
0.043	1.205	47.012	0.011	0.005	0.001	0.008	3.102	44.221	n.d.	n.d.	n.d.	n.d.	n.d.	99.636
0.035	1.259	46.713	0.013	0.001	0.000	0.009	2.465	44.495	n.d.	n.d.	n.d.	n.d.	n.d.	99.606
0.022	1.183	46.855	0.000	0.006	0.000	0.002	2.597	44.518	n.d.	n.d.	n.d.	n.d.	n.d.	99.523
0.194	0.167	87.809	0.006	0.131	0.000	0.024	63.551	30.625	n.d.	n.d.	n.d.	n.d.	n.d.	98.926
0.151	0.034	92.444	0.007	0.000	0.000	0.000	68.700	30.627	n.d.	n.d.	n.d.	n.d.	n.d.	99.532

Intrusion	Sample	Mineral	Sample Label	SiO2	TiO2	Al2O3	V2O3	Cr2O3	Nb2O3
Butler East	MM-V5-4	Magnetite	MMV5-4-mag3a	0.004	0.463	0.014	0.173	3.904	n.d.
Butler East	MM-V5-4	Magnetite	MMV5-4-mag3b	0.025	0.518	0.009	0.156	3.768	n.d.
Butler East	MM-V5-4	Magnetite	MMV5-4-mag4	0.023	0.524	0.021	0.151	3.374	n.d.
Butler East	MM-V5-4	Magnetite	MMV5-4-mag5a	0.012	0.408	0.023	0.197	3.526	n.d.
Butler East	MM-V5-4	Magnetite	MMV5-4-mag5b	0.023	0.306	0.015	0.178	2.540	n.d.
Butler East	MM-V5-4	Magnetite	MMV5-4-mag6a	0.018	0.476	0.017	0.196	3.555	n.d.
Butler East	MM-V5-4	Magnetite	MMV5-4-mag6b	0.021	0.313	0.013	0.176	1.525	n.d.
Butler East	MM-V5-4	Magnetite	MMV5-4-mag7	0.014	0.517	0.027	0.182	3.398	n.d.
Butler West	MM-117-1	Plagioclase	MM-117-1a-1	52.043	0.000	30.552	n.d.	n.d.	n.d.
Butler West	MM-117-1	Plagioclase	MM-117-1a-2	52.722	0.013	29.872	n.d.	n.d.	n.d.
Butler West	MM-117-1	Plagioclase	MM-117-1a-3	52.776	0.005	29.534	n.d.	n.d.	n.d.
Butler West	MM-117-1	Plagioclase	MM-117-1a-4	51.034	0.000	30.779	n.d.	n.d.	n.d.
Butler West	MM-117-1	Plagioclase	MM-117-1b-6	50.800	0.000	30.724	n.d.	n.d.	n.d.
Butler West	MM-117-1	Plagioclase	MM-117-1b-7	49.653	0.019	32.197	n.d.	n.d.	n.d.
Butler West	MM-117-1	Plagioclase	MM-117-1c-9	51.590	0.014	30.253	n.d.	n.d.	n.d.
Butler West	MM-117-1	Plagioclase	MM-117-1c-10	51.308	0.001	30.446	n.d.	n.d.	n.d.
Butler West	MM-117-1	Plagioclase	MM-117-1d-1	51.402	0.000	30.828	n.d.	n.d.	n.d.
Butler West	MM-117-1	Plagioclase	MM-117-1d-2	52.077	0.013	30.564	n.d.	n.d.	n.d.
Butler West	MM-117-1	Plagioclase	MM-117-1d-3	51.440	0.000	30.651	n.d.	n.d.	n.d.
Butler West	MM-117-1	Plagioclase	MM-117-1e-1	52.644	0.020	30.235	n.d.	n.d.	n.d.
Butler West	MM-117-1	Plagioclase	MM-117-1e-2	51.177	0.020	30.466	n.d.	n.d.	n.d.
Butler West	MM-117-1	Plagioclase	MM-117-1e-3	51.325	0.000	30.768	n.d.	n.d.	n.d.
Butler West	MM-117-1	Pyroxene	MM-117-1a-1green	49.891	0.331	6.780	n.d.	0.005	n.d.
Butler West	MM-117-1	Pyroxene	MM-117-1a-3green	47.010	0.374	9.452	n.d.	0.000	n.d.
Butler West	MM-117-1	Pyroxene	MM-117-1b-4green?	48.874	0.507	7.422	n.d.	0.110	n.d.
Butler West	MM-117-1	Pyroxene	MM-117-1b-5green?	48.988	0.502	8.041	n.d.	0.026	n.d.
Butler West	MM-117-1	Pyroxene	MM-117-1b-7green	42.077	0.176	11.168	n.d.	0.005	n.d.
Butler West	MM-117-1	Pyroxene	MM-117-1c-8green	49.058	0.305	7.739	n.d.	0.000	n.d.
Butler West	MM-117-1	Pyroxene	MM-117-1c-10green	49.960	0.288	6.878	n.d.	0.033	n.d.
Butler West	MM-117-1	Amphibole	MM-117-1a-1red	51.439	0.253	5.335	n.d.	0.000	n.d.
Butler West	MM-117-1	Amphibole	MM-117-1a-2red	50.602	0.250	6.603	n.d.	0.016	n.d.
Butler West	MM-117-1	Amphibole	MM-117-1a-3red	48.691	0.304	7.863	n.d.	0.004	n.d.
Butler West	MM-117-1	Amphibole	MM-117-1b-5red	50.232	0.427	6.275	n.d.	0.094	n.d.
Butler West	MM-117-1	Amphibole	MM-117-1b-6red	47.700	0.562	8.769	n.d.	0.053	n.d.
Butler West	MM-117-1	Amphibole	MM-117-1b-8red?	49.483	0.393	7.682	n.d.	0.003	n.d.
Butler West	MM-117-1	Amphibole	MM-117-1c-10red	49.555	0.357	7.401	n.d.	0.003	n.d.
Butler West	MM-117-1	Amphibole	MM-117-1c-11red	50.906	0.269	5.825	n.d.	0.021	n.d.
Butler West	MM-117-2	Magnetite	MM117-2-mag1a	0.015	0.076	0.197	1.943	0.193	n.d.
Butler West	MM-117-2	Magnetite	MM117-2-mag1b	0.031	0.071	0.198	1.925	0.193	n.d.
Butler West	MM-117-2	Magnetite	MM117-2-mag1c	0.022	0.485	0.239	1.864	0.184	n.d.
Butler West	MM-117-2	Magnetite	MM117-2-mag2a	0.033	0.091	0.243	1.917	0.185	n.d.
Butler West	MM-117-2	Magnetite	MM117-2-mag2b	0.034	0.177	0.228	1.858	0.187	n.d.
Butler West	MM-117-2	Magnetite	MM117-2-mag2c	0.015	0.377	0.231	1.849	0.191	n.d.
Butler West	MM-117-2	Magnetite	MM117-2-mag3	0.031	0.075	0.217	1.885	0.203	n.d.
Butler West	MM-117-2	Magnetite	MM117-2-mag4	0.016	0.084	0.239	1.901	0.175	n.d.
Butler West	MM-117-2	Magnetite	MM117-2-mag5a	0.018	0.078	0.305	1.815	0.181	n.d.
Butler West	MM-117-2	Magnetite	MM117-2-mag5b	0.012	0.119	0.269	1.820	0.172	n.d.
Butler West	MM-117-2	Magnetite	MM117-2-mag5c	0.018	0.138	0.274	1.811	0.185	n.d.
Butler West	MM-117-2	Magnetite	MM117-2-mag5d	0.011	0.797	0.261	1.741	0.174	n.d.
Butler West	MM-117-2	Magnetite	MM117-2-mag6	0.017	0.063	0.287	1.845	0.179	n.d.
Butler West	MM-117-2	Magnetite	MM117-2-mag7a	0.031	0.094	0.325	1.837	0.185	n.d.
Butler West	MM-117-2	Magnetite	MM117-2-mag7b	0.024	0.078	0.277	1.790	0.164	n.d.
Butler West	MM-117-2	Magnetite	MM117-2-mag7c	0.008	0.822	0.200	1.737	0.181	n.d.
Butler West	MM-117-2	Magnetite	MM117-2-mag8	0.021	0.065	0.251	1.880	0.183	n.d.
Butler West	MM-117-2	Ilmenite	MM117-2-ilm1a	0.000	50.608	0.031	0.363	0.043	0.000
Butler West	MM-117-2	Ilmenite	MM117-2-ilm1b	0.030	51.350	0.013	0.291	0.019	0.000
Butler West	MM-117-2	Ilmenite	MM117-2-ilm1c	0.013	50.800	0.012	0.351	0.026	0.000
Butler West	MM-117-2	Ilmenite	MM117-2-ilm2	0.009	51.550	0.025	0.357	0.029	0.000

MgO	MnO	FeO^t	CoO	NiO	CuO	ZnO	Fe2O3	FeO	CaO	SrO	BaO	Na2O	K2O	TOTAL
0.223	0.123	87.979	0.010	0.127	0.001	0.007	63.613	30.739	n.d.	n.d.	n.d.	n.d.	n.d.	99.402
0.145	0.175	87.190	0.004	0.127	0.009	0.009	62.913	30.581	n.d.	n.d.	n.d.	n.d.	n.d.	98.438
0.154	0.156	87.682	0.004	0.126	0.001	0.011	63.399	30.635	n.d.	n.d.	n.d.	n.d.	n.d.	98.579
0.201	0.105	88.490	0.020	0.123	0.000	0.004	64.129	30.786	n.d.	n.d.	n.d.	n.d.	n.d.	99.534
0.057	0.171	88.710	0.000	0.121	0.000	0.001	64.606	30.577	n.d.	n.d.	n.d.	n.d.	n.d.	98.595
0.176	0.143	88.561	0.008	0.137	0.000	0.018	64.080	30.902	n.d.	n.d.	n.d.	n.d.	n.d.	99.725
0.071	0.138	90.102	0.000	0.117	0.000	0.007	65.984	30.729	n.d.	n.d.	n.d.	n.d.	n.d.	99.094
0.166	0.192	88.681	0.009	0.124	0.000	0.012	64.187	30.925	n.d.	n.d.	n.d.	n.d.	n.d.	99.753
0.000	0.000	0.061	n.d.	n.d.	n.d.	n.d.	n.d.	n.d.	13.156	0.046	0.015	4.187	0.025	95.858
0.000	0.000	0.043	n.d.	n.d.	n.d.	n.d.	n.d.	n.d.	12.714	0.084	0.006	4.445	0.020	95.448
0.000	0.007	0.008	n.d.	n.d.	n.d.	n.d.	n.d.	n.d.	12.455	0.000	0.009	4.582	0.033	94.785
0.017	0.004	0.121	n.d.	n.d.	n.d.	n.d.	n.d.	n.d.	13.648	0.038	0.000	3.867	0.011	95.641
0.000	0.012	0.043	n.d.	n.d.	n.d.	n.d.	n.d.	n.d.	13.887	0.085	0.002	3.747	0.008	95.551
0.010	0.013	0.089	n.d.	n.d.	n.d.	n.d.	n.d.	n.d.	15.047	0.008	0.000	2.926	0.020	97.036
0.005	0.000	0.040	n.d.	n.d.	n.d.	n.d.	n.d.	n.d.	13.372	0.031	0.000	4.091	0.029	95.305
0.055	0.009	0.137	n.d.	n.d.	n.d.	n.d.	n.d.	n.d.	13.391	0.046	0.000	3.979	0.018	95.393
0.012	0.005	0.020	n.d.	n.d.	n.d.	n.d.	n.d.	n.d.	13.622	0.000	0.000	3.951	0.035	95.889
0.007	0.000	0.004	n.d.	n.d.	n.d.	n.d.	n.d.	n.d.	13.205	0.000	0.032	4.150	0.046	95.870
0.000	0.000	0.040	n.d.	n.d.	n.d.	n.d.	n.d.	n.d.	13.401	0.139	0.034	3.918	0.204	95.671
0.006	0.000	0.031	n.d.	n.d.	n.d.	n.d.	n.d.	n.d.	12.690	0.000	0.000	4.474	0.031	95.626
0.000	0.000	0.043	n.d.	n.d.	n.d.	n.d.	n.d.	n.d.	13.757	0.085	0.001	3.843	0.015	95.548
0.000	0.000	0.030	n.d.	n.d.	n.d.	n.d.	n.d.	n.d.	13.776	0.085	0.000	3.829	0.006	95.984
13.828	0.179	13.803	n.d.	n.d.	n.d.	n.d.	n.d.	n.d.	12.011	n.d.	n.d.	0.625	0.130	97.583
12.327	0.190	14.898	n.d.	n.d.	n.d.	n.d.	n.d.	n.d.	11.692	n.d.	n.d.	0.952	0.253	97.148
13.064	0.206	14.458	n.d.	n.d.	n.d.	n.d.	n.d.	n.d.	11.727	n.d.	n.d.	0.758	0.154	97.280
13.560	0.193	13.800	n.d.	n.d.	n.d.	n.d.	n.d.	n.d.	12.070	n.d.	n.d.	0.685	0.158	98.023
12.930	0.206	20.737	n.d.	n.d.	n.d.	n.d.	n.d.	n.d.	7.396	n.d.	n.d.	0.312	0.070	95.077
13.213	0.186	14.656	n.d.	n.d.	n.d.	n.d.	n.d.	n.d.	11.667	n.d.	n.d.	0.795	0.171	97.790
13.868	0.179	14.261	n.d.	n.d.	n.d.	n.d.	n.d.	n.d.	11.804	n.d.	n.d.	0.724	0.106	98.101
14.744	0.184	13.100	n.d.	n.d.	n.d.	n.d.	n.d.	n.d.	12.008	n.d.	n.d.	0.538	0.088	97.689
14.253	0.193	13.358	n.d.	n.d.	n.d.	n.d.	n.d.	n.d.	12.012	n.d.	n.d.	0.591	0.123	98.001
13.524	0.201	14.302	n.d.	n.d.	n.d.	n.d.	n.d.	n.d.	11.758	n.d.	n.d.	0.799	0.141	97.587
14.083	0.189	13.812	n.d.	n.d.	n.d.	n.d.	n.d.	n.d.	11.794	n.d.	n.d.	0.650	0.140	97.696
12.433	0.181	14.904	n.d.	n.d.	n.d.	n.d.	n.d.	n.d.	11.816	n.d.	n.d.	0.883	0.174	97.475
13.573	0.166	13.854	n.d.	n.d.	n.d.	n.d.	n.d.	n.d.	12.111	n.d.	n.d.	0.618	0.146	98.029
13.391	0.194	14.443	n.d.	n.d.	n.d.	n.d.	n.d.	n.d.	11.834	n.d.	n.d.	0.746	0.121	98.045
14.405	0.205	13.738	n.d.	n.d.	n.d.	n.d.	n.d.	n.d.	11.858	n.d.	n.d.	0.543	0.086	97.856
0.012	0.000	90.747	0.021	0.029	0.000	0.000	66.297	31.092	n.d.	n.d.	n.d.	n.d.	n.d.	99.875
0.022	0.003	90.611	0.022	0.031	0.007	0.000	66.203	31.041	n.d.	n.d.	n.d.	n.d.	n.d.	99.747
0.000	0.006	90.085	0.016	0.022	0.000	0.003	65.241	31.381	n.d.	n.d.	n.d.	n.d.	n.d.	99.463
0.005	0.004	90.636	0.025	0.028	0.000	0.004	66.150	31.114	n.d.	n.d.	n.d.	n.d.	n.d.	99.799
0.000	0.011	90.030	0.021	0.031	0.000	0.002	65.609	30.994	n.d.	n.d.	n.d.	n.d.	n.d.	99.152
0.000	0.003	90.078	0.013	0.027	0.000	0.003	65.398	31.232	n.d.	n.d.	n.d.	n.d.	n.d.	99.339
0.000	0.007	90.876	0.011	0.033	0.001	0.002	66.360	31.165	n.d.	n.d.	n.d.	n.d.	n.d.	99.990
0.002	0.010	90.516	0.024	0.024	0.000	0.012	66.114	31.026	n.d.	n.d.	n.d.	n.d.	n.d.	99.627
0.001	0.008	90.339	0.024	0.034	0.000	0.002	65.979	30.971	n.d.	n.d.	n.d.	n.d.	n.d.	99.416
0.000	0.005	89.974	0.022	0.029	0.000	0.013	65.683	30.872	n.d.	n.d.	n.d.	n.d.	n.d.	99.016
0.000	0.008	90.134	0.019	0.037	0.002	0.000	65.761	30.962	n.d.	n.d.	n.d.	n.d.	n.d.	99.215
0.005	0.014	89.782	0.026	0.033	0.000	0.009	64.687	31.576	n.d.	n.d.	n.d.	n.d.	n.d.	99.334
0.009	0.008	90.370	0.016	0.038	0.000	0.002	66.031	30.955	n.d.	n.d.	n.d.	n.d.	n.d.	99.450
0.012	0.009	90.257	0.013	0.032	0.000	0.000	65.859	30.997	n.d.	n.d.	n.d.	n.d.	n.d.	99.394
0.002	0.012	90.543	0.010	0.029	0.000	0.012	66.146	31.024	n.d.	n.d.	n.d.	n.d.	n.d.	99.568
0.000	0.009	90.837	0.019	0.035	0.001	0.000	65.452	31.942	n.d.	n.d.	n.d.	n.d.	n.d.	100.407
0.000	0.011	90.584	0.018	0.023	0.000	0.011	66.172	31.042	n.d.	n.d.	n.d.	n.d.	n.d.	99.677
0.082	0.929	47.553	0.019	0.003	0.000	0.000	3.492	44.411	n.d.	n.d.	n.d.	n.d.	n.d.	99.981
0.069	0.971	46.873	0.009	0.002	0.000	0.000	1.965	45.105	n.d.	n.d.	n.d.	n.d.	n.d.	99.824
0.081	0.940	47.250	0.013	0.003	0.001	0.004	2.955	44.591	n.d.	n.d.	n.d.	n.d.	n.d.	99.790
0.180	0.913	46.850	0.039	0.001	0.001	0.012	1.965	45.082	n.d.	n.d.	n.d.	n.d.	n.d.	100.163

Intrusion	Sample	Mineral	Sample Label	SiO2	TiO2	Al2O3	V2O3	Cr2O3	Nb2O3
Butler West	MM-117-2	Ilmenite	MM117-2-ilm3	0.006	50.885	0.020	0.360	0.032	0.000
Butler West	MM-117-2	Ilmenite	MM117-2-ilm4a	0.010	50.992	0.017	0.324	0.042	0.000
Butler West	MM-117-2	Ilmenite	MM117-2-ilm4b	0.026	50.617	0.035	0.289	0.025	0.000
Butler West	MM-117-2	Ilmenite	MM117-2-ilm4c	0.009	51.091	0.028	0.312	0.032	0.000
Butler West	MM-117-2	Ilmenite	MM117-2-ilm5	0.011	51.149	0.025	0.340	0.022	0.000
Butler West	MM-117-2	Ilmenite	MM117-2-ilm6	0.006	51.036	0.015	0.343	0.048	0.000
Butler West	MM-117-6	Plagioclase	MM-117-6a-1	51.510	0.000	30.889	n.d.	n.d.	n.d.
Butler West	MM-117-6	Plagioclase	MM-117-6b-3	53.295	0.024	29.873	n.d.	n.d.	n.d.
Butler West	MM-117-6	Plagioclase	MM-117-6b-2	52.755	0.041	29.674	n.d.	n.d.	n.d.
Butler West	MM-117-6	Plagioclase	MM-117-6c-5	52.908	0.000	29.669	n.d.	n.d.	n.d.
Butler West	MM-117-6	Plagioclase	MM-117-6c-6	52.623	0.011	30.039	n.d.	n.d.	n.d.
Butler West	MM-117-6	Plagioclase	MM-117-6c-7	52.970	0.005	29.747	n.d.	n.d.	n.d.
Butler West	MM-117-6	Plagioclase	MM-117-6d-1	52.934	0.014	29.709	n.d.	n.d.	n.d.
Butler West	MM-117-6	Plagioclase	MM-117-6d-2	52.901	0.025	29.530	n.d.	n.d.	n.d.
Butler West	MM-117-6	Plagioclase	MM-117-6d-3	52.815	0.012	29.675	n.d.	n.d.	n.d.
Butler West	MM-117-6	Plagioclase	MM-117-6e-1	52.727	0.000	29.489	n.d.	n.d.	n.d.
Butler West	MM-117-6	Plagioclase	MM-117-6e-2	52.363	0.021	30.059	n.d.	n.d.	n.d.
Butler West	MM-117-6	Plagioclase	MM-117-6e-3	53.034	0.000	29.518	n.d.	n.d.	n.d.
Butler West	MM-117-6	Plagioclase	MM-117-6f-1	51.511	0.049	30.386	n.d.	n.d.	n.d.
Butler West	MM-117-6	Plagioclase	MM-117-6f-2	51.828	0.034	30.337	n.d.	n.d.	n.d.
Butler West	MM-117-6	Plagioclase	MM-117-6f-3	52.916	0.002	29.611	n.d.	n.d.	n.d.
Butler West	MM-117-6	Pyroxene	MM-117-6b-1green	53.156	0.021	0.583	n.d.	0.000	n.d.
Butler West	MM-117-6	Pyroxene	MM-117-6b-2green	53.641	0.021	0.340	n.d.	0.012	n.d.
Butler West	MM-117-6	Pyroxene	MM-117-6b-3green	53.429	0.025	0.580	n.d.	0.000	n.d.
Butler West	MM-117-6	Amphibole	MM-117-6a-1red?	46.025	0.644	9.099	n.d.	0.075	n.d.
Butler West	MM-117-6	Amphibole	MM-117-6a-2red?	48.463	0.449	6.070	n.d.	0.027	n.d.
Butler West	MM-117-6	Amphibole	MM-117-6a-4red	50.802	0.334	4.342	n.d.	0.021	n.d.
Butler West	MM-117-6	Amphibole	MM-117-6a-5red	48.982	0.439	6.658	n.d.	0.024	n.d.
Butler West	MM-117-6	Amphibole	MM-117-6a-7red	53.111	0.157	2.490	n.d.	0.000	n.d.
Butler West	MM-117-6	Amphibole	MM-117-6b-9red	47.532	0.395	7.723	n.d.	0.031	n.d.
Butler West	MM-117-6	Amphibole	MM-117-6b-10red	45.171	0.315	9.710	n.d.	0.000	n.d.
Butler West	MM-117-6	Amphibole	MM-117-6c-15red?	47.905	0.347	7.624	n.d.	0.012	n.d.
Butler West	MM-117-6	Amphibole	MM-117-6c-16red	45.370	0.207	9.624	n.d.	0.000	n.d.
Butler West	MM-117-6	Amphibole	MM-117-6c-18red	43.852	0.179	11.946	n.d.	0.000	n.d.
Butler West	MM-V1-1	Magnetite	MMV1-1-mag1a	0.031	0.263	0.401	1.874	0.522	n.d.
Butler West	MM-V1-1	Magnetite	MMV1-1-mag1b	0.025	0.509	0.347	1.811	0.527	n.d.
Butler West	MM-V1-1	Magnetite	MMV1-1-mag2a	0.020	0.567	0.397	1.843	0.524	n.d.
Butler West	MM-V1-1	Magnetite	MMV1-1-mag2b	0.025	0.699	0.392	1.804	0.461	n.d.
Butler West	MM-V1-1	Magnetite	MMV1-1-mag3	0.038	0.236	0.383	1.914	0.518	n.d.
Butler West	MM-V1-1	Magnetite	MMV1-1-mag4a	0.029	0.325	0.394	1.875	0.493	n.d.
Butler West	MM-V1-1	Magnetite	MMV1-1-mag4b	0.021	0.312	0.446	1.866	0.494	n.d.
Butler West	MM-V1-1	Magnetite	MMV1-1-mag5a	0.024	0.184	0.385	1.889	0.506	n.d.
Butler West	MM-V1-1	Magnetite	MMV1-1-mag6a	0.029	0.172	0.392	1.915	0.493	n.d.
Butler West	MM-V1-1	Magnetite	MMV1-1-mag7a	0.041	0.191	0.367	1.900	0.505	n.d.
Butler West	MM-V1-1	Magnetite	MMV1-1-mag8a	0.027	0.269	0.376	1.909	0.486	n.d.
Butler West	MM-V1-1	Magnetite	MMV1-1-mag8b	0.022	0.513	0.447	1.871	0.479	n.d.
Butler West	MM-V1-1	Magnetite	MMV1-1-mag8c	0.039	0.226	0.579	1.838	0.393	n.d.
Butler West	MM-V1-1	Magnetite	MMV1-1-mag9a	0.031	0.208	0.416	1.904	0.551	n.d.
Butler West	MM-V1-1	Ilmenite	MMV1-1-ilm1a	0.014	51.924	0.025	0.165	0.027	0.000
Butler West	MM-V1-1	Ilmenite	MMV1-1-ilm3a	0.004	51.594	0.016	0.214	0.032	0.000
Butler West	MM-V1-1	Ilmenite	MMV1-1-ilm2a	0.005	51.014	0.018	0.201	0.023	0.000
Butler West	MM-V1-2	Magnetite	MMV1-2-mag1a	0.028	0.191	0.301	1.973	0.515	n.d.
Butler West	MM-V1-2	Magnetite	MMV1-2-mag1b	0.020	0.535	0.354	1.920	0.511	n.d.
Butler West	MM-V1-2	Magnetite	MMV1-2-mag2a	0.021	0.297	0.394	1.934	0.522	n.d.
Butler West	MM-V1-2	Magnetite	MMV1-2-mag3a	0.064	0.276	0.636	1.944	0.500	n.d.
Butler West	MM-V1-2	Magnetite	MMV1-2-mag3b	0.024	0.494	0.341	1.918	0.494	n.d.
Butler West	MM-V1-2	Magnetite	MMV1-2-mag4a	0.027	0.151	0.457	2.029	0.499	n.d.
Butler West	MM-V1-2	Magnetite	MMV1-2-mag4b	0.033	0.719	0.424	1.922	0.522	n.d.

MgO	MnO	FeO^t	CoO	NiO	CuO	ZnO	Fe2O3	FeO	CaO	SrO	BaO	Na2O	K2O	TOTAL
0.087	0.915	47.127	0.019	0.009	0.000	0.011	2.745	44.657	n.d.	n.d.	n.d.	n.d.	n.d.	99.746
0.032	1.040	46.579	0.013	0.000	0.000	0.002	2.031	44.752	n.d.	n.d.	n.d.	n.d.	n.d.	99.254
0.047	1.059	47.047	0.028	0.006	0.000	0.010	2.986	44.360	n.d.	n.d.	n.d.	n.d.	n.d.	99.488
0.038	1.055	46.917	0.019	0.001	0.000	0.004	2.347	44.805	n.d.	n.d.	n.d.	n.d.	n.d.	99.741
0.065	1.065	46.837	0.034	0.001	0.000	0.007	2.281	44.784	n.d.	n.d.	n.d.	n.d.	n.d.	99.785
0.056	1.070	47.041	0.030	0.008	0.000	0.012	2.623	44.681	n.d.	n.d.	n.d.	n.d.	n.d.	99.928
0.000	0.000	0.050	n.d.	n.d.	n.d.	n.d.	n.d.	n.d.	13.748	0.061	0.000	3.819	0.028	96.258
0.006	0.016	0.111	n.d.	n.d.	n.d.	n.d.	n.d.	n.d.	12.190	0.100	0.009	4.769	0.034	95.615
0.026	0.009	0.269	n.d.	n.d.	n.d.	n.d.	n.d.	n.d.	12.414	0.092	0.000	4.636	0.028	95.280
0.000	0.000	0.037	n.d.	n.d.	n.d.	n.d.	n.d.	n.d.	12.380	0.130	0.001	4.664	0.027	95.124
0.000	0.000	0.061	n.d.	n.d.	n.d.	n.d.	n.d.	n.d.	12.802	0.000	0.000	4.553	0.026	95.536
0.000	0.006	0.177	n.d.	n.d.	n.d.	n.d.	n.d.	n.d.	12.604	0.000	0.000	4.606	0.031	95.509
0.001	0.000	0.127	n.d.	n.d.	n.d.	n.d.	n.d.	n.d.	12.401	0.061	0.011	4.648	0.037	95.247
0.010	0.000	0.040	n.d.	n.d.	n.d.	n.d.	n.d.	n.d.	12.411	0.153	0.000	4.639	0.024	95.070
0.000	0.000	0.073	n.d.	n.d.	n.d.	n.d.	n.d.	n.d.	12.523	0.161	0.000	4.665	0.031	95.259
0.000	0.000	0.049	n.d.	n.d.	n.d.	n.d.	n.d.	n.d.	12.333	0.000	0.011	4.662	0.031	94.598
0.001	0.000	0.173	n.d.	n.d.	n.d.	n.d.	n.d.	n.d.	12.674	0.062	0.000	4.435	0.036	95.353
0.003	0.016	0.054	n.d.	n.d.	n.d.	n.d.	n.d.	n.d.	12.340	0.046	0.000	4.686	0.042	95.011
0.002	0.000	0.133	n.d.	n.d.	n.d.	n.d.	n.d.	n.d.	13.299	0.038	0.017	4.111	0.045	95.418
0.000	0.012	0.062	n.d.	n.d.	n.d.	n.d.	n.d.	n.d.	13.384	0.023	0.000	4.077	0.028	95.680
0.000	0.000	0.077	n.d.	n.d.	n.d.	n.d.	n.d.	n.d.	12.334	0.054	0.000	4.685	0.022	94.994
15.085	0.979	26.687	n.d.	n.d.	n.d.	n.d.	n.d.	n.d.	0.909	n.d.	n.d.	0.032	0.004	97.456
15.269	0.850	27.236	n.d.	n.d.	n.d.	n.d.	n.d.	n.d.	0.579	n.d.	n.d.	0.015	0.000	97.963
15.031	1.031	27.058	n.d.	n.d.	n.d.	n.d.	n.d.	n.d.	0.916	n.d.	n.d.	0.015	0.003	98.088
10.019	0.283	19.043	n.d.	n.d.	n.d.	n.d.	n.d.	n.d.	11.189	n.d.	n.d.	1.094	0.241	97.712
11.789	0.351	18.574	n.d.	n.d.	n.d.	n.d.	n.d.	n.d.	10.583	n.d.	n.d.	0.714	0.126	97.146
12.966	0.322	17.490	n.d.	n.d.	n.d.	n.d.	n.d.	n.d.	10.712	n.d.	n.d.	0.540	0.075	97.604
11.509	0.293	17.880	n.d.	n.d.	n.d.	n.d.	n.d.	n.d.	11.272	n.d.	n.d.	0.792	0.113	97.962
14.569	0.413	17.233	n.d.	n.d.	n.d.	n.d.	n.d.	n.d.	9.797	n.d.	n.d.	0.264	0.024	98.058
10.696	0.280	18.910	n.d.	n.d.	n.d.	n.d.	n.d.	n.d.	11.225	n.d.	n.d.	0.979	0.157	97.928
9.671	0.320	20.657	n.d.	n.d.	n.d.	n.d.	n.d.	n.d.	10.662	n.d.	n.d.	1.108	0.233	97.847
11.141	0.339	18.321	n.d.	n.d.	n.d.	n.d.	n.d.	n.d.	11.264	n.d.	n.d.	0.891	0.155	97.999
9.564	0.313	19.652	n.d.	n.d.	n.d.	n.d.	n.d.	n.d.	10.957	n.d.	n.d.	1.265	0.206	97.158
8.469	0.308	20.910	n.d.	n.d.	n.d.	n.d.	n.d.	n.d.	10.880	n.d.	n.d.	1.406	0.311	98.261
0.018	0.006	90.553	0.034	0.034	0.000	0.008	65.709	31.427	n.d.	n.d.	n.d.	n.d.	n.d.	100.328
0.010	0.000	89.670	0.017	0.033	0.000	0.000	64.754	31.404	n.d.	n.d.	n.d.	n.d.	n.d.	99.437
0.011	0.007	89.870	0.025	0.038	0.000	0.007	64.817	31.547	n.d.	n.d.	n.d.	n.d.	n.d.	99.803
0.007	0.002	89.908	0.019	0.041	0.000	0.000	64.683	31.705	n.d.	n.d.	n.d.	n.d.	n.d.	99.839
0.004	0.005	89.914	0.007	0.033	0.000	0.000	65.212	31.236	n.d.	n.d.	n.d.	n.d.	n.d.	99.586
0.009	0.001	90.027	0.013	0.032	0.000	0.011	65.224	31.338	n.d.	n.d.	n.d.	n.d.	n.d.	99.744
0.003	0.010	90.435	0.016	0.042	0.000	0.003	65.536	31.465	n.d.	n.d.	n.d.	n.d.	n.d.	100.214
0.011	0.005	90.460	0.025	0.034	0.008	0.000	65.750	31.297	n.d.	n.d.	n.d.	n.d.	n.d.	100.119
0.002	0.001	89.930	0.019	0.033	0.000	0.000	65.331	31.144	n.d.	n.d.	n.d.	n.d.	n.d.	99.532
0.016	0.012	90.432	0.011	0.038	0.000	0.008	65.701	31.314	n.d.	n.d.	n.d.	n.d.	n.d.	100.104
0.017	0.006	90.554	0.013	0.043	0.000	0.007	65.712	31.426	n.d.	n.d.	n.d.	n.d.	n.d.	100.291
0.018	0.000	90.282	0.016	0.033	0.000	0.000	65.160	31.650	n.d.	n.d.	n.d.	n.d.	n.d.	100.210
0.015	0.003	89.877	0.028	0.037	0.000	0.000	65.195	31.214	n.d.	n.d.	n.d.	n.d.	n.d.	99.567
0.013	0.004	89.925	0.010	0.039	0.000	0.006	65.266	31.198	n.d.	n.d.	n.d.	n.d.	n.d.	99.646
0.386	0.402	46.016	0.023	0.011	0.000	0.005	0.477	45.587	n.d.	n.d.	n.d.	n.d.	n.d.	99.046
0.398	0.378	46.486	0.019	0.009	0.000	0.001	1.329	45.291	n.d.	n.d.	n.d.	n.d.	n.d.	99.284
0.344	0.376	46.284	0.018	0.008	0.000	0.000	1.570	44.871	n.d.	n.d.	n.d.	n.d.	n.d.	98.448
0.000	0.004	90.301	0.019	0.041	0.000	0.000	65.607	31.267	n.d.	n.d.	n.d.	n.d.	n.d.	99.946
0.000	0.000	90.070	0.025	0.042	0.000	0.000	64.986	31.595	n.d.	n.d.	n.d.	n.d.	n.d.	99.988
0.020	0.007	89.999	0.023	0.031	0.000	0.000	65.242	31.294	n.d.	n.d.	n.d.	n.d.	n.d.	99.785
0.050	0.001	89.880	0.015	0.042	0.000	0.006	65.024	31.370	n.d.	n.d.	n.d.	n.d.	n.d.	99.929
0.001	0.000	90.116	0.029	0.039	0.000	0.019	65.096	31.542	n.d.	n.d.	n.d.	n.d.	n.d.	99.997
0.020	0.005	90.000	0.030	0.043	0.000	0.006	65.384	31.167	n.d.	n.d.	n.d.	n.d.	n.d.	99.818
0.016	0.000	89.058	0.011	0.043	0.000	0.000	63.939	31.525	n.d.	n.d.	n.d.	n.d.	n.d.	99.154

Intrusion	Sample	Mineral	Sample Label	SiO2	TiO2	Al2O3	V2O3	Cr2O3	Nb2O3
Butler West	MM-V1-2	Magnetite	MMV1-2-mag5a	0.027	0.194	0.377	2.010	0.460	n.d.
Butler West	MM-V1-2	Magnetite	MMV1-2-mag6a	0.023	0.248	0.541	2.112	0.508	n.d.
Butler West	MM-V1-2	Magnetite	MMV1-2-mag7a	0.027	0.142	0.336	1.971	0.491	n.d.
Butler West	MM-V1-2	Magnetite	MMV1-2-mag7b	0.028	0.828	0.373	1.837	0.487	n.d.
Butler West	MM-V1-2	Magnetite	MMV1-2-mag8a	0.018	0.190	0.373	2.006	0.490	n.d.
Butler West	MM-V1-2	Magnetite	MMV1-2-mag9a	0.031	0.320	0.454	1.988	0.617	n.d.
Butler West	MM-V1-2	Ilmenite	MMV1-2-ilm1a	0.011	51.358	0.037	0.213	0.024	0.000
Butler West	MM-V1-2	Ilmenite	MMV1-2-ilm2a	0.005	51.664	0.024	0.222	0.030	0.000
Butler West	MM-V1-2	Ilmenite	MMV1-2-ilm3a	0.006	51.262	0.018	0.217	0.024	0.000
Butler West	MM-V1-2	Plagioclase	MM-V1-2a-1	53.625	0.094	29.385	n.d.	n.d.	n.d.
Butler West	MM-V1-2	Plagioclase	MM-V1-2a-2	53.465	0.010	29.508	n.d.	n.d.	n.d.
Butler West	MM-V1-2	Plagioclase	MM-V1-2a-3	52.906	0.027	29.438	n.d.	n.d.	n.d.
Butler West	MM-V1-2	Plagioclase	MM-V1-2a-5	53.979	0.015	29.610	n.d.	n.d.	n.d.
Butler West	MM-V1-2	Plagioclase	MM-V1-2b-6	53.061	0.000	29.808	n.d.	n.d.	n.d.
Butler West	MM-V1-2	Plagioclase	MM-V1-2b-7(at margin)	52.875	0.000	29.870	n.d.	n.d.	n.d.
Butler West	MM-V1-2	Plagioclase	MM-V1-2b-8	52.303	0.004	30.277	n.d.	n.d.	n.d.
Butler West	MM-V1-2	Plagioclase	MM-V1-2b-9	52.876	0.000	29.896	n.d.	n.d.	n.d.
Butler West	MM-V1-2	Plagioclase	MM-V1-2b-10	53.008	0.005	29.723	n.d.	n.d.	n.d.
Butler West	MM-V1-2	Plagioclase	MM-V1-2c-12	53.452	0.022	29.664	n.d.	n.d.	n.d.
Butler West	MM-V1-2	Plagioclase	MM-V1-2c-13	53.410	0.001	29.320	n.d.	n.d.	n.d.
Butler West	MM-V1-2	Plagioclase	MM-V1-2c-14	53.075	0.000	30.020	n.d.	n.d.	n.d.
Butler West	MM-V1-2	Plagioclase	MM-V1-2d-1	53.877	0.003	29.331	n.d.	n.d.	n.d.
Butler West	MM-V1-2	Plagioclase	MM-V1-2d-2	53.402	0.000	29.275	n.d.	n.d.	n.d.
Butler West	MM-V1-2	Plagioclase	MM-V1-2d-3	48.091	0.005	32.899	n.d.	n.d.	n.d.
Butler West	MM-V1-2	Plagioclase	MM-V1-2e-1	53.052	0.012	29.556	n.d.	n.d.	n.d.
Butler West	MM-V1-2	Plagioclase	MM-V1-2e-2	53.156	0.000	29.809	n.d.	n.d.	n.d.
Butler West	MM-V1-2	Plagioclase	MM-V1-2e-3	46.542	0.012	33.960	n.d.	n.d.	n.d.
Butler West	MM-V1-2	Plagioclase	MM-V1-2f-1	53.188	0.000	29.694	n.d.	n.d.	n.d.
Butler West	MM-V1-2	Plagioclase	MM-V1-2f-2	53.103	0.000	29.583	n.d.	n.d.	n.d.
Butler West	MM-V1-2	Plagioclase	MM-V1-2f-3	53.446	0.005	29.603	n.d.	n.d.	n.d.
Butler West	MM-V1-2	Plagioclase	MM-V1-2g-1	54.000	0.026	28.972	n.d.	n.d.	n.d.
Butler West	MM-V1-2	Plagioclase	MM-V1-2g-2	53.886	0.015	29.192	n.d.	n.d.	n.d.
Butler West	MM-V1-2	Plagioclase	MM-V1-2g-3	53.104	0.034	29.963	n.d.	n.d.	n.d.
Butler West	MM-V1-2	Garnet	MM-V1-2d-gnt	37.684	0.027	21.075	n.d.	0.005	n.d.
Butler West	MM-V1-2	Garnet	MM-V1-2f-gnt	37.996	0.025	21.271	n.d.	0.010	n.d.
Butler West	MM-V1-3	Magnetite	MMV1-3-mag10a	0.032	0.098	0.238	1.984	0.309	n.d.
Butler West	MM-V1-3	Magnetite	MMV1-3-mag11a	0.020	0.179	0.203	1.908	0.332	n.d.
Butler West	MM-V1-3	Magnetite	MMV1-3-mag12a	0.015	0.105	0.244	2.008	0.312	n.d.
Butler West	MM-V1-3	Magnetite	MMV1-3-mag1a	0.033	0.084	0.253	2.138	0.283	n.d.
Butler West	MM-V1-3	Magnetite	MMV1-3-mag1b	0.021	0.469	0.600	2.056	0.270	n.d.
Butler West	MM-V1-3	Magnetite	MMV1-3-mag1c	0.049	0.187	0.397	2.017	0.273	n.d.
Butler West	MM-V1-3	Magnetite	MMV1-3-mag2a	0.022	0.131	0.303	2.163	0.316	n.d.
Butler West	MM-V1-3	Magnetite	MMV1-3-mag2b	0.019	0.917	0.192	1.971	0.316	n.d.
Butler West	MM-V1-3	Magnetite	MMV1-3-mag3a	0.032	0.115	0.467	2.209	0.331	n.d.
Butler West	MM-V1-3	Magnetite	MMV1-3-mag4a	0.043	0.249	0.229	2.148	0.301	n.d.
Butler West	MM-V1-3	Magnetite	MMV1-3-mag5a	0.019	0.050	0.217	2.100	0.320	n.d.
Butler West	MM-V1-3	Magnetite	MMV1-3-mag6a	0.022	0.086	0.232	2.079	0.319	n.d.
Butler West	MM-V1-3	Magnetite	MMV1-3-mag6b	0.020	0.498	0.527	1.991	0.330	n.d.
Butler West	MM-V1-3	Magnetite	MMV1-3-mag6c	0.029	0.094	0.306	2.006	0.369	n.d.
Butler West	MM-V1-3	Magnetite	MMV1-3-mag7a	0.024	0.117	0.392	2.140	0.304	n.d.
Butler West	MM-V1-3	Magnetite	MMV1-3-mag8a	0.021	0.184	0.280	2.039	0.316	n.d.
Butler West	MM-V1-3	Magnetite	MMV1-3-mag9a	0.021	0.069	0.217	2.069	0.311	n.d.
Butler West	MM-V1-3	Magnetite	MMV1-3-mag9b	0.029	0.555	0.317	1.947	0.320	n.d.
Butler West	MM-V1-3	Magnetite	MMV1-3-mag9c	0.027	0.079	0.267	2.012	0.321	n.d.
Butler West	MM-V1-3	Ilmenite	MMV1-3-ilm1a	0.007	50.713	0.017	0.347	0.036	0.002
Butler West	MM-V1-3	Ilmenite	MMV1-3-ilm2a	0.001	51.027	0.026	0.345	0.030	0.000
Butler West	MM-V1-3	Ilmenite	MMV1-3-ilm2b	0.018	50.786	0.033	0.303	0.023	0.000
Butler West	MM-V1-3	Ilmenite	MMV1-3-ilm2c	0.000	50.931	0.009	0.321	0.041	0.000

MgO	MnO	FeO^t	CoO	NiO	CuO	ZnO	Fe2O3	FeO	CaO	SrO	BaO	Na2O	K2O	TOTAL
0.006	0.004	90.053	0.017	0.040	0.000	0.003	65.395	31.210	n.d.	n.d.	n.d.	n.d.	n.d.	99.743
0.012	0.004	90.669	0.023	0.040	0.000	0.013	65.667	31.581	n.d.	n.d.	n.d.	n.d.	n.d.	100.772
0.004	0.000	90.112	0.010	0.034	0.000	0.000	65.516	31.160	n.d.	n.d.	n.d.	n.d.	n.d.	99.691
0.006	0.000	89.446	0.012	0.042	0.000	0.000	64.146	31.727	n.d.	n.d.	n.d.	n.d.	n.d.	99.486
0.000	0.000	90.324	0.023	0.034	0.003	0.001	65.600	31.296	n.d.	n.d.	n.d.	n.d.	n.d.	100.035
0.009	0.000	89.628	0.012	0.041	0.000	0.014	64.823	31.299	n.d.	n.d.	n.d.	n.d.	n.d.	99.609
0.256	0.332	47.155	0.027	0.003	0.000	0.010	1.976	45.377	n.d.	n.d.	n.d.	n.d.	n.d.	99.624
0.308	0.348	46.419	0.019	0.005	0.002	0.000	0.967	45.548	n.d.	n.d.	n.d.	n.d.	n.d.	99.143
0.297	0.336	46.524	0.035	0.006	0.000	0.000	1.465	45.205	n.d.	n.d.	n.d.	n.d.	n.d.	98.872
0.000	0.004	0.230	n.d.	n.d.	n.d.	n.d.	n.d.	n.d.	12.178	0.000	0.000	4.881	0.023	95.516
0.000	0.000	0.055	n.d.	n.d.	n.d.	n.d.	n.d.	n.d.	12.293	0.061	0.000	4.858	0.012	95.392
0.059	0.000	0.489	n.d.	n.d.	n.d.	n.d.	n.d.	n.d.	12.053	0.038	0.000	4.770	0.024	95.010
0.049	0.015	0.157	n.d.	n.d.	n.d.	n.d.	n.d.	n.d.	11.946	0.000	0.000	5.012	0.047	95.771
0.005	0.000	0.015	n.d.	n.d.	n.d.	n.d.	n.d.	n.d.	12.519	0.084	0.000	4.669	0.007	95.492
0.000	0.008	0.175	n.d.	n.d.	n.d.	n.d.	n.d.	n.d.	12.395	0.061	0.000	4.685	0.013	95.384
0.000	0.000	0.117	n.d.	n.d.	n.d.	n.d.	n.d.	n.d.	12.919	0.138	0.000	4.357	0.009	95.758
0.000	0.012	0.051	n.d.	n.d.	n.d.	n.d.	n.d.	n.d.	12.571	0.107	0.000	4.651	0.010	95.513
0.025	0.000	0.140	n.d.	n.d.	n.d.	n.d.	n.d.	n.d.	12.341	0.008	0.000	4.744	0.013	95.250
0.000	0.000	0.054	n.d.	n.d.	n.d.	n.d.	n.d.	n.d.	12.127	0.091	0.014	4.823	0.015	95.410
0.010	0.002	0.085	n.d.	n.d.	n.d.	n.d.	n.d.	n.d.	11.881	0.122	0.000	4.986	0.021	94.831
0.020	0.000	0.137	n.d.	n.d.	n.d.	n.d.	n.d.	n.d.	12.259	0.130	0.000	4.575	0.003	95.641
0.000	0.000	0.106	n.d.	n.d.	n.d.	n.d.	n.d.	n.d.	11.768	0.015	0.000	5.020	0.010	95.100
0.019	0.000	0.041	n.d.	n.d.	n.d.	n.d.	n.d.	n.d.	11.985	0.000	0.000	4.964	0.024	94.722
0.000	0.019	0.102	n.d.	n.d.	n.d.	n.d.	n.d.	n.d.	16.238	0.008	0.000	2.427	0.012	97.362
0.000	0.028	0.047	n.d.	n.d.	n.d.	n.d.	n.d.	n.d.	12.145	0.031	0.000	4.782	0.006	94.871
0.000	0.000	0.030	n.d.	n.d.	n.d.	n.d.	n.d.	n.d.	12.279	0.069	0.000	4.746	0.011	95.343
0.000	0.005	0.146	n.d.	n.d.	n.d.	n.d.	n.d.	n.d.	17.552	0.031	0.003	1.658	0.003	98.248
0.000	0.000	0.079	n.d.	n.d.	n.d.	n.d.	n.d.	n.d.	12.365	0.099	0.000	4.730	0.013	95.425
0.010	0.000	0.114	n.d.	n.d.	n.d.	n.d.	n.d.	n.d.	12.225	0.069	0.000	4.766	0.010	95.104
0.018	0.000	0.186	n.d.	n.d.	n.d.	n.d.	n.d.	n.d.	12.319	0.023	0.000	4.754	0.041	95.600
0.007	0.000	0.050	n.d.	n.d.	n.d.	n.d.	n.d.	n.d.	11.558	0.061	0.000	5.191	0.018	94.674
0.000	0.000	0.087	n.d.	n.d.	n.d.	n.d.	n.d.	n.d.	11.670	0.061	0.013	5.106	0.007	94.911
0.022	0.003	0.180	n.d.	n.d.	n.d.	n.d.	n.d.	n.d.	12.508	0.023	0.000	4.733	0.005	95.837
4.347	1.657	31.460	n.d.	n.d.	n.d.	n.d.	n.d.	n.d.	3.996	n.d.	n.d.	0.000	0.000	100.251
4.700	1.376	31.530	n.d.	n.d.	n.d.	n.d.	n.d.	n.d.	3.782	n.d.	n.d.	0.000	0.000	100.690
0.000	0.008	90.311	0.013	0.028	0.000	0.008	65.827	31.079	n.d.	n.d.	n.d.	n.d.	n.d.	99.624
0.005	0.011	90.438	0.017	0.012	0.000	0.000	65.867	31.170	n.d.	n.d.	n.d.	n.d.	n.d.	99.724
0.000	0.000	90.650	0.016	0.025	0.000	0.000	66.075	31.195	n.d.	n.d.	n.d.	n.d.	n.d.	99.995
0.003	0.000	89.881	0.018	0.015	0.000	0.000	65.459	30.980	n.d.	n.d.	n.d.	n.d.	n.d.	99.266
0.003	0.008	89.855	0.014	0.018	0.000	0.005	64.809	31.539	n.d.	n.d.	n.d.	n.d.	n.d.	99.812
0.000	0.003	90.280	0.007	0.019	0.000	0.000	65.554	31.294	n.d.	n.d.	n.d.	n.d.	n.d.	99.800
0.000	0.005	90.146	0.016	0.023	0.001	0.000	65.571	31.145	n.d.	n.d.	n.d.	n.d.	n.d.	99.696
0.000	0.000	89.950	0.029	0.015	0.000	0.003	64.510	31.903	n.d.	n.d.	n.d.	n.d.	n.d.	99.875
0.000	0.000	90.103	0.023	0.014	0.000	0.016	65.440	31.220	n.d.	n.d.	n.d.	n.d.	n.d.	99.867
0.002	0.007	90.411	0.026	0.023	0.003	0.005	65.638	31.350	n.d.	n.d.	n.d.	n.d.	n.d.	100.023
0.000	0.001	90.288	0.028	0.019	0.000	0.006	65.861	31.026	n.d.	n.d.	n.d.	n.d.	n.d.	99.647
0.004	0.000	89.385	0.027	0.017	0.000	0.004	65.140	30.772	n.d.	n.d.	n.d.	n.d.	n.d.	98.701
0.001	0.008	89.634	0.021	0.015	0.000	0.011	64.653	31.459	n.d.	n.d.	n.d.	n.d.	n.d.	99.534
0.000	0.002	89.582	0.021	0.014	0.004	0.006	65.226	30.891	n.d.	n.d.	n.d.	n.d.	n.d.	98.968
0.000	0.001	89.939	0.013	0.028	0.000	0.007	65.401	31.091	n.d.	n.d.	n.d.	n.d.	n.d.	99.518
0.000	0.001	90.432	0.013	0.019	0.000	0.007	65.766	31.256	n.d.	n.d.	n.d.	n.d.	n.d.	99.901
0.000	0.006	90.635	0.016	0.021	0.002	0.007	66.102	31.156	n.d.	n.d.	n.d.	n.d.	n.d.	99.997
0.001	0.010	90.202	0.019	0.023	0.000	0.001	65.110	31.616	n.d.	n.d.	n.d.	n.d.	n.d.	99.947
0.003	0.003	90.236	0.034	0.016	0.002	0.008	65.785	31.043	n.d.	n.d.	n.d.	n.d.	n.d.	99.599
0.141	0.576	47.733	0.021	0.000	0.001	0.015	3.312	44.753	n.d.	n.d.	n.d.	n.d.	n.d.	99.941
0.176	0.582	47.462	0.025	0.010	0.000	0.016	2.796	44.946	n.d.	n.d.	n.d.	n.d.	n.d.	99.980
0.174	0.586	47.202	0.026	0.004	0.000	0.016	2.721	44.754	n.d.	n.d.	n.d.	n.d.	n.d.	99.444
0.164	0.598	47.207	0.026	0.008	0.012	0.008	2.607	44.861	n.d.	n.d.	n.d.	n.d.	n.d.	99.586

Intrusion	Sample	Mineral	Sample Label	SiO2	TiO2	Al2O3	V2O3	Cr2O3	Nb2O3
Butler West	MM-V1-3	Ilmenite	MMV1-3-ilm3a	0.000	50.622	0.029	0.347	0.044	0.000
Butler West	MM-V1-3	Ilmenite	MMV1-3-ilm3b	0.002	50.826	0.016	0.332	0.046	0.000
Butler West	MM-V1-4	Magnetite	MMV1-4-mag10a	0.032	0.152	0.431	1.859	0.248	n.d.
Butler West	MM-V1-4	Magnetite	MMV1-4-mag11a	0.029	0.117	0.342	1.884	0.247	n.d.
Butler West	MM-V1-4	Magnetite	MMV1-4-mag1a	0.033	0.126	0.354	1.799	0.244	n.d.
Butler West	MM-V1-4	Magnetite	MMV1-4-mag1b	0.022	0.573	0.381	1.733	0.240	n.d.
Butler West	MM-V1-4	Magnetite	MMV1-4-mag1c	0.012	0.177	0.358	1.778	0.230	n.d.
Butler West	MM-V1-4	Magnetite	MMV1-4-mag2a	0.037	0.117	0.364	1.837	0.232	n.d.
Butler West	MM-V1-4	Magnetite	MMV1-4-mag3a	0.032	0.172	0.485	1.805	0.250	n.d.
Butler West	MM-V1-4	Magnetite	MMV1-4-mag4a	0.022	0.116	0.284	1.820	0.248	n.d.
Butler West	MM-V1-4	Magnetite	MMV1-4-mag5a	0.030	0.130	0.360	1.795	0.257	n.d.
Butler West	MM-V1-4	Magnetite	MMV1-4-mag5b	0.028	0.606	0.387	1.756	0.256	n.d.
Butler West	MM-V1-4	Magnetite	MMV1-4-mag5c	0.029	0.186	0.374	1.751	0.250	n.d.
Butler West	MM-V1-4	Magnetite	MMV1-4-mag6a	0.026	0.142	0.505	1.815	0.266	n.d.
Butler West	MM-V1-4	Magnetite	MMV1-4-mag7a	0.023	0.116	0.342	1.846	0.233	n.d.
Butler West	MM-V1-4	Magnetite	MMV1-4-mag8a	0.023	0.144	0.322	1.773	0.222	n.d.
Butler West	MM-V1-4	Magnetite	MMV1-4-mag9a	0.028	0.211	0.358	1.880	0.237	n.d.
Butler West	MM-V1-4	Magnetite	MMV1-4-mag9b	0.034	0.496	0.365	1.821	0.240	n.d.
Butler West	MM-V1-4	Magnetite	MMV1-4-mag9c	0.023	0.133	0.335	1.827	0.223	n.d.
Butler West	MM-V1-4	Ilmenite	MMV1-4-ilm1a	0.011	51.023	0.022	0.234	0.020	0.000
Butler West	MM-V1-4	Ilmenite	MMV1-4-ilm1b	0.007	50.887	0.023	0.228	0.021	0.000
Butler West	MM-V1-4	Ilmenite	MMV1-4-ilm2a	0.001	51.008	0.018	0.237	0.024	0.000
Butler West	MM-V1-4	Ilmenite	MMV1-4-ilm3a	0.000	50.769	0.019	0.213	0.028	0.000
Butler West	MM-V1-4	Ilmenite	MMV1-4-ilm4a	0.009	51.441	0.022	0.224	0.025	0.000
Butler West	MM-V1-4	Ilmenite	MMV1-4-ilm5a	0.002	50.881	0.016	0.258	0.035	0.000
Butler West	MM-V1-5	Magnetite	MMV1-5-mag10a	0.023	0.056	0.250	1.790	0.152	n.d.
Butler West	MM-V1-5	Magnetite	MMV1-5-mag11a	0.012	0.070	0.240	1.777	0.162	n.d.
Butler West	MM-V1-5	Magnetite	MMV1-5-mag12a	0.020	0.054	0.249	1.779	0.174	n.d.
Butler West	MM-V1-5	Magnetite	MMV1-5-mag13a	0.030	0.062	0.226	1.809	0.159	n.d.
Butler West	MM-V1-5	Magnetite	MMV1-5-mag1a	0.037	0.070	0.171	1.800	0.169	n.d.
Butler West	MM-V1-5	Magnetite	MMV1-5-mag2a	0.017	0.065	0.171	1.816	0.185	n.d.
Butler West	MM-V1-5	Magnetite	MMV1-5-mag2b	0.017	0.447	0.181	1.730	0.180	n.d.
Butler West	MM-V1-5	Magnetite	MMV1-5-mag2c	0.031	0.129	0.172	1.785	0.180	n.d.
Butler West	MM-V1-5	Magnetite	MMV1-5-mag3a	0.020	0.073	0.151	1.545	0.148	n.d.
Butler West	MM-V1-5	Magnetite	MMV1-5-mag3b	0.036	0.101	0.214	1.511	0.151	n.d.
Butler West	MM-V1-5	Magnetite	MMV1-5-mag4a	0.021	0.071	0.154	1.626	0.151	n.d.
Butler West	MM-V1-5	Magnetite	MMV1-5-mag5a	0.028	0.078	0.259	1.817	0.173	n.d.
Butler West	MM-V1-5	Magnetite	MMV1-5-mag5b	0.028	0.361	0.312	1.755	0.163	n.d.
Butler West	MM-V1-5	Magnetite	MMV1-5-mag6a	0.026	0.061	0.342	1.851	0.178	n.d.
Butler West	MM-V1-5	Magnetite	MMV1-5-mag6b	0.014	0.610	0.227	1.793	0.178	n.d.
Butler West	MM-V1-5	Magnetite	MMV1-5-mag7a	0.019	0.065	0.216	1.850	0.179	n.d.
Butler West	MM-V1-5	Magnetite	MMV1-5-mag8a	0.020	0.078	0.185	1.822	0.164	n.d.
Butler West	MM-V1-5	Magnetite	MMV1-5-mag9a	0.022	0.093	0.301	1.787	0.159	n.d.
Butler West	MM-V1-5	Magnetite	MMV1-5-mag9b	0.020	1.334	0.224	1.619	0.145	n.d.
Butler West	MM-V1-5	Magnetite	MMV1-5-mag9c	0.026	0.084	0.253	1.802	0.166	n.d.
Butler West	MM-V1-5	Ilmenite	MMV1-5-ilm1a	0.011	50.420	0.010	0.294	0.033	0.000
Butler West	MM-V1-5	Ilmenite	MMV1-5-ilm2a	0.002	50.320	0.006	0.273	0.020	0.000
Butler West	MM-V1-5	Ilmenite	MMV1-5-ilm3a	0.011	50.547	0.016	0.330	0.034	0.000
Butler West	MM-V1-5	Ilmenite	MMV1-5-ilm3b	0.012	50.491	0.027	0.352	0.041	0.000
Butler West	MM-V1-5	Ilmenite	MMV1-5-ilm3c	0.003	50.342	0.007	0.336	0.028	0.000
Butler West	MM-V1-5	Ilmenite	MMV1-5-ilm4a	0.015	50.877	0.016	0.284	0.031	0.000
Butler West	MM-V1-5	Ilmenite	MMV1-5-ilm4b	0.006	50.795	0.014	0.290	0.028	0.000
Butler West	MM-V1-6	Magnetite	MMV1-6-mag1a	0.038	0.039	0.074	0.000	0.003	n.d.
Butler West	MM-V1-6	Magnetite	MMV1-6-mag1b	0.038	0.043	0.081	0.008	0.005	n.d.
Butler West	MM-V1-6	Ilmenite	MMV1-6-ilm1a	0.011	51.150	0.012	0.000	0.007	0.015
Butler West	MM-V1-6	Ilmenite	MMV1-6-ilm1b	0.016	50.989	0.016	0.000	0.015	0.000
Butler West	MM-V1-6	Ilmenite	MMV1-6-ilm2a	0.016	51.092	0.018	0.001	0.000	0.010
Butler West	MM-V1-6	Ilmenite	MMV1-6-ilm3a	0.018	51.131	0.015	0.000	0.000	0.007

MgO	MnO	FeO^t	CoO	NiO	CuO	ZnO	Fe2O3	FeO	CaO	SrO	BaO	Na2O	K2O	TOTAL
0.125	0.595	47.370	0.037	0.000	0.000	0.000	3.000	44.671	n.d.	n.d.	n.d.	n.d.	n.d.	99.470
0.128	0.596	47.176	0.024	0.002	0.000	0.012	2.585	44.850	n.d.	n.d.	n.d.	n.d.	n.d.	99.419
0.041	0.005	91.051	0.025	0.031	0.000	0.004	66.329	31.368	n.d.	n.d.	n.d.	n.d.	n.d.	100.525
0.020	0.001	90.384	0.015	0.042	0.000	0.000	65.892	31.094	n.d.	n.d.	n.d.	n.d.	n.d.	99.683
0.004	0.014	90.931	0.002	0.042	0.000	0.014	66.291	31.281	n.d.	n.d.	n.d.	n.d.	n.d.	100.205
0.010	0.003	89.951	0.025	0.039	0.000	0.007	65.009	31.455	n.d.	n.d.	n.d.	n.d.	n.d.	99.497
0.006	0.003	90.510	0.019	0.042	0.000	0.005	65.960	31.159	n.d.	n.d.	n.d.	n.d.	n.d.	99.749
0.015	0.000	90.992	0.018	0.031	0.000	0.000	66.325	31.312	n.d.	n.d.	n.d.	n.d.	n.d.	100.288
0.023	0.009	90.534	0.015	0.040	0.005	0.000	65.888	31.247	n.d.	n.d.	n.d.	n.d.	n.d.	99.971
0.010	0.001	90.562	0.025	0.040	0.000	0.000	66.082	31.101	n.d.	n.d.	n.d.	n.d.	n.d.	99.749
0.030	0.004	90.464	0.025	0.045	0.000	0.000	65.975	31.099	n.d.	n.d.	n.d.	n.d.	n.d.	99.750
0.025	0.013	90.747	0.023	0.034	0.000	0.015	65.555	31.760	n.d.	n.d.	n.d.	n.d.	n.d.	100.458
0.013	0.004	90.333	0.019	0.041	0.000	0.000	65.787	31.138	n.d.	n.d.	n.d.	n.d.	n.d.	99.591
0.033	0.003	90.478	0.026	0.035	0.000	0.004	65.890	31.189	n.d.	n.d.	n.d.	n.d.	n.d.	99.935
0.010	0.008	91.220	0.017	0.044	0.000	0.014	66.545	31.342	n.d.	n.d.	n.d.	n.d.	n.d.	100.540
0.009	0.002	90.503	0.014	0.038	0.000	0.013	66.004	31.112	n.d.	n.d.	n.d.	n.d.	n.d.	99.676
0.017	0.003	90.181	0.012	0.031	0.009	0.004	65.611	31.144	n.d.	n.d.	n.d.	n.d.	n.d.	99.545
0.018	0.000	90.543	0.019	0.042	0.000	0.005	65.511	31.596	n.d.	n.d.	n.d.	n.d.	n.d.	100.147
0.008	0.001	90.485	0.020	0.035	0.000	0.006	65.975	31.120	n.d.	n.d.	n.d.	n.d.	n.d.	99.706
0.269	0.528	47.043	0.026	0.000	0.000	0.001	2.420	44.865	n.d.	n.d.	n.d.	n.d.	n.d.	99.419
0.258	0.526	47.026	0.021	0.007	0.000	0.000	2.520	44.759	n.d.	n.d.	n.d.	n.d.	n.d.	99.256
0.363	0.524	46.959	0.018	0.000	0.000	0.004	2.531	44.681	n.d.	n.d.	n.d.	n.d.	n.d.	99.410
0.072	0.515	47.634	0.032	0.002	0.000	0.010	2.958	44.972	n.d.	n.d.	n.d.	n.d.	n.d.	99.590
0.409	0.561	46.926	0.026	0.005	0.000	0.005	2.199	44.948	n.d.	n.d.	n.d.	n.d.	n.d.	99.873
0.410	0.518	47.003	0.026	0.006	0.000	0.011	2.814	44.471	n.d.	n.d.	n.d.	n.d.	n.d.	99.448
0.000	0.003	91.137	0.007	0.010	0.000	0.002	66.604	31.206	n.d.	n.d.	n.d.	n.d.	n.d.	100.103
0.000	0.004	90.776	0.001	0.015	0.000	0.000	66.343	31.080	n.d.	n.d.	n.d.	n.d.	n.d.	99.704
0.000	0.004	91.022	0.019	0.008	0.000	0.000	66.530	31.158	n.d.	n.d.	n.d.	n.d.	n.d.	99.995
0.000	0.007	91.421	0.000	0.009	0.000	0.001	66.794	31.319	n.d.	n.d.	n.d.	n.d.	n.d.	100.416
0.000	0.007	90.457	0.008	0.006	0.000	0.000	66.088	30.990	n.d.	n.d.	n.d.	n.d.	n.d.	99.346
0.000	0.001	90.976	0.006	0.008	0.000	0.009	66.505	31.134	n.d.	n.d.	n.d.	n.d.	n.d.	99.917
0.003	0.011	90.738	0.009	0.000	0.001	0.015	65.859	31.478	n.d.	n.d.	n.d.	n.d.	n.d.	99.931
0.003	0.006	90.837	0.005	0.003	0.000	0.012	66.309	31.171	n.d.	n.d.	n.d.	n.d.	n.d.	99.807
0.000	0.007	91.441	0.002	0.003	0.000	0.006	66.949	31.200	n.d.	n.d.	n.d.	n.d.	n.d.	100.104
0.007	0.007	91.069	0.013	0.005	0.000	0.028	66.619	31.125	n.d.	n.d.	n.d.	n.d.	n.d.	99.817
0.001	0.000	91.387	0.015	0.000	0.000	0.000	66.878	31.210	n.d.	n.d.	n.d.	n.d.	n.d.	100.127
0.010	0.002	91.269	0.015	0.007	0.000	0.003	66.659	31.289	n.d.	n.d.	n.d.	n.d.	n.d.	100.340
0.000	0.001	90.812	0.014	0.011	0.000	0.019	65.939	31.479	n.d.	n.d.	n.d.	n.d.	n.d.	100.083
0.017	0.008	91.168	0.011	0.005	0.000	0.006	66.564	31.273	n.d.	n.d.	n.d.	n.d.	n.d.	100.342
0.000	0.010	90.467	0.001	0.006	0.000	0.015	65.394	31.625	n.d.	n.d.	n.d.	n.d.	n.d.	99.873
0.000	0.007	91.026	0.000	0.005	0.000	0.010	66.504	31.186	n.d.	n.d.	n.d.	n.d.	n.d.	100.040
0.004	0.010	90.205	0.015	0.003	0.000	0.000	65.918	30.892	n.d.	n.d.	n.d.	n.d.	n.d.	99.110
0.000	0.006	90.695	0.019	0.016	0.000	0.001	66.215	31.114	n.d.	n.d.	n.d.	n.d.	n.d.	99.733
0.000	0.014	90.472	0.013	0.007	0.000	0.009	64.505	32.430	n.d.	n.d.	n.d.	n.d.	n.d.	100.320
0.008	0.008	91.293	0.015	0.009	0.000	0.007	66.689	31.286	n.d.	n.d.	n.d.	n.d.	n.d.	100.353
0.012	0.793	47.543	0.006	0.003	0.000	0.017	3.365	44.515	n.d.	n.d.	n.d.	n.d.	n.d.	99.479
0.016	0.821	47.260	0.000	0.002	0.000	0.000	3.178	44.400	n.d.	n.d.	n.d.	n.d.	n.d.	99.038
0.024	0.733	47.379	0.008	0.000	0.010	0.002	3.007	44.674	n.d.	n.d.	n.d.	n.d.	n.d.	99.395
0.025	0.761	46.815	0.011	0.000	0.000	0.003	2.462	44.600	n.d.	n.d.	n.d.	n.d.	n.d.	98.785
0.023	0.729	47.648	0.008	0.000	0.000	0.006	3.509	44.491	n.d.	n.d.	n.d.	n.d.	n.d.	99.482
0.071	0.742	47.462	0.015	0.004	0.000	0.018	2.884	44.867	n.d.	n.d.	n.d.	n.d.	n.d.	99.824
0.078	0.766	47.246	0.015	0.004	0.000	0.000	2.761	44.761	n.d.	n.d.	n.d.	n.d.	n.d.	99.519
0.000	0.004	93.033	0.011	0.000	0.000	0.010	68.786	31.138	n.d.	n.d.	n.d.	n.d.	n.d.	100.104
0.000	0.008	92.689	0.007	0.003	0.000	0.000	68.515	31.039	n.d.	n.d.	n.d.	n.d.	n.d.	99.747
0.033	1.761	45.809	0.012	0.000	0.000	0.024	1.850	44.145	n.d.	n.d.	n.d.	n.d.	n.d.	99.019
0.027	1.795	45.954	0.005	0.001	0.014	0.011	2.186	43.987	n.d.	n.d.	n.d.	n.d.	n.d.	99.062
0.035	1.778	46.196	0.000	0.004	0.000	0.022	2.344	44.087	n.d.	n.d.	n.d.	n.d.	n.d.	99.407
0.041	1.803	46.339	0.000	0.002	0.000	0.025	2.502	44.088	n.d.	n.d.	n.d.	n.d.	n.d.	99.632

Intrusion	Sample	Mineral	Sample Label	SiO2	TiO2	Al2O3	V2O3	Cr2O3	Nb2O3
Butler West	MM-V1-6	Ilmenite	MMV1-6-ilm4a	0.015	51.350	0.012	0.000	0.007	0.012
Butler West	MM-V8-1	Plagioclase	MM-V8-1a-1	54.149	0.014	29.274	n.d.	n.d.	n.d.
Butler West	MM-V8-1	Plagioclase	MM-V8-1a-2	54.739	0.000	29.056	n.d.	n.d.	n.d.
Butler West	MM-V8-1	Plagioclase	MM-V8-1b-3	54.396	0.023	29.012	n.d.	n.d.	n.d.
Butler West	MM-V8-1	Plagioclase	MM-V8-1b-4	54.592	0.013	29.104	n.d.	n.d.	n.d.
Butler West	MM-V8-1	Plagioclase	MM-V8-1b-5	54.052	0.014	29.063	n.d.	n.d.	n.d.
Butler West	MM-V8-1	Plagioclase	MM-V8-1c-6	54.292	0.014	29.000	n.d.	n.d.	n.d.
Butler West	MM-V8-1	Plagioclase	MM-V8-1c-7	54.896	0.012	28.616	n.d.	n.d.	n.d.
Butler West	MM-V8-1	Plagioclase	MM-V8-1c-8	54.635	0.001	28.748	n.d.	n.d.	n.d.
Butler West	MM-V8-1	Plagioclase	MM-V8-1d-1	54.334	0.007	28.800	n.d.	n.d.	n.d.
Butler West	MM-V8-1	Plagioclase	MM-V8-1d-2	54.123	0.003	29.051	n.d.	n.d.	n.d.
Butler West	MM-V8-1	Plagioclase	MM-V8-1d-3	54.300	0.017	28.889	n.d.	n.d.	n.d.
Butler West	MM-V8-1	Plagioclase	MM-V8-1e-1	54.022	0.007	29.098	n.d.	n.d.	n.d.
Butler West	MM-V8-1	Plagioclase	MM-V8-1e-2	54.109	0.039	29.094	n.d.	n.d.	n.d.
Butler West	MM-V8-1	Plagioclase	MM-V8-1e-3	53.688	0.010	29.458	n.d.	n.d.	n.d.
Butler West	MM-V8-1	Plagioclase	MM-V8-1f-1	54.519	0.000	28.970	n.d.	n.d.	n.d.
Butler West	MM-V8-1	Plagioclase	MM-V8-1f-2	54.266	0.012	28.667	n.d.	n.d.	n.d.
Butler West	MM-V8-1	Plagioclase	MM-V8-1f-3	54.332	0.019	28.628	n.d.	n.d.	n.d.
Butler West	MM-V8-1	Pyroxene	MM-V8-1a-1rgreen	43.164	0.839	11.791	n.d.	0.001	n.d.
Butler West	MM-V8-1	Pyroxene	MM-V8-1a-2rgreen	43.793	0.721	11.729	n.d.	0.009	n.d.
Butler West	MM-V8-1	Pyroxene	MM-V8-1a-3rgreen	49.139	0.402	6.006	n.d.	0.021	n.d.
Butler West	MM-V8-1	Pyroxene	MM-V8-1a-4rgreen	49.536	0.376	5.557	n.d.	0.003	n.d.
Butler West	MM-V8-1	Pyroxene	MM-V8-1b-5green	47.972	0.482	6.602	n.d.	0.029	n.d.
Butler West	MM-V8-1	Pyroxene	MM-V8-1c-8green?	45.428	0.356	9.672	n.d.	0.000	n.d.
Butler West	MM-V8-1	Amphibole	MM-V8-1a-2red	45.200	0.787	9.374	n.d.	0.007	n.d.
Butler West	MM-V8-1	Amphibole	MM-V8-1a-3red?	42.053	0.742	13.283	n.d.	0.016	n.d.
Butler West	MM-V8-1	Amphibole	MM-V8-1b-5red	43.116	0.650	11.429	n.d.	0.000	n.d.
Butler West	MM-V8-1	Amphibole	MM-V8-1b-6red	42.876	0.823	11.811	n.d.	0.008	n.d.
Butler West	MM-V8-1	Amphibole	MM-V8-1b-7red	44.055	0.524	10.827	n.d.	0.007	n.d.
Butler West	MM-V8-1	Amphibole	MM-V8-1c-9red?	46.591	0.318	8.346	n.d.	0.000	n.d.
Butler West	MM-V8-1	Amphibole	MM-V8-1c-11red?	45.451	0.416	9.567	n.d.	0.007	n.d.
Butler West	MM-V8-2	Magnetite	MMV8-2-mag1a	0.009	0.077	0.164	1.797	0.150	n.d.
Butler West	MM-V8-2	Magnetite	MMV8-2-mag1b	0.024	0.095	0.161	1.726	0.151	n.d.
Butler West	MM-V8-2	Magnetite	MMV8-2-mag2a	0.017	0.134	0.146	1.730	0.143	n.d.
Butler West	MM-V8-2	Magnetite	MMV8-2-mag2b	0.016	0.245	0.150	1.620	0.132	n.d.
Butler West	MM-V8-2	Magnetite	MMV8-2-mag2c	0.008	0.154	0.149	1.688	0.141	n.d.
Butler West	MM-V8-2	Magnetite	MMV8-2-mag3	0.019	0.061	0.163	1.777	0.148	n.d.
Butler West	MM-V8-2	Magnetite	MMV8-2-mag4a	0.016	0.045	0.153	1.621	0.150	n.d.
Butler West	MM-V8-2	Magnetite	MMV8-2-mag4b	0.007	0.196	0.148	1.599	0.139	n.d.
Butler West	MM-V8-2	Magnetite	MMV8-2-mag4c	0.024	1.231	0.151	1.390	0.121	n.d.
Butler West	MM-V8-2	Magnetite	MMV8-2-mag5	0.013	0.124	0.161	1.592	0.137	n.d.
Butler West	MM-V8-2	Magnetite	MMV8-2-mag6a	0.014	0.185	0.147	1.602	0.138	n.d.
Butler West	MM-V8-2	Magnetite	MMV8-2-mag6b	0.028	0.439	0.155	1.564	0.142	n.d.
Butler West	MM-V8-2	Magnetite	MMV8-2-mag7	0.017	0.091	0.169	1.622	0.138	n.d.
Butler West	MM-V8-2	Ilmenite	MMV8-2-ilm1	0.006	51.218	0.016	0.346	0.035	0.000
Butler West	MM-V8-2	Ilmenite	MMV8-2-ilm2	0.019	51.709	0.011	0.350	0.033	0.000
Butler West	MM-V8-2	Ilmenite	MMV8-2-ilm3	0.002	51.405	0.014	0.308	0.031	0.000
Butler West	MM-V8-2	Ilmenite	MMV8-2-ilm4a	0.004	50.962	0.013	0.341	0.039	0.000
Butler West	MM-V8-2	Ilmenite	MMV8-2-ilm4b	0.000	51.055	0.009	0.328	0.022	0.000
Butler West	MM-V8-2	Ilmenite	MMV8-2-ilm4c	0.011	51.341	0.020	0.233	0.025	0.000
Butler West	MM-V8-2	Ilmenite	MMV8-2-ilm5	0.011	50.984	0.004	0.283	0.032	0.000
Butler West	MM-V8-2	Ilmenite	MMV8-2-ilm6a	0.008	51.025	0.018	0.360	0.044	0.000
Butler West	MM-V8-2	Ilmenite	MMV8-2-ilm6b	0.016	50.827	0.012	0.349	0.028	0.000
Butler West	MM-V8-2	Ilmenite	MMV8-2-ilm7a	0.006	51.220	0.004	0.258	0.028	0.000
Butler West	MM-V8-2	Ilmenite	MMV8-2-ilm7b	0.003	51.191	0.010	0.278	0.025	0.000
Butler West	MM-V8-2	Ilmenite	MMV8-2-ilm7c	0.015	50.837	0.022	0.247	0.031	0.000
Butler West	MM-V8-2	Ilmenite	MMV8-2-ilm8	0.000	51.012	0.015	0.292	0.029	0.000
Butler West	MM-V8-3	Magnetite	MMV8-3-mag10	0.016	0.064	0.159	1.751	0.160	n.d.

MgO	MnO	FeO^t	CoO	NiO	CuO	ZnO	Fe2O3	FeO	CaO	SrO	BaO	Na2O	K2O	TOTAL
0.034	1.824	45.748	0.003	0.009	0.000	0.013	1.639	44.273	n.d.	n.d.	n.d.	n.d.	n.d.	99.191
0.000	0.009	0.105	n.d.	n.d.	n.d.	n.d.	n.d.	n.d.	11.812	0.061	0.000	5.068	0.043	95.424
0.012	0.000	0.072	n.d.	n.d.	n.d.	n.d.	n.d.	n.d.	11.322	0.000	0.000	5.304	0.037	95.201
0.020	0.007	0.301	n.d.	n.d.	n.d.	n.d.	n.d.	n.d.	11.423	0.061	0.000	5.214	0.058	95.243
0.016	0.000	0.165	n.d.	n.d.	n.d.	n.d.	n.d.	n.d.	11.398	0.000	0.028	5.189	0.042	95.288
0.032	0.000	0.267	n.d.	n.d.	n.d.	n.d.	n.d.	n.d.	11.511	0.031	0.000	5.146	0.041	94.970
0.015	0.000	0.132	n.d.	n.d.	n.d.	n.d.	n.d.	n.d.	11.514	0.115	0.000	5.199	0.046	95.082
0.024	0.002	0.148	n.d.	n.d.	n.d.	n.d.	n.d.	n.d.	11.089	0.145	0.005	5.302	0.052	94.932
0.008	0.000	0.131	n.d.	n.d.	n.d.	n.d.	n.d.	n.d.	10.981	0.176	0.000	5.406	0.026	94.680
0.000	0.000	0.100	n.d.	n.d.	n.d.	n.d.	n.d.	n.d.	11.438	0.008	0.000	5.141	0.026	94.687
0.000	0.003	0.099	n.d.	n.d.	n.d.	n.d.	n.d.	n.d.	11.456	0.023	0.000	5.116	0.042	94.758
0.016	0.000	0.139	n.d.	n.d.	n.d.	n.d.	n.d.	n.d.	11.377	0.015	0.000	5.125	0.021	94.753
0.010	0.000	0.106	n.d.	n.d.	n.d.	n.d.	n.d.	n.d.	11.469	0.084	0.000	5.119	0.035	94.796
0.011	0.003	0.170	n.d.	n.d.	n.d.	n.d.	n.d.	n.d.	11.431	0.122	0.000	5.118	0.033	94.979
0.000	0.000	0.181	n.d.	n.d.	n.d.	n.d.	n.d.	n.d.	11.706	0.092	0.000	5.042	0.014	95.135
0.000	0.000	0.064	n.d.	n.d.	n.d.	n.d.	n.d.	n.d.	11.344	0.069	0.000	5.350	0.056	94.966
0.031	0.012	0.273	n.d.	n.d.	n.d.	n.d.	n.d.	n.d.	11.251	0.008	0.005	5.458	0.081	94.520
0.078	0.000	0.444	n.d.	n.d.	n.d.	n.d.	n.d.	n.d.	11.235	0.046	0.000	5.353	0.139	94.782
8.231	0.208	20.481	n.d.	n.d.	n.d.	n.d.	n.d.	n.d.	11.582	n.d.	n.d.	1.320	0.536	98.153
8.446	0.249	20.447	n.d.	n.d.	n.d.	n.d.	n.d.	n.d.	11.533	n.d.	n.d.	1.304	0.444	98.675
11.815	0.298	18.165	n.d.	n.d.	n.d.	n.d.	n.d.	n.d.	11.561	n.d.	n.d.	0.708	0.191	98.306
11.966	0.306	17.702	n.d.	n.d.	n.d.	n.d.	n.d.	n.d.	11.569	n.d.	n.d.	0.698	0.172	97.885
11.108	0.236	17.509	n.d.	n.d.	n.d.	n.d.	n.d.	n.d.	11.302	n.d.	n.d.	0.834	0.238	96.312
9.670	0.252	19.666	n.d.	n.d.	n.d.	n.d.	n.d.	n.d.	11.558	n.d.	n.d.	1.163	0.368	98.133
9.535	0.253	19.918	n.d.	n.d.	n.d.	n.d.	n.d.	n.d.	11.604	n.d.	n.d.	1.195	0.403	98.276
7.319	0.210	21.015	n.d.	n.d.	n.d.	n.d.	n.d.	n.d.	11.545	n.d.	n.d.	1.407	0.606	98.196
8.362	0.236	20.711	n.d.	n.d.	n.d.	n.d.	n.d.	n.d.	11.627	n.d.	n.d.	1.328	0.533	97.992
8.113	0.211	20.378	n.d.	n.d.	n.d.	n.d.	n.d.	n.d.	11.547	n.d.	n.d.	1.386	0.581	97.734
8.589	0.239	20.188	n.d.	n.d.	n.d.	n.d.	n.d.	n.d.	11.539	n.d.	n.d.	1.264	0.388	97.620
10.199	0.297	19.336	n.d.	n.d.	n.d.	n.d.	n.d.	n.d.	11.596	n.d.	n.d.	1.083	0.307	98.073
9.636	0.268	19.709	n.d.	n.d.	n.d.	n.d.	n.d.	n.d.	11.594	n.d.	n.d.	1.169	0.391	98.208
0.000	0.009	90.423	0.000	0.008	0.000	0.000	66.112	30.935	n.d.	n.d.	n.d.	n.d.	n.d.	99.261
0.001	0.009	90.757	0.000	0.009	0.000	0.000	66.337	31.066	n.d.	n.d.	n.d.	n.d.	n.d.	99.579
0.000	0.005	91.266	0.000	0.000	0.000	0.005	66.676	31.270	n.d.	n.d.	n.d.	n.d.	n.d.	100.126
0.000	0.018	90.466	0.009	0.005	0.000	0.000	65.995	31.083	n.d.	n.d.	n.d.	n.d.	n.d.	99.273
0.000	0.002	90.997	0.005	0.000	0.000	0.000	66.479	31.179	n.d.	n.d.	n.d.	n.d.	n.d.	99.805
0.003	0.001	90.731	0.000	0.008	0.000	0.005	66.353	31.026	n.d.	n.d.	n.d.	n.d.	n.d.	99.564
0.008	0.008	91.224	0.006	0.004	0.000	0.006	66.819	31.100	n.d.	n.d.	n.d.	n.d.	n.d.	99.936
0.003	0.008	90.655	0.010	0.010	0.000	0.003	66.225	31.065	n.d.	n.d.	n.d.	n.d.	n.d.	99.413
0.000	0.018	90.383	0.000	0.006	0.005	0.017	64.699	32.166	n.d.	n.d.	n.d.	n.d.	n.d.	99.828
0.000	0.009	91.358	0.000	0.000	0.000	0.006	66.812	31.240	n.d.	n.d.	n.d.	n.d.	n.d.	100.094
0.005	0.018	91.440	0.024	0.002	0.000	0.000	66.821	31.314	n.d.	n.d.	n.d.	n.d.	n.d.	100.270
0.007	0.019	91.534	0.015	0.008	0.000	0.009	66.542	31.659	n.d.	n.d.	n.d.	n.d.	n.d.	100.587
0.000	0.005	91.007	0.007	0.002	0.000	0.014	66.582	31.096	n.d.	n.d.	n.d.	n.d.	n.d.	99.743
0.014	1.365	46.976	0.003	0.005	0.005	0.009	2.588	44.647	n.d.	n.d.	n.d.	n.d.	n.d.	100.257
0.009	1.368	46.872	0.000	0.002	0.000	0.007	1.944	45.122	n.d.	n.d.	n.d.	n.d.	n.d.	100.575
0.015	1.349	46.267	0.012	0.002	0.000	0.007	1.602	44.826	n.d.	n.d.	n.d.	n.d.	n.d.	99.572
0.027	1.324	46.985	0.002	0.003	0.000	0.011	2.830	44.439	n.d.	n.d.	n.d.	n.d.	n.d.	99.995
0.028	1.321	47.248	0.001	0.000	0.000	0.002	3.020	44.530	n.d.	n.d.	n.d.	n.d.	n.d.	100.317
0.014	1.388	46.167	0.000	0.000	0.000	0.012	1.575	44.750	n.d.	n.d.	n.d.	n.d.	n.d.	99.369
0.043	1.299	46.860	0.010	0.001	0.000	0.012	2.671	44.457	n.d.	n.d.	n.d.	n.d.	n.d.	99.807
0.032	1.340	46.763	0.012	0.000	0.004	0.010	2.553	44.465	n.d.	n.d.	n.d.	n.d.	n.d.	99.872
0.035	1.364	47.434	0.005	0.000	0.000	0.011	3.509	44.277	n.d.	n.d.	n.d.	n.d.	n.d.	100.433
0.088	1.339	46.805	0.005	0.001	0.000	0.000	2.497	44.558	n.d.	n.d.	n.d.	n.d.	n.d.	100.004
0.060	1.374	46.691	0.014	0.002	0.000	0.004	2.402	44.530	n.d.	n.d.	n.d.	n.d.	n.d.	99.893
0.079	1.344	46.593	0.009	0.000	0.000	0.005	2.629	44.228	n.d.	n.d.	n.d.	n.d.	n.d.	99.445
0.018	1.350	47.140	0.003	0.000	0.003	0.003	2.962	44.475	n.d.	n.d.	n.d.	n.d.	n.d.	100.162
0.006	0.010	91.178	0.010	0.004	0.004	0.000	66.707	31.154	n.d.	n.d.	n.d.	n.d.	n.d.	100.046

Intrusion	Sample	Mineral	Sample Label	SiO2	TiO2	Al2O3	V2O3	Cr2O3	Nb2O3
Butler West	MM-V8-3	Magnetite	MMV8-3-mag1a	0.036	0.131	0.115	1.714	0.147	n.d.
Butler West	MM-V8-3	Magnetite	MMV8-3-mag1b	0.016	0.376	0.079	1.622	0.144	n.d.
Butler West	MM-V8-3	Magnetite	MMV8-3-mag1c	0.022	0.123	0.109	1.704	0.150	n.d.
Butler West	MM-V8-3	Magnetite	MMV8-3-mag2	0.022	0.137	0.125	1.759	0.155	n.d.
Butler West	MM-V8-3	Magnetite	MMV8-3-mag3	0.008	0.165	0.117	1.809	0.160	n.d.
Butler West	MM-V8-3	Magnetite	MMV8-3-mag4	0.018	0.685	0.073	1.531	0.138	n.d.
Butler West	MM-V8-3	Magnetite	MMV8-3-mag5	0.022	0.159	0.104	1.694	0.150	n.d.
Butler West	MM-V8-3	Magnetite	MMV8-3-mag6	0.023	1.428	0.111	1.385	0.133	n.d.
Butler West	MM-V8-3	Magnetite	MMV8-3-mag7a	0.021	0.060	0.219	1.788	0.154	n.d.
Butler West	MM-V8-3	Magnetite	MMV8-3-mag7b	0.024	0.366	0.173	1.653	0.141	n.d.
Butler West	MM-V8-3	Magnetite	MMV8-3-mag8	0.012	0.255	0.138	1.750	0.158	n.d.
Butler West	MM-V8-3	Magnetite	MMV8-3-mag9	0.015	0.285	0.156	1.761	0.158	n.d.
Butler West	MM-V8-3	Ilmenite	MMV8-3-ilm1a	0.003	50.983	0.016	0.335	0.028	0.000
Butler West	MM-V8-3	Ilmenite	MMV8-3-ilm1b	0.027	51.392	0.020	0.252	0.017	0.000
Butler West	MM-V8-3	Ilmenite	MMV8-3-ilm2a	0.009	51.069	0.014	0.314	0.031	0.000
Butler West	MM-V8-3	Ilmenite	MMV8-3-ilm2b	0.013	51.205	0.014	0.297	0.021	0.000
Butler West	MM-V8-3	Ilmenite	MMV8-3-ilm2c	0.002	51.010	0.023	0.300	0.028	0.007
Butler West	MM-V8-3	Ilmenite	MMV8-3-ilm3	0.002	51.196	0.017	0.290	0.027	0.000
Butler West	MM-V8-3	Ilmenite	MMV8-3-ilm4	0.016	50.826	0.053	0.315	0.033	0.000
Butler West	MM-V8-3	Ilmenite	MMV8-3-ilm5a	0.004	50.847	0.015	0.344	0.031	0.000
Butler West	MM-V8-3	Ilmenite	MMV8-3-ilm5b	0.019	51.486	0.000	0.299	0.032	0.000
Butler West	MM-V8-3	Ilmenite	MMV8-3-ilm5c	0.018	51.356	0.024	0.304	0.025	0.000
Butler West	MM-V8-3	Ilmenite	MMV8-3-ilm6	0.011	51.326	0.018	0.304	0.024	0.000
Butler West	MM-V8-4	Magnetite	MMV8-4-mag1a	0.037	0.115	0.280	1.667	0.138	n.d.
Butler West	MM-V8-4	Magnetite	MMV8-4-mag1b	0.020	0.247	0.162	1.648	0.148	n.d.
Butler West	MM-V8-4	Magnetite	MMV8-4-mag1c	0.009	0.858	0.154	1.543	0.140	n.d.
Butler West	MM-V8-4	Magnetite	MMV8-4-mag2	0.021	0.098	0.180	1.677	0.145	n.d.
Butler West	MM-V8-4	Magnetite	MMV8-4-mag3	0.040	0.117	0.180	1.697	0.147	n.d.
Butler West	MM-V8-4	Magnetite	MMV8-4-mag4	0.013	0.153	0.178	1.639	0.150	n.d.
Butler West	MM-V8-4	Magnetite	MMV8-4-mag5a	0.027	0.058	0.246	1.693	0.147	n.d.
Butler West	MM-V8-4	Magnetite	MMV8-4-mag5b	0.021	0.100	0.178	1.673	0.148	n.d.
Butler West	MM-V8-4	Magnetite	MMV8-4-mag5c	0.019	0.498	0.156	1.627	0.134	n.d.
Butler West	MM-V8-4	Magnetite	MMV8-4-mag6a	0.026	0.064	0.178	1.569	0.140	n.d.
Butler West	MM-V8-4	Magnetite	MMV8-4-mag6b	0.008	0.124	0.170	1.539	0.135	n.d.
Butler West	MM-V8-4	Magnetite	MMV8-4-mag6c	0.023	0.521	0.161	1.535	0.137	n.d.
Butler West	MM-V8-4	Magnetite	MMV8-4-mag7	0.019	0.070	0.149	1.548	0.133	n.d.
Butler West	MM-V8-4	Magnetite	MMV8-4-mag8a	0.020	0.053	0.192	1.564	0.138	n.d.
Butler West	MM-V8-4	Magnetite	MMV8-4-mag8b	0.020	0.078	0.210	1.531	0.137	n.d.
Butler West	MM-V8-4	Magnetite	MMV8-4-mag8c	0.027	0.712	0.143	1.431	0.135	n.d.
Butler West	MM-V8-4	Ilmenite	MMV8-4-ilm1a	0.006	50.977	0.013	0.284	0.022	0.000
Butler West	MM-V8-4	Ilmenite	MMV8-4-ilm1b	0.012	50.974	0.015	0.281	0.019	0.000
Butler West	MM-V8-4	Ilmenite	MMV8-4-ilm1c	0.001	51.445	0.010	0.267	0.025	0.000
Butler West	MM-V8-4	Ilmenite	MMV8-4-ilm2	0.004	51.045	0.030	0.330	0.022	0.000
Butler West	MM-V8-4	Ilmenite	MMV8-4-ilm3	0.008	50.977	0.017	0.288	0.033	0.000
Butler West	MM-V8-4	Ilmenite	MMV8-4-ilm4a	0.004	50.496	0.020	0.281	0.031	0.000
Butler West	MM-V8-4	Ilmenite	MMV8-4-ilm4b	0.000	50.445	0.027	0.303	0.034	0.000
Butler West	MM-V8-4	Ilmenite	MMV8-4-ilm4c	0.013	51.098	0.011	0.255	0.017	0.000
Butler West	MM-V8-4	Ilmenite	MMV8-4-ilm4d	0.015	51.025	0.022	0.255	0.018	0.000
Butler West	MM-V8-4	Ilmenite	MMV8-4-ilm5	0.010	51.136	0.014	0.282	0.026	0.000
Butler West	MM-V8-4	Ilmenite	MMV8-4-ilm6	0.006	51.032	0.014	0.280	0.014	0.000
Thunder Bird	NO-2G21-1	Amphibole	NO-2G21-1a-1	49.549	0.348	5.845	n.d.	0.016	n.d.
Thunder Bird	NO-2G21-1	Amphibole	NO-2G21-1a-2	52.521	0.267	2.830	n.d.	0.007	n.d.
Thunder Bird	NO-2G21-1	Amphibole	NO-2G21-1a-3	50.062	0.424	5.197	n.d.	0.000	n.d.
Thunder Bird	NO-2G21-1	Amphibole	NO-2G21-1a-4	51.637	0.360	3.700	n.d.	0.004	n.d.
Thunder Bird	NO-2G21-1	Amphibole	NO-2G21-1a-5	51.350	0.271	3.896	n.d.	0.015	n.d.
Thunder Bird	NO-2G21-1	Amphibole	NO-2G21-1a-6	47.287	0.423	7.843	n.d.	0.021	n.d.
Thunder Bird	NO-2G21-1	Amphibole	NO-2G21-1a-7	47.446	0.386	7.824	n.d.	0.017	n.d.
Thunder Bird	NO-2G21-1	Amphibole	NO-2G21-1a-8	49.945	0.431	5.505	n.d.	0.035	n.d.

MgO	MnO	FeO^t	CoO	NiO	CuO	ZnO	Fe2O3	FeO	CaO	SrO	BaO	Na2O	K2O	TOTAL
0.000	0.016	91.360	0.020	0.000	0.000	0.010	66.763	31.286	n.d.	n.d.	n.d.	n.d.	n.d.	100.238
0.000	0.005	91.338	0.003	0.004	0.000	0.000	66.484	31.515	n.d.	n.d.	n.d.	n.d.	n.d.	100.248
0.000	0.004	91.249	0.008	0.001	0.000	0.023	66.713	31.220	n.d.	n.d.	n.d.	n.d.	n.d.	100.077
0.000	0.008	90.972	0.008	0.004	0.000	0.000	66.450	31.180	n.d.	n.d.	n.d.	n.d.	n.d.	99.848
0.000	0.013	91.363	0.007	0.005	0.000	0.003	66.717	31.330	n.d.	n.d.	n.d.	n.d.	n.d.	100.335
0.002	0.022	90.811	0.000	0.009	0.000	0.002	65.734	31.663	n.d.	n.d.	n.d.	n.d.	n.d.	99.877
0.008	0.014	91.078	0.016	0.008	0.000	0.008	66.564	31.184	n.d.	n.d.	n.d.	n.d.	n.d.	99.930
0.000	0.023	91.417	0.000	0.000	0.000	0.014	65.217	32.734	n.d.	n.d.	n.d.	n.d.	n.d.	101.068
0.005	0.011	91.174	0.005	0.002	0.000	0.031	66.670	31.183	n.d.	n.d.	n.d.	n.d.	n.d.	100.150
0.000	0.010	91.092	0.014	0.007	0.000	0.018	66.267	31.464	n.d.	n.d.	n.d.	n.d.	n.d.	100.137
0.000	0.007	91.338	0.006	0.002	0.000	0.002	66.574	31.434	n.d.	n.d.	n.d.	n.d.	n.d.	100.338
0.000	0.014	91.322	0.015	0.008	0.000	0.009	66.524	31.463	n.d.	n.d.	n.d.	n.d.	n.d.	100.408
0.040	1.471	47.082	0.006	0.000	0.000	0.000	3.100	44.293	n.d.	n.d.	n.d.	n.d.	n.d.	100.275
0.035	1.433	46.685	0.018	0.000	0.000	0.005	2.183	44.721	n.d.	n.d.	n.d.	n.d.	n.d.	100.103
0.041	1.456	47.021	0.002	0.000	0.000	0.003	2.922	44.392	n.d.	n.d.	n.d.	n.d.	n.d.	100.253
0.018	1.466	46.856	0.000	0.000	0.000	0.018	2.575	44.539	n.d.	n.d.	n.d.	n.d.	n.d.	100.166
0.025	1.459	47.088	0.000	0.000	0.007	0.009	3.047	44.346	n.d.	n.d.	n.d.	n.d.	n.d.	100.263
0.020	1.440	46.676	0.001	0.005	0.000	0.000	2.362	44.550	n.d.	n.d.	n.d.	n.d.	n.d.	99.911
0.060	1.434	47.177	0.000	0.000	0.017	0.005	3.358	44.155	n.d.	n.d.	n.d.	n.d.	n.d.	100.272
0.050	1.456	46.815	0.009	0.000	0.000	0.011	2.954	44.157	n.d.	n.d.	n.d.	n.d.	n.d.	99.878
0.054	1.460	46.729	0.016	0.000	0.004	0.005	2.218	44.733	n.d.	n.d.	n.d.	n.d.	n.d.	100.326
0.049	1.508	46.604	0.015	0.004	0.000	0.011	2.260	44.571	n.d.	n.d.	n.d.	n.d.	n.d.	100.144
0.026	1.477	46.658	0.007	0.000	0.000	0.002	2.257	44.627	n.d.	n.d.	n.d.	n.d.	n.d.	100.079
0.005	0.009	91.750	0.024	0.003	0.000	0.027	67.022	31.443	n.d.	n.d.	n.d.	n.d.	n.d.	100.770
0.000	0.004	91.331	0.012	0.002	0.000	0.021	66.607	31.397	n.d.	n.d.	n.d.	n.d.	n.d.	100.269
0.006	0.018	91.258	0.013	0.005	0.000	0.013	65.819	32.034	n.d.	n.d.	n.d.	n.d.	n.d.	100.612
0.003	0.013	91.286	0.005	0.000	0.000	0.000	66.743	31.230	n.d.	n.d.	n.d.	n.d.	n.d.	100.115
0.007	0.003	91.291	0.018	0.007	0.000	0.011	66.699	31.275	n.d.	n.d.	n.d.	n.d.	n.d.	100.201
0.000	0.015	90.670	0.018	0.006	0.000	0.000	66.251	31.057	n.d.	n.d.	n.d.	n.d.	n.d.	99.480
0.007	0.002	90.970	0.008	0.000	0.000	0.005	66.513	31.121	n.d.	n.d.	n.d.	n.d.	n.d.	99.827
0.001	0.007	90.630	0.016	0.003	0.000	0.000	66.258	31.010	n.d.	n.d.	n.d.	n.d.	n.d.	99.416
0.000	0.014	91.035	0.023	0.004	0.000	0.000	66.074	31.581	n.d.	n.d.	n.d.	n.d.	n.d.	100.130
0.009	0.013	90.878	0.018	0.001	0.000	0.014	66.545	31.000	n.d.	n.d.	n.d.	n.d.	n.d.	99.577
0.003	0.013	91.357	0.014	0.004	0.000	0.000	66.851	31.204	n.d.	n.d.	n.d.	n.d.	n.d.	100.065
0.000	0.014	90.908	0.015	0.000	0.000	0.002	65.964	31.553	n.d.	n.d.	n.d.	n.d.	n.d.	99.925
0.004	0.004	91.525	0.010	0.004	0.000	0.009	67.034	31.207	n.d.	n.d.	n.d.	n.d.	n.d.	100.191
0.004	0.007	91.094	0.014	0.007	0.000	0.029	66.726	31.054	n.d.	n.d.	n.d.	n.d.	n.d.	99.807
0.011	0.010	90.973	0.020	0.001	0.000	0.009	66.604	31.042	n.d.	n.d.	n.d.	n.d.	n.d.	99.673
0.000	0.009	90.910	0.009	0.009	0.000	0.025	65.764	31.735	n.d.	n.d.	n.d.	n.d.	n.d.	99.999
0.025	1.201	47.112	0.013	0.000	0.000	0.013	2.822	44.573	n.d.	n.d.	n.d.	n.d.	n.d.	99.949
0.043	1.199	46.837	0.008	0.009	0.000	0.010	2.546	44.546	n.d.	n.d.	n.d.	n.d.	n.d.	99.662
0.040	1.189	47.007	0.010	0.000	0.000	0.018	2.262	44.972	n.d.	n.d.	n.d.	n.d.	n.d.	100.239
0.039	1.241	46.735	0.000	0.000	0.000	0.001	2.384	44.590	n.d.	n.d.	n.d.	n.d.	n.d.	99.686
0.021	1.234	46.802	0.015	0.000	0.007	0.000	2.500	44.553	n.d.	n.d.	n.d.	n.d.	n.d.	99.652
0.049	1.187	47.371	0.024	0.000	0.006	0.008	3.637	44.098	n.d.	n.d.	n.d.	n.d.	n.d.	99.841
0.050	1.206	47.423	0.010	0.000	0.000	0.003	3.749	44.050	n.d.	n.d.	n.d.	n.d.	n.d.	99.877
0.059	1.192	46.959	0.013	0.000	0.000	0.019	2.584	44.634	n.d.	n.d.	n.d.	n.d.	n.d.	99.895
0.050	1.184	46.798	0.010	0.000	0.000	0.005	2.432	44.610	n.d.	n.d.	n.d.	n.d.	n.d.	99.626
0.036	1.230	46.950	0.004	0.000	0.000	0.005	2.514	44.688	n.d.	n.d.	n.d.	n.d.	n.d.	99.945
0.050	1.210	46.785	0.004	0.005	0.000	0.015	2.461	44.571	n.d.	n.d.	n.d.	n.d.	n.d.	99.662
11.727	0.279	17.369	n.d.	n.d.	n.d.	n.d.	n.d.	n.d.	11.680	n.d.	n.d.	0.695	0.097	97.605
13.388	0.267	15.980	n.d.	n.d.	n.d.	n.d.	n.d.	n.d.	11.947	n.d.	n.d.	0.380	0.035	97.622
11.824	0.281	17.565	n.d.	n.d.	n.d.	n.d.	n.d.	n.d.	11.896	n.d.	n.d.	0.648	0.056	97.953
12.808	0.286	16.709	n.d.	n.d.	n.d.	n.d.	n.d.	n.d.	11.981	n.d.	n.d.	0.510	0.037	98.032
12.898	0.250	16.414	n.d.	n.d.	n.d.	n.d.	n.d.	n.d.	11.867	n.d.	n.d.	0.474	0.049	97.484
10.052	0.223	19.089	n.d.	n.d.	n.d.	n.d.	n.d.	n.d.	11.763	n.d.	n.d.	1.003	0.139	97.843
10.235	0.247	19.182	n.d.	n.d.	n.d.	n.d.	n.d.	n.d.	11.777	n.d.	n.d.	0.948	0.127	98.189
11.826	0.263	17.793	n.d.	n.d.	n.d.	n.d.	n.d.	n.d.	11.867	n.d.	n.d.	0.713	0.101	98.479

Intrusion	Sample	Mineral	Sample Label	SiO2	TiO2	Al2O3	V2O3	Cr2O3	Nb2O3
Thunder Bird	NO-2G21-1	Amphibole	NO-2G21-1a-9	44.676	1.483	9.500	n.d.	0.019	n.d.
Thunder Bird	NO-2G21-1	Amphibole	NO-2G21-1a-10	43.759	0.589	11.176	n.d.	0.026	n.d.
Thunder Bird	NO-2G21-1	Amphibole	NO-2G21-1a-11	45.675	0.634	8.752	n.d.	0.008	n.d.
Thunder Bird	NO-2G21-1	Amphibole	NO-2G21-1a-12	40.305	0.297	15.249	n.d.	0.017	n.d.
Thunder Bird	NO-2G21-1	Amphibole	NO-2G21-1b-14	51.507	0.275	4.246	n.d.	0.009	n.d.
Thunder Bird	NO-2G21-1	Amphibole	NO-2G21-1b-15	51.296	0.179	4.254	n.d.	0.035	n.d.
Thunder Bird	NO-2G21-1	Amphibole	NO-2G21-1b-16	51.906	0.158	3.501	n.d.	0.008	n.d.
Thunder Bird	NO-2G21-1	Amphibole	NO-2G21-1b-17	50.665	0.157	5.038	n.d.	0.028	n.d.
Thunder Bird	NO-2G21-1	Amphibole	NO-2G21-1b-18	51.290	0.177	4.347	n.d.	0.005	n.d.
Thunder Bird	NO-2G21-1	Amphibole	NO-2G21-1b-19	52.299	0.139	3.393	n.d.	0.000	n.d.
Thunder Bird	NO-2G21-1	Amphibole	NO-2G21-1b-20	46.348	0.100	2.928	n.d.	0.017	n.d.
Thunder Bird	NO-2G21-1	Amphibole	NO-2G21-1b-21	51.724	0.124	3.993	n.d.	0.000	n.d.
Thunder Bird	NO-2G21-1	Amphibole	NO-2G21-1b-22	52.416	0.217	3.208	n.d.	0.001	n.d.
Thunder Bird	NO-2G21-1	Amphibole	NO-2G21-1b-23	50.971	0.131	4.663	n.d.	0.021	n.d.
Thunder Bird	NO-2G21-1	Amphibole	NO-2G21-1b-24?	41.810	0.319	13.370	n.d.	0.007	n.d.
Thunder Bird	NO-2G21-1	Amphibole	NO-2G21-1b-25?	42.547	0.362	12.990	n.d.	0.033	n.d.
Thunder Bird	NO-2G21-1	Amphibole	NO-2G21-1c-26	49.648	0.164	6.050	n.d.	0.000	n.d.
Thunder Bird	NO-2G21-1	Amphibole	NO-2G21-1c-27	48.204	0.195	7.398	n.d.	0.000	n.d.
Thunder Bird	NO-2G21-1	Amphibole	NO-2G21-1c-28	48.900	0.198	6.950	n.d.	0.025	n.d.
Thunder Bird	NO-2G21-1	Amphibole	NO-2G21-1c-29	52.204	0.095	3.181	n.d.	0.020	n.d.
Thunder Bird	NO-2G21-1	Amphibole	NO-2G21-1c-30	51.615	0.143	4.318	n.d.	0.017	n.d.
Thunder Bird	NO-2G21-1	Amphibole	NO-2G21-1c-31	47.623	0.214	7.513	n.d.	0.024	n.d.
Thunder Bird	NO-2G21-1	Amphibole	NO-2G21-1c-32	47.515	0.224	8.004	n.d.	0.008	n.d.
Thunder Bird	NO-2G21-1	Amphibole	NO-2G21-1c-33	52.380	0.105	3.708	n.d.	0.000	n.d.
Thunder Bird	NO-2G21-1	Amphibole	NO-2G21-1c-34?	41.572	0.312	13.416	n.d.	0.026	n.d.
Thunder Bird	NO-2G21-1	Amphibole	NO-2G21-1c-35	45.116	0.308	10.650	n.d.	0.033	n.d.
Thunder Bird	NO-2G21-1	Amphibole	NO-2G21-1c-36	54.286	0.046	1.871	n.d.	0.000	n.d.
Thunder Bird	NO-2G21-1	Amphibole	NO-2G21-1c-37	47.140	0.241	8.472	n.d.	0.012	n.d.
Thunder Bird	NO-2G21-10	Magnetite	NO2G21-10-mag10	0.022	0.098	0.133	1.780	0.315	n.d.
Thunder Bird	NO-2G21-10	Magnetite	NO2G21-10-mag1a	0.035	0.151	0.122	1.787	0.321	n.d.
Thunder Bird	NO-2G21-10	Magnetite	NO2G21-10-mag1b	0.009	0.741	0.098	1.780	0.388	n.d.
Thunder Bird	NO-2G21-10	Magnetite	NO2G21-10-mag1c	0.019	0.229	0.105	1.761	0.375	n.d.
Thunder Bird	NO-2G21-10	Magnetite	NO2G21-10-mag2	0.010	0.179	0.103	1.724	0.409	n.d.
Thunder Bird	NO-2G21-10	Magnetite	NO2G21-10-mag3	0.027	0.299	0.057	1.742	0.381	n.d.
Thunder Bird	NO-2G21-10	Magnetite	NO2G21-10-mag4	0.026	0.050	0.086	1.802	0.310	n.d.
Thunder Bird	NO-2G21-10	Magnetite	NO2G21-10-mag5	0.013	0.127	0.161	1.811	0.313	n.d.
Thunder Bird	NO-2G21-10	Magnetite	NO2G21-10-mag6a	0.023	0.440	0.096	1.783	0.363	n.d.
Thunder Bird	NO-2G21-10	Magnetite	NO2G21-10-mag6b	0.028	0.184	0.133	1.789	0.348	n.d.
Thunder Bird	NO-2G21-10	Magnetite	NO2G21-10-mag7	0.027	0.247	0.120	1.801	0.311	n.d.
Thunder Bird	NO-2G21-10	Magnetite	NO2G21-10-mag8	0.009	1.057	0.069	1.466	0.463	n.d.
Thunder Bird	NO-2G21-10	Magnetite	NO2G21-10-mag9	0.047	0.115	0.156	1.792	0.310	n.d.
Thunder Bird	NO-2G21-10	Ilmenite	NO2G21-10-ilm1a	0.001	50.732	0.023	0.368	0.053	0.000
Thunder Bird	NO-2G21-10	Ilmenite	NO2G21-10-ilm1b	0.001	50.582	0.010	0.373	0.043	0.000
Thunder Bird	NO-2G21-10	Ilmenite	NO2G21-10-ilm1c	0.002	50.558	0.014	0.313	0.039	0.000
Thunder Bird	NO-2G21-10	Ilmenite	NO2G21-10-ilm2a	0.010	50.744	0.011	0.318	0.043	0.000
Thunder Bird	NO-2G21-10	Ilmenite	NO2G21-10-ilm2b	0.000	50.550	0.005	0.330	0.042	0.000
Thunder Bird	NO-2G21-10	Ilmenite	NO2G21-10-ilm2c	0.010	50.796	0.006	0.315	0.060	0.000
Thunder Bird	NO-2G21-10	Ilmenite	NO2G21-10-ilm2d	0.007	50.467	0.012	0.316	0.057	0.000
Thunder Bird	NO-2G21-10	Ilmenite	NO2G21-10-ilm3	0.000	51.112	0.008	0.308	0.045	0.000
Thunder Bird	NO-2G21-10	Ilmenite	NO2G21-10-ilm4	0.018	51.207	0.008	0.320	0.031	0.000
Thunder Bird	NO-2G21-10	Ilmenite	NO2G21-10-ilm5a	0.006	50.638	0.014	0.332	0.041	0.000
Thunder Bird	NO-2G21-10	Ilmenite	NO2G21-10-ilm5b	0.000	50.836	0.014	0.349	0.050	0.000
Thunder Bird	NO-2G21-10	Ilmenite	NO2G21-10-ilm6a	0.007	51.028	0.007	0.339	0.046	0.000
Thunder Bird	NO-2G21-10	Ilmenite	NO2G21-10-ilm6b	0.001	50.906	0.000	0.379	0.047	0.000
Thunder Bird	NO-2G21-10	Ilmenite	NO2G21-10-ilm7	0.009	50.652	0.018	0.405	0.079	0.000
Thunder Bird	NO-2G21-10	Ilmenite	NO2G21-10-ilm8	0.009	50.615	0.010	0.397	0.061	0.000
Thunder Bird	NO-2G21-11	Magnetite	NO2G21-11-mag1a	0.011	0.350	0.108	1.888	0.188	n.d.
Thunder Bird	NO-2G21-11	Magnetite	NO2G21-11-mag1b	0.011	0.250	0.079	1.833	0.181	n.d.

MgO	MnO	FeO^t	CoO	NiO	CuO	ZnO	Fe2O3	FeO	CaO	SrO	BaO	Na2O	K2O	TOTAL
0.000	0.013	91.021	0.014	0.006	0.000	0.001	66.097	31.546	n.d.	n.d.	n.d.	n.d.	n.d.	100.280
0.000	0.012	90.754	0.000	0.005	0.001	0.004	65.888	31.467	n.d.	n.d.	n.d.	n.d.	n.d.	99.925
0.000	0.007	91.389	0.014	0.008	0.000	0.007	66.529	31.526	n.d.	n.d.	n.d.	n.d.	n.d.	100.585
0.000	0.010	90.894	0.009	0.013	0.000	0.014	66.074	31.440	n.d.	n.d.	n.d.	n.d.	n.d.	100.138
0.000	0.009	91.066	0.003	0.019	0.006	0.000	66.256	31.448	n.d.	n.d.	n.d.	n.d.	n.d.	100.212
0.000	0.000	90.782	0.010	0.010	0.000	0.019	66.011	31.385	n.d.	n.d.	n.d.	n.d.	n.d.	100.037
0.000	0.006	91.267	0.002	0.011	0.000	0.011	66.629	31.314	n.d.	n.d.	n.d.	n.d.	n.d.	100.278
0.001	0.007	91.239	0.006	0.008	0.000	0.013	66.022	31.832	n.d.	n.d.	n.d.	n.d.	n.d.	100.476
0.000	0.008	90.886	0.008	0.012	0.000	0.000	65.794	31.684	n.d.	n.d.	n.d.	n.d.	n.d.	100.045
0.000	0.007	91.237	0.002	0.007	0.000	0.002	66.111	31.749	n.d.	n.d.	n.d.	n.d.	n.d.	100.379
0.000	0.005	91.153	0.012	0.007	0.002	0.000	66.739	31.101	n.d.	n.d.	n.d.	n.d.	n.d.	99.809
0.000	0.000	91.247	0.000	0.000	0.000	0.006	66.256	31.629	n.d.	n.d.	n.d.	n.d.	n.d.	100.308
0.000	0.010	91.075	0.020	0.006	0.000	0.012	66.139	31.562	n.d.	n.d.	n.d.	n.d.	n.d.	100.176
0.000	0.012	90.899	0.019	0.012	0.000	0.010	65.659	31.818	n.d.	n.d.	n.d.	n.d.	n.d.	100.133
0.013	0.920	47.429	0.016	0.000	0.008	0.016	3.173	44.574	n.d.	n.d.	n.d.	n.d.	n.d.	99.803
0.013	0.926	47.234	0.020	0.002	0.000	0.011	2.568	44.923	n.d.	n.d.	n.d.	n.d.	n.d.	99.952
0.003	0.896	47.654	0.014	0.000	0.000	0.003	2.918	45.028	n.d.	n.d.	n.d.	n.d.	n.d.	100.318
0.010	0.929	47.452	0.014	0.003	0.000	0.000	2.914	44.830	n.d.	n.d.	n.d.	n.d.	n.d.	100.007
0.013	0.919	47.482	0.010	0.000	0.003	0.016	3.086	44.705	n.d.	n.d.	n.d.	n.d.	n.d.	99.965
0.013	0.921	47.658	0.017	0.000	0.000	0.002	3.462	44.543	n.d.	n.d.	n.d.	n.d.	n.d.	100.013
0.015	0.949	47.792	0.007	0.002	0.000	0.000	3.207	44.907	n.d.	n.d.	n.d.	n.d.	n.d.	100.532
0.012	0.945	47.700	0.007	0.004	0.000	0.023	3.747	44.329	n.d.	n.d.	n.d.	n.d.	n.d.	99.901
0.003	0.935	47.577	0.011	0.000	0.003	0.000	2.740	45.112	n.d.	n.d.	n.d.	n.d.	n.d.	100.369
0.018	0.922	47.119	0.006	0.002	0.000	0.010	2.487	44.881	n.d.	n.d.	n.d.	n.d.	n.d.	99.665
0.015	0.912	47.631	0.009	0.000	0.006	0.019	3.025	44.910	n.d.	n.d.	n.d.	n.d.	n.d.	100.292
0.015	0.899	47.119	0.017	0.003	0.008	0.000	2.813	44.588	n.d.	n.d.	n.d.	n.d.	n.d.	99.384
0.009	0.919	47.764	0.007	0.000	0.000	0.019	3.739	44.400	n.d.	n.d.	n.d.	n.d.	n.d.	99.922
0.006	0.919	47.630	0.017	0.000	0.000	0.015	3.326	44.637	n.d.	n.d.	n.d.	n.d.	n.d.	100.011
0.000	0.991	47.245	0.015	0.006	0.008	0.000	1.775	45.648	n.d.	n.d.	n.d.	n.d.	n.d.	100.661
0.000	0.000	0.061	n.d.	n.d.	n.d.	n.d.	n.d.	n.d.	0.317	0.000	0.000	11.872	0.046	89.175
0.008	0.003	0.102	n.d.	n.d.	n.d.	n.d.	n.d.	n.d.	0.265	0.000	0.000	11.847	0.057	89.226
15.474	0.288	13.710	n.d.	n.d.	n.d.	n.d.	n.d.	n.d.	12.161	n.d.	n.d.	0.209	0.024	98.222
15.450	0.273	13.669	n.d.	n.d.	n.d.	n.d.	n.d.	n.d.	11.967	n.d.	n.d.	0.229	0.030	98.417
11.621	0.279	17.235	n.d.	n.d.	n.d.	n.d.	n.d.	n.d.	11.709	n.d.	n.d.	0.803	0.195	97.916
15.001	0.272	14.479	n.d.	n.d.	n.d.	n.d.	n.d.	n.d.	11.951	n.d.	n.d.	0.297	0.050	98.255
16.065	0.244	13.235	n.d.	n.d.	n.d.	n.d.	n.d.	n.d.	11.951	n.d.	n.d.	0.129	0.006	97.884
16.243	0.228	12.897	n.d.	n.d.	n.d.	n.d.	n.d.	n.d.	12.219	n.d.	n.d.	0.160	0.020	98.176
17.478	0.304	11.584	n.d.	n.d.	n.d.	n.d.	n.d.	n.d.	12.193	n.d.	n.d.	0.122	0.016	98.682
16.269	0.314	13.209	n.d.	n.d.	n.d.	n.d.	n.d.	n.d.	11.991	n.d.	n.d.	0.129	0.007	98.643
16.164	0.309	12.728	n.d.	n.d.	n.d.	n.d.	n.d.	n.d.	12.334	n.d.	n.d.	0.096	0.016	98.293
15.806	0.252	13.596	n.d.	n.d.	n.d.	n.d.	n.d.	n.d.	11.975	n.d.	n.d.	0.221	0.030	98.394
15.267	0.246	13.540	n.d.	n.d.	n.d.	n.d.	n.d.	n.d.	12.158	n.d.	n.d.	0.227	0.031	97.638
16.272	0.266	12.966	n.d.	n.d.	n.d.	n.d.	n.d.	n.d.	12.207	n.d.	n.d.	0.122	0.008	98.033
15.376	0.288	13.856	n.d.	n.d.	n.d.	n.d.	n.d.	n.d.	12.151	n.d.	n.d.	0.236	0.024	98.522
9.647	0.260	19.093	n.d.	n.d.	n.d.	n.d.	n.d.	n.d.	11.461	n.d.	n.d.	1.126	0.242	97.488
15.463	0.257	13.801	n.d.	n.d.	n.d.	n.d.	n.d.	n.d.	12.279	n.d.	n.d.	0.250	0.026	98.783
0.000	0.078	12.333	n.d.	n.d.	n.d.	n.d.	n.d.	n.d.	23.241	n.d.	n.d.	0.000	0.000	97.368
0.000	0.001	0.102	n.d.	n.d.	n.d.	n.d.	n.d.	n.d.	11.862	0.000	0.000	4.861	0.087	95.186
0.000	0.002	0.102	n.d.	n.d.	n.d.	n.d.	n.d.	n.d.	12.599	0.146	0.025	4.548	0.014	95.668
0.000	0.000	0.131	n.d.	n.d.	n.d.	n.d.	n.d.	n.d.	11.875	0.015	0.000	4.907	0.038	95.228
0.004	0.000	0.052	n.d.	n.d.	n.d.	n.d.	n.d.	n.d.	12.011	0.000	0.005	4.832	0.037	95.004
0.000	0.000	0.151	n.d.	n.d.	n.d.	n.d.	n.d.	n.d.	11.973	0.000	0.000	4.891	0.028	94.580
0.000	0.000	0.122	n.d.	n.d.	n.d.	n.d.	n.d.	n.d.	11.930	0.000	0.000	4.859	0.019	94.719
0.000	0.009	0.148	n.d.	n.d.	n.d.	n.d.	n.d.	n.d.	11.700	0.053	0.012	4.900	0.022	94.190
0.018	0.000	0.095	n.d.	n.d.	n.d.	n.d.	n.d.	n.d.	11.526	0.023	0.028	5.044	0.042	94.571
0.000	0.000	0.047	n.d.	n.d.	n.d.	n.d.	n.d.	n.d.	11.996	0.054	0.013	4.833	0.034	95.148
0.022	0.000	0.129	n.d.	n.d.	n.d.	n.d.	n.d.	n.d.	11.093	0.093	0.049	5.009	0.332	94.420
0.006	0.001	0.061	n.d.	n.d.	n.d.	n.d.	n.d.	n.d.	11.568	0.085	0.004	5.099	0.020	95.057

Intrusion	Sample	Mineral	Sample Label	SiO2	TiO2	Al2O3	V2O3	Cr2O3	Nb2O3
Thunder Bird	NO-2G21-5	Pyroxene	NO-2G21-5a-3	38.253	0.006	24.833	n.d.	0.057	n.d.
Thunder Bird	NO-2G21-5	Pyroxene	NO-2G21-5a-6	38.425	0.029	26.256	n.d.	0.052	n.d.
Thunder Bird	NO-2G21-5	Pyroxene	NO-2G21-5a-9	38.289	0.016	25.131	n.d.	0.074	n.d.
Thunder Bird	NO-2G21-6	Magnetite	NO2G21-6-mag1a	0.004	0.459	0.100	1.866	0.264	n.d.
Thunder Bird	NO-2G21-6	Magnetite	NO2G21-6-mag1b	0.007	0.457	0.103	1.856	0.270	n.d.
Thunder Bird	NO-2G21-6	Magnetite	NO2G21-6-mag2a	0.016	0.607	0.096	1.879	0.288	n.d.
Thunder Bird	NO-2G21-6	Magnetite	NO2G21-6-mag2b	0.007	0.393	0.108	1.874	0.270	n.d.
Thunder Bird	NO-2G21-6	Magnetite	NO2G21-6-mag3	0.014	0.348	0.096	1.874	0.271	n.d.
Thunder Bird	NO-2G21-6	Magnetite	NO2G21-6-mag4a	0.012	0.500	0.102	1.853	0.238	n.d.
Thunder Bird	NO-2G21-6	Magnetite	NO2G21-6-mag4b	0.007	0.125	0.087	1.841	0.184	n.d.
Thunder Bird	NO-2G21-6	Magnetite	NO2G21-6-mag5a	0.005	0.347	0.098	1.642	0.238	n.d.
Thunder Bird	NO-2G21-6	Magnetite	NO2G21-6-mag5b	0.018	0.431	0.096	1.651	0.239	n.d.
Thunder Bird	NO-2G21-6	Magnetite	NO2G21-6-mag6a	0.019	0.475	0.109	1.642	0.232	n.d.
Thunder Bird	NO-2G21-6	Magnetite	NO2G21-6-mag6b	0.015	0.471	0.103	1.637	0.229	n.d.
Thunder Bird	NO-2G21-6	Magnetite	NO2G21-6-mag6c	0.020	0.677	0.098	1.636	0.257	n.d.
Thunder Bird	NO-2G21-6	Magnetite	NO2G21-6-mag7	0.020	0.483	0.109	1.634	0.229	n.d.
Thunder Bird	NO-2G21-6	Magnetite	NO2G21-6-mag8	0.014	0.437	0.096	1.656	0.228	n.d.
Thunder Bird	NO-2G21-6	Ilmenite	NO2G21-6-ilm1a	0.006	50.331	0.010	0.401	0.047	0.000
Thunder Bird	NO-2G21-6	Ilmenite	NO2G21-6-ilm1b	0.005	50.310	0.010	0.400	0.046	0.000
Thunder Bird	NO-2G21-6	Ilmenite	NO2G21-6-ilm1c	0.012	50.489	0.014	0.352	0.039	0.000
Thunder Bird	NO-2G21-6	Ilmenite	NO2G21-6-ilm2	0.003	50.466	0.010	0.396	0.044	0.000
Thunder Bird	NO-2G21-6	Ilmenite	NO2G21-6-ilm3	0.001	50.893	0.008	0.402	0.041	0.000
Thunder Bird	NO-2G21-6	Ilmenite	NO2G21-6-ilm4	0.016	50.973	0.016	0.330	0.049	0.000
Thunder Bird	NO-2G21-6	Ilmenite	NO2G21-6-ilm5	0.008	51.189	0.009	0.311	0.024	0.000
Thunder Bird	NO-2G21-6	Ilmenite	NO2G21-6-ilm6	0.018	50.290	0.009	0.362	0.042	0.000
Thunder Bird	NO-2G21-6	Ilmenite	NO2G21-6-ilm7	0.008	51.225	0.020	0.342	0.034	0.000
Thunder Bird	NO-2G21-7	Magnetite	NO2G21-7-mag10	0.023	0.106	0.051	1.753	0.904	n.d.
Thunder Bird	NO-2G21-7	Magnetite	NO2G21-7-mag11	0.023	0.286	0.039	1.678	0.940	n.d.
Thunder Bird	NO-2G21-7	Magnetite	NO2G21-7-mag12	0.021	0.116	0.064	1.738	0.682	n.d.
Thunder Bird	NO-2G21-7	Magnetite	NO2G21-7-mag1a	0.139	0.190	0.236	1.711	0.678	n.d.
Thunder Bird	NO-2G21-7	Magnetite	NO2G21-7-mag1b	0.044	0.167	0.122	1.702	0.715	n.d.
Thunder Bird	NO-2G21-7	Magnetite	NO2G21-7-mag2	0.019	0.136	0.083	1.690	0.823	n.d.
Thunder Bird	NO-2G21-7	Magnetite	NO2G21-7-mag3	0.019	0.205	0.072	1.665	0.989	n.d.
Thunder Bird	NO-2G21-7	Magnetite	NO2G21-7-mag4	0.065	0.221	0.135	1.702	0.680	n.d.
Thunder Bird	NO-2G21-7	Magnetite	NO2G21-7-mag5	0.010	0.420	0.107	1.726	0.752	n.d.
Thunder Bird	NO-2G21-7	Magnetite	NO2G21-7-mag6	0.033	0.148	0.070	1.742	0.621	n.d.
Thunder Bird	NO-2G21-7	Magnetite	NO2G21-7-mag7	0.033	0.157	0.079	1.708	0.831	n.d.
Thunder Bird	NO-2G21-7	Magnetite	NO2G21-7-mag8	0.015	0.141	0.069	1.738	0.686	n.d.
Thunder Bird	NO-2G21-7	Magnetite	NO2G21-7-mag9	0.024	0.165	0.073	1.664	0.922	n.d.
Thunder Bird	NO-2G21-7	Ilmenite	NO2G21-7-ilm1a	0.008	50.171	0.004	0.328	0.068	0.000
Thunder Bird	NO-2G21-7	Ilmenite	NO2G21-7-ilm1b	0.013	50.285	0.008	0.243	0.055	0.000
Thunder Bird	NO-2G21-7	Ilmenite	NO2G21-7-ilm1c	0.011	50.451	0.010	0.307	0.097	0.000
Thunder Bird	NO-2G21-7	Ilmenite	NO2G21-7-ilm2a	0.008	51.046	0.013	0.220	0.047	0.000
Thunder Bird	NO-2G21-7	Ilmenite	NO2G21-7-ilm2b	0.004	51.536	0.009	0.210	0.054	0.000
Thunder Bird	NO-2G21-7	Ilmenite	NO2G21-7-ilm3	0.009	50.913	0.016	0.325	0.091	0.000
Thunder Bird	NO-2G21-7	Ilmenite	NO2G21-7-ilm4a	0.008	50.442	0.008	0.353	0.063	0.000
Thunder Bird	NO-2G21-7	Ilmenite	NO2G21-7-ilm4b	0.004	51.282	0.012	0.354	0.053	0.000
Thunder Bird	NO-2G21-7	Ilmenite	NO2G21-7-ilm4c	0.015	51.319	0.013	0.243	0.058	0.000
Thunder Bird	NO-2G21-7	Ilmenite	NO2G21-7-ilm5	0.005	50.874	0.013	0.307	0.062	0.000
Thunder Bird	NO-2G21-7	Ilmenite	NO2G21-7-ilm6	0.020	51.073	0.013	0.319	0.063	0.000
Thunder Bird	NO-2G21-7	Ilmenite	NO2G21-7-ilm7	0.065	50.422	0.053	0.374	0.081	0.000
Thunder Bird	NO-2G21-9	Magnetite	NO2G21-9-mag1a	0.022	1.059	0.081	1.710	0.482	n.d.
Thunder Bird	NO-2G21-9	Magnetite	NO2G21-9-mag1b	0.022	0.723	0.074	1.676	0.500	n.d.
Thunder Bird	NO-2G21-9	Magnetite	NO2G21-9-mag2	0.016	0.561	0.051	1.729	0.575	n.d.
Thunder Bird	NO-2G21-9	Magnetite	NO2G21-9-mag3a	0.016	0.809	0.083	1.721	0.477	n.d.
Thunder Bird	NO-2G21-9	Magnetite	NO2G21-9-mag3b	0.014	0.442	0.039	1.660	0.478	n.d.
Thunder Bird	NO-2G21-9	Magnetite	NO2G21-9-mag4	0.020	0.351	0.071	1.723	0.483	n.d.
Thunder Bird	NO-2G21-9	Magnetite	NO2G21-9-mag5	0.024	0.105	0.062	1.724	0.467	n.d.

MgO	MnO	FeO^t	CoO	NiO	CuO	ZnO	Fe2O3	FeO	CaO	SrO	BaO	Na2O	K2O	TOTAL
0.018	0.052	10.818	n.d.	n.d.	n.d.	n.d.	n.d.	n.d.	23.342	n.d.	n.d.	0.000	0.000	97.379
0.003	0.118	9.338	n.d.	n.d.	n.d.	n.d.	n.d.	n.d.	23.357	n.d.	n.d.	0.000	0.000	97.578
0.000	0.074	10.141	n.d.	n.d.	n.d.	n.d.	n.d.	n.d.	23.311	n.d.	n.d.	0.000	0.000	97.036
0.000	0.013	90.873	0.000	0.011	0.000	0.007	65.924	31.554	n.d.	n.d.	n.d.	n.d.	n.d.	100.202
0.000	0.010	90.559	0.012	0.024	0.000	0.006	65.703	31.439	n.d.	n.d.	n.d.	n.d.	n.d.	99.887
0.000	0.014	90.665	0.011	0.014	0.000	0.020	65.559	31.674	n.d.	n.d.	n.d.	n.d.	n.d.	100.179
0.000	0.013	90.755	0.005	0.020	0.000	0.009	65.921	31.439	n.d.	n.d.	n.d.	n.d.	n.d.	100.059
0.000	0.012	90.805	0.014	0.029	0.000	0.007	66.022	31.398	n.d.	n.d.	n.d.	n.d.	n.d.	100.085
0.000	0.008	90.734	0.003	0.013	0.000	0.007	65.764	31.559	n.d.	n.d.	n.d.	n.d.	n.d.	100.059
0.000	0.000	90.915	0.014	0.026	0.000	0.000	66.445	31.128	n.d.	n.d.	n.d.	n.d.	n.d.	99.856
0.000	0.009	91.149	0.019	0.016	0.000	0.000	66.375	31.424	n.d.	n.d.	n.d.	n.d.	n.d.	100.173
0.000	0.007	91.174	0.003	0.021	0.000	0.000	66.247	31.565	n.d.	n.d.	n.d.	n.d.	n.d.	100.277
0.000	0.008	91.093	0.017	0.024	0.000	0.001	66.138	31.581	n.d.	n.d.	n.d.	n.d.	n.d.	100.247
0.000	0.000	91.051	0.008	0.022	0.000	0.000	66.111	31.564	n.d.	n.d.	n.d.	n.d.	n.d.	100.160
0.000	0.006	91.050	0.018	0.016	0.000	0.020	65.841	31.806	n.d.	n.d.	n.d.	n.d.	n.d.	100.395
0.000	0.012	91.016	0.018	0.016	0.001	0.006	66.075	31.561	n.d.	n.d.	n.d.	n.d.	n.d.	100.164
0.000	0.011	90.735	0.005	0.017	0.000	0.013	65.933	31.408	n.d.	n.d.	n.d.	n.d.	n.d.	99.818
0.013	0.940	47.897	0.015	0.003	0.000	0.016	4.030	44.270	n.d.	n.d.	n.d.	n.d.	n.d.	100.083
0.010	0.937	47.374	0.011	0.001	0.000	0.003	3.443	44.276	n.d.	n.d.	n.d.	n.d.	n.d.	99.452
0.015	0.975	47.153	0.018	0.000	0.000	0.003	3.068	44.392	n.d.	n.d.	n.d.	n.d.	n.d.	99.377
0.014	0.964	47.473	0.012	0.000	0.008	0.005	3.448	44.370	n.d.	n.d.	n.d.	n.d.	n.d.	99.740
0.009	0.955	47.520	0.003	0.001	0.000	0.002	3.037	44.788	n.d.	n.d.	n.d.	n.d.	n.d.	100.139
0.000	0.971	47.291	0.025	0.000	0.000	0.009	2.712	44.851	n.d.	n.d.	n.d.	n.d.	n.d.	99.952
0.007	0.973	47.182	0.006	0.000	0.000	0.003	2.375	45.045	n.d.	n.d.	n.d.	n.d.	n.d.	99.950
0.017	0.968	48.025	0.014	0.007	0.000	0.010	4.234	44.215	n.d.	n.d.	n.d.	n.d.	n.d.	100.186
0.005	0.979	47.669	0.002	0.006	0.000	0.012	2.894	45.065	n.d.	n.d.	n.d.	n.d.	n.d.	100.592
0.000	0.004	90.650	0.010	0.014	0.000	0.009	66.041	31.226	n.d.	n.d.	n.d.	n.d.	n.d.	100.141
0.000	0.007	90.745	0.004	0.023	0.000	0.004	65.892	31.454	n.d.	n.d.	n.d.	n.d.	n.d.	100.351
0.015	0.004	90.971	0.007	0.011	0.000	0.000	66.355	31.265	n.d.	n.d.	n.d.	n.d.	n.d.	100.277
0.039	0.006	90.493	0.012	0.014	0.006	0.011	65.664	31.408	n.d.	n.d.	n.d.	n.d.	n.d.	100.114
0.010	0.005	90.540	0.010	0.010	0.000	0.000	65.893	31.249	n.d.	n.d.	n.d.	n.d.	n.d.	99.927
0.000	0.004	90.609	0.000	0.020	0.000	0.009	66.009	31.214	n.d.	n.d.	n.d.	n.d.	n.d.	100.007
0.000	0.011	90.185	0.010	0.015	0.000	0.013	65.570	31.184	n.d.	n.d.	n.d.	n.d.	n.d.	99.754
0.003	0.001	90.731	0.003	0.030	0.000	0.000	65.928	31.409	n.d.	n.d.	n.d.	n.d.	n.d.	100.176
0.000	0.010	90.189	0.011	0.015	0.000	0.007	65.342	31.394	n.d.	n.d.	n.d.	n.d.	n.d.	99.794
0.000	0.000	90.432	0.007	0.019	0.000	0.007	65.896	31.139	n.d.	n.d.	n.d.	n.d.	n.d.	99.681
0.000	0.004	90.563	0.004	0.014	0.012	0.000	65.915	31.252	n.d.	n.d.	n.d.	n.d.	n.d.	100.009
0.000	0.004	90.590	0.021	0.010	0.000	0.003	66.037	31.169	n.d.	n.d.	n.d.	n.d.	n.d.	99.893
0.003	0.009	90.563	0.009	0.018	0.013	0.006	65.926	31.242	n.d.	n.d.	n.d.	n.d.	n.d.	100.074
0.018	0.973	47.816	0.021	0.001	0.003	0.014	4.150	44.082	n.d.	n.d.	n.d.	n.d.	n.d.	99.841
0.010	0.973	46.950	0.006	0.001	0.000	0.007	3.025	44.228	n.d.	n.d.	n.d.	n.d.	n.d.	98.854
0.008	0.997	46.933	0.023	0.001	0.004	0.023	2.904	44.320	n.d.	n.d.	n.d.	n.d.	n.d.	99.156
0.026	0.938	46.653	0.020	0.004	0.000	0.010	1.955	44.894	n.d.	n.d.	n.d.	n.d.	n.d.	99.181
0.014	1.002	46.782	0.000	0.002	0.000	0.015	1.643	45.303	n.d.	n.d.	n.d.	n.d.	n.d.	99.793
0.003	0.977	47.186	0.021	0.002	0.000	0.021	2.687	44.769	n.d.	n.d.	n.d.	n.d.	n.d.	99.833
0.008	0.966	48.128	0.007	0.000	0.000	0.009	4.174	44.372	n.d.	n.d.	n.d.	n.d.	n.d.	100.410
0.013	0.913	47.275	0.015	0.004	0.000	0.004	2.350	45.160	n.d.	n.d.	n.d.	n.d.	n.d.	100.164
0.015	1.037	47.102	0.011	0.000	0.000	0.004	2.241	45.085	n.d.	n.d.	n.d.	n.d.	n.d.	100.042
0.008	0.940	47.687	0.019	0.003	0.003	0.006	3.243	44.769	n.d.	n.d.	n.d.	n.d.	n.d.	100.252
0.020	0.931	47.012	0.016	0.000	0.004	0.006	2.282	44.958	n.d.	n.d.	n.d.	n.d.	n.d.	99.706
0.023	0.948	47.226	0.009	0.000	0.004	0.000	3.123	44.416	n.d.	n.d.	n.d.	n.d.	n.d.	99.518
0.000	0.010	90.675	0.007	0.015	0.000	0.010	64.942	32.240	n.d.	n.d.	n.d.	n.d.	n.d.	100.578
0.000	0.000	90.751	0.009	0.011	0.000	0.006	65.444	31.864	n.d.	n.d.	n.d.	n.d.	n.d.	100.329
0.001	0.016	91.019	0.010	0.017	0.001	0.003	65.853	31.764	n.d.	n.d.	n.d.	n.d.	n.d.	100.597
0.002	0.008	91.016	0.013	0.013	0.000	0.000	65.533	32.049	n.d.	n.d.	n.d.	n.d.	n.d.	100.724
0.000	0.006	90.904	0.011	0.010	0.000	0.000	65.979	31.536	n.d.	n.d.	n.d.	n.d.	n.d.	100.175
0.000	0.005	91.282	0.010	0.013	0.000	0.000	66.329	31.598	n.d.	n.d.	n.d.	n.d.	n.d.	100.604
0.000	0.005	91.458	0.012	0.010	0.000	0.014	66.799	31.352	n.d.	n.d.	n.d.	n.d.	n.d.	100.574

Intrusion	Sample	Mineral	Sample Label	SiO2	TiO2	Al2O3	V2O3	Cr2O3	Nb2O3
Thunder Bird	NO-2G21-9	Magnetite	NO2G21-9-mag6a	0.004	0.723	0.058	1.737	0.521	n.d.
Thunder Bird	NO-2G21-9	Magnetite	NO2G21-9-mag6b	0.019	0.296	0.032	1.636	0.501	n.d.
Thunder Bird	NO-2G21-9	Magnetite	NO2G21-9-mag7	0.022	0.083	0.073	1.808	0.424	n.d.
Thunder Bird	NO-2G21-9	Magnetite	NO2G21-9-mag8	0.019	0.973	0.063	1.729	0.594	n.d.
Thunder Bird	NO-2G21-9	Ilmenite	NO2G21-9-ilm1a	0.010	50.867	0.013	0.332	0.044	0.000
Thunder Bird	NO-2G21-9	Ilmenite	NO2G21-9-ilm1b	0.017	50.712	0.017	0.345	0.053	0.000
Thunder Bird	NO-2G21-9	Ilmenite	NO2G21-9-ilm2	0.010	50.577	0.012	0.352	0.060	0.000
Thunder Bird	NO-2G21-9	Ilmenite	NO2G21-9-ilm3	0.015	50.887	0.017	0.368	0.063	0.000
Thunder Bird	NO-2G21-9	Ilmenite	NO2G21-9-ilm4	0.003	50.835	0.011	0.382	0.074	0.000
Thunder Bird	NO-2G21-9	Ilmenite	NO2G21-9-ilm5a	0.007	50.804	0.009	0.319	0.033	0.000
Thunder Bird	NO-2G21-9	Ilmenite	NO2G21-9-ilm5b	0.013	50.962	0.037	0.357	0.063	0.000
Thunder Bird	NO-2G21-9	Ilmenite	NO2G21-9-ilm5c	0.014	51.333	0.023	0.270	0.038	0.000
Thunder Bird	NO-2G21-9	Ilmenite	NO2G21-9-ilm6	0.014	51.071	0.013	0.389	0.061	0.000
Thunder Bird	NO-2G21-9	Ilmenite	NO2G21-9-ilm7	0.008	50.592	0.004	0.361	0.057	0.000
Thunder Bird	NO-2G21-9	Ilmenite	NO2G21-9-ilm8a	0.002	50.741	0.018	0.354	0.058	0.006
Thunder Bird	NO-2G21-9	Ilmenite	NO2G21-9-ilm8b	0.008	50.703	0.010	0.334	0.055	0.000
Thunder Bird	NO-2G21-9	Ilmenite	NO2G21-9-ilm8c	0.010	50.671	0.008	0.339	0.048	0.000
Thunder Bird	NO-2G22-4	Plagioclase	NO-2G22-4a-1	68.508	0.005	19.985	n.d.	n.d.	n.d.
Thunder Bird	NO-2G22-4	Plagioclase	NO-2G22-4a-2	54.083	0.030	28.991	n.d.	n.d.	n.d.
Thunder Bird	NO-2G22-4	Plagioclase	NO-2G22-4a-3	53.864	0.051	29.164	n.d.	n.d.	n.d.
Thunder Bird	NO-2G22-4	Plagioclase	NO-2G22-4a-4	54.090	0.031	28.920	n.d.	n.d.	n.d.
Thunder Bird	NO-2G22-4	Plagioclase	NO-2G22-4a-5	53.951	0.026	28.905	n.d.	n.d.	n.d.
Thunder Bird	NO-2G22-4	Plagioclase	NO-2G22-4a-6	54.111	0.023	28.685	n.d.	n.d.	n.d.
Thunder Bird	NO-2G22-4	Plagioclase	NO-2G22-4a-7	53.936	0.059	28.760	n.d.	n.d.	n.d.
Thunder Bird	NO-2G22-4	Plagioclase	NO-2G22-4a-8	54.263	0.048	28.904	n.d.	n.d.	n.d.
Thunder Bird	NO-2G22-4	Plagioclase	NO-2G22-4a-9	54.611	0.028	29.049	n.d.	n.d.	n.d.
Thunder Bird	NO-2G22-4	Plagioclase	NO-2G22-4a-10	53.451	0.052	29.132	n.d.	n.d.	n.d.
Thunder Bird	NO-2G22-4	Plagioclase	NO-2G22-4a-11	54.302	0.039	28.902	n.d.	n.d.	n.d.
Thunder Bird	NO-2G22-4	Plagioclase	NO-2G22-4a-12	54.489	0.033	28.786	n.d.	n.d.	n.d.
Thunder Bird	NO-2G22-4	Plagioclase	NO-2G22-4a-13	54.169	0.027	29.060	n.d.	n.d.	n.d.
Thunder Bird	NO-2G22-4	Plagioclase	NO-2G22-4a-14	53.951	0.022	29.030	n.d.	n.d.	n.d.
Thunder Bird	NO-2G22-4	Plagioclase	NO-2G22-4a-15	54.350	0.020	28.976	n.d.	n.d.	n.d.
Thunder Bird	NO-2G22-4	Plagioclase	NO-2G22-4a-16	53.942	0.000	29.156	n.d.	n.d.	n.d.
Thunder Bird	NO-2G22-4	Plagioclase	NO-2G22-4b-17	54.440	0.042	28.703	n.d.	n.d.	n.d.
Thunder Bird	NO-2G22-4	Plagioclase	NO-2G22-4b-18	54.970	0.009	28.788	n.d.	n.d.	n.d.
Thunder Bird	NO-2G22-4	Plagioclase	NO-2G22-4b-19	54.352	0.048	28.763	n.d.	n.d.	n.d.
Thunder Bird	NO-2G22-4	Plagioclase	NO-2G22-4b-20	54.383	0.063	28.738	n.d.	n.d.	n.d.
Thunder Bird	NO-2G22-4	Plagioclase	NO-2G22-4b-23	54.258	0.013	29.038	n.d.	n.d.	n.d.
Thunder Bird	NO-2G22-4	Plagioclase	NO-2G22-4b-24	54.720	0.037	28.874	n.d.	n.d.	n.d.
Thunder Bird	NO-2G22-4	Plagioclase	NO-2G22-4c-27	54.066	0.038	29.221	n.d.	n.d.	n.d.
Thunder Bird	NO-2G22-4	Plagioclase	NO-2G22-4c-28	54.306	0.075	28.571	n.d.	n.d.	n.d.
Thunder Bird	NO-2G22-4	Plagioclase	NO-2G22-4c-29	54.080	0.052	28.863	n.d.	n.d.	n.d.
Thunder Bird	NO-2G22-4	Plagioclase	NO-2G22-4c-32	54.680	0.023	28.684	n.d.	n.d.	n.d.
Thunder Bird	NO-2G22-4	Plagioclase	NO-2G22-4c-33	54.584	0.044	29.043	n.d.	n.d.	n.d.
Thunder Bird	NO-2G22-4	Plagioclase	NO-2G22-4d-40	55.614	0.031	28.377	n.d.	n.d.	n.d.
Thunder Bird	NO-2G22-4	Plagioclase	NO-2G22-4d-42	54.342	0.027	28.999	n.d.	n.d.	n.d.
Thunder Bird	NO-2G22-4	Amphibole	NO-2G22-4a-1	39.650	0.255	16.103	n.d.	0.020	n.d.
Thunder Bird	NO-2G22-4	Amphibole	NO-2G22-4a-2	40.594	0.288	14.821	n.d.	0.052	n.d.
Thunder Bird	NO-2G22-4	Amphibole	NO-2G22-4a-3	39.917	0.637	15.340	n.d.	0.024	n.d.
Thunder Bird	NO-2G22-4	Amphibole	NO-2G22-4a-4	40.432	0.264	14.993	n.d.	0.051	n.d.
Thunder Bird	NO-2G22-4	Amphibole	NO-2G22-4a-5	40.136	0.302	15.738	n.d.	0.024	n.d.
Thunder Bird	NO-2G22-4	Amphibole	NO-2G22-4a-6	40.312	0.264	14.930	n.d.	0.014	n.d.
Thunder Bird	NO-2G22-4	Amphibole	NO-2G22-4b-7	39.736	0.326	16.156	n.d.	0.047	n.d.
Thunder Bird	NO-2G22-4	Amphibole	NO-2G22-4b-8	39.917	0.225	16.557	n.d.	0.050	n.d.
Thunder Bird	NO-2G22-4	Amphibole	NO-2G22-4b-9	39.950	0.318	15.330	n.d.	0.046	n.d.
Thunder Bird	NO-2G22-4	Amphibole	NO-2G22-4b-10	38.230	0.074	24.914	n.d.	0.000	n.d.
Thunder Bird	NO-2G22-4	Amphibole	NO-2G22-4b-12	39.659	0.220	16.307	n.d.	0.016	n.d.
Thunder Bird	NO-2G22-4	Amphibole	NO-2G22-4b-13	40.092	0.285	15.098	n.d.	0.029	n.d.

MgO	MnO	FeO^t	CoO	NiO	CuO	ZnO	Fe2O3	FeO	CaO	SrO	BaO	Na2O	K2O	TOTAL
0.000	0.007	91.114	0.002	0.016	0.000	0.002	65.725	31.974	n.d.	n.d.	n.d.	n.d.	n.d.	100.769
0.001	0.008	90.693	0.007	0.008	0.000	0.000	66.011	31.296	n.d.	n.d.	n.d.	n.d.	n.d.	99.815
0.000	0.009	90.936	0.016	0.015	0.000	0.003	66.427	31.165	n.d.	n.d.	n.d.	n.d.	n.d.	100.044
0.003	0.020	90.230	0.014	0.010	0.000	0.008	64.707	32.006	n.d.	n.d.	n.d.	n.d.	n.d.	100.146
0.021	0.835	47.935	0.018	0.000	0.000	0.016	3.429	44.849	n.d.	n.d.	n.d.	n.d.	n.d.	100.435
0.028	0.802	47.824	0.015	0.004	0.000	0.010	3.423	44.744	n.d.	n.d.	n.d.	n.d.	n.d.	100.170
0.009	0.811	47.715	0.010	0.000	0.000	0.015	3.414	44.643	n.d.	n.d.	n.d.	n.d.	n.d.	99.913
0.010	0.832	47.953	0.007	0.002	0.011	0.010	3.393	44.900	n.d.	n.d.	n.d.	n.d.	n.d.	100.515
0.012	0.806	48.020	0.000	0.000	0.000	0.015	3.494	44.876	n.d.	n.d.	n.d.	n.d.	n.d.	100.508
0.032	0.826	47.565	0.014	0.001	0.000	0.019	3.096	44.779	n.d.	n.d.	n.d.	n.d.	n.d.	99.939
0.037	0.790	47.503	0.020	0.006	0.000	0.013	2.837	44.950	n.d.	n.d.	n.d.	n.d.	n.d.	100.085
0.015	0.853	47.286	0.010	0.000	0.000	0.000	2.221	45.288	n.d.	n.d.	n.d.	n.d.	n.d.	100.065
0.034	0.808	47.624	0.006	0.005	0.000	0.001	2.848	45.062	n.d.	n.d.	n.d.	n.d.	n.d.	100.311
0.013	0.807	47.553	0.011	0.004	0.000	0.005	3.221	44.655	n.d.	n.d.	n.d.	n.d.	n.d.	99.738
0.029	0.841	47.520	0.017	0.001	0.000	0.008	3.119	44.713	n.d.	n.d.	n.d.	n.d.	n.d.	99.908
0.020	0.822	47.928	0.021	0.000	0.001	0.021	3.580	44.706	n.d.	n.d.	n.d.	n.d.	n.d.	100.282
0.013	0.808	47.703	0.010	0.000	0.000	0.016	3.313	44.722	n.d.	n.d.	n.d.	n.d.	n.d.	99.958
0.004	0.013	0.043	n.d.	n.d.	n.d.	n.d.	n.d.	n.d.	0.666	0.000	0.000	11.662	0.032	89.224
0.007	0.006	0.179	n.d.	n.d.	n.d.	n.d.	n.d.	n.d.	11.650	0.061	0.000	5.138	0.032	95.007
0.004	0.000	0.123	n.d.	n.d.	n.d.	n.d.	n.d.	n.d.	11.562	0.008	0.008	5.172	0.041	94.776
0.026	0.000	0.183	n.d.	n.d.	n.d.	n.d.	n.d.	n.d.	11.395	0.100	0.000	5.237	0.037	94.745
0.005	0.013	0.179	n.d.	n.d.	n.d.	n.d.	n.d.	n.d.	11.450	0.116	0.037	5.185	0.033	94.645
0.000	0.016	0.371	n.d.	n.d.	n.d.	n.d.	n.d.	n.d.	11.430	0.139	0.002	5.261	0.034	94.775
0.021	0.006	0.416	n.d.	n.d.	n.d.	n.d.	n.d.	n.d.	11.393	0.000	0.000	5.317	0.027	94.591
0.010	0.006	0.118	n.d.	n.d.	n.d.	n.d.	n.d.	n.d.	11.314	0.093	0.000	5.306	0.032	94.756
0.013	0.001	0.096	n.d.	n.d.	n.d.	n.d.	n.d.	n.d.	11.410	0.031	0.005	5.332	0.026	95.239
0.010	0.001	0.291	n.d.	n.d.	n.d.	n.d.	n.d.	n.d.	11.922	0.000	0.048	4.907	0.029	94.859
0.000	0.000	0.193	n.d.	n.d.	n.d.	n.d.	n.d.	n.d.	11.321	0.099	0.023	5.237	0.047	94.856
0.011	0.004	0.114	n.d.	n.d.	n.d.	n.d.	n.d.	n.d.	11.245	0.008	0.006	5.265	0.029	94.690
0.019	0.002	0.127	n.d.	n.d.	n.d.	n.d.	n.d.	n.d.	11.609	0.099	0.000	5.136	0.041	95.112
0.021	0.000	0.233	n.d.	n.d.	n.d.	n.d.	n.d.	n.d.	11.528	0.076	0.000	5.125	0.027	94.861
0.013	0.006	0.100	n.d.	n.d.	n.d.	n.d.	n.d.	n.d.	11.637	0.038	0.003	5.124	0.024	95.140
0.011	0.009	0.227	n.d.	n.d.	n.d.	n.d.	n.d.	n.d.	11.552	0.061	0.043	5.168	0.036	94.958
0.000	0.000	0.095	n.d.	n.d.	n.d.	n.d.	n.d.	n.d.	11.222	0.000	0.000	5.435	0.026	94.502
0.005	0.002	0.136	n.d.	n.d.	n.d.	n.d.	n.d.	n.d.	11.196	0.000	0.000	5.411	0.037	95.106
0.014	0.000	0.224	n.d.	n.d.	n.d.	n.d.	n.d.	n.d.	11.316	0.084	0.023	5.195	0.033	94.801
0.003	0.009	0.379	n.d.	n.d.	n.d.	n.d.	n.d.	n.d.	11.257	0.000	0.000	5.306	0.037	94.832
0.000	0.000	0.141	n.d.	n.d.	n.d.	n.d.	n.d.	n.d.	11.412	0.000	0.000	5.224	0.036	94.862
0.021	0.010	0.115	n.d.	n.d.	n.d.	n.d.	n.d.	n.d.	11.279	0.061	0.000	5.349	0.046	95.117
0.000	0.000	0.225	n.d.	n.d.	n.d.	n.d.	n.d.	n.d.	11.616	0.000	0.000	5.140	0.054	95.166
0.016	0.027	0.207	n.d.	n.d.	n.d.	n.d.	n.d.	n.d.	11.132	0.123	0.004	5.359	0.030	94.457
0.020	0.009	0.248	n.d.	n.d.	n.d.	n.d.	n.d.	n.d.	11.345	0.008	0.000	5.253	0.039	94.625
0.014	0.000	0.038	n.d.	n.d.	n.d.	n.d.	n.d.	n.d.	11.254	0.000	0.000	5.261	0.041	94.693
0.005	0.000	0.053	n.d.	n.d.	n.d.	n.d.	n.d.	n.d.	11.466	0.099	0.000	5.215	0.029	95.294
0.000	0.000	0.093	n.d.	n.d.	n.d.	n.d.	n.d.	n.d.	9.576	0.091	0.022	5.644	0.655	93.782
0.018	0.005	0.143	n.d.	n.d.	n.d.	n.d.	n.d.	n.d.	11.405	0.061	0.000	5.213	0.044	95.000
4.138	0.165	23.806	n.d.	n.d.	n.d.	n.d.	n.d.	n.d.	11.146	n.d.	n.d.	1.278	0.515	97.076
4.566	0.159	23.835	n.d.	n.d.	n.d.	n.d.	n.d.	n.d.	11.175	n.d.	n.d.	1.253	0.560	97.303
4.256	0.144	24.228	n.d.	n.d.	n.d.	n.d.	n.d.	n.d.	11.255	n.d.	n.d.	1.291	0.721	97.813
4.454	0.175	23.915	n.d.	n.d.	n.d.	n.d.	n.d.	n.d.	11.237	n.d.	n.d.	1.227	0.574	97.322
4.167	0.177	24.417	n.d.	n.d.	n.d.	n.d.	n.d.	n.d.	11.250	n.d.	n.d.	1.285	0.620	98.116
4.450	0.165	24.392	n.d.	n.d.	n.d.	n.d.	n.d.	n.d.	11.176	n.d.	n.d.	1.319	0.603	97.625
4.105	0.148	23.794	n.d.	n.d.	n.d.	n.d.	n.d.	n.d.	11.141	n.d.	n.d.	1.293	0.663	97.409
3.819	0.129	24.030	n.d.	n.d.	n.d.	n.d.	n.d.	n.d.	11.314	n.d.	n.d.	1.243	0.588	97.872
4.248	0.150	24.345	n.d.	n.d.	n.d.	n.d.	n.d.	n.d.	11.097	n.d.	n.d.	1.270	0.594	97.348
0.012	0.103	11.409	n.d.	n.d.	n.d.	n.d.	n.d.	n.d.	23.247	n.d.	n.d.	0.000	0.000	97.989
3.980	0.176	24.022	n.d.	n.d.	n.d.	n.d.	n.d.	n.d.	11.129	n.d.	n.d.	1.344	0.458	97.311
4.411	0.168	23.915	n.d.	n.d.	n.d.	n.d.	n.d.	n.d.	11.155	n.d.	n.d.	1.275	0.597	97.025

Intrusion	Sample	Mineral	Sample Label	SiO2	TiO2	Al2O3	V2O3	Cr2O3	Nb2O3
Thunder Bird	NO-2G22-4	Amphibole	NO-2G22-4c-19	39.828	0.279	15.273	n.d.	0.029	n.d.
Thunder Bird	NO-2G22-4	Amphibole	NO-2G22-4c-20	40.057	0.253	16.629	n.d.	0.023	n.d.
Thunder Bird	NO-2G22-4	Amphibole	NO-2G22-4c-17	42.962	0.431	12.245	n.d.	0.000	n.d.
Thunder Bird	NO-2G22-4	Amphibole	NO-2G22-4c-16	39.319	0.271	15.792	n.d.	0.031	n.d.
Thunder Bird	NO-2G22-4	Amphibole	NO-2G22-4c-14	39.480	0.251	16.305	n.d.	0.022	n.d.
Thunder Bird	NO-2G22-4	Amphibole	NO-2G22-4c-15	38.247	0.049	25.160	n.d.	0.053	n.d.
Thunder Bird	NO-2G25-3	Magnetite	NO2G25-3-mag10	0.041	0.036	0.105	2.264	0.213	n.d.
Thunder Bird	NO-2G25-3	Magnetite	NO2G25-3-mag1a	0.010	0.043	0.047	2.451	0.222	n.d.
Thunder Bird	NO-2G25-3	Magnetite	NO2G25-3-mag1b	0.007	0.052	0.044	2.463	0.212	n.d.
Thunder Bird	NO-2G25-3	Magnetite	NO2G25-3-mag1c	0.018	0.043	0.045	2.453	0.205	n.d.
Thunder Bird	NO-2G25-3	Magnetite	NO2G25-3-mag1d	0.020	0.056	0.041	2.407	0.216	n.d.
Thunder Bird	NO-2G25-3	Magnetite	NO2G25-3-mag1e	0.002	0.480	0.027	2.329	0.208	n.d.
Thunder Bird	NO-2G25-3	Magnetite	NO2G25-3-mag2a	0.026	0.037	0.050	2.358	0.214	n.d.
Thunder Bird	NO-2G25-3	Magnetite	NO2G25-3-mag2b	0.010	0.027	0.027	2.283	0.233	n.d.
Thunder Bird	NO-2G25-3	Magnetite	NO2G25-3-mag2c	0.007	0.948	0.024	2.058	0.212	n.d.
Thunder Bird	NO-2G25-3	Magnetite	NO2G25-3-mag3	0.033	0.023	0.039	2.354	0.216	n.d.
Thunder Bird	NO-2G25-3	Magnetite	NO2G25-3-mag4	0.015	0.031	0.047	2.334	0.228	n.d.
Thunder Bird	NO-2G25-3	Magnetite	NO2G25-3-mag5a	0.040	0.053	0.150	2.284	0.224	n.d.
Thunder Bird	NO-2G25-3	Magnetite	NO2G25-3-mag5b	0.012	0.037	0.073	2.262	0.225	n.d.
Thunder Bird	NO-2G25-3	Magnetite	NO2G25-3-mag5c	0.007	0.197	0.034	2.199	0.245	n.d.
Thunder Bird	NO-2G25-3	Magnetite	NO2G25-3-mag5d	0.009	0.506	0.031	2.080	0.242	n.d.
Thunder Bird	NO-2G25-3	Magnetite	NO2G25-3-mag6a	0.024	0.180	0.058	2.243	0.221	n.d.
Thunder Bird	NO-2G25-3	Magnetite	NO2G25-3-mag6b	0.025	0.141	0.068	2.188	0.212	n.d.
Thunder Bird	NO-2G25-3	Magnetite	NO2G25-3-mag6c	0.000	1.013	0.049	2.094	0.244	n.d.
Thunder Bird	NO-2G25-3	Magnetite	NO2G25-3-mag6d	0.012	0.453	0.028	2.143	0.244	n.d.
Thunder Bird	NO-2G25-3	Magnetite	NO2G25-3-mag7	0.084	0.031	0.071	2.238	0.227	n.d.
Thunder Bird	NO-2G25-3	Magnetite	NO2G25-3-mag8	0.049	0.047	0.122	2.273	0.207	n.d.
Thunder Bird	NO-2G25-3	Magnetite	NO2G25-3-mag9	0.009	0.043	0.040	2.249	0.212	n.d.
Thunder Bird	NO-2G25-3	Ilmenite	NO2G25-3-ilm1a	0.031	50.716	0.011	0.385	0.049	0.000
Thunder Bird	NO-2G25-3	Ilmenite	NO2G25-3-ilm1b	0.010	50.653	0.014	0.436	0.055	0.002
Thunder Bird	NO-2G25-3	Ilmenite	NO2G25-3-ilm1c	0.003	50.816	0.013	0.433	0.043	0.000
Thunder Bird	NO-2G25-3	Ilmenite	NO2G25-3-ilm1d	0.001	50.366	0.004	0.567	0.059	0.000
Thunder Bird	NO-2G25-3	Ilmenite	NO2G25-3-ilm2	0.005	50.320	0.003	0.523	0.050	0.000
Thunder Bird	NO-2G25-3	Ilmenite	NO2G25-3-ilm3	0.017	51.010	0.012	0.412	0.035	0.000
Thunder Bird	NO-2G25-3	Ilmenite	NO2G25-3-ilm4	0.002	51.304	0.006	0.479	0.062	0.000
Thunder Bird	NO-2G25-3	Ilmenite	NO2G25-3-ilm5	0.010	50.417	0.009	0.535	0.053	0.000
Thunder Bird	NO-2G25-3	Ilmenite	NO2G25-3-ilm6	0.009	50.619	0.006	0.457	0.043	0.000
Thunder Bird	NO-2G25-3	Ilmenite	NO2G25-3-ilm7a	0.015	50.709	0.004	0.454	0.052	0.000
Thunder Bird	NO-2G25-3	Ilmenite	NO2G25-3-ilm7b	0.000	50.489	0.016	0.458	0.050	0.000
Thunder Bird	NO-2G25-3	Ilmenite	NO2G25-3-ilm7c	0.004	50.412	0.003	0.439	0.049	0.000
Thunder Bird	NO-2G25-4	Magnetite	NO2G25-4-mag1a	0.013	0.823	0.096	1.492	0.252	n.d.
Thunder Bird	NO-2G25-4	Magnetite	NO2G25-4-mag1b	0.016	1.402	0.120	1.456	0.247	n.d.
Thunder Bird	NO-2G25-4	Magnetite	NO2G25-4-mag1c	0.019	0.725	0.092	1.481	0.237	n.d.
Thunder Bird	NO-2G25-4	Magnetite	NO2G25-4-mag1d	0.010	0.399	0.115	1.483	0.259	n.d.
Thunder Bird	NO-2G25-4	Magnetite	NO2G25-4-mag1e	0.011	0.279	0.109	1.497	0.260	n.d.
Thunder Bird	NO-2G25-4	Magnetite	NO2G25-4-mag2a	0.018	0.846	0.098	1.465	0.248	n.d.
Thunder Bird	NO-2G25-4	Magnetite	NO2G25-4-mag2b	0.000	0.229	0.106	1.487	0.243	n.d.
Thunder Bird	NO-2G25-4	Magnetite	NO2G25-4-mag2c	0.007	0.161	0.112	1.498	0.255	n.d.
Thunder Bird	NO-2G25-4	Magnetite	NO2G25-4-mag2d	0.013	0.150	0.150	1.476	0.238	n.d.
Thunder Bird	NO-2G25-4	Magnetite	NO2G25-4-mag2e	0.018	0.158	0.107	1.497	0.247	n.d.
Thunder Bird	NO-2G25-4	Magnetite	NO2G25-4-mag2f	0.022	0.226	0.090	1.443	0.237	n.d.
Thunder Bird	NO-2G25-4	Magnetite	NO2G25-4-mag3a	0.011	0.041	0.095	1.448	0.189	n.d.
Thunder Bird	NO-2G25-4	Magnetite	NO2G25-4-mag3b	0.012	0.043	0.077	1.426	0.194	n.d.
Thunder Bird	NO-2G25-4	Magnetite	NO2G25-4-mag4	0.007	0.060	0.085	1.465	0.223	n.d.
Thunder Bird	NO-2G25-4	Magnetite	NO2G25-4-mag5a	0.014	12.919	0.066	1.080	0.192	n.d.
Thunder Bird	NO-2G25-4	Magnetite	NO2G25-4-mag5b	0.014	0.338	0.087	1.462	0.244	n.d.
Thunder Bird	NO-2G25-4	Magnetite	NO2G25-4-mag5c	0.016	0.173	0.072	1.430	0.221	n.d.
Thunder Bird	NO-2G25-4	Magnetite	NO2G25-4-mag6a	0.019	0.491	0.098	1.493	0.227	n.d.

MgO	MnO	FeO^t	CoO	NiO	CuO	ZnO	Fe2O3	FeO	CaO	SrO	BaO	Na2O	K2O	TOTAL
4.089	0.176	24.656	n.d.	n.d.	n.d.	n.d.	n.d.	n.d.	11.281	n.d.	n.d.	1.250	0.647	97.508
4.005	0.145	23.854	n.d.	n.d.	n.d.	n.d.	n.d.	n.d.	11.225	n.d.	n.d.	1.201	0.562	97.954
5.878	0.183	23.522	n.d.	n.d.	n.d.	n.d.	n.d.	n.d.	11.211	n.d.	n.d.	1.170	0.377	97.979
3.948	0.133	24.349	n.d.	n.d.	n.d.	n.d.	n.d.	n.d.	11.118	n.d.	n.d.	1.364	0.568	96.893
3.970	0.158	23.634	n.d.	n.d.	n.d.	n.d.	n.d.	n.d.	11.177	n.d.	n.d.	1.299	0.642	96.938
0.008	0.142	10.971	n.d.	n.d.	n.d.	n.d.	n.d.	n.d.	23.084	n.d.	n.d.	0.000	0.006	97.720
0.009	0.006	91.119	0.006	0.017	0.000	0.011	66.496	31.286	n.d.	n.d.	n.d.	n.d.	n.d.	100.489
0.000	0.000	90.602	0.011	0.011	0.000	0.008	66.100	31.125	n.d.	n.d.	n.d.	n.d.	n.d.	100.028
0.000	0.000	90.987	0.000	0.009	0.000	0.015	66.375	31.263	n.d.	n.d.	n.d.	n.d.	n.d.	100.439
0.000	0.000	91.001	0.000	0.006	0.000	0.002	66.372	31.279	n.d.	n.d.	n.d.	n.d.	n.d.	100.423
0.000	0.004	90.172	0.002	0.005	0.000	0.000	65.754	31.006	n.d.	n.d.	n.d.	n.d.	n.d.	99.511
0.000	0.004	90.351	0.012	0.004	0.000	0.006	65.402	31.502	n.d.	n.d.	n.d.	n.d.	n.d.	99.976
0.000	0.000	89.960	0.017	0.011	0.000	0.002	65.639	30.898	n.d.	n.d.	n.d.	n.d.	n.d.	99.251
0.000	0.000	89.994	0.014	0.003	0.000	0.000	65.728	30.851	n.d.	n.d.	n.d.	n.d.	n.d.	99.176
0.000	0.013	90.218	0.007	0.013	0.000	0.003	64.775	31.933	n.d.	n.d.	n.d.	n.d.	n.d.	99.993
0.000	0.000	90.609	0.001	0.018	0.000	0.000	66.124	31.110	n.d.	n.d.	n.d.	n.d.	n.d.	99.918
0.002	0.007	90.450	0.005	0.009	0.000	0.003	66.033	31.033	n.d.	n.d.	n.d.	n.d.	n.d.	99.747
0.006	0.002	90.155	0.004	0.020	0.000	0.002	65.714	31.025	n.d.	n.d.	n.d.	n.d.	n.d.	99.524
0.005	0.011	90.703	0.009	0.020	0.000	0.000	66.246	31.094	n.d.	n.d.	n.d.	n.d.	n.d.	99.994
0.000	0.001	90.700	0.010	0.015	0.000	0.007	66.063	31.256	n.d.	n.d.	n.d.	n.d.	n.d.	100.034
0.000	0.005	89.926	0.013	0.016	0.000	0.012	65.128	31.323	n.d.	n.d.	n.d.	n.d.	n.d.	99.365
0.000	0.007	90.537	0.009	0.012	0.000	0.000	65.912	31.229	n.d.	n.d.	n.d.	n.d.	n.d.	99.895
0.007	0.003	90.067	0.014	0.021	0.000	0.003	65.650	30.995	n.d.	n.d.	n.d.	n.d.	n.d.	99.327
0.000	0.011	90.060	0.004	0.022	0.000	0.001	64.548	31.979	n.d.	n.d.	n.d.	n.d.	n.d.	99.965
0.004	0.005	90.301	0.011	0.014	0.000	0.005	65.448	31.411	n.d.	n.d.	n.d.	n.d.	n.d.	99.777
0.002	0.004	90.259	0.003	0.017	0.001	0.016	65.802	31.050	n.d.	n.d.	n.d.	n.d.	n.d.	99.546
0.032	0.005	90.420	0.001	0.018	0.000	0.001	65.959	31.069	n.d.	n.d.	n.d.	n.d.	n.d.	99.784
0.000	0.003	90.514	0.013	0.015	0.002	0.000	66.118	31.020	n.d.	n.d.	n.d.	n.d.	n.d.	99.724
0.015	1.034	47.114	0.015	0.004	0.000	0.008	2.845	44.554	n.d.	n.d.	n.d.	n.d.	n.d.	99.667
0.029	1.030	47.339	0.000	0.000	0.000	0.003	3.184	44.474	n.d.	n.d.	n.d.	n.d.	n.d.	99.890
0.041	1.036	47.302	0.000	0.000	0.013	0.006	3.036	44.570	n.d.	n.d.	n.d.	n.d.	n.d.	100.010
0.025	1.082	47.437	0.002	0.002	0.002	0.019	3.664	44.140	n.d.	n.d.	n.d.	n.d.	n.d.	99.933
0.024	1.050	47.515	0.002	0.000	0.000	0.002	3.733	44.156	n.d.	n.d.	n.d.	n.d.	n.d.	99.868
0.013	1.103	47.201	0.000	0.002	0.000	0.011	2.725	44.749	n.d.	n.d.	n.d.	n.d.	n.d.	100.089
0.025	1.099	47.516	0.000	0.001	0.014	0.015	2.837	44.963	n.d.	n.d.	n.d.	n.d.	n.d.	100.807
0.036	1.014	47.044	0.006	0.005	0.000	0.007	3.104	44.251	n.d.	n.d.	n.d.	n.d.	n.d.	99.447
0.017	1.019	46.827	0.000	0.000	0.000	0.000	2.611	44.477	n.d.	n.d.	n.d.	n.d.	n.d.	99.259
0.027	1.004	47.189	0.006	0.001	0.008	0.005	2.939	44.544	n.d.	n.d.	n.d.	n.d.	n.d.	99.768
0.026	1.008	47.453	0.000	0.000	0.000	0.010	3.464	44.336	n.d.	n.d.	n.d.	n.d.	n.d.	99.857
0.019	1.050	47.190	0.009	0.000	0.000	0.014	3.291	44.229	n.d.	n.d.	n.d.	n.d.	n.d.	99.519
0.000	0.016	91.482	0.008	0.007	0.007	0.003	66.020	32.077	n.d.	n.d.	n.d.	n.d.	n.d.	100.814
0.000	0.031	89.172	0.015	0.014	0.000	0.000	63.548	31.991	n.d.	n.d.	n.d.	n.d.	n.d.	98.840
0.000	0.010	91.421	0.004	0.009	0.000	0.000	66.094	31.950	n.d.	n.d.	n.d.	n.d.	n.d.	100.620
0.000	0.000	91.452	0.011	0.018	0.000	0.019	66.563	31.558	n.d.	n.d.	n.d.	n.d.	n.d.	100.435
0.003	0.010	91.246	0.009	0.006	0.007	0.011	66.567	31.348	n.d.	n.d.	n.d.	n.d.	n.d.	100.117
0.001	0.017	91.218	0.005	0.008	0.000	0.008	65.794	32.016	n.d.	n.d.	n.d.	n.d.	n.d.	100.524
0.004	0.002	91.114	0.000	0.005	0.000	0.003	66.545	31.236	n.d.	n.d.	n.d.	n.d.	n.d.	99.860
0.000	0.003	91.552	0.013	0.000	0.000	0.005	66.939	31.320	n.d.	n.d.	n.d.	n.d.	n.d.	100.313
0.002	0.002	91.294	0.011	0.018	0.000	0.026	66.773	31.211	n.d.	n.d.	n.d.	n.d.	n.d.	100.070
0.005	0.009	91.508	0.009	0.008	0.001	0.000	66.908	31.304	n.d.	n.d.	n.d.	n.d.	n.d.	100.271
0.000	0.010	91.226	0.004	0.014	0.000	0.000	66.627	31.275	n.d.	n.d.	n.d.	n.d.	n.d.	99.947
0.000	0.000	91.848	0.008	0.005	0.000	0.007	67.360	31.237	n.d.	n.d.	n.d.	n.d.	n.d.	100.401
0.000	0.003	91.584	0.021	0.010	0.000	0.003	67.188	31.128	n.d.	n.d.	n.d.	n.d.	n.d.	100.105
0.000	0.008	91.430	0.004	0.007	0.000	0.004	67.022	31.123	n.d.	n.d.	n.d.	n.d.	n.d.	100.008
0.011	0.377	90.563	0.005	0.004	0.000	0.014	49.683	45.858	n.d.	n.d.	n.d.	n.d.	n.d.	110.223
0.000	0.008	91.209	0.016	0.007	0.000	0.012	66.481	31.388	n.d.	n.d.	n.d.	n.d.	n.d.	100.058
0.000	0.015	91.013	0.007	0.005	0.000	0.011	66.577	31.107	n.d.	n.d.	n.d.	n.d.	n.d.	99.633
0.002	0.008	91.683	0.009	0.013	0.000	0.005	66.606	31.750	n.d.	n.d.	n.d.	n.d.	n.d.	100.721

Intrusion	Sample	Mineral	Sample Label	SiO2	TiO2	Al2O3	V2O3	Cr2O3	Nb2O3
Thunder Bird	NO-2G25-4	Magnetite	NO2G25-4-mag6b	0.015	0.551	0.082	1.503	0.231	n.d.
Thunder Bird	NO-2G25-4	Magnetite	NO2G25-4-mag6c	0.022	0.971	0.072	1.475	0.235	n.d.
Thunder Bird	NO-2G25-4	Magnetite	NO2G25-4-mag7a	0.012	0.836	0.080	1.480	0.223	n.d.
Thunder Bird	NO-2G25-4	Magnetite	NO2G25-4-mag7b	0.013	0.483	0.081	1.468	0.247	n.d.
Thunder Bird	NO-2G25-4	Magnetite	NO2G25-4-mag7c	0.018	0.100	0.063	1.504	0.244	n.d.
Thunder Bird	NO-2G25-4	Magnetite	NO2G25-4-mag8	0.011	0.351	0.075	1.511	0.199	n.d.
Thunder Bird	NO-2G25-4	Ilmenite	NO2G25-4-ilm1	0.016	51.396	0.016	0.312	0.038	0.000
Thunder Bird	NO-2G25-4	Ilmenite	NO2G25-4-ilm2	0.005	51.791	0.011	0.215	0.023	0.000
Thunder Bird	NO-2G25-4	Ilmenite	NO2G25-4-ilm3	0.009	51.386	0.008	0.298	0.039	0.000
Thunder Bird	NO-2G25-4	Ilmenite	NO2G25-4-ilm4	0.009	51.775	0.005	0.244	0.035	0.000
Thunder Bird	NO-2G25-4	Ilmenite	NO2G25-4-ilm5	0.006	50.897	0.015	0.315	0.051	0.000
Thunder Bird	NO-2G25-4	Ilmenite	NO2G25-4-ilm6	0.013	52.292	0.016	0.165	0.019	0.000
Thunder Bird	NO-2G25-5	Magnetite	NO2G25-5-mag1a	0.073	0.131	0.160	1.654	0.222	n.d.
Thunder Bird	NO-2G25-5	Magnetite	NO2G25-5-mag1b	0.030	0.369	0.044	1.632	0.241	n.d.
Thunder Bird	NO-2G25-5	Magnetite	NO2G25-5-mag1c	0.013	0.213	0.049	1.631	0.247	n.d.
Thunder Bird	NO-2G25-5	Magnetite	NO2G25-5-mag2	0.133	0.687	0.169	1.620	0.216	n.d.
Thunder Bird	NO-2G25-5	Magnetite	NO2G25-5-mag3a	0.078	0.239	0.153	1.641	0.193	n.d.
Thunder Bird	NO-2G25-5	Magnetite	NO2G25-5-mag3b	0.009	0.195	0.069	1.666	0.204	n.d.
Thunder Bird	NO-2G25-5	Magnetite	NO2G25-5-mag3c	0.014	0.106	0.074	1.645	0.216	n.d.
Thunder Bird	NO-2G25-5	Magnetite	NO2G25-5-mag3d	0.012	0.094	0.062	1.633	0.234	n.d.
Thunder Bird	NO-2G25-5	Magnetite	NO2G25-5-mag4a	0.033	0.562	0.118	1.630	0.204	n.d.
Thunder Bird	NO-2G25-5	Magnetite	NO2G25-5-mag5	0.012	0.159	0.050	1.645	0.197	n.d.
Thunder Bird	NO-2G25-5	Magnetite	NO2G25-5-mag6a	0.028	0.168	0.089	1.744	0.226	n.d.
Thunder Bird	NO-2G25-5	Magnetite	NO2G25-5-mag6b	0.015	0.081	0.070	1.732	0.262	n.d.
Thunder Bird	NO-2G25-5	Magnetite	NO2G25-5-mag6c	0.023	0.074	0.063	1.680	0.269	n.d.
Thunder Bird	NO-2G25-5	Magnetite	NO2G25-5-mag6d	0.051	0.222	0.085	1.740	0.245	n.d.
Thunder Bird	NO-2G25-5	Magnetite	NO2G25-5-mag7a	0.029	0.308	0.104	1.733	0.232	n.d.
Thunder Bird	NO-2G25-5	Magnetite	NO2G25-5-mag7b	0.028	0.347	0.083	1.722	0.227	n.d.
Thunder Bird	NO-2G25-5	Magnetite	NO2G25-5-mag8	0.019	0.167	0.042	1.697	0.232	n.d.
Thunder Bird	NO-2G25-5	Magnetite	NO2G25-5-mag9	0.024	0.246	0.081	1.742	0.233	n.d.
Thunder Bird	NO-2G25-5	Ilmenite	NO2G25-5-ilm1	0.008	51.072	0.012	0.334	0.040	0.000
Thunder Bird	NO-2G25-5	Ilmenite	NO2G25-5-ilm2	0.011	51.070	0.009	0.336	0.032	0.000
Thunder Bird	NO-2G25-5	Ilmenite	NO2G25-5-ilm3	0.012	51.381	0.012	0.304	0.039	0.000
Thunder Bird	NO-2G25-5	Ilmenite	NO2G25-5-ilm4	0.011	51.333	0.015	0.330	0.032	0.000
Thunder Bird	NO-2G25-5	Ilmenite	NO2G25-5-ilm5a	0.010	50.644	0.005	0.388	0.040	0.000
Thunder Bird	NO-2G25-5	Ilmenite	NO2G25-5-ilm5b	0.012	50.347	0.010	0.380	0.040	0.000
Thunder Bird	NO-2G25-5	Ilmenite	NO2G25-5-ilm5c	0.007	51.281	0.018	0.265	0.033	0.000
Thunder Bird	NO-2G25-5	Ilmenite	NO2G25-5-ilm6	0.000	50.998	0.005	0.357	0.047	0.000
Thunder Bird	NO-2G25-5	Ilmenite	NO2G25-5-ilm7	0.031	50.820	0.014	0.315	0.040	0.000
Thunder Bird	NO-2G25-6	Magnetite	NO2G25-6-mag1a	0.017	0.829	0.088	2.003	0.514	n.d.
Thunder Bird	NO-2G25-6	Magnetite	NO2G25-6-mag1b	0.014	0.291	0.073	2.022	0.559	n.d.
Thunder Bird	NO-2G25-6	Magnetite	NO2G25-6-mag2	0.009	0.481	0.036	1.894	0.546	n.d.
Thunder Bird	NO-2G25-6	Magnetite	NO2G25-6-mag3	0.007	0.154	0.061	1.975	0.489	n.d.
Thunder Bird	NO-2G25-6	Magnetite	NO2G25-6-mag4	0.017	0.169	0.064	2.002	0.537	n.d.
Thunder Bird	NO-2G25-6	Magnetite	NO2G25-6-mag5a	0.009	2.159	0.085	1.946	0.572	n.d.
Thunder Bird	NO-2G25-6	Magnetite	NO2G25-6-mag5b	0.036	0.194	0.080	2.033	0.631	n.d.
Thunder Bird	NO-2G25-6	Magnetite	NO2G25-6-mag5c	0.013	0.272	0.087	1.990	0.577	n.d.
Thunder Bird	NO-2G25-6	Magnetite	NO2G25-6-mag6a	0.027	6.402	0.111	1.698	0.448	n.d.
Thunder Bird	NO-2G25-6	Magnetite	NO2G25-6-mag6b	0.021	3.567	0.119	1.806	0.447	n.d.
Thunder Bird	NO-2G25-6	Magnetite	NO2G25-6-mag6c	0.017	0.436	0.107	1.853	0.517	n.d.
Thunder Bird	NO-2G25-6	Magnetite	NO2G25-6-mag6d	0.013	0.308	0.085	1.878	0.339	n.d.
Thunder Bird	NO-2G25-6	Magnetite	NO2G25-6-mag6e	0.018	0.821	0.103	1.882	0.464	n.d.
Thunder Bird	NO-2G25-6	Magnetite	NO2G25-6-mag6f	0.021	0.281	0.129	1.854	0.285	n.d.
Thunder Bird	NO-2G25-6	Magnetite	NO2G25-6-mag7a	0.002	0.810	0.095	1.902	0.457	n.d.
Thunder Bird	NO-2G25-6	Magnetite	NO2G25-6-mag7b	0.021	2.526	0.109	1.860	0.448	n.d.
Thunder Bird	NO-2G25-6	Magnetite	NO2G25-6-mag7c	0.020	0.074	0.103	1.892	0.259	n.d.
Thunder Bird	NO-2G25-6	Ilmenite	NO2G25-6-ilm1	0.005	51.601	0.009	0.329	0.056	0.000
Thunder Bird	NO-2G25-6	Ilmenite	NO2G25-6-ilm2	0.005	50.921	0.011	0.405	0.060	0.000

MgO	MnO	FeO^t	CoO	NiO	CuO	ZnO	Fe2O3	FeO	CaO	SrO	BaO	Na2O	K2O	TOTAL
0.000	0.012	91.547	0.007	0.011	0.000	0.000	66.430	31.772	n.d.	n.d.	n.d.	n.d.	n.d.	100.615
0.000	0.013	91.313	0.009	0.016	0.000	0.000	65.704	32.192	n.d.	n.d.	n.d.	n.d.	n.d.	100.709
0.000	0.000	91.495	0.000	0.011	0.000	0.008	66.021	32.089	n.d.	n.d.	n.d.	n.d.	n.d.	100.760
0.000	0.005	91.210	0.002	0.012	0.000	0.000	66.274	31.576	n.d.	n.d.	n.d.	n.d.	n.d.	100.161
0.000	0.005	91.375	0.009	0.014	0.000	0.000	66.902	31.176	n.d.	n.d.	n.d.	n.d.	n.d.	100.035
0.000	0.008	91.305	0.013	0.011	0.000	0.001	66.539	31.433	n.d.	n.d.	n.d.	n.d.	n.d.	100.152
0.005	0.936	47.100	0.004	0.005	0.000	0.006	2.027	45.276	n.d.	n.d.	n.d.	n.d.	n.d.	100.037
0.001	0.979	47.158	0.005	0.000	0.003	0.010	1.754	45.579	n.d.	n.d.	n.d.	n.d.	n.d.	100.377
0.004	0.944	47.039	0.011	0.000	0.000	0.007	1.989	45.250	n.d.	n.d.	n.d.	n.d.	n.d.	99.944
0.000	0.953	47.301	0.000	0.001	0.003	0.000	1.879	45.611	n.d.	n.d.	n.d.	n.d.	n.d.	100.514
0.003	0.935	47.271	0.014	0.004	0.001	0.003	2.732	44.813	n.d.	n.d.	n.d.	n.d.	n.d.	99.789
0.000	1.023	46.620	0.003	0.000	0.016	0.011	0.705	45.986	n.d.	n.d.	n.d.	n.d.	n.d.	100.249
0.036	0.003	91.239	0.006	0.016	0.000	0.002	66.613	31.300	n.d.	n.d.	n.d.	n.d.	n.d.	100.216
0.007	0.009	91.482	0.012	0.013	0.008	0.003	66.588	31.566	n.d.	n.d.	n.d.	n.d.	n.d.	100.522
0.010	0.006	91.194	0.011	0.005	0.000	0.011	66.604	31.264	n.d.	n.d.	n.d.	n.d.	n.d.	100.063
0.023	0.011	91.090	0.013	0.012	0.000	0.013	65.663	32.006	n.d.	n.d.	n.d.	n.d.	n.d.	100.566
0.000	0.010	91.160	0.021	0.010	0.000	0.016	66.393	31.419	n.d.	n.d.	n.d.	n.d.	n.d.	100.173
0.000	0.001	91.793	0.000	0.017	0.000	0.004	67.050	31.461	n.d.	n.d.	n.d.	n.d.	n.d.	100.676
0.000	0.007	91.456	0.006	0.019	0.000	0.002	66.919	31.241	n.d.	n.d.	n.d.	n.d.	n.d.	100.250
0.000	0.005	91.231	0.010	0.016	0.000	0.015	66.784	31.138	n.d.	n.d.	n.d.	n.d.	n.d.	100.003
0.005	0.007	91.477	0.001	0.011	0.004	0.025	66.295	31.824	n.d.	n.d.	n.d.	n.d.	n.d.	100.719
0.000	0.008	91.296	0.008	0.008	0.000	0.005	66.749	31.234	n.d.	n.d.	n.d.	n.d.	n.d.	100.076
0.005	0.008	91.714	0.000	0.014	0.000	0.002	66.956	31.466	n.d.	n.d.	n.d.	n.d.	n.d.	100.706
0.000	0.007	91.798	0.004	0.009	0.000	0.010	67.156	31.370	n.d.	n.d.	n.d.	n.d.	n.d.	100.716
0.000	0.004	91.170	0.005	0.013	0.000	0.009	66.706	31.147	n.d.	n.d.	n.d.	n.d.	n.d.	99.993
0.000	0.007	91.703	0.004	0.012	0.000	0.000	66.825	31.573	n.d.	n.d.	n.d.	n.d.	n.d.	100.764
0.000	0.003	91.091	0.002	0.011	0.000	0.001	66.288	31.444	n.d.	n.d.	n.d.	n.d.	n.d.	100.156
0.000	0.004	91.149	0.006	0.016	0.000	0.000	66.304	31.488	n.d.	n.d.	n.d.	n.d.	n.d.	100.225
0.000	0.002	91.534	0.007	0.015	0.000	0.009	66.878	31.356	n.d.	n.d.	n.d.	n.d.	n.d.	100.425
0.000	0.007	91.354	0.005	0.015	0.000	0.000	66.591	31.435	n.d.	n.d.	n.d.	n.d.	n.d.	100.379
0.000	0.960	47.432	0.009	0.000	0.002	0.000	2.744	44.963	n.d.	n.d.	n.d.	n.d.	n.d.	100.144
0.016	0.978	47.866	0.015	0.000	0.000	0.007	3.287	44.908	n.d.	n.d.	n.d.	n.d.	n.d.	100.669
0.015	0.986	47.024	0.011	0.003	0.003	0.000	2.041	45.187	n.d.	n.d.	n.d.	n.d.	n.d.	99.995
0.010	0.953	47.402	0.013	0.005	0.000	0.012	2.477	45.173	n.d.	n.d.	n.d.	n.d.	n.d.	100.364
0.024	0.983	47.967	0.011	0.005	0.000	0.011	3.853	44.500	n.d.	n.d.	n.d.	n.d.	n.d.	100.474
0.013	0.986	48.093	0.002	0.003	0.000	0.000	4.246	44.272	n.d.	n.d.	n.d.	n.d.	n.d.	100.311
0.007	0.969	47.516	0.009	0.001	0.002	0.000	2.655	45.127	n.d.	n.d.	n.d.	n.d.	n.d.	100.374
0.013	0.962	47.596	0.012	0.005	0.002	0.006	3.053	44.849	n.d.	n.d.	n.d.	n.d.	n.d.	100.309
0.010	0.984	47.649	0.004	0.006	0.001	0.005	3.258	44.717	n.d.	n.d.	n.d.	n.d.	n.d.	100.205
0.000	0.019	90.437	0.013	0.004	0.000	0.008	64.964	31.982	n.d.	n.d.	n.d.	n.d.	n.d.	100.441
0.000	0.011	90.997	0.008	0.015	0.000	0.003	66.081	31.536	n.d.	n.d.	n.d.	n.d.	n.d.	100.614
0.000	0.012	90.320	0.009	0.012	0.000	0.000	65.402	31.471	n.d.	n.d.	n.d.	n.d.	n.d.	99.872
0.000	0.002	90.689	0.009	0.024	0.000	0.018	66.106	31.206	n.d.	n.d.	n.d.	n.d.	n.d.	100.051
0.000	0.005	90.627	0.005	0.018	0.000	0.004	65.980	31.257	n.d.	n.d.	n.d.	n.d.	n.d.	100.059
0.000	0.041	89.635	0.003	0.014	0.000	0.005	62.627	33.282	n.d.	n.d.	n.d.	n.d.	n.d.	100.744
0.000	0.011	90.842	0.000	0.014	0.000	0.000	66.016	31.440	n.d.	n.d.	n.d.	n.d.	n.d.	100.455
0.000	0.013	90.493	0.003	0.017	0.000	0.011	65.738	31.342	n.d.	n.d.	n.d.	n.d.	n.d.	100.062
0.004	0.152	79.126	0.000	0.012	0.000	0.015	49.364	34.708	n.d.	n.d.	n.d.	n.d.	n.d.	92.941
0.002	0.074	87.819	0.005	0.011	0.000	0.023	59.498	34.282	n.d.	n.d.	n.d.	n.d.	n.d.	99.855
0.000	0.006	91.356	0.013	0.012	0.006	0.006	66.210	31.780	n.d.	n.d.	n.d.	n.d.	n.d.	100.963
0.006	0.005	91.651	0.011	0.018	0.000	0.007	66.677	31.654	n.d.	n.d.	n.d.	n.d.	n.d.	101.002
0.000	0.005	91.224	0.010	0.012	0.000	0.000	65.596	32.200	n.d.	n.d.	n.d.	n.d.	n.d.	101.111
0.000	0.012	91.065	0.008	0.006	0.000	0.006	66.255	31.448	n.d.	n.d.	n.d.	n.d.	n.d.	100.305
0.000	0.009	90.997	0.007	0.016	0.000	0.021	65.488	32.070	n.d.	n.d.	n.d.	n.d.	n.d.	100.877
0.000	0.050	90.783	0.000	0.018	0.000	0.015	63.043	34.056	n.d.	n.d.	n.d.	n.d.	n.d.	102.146
0.000	0.010	91.518	0.015	0.011	0.000	0.016	66.892	31.328	n.d.	n.d.	n.d.	n.d.	n.d.	100.620
0.001	1.142	47.328	0.000	0.008	0.000	0.011	2.318	45.242	n.d.	n.d.	n.d.	n.d.	n.d.	100.722
0.010	1.101	47.310	0.004	0.002	0.000	0.006	2.942	44.663	n.d.	n.d.	n.d.	n.d.	n.d.	100.130

Intrusion	Sample	Mineral	Sample Label	SiO2	TiO2	Al2O3	V2O3	Cr2O3	Nb2O3
Thunder Bird	NO-2G25-6	Ilmenite	NO2G25-6-ilm3	0.010	51.233	0.010	0.387	0.057	0.000
Thunder Bird	NO-2G25-6	Ilmenite	NO2G25-6-ilm4	0.013	49.989	0.013	0.409	0.062	0.000
Thunder Bird	NO-2G25-6	Ilmenite	NO2G25-6-ilm5	0.006	51.258	0.005	0.331	0.054	0.000
Thunder Bird	NO-2G25-6	Ilmenite	NO2G25-6-ilm6	0.006	50.600	0.017	0.407	0.064	0.000
Thunder Bird	NO-2G25-6	Ilmenite	NO2G25-6-ilm7	1.333	51.080	0.041	0.385	0.041	0.000
Thunder Bird	NO-2G46-1	Magnetite	NO2G46-1-mag1a	0.027	0.572	0.100	0.501	0.151	n.d.
Thunder Bird	NO-2G46-1	Magnetite	NO2G46-1-mag1b	0.021	0.620	0.107	0.506	0.115	n.d.
Thunder Bird	NO-2G46-1	Magnetite	NO2G46-1-mag1c	0.024	0.877	0.118	0.504	0.183	n.d.
Thunder Bird	NO-2G46-1	Magnetite	NO2G46-1-mag2	0.021	1.874	0.092	0.481	0.142	n.d.
Thunder Bird	NO-2G46-1	Magnetite	NO2G46-1-mag3a	0.007	0.352	0.113	0.511	0.113	n.d.
Thunder Bird	NO-2G46-1	Magnetite	NO2G46-1-mag3b	0.009	0.559	0.099	0.514	0.127	n.d.
Thunder Bird	NO-2G46-1	Magnetite	NO2G46-1-mag3c	0.023	0.878	0.095	0.492	0.150	n.d.
Thunder Bird	NO-2G46-1	Magnetite	NO2G46-1-mag4	0.024	1.142	0.057	0.397	0.136	n.d.
Thunder Bird	NO-2G46-1	Magnetite	NO2G46-1-mag5	0.024	0.558	0.096	0.540	0.089	n.d.
Thunder Bird	NO-2G46-1	Magnetite	NO2G46-1-mag6	0.014	0.545	0.098	0.534	0.098	n.d.
Thunder Bird	NO-2G46-1	Magnetite	NO2G46-1-mag7	0.020	1.023	0.093	0.521	0.107	n.d.
Thunder Bird	NO-2G46-1	Magnetite	NO2G46-1-mag8	0.016	0.883	0.094	0.520	0.096	n.d.
Thunder Bird	NO-2G46-1	Magnetite	NO2G46-1-mag9	0.021	1.044	0.098	0.530	0.110	n.d.
Thunder Bird	NO-2G46-1	Ilmenite	NO2G46-1-ilm1a	0.006	52.205	0.012	0.035	0.011	0.000
Thunder Bird	NO-2G46-1	Ilmenite	NO2G46-1-ilm1b	0.009	52.005	0.009	0.044	0.003	0.000
Thunder Bird	NO-2G46-1	Ilmenite	NO2G46-1-ilm1c	0.022	52.018	0.012	0.043	0.020	0.000
Thunder Bird	NO-2G46-1	Ilmenite	NO2G46-1-ilm2	0.010	51.795	0.011	0.069	0.008	0.000
Thunder Bird	NO-2G46-1	Ilmenite	NO2G46-1-ilm3	0.005	51.932	0.012	0.058	0.015	0.000
Thunder Bird	NO-2G46-1	Ilmenite	NO2G46-1-ilm4	0.010	51.388	0.011	0.076	0.012	0.000
Thunder Bird	NO-2G46-1	Ilmenite	NO2G46-1-ilm5a	0.010	52.191	0.020	0.069	0.019	0.000
Thunder Bird	NO-2G46-1	Ilmenite	NO2G46-1-ilm5b	0.010	51.444	0.015	0.069	0.011	0.000
Thunder Bird	NO-2G46-1	Ilmenite	NO2G46-1-ilm6	0.009	51.887	0.015	0.056	0.008	0.000
Thunder Bird	NO-2G46-1	Ilmenite	NO2G46-1-ilm7	0.011	51.906	0.020	0.053	0.011	0.000
Thunder Bird	NO-2G46-1	Ilmenite	NO2G46-1-ilm8	0.004	51.701	0.008	0.059	0.012	0.000
Thunder Bird	NO-2G46-1	Ilmenite	NO2G46-1-ilm9	0.002	51.564	0.007	0.075	0.005	0.000
Thunder Bird	NO-2G46-2	Magnetite	NO2G46-2-mag10	0.033	0.183	0.108	0.663	0.187	n.d.
Thunder Bird	NO-2G46-2	Magnetite	NO2G46-2-mag1a	0.026	0.343	0.098	0.679	0.201	n.d.
Thunder Bird	NO-2G46-2	Magnetite	NO2G46-2-mag2	0.027	0.224	0.105	0.678	0.240	n.d.
Thunder Bird	NO-2G46-2	Magnetite	NO2G46-2-mag3	0.028	0.347	0.085	0.641	0.259	n.d.
Thunder Bird	NO-2G46-2	Magnetite	NO2G46-2-mag4	0.021	0.320	0.092	0.647	0.261	n.d.
Thunder Bird	NO-2G46-2	Magnetite	NO2G46-2-mag5	0.022	0.792	0.100	0.648	0.211	n.d.
Thunder Bird	NO-2G46-2	Magnetite	NO2G46-2-mag6	0.025	0.250	0.117	0.653	0.366	n.d.
Thunder Bird	NO-2G46-2	Magnetite	NO2G46-2-mag7a	0.006	0.187	0.089	0.664	0.190	n.d.
Thunder Bird	NO-2G46-2	Magnetite	NO2G46-2-mag7b	0.036	0.374	0.111	0.635	0.201	n.d.
Thunder Bird	NO-2G46-2	Magnetite	NO2G46-2-mag8	0.022	0.462	0.109	0.632	0.183	n.d.
Thunder Bird	NO-2G46-2	Magnetite	NO2G46-2-mag9	0.020	0.306	0.094	0.624	0.160	n.d.
Thunder Bird	NO-2G46-2	Ilmenite	NO2G46-2-ilm1a	0.010	51.302	0.013	0.066	0.014	0.000
Thunder Bird	NO-2G46-2	Ilmenite	NO2G46-2-ilm1b	0.004	52.200	0.008	0.055	0.013	0.000
Thunder Bird	NO-2G46-2	Ilmenite	NO2G46-2-ilm1c	0.014	51.238	0.006	0.076	0.016	0.000
Thunder Bird	NO-2G46-2	Ilmenite	NO2G46-2-ilm2	0.000	51.343	0.006	0.077	0.024	0.000
Thunder Bird	NO-2G46-2	Ilmenite	NO2G46-2-ilm3	0.007	51.598	0.015	0.086	0.017	0.000
Thunder Bird	NO-2G46-2	Ilmenite	NO2G46-2-ilm4	0.005	51.633	0.013	0.093	0.014	0.000
Thunder Bird	NO-2G46-2	Ilmenite	NO2G46-2-ilm5	0.000	51.764	0.009	0.078	0.023	0.000
Thunder Bird	NO-2G46-2	Ilmenite	NO2G46-2-ilm6a	0.015	51.684	0.004	0.082	0.020	0.000
Thunder Bird	NO-2G46-2	Ilmenite	NO2G46-2-ilm6b	0.018	52.019	0.010	0.063	0.018	0.000
Thunder Bird	NO-2G46-2	Ilmenite	NO2G46-2-ilm7a	0.005	51.497	0.012	0.062	0.015	0.000
Thunder Bird	NO-2G46-2	Ilmenite	NO2G46-2-ilm7b	0.000	51.708	0.011	0.060	0.012	0.000
Thunder Bird	NO-2G46-2	Ilmenite	NO2G46-2-ilm7c	0.008	51.626	0.015	0.063	0.021	0.000
Thunder Bird	NO-2G46-2	Ilmenite	NO2G46-2-ilm8	0.002	52.060	0.019	0.082	0.025	0.000
Thunder Bird	NO-2G46-2	Ilmenite	NO2G46-2-ilm9	0.013	51.714	0.002	0.089	0.017	0.000
Thunder Bird	NO-2G46-2	Ilmenite	NO2G46-2-ilm10	0.013	51.632	0.006	0.095	0.020	0.000
Thunder Bird	NO-2G46-2	Ilmenite	NO2G46-2-ilm11	0.013	51.621	0.015	0.071	0.013	0.000
Thunder Bird	NO-2G46-3	Ilmenite	NO2G46-3-ilm1a	0.013	52.726	0.012	0.018	0.009	0.000

MgO	MnO	FeO^t	CoO	NiO	CuO	ZnO	Fe2O3	FeO	CaO	SrO	BaO	Na2O	K2O	TOTAL
0.000	1.104	47.017	0.007	0.000	0.000	0.014	2.291	44.956	n.d.	n.d.	n.d.	n.d.	n.d.	100.069
0.000	1.078	47.101	0.000	0.001	0.000	0.009	3.583	43.877	n.d.	n.d.	n.d.	n.d.	n.d.	99.034
0.009	1.039	47.143	0.010	0.003	0.011	0.009	2.368	45.012	n.d.	n.d.	n.d.	n.d.	n.d.	100.115
0.015	1.035	47.550	0.005	0.001	0.001	0.017	3.476	44.422	n.d.	n.d.	n.d.	n.d.	n.d.	100.066
0.011	1.039	47.869	0.014	0.003	0.000	0.011	1.589	46.440	n.d.	n.d.	n.d.	n.d.	n.d.	101.986
0.000	0.007	91.859	0.009	0.003	0.000	0.000	66.979	31.591	n.d.	n.d.	n.d.	n.d.	n.d.	99.940
0.000	0.005	91.893	0.003	0.010	0.000	0.016	66.967	31.635	n.d.	n.d.	n.d.	n.d.	n.d.	100.006
0.002	0.003	92.049	0.010	0.009	0.000	0.000	66.701	32.031	n.d.	n.d.	n.d.	n.d.	n.d.	100.462
0.000	0.018	91.342	0.007	0.004	0.000	0.013	64.902	32.943	n.d.	n.d.	n.d.	n.d.	n.d.	100.497
0.000	0.003	92.160	0.007	0.004	0.000	0.008	67.535	31.392	n.d.	n.d.	n.d.	n.d.	n.d.	100.044
0.000	0.012	91.892	0.011	0.009	0.000	0.022	67.081	31.532	n.d.	n.d.	n.d.	n.d.	n.d.	99.975
0.000	0.010	91.791	0.000	0.007	0.000	0.021	66.546	31.912	n.d.	n.d.	n.d.	n.d.	n.d.	100.134
0.001	0.008	91.985	0.003	0.009	0.000	0.000	66.384	32.252	n.d.	n.d.	n.d.	n.d.	n.d.	100.413
0.000	0.007	92.160	0.010	0.002	0.000	0.000	67.236	31.661	n.d.	n.d.	n.d.	n.d.	n.d.	100.222
0.000	0.007	92.316	0.014	0.002	0.000	0.000	67.387	31.681	n.d.	n.d.	n.d.	n.d.	n.d.	100.380
0.000	0.014	91.787	0.016	0.008	0.000	0.013	66.371	32.066	n.d.	n.d.	n.d.	n.d.	n.d.	100.252
0.007	0.006	92.047	0.008	0.006	0.006	0.007	66.757	31.978	n.d.	n.d.	n.d.	n.d.	n.d.	100.385
0.000	0.014	92.288	0.006	0.001	0.000	0.000	66.685	32.284	n.d.	n.d.	n.d.	n.d.	n.d.	100.793
0.033	0.825	47.031	0.010	0.005	0.000	0.011	1.097	46.044	n.d.	n.d.	n.d.	n.d.	n.d.	100.294
0.019	0.833	47.109	0.000	0.001	0.000	0.002	1.337	45.906	n.d.	n.d.	n.d.	n.d.	n.d.	100.168
0.005	0.845	46.514	0.000	0.000	0.002	0.000	0.630	45.947	n.d.	n.d.	n.d.	n.d.	n.d.	99.544
0.010	0.857	47.055	0.000	0.000	0.001	0.017	1.509	45.697	n.d.	n.d.	n.d.	n.d.	n.d.	99.984
0.025	0.835	47.708	0.000	0.000	0.000	0.007	2.099	45.819	n.d.	n.d.	n.d.	n.d.	n.d.	100.807
0.009	0.847	47.407	0.012	0.000	0.000	0.007	2.296	45.341	n.d.	n.d.	n.d.	n.d.	n.d.	100.009
0.014	0.833	46.832	0.000	0.002	0.000	0.000	0.831	46.084	n.d.	n.d.	n.d.	n.d.	n.d.	100.073
0.012	0.856	47.536	0.000	0.001	0.000	0.000	2.381	45.394	n.d.	n.d.	n.d.	n.d.	n.d.	100.193
0.015	0.862	46.889	0.001	0.003	0.000	0.001	1.237	45.776	n.d.	n.d.	n.d.	n.d.	n.d.	99.870
0.018	0.856	47.026	0.000	0.006	0.000	0.013	1.381	45.783	n.d.	n.d.	n.d.	n.d.	n.d.	100.058
0.008	0.860	47.297	0.007	0.004	0.000	0.005	1.879	45.607	n.d.	n.d.	n.d.	n.d.	n.d.	100.153
0.004	0.874	47.231	0.000	0.000	0.000	0.000	1.936	45.489	n.d.	n.d.	n.d.	n.d.	n.d.	99.956
0.000	0.003	92.081	0.005	0.006	0.000	0.009	67.579	31.273	n.d.	n.d.	n.d.	n.d.	n.d.	100.049
0.000	0.000	92.206	0.003	0.016	0.000	0.000	67.463	31.502	n.d.	n.d.	n.d.	n.d.	n.d.	100.331
0.010	0.006	92.165	0.000	0.007	0.000	0.000	67.582	31.355	n.d.	n.d.	n.d.	n.d.	n.d.	100.233
0.008	0.008	91.635	0.008	0.008	0.002	0.002	67.048	31.305	n.d.	n.d.	n.d.	n.d.	n.d.	99.749
0.000	0.004	91.785	0.000	0.012	0.000	0.000	67.182	31.334	n.d.	n.d.	n.d.	n.d.	n.d.	99.873
0.000	0.004	92.117	0.000	0.016	0.000	0.000	66.813	31.998	n.d.	n.d.	n.d.	n.d.	n.d.	100.604
0.000	0.005	92.392	0.011	0.009	0.000	0.000	67.672	31.500	n.d.	n.d.	n.d.	n.d.	n.d.	100.608
0.003	0.001	92.459	0.007	0.004	0.000	0.000	67.907	31.356	n.d.	n.d.	n.d.	n.d.	n.d.	100.414
0.000	0.007	91.879	0.004	0.009	0.000	0.011	67.179	31.431	n.d.	n.d.	n.d.	n.d.	n.d.	99.998
0.000	0.000	91.632	0.005	0.007	0.000	0.000	66.898	31.436	n.d.	n.d.	n.d.	n.d.	n.d.	99.755
0.000	0.000	92.353	0.000	0.006	0.000	0.000	67.658	31.473	n.d.	n.d.	n.d.	n.d.	n.d.	100.342
0.003	0.806	47.261	0.007	0.002	0.000	0.001	2.153	45.324	n.d.	n.d.	n.d.	n.d.	n.d.	99.701
0.001	0.860	47.255	0.000	0.000	0.000	0.018	1.320	46.067	n.d.	n.d.	n.d.	n.d.	n.d.	100.546
0.003	0.805	47.252	0.012	0.000	0.001	0.000	2.203	45.269	n.d.	n.d.	n.d.	n.d.	n.d.	99.644
0.008	0.777	47.475	0.000	0.001	0.000	0.002	2.333	45.376	n.d.	n.d.	n.d.	n.d.	n.d.	99.947
0.001	0.817	46.913	0.007	0.003	0.000	0.013	1.495	45.567	n.d.	n.d.	n.d.	n.d.	n.d.	99.627
0.000	0.817	46.989	0.000	0.001	0.007	0.003	1.533	45.610	n.d.	n.d.	n.d.	n.d.	n.d.	99.729
0.008	0.827	47.124	0.000	0.002	0.000	0.005	1.582	45.701	n.d.	n.d.	n.d.	n.d.	n.d.	99.998
0.000	0.845	46.909	0.005	0.000	0.000	0.000	1.406	45.644	n.d.	n.d.	n.d.	n.d.	n.d.	99.705
0.009	0.851	47.265	0.000	0.002	0.000	0.003	1.487	45.927	n.d.	n.d.	n.d.	n.d.	n.d.	100.407
0.006	0.793	47.161	0.005	0.000	0.000	0.012	1.851	45.495	n.d.	n.d.	n.d.	n.d.	n.d.	99.753
0.000	0.742	47.464	0.003	0.000	0.000	0.002	1.902	45.752	n.d.	n.d.	n.d.	n.d.	n.d.	100.193
0.009	0.822	46.836	0.002	0.001	0.000	0.002	1.384	45.591	n.d.	n.d.	n.d.	n.d.	n.d.	99.544
0.005	0.787	47.379	0.000	0.004	0.000	0.015	1.528	46.004	n.d.	n.d.	n.d.	n.d.	n.d.	100.531
0.004	0.810	47.222	0.013	0.000	0.000	0.002	1.705	45.688	n.d.	n.d.	n.d.	n.d.	n.d.	100.057
0.007	0.788	47.725	0.006	0.000	0.000	0.012	2.330	45.629	n.d.	n.d.	n.d.	n.d.	n.d.	100.537
0.000	0.768	47.707	0.016	0.003	0.000	0.002	2.288	45.648	n.d.	n.d.	n.d.	n.d.	n.d.	100.458
0.033	1.790	45.668	0.001	0.001	0.000	0.024	0.137	45.545	n.d.	n.d.	n.d.	n.d.	n.d.	100.309

Intrusion	Sample	Mineral	Sample Label	SiO2	TiO2	Al2O3	V2O3	Cr2O3	Nb2O3
Thunder Bird	NO-2G46-3	Ilmenite	NO2G46-3-ilm1b	0.004	52.247	0.009	0.017	0.003	0.000
Thunder Bird	NO-2G46-3	Ilmenite	NO2G46-3-ilm1c	0.027	51.920	0.010	0.022	0.003	0.000
Thunder Bird	NO-2G46-3	Ilmenite	NO2G46-3-ilm1d	0.006	52.426	0.009	0.018	0.012	0.000
Thunder Bird	NO-2G46-3	Ilmenite	NO2G46-3-ilm1e	0.003	52.070	0.013	0.011	0.006	0.000
Thunder Bird	NO-2G46-3	Ilmenite	NO2G46-3-ilm1f	0.020	52.291	0.017	0.024	0.000	0.000
Thunder Bird	NO-2G46-3	Ilmenite	NO2G46-3-ilm2	0.041	52.111	0.017	0.001	0.007	0.000
Thunder Bird	NO-2G46-3	Ilmenite	NO2G46-3-ilm3a	0.010	52.343	0.012	0.018	0.004	0.000
Thunder Bird	NO-2G46-3	Ilmenite	NO2G46-3-ilm3b	0.010	52.017	0.016	0.030	0.012	0.000
Thunder Bird	NO-2G46-3	Ilmenite	NO2G46-3-ilm3c	0.026	52.485	0.006	0.008	0.000	0.000
Thunder Bird	NO-2G46-3	Ilmenite	NO2G46-3-ilm4a	0.004	52.294	0.017	0.008	0.000	0.000
Thunder Bird	NO-2G46-3	Ilmenite	NO2G46-3-ilm4b	0.002	51.960	0.015	0.005	0.006	0.000
Thunder Bird	NO-2G46-3	Ilmenite	NO2G46-3-ilm4c	0.007	52.276	0.013	0.005	0.000	0.004
Thunder Bird	NO-2G46-3	Ilmenite	NO2G46-3-ilm4d	0.018	52.707	0.005	0.000	0.004	0.000
Thunder Bird	NO-2G46-3	Ilmenite	NO2G46-3-ilm4e	0.006	52.216	0.003	0.000	0.008	0.000
Thunder Bird	NO-2G46-3	Ilmenite	NO2G46-3-ilm4f	0.016	52.393	0.022	0.000	0.018	0.000
Thunder Bird	NO-2G46-3	Ilmenite	NO2G46-3-ilm4g	0.011	52.552	0.010	0.000	0.004	0.000
Thunder Bird	NO-2G46-3	Ilmenite	NO2G46-3-ilm4h	0.006	52.156	0.017	0.015	0.011	0.000
Thunder Bird	NO-2G46-3	Plagioclase	NO-2G46-3a-7	55.533	0.029	28.008	n.d.	n.d.	n.d.
Thunder Bird	NO-2G46-3	Plagioclase	NO-2G46-3a-8	55.106	0.019	28.483	n.d.	n.d.	n.d.
Thunder Bird	NO-2G46-3	Plagioclase	NO-2G46-3a-9	55.345	0.038	28.459	n.d.	n.d.	n.d.
Thunder Bird	NO-2G46-3	Plagioclase	NO-2G46-3a-10	55.422	0.044	28.141	n.d.	n.d.	n.d.
Thunder Bird	NO-2G46-3	Plagioclase	NO-2G46-3a-6	56.022	0.011	27.627	n.d.	n.d.	n.d.
Thunder Bird	NO-2G46-3	Plagioclase	NO-2G46-3b-28	56.236	0.011	27.792	n.d.	n.d.	n.d.
Thunder Bird	NO-2G46-3	Plagioclase	NO-2G46-3b-29	54.800	0.027	28.503	n.d.	n.d.	n.d.
Thunder Bird	NO-2G46-3	Plagioclase	NO-2G46-3b-27	55.040	0.040	28.525	n.d.	n.d.	n.d.
Thunder Bird	NO-2G46-3	Plagioclase	NO-2G46-3b-20	55.314	0.051	28.531	n.d.	n.d.	n.d.
Thunder Bird	NO-2G46-3	Plagioclase	NO-2G46-3b-21	56.127	0.042	27.917	n.d.	n.d.	n.d.
Thunder Bird	NO-2G46-3	Plagioclase	NO-2G46-3b-22	56.107	0.022	27.857	n.d.	n.d.	n.d.
Thunder Bird	NO-2G46-3	Plagioclase	NO-2G46-3d-1	55.037	0.065	28.306	n.d.	n.d.	n.d.
Thunder Bird	NO-2G46-3	Plagioclase	NO-2G46-3d-2	55.399	0.012	28.197	n.d.	n.d.	n.d.
Thunder Bird	NO-2G46-3	Plagioclase	NO-2G46-3e-1	55.295	0.024	28.340	n.d.	n.d.	n.d.
Thunder Bird	NO-2G46-3	Plagioclase	NO-2G46-3e-2	55.481	0.000	28.020	n.d.	n.d.	n.d.
Thunder Bird	NO-2G46-3	Plagioclase	NO-2G47-3b-14	56.256	0.009	27.915	n.d.	n.d.	n.d.
Thunder Bird	NO-2G46-3	Plagioclase	NO-2G47-3b-15	55.738	0.037	27.903	n.d.	n.d.	n.d.
Thunder Bird	NO-2G46-3	Plagioclase	NO-2G47-3b-16	55.827	0.054	27.856	n.d.	n.d.	n.d.
Thunder Bird	NO-2G46-3	Plagioclase	NO-2G47-3b-17	55.904	0.045	27.864	n.d.	n.d.	n.d.
Thunder Bird	NO-2G46-3	Plagioclase	NO-2G47-3b-18	55.571	0.035	28.113	n.d.	n.d.	n.d.
Thunder Bird	NO-2G46-3	Plagioclase	NO-2G47-3c-21	55.983	0.038	27.961	n.d.	n.d.	n.d.
Thunder Bird	NO-2G46-3	Plagioclase	NO-2G47-3c-22	55.878	0.029	27.876	n.d.	n.d.	n.d.
Thunder Bird	NO-2G46-3	Plagioclase	NO-2G47-3c-23	55.768	0.015	28.043	n.d.	n.d.	n.d.
Thunder Bird	NO-2G46-3	Plagioclase	NO-2G47-3c-24	55.722	0.019	27.835	n.d.	n.d.	n.d.
Thunder Bird	NO-2G46-3	Plagioclase	NO-2G47-3c-25	55.766	0.019	28.065	n.d.	n.d.	n.d.
Thunder Bird	NO-2G46-3	Plagioclase	NO-2G47-3c-26	55.925	0.031	28.164	n.d.	n.d.	n.d.
Thunder Bird	NO-2G46-3	Plagioclase	NO-2G47-3c-27	55.839	0.009	27.984	n.d.	n.d.	n.d.
Thunder Bird	NO-2G46-3	Plagioclase	NO-2G47-3d-1	55.278	0.000	28.366	n.d.	n.d.	n.d.
Thunder Bird	NO-2G46-3	Plagioclase	NO-2G47-3d-2	55.664	0.048	28.319	n.d.	n.d.	n.d.
Thunder Bird	NO-2G46-3	Plagioclase	NO-2G47-3e-1	55.669	0.020	27.812	n.d.	n.d.	n.d.
Thunder Bird	NO-2G46-3	Plagioclase	NO-2G47-3e-2	55.869	0.030	27.828	n.d.	n.d.	n.d.
Thunder Bird	NO-2G46-3	Plagioclase	NO-2G47-3e-3	55.558	0.032	27.770	n.d.	n.d.	n.d.
Thunder Bird	NO-2G46-3	Plagioclase	NO-2G47-3f-1	56.141	0.037	27.742	n.d.	n.d.	n.d.
Thunder Bird	NO-2G46-3	Plagioclase	NO-2G47-3f-2	55.948	0.040	27.887	n.d.	n.d.	n.d.
Thunder Bird	NO-2G46-3	Plagioclase	NO-2G47-3f-3	55.480	0.049	28.333	n.d.	n.d.	n.d.
Thunder Bird	NO-2G46-3	Plagioclase	NO-2G47-3g-1	55.620	0.055	27.909	n.d.	n.d.	n.d.
Thunder Bird	NO-2G46-3	Plagioclase	NO-2G47-3g-2	56.081	0.026	27.804	n.d.	n.d.	n.d.
Thunder Bird	NO-2G46-3	Plagioclase	NO-2G47-3g-3	55.712	0.037	27.671	n.d.	n.d.	n.d.
Thunder Bird	NO-2G46-3	Pyroxene	NO-2G46-3a-2	45.587	0.279	8.727	n.d.	0.006	n.d.
Thunder Bird	NO-2G46-3	Pyroxene	NO-2G46-3a-4	50.728	0.647	2.519	n.d.	0.002	n.d.
Thunder Bird	NO-2G46-3	Pyroxene	NO-2G46-3c-10? gr	50.655	0.092	2.213	n.d.	0.000	n.d.

MgO	MnO	FeO^t	CoO	NiO	CuO	ZnO	Fe2O3	FeO	CaO	SrO	BaO	Na2O	K2O	TOTAL
0.025	1.829	45.946	0.011	0.002	0.000	0.014	0.967	45.076	n.d.	n.d.	n.d.	n.d.	n.d.	100.204
0.031	1.872	45.362	0.005	0.000	0.004	0.007	0.663	44.766	n.d.	n.d.	n.d.	n.d.	n.d.	99.329
0.033	1.799	46.100	0.000	0.001	0.000	0.017	0.929	45.265	n.d.	n.d.	n.d.	n.d.	n.d.	100.514
0.033	1.819	45.349	0.003	0.000	0.012	0.019	0.492	44.906	n.d.	n.d.	n.d.	n.d.	n.d.	99.387
0.029	1.836	45.603	0.010	0.000	0.000	0.009	0.528	45.128	n.d.	n.d.	n.d.	n.d.	n.d.	99.892
0.016	1.961	45.406	0.006	0.003	0.000	0.012	0.578	44.886	n.d.	n.d.	n.d.	n.d.	n.d.	99.639
0.018	1.840	45.442	0.004	0.001	0.000	0.011	0.290	45.181	n.d.	n.d.	n.d.	n.d.	n.d.	99.732
0.032	1.844	45.826	0.000	0.000	0.006	0.025	1.089	44.846	n.d.	n.d.	n.d.	n.d.	n.d.	99.927
0.028	1.905	45.371	0.001	0.000	0.000	0.019	0.144	45.241	n.d.	n.d.	n.d.	n.d.	n.d.	99.863
0.041	1.540	45.772	0.012	0.002	0.005	0.021	0.446	45.371	n.d.	n.d.	n.d.	n.d.	n.d.	99.761
0.039	1.519	45.873	0.010	0.000	0.000	0.007	0.844	45.114	n.d.	n.d.	n.d.	n.d.	n.d.	99.521
0.040	1.522	46.001	0.008	0.004	0.003	0.019	0.686	45.384	n.d.	n.d.	n.d.	n.d.	n.d.	99.971
0.053	1.514	46.354	0.000	0.000	0.000	0.020	0.635	45.783	n.d.	n.d.	n.d.	n.d.	n.d.	100.739
0.049	1.533	46.132	0.000	0.000	0.003	0.016	0.907	45.316	n.d.	n.d.	n.d.	n.d.	n.d.	100.057
0.057	1.523	45.760	0.008	0.003	0.008	0.023	0.332	45.461	n.d.	n.d.	n.d.	n.d.	n.d.	99.864
0.045	1.545	46.007	0.009	0.000	0.001	0.010	0.433	45.617	n.d.	n.d.	n.d.	n.d.	n.d.	100.237
0.029	1.556	46.155	0.001	0.003	0.000	0.003	0.968	45.284	n.d.	n.d.	n.d.	n.d.	n.d.	100.049
0.000	0.008	0.093	n.d.	n.d.	n.d.	n.d.	n.d.	n.d.	10.321	0.069	0.000	5.862	0.034	94.061
0.000	0.000	0.034	n.d.	n.d.	n.d.	n.d.	n.d.	n.d.	10.677	0.130	0.020	5.636	0.024	94.449
0.007	0.000	0.089	n.d.	n.d.	n.d.	n.d.	n.d.	n.d.	10.794	0.038	0.000	5.560	0.037	94.770
0.014	0.001	0.047	n.d.	n.d.	n.d.	n.d.	n.d.	n.d.	10.330	0.168	0.000	5.881	0.019	94.167
0.001	0.000	0.097	n.d.	n.d.	n.d.	n.d.	n.d.	n.d.	9.923	0.053	0.000	6.098	0.006	93.734
0.002	0.003	0.019	n.d.	n.d.	n.d.	n.d.	n.d.	n.d.	10.067	0.069	0.000	6.073	0.023	94.199
0.000	0.001	0.060	n.d.	n.d.	n.d.	n.d.	n.d.	n.d.	10.850	0.099	0.000	5.576	0.036	94.340
0.000	0.000	0.079	n.d.	n.d.	n.d.	n.d.	n.d.	n.d.	10.740	0.099	0.005	5.548	0.020	94.523
0.000	0.009	0.102	n.d.	n.d.	n.d.	n.d.	n.d.	n.d.	10.794	0.053	0.011	5.555	0.025	94.854
0.000	0.000	0.053	n.d.	n.d.	n.d.	n.d.	n.d.	n.d.	10.151	0.015	0.000	6.065	0.019	94.305
0.000	0.010	0.026	n.d.	n.d.	n.d.	n.d.	n.d.	n.d.	10.147	0.015	0.028	6.029	0.009	94.184
0.000	0.018	0.073	n.d.	n.d.	n.d.	n.d.	n.d.	n.d.	10.875	0.107	0.000	5.572	0.030	94.481
0.000	0.000	0.195	n.d.	n.d.	n.d.	n.d.	n.d.	n.d.	10.491	0.107	0.035	5.766	0.024	94.401
0.000	0.003	0.069	n.d.	n.d.	n.d.	n.d.	n.d.	n.d.	10.635	0.099	0.000	5.670	0.034	94.465
0.003	0.000	0.053	n.d.	n.d.	n.d.	n.d.	n.d.	n.d.	10.385	0.030	0.000	5.929	0.025	93.972
0.002	0.003	0.095	n.d.	n.d.	n.d.	n.d.	n.d.	n.d.	10.194	0.068	0.000	6.062	0.024	94.542
0.028	0.008	0.144	n.d.	n.d.	n.d.	n.d.	n.d.	n.d.	10.224	0.023	0.006	5.994	0.018	94.105
0.004	0.000	0.091	n.d.	n.d.	n.d.	n.d.	n.d.	n.d.	10.201	0.061	0.037	5.970	0.012	94.094
0.001	0.012	0.065	n.d.	n.d.	n.d.	n.d.	n.d.	n.d.	10.153	0.068	0.000	5.977	0.016	94.112
0.018	0.004	0.104	n.d.	n.d.	n.d.	n.d.	n.d.	n.d.	10.376	0.015	0.000	5.771	0.022	94.236
0.010	0.005	0.067	n.d.	n.d.	n.d.	n.d.	n.d.	n.d.	10.192	0.000	0.000	5.902	0.025	94.256
0.017	0.000	0.070	n.d.	n.d.	n.d.	n.d.	n.d.	n.d.	10.258	0.000	0.000	5.881	0.019	94.128
0.006	0.000	0.059	n.d.	n.d.	n.d.	n.d.	n.d.	n.d.	10.371	0.122	0.000	5.844	0.013	94.384
0.000	0.003	0.176	n.d.	n.d.	n.d.	n.d.	n.d.	n.d.	10.084	0.046	0.000	5.934	0.008	93.885
0.000	0.013	0.033	n.d.	n.d.	n.d.	n.d.	n.d.	n.d.	10.484	0.069	0.000	5.868	0.000	94.449
0.000	0.000	0.074	n.d.	n.d.	n.d.	n.d.	n.d.	n.d.	10.321	0.053	0.000	5.953	0.028	94.568
0.001	0.001	0.060	n.d.	n.d.	n.d.	n.d.	n.d.	n.d.	10.264	0.000	0.029	5.965	0.018	94.158
0.000	0.002	0.115	n.d.	n.d.	n.d.	n.d.	n.d.	n.d.	10.669	0.000	0.000	5.716	0.000	94.430
0.000	0.000	0.150	n.d.	n.d.	n.d.	n.d.	n.d.	n.d.	10.560	0.213	0.000	5.801	0.023	94.954
0.008	0.000	0.083	n.d.	n.d.	n.d.	n.d.	n.d.	n.d.	10.177	0.091	0.003	5.973	0.008	93.860
0.001	0.000	0.061	n.d.	n.d.	n.d.	n.d.	n.d.	n.d.	10.191	0.053	0.025	6.029	0.025	94.033
0.000	0.003	0.094	n.d.	n.d.	n.d.	n.d.	n.d.	n.d.	10.282	0.107	0.000	5.946	0.023	93.846
0.000	0.007	0.057	n.d.	n.d.	n.d.	n.d.	n.d.	n.d.	10.025	0.137	0.000	6.083	0.019	94.146
0.000	0.000	0.052	n.d.	n.d.	n.d.	n.d.	n.d.	n.d.	10.180	0.054	0.000	6.060	0.022	94.161
0.000	0.000	0.099	n.d.	n.d.	n.d.	n.d.	n.d.	n.d.	10.368	0.107	0.000	5.873	0.017	94.436
0.000	0.000	0.094	n.d.	n.d.	n.d.	n.d.	n.d.	n.d.	10.263	0.046	0.000	5.956	0.019	93.987
0.000	0.013	0.093	n.d.	n.d.	n.d.	n.d.	n.d.	n.d.	10.108	0.038	0.013	6.004	0.018	94.163
0.000	0.000	0.146	n.d.	n.d.	n.d.	n.d.	n.d.	n.d.	10.132	0.068	0.000	5.967	0.013	93.766
7.443	0.358	24.309	n.d.	n.d.	n.d.	n.d.	n.d.	n.d.	10.057	n.d.	n.d.	1.055	0.201	98.022
10.130	0.785	28.312	n.d.	n.d.	n.d.	n.d.	n.d.	n.d.	5.040	n.d.	n.d.	0.470	0.044	98.677
10.517	0.881	29.165	n.d.	n.d.	n.d.	n.d.	n.d.	n.d.	4.007	n.d.	n.d.	0.324	0.054	97.908

Intrusion	Sample	Mineral	Sample Label	SiO2	TiO2	Al2O3	V2O3	Cr2O3	Nb2O3
Thunder Bird	NO-2G46-3	Pyroxene	NO-2G46-3c-10? red	47.662	0.187	6.376	n.d.	0.031	n.d.
Thunder Bird	NO-2G46-3	Amphibole	NO-2G46-3b-1	39.792	0.430	15.738	n.d.	0.030	n.d.
Thunder Bird	NO-2G46-3	Amphibole	NO-2G46-3b-2	39.520	0.066	16.592	n.d.	0.005	n.d.
Thunder Bird	NO-2G46-3	Amphibole	NO-2G46-3b-4	43.413	0.383	10.917	n.d.	0.000	n.d.
Thunder Bird	NO-2G46-3	Amphibole	NO-2G46-3c-16?	40.024	0.230	15.672	n.d.	0.000	n.d.
Thunder Bird	NO-2G46-3	Amphibole	NO-2G47-3b-3	38.256	0.367	18.690	n.d.	0.018	n.d.
Thunder Bird	NO-2G46-3	Amphibole	NO-2G47-3b-2	39.237	0.005	18.640	n.d.	0.005	n.d.
Thunder Bird	NO-2G46-3	Amphibole	NO-2G47-3b-1	37.978	0.109	19.311	n.d.	0.008	n.d.
Thunder Bird	NO-2G47-2	Plagioclase	NO-2G47-2a-1	55.316	0.038	27.987	n.d.	n.d.	n.d.
Thunder Bird	NO-2G47-2	Plagioclase	NO-2G47-2a-2	55.590	0.022	28.181	n.d.	n.d.	n.d.
Thunder Bird	NO-2G47-2	Plagioclase	NO-2G47-2a-3	55.946	0.000	28.051	n.d.	n.d.	n.d.
Thunder Bird	NO-2G47-2	Plagioclase	NO-2G47-2a-4	55.503	0.025	27.989	n.d.	n.d.	n.d.
Thunder Bird	NO-2G47-2	Plagioclase	NO-2G47-2a-5	55.776	0.023	27.682	n.d.	n.d.	n.d.
Thunder Bird	NO-2G47-2	Plagioclase	NO-2G47-2a-6	53.864	0.000	29.350	n.d.	n.d.	n.d.
Thunder Bird	NO-2G47-2	Plagioclase	NO-2G47-2a-8	56.000	0.020	27.877	n.d.	n.d.	n.d.
Thunder Bird	NO-2G47-2	Plagioclase	NO-2G47-2a-10	55.702	0.030	27.944	n.d.	n.d.	n.d.
Thunder Bird	NO-2G47-2	Plagioclase	NO-2G47-2c-1	55.373	0.018	28.039	n.d.	n.d.	n.d.
Thunder Bird	NO-2G47-2	Plagioclase	NO-2G47-2c-2	55.368	0.028	27.860	n.d.	n.d.	n.d.
Thunder Bird	NO-2G47-2	Plagioclase	NO-2G47-2c-3	55.590	0.000	27.898	n.d.	n.d.	n.d.
Thunder Bird	NO-2G47-2	Plagioclase	NO-2G47-2d-1	55.541	0.000	27.995	n.d.	n.d.	n.d.
Thunder Bird	NO-2G47-2	Plagioclase	NO-2G47-2d-2	55.489	0.116	27.813	n.d.	n.d.	n.d.
Thunder Bird	NO-2G47-2	Plagioclase	NO-2G47-2d-3	55.376	0.036	28.255	n.d.	n.d.	n.d.
Thunder Bird	NO-2G47-2	Plagioclase	NO-2G47-2e-1	55.667	0.023	27.927	n.d.	n.d.	n.d.
Thunder Bird	NO-2G47-2	Plagioclase	NO-2G47-2e-2	55.441	0.018	28.020	n.d.	n.d.	n.d.
Thunder Bird	NO-2G47-2	Plagioclase	NO-2G47-2e-3	55.573	0.045	28.007	n.d.	n.d.	n.d.
Thunder Bird	NO-2G47-2	Pyroxene	NO-2G47-2b-10	46.170	0.385	8.143	n.d.	0.000	n.d.
Thunder Bird	NO-2G47-2	Pyroxene	NO-2G47-2b-9	49.608	0.236	4.876	n.d.	0.001	n.d.
Thunder Bird	NO-2G47-2	Pyroxene	NO-2G47-2b-8	48.607	0.175	5.977	n.d.	0.011	n.d.
Thunder Bird	NO-2G47-2	Pyroxene	NO-2G47-2b-7	46.881	0.659	6.978	n.d.	0.019	n.d.
Thunder Bird	NO-2G47-2	Pyroxene	NO-2G47-2a-6	48.645	0.300	5.871	n.d.	0.017	n.d.
Thunder Bird	NO-2G47-2	Pyroxene	NO-2G47-2a-5?	47.767	0.316	7.203	n.d.	0.021	n.d.
Thunder Bird	NO-2G47-2	Pyroxene	NO-2G47-2a-4?	49.387	0.236	4.934	n.d.	0.008	n.d.
Thunder Bird	NO-2G47-2	Pyroxene	NO-2G47-2a-1	50.821	0.172	3.963	n.d.	0.015	n.d.
Thunder Bird	NO-2G47-2	Pyroxene	NO-2G47-2a-2	52.607	0.093	2.453	n.d.	0.015	n.d.
Thunder Bird	NO-2G47-2	Pyroxene	NO-2G47-2a-3?	47.089	0.430	7.541	n.d.	0.030	n.d.
Thunder Bird	NO-2G47-2	Amphibole	NO-2G47-2b-4red	45.509	1.290	8.150	n.d.	0.011	n.d.
Thunder Bird	NO-2G47-2	Amphibole	NO-2G47-2b-3red	50.913	0.183	4.106	n.d.	0.020	n.d.
Thunder Bird	NO-2G47-2	Amphibole	NO-2G47-2b-2red	46.529	0.614	7.736	n.d.	0.012	n.d.
Thunder Bird	NO-2G47-5	Plagioclase	NO-2G47-5a-1	56.215	0.025	27.604	n.d.	n.d.	n.d.
Thunder Bird	NO-2G47-5	Plagioclase	NO-2G47-5a-4	56.119	0.035	27.660	n.d.	n.d.	n.d.
Thunder Bird	NO-2G47-5	Plagioclase	NO-2G47-5a-7	56.099	0.024	27.575	n.d.	n.d.	n.d.
Thunder Bird	NO-2G47-5	Plagioclase	NO-2G47-5a-10	56.416	0.026	27.587	n.d.	n.d.	n.d.
Thunder Bird	NO-2G47-5	Plagioclase	NO-2G47-5a-13	55.886	0.027	27.775	n.d.	n.d.	n.d.
Thunder Bird	NO-2G47-5	Plagioclase	NO-2G47-5b-17	56.099	0.036	27.603	n.d.	n.d.	n.d.
Thunder Bird	NO-2G47-5	Plagioclase	NO-2G47-5b-18	56.229	0.035	27.550	n.d.	n.d.	n.d.
Thunder Bird	NO-2G47-5	Plagioclase	NO-2G47-5b-19	56.395	0.032	27.617	n.d.	n.d.	n.d.
Thunder Bird	NO-2G47-5	Plagioclase	NO-2G47-5c-21	56.312	0.000	27.785	n.d.	n.d.	n.d.
Thunder Bird	NO-2G47-5	Plagioclase	NO-2G47-5c-22	56.146	0.030	27.837	n.d.	n.d.	n.d.
Thunder Bird	NO-2G47-5	Plagioclase	NO-2G47-5d-1	55.377	0.007	28.087	n.d.	n.d.	n.d.
Thunder Bird	NO-2G47-5	Plagioclase	NO-2G47-5d-2	55.417	0.012	28.172	n.d.	n.d.	n.d.
Thunder Bird	NO-2G47-5	Plagioclase	NO-2G47-5d-3	56.119	0.022	27.349	n.d.	n.d.	n.d.
Thunder Bird	NO-2G47-5	Plagioclase	NO-2G47-5e-1	55.913	0.037	27.831	n.d.	n.d.	n.d.
Thunder Bird	NO-2G47-5	Plagioclase	NO-2G47-5e-2	56.401	0.030	27.228	n.d.	n.d.	n.d.
Thunder Bird	NO-2G47-5	Plagioclase	NO-2G47-5e-3	55.994	0.026	27.908	n.d.	n.d.	n.d.
Thunder Bird	NO-2G47-5	Pyroxene	NO-2G47-5b-6	51.904	0.226	1.016	n.d.	0.007	n.d.
Thunder Bird	NO-2G47-5	Pyroxene	NO-2G47-5b-3	50.846	0.546	1.431	n.d.	0.029	n.d.
Thunder Bird	NO-2G47-5	Pyroxene	NO-2G47-5b-2	51.034	0.503	1.411	n.d.	0.008	n.d.
Thunder Bird	NO-2G47-5	Pyroxene	NO-2G47-5b-1	51.707	0.218	1.105	n.d.	0.003	n.d.

MgO	MnO	FeO^t	CoO	NiO	CuO	ZnO	Fe2O3	FeO	CaO	SrO	BaO	Na2O	K2O	TOTAL
9.056	0.278	21.731	n.d.	n.d.	n.d.	n.d.	n.d.	n.d.	11.331	n.d.	n.d.	0.878	0.137	97.667
4.283	0.222	23.606	n.d.	n.d.	n.d.	n.d.	n.d.	n.d.	11.249	n.d.	n.d.	1.698	0.409	97.457
4.475	0.260	23.895	n.d.	n.d.	n.d.	n.d.	n.d.	n.d.	10.863	n.d.	n.d.	1.963	0.372	98.011
6.181	0.262	23.788	n.d.	n.d.	n.d.	n.d.	n.d.	n.d.	11.045	n.d.	n.d.	1.300	0.296	97.585
4.775	0.243	23.461	n.d.	n.d.	n.d.	n.d.	n.d.	n.d.	10.939	n.d.	n.d.	1.758	0.352	97.454
3.140	0.194	24.277	n.d.	n.d.	n.d.	n.d.	n.d.	n.d.	10.750	n.d.	n.d.	1.753	0.457	97.902
3.115	0.241	24.102	n.d.	n.d.	n.d.	n.d.	n.d.	n.d.	10.603	n.d.	n.d.	1.871	0.262	98.081
2.955	0.184	24.495	n.d.	n.d.	n.d.	n.d.	n.d.	n.d.	11.060	n.d.	n.d.	1.763	0.487	98.350
0.008	0.005	0.043	n.d.	n.d.	n.d.	n.d.	n.d.	n.d.	10.523	0.000	0.000	5.819	0.014	93.920
0.000	0.000	0.098	n.d.	n.d.	n.d.	n.d.	n.d.	n.d.	10.249	0.000	0.012	5.741	0.131	94.140
0.000	0.000	0.025	n.d.	n.d.	n.d.	n.d.	n.d.	n.d.	10.172	0.000	0.000	5.891	0.018	94.194
0.000	0.011	0.024	n.d.	n.d.	n.d.	n.d.	n.d.	n.d.	10.182	0.046	0.000	5.887	0.019	93.780
0.000	0.000	0.037	n.d.	n.d.	n.d.	n.d.	n.d.	n.d.	10.173	0.084	0.002	5.947	0.012	93.775
0.000	0.000	0.152	n.d.	n.d.	n.d.	n.d.	n.d.	n.d.	11.678	0.054	0.000	5.060	0.018	95.098
0.006	0.000	0.017	n.d.	n.d.	n.d.	n.d.	n.d.	n.d.	10.074	0.000	0.000	6.033	0.012	93.994
0.016	0.000	0.045	n.d.	n.d.	n.d.	n.d.	n.d.	n.d.	10.250	0.030	0.000	5.944	0.022	94.017
0.009	0.013	0.031	n.d.	n.d.	n.d.	n.d.	n.d.	n.d.	10.455	0.160	0.032	5.833	0.029	94.098
0.003	0.018	0.025	n.d.	n.d.	n.d.	n.d.	n.d.	n.d.	10.280	0.145	0.000	5.816	0.021	93.727
0.000	0.024	0.087	n.d.	n.d.	n.d.	n.d.	n.d.	n.d.	10.231	0.114	0.000	5.941	0.006	93.944
0.004	0.007	0.037	n.d.	n.d.	n.d.	n.d.	n.d.	n.d.	10.224	0.153	0.000	5.896	0.022	93.961
0.011	0.008	0.138	n.d.	n.d.	n.d.	n.d.	n.d.	n.d.	10.218	0.031	0.005	5.846	0.020	93.824
0.001	0.014	0.081	n.d.	n.d.	n.d.	n.d.	n.d.	n.d.	10.425	0.069	0.000	5.741	0.021	94.257
0.000	0.000	0.013	n.d.	n.d.	n.d.	n.d.	n.d.	n.d.	10.221	0.077	0.000	5.905	0.008	93.928
0.000	0.000	0.036	n.d.	n.d.	n.d.	n.d.	n.d.	n.d.	10.284	0.000	0.000	5.958	0.014	93.799
0.000	0.000	0.116	n.d.	n.d.	n.d.	n.d.	n.d.	n.d.	10.388	0.062	0.043	5.907	0.029	94.191
7.826	0.279	22.728	n.d.	n.d.	n.d.	n.d.	n.d.	n.d.	11.608	n.d.	n.d.	0.947	0.156	98.242
9.798	0.291	20.632	n.d.	n.d.	n.d.	n.d.	n.d.	n.d.	11.639	n.d.	n.d.	0.488	0.074	97.643
9.069	0.299	21.511	n.d.	n.d.	n.d.	n.d.	n.d.	n.d.	11.607	n.d.	n.d.	0.592	0.104	97.952
7.835	0.274	22.750	n.d.	n.d.	n.d.	n.d.	n.d.	n.d.	11.678	n.d.	n.d.	0.801	0.179	98.054
9.226	0.330	21.503	n.d.	n.d.	n.d.	n.d.	n.d.	n.d.	11.781	n.d.	n.d.	0.662	0.097	98.432
8.749	0.293	21.056	n.d.	n.d.	n.d.	n.d.	n.d.	n.d.	11.740	n.d.	n.d.	0.798	0.117	98.060
9.997	0.294	20.594	n.d.	n.d.	n.d.	n.d.	n.d.	n.d.	12.034	n.d.	n.d.	0.561	0.072	98.117
10.408	0.277	20.253	n.d.	n.d.	n.d.	n.d.	n.d.	n.d.	11.886	n.d.	n.d.	0.408	0.058	98.261
11.128	0.332	19.704	n.d.	n.d.	n.d.	n.d.	n.d.	n.d.	12.127	n.d.	n.d.	0.255	0.055	98.769
8.229	0.268	22.124	n.d.	n.d.	n.d.	n.d.	n.d.	n.d.	11.682	n.d.	n.d.	0.839	0.132	98.364
7.273	0.319	22.860	n.d.	n.d.	n.d.	n.d.	n.d.	n.d.	11.600	n.d.	n.d.	0.967	0.237	98.216
10.098	0.297	20.706	n.d.	n.d.	n.d.	n.d.	n.d.	n.d.	11.831	n.d.	n.d.	0.450	0.063	98.667
7.853	0.296	22.834	n.d.	n.d.	n.d.	n.d.	n.d.	n.d.	11.709	n.d.	n.d.	0.860	0.214	98.657
0.010	0.006	0.087	n.d.	n.d.	n.d.	n.d.	n.d.	n.d.	9.974	0.000	0.000	6.122	0.012	93.921
0.008	0.000	0.108	n.d.	n.d.	n.d.	n.d.	n.d.	n.d.	9.856	0.008	0.000	6.084	0.061	93.794
0.000	0.000	0.111	n.d.	n.d.	n.d.	n.d.	n.d.	n.d.	9.702	0.023	0.000	6.158	0.042	93.534
0.004	0.001	0.140	n.d.	n.d.	n.d.	n.d.	n.d.	n.d.	9.740	0.061	0.000	6.150	0.030	93.975
0.000	0.000	0.062	n.d.	n.d.	n.d.	n.d.	n.d.	n.d.	10.012	0.023	0.038	6.041	0.013	93.785
0.000	0.000	0.087	n.d.	n.d.	n.d.	n.d.	n.d.	n.d.	9.827	0.000	0.000	6.148	0.018	93.652
0.012	0.000	0.131	n.d.	n.d.	n.d.	n.d.	n.d.	n.d.	9.873	0.030	0.045	6.079	0.013	93.860
0.000	0.007	0.168	n.d.	n.d.	n.d.	n.d.	n.d.	n.d.	9.851	0.000	0.026	6.149	0.029	94.070
0.000	0.000	0.090	n.d.	n.d.	n.d.	n.d.	n.d.	n.d.	9.860	0.030	0.000	6.201	0.008	94.077
0.000	0.000	0.096	n.d.	n.d.	n.d.	n.d.	n.d.	n.d.	9.938	0.000	0.042	5.986	0.018	94.047
0.011	0.003	0.076	n.d.	n.d.	n.d.	n.d.	n.d.	n.d.	10.540	0.084	0.002	5.789	0.029	94.185
0.000	0.000	0.034	n.d.	n.d.	n.d.	n.d.	n.d.	n.d.	10.423	0.106	0.003	5.779	0.014	94.164
0.009	0.005	0.185	n.d.	n.d.	n.d.	n.d.	n.d.	n.d.	9.745	0.083	0.006	6.184	0.041	93.517
0.029	0.000	0.032	n.d.	n.d.	n.d.	n.d.	n.d.	n.d.	9.989	0.000	0.000	6.056	0.017	93.831
0.027	0.011	0.601	n.d.	n.d.	n.d.	n.d.	n.d.	n.d.	9.703	0.000	0.000	6.286	0.035	94.001
0.021	0.009	0.118	n.d.	n.d.	n.d.	n.d.	n.d.	n.d.	10.162	0.129	0.000	5.968	0.017	94.367
10.854	0.312	14.274	n.d.	n.d.	n.d.	n.d.	n.d.	n.d.	21.694	n.d.	n.d.	0.181	0.003	100.471
9.977	0.376	16.394	n.d.	n.d.	n.d.	n.d.	n.d.	n.d.	20.274	n.d.	n.d.	0.213	0.000	100.086
9.757	0.413	15.461	n.d.	n.d.	n.d.	n.d.	n.d.	n.d.	21.390	n.d.	n.d.	0.225	0.013	100.215
10.881	0.353	14.754	n.d.	n.d.	n.d.	n.d.	n.d.	n.d.	20.952	n.d.	n.d.	0.206	0.000	100.179

Intrusion	Sample	Mineral	Sample Label	SiO2	TiO2	Al2O3	V2O3	Cr2O3	Nb2O3
Thunder Bird	NO-2G47-5	Pyroxene	NO-2G47-5c-13	51.010	0.477	1.485	n.d.	0.025	n.d.
Thunder Bird	NO-2G47-5	Pyroxene	NO-2G47-5c-10	51.742	0.214	0.972	n.d.	0.023	n.d.
Thunder Bird	NO-2G47-5	Pyroxene	NO-2G47-5c-9	51.433	0.387	1.041	n.d.	0.012	n.d.
Thunder Bird	NO-2G47-6	Magnetite	NO2G47-6-mag1	0.018	0.792	0.089	0.375	0.316	n.d.
Thunder Bird	NO-2G47-6	Magnetite	NO2G47-6-mag2	0.016	0.642	0.058	0.375	0.296	n.d.
Thunder Bird	NO-2G47-6	Magnetite	NO2G47-6-mag3	0.016	0.861	0.053	0.383	0.288	n.d.
Thunder Bird	NO-2G47-6	Magnetite	NO2G47-6-mag4	0.022	2.445	0.049	0.217	0.150	n.d.
Thunder Bird	NO-2G47-6	Magnetite	NO2G47-6-mag5a	0.046	0.425	0.145	0.642	0.090	n.d.
Thunder Bird	NO-2G47-6	Magnetite	NO2G47-6-mag5b	0.046	0.719	0.159	0.614	0.086	n.d.
Thunder Bird	NO-2G47-6	Magnetite	NO2G47-6-mag5c	0.062	0.496	0.114	0.620	0.119	n.d.
Thunder Bird	NO-2G47-6	Magnetite	NO2G47-6-mag6	0.061	0.264	0.099	0.507	0.177	n.d.
Thunder Bird	NO-2G47-6	Magnetite	NO2G47-6-mag7	0.183	0.430	0.123	0.509	0.179	n.d.
Thunder Bird	NO-2G47-6	Ilmenite	NO2G47-6-ilm1a	0.000	51.581	0.012	0.017	0.001	0.000
Thunder Bird	NO-2G47-6	Ilmenite	NO2G47-6-ilm1b	0.000	51.278	0.012	0.016	0.013	0.000
Thunder Bird	NO-2G47-6	Ilmenite	NO2G47-6-ilm1c	0.012	51.279	0.019	0.009	0.005	0.000
Thunder Bird	NO-2G47-6	Ilmenite	NO2G47-6-ilm2a	0.007	51.427	0.017	0.031	0.017	0.000
Thunder Bird	NO-2G47-6	Ilmenite	NO2G47-6-ilm2b	0.006	51.425	0.013	0.021	0.014	0.000
Thunder Bird	NO-2G47-6	Ilmenite	NO2G47-6-ilm2c	0.012	52.143	0.013	0.011	0.020	0.000
Thunder Bird	NO-2G47-6	Ilmenite	NO2G47-6-ilm3	0.006	51.523	0.002	0.024	0.028	0.000
Thunder Bird	NO-2G47-6	Ilmenite	NO2G47-6-ilm4a	0.007	52.147	0.000	0.048	0.021	0.000
Thunder Bird	NO-2G47-6	Ilmenite	NO2G47-6-ilm4b	0.004	51.304	0.014	0.044	0.007	0.006
Thunder Bird	NO-2G47-6	Ilmenite	NO2G47-6-ilm4c	0.011	51.433	0.015	0.041	0.001	0.000
Thunder Bird	NO-2G47-6	Ilmenite	NO2G47-6-ilm4d	0.000	51.609	0.012	0.046	0.008	0.000
Thunder Bird	NO-2G47-6	Ilmenite	NO2G47-6-ilm5	0.000	51.777	0.014	0.068	0.011	0.000
Thunder Bird	NO-2G47-6	Ilmenite	NO2G47-6-ilm6a	0.008	50.565	0.013	0.066	0.019	0.000
Thunder Bird	NO-2G47-6	Ilmenite	NO2G47-6-ilm6b	0.013	51.460	0.016	0.040	0.010	0.000
Thunder Bird	NO-2G47-7	Magnetite	NO2G47-7-mag1a	0.043	0.091	0.131	0.477	0.058	n.d.
Thunder Bird	NO-2G47-7	Magnetite	NO2G47-7-mag1b	0.041	0.093	0.131	0.471	0.060	n.d.
Thunder Bird	NO-2G47-7	Magnetite	NO2G47-7-mag2a	0.089	0.154	0.187	0.479	0.068	n.d.
Thunder Bird	NO-2G47-7	Magnetite	NO2G47-7-mag2b	0.040	0.147	0.133	0.476	0.064	n.d.
Thunder Bird	NO-2G47-7	Magnetite	NO2G47-7-mag2c	0.104	0.272	0.131	0.470	0.081	n.d.
Thunder Bird	NO-2G47-7	Magnetite	NO2G47-7-mag3	0.036	0.166	0.121	0.385	0.088	n.d.
Thunder Bird	NO-2G47-7	Magnetite	NO2G47-7-mag4	0.046	0.200	0.122	0.446	0.081	n.d.
Thunder Bird	NO-2G47-7	Magnetite	NO2G47-7-mag5	0.031	0.303	0.106	0.490	0.121	n.d.
Thunder Bird	NO-2G47-7	Magnetite	NO2G47-7-mag6a	0.065	0.222	0.203	0.559	0.088	n.d.
Thunder Bird	NO-2G47-7	Magnetite	NO2G47-7-mag6b	0.076	0.270	0.165	0.555	0.086	n.d.
Thunder Bird	NO-2G47-7	Magnetite	NO2G47-7-mag6c	0.031	0.267	0.098	0.586	0.088	n.d.
Thunder Bird	NO-2G47-7	Magnetite	NO2G47-7-mag6d	0.030	0.475	0.125	0.570	0.070	n.d.
Thunder Bird	NO-2G47-7	Magnetite	NO2G47-7-mag7	0.073	0.188	0.112	0.429	0.094	n.d.
Thunder Bird	NO-2G47-7	Ilmenite	NO2G47-7-ilm1a	0.007	51.665	0.020	0.036	0.014	0.000
Thunder Bird	NO-2G47-7	Ilmenite	NO2G47-7-ilm1b	0.010	51.073	0.007	0.041	0.006	0.000
Thunder Bird	NO-2G47-7	Ilmenite	NO2G47-7-ilm1c	0.007	51.495	0.009	0.028	0.009	0.000
Thunder Bird	NO-2G47-7	Ilmenite	NO2G47-7-ilm1d	0.000	51.712	0.014	0.012	0.004	0.000
Thunder Bird	NO-2G47-7	Ilmenite	NO2G47-7-ilm2a	0.006	50.932	0.010	0.039	0.001	0.000
Thunder Bird	NO-2G47-7	Ilmenite	NO2G47-7-ilm2b	0.023	51.813	0.011	0.025	0.010	0.000
Thunder Bird	NO-2G47-7	Ilmenite	NO2G47-7-ilm3	0.011	51.772	0.015	0.047	0.009	0.000
Thunder Bird	NO-2G47-7	Ilmenite	NO2G47-7-ilm4	0.000	51.653	0.005	0.039	0.010	0.000
Thunder Bird	NO-2G47-7	Ilmenite	NO2G47-7-ilm5a	0.003	51.555	0.010	0.060	0.018	0.000
Thunder Bird	NO-2G47-7	Ilmenite	NO2G47-7-ilm5b	0.006	51.485	0.034	0.050	0.010	0.000
Thunder Bird	NO-2G47-7	Ilmenite	NO2G47-7-ilm5c	0.003	51.577	0.012	0.060	0.000	0.000
Thunder Bird	NO-2G47-7	Ilmenite	NO2G47-7-ilm6	0.011	51.615	0.007	0.075	0.011	0.000
Thunder Bird	NO-2G47-7	Ilmenite	NO2G47-7-ilm7	0.000	51.954	0.013	0.056	0.015	0.000
Thunder Bird	NO-2G47-7	Ilmenite	NO2G47-7-ilm8	0.020	51.212	0.009	0.047	0.000	0.000
Thunder Bird	NO-2G47-8	Magnetite	NO2G47-8-mag1a	0.078	0.424	0.118	0.282	0.045	n.d.
Thunder Bird	NO-2G47-8	Magnetite	NO2G47-8-mag1b	0.103	0.891	0.133	0.280	0.045	n.d.
Thunder Bird	NO-2G47-8	Magnetite	NO2G47-8-mag1c	0.022	0.846	0.033	0.278	0.048	n.d.
Thunder Bird	NO-2G47-8	Magnetite	NO2G47-8-mag2	0.035	0.562	0.071	0.250	0.057	n.d.
Thunder Bird	NO-2G47-8	Magnetite	NO2G47-8-mag3	0.027	0.497	0.074	0.277	0.052	n.d.

MgO	MnO	FeO^t	CoO	NiO	CuO	ZnO	Fe2O3	FeO	CaO	SrO	BaO	Na2O	K2O	TOTAL
10.219	0.398	15.583	n.d.	n.d.	n.d.	n.d.	n.d.	n.d.	20.710	n.d.	n.d.	0.212	0.000	100.119
10.865	0.361	15.399	n.d.	n.d.	n.d.	n.d.	n.d.	n.d.	20.917	n.d.	n.d.	0.183	0.006	100.682
10.393	0.384	15.560	n.d.	n.d.	n.d.	n.d.	n.d.	n.d.	21.275	n.d.	n.d.	0.206	0.005	100.696
0.000	0.005	92.254	0.007	0.002	0.000	0.000	66.983	31.982	n.d.	n.d.	n.d.	n.d.	n.d.	100.569
0.000	0.006	91.958	0.001	0.000	0.000	0.002	66.987	31.683	n.d.	n.d.	n.d.	n.d.	n.d.	100.066
0.000	0.011	91.797	0.011	0.002	0.000	0.000	66.589	31.879	n.d.	n.d.	n.d.	n.d.	n.d.	100.094
0.000	0.018	91.643	0.010	0.001	0.000	0.000	64.467	33.635	n.d.	n.d.	n.d.	n.d.	n.d.	101.014
0.000	0.006	92.071	0.009	0.000	0.000	0.003	67.245	31.563	n.d.	n.d.	n.d.	n.d.	n.d.	100.174
0.000	0.014	91.930	0.007	0.008	0.000	0.019	66.773	31.847	n.d.	n.d.	n.d.	n.d.	n.d.	100.292
0.000	0.004	91.987	0.011	0.000	0.000	0.014	67.081	31.627	n.d.	n.d.	n.d.	n.d.	n.d.	100.148
0.000	0.005	92.203	0.000	0.004	0.000	0.000	67.566	31.407	n.d.	n.d.	n.d.	n.d.	n.d.	100.090
0.000	0.000	91.613	0.007	0.000	0.000	0.021	66.690	31.605	n.d.	n.d.	n.d.	n.d.	n.d.	99.747
0.069	0.832	47.932	0.000	0.003	0.000	0.000	2.785	45.426	n.d.	n.d.	n.d.	n.d.	n.d.	100.726
0.066	0.838	47.477	0.000	0.000	0.000	0.014	2.594	45.143	n.d.	n.d.	n.d.	n.d.	n.d.	99.974
0.064	0.826	47.062	0.002	0.000	0.000	0.000	2.087	45.184	n.d.	n.d.	n.d.	n.d.	n.d.	99.487
0.036	0.822	47.468	0.004	0.000	0.000	0.011	2.350	45.354	n.d.	n.d.	n.d.	n.d.	n.d.	100.075
0.028	0.830	47.119	0.008	0.000	0.024	0.011	1.987	45.331	n.d.	n.d.	n.d.	n.d.	n.d.	99.698
0.039	0.820	47.407	0.000	0.000	0.000	0.000	1.548	46.014	n.d.	n.d.	n.d.	n.d.	n.d.	100.620
0.045	0.844	47.461	0.001	0.000	0.000	0.016	2.292	45.399	n.d.	n.d.	n.d.	n.d.	n.d.	100.180
0.044	0.850	47.319	0.005	0.003	0.000	0.012	1.517	45.954	n.d.	n.d.	n.d.	n.d.	n.d.	100.608
0.044	0.854	47.150	0.012	0.001	0.000	0.016	2.190	45.180	n.d.	n.d.	n.d.	n.d.	n.d.	99.675
0.029	0.850	47.822	0.004	0.000	0.000	0.002	2.741	45.356	n.d.	n.d.	n.d.	n.d.	n.d.	100.483
0.020	0.834	47.659	0.012	0.000	0.000	0.015	2.384	45.514	n.d.	n.d.	n.d.	n.d.	n.d.	100.454
0.014	0.900	47.182	0.011	0.002	0.000	0.006	1.740	45.616	n.d.	n.d.	n.d.	n.d.	n.d.	100.159
0.027	0.839	47.659	0.003	0.005	0.011	0.019	3.447	44.558	n.d.	n.d.	n.d.	n.d.	n.d.	99.579
0.022	0.842	47.041	0.004	0.000	0.000	0.005	1.823	45.401	n.d.	n.d.	n.d.	n.d.	n.d.	99.636
0.000	0.004	91.981	0.004	0.000	0.000	0.003	67.701	31.063	n.d.	n.d.	n.d.	n.d.	n.d.	99.575
0.000	0.004	92.287	0.017	0.003	0.000	0.001	67.940	31.154	n.d.	n.d.	n.d.	n.d.	n.d.	99.915
0.008	0.008	91.940	0.008	0.000	0.002	0.006	67.491	31.211	n.d.	n.d.	n.d.	n.d.	n.d.	99.711
0.000	0.004	91.972	0.000	0.001	0.000	0.000	67.618	31.129	n.d.	n.d.	n.d.	n.d.	n.d.	99.612
0.002	0.002	91.807	0.006	0.002	0.000	0.007	67.224	31.319	n.d.	n.d.	n.d.	n.d.	n.d.	99.619
0.000	0.010	91.738	0.000	0.002	0.000	0.008	67.467	31.031	n.d.	n.d.	n.d.	n.d.	n.d.	99.314
0.005	0.000	92.331	0.008	0.000	0.000	0.001	67.822	31.304	n.d.	n.d.	n.d.	n.d.	n.d.	100.035
0.000	0.012	91.752	0.004	0.003	0.000	0.000	67.262	31.229	n.d.	n.d.	n.d.	n.d.	n.d.	99.561
0.020	0.000	91.824	0.000	0.003	0.000	0.022	67.329	31.241	n.d.	n.d.	n.d.	n.d.	n.d.	99.752
0.000	0.000	91.731	0.013	0.007	0.000	0.016	67.180	31.282	n.d.	n.d.	n.d.	n.d.	n.d.	99.650
0.000	0.003	91.701	0.008	0.006	0.000	0.001	67.253	31.186	n.d.	n.d.	n.d.	n.d.	n.d.	99.527
0.003	0.000	91.980	0.011	0.001	0.000	0.006	67.186	31.526	n.d.	n.d.	n.d.	n.d.	n.d.	100.002
0.000	0.001	92.181	0.000	0.008	0.000	0.002	67.681	31.281	n.d.	n.d.	n.d.	n.d.	n.d.	99.869
0.003	0.850	47.141	0.000	0.000	0.003	0.025	1.727	45.587	n.d.	n.d.	n.d.	n.d.	n.d.	99.937
0.012	0.855	47.609	0.000	0.000	0.000	0.000	2.831	45.062	n.d.	n.d.	n.d.	n.d.	n.d.	99.897
0.009	0.870	46.719	0.016	0.005	0.000	0.004	1.461	45.404	n.d.	n.d.	n.d.	n.d.	n.d.	99.317
0.001	0.894	46.845	0.001	0.001	0.000	0.000	1.380	45.603	n.d.	n.d.	n.d.	n.d.	n.d.	99.622
0.025	0.862	47.563	0.000	0.003	0.000	0.014	2.976	44.885	n.d.	n.d.	n.d.	n.d.	n.d.	99.753
0.015	0.901	46.408	0.002	0.000	0.000	0.001	0.800	45.688	n.d.	n.d.	n.d.	n.d.	n.d.	99.289
0.010	0.921	46.887	0.006	0.003	0.001	0.009	1.418	45.611	n.d.	n.d.	n.d.	n.d.	n.d.	99.833
0.007	0.877	47.255	0.008	0.001	0.010	0.009	1.914	45.533	n.d.	n.d.	n.d.	n.d.	n.d.	100.066
0.032	0.842	47.298	0.000	0.000	0.002	0.014	2.053	45.450	n.d.	n.d.	n.d.	n.d.	n.d.	100.040
0.033	0.846	46.553	0.011	0.000	0.000	0.019	1.313	45.372	n.d.	n.d.	n.d.	n.d.	n.d.	99.179
0.031	0.840	47.323	0.011	0.000	0.000	0.006	2.057	45.472	n.d.	n.d.	n.d.	n.d.	n.d.	100.069
0.006	0.884	46.593	0.010	0.000	0.003	0.002	1.195	45.518	n.d.	n.d.	n.d.	n.d.	n.d.	99.337
0.015	0.872	46.281	0.000	0.008	0.000	0.008	0.529	45.805	n.d.	n.d.	n.d.	n.d.	n.d.	99.275
0.020	0.835	46.710	0.005	0.000	0.001	0.012	1.691	45.189	n.d.	n.d.	n.d.	n.d.	n.d.	99.040
0.011	0.006	91.600	0.010	0.006	0.000	0.000	67.016	31.299	n.d.	n.d.	n.d.	n.d.	n.d.	99.294
0.027	0.011	90.763	0.010	0.004	0.000	0.008	65.751	31.600	n.d.	n.d.	n.d.	n.d.	n.d.	98.863
0.001	0.010	92.030	0.004	0.003	0.000	0.004	66.902	31.831	n.d.	n.d.	n.d.	n.d.	n.d.	99.982
0.009	0.009	92.184	0.020	0.007	0.000	0.000	67.380	31.555	n.d.	n.d.	n.d.	n.d.	n.d.	99.955
0.000	0.013	92.452	0.016	0.001	0.000	0.000	67.654	31.576	n.d.	n.d.	n.d.	n.d.	n.d.	100.187

Intrusion	Sample	Mineral	Sample Label	SiO2	TiO2	Al2O3	V2O3	Cr2O3	Nb2O3
Thunder Bird	NO-2G47-8	Magnetite	NO2G47-8-mag4	0.031	0.062	0.036	0.252	0.022	n.d.
Thunder Bird	NO-2G47-8	Magnetite	NO2G47-8-mag5	0.068	1.270	0.043	0.227	0.046	n.d.
Thunder Bird	NO-2G47-8	Magnetite	NO2G47-8-mag6	0.022	0.610	0.064	0.273	0.071	n.d.
Thunder Bird	NO-2G47-8	Magnetite	NO2G47-8-mag7	0.012	0.494	0.073	0.246	0.066	n.d.
Thunder Bird	NO-2G47-8	Magnetite	NO2G47-8-mag8a	0.019	0.545	0.069	0.306	0.045	n.d.
Thunder Bird	NO-2G47-8	Magnetite	NO2G47-8-mag8b	0.041	0.948	0.067	0.300	0.041	n.d.
Thunder Bird	NO-2G47-8	Magnetite	NO2G47-8-mag8c	0.225	0.487	0.070	0.311	0.048	n.d.
Thunder Bird	NO-2G47-8	Magnetite	NO2G47-8-mag8d	0.020	1.028	0.065	0.301	0.047	n.d.
Thunder Bird	NO-2G47-8	Ilmenite	NO2G47-8-ilm1a	0.014	51.368	0.003	0.022	0.001	0.000
Thunder Bird	NO-2G47-8	Ilmenite	NO2G47-8-ilm1b	0.006	51.025	0.014	0.024	0.000	0.000
Thunder Bird	NO-2G47-8	Ilmenite	NO2G47-8-ilm1c	0.003	51.726	0.007	0.017	0.001	0.000
Thunder Bird	NO-2G47-8	Ilmenite	NO2G47-8-ilm1d	0.005	51.720	0.011	0.028	0.002	0.000
Thunder Bird	NO-2G47-8	Ilmenite	NO2G47-8-ilm1e	0.004	51.806	0.010	0.023	0.007	0.000
Thunder Bird	NO-2G47-8	Ilmenite	NO2G47-8-ilm1f	0.007	51.948	0.011	0.031	0.005	0.000
Thunder Bird	NO-2G47-8	Ilmenite	NO2G47-8-ilm2	0.016	51.357	0.010	0.038	0.005	0.000
Thunder Bird	NO-2G47-8	Ilmenite	NO2G47-8-ilm3	0.014	51.374	0.012	0.043	0.002	0.000
Thunder Bird	NO-2G47-8	Ilmenite	NO2G47-8-ilm4	0.004	51.498	0.011	0.029	0.011	0.005
Thunder Bird	NO-2G47-8	Ilmenite	NO2G47-8-ilm5a	0.000	51.701	0.014	0.013	0.008	0.000
Thunder Bird	NO-2G47-8	Ilmenite	NO2G47-8-ilm5b	0.010	51.429	0.011	0.020	0.003	0.000
Thunder Bird	NO-2G47-8	Ilmenite	NO2G47-8-ilm5c	0.008	51.459	0.013	0.017	0.007	0.000
Thunder Bird	NO-2G47-8	Ilmenite	NO2G47-8-ilm6	0.004	51.093	0.010	0.035	0.009	0.000
Thunder Bird	NO-2G47-8	Ilmenite	NO2G47-8-ilm7	0.014	51.467	0.011	0.040	0.000	0.000
Thunder Bird	NO-2G47-9	Magnetite	NO2G47-9-mag10a	0.030	0.186	0.082	0.142	0.021	n.d.
Thunder Bird	NO-2G47-9	Magnetite	NO2G47-9-mag10b	0.038	0.620	0.058	0.129	0.015	n.d.
Thunder Bird	NO-2G47-9	Magnetite	NO2G47-9-mag1a	0.051	0.805	0.089	0.125	0.021	n.d.
Thunder Bird	NO-2G47-9	Magnetite	NO2G47-9-mag1b	0.044	0.402	0.078	0.128	0.017	n.d.
Thunder Bird	NO-2G47-9	Magnetite	NO2G47-9-mag2	0.023	0.374	0.086	0.129	0.022	n.d.
Thunder Bird	NO-2G47-9	Magnetite	NO2G47-9-mag3	0.046	0.817	0.070	0.123	0.028	n.d.
Thunder Bird	NO-2G47-9	Magnetite	NO2G47-9-mag4	0.044	0.463	0.065	0.125	0.027	n.d.
Thunder Bird	NO-2G47-9	Magnetite	NO2G47-9-mag5	0.058	0.257	0.081	0.137	0.021	n.d.
Thunder Bird	NO-2G47-9	Magnetite	NO2G47-9-mag6	0.027	0.138	0.080	0.149	0.013	n.d.
Thunder Bird	NO-2G47-9	Magnetite	NO2G47-9-mag7	0.044	0.160	0.077	0.144	0.021	n.d.
Thunder Bird	NO-2G47-9	Magnetite	NO2G47-9-mag8	0.037	0.149	0.070	0.144	0.025	n.d.
Thunder Bird	NO-2G47-9	Magnetite	NO2G47-9-mag9	0.033	0.157	0.069	0.134	0.024	n.d.
Thunder Bird	NO-2G47-9	Ilmenite	NO2G47-9-ilm1a	0.011	51.442	0.002	0.000	0.004	0.000
Thunder Bird	NO-2G47-9	Ilmenite	NO2G47-9-ilm1b	0.010	51.715	0.019	0.000	0.000	0.000
Thunder Bird	NO-2G47-9	Ilmenite	NO2G47-9-ilm1c	0.010	52.107	0.014	0.000	0.000	0.000
Thunder Bird	NO-2G47-9	Ilmenite	NO2G47-9-ilm1d	0.007	51.179	0.005	0.000	0.002	0.000
Thunder Bird	NO-2G47-9	Ilmenite	NO2G47-9-ilm2a	0.003	51.602	0.008	0.000	0.000	0.000
Thunder Bird	NO-2G47-9	Ilmenite	NO2G47-9-ilm2b	0.025	51.638	0.017	0.000	0.003	0.000
Thunder Bird	NO-2G47-9	Ilmenite	NO2G47-9-ilm3	0.039	51.292	0.014	0.000	0.003	0.000
Thunder Bird	NO-2G47-9	Ilmenite	NO2G47-9-ilm4	0.004	51.568	0.013	0.000	0.000	0.000
Thunder Bird	NO-2G47-9	Ilmenite	NO2G47-9-ilm5	0.005	51.287	0.007	0.000	0.000	0.000
Thunder Bird	NO-2G47-9	Ilmenite	NO2G47-9-ilm6a	0.012	51.294	0.012	0.001	0.002	0.000
Thunder Bird	NO-2G47-9	Ilmenite	NO2G47-9-ilm6b	0.012	51.242	0.005	0.000	0.000	0.000
Thunder Bird	NO-2G47-9	Ilmenite	NO2G47-9-ilm6c	0.006	51.161	0.012	0.000	0.008	0.000
Thunder Bird	NO-2G47-9	Ilmenite	NO2G47-9-ilm7a	0.000	51.611	0.014	0.000	0.000	0.000
Thunder Bird	NO-2G47-9	Ilmenite	NO2G47-9-ilm7b	0.014	51.593	0.015	0.000	0.000	0.000
Thunder Bird	NO-2G47-9	Ilmenite	NO2G47-9-ilm7c	0.007	51.817	0.016	0.000	0.000	0.000
Thunder Bird	NO-2G47-9	Ilmenite	NO2G47-9-ilm7d	0.022	51.342	0.013	0.000	0.000	0.000
Thunder Bird	NO-2G47-9	Ilmenite	NO2G47-9-ilm8	0.013	51.384	0.010	0.000	0.000	0.000
Thunder Bird	NO-2G47-9	Ilmenite	NO2G47-9-ilm9	0.008	51.792	0.007	0.000	0.000	0.000
Thunder Bird	NO-2G47-9	Ilmenite	NO2G47-9-ilm10a	0.015	51.327	0.015	0.000	0.004	0.000
Thunder Bird	NO-2G47-9	Ilmenite	NO2G47-9-ilm10b	0.030	51.067	0.010	0.000	0.001	0.000
Thunder Bird	NO-2G47-9	Ilmenite	NO2G47-9-ilm10c	0.021	51.395	0.009	0.000	0.004	0.000

MgO	MnO	FeO^t	CoO	NiO	CuO	ZnO	Fe2O3	FeO	CaO	SrO	BaO	Na2O	K2O	TOTAL
0.000	0.007	92.370	0.004	0.000	0.000	0.000	68.191	31.011	n.d.	n.d.	n.d.	n.d.	n.d.	99.616
0.000	0.011	92.116	0.016	0.002	0.000	0.009	66.343	32.420	n.d.	n.d.	n.d.	n.d.	n.d.	100.455
0.000	0.004	91.382	0.013	0.000	0.000	0.006	66.714	31.352	n.d.	n.d.	n.d.	n.d.	n.d.	99.129
0.000	0.004	92.321	0.010	0.003	0.000	0.001	67.585	31.507	n.d.	n.d.	n.d.	n.d.	n.d.	100.001
0.002	0.007	92.229	0.003	0.000	0.000	0.004	67.424	31.560	n.d.	n.d.	n.d.	n.d.	n.d.	99.984
0.000	0.009	91.744	0.009	0.000	0.000	0.003	66.496	31.910	n.d.	n.d.	n.d.	n.d.	n.d.	99.824
0.036	0.018	91.752	0.000	0.001	0.008	0.005	66.838	31.611	n.d.	n.d.	n.d.	n.d.	n.d.	99.658
0.000	0.008	91.879	0.001	0.001	0.000	0.000	66.518	32.026	n.d.	n.d.	n.d.	n.d.	n.d.	100.015
0.026	0.972	47.093	0.007	0.004	0.000	0.012	2.140	45.167	n.d.	n.d.	n.d.	n.d.	n.d.	99.736
0.024	0.933	46.733	0.006	0.001	0.007	0.020	2.056	44.883	n.d.	n.d.	n.d.	n.d.	n.d.	98.999
0.029	0.926	47.198	0.004	0.000	0.000	0.000	1.848	45.535	n.d.	n.d.	n.d.	n.d.	n.d.	100.096
0.013	0.912	47.258	0.014	0.000	0.000	0.010	1.891	45.556	n.d.	n.d.	n.d.	n.d.	n.d.	100.163
0.025	0.947	47.025	0.008	0.006	0.000	0.012	1.613	45.574	n.d.	n.d.	n.d.	n.d.	n.d.	100.035
0.025	0.967	47.269	0.030	0.000	0.000	0.015	1.781	45.667	n.d.	n.d.	n.d.	n.d.	n.d.	100.486
0.017	0.966	47.158	0.017	0.004	0.000	0.000	2.195	45.183	n.d.	n.d.	n.d.	n.d.	n.d.	99.808
0.004	0.995	46.820	0.013	0.001	0.000	0.003	1.807	45.194	n.d.	n.d.	n.d.	n.d.	n.d.	99.462
0.019	0.919	47.443	0.007	0.000	0.000	0.024	2.346	45.332	n.d.	n.d.	n.d.	n.d.	n.d.	100.205
0.030	0.924	47.277	0.000	0.000	0.000	0.005	1.966	45.508	n.d.	n.d.	n.d.	n.d.	n.d.	100.169
0.029	0.915	47.085	0.013	0.000	0.000	0.012	2.019	45.268	n.d.	n.d.	n.d.	n.d.	n.d.	99.729
0.019	0.958	47.077	0.009	0.004	0.000	0.000	2.000	45.277	n.d.	n.d.	n.d.	n.d.	n.d.	99.771
0.012	1.000	46.793	0.011	0.000	0.000	0.011	2.098	44.906	n.d.	n.d.	n.d.	n.d.	n.d.	99.188
0.020	0.967	47.133	0.007	0.000	0.000	0.011	2.063	45.277	n.d.	n.d.	n.d.	n.d.	n.d.	99.877
0.000	0.013	92.436	0.003	0.000	0.000	0.002	68.097	31.162	n.d.	n.d.	n.d.	n.d.	n.d.	99.738
0.001	0.013	91.912	0.010	0.013	0.000	0.018	67.162	31.479	n.d.	n.d.	n.d.	n.d.	n.d.	99.556
0.011	0.014	92.688	0.004	0.011	0.000	0.003	67.449	31.997	n.d.	n.d.	n.d.	n.d.	n.d.	100.580
0.000	0.007	92.368	0.009	0.000	0.000	0.000	67.741	31.414	n.d.	n.d.	n.d.	n.d.	n.d.	99.840
0.002	0.015	92.080	0.000	0.000	0.000	0.006	67.602	31.251	n.d.	n.d.	n.d.	n.d.	n.d.	99.510
0.001	0.016	92.096	0.013	0.000	0.004	0.001	66.999	31.810	n.d.	n.d.	n.d.	n.d.	n.d.	99.928
0.001	0.009	92.414	0.010	0.000	0.000	0.010	67.708	31.490	n.d.	n.d.	n.d.	n.d.	n.d.	99.952
0.001	0.009	92.399	0.007	0.009	0.008	0.000	67.940	31.266	n.d.	n.d.	n.d.	n.d.	n.d.	99.794
0.000	0.000	92.642	0.000	0.000	0.000	0.000	68.307	31.179	n.d.	n.d.	n.d.	n.d.	n.d.	99.893
0.000	0.012	92.447	0.014	0.003	0.000	0.002	68.126	31.146	n.d.	n.d.	n.d.	n.d.	n.d.	99.750
0.000	0.008	92.407	0.009	0.000	0.000	0.000	68.116	31.116	n.d.	n.d.	n.d.	n.d.	n.d.	99.674
0.000	0.000	92.413	0.000	0.008	0.000	0.012	68.122	31.116	n.d.	n.d.	n.d.	n.d.	n.d.	99.675
0.047	1.204	46.547	0.009	0.001	0.000	0.007	1.760	44.963	n.d.	n.d.	n.d.	n.d.	n.d.	99.450
0.055	1.234	47.069	0.018	0.000	0.000	0.008	2.128	45.154	n.d.	n.d.	n.d.	n.d.	n.d.	100.341
0.045	1.221	46.441	0.013	0.000	0.000	0.009	0.999	45.542	n.d.	n.d.	n.d.	n.d.	n.d.	99.960
0.041	1.219	46.321	0.000	0.000	0.008	0.004	1.777	44.722	n.d.	n.d.	n.d.	n.d.	n.d.	98.964
0.054	1.162	46.696	0.001	0.000	0.000	0.014	1.740	45.130	n.d.	n.d.	n.d.	n.d.	n.d.	99.714
0.065	1.219	46.159	0.013	0.000	0.000	0.005	1.168	45.108	n.d.	n.d.	n.d.	n.d.	n.d.	99.261
0.048	1.234	46.360	0.008	0.000	0.000	0.000	1.692	44.838	n.d.	n.d.	n.d.	n.d.	n.d.	99.167
0.044	1.220	46.765	0.008	0.003	0.006	0.017	1.915	45.042	n.d.	n.d.	n.d.	n.d.	n.d.	99.840
0.041	1.230	46.875	0.007	0.002	0.008	0.000	2.305	44.801	n.d.	n.d.	n.d.	n.d.	n.d.	99.693
0.041	1.214	46.374	0.000	0.003	0.000	0.002	1.701	44.843	n.d.	n.d.	n.d.	n.d.	n.d.	99.125
0.053	1.210	46.703	0.005	0.001	0.001	0.000	2.141	44.777	n.d.	n.d.	n.d.	n.d.	n.d.	99.446
0.046	1.202	46.470	0.011	0.006	0.004	0.008	1.970	44.697	n.d.	n.d.	n.d.	n.d.	n.d.	99.131
0.062	1.228	46.218	0.000	0.005	0.000	0.000	1.285	45.062	n.d.	n.d.	n.d.	n.d.	n.d.	99.267
0.052	1.222	46.414	0.010	0.002	0.000	0.021	1.503	45.061	n.d.	n.d.	n.d.	n.d.	n.d.	99.494
0.049	1.205	46.501	0.010	0.000	0.000	0.002	1.340	45.296	n.d.	n.d.	n.d.	n.d.	n.d.	99.741
0.059	1.247	46.448	0.000	0.006	0.000	0.013	1.809	44.820	n.d.	n.d.	n.d.	n.d.	n.d.	99.331
0.043	1.229	46.774	0.016	0.000	0.000	0.017	2.104	44.881	n.d.	n.d.	n.d.	n.d.	n.d.	99.697
0.041	1.263	46.773	0.006	0.000	0.000	0.017	1.725	45.220	n.d.	n.d.	n.d.	n.d.	n.d.	100.080
0.025	1.232	46.664	0.001	0.000	0.000	0.000	1.971	44.890	n.d.	n.d.	n.d.	n.d.	n.d.	99.480
0.028	1.256	46.102	0.000	0.003	0.000	0.007	1.629	44.637	n.d.	n.d.	n.d.	n.d.	n.d.	98.667
0.030	1.211	46.759	0.004	0.003	0.000	0.000	1.993	44.965	n.d.	n.d.	n.d.	n.d.	n.d.	99.636

Appendix D

Whole rock and trace element geochemistry

Sample	Intrusion	Depth (m)	SG	Au	Ir	Pd
				ppb	ppb	ppb
				Ni-S Fire Assay	Ni-S Fire Assay	Ni-S Fire Assay
MM-V1-1	Butler West	15.14	4.58	0.44	0.02	0.32
MM-V1-2	Butler West	16.02	3.8	<0.22	0.01	0.16
MM-V1-3	Butler West	35.09	3.09	<0.22	0.01	<0.12
MM-V1-4	Butler West	36.78	4.57	0.31	0.01	0.54
MM-V1-5	Butler West	64.88	4.47	0.61	0.01	0.32
MM-V1-6	Butler West	120.14	2.72	<0.22	0.01	<0.12
MM-V2-1	Butler West	16.28	4.01	1.79	0.03	0.94
MM-V2-2	Butler West	62.3	4.71	0.54	0.04	0.95
MM-V2-3	Butler West	63.34	4.59	0.87	0.05	0.87
MM-V2-4	Butler West	76.64	3.32	0.92	0.02	0.19
MM-V2-5	Butler West	89.41	3.3	0.47	0.01	<0.12
MM-V2-6	Butler West	108.13	1.66	3.21	0.01	0.16
MM-V4-1	Butler East	18.5	3.96	31.8	0.08	3.07
MM-V4-2	Butler East	54.04	4.23	0.85	0.1	1.77
MM-V4-3	Butler East	63.73	4.14	2.48	0.04	2.29
MM-V4-4	Butler East	64.5	3.59	1.31	0.03	3.78
MM-V4-5	Butler East	109.09	3.12	0.24	0.01	0.24
MM-V4-6	Butler East	147.21	3.07	11.8	0.02	2.51
MM-V4-7	Butler East	162	3.15	3.9	0.04	0.16
MM-V5-1	Butler East	85.5	3.53	0.72	0.04	1.98
MM-V5-2	Butler East	86.27	3.56	2.61	0.14	4.13
MM-V5-3	Butler East	108.17	4.34	1.23	0.18	10.6
MM-V5-4	Butler East	168	3.1	0.94	3.75	8.8
MM-V5-5	Butler East	179	2.91	1.16	4.49	1.36
MM-V5-6	Butler East	192	2.81	13.7	0.13	8.07
MM-V5-7	Butler East	244.47	3.2	2.59	0.19	4.02
MM-V8-1	Butler West	39.3	3.11	0.45	0.01	<0.12
MM-V8-2	Butler West	40.15	3.39	0.81	0.01	<0.12
MM-V8-3	Butler West	41.91	3.14	0.35	0.01	<0.12
MM-V8-4	Butler West	42.46	3.81	0.8	0.02	0.15
MM-V8-5	Butler West	115.11	3.13	0.65	0.01	<0.12
MM-60-1	Butler West	67.5	4.39	0.97	0.01	0.17
MM-60-2	Butler West	68.17	3.58	1.55	0.01	0.3
MM-60-3	Butler West	72.2	3.36	0.87	0.01	<0.12
MM-60-4	Butler West	118.87	3.02	0.45	0.01	<0.12
MM-60-5	Butler West	155.28	2.82	0.71	0.07	0.13
MM-70-1	Butler East	104.25	4.64	3.66	0.04	0.58
MM-70-2	Butler East	139.73	3.44	3.35	0.02	0.2
MM-70-3	Butler East	125	3.54	2.29	0.01	0.2
MM-70-4	Butler East	129.75	3.36	1.14	0.01	<0.12
MM-70-5	Butler East	159.06	3.64	2.54	0.01	<0.12
MM-71B-1	Butler East	17.3	3.34	4.83	0.01	<0.12
MM-71B-2	Butler East	55.33	3.21	1.48	<0.01	<0.12
MM-71B-3	Butler East	150.39	3.08	1.03	0.01	<0.12

Pt	Rh	Ru	Ba	Be	Bi	Cd	Ce	Co
ppb	ppb	ppb	ppm	ppm	ppm	ppm	ppm	ppm
Ni-S Fire Assay	Ni-S Fire Assay	Ni-S Fire Assay	ICP-MS	ICP-MS	ICP-MS	ICP-MS	ICP-MS	ICP-MS
1.57	0.03	0.61	72.6	0.08	<0.15	0.023	0.47	>187
0.59	0.02	0.37	18.3	0.13	<0.15	0.053	1.47	181.65
0.36	0.02	<0.08	64.8	0.23	<0.15	0.065	3.14	96.96
0.59	0.04	0.25	159.1	0.05	<0.15	0.023	0.56	>187
0.46	0.02	<0.08	40.9	0.06	<0.15	0.063	1.45	>187
0.21	<0.02	<0.08	104.3	0.38	<0.15	0.045	5.35	9.29
1.11	0.05	<0.08	45	0.06	<0.15	0.035	0.73	160.98
1.14	0.05	0.1	1.8	0.05	<0.15	0.052	1.22	117.67
0.88	0.09	0.15	1	0.04	<0.15	0.023	1.03	106.56
0.55	0.03	<0.08	402	0.19	<0.15	0.033	2.87	95.07
<0.17	<0.02	<0.08	79.2	0.16	<0.15	0.044	3.73	115.17
0.34	<0.02	<0.08	262.5	0.22	<0.15	0.027	3.77	44.88
0.52	0.12	0.13	2.6	0.05	0.51	>4	0.33	>187
2.35	0.11	0.19	43.4	0.13	0.24	0.441	1.56	>187
1.74	0.06	<0.08	93.1	0.08	<0.15	0.114	1.97	>187
1.96	0.09	<0.08	178.6	0.17	<0.15	0.086	2.16	130.33
0.19	<0.02	<0.08	170.6	0.23	<0.15	0.102	6.24	83.6
0.66	<0.02	<0.08	33.2	0.06	0.38	0.382	1.92	>187
0.64	0.04	<0.08	50.3	0.31	<0.15	0.095	4.13	56.06
1.04	0.06	0.09	254.8	0.46	0.29	0.048	2.36	129.8
4.52	0.24	<0.08	192	0.52	0.17	0.04	2.37	137.82
8.18	0.31	0.16	4.5	0.08	<0.15	0.025	1.52	>187
30.5	5	10.4	1.1	0.05	<0.15	<0.013	0.87	78.16
2.35	1.38	7.94	1.3	0.12	0.19	0.024	1.88	79.67
6.62	0.23	0.09	96.1	0.46	0.15	0.06	4.05	54.71
6.47	0.4	0.39	185.7	0.2	<0.15	0.062	1.41	74.97
0.22	0.02	<0.08	55.1	0.18	<0.15	0.077	8.33	91.17
0.32	0.02	<0.08	43.9	0.17	0.2	0.096	2.54	134.42
0.41	0.03	<0.08	66.2	0.14	<0.15	0.092	2.63	103.04
0.3	0.04	<0.08	93.7	0.1	<0.15	0.063	2.97	>187
0.29	0.03	<0.08	86.6	0.14	0.18	0.075	2.32	93.04
0.27	0.06	<0.08	8	<0.04	<0.15	0.055	1.35	>187
0.26	0.05	<0.08	47.2	0.14	<0.15	0.106	2.36	177.77
0.22	0.03	<0.08	54.8	0.22	<0.15	0.134	7.25	107.35
0.19	0.03	<0.08	61.8	0.24	<0.15	0.071	6.59	72.51
0.43	0.06	<0.08	82.5	0.36	<0.15	0.038	6.02	21.28
1.14	0.05	<0.08	8.2	<0.04	<0.15	0.036	0.76	>187
1.02	0.02	<0.08	43.1	0.18	<0.15	0.079	2.37	149.56
0.93	0.02	<0.08	58.8	0.19	<0.15	0.061	2	143.51
0.19	<0.02	<0.08	70.1	0.2	<0.15	0.115	4.35	116.72
0.23	<0.02	<0.08	81.7	0.26	0.15	0.084	2.81	145.2
<0.17	<0.02	<0.08	27.8	0.21	<0.15	0.089	2.41	128.62
<0.17	<0.02	<0.08	92.7	0.34	<0.15	0.142	7.41	71.59
<0.17	<0.02	<0.08	68	0.58	<0.15	0.131	13.26	16.31

Cs	Cu	Dy	Er	Eu	Ga	Gd	Hf	Ho	In	La	Li
ppm	ppm	ppm	ppm	ppm	ppm	ppm	ppm	ppm	ppm	ppm	ppm
ICP-MS	ICP-MS	ICP-MS	ICP-MS	ICP-MS	ICP-MS	ICP-MS	ICP-MS	ICP-MS	ICP-MS	ICP-MS	ICP-MS
1.075	21.5	0.073	0.053	0.0549	47.28	0.061	0.53	0.0168	0.0729	0.24	6.8
0.272	8.1	0.142	0.085	0.2033	36.63	0.137	0.43	0.0303	0.0647	0.78	8.3
0.336	4.9	0.403	0.257	0.325	24.46	0.309	0.29	0.0838	0.0409	1.76	14.1
1.843	3.8	0.061	0.053	0.0112	44.96	0.043	0.57	0.0164	0.0719	0.34	9.1
0.439	201.4	0.206	0.141	0.0631	41.1	0.168	0.64	0.0459	0.0947	0.78	21.4
0.292	39.1	0.269	0.169	0.5259	22.51	0.292	0.66	0.0562	0.0066	3.28	7.3
1.478	196.2	0.091	0.059	0.1123	36.49	0.075	0.31	0.02	0.0489	0.42	32.9
0.034	148.7	0.056	0.038	0.0308	45.1	0.067	0.45	0.0127	0.0194	1.05	20.9
<0.013	39.4	0.057	0.032	0.0245	43.84	0.093	0.52	0.0114	0.0283	0.76	19.8
0.272	153.5	0.34	0.199	0.3884	28.9	0.334	0.32	0.0698	0.0394	1.34	19.4
0.313	52.1	1.069	0.695	0.3329	18.13	0.834	0.47	0.2275	0.0519	1.68	18.1
0.407	56.5	0.582	0.364	0.5297	20.11	0.521	0.32	0.1241	0.0366	1.97	15.4
0.072	576.3	0.258	0.31	0.0173	34.57	0.128	0.33	0.0758	0.7936	0.16	5.5
3.084	126.2	0.146	0.095	0.0903	39.49	0.133	0.42	0.0315	0.1403	0.76	28.5
1.852	129.9	0.188	0.132	0.1177	40.46	0.154	0.48	0.0393	0.0875	1.09	22.9
3.167	137.9	0.278	0.19	0.2415	33.24	0.24	0.44	0.0604	0.0752	1.36	32
0.729	43	1.98	1.245	0.6082	16.09	1.669	0.73	0.4199	0.0538	2.63	18.1
1.336	1778.5	0.338	0.2	0.0603	5.26	0.221	0.14	0.0683	0.0608	0.87	11.9
0.213	29.8	0.585	0.36	0.8252	29.65	0.564	0.62	0.127	0.0396	2.1	7.3
6.755	72.9	0.721	0.497	0.528	30.99	0.51	0.5	0.1576	0.0874	0.98	55.5
5.694	161.6	0.642	0.418	0.3302	31.85	0.48	0.5	0.1408	0.0793	0.97	46.5
0.084	203.5	0.362	0.236	0.1273	40.88	0.301	0.68	0.0787	0.1026	0.66	9.6
0.075	2.7	0.088	0.076	0.0232	14.54	0.117	0.18	0.0216	0.0459	0.34	4.7
0.052	41.5	0.329	0.243	0.0234	7.07	0.273	0.27	0.0722	0.0332	1.1	0.4
0.43	492.3	0.881	0.711	0.5052	13.61	0.598	0.37	0.2086	0.0944	2.01	46.5
0.918	225	0.237	0.138	0.3306	25.88	0.203	0.21	0.05	0.0332	0.75	16.1
0.083	125.6	1.008	0.617	0.3772	18.26	0.871	0.53	0.2089	0.0485	4.31	8.9
0.15	250.2	0.665	0.413	0.2705	23.67	0.518	0.44	0.1402	0.0558	1.34	10.7
0.121	160.5	0.902	0.582	0.3379	17.06	0.729	0.28	0.1916	0.0423	1.26	7.8
0.567	278.9	0.38	0.245	0.1683	31.31	0.346	0.47	0.0828	0.0597	1.55	20.4
0.118	160.1	0.82	0.526	0.39	19.3	0.661	0.27	0.1741	0.0371	1.28	12.6
0.105	127.4	0.178	0.106	0.0625	41.58	0.194	0.48	0.037	0.0765	0.82	6.5
0.322	264.4	0.775	0.497	0.253	24.86	0.619	0.41	0.1662	0.062	1.19	21.3
0.222	252.6	1.591	1.002	0.429	19.52	1.374	1.07	0.3417	0.0576	3.27	11
0.18	40.4	1.194	0.742	0.5593	17.71	1.054	0.56	0.2477	0.0337	3.27	22
0.325	28.1	0.614	0.37	0.4668	20.9	0.607	0.64	0.1262	0.0178	3.05	7.9
0.232	250.8	0.082	0.056	0.0229	42.27	0.064	0.68	0.0178	0.3386	0.49	15.2
0.439	108.1	0.369	0.23	0.3412	31.4	0.316	0.59	0.0763	0.0572	1.25	9.9
1.129	122.2	0.231	0.142	0.3301	33.91	0.222	0.59	0.0471	0.0497	1.22	12.2
0.692	62.7	0.697	0.455	0.5071	28.71	0.644	0.66	0.1476	0.0542	2.28	17.1
1.016	105	0.381	0.245	0.3668	33.36	0.353	0.65	0.0833	0.0773	1.9	12.2
0.377	32.1	0.461	0.323	0.5776	17.45	0.381	0.35	0.1002	0.0394	1.14	17.5
0.457	26.1	1.818	1.087	1.0063	19.34	1.571	0.71	0.3758	0.0606	3.52	14.6
0.117	7.8	2.466	1.246	1.8407	23.98	2.893	0.51	0.4678	0.0569	5.68	9.2

Lu	Mo	Nb	Nd	Ni	Pb	Pr	Rb	Sb	Sc	Sm	Sn
ppm	ppm	ppm	ppm	ppm	ppm	ppm	ppm	ppm	ppm	ppm	ppm
ICP-MS	ICP-MS	ICP-MS	ICP-MS	ICP-MS	ICP-MS	ICP-MS	ICP-MS	ICP-MS	ICP-MS	ICP-MS	ICP-MS
0.0121	0.61	1.802	0.24	302.8	<0.6	0.058	14.47	<0.04	24.1	0.056	0.32
0.0145	0.53	1.244	0.66	202.8	1.6	0.182	3.73	<0.04	18.8	0.141	0.28
0.0426	0.63	0.742	1.32	86.9	2.1	0.336	9.57	<0.04	20	0.285	0.32
0.0121	0.56	1.822	0.22	301.7	<0.6	0.06	39	<0.04	26.6	0.048	0.34
0.0228	0.56	2.43	0.62	193.6	1.1	0.157	9.41	0.14	31.1	0.142	0.62
0.025	0.67	0.333	1.98	9	2.7	0.556	12.49	<0.04	2.8	0.335	0.16
0.0094	0.41	1.129	0.33	300.8	1.1	0.087	16.8	<0.04	23.9	0.069	0.36
0.0072	0.5	1.353	0.42	490.8	1.4	0.118	0.64	0.05	27.8	0.071	0.41
0.0051	0.4	1.471	0.41	272.8	0.6	0.107	0.3	0.05	26.9	0.089	0.51
0.0251	0.76	1.099	1.53	130.8	2.8	0.386	51.12	0.07	18.9	0.344	0.25
0.1119	0.4	1.094	2.14	61.8	1.5	0.495	10.55	0.08	48.2	0.635	0.24
0.0523	1.85	0.926	1.81	33.1	3.1	0.477	39.71	0.07	19.3	0.446	0.55
0.0981	0.33	0.834	0.18	614.6	1.6	0.042	0.55	<0.04	32.9	0.066	0.53
0.0159	0.51	1.172	0.59	333.1	5.9	0.176	32.94	0.11	27.1	0.146	0.53
0.023	1.18	1.41	0.77	254.2	4.1	0.218	30.32	0.06	26.1	0.169	0.66
0.0348	0.95	1.129	1.03	157.9	7.2	0.268	55.81	0.08	20.6	0.247	0.67
0.1786	0.35	1.122	4.45	52.3	1.3	0.932	18.84	0.04	56.4	1.305	0.27
0.0351	4.19	0.371	0.83	110.5	1.5	0.236	13.57	<0.04	9.4	0.163	0.16
0.0516	2.92	2.302	2.21	20	3.4	0.534	2.33	0.04	15.1	0.509	0.34
0.0693	0.77	1.715	1.25	133.1	6.5	0.288	124.94	0.05	28.7	0.402	0.73
0.055	1.15	1.974	1.25	203.5	5.3	0.287	103.62	0.06	29.1	0.379	1.17
0.0365	0.49	2.971	0.8	293.3	2	0.195	1.2	0.08	35.2	0.232	0.64
0.0475	0.87	0.589	0.44	977.6	<0.6	0.097	1	0.32	9.1	0.106	0.23
0.0725	0.19	1.1	0.9	1434.9	1.3	0.211	0.5	0.19	6.3	0.236	0.28
0.1444	1.11	0.576	1.98	129.6	3	0.515	12.23	0.04	32	0.519	0.34
0.021	0.82	0.481	0.69	156.7	2.3	0.184	78.37	0.07	15.5	0.183	0.43
0.0914	0.44	0.846	3.25	44	1.5	0.922	5.38	<0.04	47.2	0.736	0.32
0.0639	0.56	0.825	1.37	70.2	1.7	0.32	8.19	<0.04	45.7	0.397	0.36
0.0846	0.47	0.273	1.61	46.4	2	0.359	8.29	<0.04	52.3	0.516	<0.16
0.0369	0.4	1.212	1.31	98.6	1.5	0.347	24.82	<0.04	36.8	0.322	0.31
0.0755	0.34	0.337	1.51	40.6	1.4	0.337	7.13	<0.04	47.5	0.475	0.16
0.0147	0.43	2.043	0.62	154.9	1.2	0.154	1.99	0.05	34.2	0.154	0.48
0.069	0.32	1.051	1.52	95.9	2.5	0.327	7.35	0.06	46.9	0.471	0.31
0.1489	0.63	3.049	4.13	94.2	4.2	0.966	6.54	0.1	47.1	1.128	0.35
0.1074	0.36	0.896	3.63	64.4	2.6	0.864	7.12	0.04	24.8	0.889	0.2
0.0495	0.39	0.683	2.83	20.3	4.4	0.733	8.46	0.06	5.9	0.6	0.22
0.0125	1.33	2.063	0.33	88.8	<0.6	0.081	3.16	<0.04	24.7	0.067	1.18
0.0346	0.65	1.681	1.23	56.7	2.3	0.281	6.09	0.05	20.3	0.3	0.34
0.0213	1.41	1.837	0.89	58.7	3.2	0.215	14.48	0.04	16.5	0.187	0.4
0.0646	0.65	1.777	2.34	17.9	2.8	0.537	12.71	<0.04	21.4	0.537	0.39
0.0356	0.65	2.063	1.35	60.1	2.8	0.33	12.56	0.08	21	0.311	0.62
0.061	0.59	1.377	1.39	12.5	2	0.315	5.25	0.07	16.1	0.359	<0.16
0.1611	0.54	1.765	4.69	5	3.2	1	14.74	0.05	45.8	1.243	<0.16
0.1747	0.56	1.188	9.85	3.1	3.6	1.929	3.23	0.06	52.4	2.495	<0.16

Sr	Ta	Tb	Th	Tl	Tm	U	W	Y	Yb	Zn	Zr
ppm	ppm	ppm	ppm	ppm	ppm	ppm	ppm	ppm	ppm	ppm	ppm
ICP-MS	ICP-MS	ICP-MS	ICP-MS	ICP-MS	ICP-MS	ICP-MS	ICP-MS	ICP-MS	ICP-MS	ICP-MS	ICP-MS
12.6	0.141	0.0095	0.043	0.136	0.0095	0.04	0.09	0.42	0.067	321	16
158	0.104	0.0206	0.179	0.028	0.0133	0.048	0.14	0.72	0.097	197	13
207.7	0.06	0.0531	0.51	0.07	0.0409	0.18	0.17	2.11	0.277	102	10
5.2	0.14	0.0087	0.065	0.315	0.0097	0.114	0.18	0.41	0.07	305	17
5.3	0.19	0.0307	0.08	0.081	0.0216	0.053	0.11	1.1	0.14	331	19
306.4	0.048	0.0436	1.584	0.051	0.0237	0.481	0.06	1.45	0.16	19	23
113.2	0.09	0.014	0.028	0.176	0.0094	0.023	0.48	0.48	0.061	204	8
12.5	0.113	0.0086	0.042	<0.005	0.0058	2.239	0.59	0.4	0.04	201	13
6.5	0.126	0.0103	0.019	0.024	0.0045	0.257	0.76	0.42	0.032	451	15
294.5	0.077	0.0539	0.04	0.291	0.0281	0.074	0.2	1.72	0.176	78	10
75.1	0.075	0.1501	0.149	0.065	0.1051	0.228	0.3	5.8	0.7	82	16
245.7	0.066	0.0888	0.211	0.265	0.0525	0.15	0.55	2.95	0.363	41	10
2.1	0.06	0.028	0.034	0.011	0.0601	0.018	0.1	2	0.522	4409	9
87.7	0.093	0.0241	0.042	0.242	0.0141	0.12	0.45	0.79	0.104	270	13
76.1	0.129	0.0273	0.196	0.245	0.0189	0.23	0.88	1.11	0.138	291	14
165.4	0.132	0.0408	0.802	0.402	0.0311	0.542	0.68	1.72	0.219	208	13
184.5	0.069	0.2927	0.3	0.107	0.1797	0.091	0.13	10.35	1.191	97	25
12.1	0.037	0.0466	0.173	0.12	0.0316	0.092	1.45	1.63	0.212	201	<6
316	0.171	0.0938	0.22	0.019	0.0526	0.097	1.22	3.03	0.336	124	21
141.1	0.136	0.0976	0.055	0.939	0.0736	0.127	0.73	3.86	0.448	128	14
131.8	0.15	0.093	0.054	0.675	0.0582	0.086	0.64	3.46	0.373	160	16
52.7	0.227	0.0545	0.046	0.015	0.0346	0.08	0.26	1.94	0.238	123	21
3.2	0.053	0.0124	0.114	0.018	0.0167	0.033	0.32	0.73	0.178	48	8
6.5	0.08	0.0494	0.129	0.104	0.0439	0.075	0.2	1.92	0.369	101	10
132.3	0.068	0.1129	0.236	0.073	0.1165	0.472	0.14	5.36	0.86	122	13
255	0.033	0.0325	0.046	0.446	0.0217	0.16	0.61	1.17	0.139	88	6
168.9	0.064	0.1455	1.078	0.028	0.0914	0.272	0.15	5.29	0.601	90	18
136.3	0.062	0.0937	0.45	0.049	0.0633	0.182	0.49	3.48	0.405	140	15
162.2	<0.023	0.1275	0.173	0.039	0.084	0.065	0.05	4.58	0.554	86	8
53.8	0.087	0.0566	0.404	0.12	0.0359	0.208	0.08	2.03	0.243	205	16
177.2	0.024	0.1175	0.046	0.03	0.076	0.034	0.34	4.34	0.488	84	8
27.1	0.171	0.0289	0.027	0.025	0.015	0.028	0.47	1.12	0.099	310	13
63	0.078	0.1119	0.119	0.064	0.0708	0.049	0.19	4.23	0.478	174	12
140.1	0.204	0.24	1.237	0.048	0.1471	0.346	0.12	8.22	0.991	127	37
215.8	0.064	0.1752	0.614	0.042	0.1067	0.167	0.09	6.12	0.716	74	20
326.6	0.061	0.0961	0.886	0.051	0.0519	0.27	0.07	3.15	0.345	29	24
10.2	0.172	0.0118	0.083	0.034	0.0093	0.148	3.95	0.43	0.066	975	20
196	0.134	0.0545	0.135	0.06	0.0336	0.061	0.54	1.83	0.222	201	18
200.8	0.146	0.0336	0.091	0.126	0.0209	0.102	0.93	1.2	0.146	190	19
217.9	0.131	0.1054	0.296	0.099	0.0645	0.136	0.2	3.72	0.428	178	22
216.3	0.154	0.058	0.181	0.107	0.035	0.129	0.72	2.05	0.235	204	22
40	0.097	0.068	0.139	0.058	0.0489	0.045	0.38	2.47	0.353	178	12
194.7	0.122	0.2653	0.335	0.126	0.1591	0.135	0.29	9.05	1.051	128	24
333.1	0.081	0.4164	0.343	0.03	0.1665	0.116	0.24	11.18	1.052	117	17

Al2O3	CaO	Fe2O3	K2O	LOI	MgO	MnO	Na2O	P2O5	SiO2	TiO2	Total	CO2	S
%	%	%	%	%	%	%	%	%	%	%	%	%	%
XRF	XRF	XRF	XRF	XRF	XRF	XRF	XRF	XRF	XRF	XRF	XRF	XRF	XRF
5.63	1.036	74.86	0.37	-2.74	1.76	0.152	0.17	<0.002	6.68	11.06	98.98	0.08	0.03
13.33	5.074	49.78	0.13	-1.75	1.99	0.182	1.32	0.004	22.27	7.1	99.43	0.09	0.01
17.71	8.198	22.73	0.32	-0.08	3.94	0.141	2.72	0.004	41.54	2.76	99.98	0.09	0.01
4.76	0.215	76.39	0.94	-2.64	2.13	0.16	0.13	0.002	5.31	11.25	98.65	0.06	0.01
4.72	0.759	74.11	0.23	-1.66	2.28	0.25	0.12	0.003	6.37	12.01	99.19	0.12	0.4
26.97	11.037	2.13	0.31	1.04	0.53	0.024	4.29	0.018	53.6	0.13	100.08	0.29	0.04
10.9	3.782	58.56	0.33	-1.01	2.2	0.209	0.88	0.002	16.74	7.15	99.74	0.1	0.19
3.99	0.658	79	0.01	-1.36	1.59	0.261	0.04	<0.002	3.85	10.85	98.89	0.23	0.51
3.83	1.763	77.57	<0.01	-1.1	1.42	0.246	0.02	<0.002	2.56	11.69	98	1.32	0.15
17.73	7.179	28.74	1.77	1.53	1.61	0.149	1.9	0.004	33.34	5.2	99.15	0.12	0.36
10.86	8.307	25.84	0.48	1.64	7.49	0.259	1.12	0.012	40.84	3.31	100.16	0.1	0.2
20.78	10.904	11.57	1.43	1.94	2.98	0.137	2.64	0.011	45.1	2.38	99.87	0.45	0.14
2.92	0.174	62.08	0.01	5.05	8.62	0.167	0.05	0.002	17.94	2.69	99.7	0.13	12.4
6.9	2.401	68.71	0.85	-0.74	2.91	0.242	0.06	0.002	10.1	7.6	99.04	0.04	0.23
7.27	2.952	65.97	1	-1.01	2.66	0.233	0.11	0.002	11.55	8.76	99.5	0.03	0.41
13.38	5.573	43.35	1.92	0.44	2.73	0.191	1.06	0.005	24.73	5.83	99.21	0.09	0.83
11.63	10.187	18.6	0.67	1.21	8.25	0.247	1.67	0.02	46.77	1.37	100.62	0.11	0.2
3.47	0.441	32.79	0.56	5.19	1.23	0.152	0.53	0.007	53.61	0.9	98.88	0.22	13.5
18.83	8.006	25.23	0.19	-0.45	1.16	0.18	3.33	0.027	38.73	5.09	100.32	0.25	0.25
10.12	7.163	43	3.32	3.8	2.92	0.269	0.78	0.008	20.97	6.64	98.99	4.57	0.19
10.24	5.114	45.96	2.58	2.44	3.16	0.259	0.84	0.007	21.7	6.61	98.91	2.95	0.25
4.75	1.84	71.27	0.04	-1.35	2.59	0.31	0.13	0.004	8.17	10.74	98.49	0.02	0.23
1.25	0.075	34.11	0.01	7.74	27.51	0.105	<0.02	0.017	28.61	0.29	99.69	0.09	0.05
1.16	1.042	21.74	0.01	9.08	29.68	0.149	<0.02	0.016	36.42	0.14	99.41	1.18	0.16
14.23	7.763	12.78	0.56	10.25	8.99	0.236	1.18	0.014	42.61	0.39	99	5.59	0.08
19.41	7.707	23.88	2.41	1.86	2.28	0.125	1.98	0.003	37.13	2.83	99.62	0.37	0.19
14.68	10.273	17.81	0.36	0.44	5.75	0.2	2.34	0.008	46.65	1.84	100.35	0.24	0.27
12.25	8.018	32.41	0.37	0.08	5.02	0.238	1.84	0.004	35.86	4.85	100.94	0.1	0.63
14.32	10.584	17.83	0.31	0.58	6.45	0.176	2.02	0.004	46.12	1.78	100.17	0.14	0.4
8.24	4.006	55.05	0.63	-0.82	3.38	0.296	0.87	0.004	19.61	9.19	100.46	0.12	0.7
15.34	10.822	17.8	0.46	0.46	5.63	0.203	2.05	0.005	44.38	1.96	99.11	0.17	0.31
4.42	1.084	75.32	0.04	-1.45	2.26	0.295	0.03	0.002	5.58	12.1	99.68	0.11	0.39
10.05	7.016	39.31	0.34	0.1	5.23	0.259	1.12	0.004	29.94	6.03	99.4	0.25	0.62
12.11	9.216	24.95	0.38	0.86	5.39	0.244	1.23	0.014	42.22	3.45	100.06	0.14	0.29
18.32	9.978	14.21	0.4	1.15	5.47	0.183	2.46	0.015	47.51	0.78	100.48	0.19	0.09
25.55	10.982	5.17	0.41	1.29	1.66	0.058	3.87	0.032	51.55	0.23	100.8	0.16	0.05
3.82	0.353	80.38	0.1	-2.14	1.69	0.267	0.04	0.003	3.32	11.42	99.25	0.05	0.87
14.79	6.322	39.88	0.23	0.25	1.73	0.169	2.05	0.008	28.55	6.21	100.19	0.71	0.66
14.27	5.505	43.65	0.46	-0.45	1.34	0.181	1.96	0.006	25.97	6.97	99.86	0.31	0.71
15.06	6.809	33.73	0.5	-0.11	2.38	0.189	2.36	0.024	33.06	5.81	99.81	0.27	0.43
12.74	5.264	46.12	0.4	-0.64	1.71	0.225	1.78	0.011	24.5	7.49	99.6	0.05	0.8
11.68	5.177	34.34	0.25	1.62	6.55	0.353	0.94	0.024	36.53	2.93	100.39	0.11	0.26
13.15	9.04	23.93	0.82	0.3	4.51	0.286	2.2	0.04	43.39	2.61	100.28	0.12	0.18
16.29	8.622	20.63	0.36	-0.09	1.31	0.309	3.53	0.423	47.74	1.43	100.55	0.14	0.07

Al	Ba	Be	Ca	Co	Cr	Cu	Fe	K	Li	Mg
ppm	ppm	ppm	ppm	ppm	ppm	ppm	ppm	ppm	ppm	ppm
ICP-AES	ICP-AES	ICP-AES	ICP-AES	ICP-AES	ICP-AES	ICP-AES	ICP-AES	ICP-AES	ICP-AES	ICP-AES
25429	65	4	5683	205	1318	<6	>95000	2926	7	8468
61650	21	3	29193	143	832	<6	>95000	1051	8	10026
82414	55	1	48550	78	111	<6	>95000	2513	13	20707
22112	133	5	1172	214	330	<6	>95000	7226	9	10714
21245	40	5	4106	189	32	158	>95000	1717	21	11026
>110000	94	1	61631	8	15	32	13496	2419	7	2737
48883	43	2	21046	130	789	156	>95000	2492	33	10828
18127	12	4	3522	98	1744	110	>95000	<70	22	7596
17433	11	5	9395	92	1245	13	>95000	<70	21	6893
81782	325	2	42566	80	40	130	>95000	13444	20	8695
50022	66	1	47386	91	76	35	>95000	3480	18	39816
97058	214	1	65069	38	38	46	71094	11249	16	15979
12986	9	1	950	352	26	473	>95000	<70	5	42863
33009	42	3	13515	173	798	89	>95000	7045	29	15384
34364	80	3	16818	165	216	94	>95000	7887	23	13531
61428	142	2	31762	103	149	106	>95000	14274	31	14010
53778	139	1	58384	66	34	29	>95000	4837	18	43841
15846	31	<1	2700	385	21	1547	>95000	4128	12	6252
88156	44	2	48271	48	83	18	>95000	1341	8	6076
46384	197	3	40240	104	46	50	>95000	24986	57	14745
46768	153	3	29040	110	28	128	>95000	19346	46	15905
22681	12	5	10487	180	336	155	>95000	329	10	13416
5646	4	<1	423	63	3383	<6	>95000	<70	4	140134
5308	3	<1	5882	68	4457	30	>95000	<70	<1	149304
65948	78	1	45800	45	131	440	76331	4331	41	48925
87408	152	1	45556	63	1270	196	>95000	17790	15	11696
67729	46	1	59534	73	13	104	>95000	2708	8	30504
56476	38	2	46111	107	12	212	>95000	2857	11	26269
66787	56	1	62061	86	11	138	>95000	2460	8	34915
37137	79	4	22162	166	19	229	>95000	4812	20	16760
71592	72	1	63056	74	9	132	>95000	3543	12	30368
19621	15	5	5801	185	27	89	>95000	321	7	10806
45908	42	2	39838	140	15	219	>95000	2628	21	27037
56975	47	2	53795	89	16	224	>95000	2700	12	29028
84906	51	1	58714	58	12	29	84381	3139	21	29357
>110000	76	1	59571	17	12	21	32068	3194	9	8677
17587	16	5	1918	171	90	202	>95000	649	16	8279
67571	39	2	36506	122	84	85	>95000	1706	11	8782
66241	53	3	32404	122	109	98	>95000	3579	13	6913
68647	60	2	39410	94	14	42	>95000	3678	17	12185
57613	68	3	29651	117	19	76	>95000	2882	12	8534
52862	26	1	29868	103	2	15	>95000	1859	17	33977
62547	80	2	53679	59	3	13	>95000	6542	15	24263
74503	58	1	50966	14	4	<6	>95000	2672	9	6755

Mn	Na	Ni	P	Pb	Sc	Sr	Ti	V	Y	As	Ba
ppm	ppm	ppm	ppm	ppm	ppm	ppm	ppm	ppm	ppm	ppm	ppm
ICP-AES	ICP-AES	ICP-AES	ICP-AES	ICP-AES	ICP-AES	ICP-AES	ICP-AES	ICP-AES	ICP-AES	XRF	XRF
890	1302	228	188	58	17	10	56338	6098	<1	20	50
1142	10653	156	127	38	15	145	37894	4121	<1	10	<8
900	21307	69	55	<15	15	188	15457	1570	1	6	65
941	801	232	204	67	19	4	58230	6216	<1	16	153
1522	928	146	176	62	23	4	60316	5303	<1	19	<8
154	>31000	6	21	<15	2	296	686	42	2	<6	104
1267	7043	237	131	47	18	104	36786	4771	<1	12	42
1580	<500	383	189	64	20	11	55256	6877	<1	25	<8
1470	<500	217	213	69	20	5	59927	6730	<1	20	<8
1020	15020	109	57	24	15	273	29926	2297	1	11	462
1660	8921	46	101	18	37	68	17846	1000	5	10	80
921	20804	25	42	<15	16	232	13291	571	3	7	253
1010	588	468	129	52	24	<2	14190	1390	<1	14	<8
1482	<500	254	161	60	19	80	39779	4748	<1	23	33
1442	842	194	155	57	19	70	46339	4862	<1	15	91
1154	8530	123	96	41	15	148	30681	3129	1	9	207
1604	13257	40	106	<15	44	167	7624	570	9	13	155
991	4254	90	<15	27	6	11	4412	199	1	12	11
1168	25904	16	129	17	12	297	28030	667	2	10	29
1657	6299	103	124	41	22	129	34781	3044	2	8	309
1583	6775	156	129	45	22	120	35258	3168	2	12	227
1884	1051	218	178	63	26	47	55397	5201	<1	16	<8
621	<500	745	140	26	6	2	1492	329	<1	9	<8
944	<500	1161	107	24	4	5	710	108	1	11	<8
1553	9690	105	24	<15	26	120	1975	144	5	6	80
812	15275	130	26	<15	13	232	15902	1552	1	11	199
1282	18324	32	48	<15	38	154	10174	722	4	7	36
1512	14664	53	74	26	36	126	26221	1956	2	10	25
1161	16203	36	29	<15	44	152	10064	760	4	10	42
1786	6967	73	118	49	28	50	46787	3551	<1	15	88
1321	16614	31	<15	<15	37	160	10840	840	4	8	67
1732	<500	113	188	63	25	24	59704	5408	<1	17	<8
1633	9067	71	88	38	37	58	32295	2331	3	12	24
1611	10263	75	84	22	39	132	19274	1081	7	7	42
1192	19210	49	51	<15	20	196	3940	216	5	6	50
359	28963	14	89	<15	5	314	1180	49	3	7	89
1574	<500	67	194	69	18	9	58040	5518	<1	21	<8
1048	16263	45	114	30	16	184	33295	2311	1	9	28
1133	15771	46	103	36	13	191	37718	2565	<1	16	47
1199	18502	12	144	28	17	198	31396	1507	3	10	66
1376	13937	43	138	37	16	194	39057	2662	1	10	69
2246	7518	7	172	27	12	37	15846	216	2	13	13
1878	17700	<2	182	20	38	181	14638	67	8	10	101
2039	26346	<2	1476	18	44	308	7922	3	10	9	51

Cr	Ga	Nb	Pb	Rb	Sr	Th	Y	Zr
ppm	ppm	ppm	ppm	ppm	ppm	ppm	ppm	ppm
XRF	XRF	XRF	XRF	XRF	XRF	XRF	XRF	XRF
2307	50	2	3	16	13	2	<0.7	17
1271	38	2	4	5	186	2	1	13
140	25	1	5	12	226	2	2	10
463	47	2	4	42	6	<1.5	1	17
<9	42	3	3	11	6	<1.5	1	20
20	23	1	5	15	339	3	1	21
1287	39	2	5	23	138	<1.5	<0.7	11
3136	46	2	5	1	15	3	2	14
2221	48	2	3	1	8	2	1	17
36	33	1	6	67	336	<1.5	1	8
91	21	1	5	12	80	<1.5	6	15
40	22	1	5	45	261	<1.5	2	9
62	34	1	6	2	1	2	3	11
1377	49	1	11	40	110	<1.5	<0.7	13
302	47	2	7	35	90	2	<0.7	15
200	39	1	12	65	192	2	2	12
41	17	1	5	21	197	<1.5	10	21
116	7	1	4	15	13	<1.5	1	4
102	34	3	7	5	359	2	3	21
36	40	2	11	151	164	2	3	16
<9	41	3	8	121	155	2	3	18
512	51	3	5	2	68	4	2	30
>4000	19	1	3	2	3	<1.5	<0.7	5
>4000	9	1	5	1	7	2	2	8
166	15	1	5	13	133	<1.5	5	13
1738	30	1	6	106	291	2	<0.7	4
15	20	1	5	7	179	2	6	20
<9	26	1	5	10	150	<1.5	3	14
15	19	<0.7	5	10	177	2	4	7
<9	35	2	6	28	63	2	2	16
<9	21	<0.7	4	9	184	<1.5	4	6
<9	47	2	5	2	32	4	2	18
<9	29	1	6	9	72	<1.5	5	13
16	22	3	6	8	154	3	9	43
19	19	1	6	9	224	2	6	18
17	22	1	6	11	359	<1.5	4	23
49	44	3	3	4	13	2	1	20
104	35	2	6	9	235	<1.5	2	17
142	38	2	8	20	248	<1.5	<0.7	17
12	33	2	6	16	256	<1.5	4	23
<9	40	2	5	16	255	<1.5	1	20
<9	20	1	5	6	43	<1.5	3	13
<9	21	2	7	17	203	<1.5	9	24
<9	26	1	7	6	366	2	12	17

Sample	Intrusion	Depth (m)	SG	Au	Ir	Pd
MM-110-1	Butler East	19.83	4.37	1.37	0.08	1.89
MM-110-2	Butler East	37.84	2.89	0.54	0.01	0.21
MM-110-3	Butler East	115.82	3.45	0.54	0.01	0.23
MM-110-4	Butler East	146	3.44	4.75	0.2	5.79
MM-117-1	Butler West	30.18	2.82	0.44	0.03	0.71
MM-117-2	Butler West	57.51	3.33	0.65	0.06	5.45
MM-117-3	Butler West	63.6	4.73	1.92	0.02	0.74
MM-117-4	Butler West	109.95	3.2	0.79	0.04	<0.12
MM-117-5	Butler West	199.84	2.94	0.6	0.02	<0.12
MM-117-6	Butler West	200.46	3.08	0.69	0.01	<0.12
NO-2G21-1	Thunderbird	49.92	3.2	0.73	0.01	<0.12
NO-2G21-2	Thunderbird	139.6	3.36	1.99	0.01	0.4
NO-2G21-3	Thunderbird	211.4	3.03	1.61	0.03	1.5
NO-2G21-4	Thunderbird	276	3.93	19.9	0.6	8.28
NO-2G21-5	Thunderbird	294.57	3.75	6.65	0.03	0.72
NO-2G21-6	Thunderbird	400	3.74	29.7	0.01	0.39
NO-2G21-7	Thunderbird	429	3.97	7.42	0.53	8.97
NO-2G21-8	Thunderbird	429.23	3.3	5.11	0.23	3.22
NO-2G21-9	Thunderbird	439.19	4.09	23.9	0.48	5.58
NO-2G21-10	Thunderbird	447.56	3.53	7.89	0.04	1.14
NO-2G21-11	Thunderbird	456	3.43	2.59	0.02	0.41
NO-2G21-12	Thunderbird	493.06	4.22	1.61	0.02	0.59
NO-2G21-13	Thunderbird	537	3.22	0.85	0.02	<0.12
NO-2G22-1	Thunderbird	36	3.64	8.23	0.28	14.1
NO-2G22-2	Thunderbird	33.66	3.13	0.47	0.01	<0.12
NO-2G22-3	Thunderbird	73.3	3.78	3.3	2.62	64.5
NO-2G22-4	Thunderbird	107.45	3.21	0.6	0.02	0.28
NO-2G22-5	Thunderbird	152.03	3.05	0.6	0.01	0.15
NO-2G22-6	Thunderbird	159	3.19	0.58	0.01	0.13
NO-2G25-1	Thunderbird	27.22	3.21	1.03	0.01	0.12
NO-2G25-2	Thunderbird	95.62	3.26	0.99	0.01	<0.12
NO-2G25-3	Thunderbird	156.1	3.13	3.24	0.01	0.23
NO-2G25-4	Thunderbird	193.4	3.66	9.05	0.05	1.95
NO-2G25-5	Thunderbird	197.61	4.13	1.89	0.07	2.51
NO-2G25-6	Thunderbird	219.86	4.14	6.17	0.18	2.61
NO-2G25-7	Thunderbird	231.8	3.81	2.09	0.15	2.41
NO-2G25-8	Thunderbird	247	3.16	1.02	0.01	0.3
NO-2G25-9	Thunderbird	309.74	3.31	0.65	0.01	0.15
NO-2G25-10	Thunderbird	450.21	3.13	0.44	<0.01	<0.12
NO-2G46-1	Thunderbird	62.96	4.11	1.65	0.03	1.01
NO-2G46-2	Thunderbird	66.91	3.92	0.91	0.13	4.02
NO-2G46-3	Thunderbird	105	3.13	0.78	0.01	<0.12
NO-2G46-4	Thunderbird	107.65	3.13	0.49	<0.01	<0.12
NO-2G46-5	Thunderbird	110	3.3	0.46	0.02	0.21
NO-2G46-6	Thunderbird	147.67	3.37	0.66	0.01	0.15
NO-2G47-1	Thunderbird	51.68	3.36	0.75	0.01	<0.12

Pt	Rh	Ru	Ba	Be	Bi	Cd	Ce	Co
2.14	0.12	0.21	73.6	0.05	<0.15	0.137	1.89	179.74
0.31	0.02	<0.08	810.4	1.06	<0.15	0.144	108.7	31.42
0.42	<0.02	<0.08	96.6	0.18	0.43	1.635	5.61	117.13
5.55	0.29	0.47	161.4	0.31	0.18	0.812	3.43	154.99
1.06	0.04	<0.08	38	0.39	0.15	0.068	3.46	39.69
4.43	0.13	0.1	16.5	0.21	0.19	0.083	6.49	88.84
0.87	0.03	0.08	1.6	0.04	<0.15	0.032	0.56	>187
<0.17	0.04	<0.08	40.2	0.22	0.4	0.102	5.78	116.04
0.19	0.02	<0.08	58.4	0.29	0.36	0.065	3.88	56.69
0.26	<0.02	<0.08	45.9	0.17	0.31	0.078	4.14	86.46
<0.17	0.02	<0.08	35.7	0.18	<0.15	0.074	1.77	78.28
0.21	0.03	<0.08	5.5	0.11	<0.15	0.089	1.69	118.24
1.49	0.05	<0.08	76	0.24	<0.15	0.043	1.37	83.09
10.7	0.57	1.25	4.3	0.1	<0.15	0.088	0.54	185.02
0.79	0.04	<0.08	29.7	0.11	<0.15	0.104	0.92	156.52
0.36	0.03	<0.08	30.8	0.1	<0.15	0.138	0.84	172.71
8.63	0.57	1.11	3.6	0.06	<0.15	0.079	0.78	>187
4.62	0.22	0.4	61	0.22	<0.15	0.104	1.6	108.9
7.04	0.46	0.92	<0.8	0.05	<0.15	0.049	0.45	>187
1.96	0.06	0.08	71.6	0.14	<0.15	0.071	0.87	138.36
0.28	0.02	<0.08	14.7	0.14	<0.15	0.04	1.15	163.41
0.45	0.03	<0.08	4.2	0.08	<0.15	0.023	0.7	>187
<0.17	<0.02	<0.08	23.2	0.15	<0.15	0.066	1.52	95.38
21.8	0.79	1.25	12.1	0.12	<0.15	0.101	1.04	128.86
<0.17	<0.02	<0.08	24.3	0.21	<0.15	0.072	2.42	76.22
21.9	3.88	9.21	4.1	0.08	0.49	0.055	8.64	>187
0.33	0.03	<0.08	35.5	0.21	<0.15	0.058	1.46	87.37
0.22	<0.02	<0.08	41.5	0.25	<0.15	0.087	3.11	57.39
0.18	<0.02	<0.08	23.1	0.19	<0.15	0.088	1.74	86.34
0.62	0.04	0.09	26.2	0.19	<0.15	0.057	1.56	90.9
0.43	0.04	<0.08	13	0.13	<0.15	0.056	1.61	111.42
0.65	0.05	<0.08	53.8	0.17	<0.15	0.031	2.12	81.21
2.16	0.11	0.1	41.6	0.12	<0.15	0.053	1.06	173.26
1.23	0.14	0.22	1.3	0.08	<0.15	0.091	0.5	>187
3.51	0.23	0.36	2.5	0.07	<0.15	1.283	0.48	>187
3	0.28	0.38	2.3	0.07	<0.15	0.046	0.87	>187
0.73	0.07	<0.08	142.8	0.24	<0.15	0.046	1.47	78.42
0.19	0.05	<0.08	9.4	0.11	<0.15	0.088	1.44	118.17
<0.17	0.04	<0.08	29.1	0.25	<0.15	0.059	2.05	70.28
2.18	0.11	<0.08	11.5	0.12	<0.15	0.027	1.46	156.93
7.25	0.29	0.11	19.4	0.12	<0.15	0.032	0.9	124.04
<0.17	0.05	<0.08	50.1	0.29	0.16	0.056	3.21	64.45
<0.17	0.04	<0.08	39.5	0.28	<0.15	0.058	15.74	75.67
0.98	0.05	<0.08	23.8	0.17	<0.15	0.043	23.7	96.12
0.17	0.04	<0.08	25.3	0.19	<0.15	0.046	33.96	87.17
<0.17	0.03	<0.08	14.5	0.19	<0.15	0.046	1.85	110.45

Cs	Cu	Dy	Er	Eu	Ga	Gd	Hf	Ho	In	La	Li
2.347	183.9	0.056	0.036	0.0397	40.97	0.067	0.42	0.012	0.1381	1.03	18.8
0.704	46.7	5.177	2.423	2.7896	19.93	7.616	4.12	0.927	0.0624	52.88	34.1
0.722	593.1	1.133	0.83	0.2771	20.69	0.864	0.65	0.2612	0.7097	2.59	10.6
2.962	433.4	0.388	0.241	0.1996	28.41	0.325	0.33	0.0812	0.1171	1.96	32.8
0.403	51	0.495	0.307	0.3319	19.59	0.462	0.19	0.1064	0.025	1.83	13.6
0.07	232.6	2.82	1.703	0.478	12	2.282	0.7	0.5903	0.0898	2.73	7.9
<0.013	223.5	0.102	0.069	0.0171	45.59	0.08	0.39	0.0212	0.0796	0.27	3.2
0.193	212.3	1.782	1.101	0.5068	15.15	1.539	0.69	0.3739	0.057	2.4	16.4
0.367	65.8	0.823	0.546	0.6375	19.07	0.696	0.48	0.1756	0.03	2.04	19.7
0.22	151.9	1.49	0.948	0.5183	17.21	1.199	0.64	0.318	0.0454	1.92	10.3
0.121	61.2	0.861	0.559	0.4031	18.52	0.728	0.3	0.1872	0.0495	0.77	5.4
0.231	91.7	1.292	0.843	0.2954	15.35	1.009	0.37	0.2805	0.0568	0.59	1.8
1.138	188.9	0.156	0.091	0.3104	29.79	0.149	0.22	0.0315	0.0203	0.77	3.5
0.177	492.7	0.099	0.066	0.1022	37	0.087	0.39	0.0219	0.072	0.28	0.9
0.423	292.9	0.08	0.054	0.1397	33.95	0.085	0.34	0.0173	0.0438	0.48	5.7
0.431	637.9	0.16	0.099	0.1547	33.15	0.131	0.32	0.0337	0.0596	0.42	2.5
0.584	372.4	0.118	0.074	0.0915	37.85	0.105	0.37	0.0259	0.0711	0.43	3.1
0.722	337.3	0.24	0.153	0.2746	28.84	0.243	0.32	0.0548	0.0324	0.74	3.5
0.134	346.7	0.113	0.087	0.0238	37.57	0.092	0.36	0.0281	0.0665	0.22	3.2
0.79	250.1	0.141	0.085	0.1808	33.68	0.12	0.32	0.0283	0.0409	0.44	4.3
0.473	258.6	0.194	0.13	0.1898	33.78	0.177	0.33	0.0423	0.0415	0.62	3.9
1.15	207.6	0.181	0.119	0.1021	37.05	0.127	0.41	0.0357	0.0588	0.34	3
0.207	58.5	0.98	0.631	0.3452	17.14	0.749	0.27	0.2075	0.0477	0.66	3
0.549	622.8	0.528	0.315	0.2342	24.41	0.413	0.34	0.1053	0.0595	0.43	8.3
0.146	79.1	1.094	0.706	0.4436	15.26	0.923	0.33	0.2349	0.0447	1.02	6.3
0.843	1225.5	0.651	0.376	0.5083	20.15	0.762	0.5	0.1363	0.0329	5.49	2.5
0.359	78.4	0.364	0.228	0.4164	25.55	0.317	0.36	0.0773	0.0375	0.74	6
0.474	51	1.084	0.65	0.6849	19.57	0.946	0.38	0.2309	0.0453	1.43	5.9
0.117	45.7	0.58	0.356	0.5741	20.07	0.51	0.28	0.1171	0.0375	0.87	5.5
0.101	82.1	1.056	0.67	0.366	17.96	0.871	0.29	0.2248	0.0485	0.65	5
0.109	89.9	1.148	0.73	0.3142	17.02	0.89	0.36	0.2417	0.0532	0.69	2.7
0.593	173.9	0.525	0.337	0.3399	22.26	0.445	0.29	0.1122	0.0271	1.05	6.8
0.872	201.6	0.167	0.092	0.2005	32.79	0.142	0.33	0.0336	0.0536	0.53	2.2
0.423	227.8	0.12	0.08	0.0936	39.23	0.093	0.41	0.0252	0.0738	0.24	2.4
1.317	252.9	0.149	0.106	0.0097	36.1	0.117	0.38	0.0322	0.0507	0.21	4.1
0.721	306.4	0.286	0.176	0.1669	33.98	0.237	0.35	0.0574	0.0637	0.44	2.2
0.964	135.7	0.233	0.152	0.3682	26.94	0.227	0.21	0.0497	0.0321	0.71	2.8
0.197	62.5	1.256	0.825	0.2603	14.88	0.939	0.35	0.2703	0.0582	0.51	2.7
0.206	42.7	0.988	0.645	0.4885	18.31	0.831	0.31	0.2163	0.0475	0.93	3.4
0.099	360.7	0.224	0.129	0.2672	31.72	0.232	0.61	0.0437	0.0697	0.74	3.9
0.092	197.3	0.171	0.11	0.2901	31.04	0.179	0.56	0.037	0.0617	0.44	3.9
0.1	36.4	0.736	0.436	0.7746	19.35	0.729	0.32	0.1545	0.0277	1.46	8.3
0.152	20.1	3.027	1.405	1.4909	19.52	3.972	0.28	0.5547	0.023	6.29	9.8
0.383	34.5	4.664	2.188	1.9637	17.53	6.432	0.2	0.8715	0.0261	9.01	5.4
1.087	95.4	6.617	2.877	2.4633	18.13	9.453	0.22	1.2071	0.0266	12.4	3.2
0.095	104.1	0.557	0.328	0.5091	18.09	0.492	0.34	0.1119	0.0366	0.78	3.9

Lu	Mo	Nb	Nd	Ni	Pb	Pr	Rb	Sb	Sc	Sm	Sn
0.0091	0.69	1.233	0.6	394.9	6.2	0.184	36.9	0.06	21.7	0.092	0.17
0.2851	0.42	5.104	55.91	65.3	7.6	13.548	38.45	0.05	17.8	10.303	1.16
0.1455	2.19	1.516	3.01	38	7	0.722	39.67	0.04	44.2	0.735	0.79
0.0398	2	0.777	1.39	292.1	6.6	0.37	57.58	0.13	25.9	0.296	0.48
0.046	0.32	0.352	1.65	78	2.3	0.433	3.97	<0.04	20	0.406	0.38
0.2413	0.45	1.311	5.37	261.1	0.7	1.039	1.28	0.08	>63	1.709	0.24
0.0106	0.31	1.244	0.3	507.7	0.6	0.073	0.4	<0.04	29.6	0.077	0.33
0.1595	0.43	1.061	4.15	82.5	1.1	0.86	6.83	0.04	52.7	1.181	0.25
0.0822	1.53	0.621	2.15	41.4	2.1	0.499	7.59	0.06	25	0.568	0.23
0.135	0.55	0.907	2.82	69.9	1.5	0.591	4.16	0.05	53.8	0.894	0.19
0.083	0.69	0.441	1.42	20.6	1	0.28	2.14	0.2	46.9	0.469	0.22
0.1211	0.46	0.431	1.74	48.7	<0.6	0.313	0.69	0.4	>63	0.673	0.25
0.0133	0.47	0.477	0.67	119.4	1.2	0.155	10.31	0.29	6.6	0.152	0.2
0.0107	0.21	0.945	0.25	435.5	0.8	0.064	0.5	0.15	20.5	0.065	0.47
0.0098	0.25	0.855	0.4	318.1	0.7	0.103	2.25	0.17	16.2	0.085	0.41
0.016	0.2	0.789	0.45	354.9	1	0.104	1.99	0.2	17.2	0.106	0.39
0.0136	0.18	0.923	0.42	370.1	0.6	0.1	0.61	0.24	21	0.093	0.55
0.0223	0.23	0.671	0.85	235	1.2	0.206	6.93	0.23	5.4	0.212	0.43
0.0154	0.16	1.043	0.25	373	<0.6	0.056	0.3	0.14	23.7	0.075	0.37
0.0125	0.27	0.808	0.5	228.6	1	0.108	8.8	0.23	7.2	0.113	0.41
0.0188	0.22	0.82	0.6	266.9	1	0.14	0.91	0.26	17.9	0.151	0.38
0.0161	0.19	1.246	0.42	199.3	<0.6	0.092	0.76	0.13	22.6	0.105	0.44
0.0926	0.44	0.332	1.44	35.3	<0.6	0.265	0.64	0.17	51.2	0.504	0.75
0.0455	0.21	0.811	0.87	413.6	0.9	0.163	1.46	0.12	45	0.31	0.24
0.1061	0.27	0.471	2.01	101.7	0.9	0.386	1.01	0.14	52.6	0.66	0.21
0.055	0.78	1.706	3.87	641.7	64.8	0.941	1.31	0.32	30.3	0.674	0.36
0.0345	0.32	1.043	0.87	86.4	0.8	0.191	0.99	0.11	20.7	0.248	0.26
0.0929	0.27	0.594	2.34	33.7	1.8	0.469	1.86	0.23	46.7	0.712	0.2
0.0538	0.29	0.64	1.26	46.3	1.5	0.27	1.06	0.17	34.1	0.387	0.16
0.09	0.26	0.325	1.56	27.8	1	0.273	1.19	0.17	53.2	0.548	0.22
0.1073	0.37	0.423	1.63	50.4	<0.6	0.301	0.86	0.19	58.4	0.619	0.27
0.0462	0.26	0.631	1.22	90.1	0.7	0.278	3.9	0.34	25.6	0.346	0.41
0.0153	0.21	0.829	0.53	294.8	1.3	0.136	5.6	0.34	12.1	0.123	0.51
0.0146	0.16	1.193	0.29	360.3	<0.6	0.061	0.47	0.17	23.4	0.076	0.63
0.0163	0.1	1.152	0.29	333.5	1.1	0.067	0.76	0.29	21.5	0.092	0.41
0.0268	0.19	0.853	0.63	383.8	0.6	0.127	0.53	0.38	24.7	0.176	0.59
0.0192	0.28	0.471	0.85	125.6	0.8	0.191	5.79	0.47	9.3	0.195	0.33
0.1158	0.28	0.397	1.61	45.4	<0.6	0.284	0.76	0.18	>63	0.631	0.24
0.0938	0.4	0.427	1.69	9.7	0.8	0.331	1.11	0.14	49.3	0.571	0.18
0.0215	1.02	3.181	0.84	244.4	2.1	0.189	1.43	0.18	28.7	0.215	0.26
0.0173	0.94	3.037	0.57	227	1	0.126	2.21	0.09	25.5	0.148	0.2
0.0662	0.28	0.694	2.24	29.6	1.5	0.468	2.58	0.06	22.5	0.591	0.17
0.1318	0.27	0.65	12.53	10.8	0.8	2.376	3.37	0.05	15.7	3.28	0.21
0.1912	0.33	0.754	20.11	25.3	<0.6	3.719	3.32	0.08	13.4	5.252	<0.16
0.2184	0.41	0.742	29.39	41.2	6.8	5.41	2.7	0.07	12.1	7.708	0.74
0.056	0.38	1.026	1.35	48.4	1	0.273	1	0.05	25.7	0.399	0.2

Sr	Ta	Tb	Th	Tl	Tm	U	W	Y	Yb	Zn	Zr
33.2	0.094	0.0097	0.075	0.302	0.0063	0.259	1.14	0.33	0.047	562	12
866.1	0.236	0.9538	5.006	0.263	0.3242	0.67	0.11	23.75	1.996	107	179
56.5	0.097	0.1602	0.442	0.248	0.1313	0.178	0.43	6.63	0.895	1376	22
163.5	0.058	0.0567	0.133	0.437	0.0382	0.188	1.53	2.09	0.25	295	10
306.9	<0.023	0.0751	0.121	0.019	0.0453	0.073	0.08	2.67	0.298	34	6
71.5	0.093	0.4004	0.305	0.036	0.2483	0.096	1.07	14.42	1.616	84	21
3.1	0.098	0.0148	0.053	0.032	0.0101	0.015	0.17	0.55	0.07	315	11
102.2	0.071	0.2626	0.276	0.059	0.1605	0.084	0.19	9.23	1.03	103	24
279.4	0.044	0.119	0.22	0.057	0.0792	0.064	0.19	4.49	0.545	82	18
189.6	0.064	0.2143	0.225	0.031	0.135	0.07	0.39	7.75	0.897	103	22
224.8	0.028	0.1241	0.064	0.022	0.0792	0.019	0.44	4.89	0.524	94	9
63.1	0.034	0.181	0.04	0.006	0.123	0.016	0.55	7.28	0.789	118	10
336.7	0.035	0.0235	0.04	0.052	0.0134	0.024	0.69	0.9	0.086	58	8
67.7	0.075	0.0154	<0.018	0.007	0.0115	<0.011	1.1	0.58	0.074	207	11
156.2	0.066	0.0142	0.023	0.011	0.008	0.012	0.83	0.46	0.056	180	10
143.7	0.064	0.0246	0.027	0.015	0.0143	0.011	1.61	0.87	0.102	174	9
71	0.074	0.0189	0.054	<0.005	0.0116	0.012	1.3	0.66	0.08	240	11
258.3	0.053	0.0389	0.077	0.041	0.0222	0.026	0.43	1.44	0.153	137	10
14.9	0.078	0.0171	<0.018	<0.005	0.0139	<0.011	2.7	0.72	0.097	179	10
200.5	0.062	0.0221	0.035	0.05	0.0121	0.035	1.21	0.79	0.088	160	10
194.2	0.062	0.0306	0.042	0.006	0.0192	0.013	1.59	1.12	0.128	173	10
65.7	0.092	0.0249	0.023	0.005	0.0159	0.015	2.16	0.97	0.105	161	13
187.6	0.024	0.1377	0.021	0.008	0.0917	<0.011	0.36	5.56	0.612	95	7
114.4	0.063	0.0749	0.025	0.02	0.0436	<0.011	0.18	2.84	0.307	91	10
178.5	0.031	0.1658	0.07	0.013	0.101	0.02	0.05	6.44	0.677	91	10
17.9	0.106	0.1058	0.056	0.283	0.054	0.106	1.38	4	0.341	48	17
217.7	0.077	0.0531	0.04	0.01	0.0318	0.015	0.11	2.01	0.23	184	11
327.2	0.042	0.1593	0.094	0.015	0.0947	0.028	<0.05	6.05	0.617	87	12
269.7	0.047	0.0818	0.062	0.013	0.0496	0.017	0.06	3.2	0.336	116	9
189	0.024	0.1544	<0.018	0.028	0.0947	<0.011	0.33	5.85	0.643	84	8
90.3	0.031	0.1667	0.023	0.01	0.106	<0.011	0.48	6.42	0.719	115	9
198.3	0.049	0.0784	0.09	0.018	0.0486	0.033	0.63	3.05	0.317	48	8
191.9	0.066	0.0242	0.041	0.035	0.014	0.011	1.21	0.86	0.099	142	10
61.6	0.089	0.0172	<0.018	0.007	0.0131	<0.011	1.28	0.77	0.086	195	13
6	0.091	0.0238	<0.018	0.016	0.0165	0.012	2.74	0.92	0.117	777	11
142.3	0.066	0.0386	0.021	0.012	0.0253	<0.011	1.69	1.55	0.168	183	10
286.6	0.034	0.0378	0.033	0.033	0.0211	0.012	1.24	1.36	0.136	33	7
17.7	0.03	0.1843	0.019	0.009	0.1175	<0.011	0.5	7.05	0.786	124	10
220.4	0.033	0.1441	0.058	0.012	0.0929	0.016	0.37	5.75	0.625	98	9
14.3	0.233	0.0338	0.037	0.149	0.0199	0.011	0.42	1.23	0.127	166	19
42.8	0.222	0.028	<0.018	0.034	0.0166	<0.011	0.32	0.98	0.115	156	17
274.2	0.047	0.1188	0.118	0.022	0.0623	0.034	0.37	4.15	0.413	103	12
257.1	0.045	0.5206	0.203	0.023	0.1654	0.064	0.16	15.46	0.977	113	10
152.9	0.05	0.8334	0.184	0.025	0.2541	0.074	0.16	24.06	1.378	140	7
166.1	0.05	1.1961	0.212	0.044	0.3122	0.086	0.06	33.21	1.61	144	8
164.5	0.075	0.083	0.077	0.145	0.0503	0.022	0.13	3.07	0.339	158	11

Al2O3	CaO	Fe2O3	K2O	LOI	MgO	MnO	Na2O	P2O5	SiO2	TiO2	Total	CO2	S
5.18	1.143	73.35	1.19	-1.46	2.53	0.284	0.08	0.003	8.27	8.01	98.58	0.08	0.35
17.13	7.823	9.69	1.68	1.4	4.78	0.132	3.65	0.495	52.1	1.17	100.05	0.55	0.22
8.78	2.957	31.79	1.01	1.77	11	0.242	0.54	0.052	39.97	1.71	99.82	0.28	1.78
12.63	4.008	38.11	1.81	1.88	5.19	0.202	0.95	0.005	29.15	3.77	97.71	1.15	0.48
23.48	12.397	6.27	0.18	1.29	3.94	0.079	2.92	0.007	49.99	0.18	100.73	0.48	0.05
5.53	16.228	20.54	0.11	0.73	8.76	0.275	0.54	0.017	44.84	2.9	100.47	0.47	0.34
4.39	0.324	79.8	0.01	-2.24	2.4	0.247	0.04	0.002	2.49	10.68	98.14	0.09	0.14
10.52	9.627	23.97	0.25	1.11	7.68	0.261	1.25	0.021	43.37	2.11	100.17	0.34	0.62
19.77	10.38	13.04	0.36	1.05	4.22	0.179	2.87	0.017	47.6	1.13	100.62	0.3	0.16
13.61	10.542	19.96	0.22	0.44	6.2	0.242	1.85	0.018	45.15	2.33	100.56	0.17	0.34
14.01	11.145	19.71	0.2	1.48	6.08	0.225	1.74	0.007	42.5	2.14	99.24	0.31	0.33
6.66	9.72	28.62	0.08	1.11	9.72	0.272	0.41	0.003	39.95	2.71	99.26	0.16	0.37
22.19	10.481	16.1	0.4	2.62	0.79	0.066	3.57	0.006	40.75	1.9	98.87	1.76	0.5
8.83	3.153	62.7	0.06	0.67	2.27	0.2	0.56	0.003	12.65	7.25	98.35	0.77	0.61
12.21	4.952	52.45	0.08	0.37	1.96	0.19	1.1	0.003	19.43	5.92	98.67	0.06	0.35
12.59	5.234	50.35	0.09	0.5	1.85	0.162	1.24	0.004	20.69	5.66	98.37	0.03	0.51
8.89	3.155	62.58	0.03	1	2.32	0.204	0.23	0.003	12.68	7.07	98.16	0.83	0.38
17.79	7.568	31.53	0.26	1.84	1.63	0.126	2.56	0.011	31.78	3.44	98.54	0.91	0.35
6.79	3.585	66.42	<0.01	1.32	2.27	0.208	<0.02	0.002	9.56	8.12	98.27	2.73	0.58
15.24	6.082	42.56	0.33	1.08	1.59	0.141	1.75	0.004	25.46	5.03	99.27	0.39	0.31
13.93	6.302	44.56	0.05	1.14	1.88	0.164	1.46	0.005	24	5.32	98.81	0.34	0.88
8.31	2.66	63.62	0.02	0.12	2.16	0.193	0.41	0.002	13.1	7.95	98.55	0.05	0.89
11.72	10.313	21.63	0.21	1.21	7.67	0.231	1.53	0.004	43.13	1.97	99.62	0.05	0.27
9.1	6.784	43.08	0.13	0.68	4.86	0.281	0.85	0.005	27.05	6.47	99.29	0.16	0.93
11.65	10.023	19.81	0.12	1.49	7.93	0.249	1.61	0.011	44.82	1.7	99.41	0.15	0.26
3.48	8.161	51.55	0.05	4.66	2.54	0.309	0.11	0.006	13.45	10.12	94.14	4.97	6.7
16.16	7.559	28.44	0.12	1.91	2.21	0.172	2.98	0.007	33.74	5.19	98.49	1.78	0.48
15.56	10.606	16.36	0.18	2.46	4.38	0.188	2.4	0.019	44.82	2.3	99.27	1.64	0.34
14.25	7.81	24.84	0.19	1.68	4.51	0.243	2.32	0.017	39.25	3.78	98.89	0.91	0.31
12.41	10.973	21.11	0.21	1.31	6.86	0.221	1.58	0.002	42.64	2.12	99.44	0.52	0.37
9.43	10.096	25.68	0.2	1.59	8.39	0.239	0.73	0.004	40.56	2.42	99.34	0.83	0.46
15.67	8.584	24.23	0.18	4.66	3.52	0.135	1.93	0.005	36.71	2.78	98.4	3.18	0.53
14.09	6.375	45.07	0.18	1.02	1.63	0.16	1.35	0.005	23.47	5.51	98.86	0.05	0.89
7.24	3.298	66.18	0.02	0.77	2.39	0.211	0.04	0.002	10.17	8.23	98.55	0.84	0.95
5.71	3.766	69.27	0.02	1.64	2.21	0.227	<0.02	0.002	6.36	8.8	98.01	2.82	0.36
10.62	4.875	52.91	0.01	1.25	2.83	0.188	0.19	0.004	19.58	6.19	98.65	0.11	1.43
21.22	9.895	19.46	0.32	2.25	1.1	0.087	3.11	0.006	39.3	2.3	99.05	0.04	0.46
6.79	10.219	27.48	0.11	1.29	9.66	0.273	0.57	0.003	40.2	2.53	99.13	0.84	0.35
13.9	10.777	17.43	0.13	2.75	5.76	0.207	2.03	0.006	44.09	1.87	98.95	1.4	0.26
6.33	2.431	59.59	0.13	-0.43	2.01	0.321	0.41	0.02	12.6	15.43	98.85	0.11	1.1
7.88	2.913	55.92	0.16	-0.46	1.82	0.301	0.71	0.013	15.08	14.66	99	0.14	0.6
15.53	8.068	21.21	0.27	1.27	4.92	0.249	2.81	0.113	43.43	1.99	99.86	0.05	0.09
14.43	8.844	22.2	0.23	1.74	4.95	0.228	2.74	1.79	40	2.14	99.29	0.29	0.04
11.22	8.644	29.95	0.18	1.69	5.95	0.286	1.55	2.957	33.7	3.26	99.39	0.05	0.09
10.2	9.85	34.37	0.18	1.83	3.7	0.292	1.4	4.501	26.89	5.98	99.19	0.59	0.38
11.15	5.927	32.95	0.16	1.34	5.93	0.323	1.84	0.055	35.05	4.22	98.95	0.04	0.49

Al	Ba	Be	Ca	Co	Cr	Cu	Fe	K	Li	Mg
23623	66	3	6308	145	954	143	>95000	8939	19	12398
79203	663	2	46971	26	71	36	59366	13113	34	25960
39813	81	1	17192	93	12	502	>95000	7359	10	58957
59549	133	2	23915	128	2787	384	>95000	14352	32	28002
107465	32	1	72734	31	36	40	36314	1265	13	20365
26177	15	2	84366	70	94	197	>95000	595	8	46539
20084	12	4	1742	219	463	168	>95000	<70	3	11782
48674	35	1	54843	90	13	172	>95000	1797	16	40565
91507	50	1	61438	46	42	52	78606	2093	19	22542
64573	40	1	62092	71	94	128	>95000	1571	10	33877
68152	34	1	65174	72	18	43	>95000	1542	6	33195
32770	8	1	56437	108	22	67	>95000	554	2	53430
>110000	81	1	71645	78	67	158	>95000	3362	4	4347
42135	12	2	17911	175	2408	418	>95000	96	1	11709
59438	34	2	29363	151	540	249	>95000	556	7	10206
59606	34	2	29289	161	222	555	>95000	628	3	9898
43183	12	2	18409	189	2319	313	>95000	<70	4	12108
81175	69	1	45070	107	925	289	>95000	1918	4	6846
32044	10	2	20167	190	1173	283	>95000	<70	4	11415
71738	80	2	36344	133	436	201	>95000	2438	5	7461
67275	20	2	37318	151	68	209	>95000	217	4	9772
40452	13	2	15480	186	63	158	>95000	<70	3	11206
56556	23	1	59546	87	24	40	>95000	853	3	41661
44652	16	2	39694	123	965	545	>95000	903	10	26104
57317	24	1	59682	70	35	61	>95000	740	7	43622
17458	10	3	48128	466	1283	1126	>95000	325	3	13773
77314	35	2	44922	85	31	57	>95000	748	7	11618
74890	39	1	62553	54	59	36	>95000	1246	6	23399
68710	23	1	46207	81	27	28	>95000	993	6	24258
60701	26	1	63928	83	15	60	>95000	1280	5	37370
46549	15	1	59215	102	17	68	>95000	863	3	46047
69953	51	1	47400	77	35	141	>95000	1222	7	17757
67889	45	2	37630	164	249	165	>95000	1342	3	7939
35292	11	2	18781	204	246	171	>95000	<70	3	12400
26972	12	2	20668	170	1216	194	>95000	<70	5	10934
50414	9	2	27676	188	294	245	>95000	<70	2	14384
101158	132	1	59563	76	50	112	>95000	2457	3	5012
32825	12	1	57339	105	18	41	>95000	798	3	51553
70100	29	1	65061	67	8	29	>95000	960	4	32410
31432	15	6	14134	150	179	287	>95000	883	4	10583
38687	22	5	16595	127	387	154	>95000	1137	5	9384
78811	49	1	49722	62	7	23	>95000	1865	9	27695
70915	37	1	52395	69	5	7	>95000	1703	10	26972
55721	24	1	50814	88	5	17	>95000	1340	6	32714
50077	25	2	56111	84	23	72	>95000	1131	4	19793
55370	16	1	34725	101	3	77	>95000	1187	4	32389

Mn	Na	Ni	P	Pb	Sc	Sr	Ti	V	Y	As	Ba
1696	<500	312	176	68	16	31	41397	5385	<1	19	68
878	27465	52	1746	<15	14	755	5688	155	22	8	981
1563	4341	27	207	29	34	52	9259	466	5	11	84
1278	7757	238	62	29	21	151	20749	2456	1	16	197
504	22695	60	<15	<15	17	271	830	104	2	8	26
1764	4899	204	101	20	62	63	15677	570	12	10	<8
1502	<500	384	180	65	21	2	54874	6858	<1	19	<8
1680	10513	62	113	16	39	91	11525	358	8	9	15
1217	22642	32	53	<15	19	255	5443	221	4	11	37
1628	15377	54	88	15	42	176	13269	463	7	6	29
1693	12486	16	96	15	40	218	12019	783	4	8	33
2038	3319	40	110	25	57	63	15191	1329	5	15	<8
578	27616	109	41	<15	7	354	12597	1317	<1	7	81
1408	4235	389	174	46	16	66	38512	4683	<1	9	<8
1389	8132	291	147	42	13	158	32712	4335	<1	11	25
1181	8891	323	110	39	15	142	30376	3796	<1	<6	32
1463	1849	334	184	48	17	71	38346	4835	<1	14	<8
916	17565	223	99	18	8	261	19116	2357	<1	6	78
1405	<500	326	185	57	19	14	41718	5037	<1	12	<8
1019	12348	210	133	31	11	201	27782	3347	<1	8	110
1180	10569	235	130	38	15	189	29107	3339	<1	9	12
1387	3188	173	211	57	18	65	42947	4712	<1	56	<8
1726	11135	29	74	18	43	181	10931	896	4	14	19
2068	6502	373	122	39	39	114	35431	1187	1	7	12
1899	11686	90	107	<15	45	176	9759	379	5	<6	27
2249	1056	574	114	105	25	17	52762	2674	2	8	<8
1290	20240	79	110	19	18	212	28456	1334	1	9	27
1404	16561	27	118	<15	41	319	12840	181	5	9	41
1831	16297	38	144	17	29	264	21084	255	2	12	12
1679	11574	22	66	19	46	186	11887	974	4	10	23
1841	5705	42	81	26	50	90	13698	1211	5	8	9
946	12608	81	66	15	22	198	14473	1544	2	7	55
1152	9975	270	137	38	12	196	30512	3322	<1	<6	48
1475	<500	302	198	57	18	60	43712	4953	<1	16	<8
1541	<500	277	203	57	17	5	45446	5499	<1	11	<8
1309	1522	331	162	39	20	137	32859	3705	<1	9	<8
654	21552	116	48	<15	8	285	13163	1398	1	14	163
1940	4389	37	106	29	55	17	13761	1191	5	<6	<8
1623	15110	6	60	16	43	220	10873	510	5	8	17
2274	3365	199	281	62	22	14	80032	1145	<1	8	<8
2147	5423	195	235	53	21	43	76013	1380	<1	28	12
1933	20456	27	496	<15	20	281	11858	168	3	6	43
1708	19333	8	>6400	<15	13	254	11999	59	13	<6	19
2152	11582	20	>6400	29	10	152	18512	65	20	6	<8
2127	10410	33	>6400	34	10	163	31364	209	27	8	9
2369	13433	39	301	26	21	162	23415	251	2	7	<8

Cr	Ga	Nb	Pb	Rb	Sr	Th	Y	Zr
1617	45	2	10	45	40	2	<0.7	13
83	21	6	10	43	899	6	23	160
15	21	2	10	44	63	<1.5	7	23
3687	33	1	12	70	196	2	1	11
43	20	<0.7	4	6	305	<1.5	3	4
119	13	1	3	2	72	2	15	23
726	51	1	3	<0.8	3	<1.5	1	14
11	17	1	4	8	108	2	10	19
51	21	1	5	10	293	2	5	11
109	18	1	4	6	205	2	8	15
31	20	<0.7	3	3	236	<1.5	4	6
43	17	<0.7	4	1	69	2	7	9
79	29	1	2	11	340	<1.5	<0.7	4
>4000	44	<0.7	4	1	77	<1.5	<0.7	10
867	41	<0.7	2	3	185	<1.5	<0.7	9
349	42	1	3	3	179	2	<0.7	9
3740	44	<0.7	3	<0.8	81	<1.5	<0.7	11
1306	33	<0.7	3	9	299	2	<0.7	8
1899	43	2	4	<0.8	18	2	<0.7	13
660	39	1	4	11	234	3	<0.7	9
113	41	<0.7	4	1	214	3	<0.7	10
94	43	1	3	1	76	<1.5	<0.7	13
44	18	<0.7	4	2	201	<1.5	5	6
1429	28	<0.7	4	2	129	2	2	8
50	17	<0.7	3	2	189	2	6	9
2066	21	1	69	<0.8	18	2	3	17
49	29	1	2	2	239	<1.5	2	10
77	21	1	3	4	347	2	5	11
38	23	1	4	3	288	2	2	7
36	19	<0.7	2	2	200	2	6	6
30	19	<0.7	3	1	97	2	6	8
56	28	1	4	6	236	<1.5	2	6
393	40	1	3	7	223	3	<0.7	9
413	45	1	3	<0.8	70	2	<0.7	13
2117	41	1	4	<0.8	7	3	<0.7	13
459	41	<0.7	3	1	159	2	1	10
77	29	<0.7	3	8	310	2	<0.7	5
34	16	<0.7	3	1	18	2	7	9
15	19	<0.7	2	2	225	2	5	7
280	35	4	6	1	17	3	1	20
633	37	4	5	3	49	3	<0.7	19
11	20	<0.7	3	4	297	<1.5	3	9
<9	21	<0.7	<1.7	4	274	2	15	8
<9	19	<0.7	3	4	160	<1.5	25	6
30	20	<0.7	8	4	181	<1.5	36	6
<9	20	<0.7	3	2	179	<1.5	1	10

Sample	Intrusion	Depth (m)	SG	Au	Ir	Pd
NO-2G47-2	Thunderbird	63.07	2.98	0.38	0.05	1.66
NO-2G47-3	Thunderbird	84.15	3.35	0.29	0.01	<0.12
NO-2G47-4	Thunderbird	89.5	3.45	0.36	0.01	<0.12
NO-2G47-4B	Thunderbird	179	3.34	0.62	<0.01	<0.12
NO-2G47-5	Thunderbird	233.78	3.38	0.85	<0.01	<0.12
NO-2G47-6	Thunderbird	311.3	3.75	0.65	0.08	0.52
NO-2G47-7	Thunderbird	311.58	3.12	0.61	0.01	0.22
NO-2G47-8	Thunderbird	320.76	3.65	0.96	0.01	0.39
NO-2G47-9	Thunderbird	346.57	3.39	0.66	<0.01	<0.12
NO-2G47-10	Thunderbird	355	3.12	0.59	0.01	<0.12

Pt	Rh	Ru	Ba	Be	Bi	Cd	Ce	Co
1.17	0.13	0.12	90.1	0.37	<0.15	0.05	4.62	37.01
0.32	0.03	<0.08	48.6	0.21	<0.15	0.037	1.77	98.66
0.23	0.03	<0.08	26.9	0.2	<0.15	0.05	1.38	103.34
0.19	0.02	<0.08	32.1	0.24	<0.15	0.07	1.52	90.65
<0.17	0.03	<0.08	21.8	0.18	<0.15	0.054	18.58	87.29
1.46	0.12	<0.08	20.9	0.13	<0.15	0.034	1.34	118.02
0.53	0.04	<0.08	69.1	0.28	<0.15	0.043	6.11	64.45
0.35	0.04	<0.08	16.2	0.19	<0.15	0.042	1.24	112.64
0.18	0.02	<0.08	15.9	0.21	<0.15	0.071	1.93	88.56
<0.17	<0.02	<0.08	178.1	0.18	<0.15	0.031	27.98	72.03

Cs	Cu	Dy	Er	Eu	Ga	Gd	Hf	Ho	In	La	Li
0.769	34.2	1.321	0.767	0.9966	21.42	1.234	0.38	0.2644	0.0403	2.1	12.3
0.088	53.8	0.267	0.169	0.5639	21.38	0.259	0.36	0.0582	0.0347	0.88	2.7
0.07	66.6	0.174	0.121	0.4973	25.75	0.173	0.38	0.0374	0.0406	0.68	4.6
0.056	61.4	0.336	0.211	0.5913	21.82	0.306	0.27	0.0719	0.0355	0.74	6.5
0.074	68.6	3.695	1.689	1.5578	14.43	5.147	0.17	0.6759	0.027	7	2.4
0.2	88.6	0.167	0.159	0.4194	28.71	0.141	1.65	0.0425	0.0505	0.79	7.3
0.192	60.8	0.749	0.419	0.9888	28.04	0.798	0.54	0.1527	0.0308	3.1	6.4
0.081	57.9	0.206	0.138	0.4295	25.78	0.173	0.58	0.0461	0.0489	0.78	6.1
0.08	68.3	0.481	0.279	0.6646	20.03	0.447	0.25	0.0942	0.0315	0.95	8.2
3.403	66.9	5.41	2.478	2.0382	17.94	7.362	0.27	0.9971	0.0267	10.73	8.8

Lu	Mo	Nb	Nd	Ni	Pb	Pr	Rb	Sb	Sc	Sm	Sn
0.1084	0.37	0.729	3.33	21.2	2.1	0.676	11.67	0.08	43.4	0.949	1.71
0.0331	0.45	1.327	0.97	49	1.3	0.228	6.99	<0.04	16.3	0.227	1.28
0.0208	0.45	1.663	0.76	47.9	<0.6	0.178	1.38	0.05	16.4	0.175	0.2
0.0363	0.35	0.982	0.92	38.6	<0.6	0.206	1.41	0.08	22.4	0.252	0.21
0.144	0.41	0.508	15.95	15.4	<0.6	2.93	0.82	0.07	23.1	4.159	<0.16
0.0429	1.05	2.824	0.6	51.4	<0.6	0.148	1.35	0.04	21	0.133	0.18
0.0536	0.73	1.619	3.2	25.1	0.9	0.77	2.1	0.04	12	0.752	0.34
0.0302	0.79	2.152	0.59	33.7	0.9	0.133	0.9	0.06	21.7	0.144	0.19
0.0439	0.44	1.004	1.38	29.4	<0.6	0.284	0.83	0.09	22.6	0.377	<0.16
0.1982	0.33	0.931	23.47	13.6	2.5	4.729	27.11	<0.04	20.9	6.016	0.19

Sr	Ta	Tb	Th	Tl	Tm	U	W	Y	Yb	Zn	Zr
384.1	0.043	0.1935	0.053	0.066	0.1067	0.02	0.26	7.06	0.686	69	12
201	0.09	0.0394	0.044	0.041	0.0278	0.016	<0.05	1.55	0.196	152	12
208.9	0.122	0.0265	0.055	0.016	0.0166	0.018	<0.05	1	0.124	176	13
205.1	0.071	0.0524	0.053	0.023	0.0325	0.017	0.31	1.94	0.223	173	9
173.3	0.037	0.6639	0.139	0.007	0.1908	0.055	0.06	18.94	1.021	147	6
89.8	0.215	0.0232	0.119	0.024	0.0277	0.088	0.3	1.12	0.221	245	76
377.8	0.123	0.1202	0.841	0.012	0.0564	0.166	0.3	4.07	0.373	139	18
43.1	0.159	0.0313	0.091	0.033	0.0233	0.047	0.08	1.21	0.171	265	22
104.3	0.073	0.0713	0.04	0.009	0.0382	0.013	0.12	2.44	0.27	179	8
102.5	0.067	0.9547	0.238	0.161	0.2735	0.09	0.94	27.88	1.449	133	9

Al2O3	CaO	Fe2O3	K2O	LOI	MgO	MnO	Na2O	P2O5	SiO2	TiO2	Total	CO2	S
18.43	10.653	12.35	0.53	1.31	3.3	0.157	3.22	0.075	48.2	1.59	99.82	0.13	0.13
13.1	5.28	33.92	0.3	1.01	4.43	0.297	1.66	0.038	33.99	5.2	99.23	0.13	0.26
12.83	4.902	38.06	0.16	0.79	3.06	0.263	1.91	0.022	29	7.98	98.98	0.12	0.33
13.34	6.325	31.07	0.16	0.88	4.5	0.28	2.08	0.021	36.02	4.85	99.53	0.07	0.3
10.22	8.814	32.41	0.07	0.17	5.59	0.369	1.57	2.555	35.17	2.92	99.86	0.36	0.36
9.74	3.687	47.9	0.16	-0.69	1.63	0.279	1.17	0.014	22.77	12.41	99.07	0.07	0.49
18.51	6.967	22.76	0.18	-0.03	0.95	0.141	3.9	0.113	40.49	5.6	99.58	0.28	0.31
9.38	3.695	45.74	0.17	-0.18	2.41	0.312	0.86	0.014	24.59	11.91	98.9	0.1	0.29
12.25	6.018	34.32	0.2	0.69	3.92	0.334	1.55	0.055	34.32	5.79	99.45	0.03	0.34
11.45	7.811	29.08	0.67	5.05	3.54	0.277	1.35	3.053	32.11	4.24	98.63	3.16	0.32

Al	Ba	Be	Ca	Co	Cr	Cu	Fe	K	Li	Mg
91057	82	1	64163	34	110	22	79105	4012	13	17933
66200	47	2	31816	94	21	33	>95000	2159	3	24103
62885	27	2	28851	99	29	43	>95000	1185	5	16257
66865	32	2	38030	86	6	41	>95000	1181	8	24768
49792	23	1	50249	81	5	48	>95000	528	3	29872
47239	22	4	21190	117	59	59	>95000	1113	8	8429
94073	65	2	44013	64	27	44	>95000	1332	7	5161
45976	18	4	21258	109	30	32	>95000	1293	7	12821
61626	17	2	36378	86	7	46	>95000	1520	9	21674
57208	160	2	46808	68	5	46	>95000	5191	10	19563

Mn	Na	Ni	P	Pb	Sc	Sr	Ti	V	Y	As	Ba
1223	22737	17	316	<15	37	373	9143	91	6	<6	85
2197	12525	42	258	28	13	203	29858	316	<1	9	31
1932	13939	40	230	35	13	209	43531	447	<1	8	<8
2121	15386	33	197	27	19	207	27725	208	1	10	15
2699	11421	11	>6400	26	19	174	16043	51	15	7	9
1997	8685	43	219	45	17	88	65569	767	<1	14	<8
1129	27620	21	489	16	10	378	33230	373	3	<6	59
2166	6401	27	223	48	17	42	60657	430	<1	9	<8
2466	11698	23	319	30	19	107	31675	138	1	<6	<8
2079	9978	11	>6400	26	17	101	23386	62	23	7	192

Cr	Ga	Nb	Pb	Rb	Sr	Th	Y	Zr
127	22	1	2	13	390	<1.5	6	9
29	25	1	3	9	223	<1.5	<0.7	9
39	30	1	3	2	235	<1.5	<0.7	11
<9	23	<0.7	3	2	222	<1.5	1	8
<9	17	<0.7	2	2	198	<1.5	21	3
77	32	2	5	1	98	<1.5	1	78
33	29	1	<1.7	4	406	<1.5	2	17
37	31	1	3	<0.8	50	<1.5	1	25
<9	22	<0.7	2	1	117	<1.5	2	6
<9	19	1	5	28	107	2	29	9

Appendix E

Samarium- Neodymium Isotope geochemistry

Sample Name	Sample Wt.	Spike Wt.	Nd	Sm	Eps Nd (CHUR)	Model Age
	(grams)	(grams)	(ppm)	(ppm)	(T=2735 Ma.)	
MM-V5-1	0.9997	0.0800	1.0973	0.3432	-2.80	4578
MM-V8-4	1.3893	0.0816	1.2681	0.2903	-3.33	3398
MM-117-7	0.8014	0.0860	2.3730	0.7029	4.01	2565
NO-2G46-6	0.1152	0.1178	28.5985	7.5828	0.44	3133
MM-V8-2	0.6907	0.0811	1.2367	0.3527	-0.28	3379
NO-2G47-2	0.6713	0.0804	3.3615	0.9574	1.53	3048
NO-2G47-5	0.1394	0.0810	16.4976	4.3744	0.44	3132
MM-60-4	0.5405	0.0803	2.8634	0.6907	1.90	2885
MM-110-03	0.0399	0.0806	2.6502	0.6174	11.24	1896
MM-V2-5	0.2488	0.0180	*1.5660*	0.3733	1.61	2913
MM-110-04	0.2508	0.0203	*1.2977*	0.2708	4.86	2594
NO-2G22-2	0.2501	0.0205	*1.9428*	0.6549	0.42	4831
NO-2G46-3	0.2492	0.0201	*2.0990*	0.5827	0.03	3265
MM-V4-1	1.2275	0.0756	0.1303	0.0473	8.76	10187
MM-V4-6	0.5062	0.0803	0.4587	0.1252	5.52	2379

Sample Name	AGE	146/144Nd	148/144Nd	143/144Nd	147/149Sm	152/149 Sm
MM-V5-1	2735	0.7219	0.71527	0.513242	0.28648	0.50422
MM-V8-4	2735	0.7219	0.54258	0.511979	0.31764	0.5574
MM-117-7	2735	0.7219	0.53575	0.513072	0.38381	0.67348
NO-2G46-6	2735	0.7219	0.474124	0.512437	0.41514	0.72827
MM-V8-2	2735	0.7219	0.8575	0.513337	0.21817	0.38542
NO-2G47-2	2735	0.7219	0.47321	0.512705	0.43451	0.76283
NO-2G47-5	2735	0.7219	0.470685	0.512431	0.41844	0.73635
MM-60-4	2735	0.7219	0.578677	0.512446	0.30419	0.53364
MM-110-03	2735	0.7219	4.993	0.521486	0.03002	0.0533
MM-V2-5	*2735*	*0.7219*	*0.541448*	*0.512331*	*0.32763*	*0.5748*
MM-110-04	*2735*	*0.7219*	*0.64673*	*0.512369*	*0.23795*	*0.41773*
NO-2G22-2	*2735*	*0.7219*	*0.516395*	*0.513299*	*0.43443*	*0.76036*
NO-2G46-3	*2735*	*0.7219*	*0.491284*	*0.512584*	*0.40768*	*0.71961*
MM-V4-1	2735	0.7219	3.2402	0.519223	0.068	0.11955
MM-V4-6	2735	0.7219	2.45	0.52	0.07	0.12

Sample Name	143Nd/144Nd	147Sm/144Nd	143Nd/144Nd			
			(initial)			
MM-V5-1	0.512358136	0.1890958	0.508945368			
MM-V8-4	0.511416615	0.13842047	0.508918426			
MM-117-7	0.512524127	0.17907442	0.509292223			
NO-2G46-6	0.512003385	0.1602994	0.509110329			
MM-V8-2	0.512185667	0.17241425	0.509073964			
NO-2G47-2	0.51227	0.17219656	0.509165649			
NO-2G47-5	0.512003803	0.16030553	0.509110636			
MM-60-4	0.511816737	0.14583737	0.509184689			
MM-110-03	0.512202242	0.1408539	0.509660135			
MM-V2-5	*0.511771298*	0.14412636	0.50917013			
MM-110-04	*0.511611866*	0.12614507	0.509335222			
NO-2G22-2	*0.512787615*	0.20379988	0.50910947			
NO-2G46-3	*0.512118511*	0.1678269	0.5090896			
MM-V4-1	0.513495762	0.21952696	0.509533777			
MM-V4-6	0.51	0.1649765	0.509368931			

Appendix F

Mineral Calculations

Assumptions for amphibole recalculations:

Orthorhombic?	False
Use initial $M^{3+}/\Sigma M$?	False
Estimate OH=2-2Ti?	True
Require initial H_2O+?	False
Require Si–K<=16?	True
Require Si–Ca & Li<=15?	True
Require Si–Mg & Li>=13?	False
Require Si–Na>=15?	True

Sample Data				**Mole Cation**					
Analysis point	Intrusion/Phase	Sample	Mineral	SiO2	TiO2	Al2O3	MgO	CaO	MnO
NO-2G22-4a-1	Thunderbird-V	NO-2G22-4	Feldspar	1.140	0.000	0.392	0.000	0.012	0.000
NO-2G22-4a-2	Thunderbird-V	NO-2G22-4	Feldspar	0.900	0.000	0.569	0.000	0.208	0.000
NO-2G22-4a-3	Thunderbird-V	NO-2G22-4	Feldspar	0.896	0.001	0.572	0.000	0.206	0.000
NO-2G22-4a-4	Thunderbird-V	NO-2G22-4	Feldspar	0.900	0.000	0.567	0.001	0.203	0.000
NO-2G22-4a-5	Thunderbird-V	NO-2G22-4	Feldspar	0.898	0.000	0.567	0.000	0.204	0.000
NO-2G22-4a-6	Thunderbird-V	NO-2G22-4	Feldspar	0.901	0.000	0.563	0.000	0.204	0.000
NO-2G22-4a-7	Thunderbird-V	NO-2G22-4	Feldspar	0.898	0.001	0.564	0.001	0.203	0.000
NO-2G22-4a-8	Thunderbird-V	NO-2G22-4	Feldspar	0.903	0.001	0.567	0.000	0.202	0.000
NO-2G22-4a-9	Thunderbird-V	NO-2G22-4	Feldspar	0.909	0.000	0.570	0.000	0.203	0.000
NO-2G22-4a-10	Thunderbird-V	NO-2G22-4	Feldspar	0.890	0.001	0.571	0.000	0.213	0.000
NO-2G22-4a-11	Thunderbird-V	NO-2G22-4	Feldspar	0.904	0.000	0.567	0.000	0.202	0.000
NO-2G22-4a-12	Thunderbird-V	NO-2G22-4	Feldspar	0.907	0.000	0.565	0.000	0.201	0.000
NO-2G22-4a-13	Thunderbird-V	NO-2G22-4	Feldspar	0.902	0.000	0.570	0.000	0.207	0.000
NO-2G22-4a-14	Thunderbird-V	NO-2G22-4	Feldspar	0.898	0.000	0.569	0.001	0.206	0.000
NO-2G22-4a-15	Thunderbird-V	NO-2G22-4	Feldspar	0.905	0.000	0.568	0.000	0.208	0.000
NO-2G22-4a-16	Thunderbird-V	NO-2G22-4	Feldspar	0.898	0.000	0.572	0.000	0.206	0.000
NO-2G22-4b-17	Thunderbird-V	NO-2G22-4	Feldspar	0.906	0.001	0.563	0.000	0.200	0.000
NO-2G22-4b-18	Thunderbird-V	NO-2G22-4	Feldspar	0.915	0.000	0.565	0.000	0.200	0.000
NO-2G22-4b-19	Thunderbird-V	NO-2G22-4	Feldspar	0.905	0.001	0.564	0.000	0.202	0.000
NO-2G22-4b-20	Thunderbird-V	NO-2G22-4	Feldspar	0.905	0.001	0.564	0.000	0.201	0.000
NO-2G22-4b-23	Thunderbird-V	NO-2G22-4	Feldspar	0.903	0.000	0.570	0.000	0.203	0.000
NO-2G22-4b-24	Thunderbird-V	NO-2G22-4	Feldspar	0.911	0.000	0.566	0.001	0.201	0.000
NO-2G22-4c-27	Thunderbird-V	NO-2G22-4	Feldspar	0.900	0.000	0.573	0.000	0.207	0.000
NO-2G22-4c-28	Thunderbird-V	NO-2G22-4	Feldspar	0.904	0.001	0.560	0.000	0.199	0.000
NO-2G22-4c-29	Thunderbird-V	NO-2G22-4	Feldspar	0.900	0.001	0.566	0.000	0.202	0.000
NO-2G22-4c-32	Thunderbird-V	NO-2G22-4	Feldspar	0.910	0.000	0.563	0.000	0.201	0.000
NO-2G22-4c-33	Thunderbird-V	NO-2G22-4	Feldspar	0.908	0.001	0.570	0.000	0.204	0.000
NO-2G22-4d-40	Thunderbird-V	NO-2G22-4	Feldspar	0.926	0.000	0.557	0.000	0.171	0.000
NO-2G22-4d-42	Thunderbird-V	NO-2G22-4	Feldspar	0.904	0.000	0.569	0.000	0.203	0.000
NO-2G21-2c-2	Thunderbird-V	NO-2G21-2	Feldspar	1.149	0.000	0.388	0.000	0.006	0.000
NO-2G21-2c-3	Thunderbird-V	NO-2G21-2	Feldspar	1.158	0.000	0.378	0.000	0.005	0.000
NO-2G21-5a-1	Thunderbird-V	NO-2G21-5	Feldspar	0.895	0.001	0.576	0.000	0.212	0.000
NO-2G21-5a-2	Thunderbird-V	NO-2G21-5	Feldspar	0.881	0.000	0.586	0.000	0.225	0.000
NO-2G21-5b-1	Thunderbird-V	NO-2G21-5	Feldspar	0.895	0.001	0.576	0.000	0.212	0.000
NO-2G21-5b-2	Thunderbird-V	NO-2G21-5	Feldspar	0.890	0.001	0.577	0.000	0.214	0.000
NO-2G21-5b-3	Thunderbird-V	NO-2G21-5	Feldspar	0.886	0.000	0.573	0.000	0.214	0.000
NO-2G21-5c-1	Thunderbird-V	NO-2G21-5	Feldspar	0.887	0.000	0.576	0.000	0.213	0.000
NO-2G21-5c-2	Thunderbird-V	NO-2G21-5	Feldspar	0.886	0.001	0.569	0.000	0.209	0.000
NO-2G21-5c-3	Thunderbird-V	NO-2G21-5	Feldspar	0.897	0.001	0.568	0.000	0.206	0.000
NO-2G21-5d-1	Thunderbird-V	NO-2G21-5	Feldspar	0.893	0.000	0.576	0.000	0.214	0.000
NO-2G21-5d-2	Thunderbird-V	NO-2G21-5	Feldspar	0.896	0.000	0.573	0.001	0.198	0.000
NO-2G21-5d-3	Thunderbird-V	NO-2G21-5	Feldspar	0.902	0.000	0.572	0.000	0.206	0.000
NO-2G46-3a-7	Thunderbird-P	NO-2G46-3	Feldspar	0.924	0.000	0.549	0.000	0.184	0.000
NO-2G46-3a-8	Thunderbird-P	NO-2G46-3	Feldspar	0.917	0.000	0.559	0.000	0.190	0.000
NO-2G46-3a-9	Thunderbird-P	NO-2G46-3	Feldspar	0.921	0.000	0.558	0.000	0.192	0.000

Sample Data							**Mole oxygen**					
Analysis point	FeOt	SrO	BaO	Na2O	K2O	Total	SiO2	TiO2	Al2O3	MgO	CaO	MnO
NO-2G22-4a-1	0.001	0.000	0.000	0.376	0.001	1.922	2.280	0.000	0.588	0.000	0.012	0.000
NO-2G22-4a-2	0.002	0.001	0.000	0.166	0.001	1.846	1.800	0.001	0.853	0.000	0.208	0.000
NO-2G22-4a-3	0.002	0.000	0.000	0.167	0.001	1.845	1.793	0.001	0.858	0.000	0.206	0.000
NO-2G22-4a-4	0.002	0.001	0.000	0.169	0.001	1.845	1.800	0.001	0.851	0.001	0.203	0.000
NO-2G22-4a-5	0.002	0.001	0.000	0.167	0.001	1.841	1.796	0.001	0.850	0.000	0.204	0.000
NO-2G22-4a-5	0.005	0.001	0.000	0.170	0.001	1.844	1.801	0.001	0.844	0.000	0.204	0.000
NO-2G22-4a-7	0.005	0.000	0.000	0.172	0.001	1.844	1.795	0.001	0.846	0.001	0.203	0.000
NO-2G22-4a-8	0.001	0.001	0.000	0.171	0.001	1.847	1.806	0.001	0.850	0.000	0.202	0.000
NO-2G22-4a-9	0.001	0.000	0.000	0.172	0.001	1.857	1.818	0.001	0.855	0.000	0.203	0.000
NO-2G22-4a-10	0.004	0.000	0.000	0.158	0.001	1.837	1.779	0.001	0.857	0.000	0.213	0.000
NO-2G22-4a-11	0.002	0.001	0.000	0.169	0.001	1.847	1.808	0.001	0.850	0.000	0.202	0.000
NO-2G22-4a-12	0.001	0.000	0.000	0.170	0.001	1.845	1.814	0.001	0.847	0.000	0.201	0.000
NO-2G22-4a-13	0.002	0.001	0.000	0.166	0.001	1.849	1.803	0.001	0.855	0.000	0.207	0.000
NO-2G22-4a-14	0.003	0.001	0.000	0.165	0.001	1.843	1.796	0.001	0.854	0.001	0.206	0.000
NO-2G22-4a-15	0.001	0.000	0.000	0.165	0.001	1.849	1.809	0.001	0.853	0.000	0.208	0.000
NO-2G22-4a-16	0.003	0.001	0.000	0.167	0.001	1.847	1.796	0.000	0.858	0.000	0.206	0.000
NO-2G22-4b-17	0.001	0.000	0.000	0.175	0.001	1.847	1.812	0.001	0.845	0.000	0.200	0.000
NO-2G22-4b-18	0.002	0.000	0.000	0.175	0.001	1.857	1.830	0.000	0.847	0.000	0.200	0.000
NO-2G22-4b-19	0.003	0.001	0.000	0.168	0.001	1.844	1.809	0.001	0.846	0.000	0.202	0.000
NO-2G22-4b-20	0.005	0.000	0.000	0.171	0.001	1.847	1.810	0.002	0.846	0.000	0.201	0.000
NO-2G22-4b-23	0.002	0.000	0.000	0.169	0.001	1.847	1.806	0.000	0.854	0.000	0.203	0.000
NO-2G22-4b-24	0.001	0.001	0.000	0.173	0.001	1.855	1.821	0.001	0.850	0.001	0.201	0.000
NO-2G22-4c-27	0.003	0.000	0.000	0.166	0.001	1.850	1.800	0.001	0.860	0.000	0.207	0.000
NO-2G22-4c-28	0.003	0.001	0.000	0.173	0.001	1.842	1.808	0.002	0.841	0.000	0.199	0.000
NO-2G22-4c-29	0.003	0.000	0.000	0.170	0.001	1.843	1.800	0.001	0.849	0.000	0.202	0.000
NO-2G22-4c-32	0.000	0.000	0.000	0.170	0.001	1.845	1.820	0.001	0.844	0.000	0.201	0.000
NO-2G22-4c-33	0.001	0.001	0.000	0.168	0.001	1.854	1.817	0.001	0.855	0.000	0.204	0.000
NO-2G22-4d-40	0.001	0.001	0.000	0.182	0.014	1.852	1.851	0.001	0.835	0.000	0.171	0.000
NO-2G22-4d-42	0.002	0.001	0.000	0.168	0.001	1.849	1.809	0.001	0.853	0.000	0.203	0.000
NO-2G21-2c-2	0.001	0.000	0.000	0.383	0.001	1.927	2.298	0.000	0.582	0.000	0.006	0.000
NO-2G21-2c-3	0.001	0.000	0.000	0.382	0.001	1.926	2.315	0.000	0.568	0.000	0.005	0.000
NO-2G21-5a-1	0.001	0.000	0.000	0.157	0.002	1.844	1.791	0.001	0.864	0.000	0.212	0.000
NO-2G21-5a-2	0.001	0.001	0.000	0.147	0.000	1.842	1.763	0.000	0.878	0.000	0.225	0.000
NO-2G21-5b-1	0.002	0.000	0.000	0.158	0.001	1.845	1.790	0.001	0.865	0.000	0.212	0.000
NO-2G21-5b-2	0.001	0.000	0.000	0.156	0.001	1.839	1.780	0.001	0.866	0.000	0.214	0.000
NO-2G21-5b-3	0.002	0.000	0.000	0.158	0.001	1.833	1.772	0.001	0.859	0.000	0.214	0.000
NO-2G21-5c-1	0.002	0.000	0.000	0.157	0.000	1.834	1.774	0.001	0.864	0.000	0.213	0.000
NO-2G21-5c-2	0.002	0.001	0.000	0.158	0.000	1.825	1.771	0.001	0.854	0.000	0.209	0.000
NO-2G21-5c-3	0.001	0.000	0.000	0.163	0.001	1.837	1.795	0.001	0.852	0.000	0.206	0.000
NO-2G21-5d-1	0.001	0.001	0.000	0.156	0.001	1.841	1.786	0.001	0.864	0.000	0.214	0.000
NO-2G21-5d-2	0.002	0.001	0.000	0.162	0.007	1.839	1.791	0.001	0.860	0.001	0.198	0.000
NO-2G21-5d-3	0.001	0.001	0.000	0.165	0.000	1.847	1.804	0.000	0.857	0.000	0.206	0.000
NO-2G46-3a-7	0.001	0.001	0.000	0.189	0.001	1.850	1.849	0.001	0.824	0.000	0.184	0.000
NO-2G46-3a-8	0.000	0.001	0.000	0.182	0.001	1.851	1.834	0.000	0.838	0.000	0.190	0.000
NO-2G46-3a-9	0.001	0.000	0.000	0.179	0.001	1.854	1.842	0.001	0.837	0.000	0.192	0.000

Sample Data							**Norm Cations**					
Analysis point	FeOt	SrO	BaO	Na2O	K2O	Total	SiO2	TiO2	Al2O3	MgO	CaO	MnO
NO-2G22-4a-1	0.001	0.000	0.000	0.188	0.000	3.070	2.971	0.000	1.020	0.000	0.031	0.000
NO-2G22-4a-2	0.003	0.001	0.000	0.083	0.000	2.949	2.442	0.001	1.543	0.000	0.564	0.000
NO-2G22-4a-3	0.002	0.000	0.000	0.083	0.000	2.945	2.435	0.002	1.554	0.000	0.560	0.000
NO-2G22-4a-4	0.003	0.001	0.000	0.084	0.000	2.945	2.445	0.001	1.541	0.002	0.552	0.000
NO-2G22-4a-5	0.003	0.001	0.000	0.084	0.000	2.940	2.443	0.001	1.543	0.000	0.556	0.000
NO-2G22-4a-5	0.007	0.001	0.000	0.085	0.000	2.943	2.448	0.001	1.529	0.000	0.554	0.001
NO-2G22-4a-7	0.008	0.000	0.000	0.086	0.000	2.941	2.442	0.002	1.535	0.001	0.553	0.000
NO-2G22-4a-8	0.002	0.001	0.000	0.086	0.000	2.949	2.450	0.002	1.538	0.001	0.547	0.000
NO-2G22-4a-9	0.002	0.000	0.000	0.086	0.000	2.965	2.452	0.001	1.537	0.001	0.549	0.000
NO-2G22-4a-10	0.005	0.000	0.000	0.079	0.000	2.936	2.424	0.002	1.557	0.001	0.579	0.000
NO-2G22-4a-11	0.004	0.001	0.000	0.084	0.000	2.950	2.450	0.001	1.537	0.000	0.547	0.000
NO-2G22-4a-12	0.002	0.000	0.000	0.085	0.000	2.950	2.459	0.001	1.531	0.001	0.544	0.000
NO-2G22-4a-13	0.002	0.001	0.000	0.083	0.000	2.953	2.442	0.001	1.544	0.001	0.561	0.000
NO-2G22-4a-14	0.004	0.001	0.000	0.083	0.000	2.945	2.439	0.001	1.547	0.001	0.558	0.000
NO-2G22-4a-15	0.002	0.000	0.000	0.083	0.000	2.955	2.449	0.001	1.539	0.001	0.562	0.000
NO-2G22-4a-16	0.004	0.001	0.000	0.083	0.000	2.949	2.436	0.000	1.552	0.001	0.559	0.000
NO-2G22-4b-17	0.002	0.000	0.000	0.088	0.000	2.948	2.459	0.001	1.528	0.000	0.543	0.000
NO-2G22-4b-18	0.003	0.000	0.000	0.087	0.000	2.967	2.467	0.000	1.523	0.000	0.538	0.000
NO-2G22-4b-19	0.004	0.001	0.000	0.084	0.000	2.948	2.455	0.002	1.531	0.001	0.548	0.000
NO-2G22-4b-20	0.007	0.000	0.000	0.086	0.000	2.951	2.453	0.002	1.528	0.000	0.544	0.000
NO-2G22-4b-23	0.003	0.000	0.000	0.084	0.000	2.952	2.448	0.000	1.544	0.000	0.552	0.000
NO-2G22-4b-24	0.002	0.001	0.000	0.086	0.000	2.963	2.459	0.001	1.529	0.001	0.543	0.000
NO-2G22-4c-27	0.004	0.000	0.000	0.083	0.001	2.955	2.436	0.001	1.552	0.000	0.561	0.000
NO-2G22-4c-28	0.004	0.001	0.000	0.086	0.000	2.941	2.458	0.003	1.524	0.001	0.540	0.001
NO-2G22-4c-29	0.005	0.000	0.000	0.085	0.000	2.944	2.446	0.002	1.539	0.001	0.550	0.000
NO-2G22-4c-32	0.001	0.000	0.000	0.085	0.000	2.952	2.467	0.001	1.525	0.001	0.544	0.000
NO-2G22-4c-33	0.001	0.001	0.000	0.084	0.000	2.964	2.452	0.001	1.538	0.000	0.552	0.000
NO-2G22-4d-40	0.002	0.001	0.000	0.091	0.007	2.958	2.503	0.001	1.505	0.000	0.462	0.000
NO-2G22-4d-42	0.003	0.001	0.000	0.084	0.000	2.955	2.449	0.001	1.540	0.001	0.551	0.000
NO-2G21-2c-2	0.001	0.000	0.000	0.192	0.000	3.078	2.986	0.000	1.008	0.000	0.015	0.000
NO-2G21-2c-3	0.002	0.000	0.000	0.191	0.001	3.082	3.005	0.000	0.983	0.001	0.012	0.000
NO-2G21-5a-1	0.002	0.000	0.000	0.078	0.001	2.949	2.429	0.002	1.563	0.000	0.574	0.000
NO-2G21-5a-2	0.002	0.001	0.000	0.073	0.000	2.943	2.396	0.001	1.592	0.000	0.611	0.000
NO-2G21-5b-1	0.002	0.000	0.000	0.079	0.000	2.950	2.427	0.002	1.564	0.000	0.574	0.000
NO-2G21-5b-2	0.001	0.000	0.000	0.078	0.000	2.940	2.421	0.002	1.571	0.000	0.583	0.000
NO-2G21-5b-3	0.003	0.000	0.000	0.079	0.000	2.927	2.421	0.001	1.565	0.000	0.583	0.000
NO-2G21-5c-1	0.002	0.000	0.000	0.078	0.000	2.932	2.420	0.001	1.571	0.000	0.581	0.000
NO-2G21-5c-2	0.003	0.001	0.000	0.079	0.000	2.918	2.429	0.001	1.561	0.000	0.572	0.000
NO-2G21-5c-3	0.002	0.000	0.000	0.081	0.000	2.938	2.444	0.001	1.547	0.001	0.560	0.000
NO-2G21-5d-1	0.001	0.001	0.000	0.078	0.000	2.945	2.427	0.001	1.565	0.000	0.581	0.000
NO-2G21-5d-2	0.002	0.001	0.000	0.081	0.004	2.939	2.438	0.001	1.561	0.001	0.539	0.000
NO-2G21-5d-3	0.001	0.001	0.000	0.082	0.000	2.952	2.444	0.000	1.549	0.000	0.559	0.000
NO-2G46-3a-7	0.002	0.001	0.000	0.095	0.000	2.955	2.502	0.001	1.487	0.000	0.498	0.000
NO-2G46-3a-8	0.001	0.001	0.000	0.091	0.000	2.956	2.482	0.001	1.512	0.000	0.515	0.000
NO-2G46-3a-9	0.002	0.000	0.000	0.090	0.000	2.965	2.485	0.001	1.506	0.000	0.519	0.000

Sample Data						**Norm Oxygen**						
Analysis point	SrO	BaO	Na2O	K2O	Total	SiO2	TiO2	Al2O3	MgO	CaO	MnO	FeOt
NO-2G22-4a-1	0.000	0.000	0.981	0.002	5.007	5.942	0.000	1.530	0.000	0.031	0.000	0.002
NO-2G22-4a-2	0.002	0.000	0.450	0.002	5.009	4.883	0.002	2.314	0.000	0.564	0.000	0.009
NO-2G22-4a-3	0.000	0.000	0.453	0.002	5.012	4.871	0.003	2.331	0.000	0.560	0.000	0.006
NO-2G22-4a-4	0.003	0.000	0.459	0.002	5.011	4.890	0.002	2.311	0.002	0.552	0.000	0.009
NO-2G22-4a-5	0.003	0.001	0.455	0.002	5.010	4.886	0.002	2.314	0.000	0.556	0.000	0.009
NO-2G22-4a-5	0.004	0.000	0.461	0.002	5.012	4.896	0.002	2.294	0.000	0.554	0.001	0.019
NO-2G22-4a-7	0.000	0.000	0.467	0.002	5.016	4.884	0.004	2.302	0.001	0.553	0.000	0.021
NO-2G22-4a-8	0.002	0.000	0.464	0.002	5.011	4.900	0.003	2.307	0.001	0.547	0.000	0.006
NO-2G22-4a-9	0.001	0.000	0.464	0.001	5.010	4.904	0.002	2.306	0.001	0.549	0.000	0.005
NO-2G22-4a-10	0.000	0.001	0.431	0.002	5.007	4.848	0.004	2.336	0.001	0.579	0.000	0.015
NO-2G22-4a-11	0.003	0.000	0.458	0.003	5.007	4.901	0.003	2.306	0.000	0.547	0.000	0.010
NO-2G22-4a-12	0.000	0.000	0.461	0.002	5.003	4.919	0.002	2.297	0.001	0.544	0.000	0.006
NO-2G22-4a-13	0.003	0.000	0.449	0.002	5.008	4.885	0.002	2.316	0.001	0.561	0.000	0.006
NO-2G22-4a-14	0.002	0.000	0.449	0.002	5.008	4.879	0.001	2.320	0.001	0.558	0.000	0.012
NO-2G22-4a-15	0.001	0.000	0.448	0.001	5.004	4.897	0.001	2.308	0.001	0.562	0.000	0.005
NO-2G22-4a-16	0.002	0.001	0.452	0.002	5.012	4.871	0.000	2.327	0.001	0.559	0.000	0.012
NO-2G22-4b-17	0.000	0.000	0.476	0.001	5.013	4.918	0.003	2.292	0.000	0.543	0.000	0.005
NO-2G22-4b-18	0.000	0.000	0.471	0.002	5.006	4.934	0.001	2.284	0.000	0.538	0.000	0.007
NO-2G22-4b-19	0.002	0.000	0.455	0.002	5.003	4.909	0.003	2.296	0.001	0.548	0.000	0.011
NO-2G22-4b-20	0.000	0.000	0.464	0.002	5.007	4.907	0.004	2.292	0.000	0.544	0.000	0.019
NO-2G22-4b-23	0.000	0.000	0.457	0.002	5.007	4.895	0.001	2.316	0.000	0.552	0.000	0.007
NO-2G22-4b-24	0.002	0.000	0.466	0.003	5.008	4.917	0.003	2.294	0.001	0.543	0.000	0.006
NO-2G22-4c-27	0.000	0.000	0.449	0.003	5.009	4.872	0.003	2.327	0.000	0.561	0.000	0.011
NO-2G22-4c-28	0.003	0.000	0.470	0.002	5.010	4.917	0.005	2.286	0.001	0.540	0.001	0.011
NO-2G22-4c-29	0.000	0.000	0.461	0.002	5.010	4.893	0.004	2.308	0.001	0.550	0.000	0.013
NO-2G22-4c-32	0.000	0.000	0.460	0.002	5.001	4.933	0.002	2.287	0.001	0.544	0.000	0.002
NO-2G22-4c-33	0.003	0.000	0.454	0.002	5.004	4.905	0.003	2.307	0.000	0.552	0.000	0.003
NO-2G22-4d-40	0.002	0.000	0.492	0.038	5.007	5.006	0.002	2.258	0.000	0.462	0.000	0.005
NO-2G22-4d-42	0.002	0.000	0.455	0.003	5.007	4.898	0.002	2.310	0.001	0.551	0.000	0.007
NO-2G21-2c-2	0.000	0.000	0.996	0.003	5.008	5.971	0.000	1.512	0.000	0.015	0.000	0.003
NO-2G21-2c-3	0.000	0.000	0.992	0.003	5.000	6.011	0.000	1.474	0.001	0.012	0.000	0.005
NO-2G21-5a-1	0.000	0.000	0.426	0.005	5.001	4.858	0.003	2.345	0.000	0.574	0.000	0.005
NO-2G21-5a-2	0.004	0.000	0.399	0.001	5.006	4.791	0.001	2.388	0.000	0.611	0.000	0.005
NO-2G21-5b-1	0.000	0.000	0.429	0.002	5.003	4.854	0.004	2.345	0.000	0.574	0.000	0.007
NO-2G21-5b-2	0.000	0.000	0.424	0.002	5.004	4.842	0.003	2.356	0.000	0.583	0.000	0.003
NO-2G21-5b-3	0.000	0.000	0.431	0.002	5.009	4.842	0.002	2.348	0.000	0.583	0.000	0.008
NO-2G21-5c-1	0.000	0.000	0.428	0.001	5.006	4.840	0.002	2.357	0.000	0.581	0.000	0.006
NO-2G21-5c-2	0.001	0.000	0.434	0.001	5.005	4.857	0.003	2.341	0.000	0.572	0.000	0.008
NO-2G21-5c-3	0.001	0.000	0.443	0.002	5.003	4.887	0.003	2.320	0.001	0.560	0.000	0.005
NO-2G21-5d-1	0.001	0.000	0.424	0.002	5.002	4.853	0.002	2.347	0.000	0.581	0.000	0.002
NO-2G21-5d-2	0.002	0.001	0.440	0.019	5.007	4.876	0.003	2.342	0.001	0.539	0.000	0.007
NO-2G21-5d-3	0.002	0.000	0.446	0.001	5.004	4.888	0.001	2.323	0.000	0.559	0.000	0.003
NO-2G46-3a-7	0.002	0.000	0.512	0.002	5.008	5.005	0.002	2.231	0.000	0.498	0.000	0.005
NO-2G46-3a-8	0.003	0.000	0.492	0.001	5.008	4.964	0.001	2.268	0.000	0.515	0.000	0.002
NO-2G46-3a-9	0.001	0.000	0.484	0.002	5.002	4.970	0.003	2.259	0.000	0.519	0.000	0.005

		Sample Data			Atom units							
SrO	BaO	Analysis point	K2O	Total	SiO2	TiO2	Al2O3	MgO	CaO	MnO	FeOt	SrO
0.000	0.000	NO-2G22-4a-1	0.001	8.488	2.971	0.000	1.020	0.000	0.031	0.000	0.001	0.000
0.002	0.000	NO-2G22-4a-2	0.001	8.000	2.442	0.001	1.543	0.000	0.564	0.000	0.006	0.002
0.000	0.000	NO-2G22-4a-3	0.001	8.000	2.435	0.002	1.554	0.000	0.560	0.000	0.004	0.000
0.003	0.000	NO-2G22-4a-4	0.001	8.000	2.445	0.001	1.541	0.002	0.552	0.000	0.006	0.003
0.003	0.001	NO-2G22-4a-5	0.001	8.000	2.443	0.001	1.543	0.000	0.556	0.000	0.006	0.003
0.004	0.000	NO-2G22-4a-5	0.001	8.000	2.448	0.001	1.529	0.000	0.554	0.001	0.013	0.004
0.000	0.000	NO-2G22-4a-7	0.001	8.000	2.442	0.002	1.535	0.001	0.553	0.000	0.014	0.000
0.002	0.000	NO-2G22-4a-8	0.001	8.000	2.450	0.002	1.538	0.001	0.547	0.000	0.004	0.002
0.001	0.000	NO-2G22-4a-9	0.001	8.000	2.452	0.001	1.537	0.001	0.549	0.000	0.003	0.001
0.000	0.001	NO-2G22-4a-10	0.001	8.000	2.424	0.002	1.557	0.001	0.579	0.000	0.010	0.000
0.003	0.000	NO-2G22-4a-11	0.001	8.000	2.450	0.001	1.537	0.000	0.547	0.000	0.007	0.003
0.000	0.000	NO-2G22-4a-12	0.001	8.000	2.459	0.001	1.531	0.001	0.544	0.000	0.004	0.000
0.003	0.000	NO-2G22-4a-13	0.001	8.000	2.442	0.001	1.544	0.001	0.561	0.000	0.004	0.003
0.002	0.000	NO-2G22-4a-14	0.001	8.000	2.439	0.001	1.547	0.001	0.558	0.000	0.008	0.002
0.001	0.000	NO-2G22-4a-15	0.001	8.000	2.449	0.001	1.539	0.001	0.562	0.000	0.003	0.001
0.002	0.001	NO-2G22-4a-16	0.001	8.000	2.436	0.000	1.552	0.001	0.559	0.000	0.008	0.002
0.000	0.000	NO-2G22-4b-17	0.001	8.000	2.459	0.001	1.528	0.000	0.543	0.000	0.003	0.000
0.000	0.000	NO-2G22-4b-18	0.001	8.000	2.467	0.000	1.523	0.000	0.538	0.000	0.005	0.000
0.002	0.000	NO-2G22-4b-19	0.001	8.000	2.455	0.002	1.531	0.001	0.548	0.000	0.008	0.002
0.000	0.000	NO-2G22-4b-20	0.001	8.000	2.453	0.002	1.528	0.000	0.544	0.000	0.013	0.000
0.000	0.000	NO-2G22-4b-23	0.001	8.000	2.448	0.000	1.544	0.000	0.552	0.000	0.005	0.000
0.002	0.000	NO-2G22-4b-24	0.001	8.000	2.459	0.001	1.529	0.001	0.543	0.000	0.004	0.002
0.000	0.000	NO-2G22-4c-27	0.002	8.000	2.436	0.001	1.552	0.000	0.561	0.000	0.008	0.000
0.003	0.000	NO-2G22-4c-28	0.001	8.000	2.458	0.003	1.524	0.001	0.540	0.001	0.007	0.003
0.000	0.000	NO-2G22-4c-29	0.001	8.000	2.446	0.002	1.539	0.001	0.550	0.000	0.008	0.000
0.000	0.000	NO-2G22-4c-32	0.001	8.000	2.467	0.001	1.525	0.001	0.544	0.000	0.001	0.000
0.003	0.000	NO-2G22-4c-33	0.001	8.000	2.452	0.001	1.538	0.000	0.552	0.000	0.002	0.003
0.002	0.000	NO-2G22-4d-40	0.019	8.000	2.503	0.001	1.505	0.000	0.462	0.000	0.003	0.002
0.002	0.000	NO-2G22-4d-42	0.001	8.000	2.449	0.001	1.540	0.001	0.551	0.000	0.005	0.002
0.000	0.000	NO-2G21-2c-2	0.001	8.000	2.986	0.000	1.008	0.000	0.015	0.000	0.002	0.000
0.000	0.000	NO-2G21-2c-3	0.002	8.000	3.005	0.000	0.983	0.001	0.012	0.000	0.003	0.000
0.000	0.000	NO-2G21-5a-1	0.003	8.000	2.429	0.002	1.563	0.000	0.574	0.000	0.003	0.000
0.004	0.000	NO-2G21-5a-2	0.000	8.000	2.396	0.001	1.592	0.000	0.611	0.000	0.003	0.004
0.000	0.000	NO-2G21-5b-1	0.001	8.000	2.427	0.002	1.564	0.000	0.574	0.000	0.004	0.000
0.000	0.000	NO-2G21-5b-2	0.001	8.000	2.421	0.002	1.571	0.000	0.583	0.000	0.002	0.000
0.000	0.000	NO-2G21-5b-3	0.001	8.000	2.421	0.001	1.565	0.000	0.583	0.000	0.005	0.000
0.000	0.000	NO-2G21-5c-1	0.001	8.000	2.420	0.001	1.571	0.000	0.581	0.000	0.004	0.000
0.001	0.000	NO-2G21-5c-2	0.001	8.000	2.429	0.001	1.561	0.000	0.572	0.000	0.005	0.001
0.001	0.000	NO-2G21-5c-3	0.001	8.000	2.444	0.001	1.547	0.001	0.560	0.000	0.003	0.001
0.001	0.000	NO-2G21-5d-1	0.001	8.000	2.427	0.001	1.565	0.000	0.581	0.000	0.002	0.001
0.002	0.001	NO-2G21-5d-2	0.010	8.000	2.438	0.001	1.561	0.001	0.539	0.000	0.004	0.002
0.002	0.000	NO-2G21-5d-3	0.001	8.000	2.444	0.000	1.549	0.000	0.559	0.000	0.002	0.002
0.002	0.000	NO-2G46-3a-7	0.001	8.000	2.502	0.001	1.487	0.000	0.498	0.000	0.003	0.002
0.003	0.000	NO-2G46-3a-8	0.001	8.000	2.482	0.001	1.512	0.000	0.515	0.000	0.001	0.003
0.001	0.000	NO-2G46-3a-9	0.001	8.000	2.485	0.001	1.506	0.000	0.519	0.000	0.003	0.001

Sample Data				**Norm oxygen**								
Analysis point	Na2O	K2O	Total	SiO2	TiO2	Al2O3	MgO	CaO	MnO	FeOt	SrO	BaO
NO-2G22-4a-1	0.981	0.002	5.007	5.942	0.000	1.530	0.000	0.031	0.000	0.002	0.000	0.000
NO-2G22-4a-2	0.450	0.002	5.009	4.883	0.002	2.314	0.000	0.564	0.000	0.009	0.002	0.000
NO-2G22-4a-3	0.453	0.002	5.012	4.871	0.003	2.331	0.000	0.560	0.000	0.006	0.000	0.000
NO-2G22-4a-4	0.459	0.002	5.011	4.890	0.002	2.311	0.002	0.552	0.000	0.009	0.003	0.000
NO-2G22-4a-5	0.455	0.002	5.010	4.886	0.002	2.314	0.000	0.556	0.000	0.009	0.003	0.001
NO-2G22-4a-5	0.461	0.002	5.012	4.896	0.002	2.294	0.000	0.554	0.001	0.019	0.004	0.000
NO-2G22-4a-7	0.467	0.002	5.016	4.884	0.004	2.302	0.001	0.553	0.000	0.021	0.000	0.000
NO-2G22-4a-8	0.464	0.002	5.011	4.900	0.003	2.307	0.001	0.547	0.000	0.006	0.002	0.000
NO-2G22-4a-9	0.464	0.001	5.010	4.904	0.002	2.306	0.001	0.549	0.000	0.005	0.001	0.000
NO-2G22-4a-10	0.431	0.002	5.007	4.848	0.004	2.336	0.001	0.579	0.000	0.015	0.000	0.001
NO-2G22-4a-11	0.458	0.003	5.007	4.901	0.003	2.306	0.000	0.547	0.000	0.010	0.003	0.000
NO-2G22-4a-12	0.461	0.002	5.003	4.919	0.002	2.297	0.001	0.544	0.000	0.006	0.000	0.000
NO-2G22-4a-13	0.449	0.002	5.008	4.885	0.002	2.316	0.001	0.561	0.000	0.006	0.003	0.000
NO-2G22-4a-14	0.449	0.002	5.008	4.879	0.001	2.320	0.001	0.558	0.000	0.012	0.002	0.000
NO-2G22-4a-15	0.448	0.001	5.004	4.897	0.001	2.308	0.001	0.562	0.000	0.005	0.001	0.000
NO-2G22-4a-16	0.452	0.002	5.012	4.871	0.000	2.327	0.001	0.559	0.000	0.012	0.002	0.001
NO-2G22-4b-17	0.476	0.001	5.013	4.918	0.003	2.292	0.000	0.543	0.000	0.005	0.000	0.000
NO-2G22-4b-18	0.471	0.002	5.006	4.934	0.001	2.284	0.000	0.538	0.000	0.007	0.000	0.000
NO-2G22-4b-19	0.455	0.002	5.003	4.909	0.003	2.296	0.001	0.548	0.000	0.011	0.002	0.000
NO-2G22-4b-20	0.464	0.002	5.007	4.907	0.004	2.292	0.000	0.544	0.000	0.019	0.000	0.000
NO-2G22-4b-23	0.457	0.002	5.007	4.895	0.001	2.316	0.000	0.552	0.000	0.007	0.000	0.000
NO-2G22-4b-24	0.466	0.003	5.008	4.917	0.003	2.294	0.001	0.543	0.000	0.006	0.002	0.000
NO-2G22-4c-27	0.449	0.003	5.009	4.872	0.003	2.327	0.000	0.561	0.000	0.011	0.000	0.000
NO-2G22-4c-28	0.470	0.002	5.010	4.917	0.005	2.286	0.001	0.540	0.001	0.011	0.003	0.000
NO-2G22-4c-29	0.461	0.002	5.010	4.893	0.004	2.308	0.001	0.550	0.000	0.013	0.000	0.000
NO-2G22-4c-32	0.460	0.002	5.001	4.933	0.002	2.287	0.001	0.544	0.000	0.002	0.000	0.000
NO-2G22-4c-33	0.454	0.002	5.004	4.905	0.003	2.307	0.000	0.552	0.000	0.003	0.003	0.000
NO-2G22-4d-40	0.492	0.038	5.007	5.006	0.002	2.258	0.000	0.462	0.000	0.005	0.002	0.000
NO-2G22-4d-42	0.455	0.003	5.007	4.898	0.002	2.310	0.001	0.551	0.000	0.007	0.002	0.000
NO-2G21-2c-2	0.996	0.003	5.008	5.971	0.000	1.512	0.000	0.015	0.000	0.003	0.000	0.000
NO-2G21-2c-3	0.992	0.003	5.000	6.011	0.000	1.474	0.001	0.012	0.000	0.005	0.000	0.000
NO-2G21-5a-1	0.426	0.005	5.001	4.858	0.003	2.345	0.000	0.574	0.000	0.005	0.000	0.000
NO-2G21-5a-2	0.399	0.001	5.006	4.791	0.001	2.388	0.000	0.611	0.000	0.005	0.004	0.000
NO-2G21-5b-1	0.429	0.002	5.003	4.854	0.004	2.345	0.000	0.574	0.000	0.007	0.000	0.000
NO-2G21-5b-2	0.424	0.002	5.004	4.842	0.003	2.356	0.000	0.583	0.000	0.003	0.000	0.000
NO-2G21-5b-3	0.431	0.002	5.009	4.842	0.002	2.348	0.000	0.583	0.000	0.008	0.000	0.000
NO-2G21-5c-1	0.428	0.001	5.006	4.840	0.002	2.357	0.000	0.581	0.000	0.006	0.000	0.000
NO-2G21-5c-2	0.434	0.001	5.005	4.857	0.003	2.341	0.000	0.572	0.000	0.008	0.001	0.000
NO-2G21-5c-3	0.443	0.002	5.003	4.887	0.003	2.320	0.001	0.560	0.000	0.005	0.001	0.000
NO-2G21-5d-1	0.424	0.002	5.002	4.853	0.002	2.347	0.000	0.581	0.000	0.002	0.001	0.000
NO-2G21-5d-2	0.440	0.019	5.007	4.876	0.003	2.342	0.001	0.539	0.000	0.007	0.002	0.001
NO-2G21-5d-3	0.446	0.001	5.004	4.888	0.001	2.323	0.000	0.559	0.000	0.003	0.002	0.000
NO-2G46-3a-7	0.512	0.002	5.008	5.005	0.002	2.231	0.000	0.498	0.000	0.005	0.002	0.000
NO-2G46-3a-8	0.492	0.001	5.008	4.964	0.001	2.268	0.000	0.515	0.000	0.002	0.003	0.000
NO-2G46-3a-9	0.484	0.002	5.002	4.970	0.003	2.259	0.000	0.519	0.000	0.005	0.001	0.000

Sample Data			**End Member**		
Analysis point	Na2O	K2O	Anorthite	Albite	Orthoclase
NO-2G22-4a-1	0.981	0.001	3.1	96.8	0.2
NO-2G22-4a-2	0.225	0.001	55.5	44.3	0.2
NO-2G22-4a-3	0.227	0.001	55.1	44.6	0.2
NO-2G22-4a-4	0.230	0.001	54.5	45.3	0.2
NO-2G22-4a-5	0.228	0.001	54.9	45.0	0.2
NO-2G22-4a-5	0.231	0.001	54.5	45.4	0.2
NO-2G22-4a-7	0.233	0.001	54.1	45.7	0.2
NO-2G22-4a-8	0.232	0.001	54.0	45.8	0.2
NO-2G22-4a-9	0.232	0.001	54.1	45.8	0.1
NO-2G22-4a-10	0.216	0.001	57.2	42.6	0.2
NO-2G22-4a-11	0.229	0.001	54.3	45.4	0.3
NO-2G22-4a-12	0.230	0.001	54.0	45.8	0.2
NO-2G22-4a-13	0.224	0.001	55.4	44.4	0.2
NO-2G22-4a-14	0.225	0.001	55.3	44.5	0.2
NO-2G22-4a-15	0.224	0.001	55.6	44.3	0.1
NO-2G22-4a-16	0.226	0.001	55.1	44.6	0.2
NO-2G22-4b-17	0.238	0.001	53.2	46.6	0.1
NO-2G22-4b-18	0.235	0.001	53.2	46.6	0.2
NO-2G22-4b-19	0.227	0.001	54.5	45.3	0.2
NO-2G22-4b-20	0.232	0.001	53.9	45.9	0.2
NO-2G22-4b-23	0.228	0.001	54.6	45.2	0.2
NO-2G22-4b-24	0.233	0.001	53.7	46.1	0.3
NO-2G22-4c-27	0.224	0.002	55.4	44.3	0.3
NO-2G22-4c-28	0.235	0.001	53.4	46.5	0.2
NO-2G22-4c-29	0.230	0.001	54.3	45.5	0.2
NO-2G22-4c-32	0.230	0.001	54.0	45.7	0.2
NO-2G22-4c-33	0.227	0.001	54.8	45.1	0.2
NO-2G22-4d-40	0.246	0.019	46.6	49.7	3.8
NO-2G22-4d-42	0.228	0.001	54.6	45.2	0.3
NO-2G21-2c-2	0.498	0.001	1.5	98.3	0.3
NO-2G21-2c-3	0.496	0.002	1.2	98.5	0.3
NO-2G21-5a-1	0.213	0.003	57.1	42.4	0.5
NO-2G21-5a-2	0.199	0.000	60.4	39.5	0.1
NO-2G21-5b-1	0.215	0.001	57.1	42.7	0.2
NO-2G21-5b-2	0.212	0.001	57.7	42.0	0.2
NO-2G21-5b-3	0.216	0.001	57.4	42.4	0.2
NO-2G21-5c-1	0.214	0.001	57.5	42.4	0.1
NO-2G21-5c-2	0.217	0.001	56.8	43.1	0.1
NO-2G21-5c-3	0.222	0.001	55.7	44.1	0.2
NO-2G21-5d-1	0.212	0.001	57.7	42.1	0.2
NO-2G21-5d-2	0.220	0.010	54.0	44.1	1.9
NO-2G21-5d-3	0.223	0.001	55.6	44.3	0.1
NO-2G46-3a-7	0.256	0.001	49.2	50.6	0.2
NO-2G46-3a-8	0.246	0.001	51.1	48.8	0.1
NO-2G46-3a-9	0.242	0.001	51.6	48.1	0.2

Sample Data				**Mole Cation**					
Analysis point	Intrusion/Phase	Sample	Mineral	SiO2	TiO2	Al2O3	MgO	CaO	MnO
NO-2G46-3a-9	Thunderbird-P	NO-2G46-3	Feldspar	0.921	0.000	0.558	0.000	0.192	0.000
NO-2G46-3a-6	Thunderbird-P	NO-2G46-3	Feldspar	0.932	0.000	0.542	0.000	0.177	0.000
NO-2G46-3b-28	Thunderbird-P	NO-2G46-3	Feldspar	0.936	0.000	0.545	0.000	0.180	0.000
NO-2G46-3b-29	Thunderbird-P	NO-2G46-3	Feldspar	0.912	0.000	0.559	0.000	0.193	0.000
NO-2G46-3b-27	Thunderbird-P	NO-2G46-3	Feldspar	0.916	0.001	0.560	0.000	0.192	0.000
NO-2G46-3b-20	Thunderbird-P	NO-2G46-3	Feldspar	0.921	0.001	0.560	0.000	0.192	0.000
NO-2G46-3b-21	Thunderbird-P	NO-2G46-3	Feldspar	0.934	0.001	0.548	0.000	0.181	0.000
NO-2G46-3b-22	Thunderbird-P	NO-2G46-3	Feldspar	0.934	0.000	0.546	0.000	0.181	0.000
NO-2G46-3d-1	Thunderbird-P	NO-2G46-3	Feldspar	0.916	0.001	0.555	0.000	0.194	0.000
NO-2G46-3d-2	Thunderbird-P	NO-2G46-3	Feldspar	0.922	0.000	0.553	0.000	0.187	0.000
NO-2G46-3e-1	Thunderbird-P	NO-2G46-3	Feldspar	0.920	0.000	0.556	0.000	0.190	0.000
NO-2G46-3e-2	Thunderbird-P	NO-2G46-3	Feldspar	0.923	0.000	0.550	0.000	0.185	0.000
NO-2G47-3b-14	Thunderbird-P	NO-2G47-3	Feldspar	0.936	0.000	0.548	0.000	0.182	0.000
NO-2G47-3b-15	Thunderbird-P	NO-2G47-3	Feldspar	0.928	0.000	0.547	0.001	0.182	0.000
NO-2G47-3b-16	Thunderbird-P	NO-2G47-3	Feldspar	0.929	0.001	0.546	0.000	0.182	0.000
NO-2G47-3b-17	Thunderbird-P	NO-2G47-3	Feldspar	0.930	0.001	0.547	0.000	0.181	0.000
NO-2G47-3b-18	Thunderbird-P	NO-2G47-3	Feldspar	0.925	0.000	0.551	0.000	0.185	0.000
NO-2G47-3c-21	Thunderbird-P	NO-2G47-3	Feldspar	0.932	0.000	0.548	0.000	0.182	0.000
NO-2G47-3c-22	Thunderbird-P	NO-2G47-3	Feldspar	0.930	0.000	0.547	0.000	0.183	0.000
NO-2G47-3c-23	Thunderbird-P	NO-2G47-3	Feldspar	0.928	0.000	0.550	0.000	0.185	0.000
NO-2G47-3c-24	Thunderbird-P	NO-2G47-3	Feldspar	0.927	0.000	0.546	0.000	0.180	0.000
NO-2G47-3c-25	Thunderbird-P	NO-2G47-3	Feldspar	0.928	0.000	0.551	0.000	0.187	0.000
NO-2G47-3c-26	Thunderbird-P	NO-2G47-3	Feldspar	0.931	0.000	0.552	0.000	0.184	0.000
NO-2G47-3c-27	Thunderbird-P	NO-2G47-3	Feldspar	0.929	0.000	0.549	0.000	0.183	0.000
NO-2G47-3d-1	Thunderbird-P	NO-2G47-3	Feldspar	0.920	0.000	0.556	0.000	0.190	0.000
NO-2G47-3d-2	Thunderbird-P	NO-2G47-3	Feldspar	0.926	0.001	0.555	0.000	0.188	0.000
NO-2G47-3e-1	Thunderbird-P	NO-2G47-3	Feldspar	0.927	0.000	0.546	0.000	0.181	0.000
NO-2G47-3e-2	Thunderbird-P	NO-2G47-3	Feldspar	0.930	0.000	0.546	0.000	0.182	0.000
NO-2G47-3e-3	Thunderbird-P	NO-2G47-3	Feldspar	0.925	0.000	0.545	0.000	0.183	0.000
NO-2G47-3f-1	Thunderbird-P	NO-2G47-3	Feldspar	0.934	0.000	0.544	0.000	0.179	0.000
NO-2G47-3f-2	Thunderbird-P	NO-2G47-3	Feldspar	0.931	0.001	0.547	0.000	0.182	0.000
NO-2G47-3f-3	Thunderbird-P	NO-2G47-3	Feldspar	0.923	0.001	0.556	0.000	0.185	0.000
NO-2G47-3g-1	Thunderbird-P	NO-2G47-3	Feldspar	0.926	0.001	0.547	0.000	0.183	0.000
NO-2G47-3g-2	Thunderbird-P	NO-2G47-3	Feldspar	0.933	0.000	0.545	0.000	0.180	0.000
NO-2G47-3g-3	Thunderbird-P	NO-2G47-3	Feldspar	0.927	0.000	0.543	0.000	0.181	0.000
NO-2G47-2a-1	Thunderbird-P	NO-2G47-2	Feldspar	0.921	0.000	0.549	0.000	0.188	0.000
NO-2G47-2a-2	Thunderbird-P	NO-2G47-2	Feldspar	0.925	0.000	0.553	0.000	0.183	0.000
NO-2G47-2a-3	Thunderbird-P	NO-2G47-2	Feldspar	0.931	0.000	0.550	0.000	0.181	0.000
NO-2G47-2a-4	Thunderbird-P	NO-2G47-2	Feldspar	0.924	0.000	0.549	0.000	0.182	0.000
NO-2G47-2a-5	Thunderbird-P	NO-2G47-2	Feldspar	0.928	0.000	0.543	0.000	0.181	0.000
NO-2G47-2a-6	Thunderbird-P	NO-2G47-2	Feldspar	0.896	0.000	0.576	0.000	0.208	0.000
NO-2G47-2a-8	Thunderbird-P	NO-2G47-2	Feldspar	0.932	0.000	0.547	0.000	0.180	0.000
NO-2G47-2a-10	Thunderbird-P	NO-2G47-2	Feldspar	0.927	0.000	0.548	0.000	0.183	0.000
NO-2G47-2c-1	Thunderbird-P	NO-2G47-2	Feldspar	0.922	0.000	0.550	0.000	0.186	0.000
NO-2G47-2c-2	Thunderbird-P	NO-2G47-2	Feldspar	0.922	0.000	0.546	0.000	0.183	0.000

Sample Data							**Mole oxygen**					
Analysis point	FeOt	SrO	BaO	Na2O	K2O	Total	SiO2	TiO2	Al2O3	MgO	CaO	MnO
NO-2G46-3a-9	0.001	0.000	0.000	0.179	0.001	1.854	1.842	0.001	0.837	0.000	0.192	0.000
NO-2G46-3a-6	0.001	0.001	0.000	0.197	0.000	1.850	1.865	0.000	0.813	0.000	0.177	0.000
NO-2G46-3b-28	0.000	0.001	0.000	0.196	0.000	1.858	1.872	0.000	0.818	0.000	0.180	0.000
NO-2G46-3b-29	0.001	0.001	0.000	0.180	0.001	1.847	1.824	0.001	0.839	0.000	0.193	0.000
NO-2G46-3b-27	0.001	0.001	0.000	0.179	0.000	1.849	1.832	0.001	0.839	0.000	0.192	0.000
NO-2G46-3b-20	0.001	0.001	0.000	0.179	0.001	1.855	1.841	0.001	0.839	0.000	0.192	0.000
NO-2G46-3b-21	0.001	0.000	0.000	0.196	0.000	1.860	1.868	0.001	0.821	0.000	0.181	0.000
NO-2G46-3b-22	0.000	0.000	0.000	0.195	0.000	1.857	1.868	0.001	0.820	0.000	0.181	0.000
NO-2G46-3d-1	0.001	0.001	0.000	0.180	0.001	1.849	1.832	0.002	0.833	0.000	0.194	0.000
NO-2G46-3d-2	0.002	0.001	0.000	0.186	0.001	1.853	1.844	0.000	0.830	0.000	0.187	0.000
NO-2G46-3e-1	0.001	0.001	0.000	0.183	0.001	1.852	1.841	0.001	0.834	0.000	0.190	0.000
NO-2G46-3e-2	0.001	0.000	0.000	0.191	0.001	1.851	1.847	0.000	0.824	0.000	0.185	0.000
NO-2G47-3b-14	0.001	0.001	0.000	0.196	0.001	1.864	1.873	0.000	0.821	0.000	0.182	0.000
NO-2G47-3b-15	0.002	0.000	0.000	0.193	0.000	1.854	1.855	0.001	0.821	0.001	0.182	0.000
NO-2G47-3b-16	0.001	0.001	0.000	0.193	0.000	1.853	1.858	0.001	0.820	0.000	0.182	0.000
NO-2G47-3b-17	0.001	0.001	0.000	0.193	0.000	1.853	1.861	0.001	0.820	0.000	0.181	0.000
NO-2G47-3b-18	0.001	0.000	0.000	0.186	0.000	1.850	1.850	0.001	0.827	0.000	0.185	0.000
NO-2G47-3c-21	0.001	0.000	0.000	0.190	0.001	1.855	1.863	0.001	0.823	0.000	0.182	0.000
NO-2G47-3c-22	0.001	0.000	0.000	0.190	0.000	1.852	1.860	0.001	0.820	0.000	0.183	0.000
NO-2G47-3c-23	0.001	0.001	0.000	0.189	0.000	1.854	1.856	0.000	0.825	0.000	0.185	0.000
NO-2G47-3c-24	0.002	0.000	0.000	0.191	0.000	1.848	1.855	0.000	0.819	0.000	0.180	0.000
NO-2G47-3c-25	0.000	0.001	0.000	0.189	0.000	1.856	1.856	0.000	0.826	0.000	0.187	0.000
NO-2G47-3c-26	0.001	0.001	0.000	0.192	0.001	1.862	1.862	0.001	0.829	0.000	0.184	0.000
NO-2G47-3c-27	0.001	0.000	0.000	0.192	0.000	1.855	1.859	0.000	0.823	0.000	0.183	0.000
NO-2G47-3d-1	0.001	0.000	0.000	0.184	0.000	1.853	1.840	0.000	0.835	0.000	0.190	0.000
NO-2G47-3d-2	0.002	0.002	0.000	0.187	0.000	1.862	1.853	0.001	0.833	0.000	0.188	0.000
NO-2G47-3e-1	0.001	0.001	0.000	0.193	0.000	1.849	1.853	0.001	0.818	0.000	0.181	0.000
NO-2G47-3e-2	0.001	0.001	0.000	0.195	0.001	1.854	1.860	0.001	0.819	0.000	0.182	0.000
NO-2G47-3e-3	0.001	0.001	0.000	0.192	0.000	1.848	1.849	0.001	0.817	0.000	0.183	0.000
NO-2G47-3f-1	0.001	0.001	0.000	0.196	0.000	1.857	1.869	0.001	0.816	0.000	0.179	0.000
NO-2G47-3f-2	0.001	0.001	0.000	0.196	0.000	1.857	1.862	0.001	0.821	0.000	0.182	0.000
NO-2G47-3f-3	0.001	0.001	0.000	0.190	0.000	1.857	1.847	0.001	0.834	0.000	0.185	0.000
NO-2G47-3g-1	0.001	0.000	0.000	0.192	0.000	1.851	1.851	0.001	0.821	0.000	0.183	0.000
NO-2G47-3g-2	0.001	0.000	0.000	0.194	0.000	1.855	1.867	0.001	0.818	0.000	0.180	0.000
NO-2G47-3g-3	0.002	0.001	0.000	0.193	0.000	1.846	1.854	0.001	0.814	0.000	0.181	0.000
NO-2G47-2a-1	0.001	0.000	0.000	0.188	0.000	1.847	1.841	0.001	0.823	0.000	0.188	0.000
NO-2G47-2a-2	0.001	0.000	0.000	0.185	0.003	1.850	1.850	0.001	0.829	0.000	0.183	0.000
NO-2G47-2a-3	0.000	0.000	0.000	0.190	0.000	1.854	1.862	0.000	0.825	0.000	0.181	0.000
NO-2G47-2a-4	0.000	0.000	0.000	0.190	0.000	1.846	1.848	0.001	0.824	0.000	0.182	0.000
NO-2G47-2a-5	0.000	0.001	0.000	0.192	0.000	1.846	1.857	0.001	0.814	0.000	0.181	0.000
NO-2G47-2a-6	0.002	0.001	0.000	0.163	0.000	1.847	1.793	0.000	0.864	0.000	0.208	0.000
NO-2G47-2a-8	0.000	0.000	0.000	0.195	0.000	1.854	1.864	0.001	0.820	0.000	0.180	0.000
NO-2G47-2a-10	0.001	0.000	0.000	0.192	0.000	1.852	1.854	0.001	0.822	0.000	0.183	0.000
NO-2G47-2c-1	0.000	0.002	0.000	0.188	0.001	1.850	1.843	0.000	0.825	0.000	0.186	0.000
NO-2G47-2c-2	0.000	0.001	0.000	0.188	0.000	1.842	1.843	0.001	0.820	0.000	0.183	0.000

Sample Data							**Norm Cations**					
Analysis point	FeOt	SrO	BaO	Na2O	K2O	Total	SiO2	TiO2	Al2O3	MgO	CaO	MnO
NO-2G46-3a-9	0.002	0.000	0.000	0.090	0.000	2.965	2.485	0.001	1.506	0.000	0.519	0.000
NO-2G46-3a-6	0.002	0.001	0.000	0.098	0.000	2.956	2.524	0.000	1.467	0.000	0.479	0.000
NO-2G46-3b-28	0.000	0.001	0.000	0.098	0.000	2.969	2.522	0.000	1.469	0.000	0.484	0.000
NO-2G46-3b-29	0.001	0.001	0.000	0.090	0.000	2.949	2.474	0.001	1.517	0.000	0.525	0.000
NO-2G46-3b-27	0.001	0.001	0.000	0.090	0.000	2.956	2.479	0.001	1.514	0.000	0.518	0.000
NO-2G46-3b-20	0.002	0.001	0.000	0.090	0.000	2.967	2.482	0.002	1.509	0.000	0.519	0.000
NO-2G46-3b-21	0.001	0.000	0.000	0.098	0.000	2.971	2.515	0.001	1.475	0.000	0.487	0.000
NO-2G46-3b-22	0.000	0.000	0.000	0.097	0.000	2.967	2.518	0.001	1.473	0.000	0.488	0.000
NO-2G46-3d-1	0.001	0.001	0.000	0.090	0.000	2.953	2.481	0.002	1.504	0.000	0.525	0.001
NO-2G46-3d-2	0.004	0.001	0.000	0.093	0.000	2.959	2.493	0.000	1.495	0.000	0.506	0.000
NO-2G46-3e-1	0.001	0.001	0.000	0.091	0.000	2.959	2.488	0.001	1.503	0.000	0.513	0.000
NO-2G46-3e-2	0.001	0.000	0.000	0.096	0.000	2.954	2.501	0.000	1.489	0.000	0.502	0.000
NO-2G47-3b-14	0.002	0.001	0.000	0.098	0.000	2.977	2.516	0.000	1.472	0.000	0.489	0.000
NO-2G47-3b-15	0.003	0.000	0.000	0.097	0.000	2.960	2.507	0.001	1.479	0.002	0.493	0.000
NO-2G47-3b-16	0.002	0.001	0.000	0.096	0.000	2.960	2.511	0.002	1.477	0.000	0.492	0.000
NO-2G47-3b-17	0.001	0.001	0.000	0.096	0.000	2.962	2.513	0.002	1.476	0.000	0.489	0.000
NO-2G47-3b-18	0.002	0.000	0.000	0.093	0.000	2.959	2.501	0.001	1.491	0.001	0.500	0.000
NO-2G47-3c-21	0.001	0.000	0.000	0.095	0.000	2.966	2.513	0.001	1.479	0.001	0.490	0.000
NO-2G47-3c-22	0.001	0.000	0.000	0.095	0.000	2.961	2.513	0.001	1.478	0.001	0.494	0.000
NO-2G47-3c-23	0.001	0.001	0.000	0.094	0.000	2.964	2.505	0.001	1.485	0.000	0.499	0.000
NO-2G47-3c-24	0.003	0.000	0.000	0.096	0.000	2.954	2.512	0.001	1.479	0.000	0.487	0.000
NO-2G47-3c-25	0.001	0.001	0.000	0.095	0.000	2.966	2.504	0.001	1.485	0.000	0.504	0.000
NO-2G47-3c-26	0.001	0.001	0.000	0.096	0.000	2.973	2.504	0.001	1.486	0.000	0.495	0.000
NO-2G47-3c-27	0.001	0.000	0.000	0.096	0.000	2.963	2.509	0.000	1.482	0.000	0.494	0.000
NO-2G47-3d-1	0.002	0.000	0.000	0.092	0.000	2.959	2.487	0.000	1.504	0.000	0.514	0.000
NO-2G47-3d-2	0.003	0.002	0.000	0.094	0.000	2.974	2.492	0.002	1.494	0.000	0.506	0.000
NO-2G47-3e-1	0.002	0.001	0.000	0.096	0.000	2.952	2.511	0.001	1.478	0.001	0.492	0.000
NO-2G47-3e-2	0.001	0.001	0.000	0.097	0.000	2.960	2.513	0.001	1.475	0.000	0.491	0.000
NO-2G47-3e-3	0.002	0.001	0.000	0.096	0.000	2.950	2.508	0.001	1.477	0.000	0.497	0.000
NO-2G47-3f-1	0.001	0.001	0.000	0.098	0.000	2.966	2.521	0.001	1.468	0.000	0.482	0.000
NO-2G47-3f-2	0.001	0.001	0.000	0.098	0.000	2.965	2.513	0.001	1.476	0.000	0.490	0.000
NO-2G47-3f-3	0.002	0.001	0.000	0.095	0.000	2.964	2.492	0.002	1.500	0.000	0.499	0.000
NO-2G47-3g-1	0.002	0.000	0.000	0.096	0.000	2.955	2.506	0.002	1.482	0.000	0.495	0.000
NO-2G47-3g-2	0.002	0.000	0.000	0.097	0.000	2.965	2.518	0.001	1.471	0.000	0.486	0.000
NO-2G47-3g-3	0.003	0.001	0.000	0.096	0.000	2.950	2.514	0.001	1.472	0.000	0.490	0.000
NO-2G47-2a-1	0.001	0.000	0.000	0.094	0.000	2.948	2.498	0.001	1.490	0.001	0.509	0.000
NO-2G47-2a-2	0.002	0.000	0.000	0.093	0.001	2.959	2.502	0.001	1.495	0.000	0.494	0.000
NO-2G47-2a-3	0.000	0.000	0.000	0.095	0.000	2.965	2.513	0.000	1.485	0.000	0.489	0.000
NO-2G47-2a-4	0.000	0.000	0.000	0.095	0.000	2.949	2.506	0.001	1.489	0.000	0.492	0.000
NO-2G47-2a-5	0.001	0.001	0.000	0.096	0.000	2.951	2.517	0.001	1.472	0.000	0.492	0.000
NO-2G47-2a-6	0.003	0.001	0.000	0.082	0.000	2.950	2.431	0.000	1.561	0.000	0.565	0.000
NO-2G47-2a-8	0.000	0.000	0.000	0.097	0.000	2.962	2.517	0.001	1.477	0.000	0.485	0.000
NO-2G47-2a-10	0.001	0.000	0.000	0.096	0.000	2.958	2.508	0.001	1.483	0.001	0.494	0.000
NO-2G47-2c-1	0.001	0.002	0.000	0.094	0.000	2.952	2.497	0.001	1.490	0.001	0.505	0.000
NO-2G47-2c-2	0.000	0.001	0.000	0.094	0.000	2.943	2.505	0.001	1.486	0.000	0.498	0.001

Sample Data						**Norm Oxygen**								
Analysis point	SrO	BaO	Na2O	K2O	Total	SiO2	TiO2	Al2O3	MgO	CaO	MnO	FeOt	SrO	BaO
NO-2G46-3a-9	0.001	0.000	0.484	0.002	5.002	4.970	0.003	2.259	0.000	0.519	0.000	0.005	0.001	0.000
NO-2G46-3a-6	0.001	0.000	0.533	0.000	5.007	5.047	0.001	2.200	0.000	0.479	0.000	0.005	0.001	0.000
NO-2G46-3b-28	0.002	0.000	0.528	0.001	5.007	5.044	0.001	2.204	0.000	0.484	0.000	0.001	0.002	0.000
NO-2G46-3b-29	0.003	0.000	0.488	0.002	5.011	4.948	0.002	2.275	0.000	0.525	0.000	0.003	0.003	0.000
NO-2G46-3b-27	0.003	0.000	0.484	0.001	5.004	4.958	0.003	2.271	0.000	0.518	0.000	0.004	0.003	0.000
NO-2G46-3b-20	0.001	0.000	0.483	0.001	5.002	4.965	0.003	2.264	0.000	0.519	0.000	0.005	0.001	0.000
NO-2G46-3b-21	0.000	0.000	0.527	0.001	5.009	5.031	0.003	2.212	0.000	0.487	0.000	0.003	0.000	0.000
NO-2G46-3b-22	0.000	0.000	0.525	0.001	5.007	5.036	0.001	2.210	0.000	0.488	0.000	0.001	0.000	0.000
NO-2G46-3d-1	0.003	0.000	0.487	0.002	5.008	4.963	0.004	2.256	0.000	0.525	0.001	0.004	0.003	0.000
NO-2G46-3d-2	0.003	0.001	0.503	0.001	5.008	4.985	0.001	2.243	0.000	0.506	0.000	0.010	0.003	0.001
NO-2G46-3e-1	0.003	0.000	0.495	0.002	5.007	4.977	0.002	2.255	0.000	0.513	0.000	0.004	0.003	0.000
NO-2G46-3e-2	0.001	0.000	0.518	0.001	5.014	5.002	0.000	2.233	0.000	0.502	0.000	0.003	0.001	0.000
NO-2G47-3b-14	0.002	0.000	0.526	0.001	5.009	5.033	0.001	2.208	0.000	0.489	0.000	0.005	0.002	0.000
NO-2G47-3b-15	0.001	0.000	0.523	0.001	5.012	5.014	0.003	2.219	0.002	0.493	0.000	0.007	0.001	0.000
NO-2G47-3b-16	0.002	0.001	0.521	0.001	5.008	5.022	0.004	2.215	0.000	0.492	0.000	0.005	0.002	0.001
NO-2G47-3b-17	0.002	0.000	0.521	0.001	5.007	5.027	0.003	2.215	0.000	0.489	0.000	0.003	0.002	0.000
NO-2G47-3b-18	0.000	0.000	0.504	0.001	5.003	5.001	0.002	2.237	0.001	0.500	0.000	0.005	0.000	0.000
NO-2G47-3c-21	0.000	0.000	0.514	0.001	5.002	5.026	0.003	2.219	0.001	0.490	0.000	0.003	0.000	0.000
NO-2G47-3c-22	0.000	0.000	0.513	0.001	5.003	5.026	0.002	2.216	0.001	0.494	0.000	0.004	0.000	0.000
NO-2G47-3c-23	0.003	0.000	0.509	0.001	5.005	5.011	0.001	2.227	0.000	0.499	0.000	0.003	0.003	0.000
NO-2G47-3c-24	0.001	0.000	0.519	0.000	5.005	5.024	0.001	2.218	0.000	0.487	0.000	0.009	0.001	0.000
NO-2G47-3c-25	0.002	0.000	0.511	0.000	5.008	5.007	0.001	2.228	0.000	0.504	0.000	0.002	0.002	0.000
NO-2G47-3c-26	0.001	0.000	0.517	0.002	5.009	5.009	0.002	2.230	0.000	0.495	0.000	0.004	0.001	0.000
NO-2G47-3c-27	0.000	0.001	0.520	0.001	5.009	5.018	0.001	2.223	0.000	0.494	0.000	0.003	0.000	0.001
NO-2G47-3d-1	0.000	0.000	0.499	0.000	5.008	4.974	0.000	2.256	0.000	0.514	0.000	0.006	0.000	0.000
NO-2G47-3d-2	0.006	0.000	0.503	0.001	5.009	4.984	0.003	2.241	0.000	0.506	0.000	0.008	0.006	0.000
NO-2G47-3e-1	0.002	0.000	0.522	0.000	5.010	5.021	0.001	2.217	0.001	0.492	0.000	0.004	0.002	0.000
NO-2G47-3e-2	0.001	0.000	0.526	0.001	5.011	5.026	0.002	2.213	0.000	0.491	0.000	0.003	0.001	0.000
NO-2G47-3e-3	0.003	0.000	0.520	0.001	5.012	5.016	0.002	2.216	0.000	0.497	0.000	0.005	0.003	0.000
NO-2G47-3f-1	0.004	0.000	0.530	0.001	5.008	5.041	0.002	2.202	0.000	0.482	0.000	0.003	0.004	0.000
NO-2G47-3f-2	0.001	0.000	0.528	0.001	5.012	5.025	0.003	2.214	0.000	0.490	0.000	0.003	0.001	0.000
NO-2G47-3f-3	0.003	0.000	0.511	0.001	5.011	4.984	0.003	2.250	0.000	0.499	0.000	0.005	0.003	0.000
NO-2G47-3g-1	0.001	0.000	0.520	0.001	5.011	5.011	0.004	2.223	0.000	0.495	0.000	0.005	0.001	0.000
NO-2G47-3g-2	0.001	0.000	0.523	0.001	5.005	5.036	0.002	2.207	0.000	0.486	0.000	0.005	0.001	0.000
NO-2G47-3g-3	0.002	0.000	0.522	0.001	5.007	5.029	0.003	2.208	0.000	0.490	0.000	0.007	0.002	0.000
NO-2G47-2a-1	0.000	0.000	0.509	0.001	5.010	4.996	0.003	2.234	0.001	0.509	0.000	0.002	0.000	0.000
NO-2G47-2a-2	0.000	0.000	0.501	0.008	5.003	5.003	0.001	2.242	0.000	0.494	0.000	0.005	0.000	0.000
NO-2G47-2a-3	0.000	0.000	0.513	0.001	5.002	5.025	0.000	2.227	0.000	0.489	0.000	0.001	0.000	0.000
NO-2G47-2a-4	0.001	0.000	0.515	0.001	5.007	5.011	0.002	2.234	0.000	0.492	0.000	0.001	0.001	0.000
NO-2G47-2a-5	0.002	0.000	0.520	0.001	5.006	5.034	0.002	2.208	0.000	0.492	0.000	0.002	0.002	0.000
NO-2G47-2a-6	0.001	0.000	0.443	0.001	5.008	4.862	0.000	2.342	0.000	0.565	0.000	0.008	0.001	0.000
NO-2G47-2a-8	0.000	0.000	0.526	0.001	5.007	5.034	0.001	2.215	0.000	0.485	0.000	0.001	0.000	0.000
NO-2G47-2a-10	0.001	0.000	0.519	0.001	5.009	5.015	0.002	2.224	0.001	0.494	0.000	0.002	0.001	0.000
NO-2G47-2c-1	0.004	0.001	0.510	0.002	5.012	4.995	0.001	2.236	0.001	0.505	0.000	0.002	0.004	0.001
NO-2G47-2c-2	0.004	0.000	0.510	0.001	5.007	5.010	0.002	2.228	0.000	0.498	0.001	0.001	0.004	0.000

Sample Data			**Atom units**							
Analysis point	K2O	Total	SiO2	TiO2	Al2O3	MgO	CaO	MnO	FeOt	SrO
NO-2G46-3a-9	0.001	8.000	2.485	0.001	1.506	0.000	0.519	0.000	0.003	0.001
NO-2G46-3a-6	0.000	8.000	2.524	0.000	1.467	0.000	0.479	0.000	0.003	0.001
NO-2G46-3b-28	0.001	8.000	2.522	0.000	1.469	0.000	0.484	0.000	0.001	0.002
NO-2G46-3b-29	0.001	8.000	2.474	0.001	1.517	0.000	0.525	0.000	0.002	0.003
NO-2G46-3b-27	0.001	8.000	2.479	0.001	1.514	0.000	0.518	0.000	0.003	0.003
NO-2G46-3b-20	0.001	8.000	2.482	0.002	1.509	0.000	0.519	0.000	0.003	0.001
NO-2G46-3b-21	0.001	8.000	2.515	0.001	1.475	0.000	0.487	0.000	0.002	0.000
NO-2G46-3b-22	0.000	8.000	2.518	0.001	1.473	0.000	0.488	0.000	0.001	0.000
NO-2G46-3d-1	0.001	8.000	2.481	0.002	1.504	0.000	0.525	0.001	0.002	0.003
NO-2G46-3d-2	0.001	8.000	2.493	0.000	1.495	0.000	0.506	0.000	0.007	0.003
NO-2G46-3e-1	0.001	8.000	2.488	0.001	1.503	0.000	0.513	0.000	0.002	0.003
NO-2G46-3e-2	0.001	8.000	2.501	0.000	1.489	0.000	0.502	0.000	0.002	0.001
NO-2G47-3b-14	0.001	8.000	2.516	0.000	1.472	0.000	0.489	0.000	0.003	0.002
NO-2G47-3b-15	0.001	8.000	2.507	0.001	1.479	0.002	0.493	0.000	0.005	0.001
NO-2G47-3b-16	0.000	8.000	2.511	0.002	1.477	0.000	0.492	0.000	0.003	0.002
NO-2G47-3b-17	0.000	8.000	2.513	0.002	1.476	0.000	0.489	0.000	0.002	0.002
NO-2G47-3b-18	0.001	8.000	2.501	0.001	1.491	0.001	0.500	0.000	0.004	0.000
NO-2G47-3c-21	0.001	8.000	2.513	0.001	1.479	0.001	0.490	0.000	0.002	0.000
NO-2G47-3c-22	0.001	8.000	2.513	0.001	1.478	0.001	0.494	0.000	0.002	0.000
NO-2G47-3c-23	0.000	8.000	2.505	0.001	1.485	0.000	0.499	0.000	0.002	0.003
NO-2G47-3c-24	0.000	8.000	2.512	0.001	1.479	0.000	0.487	0.000	0.006	0.001
NO-2G47-3c-25	0.000	8.000	2.504	0.001	1.485	0.000	0.504	0.000	0.001	0.002
NO-2G47-3c-26	0.001	8.000	2.504	0.001	1.486	0.000	0.495	0.000	0.002	0.001
NO-2G47-3c-27	0.001	8.000	2.509	0.000	1.482	0.000	0.494	0.000	0.002	0.000
NO-2G47-3d-1	0.000	8.000	2.487	0.000	1.504	0.000	0.514	0.000	0.004	0.000
NO-2G47-3d-2	0.001	8.000	2.492	0.002	1.494	0.000	0.506	0.000	0.005	0.006
NO-2G47-3e-1	0.000	8.000	2.511	0.001	1.478	0.001	0.492	0.000	0.003	0.002
NO-2G47-3e-2	0.001	8.000	2.513	0.001	1.475	0.000	0.491	0.000	0.002	0.001
NO-2G47-3e-3	0.001	8.000	2.508	0.001	1.477	0.000	0.497	0.000	0.003	0.003
NO-2G47-3f-1	0.001	8.000	2.521	0.001	1.468	0.000	0.482	0.000	0.002	0.004
NO-2G47-3f-2	0.001	8.000	2.513	0.001	1.476	0.000	0.490	0.000	0.002	0.001
NO-2G47-3f-3	0.000	8.000	2.492	0.002	1.500	0.000	0.499	0.000	0.003	0.003
NO-2G47-3g-1	0.001	8.000	2.506	0.002	1.482	0.000	0.495	0.000	0.003	0.001
NO-2G47-3g-2	0.001	8.000	2.518	0.001	1.471	0.000	0.486	0.000	0.003	0.001
NO-2G47-3g-3	0.000	8.000	2.514	0.001	1.472	0.000	0.490	0.000	0.005	0.002
NO-2G47-2a-1	0.000	8.000	2.498	0.001	1.490	0.001	0.509	0.000	0.001	0.000
NO-2G47-2a-2	0.004	8.000	2.502	0.001	1.495	0.000	0.494	0.000	0.003	0.000
NO-2G47-2a-3	0.001	8.000	2.513	0.000	1.485	0.000	0.489	0.000	0.001	0.000
NO-2G47-2a-4	0.001	8.000	2.506	0.001	1.489	0.000	0.492	0.000	0.001	0.001
NO-2G47-2a-5	0.000	8.000	2.517	0.001	1.472	0.000	0.492	0.000	0.001	0.002
NO-2G47-2a-6	0.001	8.000	2.431	0.000	1.561	0.000	0.565	0.000	0.005	0.001
NO-2G47-2a-8	0.000	8.000	2.517	0.001	1.477	0.000	0.485	0.000	0.001	0.000
NO-2G47-2a-10	0.001	8.000	2.508	0.001	1.483	0.001	0.494	0.000	0.002	0.001
NO-2G47-2c-1	0.001	8.000	2.497	0.001	1.490	0.001	0.505	0.000	0.001	0.004
NO-2G47-2c-2	0.001	8.000	2.505	0.001	1.486	0.000	0.498	0.001	0.001	0.004

Sample Data				**Norm oxygen**								
Analysis point	Na2O	K2O	Total	SiO2	TiO2	Al2O3	MgO	CaO	MnO	FeOt	SrO	BaO
NO-2G46-3a-9	0.484	0.002	5.002	4.970	0.003	2.259	0.000	0.519	0.000	0.005	0.001	0.000
NO-2G46-3a-6	0.533	0.000	5.007	5.047	0.001	2.200	0.000	0.479	0.000	0.005	0.001	0.000
NO-2G46-3b-28	0.528	0.001	5.007	5.044	0.001	2.204	0.000	0.484	0.000	0.001	0.002	0.000
NO-2G46-3b-29	0.488	0.002	5.011	4.948	0.002	2.275	0.000	0.525	0.000	0.003	0.003	0.000
NO-2G46-3b-27	0.484	0.001	5.004	4.958	0.003	2.271	0.000	0.518	0.000	0.004	0.003	0.000
NO-2G46-3b-20	0.483	0.001	5.002	4.965	0.003	2.264	0.000	0.519	0.000	0.005	0.001	0.000
NO-2G46-3b-21	0.527	0.001	5.009	5.031	0.003	2.212	0.000	0.487	0.000	0.003	0.000	0.000
NO-2G46-3b-22	0.525	0.001	5.007	5.036	0.001	2.210	0.000	0.488	0.000	0.001	0.000	0.000
NO-2G46-3d-1	0.487	0.002	5.008	4.963	0.004	2.256	0.000	0.525	0.001	0.004	0.003	0.000
NO-2G46-3d-2	0.503	0.001	5.008	4.985	0.001	2.243	0.000	0.506	0.000	0.010	0.003	0.001
NO-2G46-3e-1	0.495	0.002	5.007	4.977	0.002	2.255	0.000	0.513	0.000	0.004	0.003	0.000
NO-2G46-3e-2	0.518	0.001	5.014	5.002	0.000	2.233	0.000	0.502	0.000	0.003	0.001	0.000
NO-2G47-3b-14	0.526	0.001	5.009	5.033	0.001	2.208	0.000	0.489	0.000	0.005	0.002	0.000
NO-2G47-3b-15	0.523	0.001	5.012	5.014	0.003	2.219	0.002	0.493	0.000	0.007	0.001	0.000
NO-2G47-3b-16	0.521	0.001	5.008	5.022	0.004	2.215	0.000	0.492	0.000	0.005	0.002	0.001
NO-2G47-3b-17	0.521	0.001	5.007	5.027	0.003	2.215	0.000	0.489	0.000	0.003	0.002	0.000
NO-2G47-3b-18	0.504	0.001	5.003	5.001	0.002	2.237	0.001	0.500	0.000	0.005	0.000	0.000
NO-2G47-3c-21	0.514	0.001	5.002	5.026	0.003	2.219	0.001	0.490	0.000	0.003	0.000	0.000
NO-2G47-3c-22	0.513	0.001	5.003	5.026	0.002	2.216	0.001	0.494	0.000	0.004	0.000	0.000
NO-2G47-3c-23	0.509	0.001	5.005	5.011	0.001	2.227	0.000	0.499	0.000	0.003	0.003	0.000
NO-2G47-3c-24	0.519	0.000	5.005	5.024	0.001	2.218	0.000	0.487	0.000	0.009	0.001	0.000
NO-2G47-3c-25	0.511	0.000	5.008	5.007	0.001	2.228	0.000	0.504	0.000	0.002	0.002	0.000
NO-2G47-3c-26	0.517	0.002	5.009	5.009	0.002	2.230	0.000	0.495	0.000	0.004	0.001	0.000
NO-2G47-3c-27	0.520	0.001	5.009	5.018	0.001	2.223	0.000	0.494	0.000	0.003	0.000	0.001
NO-2G47-3d-1	0.499	0.000	5.008	4.974	0.000	2.256	0.000	0.514	0.000	0.006	0.000	0.000
NO-2G47-3d-2	0.503	0.001	5.009	4.984	0.003	2.241	0.000	0.506	0.000	0.008	0.006	0.000
NO-2G47-3e-1	0.522	0.000	5.010	5.021	0.001	2.217	0.001	0.492	0.000	0.004	0.002	0.000
NO-2G47-3e-2	0.526	0.001	5.011	5.026	0.002	2.213	0.000	0.491	0.000	0.003	0.001	0.000
NO-2G47-3e-3	0.520	0.001	5.012	5.016	0.002	2.216	0.000	0.497	0.000	0.005	0.003	0.000
NO-2G47-3f-1	0.530	0.001	5.008	5.041	0.002	2.202	0.000	0.482	0.000	0.003	0.004	0.000
NO-2G47-3f-2	0.528	0.001	5.012	5.025	0.003	2.214	0.000	0.490	0.000	0.003	0.001	0.000
NO-2G47-3f-3	0.511	0.001	5.011	4.984	0.003	2.250	0.000	0.499	0.000	0.005	0.003	0.000
NO-2G47-3g-1	0.520	0.001	5.011	5.011	0.004	2.223	0.000	0.495	0.000	0.005	0.001	0.000
NO-2G47-3g-2	0.523	0.001	5.005	5.036	0.002	2.207	0.000	0.486	0.000	0.005	0.001	0.000
NO-2G47-3g-3	0.522	0.001	5.007	5.029	0.003	2.208	0.000	0.490	0.000	0.007	0.002	0.000
NO-2G47-2a-1	0.509	0.001	5.010	4.996	0.003	2.234	0.001	0.509	0.000	0.002	0.000	0.000
NO-2G47-2a-2	0.501	0.008	5.003	5.003	0.001	2.242	0.000	0.494	0.000	0.005	0.000	0.000
NO-2G47-2a-3	0.513	0.001	5.002	5.025	0.000	2.227	0.000	0.489	0.000	0.001	0.000	0.000
NO-2G47-2a-4	0.515	0.001	5.007	5.011	0.002	2.234	0.000	0.492	0.000	0.001	0.001	0.000
NO-2G47-2a-5	0.520	0.001	5.006	5.034	0.002	2.208	0.000	0.492	0.000	0.002	0.002	0.000
NO-2G47-2a-6	0.443	0.001	5.008	4.862	0.000	2.342	0.000	0.565	0.000	0.008	0.001	0.000
NO-2G47-2a-8	0.526	0.001	5.007	5.034	0.001	2.215	0.000	0.485	0.000	0.001	0.000	0.000
NO-2G47-2a-10	0.519	0.001	5.009	5.015	0.002	2.224	0.001	0.494	0.000	0.002	0.001	0.000
NO-2G47-2c-1	0.510	0.002	5.012	4.995	0.001	2.236	0.001	0.505	0.000	0.002	0.004	0.001
NO-2G47-2c-2	0.510	0.001	5.007	5.010	0.002	2.228	0.000	0.498	0.001	0.001	0.004	0.000

Sample Data			**End Member**		
Analysis point	Na2O	K2O	Anorthite	Albite	Orthoclase
NO-2G46-3a-9	0.242	0.001	51.6	48.1	0.2
NO-2G46-3a-6	0.266	0.000	47.3	52.6	0.0
NO-2G46-3b-28	0.264	0.001	47.7	52.1	0.1
NO-2G46-3b-29	0.244	0.001	51.7	48.1	0.2
NO-2G46-3b-27	0.242	0.001	51.6	48.3	0.1
NO-2G46-3b-20	0.242	0.001	51.7	48.2	0.1
NO-2G46-3b-21	0.264	0.001	48.0	51.9	0.1
NO-2G46-3b-22	0.262	0.000	48.2	51.8	0.1
NO-2G46-3d-1	0.244	0.001	51.8	48.0	0.2
NO-2G46-3d-2	0.251	0.001	50.1	49.8	0.1
NO-2G46-3e-1	0.247	0.001	50.8	49.0	0.2
NO-2G46-3e-2	0.259	0.001	49.1	50.7	0.1
NO-2G47-3b-14	0.263	0.001	48.1	51.8	0.1
NO-2G47-3b-15	0.261	0.001	48.5	51.4	0.1
NO-2G47-3b-16	0.260	0.000	48.5	51.4	0.1
NO-2G47-3b-17	0.261	0.000	48.4	51.5	0.1
NO-2G47-3b-18	0.252	0.001	49.8	50.1	0.1
NO-2G47-3c-21	0.257	0.001	48.8	51.1	0.1
NO-2G47-3c-22	0.256	0.001	49.0	50.9	0.1
NO-2G47-3c-23	0.255	0.000	49.5	50.5	0.1
NO-2G47-3c-24	0.259	0.000	48.4	51.5	0.0
NO-2G47-3c-25	0.255	0.000	49.7	50.3	0.0
NO-2G47-3c-26	0.258	0.001	48.9	51.0	0.2
NO-2G47-3c-27	0.260	0.001	48.7	51.2	0.1
NO-2G47-3d-1	0.249	0.000	50.8	49.2	0.0
NO-2G47-3d-2	0.252	0.001	50.1	49.8	0.1
NO-2G47-3e-1	0.261	0.000	48.5	51.5	0.0
NO-2G47-3e-2	0.263	0.001	48.2	51.6	0.1
NO-2G47-3e-3	0.260	0.001	48.8	51.1	0.1
NO-2G47-3f-1	0.265	0.001	47.6	52.3	0.1
NO-2G47-3f-2	0.264	0.001	48.1	51.8	0.1
NO-2G47-3f-3	0.256	0.000	49.3	50.6	0.1
NO-2G47-3g-1	0.260	0.001	48.7	51.2	0.1
NO-2G47-3g-2	0.261	0.001	48.1	51.8	0.1
NO-2G47-3g-3	0.261	0.000	48.4	51.6	0.1
NO-2G47-2a-1	0.255	0.000	49.9	50.0	0.1
NO-2G47-2a-2	0.250	0.004	49.3	50.0	0.8
NO-2G47-2a-3	0.256	0.001	48.8	51.1	0.1
NO-2G47-2a-4	0.258	0.001	48.8	51.1	0.1
NO-2G47-2a-5	0.260	0.000	48.6	51.4	0.1
NO-2G47-2a-6	0.221	0.001	56.0	43.9	0.1
NO-2G47-2a-8	0.263	0.000	48.0	52.0	0.1
NO-2G47-2a-10	0.259	0.001	48.7	51.1	0.1
NO-2G47-2c-1	0.255	0.001	49.7	50.2	0.2
NO-2G47-2c-2	0.255	0.001	49.4	50.5	0.1

Sample Data				**Mole Cation**					
Analysis point	Intrusion/Phase	Sample	Mineral	SiO2	TiO2	Al2O3	MgO	CaO	MnO
NO-2G47-2c-3	Thunderbird-P	NO-2G47-2	Feldspar	0.925	0.000	0.547	0.000	0.182	0.000
NO-2G47-2d-1	Thunderbird-P	NO-2G47-2	Feldspar	0.924	0.000	0.549	0.000	0.182	0.000
NO-2G47-2d-2	Thunderbird-P	NO-2G47-2	Feldspar	0.924	0.001	0.546	0.000	0.182	0.000
NO-2G47-2d-3	Thunderbird-P	NO-2G47-2	Feldspar	0.922	0.000	0.554	0.000	0.186	0.000
NO-2G47-2e-1	Thunderbird-P	NO-2G47-2	Feldspar	0.926	0.000	0.548	0.000	0.182	0.000
NO-2G47-2e-2	Thunderbird-P	NO-2G47-2	Feldspar	0.923	0.000	0.550	0.000	0.183	0.000
NO-2G47-2e-3	Thunderbird-P	NO-2G47-2	Feldspar	0.925	0.001	0.549	0.000	0.185	0.000
NO-2G47-5a-1	Thunderbird-P	NO-2G47-5	Feldspar	0.936	0.000	0.541	0.000	0.178	0.000
NO-2G47-5a-4	Thunderbird-P	NO-2G47-5	Feldspar	0.934	0.000	0.543	0.000	0.176	0.000
NO-2G47-5a-7	Thunderbird-P	NO-2G47-5	Feldspar	0.934	0.000	0.541	0.000	0.173	0.000
NO-2G47-5a-10	Thunderbird-P	NO-2G47-5	Feldspar	0.939	0.000	0.541	0.000	0.174	0.000
NO-2G47-5a-13	Thunderbird-P	NO-2G47-5	Feldspar	0.930	0.000	0.545	0.000	0.179	0.000
NO-2G47-5b-17	Thunderbird-P	NO-2G47-5	Feldspar	0.934	0.000	0.541	0.000	0.175	0.000
NO-2G47-5b-18	Thunderbird-P	NO-2G47-5	Feldspar	0.936	0.000	0.540	0.000	0.176	0.000
NO-2G47-5b-19	Thunderbird-P	NO-2G47-5	Feldspar	0.939	0.000	0.542	0.000	0.176	0.000
NO-2G47-5c-21	Thunderbird-P	NO-2G47-5	Feldspar	0.937	0.000	0.545	0.000	0.176	0.000
NO-2G47-5c-22	Thunderbird-P	NO-2G47-5	Feldspar	0.934	0.000	0.546	0.000	0.177	0.000
NO-2G47-5d-1	Thunderbird-P	NO-2G47-5	Feldspar	0.922	0.000	0.551	0.000	0.188	0.000
NO-2G47-5d-2	Thunderbird-P	NO-2G47-5	Feldspar	0.922	0.000	0.553	0.000	0.186	0.000
NO-2G47-5d-3	Thunderbird-P	NO-2G47-5	Feldspar	0.934	0.000	0.536	0.000	0.174	0.000
NO-2G47-5e-1	Thunderbird-P	NO-2G47-5	Feldspar	0.931	0.000	0.546	0.001	0.178	0.000
NO-2G47-5e-2	Thunderbird-P	NO-2G47-5	Feldspar	0.939	0.000	0.534	0.001	0.173	0.000
NO-2G47-5e-3	Thunderbird-P	NO-2G47-5	Feldspar	0.932	0.000	0.547	0.001	0.181	0.000
MM-71B-2a-1	Butler East	MM-71B-2	Feldspar	0.981	0.000	0.512	0.000	0.140	0.000
MM-71B-2a-2	Butler East	MM-71B-2	Feldspar	0.959	0.000	0.532	0.000	0.162	0.000
MM-71B-2a-3	Butler East	MM-71B-2	Feldspar	0.964	0.000	0.525	0.000	0.158	0.000
MM-71B-2a-4	Butler East	MM-71B-2	Feldspar	0.927	0.000	0.552	0.000	0.186	0.000
MM-71B-2a-5	Butler East	MM-71B-2	Feldspar	0.919	0.000	0.555	0.000	0.189	0.000
MM-71B-2c-6	Butler East	MM-71B-2	Feldspar	0.927	0.000	0.551	0.000	0.185	0.000
MM-71B-2c-7	Butler East	MM-71B-2	Feldspar	0.917	0.000	0.557	0.000	0.190	0.000
MM-71B-2c-8	Butler East	MM-71B-2	Feldspar	0.929	0.000	0.547	0.000	0.181	0.000
MM-71B-2d-1	Butler East	MM-71B-2	Feldspar	0.974	0.000	0.517	0.000	0.142	0.000
MM-71B-2d-2	Butler East	MM-71B-2	Feldspar	0.973	0.000	0.515	0.000	0.146	0.000
MM-71B-2d-3	Butler East	MM-71B-2	Feldspar	0.970	0.000	0.518	0.001	0.148	0.000
MM-71B-2e-1	Butler East	MM-71B-2	Feldspar	0.921	0.000	0.552	0.000	0.186	0.000
MM-71B-2e-2	Butler East	MM-71B-2	Feldspar	0.949	0.000	0.536	0.000	0.165	0.000
MM-71B-2e-3	Butler East	MM-71B-2	Feldspar	1.019	0.000	0.479	0.000	0.108	0.000
MM-71B-2f-1	Butler East	MM-71B-2	Feldspar	0.939	0.000	0.539	0.000	0.174	0.000
MM-71B-2f-2	Butler East	MM-71B-2	Feldspar	0.971	0.000	0.516	0.000	0.144	0.000
MM-71B-2f-3	Butler East	MM-71B-2	Feldspar	0.983	0.000	0.514	0.000	0.140	0.000
MM-117-1a-1	Butler West	MM-117-1	Feldspar	0.866	0.000	0.599	0.000	0.235	0.000
MM-117-1a-2	Butler West	MM-117-1	Feldspar	0.877	0.000	0.586	0.000	0.227	0.000
MM-117-1a-3	Butler West	MM-117-1	Feldspar	0.878	0.000	0.579	0.000	0.222	0.000
MM-117-1a-4	Butler West	MM-117-1	Feldspar	0.849	0.000	0.604	0.000	0.243	0.000
MM-117-1b-6	Butler West	MM-117-1	Feldspar	0.845	0.000	0.603	0.000	0.248	0.000

Sample Data							**Mole oxygen**					
Analysis point	FeOt	SrO	BaO	Na2O	K2O	Total	SiO2	TiO2	Al2O3	MgO	CaO	MnO
NO-2G47-2c-3	0.001	0.001	0.000	0.192	0.000	1.849	1.850	0.000	0.821	0.000	0.182	0.000
NO-2G47-2d-1	0.000	0.001	0.000	0.190	0.000	1.849	1.849	0.000	0.824	0.000	0.182	0.000
NO-2G47-2d-2	0.002	0.000	0.000	0.189	0.000	1.844	1.847	0.003	0.818	0.000	0.182	0.000
NO-2G47-2d-3	0.001	0.001	0.000	0.185	0.000	1.850	1.843	0.001	0.831	0.000	0.186	0.000
NO-2G47-2e-1	0.000	0.001	0.000	0.191	0.000	1.848	1.853	0.001	0.822	0.000	0.182	0.000
NO-2G47-2e-2	0.000	0.000	0.000	0.192	0.000	1.849	1.845	0.000	0.824	0.000	0.183	0.000
NO-2G47-2e-3	0.001	0.001	0.000	0.191	0.001	1.854	1.850	0.001	0.824	0.000	0.185	0.000
NO-2G47-5a-1	0.001	0.000	0.000	0.198	0.000	1.854	1.871	0.001	0.812	0.000	0.178	0.000
NO-2G47-5a-4	0.001	0.000	0.000	0.196	0.001	1.852	1.868	0.001	0.814	0.000	0.176	0.000
NO-2G47-5a-7	0.001	0.000	0.000	0.199	0.001	1.849	1.867	0.001	0.811	0.000	0.173	0.000
NO-2G47-5a-10	0.002	0.001	0.000	0.198	0.001	1.856	1.878	0.001	0.812	0.000	0.174	0.000
NO-2G47-5a-13	0.001	0.000	0.000	0.195	0.000	1.850	1.860	0.001	0.817	0.000	0.179	0.000
NO-2G47-5b-17	0.001	0.000	0.000	0.198	0.000	1.851	1.867	0.001	0.812	0.000	0.175	0.000
NO-2G47-5b-18	0.002	0.000	0.000	0.196	0.000	1.852	1.872	0.001	0.811	0.000	0.176	0.000
NO-2G47-5b-19	0.002	0.000	0.000	0.198	0.001	1.858	1.877	0.001	0.813	0.000	0.176	0.000
NO-2G47-5c-21	0.001	0.000	0.000	0.200	0.000	1.860	1.874	0.000	0.818	0.000	0.176	0.000
NO-2G47-5c-22	0.001	0.000	0.000	0.193	0.000	1.853	1.869	0.001	0.819	0.000	0.177	0.000
NO-2G47-5d-1	0.001	0.001	0.000	0.187	0.001	1.850	1.843	0.000	0.826	0.000	0.188	0.000
NO-2G47-5d-2	0.000	0.001	0.000	0.186	0.000	1.849	1.845	0.000	0.829	0.000	0.186	0.000
NO-2G47-5d-3	0.002	0.001	0.000	0.200	0.001	1.848	1.868	0.001	0.805	0.000	0.174	0.000
NO-2G47-5e-1	0.000	0.000	0.000	0.195	0.000	1.852	1.861	0.001	0.819	0.001	0.178	0.000
NO-2G47-5e-2	0.008	0.000	0.000	0.203	0.001	1.858	1.877	0.001	0.801	0.001	0.173	0.000
NO-2G47-5e-3	0.001	0.001	0.000	0.193	0.000	1.857	1.864	0.001	0.821	0.001	0.181	0.000
MM-71B-2a-1	0.000	0.001	0.000	0.237	0.001	1.873	1.963	0.000	0.768	0.000	0.140	0.000
MM-71B-2a-2	0.001	0.001	0.000	0.211	0.001	1.867	1.919	0.000	0.797	0.000	0.162	0.000
MM-71B-2a-3	0.000	0.002	0.000	0.221	0.001	1.871	1.928	0.000	0.788	0.000	0.158	0.000
MM-71B-2a-4	0.001	0.000	0.000	0.188	0.001	1.855	1.854	0.000	0.829	0.000	0.186	0.000
MM-71B-2a-5	0.001	0.001	0.000	0.186	0.001	1.851	1.838	0.000	0.832	0.000	0.189	0.000
MM-71B-2c-6	0.001	0.001	0.000	0.188	0.001	1.855	1.855	0.000	0.826	0.000	0.185	0.000
MM-71B-2c-7	0.002	0.000	0.000	0.183	0.001	1.850	1.834	0.001	0.835	0.000	0.190	0.000
MM-71B-2c-8	0.001	0.001	0.000	0.192	0.001	1.850	1.857	0.000	0.820	0.000	0.181	0.000
MM-71B-2d-1	0.000	0.001	0.000	0.234	0.001	1.870	1.948	0.000	0.776	0.000	0.142	0.000
MM-71B-2d-2	0.000	0.001	0.000	0.232	0.001	1.869	1.946	0.000	0.772	0.000	0.146	0.000
MM-71B-2d-3	0.001	0.001	0.000	0.228	0.001	1.869	1.941	0.000	0.777	0.001	0.148	0.000
MM-71B-2e-1	0.001	0.002	0.000	0.185	0.001	1.848	1.841	0.000	0.828	0.000	0.186	0.000
MM-71B-2e-2	0.001	0.001	0.000	0.210	0.001	1.862	1.899	0.000	0.804	0.000	0.165	0.000
MM-71B-2e-3	0.001	0.001	0.000	0.270	0.001	1.878	2.038	0.000	0.718	0.000	0.108	0.000
MM-71B-2f-1	0.000	0.001	0.000	0.199	0.001	1.853	1.878	0.000	0.808	0.000	0.174	0.000
MM-71B-2f-2	0.001	0.001	0.000	0.228	0.001	1.862	1.943	0.000	0.773	0.000	0.144	0.000
MM-71B-2f-3	0.002	0.001	0.000	0.235	0.001	1.877	1.966	0.000	0.772	0.000	0.140	0.000
MM-117-1a-1	0.001	0.000	0.000	0.135	0.001	1.837	1.732	0.000	0.899	0.000	0.235	0.000
MM-117-1a-2	0.001	0.001	0.000	0.143	0.000	1.836	1.755	0.000	0.879	0.000	0.227	0.000
MM-117-1a-3	0.000	0.000	0.000	0.148	0.001	1.829	1.757	0.000	0.869	0.000	0.222	0.000
MM-117-1a-4	0.002	0.000	0.000	0.125	0.000	1.824	1.699	0.000	0.906	0.000	0.243	0.000

Sample Data							**Norm Cations**					
Analysis point	FeOt	SrO	BaO	Na2O	K2O	Total	SiO2	TiO2	Al2O3	MgO	CaO	MnO
NO-2G47-2c-3	0.002	0.001	0.000	0.096	0.000	2.953	2.507	0.000	1.483	0.000	0.494	0.001
NO-2G47-2d-1	0.001	0.001	0.000	0.095	0.000	2.953	2.505	0.000	1.488	0.000	0.494	0.000
NO-2G47-2d-2	0.003	0.000	0.000	0.094	0.000	2.948	2.506	0.004	1.480	0.001	0.494	0.000
NO-2G47-2d-3	0.002	0.001	0.000	0.093	0.000	2.957	2.494	0.001	1.500	0.000	0.503	0.001
NO-2G47-2e-1	0.000	0.001	0.000	0.095	0.000	2.954	2.509	0.001	1.484	0.000	0.494	0.000
NO-2G47-2e-2	0.001	0.000	0.000	0.096	0.000	2.951	2.502	0.001	1.490	0.000	0.497	0.000
NO-2G47-2e-3	0.002	0.001	0.000	0.095	0.000	2.959	2.501	0.002	1.485	0.000	0.501	0.000
NO-2G47-5a-1	0.002	0.000	0.000	0.099	0.000	2.963	2.526	0.001	1.462	0.001	0.480	0.000
NO-2G47-5a-4	0.002	0.000	0.000	0.098	0.001	2.960	2.525	0.001	1.467	0.001	0.475	0.000
NO-2G47-5a-7	0.002	0.000	0.000	0.099	0.000	2.954	2.528	0.001	1.465	0.000	0.468	0.000
NO-2G47-5a-10	0.003	0.001	0.000	0.099	0.000	2.967	2.532	0.001	1.459	0.000	0.468	0.000
NO-2G47-5a-13	0.001	0.000	0.000	0.097	0.000	2.956	2.517	0.001	1.475	0.000	0.483	0.000
NO-2G47-5b-17	0.002	0.000	0.000	0.099	0.000	2.957	2.526	0.001	1.465	0.000	0.474	0.000
NO-2G47-5b-18	0.002	0.000	0.000	0.098	0.000	2.961	2.529	0.001	1.460	0.001	0.476	0.000
NO-2G47-5b-19	0.003	0.000	0.000	0.099	0.000	2.969	2.529	0.001	1.460	0.000	0.473	0.000
NO-2G47-5c-21	0.002	0.000	0.000	0.100	0.000	2.970	2.525	0.000	1.468	0.000	0.474	0.000
NO-2G47-5c-22	0.002	0.000	0.000	0.097	0.000	2.965	2.521	0.001	1.473	0.000	0.478	0.000
NO-2G47-5d-1	0.001	0.001	0.000	0.093	0.000	2.954	2.496	0.000	1.492	0.001	0.509	0.000
NO-2G47-5d-2	0.001	0.001	0.000	0.093	0.000	2.955	2.497	0.000	1.496	0.000	0.503	0.000
NO-2G47-5d-3	0.003	0.001	0.000	0.100	0.000	2.952	2.531	0.001	1.454	0.001	0.471	0.000
NO-2G47-5e-1	0.001	0.000	0.000	0.098	0.000	2.958	2.517	0.001	1.476	0.002	0.482	0.000
NO-2G47-5e-2	0.011	0.000	0.000	0.101	0.000	2.966	2.532	0.001	1.440	0.002	0.467	0.000
NO-2G47-5e-3	0.002	0.001	0.000	0.096	0.000	2.967	2.512	0.001	1.476	0.001	0.489	0.000
MM-71B-2a-1	0.001	0.001	0.000	0.118	0.001	2.991	2.625	0.000	1.369	0.000	0.374	0.000
MM-71B-2a-2	0.001	0.001	0.000	0.106	0.000	2.987	2.570	0.000	1.424	0.000	0.434	0.000
MM-71B-2a-3	0.000	0.002	0.000	0.111	0.000	2.987	2.582	0.000	1.407	0.000	0.423	0.000
MM-71B-2a-4	0.001	0.000	0.000	0.094	0.000	2.964	2.502	0.000	1.491	0.000	0.502	0.000
MM-71B-2a-5	0.001	0.001	0.000	0.093	0.000	2.955	2.488	0.000	1.503	0.000	0.511	0.000
MM-71B-2c-6	0.001	0.001	0.000	0.094	0.000	2.963	2.504	0.000	1.487	0.000	0.499	0.000
MM-71B-2c-7	0.002	0.000	0.000	0.091	0.000	2.955	2.483	0.001	1.508	0.000	0.515	0.000
MM-71B-2c-8	0.001	0.001	0.000	0.096	0.000	2.956	2.513	0.000	1.479	0.000	0.489	0.000
MM-71B-2d-1	0.000	0.001	0.000	0.117	0.001	2.985	2.610	0.000	1.387	0.000	0.380	0.000
MM-71B-2d-2	0.000	0.001	0.000	0.116	0.001	2.983	2.609	0.000	1.380	0.000	0.393	0.000
MM-71B-2d-3	0.002	0.001	0.000	0.114	0.000	2.985	2.601	0.000	1.389	0.002	0.398	0.000
MM-71B-2e-1	0.001	0.002	0.000	0.093	0.001	2.952	2.495	0.000	1.496	0.000	0.505	0.000
MM-71B-2e-2	0.001	0.001	0.000	0.105	0.000	2.974	2.554	0.000	1.442	0.000	0.443	0.000
MM-71B-2e-3	0.001	0.001	0.000	0.135	0.000	3.002	2.716	0.000	1.276	0.000	0.287	0.000
MM-71B-2f-1	0.000	0.001	0.000	0.099	0.000	2.961	2.537	0.000	1.456	0.000	0.470	0.000
MM-71B-2f-2	0.001	0.001	0.000	0.114	0.000	2.977	2.610	0.000	1.386	0.000	0.388	0.000
MM-71B-2f-3	0.003	0.001	0.000	0.118	0.001	3.001	2.621	0.000	1.371	0.000	0.373	0.000
MM-117-1a-1	0.001	0.000	0.000	0.068	0.000	2.935	2.361	0.000	1.633	0.000	0.639	0.000
MM-117-1a-2	0.001	0.001	0.000	0.072	0.000	2.934	2.392	0.000	1.597	0.000	0.618	0.000
MM-117-1a-3	0.000	0.000	0.000	0.074	0.000	2.923	2.404	0.000	1.586	0.000	0.608	0.000
MM-117-1a-4	0.002	0.000	0.000	0.062	0.000	2.913	2.332	0.000	1.658	0.001	0.668	0.000
MM-117-1b-6	0.001	0.001	0.000	0.060	0.000	2.905	2.328	0.000	1.660	0.000	0.682	0.000

Sample Data						**Norm Oxygen**								
Analysis point	SrO	BaO	Na2O	K2O	Total	SiO2	TiO2	Al2O3	MgO	CaO	MnO	FeOt	SrO	BaO
NO-2G47-2c-3	0.003	0.000	0.519	0.000	5.010	5.013	0.000	2.224	0.000	0.494	0.001	0.004	0.003	0.000
NO-2G47-2d-1	0.004	0.000	0.516	0.001	5.009	5.009	0.000	2.232	0.000	0.494	0.000	0.002	0.004	0.000
NO-2G47-2d-2	0.001	0.000	0.512	0.001	5.004	5.012	0.008	2.220	0.001	0.494	0.000	0.007	0.001	0.000
NO-2G47-2d-3	0.002	0.000	0.501	0.001	5.005	4.987	0.002	2.249	0.000	0.503	0.001	0.004	0.002	0.000
NO-2G47-2e-1	0.002	0.000	0.516	0.000	5.006	5.018	0.002	2.225	0.000	0.494	0.000	0.001	0.002	0.000
NO-2G47-2e-2	0.000	0.000	0.521	0.001	5.013	5.003	0.001	2.235	0.000	0.497	0.000	0.002	0.000	0.000
NO-2G47-2e-3	0.002	0.001	0.515	0.002	5.012	5.001	0.003	2.228	0.000	0.501	0.000	0.006	0.002	0.001
NO-2G47-5a-1	0.000	0.000	0.533	0.001	5.007	5.053	0.002	2.193	0.001	0.480	0.000	0.004	0.000	0.000
NO-2G47-5a-4	0.000	0.000	0.531	0.004	5.006	5.049	0.002	2.200	0.001	0.475	0.000	0.005	0.000	0.000
NO-2G47-5a-7	0.001	0.000	0.538	0.002	5.007	5.056	0.002	2.197	0.000	0.468	0.000	0.006	0.001	0.000
NO-2G47-5a-10	0.002	0.000	0.535	0.002	5.004	5.064	0.002	2.189	0.000	0.468	0.000	0.007	0.002	0.000
NO-2G47-5a-13	0.001	0.001	0.528	0.001	5.008	5.035	0.002	2.212	0.000	0.483	0.000	0.003	0.001	0.001
NO-2G47-5b-17	0.000	0.000	0.537	0.001	5.007	5.053	0.002	2.198	0.000	0.474	0.000	0.004	0.000	0.000
NO-2G47-5b-18	0.001	0.001	0.530	0.001	5.003	5.057	0.002	2.190	0.001	0.476	0.000	0.007	0.001	0.001
NO-2G47-5b-19	0.000	0.000	0.535	0.002	5.006	5.058	0.002	2.189	0.000	0.473	0.000	0.009	0.000	0.000
NO-2G47-5c-21	0.001	0.000	0.539	0.000	5.010	5.049	0.000	2.202	0.000	0.474	0.000	0.005	0.001	0.000
NO-2G47-5c-22	0.000	0.001	0.521	0.001	5.000	5.043	0.002	2.210	0.000	0.478	0.000	0.005	0.000	0.001
NO-2G47-5d-1	0.002	0.000	0.506	0.002	5.010	4.992	0.000	2.238	0.001	0.509	0.000	0.004	0.002	0.000
NO-2G47-5d-2	0.003	0.000	0.505	0.001	5.007	4.994	0.001	2.244	0.000	0.503	0.000	0.002	0.003	0.000
NO-2G47-5d-3	0.002	0.000	0.541	0.002	5.009	5.063	0.001	2.181	0.001	0.471	0.000	0.009	0.002	0.000
NO-2G47-5e-1	0.000	0.000	0.528	0.001	5.008	5.033	0.003	2.214	0.002	0.482	0.000	0.002	0.000	0.000
NO-2G47-5e-2	0.000	0.000	0.547	0.002	5.011	5.063	0.002	2.161	0.002	0.467	0.000	0.030	0.000	0.000
NO-2G47-5e-3	0.003	0.000	0.519	0.001	5.007	5.025	0.002	2.214	0.001	0.489	0.000	0.006	0.003	0.000
MM-71B-2a-1	0.003	0.000	0.634	0.003	5.008	5.249	0.000	2.054	0.000	0.374	0.000	0.002	0.003	0.000
MM-71B-2a-2	0.004	0.000	0.566	0.002	5.002	5.140	0.000	2.136	0.000	0.434	0.000	0.002	0.004	0.000
MM-71B-2a-3	0.004	0.000	0.593	0.002	5.012	5.163	0.001	2.110	0.000	0.423	0.000	0.001	0.004	0.000
MM-71B-2a-4	0.001	0.000	0.507	0.002	5.006	5.005	0.000	2.236	0.000	0.502	0.000	0.002	0.001	0.000
MM-71B-2a-5	0.002	0.000	0.504	0.003	5.013	4.976	0.000	2.254	0.000	0.511	0.000	0.004	0.002	0.000
MM-71B-2c-6	0.004	0.000	0.509	0.003	5.007	5.008	0.000	2.231	0.000	0.499	0.000	0.002	0.004	0.000
MM-71B-2c-7	0.001	0.000	0.495	0.002	5.009	4.965	0.002	2.262	0.000	0.515	0.000	0.006	0.001	0.000
MM-71B-2c-8	0.002	0.000	0.520	0.002	5.007	5.027	0.000	2.219	0.000	0.489	0.000	0.003	0.002	0.000
MM-71B-2d-1	0.003	0.000	0.629	0.003	5.012	5.220	0.000	2.080	0.000	0.380	0.000	0.001	0.003	0.000
MM-71B-2d-2	0.004	0.000	0.623	0.003	5.013	5.218	0.001	2.070	0.000	0.393	0.000	0.001	0.004	0.000
MM-71B-2d-3	0.003	0.000	0.611	0.002	5.009	5.202	0.001	2.084	0.002	0.398	0.000	0.005	0.003	0.000
MM-71B-2e-1	0.005	0.000	0.502	0.003	5.008	4.990	0.000	2.245	0.000	0.505	0.000	0.002	0.005	0.000
MM-71B-2e-2	0.002	0.000	0.564	0.002	5.008	5.107	0.000	2.163	0.000	0.443	0.000	0.002	0.002	0.000
MM-71B-2e-3	0.003	0.000	0.719	0.002	5.006	5.432	0.000	1.914	0.000	0.287	0.000	0.004	0.003	0.000
MM-71B-2f-1	0.004	0.000	0.537	0.001	5.005	5.073	0.000	2.183	0.000	0.470	0.000	0.000	0.004	0.000
MM-71B-2f-2	0.003	0.000	0.612	0.003	5.003	5.221	0.000	2.078	0.000	0.388	0.000	0.003	0.003	0.000
MM-71B-2f-3	0.003	0.000	0.627	0.004	5.006	5.242	0.000	2.057	0.000	0.373	0.000	0.009	0.003	0.000
MM-117-1a-1	0.001	0.000	0.368	0.001	5.007	4.721	0.000	2.450	0.000	0.639	0.000	0.003	0.001	0.000
MM-117-1a-2	0.002	0.000	0.391	0.001	5.004	4.784	0.001	2.396	0.000	0.618	0.000	0.002	0.002	0.000
MM-117-1a-3	0.000	0.000	0.405	0.002	5.006	4.809	0.000	2.379	0.000	0.608	0.000	0.000	0.000	0.000
MM-117-1a-4	0.001	0.000	0.343	0.001	5.008	4.665	0.000	2.487	0.001	0.668	0.000	0.006	0.001	0.000
MM-117-1b-6	0.002	0.000	0.333	0.000	5.008	4.657	0.000	2.490	0.000	0.682	0.000	0.002	0.002	0.000

Sample Data			**Atom units**							
Analysis point	K2O	Total	SiO2	TiO2	Al2O3	MgO	CaO	MnO	FeOt	SrO
NO-2G47-2c-3	0.000	8.000	2.507	0.000	1.483	0.000	0.494	0.001	0.003	0.003
NO-2G47-2d-1	0.001	8.000	2.505	0.000	1.488	0.000	0.494	0.000	0.001	0.004
NO-2G47-2d-2	0.001	8.000	2.506	0.004	1.480	0.001	0.494	0.000	0.005	0.001
NO-2G47-2d-3	0.001	8.000	2.494	0.001	1.500	0.000	0.503	0.001	0.003	0.002
NO-2G47-2e-1	0.000	8.000	2.509	0.001	1.484	0.000	0.494	0.000	0.000	0.002
NO-2G47-2e-2	0.000	8.000	2.502	0.001	1.490	0.000	0.497	0.000	0.001	0.000
NO-2G47-2e-3	0.001	8.000	2.501	0.002	1.485	0.000	0.501	0.000	0.004	0.002
NO-2G47-5a-1	0.000	8.000	2.526	0.001	1.462	0.001	0.480	0.000	0.003	0.000
NO-2G47-5a-4	0.002	8.000	2.525	0.001	1.467	0.001	0.475	0.000	0.004	0.000
NO-2G47-5a-7	0.001	8.000	2.528	0.001	1.465	0.000	0.468	0.000	0.004	0.001
NO-2G47-5a-10	0.001	8.000	2.532	0.001	1.459	0.000	0.468	0.000	0.005	0.002
NO-2G47-5a-13	0.000	8.000	2.517	0.001	1.475	0.000	0.483	0.000	0.002	0.001
NO-2G47-5b-17	0.001	8.000	2.526	0.001	1.465	0.000	0.474	0.000	0.003	0.000
NO-2G47-5b-18	0.000	8.000	2.529	0.001	1.460	0.001	0.476	0.000	0.004	0.001
NO-2G47-5b-19	0.001	8.000	2.529	0.001	1.460	0.000	0.473	0.000	0.006	0.000
NO-2G47-5c-21	0.000	8.000	2.525	0.000	1.468	0.000	0.474	0.000	0.003	0.001
NO-2G47-5c-22	0.001	8.000	2.521	0.001	1.473	0.000	0.478	0.000	0.003	0.000
NO-2G47-5d-1	0.001	8.000	2.496	0.000	1.492	0.001	0.509	0.000	0.003	0.002
NO-2G47-5d-2	0.000	8.000	2.497	0.000	1.496	0.000	0.503	0.000	0.001	0.003
NO-2G47-5d-3	0.001	8.000	2.531	0.001	1.454	0.001	0.471	0.000	0.006	0.002
NO-2G47-5e-1	0.000	8.000	2.517	0.001	1.476	0.002	0.482	0.000	0.001	0.000
NO-2G47-5e-2	0.001	8.000	2.532	0.001	1.440	0.002	0.467	0.000	0.020	0.000
NO-2G47-5e-3	0.000	8.000	2.512	0.001	1.476	0.001	0.489	0.000	0.004	0.003
MM-71B-2a-1	0.001	8.000	2.625	0.000	1.369	0.000	0.374	0.000	0.001	0.003
MM-71B-2a-2	0.001	8.000	2.570	0.000	1.424	0.000	0.434	0.000	0.002	0.004
MM-71B-2a-3	0.001	8.000	2.582	0.000	1.407	0.000	0.423	0.000	0.001	0.004
MM-71B-2a-4	0.001	8.000	2.502	0.000	1.491	0.000	0.502	0.000	0.002	0.001
MM-71B-2a-5	0.001	8.000	2.488	0.000	1.503	0.000	0.511	0.000	0.003	0.002
MM-71B-2c-6	0.001	8.000	2.504	0.000	1.487	0.000	0.499	0.000	0.002	0.004
MM-71B-2c-7	0.001	8.000	2.483	0.001	1.508	0.000	0.515	0.000	0.004	0.001
MM-71B-2c-8	0.001	8.000	2.513	0.000	1.479	0.000	0.489	0.000	0.002	0.002
MM-71B-2d-1	0.001	8.000	2.610	0.000	1.387	0.000	0.380	0.000	0.001	0.003
MM-71B-2d-2	0.002	8.000	2.609	0.000	1.380	0.000	0.393	0.000	0.001	0.004
MM-71B-2d-3	0.001	8.000	2.601	0.000	1.389	0.002	0.398	0.000	0.003	0.003
MM-71B-2e-1	0.001	8.000	2.495	0.000	1.496	0.000	0.505	0.000	0.002	0.005
MM-71B-2e-2	0.001	8.000	2.554	0.000	1.442	0.000	0.443	0.000	0.001	0.002
MM-71B-2e-3	0.001	8.000	2.716	0.000	1.276	0.000	0.287	0.000	0.002	0.003
MM-71B-2f-1	0.001	8.000	2.537	0.000	1.456	0.000	0.470	0.000	0.000	0.004
MM-71B-2f-2	0.001	8.000	2.610	0.000	1.386	0.000	0.388	0.000	0.002	0.003
MM-71B-2f-3	0.002	8.000	2.621	0.000	1.371	0.000	0.373	0.000	0.006	0.003
MM-117-1a-1	0.001	8.000	2.361	0.000	1.633	0.000	0.639	0.000	0.002	0.001
MM-117-1a-2	0.001	8.000	2.392	0.000	1.597	0.000	0.618	0.000	0.001	0.002
MM-117-1a-3	0.001	8.000	2.404	0.000	1.586	0.000	0.608	0.000	0.000	0.000
MM-117-1a-4	0.000	8.000	2.332	0.000	1.658	0.001	0.668	0.000	0.004	0.001
MM-117-1b-6	0.000	8.000	2.328	0.000	1.660	0.000	0.682	0.000	0.001	0.002

Sample Data				**Norm oxygen**								
Analysis point	Na2O	K2O	Total	SiO2	TiO2	Al2O3	MgO	CaO	MnO	FeOt	SrO	BaO
NO-2G47-2c-3	0.519	0.000	5.010	5.013	0.000	2.224	0.000	0.494	0.001	0.004	0.003	0.000
NO-2G47-2d-1	0.516	0.001	5.009	5.009	0.000	2.232	0.000	0.494	0.000	0.002	0.004	0.000
NO-2G47-2d-2	0.512	0.001	5.004	5.012	0.008	2.220	0.001	0.494	0.000	0.007	0.001	0.000
NO-2G47-2d-3	0.501	0.001	5.005	4.987	0.002	2.249	0.000	0.503	0.001	0.004	0.002	0.000
NO-2G47-2e-1	0.516	0.000	5.006	5.018	0.002	2.225	0.000	0.494	0.000	0.001	0.002	0.000
NO-2G47-2e-2	0.521	0.001	5.013	5.003	0.001	2.235	0.000	0.497	0.000	0.002	0.000	0.000
NO-2G47-2e-3	0.515	0.002	5.012	5.001	0.003	2.228	0.000	0.501	0.000	0.006	0.002	0.001
NO-2G47-5a-1	0.533	0.001	5.007	5.053	0.002	2.193	0.001	0.480	0.000	0.004	0.000	0.000
NO-2G47-5a-4	0.531	0.004	5.006	5.049	0.002	2.200	0.001	0.475	0.000	0.005	0.000	0.000
NO-2G47-5a-7	0.538	0.002	5.007	5.056	0.002	2.197	0.000	0.468	0.000	0.006	0.001	0.000
NO-2G47-5a-10	0.535	0.002	5.004	5.064	0.002	2.189	0.000	0.468	0.000	0.007	0.002	0.000
NO-2G47-5a-13	0.528	0.001	5.008	5.035	0.002	2.212	0.000	0.483	0.000	0.003	0.001	0.001
NO-2G47-5b-17	0.537	0.001	5.007	5.053	0.002	2.198	0.000	0.474	0.000	0.004	0.000	0.000
NO-2G47-5b-18	0.530	0.001	5.003	5.057	0.002	2.190	0.001	0.476	0.000	0.007	0.001	0.001
NO-2G47-5b-19	0.535	0.002	5.006	5.058	0.002	2.189	0.000	0.473	0.000	0.009	0.000	0.000
NO-2G47-5c-21	0.539	0.000	5.010	5.049	0.000	2.202	0.000	0.474	0.000	0.005	0.001	0.000
NO-2G47-5c-22	0.521	0.001	5.000	5.043	0.002	2.210	0.000	0.478	0.000	0.005	0.000	0.001
NO-2G47-5d-1	0.506	0.002	5.010	4.992	0.000	2.238	0.001	0.509	0.000	0.004	0.002	0.000
NO-2G47-5d-2	0.505	0.001	5.007	4.994	0.001	2.244	0.000	0.503	0.000	0.002	0.003	0.000
NO-2G47-5d-3	0.541	0.002	5.009	5.063	0.001	2.181	0.001	0.471	0.000	0.009	0.002	0.000
NO-2G47-5e-1	0.528	0.001	5.008	5.033	0.003	2.214	0.002	0.482	0.000	0.002	0.000	0.000
NO-2G47-5e-2	0.547	0.002	5.011	5.063	0.002	2.161	0.002	0.467	0.000	0.030	0.000	0.000
NO-2G47-5e-3	0.519	0.001	5.007	5.025	0.002	2.214	0.001	0.489	0.000	0.006	0.003	0.000
MM-71B-2a-1	0.634	0.003	5.008	5.249	0.000	2.054	0.000	0.374	0.000	0.002	0.003	0.000
MM-71B-2a-2	0.566	0.002	5.002	5.140	0.000	2.136	0.000	0.434	0.000	0.002	0.004	0.000
MM-71B-2a-3	0.593	0.002	5.012	5.163	0.001	2.110	0.000	0.423	0.000	0.001	0.004	0.000
MM-71B-2a-4	0.507	0.002	5.006	5.005	0.000	2.236	0.000	0.502	0.000	0.002	0.001	0.000
MM-71B-2a-5	0.504	0.003	5.013	4.976	0.000	2.254	0.000	0.511	0.000	0.004	0.002	0.000
MM-71B-2c-6	0.509	0.003	5.007	5.008	0.000	2.231	0.000	0.499	0.000	0.002	0.004	0.000
MM-71B-2c-7	0.495	0.002	5.009	4.965	0.002	2.262	0.000	0.515	0.000	0.006	0.001	0.000
MM-71B-2c-8	0.520	0.002	5.007	5.027	0.000	2.219	0.000	0.489	0.000	0.003	0.002	0.000
MM-71B-2d-1	0.629	0.003	5.012	5.220	0.000	2.080	0.000	0.380	0.000	0.001	0.003	0.000
MM-71B-2d-2	0.623	0.003	5.013	5.218	0.001	2.070	0.000	0.393	0.000	0.001	0.004	0.000
MM-71B-2d-3	0.611	0.002	5.009	5.202	0.001	2.084	0.002	0.398	0.000	0.005	0.003	0.000
MM-71B-2e-1	0.502	0.003	5.008	4.990	0.000	2.245	0.000	0.505	0.000	0.002	0.005	0.000
MM-71B-2e-2	0.564	0.002	5.008	5.107	0.000	2.163	0.000	0.443	0.000	0.002	0.002	0.000
MM-71B-2e-3	0.719	0.002	5.006	5.432	0.000	1.914	0.000	0.287	0.000	0.004	0.003	0.000
MM-71B-2f-1	0.537	0.001	5.005	5.073	0.000	2.183	0.000	0.470	0.000	0.000	0.004	0.000
MM-71B-2f-2	0.612	0.003	5.003	5.221	0.000	2.078	0.000	0.388	0.000	0.003	0.003	0.000
MM-71B-2f-3	0.627	0.004	5.006	5.242	0.000	2.057	0.000	0.373	0.000	0.009	0.003	0.000
MM-117-1a-1	0.368	0.001	5.007	4.721	0.000	2.450	0.000	0.639	0.000	0.003	0.001	0.000
MM-117-1a-2	0.391	0.001	5.004	4.784	0.001	2.396	0.000	0.618	0.000	0.002	0.002	0.000
MM-117-1a-3	0.405	0.002	5.006	4.809	0.000	2.379	0.000	0.608	0.000	0.000	0.000	0.000
MM-117-1a-4	0.343	0.001	5.008	4.665	0.000	2.487	0.001	0.668	0.000	0.006	0.001	0.000
MM-117-1b-6	0.333	0.000	5.008	4.657	0.000	2.490	0.000	0.682	0.000	0.002	0.002	0.000

Sample Data			**End Member**		
Analysis point	Na2O	K2O	Anorthite	Albite	Orthoclase
NO-2G47-2c-3	0.260	0.000	48.7	51.2	0.0
NO-2G47-2d-1	0.258	0.001	48.9	51.0	0.1
NO-2G47-2d-2	0.256	0.001	49.1	50.8	0.1
NO-2G47-2d-3	0.251	0.001	50.0	49.9	0.1
NO-2G47-2e-1	0.258	0.000	48.9	51.1	0.0
NO-2G47-2e-2	0.261	0.000	48.8	51.1	0.1
NO-2G47-2e-3	0.258	0.001	49.2	50.6	0.2
NO-2G47-5a-1	0.267	0.000	47.3	52.6	0.1
NO-2G47-5a-4	0.265	0.002	47.1	52.6	0.3
NO-2G47-5a-7	0.269	0.001	46.4	53.3	0.2
NO-2G47-5a-10	0.268	0.001	46.6	53.2	0.2
NO-2G47-5a-13	0.264	0.000	47.8	52.2	0.1
NO-2G47-5b-17	0.268	0.001	46.9	53.0	0.1
NO-2G47-5b-18	0.265	0.000	47.3	52.7	0.1
NO-2G47-5b-19	0.267	0.001	46.9	53.0	0.2
NO-2G47-5c-21	0.270	0.000	46.7	53.2	0.0
NO-2G47-5c-22	0.261	0.001	47.8	52.1	0.1
NO-2G47-5d-1	0.253	0.001	50.1	49.8	0.2
NO-2G47-5d-2	0.252	0.000	49.9	50.0	0.1
NO-2G47-5d-3	0.270	0.001	46.4	53.3	0.2
NO-2G47-5e-1	0.264	0.000	47.6	52.3	0.1
NO-2G47-5e-2	0.274	0.001	45.9	53.9	0.2
NO-2G47-5e-3	0.260	0.000	48.4	51.5	0.1
MM-71B-2a-1	0.317	0.001	37.0	62.7	0.3
MM-71B-2a-2	0.283	0.001	43.3	56.5	0.2
MM-71B-2a-3	0.296	0.001	41.5	58.2	0.2
MM-71B-2a-4	0.253	0.001	49.7	50.2	0.2
MM-71B-2a-5	0.252	0.001	50.2	49.5	0.3
MM-71B-2c-6	0.254	0.001	49.4	50.4	0.3
MM-71B-2c-7	0.247	0.001	50.9	48.9	0.2
MM-71B-2c-8	0.260	0.001	48.4	51.5	0.2
MM-71B-2d-1	0.314	0.001	37.6	62.1	0.3
MM-71B-2d-2	0.312	0.002	38.5	61.1	0.3
MM-71B-2d-3	0.305	0.001	39.3	60.4	0.2
MM-71B-2e-1	0.251	0.001	50.0	49.7	0.3
MM-71B-2e-2	0.282	0.001	43.9	55.9	0.2
MM-71B-2e-3	0.360	0.001	28.5	71.3	0.2
MM-71B-2f-1	0.269	0.001	46.6	53.3	0.1
MM-71B-2f-2	0.306	0.001	38.7	61.0	0.3
MM-71B-2f-3	0.313	0.002	37.1	62.5	0.4
MM-117-1a-1	0.184	0.001	63.4	36.5	0.1
MM-117-1a-2	0.196	0.001	61.2	38.7	0.1
MM-117-1a-3	0.202	0.001	59.9	39.9	0.2
MM-117-1a-4	0.171	0.000	66.1	33.9	0.1
MM-117-1b-6	0.166	0.000	67.2	32.8	0.0

Sample Data				**Mole Cation**					
Analysis point	Intrusion/Phase	Sample	Mineral	SiO2	TiO2	Al2O3	MgO	CaO	MnO
MM-117-1b-7	Butler West	MM-117-1	Feldspar	0.826	0.000	0.632	0.000	0.268	0.000
MM-117-1c-9	Butler West	MM-117-1	Feldspar	0.859	0.000	0.593	0.000	0.238	0.000
MM-117-1c-10	Butler West	MM-117-1	Feldspar	0.854	0.000	0.597	0.001	0.239	0.000
MM-117-1d-1	Butler West	MM-117-1	Feldspar	0.855	0.000	0.605	0.000	0.243	0.000
MM-117-1d-2	Butler West	MM-117-1	Feldspar	0.867	0.000	0.600	0.000	0.235	0.000
MM-117-1d-3	Butler West	MM-117-1	Feldspar	0.856	0.000	0.601	0.000	0.239	0.000
MM-117-1e-1	Butler West	MM-117-1	Feldspar	0.876	0.000	0.593	0.000	0.226	0.000
MM-117-1e-2	Butler West	MM-117-1	Feldspar	0.852	0.000	0.598	0.000	0.245	0.000
MM-117-1e-3	Butler West	MM-117-1	Feldspar	0.854	0.000	0.604	0.000	0.246	0.000
MM-117-6a-1	Butler West	MM-117-6	Feldspar	0.857	0.000	0.606	0.000	0.245	0.000
MM-117-6b-3	Butler West	MM-117-6	Feldspar	0.887	0.000	0.586	0.000	0.217	0.000
MM-117-6b-2	Butler West	MM-117-6	Feldspar	0.878	0.001	0.582	0.001	0.221	0.000
MM-117-6c-5	Butler West	MM-117-6	Feldspar	0.881	0.000	0.582	0.000	0.221	0.000
MM-117-6c-6	Butler West	MM-117-6	Feldspar	0.876	0.000	0.589	0.000	0.228	0.000
MM-117-6c-7	Butler West	MM-117-6	Feldspar	0.882	0.000	0.583	0.000	0.225	0.000
MM-117-6d-1	Butler West	MM-117-6	Feldspar	0.881	0.000	0.583	0.000	0.221	0.000
MM-117-6d-2	Butler West	MM-117-6	Feldspar	0.880	0.000	0.579	0.000	0.221	0.000
MM-117-6d-3	Butler West	MM-117-6	Feldspar	0.879	0.000	0.582	0.000	0.223	0.000
MM-117-6e-1	Butler West	MM-117-6	Feldspar	0.878	0.000	0.578	0.000	0.220	0.000
MM-117-6e-2	Butler West	MM-117-6	Feldspar	0.871	0.000	0.590	0.000	0.226	0.000
MM-117-6e-3	Butler West	MM-117-6	Feldspar	0.883	0.000	0.579	0.000	0.220	0.000
MM-117-6f-1	Butler West	MM-117-6	Feldspar	0.857	0.001	0.596	0.000	0.237	0.000
MM-117-6f-2	Butler West	MM-117-6	Feldspar	0.863	0.000	0.595	0.000	0.239	0.000
MM-117-6f-3	Butler West	MM-117-6	Feldspar	0.881	0.000	0.581	0.000	0.220	0.000
MM-70-2a-1	Butler East	MM-70-2	Feldspar	0.896	0.000	0.570	0.000	0.208	0.000
MM-70-2a-2	Butler East	MM-70-2	Feldspar	0.899	0.001	0.566	0.000	0.203	0.000
MM-70-2a-3	Butler East	MM-70-2	Feldspar	0.917	0.000	0.554	0.000	0.193	0.000
MM-70-2a-4	Butler East	MM-70-2	Feldspar	0.901	0.000	0.563	0.000	0.200	0.000
MM-70-2b-9	Butler East	MM-70-2	Feldspar	0.850	0.000	0.610	0.000	0.250	0.000
MM-70-2b-10	Butler East	MM-70-2	Feldspar	0.901	0.000	0.570	0.000	0.206	0.000
MM-70-2b-11	Butler East	MM-70-2	Feldspar	0.898	0.000	0.567	0.000	0.206	0.000
MM-70-2c-14	Butler East	MM-70-2	Feldspar	0.905	0.000	0.567	0.000	0.201	0.000
MM-70-2c-15	Butler East	MM-70-2	Feldspar	0.899	0.000	0.563	0.000	0.206	0.000
MM-70-2c-16	Butler East	MM-70-2	Feldspar	0.876	0.000	0.595	0.000	0.226	0.000
MM-70-2d-1	Butler East	MM-70-2	Feldspar	0.902	0.000	0.566	0.000	0.200	0.000
MM-70-2d-2	Butler East	MM-70-2	Feldspar	0.899	0.000	0.573	0.001	0.208	0.000
MM-70-2d-3	Butler East	MM-70-2	Feldspar	0.888	0.000	0.582	0.000	0.219	0.000
MM-70-2e-1	Butler East	MM-70-2	Feldspar	0.893	0.000	0.570	0.000	0.211	0.000
MM-70-2e-2	Butler East	MM-70-2	Feldspar	0.907	0.000	0.564	0.000	0.201	0.000
MM-70-2e-3	Butler East	MM-70-2	Feldspar	0.892	0.000	0.578	0.000	0.220	0.000
MM-70-2f-1	Butler East	MM-70-2	Feldspar	0.798	0.000	0.655	0.000	0.295	0.000
MM-70-2f-2	Butler East	MM-70-2	Feldspar	0.904	0.000	0.569	0.000	0.208	0.000
MM-70-2f-3	Butler East	MM-70-2	Feldspar	0.899	0.000	0.570	0.000	0.208	0.000
MM-V1-2a-1	Butler West	MM-V1-2	Feldspar	0.892	0.001	0.576	0.000	0.217	0.000
MM-V1-2a-2	Butler West	MM-V1-2	Feldspar	0.890	0.000	0.579	0.000	0.219	0.000

Sample Data							**Mole oxygen**					
Analysis point	FeOt	SrO	BaO	Na2O	K2O	Total	SiO2	TiO2	Al2O3	MgO	CaO	MnO
MM-117-1b-7	0.001	0.000	0.000	0.094	0.000	1.823	1.653	0.000	0.947	0.000	0.268	0.000
MM-117-1c-9	0.001	0.000	0.000	0.132	0.001	1.824	1.717	0.000	0.890	0.000	0.238	0.000
MM-117-1c-10	0.002	0.000	0.000	0.128	0.000	1.822	1.708	0.000	0.896	0.001	0.239	0.000
MM-117-1d-1	0.000	0.000	0.000	0.127	0.001	1.832	1.711	0.000	0.907	0.000	0.243	0.000
MM-117-1d-2	0.000	0.000	0.000	0.134	0.001	1.837	1.733	0.000	0.899	0.000	0.235	0.000
MM-117-1d-3	0.001	0.001	0.000	0.126	0.004	1.829	1.712	0.000	0.902	0.000	0.239	0.000
MM-117-1e-1	0.000	0.000	0.000	0.144	0.001	1.841	1.752	0.001	0.890	0.000	0.226	0.000
MM-117-1e-2	0.001	0.001	0.000	0.124	0.000	1.821	1.704	0.001	0.896	0.000	0.245	0.000
MM-117-1e-3	0.000	0.001	0.000	0.124	0.000	1.828	1.708	0.000	0.905	0.000	0.246	0.000
MM-117-6a-1	0.001	0.001	0.000	0.123	0.001	1.833	1.715	0.000	0.909	0.000	0.245	0.000
MM-117-6b-3	0.001	0.001	0.000	0.154	0.001	1.848	1.774	0.001	0.879	0.000	0.217	0.000
MM-117-6b-2	0.003	0.001	0.000	0.150	0.001	1.837	1.756	0.001	0.873	0.001	0.221	0.000
MM-117-6c-5	0.000	0.001	0.000	0.151	0.001	1.836	1.761	0.000	0.873	0.000	0.221	0.000
MM-117-6c-6	0.001	0.000	0.000	0.147	0.001	1.842	1.752	0.000	0.884	0.000	0.228	0.000
MM-117-6c-7	0.002	0.000	0.000	0.149	0.001	1.841	1.763	0.000	0.875	0.000	0.225	0.000
MM-117-6d-1	0.002	0.001	0.000	0.150	0.001	1.838	1.762	0.000	0.874	0.000	0.221	0.000
MM-117-6d-2	0.001	0.001	0.000	0.150	0.001	1.834	1.761	0.001	0.869	0.000	0.221	0.000
MM-117-6d-3	0.001	0.002	0.000	0.151	0.001	1.838	1.758	0.000	0.873	0.000	0.223	0.000
MM-117-6e-1	0.001	0.000	0.000	0.150	0.001	1.828	1.755	0.000	0.868	0.000	0.220	0.000
MM-117-6e-2	0.002	0.001	0.000	0.143	0.001	1.834	1.743	0.001	0.884	0.000	0.226	0.000
MM-117-6e-3	0.001	0.000	0.000	0.151	0.001	1.835	1.765	0.000	0.869	0.000	0.220	0.000
MM-117-6f-1	0.002	0.000	0.000	0.133	0.001	1.827	1.715	0.001	0.894	0.000	0.237	0.000
MM-117-6f-2	0.001	0.000	0.000	0.132	0.001	1.830	1.725	0.001	0.893	0.000	0.239	0.000
MM-117-6f-3	0.001	0.001	0.000	0.151	0.000	1.835	1.761	0.000	0.871	0.000	0.220	0.000
MM-70-2a-1	0.000	0.000	0.000	0.166	0.001	1.841	1.792	0.000	0.854	0.000	0.208	0.000
MM-70-2a-2	0.002	0.000	0.000	0.169	0.001	1.842	1.799	0.002	0.849	0.000	0.203	0.000
MM-70-2a-3	0.001	0.001	0.000	0.181	0.001	1.846	1.834	0.000	0.831	0.000	0.193	0.000
MM-70-2a-4	0.001	0.001	0.000	0.174	0.001	1.841	1.803	0.001	0.844	0.000	0.200	0.000
MM-70-2b-9	0.001	0.000	0.000	0.121	0.000	1.833	1.699	0.000	0.914	0.000	0.250	0.000
MM-70-2b-10	0.001	0.001	0.000	0.168	0.000	1.847	1.803	0.000	0.855	0.000	0.206	0.000
MM-70-2b-11	0.002	0.001	0.000	0.167	0.001	1.843	1.796	0.001	0.851	0.000	0.206	0.000
MM-70-2c-14	0.001	0.000	0.000	0.174	0.001	1.850	1.811	0.000	0.851	0.000	0.201	0.000
MM-70-2c-15	0.000	0.000	0.000	0.170	0.001	1.839	1.799	0.000	0.845	0.000	0.206	0.000
MM-70-2c-16	0.001	0.000	0.000	0.147	0.001	1.847	1.753	0.001	0.892	0.000	0.226	0.000
MM-70-2d-1	0.001	0.000	0.000	0.172	0.001	1.842	1.804	0.000	0.849	0.000	0.200	0.000
MM-70-2d-2	0.003	0.000	0.000	0.163	0.001	1.849	1.799	0.001	0.860	0.001	0.208	0.000
MM-70-2d-3	0.002	0.000	0.000	0.153	0.001	1.845	1.775	0.000	0.873	0.000	0.219	0.000
MM-70-2e-1	0.000	0.001	0.000	0.163	0.001	1.838	1.785	0.000	0.854	0.000	0.211	0.000
MM-70-2e-2	0.001	0.001	0.000	0.170	0.001	1.845	1.814	0.000	0.845	0.000	0.201	0.000
MM-70-2e-3	0.002	0.001	0.000	0.157	0.001	1.849	1.783	0.000	0.867	0.000	0.220	0.000
MM-70-2f-1	0.001	0.000	0.000	0.068	0.000	1.817	1.596	0.000	0.982	0.000	0.295	0.000
MM-70-2f-2	0.001	0.000	0.000	0.164	0.001	1.847	1.808	0.000	0.853	0.000	0.208	0.000
MM-70-2f-3	0.001	0.000	0.000	0.163	0.001	1.843	1.798	0.000	0.855	0.000	0.208	0.000
MM-V1-2a-1	0.003	0.000	0.000	0.158	0.000	1.848	1.785	0.002	0.865	0.000	0.217	0.000
MM-V1-2a-2	0.001	0.001	0.000	0.157	0.000	1.846	1.780	0.000	0.868	0.000	0.219	0.000

Sample Data							**Norm Cations**					
Analysis point	FeOt	SrO	BaO	Na2O	K2O	Total	SiO2	TiO2	Al2O3	MgO	CaO	MnO
MM-117-1b-7	0.002	0.000	0.000	0.047	0.000	2.919	2.265	0.001	1.731	0.001	0.735	0.001
MM-117-1c-9	0.001	0.000	0.000	0.066	0.000	2.914	2.358	0.000	1.629	0.000	0.655	0.000
MM-117-1c-10	0.003	0.000	0.000	0.064	0.000	2.911	2.346	0.000	1.641	0.004	0.656	0.000
MM-117-1d-1	0.000	0.000	0.000	0.064	0.000	2.926	2.339	0.000	1.653	0.001	0.664	0.000
MM-117-1d-2	0.000	0.000	0.000	0.067	0.000	2.936	2.361	0.000	1.633	0.000	0.642	0.000
MM-117-1d-3	0.001	0.001	0.000	0.063	0.002	2.921	2.345	0.000	1.647	0.000	0.655	0.000
MM-117-1e-1	0.001	0.000	0.000	0.072	0.000	2.942	2.383	0.001	1.613	0.000	0.615	0.000
MM-117-1e-2	0.001	0.001	0.000	0.062	0.000	2.910	2.342	0.001	1.643	0.000	0.675	0.000
MM-117-1e-3	0.001	0.001	0.000	0.062	0.000	2.923	2.338	0.000	1.652	0.000	0.672	0.000
MM-117-6a-1	0.001	0.001	0.000	0.062	0.000	2.932	2.339	0.000	1.653	0.000	0.669	0.000
MM-117-6b-3	0.002	0.001	0.000	0.077	0.000	2.952	2.404	0.001	1.588	0.000	0.589	0.001
MM-117-6b-2	0.005	0.001	0.000	0.075	0.000	2.933	2.395	0.001	1.587	0.002	0.604	0.000
MM-117-6c-5	0.001	0.001	0.000	0.075	0.000	2.932	2.402	0.000	1.588	0.000	0.602	0.000
MM-117-6c-6	0.001	0.000	0.000	0.073	0.000	2.939	2.384	0.000	1.604	0.000	0.621	0.000
MM-117-6c-7	0.003	0.000	0.000	0.074	0.000	2.941	2.398	0.000	1.587	0.000	0.611	0.000
MM-117-6d-1	0.002	0.001	0.000	0.075	0.000	2.936	2.400	0.000	1.588	0.000	0.603	0.000
MM-117-6d-2	0.001	0.001	0.000	0.075	0.000	2.929	2.405	0.001	1.582	0.001	0.604	0.000
MM-117-6d-3	0.001	0.002	0.000	0.075	0.000	2.933	2.397	0.000	1.588	0.000	0.609	0.000
MM-117-6e-1	0.001	0.000	0.000	0.075	0.000	2.919	2.405	0.000	1.585	0.000	0.603	0.000
MM-117-6e-2	0.003	0.001	0.000	0.072	0.000	2.930	2.380	0.001	1.610	0.000	0.617	0.000
MM-117-6e-3	0.001	0.000	0.000	0.076	0.000	2.932	2.409	0.000	1.580	0.000	0.600	0.001
MM-117-6f-1	0.002	0.000	0.000	0.066	0.000	2.917	2.351	0.002	1.635	0.000	0.650	0.000
MM-117-6f-2	0.001	0.000	0.000	0.066	0.000	2.925	2.359	0.001	1.628	0.000	0.653	0.000
MM-117-6f-3	0.001	0.001	0.000	0.076	0.000	2.930	2.404	0.000	1.586	0.000	0.600	0.000
MM-70-2a-1	0.000	0.000	0.000	0.083	0.000	2.938	2.439	0.000	1.551	0.000	0.566	0.000
MM-70-2a-2	0.003	0.000	0.000	0.085	0.000	2.941	2.446	0.002	1.540	0.000	0.553	0.001
MM-70-2a-3	0.001	0.001	0.000	0.090	0.000	2.950	2.487	0.000	1.502	0.000	0.522	0.000
MM-70-2a-4	0.002	0.001	0.000	0.087	0.000	2.937	2.455	0.001	1.533	0.000	0.545	0.000
MM-70-2b-9	0.002	0.000	0.000	0.061	0.000	2.927	2.322	0.000	1.666	0.000	0.684	0.000
MM-70-2b-10	0.001	0.001	0.000	0.084	0.000	2.949	2.445	0.000	1.546	0.000	0.557	0.000
MM-70-2b-11	0.002	0.001	0.000	0.084	0.000	2.941	2.442	0.001	1.543	0.000	0.561	0.000
MM-70-2c-14	0.001	0.000	0.000	0.087	0.001	2.952	2.454	0.000	1.537	0.000	0.546	0.000
MM-70-2c-15	0.001	0.000	0.000	0.085	0.000	2.936	2.451	0.000	1.535	0.000	0.562	0.000
MM-70-2c-16	0.002	0.000	0.000	0.073	0.000	2.948	2.378	0.001	1.614	0.000	0.614	0.000
MM-70-2d-1	0.002	0.000	0.000	0.086	0.000	2.941	2.453	0.000	1.539	0.000	0.544	0.000
MM-70-2d-2	0.004	0.000	0.000	0.082	0.000	2.954	2.435	0.001	1.552	0.002	0.563	0.000
MM-70-2d-3	0.004	0.000	0.000	0.077	0.000	2.948	2.409	0.000	1.579	0.000	0.594	0.000
MM-70-2e-1	0.001	0.001	0.000	0.081	0.000	2.934	2.434	0.000	1.553	0.000	0.576	0.000
MM-70-2e-2	0.002	0.001	0.000	0.085	0.001	2.949	2.460	0.000	1.529	0.001	0.545	0.000
MM-70-2e-3	0.003	0.001	0.000	0.078	0.000	2.952	2.416	0.000	1.566	0.000	0.595	0.000
MM-70-2f-1	0.001	0.000	0.000	0.034	0.000	2.909	2.195	0.000	1.801	0.000	0.812	0.000
MM-70-2f-2	0.001	0.000	0.000	0.082	0.000	2.953	2.449	0.000	1.541	0.001	0.563	0.000
MM-70-2f-3	0.001	0.000	0.000	0.081	0.000	2.946	2.441	0.001	1.549	0.001	0.566	0.000
MM-V1-2a-1	0.004	0.000	0.000	0.079	0.000	2.952	2.418	0.003	1.562	0.000	0.588	0.000
MM-V1-2a-2	0.001	0.001	0.000	0.078	0.000	2.947	2.415	0.000	1.571	0.000	0.595	0.000

Sample Data						**Norm Oxygen**								
Analysis point	SrO	BaO	Na2O	K2O	Total	SiO2	TiO2	Al2O3	MgO	CaO	MnO	FeOt	SrO	BaO
MM-117-1b-7	0.000	0.000	0.259	0.001	4.997	4.530	0.001	2.597	0.001	0.735	0.001	0.005	0.000	0.000
MM-117-1c-9	0.001	0.000	0.362	0.002	5.009	4.715	0.001	2.444	0.000	0.655	0.000	0.002	0.001	0.000
MM-117-1c-10	0.001	0.000	0.353	0.001	5.008	4.693	0.000	2.462	0.004	0.656	0.000	0.007	0.001	0.000
MM-117-1d-1	0.000	0.000	0.349	0.002	5.009	4.678	0.000	2.480	0.001	0.664	0.000	0.001	0.000	0.000
MM-117-1d-2	0.000	0.001	0.365	0.003	5.005	4.723	0.001	2.450	0.000	0.642	0.000	0.000	0.000	0.001
MM-117-1d-3	0.004	0.001	0.346	0.012	5.010	4.690	0.000	2.470	0.000	0.655	0.000	0.002	0.004	0.001
MM-117-1e-1	0.000	0.000	0.393	0.002	5.007	4.765	0.001	2.419	0.000	0.615	0.000	0.002	0.000	0.000
MM-117-1e-2	0.002	0.000	0.341	0.001	5.006	4.684	0.001	2.465	0.000	0.675	0.000	0.002	0.002	0.000
MM-117-1e-3	0.002	0.000	0.338	0.000	5.005	4.676	0.000	2.478	0.000	0.672	0.000	0.002	0.002	0.000
MM-117-6a-1	0.002	0.000	0.336	0.002	5.002	4.678	0.000	2.480	0.000	0.669	0.000	0.003	0.002	0.000
MM-117-6b-3	0.003	0.000	0.417	0.002	5.009	4.808	0.002	2.382	0.000	0.589	0.001	0.006	0.003	0.000
MM-117-6b-2	0.002	0.000	0.408	0.002	5.010	4.789	0.003	2.381	0.002	0.604	0.000	0.014	0.002	0.000
MM-117-6c-5	0.003	0.000	0.411	0.002	5.009	4.805	0.000	2.382	0.000	0.602	0.000	0.002	0.003	0.000
MM-117-6c-6	0.000	0.000	0.400	0.002	5.013	4.768	0.001	2.406	0.000	0.621	0.000	0.003	0.000	0.000
MM-117-6c-7	0.000	0.000	0.404	0.002	5.009	4.796	0.000	2.381	0.000	0.611	0.000	0.009	0.000	0.000
MM-117-6d-1	0.002	0.000	0.409	0.002	5.008	4.801	0.001	2.382	0.000	0.603	0.000	0.007	0.002	0.000
MM-117-6d-2	0.004	0.000	0.409	0.001	5.008	4.809	0.002	2.373	0.001	0.604	0.000	0.002	0.004	0.000
MM-117-6d-3	0.004	0.000	0.411	0.002	5.013	4.795	0.001	2.381	0.000	0.609	0.000	0.004	0.004	0.000
MM-117-6e-1	0.000	0.000	0.412	0.002	5.009	4.810	0.000	2.378	0.000	0.603	0.000	0.003	0.000	0.000
MM-117-6e-2	0.002	0.000	0.391	0.002	5.008	4.759	0.001	2.415	0.000	0.617	0.000	0.009	0.002	0.000
MM-117-6e-3	0.001	0.000	0.413	0.002	5.008	4.817	0.000	2.370	0.000	0.600	0.001	0.003	0.001	0.000
MM-117-6f-1	0.001	0.000	0.364	0.003	5.011	4.703	0.003	2.452	0.000	0.650	0.000	0.007	0.001	0.000
MM-117-6f-2	0.001	0.000	0.360	0.002	5.005	4.719	0.002	2.441	0.000	0.653	0.000	0.003	0.001	0.000
MM-117-6f-3	0.001	0.000	0.413	0.001	5.008	4.809	0.000	2.378	0.000	0.600	0.000	0.004	0.001	0.000
MM-70-2a-1	0.000	0.000	0.452	0.002	5.012	4.878	0.000	2.327	0.000	0.566	0.000	0.001	0.000	0.000
MM-70-2a-2	0.000	0.000	0.461	0.003	5.011	4.892	0.005	2.310	0.000	0.553	0.001	0.008	0.000	0.000
MM-70-2a-3	0.002	0.000	0.490	0.002	5.007	4.974	0.000	2.253	0.000	0.522	0.000	0.002	0.002	0.000
MM-70-2a-4	0.002	0.000	0.474	0.002	5.014	4.911	0.001	2.299	0.000	0.545	0.000	0.004	0.002	0.000
MM-70-2b-9	0.001	0.000	0.332	0.001	5.009	4.645	0.001	2.499	0.000	0.684	0.000	0.005	0.001	0.000
MM-70-2b-10	0.003	0.000	0.456	0.001	5.010	4.890	0.000	2.319	0.000	0.557	0.000	0.002	0.003	0.000
MM-70-2b-11	0.003	0.000	0.455	0.003	5.013	4.884	0.001	2.314	0.000	0.561	0.000	0.006	0.003	0.000
MM-70-2c-14	0.000	0.000	0.470	0.003	5.013	4.908	0.000	2.306	0.000	0.546	0.000	0.003	0.000	0.000
MM-70-2c-15	0.000	0.000	0.462	0.002	5.013	4.902	0.000	2.302	0.000	0.562	0.000	0.001	0.000	0.000
MM-70-2c-16	0.000	0.000	0.398	0.002	5.012	4.757	0.001	2.422	0.000	0.614	0.000	0.005	0.000	0.000
MM-70-2d-1	0.000	0.000	0.468	0.002	5.011	4.907	0.000	2.309	0.000	0.544	0.000	0.005	0.000	0.000
MM-70-2d-2	0.001	0.000	0.442	0.002	5.006	4.871	0.002	2.328	0.002	0.563	0.000	0.011	0.001	0.000
MM-70-2d-3	0.000	0.000	0.416	0.002	5.007	4.819	0.001	2.368	0.000	0.594	0.000	0.010	0.000	0.000
MM-70-2e-1	0.002	0.000	0.444	0.002	5.012	4.867	0.000	2.330	0.000	0.576	0.000	0.002	0.002	0.000
MM-70-2e-2	0.002	0.000	0.462	0.003	5.006	4.921	0.000	2.293	0.001	0.545	0.000	0.005	0.002	0.000
MM-70-2e-3	0.002	0.000	0.425	0.002	5.012	4.833	0.000	2.349	0.000	0.595	0.000	0.007	0.002	0.000
MM-70-2f-1	0.000	0.000	0.187	0.000	4.997	4.390	0.000	2.701	0.000	0.812	0.000	0.003	0.000	0.000
MM-70-2f-2	0.000	0.000	0.445	0.002	5.003	4.897	0.000	2.311	0.001	0.563	0.000	0.004	0.000	0.000
MM-70-2f-3	0.000	0.001	0.442	0.003	5.005	4.882	0.001	2.323	0.001	0.566	0.000	0.004	0.000	0.001
MM-V1-2a-1	0.000	0.000	0.427	0.001	5.008	4.837	0.006	2.343	0.000	0.588	0.000	0.012	0.000	0.000
MM-V1-2a-2	0.002	0.000	0.425	0.001	5.011	4.830	0.001	2.356	0.000	0.595	0.000	0.003	0.002	0.000

Sample Data			**Atom units**							
Analysis point	K2O	Total	SiO2	TiO2	Al2O3	MgO	CaO	MnO	FeOt	SrO
MM-117-1b-7	0.001	8.000	2.265	0.001	1.731	0.001	0.735	0.001	0.003	0.000
MM-117-1c-9	0.001	8.000	2.358	0.000	1.629	0.000	0.655	0.000	0.001	0.001
MM-117-1c-10	0.001	8.000	2.346	0.000	1.641	0.004	0.656	0.000	0.005	0.001
MM-117-1d-1	0.001	8.000	2.339	0.000	1.653	0.001	0.664	0.000	0.001	0.000
MM-117-1d-2	0.001	8.000	2.361	0.000	1.633	0.000	0.642	0.000	0.000	0.000
MM-117-1d-3	0.006	8.000	2.345	0.000	1.647	0.000	0.655	0.000	0.001	0.004
MM-117-1e-1	0.001	8.000	2.383	0.001	1.613	0.000	0.615	0.000	0.001	0.000
MM-117-1e-2	0.000	8.000	2.342	0.001	1.643	0.000	0.675	0.000	0.001	0.002
MM-117-1e-3	0.000	8.000	2.338	0.000	1.652	0.000	0.672	0.000	0.001	0.002
MM-117-6a-1	0.001	8.000	2.339	0.000	1.653	0.000	0.669	0.000	0.002	0.002
MM-117-6b-3	0.001	8.000	2.404	0.001	1.588	0.000	0.589	0.001	0.004	0.003
MM-117-6b-2	0.001	8.000	2.395	0.001	1.587	0.002	0.604	0.000	0.009	0.002
MM-117-6c-5	0.001	8.000	2.402	0.000	1.588	0.000	0.602	0.000	0.001	0.003
MM-117-6c-6	0.001	8.000	2.384	0.000	1.604	0.000	0.621	0.000	0.002	0.000
MM-117-6c-7	0.001	8.000	2.398	0.000	1.587	0.000	0.611	0.000	0.006	0.000
MM-117-6d-1	0.001	8.000	2.400	0.000	1.588	0.000	0.603	0.000	0.004	0.002
MM-117-6d-2	0.001	8.000	2.405	0.001	1.582	0.001	0.604	0.000	0.001	0.004
MM-117-6d-3	0.001	8.000	2.397	0.000	1.588	0.000	0.609	0.000	0.002	0.004
MM-117-6e-1	0.001	8.000	2.405	0.000	1.585	0.000	0.603	0.000	0.002	0.000
MM-117-6e-2	0.001	8.000	2.380	0.001	1.610	0.000	0.617	0.000	0.006	0.002
MM-117-6e-3	0.001	8.000	2.409	0.000	1.580	0.000	0.600	0.001	0.002	0.001
MM-117-6f-1	0.001	8.000	2.351	0.002	1.635	0.000	0.650	0.000	0.005	0.001
MM-117-6f-2	0.001	8.000	2.359	0.001	1.628	0.000	0.653	0.000	0.002	0.001
MM-117-6f-3	0.001	8.000	2.404	0.000	1.586	0.000	0.600	0.000	0.003	0.001
MM-70-2a-1	0.001	8.000	2.439	0.000	1.551	0.000	0.566	0.000	0.001	0.000
MM-70-2a-2	0.001	8.000	2.446	0.002	1.540	0.000	0.553	0.001	0.005	0.000
MM-70-2a-3	0.001	8.000	2.487	0.000	1.502	0.000	0.522	0.000	0.001	0.002
MM-70-2a-4	0.001	8.000	2.455	0.001	1.533	0.000	0.545	0.000	0.003	0.002
MM-70-2b-9	0.000	8.000	2.322	0.000	1.666	0.000	0.684	0.000	0.003	0.001
MM-70-2b-10	0.001	8.000	2.445	0.000	1.546	0.000	0.557	0.000	0.001	0.003
MM-70-2b-11	0.001	8.000	2.442	0.001	1.543	0.000	0.561	0.000	0.004	0.003
MM-70-2c-14	0.001	8.000	2.454	0.000	1.537	0.000	0.546	0.000	0.002	0.000
MM-70-2c-15	0.001	8.000	2.451	0.000	1.535	0.000	0.562	0.000	0.001	0.000
MM-70-2c-16	0.001	8.000	2.378	0.001	1.614	0.000	0.614	0.000	0.003	0.000
MM-70-2d-1	0.001	8.000	2.453	0.000	1.539	0.000	0.544	0.000	0.003	0.000
MM-70-2d-2	0.001	8.000	2.435	0.001	1.552	0.002	0.563	0.000	0.007	0.001
MM-70-2d-3	0.001	8.000	2.409	0.000	1.579	0.000	0.594	0.000	0.006	0.000
MM-70-2e-1	0.001	8.000	2.434	0.000	1.553	0.000	0.576	0.000	0.001	0.002
MM-70-2e-2	0.002	8.000	2.460	0.000	1.529	0.001	0.545	0.000	0.004	0.002
MM-70-2e-3	0.001	8.000	2.416	0.000	1.566	0.000	0.595	0.000	0.005	0.002
MM-70-2f-1	0.000	8.000	2.195	0.000	1.801	0.000	0.812	0.000	0.002	0.000
MM-70-2f-2	0.001	8.000	2.449	0.000	1.541	0.001	0.563	0.000	0.002	0.000
MM-70-2f-3	0.001	8.000	2.441	0.001	1.549	0.001	0.566	0.000	0.002	0.000
MM-V1-2a-1	0.001	8.000	2.418	0.003	1.562	0.000	0.588	0.000	0.008	0.000
MM-V1-2a-2	0.000	8.000	2.415	0.000	1.571	0.000	0.595	0.000	0.002	0.002

Sample Data				**Norm oxygen**								
Analysis point	Na2O	K2O	Total	SiO2	TiO2	Al2O3	MgO	CaO	MnO	FeOt	SrO	BaO
MM-117-1b-7	0.259	0.001	4.997	4.530	0.001	2.597	0.001	0.735	0.001	0.005	0.000	0.000
MM-117-1c-9	0.362	0.002	5.009	4.715	0.001	2.444	0.000	0.655	0.000	0.002	0.001	0.000
MM-117-1c-10	0.353	0.001	5.008	4.693	0.000	2.462	0.004	0.656	0.000	0.007	0.001	0.000
MM-117-1d-1	0.349	0.002	5.009	4.678	0.000	2.480	0.001	0.664	0.000	0.001	0.000	0.000
MM-117-1d-2	0.365	0.003	5.005	4.723	0.001	2.450	0.000	0.642	0.000	0.000	0.000	0.001
MM-117-1d-3	0.346	0.012	5.010	4.690	0.000	2.470	0.000	0.655	0.000	0.002	0.004	0.001
MM-117-1e-1	0.393	0.002	5.007	4.765	0.001	2.419	0.000	0.615	0.000	0.002	0.000	0.000
MM-117-1e-2	0.341	0.001	5.006	4.684	0.001	2.465	0.000	0.675	0.000	0.002	0.002	0.000
MM-117-1e-3	0.338	0.000	5.005	4.676	0.000	2.478	0.000	0.672	0.000	0.002	0.002	0.000
MM-117-6a-1	0.336	0.002	5.002	4.678	0.000	2.480	0.000	0.669	0.000	0.003	0.002	0.000
MM-117-6b-3	0.417	0.002	5.009	4.808	0.002	2.382	0.000	0.589	0.001	0.006	0.003	0.000
MM-117-6b-2	0.408	0.002	5.010	4.789	0.003	2.381	0.002	0.604	0.000	0.014	0.002	0.000
MM-117-6c-5	0.411	0.002	5.009	4.805	0.000	2.382	0.000	0.602	0.000	0.002	0.003	0.000
MM-117-6c-6	0.400	0.002	5.013	4.768	0.001	2.406	0.000	0.621	0.000	0.003	0.000	0.000
MM-117-6c-7	0.404	0.002	5.009	4.796	0.000	2.381	0.000	0.611	0.000	0.009	0.000	0.000
MM-117-6d-1	0.409	0.002	5.008	4.801	0.001	2.382	0.000	0.603	0.000	0.007	0.002	0.000
MM-117-6d-2	0.409	0.001	5.008	4.809	0.002	2.373	0.001	0.604	0.000	0.002	0.004	0.000
MM-117-6d-3	0.411	0.002	5.013	4.795	0.001	2.381	0.000	0.609	0.000	0.004	0.004	0.000
MM-117-6e-1	0.412	0.002	5.009	4.810	0.000	2.378	0.000	0.603	0.000	0.003	0.000	0.000
MM-117-6e-2	0.391	0.002	5.008	4.759	0.001	2.415	0.000	0.617	0.000	0.009	0.002	0.000
MM-117-6e-3	0.413	0.002	5.008	4.817	0.000	2.370	0.000	0.600	0.001	0.003	0.001	0.000
MM-117-6f-1	0.364	0.003	5.011	4.703	0.003	2.452	0.000	0.650	0.000	0.007	0.001	0.000
MM-117-6f-2	0.360	0.002	5.005	4.719	0.002	2.441	0.000	0.653	0.000	0.003	0.001	0.000
MM-117-6f-3	0.413	0.001	5.008	4.809	0.000	2.378	0.000	0.600	0.000	0.004	0.001	0.000
MM-70-2a-1	0.452	0.002	5.012	4.878	0.000	2.327	0.000	0.566	0.000	0.001	0.000	0.000
MM-70-2a-2	0.461	0.003	5.011	4.892	0.005	2.310	0.000	0.553	0.001	0.008	0.000	0.000
MM-70-2a-3	0.490	0.002	5.007	4.974	0.000	2.253	0.000	0.522	0.000	0.002	0.002	0.000
MM-70-2a-4	0.474	0.002	5.014	4.911	0.001	2.299	0.000	0.545	0.000	0.004	0.002	0.000
MM-70-2b-9	0.332	0.001	5.009	4.645	0.001	2.499	0.000	0.684	0.000	0.005	0.001	0.000
MM-70-2b-10	0.456	0.001	5.010	4.890	0.000	2.319	0.000	0.557	0.000	0.002	0.003	0.000
MM-70-2b-11	0.455	0.003	5.013	4.884	0.001	2.314	0.000	0.561	0.000	0.006	0.003	0.000
MM-70-2c-14	0.470	0.003	5.013	4.908	0.000	2.306	0.000	0.546	0.000	0.003	0.000	0.000
MM-70-2c-15	0.462	0.002	5.013	4.902	0.000	2.302	0.000	0.562	0.000	0.001	0.000	0.000
MM-70-2c-16	0.398	0.002	5.012	4.757	0.001	2.422	0.000	0.614	0.000	0.005	0.000	0.000
MM-70-2d-1	0.468	0.002	5.011	4.907	0.000	2.309	0.000	0.544	0.000	0.005	0.000	0.000
MM-70-2d-2	0.442	0.002	5.006	4.871	0.002	2.328	0.002	0.563	0.000	0.011	0.001	0.000
MM-70-2d-3	0.416	0.002	5.007	4.819	0.001	2.368	0.000	0.594	0.000	0.010	0.000	0.000
MM-70-2e-1	0.444	0.002	5.012	4.867	0.000	2.330	0.000	0.576	0.000	0.002	0.002	0.000
MM-70-2e-2	0.462	0.003	5.006	4.921	0.000	2.293	0.001	0.545	0.000	0.005	0.002	0.000
MM-70-2e-3	0.425	0.002	5.012	4.833	0.000	2.349	0.000	0.595	0.000	0.007	0.002	0.000
MM-70-2f-1	0.187	0.000	4.997	4.390	0.000	2.701	0.000	0.812	0.000	0.003	0.000	0.000
MM-70-2f-2	0.445	0.002	5.003	4.897	0.000	2.311	0.001	0.563	0.000	0.004	0.000	0.000
MM-70-2f-3	0.442	0.003	5.005	4.882	0.001	2.323	0.001	0.566	0.000	0.004	0.000	0.001
MM-V1-2a-1	0.427	0.001	5.008	4.837	0.006	2.343	0.000	0.588	0.000	0.012	0.000	0.000
MM-V1-2a-2	0.425	0.001	5.011	4.830	0.001	2.356	0.000	0.595	0.000	0.003	0.002	0.000

Sample Data			**End Member**		
Analysis point	Na2O	K2O	Anorthite	Albite	Orthoclase
MM-117-1b-7	0.129	0.001	73.9	26.0	0.1
MM-117-1c-9	0.181	0.001	64.3	35.6	0.2
MM-117-1c-10	0.176	0.001	65.0	34.9	0.1
MM-117-1d-1	0.174	0.001	65.4	34.4	0.2
MM-117-1d-2	0.182	0.001	63.6	36.2	0.3
MM-117-1d-3	0.173	0.006	64.6	34.2	1.2
MM-117-1e-1	0.196	0.001	60.9	38.9	0.2
MM-117-1e-2	0.170	0.000	66.4	33.5	0.1
MM-117-1e-3	0.169	0.000	66.5	33.5	0.0
MM-117-6a-1	0.168	0.001	66.4	33.4	0.2
MM-117-6b-3	0.209	0.001	58.4	41.4	0.2
MM-117-6b-2	0.204	0.001	59.6	40.3	0.2
MM-117-6c-5	0.205	0.001	59.4	40.5	0.2
MM-117-6c-6	0.200	0.001	60.8	39.1	0.1
MM-117-6c-7	0.202	0.001	60.1	39.7	0.2
MM-117-6d-1	0.204	0.001	59.5	40.3	0.2
MM-117-6d-2	0.204	0.001	59.6	40.3	0.1
MM-117-6d-3	0.205	0.001	59.6	40.2	0.2
MM-117-6e-1	0.206	0.001	59.3	40.5	0.2
MM-117-6e-2	0.195	0.001	61.1	38.7	0.2
MM-117-6e-3	0.206	0.001	59.1	40.6	0.2
MM-117-6f-1	0.182	0.001	64.0	35.8	0.3
MM-117-6f-2	0.180	0.001	64.4	35.5	0.2
MM-117-6f-3	0.206	0.001	59.2	40.7	0.1
MM-70-2a-1	0.226	0.001	55.5	44.3	0.2
MM-70-2a-2	0.230	0.001	54.4	45.3	0.3
MM-70-2a-3	0.245	0.001	51.5	48.3	0.2
MM-70-2a-4	0.237	0.001	53.4	46.4	0.2
MM-70-2b-9	0.166	0.000	67.3	32.7	0.1
MM-70-2b-10	0.228	0.001	55.0	44.9	0.1
MM-70-2b-11	0.228	0.001	55.1	44.7	0.2
MM-70-2c-14	0.235	0.001	53.6	46.2	0.3
MM-70-2c-15	0.231	0.001	54.8	45.1	0.2
MM-70-2c-16	0.199	0.001	60.6	39.2	0.2
MM-70-2d-1	0.234	0.001	53.6	46.1	0.2
MM-70-2d-2	0.221	0.001	55.9	43.9	0.2
MM-70-2d-3	0.208	0.001	58.7	41.1	0.2
MM-70-2e-1	0.222	0.001	56.4	43.4	0.2
MM-70-2e-2	0.231	0.002	54.0	45.7	0.3
MM-70-2e-3	0.213	0.001	58.2	41.6	0.2
MM-70-2f-1	0.094	0.000	81.3	18.7	0.0
MM-70-2f-2	0.223	0.001	55.7	44.1	0.2
MM-70-2f-3	0.221	0.001	56.0	43.7	0.3
MM-V1-2a-1	0.213	0.001	57.9	42.0	0.1
MM-V1-2a-2	0.213	0.000	58.3	41.7	0.1

Sample Data				**Mole Cation**					
Analysis point	Intrusion/Phase	Sample	Mineral	SiO2	TiO2	Al2O3	MgO	CaO	MnO
MM-V1-2a-3	Butler West	MM-V1-2	Feldspar	0.881	0.000	0.577	0.001	0.215	0.000
MM-V1-2a-5	Butler West	MM-V1-2	Feldspar	0.898	0.000	0.581	0.001	0.213	0.000
MM-V1-2b-6	Butler West	MM-V1-2	Feldspar	0.883	0.000	0.585	0.000	0.223	0.000
MM-V1-2b-7	Butler West	MM-V1-2	Feldspar	0.880	0.000	0.586	0.000	0.221	0.000
MM-V1-2b-8	Butler West	MM-V1-2	Feldspar	0.870	0.000	0.594	0.000	0.230	0.000
MM-V1-2b-9	Butler West	MM-V1-2	Feldspar	0.880	0.000	0.586	0.000	0.224	0.000
MM-V1-2b-10	Butler West	MM-V1-2	Feldspar	0.882	0.000	0.583	0.001	0.220	0.000
MM-V1-2c-12	Butler West	MM-V1-2	Feldspar	0.890	0.000	0.582	0.000	0.216	0.000
MM-V1-2c-13	Butler West	MM-V1-2	Feldspar	0.889	0.000	0.575	0.000	0.212	0.000
MM-V1-2c-14	Butler West	MM-V1-2	Feldspar	0.883	0.000	0.589	0.000	0.219	0.000
MM-V1-2d-1	Butler West	MM-V1-2	Feldspar	0.897	0.000	0.575	0.000	0.210	0.000
MM-V1-2d-2	Butler West	MM-V1-2	Feldspar	0.889	0.000	0.574	0.000	0.214	0.000
MM-V1-2d-3	Butler West	MM-V1-2	Feldspar	0.800	0.000	0.645	0.000	0.290	0.000
MM-V1-2e-1	Butler West	MM-V1-2	Feldspar	0.883	0.000	0.580	0.000	0.217	0.000
MM-V1-2e-2	Butler West	MM-V1-2	Feldspar	0.885	0.000	0.585	0.000	0.219	0.000
MM-V1-2e-3	Butler West	MM-V1-2	Feldspar	0.775	0.000	0.666	0.000	0.313	0.000
MM-V1-2f-1	Butler West	MM-V1-2	Feldspar	0.885	0.000	0.582	0.000	0.220	0.000
MM-V1-2f-2	Butler West	MM-V1-2	Feldspar	0.884	0.000	0.580	0.000	0.218	0.000
MM-V1-2f-3	Butler West	MM-V1-2	Feldspar	0.890	0.000	0.581	0.000	0.220	0.000
MM-V1-2g-1	Butler West	MM-V1-2	Feldspar	0.899	0.000	0.568	0.000	0.206	0.000
MM-V1-2g-2	Butler West	MM-V1-2	Feldspar	0.897	0.000	0.573	0.000	0.208	0.000
MM-V1-2g-3	Butler West	MM-V1-2	Feldspar	0.884	0.000	0.588	0.001	0.223	0.000
MM-V4-7a-1	Butler East	MM-V4-7	Feldspar	0.915	0.001	0.561	0.000	0.194	0.000
MM-V4-7a-2	Butler East	MM-V4-7	Feldspar	0.917	0.000	0.557	0.000	0.195	0.000
MM-V4-7a-3	Butler East	MM-V4-7	Feldspar	0.922	0.000	0.557	0.000	0.190	0.000
MM-V4-7b-4	Butler East	MM-V4-7	Feldspar	0.921	0.000	0.561	0.000	0.191	0.000
MM-V4-7b-5	Butler East	MM-V4-7	Feldspar	0.919	0.000	0.556	0.000	0.193	0.000
MM-V4-7b-6	Butler East	MM-V4-7	Feldspar	0.919	0.000	0.559	0.000	0.194	0.000
MM-V4-7b-7	Butler East	MM-V4-7	Feldspar	0.924	0.000	0.555	0.000	0.190	0.000
MM-V4-7c-9	Butler East	MM-V4-7	Feldspar	0.916	0.000	0.562	0.000	0.197	0.000
MM-V4-7c-10	Butler East	MM-V4-7	Feldspar	0.914	0.000	0.564	0.000	0.199	0.000
MM-V4-7c-11	Butler East	MM-V4-7	Feldspar	0.920	0.000	0.560	0.000	0.194	0.000
MM-V4-7d-1	Butler East	MM-V4-7	Feldspar	0.920	0.000	0.561	0.000	0.193	0.000
MM-V4-7d-2	Butler East	MM-V4-7	Feldspar	0.915	0.000	0.562	0.000	0.197	0.000
MM-V4-7d-3	Butler East	MM-V4-7	Feldspar	0.912	0.000	0.567	0.000	0.201	0.000
MM-V4-7e-1	Butler East	MM-V4-7	Feldspar	0.919	0.000	0.557	0.000	0.193	0.000
MM-V4-7e-2	Butler East	MM-V4-7	Feldspar	0.917	0.000	0.557	0.000	0.192	0.000
MM-V4-7e-3	Butler East	MM-V4-7	Feldspar	0.919	0.000	0.560	0.000	0.195	0.000
MM-V4-7f-1	Butler East	MM-V4-7	Feldspar	0.916	0.000	0.561	0.000	0.195	0.000
MM-V4-7f-2	Butler East	MM-V4-7	Feldspar	0.922	0.000	0.557	0.000	0.192	0.000
MM-V4-7f-3	Butler East	MM-V4-7	Feldspar	0.910	0.001	0.567	0.000	0.199	0.000
MM-V8-1a-1	Butler West	MM-V8-1	Feldspar	0.901	0.000	0.574	0.000	0.211	0.000
MM-V8-1a-2	Butler West	MM-V8-1	Feldspar	0.911	0.000	0.570	0.000	0.202	0.000
MM-V8-1b-3	Butler West	MM-V8-1	Feldspar	0.905	0.000	0.569	0.000	0.204	0.000
MM-V8-1b-4	Butler West	MM-V8-1	Feldspar	0.909	0.000	0.571	0.000	0.203	0.000

Sample Data							**Mole oxygen**					
Analysis point	FeOt	SrO	BaO	Na2O	K2O	Total	SiO2	TiO2	Al2O3	MgO	CaO	MnO
MM-V1-2a-3	0.006	0.000	0.000	0.154	0.001	1.836	1.761	0.001	0.866	0.001	0.215	0.000
MM-V1-2a-5	0.002	0.000	0.000	0.162	0.001	1.859	1.797	0.000	0.871	0.001	0.213	0.000
MM-V1-2b-6	0.000	0.001	0.000	0.151	0.000	1.843	1.766	0.000	0.877	0.000	0.223	0.000
MM-V1-2b-7	0.002	0.001	0.000	0.151	0.000	1.841	1.760	0.000	0.879	0.000	0.221	0.000
MM-V1-2b-8	0.001	0.001	0.000	0.141	0.000	1.838	1.741	0.000	0.891	0.000	0.230	0.000
MM-V1-2b-9	0.001	0.001	0.000	0.150	0.000	1.843	1.760	0.000	0.880	0.000	0.224	0.000
MM-V1-2b-10	0.002	0.000	0.000	0.153	0.000	1.841	1.764	0.000	0.875	0.001	0.220	0.000
MM-V1-2c-12	0.001	0.001	0.000	0.156	0.000	1.846	1.779	0.001	0.873	0.000	0.216	0.000
MM-V1-2c-13	0.001	0.001	0.000	0.161	0.000	1.840	1.778	0.000	0.863	0.000	0.212	0.000
MM-V1-2c-14	0.002	0.001	0.000	0.148	0.000	1.842	1.767	0.000	0.883	0.000	0.219	0.000
MM-V1-2d-1	0.001	0.000	0.000	0.162	0.000	1.846	1.793	0.000	0.863	0.000	0.210	0.000
MM-V1-2d-2	0.001	0.000	0.000	0.160	0.001	1.838	1.778	0.000	0.861	0.000	0.214	0.000
MM-V1-2d-3	0.001	0.000	0.000	0.078	0.000	1.816	1.601	0.000	0.968	0.000	0.290	0.000
MM-V1-2e-1	0.001	0.000	0.000	0.154	0.000	1.835	1.766	0.000	0.870	0.000	0.217	0.000
MM-V1-2e-2	0.000	0.001	0.000	0.153	0.000	1.843	1.769	0.000	0.877	0.000	0.219	0.000
MM-V1-2e-3	0.002	0.000	0.000	0.054	0.000	1.810	1.549	0.000	0.999	0.000	0.313	0.000
MM-V1-2f-1	0.001	0.001	0.000	0.153	0.000	1.843	1.770	0.000	0.874	0.000	0.220	0.000
MM-V1-2f-2	0.001	0.001	0.000	0.154	0.000	1.838	1.768	0.000	0.870	0.000	0.218	0.000
MM-V1-2f-3	0.002	0.000	0.000	0.153	0.001	1.847	1.779	0.000	0.871	0.000	0.220	0.000
MM-V1-2g-1	0.001	0.001	0.000	0.168	0.000	1.843	1.797	0.001	0.852	0.000	0.206	0.000
MM-V1-2g-2	0.001	0.001	0.000	0.165	0.000	1.844	1.794	0.000	0.859	0.000	0.208	0.000
MM-V1-2g-3	0.002	0.000	0.000	0.153	0.000	1.851	1.768	0.001	0.882	0.001	0.223	0.000
MM-V4-7a-1	0.001	0.000	0.000	0.178	0.001	1.851	1.830	0.001	0.841	0.000	0.194	0.000
MM-V4-7a-2	0.001	0.000	0.000	0.179	0.001	1.849	1.834	0.000	0.835	0.000	0.195	0.000
MM-V4-7a-3	0.001	0.000	0.000	0.184	0.001	1.854	1.845	0.000	0.835	0.000	0.190	0.000
MM-V4-7b-4	0.001	0.000	0.000	0.181	0.001	1.856	1.842	0.000	0.841	0.000	0.191	0.000
MM-V4-7b-5	0.000	0.000	0.000	0.179	0.001	1.848	1.838	0.000	0.834	0.000	0.193	0.000
MM-V4-7b-6	0.001	0.000	0.000	0.179	0.001	1.854	1.839	0.000	0.839	0.000	0.194	0.000
MM-V4-7b-7	0.000	0.001	0.000	0.183	0.001	1.854	1.847	0.000	0.833	0.000	0.190	0.000
MM-V4-7c-9	0.001	0.000	0.000	0.173	0.001	1.851	1.831	0.000	0.843	0.000	0.197	0.000
MM-V4-7c-10	0.000	0.001	0.000	0.173	0.001	1.851	1.828	0.000	0.846	0.000	0.199	0.000
MM-V4-7c-11	0.000	0.001	0.000	0.179	0.001	1.855	1.840	0.000	0.840	0.000	0.194	0.000
MM-V4-7d-1	0.000	0.001	0.000	0.180	0.001	1.855	1.840	0.000	0.841	0.000	0.193	0.000
MM-V4-7d-2	0.000	0.001	0.000	0.176	0.001	1.852	1.830	0.001	0.842	0.000	0.197	0.000
MM-V4-7d-3	0.001	0.001	0.000	0.172	0.001	1.856	1.824	0.000	0.851	0.000	0.201	0.000
MM-V4-7e-1	0.001	0.001	0.000	0.181	0.001	1.852	1.839	0.000	0.835	0.000	0.193	0.000
MM-V4-7e-2	0.001	0.001	0.000	0.179	0.001	1.848	1.834	0.000	0.835	0.000	0.192	0.000
MM-V4-7e-3	0.001	0.000	0.000	0.176	0.001	1.853	1.838	0.001	0.841	0.000	0.195	0.000
MM-V4-7f-1	0.001	0.000	0.000	0.176	0.001	1.850	1.833	0.000	0.842	0.000	0.195	0.000
MM-V4-7f-2	0.001	0.000	0.000	0.181	0.001	1.854	1.844	0.000	0.836	0.000	0.192	0.000
MM-V4-7f-3	0.002	0.000	0.000	0.174	0.001	1.853	1.819	0.001	0.850	0.000	0.199	0.000
MM-V8-1a-1	0.001	0.001	0.000	0.164	0.001	1.853	1.802	0.000	0.861	0.000	0.211	0.000
MM-V8-1a-2	0.001	0.000	0.000	0.171	0.001	1.856	1.822	0.000	0.855	0.000	0.202	0.000
MM-V8-1b-3	0.004	0.001	0.000	0.168	0.001	1.853	1.811	0.001	0.854	0.000	0.204	0.000
MM-V8-1b-4	0.002	0.000	0.000	0.167	0.001	1.854	1.817	0.000	0.856	0.000	0.203	0.000

Sample Data							**Norm Cations**					
Analysis point	FeOt	SrO	BaO	Na2O	K2O	Total	SiO2	TiO2	Al2O3	MgO	CaO	MnO
MM-V1-2a-3	0.009	0.000	0.000	0.077	0.000	2.931	2.403	0.001	1.576	0.004	0.587	0.000
MM-V1-2a-5	0.003	0.000	0.000	0.081	0.000	2.967	2.422	0.001	1.566	0.003	0.574	0.001
MM-V1-2b-6	0.000	0.001	0.000	0.075	0.000	2.943	2.400	0.000	1.589	0.000	0.607	0.000
MM-V1-2b-7	0.003	0.001	0.000	0.076	0.000	2.940	2.395	0.000	1.595	0.000	0.602	0.000
MM-V1-2b-8	0.002	0.001	0.000	0.070	0.000	2.936	2.372	0.000	1.618	0.000	0.628	0.000
MM-V1-2b-9	0.001	0.001	0.000	0.075	0.000	2.941	2.394	0.000	1.595	0.000	0.610	0.000
MM-V1-2b-10	0.003	0.000	0.000	0.077	0.000	2.939	2.401	0.000	1.587	0.002	0.599	0.000
MM-V1-2c-12	0.001	0.001	0.000	0.078	0.000	2.949	2.414	0.001	1.579	0.000	0.587	0.000
MM-V1-2c-13	0.002	0.001	0.000	0.080	0.000	2.936	2.422	0.000	1.567	0.001	0.577	0.000
MM-V1-2c-14	0.003	0.001	0.000	0.074	0.000	2.947	2.398	0.000	1.599	0.001	0.593	0.000
MM-V1-2d-1	0.002	0.000	0.000	0.081	0.000	2.950	2.432	0.000	1.560	0.000	0.569	0.000
MM-V1-2d-2	0.001	0.000	0.000	0.080	0.000	2.934	2.423	0.000	1.566	0.001	0.583	0.000
MM-V1-2d-3	0.002	0.000	0.000	0.039	0.000	2.900	2.208	0.000	1.780	0.000	0.799	0.001
MM-V1-2e-1	0.001	0.000	0.000	0.077	0.000	2.931	2.410	0.000	1.582	0.000	0.591	0.001
MM-V1-2e-2	0.001	0.001	0.000	0.077	0.000	2.943	2.405	0.000	1.589	0.000	0.595	0.000
MM-V1-2e-3	0.003	0.000	0.000	0.027	0.000	2.892	2.143	0.000	1.843	0.000	0.866	0.000
MM-V1-2f-1	0.001	0.001	0.000	0.076	0.000	2.944	2.406	0.000	1.583	0.000	0.599	0.000
MM-V1-2f-2	0.002	0.001	0.000	0.077	0.000	2.936	2.408	0.000	1.581	0.001	0.594	0.000
MM-V1-2f-3	0.003	0.000	0.000	0.077	0.000	2.951	2.411	0.000	1.574	0.001	0.595	0.000
MM-V1-2g-1	0.001	0.001	0.000	0.084	0.000	2.942	2.444	0.001	1.545	0.000	0.560	0.000
MM-V1-2g-2	0.002	0.001	0.000	0.082	0.000	2.946	2.436	0.001	1.555	0.000	0.565	0.000
MM-V1-2g-3	0.003	0.000	0.000	0.076	0.000	2.954	2.394	0.001	1.592	0.001	0.604	0.000
MM-V4-7a-1	0.002	0.000	0.000	0.089	0.000	2.958	2.475	0.001	1.516	0.001	0.524	0.000
MM-V4-7a-2	0.001	0.000	0.000	0.090	0.000	2.955	2.483	0.000	1.507	0.000	0.527	0.001
MM-V4-7a-3	0.002	0.000	0.000	0.092	0.000	2.963	2.490	0.000	1.503	0.000	0.512	0.000
MM-V4-7b-4	0.001	0.000	0.000	0.091	0.001	2.967	2.484	0.000	1.512	0.000	0.514	0.000
MM-V4-7b-5	0.000	0.000	0.000	0.089	0.000	2.955	2.487	0.000	1.505	0.001	0.522	0.000
MM-V4-7b-6	0.001	0.000	0.000	0.089	0.001	2.964	2.482	0.000	1.510	0.000	0.524	0.000
MM-V4-7b-7	0.001	0.001	0.000	0.091	0.000	2.963	2.494	0.000	1.499	0.000	0.512	0.000
MM-V4-7c-9	0.001	0.000	0.000	0.087	0.001	2.960	2.474	0.000	1.520	0.000	0.532	0.000
MM-V4-7c-10	0.000	0.001	0.000	0.086	0.000	2.960	2.470	0.000	1.524	0.000	0.537	0.000
MM-V4-7c-11	0.001	0.001	0.000	0.089	0.000	2.966	2.482	0.000	1.511	0.000	0.523	0.001
MM-V4-7d-1	0.000	0.001	0.000	0.090	0.000	2.965	2.482	0.000	1.513	0.000	0.520	0.000
MM-V4-7d-2	0.001	0.001	0.000	0.088	0.000	2.960	2.473	0.001	1.518	0.000	0.532	0.000
MM-V4-7d-3	0.002	0.001	0.000	0.086	0.001	2.966	2.461	0.000	1.530	0.000	0.543	0.000
MM-V4-7e-1	0.001	0.001	0.000	0.090	0.000	2.959	2.486	0.000	1.505	0.000	0.522	0.000
MM-V4-7e-2	0.001	0.001	0.000	0.090	0.000	2.953	2.483	0.000	1.508	0.000	0.520	0.000
MM-V4-7e-3	0.002	0.000	0.000	0.088	0.000	2.964	2.480	0.001	1.512	0.000	0.527	0.000
MM-V4-7f-1	0.001	0.000	0.000	0.088	0.000	2.959	2.478	0.001	1.517	0.000	0.528	0.000
MM-V4-7f-2	0.001	0.000	0.000	0.091	0.001	2.964	2.489	0.000	1.504	0.000	0.517	0.000
MM-V4-7f-3	0.003	0.000	0.000	0.087	0.000	2.960	2.458	0.002	1.531	0.001	0.539	0.000
MM-V8-1a-1	0.002	0.001	0.000	0.082	0.000	2.960	2.436	0.000	1.552	0.000	0.569	0.000
MM-V8-1a-2	0.001	0.000	0.000	0.086	0.000	2.966	2.457	0.000	1.537	0.001	0.544	0.000
MM-V8-1b-3	0.006	0.001	0.000	0.084	0.001	2.960	2.447	0.001	1.538	0.001	0.550	0.000
MM-V8-1b-4	0.003	0.000	0.000	0.084	0.000	2.965	2.452	0.000	1.540	0.001	0.548	0.000

Sample Data						**Norm Oxygen**								
Analysis point	SrO	BaO	Na2O	K2O	Total	SiO2	TiO2	Al2O3	MgO	CaO	MnO	FeOt	SrO	BaO
MM-V1-2a-3	0.001	0.000	0.420	0.001	5.010	4.807	0.002	2.364	0.004	0.587	0.000	0.025	0.001	0.000
MM-V1-2a-5	0.000	0.000	0.436	0.003	5.011	4.844	0.001	2.349	0.003	0.574	0.001	0.008	0.000	0.000
MM-V1-2b-6	0.002	0.000	0.410	0.000	5.010	4.801	0.000	2.384	0.000	0.607	0.000	0.001	0.002	0.000
MM-V1-2b-7	0.002	0.000	0.411	0.001	5.011	4.790	0.000	2.392	0.000	0.602	0.000	0.009	0.002	0.000
MM-V1-2b-8	0.004	0.000	0.383	0.001	5.009	4.743	0.000	2.427	0.000	0.628	0.000	0.006	0.004	0.000
MM-V1-2b-9	0.003	0.000	0.408	0.001	5.012	4.787	0.000	2.393	0.000	0.610	0.000	0.003	0.003	0.000
MM-V1-2b-10	0.000	0.000	0.417	0.001	5.011	4.803	0.000	2.380	0.002	0.599	0.000	0.007	0.000	0.000
MM-V1-2c-12	0.002	0.000	0.422	0.001	5.007	4.827	0.001	2.368	0.000	0.587	0.000	0.003	0.002	0.000
MM-V1-2c-13	0.003	0.000	0.438	0.001	5.013	4.844	0.000	2.351	0.001	0.577	0.000	0.004	0.003	0.000
MM-V1-2c-14	0.003	0.000	0.401	0.000	5.001	4.796	0.000	2.398	0.001	0.593	0.000	0.007	0.003	0.000
MM-V1-2d-1	0.000	0.000	0.439	0.001	5.006	4.864	0.000	2.341	0.000	0.569	0.000	0.005	0.000	0.000
MM-V1-2d-2	0.000	0.000	0.437	0.001	5.012	4.846	0.000	2.348	0.001	0.583	0.000	0.002	0.000	0.000
MM-V1-2d-3	0.000	0.000	0.216	0.001	5.008	4.416	0.000	2.670	0.000	0.799	0.001	0.005	0.000	0.000
MM-V1-2e-1	0.001	0.000	0.421	0.000	5.009	4.820	0.001	2.373	0.000	0.591	0.001	0.002	0.001	0.000
MM-V1-2e-2	0.002	0.000	0.416	0.001	5.009	4.809	0.000	2.384	0.000	0.595	0.000	0.002	0.002	0.000
MM-V1-2e-3	0.001	0.000	0.148	0.000	5.007	4.286	0.001	2.764	0.000	0.866	0.000	0.008	0.001	0.000
MM-V1-2f-1	0.003	0.000	0.415	0.001	5.009	4.812	0.000	2.375	0.000	0.599	0.000	0.004	0.003	0.000
MM-V1-2f-2	0.002	0.000	0.419	0.001	5.009	4.816	0.000	2.372	0.001	0.594	0.000	0.006	0.002	0.000
MM-V1-2f-3	0.001	0.000	0.416	0.002	5.007	4.823	0.000	2.361	0.001	0.595	0.000	0.009	0.001	0.000
MM-V1-2g-1	0.002	0.000	0.455	0.001	5.010	4.887	0.002	2.318	0.000	0.560	0.000	0.003	0.002	0.000
MM-V1-2g-2	0.002	0.000	0.447	0.000	5.009	4.871	0.001	2.333	0.000	0.565	0.000	0.004	0.002	0.000
MM-V1-2g-3	0.001	0.000	0.414	0.000	5.013	4.788	0.002	2.388	0.001	0.604	0.000	0.009	0.001	0.000
MM-V4-7a-1	0.000	0.000	0.483	0.002	5.006	4.951	0.003	2.274	0.001	0.524	0.000	0.005	0.000	0.000
MM-V4-7a-2	0.000	0.000	0.485	0.002	5.006	4.965	0.000	2.260	0.000	0.527	0.001	0.004	0.000	0.000
MM-V4-7a-3	0.000	0.000	0.496	0.002	5.006	4.981	0.000	2.254	0.000	0.512	0.000	0.004	0.000	0.000
MM-V4-7b-4	0.000	0.000	0.489	0.003	5.005	4.968	0.000	2.269	0.000	0.514	0.000	0.002	0.000	0.000
MM-V4-7b-5	0.001	0.000	0.484	0.003	5.003	4.975	0.000	2.258	0.001	0.522	0.000	0.001	0.001	0.000
MM-V4-7b-6	0.001	0.000	0.483	0.003	5.006	4.963	0.000	2.265	0.000	0.524	0.000	0.003	0.001	0.000
MM-V4-7b-7	0.002	0.000	0.494	0.003	5.004	4.987	0.000	2.249	0.000	0.512	0.000	0.001	0.002	0.000
MM-V4-7c-9	0.001	0.000	0.468	0.003	5.001	4.948	0.001	2.279	0.000	0.532	0.000	0.002	0.001	0.000
MM-V4-7c-10	0.002	0.000	0.467	0.002	5.002	4.941	0.000	2.285	0.000	0.537	0.000	0.001	0.002	0.000
MM-V4-7c-11	0.002	0.000	0.482	0.002	5.004	4.963	0.000	2.266	0.000	0.523	0.001	0.002	0.002	0.000
MM-V4-7d-1	0.002	0.000	0.484	0.003	5.005	4.963	0.000	2.270	0.000	0.520	0.000	0.001	0.002	0.000
MM-V4-7d-2	0.002	0.000	0.476	0.002	5.006	4.946	0.002	2.277	0.000	0.532	0.000	0.002	0.002	0.000
MM-V4-7d-3	0.002	0.000	0.464	0.003	5.006	4.921	0.000	2.295	0.000	0.543	0.000	0.005	0.002	0.000
MM-V4-7e-1	0.001	0.000	0.488	0.002	5.006	4.971	0.000	2.258	0.000	0.522	0.000	0.002	0.001	0.000
MM-V4-7e-2	0.003	0.000	0.485	0.003	5.005	4.967	0.000	2.263	0.000	0.520	0.000	0.003	0.003	0.000
MM-V4-7e-3	0.000	0.000	0.475	0.002	5.000	4.959	0.002	2.268	0.000	0.527	0.000	0.004	0.000	0.000
MM-V4-7f-1	0.000	0.000	0.475	0.002	5.001	4.955	0.001	2.275	0.000	0.528	0.000	0.002	0.000	0.000
MM-V4-7f-2	0.000	0.000	0.490	0.003	5.005	4.977	0.000	2.256	0.000	0.517	0.000	0.002	0.000	0.000
MM-V4-7f-3	0.000	0.000	0.470	0.002	5.008	4.916	0.003	2.297	0.001	0.539	0.000	0.008	0.000	0.000
MM-V8-1a-1	0.002	0.000	0.442	0.002	5.008	4.872	0.001	2.328	0.000	0.569	0.000	0.005	0.002	0.000
MM-V8-1a-2	0.000	0.000	0.462	0.002	5.005	4.914	0.000	2.306	0.001	0.544	0.000	0.004	0.000	0.000
MM-V8-1b-3	0.002	0.000	0.455	0.003	5.007	4.893	0.002	2.307	0.001	0.550	0.000	0.015	0.002	0.000
MM-V8-1b-4	0.000	0.000	0.452	0.002	5.002	4.903	0.001	2.311	0.001	0.548	0.000	0.008	0.000	0.000

Sample Data			**Atom units**							
Analysis point	K2O	Total	SiO2	TiO2	Al2O3	MgO	CaO	MnO	FeOt	SrO
MM-V1-2a-3	0.001	8.000	2.403	0.001	1.576	0.004	0.587	0.000	0.017	0.001
MM-V1-2a-5	0.001	8.000	2.422	0.001	1.566	0.003	0.574	0.001	0.005	0.000
MM-V1-2b-6	0.000	8.000	2.400	0.000	1.589	0.000	0.607	0.000	0.001	0.002
MM-V1-2b-7	0.000	8.000	2.395	0.000	1.595	0.000	0.602	0.000	0.006	0.002
MM-V1-2b-8	0.000	8.000	2.372	0.000	1.618	0.000	0.628	0.000	0.004	0.004
MM-V1-2b-9	0.000	8.000	2.394	0.000	1.595	0.000	0.610	0.000	0.002	0.003
MM-V1-2b-10	0.000	8.000	2.401	0.000	1.587	0.002	0.599	0.000	0.005	0.000
MM-V1-2c-12	0.000	8.000	2.414	0.001	1.579	0.000	0.587	0.000	0.002	0.002
MM-V1-2c-13	0.001	8.000	2.422	0.000	1.567	0.001	0.577	0.000	0.003	0.003
MM-V1-2c-14	0.000	8.000	2.398	0.000	1.599	0.001	0.593	0.000	0.005	0.003
MM-V1-2d-1	0.000	8.000	2.432	0.000	1.560	0.000	0.569	0.000	0.004	0.000
MM-V1-2d-2	0.001	8.000	2.423	0.000	1.566	0.001	0.583	0.000	0.001	0.000
MM-V1-2d-3	0.000	8.000	2.208	0.000	1.780	0.000	0.799	0.001	0.004	0.000
MM-V1-2e-1	0.000	8.000	2.410	0.000	1.582	0.000	0.591	0.001	0.002	0.001
MM-V1-2e-2	0.000	8.000	2.405	0.000	1.589	0.000	0.595	0.000	0.001	0.002
MM-V1-2e-3	0.000	8.000	2.143	0.000	1.843	0.000	0.866	0.000	0.005	0.001
MM-V1-2f-1	0.000	8.000	2.406	0.000	1.583	0.000	0.599	0.000	0.003	0.003
MM-V1-2f-2	0.000	8.000	2.408	0.000	1.581	0.001	0.594	0.000	0.004	0.002
MM-V1-2f-3	0.001	8.000	2.411	0.000	1.574	0.001	0.595	0.000	0.006	0.001
MM-V1-2g-1	0.001	8.000	2.444	0.001	1.545	0.000	0.560	0.000	0.002	0.002
MM-V1-2g-2	0.000	8.000	2.436	0.001	1.555	0.000	0.565	0.000	0.003	0.002
MM-V1-2g-3	0.000	8.000	2.394	0.001	1.592	0.001	0.604	0.000	0.006	0.001
MM-V4-7a-1	0.001	8.000	2.475	0.001	1.516	0.001	0.524	0.000	0.003	0.000
MM-V4-7a-2	0.001	8.000	2.483	0.000	1.507	0.000	0.527	0.001	0.002	0.000
MM-V4-7a-3	0.001	8.000	2.490	0.000	1.503	0.000	0.512	0.000	0.003	0.000
MM-V4-7b-4	0.002	8.000	2.484	0.000	1.512	0.000	0.514	0.000	0.001	0.000
MM-V4-7b-5	0.001	8.000	2.487	0.000	1.505	0.001	0.522	0.000	0.001	0.001
MM-V4-7b-6	0.002	8.000	2.482	0.000	1.510	0.000	0.524	0.000	0.002	0.001
MM-V4-7b-7	0.001	8.000	2.494	0.000	1.499	0.000	0.512	0.000	0.001	0.002
MM-V4-7c-9	0.002	8.000	2.474	0.000	1.520	0.000	0.532	0.000	0.002	0.001
MM-V4-7c-10	0.001	8.000	2.470	0.000	1.524	0.000	0.537	0.000	0.001	0.002
MM-V4-7c-11	0.001	8.000	2.482	0.000	1.511	0.000	0.523	0.001	0.001	0.002
MM-V4-7d-1	0.001	8.000	2.482	0.000	1.513	0.000	0.520	0.000	0.001	0.002
MM-V4-7d-2	0.001	8.000	2.473	0.001	1.518	0.000	0.532	0.000	0.001	0.002
MM-V4-7d-3	0.001	8.000	2.461	0.000	1.530	0.000	0.543	0.000	0.003	0.002
MM-V4-7e-1	0.001	8.000	2.486	0.000	1.505	0.000	0.522	0.000	0.001	0.001
MM-V4-7e-2	0.001	8.000	2.483	0.000	1.508	0.000	0.520	0.000	0.002	0.003
MM-V4-7e-3	0.001	8.000	2.480	0.001	1.512	0.000	0.527	0.000	0.003	0.000
MM-V4-7f-1	0.001	8.000	2.478	0.001	1.517	0.000	0.528	0.000	0.001	0.000
MM-V4-7f-2	0.001	8.000	2.489	0.000	1.504	0.000	0.517	0.000	0.001	0.000
MM-V4-7f-3	0.001	8.000	2.458	0.002	1.531	0.001	0.539	0.000	0.005	0.000
MM-V8-1a-1	0.001	8.000	2.436	0.000	1.552	0.000	0.569	0.000	0.004	0.002
MM-V8-1a-2	0.001	8.000	2.457	0.000	1.537	0.001	0.544	0.000	0.002	0.000
MM-V8-1b-3	0.002	8.000	2.447	0.001	1.538	0.001	0.550	0.000	0.010	0.002
MM-V8-1b-4	0.001	8.000	2.452	0.000	1.540	0.001	0.548	0.000	0.006	0.000

Sample Data				**Norm oxygen**								
Analysis point	Na2O	K2O	Total	SiO2	TiO2	Al2O3	MgO	CaO	MnO	FeOt	SrO	BaO
MM-V1-2a-3	0.420	0.001	5.010	4.807	0.002	2.364	0.004	0.587	0.000	0.025	0.001	0.000
MM-V1-2a-5	0.436	0.003	5.011	4.844	0.001	2.349	0.003	0.574	0.001	0.008	0.000	0.000
MM-V1-2b-6	0.410	0.000	5.010	4.801	0.000	2.384	0.000	0.607	0.000	0.001	0.002	0.000
MM-V1-2b-7	0.411	0.001	5.011	4.790	0.000	2.392	0.000	0.602	0.000	0.009	0.002	0.000
MM-V1-2b-8	0.383	0.001	5.009	4.743	0.000	2.427	0.000	0.628	0.000	0.006	0.004	0.000
MM-V1-2b-9	0.408	0.001	5.012	4.787	0.000	2.393	0.000	0.610	0.000	0.003	0.003	0.000
MM-V1-2b-10	0.417	0.001	5.011	4.803	0.000	2.380	0.002	0.599	0.000	0.007	0.000	0.000
MM-V1-2c-12	0.422	0.001	5.007	4.827	0.001	2.368	0.000	0.587	0.000	0.003	0.002	0.000
MM-V1-2c-13	0.438	0.001	5.013	4.844	0.000	2.351	0.001	0.577	0.000	0.004	0.003	0.000
MM-V1-2c-14	0.401	0.000	5.001	4.796	0.000	2.398	0.001	0.593	0.000	0.007	0.003	0.000
MM-V1-2d-1	0.439	0.001	5.006	4.864	0.000	2.341	0.000	0.569	0.000	0.005	0.000	0.000
MM-V1-2d-2	0.437	0.001	5.012	4.846	0.000	2.348	0.001	0.583	0.000	0.002	0.000	0.000
MM-V1-2d-3	0.216	0.001	5.008	4.416	0.000	2.670	0.000	0.799	0.001	0.005	0.000	0.000
MM-V1-2e-1	0.421	0.000	5.009	4.820	0.001	2.373	0.000	0.591	0.001	0.002	0.001	0.000
MM-V1-2e-2	0.416	0.001	5.009	4.809	0.000	2.384	0.000	0.595	0.000	0.002	0.002	0.000
MM-V1-2e-3	0.148	0.000	5.007	4.286	0.001	2.764	0.000	0.866	0.000	0.008	0.001	0.000
MM-V1-2f-1	0.415	0.001	5.009	4.812	0.000	2.375	0.000	0.599	0.000	0.004	0.003	0.000
MM-V1-2f-2	0.419	0.001	5.009	4.816	0.000	2.372	0.001	0.594	0.000	0.006	0.002	0.000
MM-V1-2f-3	0.416	0.002	5.007	4.823	0.000	2.361	0.001	0.595	0.000	0.009	0.001	0.000
MM-V1-2g-1	0.455	0.001	5.010	4.887	0.002	2.318	0.000	0.560	0.000	0.003	0.002	0.000
MM-V1-2g-2	0.447	0.000	5.009	4.871	0.001	2.333	0.000	0.565	0.000	0.004	0.002	0.000
MM-V1-2g-3	0.414	0.000	5.013	4.788	0.002	2.388	0.001	0.604	0.000	0.009	0.001	0.000
MM-V4-7a-1	0.483	0.002	5.006	4.951	0.003	2.274	0.001	0.524	0.000	0.005	0.000	0.000
MM-V4-7a-2	0.485	0.002	5.006	4.965	0.000	2.260	0.000	0.527	0.001	0.004	0.000	0.000
MM-V4-7a-3	0.496	0.002	5.006	4.981	0.000	2.254	0.000	0.512	0.000	0.004	0.000	0.000
MM-V4-7b-4	0.489	0.003	5.005	4.968	0.000	2.269	0.000	0.514	0.000	0.002	0.000	0.000
MM-V4-7b-5	0.484	0.003	5.003	4.975	0.000	2.258	0.001	0.522	0.000	0.001	0.001	0.000
MM-V4-7b-6	0.483	0.003	5.006	4.963	0.000	2.265	0.000	0.524	0.000	0.003	0.001	0.000
MM-V4-7b-7	0.494	0.003	5.004	4.987	0.000	2.249	0.000	0.512	0.000	0.001	0.002	0.000
MM-V4-7c-9	0.468	0.003	5.001	4.948	0.001	2.279	0.000	0.532	0.000	0.002	0.001	0.000
MM-V4-7c-10	0.467	0.002	5.002	4.941	0.000	2.285	0.000	0.537	0.000	0.001	0.002	0.000
MM-V4-7c-11	0.482	0.002	5.004	4.963	0.000	2.266	0.000	0.523	0.001	0.002	0.002	0.000
MM-V4-7d-1	0.484	0.003	5.005	4.963	0.000	2.270	0.000	0.520	0.000	0.001	0.002	0.000
MM-V4-7d-2	0.476	0.002	5.006	4.946	0.002	2.277	0.000	0.532	0.000	0.002	0.002	0.000
MM-V4-7d-3	0.464	0.003	5.006	4.921	0.000	2.295	0.000	0.543	0.000	0.005	0.002	0.000
MM-V4-7e-1	0.488	0.002	5.006	4.971	0.000	2.258	0.000	0.522	0.000	0.002	0.001	0.000
MM-V4-7e-2	0.485	0.003	5.005	4.967	0.000	2.263	0.000	0.520	0.000	0.003	0.003	0.000
MM-V4-7e-3	0.475	0.002	5.000	4.959	0.002	2.268	0.000	0.527	0.000	0.004	0.000	0.000
MM-V4-7f-1	0.475	0.002	5.001	4.955	0.001	2.275	0.000	0.528	0.000	0.002	0.000	0.000
MM-V4-7f-2	0.490	0.003	5.005	4.977	0.000	2.256	0.000	0.517	0.000	0.002	0.000	0.000
MM-V4-7f-3	0.470	0.002	5.008	4.916	0.003	2.297	0.001	0.539	0.000	0.008	0.000	0.000
MM-V8-1a-1	0.442	0.002	5.008	4.872	0.001	2.328	0.000	0.569	0.000	0.005	0.002	0.000
MM-V8-1a-2	0.462	0.002	5.005	4.914	0.000	2.306	0.001	0.544	0.000	0.004	0.000	0.000
MM-V8-1b-3	0.455	0.003	5.007	4.893	0.002	2.307	0.001	0.550	0.000	0.015	0.002	0.000
MM-V8-1b-4	0.452	0.002	5.002	4.903	0.001	2.311	0.001	0.548	0.000	0.008	0.000	0.000

Sample Data			**End Member**		
Analysis point	Na2O	K2O	Anorthite	Albite	Orthoclase
MM-V1-2a-3	0.210	0.001	58.2	41.7	0.1
MM-V1-2a-5	0.218	0.001	56.7	43.0	0.3
MM-V1-2b-6	0.205	0.000	59.7	40.3	0.0
MM-V1-2b-7	0.206	0.000	59.3	40.6	0.1
MM-V1-2b-8	0.192	0.000	62.1	37.9	0.1
MM-V1-2b-9	0.204	0.000	59.9	40.1	0.1
MM-V1-2b-10	0.208	0.000	58.9	41.0	0.1
MM-V1-2c-12	0.211	0.000	58.1	41.8	0.1
MM-V1-2c-13	0.219	0.001	56.8	43.1	0.1
MM-V1-2c-14	0.200	0.000	59.7	40.3	0.0
MM-V1-2d-1	0.220	0.000	56.4	43.5	0.1
MM-V1-2d-2	0.218	0.001	57.1	42.8	0.1
MM-V1-2d-3	0.108	0.000	78.7	21.3	0.1
MM-V1-2e-1	0.211	0.000	58.4	41.6	0.0
MM-V1-2e-2	0.208	0.000	58.8	41.1	0.1
MM-V1-2e-3	0.074	0.000	85.4	14.6	0.0
MM-V1-2f-1	0.207	0.000	59.0	40.9	0.1
MM-V1-2f-2	0.210	0.000	58.6	41.3	0.1
MM-V1-2f-3	0.208	0.001	58.7	41.0	0.2
MM-V1-2g-1	0.228	0.001	55.1	44.8	0.1
MM-V1-2g-2	0.224	0.000	55.8	44.2	0.0
MM-V1-2g-3	0.207	0.000	59.3	40.6	0.0
MM-V4-7a-1	0.241	0.001	51.9	47.9	0.2
MM-V4-7a-2	0.242	0.001	52.0	47.8	0.2
MM-V4-7a-3	0.248	0.001	50.7	49.1	0.2
MM-V4-7b-4	0.244	0.002	51.1	48.5	0.3
MM-V4-7b-5	0.242	0.001	51.7	48.0	0.3
MM-V4-7b-6	0.242	0.002	51.9	47.8	0.3
MM-V4-7b-7	0.247	0.001	50.8	49.0	0.3
MM-V4-7c-9	0.234	0.002	53.0	46.7	0.3
MM-V4-7c-10	0.233	0.001	53.4	46.4	0.2
MM-V4-7c-11	0.241	0.001	52.0	47.8	0.2
MM-V4-7d-1	0.242	0.001	51.7	48.1	0.3
MM-V4-7d-2	0.238	0.001	52.7	47.1	0.2
MM-V4-7d-3	0.232	0.001	53.8	46.0	0.3
MM-V4-7e-1	0.244	0.001	51.6	48.3	0.2
MM-V4-7e-2	0.243	0.001	51.6	48.1	0.3
MM-V4-7e-3	0.238	0.001	52.5	47.3	0.2
MM-V4-7f-1	0.238	0.001	52.5	47.3	0.2
MM-V4-7f-2	0.245	0.001	51.2	48.5	0.3
MM-V4-7f-3	0.235	0.001	53.3	46.5	0.2
MM-V8-1a-1	0.221	0.001	56.2	43.6	0.2
MM-V8-1a-2	0.231	0.001	54.0	45.8	0.2
MM-V8-1b-3	0.227	0.002	54.6	45.1	0.3
MM-V8-1b-4	0.226	0.001	54.7	45.1	0.2

Sample Data				**Mole Cation**					
Analysis point	Intrusion/Phase	Sample	Mineral	SiO2	TiO2	Al2O3	MgO	CaO	MnO
MM-V8-1b-5	Butler West	MM-V8-1	Feldspar	0.900	0.000	0.570	0.001	0.205	0.000
MM-V8-1c-6	Butler West	MM-V8-1	Feldspar	0.904	0.000	0.569	0.000	0.205	0.000
MM-V8-1c-7	Butler West	MM-V8-1	Feldspar	0.914	0.000	0.561	0.001	0.198	0.000
MM-V8-1c-8	Butler West	MM-V8-1	Feldspar	0.909	0.000	0.564	0.000	0.196	0.000
MM-V8-1d-1	Butler West	MM-V8-1	Feldspar	0.904	0.000	0.565	0.000	0.204	0.000
MM-V8-1d-2	Butler West	MM-V8-1	Feldspar	0.901	0.000	0.570	0.000	0.204	0.000
MM-V8-1d-3	Butler West	MM-V8-1	Feldspar	0.904	0.000	0.567	0.000	0.203	0.000
MM-V8-1e-1	Butler West	MM-V8-1	Feldspar	0.899	0.000	0.571	0.000	0.205	0.000
MM-V8-1e-2	Butler West	MM-V8-1	Feldspar	0.901	0.000	0.571	0.000	0.204	0.000
MM-V8-1e-3	Butler West	MM-V8-1	Feldspar	0.894	0.000	0.578	0.000	0.209	0.000
MM-V8-1f-1	Butler West	MM-V8-1	Feldspar	0.907	0.000	0.568	0.000	0.202	0.000
MM-V8-1f-2	Butler West	MM-V8-1	Feldspar	0.903	0.000	0.562	0.001	0.201	0.000
MM-V8-1f-3	Butler West	MM-V8-1	Feldspar	0.904	0.000	0.562	0.002	0.200	0.000
Sample Data				**Mole Cation**					
Analysis point	Intrusion/Phase	Sample	Mineral	SiO2	TiO2	Al2O3	Cr2O3	MgO	CaO
NO-2G21-2a-1	Thunderbird-V	NO-2G21-2	Pyroxene	0.906	0.002	0.035	0.000	0.384	0.217
NO-2G21-2a-3	Thunderbird-V	NO-2G21-2	Pyroxene	0.911	0.002	0.037	0.000	0.383	0.213
NO-2G21-2a-5	Thunderbird-V	NO-2G21-2	Pyroxene	0.815	0.007	0.129	0.000	0.288	0.209
NO-2G21-2a-7	Thunderbird-V	NO-2G21-2	Pyroxene	0.889	0.001	0.053	0.000	0.372	0.213
NO-2G21-2a-9	Thunderbird-V	NO-2G21-2	Pyroxene	0.916	0.001	0.023	0.000	0.399	0.213
NO-2G21-2a-10	Thunderbird-V	NO-2G21-2	Pyroxene	0.915	0.001	0.027	0.000	0.403	0.218
NO-2G21-2a-11	Thunderbird-V	NO-2G21-2	Pyroxene	0.936	0.001	0.013	0.000	0.434	0.217
NO-2G21-2a-13?	Thunderbird-V	NO-2G21-2	Pyroxene	0.919	0.007	0.019	0.000	0.404	0.214
NO-2G21-2a-14	Thunderbird-V	NO-2G21-2	Pyroxene	0.927	0.001	0.017	0.000	0.401	0.220
NO-2G21-2a-16	Thunderbird-V	NO-2G21-2	Pyroxene	0.908	0.001	0.036	0.000	0.392	0.214
NO-2G21-2b-23?	Thunderbird-V	NO-2G21-2	Pyroxene	0.898	0.001	0.042	0.000	0.379	0.217
NO-2G21-2b-24?	Thunderbird-V	NO-2G21-2	Pyroxene	0.914	0.000	0.024	0.000	0.404	0.218
NO-2G21-2b-26	Thunderbird-V	NO-2G21-2	Pyroxene	0.903	0.001	0.044	0.000	0.381	0.217
NO-2G21-2b-26	Thunderbird-V	NO-2G21-2	Pyroxene	0.766	0.003	0.184	0.000	0.239	0.204
NO-2G21-2c-31?	Thunderbird-V	NO-2G21-2	Pyroxene	0.906	0.001	0.043	0.000	0.384	0.219
NO-2G21-2c-32	Thunderbird-V	NO-2G21-2	Pyroxene	0.634	0.001	0.460	0.001	0.000	0.414
NO-2G21-5a-3	Thunderbird-V	NO-2G21-5	Pyroxene	0.637	0.000	0.487	0.001	0.000	0.416
NO-2G21-5a-6	Thunderbird-V	NO-2G21-5	Pyroxene	0.640	0.000	0.515	0.001	0.000	0.416
NO-2G21-5a-9	Thunderbird-V	NO-2G21-5	Pyroxene	0.637	0.000	0.493	0.001	0.000	0.416
NO-2G46-3a-2	Thunderbird-P	NO-2G46-3	Pyroxene	0.759	0.003	0.171	0.000	0.185	0.179
NO-2G46-3a-4	Thunderbird-P	NO-2G46-3	Pyroxene	0.844	0.008	0.049	0.000	0.251	0.090
NO-2G46-3c-10?	Thunderbird-P	NO-2G46-3	Pyroxene	0.843	0.001	0.043	0.000	0.261	0.071
NO-2G46-3c-10?	Thunderbird-P	NO-2G46-3	Pyroxene	0.793	0.002	0.125	0.000	0.225	0.202
NO-2G47-5b-6	Thunderbird-P	NO-2G47-5	Pyroxene	0.864	0.003	0.020	0.000	0.269	0.387
NO-2G47-5b-3	Thunderbird-P	NO-2G47-5	Pyroxene	0.846	0.007	0.028	0.000	0.248	0.362
NO-2G47-5b-2	Thunderbird-P	NO-2G47-5	Pyroxene	0.849	0.006	0.028	0.000	0.242	0.381
NO-2G47-5b-1	Thunderbird-P	NO-2G47-5	Pyroxene	0.861	0.003	0.022	0.000	0.270	0.374
NO-2G47-5c-13	Thunderbird-P	NO-2G47-5	Pyroxene	0.849	0.006	0.029	0.000	0.254	0.369
NO-2G47-5c-10	Thunderbird-P	NO-2G47-5	Pyroxene	0.861	0.003	0.019	0.000	0.270	0.373
NO-2G47-5c-9	Thunderbird-P	NO-2G47-5	Pyroxene	0.856	0.005	0.020	0.000	0.258	0.379

Sample Data							**Mole oxygen**					
Analysis point	FeOt	SrO	BaO	Na2O	K2O	Total	SiO2	TiO2	Al2O3	MgO	CaO	MnO
MM-V8-1b-5	0.003	0.000	0.000	0.166	0.001	1.846	1.799	0.000	0.855	0.001	0.205	0.000
MM-V8-1c-6	0.002	0.001	0.000	0.168	0.001	1.850	1.807	0.000	0.853	0.000	0.205	0.000
MM-V8-1c-7	0.002	0.001	0.000	0.171	0.001	1.849	1.827	0.000	0.842	0.001	0.198	0.000
MM-V8-1c-8	0.002	0.002	0.000	0.174	0.001	1.848	1.819	0.000	0.846	0.000	0.196	0.000
MM-V8-1d-1	0.001	0.000	0.000	0.166	0.001	1.841	1.809	0.000	0.847	0.000	0.204	0.000
MM-V8-1d-2	0.001	0.000	0.000	0.165	0.001	1.842	1.802	0.000	0.855	0.000	0.204	0.000
MM-V8-1d-3	0.002	0.000	0.000	0.165	0.000	1.842	1.807	0.000	0.850	0.000	0.203	0.000
MM-V8-1e-1	0.001	0.001	0.000	0.165	0.001	1.843	1.798	0.000	0.856	0.000	0.205	0.000
MM-V8-1e-2	0.002	0.001	0.000	0.165	0.001	1.845	1.801	0.001	0.856	0.000	0.204	0.000
MM-V8-1e-3	0.002	0.001	0.000	0.163	0.000	1.846	1.787	0.000	0.867	0.000	0.209	0.000
MM-V8-1f-1	0.001	0.001	0.000	0.173	0.001	1.853	1.815	0.000	0.852	0.000	0.202	0.000
MM-V8-1f-2	0.003	0.000	0.000	0.176	0.002	1.849	1.806	0.000	0.843	0.001	0.201	0.000
MM-V8-1f-3	0.006	0.000	0.000	0.173	0.003	1.850	1.809	0.000	0.842	0.002	0.200	0.000
Sample Data							**Mole oxygen**					
Analysis point	MnO	FeO2C	FeO	Na2O	K2O	Total	SiO2	TiO2	Al2O3	Cr2O3	MgO	CaO
NO-2G21-2a-1	0.004	0.000	0.191	0.007	0.001	1.746	1.811	0.004	0.053	0.000	0.384	0.217
NO-2G21-2a-3	0.004	0.000	0.190	0.007	0.001	1.749	1.821	0.004	0.056	0.000	0.383	0.213
NO-2G21-2a-5	0.004	0.000	0.240	0.026	0.004	1.722	1.630	0.013	0.193	0.000	0.288	0.209
NO-2G21-2a-7	0.004	0.000	0.202	0.010	0.001	1.744	1.777	0.002	0.080	0.000	0.372	0.213
NO-2G21-2a-9	0.003	0.000	0.184	0.004	0.000	1.743	1.832	0.001	0.034	0.000	0.399	0.213
NO-2G21-2a-10	0.003	0.000	0.180	0.005	0.000	1.752	1.829	0.001	0.041	0.000	0.403	0.218
NO-2G21-2a-11	0.004	0.000	0.161	0.004	0.000	1.771	1.873	0.001	0.020	0.000	0.434	0.217
NO-2G21-2a-13?	0.004	0.000	0.184	0.004	0.000	1.755	1.837	0.013	0.029	0.000	0.404	0.214
NO-2G21-2a-14	0.004	0.000	0.177	0.003	0.000	1.751	1.855	0.001	0.026	0.000	0.401	0.220
NO-2G21-2a-16	0.004	0.000	0.189	0.007	0.001	1.752	1.817	0.003	0.054	0.000	0.392	0.214
NO-2G21-2b-23?	0.003	0.000	0.188	0.007	0.001	1.736	1.796	0.002	0.062	0.000	0.379	0.217
NO-2G21-2b-24?	0.004	0.000	0.180	0.004	0.000	1.748	1.829	0.001	0.036	0.000	0.404	0.218
NO-2G21-2b-26	0.004	0.000	0.193	0.008	0.001	1.751	1.806	0.002	0.066	0.000	0.381	0.217
NO-2G21-2b-26	0.004	0.000	0.266	0.036	0.005	1.708	1.532	0.006	0.276	0.000	0.239	0.204
NO-2G21-2c-31?	0.004	0.000	0.192	0.008	0.001	1.757	1.812	0.002	0.064	0.000	0.384	0.219
NO-2G21-2c-32	0.001	0.000	0.172	0.000	0.000	1.684	1.269	0.002	0.690	0.001	0.000	0.414
NO-2G21-5a-3	0.001	0.000	0.151	0.000	0.000	1.693	1.273	0.000	0.731	0.001	0.000	0.416
NO-2G21-5a-6	0.002	0.000	0.130	0.000	0.000	1.704	1.279	0.001	0.773	0.001	0.000	0.416
NO-2G21-5a-9	0.001	0.000	0.141	0.000	0.000	1.689	1.275	0.000	0.739	0.001	0.000	0.416
NO-2G46-3a-2	0.005	0.000	0.338	0.034	0.004	1.679	1.517	0.007	0.257	0.000	0.185	0.179
NO-2G46-3a-4	0.011	0.000	0.394	0.015	0.001	1.664	1.689	0.016	0.074	0.000	0.251	0.090
NO-2G46-3c-10?	0.012	0.000	0.406	0.010	0.001	1.650	1.686	0.002	0.065	0.000	0.261	0.071
NO-2G46-3c-10?	0.004	0.000	0.302	0.028	0.003	1.685	1.587	0.005	0.188	0.001	0.225	0.202
NO-2G47-5b-6	0.004	0.000	0.199	0.006	0.000	1.752	1.728	0.006	0.030	0.000	0.269	0.387
NO-2G47-5b-3	0.005	0.000	0.228	0.007	0.000	1.731	1.692	0.014	0.042	0.001	0.248	0.362
NO-2G47-5b-2	0.006	0.000	0.215	0.007	0.000	1.736	1.699	0.013	0.042	0.000	0.242	0.381
NO-2G47-5b-1	0.005	0.000	0.205	0.007	0.000	1.746	1.721	0.005	0.033	0.000	0.270	0.374
NO-2G47-5c-13	0.006	0.000	0.217	0.007	0.000	1.737	1.698	0.012	0.044	0.000	0.254	0.369
NO-2G47-5c-10	0.005	0.000	0.214	0.006	0.000	1.751	1.722	0.005	0.029	0.000	0.270	0.373
NO-2G47-5c-9	0.005	0.000	0.217	0.007	0.000	1.747	1.712	0.010	0.031	0.000	0.258	0.379

Sample Data							**Norm Cations**					
Analysis point	FeOt	SrO	BaO	Na2O	K2O	Total	SiO2	TiO2	Al2O3	MgO	CaO	MnO
MM-V8-1b-5	0.005	0.000	0.000	0.083	0.000	2.950	2.440	0.000	1.546	0.002	0.557	0.000
MM-V8-1c-6	0.002	0.001	0.000	0.084	0.000	2.954	2.447	0.000	1.540	0.001	0.556	0.000
MM-V8-1c-7	0.003	0.001	0.000	0.086	0.001	2.958	2.471	0.000	1.518	0.002	0.535	0.000
MM-V8-1c-8	0.002	0.002	0.000	0.087	0.000	2.952	2.464	0.000	1.528	0.001	0.531	0.000
MM-V8-1d-1	0.002	0.000	0.000	0.083	0.000	2.945	2.456	0.000	1.534	0.000	0.554	0.000
MM-V8-1d-2	0.002	0.000	0.000	0.083	0.000	2.946	2.446	0.000	1.548	0.000	0.555	0.000
MM-V8-1d-3	0.003	0.000	0.000	0.083	0.000	2.947	2.453	0.001	1.538	0.001	0.551	0.000
MM-V8-1e-1	0.002	0.001	0.000	0.083	0.000	2.945	2.442	0.000	1.550	0.001	0.556	0.000
MM-V8-1e-2	0.003	0.001	0.000	0.083	0.000	2.950	2.443	0.001	1.548	0.001	0.553	0.000
MM-V8-1e-3	0.003	0.001	0.000	0.081	0.000	2.949	2.424	0.000	1.568	0.000	0.566	0.000
MM-V8-1f-1	0.001	0.001	0.000	0.086	0.001	2.958	2.454	0.000	1.537	0.000	0.547	0.000
MM-V8-1f-2	0.005	0.000	0.000	0.088	0.001	2.946	2.453	0.000	1.527	0.002	0.545	0.000
MM-V8-1f-3	0.008	0.000	0.000	0.086	0.001	2.950	2.452	0.001	1.523	0.005	0.543	0.000
Sample Data							**Norm Cations**					
Analysis point	MnO	FeO2C	FeO	Na2O	K2O	Total	SiO2	TiO2	Al2O3	Cr2O3	MgO	CaO
NO-2G21-2a-1	0.004	0.000	0.191	0.003	0.000	2.667	2.075	0.004	0.081	0.000	0.880	0.497
NO-2G21-2a-3	0.004	0.000	0.190	0.004	0.000	2.677	2.083	0.005	0.086	0.000	0.877	0.488
NO-2G21-2a-5	0.004	0.000	0.240	0.013	0.002	2.593	1.894	0.016	0.299	0.000	0.670	0.485
NO-2G21-2a-7	0.004	0.000	0.202	0.005	0.001	2.655	2.038	0.003	0.122	0.001	0.853	0.489
NO-2G21-2a-9	0.003	0.000	0.184	0.002	0.000	2.669	2.102	0.002	0.052	0.000	0.915	0.489
NO-2G21-2a-10	0.003	0.000	0.180	0.003	0.000	2.678	2.089	0.002	0.062	0.000	0.920	0.497
NO-2G21-2a-11	0.004	0.000	0.161	0.002	0.000	2.713	2.115	0.001	0.030	0.000	0.979	0.491
NO-2G21-2a-13?	0.004	0.000	0.184	0.002	0.000	2.688	2.094	0.015	0.044	0.000	0.920	0.487
NO-2G21-2a-14	0.004	0.000	0.177	0.002	0.000	2.686	2.118	0.001	0.040	0.000	0.916	0.502
NO-2G21-2a-16	0.004	0.000	0.189	0.004	0.000	2.676	2.074	0.003	0.082	0.000	0.895	0.488
NO-2G21-2b-23?	0.003	0.000	0.188	0.004	0.000	2.652	2.069	0.002	0.096	0.001	0.873	0.499
NO-2G21-2b-24?	0.004	0.000	0.180	0.002	0.000	2.673	2.092	0.001	0.054	0.000	0.924	0.498
NO-2G21-2b-26	0.004	0.000	0.193	0.004	0.000	2.673	2.062	0.003	0.101	0.000	0.871	0.495
NO-2G21-2b-26	0.004	0.000	0.266	0.018	0.003	2.548	1.794	0.007	0.431	0.001	0.561	0.479
NO-2G21-2c-31?	0.004	0.000	0.192	0.004	0.000	2.681	2.063	0.002	0.098	0.000	0.873	0.498
NO-2G21-2c-32	0.001	0.000	0.172	0.000	0.000	2.549	1.507	0.002	1.093	0.002	0.000	0.985
NO-2G21-5a-3	0.001	0.000	0.151	0.000	0.000	2.573	1.505	0.000	1.151	0.002	0.001	0.984
NO-2G21-5a-6	0.002	0.000	0.130	0.000	0.000	2.602	1.501	0.001	1.209	0.002	0.000	0.978
NO-2G21-5a-9	0.001	0.000	0.141	0.000	0.000	2.574	1.509	0.000	1.167	0.002	0.000	0.984
NO-2G46-3a-2	0.005	0.000	0.338	0.017	0.002	2.508	1.807	0.008	0.408	0.000	0.440	0.427
NO-2G46-3a-4	0.011	0.000	0.394	0.008	0.000	2.533	2.029	0.019	0.119	0.000	0.604	0.216
NO-2G46-3c-10?	0.012	0.000	0.406	0.005	0.001	2.510	2.044	0.003	0.105	0.000	0.633	0.173
NO-2G46-3c-10?	0.004	0.000	0.302	0.014	0.001	2.528	1.883	0.006	0.297	0.001	0.533	0.480
NO-2G47-5b-6	0.004	0.000	0.199	0.003	0.000	2.626	1.972	0.006	0.046	0.000	0.615	0.883
NO-2G47-5b-3	0.005	0.000	0.228	0.003	0.000	2.595	1.956	0.016	0.065	0.001	0.572	0.835
NO-2G47-5b-2	0.006	0.000	0.215	0.004	0.000	2.601	1.958	0.015	0.064	0.000	0.558	0.879
NO-2G47-5b-1	0.005	0.000	0.205	0.003	0.000	2.616	1.972	0.006	0.050	0.000	0.619	0.856
NO-2G47-5c-13	0.006	0.000	0.217	0.003	0.000	2.603	1.955	0.014	0.067	0.001	0.584	0.851
NO-2G47-5c-10	0.005	0.000	0.214	0.003	0.000	2.622	1.967	0.006	0.044	0.001	0.616	0.852
NO-2G47-5c-9	0.005	0.000	0.217	0.003	0.000	2.615	1.960	0.011	0.047	0.000	0.590	0.868

Sample Data						**Norm Oxygen**								
Analysis point	SrO	BaO	Na2O	K2O	Total	SiO2	TiO2	Al2O3	MgO	CaO	MnO	FeOt	SrO	BaO
MM-V8-1b-5	0.001	0.000	0.450	0.002	5.008	4.880	0.001	2.319	0.002	0.557	0.000	0.014	0.001	0.000
MM-V8-1c-6	0.003	0.000	0.454	0.003	5.009	4.893	0.001	2.310	0.001	0.556	0.000	0.007	0.003	0.000
MM-V8-1c-7	0.004	0.000	0.463	0.003	5.000	4.942	0.001	2.277	0.002	0.535	0.000	0.008	0.004	0.000
MM-V8-1c-8	0.005	0.000	0.473	0.001	5.007	4.928	0.000	2.292	0.001	0.531	0.000	0.007	0.005	0.000
MM-V8-1d-1	0.000	0.000	0.451	0.001	5.001	4.913	0.000	2.302	0.000	0.554	0.000	0.005	0.000	0.000
MM-V8-1d-2	0.001	0.000	0.448	0.002	5.004	4.893	0.000	2.321	0.000	0.555	0.000	0.005	0.001	0.000
MM-V8-1d-3	0.000	0.000	0.449	0.001	5.000	4.907	0.001	2.308	0.001	0.551	0.000	0.007	0.000	0.000
MM-V8-1e-1	0.002	0.000	0.449	0.002	5.006	4.885	0.000	2.326	0.001	0.556	0.000	0.005	0.002	0.000
MM-V8-1e-2	0.003	0.000	0.448	0.002	5.004	4.885	0.003	2.322	0.001	0.553	0.000	0.009	0.003	0.000
MM-V8-1e-3	0.002	0.000	0.441	0.001	5.010	4.849	0.001	2.352	0.000	0.566	0.000	0.009	0.002	0.000
MM-V8-1f-1	0.002	0.000	0.467	0.003	5.012	4.908	0.000	2.305	0.000	0.547	0.000	0.003	0.002	0.000
MM-V8-1f-2	0.000	0.000	0.478	0.005	5.020	4.905	0.001	2.291	0.002	0.545	0.000	0.014	0.000	0.000
MM-V8-1f-3	0.001	0.000	0.468	0.008	5.017	4.904	0.001	2.284	0.005	0.543	0.000	0.023	0.001	0.000
Sample Data						**Norm Oxygen**								
Analysis point	FeO2C	FeO	Na2O	K2O	Total	SiO2	TiO2	Al2O3	Cr2O3	MgO	CaO	MnO	FeO2C	FeO
NO-2G21-2a-1	0.000	0.437	0.015	0.001	4.000	4.150	0.008	0.121	0.000	0.880	0.497	0.014	0.000	0.437
NO-2G21-2a-3	0.000	0.435	0.017	0.001	4.000	4.165	0.009	0.128	0.000	0.877	0.488	0.013	0.000	0.435
NO-2G21-2a-5	0.000	0.557	0.060	0.010	4.000	3.788	0.031	0.448	0.000	0.670	0.485	0.014	0.000	0.557
NO-2G21-2a-7	0.000	0.462	0.022	0.002	4.000	4.075	0.005	0.183	0.001	0.853	0.489	0.013	0.000	0.462
NO-2G21-2a-9	0.000	0.423	0.010	0.000	4.000	4.205	0.003	0.078	0.000	0.915	0.489	0.012	0.000	0.423
NO-2G21-2a-10	0.000	0.410	0.012	0.001	4.000	4.177	0.003	0.093	0.000	0.920	0.497	0.011	0.000	0.410
NO-2G21-2a-11	0.000	0.364	0.009	0.001	4.000	4.229	0.003	0.045	0.000	0.979	0.491	0.015	0.000	0.364
NO-2G21-2a-13?	0.000	0.419	0.009	0.000	4.000	4.188	0.031	0.066	0.000	0.920	0.487	0.015	0.000	0.419
NO-2G21-2a-14	0.000	0.405	0.007	0.001	4.000	4.236	0.002	0.060	0.000	0.916	0.502	0.015	0.000	0.405
NO-2G21-2a-16	0.000	0.432	0.016	0.001	4.000	4.148	0.006	0.123	0.000	0.895	0.488	0.012	0.000	0.432
NO-2G21-2b-23?	0.000	0.434	0.017	0.002	4.000	4.138	0.004	0.144	0.001	0.873	0.499	0.012	0.000	0.434
NO-2G21-2b-24?	0.000	0.413	0.009	0.000	4.000	4.184	0.002	0.081	0.000	0.924	0.498	0.013	0.000	0.413
NO-2G21-2b-26	0.000	0.440	0.017	0.001	4.000	4.125	0.005	0.151	0.000	0.871	0.495	0.014	0.000	0.440
NO-2G21-2b-26	0.000	0.622	0.085	0.012	4.000	3.588	0.015	0.646	0.001	0.561	0.479	0.013	0.000	0.622
NO-2G21-2c-31?	0.000	0.437	0.018	0.001	4.000	4.126	0.004	0.147	0.000	0.873	0.498	0.012	0.000	0.437
NO-2G21-2c-32	0.000	0.408	0.000	0.000	4.000	3.015	0.004	1.640	0.002	0.000	0.985	0.004	0.000	0.408
NO-2G21-5a-3	0.000	0.356	0.000	0.000	4.000	3.009	0.000	1.727	0.002	0.001	0.984	0.003	0.000	0.356
NO-2G21-5a-6	0.000	0.305	0.000	0.000	4.000	3.003	0.002	1.814	0.002	0.000	0.978	0.006	0.000	0.305
NO-2G21-5a-9	0.000	0.334	0.000	0.000	4.000	3.018	0.001	1.751	0.002	0.000	0.984	0.004	0.000	0.334
NO-2G46-3a-2	0.000	0.806	0.081	0.010	4.000	3.615	0.017	0.612	0.000	0.440	0.427	0.018	0.000	0.806
NO-2G46-3a-4	0.000	0.947	0.036	0.002	4.000	4.058	0.039	0.178	0.000	0.604	0.216	0.040	0.000	0.947
NO-2G46-3c-10?	0.000	0.984	0.025	0.003	4.000	4.088	0.006	0.158	0.000	0.633	0.173	0.045	0.000	0.984
NO-2G46-3c-10?	0.000	0.718	0.067	0.007	4.000	3.765	0.011	0.445	0.001	0.533	0.480	0.014	0.000	0.718
NO-2G47-5b-6	0.000	0.454	0.013	0.000	4.000	3.945	0.013	0.068	0.000	0.615	0.883	0.015	0.000	0.454
NO-2G47-5b-3	0.000	0.527	0.016	0.000	4.000	3.911	0.032	0.097	0.001	0.572	0.835	0.018	0.000	0.527
NO-2G47-5b-2	0.000	0.496	0.017	0.001	4.000	3.915	0.029	0.096	0.000	0.558	0.879	0.020	0.000	0.496
NO-2G47-5b-1	0.000	0.471	0.015	0.000	4.000	3.944	0.013	0.075	0.000	0.619	0.856	0.017	0.000	0.471
NO-2G47-5c-13	0.000	0.500	0.016	0.000	4.000	3.911	0.028	0.101	0.001	0.584	0.851	0.019	0.000	0.500
NO-2G47-5c-10	0.000	0.490	0.013	0.000	4.000	3.934	0.012	0.065	0.001	0.616	0.852	0.017	0.000	0.490
NO-2G47-5c-9	0.000	0.496	0.015	0.000	4.000	3.919	0.022	0.070	0.000	0.590	0.868	0.019	0.000	0.496

Sample Data			**Atom units**							
Analysis point	K2O	Total	SiO2	TiO2	Al2O3	MgO	CaO	MnO	FeOt	SrO
MM-V8-1b-5	0.001	8.000	2.440	0.000	1.546	0.002	0.557	0.000	0.009	0.001
MM-V8-1c-6	0.001	8.000	2.447	0.000	1.540	0.001	0.556	0.000	0.004	0.003
MM-V8-1c-7	0.001	8.000	2.471	0.000	1.518	0.002	0.535	0.000	0.005	0.004
MM-V8-1c-8	0.001	8.000	2.464	0.000	1.528	0.001	0.531	0.000	0.004	0.005
MM-V8-1d-1	0.001	8.000	2.456	0.000	1.534	0.000	0.554	0.000	0.003	0.000
MM-V8-1d-2	0.001	8.000	2.446	0.000	1.548	0.000	0.555	0.000	0.003	0.001
MM-V8-1d-3	0.001	8.000	2.453	0.001	1.538	0.001	0.551	0.000	0.005	0.000
MM-V8-1e-1	0.001	8.000	2.442	0.000	1.550	0.001	0.556	0.000	0.004	0.002
MM-V8-1e-2	0.001	8.000	2.443	0.001	1.548	0.001	0.553	0.000	0.006	0.003
MM-V8-1e-3	0.000	8.000	2.424	0.000	1.568	0.000	0.566	0.000	0.006	0.002
MM-V8-1f-1	0.002	8.000	2.454	0.000	1.537	0.000	0.547	0.000	0.002	0.002
MM-V8-1f-2	0.002	8.000	2.453	0.000	1.527	0.002	0.545	0.000	0.009	0.000
MM-V8-1f-3	0.004	8.000	2.452	0.001	1.523	0.005	0.543	0.000	0.015	0.001

Sample Data			**Atom units**							
Analysis point	K2O	Total	SiO2	TiO2	Al2O3	Cr2O3	MgO	CaO	MnO	FeO2C
NO-2G21-2a-1	0.001	6.116	2.075	0.004	0.081	0.000	0.880	0.497	0.009	0.000
NO-2G21-2a-3	0.001	6.125	2.083	0.005	0.086	0.000	0.877	0.488	0.009	0.000
NO-2G21-2a-5	0.005	6.029	1.894	0.016	0.299	0.000	0.670	0.485	0.009	0.000
NO-2G21-2a-7	0.001	6.093	2.038	0.003	0.122	0.001	0.853	0.489	0.009	0.000
NO-2G21-2a-9	0.000	6.129	2.102	0.002	0.052	0.000	0.915	0.489	0.008	0.000
NO-2G21-2a-10	0.000	6.118	2.089	0.002	0.062	0.000	0.920	0.497	0.007	0.000
NO-2G21-2a-11	0.000	6.131	2.115	0.001	0.030	0.000	0.979	0.491	0.010	0.000
NO-2G21-2a-13?	0.000	6.131	2.094	0.015	0.044	0.000	0.920	0.487	0.010	0.000
NO-2G21-2a-14	0.000	6.140	2.118	0.001	0.040	0.000	0.916	0.502	0.010	0.000
NO-2G21-2a-16	0.001	6.113	2.074	0.003	0.082	0.000	0.895	0.488	0.008	0.000
NO-2G21-2b-23?	0.001	6.114	2.069	0.002	0.096	0.001	0.873	0.499	0.008	0.000
NO-2G21-2b-24?	0.000	6.120	2.092	0.001	0.054	0.000	0.924	0.498	0.009	0.000
NO-2G21-2b-26	0.001	6.111	2.062	0.003	0.101	0.000	0.871	0.495	0.009	0.000
NO-2G21-2b-26	0.006	5.972	1.794	0.007	0.431	0.001	0.561	0.479	0.009	0.000
NO-2G21-2c-31?	0.001	6.108	2.063	0.002	0.098	0.000	0.873	0.498	0.008	0.000
NO-2G21-2c-32	0.000	6.057	1.507	0.002	1.093	0.002	0.000	0.985	0.003	0.000
NO-2G21-5a-3	0.000	6.081	1.505	0.000	1.151	0.002	0.001	0.984	0.002	0.000
NO-2G21-5a-6	0.000	6.109	1.501	0.001	1.209	0.002	0.000	0.978	0.004	0.000
NO-2G21-5a-9	0.000	6.094	1.509	0.000	1.167	0.002	0.000	0.984	0.002	0.000
NO-2G46-3a-2	0.005	5.980	1.807	0.008	0.408	0.000	0.440	0.427	0.012	0.000
NO-2G46-3a-4	0.001	6.102	2.029	0.019	0.119	0.000	0.604	0.216	0.027	0.000
NO-2G46-3c-10?	0.001	6.100	2.044	0.003	0.105	0.000	0.633	0.173	0.030	0.000
NO-2G46-3c-10?	0.003	6.004	1.883	0.006	0.297	0.001	0.533	0.480	0.009	0.000
NO-2G47-5b-6	0.000	6.000	1.972	0.006	0.046	0.000	0.615	0.883	0.010	0.000
NO-2G47-5b-3	0.000	6.002	1.956	0.016	0.065	0.001	0.572	0.835	0.012	0.000
NO-2G47-5b-2	0.000	6.002	1.958	0.015	0.064	0.000	0.558	0.879	0.013	0.000
NO-2G47-5b-1	0.000	6.001	1.972	0.006	0.050	0.000	0.619	0.856	0.011	0.000
NO-2G47-5c-13	0.000	6.001	1.955	0.014	0.067	0.001	0.584	0.851	0.013	0.000
NO-2G47-5c-10	0.000	5.994	1.967	0.006	0.044	0.001	0.616	0.852	0.012	0.000
NO-2G47-5c-9	0.000	5.992	1.960	0.011	0.047	0.000	0.590	0.868	0.012	0.000

Sample Data				**Norm oxygen**								
Analysis point	Na2O	K2O	Total	SiO2	TiO2	Al2O3	MgO	CaO	MnO	FeOt	SrO	BaO
MM-V8-1b-5	0.450	0.002	5.008	4.880	0.001	2.319	0.002	0.557	0.000	0.014	0.001	0.000
MM-V8-1c-6	0.454	0.003	5.009	4.893	0.001	2.310	0.001	0.556	0.000	0.007	0.003	0.000
MM-V8-1c-7	0.463	0.003	5.000	4.942	0.001	2.277	0.002	0.535	0.000	0.008	0.004	0.000
MM-V8-1c-8	0.473	0.001	5.007	4.928	0.000	2.292	0.001	0.531	0.000	0.007	0.005	0.000
MM-V8-1d-1	0.451	0.001	5.001	4.913	0.000	2.302	0.000	0.554	0.000	0.005	0.000	0.000
MM-V8-1d-2	0.448	0.002	5.004	4.893	0.000	2.321	0.000	0.555	0.000	0.005	0.001	0.000
MM-V8-1d-3	0.449	0.001	5.000	4.907	0.001	2.308	0.001	0.551	0.000	0.007	0.000	0.000
MM-V8-1e-1	0.449	0.002	5.006	4.885	0.000	2.326	0.001	0.556	0.000	0.005	0.002	0.000
MM-V8-1e-2	0.448	0.002	5.004	4.885	0.003	2.322	0.001	0.553	0.000	0.009	0.003	0.000
MM-V8-1e-3	0.441	0.001	5.010	4.849	0.001	2.352	0.000	0.566	0.000	0.009	0.002	0.000
MM-V8-1f-1	0.467	0.003	5.012	4.908	0.000	2.305	0.000	0.547	0.000	0.003	0.002	0.000
MM-V8-1f-2	0.478	0.005	5.020	4.905	0.001	2.291	0.002	0.545	0.000	0.014	0.000	0.000
MM-V8-1f-3	0.468	0.008	5.017	4.904	0.001	2.284	0.005	0.543	0.000	0.023	0.001	0.000
Sample Data				**Norm oxygen**								
Analysis point	Na2O	K2O	Total	SiO2	TiO2	Al2O3	Cr2O3	MgO	CaO	MnO	FeO2C	FeO
NO-2G21-2a-1	0.015	0.001	4.000	4.150	0.008	0.121	0.000	0.880	0.497	0.014	0.000	0.437
NO-2G21-2a-3	0.017	0.001	4.000	4.165	0.009	0.128	0.000	0.877	0.488	0.013	0.000	0.435
NO-2G21-2a-5	0.060	0.010	4.000	3.788	0.031	0.448	0.000	0.670	0.485	0.014	0.000	0.557
NO-2G21-2a-7	0.022	0.002	4.000	4.075	0.005	0.183	0.001	0.853	0.489	0.013	0.000	0.462
NO-2G21-2a-9	0.010	0.000	4.000	4.205	0.003	0.078	0.000	0.915	0.489	0.012	0.000	0.423
NO-2G21-2a-10	0.012	0.001	4.000	4.177	0.003	0.093	0.000	0.920	0.497	0.011	0.000	0.410
NO-2G21-2a-11	0.009	0.001	4.000	4.229	0.003	0.045	0.000	0.979	0.491	0.015	0.000	0.364
NO-2G21-2a-13?	0.009	0.000	4.000	4.188	0.031	0.066	0.000	0.920	0.487	0.015	0.000	0.419
NO-2G21-2a-14	0.007	0.001	4.000	4.236	0.002	0.060	0.000	0.916	0.502	0.015	0.000	0.405
NO-2G21-2a-16	0.016	0.001	4.000	4.148	0.006	0.123	0.000	0.895	0.488	0.012	0.000	0.432
NO-2G21-2b-23?	0.017	0.002	4.000	4.138	0.004	0.144	0.001	0.873	0.499	0.012	0.000	0.434
NO-2G21-2b-24?	0.009	0.000	4.000	4.184	0.002	0.081	0.000	0.924	0.498	0.013	0.000	0.413
NO-2G21-2b-26	0.017	0.001	4.000	4.125	0.005	0.151	0.000	0.871	0.495	0.014	0.000	0.440
NO-2G21-2b-26	0.085	0.012	4.000	3.588	0.015	0.646	0.001	0.561	0.479	0.013	0.000	0.622
NO-2G21-2c-31?	0.018	0.001	4.000	4.126	0.004	0.147	0.000	0.873	0.498	0.012	0.000	0.437
NO-2G21-2c-32	0.000	0.000	4.000	3.015	0.004	1.640	0.002	0.000	0.985	0.004	0.000	0.408
NO-2G21-5a-3	0.000	0.000	4.000	3.009	0.000	1.727	0.002	0.001	0.984	0.003	0.000	0.356
NO-2G21-5a-6	0.000	0.000	4.000	3.003	0.002	1.814	0.002	0.000	0.978	0.006	0.000	0.305
NO-2G21-5a-9	0.000	0.000	4.000	3.018	0.001	1.751	0.002	0.000	0.984	0.004	0.000	0.334
NO-2G46-3a-2	0.081	0.010	4.000	3.615	0.017	0.612	0.000	0.440	0.427	0.018	0.000	0.806
NO-2G46-3a-4	0.036	0.002	4.000	4.058	0.039	0.178	0.000	0.604	0.216	0.040	0.000	0.947
NO-2G46-3c-10?	0.025	0.003	4.000	4.088	0.006	0.158	0.000	0.633	0.173	0.045	0.000	0.984
NO-2G46-3c-10?	0.067	0.007	4.000	3.765	0.011	0.445	0.001	0.533	0.480	0.014	0.000	0.718
NO-2G47-5b-6	0.013	0.000	4.000	3.945	0.013	0.068	0.000	0.615	0.883	0.015	0.000	0.454
NO-2G47-5b-3	0.016	0.000	4.000	3.911	0.032	0.097	0.001	0.572	0.835	0.018	0.000	0.527
NO-2G47-5b-2	0.017	0.001	4.000	3.915	0.029	0.096	0.000	0.558	0.879	0.020	0.000	0.496
NO-2G47-5b-1	0.015	0.000	4.000	3.944	0.013	0.075	0.000	0.619	0.856	0.017	0.000	0.471
NO-2G47-5c-13	0.016	0.000	4.000	3.911	0.028	0.101	0.001	0.584	0.851	0.019	0.000	0.500
NO-2G47-5c-10	0.013	0.000	4.000	3.934	0.012	0.065	0.001	0.616	0.852	0.017	0.000	0.490
NO-2G47-5c-9	0.015	0.000	4.000	3.919	0.022	0.070	0.000	0.590	0.868	0.019	0.000	0.496

Sample Data			**End Member**		
Analysis point	Na2O	K2O	Anorthite	Albite	Orthoclase
MM-V8-1b-5	0.225	0.001	55.2	44.6	0.2
MM-V8-1c-6	0.227	0.001	54.9	44.9	0.3
MM-V8-1c-7	0.231	0.001	53.5	46.2	0.3
MM-V8-1c-8	0.236	0.001	52.8	47.0	0.1
MM-V8-1d-1	0.225	0.001	55.1	44.8	0.1
MM-V8-1d-2	0.224	0.001	55.2	44.6	0.2
MM-V8-1d-3	0.224	0.001	55.0	44.9	0.1
MM-V8-1e-1	0.224	0.001	55.2	44.6	0.2
MM-V8-1e-2	0.224	0.001	55.1	44.7	0.2
MM-V8-1e-3	0.221	0.000	56.2	43.8	0.1
MM-V8-1f-1	0.233	0.002	53.8	45.9	0.3
MM-V8-1f-2	0.239	0.002	53.0	46.5	0.5
MM-V8-1f-3	0.234	0.004	53.3	45.9	0.8
Sample Data			**End Member**		
Analysis point	Na2O	K2O	Wollastonite	Enstatite	Ferrosilite
NO-2G21-2a-1	0.008	0.001	27.4	48.5	24.1
NO-2G21-2a-3	0.008	0.001	27.1	48.7	24.2
NO-2G21-2a-5	0.030	0.005	28.3	39.1	32.5
NO-2G21-2a-7	0.011	0.001	27.1	47.3	25.6
NO-2G21-2a-9	0.005	0.000	26.8	50.1	23.1
NO-2G21-2a-10	0.006	0.000	27.2	50.4	22.4
NO-2G21-2a-11	0.004	0.000	26.8	53.4	19.8
NO-2G21-2a-13?	0.005	0.000	26.7	50.4	22.9
NO-2G21-2a-14	0.004	0.000	27.6	50.2	22.2
NO-2G21-2a-16	0.008	0.001	26.9	49.3	23.8
NO-2G21-2b-23?	0.008	0.001	27.7	48.3	24.0
NO-2G21-2b-24?	0.005	0.000	27.1	50.3	22.5
NO-2G21-2b-26	0.009	0.001	27.4	48.2	24.4
NO-2G21-2b-26	0.043	0.006	28.8	33.7	37.5
NO-2G21-2c-31?	0.009	0.001	27.6	48.3	24.2
NO-2G21-2c-32	0.000	0.000	70.7	0.0	29.3
NO-2G21-5a-3	0.000	0.000	73.4	0.1	26.5
NO-2G21-5a-6	0.000	0.000	76.2	0.0	23.8
NO-2G21-5a-9	0.000	0.000	74.7	0.0	25.3
NO-2G46-3a-2	0.041	0.005	25.5	26.3	48.2
NO-2G46-3a-4	0.018	0.001	12.2	34.2	53.6
NO-2G46-3c-10?	0.013	0.001	9.7	35.3	55.0
NO-2G46-3c-10?	0.034	0.003	27.7	30.8	41.5
NO-2G47-5b-6	0.007	0.000	45.3	31.5	23.2
NO-2G47-5b-3	0.008	0.000	43.2	29.6	27.3
NO-2G47-5b-2	0.008	0.000	45.5	28.9	25.7
NO-2G47-5b-1	0.008	0.000	44.0	31.8	24.2
NO-2G47-5c-13	0.008	0.000	44.0	30.2	25.8
NO-2G47-5c-10	0.007	0.000	43.5	31.5	25.0
NO-2G47-5c-9	0.008	0.000	44.4	30.2	25.4

Sample Data				**Mole Cation**					
Analysis point	Intrusion/Phase	Sample	Mineral	SiO2	TiO2	Al2O3	Cr2O3	MgO	CaO
NO-2G47-2b-10	Thunderbird-P	NO-2G47-2	Pyroxene	0.768	0.005	0.160	0.000	0.194	0.207
NO-2G47-2b-9	Thunderbird-P	NO-2G47-2	Pyroxene	0.826	0.003	0.096	0.000	0.243	0.208
NO-2G47-2b-8	Thunderbird-P	NO-2G47-2	Pyroxene	0.809	0.002	0.117	0.000	0.225	0.207
NO-2G47-2b-7	Thunderbird-P	NO-2G47-2	Pyroxene	0.780	0.008	0.137	0.000	0.194	0.208
NO-2G47-2a-6	Thunderbird-P	NO-2G47-2	Pyroxene	0.810	0.004	0.115	0.000	0.229	0.210
NO-2G47-2a-5?	Thunderbird-P	NO-2G47-2	Pyroxene	0.795	0.004	0.141	0.000	0.217	0.209
NO-2G47-2a-4?	Thunderbird-P	NO-2G47-2	Pyroxene	0.822	0.003	0.097	0.000	0.248	0.215
NO-2G47-2a-1	Thunderbird-P	NO-2G47-2	Pyroxene	0.846	0.002	0.078	0.000	0.258	0.212
NO-2G47-2a-2	Thunderbird-P	NO-2G47-2	Pyroxene	0.876	0.001	0.048	0.000	0.276	0.216
NO-2G47-2a-3?	Thunderbird-P	NO-2G47-2	Pyroxene	0.784	0.005	0.148	0.000	0.204	0.208
MM-117-1a-1	Butler West	MM-117-1	Pyroxene	0.830	0.004	0.133	0.000	0.343	0.214
MM-117-1a-3	Butler West	MM-117-1	Pyroxene	0.782	0.005	0.185	0.000	0.306	0.208
MM-117-1b-4	Butler West	MM-117-1	Pyroxene	0.813	0.006	0.146	0.001	0.324	0.209
MM-117-1b-5	Butler West	MM-117-1	Pyroxene	0.815	0.006	0.158	0.000	0.336	0.215
MM-117-1b-7	Butler West	MM-117-1	Pyroxene	0.700	0.002	0.219	0.000	0.321	0.132
MM-117-1c-8	Butler West	MM-117-1	Pyroxene	0.816	0.004	0.152	0.000	0.328	0.208
MM-117-1c-10	Butler West	MM-117-1	Pyroxene	0.831	0.004	0.135	0.000	0.344	0.210
MM-117-6b-1	Butler West	MM-117-6	Pyroxene	0.885	0.000	0.011	0.000	0.374	0.016
MM-117-6b-2	Butler West	MM-117-6	Pyroxene	0.893	0.000	0.007	0.000	0.379	0.010
MM-117-6b-3	Butler West	MM-117-6	Pyroxene	0.889	0.000	0.011	0.000	0.373	0.016
MM-V4-1a-1	Butler East	MM-V4-1	Pyroxene	0.938	0.001	0.038	0.000	0.611	0.008
MM-V4-1a-2	Butler East	MM-V4-1	Pyroxene	0.929	0.000	0.040	0.000	0.606	0.009
MM-V4-1a-3	Butler East	MM-V4-1	Pyroxene	0.939	0.001	0.037	0.000	0.605	0.008
MM-V4-1a-6	Butler East	MM-V4-1	Pyroxene	0.933	0.001	0.038	0.000	0.603	0.009
MM-V4-1b-7	Butler East	MM-V4-1	Pyroxene	0.929	0.001	0.044	0.000	0.594	0.009
MM-V4-1b-8	Butler East	MM-V4-1	Pyroxene	0.926	0.001	0.043	0.000	0.608	0.009
MM-V4-1b-10	Butler East	MM-V4-1	Pyroxene	0.930	0.001	0.044	0.000	0.587	0.010
MM-V4-1c-11	Butler East	MM-V4-1	Pyroxene	0.921	0.001	0.039	0.000	0.575	0.008
MM-V4-1c-12	Butler East	MM-V4-1	Pyroxene	0.945	0.000	0.028	0.000	0.615	0.008
MM-V4-1c-13	Butler East	MM-V4-1	Pyroxene	0.920	0.001	0.034	0.000	0.592	0.007
MM-V4-1c-14	Butler East	MM-V4-1	Pyroxene	0.934	0.000	0.041	0.000	0.610	0.009
MM-V4-7a-1	Butler East	MM-V4-7	Pyroxene	0.706	0.012	0.258	0.000	0.180	0.190
MM-V4-7a-2	Butler East	MM-V4-7	Pyroxene	0.707	0.011	0.258	0.000	0.189	0.184
MM-V4-7a-3	Butler East	MM-V4-7	Pyroxene	0.709	0.011	0.258	0.000	0.197	0.190
MM-V8-1a-1	Butler West	MM-V8-1	Pyroxene	0.718	0.011	0.231	0.000	0.204	0.207
MM-V8-1a-2	Butler West	MM-V8-1	Pyroxene	0.729	0.009	0.230	0.000	0.210	0.206
MM-V8-1a-3	Butler West	MM-V8-1	Pyroxene	0.818	0.005	0.118	0.000	0.293	0.206
MM-V8-1a-4	Butler West	MM-V8-1	Pyroxene	0.824	0.005	0.109	0.000	0.297	0.206
MM-V8-1b-5	Butler West	MM-V8-1	Pyroxene	0.798	0.006	0.130	0.000	0.276	0.202
MM-V8-1c-8	Butler West	MM-V8-1	Pyroxene	0.756	0.004	0.190	0.000	0.240	0.206

Sample Data							**Mole oxygen**					
Analysis point	MnO	FeO2C	FeO	Na2O	K2O	Total	SiO2	TiO2	Al2O3	Cr2O3	MgO	CaO
NO-2G47-2b-10	0.004	0.000	0.316	0.031	0.003	1.688	1.537	0.010	0.240	0.000	0.194	0.207
NO-2G47-2b-9	0.004	0.000	0.287	0.016	0.002	1.683	1.651	0.006	0.143	0.000	0.243	0.208
NO-2G47-2b-8	0.004	0.000	0.299	0.019	0.002	1.685	1.618	0.004	0.176	0.000	0.225	0.207
NO-2G47-2b-7	0.004	0.000	0.317	0.026	0.004	1.678	1.561	0.016	0.205	0.000	0.194	0.208
NO-2G47-2a-6	0.005	0.000	0.299	0.021	0.002	1.695	1.619	0.008	0.173	0.000	0.229	0.210
NO-2G47-2a-5?	0.004	0.000	0.293	0.026	0.002	1.692	1.590	0.008	0.212	0.000	0.217	0.209
NO-2G47-2a-4?	0.004	0.000	0.287	0.018	0.002	1.695	1.644	0.006	0.145	0.000	0.248	0.215
NO-2G47-2a-1	0.004	0.000	0.282	0.013	0.001	1.696	1.692	0.004	0.117	0.000	0.258	0.212
NO-2G47-2a-2	0.005	0.000	0.274	0.008	0.001	1.706	1.751	0.002	0.072	0.000	0.276	0.216
NO-2G47-2a-3?	0.004	0.000	0.308	0.027	0.003	1.691	1.567	0.011	0.222	0.001	0.204	0.208
MM-117-1a-1	0.003	0.000	0.192	0.020	0.003	1.742	1.661	0.008	0.199	0.000	0.343	0.214
MM-117-1a-3	0.003	0.000	0.207	0.031	0.005	1.733	1.565	0.009	0.278	0.000	0.306	0.208
MM-117-1b-4	0.003	0.000	0.201	0.024	0.003	1.732	1.627	0.013	0.218	0.002	0.324	0.209
MM-117-1b-5	0.003	0.000	0.192	0.022	0.003	1.752	1.631	0.013	0.237	0.001	0.336	0.215
MM-117-1b-7	0.003	0.000	0.289	0.010	0.001	1.677	1.401	0.004	0.329	0.000	0.321	0.132
MM-117-1c-8	0.003	0.000	0.204	0.026	0.004	1.744	1.633	0.008	0.228	0.000	0.328	0.208
MM-117-1c-10	0.003	0.000	0.198	0.023	0.002	1.752	1.663	0.007	0.202	0.001	0.344	0.210
MM-117-6b-1	0.014	0.000	0.371	0.001	0.000	1.673	1.769	0.001	0.017	0.000	0.374	0.016
MM-117-6b-2	0.012	0.000	0.379	0.000	0.000	1.681	1.786	0.001	0.010	0.000	0.379	0.010
MM-117-6b-3	0.015	0.000	0.377	0.000	0.000	1.682	1.778	0.001	0.017	0.000	0.373	0.016
MM-V4-1a-1	0.006	0.000	0.197	0.006	0.000	1.806	1.876	0.001	0.057	0.000	0.611	0.008
MM-V4-1a-2	0.005	0.000	0.195	0.008	0.000	1.792	1.857	0.001	0.060	0.000	0.606	0.009
MM-V4-1a-3	0.005	0.000	0.203	0.006	0.000	1.805	1.877	0.001	0.056	0.000	0.605	0.008
MM-V4-1a-6	0.005	0.000	0.202	0.006	0.000	1.798	1.866	0.002	0.057	0.000	0.603	0.009
MM-V4-1b-7	0.005	0.000	0.198	0.009	0.000	1.789	1.858	0.001	0.066	0.000	0.594	0.009
MM-V4-1b-8	0.006	0.000	0.198	0.009	0.000	1.799	1.852	0.002	0.064	0.000	0.608	0.009
MM-V4-1b-10	0.005	0.000	0.201	0.015	0.001	1.793	1.860	0.003	0.066	0.000	0.587	0.010
MM-V4-1c-11	0.006	0.000	0.221	0.007	0.000	1.778	1.843	0.002	0.059	0.000	0.575	0.008
MM-V4-1c-12	0.005	0.000	0.199	0.005	0.000	1.805	1.890	0.001	0.042	0.000	0.615	0.008
MM-V4-1c-13	0.005	0.000	0.223	0.006	0.000	1.787	1.839	0.001	0.051	0.000	0.592	0.007
MM-V4-1c-14	0.005	0.000	0.197	0.008	0.000	1.803	1.867	0.001	0.061	0.000	0.610	0.009
MM-V4-7a-1	0.004	0.000	0.291	0.053	0.012	1.707	1.413	0.024	0.387	0.000	0.180	0.190
MM-V4-7a-2	0.005	0.000	0.290	0.050	0.011	1.706	1.415	0.022	0.387	0.000	0.189	0.184
MM-V4-7a-3	0.004	0.000	0.284	0.051	0.011	1.716	1.418	0.021	0.388	0.000	0.197	0.190
MM-V8-1a-1	0.003	0.000	0.285	0.043	0.011	1.713	1.437	0.021	0.347	0.000	0.204	0.207
MM-V8-1a-2	0.004	0.000	0.285	0.042	0.009	1.723	1.458	0.018	0.345	0.000	0.210	0.206
MM-V8-1a-3	0.004	0.000	0.253	0.023	0.004	1.724	1.636	0.010	0.177	0.000	0.293	0.206
MM-V8-1a-4	0.004	0.000	0.246	0.023	0.004	1.718	1.649	0.009	0.164	0.000	0.297	0.206
MM-V8-1b-5	0.003	0.000	0.244	0.027	0.005	1.690	1.597	0.012	0.194	0.001	0.276	0.202
MM-V8-1c-8	0.004	0.000	0.274	0.038	0.008	1.719	1.512	0.009	0.285	0.000	0.240	0.206

Sample Data							**Norm Cations**					
Analysis point	MnO	FeO2C	FeO	Na2O	K2O	Total	SiO2	TiO2	Al2O3	Cr2O3	MgO	CaO
NO-2G47-2b-10	0.004	0.000	0.316	0.015	0.002	2.524	1.821	0.011	0.378	0.000	0.460	0.490
NO-2G47-2b-9	0.004	0.000	0.287	0.008	0.001	2.551	1.962	0.007	0.227	0.000	0.578	0.493
NO-2G47-2b-8	0.004	0.000	0.299	0.010	0.001	2.545	1.920	0.005	0.278	0.000	0.534	0.491
NO-2G47-2b-7	0.004	0.000	0.317	0.013	0.002	2.521	1.859	0.020	0.326	0.001	0.463	0.496
NO-2G47-2a-6	0.005	0.000	0.299	0.011	0.001	2.554	1.910	0.009	0.272	0.001	0.540	0.496
NO-2G47-2a-5?	0.004	0.000	0.293	0.013	0.001	2.548	1.879	0.009	0.334	0.001	0.513	0.495
NO-2G47-2a-4?	0.004	0.000	0.287	0.009	0.001	2.558	1.940	0.007	0.228	0.000	0.585	0.506
NO-2G47-2a-1	0.004	0.000	0.282	0.007	0.001	2.576	1.995	0.005	0.183	0.000	0.609	0.500
NO-2G47-2a-2	0.005	0.000	0.274	0.004	0.001	2.602	2.053	0.003	0.113	0.000	0.647	0.507
NO-2G47-2a-3?	0.004	0.000	0.308	0.014	0.001	2.540	1.853	0.013	0.350	0.001	0.483	0.493
MM-117-1a-1	0.003	0.000	0.192	0.010	0.001	2.632	1.906	0.010	0.305	0.000	0.788	0.492
MM-117-1a-3	0.003	0.000	0.207	0.015	0.003	2.595	1.806	0.011	0.428	0.000	0.706	0.481
MM-117-1b-4	0.003	0.000	0.201	0.012	0.002	2.611	1.879	0.015	0.336	0.003	0.749	0.483
MM-117-1b-5	0.003	0.000	0.192	0.011	0.002	2.640	1.862	0.014	0.360	0.001	0.768	0.492
MM-117-1b-7	0.003	0.000	0.289	0.005	0.001	2.484	1.670	0.005	0.522	0.000	0.765	0.314
MM-117-1c-8	0.003	0.000	0.204	0.013	0.002	2.625	1.873	0.009	0.348	0.000	0.752	0.477
MM-117-1c-10	0.003	0.000	0.198	0.012	0.001	2.642	1.899	0.008	0.308	0.001	0.786	0.481
MM-117-6b-1	0.014	0.000	0.371	0.001	0.000	2.563	2.115	0.001	0.027	0.000	0.895	0.039
MM-117-6b-2	0.012	0.000	0.379	0.000	0.000	2.577	2.125	0.001	0.016	0.000	0.902	0.025
MM-117-6b-3	0.015	0.000	0.377	0.000	0.000	2.577	2.115	0.001	0.027	0.000	0.887	0.039
MM-V4-1a-1	0.006	0.000	0.197	0.003	0.000	2.760	2.077	0.001	0.084	0.000	1.353	0.019
MM-V4-1a-2	0.005	0.000	0.195	0.004	0.000	2.737	2.073	0.001	0.089	0.000	1.354	0.020
MM-V4-1a-3	0.005	0.000	0.203	0.003	0.000	2.759	2.080	0.001	0.082	0.001	1.341	0.018
MM-V4-1a-6	0.005	0.000	0.202	0.003	0.000	2.748	2.076	0.002	0.085	0.000	1.342	0.020
MM-V4-1b-7	0.005	0.000	0.198	0.004	0.000	2.736	2.077	0.001	0.098	0.000	1.328	0.021
MM-V4-1b-8	0.006	0.000	0.198	0.004	0.000	2.743	2.060	0.002	0.095	0.000	1.352	0.019
MM-V4-1b-10	0.005	0.000	0.201	0.007	0.000	2.739	2.075	0.003	0.098	0.000	1.310	0.021
MM-V4-1c-11	0.006	0.000	0.221	0.003	0.000	2.716	2.073	0.002	0.088	0.000	1.294	0.018
MM-V4-1c-12	0.005	0.000	0.199	0.002	0.000	2.762	2.093	0.001	0.061	0.000	1.363	0.018
MM-V4-1c-13	0.005	0.000	0.223	0.003	0.000	2.721	2.058	0.001	0.076	0.000	1.325	0.015
MM-V4-1c-14	0.005	0.000	0.197	0.004	0.000	2.753	2.072	0.001	0.090	0.000	1.353	0.019
MM-V4-7a-1	0.004	0.000	0.291	0.027	0.006	2.522	1.655	0.028	0.605	0.000	0.422	0.446
MM-V4-7a-2	0.005	0.000	0.290	0.025	0.006	2.523	1.659	0.026	0.605	0.000	0.444	0.431
MM-V4-7a-3	0.004	0.000	0.284	0.026	0.006	2.534	1.653	0.025	0.602	0.000	0.460	0.444
MM-V8-1a-1	0.003	0.000	0.285	0.021	0.006	2.530	1.678	0.025	0.540	0.000	0.477	0.482
MM-V8-1a-2	0.004	0.000	0.285	0.021	0.005	2.550	1.692	0.021	0.534	0.000	0.487	0.477
MM-V8-1a-3	0.004	0.000	0.253	0.011	0.002	2.593	1.897	0.012	0.273	0.001	0.680	0.478
MM-V8-1a-4	0.004	0.000	0.246	0.011	0.002	2.589	1.919	0.011	0.254	0.000	0.691	0.480
MM-V8-1b-5	0.003	0.000	0.244	0.013	0.003	2.544	1.889	0.014	0.306	0.001	0.652	0.477
MM-V8-1c-8	0.004	0.000	0.274	0.019	0.004	2.552	1.759	0.010	0.441	0.000	0.558	0.480

Sample Data						**Norm Oxygen**								
Analysis point	FeO2C	FeO	Na2O	K2O	Total	SiO2	TiO2	Al2O3	Cr2O3	MgO	CaO	MnO	FeO2C	FeO
NO-2G47-2b-10	0.000	0.750	0.072	0.008	4.000	3.641	0.023	0.568	0.000	0.460	0.490	0.014	0.000	0.750
NO-2G47-2b-9	0.000	0.682	0.037	0.004	4.000	3.923	0.014	0.341	0.000	0.578	0.493	0.015	0.000	0.682
NO-2G47-2b-8	0.000	0.711	0.045	0.005	4.000	3.840	0.010	0.417	0.000	0.534	0.491	0.015	0.000	0.711
NO-2G47-2b-7	0.000	0.755	0.062	0.009	4.000	3.719	0.039	0.489	0.001	0.463	0.496	0.014	0.000	0.755
NO-2G47-2a-6	0.000	0.706	0.050	0.005	4.000	3.821	0.018	0.408	0.001	0.540	0.496	0.016	0.000	0.706
NO-2G47-2a-5?	0.000	0.693	0.061	0.006	4.000	3.758	0.019	0.501	0.001	0.513	0.495	0.015	0.000	0.693
NO-2G47-2a-4?	0.000	0.676	0.043	0.004	4.000	3.880	0.014	0.343	0.000	0.585	0.506	0.015	0.000	0.676
NO-2G47-2a-1	0.000	0.665	0.031	0.003	4.000	3.989	0.010	0.275	0.000	0.609	0.500	0.014	0.000	0.665
NO-2G47-2a-2	0.000	0.643	0.019	0.003	4.000	4.106	0.005	0.169	0.000	0.647	0.507	0.016	0.000	0.643
NO-2G47-2a-3?	0.000	0.728	0.064	0.007	4.000	3.707	0.025	0.525	0.001	0.483	0.493	0.013	0.000	0.728
MM-117-1a-1	0.000	0.441	0.046	0.006	4.000	3.812	0.019	0.458	0.000	0.788	0.492	0.009	0.000	0.441
MM-117-1a-3	0.000	0.479	0.071	0.012	4.000	3.612	0.022	0.642	0.000	0.706	0.481	0.009	0.000	0.479
MM-117-1b-4	0.000	0.465	0.056	0.008	4.000	3.757	0.029	0.504	0.003	0.749	0.483	0.010	0.000	0.465
MM-117-1b-5	0.000	0.439	0.050	0.008	4.000	3.724	0.029	0.540	0.001	0.768	0.492	0.009	0.000	0.439
MM-117-1b-7	0.000	0.688	0.024	0.004	4.000	3.340	0.011	0.784	0.000	0.765	0.314	0.010	0.000	0.688
MM-117-1c-8	0.000	0.468	0.059	0.008	4.000	3.746	0.018	0.522	0.000	0.752	0.477	0.009	0.000	0.468
MM-117-1c-10	0.000	0.453	0.053	0.005	4.000	3.798	0.016	0.462	0.001	0.786	0.481	0.009	0.000	0.453
MM-117-6b-1	0.000	0.888	0.002	0.000	4.000	4.230	0.001	0.041	0.000	0.895	0.039	0.049	0.000	0.888
MM-117-6b-2	0.000	0.902	0.001	0.000	4.000	4.250	0.001	0.024	0.000	0.902	0.025	0.043	0.000	0.902
MM-117-6b-3	0.000	0.896	0.001	0.000	4.000	4.230	0.001	0.041	0.000	0.887	0.039	0.052	0.000	0.896
MM-V4-1a-1	0.000	0.437	0.014	0.001	4.000	4.155	0.003	0.126	0.000	1.353	0.019	0.018	0.000	0.437
MM-V4-1a-2	0.000	0.435	0.017	0.000	4.000	4.146	0.002	0.133	0.000	1.354	0.020	0.017	0.000	0.435
MM-V4-1a-3	0.000	0.450	0.014	0.000	4.000	4.161	0.003	0.123	0.001	1.341	0.018	0.017	0.000	0.450
MM-V4-1a-6	0.000	0.449	0.014	0.000	4.000	4.152	0.004	0.127	0.000	1.342	0.020	0.018	0.000	0.449
MM-V4-1b-7	0.000	0.443	0.020	0.000	4.000	4.155	0.003	0.147	0.000	1.328	0.021	0.017	0.000	0.443
MM-V4-1b-8	0.000	0.439	0.019	0.000	4.000	4.120	0.004	0.143	0.000	1.352	0.019	0.018	0.000	0.439
MM-V4-1b-10	0.000	0.447	0.033	0.002	4.000	4.150	0.006	0.146	0.000	1.310	0.021	0.016	0.000	0.447
MM-V4-1c-11	0.000	0.497	0.015	0.000	4.000	4.146	0.004	0.132	0.000	1.294	0.018	0.019	0.000	0.497
MM-V4-1c-12	0.000	0.441	0.011	0.000	4.000	4.187	0.002	0.092	0.000	1.363	0.018	0.016	0.000	0.441
MM-V4-1c-13	0.000	0.498	0.014	0.000	4.000	4.117	0.003	0.115	0.000	1.325	0.015	0.018	0.000	0.498
MM-V4-1c-14	0.000	0.437	0.017	0.000	4.000	4.143	0.002	0.135	0.000	1.353	0.019	0.018	0.000	0.437
MM-V4-7a-1	0.000	0.682	0.124	0.028	4.000	3.310	0.055	0.907	0.000	0.422	0.446	0.015	0.000	0.682
MM-V4-7a-2	0.000	0.679	0.118	0.026	4.000	3.318	0.052	0.908	0.000	0.444	0.431	0.017	0.000	0.679
MM-V4-7a-3	0.000	0.662	0.120	0.026	4.000	3.306	0.049	0.904	0.000	0.460	0.444	0.014	0.000	0.662
MM-V8-1a-1	0.000	0.666	0.099	0.027	4.000	3.355	0.049	0.810	0.000	0.477	0.482	0.010	0.000	0.666
MM-V8-1a-2	0.000	0.661	0.098	0.022	4.000	3.384	0.042	0.801	0.000	0.487	0.477	0.012	0.000	0.661
MM-V8-1a-3	0.000	0.587	0.053	0.009	4.000	3.795	0.023	0.410	0.001	0.680	0.478	0.015	0.000	0.587
MM-V8-1a-4	0.000	0.574	0.052	0.009	4.000	3.839	0.022	0.381	0.000	0.691	0.480	0.015	0.000	0.574
MM-V8-1b-5	0.000	0.577	0.064	0.012	4.000	3.778	0.029	0.460	0.001	0.652	0.477	0.012	0.000	0.577
MM-V8-1c-8	0.000	0.637	0.087	0.018	4.000	3.519	0.021	0.662	0.000	0.558	0.480	0.012	0.000	0.637

Sample Data			**Atom units**							
Analysis point	K2O	Total	SiO2	TiO2	Al2O3	Cr2O3	MgO	CaO	MnO	FeO2C
NO-2G47-2b-10	0.004	5.986	1.821	0.011	0.378	0.000	0.460	0.490	0.009	0.000
NO-2G47-2b-9	0.002	6.067	1.962	0.007	0.227	0.000	0.578	0.493	0.010	0.000
NO-2G47-2b-8	0.003	6.044	1.920	0.005	0.278	0.000	0.534	0.491	0.010	0.000
NO-2G47-2b-7	0.005	6.012	1.859	0.020	0.326	0.001	0.463	0.496	0.009	0.000
NO-2G47-2a-6	0.002	6.033	1.910	0.009	0.272	0.001	0.540	0.496	0.011	0.000
NO-2G47-2a-5?	0.003	6.027	1.879	0.009	0.334	0.001	0.513	0.495	0.010	0.000
NO-2G47-2a-4?	0.002	6.043	1.940	0.007	0.228	0.000	0.585	0.506	0.010	0.000
NO-2G47-2a-1	0.001	6.079	1.995	0.005	0.183	0.000	0.609	0.500	0.009	0.000
NO-2G47-2a-2	0.001	6.107	2.053	0.003	0.113	0.000	0.647	0.507	0.011	0.000
NO-2G47-2a-3?	0.003	6.010	1.853	0.013	0.350	0.001	0.483	0.493	0.009	0.000
MM-117-1a-1	0.003	6.045	1.906	0.010	0.305	0.000	0.788	0.492	0.006	0.000
MM-117-1a-3	0.006	5.992	1.806	0.011	0.428	0.000	0.706	0.481	0.006	0.000
MM-117-1b-4	0.004	6.033	1.879	0.015	0.336	0.003	0.749	0.483	0.007	0.000
MM-117-1b-5	0.004	6.030	1.862	0.014	0.360	0.001	0.768	0.492	0.006	0.000
MM-117-1b-7	0.002	5.926	1.670	0.005	0.522	0.000	0.765	0.314	0.007	0.000
MM-117-1c-8	0.004	6.025	1.873	0.009	0.348	0.000	0.752	0.477	0.006	0.000
MM-117-1c-10	0.003	6.035	1.899	0.008	0.308	0.001	0.786	0.481	0.006	0.000
MM-117-6b-1	0.000	6.144	2.115	0.001	0.027	0.000	0.895	0.039	0.033	0.000
MM-117-6b-2	0.000	6.147	2.125	0.001	0.016	0.000	0.902	0.025	0.029	0.000
MM-117-6b-3	0.000	6.146	2.115	0.001	0.027	0.000	0.887	0.039	0.035	0.000
MM-V4-1a-1	0.000	6.120	2.077	0.001	0.084	0.000	1.353	0.019	0.012	0.000
MM-V4-1a-2	0.000	6.115	2.073	0.001	0.089	0.000	1.354	0.020	0.011	0.000
MM-V4-1a-3	0.000	6.121	2.080	0.001	0.082	0.001	1.341	0.018	0.011	0.000
MM-V4-1a-6	0.000	6.119	2.076	0.002	0.085	0.000	1.342	0.020	0.012	0.000
MM-V4-1b-7	0.000	6.124	2.077	0.001	0.098	0.000	1.328	0.021	0.011	0.000
MM-V4-1b-8	0.000	6.106	2.060	0.002	0.095	0.000	1.352	0.019	0.012	0.000
MM-V4-1b-10	0.001	6.115	2.075	0.003	0.098	0.000	1.310	0.021	0.011	0.000
MM-V4-1c-11	0.000	6.117	2.073	0.002	0.088	0.000	1.294	0.018	0.013	0.000
MM-V4-1c-12	0.000	6.125	2.093	0.001	0.061	0.000	1.363	0.018	0.011	0.000
MM-V4-1c-13	0.000	6.097	2.058	0.001	0.076	0.000	1.325	0.015	0.012	0.000
MM-V4-1c-14	0.000	6.115	2.072	0.001	0.090	0.000	1.353	0.019	0.012	0.000
MM-V4-7a-1	0.014	5.914	1.655	0.028	0.605	0.000	0.422	0.446	0.010	0.000
MM-V4-7a-2	0.013	5.921	1.659	0.026	0.605	0.000	0.444	0.431	0.011	0.000
MM-V4-7a-3	0.013	5.911	1.653	0.025	0.602	0.000	0.460	0.444	0.009	0.000
MM-V8-1a-1	0.013	5.913	1.678	0.025	0.540	0.000	0.477	0.482	0.007	0.000
MM-V8-1a-2	0.011	5.924	1.692	0.021	0.534	0.000	0.487	0.477	0.008	0.000
MM-V8-1a-3	0.005	6.019	1.897	0.012	0.273	0.001	0.680	0.478	0.010	0.000
MM-V8-1a-4	0.004	6.032	1.919	0.011	0.254	0.000	0.691	0.480	0.010	0.000
MM-V8-1b-5	0.006	6.023	1.889	0.014	0.306	0.001	0.652	0.477	0.008	0.000
MM-V8-1c-8	0.009	5.942	1.759	0.010	0.441	0.000	0.558	0.480	0.008	0.000

Sample Data				**Norm oxygen**								
Analysis point	Na2O	K2O	Total	SiO2	TiO2	Al2O3	Cr2O3	MgO	CaO	MnO	FeO2C	FeO
NO-2G47-2b-10	0.072	0.008	4.000	3.641	0.023	0.568	0.000	0.460	0.490	0.014	0.000	0.750
NO-2G47-2b-9	0.037	0.004	4.000	3.923	0.014	0.341	0.000	0.578	0.493	0.015	0.000	0.682
NO-2G47-2b-8	0.045	0.005	4.000	3.840	0.010	0.417	0.000	0.534	0.491	0.015	0.000	0.711
NO-2G47-2b-7	0.062	0.009	4.000	3.719	0.039	0.489	0.001	0.463	0.496	0.014	0.000	0.755
NO-2G47-2a-6	0.050	0.005	4.000	3.821	0.018	0.408	0.001	0.540	0.496	0.016	0.000	0.706
NO-2G47-2a-5?	0.061	0.006	4.000	3.758	0.019	0.501	0.001	0.513	0.495	0.015	0.000	0.693
NO-2G47-2a-4?	0.043	0.004	4.000	3.880	0.014	0.343	0.000	0.585	0.506	0.015	0.000	0.676
NO-2G47-2a-1	0.031	0.003	4.000	3.989	0.010	0.275	0.000	0.609	0.500	0.014	0.000	0.665
NO-2G47-2a-2	0.019	0.003	4.000	4.106	0.005	0.169	0.000	0.647	0.507	0.016	0.000	0.643
NO-2G47-2a-3?	0.064	0.007	4.000	3.707	0.025	0.525	0.001	0.483	0.493	0.013	0.000	0.728
MM-117-1a-1	0.046	0.006	4.000	3.812	0.019	0.458	0.000	0.788	0.492	0.009	0.000	0.441
MM-117-1a-3	0.071	0.012	4.000	3.612	0.022	0.642	0.000	0.706	0.481	0.009	0.000	0.479
MM-117-1b-4	0.056	0.008	4.000	3.757	0.029	0.504	0.003	0.749	0.483	0.010	0.000	0.465
MM-117-1b-5	0.050	0.008	4.000	3.724	0.029	0.540	0.001	0.768	0.492	0.009	0.000	0.439
MM-117-1b-7	0.024	0.004	4.000	3.340	0.011	0.784	0.000	0.765	0.314	0.010	0.000	0.688
MM-117-1c-8	0.059	0.008	4.000	3.746	0.018	0.522	0.000	0.752	0.477	0.009	0.000	0.468
MM-117-1c-10	0.053	0.005	4.000	3.798	0.016	0.462	0.001	0.786	0.481	0.009	0.000	0.453
MM-117-6b-1	0.002	0.000	4.000	4.230	0.001	0.041	0.000	0.895	0.039	0.049	0.000	0.888
MM-117-6b-2	0.001	0.000	4.000	4.250	0.001	0.024	0.000	0.902	0.025	0.043	0.000	0.902
MM-117-6b-3	0.001	0.000	4.000	4.230	0.001	0.041	0.000	0.887	0.039	0.052	0.000	0.896
MM-V4-1a-1	0.014	0.001	4.000	4.155	0.003	0.126	0.000	1.353	0.019	0.018	0.000	0.437
MM-V4-1a-2	0.017	0.000	4.000	4.146	0.002	0.133	0.000	1.354	0.020	0.017	0.000	0.435
MM-V4-1a-3	0.014	0.000	4.000	4.161	0.003	0.123	0.001	1.341	0.018	0.017	0.000	0.450
MM-V4-1a-6	0.014	0.000	4.000	4.152	0.004	0.127	0.000	1.342	0.020	0.018	0.000	0.449
MM-V4-1b-7	0.020	0.000	4.000	4.155	0.003	0.147	0.000	1.328	0.021	0.017	0.000	0.443
MM-V4-1b-8	0.019	0.000	4.000	4.120	0.004	0.143	0.000	1.352	0.019	0.018	0.000	0.439
MM-V4-1b-10	0.033	0.002	4.000	4.150	0.006	0.146	0.000	1.310	0.021	0.016	0.000	0.447
MM-V4-1c-11	0.015	0.000	4.000	4.146	0.004	0.132	0.000	1.294	0.018	0.019	0.000	0.497
MM-V4-1c-12	0.011	0.000	4.000	4.187	0.002	0.092	0.000	1.363	0.018	0.016	0.000	0.441
MM-V4-1c-13	0.014	0.000	4.000	4.117	0.003	0.115	0.000	1.325	0.015	0.018	0.000	0.498
MM-V4-1c-14	0.017	0.000	4.000	4.143	0.002	0.135	0.000	1.353	0.019	0.018	0.000	0.437
MM-V4-7a-1	0.124	0.028	4.000	3.310	0.055	0.907	0.000	0.422	0.446	0.015	0.000	0.682
MM-V4-7a-2	0.118	0.026	4.000	3.318	0.052	0.908	0.000	0.444	0.431	0.017	0.000	0.679
MM-V4-7a-3	0.120	0.026	4.000	3.306	0.049	0.904	0.000	0.460	0.444	0.014	0.000	0.662
MM-V8-1a-1	0.099	0.027	4.000	3.355	0.049	0.810	0.000	0.477	0.482	0.010	0.000	0.666
MM-V8-1a-2	0.098	0.022	4.000	3.384	0.042	0.801	0.000	0.487	0.477	0.012	0.000	0.661
MM-V8-1a-3	0.053	0.009	4.000	3.795	0.023	0.410	0.001	0.680	0.478	0.015	0.000	0.587
MM-V8-1a-4	0.052	0.009	4.000	3.839	0.022	0.381	0.000	0.691	0.480	0.015	0.000	0.574
MM-V8-1b-5	0.064	0.012	4.000	3.778	0.029	0.460	0.001	0.652	0.477	0.012	0.000	0.577
MM-V8-1c-8	0.087	0.018	4.000	3.519	0.021	0.662	0.000	0.558	0.480	0.012	0.000	0.637

Sample Data			**End Member**		
Analysis point	Na2O	K2O	Wollastonite	Enstatite	Ferrosilite
NO-2G47-2b-10	0.036	0.004	28.8	27.1	44.1
NO-2G47-2b-9	0.019	0.002	28.1	32.9	38.9
NO-2G47-2b-8	0.023	0.003	28.3	30.8	40.9
NO-2G47-2b-7	0.031	0.005	29.0	27.0	44.0
NO-2G47-2a-6	0.025	0.002	28.5	31.0	40.5
NO-2G47-2a-5?	0.030	0.003	29.1	30.2	40.7
NO-2G47-2a-4?	0.021	0.002	28.6	33.1	38.3
NO-2G47-2a-1	0.016	0.001	28.2	34.3	37.5
NO-2G47-2a-2	0.010	0.001	28.2	36.0	35.8
NO-2G47-2a-3?	0.032	0.003	28.9	28.3	42.7
MM-117-1a-1	0.023	0.003	28.6	45.8	25.6
MM-117-1a-3	0.035	0.006	28.9	42.4	28.7
MM-117-1b-4	0.028	0.004	28.5	44.1	27.4
MM-117-1b-5	0.025	0.004	28.9	45.2	25.8
MM-117-1b-7	0.012	0.002	17.8	43.3	38.9
MM-117-1c-8	0.029	0.004	28.1	44.3	27.6
MM-117-1c-10	0.027	0.003	28.0	45.7	26.4
MM-117-6b-1	0.001	0.000	2.1	49.1	48.8
MM-117-6b-2	0.001	0.000	1.3	49.3	49.3
MM-117-6b-3	0.001	0.000	2.1	48.7	49.2
MM-V4-1a-1	0.007	0.000	1.0	74.8	24.2
MM-V4-1a-2	0.008	0.000	1.1	74.8	24.0
MM-V4-1a-3	0.007	0.000	1.0	74.1	24.9
MM-V4-1a-6	0.007	0.000	1.1	74.1	24.8
MM-V4-1b-7	0.010	0.000	1.2	74.1	24.7
MM-V4-1b-8	0.010	0.000	1.1	74.7	24.3
MM-V4-1b-10	0.016	0.001	1.2	73.6	25.2
MM-V4-1c-11	0.007	0.000	1.0	71.5	27.5
MM-V4-1c-12	0.005	0.000	1.0	74.8	24.2
MM-V4-1c-13	0.007	0.000	0.8	72.1	27.1
MM-V4-1c-14	0.009	0.000	1.1	74.8	24.1
MM-V4-7a-1	0.062	0.014	28.8	27.2	44.0
MM-V4-7a-2	0.059	0.013	27.7	28.6	43.7
MM-V4-7a-3	0.060	0.013	28.3	29.4	42.3
MM-V8-1a-1	0.050	0.013	29.7	29.3	41.0
MM-V8-1a-2	0.049	0.011	29.4	29.9	40.7
MM-V8-1a-3	0.027	0.005	27.4	39.0	33.6
MM-V8-1a-4	0.026	0.004	27.5	39.6	32.9
MM-V8-1b-5	0.032	0.006	28.0	38.2	33.8
MM-V8-1c-8	0.044	0.009	28.6	33.3	38.0

Analysis	Mineral	Intrusion/Phase	Sample	SiO_2	TiO_2	Al_2O_3	Cr_2O_3	MnO
NO-2G21-1a-1	Amphibole	Thunderbird-V	NO-2G21-1	49.549	0.348	5.845	0.016	0.279
NO-2G21-1a-2	Amphibole	Thunderbird-V	NO-2G21-1	52.521	0.267	2.830	0.007	0.267
NO-2G21-1a-3	Amphibole	Thunderbird-V	NO-2G21-1	50.062	0.424	5.197	0.000	0.281
NO-2G21-1a-4	Amphibole	Thunderbird-V	NO-2G21-1	51.637	0.360	3.700	0.004	0.286
NO-2G21-1a-5	Amphibole	Thunderbird-V	NO-2G21-1	51.350	0.271	3.896	0.015	0.250
NO-2G21-1a-6	Amphibole	Thunderbird-V	NO-2G21-1	47.287	0.423	7.843	0.021	0.223
NO-2G21-1a-7	Amphibole	Thunderbird-V	NO-2G21-1	47.446	0.386	7.824	0.017	0.247
NO-2G21-1a-8	Amphibole	Thunderbird-V	NO-2G21-1	49.945	0.431	5.505	0.035	0.263
NO-2G21-1a-9	Amphibole	Thunderbird-V	NO-2G21-1	44.676	1.483	9.500	0.019	0.269
NO-2G21-1a-10	Amphibole	Thunderbird-V	NO-2G21-1	43.759	0.589	11.176	0.026	0.245
NO-2G21-1a-11	Amphibole	Thunderbird-V	NO-2G21-1	45.675	0.634	8.752	0.008	0.264
NO-2G21-1a-12	Amphibole	Thunderbird-V	NO-2G21-1	40.305	0.297	15.249	0.017	0.247
NO-2G21-1b-14	Amphibole	Thunderbird-V	NO-2G21-1	51.507	0.275	4.246	0.009	0.282
NO-2G21-1b-15	Amphibole	Thunderbird-V	NO-2G21-1	51.296	0.179	4.254	0.035	0.251
NO-2G21-1b-16	Amphibole	Thunderbird-V	NO-2G21-1	51.906	0.158	3.501	0.008	0.269
NO-2G21-1b-17	Amphibole	Thunderbird-V	NO-2G21-1	50.665	0.157	5.038	0.028	0.240
NO-2G21-1b-18	Amphibole	Thunderbird-V	NO-2G21-1	51.290	0.177	4.347	0.005	0.261
NO-2G21-1b-19	Amphibole	Thunderbird-V	NO-2G21-1	52.299	0.139	3.393	0.000	0.246
NO-2G21-1b-20	Amphibole	Thunderbird-V	NO-2G21-1	46.348	0.100	2.928	0.017	0.287
NO-2G21-1b-21	Amphibole	Thunderbird-V	NO-2G21-1	51.724	0.124	3.993	0.000	0.243
NO-2G21-1b-22	Amphibole	Thunderbird-V	NO-2G21-1	52.416	0.217	3.208	0.001	0.268
NO-2G21-1b-23	Amphibole	Thunderbird-V	NO-2G21-1	50.971	0.131	4.663	0.021	0.242
NO-2G21-1b-24?	Amphibole	Thunderbird-V	NO-2G21-1	41.810	0.319	13.370	0.007	0.240
NO-2G21-1b-25?	Amphibole	Thunderbird-V	NO-2G21-1	42.547	0.362	12.990	0.033	0.247
NO-2G21-1c-26	Amphibole	Thunderbird-V	NO-2G21-1	49.648	0.164	6.050	0.000	0.229
NO-2G21-1c-27	Amphibole	Thunderbird-V	NO-2G21-1	48.204	0.195	7.398	0.000	0.244
NO-2G21-1c-28	Amphibole	Thunderbird-V	NO-2G21-1	48.900	0.198	6.950	0.025	0.234
NO-2G21-1c-29	Amphibole	Thunderbird-V	NO-2G21-1	52.204	0.095	3.181	0.020	0.274
NO-2G21-1c-30	Amphibole	Thunderbird-V	NO-2G21-1	51.615	0.143	4.318	0.017	0.270
NO-2G21-1c-31	Amphibole	Thunderbird-V	NO-2G21-1	47.623	0.214	7.513	0.024	0.243
NO-2G21-1c-32	Amphibole	Thunderbird-V	NO-2G21-1	47.515	0.224	8.004	0.008	0.226
NO-2G21-1c-33	Amphibole	Thunderbird-V	NO-2G21-1	52.380	0.105	3.708	0.000	0.262
NO-2G21-1c-34?	Amphibole	Thunderbird-V	NO-2G21-1	41.572	0.312	13.416	0.026	0.219
NO-2G21-1c-35	Amphibole	Thunderbird-V	NO-2G21-1	45.116	0.308	10.650	0.033	0.212
NO-2G21-1c-36	Amphibole	Thunderbird-V	NO-2G21-1	54.286	0.046	1.871	0.000	0.261
NO-2G21-1c-37	Amphibole	Thunderbird-V	NO-2G21-1	47.140	0.241	8.472	0.012	0.241
NO-2G22-4a-1	Amphibole	Thunderbird-V	NO-2G22-4	39.650	0.255	16.103	0.020	0.165
NO-2G22-4a-2	Amphibole	Thunderbird-V	NO-2G22-4	40.594	0.288	14.821	0.052	0.159
NO-2G22-4a-3	Amphibole	Thunderbird-V	NO-2G22-4	39.917	0.637	15.340	0.024	0.144

Analysis	Fe_2O_3	MgO	CaO	Na_2O	K_2O	O=F,Cl (calc)	Initial Total
NO-2G21-1a-1	17.369	11.727	11.680	0.695	0.097	0.00	97.61
NO-2G21-1a-2	15.980	13.388	11.947	0.380	0.035	0.00	97.62
NO-2G21-1a-3	17.565	11.824	11.896	0.648	0.056	0.00	97.95
NO-2G21-1a-4	16.709	12.808	11.981	0.510	0.037	0.00	98.03
NO-2G21-1a-5	16.414	12.898	11.867	0.474	0.049	0.00	97.48
NO-2G21-1a-6	19.089	10.052	11.763	1.003	0.139	0.00	97.84
NO-2G21-1a-7	19.182	10.235	11.777	0.948	0.127	0.00	98.19
NO-2G21-1a-8	17.793	11.826	11.867	0.713	0.101	0.00	98.48
NO-2G21-1a-9	20.089	8.818	11.276	1.171	0.283	0.00	97.58
NO-2G21-1a-10	21.109	8.171	11.506	1.269	0.274	0.00	98.12
NO-2G21-1a-11	20.557	9.175	11.486	1.293	0.263	0.00	98.11
NO-2G21-1a-12	22.522	5.722	11.385	1.549	0.582	0.00	97.88
NO-2G21-1b-14	16.557	13.001	12.008	0.518	0.060	0.00	98.46
NO-2G21-1b-15	16.744	12.816	12.008	0.506	0.061	0.00	98.15
NO-2G21-1b-16	16.337	13.346	11.959	0.440	0.046	0.00	97.97
NO-2G21-1b-17	17.017	12.486	12.053	0.566	0.066	0.00	98.32
NO-2G21-1b-18	16.876	12.744	11.894	0.485	0.072	0.00	98.15
NO-2G21-1b-19	16.032	13.543	12.083	0.366	0.032	0.00	98.13
NO-2G21-1b-20	14.121	12.161	16.422	0.316	0.030	0.00	92.73
NO-2G21-1b-21	16.556	13.024	11.847	0.455	0.060	0.00	98.03
NO-2G21-1b-22	16.093	13.598	11.895	0.390	0.036	0.00	98.12
NO-2G21-1b-23	16.782	12.621	12.033	0.513	0.054	0.00	98.03
NO-2G21-1b-24?	21.749	6.758	11.548	1.399	0.405	0.00	97.61
NO-2G21-1b-25?	21.586	6.995	11.414	1.401	0.366	0.00	97.94
NO-2G21-1c-26	17.758	11.821	12.044	0.666	0.072	0.00	98.45
NO-2G21-1c-27	18.709	10.741	11.760	0.822	0.149	0.00	98.22
NO-2G21-1c-28	17.958	10.863	11.885	0.794	0.114	0.00	97.92
NO-2G21-1c-29	16.003	13.351	12.114	0.373	0.044	0.00	97.66
NO-2G21-1c-30	16.554	12.878	12.046	0.510	0.070	0.00	98.42
NO-2G21-1c-31	18.734	10.345	11.710	0.915	0.154	0.00	97.48
NO-2G21-1c-32	18.987	10.394	11.764	0.957	0.159	0.00	98.24
NO-2G21-1c-33	16.004	13.517	12.179	0.406	0.052	0.00	98.61
NO-2G21-1c-34?	22.043	6.692	11.540	1.416	0.445	0.00	97.68
NO-2G21-1c-35	20.298	8.634	11.592	1.140	0.254	0.00	98.24
NO-2G21-1c-36	14.674	14.975	12.176	0.198	0.022	0.00	98.51
NO-2G21-1c-37	19.291	10.085	11.807	0.931	0.209	0.00	98.43
NO-2G22-4a-1	23.806	4.138	11.146	1.278	0.515	0.00	97.08
NO-2G22-4a-2	23.835	4.566	11.175	1.253	0.560	0.00	97.30
NO-2G22-4a-3	24.228	4.256	11.255	1.291	0.721	0.00	97.81

			OUTPUT		
Analysis	$Fe^{3+}/\Sigma Fe$ initial	$Mn^{3+}/\Sigma Mn$ initial	$Fe^{3+}/\Sigma Fe$ used	$Mn^{3+}/\Sigma Mn$ used	MnO
NO-2G21-1a-1	1.000	0.000	0.054	0.000	0.28
NO-2G21-1a-2	1.000	0.000	0.029	0.000	0.27
NO-2G21-1a-3	1.000	0.000	0.043	0.000	0.28
NO-2G21-1a-4	1.000	0.000	0.035	0.000	0.29
NO-2G21-1a-5	1.000	0.000	0.043	0.000	0.25
NO-2G21-1a-6	1.000	0.000	0.041	0.000	0.22
NO-2G21-1a-7	1.000	0.000	0.054	0.000	0.25
NO-2G21-1a-8	1.000	0.000	0.052	0.000	0.26
NO-2G21-1a-9	1.000	0.000	0.115	0.000	0.27
NO-2G21-1a-10	1.000	0.000	0.098	0.000	0.25
NO-2G21-1a-11	1.000	0.000	0.069	0.000	0.26
NO-2G21-1a-12	1.000	0.000	0.065	0.000	0.25
NO-2G21-1b-14	1.000	0.000	0.048	0.000	0.28
NO-2G21-1b-15	1.000	0.000	0.041	0.000	0.25
NO-2G21-1b-16	1.000	0.000	0.049	0.000	0.27
NO-2G21-1b-17	1.000	0.000	0.043	0.000	0.24
NO-2G21-1b-18	1.000	0.000	0.049	0.000	0.26
NO-2G21-1b-19	1.000	0.000	0.041	0.000	0.25
NO-2G21-1b-20	1.000	0.000	0.189	0.000	0.29
NO-2G21-1b-21	1.000	0.000	0.049	0.000	0.24
NO-2G21-1b-22	1.000	0.000	0.054	0.000	0.27
NO-2G21-1b-23	1.000	0.000	0.038	0.000	0.24
NO-2G21-1b-24?	1.000	0.000	0.067	0.000	0.24
NO-2G21-1b-25?	1.000	0.000	0.060	0.000	0.25
NO-2G21-1c-26	1.000	0.000	0.047	0.000	0.23
NO-2G21-1c-27	1.000	0.000	0.055	0.000	0.24
NO-2G21-1c-28	1.000	0.000	0.023	0.000	0.23
NO-2G21-1c-29	1.000	0.000	0.023	0.000	0.27
NO-2G21-1c-30	1.000	0.000	0.034	0.000	0.27
NO-2G21-1c-31	1.000	0.000	0.041	0.000	0.24
NO-2G21-1c-32	1.000	0.000	0.053	0.000	0.23
NO-2G21-1c-33	1.000	0.000	0.034	0.000	0.26
NO-2G21-1c-34?	1.000	0.000	0.075	0.000	0.22
NO-2G21-1c-35	1.000	0.000	0.055	0.000	0.21
NO-2G21-1c-36	1.000	0.000	0.041	0.000	0.26
NO-2G21-1c-37	1.000	0.000	0.054	0.000	0.24
NO-2G22-4a-1	1.000	0.000	0.046	0.000	0.17
NO-2G22-4a-2	1.000	0.000	0.041	0.000	0.16
NO-2G22-4a-3	1.000	0.000	0.052	0.000	0.14

Analysis	Mn_2O_3	FeO	Fe_2O_3	H_2O+	Total	Group	Subgroup of (OH,F,Cl)
NO-2G21-1a-1	0.00	14.79	0.94	1.97	97.93	OH,F,Cl	Ca
NO-2G21-1a-2	0.00	13.96	0.46	2.01	98.08	OH,F,Cl	Ca
NO-2G21-1a-3	0.00	15.13	0.76	1.95	98.22	OH,F,Cl	Ca
NO-2G21-1a-4	0.00	14.51	0.59	1.98	98.40	OH,F,Cl	Ca
NO-2G21-1a-5	0.00	14.13	0.71	2.00	97.91	OH,F,Cl	Ca
NO-2G21-1a-6	0.00	16.47	0.78	1.93	97.94	OH,F,Cl	Ca
NO-2G21-1a-7	0.00	16.33	1.04	1.94	98.31	OH,F,Cl	Ca
NO-2G21-1a-8	0.00	15.18	0.93	1.95	98.74	OH,F,Cl	Ca
NO-2G21-1a-9	0.00	16.00	2.31	1.66	97.46	OH,F,Cl	Ca
NO-2G21-1a-10	0.00	17.13	2.07	1.87	98.09	OH,F,Cl	Ca
NO-2G21-1a-11	0.00	17.22	1.42	1.86	98.05	OH,F,Cl	Ca
NO-2G21-1a-12	0.00	18.95	1.46	1.91	97.68	OH,F,Cl	Ca
NO-2G21-1b-14	0.00	14.18	0.80	2.00	98.88	OH,F,Cl	Ca
NO-2G21-1b-15	0.00	14.45	0.69	2.02	98.56	OH,F,Cl	Ca
NO-2G21-1b-16	0.00	13.98	0.80	2.03	98.44	OH,F,Cl	Ca
NO-2G21-1b-17	0.00	14.65	0.73	2.02	98.71	OH,F,Cl	Ca
NO-2G21-1b-18	0.00	14.44	0.83	2.02	98.56	OH,F,Cl	Ca
NO-2G21-1b-19	0.00	13.83	0.66	2.04	98.63	OH,F,Cl	Ca
NO-2G21-1b-20	0.00	10.31	2.67	2.01	93.59	OH,F,Cl	Ca
NO-2G21-1b-21	0.00	14.17	0.81	2.04	98.49	OH,F,Cl	Ca
NO-2G21-1b-22	0.00	13.70	0.87	2.02	98.62	OH,F,Cl	Ca
NO-2G21-1b-23	0.00	14.53	0.64	2.03	98.44	OH,F,Cl	Ca
NO-2G21-1b-24?	0.00	18.26	1.46	1.92	97.49	OH,F,Cl	Ca
NO-2G21-1b-25?	0.00	18.26	1.30	1.91	97.82	OH,F,Cl	Ca
NO-2G21-1c-26	0.00	15.23	0.84	2.01	98.77	OH,F,Cl	Ca
NO-2G21-1c-27	0.00	15.91	1.03	1.99	98.44	OH,F,Cl	Ca
NO-2G21-1c-28	0.00	15.79	0.41	2.00	98.16	OH,F,Cl	Ca
NO-2G21-1c-29	0.00	14.07	0.37	2.05	98.14	OH,F,Cl	Ca
NO-2G21-1c-30	0.00	14.39	0.56	2.03	98.85	OH,F,Cl	Ca
NO-2G21-1c-31	0.00	16.17	0.77	1.98	97.66	OH,F,Cl	Ca
NO-2G21-1c-32	0.00	16.18	1.01	1.98	98.42	OH,F,Cl	Ca
NO-2G21-1c-33	0.00	13.91	0.54	2.05	99.11	OH,F,Cl	Ca
NO-2G21-1c-34?	0.00	18.35	1.65	1.91	97.55	OH,F,Cl	Ca
NO-2G21-1c-35	0.00	17.26	1.12	1.94	98.26	OH,F,Cl	Ca
NO-2G21-1c-36	0.00	12.66	0.60	2.08	99.18	OH,F,Cl	Ca
NO-2G21-1c-37	0.00	16.42	1.04	1.97	98.57	OH,F,Cl	Ca
NO-2G22-4a-1	0.00	20.44	1.10	1.91	96.71	OH,F,Cl	Ca
NO-2G22-4a-2	0.00	20.57	0.98	1.90	96.91	OH,F,Cl	Ca
NO-2G22-4a-3	0.00	20.67	1.26	1.81	97.32	OH,F,Cl	Ca

		T (ideally 8 apfu)			C (ideal
Analysis	**Species**	Si	Al	T subtotal	Ti
NO-2G21-1a-1	magnesio-hornblende	7.395	0.605	8.000	0.039
NO-2G21-1a-2	actinolite	7.752	0.248	8.000	0.030
NO-2G21-1a-3	actinolite	7.457	0.543	8.000	0.048
NO-2G21-1a-4	actinolite	7.634	0.366	8.000	0.040
NO-2G21-1a-5	actinolite	7.616	0.384	8.000	0.030
NO-2G21-1a-6	magnesio-hornblende	7.142	0.858	8.000	0.048
NO-2G21-1a-7	magnesio-hornblende	7.135	0.865	8.000	0.044
NO-2G21-1a-8	actinolite	7.409	0.591	8.000	0.048
NO-2G21-1a-9	magnesio-hornblende	6.849	1.151	8.000	0.171
NO-2G21-1a-10	ferro-hornblende	6.686	1.314	8.000	0.068
NO-2G21-1a-11	ferro-hornblende	6.960	1.040	8.000	0.073
NO-2G21-1a-12	ferro-pargasite	6.258	1.742	8.000	0.035
NO-2G21-1b-14	actinolite	7.569	0.431	8.000	0.030
NO-2G21-1b-15	actinolite	7.569	0.431	8.000	0.020
NO-2G21-1b-16	actinolite	7.647	0.353	8.000	0.018
NO-2G21-1b-17	actinolite	7.480	0.520	8.000	0.017
NO-2G21-1b-18	actinolite	7.567	0.433	8.000	0.020
NO-2G21-1b-19	actinolite	7.675	0.325	8.000	0.015
NO-2G21-1b-20	edenite	7.307	0.544	8.000	
NO-2G21-1b-21	actinolite	7.618	0.382	8.000	0.014
NO-2G21-1b-22	actinolite	7.691	0.309	8.000	0.024
NO-2G21-1b-23	actinolite	7.533	0.467	8.000	0.015
NO-2G21-1b-24?	ferro-hornblende	6.468	1.532	8.000	0.037
NO-2G21-1b-25?	ferro-hornblende	6.543	1.457	8.000	0.042
NO-2G21-1c-26	magnesio-hornblende	7.357	0.643	8.000	0.018
NO-2G21-1c-27	magnesio-hornblende	7.208	0.792	8.000	0.022
NO-2G21-1c-28	magnesio-hornblende	7.308	0.692	8.000	0.022
NO-2G21-1c-29	actinolite	7.706	0.294	8.000	0.011
NO-2G21-1c-30	actinolite	7.584	0.416	8.000	0.016
NO-2G21-1c-31	magnesio-hornblende	7.194	0.806	8.000	0.024
NO-2G21-1c-32	magnesio-hornblende	7.127	0.873	8.000	0.025
NO-2G21-1c-33	actinolite	7.650	0.350	8.000	0.012
NO-2G21-1c-34?	ferro-hornblende	6.438	1.562	8.000	0.036
NO-2G21-1c-35	ferro-hornblende	6.837	1.163	8.000	0.035
NO-2G21-1c-36	actinolite	7.854	0.146	8.000	0.005
NO-2G21-1c-37	magnesio-hornblende	7.073	0.927	8.000	0.027
NO-2G22-4a-1	ferro-hornblende	6.241	1.759	8.000	0.030
NO-2G22-4a-2	ferro-hornblende	6.375	1.625	8.000	0.034
NO-2G22-4a-3	ferro-pargasite	6.271	1.729	8.000	0.075

ly 5 apfu)							
Analysis	Al	Cr	Fe^{3+}	Mn^{2+}	Fe^{2+}	Mg	C subtotal
NO-2G21-1a-1	0.423	0.002	0.106		1.821	2.609	5.000
NO-2G21-1a-2	0.244	0.001	0.052	0.005	1.723	2.946	5.001
NO-2G21-1a-3	0.369		0.085		1.873	2.626	5.001
NO-2G21-1a-4	0.278		0.066		1.792	2.823	4.999
NO-2G21-1a-5	0.297	0.002	0.079		1.740	2.852	5.000
NO-2G21-1a-6	0.538	0.003	0.090		2.058	2.263	5.000
NO-2G21-1a-7	0.522	0.002	0.116		2.021	2.295	5.000
NO-2G21-1a-8	0.371	0.004	0.104		1.858	2.615	5.000
NO-2G21-1a-9	0.565	0.002	0.266		1.981	2.015	5.000
NO-2G21-1a-10	0.698	0.003	0.238		2.131	1.861	4.999
NO-2G21-1a-11	0.532	0.001	0.162		2.149	2.084	5.001
NO-2G21-1a-12	1.049	0.002	0.171		2.418	1.325	5.000
NO-2G21-1b-14	0.304	0.001	0.088		1.729	2.848	5.000
NO-2G21-1b-15	0.309	0.004	0.077		1.770	2.819	4.999
NO-2G21-1b-16	0.255	0.001	0.088		1.707	2.931	5.000
NO-2G21-1b-17	0.356	0.003	0.081		1.793	2.748	4.998
NO-2G21-1b-18	0.323	0.001	0.093		1.761	2.803	5.001
NO-2G21-1b-19	0.262		0.072		1.688	2.963	5.000
NO-2G21-1b-20		0.002	0.179	0.038	1.359	2.858	4.436
NO-2G21-1b-21	0.312		0.089		1.726	2.860	5.001
NO-2G21-1b-22	0.246		0.097		1.659	2.974	5.000
NO-2G21-1b-23	0.345	0.002	0.071		1.786	2.781	5.000
NO-2G21-1b-24?	0.905	0.001	0.169		2.329	1.558	4.999
NO-2G21-1b-25?	0.898	0.004	0.150		2.303	1.604	5.001
NO-2G21-1c-26	0.414		0.094		1.863	2.611	5.000
NO-2G21-1c-27	0.512		0.115		1.957	2.394	5.000
NO-2G21-1c-28	0.532	0.003	0.047	0.003	1.972	2.420	4.999
NO-2G21-1c-29	0.260	0.002	0.040	0.012	1.738	2.938	5.001
NO-2G21-1c-30	0.332	0.002	0.062		1.768	2.821	5.001
NO-2G21-1c-31	0.531	0.003	0.087		2.025	2.330	5.000
NO-2G21-1c-32	0.542	0.001	0.113		1.995	2.324	5.000
NO-2G21-1c-33	0.288		0.059		1.698	2.943	5.000
NO-2G21-1c-34?	0.886	0.003	0.194		2.336	1.545	5.000
NO-2G21-1c-35	0.740	0.004	0.127		2.143	1.951	5.000
NO-2G21-1c-36	0.173		0.065		1.527	3.230	5.000
NO-2G21-1c-37	0.571	0.001	0.118		2.027	2.256	5.000
NO-2G22-4a-1	1.228	0.002	0.130		2.639	0.971	5.000
NO-2G22-4a-2	1.118	0.006	0.116		2.657	1.069	5.000
NO-2G22-4a-3	1.111	0.003	0.148		2.665	0.997	4.999

	B (ideally 2 apfu)					A (from 0 to 1 apfu)		
Analysis	Mn^{2+}	Fe^{2+}	Ca	Na	B subtotal	Ca	Na	K
NO-2G21-1a-1	0.035	0.024	1.868	0.073	2.000		0.128	0.018
NO-2G21-1a-2	0.029		1.889	0.082	2.000		0.027	0.007
NO-2G21-1a-3	0.035	0.012	1.899	0.054	2.000		0.133	0.011
NO-2G21-1a-4	0.036	0.001	1.898	0.066	2.001		0.080	0.007
NO-2G21-1a-5	0.031	0.013	1.886	0.070	2.000		0.066	0.009
NO-2G21-1a-6	0.029	0.021	1.904	0.046	2.000		0.247	0.027
NO-2G21-1a-7	0.031	0.033	1.898	0.038	2.000		0.238	0.024
NO-2G21-1a-8	0.033	0.025	1.886	0.056	2.000		0.149	0.019
NO-2G21-1a-9	0.035	0.071	1.852	0.042	2.000		0.306	0.055
NO-2G21-1a-10	0.032	0.057	1.884	0.027	2.000		0.349	0.053
NO-2G21-1a-11	0.034	0.047	1.875	0.044	2.000		0.338	0.051
NO-2G21-1a-12	0.032	0.042	1.894	0.031	1.999		0.435	0.115
NO-2G21-1b-14	0.035	0.014	1.891	0.060	2.000		0.087	0.011
NO-2G21-1b-15	0.031	0.012	1.899	0.058	2.000		0.087	0.011
NO-2G21-1b-16	0.034	0.016	1.888	0.063	2.001		0.063	0.009
NO-2G21-1b-17	0.030	0.016	1.907	0.048	2.001		0.114	0.012
NO-2G21-1b-18	0.033	0.020	1.880	0.068	2.001		0.071	0.014
NO-2G21-1b-19	0.031	0.010	1.900	0.059	2.000		0.045	0.006
NO-2G21-1b-20			2.000		2.000	0.774	0.097	0.006
NO-2G21-1b-21	0.030	0.020	1.870	0.080	2.000		0.050	0.011
NO-2G21-1b-22	0.033	0.021	1.870	0.076	2.000		0.035	0.007
NO-2G21-1b-23	0.030	0.010	1.905	0.055	2.000		0.092	0.010
NO-2G21-1b-24?	0.031	0.033	1.914	0.021	1.999		0.398	0.080
NO-2G21-1b-25?	0.032	0.045	1.881	0.042	2.000		0.376	0.072
NO-2G21-1c-26	0.029	0.024	1.912	0.035	2.000		0.156	0.014
NO-2G21-1c-27	0.031	0.034	1.884	0.051	2.000		0.187	0.028
NO-2G21-1c-28	0.026		1.903	0.071	2.000		0.159	0.022
NO-2G21-1c-29	0.022		1.916	0.062	2.000		0.045	0.008
NO-2G21-1c-30	0.034	0.001	1.896	0.069	2.000		0.076	0.013
NO-2G21-1c-31	0.031	0.018	1.895	0.056	2.000		0.212	0.030
NO-2G21-1c-32	0.029	0.035	1.891	0.046	2.001		0.233	0.030
NO-2G21-1c-33	0.032	0.001	1.906	0.061	2.000		0.054	0.010
NO-2G21-1c-34?	0.029	0.040	1.915	0.017	2.001		0.408	0.088
NO-2G21-1c-35	0.027	0.044	1.882	0.046	1.999		0.289	0.049
NO-2G21-1c-36	0.032	0.005	1.887	0.056	1.980			0.004
NO-2G21-1c-37	0.031	0.034	1.898	0.037	2.000		0.234	0.040
NO-2G22-4a-1	0.022	0.051	1.880	0.047	2.000		0.343	0.103
NO-2G22-4a-2	0.021	0.044	1.880	0.054	1.999		0.327	0.112
NO-2G22-4a-3	0.019	0.051	1.895	0.036	2.001		0.358	0.145

			W (ideally 2 apfu)				Warnings
Analysis	A subtotal	**O**	OH	O	W subtotal	Sum **T,C,B,A**	Final Total <98 or >102 wt%
NO-2G21-1a-1	0.146	22.000	1.922	0.078	2.000	15.146	low total 97.93
NO-2G21-1a-2	0.034	22.000	1.941	0.059	2.000	15.035	
NO-2G21-1a-3	0.144	22.000	1.905	0.095	2.000	15.145	
NO-2G21-1a-4	0.087	22.000	1.920	0.080	2.000	15.087	
NO-2G21-1a-5	0.075	22.000	1.939	0.061	2.000	15.075	low total 97.91
NO-2G21-1a-6	0.274	22.000	1.904	0.096	2.000	15.274	low total 97.94
NO-2G21-1a-7	0.262	22.000	1.913	0.087	2.000	15.262	
NO-2G21-1a-8	0.168	22.000	1.904	0.096	2.000	15.168	
NO-2G21-1a-9	0.361	22.000	1.657	0.343	2.000	15.361	low total 97.46
NO-2G21-1a-10	0.402	22.000	1.864	0.136	2.000	15.401	
NO-2G21-1a-11	0.389	22.000	1.854	0.146	2.000	15.390	
NO-2G21-1a-12	0.550	22.000	1.930	0.070	2.000	15.549	low total 97.68
NO-2G21-1b-14	0.098	22.000	1.939	0.061	2.000	15.098	
NO-2G21-1b-15	0.098	22.000	1.960	0.040	2.000	15.097	
NO-2G21-1b-16	0.072	22.000	1.965	0.035	2.000	15.073	
NO-2G21-1b-17	0.126	22.000	1.965	0.035	2.000	15.125	
NO-2G21-1b-18	0.085	22.000	1.961	0.039	2.000	15.087	
NO-2G21-1b-19	0.051	22.000	1.969	0.031	2.000	15.051	
NO-2G21-1b-20	0.877	22.000	1.976	0.024	2.000	15.313	low total 93.59
NO-2G21-1b-21	0.061	22.000	1.972	0.028	2.000	15.062	
NO-2G21-1b-22	0.042	22.000	1.952	0.048	2.000	15.042	
NO-2G21-1b-23	0.102	22.000	1.971	0.029	2.000	15.102	
NO-2G21-1b-24?	0.478	22.000	1.926	0.074	2.000	15.476	low total 97.49
NO-2G21-1b-25?	0.448	22.000	1.916	0.084	2.000	15.449	low total 97.82
NO-2G21-1c-26	0.170	22.000	1.963	0.037	2.000	15.170	
NO-2G21-1c-27	0.215	22.000	1.956	0.044	2.000	15.215	
NO-2G21-1c-28	0.181	22.000	1.955	0.045	2.000	15.180	
NO-2G21-1c-29	0.053	22.000	1.979	0.021	2.000	15.054	
NO-2G21-1c-30	0.089	22.000	1.968	0.032	2.000	15.090	
NO-2G21-1c-31	0.242	22.000	1.951	0.049	2.000	15.242	low total 97.66
NO-2G21-1c-32	0.263	22.000	1.949	0.051	2.000	15.264	
NO-2G21-1c-33	0.064	22.000	1.977	0.023	2.000	15.064	
NO-2G21-1c-34?	0.496	22.000	1.927	0.073	2.000	15.497	low total 97.55
NO-2G21-1c-35	0.338	22.000	1.930	0.070	2.000	15.337	
NO-2G21-1c-36	0.004	22.000	1.990	0.010	2.000	14.984	
NO-2G21-1c-37	0.274	22.000	1.945	0.055	2.000	15.274	
NO-2G22-4a-1	0.446	22.000	1.940	0.060	2.000	15.446	low total 96.71
NO-2G22-4a-2	0.439	22.000	1.932	0.068	2.000	15.438	low total 96.91
NO-2G22-4a-3	0.503	22.000	1.849	0.151	2.000	15.503	low total 97.32

Analysis	A>1	B< >2	C< >5	T< >8	W< >2	Initial $M^{3+}/\Sigma M$ and Manual normalization(s) both entered as TRUE
NO-2G21-1a-1						
NO-2G21-1a-2						
NO-2G21-1a-3						
NO-2G21-1a-4						
NO-2G21-1a-5						
NO-2G21-1a-6						
NO-2G21-1a-7						
NO-2G21-1a-8						
NO-2G21-1a-9						
NO-2G21-1a-10						
NO-2G21-1a-11						
NO-2G21-1a-12						
NO-2G21-1b-14						
NO-2G21-1b-15						
NO-2G21-1b-16						
NO-2G21-1b-17						
NO-2G21-1b-18						
NO-2G21-1b-19						
NO-2G21-1b-20			low C sum: 4.436			
NO-2G21-1b-21						
NO-2G21-1b-22						
NO-2G21-1b-23						
NO-2G21-1b-24?						
NO-2G21-1b-25?						
NO-2G21-1c-26						
NO-2G21-1c-27						
NO-2G21-1c-28						
NO-2G21-1c-29						
NO-2G21-1c-30						
NO-2G21-1c-31						
NO-2G21-1c-32						
NO-2G21-1c-33						
NO-2G21-1c-34?						
NO-2G21-1c-35						
NO-2G21-1c-36		low B sum: 1.98				
NO-2G21-1c-37						
NO-2G22-4a-1						
NO-2G22-4a-2						
NO-2G22-4a-3						

Analysis	^{A}Ca or ^{A}Li present	sum of high-valence C cations (M^{3+},M^{4+}) >2
NO-2G21-1a-1		
NO-2G21-1a-2		
NO-2G21-1a-3		
NO-2G21-1a-4		
NO-2G21-1a-5		
NO-2G21-1a-6		
NO-2G21-1a-7		
NO-2G21-1a-8		
NO-2G21-1a-9		
NO-2G21-1a-10		
NO-2G21-1a-11		
NO-2G21-1a-12		
NO-2G21-1b-14		
NO-2G21-1b-15		
NO-2G21-1b-16		
NO-2G21-1b-17		
NO-2G21-1b-18		
NO-2G21-1b-19		
NO-2G21-1b-20	non-standard A cation; check data	
NO-2G21-1b-21		
NO-2G21-1b-22		
NO-2G21-1b-23		
NO-2G21-1b-24?		
NO-2G21-1b-25?		
NO-2G21-1c-26		
NO-2G21-1c-27		
NO-2G21-1c-28		
NO-2G21-1c-29		
NO-2G21-1c-30		
NO-2G21-1c-31		
NO-2G21-1c-32		
NO-2G21-1c-33		
NO-2G21-1c-34?		
NO-2G21-1c-35		
NO-2G21-1c-36		
NO-2G21-1c-37		
NO-2G22-4a-1		
NO-2G22-4a-2		
NO-2G22-4a-3		

Analysis	Mineral	Intrusion/Phase	Sample	SiO_2	TiO_2	Al_2O_3	Cr_2O_3	MnO
NO-2G22-4a-4	Amphibole	Thunderbird-V	NO-2G22-4	40.432	0.264	14.993	0.051	0.175
NO-2G22-4a-5	Amphibole	Thunderbird-V	NO-2G22-4	40.136	0.302	15.738	0.024	0.177
NO-2G22-4a-6	Amphibole	Thunderbird-V	NO-2G22-4	40.312	0.264	14.930	0.014	0.165
NO-2G22-4b-7	Amphibole	Thunderbird-V	NO-2G22-4	39.736	0.326	16.156	0.047	0.148
NO-2G22-4b-8	Amphibole	Thunderbird-V	NO-2G22-4	39.917	0.225	16.557	0.050	0.129
NO-2G22-4b-9	Amphibole	Thunderbird-V	NO-2G22-4	39.950	0.318	15.330	0.046	0.150
NO-2G22-4b-10	Amphibole	Thunderbird-V	NO-2G22-4	38.230	0.074	24.914	0.000	0.103
NO-2G22-4b-12	Amphibole	Thunderbird-V	NO-2G22-4	39.659	0.220	16.307	0.016	0.176
NO-2G22-4b-13	Amphibole	Thunderbird-V	NO-2G22-4	40.092	0.285	15.098	0.029	0.168
NO-2G22-4c-19	Amphibole	Thunderbird-V	NO-2G22-4	39.828	0.279	15.273	0.029	0.176
NO-2G22-4c-20	Amphibole	Thunderbird-V	NO-2G22-4	40.057	0.253	16.629	0.023	0.145
NO-2G22-4c-17	Amphibole	Thunderbird-V	NO-2G22-4	42.962	0.431	12.245	0.000	0.183
NO-2G22-4c-16	Amphibole	Thunderbird-V	NO-2G22-4	39.319	0.271	15.792	0.031	0.133
NO-2G22-4c-14	Amphibole	Thunderbird-V	NO-2G22-4	39.480	0.251	16.305	0.022	0.158
NO-2G22-4c-15	Amphibole	Thunderbird-V	NO-2G22-4	38.247	0.049	25.160	0.053	0.142
NO-2G46-3b-1	Amphibole	Thunderbird-P	NO-2G46-3	39.792	0.430	15.738	0.030	0.222
NO-2G46-3b-2	Amphibole	Thunderbird-P	NO-2G46-3	39.520	0.066	16.592	0.005	0.260
NO-2G46-3b-4	Amphibole	Thunderbird-P	NO-2G46-3	43.413	0.383	10.917	0.000	0.262
NO-2G46-3c-16?	Amphibole	Thunderbird-P	NO-2G46-3	40.024	0.230	15.672	0.000	0.243
NO-2G47-3b-3	Amphibole	Thunderbird-P	NO-2G47-3	38.256	0.367	18.690	0.018	0.194
NO-2G47-3b-2	Amphibole	Thunderbird-P	NO-2G47-3	39.237	0.005	18.640	0.005	0.241
NO-2G47-3b-1	Amphibole	Thunderbird-P	NO-2G47-3	37.978	0.109	19.311	0.008	0.184
NO-2G47-2b-4red	Amphibole	Thunderbird-P	NO-2G47-2	45.509	1.290	8.150	0.011	0.319
NO-2G47-2b-3red	Amphibole	Thunderbird-P	NO-2G47-2	50.913	0.183	4.106	0.020	0.297
NO-2G47-2b-2red	Amphibole	Thunderbird-P	NO-2G47-2	46.529	0.614	7.736	0.012	0.296
MM-71B-2a-1red	Amphibole	Butler East	MM-71B-2	41.387	1.268	11.782	0.006	0.282
MM-71B-2a-3red	Amphibole	Butler East	MM-71B-2	42.180	1.270	11.215	0.004	0.282
MM-71B-2b-5red	Amphibole	Butler East	MM-71B-2	42.200	0.770	10.584	0.000	0.295
MM-71B-2a-2red	Amphibole	Butler East	MM-71B-2	41.533	1.243	11.482	0.002	0.292
MM-71B-2b-7red	Amphibole	Butler East	MM-71B-2	42.385	0.964	10.917	0.000	0.300
MM-71B-2b-9red	Amphibole	Butler East	MM-71B-2	42.189	0.621	10.875	0.004	0.308
MM-71B-2a-4red	Amphibole	Butler East	MM-71B-2	41.518	1.295	11.859	0.022	0.277
MM-71B-2c-12red	Amphibole	Butler East	MM-71B-2	42.027	0.982	11.002	0.000	0.323
MM-71B-2c-15red	Amphibole	Butler East	MM-71B-2	40.989	1.353	11.844	0.001	0.286
MM-117-1a-1red	Amphibole	Butler West	MM-117-1	51.439	0.253	5.335	0.000	0.184
MM-117-1a-2red	Amphibole	Butler West	MM-117-1	50.602	0.250	6.603	0.016	0.193
MM-117-1a-3red	Amphibole	Butler West	MM-117-1	48.691	0.304	7.863	0.004	0.201
MM-117-1b-5red	Amphibole	Butler West	MM-117-1	50.232	0.427	6.275	0.094	0.189

Analysis	Fe_2O_3	MgO	CaO	Na_2O	K_2O	O=F,Cl (calc)	Initial Total
NO-2G22-4a-4	23.915	4.454	11.237	1.227	0.574	0.00	97.32
NO-2G22-4a-5	24.417	4.167	11.250	1.285	0.620	0.00	98.12
NO-2G22-4a-6	24.392	4.450	11.176	1.319	0.603	0.00	97.63
NO-2G22-4b-7	23.794	4.105	11.141	1.293	0.663	0.00	97.41
NO-2G22-4b-8	24.030	3.819	11.314	1.243	0.588	0.00	97.87
NO-2G22-4b-9	24.345	4.248	11.097	1.270	0.594	0.00	97.35
NO-2G22-4b-10	11.409	0.012	23.247	0.000	0.000	0.00	97.99
NO-2G22-4b-12	24.022	3.980	11.129	1.344	0.458	0.00	97.31
NO-2G22-4b-13	23.915	4.411	11.155	1.275	0.597	0.00	97.03
NO-2G22-4c-19	24.656	4.089	11.281	1.250	0.647	0.00	97.51
NO-2G22-4c-20	23.854	4.005	11.225	1.201	0.562	0.00	97.95
NO-2G22-4c-17	23.522	5.878	11.211	1.170	0.377	0.00	97.98
NO-2G22-4c-16	24.349	3.948	11.118	1.364	0.568	0.00	96.89
NO-2G22-4c-14	23.634	3.970	11.177	1.299	0.642	0.00	96.94
NO-2G22-4c-15	10.971	0.008	23.084	0.000	0.006	0.00	97.72
NO-2G46-3b-1	23.606	4.283	11.249	1.698	0.409	0.00	97.46
NO-2G46-3b-2	23.895	4.475	10.863	1.963	0.372	0.00	98.01
NO-2G46-3b-4	23.788	6.181	11.045	1.300	0.296	0.00	97.59
NO-2G46-3c-16?	23.461	4.775	10.939	1.758	0.352	0.00	97.45
NO-2G47-3b-3	24.277	3.140	10.750	1.753	0.457	0.00	97.90
NO-2G47-3b-2	24.102	3.115	10.603	1.871	0.262	0.00	98.08
NO-2G47-3b-1	24.495	2.955	11.060	1.763	0.487	0.00	98.35
NO-2G47-2b-4red	22.860	7.273	11.600	0.967	0.237	0.00	98.22
NO-2G47-2b-3red	20.706	10.098	11.831	0.450	0.063	0.00	98.67
NO-2G47-2b-2red	22.834	7.853	11.709	0.860	0.214	0.00	98.66
MM-71B-2a-1red	24.448	5.580	11.004	1.345	0.832	0.00	97.93
MM-71B-2a-3red	24.455	5.873	10.928	1.292	0.769	0.00	98.27
MM-71B-2b-5red	24.785	5.942	10.829	1.312	0.760	0.00	97.48
MM-71B-2a-2red	24.445	5.635	10.984	1.388	0.846	0.00	97.85
MM-71B-2b-7red	24.940	5.880	10.981	1.304	0.756	0.00	98.43
MM-71B-2b-9red	25.065	5.935	10.914	1.367	0.774	0.00	98.05
MM-71B-2a-4red	24.489	5.557	11.038	1.379	0.848	0.00	98.28
MM-71B-2c-12red	24.619	5.588	11.098	1.383	0.859	0.00	97.88
MM-71B-2c-15red	24.718	5.315	10.963	1.369	0.963	0.00	97.80
MM-117-1a-1red	13.100	14.744	12.008	0.538	0.088	0.00	97.69
MM-117-1a-2red	13.358	14.253	12.012	0.591	0.123	0.00	98.00
MM-117-1a-3red	14.302	13.524	11.758	0.799	0.141	0.00	97.59
MM-117-1b-5red	13.812	14.083	11.794	0.650	0.140	0.00	97.70

			OUTPUT		
Analysis	$Fe^{3+}/\Sigma Fe$ initial	$Mn^{3+}/\Sigma Mn$ initial	$Fe^{3+}/\Sigma Fe$ used	$Mn^{3+}/\Sigma Mn$ used	MnO
NO-2G22-4a-4	1.000	0.000	0.039	0.000	0.18
NO-2G22-4a-5	1.000	0.000	0.045	0.000	0.18
NO-2G22-4a-6	1.000	0.000	0.047	0.000	0.17
NO-2G22-4b-7	1.000	0.000	0.042	0.000	0.15
NO-2G22-4b-8	1.000	0.000	0.032	0.000	0.13
NO-2G22-4b-9	1.000	0.000	0.053	0.000	0.15
NO-2G22-4b-10	1.000	0.000	0.084	0.000	0.10
NO-2G22-4b-12	1.000	0.000	0.045	0.000	0.18
NO-2G22-4b-13	1.000	0.000	0.043	0.000	0.17
NO-2G22-4c-19	1.000	0.000	0.049	0.000	0.18
NO-2G22-4c-20	1.000	0.000	0.042	0.000	0.15
NO-2G22-4c-17	1.000	0.000	0.050	0.000	0.18
NO-2G22-4c-16	1.000	0.000	0.045	0.000	0.13
NO-2G22-4c-14	1.000	0.000	0.034	0.000	0.16
NO-2G22-4c-15	1.000	0.000	0.066	0.000	0.14
NO-2G46-3b-1	1.000	0.000	0.031	0.000	0.22
NO-2G46-3b-2	1.000	0.000	0.057	0.000	0.26
NO-2G46-3b-4	1.000	0.000	0.053	0.000	0.26
NO-2G46-3c-16?	1.000	0.000	0.054	0.000	0.24
NO-2G47-3b-3	1.000	0.000	0.058	0.000	0.19
NO-2G47-3b-2	1.000	0.000	0.044	0.000	0.24
NO-2G47-3b-1	1.000	0.000	0.045	0.000	0.18
NO-2G47-2b-4red	1.000	0.000	0.055	0.000	0.32
NO-2G47-2b-3red	1.000	0.000	0.012	0.000	0.30
NO-2G47-2b-2red	1.000	0.000	0.043	0.000	0.30
MM-71B-2a-1red	1.000	0.000	0.093	0.000	0.28
MM-71B-2a-3red	1.000	0.000	0.095	0.000	0.28
MM-71B-2b-5red	1.000	0.000	0.084	0.000	0.30
MM-71B-2a-2red	1.000	0.000	0.086	0.000	0.29
MM-71B-2b-7red	1.000	0.000	0.090	0.000	0.30
MM-71B-2b-9red	1.000	0.000	0.086	0.000	0.31
MM-71B-2a-4red	1.000	0.000	0.088	0.000	0.28
MM-71B-2c-12red	1.000	0.000	0.059	0.000	0.32
MM-71B-2c-15red	1.000	0.000	0.091	0.000	0.29
MM-117-1a-1red	1.000	0.000	0.077	0.000	0.18
MM-117-1a-2red	1.000	0.000	0.083	0.000	0.19
MM-117-1a-3red	1.000	0.000	0.127	0.000	0.20
MM-117-1b-5red	1.000	0.000	0.102	0.000	0.19

Analysis	Mn_2O_3	FeO	Fe_2O_3	H_2O+	Total	Group	Subgroup of (OH,F,Cl)
NO-2G22-4a-4	0.00	20.68	0.93	1.91	96.93	OH,F,Cl	Ca
NO-2G22-4a-5	0.00	20.98	1.10	1.90	97.68	OH,F,Cl	Ca
NO-2G22-4a-6	0.00	20.92	1.15	1.90	97.20	OH,F,Cl	Ca
NO-2G22-4b-7	0.00	20.51	1.00	1.89	97.02	OH,F,Cl	Ca
NO-2G22-4b-8	0.00	20.93	0.77	1.92	97.46	OH,F,Cl	Ca
NO-2G22-4b-9	0.00	20.75	1.29	1.89	96.93	OH,F,Cl	Ca
NO-2G22-4b-10	0.00	9.40	0.96	2.02	98.96	OH,F,Cl	Ca
NO-2G22-4b-12	0.00	20.64	1.08	1.92	96.93	OH,F,Cl	Ca
NO-2G22-4b-13	0.00	20.59	1.03	1.90	96.63	OH,F,Cl	Ca
NO-2G22-4c-19	0.00	21.10	1.21	1.90	97.06	OH,F,Cl	Ca
NO-2G22-4c-20	0.00	20.56	1.00	1.92	97.59	OH,F,Cl	Ca
NO-2G22-4c-17	0.00	20.11	1.18	1.88	97.62	OH,F,Cl	Ca
NO-2G22-4c-16	0.00	20.92	1.10	1.90	96.46	OH,F,Cl	Ca
NO-2G22-4c-14	0.00	20.54	0.80	1.91	96.56	OH,F,Cl	Ca
NO-2G22-4c-15	0.00	9.22	0.72	2.03	98.72	OH,F,Cl	Ca
NO-2G46-3b-1	0.00	20.58	0.73	1.87	97.04	OH,F,Cl	Ca
NO-2G46-3b-2	0.00	20.28	1.36	1.95	97.70	OH,F,Cl	Ca
NO-2G46-3b-4	0.00	20.27	1.26	1.89	97.22	OH,F,Cl	Ca
NO-2G46-3c-16?	0.00	19.97	1.27	1.92	97.15	OH,F,Cl	Ca
NO-2G47-3b-3	0.00	20.58	1.41	1.88	97.49	OH,F,Cl	Ca
NO-2G47-3b-2	0.00	20.73	1.06	1.98	97.75	OH,F,Cl	Ca
NO-2G47-3b-1	0.00	21.05	1.10	1.94	97.95	OH,F,Cl	Ca
NO-2G47-2b-4red	0.00	19.44	1.26	1.69	97.74	OH,F,Cl	Ca
NO-2G47-2b-3red	0.00	18.41	0.25	1.99	98.61	OH,F,Cl	Ca
NO-2G47-2b-2red	0.00	19.66	0.98	1.85	98.32	OH,F,Cl	Ca
MM-71B-2a-1red	0.00	19.95	2.27	1.66	97.37	OH,F,Cl	Ca
MM-71B-2a-3red	0.00	19.91	2.32	1.67	97.72	OH,F,Cl	Ca
MM-71B-2b-5red	0.00	20.43	2.08	1.78	96.98	OH,F,Cl	Ca
MM-71B-2a-2red	0.00	20.10	2.10	1.67	97.28	OH,F,Cl	Ca
MM-71B-2b-7red	0.00	20.42	2.25	1.74	97.89	OH,F,Cl	Ca
MM-71B-2b-9red	0.00	20.61	2.16	1.81	97.57	OH,F,Cl	Ca
MM-71B-2a-4red	0.00	20.10	2.16	1.66	97.70	OH,F,Cl	Ca
MM-71B-2c-12red	0.00	20.85	1.45	1.73	97.29	OH,F,Cl	Ca
MM-71B-2c-15red	0.00	20.22	2.25	1.63	97.18	OH,F,Cl	Ca
MM-117-1a-1red	0.00	10.88	1.01	2.04	98.52	OH,F,Cl	Ca
MM-117-1a-2red	0.00	11.02	1.11	2.03	98.80	OH,F,Cl	Ca
MM-117-1a-3red	0.00	11.24	1.82	2.01	98.35	OH,F,Cl	Ca
MM-117-1b-5red	0.00	11.16	1.41	1.99	98.44	OH,F,Cl	Ca

		T (ideally 8 apfu)			C (ideal
Analysis	Species	Si	Al	T subtotal	Ti
NO-2G22-4a-4	ferro-hornblende	6.354	1.646	8.000	0.031
NO-2G22-4a-5	ferro-hornblende	6.271	1.729	8.000	0.036
NO-2G22-4a-6	ferro-hornblende	6.332	1.668	8.000	0.031
NO-2G22-4b-7	ferro-hornblende	6.240	1.760	8.000	0.039
NO-2G22-4b-8	ferro-hornblende	6.237	1.763	8.000	0.026
NO-2G22-4b-9	ferro-hornblende	6.291	1.709	8.000	0.038
NO-2G22-4b-10	ferro-sadanagaite	5.690	2.310	8.000	0.008
NO-2G22-4b-12	ferro-hornblende	6.230	1.770	8.000	0.026
NO-2G22-4b-13	ferro-hornblende	6.325	1.675	8.000	0.034
NO-2G22-4c-19	ferro-hornblende	6.280	1.720	8.000	0.033
NO-2G22-4c-20	ferro-hornblende	6.238	1.762	8.000	0.030
NO-2G22-4c-17	ferro-hornblende	6.661	1.339	8.000	0.050
NO-2G22-4c-16	ferro-hornblende	6.231	1.769	8.000	0.032
NO-2G22-4c-14	ferro-hornblende	6.229	1.771	8.000	0.030
NO-2G22-4c-15	ferro-sadanagaite	5.695	2.305	8.000	0.005
NO-2G46-3b-1	ferro-pargasite	6.254	1.746	8.000	0.051
NO-2G46-3b-2	ferro-pargasite	6.159	1.841	8.000	0.008
NO-2G46-3b-4	ferro-hornblende	6.769	1.231	8.000	0.045
NO-2G46-3c-16?	ferro-pargasite	6.261	1.739	8.000	0.027
NO-2G47-3b-3	ferro-sadanagaite	5.985	2.015	8.000	0.043
NO-2G47-3b-2	ferro-tschermakite	6.091	1.909	8.000	0.001
NO-2G47-3b-1	ferro-sadanagaite	5.923	2.077	8.000	0.013
NO-2G47-2b-4red	ferro-hornblende	7.039	0.961	8.000	0.150
NO-2G47-2b-3red	ferro-actinolite	7.635	0.365	8.000	0.021
NO-2G47-2b-2red	ferro-hornblende	7.123	0.877	8.000	0.071
MM-71B-2a-1red	ferro-pargasite	6.520	1.480	8.000	0.150
MM-71B-2a-3red	ferro-hornblende	6.606	1.394	8.000	0.150
MM-71B-2b-5red	ferro-pargasite	6.666	1.334	8.000	0.092
MM-71B-2a-2red	ferro-pargasite	6.552	1.448	8.000	0.148
MM-71B-2b-7red	ferro-hornblende	6.635	1.365	8.000	0.114
MM-71B-2b-9red	ferro-pargasite	6.630	1.370	8.000	0.073
MM-71B-2a-4red	ferro-pargasite	6.520	1.480	8.000	0.153
MM-71B-2c-12red	ferro-pargasite	6.634	1.366	8.000	0.117
MM-71B-2c-15red	ferro-pargasite	6.491	1.509	8.000	0.161
MM-117-1a-1red	actinolite	7.473	0.527	8.000	0.028
MM-117-1a-2red	magnesio-hornblende	7.344	0.656	8.000	0.027
MM-117-1a-3red	magnesio-hornblende	7.144	0.856	8.000	0.034
MM-117-1b-5red	magnesio-hornblende	7.339	0.661	8.000	0.047

ly 5 apfu)							
Analysis	Al	Cr	Fe^{3+}	Mn^{2+}	Fe^{2+}	Mg	C subtotal
NO-2G22-4a-4	1.130	0.006	0.111		2.677	1.043	4.998
NO-2G22-4a-5	1.170	0.003	0.130		2.691	0.971	5.001
NO-2G22-4a-6	1.096	0.002	0.136		2.694	1.042	5.001
NO-2G22-4b-7	1.229	0.006	0.118		2.647	0.961	5.000
NO-2G22-4b-8	1.286	0.006	0.089		2.703	0.890	5.000
NO-2G22-4b-9	1.136	0.006	0.152		2.671	0.997	5.000
NO-2G22-4b-10	2.061		0.108	0.013	1.170	0.003	3.363
NO-2G22-4b-12	1.249	0.002	0.128		2.663	0.932	5.000
NO-2G22-4b-13	1.132	0.004	0.122		2.672	1.037	5.001
NO-2G22-4c-19	1.118	0.004	0.144		2.740	0.961	5.000
NO-2G22-4c-20	1.290	0.003	0.118		2.631	0.930	5.002
NO-2G22-4c-17	0.899		0.136		2.556	1.359	5.000
NO-2G22-4c-16	1.181	0.004	0.131		2.719	0.933	5.000
NO-2G22-4c-14	1.260	0.003	0.096		2.678	0.934	5.001
NO-2G22-4c-15	2.110	0.006	0.081	0.018	1.148	0.002	3.370
NO-2G46-3b-1	1.169	0.004	0.088		2.685	1.004	5.001
NO-2G46-3b-2	1.206	0.001	0.159		2.587	1.040	5.001
NO-2G46-3b-4	0.775		0.147		2.596	1.437	5.000
NO-2G46-3c-16?	1.150		0.150		2.560	1.114	5.001
NO-2G47-3b-3	1.432	0.002	0.166		2.624	0.732	4.999
NO-2G47-3b-2	1.501	0.001	0.124		2.653	0.721	5.001
NO-2G47-3b-1	1.473	0.001	0.129		2.697	0.687	5.000
NO-2G47-2b-4red	0.524	0.001	0.145		2.502	1.677	4.999
NO-2G47-2b-3red	0.360	0.002	0.028	0.023	2.309	2.257	5.000
NO-2G47-2b-2red	0.519	0.001	0.113		2.503	1.792	4.999
MM-71B-2a-1red	0.707	0.001	0.271		2.560	1.310	4.999
MM-71B-2a-3red	0.675		0.274		2.530	1.371	5.000
MM-71B-2b-5red	0.637		0.248		2.624	1.399	5.000
MM-71B-2a-2red	0.687		0.249		2.590	1.325	4.999
MM-71B-2b-7red	0.648		0.264		2.602	1.372	5.000
MM-71B-2b-9red	0.644		0.254		2.638	1.390	4.999
MM-71B-2a-4red	0.715	0.003	0.255		2.574	1.301	5.001
MM-71B-2c-12red	0.681		0.172		2.715	1.315	5.000
MM-71B-2c-15red	0.702		0.267		2.615	1.255	5.000
MM-117-1a-1red	0.386		0.110		1.282	3.193	4.999
MM-117-1a-2red	0.473	0.002	0.121		1.294	3.084	5.001
MM-117-1a-3red	0.504		0.200		1.304	2.958	5.000
MM-117-1b-5red	0.420	0.011	0.154		1.301	3.067	5.000

	B (ideally 2 apfu)					A (from 0 to 1 apfu)		
Analysis	Mn^{2+}	Fe^{2+}	Ca	Na	B subtotal	Ca	Na	K
NO-2G22-4a-4	0.023	0.039	1.892	0.045	1.999		0.329	0.115
NO-2G22-4a-5	0.023	0.050	1.883	0.043	1.999		0.346	0.124
NO-2G22-4a-6	0.022	0.054	1.881	0.044	2.001		0.358	0.121
NO-2G22-4b-7	0.020	0.046	1.874	0.059	1.999		0.334	0.133
NO-2G22-4b-8	0.017	0.033	1.894	0.056	2.000		0.321	0.117
NO-2G22-4b-9	0.020	0.062	1.872	0.046	2.000		0.342	0.119
NO-2G22-4b-10			2.000		2.000	1.708		
NO-2G22-4b-12	0.023	0.049	1.873	0.055	2.000		0.355	0.092
NO-2G22-4b-13	0.022	0.046	1.886	0.046	2.000		0.344	0.120
NO-2G22-4c-19	0.024	0.042	1.906	0.029	2.001		0.353	0.130
NO-2G22-4c-20	0.019	0.047	1.873	0.061	2.000		0.302	0.112
NO-2G22-4c-17	0.024	0.052	1.862	0.061	1.999		0.291	0.075
NO-2G22-4c-16	0.018	0.054	1.888	0.041	2.001		0.378	0.115
NO-2G22-4c-14	0.021	0.033	1.889	0.057	2.000		0.340	0.129
NO-2G22-4c-15			2.000		2.000	1.683		0.001
NO-2G46-3b-1	0.030	0.019	1.894	0.057	2.000		0.460	0.082
NO-2G46-3b-2	0.034	0.056	1.814	0.096	2.000		0.497	0.074
NO-2G46-3b-4	0.035	0.048	1.845	0.072	2.000		0.321	0.059
NO-2G46-3c-16?	0.032	0.052	1.833	0.082	1.999		0.451	0.070
NO-2G47-3b-3	0.026	0.068	1.802	0.104	2.000		0.428	0.091
NO-2G47-3b-2	0.032	0.039	1.764	0.166	2.001		0.397	0.052
NO-2G47-3b-1	0.024	0.049	1.848	0.078	1.999		0.455	0.097
NO-2G47-2b-4red	0.042	0.013	1.922	0.023	2.000		0.267	0.047
NO-2G47-2b-3red	0.015		1.901	0.084	2.000		0.047	0.012
NO-2G47-2b-2red	0.038	0.014	1.921	0.027	2.000		0.228	0.042
MM-71B-2a-1red	0.038	0.067	1.857	0.038	2.000		0.373	0.167
MM-71B-2a-3red	0.037	0.079	1.834	0.050	2.000		0.342	0.154
MM-71B-2b-5red	0.039	0.074	1.833	0.053	1.999		0.349	0.153
MM-71B-2a-2red	0.039	0.063	1.857	0.042	2.001		0.383	0.170
MM-71B-2b-7red	0.040	0.072	1.842	0.047	2.001		0.349	0.151
MM-71B-2b-9red	0.041	0.072	1.838	0.050	2.001		0.367	0.155
MM-71B-2a-4red	0.037	0.065	1.857	0.041	2.000		0.379	0.170
MM-71B-2c-12red	0.043	0.038	1.877	0.042	2.000		0.381	0.173
MM-71B-2c-15red	0.038	0.064	1.860	0.037	1.999		0.383	0.195
MM-117-1a-1red	0.023	0.039	1.869	0.069	2.000		0.083	0.016
MM-117-1a-2red	0.024	0.044	1.868	0.064	2.000		0.102	0.023
MM-117-1a-3red	0.025	0.075	1.848	0.051	1.999		0.176	0.026
MM-117-1b-5red	0.023	0.063	1.846	0.067	1.999		0.117	0.026

			W (ideally 2 apfu)				Warnings
Analysis	A subtotal	**O**	OH	O	W subtotal	Sum **T,C,B,A**	Final Total <98 or >102 wt%
NO-2G22-4a-4	0.444	22.000	1.937	0.063	2.000	15.441	low total 96.93
NO-2G22-4a-5	0.470	22.000	1.929	0.071	2.000	15.470	low total 97.68
NO-2G22-4a-6	0.479	22.000	1.937	0.063	2.000	15.481	low total 97.2
NO-2G22-4b-7	0.467	22.000	1.923	0.077	2.000	15.466	low total 97.02
NO-2G22-4b-8	0.438	22.000	1.947	0.053	2.000	15.438	low total 97.46
NO-2G22-4b-9	0.461	22.000	1.925	0.075	2.000	15.461	low total 96.93
NO-2G22-4b-10	1.708	22.000	1.983	0.017	2.000	15.071	
NO-2G22-4b-12	0.447	22.000	1.948	0.052	2.000	15.447	low total 96.93
NO-2G22-4b-13	0.464	22.000	1.932	0.068	2.000	15.465	low total 96.63
NO-2G22-4c-19	0.483	22.000	1.934	0.066	2.000	15.484	low total 97.06
NO-2G22-4c-20	0.414	22.000	1.941	0.059	2.000	15.416	low total 97.59
NO-2G22-4c-17	0.366	22.000	1.899	0.101	2.000	15.365	low total 97.62
NO-2G22-4c-16	0.493	22.000	1.935	0.065	2.000	15.494	low total 96.46
NO-2G22-4c-14	0.469	22.000	1.940	0.060	2.000	15.470	low total 96.56
NO-2G22-4c-15	1.684	22.000	1.989	0.011	2.000	15.054	
NO-2G46-3b-1	0.542	22.000	1.898	0.102	2.000	15.543	low total 97.04
NO-2G46-3b-2	0.571	22.000	1.984	0.016	2.000	15.572	low total 97.7
NO-2G46-3b-4	0.380	22.000	1.910	0.090	2.000	15.380	low total 97.22
NO-2G46-3c-16?	0.521	22.000	1.946	0.054	2.000	15.521	low total 97.15
NO-2G47-3b-3	0.519	22.000	1.913	0.087	2.000	15.518	low total 97.49
NO-2G47-3b-2	0.449	22.000	1.999	0.001	2.000	15.451	low total 97.75
NO-2G47-3b-1	0.552	22.000	1.974	0.026	2.000	15.551	low total 97.95
NO-2G47-2b-4red	0.314	22.000	1.699	0.301	2.000	15.313	low total 97.74
NO-2G47-2b-3red	0.059	22.000	1.959	0.041	2.000	15.059	
NO-2G47-2b-2red	0.270	22.000	1.858	0.142	2.000	15.269	
MM-71B-2a-1red	0.540	22.000	1.699	0.301	2.000	15.539	low total 97.37
MM-71B-2a-3red	0.496	22.000	1.700	0.300	2.000	15.496	low total 97.72
MM-71B-2b-5red	0.502	22.000	1.817	0.183	2.000	15.501	low total 96.98
MM-71B-2a-2red	0.553	22.000	1.704	0.296	2.000	15.553	low total 97.28
MM-71B-2b-7red	0.500	22.000	1.773	0.227	2.000	15.501	low total 97.89
MM-71B-2b-9red	0.522	22.000	1.853	0.147	2.000	15.522	low total 97.57
MM-71B-2a-4red	0.549	22.000	1.694	0.306	2.000	15.550	low total 97.7
MM-71B-2c-12red	0.554	22.000	1.766	0.234	2.000	15.554	low total 97.29
MM-71B-2c-15red	0.578	22.000	1.677	0.323	2.000	15.577	low total 97.18
MM-117-1a-1red	0.099	22.000	1.945	0.055	2.000	15.098	
MM-117-1a-2red	0.125	22.000	1.945	0.055	2.000	15.126	
MM-117-1a-3red	0.202	22.000	1.933	0.067	2.000	15.201	
MM-117-1b-5red	0.143	22.000	1.906	0.094	2.000	15.142	

Analysis	A>1	B< >2	C< >5	T< >8	W< >2	Initial $M^{3+}/\Sigma M$ and Manual normalization(s) both entered as TRUE
NO-2G22-4a-4						
NO-2G22-4a-5						
NO-2G22-4a-6						
NO-2G22-4b-7						
NO-2G22-4b-8						
NO-2G22-4b-9						
NO-2G22-4b-10	high A sum: 1.708		low C sum: 3.363			
NO-2G22-4b-12						
NO-2G22-4b-13						
NO-2G22-4c-19						
NO-2G22-4c-20						
NO-2G22-4c-17						
NO-2G22-4c-16						
NO-2G22-4c-14						
NO-2G22-4c-15	high A sum: 1.684		low C sum: 3.37			
NO-2G46-3b-1						
NO-2G46-3b-2						
NO-2G46-3b-4						
NO-2G46-3c-16?						
NO-2G47-3b-3						
NO-2G47-3b-2						
NO-2G47-3b-1						
NO-2G47-2b-4red						
NO-2G47-2b-3red						
NO-2G47-2b-2red						
MM-71B-2a-1red						
MM-71B-2a-3red						
MM-71B-2b-5red						
MM-71B-2a-2red						
MM-71B-2b-7red						
MM-71B-2b-9red						
MM-71B-2a-4red						
MM-71B-2c-12red						
MM-71B-2c-15red						
MM-117-1a-1red						
MM-117-1a-2red						
MM-117-1a-3red						
MM-117-1b-5red						

Analysis	^{A}Ca or ^{A}Li present	sum of high-valence C cations (M^{3+},M^{4+}) >2
NO-2G22-4a-4		
NO-2G22-4a-5		
NO-2G22-4a-6		
NO-2G22-4b-7		
NO-2G22-4b-8		
NO-2G22-4b-9		
NO-2G22-4b-10	non-standard A cation; check data	high valence C cations exceed 2 apfu: 2.177; check data
NO-2G22-4b-12		
NO-2G22-4b-13		
NO-2G22-4c-19		
NO-2G22-4c-20		
NO-2G22-4c-17		
NO-2G22-4c-16		
NO-2G22-4c-14		
NO-2G22-4c-15	non-standard A cation; check data	high valence C cations exceed 2 apfu: 2.202; check data
NO-2G46-3b-1		
NO-2G46-3b-2		
NO-2G46-3b-4		
NO-2G46-3c-16?		
NO-2G47-3b-3		
NO-2G47-3b-2		
NO-2G47-3b-1		
NO-2G47-2b-4red		
NO-2G47-2b-3red		
NO-2G47-2b-2red		
MM-71B-2a-1red		
MM-71B-2a-3red		
MM-71B-2b-5red		
MM-71B-2a-2red		
MM-71B-2b-7red		
MM-71B-2b-9red		
MM-71B-2a-4red		
MM-71B-2c-12red		
MM-71B-2c-15red		
MM-117-1a-1red		
MM-117-1a-2red		
MM-117-1a-3red		
MM-117-1b-5red		

Analysis	Mineral	Intrusion/Phase	Sample	SiO_2	TiO_2	Al_2O_3	Cr_2O_3	MnO
MM-117-1b-6red	Amphibole	Butler West	MM-117-1	47.700	0.562	8.769	0.053	0.181
MM-117-1b-8red?	Amphibole	Butler West	MM-117-1	49.483	0.393	7.682	0.003	0.166
MM-117-1c-10red	Amphibole	Butler West	MM-117-1	49.555	0.357	7.401	0.003	0.194
MM-117-1c-11red	Amphibole	Butler West	MM-117-1	50.906	0.269	5.825	0.021	0.205
MM-117-6a-1red?	Amphibole	Butler West	MM-117-6	46.025	0.644	9.099	0.075	0.283
MM-117-6a-2red?	Amphibole	Butler West	MM-117-6	48.463	0.449	6.070	0.027	0.351
MM-117-6a-4red	Amphibole	Butler West	MM-117-6	50.802	0.334	4.342	0.021	0.322
MM-117-6a-5red	Amphibole	Butler West	MM-117-6	48.982	0.439	6.658	0.024	0.293
MM-117-6a-7red	Amphibole	Butler West	MM-117-6	53.111	0.157	2.490	0.000	0.413
MM-117-6b-9red	Amphibole	Butler West	MM-117-6	47.532	0.395	7.723	0.031	0.280
MM-117-6b-10red	Amphibole	Butler West	MM-117-6	45.171	0.315	9.710	0.000	0.320
MM-117-6c-15red?	Amphibole	Butler West	MM-117-6	47.905	0.347	7.624	0.012	0.339
MM-117-6c-16red	Amphibole	Butler West	MM-117-6	45.370	0.207	9.624	0.000	0.313
MM-117-6c-18red	Amphibole	Butler West	MM-117-6	43.852	0.179	11.946	0.000	0.308
MM-70-2a-1red	Amphibole	Butler East	MM-70-2	42.545	0.617	13.733	0.032	0.343
MM-70-2a-2red	Amphibole	Butler East	MM-70-2	43.044	0.502	13.411	0.007	0.377
MM-70-2a-3red	Amphibole	Butler East	MM-70-2	41.173	0.586	16.196	0.003	0.272
MM-V4-7a-1red	Amphibole	Butler East	MM-V4-7	41.930	0.691	14.046	0.006	0.217
MM-V4-7a-2red	Amphibole	Butler East	MM-V4-7	42.504	0.892	13.132	0.000	0.320
MM-V4-7a-3red	Amphibole	Butler East	MM-V4-7	42.340	1.030	12.817	0.000	0.285
MM-V4-7b-4red	Amphibole	Butler East	MM-V4-7	41.944	0.955	13.391	0.018	0.302
MM-V4-7b-5red?	Amphibole	Butler East	MM-V4-7	42.637	0.734	13.098	0.000	0.322
MM-V4-7b-6red	Amphibole	Butler East	MM-V4-7	42.277	0.817	13.368	0.012	0.290
MM-V4-7c-7red	Amphibole	Butler East	MM-V4-7	41.786	0.622	14.023	0.000	0.335
MM-V4-7c-8red	Amphibole	Butler East	MM-V4-7	41.539	0.634	14.170	0.004	0.268
MM-V8-1a-2red	Amphibole	Butler West	MM-V8-1	45.200	0.787	9.374	0.007	0.253
MM-V8-1a-3red?	Amphibole	Butler West	MM-V8-1	42.053	0.742	13.283	0.016	0.210
MM-V8-1b-5red	Amphibole	Butler West	MM-V8-1	43.116	0.650	11.429	0.000	0.236
MM-V8-1b-6red	Amphibole	Butler West	MM-V8-1	42.876	0.823	11.811	0.008	0.211
MM-V8-1b-7red	Amphibole	Butler West	MM-V8-1	44.055	0.524	10.827	0.007	0.239
MM-V8-1c-9red?	Amphibole	Butler West	MM-V8-1	46.591	0.318	8.346	0.000	0.297
MM-V8-1c-11red?	Amphibole	Butler West	MM-V8-1	45.451	0.416	9.567	0.007	0.268

Analysis	Fe_2O_3	MgO	CaO	Na_2O	K_2O	O=F,Cl (calc)	Initial Total
MM-117-1b-6red	14.904	12.433	11.816	0.883	0.174	0.00	97.48
MM-117-1b-8red?	13.854	13.573	12.111	0.618	0.146	0.00	98.03
MM-117-1c-10red	14.443	13.391	11.834	0.746	0.121	0.00	98.05
MM-117-1c-11red	13.738	14.405	11.858	0.543	0.086	0.00	97.86
MM-117-6a-1red?	19.043	10.019	11.189	1.094	0.241	0.00	97.71
MM-117-6a-2red?	18.574	11.789	10.583	0.714	0.126	0.00	97.15
MM-117-6a-4red	17.490	12.966	10.712	0.540	0.075	0.00	97.60
MM-117-6a-5red	17.880	11.509	11.272	0.792	0.113	0.00	97.96
MM-117-6a-7red	17.233	14.569	9.797	0.264	0.024	0.00	98.06
MM-117-6b-9red	18.910	10.696	11.225	0.979	0.157	0.00	97.93
MM-117-6b-10red	20.657	9.671	10.662	1.108	0.233	0.00	97.85
MM-117-6c-15red?	18.321	11.141	11.264	0.891	0.155	0.00	98.00
MM-117-6c-16red	19.652	9.564	10.957	1.265	0.206	0.00	97.16
MM-117-6c-18red	20.910	8.469	10.880	1.406	0.311	0.00	98.26
MM-70-2a-1red	22.102	7.894	8.969	1.456	0.360	0.00	98.05
MM-70-2a-2red	23.439	7.734	8.524	1.336	0.318	0.00	98.69
MM-70-2a-3red	22.786	5.795	10.120	1.743	0.376	0.00	99.05
MM-V4-7a-1red	21.670	6.653	11.060	1.478	0.564	0.00	98.32
MM-V4-7a-2red	21.436	6.986	10.410	1.687	0.533	0.00	97.90
MM-V4-7a-3red	21.709	6.798	10.684	1.573	0.495	0.00	97.73
MM-V4-7b-4red	21.452	7.078	10.585	1.736	0.520	0.00	97.98
MM-V4-7b-5red?	21.003	7.694	9.919	1.628	0.514	0.00	97.55
MM-V4-7b-6red	20.759	7.355	10.752	1.759	0.541	0.00	97.93
MM-V4-7c-7red	21.721	6.679	10.569	1.787	0.507	0.00	98.03
MM-V4-7c-8red	20.207	7.424	11.000	1.706	0.578	0.00	97.53
MM-V8-1a-2red	19.918	9.535	11.604	1.195	0.403	0.00	98.28
MM-V8-1a-3red?	21.015	7.319	11.545	1.407	0.606	0.00	98.20
MM-V8-1b-5red	20.711	8.362	11.627	1.328	0.533	0.00	97.99
MM-V8-1b-6red	20.378	8.113	11.547	1.386	0.581	0.00	97.73
MM-V8-1b-7red	20.188	8.589	11.539	1.264	0.388	0.00	97.62
MM-V8-1c-9red?	19.336	10.199	11.596	1.083	0.307	0.00	98.07
MM-V8-1c-11red?	19.709	9.636	11.594	1.169	0.391	0.00	98.21

			OUTPUT		
Analysis	$Fe^{3+}/\Sigma Fe$ initial	$Mn^{3+}/\Sigma Mn$ initial	$Fe^{3+}/\Sigma Fe$ used	$Mn^{3+}/\Sigma Mn$ used	MnO
MM-117-1b-6red	1.000	0.000	0.093	0.000	0.18
MM-117-1b-8red?	1.000	0.000	0.084	0.000	0.17
MM-117-1c-10red	1.000	0.000	0.091	0.000	0.19
MM-117-1c-11red	1.000	0.000	0.102	0.000	0.21
MM-117-6a-1red?	1.000	0.000	0.104	0.000	0.28
MM-117-6a-2red?	1.000	0.000	0.164	0.000	0.35
MM-117-6a-4red	1.000	0.000	0.151	0.000	0.32
MM-117-6a-5red	1.000	0.000	0.094	0.000	0.29
MM-117-6a-7red	1.000	0.000	0.243	0.000	0.41
MM-117-6b-9red	1.000	0.000	0.095	0.000	0.28
MM-117-6b-10red	1.000	0.000	0.165	0.000	0.32
MM-117-6c-15red?	1.000	0.000	0.103	0.000	0.34
MM-117-6c-16red	1.000	0.000	0.097	0.000	0.31
MM-117-6c-18red	1.000	0.000	0.108	0.000	0.31
MM-70-2a-1red	1.000	0.000	0.225	0.000	0.34
MM-70-2a-2red	1.000	0.000	0.246	0.000	0.38
MM-70-2a-3red	1.000	0.000	0.124	0.000	0.27
MM-V4-7a-1red	1.000	0.000	0.076	0.000	0.22
MM-V4-7a-2red	1.000	0.000	0.098	0.000	0.32
MM-V4-7a-3red	1.000	0.000	0.088	0.000	0.29
MM-V4-7b-4red	1.000	0.000	0.104	0.000	0.30
MM-V4-7b-5red?	1.000	0.000	0.142	0.000	0.32
MM-V4-7b-6red	1.000	0.000	0.087	0.000	0.29
MM-V4-7c-7red	1.000	0.000	0.091	0.000	0.34
MM-V4-7c-8red	1.000	0.000	0.082	0.000	0.27
MM-V8-1a-2red	1.000	0.000	0.103	0.000	0.25
MM-V8-1a-3red?	1.000	0.000	0.082	0.000	0.21
MM-V8-1b-5red	1.000	0.000	0.103	0.000	0.24
MM-V8-1b-6red	1.000	0.000	0.083	0.000	0.21
MM-V8-1b-7red	1.000	0.000	0.074	0.000	0.24
MM-V8-1c-9red?	1.000	0.000	0.073	0.000	0.30
MM-V8-1c-11red?	1.000	0.000	0.086	0.000	0.27

Analysis	Mn_2O_3	FeO	Fe_2O_3	H_2O+	Total	Group	Subgroup of (OH,F,Cl)
MM-117-1b-6red	0.00	12.16	1.39	1.94	98.06	OH,F,Cl	Ca
MM-117-1b-8red?	0.00	11.42	1.16	1.99	98.75	OH,F,Cl	Ca
MM-117-1c-10red	0.00	11.81	1.31	2.00	98.73	OH,F,Cl	Ca
MM-117-1c-11red	0.00	11.10	1.40	2.03	98.65	OH,F,Cl	Ca
MM-117-6a-1red?	0.00	15.35	1.98	1.88	97.88	OH,F,Cl	Ca
MM-117-6a-2red?	0.00	13.97	3.05	1.94	97.53	OH,F,Cl	Ca
MM-117-6a-4red	0.00	13.36	2.64	1.99	98.11	OH,F,Cl	Ca
MM-117-6a-5red	0.00	14.58	1.68	1.95	98.29	OH,F,Cl	Ca
MM-117-6a-7red	0.00	11.74	4.19	2.05	98.80	OH,F,Cl	Ca
MM-117-6b-9red	0.00	15.40	1.80	1.94	98.15	OH,F,Cl	Ca
MM-117-6b-10red	0.00	15.52	3.41	1.95	98.07	OH,F,Cl	Ca
MM-117-6c-15red?	0.00	14.79	1.89	1.96	98.31	OH,F,Cl	Ca
MM-117-6c-16red	0.00	15.97	1.91	1.98	97.36	OH,F,Cl	Ca
MM-117-6c-18red	0.00	16.78	2.26	1.97	98.36	OH,F,Cl	Ca
MM-70-2a-1red	0.00	15.41	4.97	1.87	98.21	OH,F,Cl	Ca
MM-70-2a-2red	0.00	15.90	5.77	1.90	98.82	OH,F,Cl	Ca
MM-70-2a-3red	0.00	17.96	2.83	1.86	98.91	OH,F,Cl	Ca
MM-V4-7a-1red	0.00	18.02	1.65	1.83	98.14	OH,F,Cl	Ca
MM-V4-7a-2red	0.00	17.40	2.10	1.79	97.75	OH,F,Cl	Ca
MM-V4-7a-3red	0.00	17.82	1.91	1.75	97.50	OH,F,Cl	Ca
MM-V4-7b-4red	0.00	17.30	2.23	1.77	97.83	OH,F,Cl	Ca
MM-V4-7b-5red?	0.00	16.22	2.98	1.84	97.58	OH,F,Cl	Ca
MM-V4-7b-6red	0.00	17.05	1.81	1.81	97.84	OH,F,Cl	Ca
MM-V4-7c-7red	0.00	17.77	1.98	1.85	97.90	OH,F,Cl	Ca
MM-V4-7c-8red	0.00	16.69	1.66	1.85	97.52	OH,F,Cl	Ca
MM-V8-1a-2red	0.00	16.08	2.05	1.83	98.32	OH,F,Cl	Ca
MM-V8-1a-3red?	0.00	17.36	1.72	1.82	98.08	OH,F,Cl	Ca
MM-V8-1b-5red	0.00	16.72	2.13	1.85	97.98	OH,F,Cl	Ca
MM-V8-1b-6red	0.00	16.81	1.69	1.81	97.67	OH,F,Cl	Ca
MM-V8-1b-7red	0.00	16.82	1.49	1.89	97.64	OH,F,Cl	Ca
MM-V8-1c-9red?	0.00	16.13	1.41	1.95	98.23	OH,F,Cl	Ca
MM-V8-1c-11red?	0.00	16.21	1.70	1.92	98.32	OH,F,Cl	Ca

		T (ideally 8 apfu)			C (ideal
Analysis	**Species**	Si	Al	T subtotal	Ti
MM-117-1b-6red	magnesio-hornblende	7.058	0.942	8.000	0.063
MM-117-1b-8red?	magnesio-hornblende	7.215	0.785	8.000	0.043
MM-117-1c-10red	magnesio-hornblende	7.240	0.760	8.000	0.039
MM-117-1c-11red	magnesio-hornblende	7.404	0.596	8.000	0.029
MM-117-6a-1red?	magnesio-hornblende	6.957	1.043	8.000	0.073
MM-117-6a-2red?	magnesio-hornblende	7.279	0.721	8.000	0.051
MM-117-6a-4red	magnesio-ferri-hornblende	7.521	0.479	8.000	0.037
MM-117-6a-5red	magnesio-hornblende	7.292	0.708	8.000	0.049
MM-117-6a-7red	magnesio-ferri-hornblende	7.725	0.275	8.000	0.017
MM-117-6b-9red	magnesio-hornblende	7.135	0.865	8.000	0.045
MM-117-6b-10red	magnesio-hornblende	6.839	1.161	8.000	0.036
MM-117-6c-15red?	magnesio-hornblende	7.155	0.845	8.000	0.039
MM-117-6c-16red	magnesio-hornblende	6.909	1.091	8.000	0.024
MM-117-6c-18red	ferro-hornblende	6.651	1.349	8.000	0.020
MM-70-2a-1red	magnesio-hornblende	6.451	1.549	8.000	0.070
MM-70-2a-2red	tschermakite	6.493	1.507	8.000	0.057
MM-70-2a-3red	ferro-hornblende	6.260	1.740	8.000	0.067
MM-V4-7a-1red	ferro-hornblende	6.434	1.566	8.000	0.080
MM-V4-7a-2red	ferro-hornblende	6.533	1.467	8.000	0.103
MM-V4-7a-3red	ferro-hornblende	6.543	1.457	8.000	0.120
MM-V4-7b-4red	ferro-pargasite	6.455	1.545	8.000	0.111
MM-V4-7b-5red?	ferro-hornblende	6.529	1.471	8.000	0.085
MM-V4-7b-6red	ferro-pargasite	6.487	1.513	8.000	0.094
MM-V4-7c-7red	ferro-pargasite	6.427	1.573	8.000	0.072
MM-V4-7c-8red	ferro-pargasite	6.389	1.611	8.000	0.073
MM-V8-1a-2red	magnesio-hornblende	6.857	1.143	8.000	0.090
MM-V8-1a-3red?	ferro-pargasite	6.455	1.545	8.000	0.086
MM-V8-1b-5red	ferro-hornblende	6.608	1.392	8.000	0.075
MM-V8-1b-6red	ferro-pargasite	6.592	1.408	8.000	0.095
MM-V8-1b-7red	ferro-hornblende	6.744	1.256	8.000	0.060
MM-V8-1c-9red?	magnesio-hornblende	7.032	0.968	8.000	0.036
MM-V8-1c-11red?	magnesio-hornblende	6.878	1.122	8.000	0.047

ly 5 apfu)							
Analysis	Al	Cr	Fe^{3+}	Mn^{2+}	Fe^{2+}	Mg	C subtotal
MM-117-1b-6red	0.587	0.006	0.154		1.448	2.743	5.001
MM-117-1b-8red?	0.535		0.127		1.344	2.950	4.999
MM-117-1c-10red	0.514		0.145		1.385	2.916	4.999
MM-117-1c-11red	0.403	0.002	0.153		1.289	3.123	4.999
MM-117-6a-1red?	0.578	0.009	0.224		1.858	2.258	5.000
MM-117-6a-2red?	0.353	0.003	0.345		1.608	2.640	5.000
MM-117-6a-4red	0.278	0.002	0.294		1.526	2.862	4.999
MM-117-6a-5red	0.460	0.003	0.188		1.746	2.554	5.000
MM-117-6a-7red	0.152		0.458		1.214	3.159	5.000
MM-117-6b-9red	0.502	0.004	0.203		1.853	2.394	5.001
MM-117-6b-10red	0.572		0.388		1.821	2.183	5.000
MM-117-6c-15red?	0.497	0.001	0.212		1.769	2.481	4.999
MM-117-6c-16red	0.637		0.217		1.951	2.171	5.000
MM-117-6c-18red	0.786		0.258		2.020	1.915	4.999
MM-70-2a-1red	0.906	0.004	0.567		1.669	1.784	5.000
MM-70-2a-2red	0.878	0.001	0.654		1.672	1.739	5.001
MM-70-2a-3red	1.162		0.324		2.133	1.313	4.999
MM-V4-7a-1red	0.974	0.001	0.191		2.233	1.522	5.001
MM-V4-7a-2red	0.912		0.244		2.140	1.601	5.000
MM-V4-7a-3red	0.877		0.223		2.214	1.566	5.000
MM-V4-7b-4red	0.884	0.002	0.257		2.121	1.624	4.999
MM-V4-7b-5red?	0.894		0.345		1.921	1.757	5.002
MM-V4-7b-6red	0.904	0.001	0.209		2.109	1.682	4.999
MM-V4-7c-7red	0.969		0.230		2.198	1.531	5.000
MM-V4-7c-8red	0.958		0.191		2.075	1.702	4.999
MM-V8-1a-2red	0.533	0.001	0.234		1.986	2.156	5.000
MM-V8-1a-3red?	0.858	0.002	0.199		2.180	1.675	5.000
MM-V8-1b-5red	0.673		0.246		2.096	1.911	5.001
MM-V8-1b-6red	0.732	0.001	0.197		2.115	1.860	5.000
MM-V8-1b-7red	0.697	0.001	0.173		2.109	1.960	5.000
MM-V8-1c-9red?	0.517		0.161		1.991	2.295	5.000
MM-V8-1c-11red?	0.584	0.001	0.192		2.003	2.174	5.001

	B (ideally 2 apfu)					A (from 0 to 1 apfu)		
Analysis	Mn^{2+}	Fe^{2+}	Ca	Na	B subtotal	Ca	Na	K
MM-117-1b-6red	0.023	0.058	1.873	0.046	2.000		0.208	0.033
MM-117-1b-8red?	0.020	0.048	1.892	0.039	1.999		0.135	0.027
MM-117-1c-10red	0.024	0.058	1.852	0.066	2.000		0.145	0.023
MM-117-1c-11red	0.025	0.061	1.848	0.065	1.999		0.088	0.016
MM-117-6a-1red?	0.036	0.084	1.812	0.068	2.000		0.253	0.046
MM-117-6a-2red?	0.045	0.146	1.703	0.106	2.000		0.102	0.024
MM-117-6a-4red	0.040	0.128	1.699	0.132	1.999		0.023	0.014
MM-117-6a-5red	0.037	0.069	1.798	0.096	2.000		0.133	0.021
MM-117-6a-7red	0.051	0.215	1.527	0.074	1.867			0.004
MM-117-6b-9red	0.036	0.080	1.805	0.079	2.000		0.206	0.030
MM-117-6b-10red	0.041	0.144	1.730	0.085	2.000		0.240	0.045
MM-117-6c-15red?	0.043	0.078	1.803	0.077	2.001		0.181	0.030
MM-117-6c-16red	0.040	0.084	1.788	0.088	2.000		0.285	0.040
MM-117-6c-18red	0.040	0.108	1.768	0.084	2.000		0.329	0.060
MM-70-2a-1red	0.044	0.286	1.457	0.213	2.000		0.215	0.070
MM-70-2a-2red	0.048	0.335	1.378	0.239	2.000		0.152	0.061
MM-70-2a-3red	0.035	0.150	1.649	0.166	2.000		0.347	0.073
MM-V4-7a-1red	0.028	0.079	1.818	0.075	2.000		0.365	0.110
MM-V4-7a-2red	0.042	0.096	1.714	0.148	2.000		0.355	0.105
MM-V4-7a-3red	0.037	0.088	1.769	0.106	2.000		0.365	0.098
MM-V4-7b-4red	0.039	0.106	1.745	0.110	2.000		0.408	0.102
MM-V4-7b-5red?	0.042	0.155	1.628	0.176	2.001		0.308	0.100
MM-V4-7b-6red	0.038	0.079	1.768	0.115	2.000		0.408	0.106
MM-V4-7c-7red	0.044	0.086	1.742	0.129	2.001		0.404	0.099
MM-V4-7c-8red	0.035	0.072	1.813	0.080	2.000		0.429	0.113
MM-V8-1a-2red	0.033	0.054	1.886	0.027	2.000		0.324	0.078
MM-V8-1a-3red?	0.027	0.048	1.899	0.026	2.000		0.393	0.119
MM-V8-1b-5red	0.031	0.047	1.909	0.013	2.000		0.382	0.104
MM-V8-1b-6red	0.027	0.046	1.902	0.025	2.000		0.389	0.114
MM-V8-1b-7red	0.031	0.044	1.893	0.033	2.001		0.343	0.076
MM-V8-1c-9red?	0.038	0.044	1.875	0.043	2.000		0.274	0.059
MM-V8-1c-11red?	0.034	0.050	1.880	0.036	2.000		0.307	0.075

			W (ideally 2 apfu)				Warnings
Analysis	A subtotal	**O**	OH	O	W subtotal	Sum **T,C,B,A**	Final Total <98 or >102 wt%
MM-117-1b-6red	0.241	22.000	1.875	0.125	2.000	15.242	
MM-117-1b-8red?	0.162	22.000	1.914	0.086	2.000	15.160	
MM-117-1c-10red	0.168	22.000	1.921	0.079	2.000	15.167	
MM-117-1c-11red	0.104	22.000	1.941	0.059	2.000	15.102	
MM-117-6a-1red?	0.299	22.000	1.853	0.147	2.000	15.299	low total 97.88
MM-117-6a-2red?	0.126	22.000	1.898	0.102	2.000	15.126	low total 97.53
MM-117-6a-4red	0.037	22.000	1.925	0.075	2.000	15.035	
MM-117-6a-5red	0.154	22.000	1.901	0.099	2.000	15.154	
MM-117-6a-7red	0.004	22.000	1.966	0.034	2.000	14.871	
MM-117-6b-9red	0.236	22.000	1.911	0.089	2.000	15.237	
MM-117-6b-10red	0.285	22.000	1.928	0.072	2.000	15.285	
MM-117-6c-15red?	0.211	22.000	1.922	0.078	2.000	15.211	
MM-117-6c-16red	0.325	22.000	1.952	0.048	2.000	15.325	low total 97.36
MM-117-6c-18red	0.389	22.000	1.959	0.041	2.000	15.388	
MM-70-2a-1red	0.285	22.000	1.859	0.141	2.000	15.285	
MM-70-2a-2red	0.213	22.000	1.886	0.114	2.000	15.214	
MM-70-2a-3red	0.420	22.000	1.866	0.134	2.000	15.419	
MM-V4-7a-1red	0.475	22.000	1.840	0.160	2.000	15.476	
MM-V4-7a-2red	0.460	22.000	1.793	0.207	2.000	15.460	low total 97.75
MM-V4-7a-3red	0.463	22.000	1.760	0.240	2.000	15.463	low total 97.5
MM-V4-7b-4red	0.510	22.000	1.778	0.222	2.000	15.509	low total 97.83
MM-V4-7b-5red?	0.408	22.000	1.831	0.169	2.000	15.411	low total 97.58
MM-V4-7b-6red	0.514	22.000	1.811	0.189	2.000	15.513	low total 97.84
MM-V4-7c-7red	0.503	22.000	1.856	0.144	2.000	15.504	low total 97.9
MM-V4-7c-8red	0.542	22.000	1.853	0.147	2.000	15.541	low total 97.52
MM-V8-1a-2red	0.402	22.000	1.820	0.180	2.000	15.402	
MM-V8-1a-3red?	0.512	22.000	1.828	0.172	2.000	15.512	
MM-V8-1b-5red	0.486	22.000	1.850	0.150	2.000	15.487	low total 97.98
MM-V8-1b-6red	0.503	22.000	1.809	0.191	2.000	15.503	low total 97.67
MM-V8-1b-7red	0.419	22.000	1.879	0.121	2.000	15.420	low total 97.64
MM-V8-1c-9red?	0.333	22.000	1.928	0.072	2.000	15.333	
MM-V8-1c-11red?	0.382	22.000	1.905	0.095	2.000	15.383	

Analysis	A>1	B< >2	C< >5	T< >8	W< >2	Initial $M^{3+}/\Sigma M$ and Manual normalization(s) both entered as TRUE
MM-117-1b-6red						
MM-117-1b-8red?						
MM-117-1c-10red						
MM-117-1c-11red						
MM-117-6a-1red?						
MM-117-6a-2red?						
MM-117-6a-4red						
MM-117-6a-5red						
MM-117-6a-7red		low B sum: 1.867				
MM-117-6b-9red						
MM-117-6b-10red						
MM-117-6c-15red?						
MM-117-6c-16red						
MM-117-6c-18red						
MM-70-2a-1red						
MM-70-2a-2red						
MM-70-2a-3red						
MM-V4-7a-1red						
MM-V4-7a-2red						
MM-V4-7a-3red						
MM-V4-7b-4red						
MM-V4-7b-5red?						
MM-V4-7b-6red						
MM-V4-7c-7red						
MM-V4-7c-8red						
MM-V8-1a-2red						
MM-V8-1a-3red?						
MM-V8-1b-5red						
MM-V8-1b-6red						
MM-V8-1b-7red						
MM-V8-1c-9red?						
MM-V8-1c-11red?						

Analysis	^{A}Ca or ^{A}Li present	sum of high-valence C cations (M^{3+},M^{4+}) >2
MM-117-1b-6red		
MM-117-1b-8red?		
MM-117-1c-10red		
MM-117-1c-11red		
MM-117-6a-1red?		
MM-117-6a-2red?		
MM-117-6a-4red		
MM-117-6a-5red		
MM-117-6a-7red		
MM-117-6b-9red		
MM-117-6b-10red		
MM-117-6c-15red?		
MM-117-6c-16red		
MM-117-6c-18red		
MM-70-2a-1red		
MM-70-2a-2red		
MM-70-2a-3red		
MM-V4-7a-1red		
MM-V4-7a-2red		
MM-V4-7a-3red		
MM-V4-7b-4red		
MM-V4-7b-5red?		
MM-V4-7b-6red		
MM-V4-7c-7red		
MM-V4-7c-8red		
MM-V8-1a-2red		
MM-V8-1a-3red?		
MM-V8-1b-5red		
MM-V8-1b-6red		
MM-V8-1b-7red		
MM-V8-1c-9red?		
MM-V8-1c-11red?		